

THE JOURNAL OF PHYSICAL CHEMISTRY

Volume 68, Number 11 November, 1964

Thermodynamic Properties of the Vapor Phase of Sodium Tetrachloroferrate(III)	R. Ronald Richards and N. W. Gregory	3089
Logarithmic Distribution Functions for Colloidal Particles	W. F. Espenscheid, M. Kerker, and E. Matijević	3093
High Pressure Mass Spectrometric Study of Alkanes	M. S. B. Munson, J. L. Franklin, and F. H. Field	3098
The Radiolysis of Aqueous Perchloric Acid Solutions	D. Katakis and A. O. Allen	3107
Tritium β -Radiation-Induced Isotopic Exchange with Water Vapor	John Y. Yang and L. H. Gevantman	3115
Extraction of Hexavalent Uranium by Trilaurylamine Nitrate	P. J. Lloyd and E. A. Mason	3120
Oxidation of Hydrocarbons Adsorbed on Oxide Catalysts Induced by Cobalt-60 γ -Rays	Harold W. Kohn	3129
Temperature Dependence of the Unperturbed Dimensions of Polystyrene	T. A. Orofino and A. Ciferri	3136
Classical Unimolecular Rate Theory. II. Effect of the Distribution of Initial Conditions	Roger C. Baetzold and David J. Wilson	3141
On Planetary Electron Corrections to Electron Diffraction Intensity Data	T. Iijima and R. A. Bonham	3146
Chemical Properties of Carbamoylpyridinium Compounds; Ionic Decomposition in Nonhydroxylic Organic Solvents	S. L. Johnson and K. A. Rumon	3149
The Effect of Substitution on the Ionization Potentials of Free Radicals and Molecules. VII. Theoretical Rationalization for Differing Correlations Found for Bond Dissociation Energies with Ionization Potentials and Electron Affinities of Organic or Inorganic Radicals	Joyce J. Kaufman	3155
Equation of State and Related Properties of Polymer and Oligomer Liquids	V. S. Nanda and Robert Simha	3158
Carbon-13 Proton Spin Coupling Constants in Heteroaromatic Molecules	Kazuo Tori and Toshio Nakagawa	3163
Shock Tube Study of the Acetylene-Oxygen Reaction	R. F. Stubbeman and W. C. Gardiner, Jr.	3169
Catalytic Deuterium Exchange Reactions with Organics. XIV. Distinction between Associative and Dissociative π -Complex Substitution Mechanisms	J. L. Garnett and W. A. Sollich-Baumgartner	3177
Isotope Effects in the Hydrogen Abstraction from Aliphatic Compounds by Radiolytically Produced Hydrogen Atoms in Aqueous Solutions	M. Anbar and D. Meyerstein	3184
A Correlation between Vibrational Isotope Shifts and Mass Spectral Fragmentation Patterns	Walter J. Lehmann	3188
Energetics of Some Gaseous Oxygenated Organic Ions	M. S. B. Munson and J. L. Franklin	3191
The Nature of the Acidic Sites on a Silica-Alumina. Characterization by Infrared Spectroscopic Studies of Trimethylamine and Pyridine Chemisorption	Michael R. Basila, Theodore R. Kantner, and Kee H. Rhee	3197
Spin-Spin Coupling in the Tetrafluoroborate Ion	Karl Kuhlmann and David M. Grant	3208
Radiolysis of Cyclohexene. III. Cyclohexene- d_{10}	B. R. Wakeford and G. R. Freeman	3214
A Surface Tension Study of the Interaction of Dimethyldodecylamine Oxide with Potassium Dodecanesulfonate in Dilute Aqueous Solution	Milton J. Rosen, David Friedman, and Michael Gross	3219
Hydrogen Bonding in Nitro Compounds	H. E. Ungnade, E. M. Roberts, and L. W. Kissinger	3225
Vaporization Reactions in the Copper Chloride-Chlorine System	Robert R. Hammer and N. W. Gregory	3229
Acid Dissociation and Proton Transfer of <i>p</i> -Toluidinium Ion and Dimethylphenylphosphonium Ion in Methanol	M. Cocivera, Ernest Grunwald, and Charles F. Jumper	3234
The Heat Capacity of and the Entropy Change in a Monolayer of Oxygen Chemisorbed on Platinum Black from 15 to 300°K.	R. A. Fisher, H. Chon, and J. G. Aston	3240
A Calorimetric Study of the Transformation of Some Metastable Modifications of Alumina to α -Alumina	T. Yokokawa and O. J. Kleppa	3246

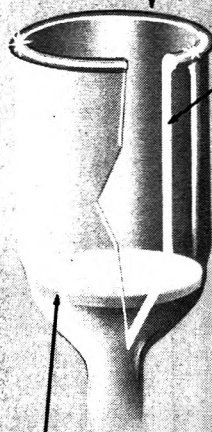
You get more of the better things first from **KIMBLE**

FOR EXAMPLE, BETTER

Kimflow® Fritted Ware

Better because . . . you can be sure of the most exactly controlled porosities in the industry. Permanently stained porosity markings give you rapid, visual identification.

Heavy, uniformly glazed rim prevents chipping and cracking



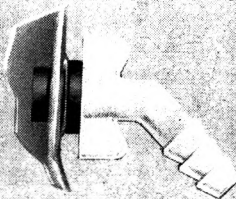
Heavy-duty wall

Maximum surface hardness

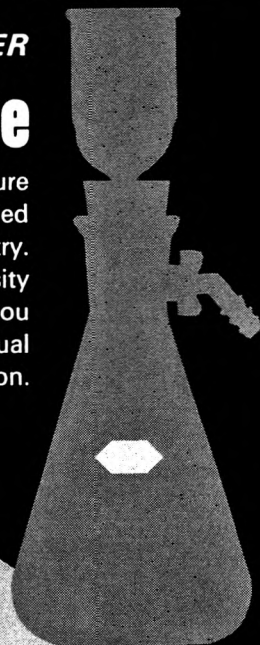


Precision-made disc for: Controlled correct porosity . . . Maximum filtering area


Seal achieved without altering porosity of disc

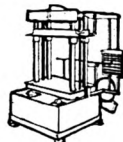


Note flexible polypropylene sidearm



OWENS-ILLINOIS

maker of Kimble Products
Toledo 1, Ohio 



Look to



America's
Leading Supplier
of Testing and
Laboratory Equipment

**MORE THAN 1,500
TESTING MACHINES
AVAILABLE FROM TMI**

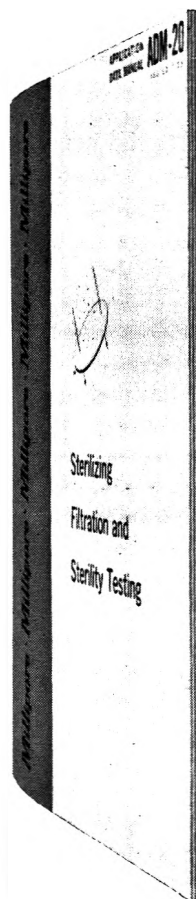
Ask for New 450 page Equipment Directory

Also

- Custom Design and Manufacturing
- Technical Assistance on Testing Problems
- Repair and Calibration

TESTING MACHINES INC.

MINEOLA, NEW YORK • Phone 516-747-7466



Worth writing for

30 PAGES — FREE OF CHARGE

ADM-20, "Sterilizing Filtration and Sterility Testing" describes techniques for using Millipore filters to sterilize pharmaceutical and biological solutions. Includes new MF technique for sterility testing of antibiotics in accordance with F.D.A. regulations. To get a copy of this manual, write to

Millipore® FILTER CORPORATION

180 Ashby Road Bedford, Mass.

Millipore® filters are cellulose plastic porous membranes made in twelve pore-size grades from 8 microns down to 10 millimicrons. In microfiltration or analysis, all matter larger than the filter pore size is screened from fluids and retained on the filter surface.

Heat Capacity of Cobalt(II) Bromide from 74 to 450° and a Structural Change in the Vicinity of 370°	Theodore J. Wydeven and N. W. Gregory	3249
Flash Photolysis in Thin Films of Gelatin and Other Polymers	A. V. Buettner	3253
The Crystal Structure of Strontium Bromide Monohydrate	Maurice Dyke and Ronald L. Sass	3259
Significant Structure Theory of Transport Phenomena	Teresa S. Ree, Taikyue Ree, and Henry Eyring	3262
Kinetic Studies of the Selectivity of Xylene Isomerization over Silica-Alumina Catalyst	A. J. Silvestri and C. D. Prater	3268
Spin-Free Quantum Chemistry. II. Three-Electron Systems	F. A. Matsen	3282
The Radiation Chemistry of Organic Liquid Mixtures. II	J. F. Merklin and S. Lipsky	3297
Kinetic Salt Effects in Concentrated Solutions of Supporting Electrolyte. The Reaction between the Bromopentaamminecobalt(III) and Hydroxyl Ions	Berta Perlmutter-Hayman and Yael Weissmann	3307
Relative Cation Mobilities in Potassium Chloride-Lithium Chloride Melts	Cornelius T. Moynihan and Richard W. Laity	3312
Transient Species Observed in the Catalyzed Decomposition of Ammonia	Charles E. Melton and Paul H. Emmett	3318
Substituent Effects on Intramolecular Energy Transfer. II. Fluorescence Spectra of Europium and Terbium β -Diketone Chelates	N. Filipescu, W. F. Sager, and F. A. Serafin	3324
Chronopotentiometric Study of Anionic Diffusion in the Potassium-Liquid Ammonia System	Roger P. Gordon and Benson Ross Sundheim	3347
Heats of Formation of Some Hexavalent Uranium Compounds	E. H. P. Cordfunke	3353
Mercaptan Inhibition of the Decay of a Smooth Platinum Cathode	Joel Jacknow, Henry Eyring, and Terrell N. Andersen	3357
Faradaic Impedance at Platinum Microelectrodes. Behavior of the Iodide-Iodine Oxidation-Reduction Couple	A. B. Thomas and R. J. Brodd	3363
Extensions of the Steady-State Rate Law for the Fumarase Reaction	Mildred Taraszka and Robert A. Alberty	3368
Self-Dissociative Equilibria in Molten Phosphoric Acid	Ronald A. Munson	3374
Solute Diffusional Specificity in Hydrogen-Bonding Systems	Samuel B. Horowitz and I. Robert Fenichel	3378
The Nucleation of Long-Chain Molecules	L. Mandelkern, J. G. Fatou, and C. Howard	3386
Kinetics of the Acid-Catalyzed Hydrolysis of Acetal in Dimethyl Sulfoxide-Water Solvents at 15, 25, and 35°	Richard K. Wolford	3392
Water Adsorption on Molybdenum Disulfide Containing Surface Contaminants	R. R. M. Johnston and A. J. W. Moore	3399
Dipole Association	Claude Treiner, James F. Skinner, and Raymond M. Fuoss	3406
Classical Model for Free Radical Formation	H. Shin	3410
Dynamic Mechanical Properties of Cross-Linked Rubbers. I. Effects of Cross-Link Spacing in Natural Rubber	John D. Ferry, Ralph G. Mancke, Etsuji Maekawa, Yasuji Oyanagi, and Ray A. Dickie	3414
Viscosity of Metallic Mercury (and Its Saturated Vapor) over Its Entire Liquid Range, <i>i.e.</i> , from Its Melting Point (234.3°K.) to Its Critical Point (1733°K.), and an Estimate of Its Critical Viscosity	A. V. Grosse	3419

NOTES

An Electron Spin Resonance Study of the Anion Radical of Benzocyclobutadienoquinone	David H. Geske and Alan L. Balch	3423
Heat of Formation of $MgAl_2O_4$	Robert L. Altman	3425
A Solid Benzene-Tetra- <i>n</i> -butylammonium Nitrate Complex	Thomas J. Plati and Edward G. Taylor	3426
Kinetics of <i>n</i> -Paraffin Sorption in the Natural Zeolite Erionite	R. M. Barrer and D. L. Peterson	3427
Proton-Proton Spin Coupling Constants in Ethyl Derivatives	S. Ebersole, S. Castellano, and A. A. Bothner-By	3430
Interchange of <i>cis</i> and <i>trans</i> Chemical Shifts in Symmetrically Substituted Amides	A. Greenville Whittaker, D. W. Moore, and S. Siegel	3431
Surface Tensions of Binary Mixtures of Isooctane with Benzene, Cyclohexane, and <i>n</i> -Dodecane at 30°	Hiram Butler Evans, Jr., and H. Lawrence Clever	3433
Thermodynamics of Ionization and Tautomerism of Aqueous Pyridine Monocarboxylic Acids	Frank J. Millero, J. C. Ahluwalia, and Loren G. Hepler	3435

You get more of the better things first from **KIMBLE**

FOR EXAMPLE, BETTER

SAFE-GARD Pipets

Better because . . . you get color coding for rapid, errorless sorting, plus SAFE-GARD® tip for protection and long life — all at no extra cost. Pipets also resist fogging and etching.



Uniform O.D. and I.D. for trouble-free use with plugging machine

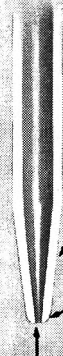
Designed with precise seat for cotton plug

Color-coded for instant size identity

Bold size identification

N-51A glass provides best known resistance to chemical attack and scratching

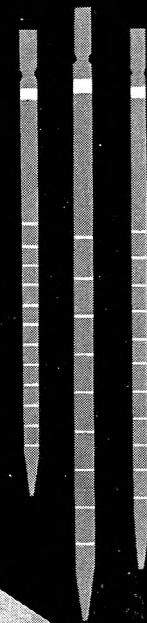
Permanent scale . . . Ratio of I.D. to scale length controlled for optimum separation of subdivisions



Tempered tip for high impact strength

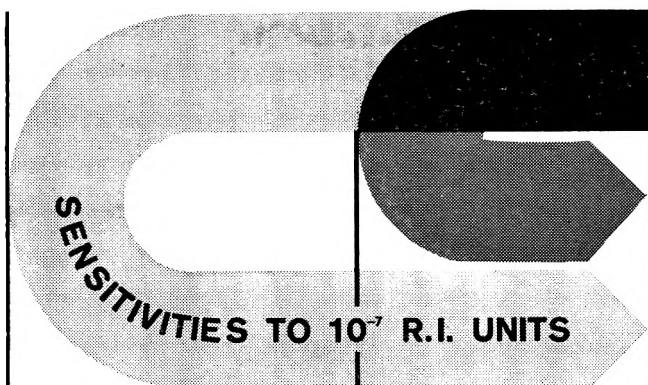
Glazed tip won't harbor impurities

Controlled orifice for correct delivery time and highest accuracy



OWENS-ILLINOIS

maker of Kimble Products
Toledo 1, Ohio



DIFFERENTIAL REFRACTOMETERS

MEASURE:

Small refractive index differences between Solvents and Solutions;

Concentrations;

Refractive index increments for use in light scattering, ultracentrifugation, streaming birefringence, electrophoresis, diffusion.

A complete line of manual, automatic indicating, and recording models is available. Write for descriptive Bulletin R-2000.

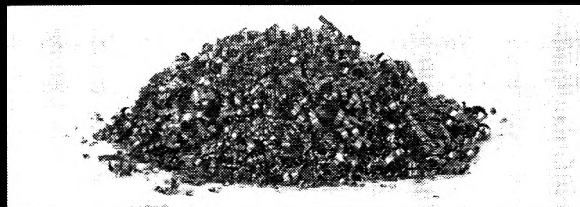


PHOENIX PRECISION INSTRUMENT COMPANY

A subsidiary of CENCO INSTRUMENTS CORP.

3803-05 N. 5TH ST., PHILA., PENNA., 19140, U.S.A.

HIGH PURITY RARE EARTH METALS



High purity rare earth metals of these properties can be used in pure form or in alloys — also can be machined, rolled or cast.

Properties of DYSPROSIUM

OTHER METALS PRODUCED	Density	8.6
	Brinell Hardness	50
	Melting Point °F	2700
YTTRIUM	Boiling Point	4710
	Electrical Resistivity (55 F)	56
GADOLINIUM	Thermal Conductivity (55 F)	7.0
PRAESODYMIUM	Thermal Neutron X-section	1100
NEODYMIUM	Ultimate Tensile Strength psi	37,000
LANTHANUM	Yield Strength (as cast) psi	33,000
	CHROMIUM	Ductile, Machinable

For further information send for brochure.

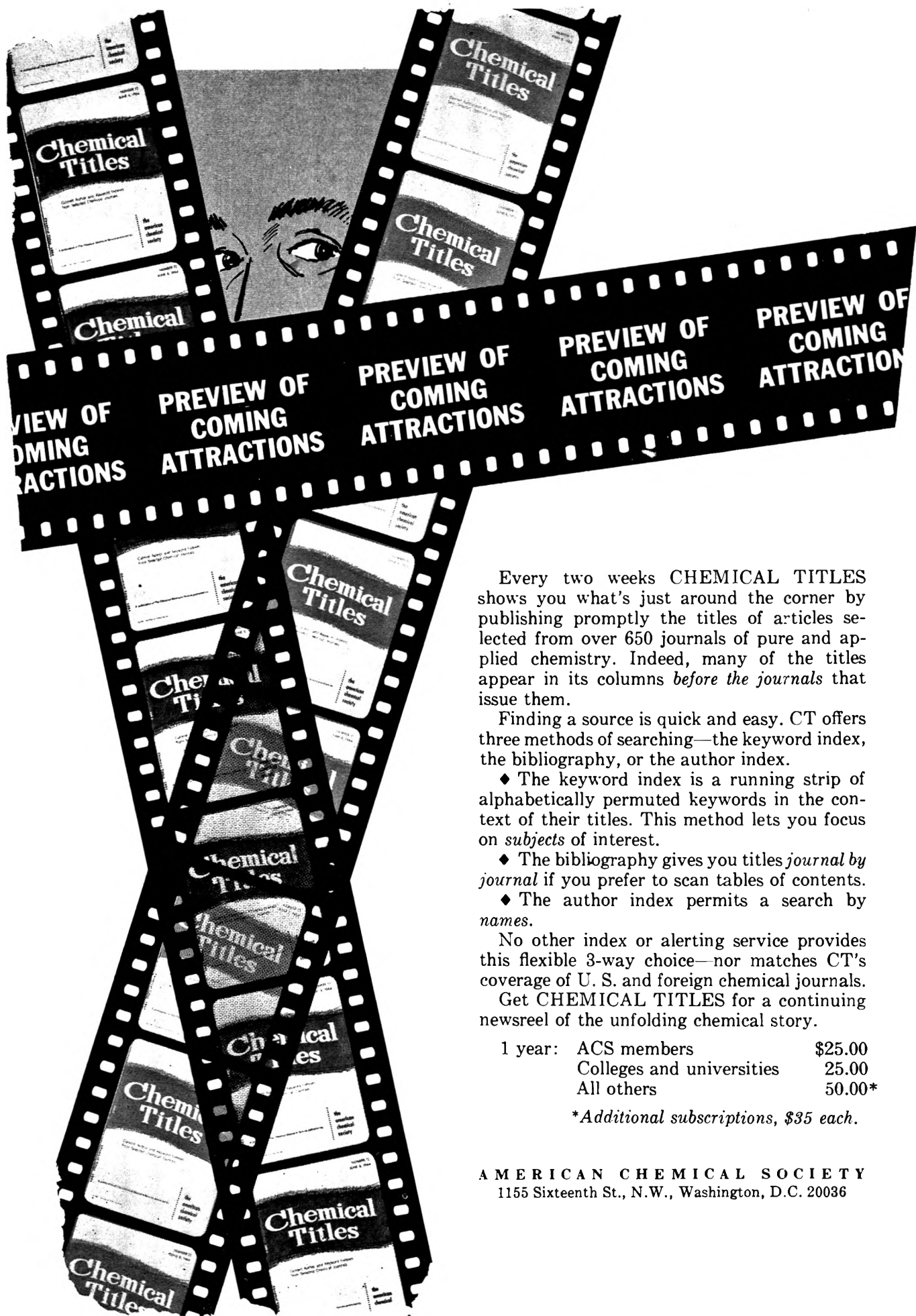
LUNEX COMPANY
PLEASANT VALLEY 1, IOWA

.....	Homer Jacobson and Herbert Dubno	3437
Reaction of Hydroxylamine with Thioesters	R. Bruce Martin and Laura P. Henkle	3438

Important Notice to Authors

Professor Frederick T. Wall officially will assume the editorship of *The Journal of Physical Chemistry* effective January 1, 1965. New manuscripts submitted to *The Journal of Physical Chemistry* after December 1, 1964 should be sent directly to Professor Wall addressed as follows:

Dr. Frederick T. Wall, Editor, *The Journal of Physical Chemistry*
Department of Chemistry, University of California
Santa Barbara, California



Every two weeks CHEMICAL TITLES shows you what's just around the corner by publishing promptly the titles of articles selected from over 650 journals of pure and applied chemistry. Indeed, many of the titles appear in its columns *before the journals* that issue them.

Finding a source is quick and easy. CT offers three methods of searching—the keyword index, the bibliography, or the author index.

- ◆ The keyword index is a running strip of alphabetically permuted keywords in the context of their titles. This method lets you focus on *subjects* of interest.

- ◆ The bibliography gives you titles *journal by journal* if you prefer to scan tables of contents.

- ◆ The author index permits a search by *names*.

No other index or alerting service provides this flexible 3-way choice—nor matches CT's coverage of U. S. and foreign chemical journals.

Get CHEMICAL TITLES for a continuing newsreel of the unfolding chemical story.

1 year:	ACS members	\$25.00
	Colleges and universities	25.00
	All others	50.00*

*Additional subscriptions, \$35 each.

AMERICAN CHEMICAL SOCIETY
1155 Sixteenth St., N.W., Washington, D.C. 20036

THE JOURNAL OF PHYSICAL CHEMISTRY

Registered in U. S. Patent Office © Copyright, 1964, by the American Chemical Society

VOLUME 68, NUMBER 11 NOVEMBER 16, 1964

Thermodynamic Properties of the Vapor Phase of Sodium Tetrachloroferrate(III)

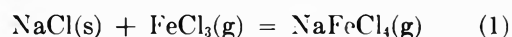
by R. Ronald Richards and N. W. Gregory

Department of Chemistry, University of Washington, Seattle, Washington 98105 (Received July 15, 1964)

Thermodynamic properties of $\text{NaFeCl}_4(\text{g})$ relative to values for ferric chloride vapor and solid sodium chloride have been determined by study of the equilibrium between these substances, using a transpiration method. Bond energies and structural characteristics of the molecules are considered.

Studies of the system sodium chloride–ferric chloride have been published by Johnstone, *et al.*,¹ Morozov and Toptygin,² and Cook and Dunn.³ It was observed by the earlier workers that the vapor pressure of ferric chloride above its liquid, particularly in the vicinity of 40–50 mole % sodium chloride, falls rapidly as sodium chloride is added; the decrease is much greater than expected from simple mixing effects. Cook and Dunn demonstrated the existence of sodium tetrachloroferrate as a solid phase by analysis of cooling curves and X-ray powder patterns. Their phase study indicates a congruent melting point at 163°. The vapor pressure of NaFeCl_4 above the melt has been reported by Cook and Dunn³ and by Korshunov, *et al.*⁴ Whereas, together with heat of solution, heat of fusion, and heat capacity data also provided by Cook and Dunn, one can use the liquid phase vaporization data to calculate thermodynamic properties of the vapor, a considerable uncertainty arises from the combination of uncertainties in the numerous thermo-

chemical equations required and lack of knowledge of activities in the liquid solution with ferric chloride. Morozov and Toptygin,² in a phase study, found that virtually pure sodium chloride exists in equilibrium with the melt on the sodium chloride-rich side of the phase diagram. In view of this we have undertaken an experimental study of the reaction



as a direct means of determining the thermodynamic properties of the addition compound. With the activity of sodium chloride at unity and its thermo-

(1) H. F. Johnstone and R. W. Darbyshire, *Ind. Eng. Chem.*, **34**, 280 (1942); H. F. Johnstone, H. C. Weingartner, and W. E. Winsche, *J. Am. Chem. Soc.*, **64**, 241 (1942).

(2) I. S. Morozov and D. Y. Toptygin, *Zh. Neorgan. Khim.*, **2**, 2129 (1957).

(3) C. M. Cook and W. E. Dunn, *J. Phys. Chem.*, **65**, 1505 (1961).

(4) B. G. Korshunov, I. S. Morozov, V. I. Ionov, and M. A. Zorina, *Izv. Vysshikh Uchebn. Zavedenii, Tsvetn. Met.*, **3**, 5, 67 (1960).

dynamic properties well known, the properties of NaFeCl_4 relative to those of FeCl_3 can be determined.

Experimental

A transpiration method with argon as the principal carrier gas was used. The apparatus, Fig. 1, and procedure were similar to that described previously.⁵

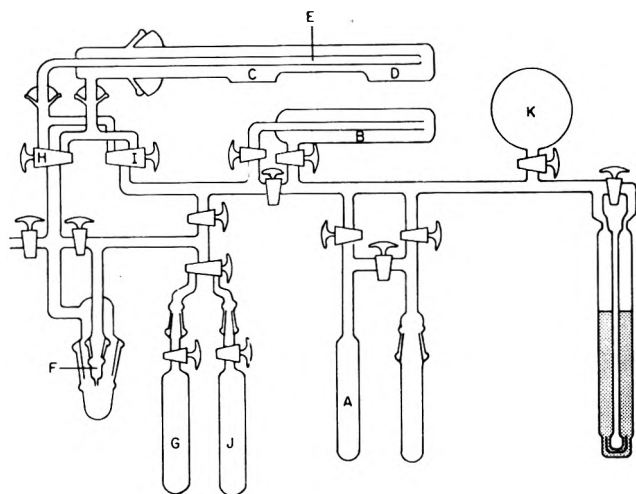


Figure 1. Transpiration apparatus.

Argon (Matheson 99.99%) condensed in tube A, which was then immersed in boiling liquid oxygen, served as a source of gas at a pressure of *ca.* 100 cm. The flow rate was controlled with a capillary restriction F beyond which argon was condensed in tube G, or J, cooled with liquid nitrogen. The argon first passed through tube B containing CuCl_2 heated to the vicinity of $410\text{--}440^\circ$ to introduce (by decomposition to CuCl) a partial pressure of 0.5 to 3.6 mm. of chlorine to prevent subsequent decomposition of ferric chloride. This gas mixture then passed over a sample of $\text{FeCl}_3(\text{s})$ at C, held at various temperatures around 175° to introduce the desired partial pressure of ferric chloride, adjacent to the main reactor D containing NaCl . The temperature of the sodium chloride in D was held at various values ranging from 350 to 530° for the equilibrium study.

The equilibrium mixture of gases left the reaction chamber *via* the small removable exit tube E in the center; the NaFeCl_4 condensed near the junction of the furnace surrounding D and the separate furnace surrounding C; the ferric chloride condensed at the outer end of furnace C; the argon and chlorine continued on through the capillary orifice and into the liquid nitrogen-cooled trap G. Temperatures were held to within $\pm 1.5^\circ$ of the desired value during the 1 to

16-hr. runs. During the period the samples were brought to reaction temperatures, argon flow was reversed by means of stopcocks H and I so as to enter the reaction zone through the exit tube; the argon during this warm-up period was collected in the alternate trap J. When steady flow conditions, pressures, and temperatures were established, the stopcocks were quickly reversed to begin the run.

Eastman practical anhydrous FeCl_3 , or, in many experiments, material prepared by reaction of analytical grade iron wire with chlorine, was used. Samples were sublimed into place under vacuum from a side arm which was subsequently sealed off. Analytical grade sodium chloride, degassed before a run, was used. In general a given set of starting materials served for four or five runs; results from many independent samples were compared.

Traces of ferric oxide were observed in the system after a run. A number of experiments were conducted in which the argon was initially bubbled through liquid potassium to ensure removal of water. Results, when this precaution was taken, did not differ from those when argon was taken directly from a fresh sample condensed from the commercial cylinder; hence most of the experiments were conducted without additional purification precautions. The reactor was always thoroughly evacuated and baked out before a run. No dependence of results on the presence of oxide could be detected.

It was found that results were more consistent, and independent of flow rate, varying from 3 to 30 ml. min.^{-1} (calculated at 0° and 1 atm. (STP)), when ferric chloride pressures were high enough to cause some condensation of yellow liquid complex in the forepart of the reaction vessel D; the sodium chloride at the end of the reactor remained white with no trace of complex visible. Most of the experiments were conducted with some complex mixed with the sodium chloride. In some cases, to approach equilibrium in the opposite direction, argon and chlorine, without added ferric chloride, were allowed to flow over a mixture of previously formed complex and solid sodium chloride.

From the exit stream, the ferric chloride condensed as platelets; NaFeCl_4 condensed as liquid droplets which solidified as the furnaces were removed at the end of a run. In some cases the two deposits were separated and analyzed separately; in others they were dissolved in the same solution, and total iron and total sodium were determined. At the conclusion of a run, the vessel was left filled with argon, the

(5) L. E. Wilson and N. W. Gregory, *J. Phys. Chem.*, **62**, 433 (1958).

inner collector tube E removed quickly, and the apparatus resealed.

The condensates were washed out of the exit tube with water. An aliquot was acidified with a few drops of concentrated hydrochloric acid and the ferric ion reduced to ferrous with hydroxylamine hydrochloride. The acid seemed to ensure complete reduction. The ferrous ion was then complexed with 1,10-phenanthroline and determined colorimetrically by the standard procedure.⁶ The sodium content in another aliquot was determined using a Beckman DU flame photometer with photomultiplier attachment. Ferric chloride in the concentration present does not interfere.⁷ The aqueous solutions varied in sodium content from 2.5 to 28 p.p.m.; care was taken to avoid contamination.

Chlorine pressures were calculated from the number of moles of chlorine transported, determined by solution of the condensed sample in aqueous potassium iodide and titration of the liberated iodine by an amperometric dead-stop method.⁸ Amounts of argon were determined by expansion of the collected sample into a calibrated volume K, Fig. 1, and measurement of the gas pressure.

The equations of Merten predict that error caused by diffusion will be negligible in our apparatus.⁹ This was verified experimentally in a zero flow rate "run" at 530° under normal reaction conditions; the amount of iron which diffused into the collector tube was found to be only 0.5% of that collected in a regular low flow rate experiment.

Results and Discussion

Results are shown in Table I, with values of the equilibrium constant calculated on the basis that all the sodium was transported as sodium tetrachloroferrate. Sodium chloride is not significantly volatile at these temperatures.¹⁰ The number of moles of sodium was subtracted from the total number of moles of iron to obtain the total number of moles of iron transported as ferric chloride monomer and dimer. The partial pressure of ferrous chloride can be shown to be negligible.^{5,11} The partial pressures of the various gases were calculated from the number of moles determined analytically from the simple expression $P_i = X_i P_t$, where the total pressure, P_t , and total number of moles for the evaluation of the mole fraction X_i were taken as those of argon, since $n_{Ar} \gg n_{FeCl_3} + n_{Fe_2Cl_6} + n_{NaFeCl_4} + \dots$. The breakdown of the number of moles of iron into partial pressures of monomer and dimer, respectively, was carried out using the equation, $\log(P_{FeCl_3}^2/P_{Fe_2Cl_6}) = 6907T^{-1} + 9.391$, based on data of Kangro and Bernstorff.^{5,12}

It may be seen (Table I) that in five of the seven experiments in which the $NaFeCl_4$ and $FeCl_3$ deposits were analyzed separately, the atomic ratio of Na to Fe in the former corresponds very closely to 1:1; in the other two, the experimental result indicates the ratio is slightly larger. We have taken this as evidence that the principal sodium-containing species in the vapor phase is Na_2FeCl_4 . Polymers in significant quantities are not believed to be present because of the relationship of the amount of complex and of $FeCl_3(g)$. The equilibrium constant based on $(NaFeCl_4)_2$, for example, requires the partial pressure of this species to be proportional to the square of the pressure of $FeCl_3$. Data in Table I show this dimeric species cannot be the dominant one. A similar argument may be given for higher polymers. Species such as Na_2FeCl_5 and Na_3FeCl_6 cannot be ruled out on similar grounds; however, the composition of the condensed complex suggests that, if such species are present, their partial pressures must be very small.

From the slope of a $\ln K$ vs. T^{-1} plot, the enthalpy change for reaction 1 was found to be 3.7 ± 1 kcal.; the corresponding entropy change is 6.5 ± 1.5 cal. deg.⁻¹, taken as representative of a temperature of 450°. The enthalpy change for (1), estimated by combination of thermochemical equations based on earlier data, indicated in the introduction, is 2.7 ± 6 kcal., in good general agreement.

Kelley has pointed out that a rather large uncertainty exists in the published thermodynamic properties of $FeCl_3(g)$.¹³ Using his recommended values and data from ref. 12, 101 and 28.7 cal. deg.⁻¹ mole⁻¹ have been taken as S° of $FeCl_3(g)$ and $NaCl(s)$, respectively, at 723°K. These, together with our experimental result, give 136 cal. deg.⁻¹ mole⁻¹ for the standard entropy of $NaFeCl_4(g)$ at 723°K. Without information on the vibrational frequencies, meaningful values of the entropy cannot be calculated on a statistical basis because the vibrational contribution is so large. We

(6) H. H. Willard, L. L. Meritt, and J. A. Dean, "Instrumental Methods of Analysis," 3rd Ed., D. Van Nostrand Co., New York, N. Y., 1958, p. 58.

(7) J. A. Dean, "Flame Photometry," McGraw-Hill Book Co., New York, N. Y., 1960, pp. 110-122, 164, 165.

(8) G. Wernimont and F. J. Hopkinson, *Ind. Eng. Chem., Anal. Ed.*, **12**, 308 (1940).

(9) U. Merten, *J. Phys. Chem.*, **63**, 443 (1959).

(10) E. F. Frock and W. H. Rodebush, *J. Am. Chem. Soc.*, **48**, 2522 (1926).

(11) R. J. Sime and N. W. Gregory, *J. Phys. Chem.*, **64**, 86 (1960).

(12) W. Kangro and H. Bernstorff, *Z. anorg. allgem. Chem.*, **263**, 316 (1950).

(13) K. K. Kelley, "Contributions to the Data on Theoretical Metallurgy," U. S. Bureau of Mines Bulletin 584 (1960) and 592 (1961), U. S. Government Printing Office, Washington, D. C.

Table I: Results of Equilibrium Study of Reaction 1

Temp., °C.	Flow rate, cm. ³ min. ⁻¹ at STP	Argon pressure, cm.	mmoles transported					Calcd. pressures, mm. × 10 ²		Equilibrium constant K = P(NaFeCl ₄) P(FeCl ₃)
			Ar	Na as NaFeCl ₄ , × 10 ⁴	Fe as FeCl ₃ , × 10 ⁴	Fe as NaFeCl ₄ , × 10 ⁴	Total Fe, × 10 ⁴	FeCl ₃	NaFeCl ₄	
350 ^a	10.1	103.6	364	2.96	6.76	6.54	8.43	1.29 ^a
350	10.0	103.0	436	3.87	4.98	3.85	8.83	6.95	8.89	1.28
400	10.0	98.9	241	7.70	13.6	18.9	31.6	1.67
400	15.8	99.8	254	13.1	24.0	29.7	51.5	1.73
400	17.7	96.4	284	11.5	9.71	11.5	21.2	24.2	39.0	1.62
400	21.3	93.6	399	9.66	8.06	8.78	17.84	13.9	22.6	1.63
400	30.1	95.2	362	19.4	36.6	30.9	51.0	1.65
450	10.3	100.5	111	19.5	31.7	88.4	177	2.00
450	16.8	97.2	135	25.0	15.0	25.1	40.1	90.4	180	1.99
450	18.0	95.1	104	17.1	10.4	17.0	27.4	76.8	156	2.04
500	3.36	102.0	71.9	4.35	6.19	25.6	61.8	2.41
500	10.0	99.3	121	7.56	4.2	6.76	10.96	27.4	62.0	2.26
500	10.9	102.5	127	9.90	9.90	23.7	55.8	2.36
500	15.7	95.2	105	32.6	21.4	32.6	54.0	144	331	2.30
500	17.0	97.1	137	14.3	21.3	48.0	101	2.11
500	26.0	85.4	75.5	9.21	13.5	47.0	104	2.21
530 ^a	9.69	100.4	25.9	30.6	44.5	471	1190	2.52 ^a
530	10.2	100.5	136	6.61	9.14	18.6	48.9	2.63
530	10.6	103.8	157	3.95	5.38	16.7	41.6	2.49
530	16.6	96.8	111	3.95	5.38	12.5	34.4	2.75
530 ^a	22.9	91.8	61.2	87.0	126	503	1300	2.59 ^a

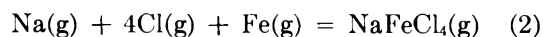
^a Points determined without prior introduction of ferric chloride into carrier gas.

have made some estimates, however, which suggest that our value is reasonable. The combined translational and rotational contribution is expected to be of the order of 77 cal. deg.⁻¹ mole⁻¹. The rotational contribution of ca. 30 was based on a model in which the four chlorine atoms are arranged tetrahedrally about the iron atom (at the same distance found in the solid in a crystal structure determination to be reported from this laboratory) with the sodium atom near the center of one of the faces of the tetrahedron at a distance of 2.5 Å. from each of the neighboring chlorine atoms. If one assumes an electronic contribution of about 5, associated with the unpaired electrons of iron(III), this leaves 54 cal. deg.⁻¹ mole⁻¹ to be contributed by the vibrational partition functions, an average of 4.5 for each degree of freedom. This average corresponds to a frequency of the order of 140 cm.⁻¹.

Woodward and Taylor¹⁴ have observed the Raman spectra of an ethereal extract of an aqueous solution of FeCl₃·HCl; they have assigned frequencies for the solvated tetrachloroferrate ion of 106(2), 133(3), 330, and 385(3) cm.⁻¹. If these values are used to estimate the contribution of nine of the degrees of freedom for the vapor molecule NaFeCl₄, the remaining contribution to the entropy from the additional three degrees of freedom (associated with the presence of the

sodium atom) would have to be ca. 20, which would require three frequencies of the order of 50 cm.⁻¹. One would certainly expect some change in the Woodward-Taylor frequencies for NaFeCl₄; however, even frequencies of the order of 50 cm.⁻¹ appear not unreasonable when compared with values for bending frequencies in some of the transition metal halides.¹⁵

Using an estimate mean value of ΔC_p for (1) of -1 cal. deg.⁻¹, the enthalpy change at 298.2°K. is found to be 4.1 kcal. This, together with data from ref. 5 and NBS Circular 500,¹⁶ leads to a value of -392 kcal. for ΔH₂₉₈^o for reaction 2.



If the sodium-chlorine bond energy in the complex is assumed to be roughly the same as that in sodium chloride, an average value of 73.4 kcal. is obtained for the Fe-Cl bonds. The value of the latter in FeCl₃(g) is 81 kcal. and in Fe₂Cl₆(g) an average of 65 kcal. It is

(14) J. A. Woodward and M. J. Taylor, *J. Chem. Soc.*, 4473 (1960).

(15) L. Brewer, G. R. Somayajulu, and E. Brackett, *Chem. Rev.*, **63**, 111 (1963).

(16) D. D. Wagman, W. H. Evans, S. Levine, and I. Jaffe, "Selected Values of Chemical Thermodynamic Properties," National Bureau of Standards Circular 500, U. S. Government Printing Office, Washington, D. C., 1952.

interesting to note that if a structure in which the sodium is bridged to the iron in FeCl_4^- through interaction with two chlorines is considered, the average energy for the six bonds in the same as the average of the eight Fe-Cl bonds in Fe_2Cl_6 .

The standard heat of formation of $\text{NaFeCl}_4(\text{g})$ at 298°K., calculated using -60 ± 3 kcal. as ΔH°

for $\text{FeCl}_3(\text{g})$ ^{5,12} and -98.2 kcal. for NaCl ,¹⁶ is -154 ± 4 kcal. mole⁻¹.

Acknowledgment. This work was supported in part by grants from the National Science Foundation and from the U. S. Army Research Office (Durham), which we acknowledge with thanks.

Logarithmic Distribution Functions for Colloidal Particles^{1a}

by W. F. Espenscheid,^{1b} M. Kerker, and E. Matijević

Chemistry Department, Clarkson College of Technology, Potsdam, New York (Received July 13, 1964)

The distribution function used in earlier light-scattering studies had been erroneously termed a *logarithmic normal distribution* when, in fact, this was a new distribution function with different parameters and properties. This new function, called a *zeroth-order logarithmic distribution*, is described herein. Since one of the parameters is the modal value of the variable, this new function permits exploration of the effect of changing the breadth of the distribution while keeping the mode invariant. A generalized logarithmic function is described which permits selection of other moments of the distribution as the size parameter appearing explicitly in the distribution function.

In a recent series of papers from this laboratory, the particle size distribution of a variety of colloids has been determined by comparison of the polarization of the scattered light with theoretical calculations. These calculations assumed that the particle sizes could be represented by a two-parameter distribution function which we had called a *logarithmic normal distribution*.²⁻⁴ For each particular system, a "solution" consisted in determining the values of the distribution parameters which gave theoretical light-scattering functions in agreement with the experimental data. This approach has also been followed by Heller and his collaborators with different experiments and a different distribution function than utilized by us.⁵

It has become apparent to us that the distribution function which we had used is actually a new distribution function, rather than the logarithmic normal distribution, and that the parameters in question stand

for physical quantities different from those stated. We would like to clarify the matter in this paper by describing in detail some of the properties of this new distribution and by comparing it with the logarithmic normal distribution. We will then write the expression for a generalized logarithmic distribution function which may be reduced to the logarithmic normal distribution or to the one used by us. For reasons which

(1) (a) Supported in part by research grant AF-0048 from the Division of Air Pollution of the Public Health Service; (b) Socony-Mobil Fellow; part of a Ph.D. Thesis by W. F. Espenscheid.

(2) (a) M. Kerker, E. Daby, G. L. Cohen, J. P. Kratochvil, and E. Matijević, *J. Phys. Chem.*, **67**, 2105 (1963); (b) M. Kerker, E. Matijević, W. F. Espenscheid, W. A. Farone, and S. Kitani, *J. Colloid Sci.*, **19**, 213 (1964).

(3) E. Matijević, S. Kitani and M. Kerker, *ibid.*, **19**, 223 (1964).

(4) W. F. Espenscheid, E. Matijević, and M. Kerker, *J. Phys. Chem.*, **68**, 2831 (1964).

(5) W. Heller and M. L. Wallach, *ibid.*, **67**, 2577 (1963); H. L. Bhatnagar and W. Heller, *J. Chem. Phys.*, **40**, 480 (1964).

will become obvious, we call this a *zeroth-order logarithmic distribution*. Other workers in colloid science may find this distribution advantageous for their purposes, so we are hopeful that, in addition to correcting misstatements in our earlier work, this paper may also serve a more general purpose.

A distribution or frequency function, $p(r)$, will be defined by

$$P(r) = \int_r^{r+\Delta r} p(r)dr \quad (1)$$

where $P(r)$ gives the fraction of the population with values of the parameter r between r and $r + \Delta r$. The function is *normalized* if the value of the integral over all possible values of r is unity. Undoubtedly, the best known distribution function is the *normal distribution*

$$p(r) = \frac{1}{\sqrt{2\pi}\sigma} \exp \frac{-(r - \bar{r})^2}{2\sigma^2} \quad (2)$$

where the two parameters, \bar{r} and σ , are the mean value and the standard deviation of r , defined by

$$\bar{r} = \int_{-\infty}^{\infty} rp(r)dr \quad (3)$$

and

$$\sigma^2 = \int_{-\infty}^{\infty} (r - \bar{r})^2 p(r)dr \quad (4)$$

Here, the exponential factor in the distribution describes a Gaussian curve, and the pre-exponential factor normalizes the expression. Because of the symmetry of this distribution, two other parameters of interest, the modal value, r_M , and the median, r_m , are identical with the mean. The mode is the value of r at the maximum frequency; the median is the value below which 50% of the population falls.

Obviously, a normal distribution cannot represent a distribution of particle sizes because it admits negative values of r . In addition, unlike the symmetrical normal distribution, naturally occurring populations are frequently positively skewed. A satisfactory representative of many such populations is the logarithmic normal distribution

$$p(r) = \frac{1}{\sqrt{2\pi}\sigma_g r} \exp \frac{-(\ln r - \ln r_m)^2}{2\sigma_g^2} \quad (5)$$

In this distribution, it is $\ln r$ rather than r which is normally distributed, so that

$$\ln r_m = \int_0^{\infty} \ln rp(r)dr \quad (6)$$

and

$$\sigma_g^2 = \int_0^{\infty} (\ln r - \ln r_m)^2 p(r)dr \quad (7)$$

Thus, $\ln r_m$ is the mean value of $\ln r$ and r_m is, in this case, both the median and the geometric mean value of r

$$r_g = r_m = (r_1 \cdot r_2 \cdot r_3 \cdots r_n)^{1/n} \quad (8)$$

The second parameter of this distribution, σ_g , is the standard deviation of $\ln r$. Its antilogarithm is the geometric mean standard deviation. The mode, the median, and the mean are related to the geometric mean by

$$\ln r_M = \ln r_g - \sigma_g^2 \quad (9)$$

$$\ln r_m = \ln r_g \quad (10)$$

$$\ln r = \ln r_g + \sigma_g^2/2 \quad (11)$$

Figure 1 shows the frequency curves for three logarithmic normal distributions for which $r_m = r_g = 3.0$ and $\sigma_g = 0.1, 0.2, 0.3$, and 0.5 . All three curves have the same values of r_m . The skewness of the distribution depends upon σ_g , and, for sufficiently small values of σ_g , there is so little skewness that the frequency curve

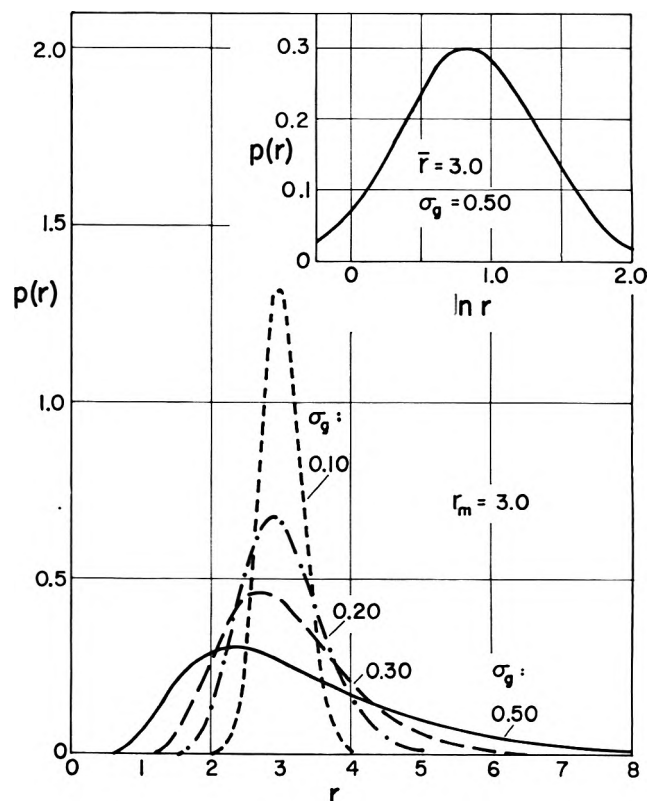


Figure 1. Distribution curves for the logarithmic normal distribution, eq. 5, with $r_m = r_g = 3.0$ and $\sigma_g = 0.1, 0.2, 0.3$, and 0.5 . In the inset, the frequency is plotted vs. $\ln r$ for one case.

can be closely approximated by a normal distribution. As a general rule for practical work, both r and $\log r$ can be considered to be normally distributed as long as $\sigma_r < 0.14$.⁶ Another feature of this distribution is the movement of the modal value of r toward smaller values as σ_r increased for a fixed value of r_m .

Although we had termed the distribution used in our earlier cited work, a logarithmic normal distribution, in actual fact, we had used the frequency function

$$[p(r)] = \frac{1}{\sqrt{2\pi}\sigma_0} \exp \frac{-(\ln r - \ln r_M)^2}{2\sigma_0^2} \quad (12)$$

Meehan and Beattie, who also claimed to have utilized a logarithmic normal distribution for analysis of particle size by light scattering, have made a similar error.⁷ The above expression will lead to the same value of $p(r)$ as a logarithmic normal distribution only if it is integrated with respect to $\ln r$, rather than with respect to r as indicated by eq. 1. As it now stands, the expression given by eq. 12 must be normalized in order to convert it into a true frequency function so that

$$p(r) = \frac{\exp -(\ln r - \ln r_M)^2 / (2\sigma_0^2)}{\int_0^\infty \exp -(\ln r - \ln r_M)^2 / (2\sigma_0^2) dr} = \frac{\exp -(\ln r - \ln r_M)^2 / (2\sigma_0^2)}{\sqrt{2\pi}\sigma_0 r_M \exp(\sigma_0^2/2)} \quad (13)$$

The evaluation of the integral in the denominator is described in the Appendix.

This new distribution will be called a *zeroth-order logarithmic distribution*. It is defined by two parameters, r_M , which is the modal value of r , and σ_0 , which is a measure of the width and the skewness of the distribution. This latter parameter is related to the standard deviation in a manner which will be described below. It will be termed the zeroth-order logarithmic standard deviation.

The frequency function for the zeroth-order logarithmic distribution is plotted in Fig. 2 for $r_M = 3.0$ and $\sigma_0 = 0.1, 0.2, 0.3,$ and 0.5 . Perhaps the most interesting feature here is that *the modal value of r is fixed, while the width of the distribution changes*. It offers the interesting possibility of exploring the effect of changing the breadth of the distribution while keeping the mode invariant.

The relation between the modal value of r and the mean value can be shown to be (see Appendix)

$$\ln \bar{r} = \ln r_M + 3\sigma_0^2/2 \quad (14)$$

The standard deviation is given by (see Appendix)

$$\begin{aligned} \sigma &= r_M [e^{4\sigma_0^2} - e^{3\sigma_0^2}]^{1/2} \\ &= r_M \sigma_0 \left(1 + \frac{7\sigma_0^2}{2!} + \frac{37\sigma_0^4}{3!} + \dots \right)^{1/2} \quad (15) \end{aligned}$$

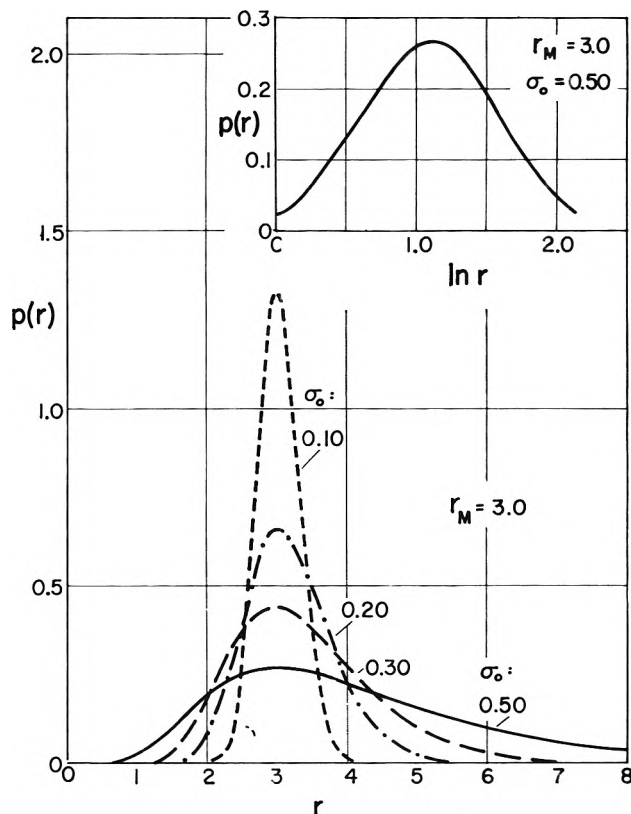


Figure 2. Distribution curves for the zeroth-order logarithmic distribution, eq. 13, with $r_M = 3.0$ and $\sigma_0 = 0.1, 0.2, 0.3,$ and 0.5 . In the inset, the frequency is plotted vs. $\ln r$ for one case.

so that for $\sigma_0 \ll 1$

$$\sigma = r_M \sigma_0 \quad (16)$$

Thus, for a sufficiently narrow distribution, σ_0 approximates the coefficient of variation

$$\sigma_0 \cong C = \frac{\sigma}{r} \cong \frac{\sigma}{r_M} \quad (\sigma_0 \ll 1) \quad (17)$$

For some purposes C may be considered to be a measure of the degree of polydispersion of the distribution. On the other hand, if we think of the polydispersion as determined by the linear width of the distribution, then the product $r_M \sigma_0$ may be taken as the measure of polydispersion.

The validity of eq. 16 has been checked by calculating the frequencies for a number of combinations of r_M and σ_0 and by then obtaining from these, the corresponding values of the usual standard deviation, σ .

(6) A. Hald, "Statistical Theory with Engineering Applications," John Wiley and Sons, Inc., New York, N. Y., 1962.

(7) E. J. Meehan and W. H. Beattie, *J. Phys. Chem.*, **64**, 1006 (1960).

The values of r_M and σ_0 were selected to correspond to the range actually encountered in the colloidal systems we have studied. The results, shown in Table I, verify that eq. 16 is indeed valid for these combinations of r_M and σ_0 .

Table I: Test of Validity of the Equation $\sigma = r_M \sigma_0$

r_M	σ_0	$r_M \sigma_0$	σ
2	0.200	0.40	0.42
4	0.100	0.40	0.40
6	0.065	0.39	0.39
8	0.050	0.40	0.40
6	0.100	0.60	0.60
8	0.100	0.80	0.80

Actually, each of the logarithmic distributions discussed above is a special case of a general family of logarithmically skewed distributions represented by

$$p_n(r) = C_n r^n \exp \frac{-(\ln r - \ln r_n)^2}{2\sigma_n^2} \quad (18)$$

where C_n is the normalizing factor. The quantities r_n , σ_n , and n will not be defined as yet, except to say that r_n locates one of the principal features of the distribution (median, mean, mode, etc.) and σ_n determines the spread of the distribution. In order to obtain C_n , it is necessary to evaluate the definite integral

$$G_n(r) = \frac{1}{C_n} = \int_0^\infty r^n \exp \frac{-(\ln r - \ln r_n)^2}{2\sigma_n^2} dr \quad (19)$$

and this result is (see Appendix)

$$G_n(r) = \sqrt{2\pi}\sigma_n r_n^{n+1} \exp[(n+1)^2\sigma_n^2/2] \quad (20)$$

so that

$$p_n(r) = \frac{r^n \exp -(\ln r - \ln r_n)^2/(2\sigma_n^2)}{\sqrt{2\pi}\sigma_n r_n^{n+1} \exp[(n+1)^2\sigma_n^2/2]} \quad (21)$$

It is immediately apparent that when $n = -1$, eq. 21 reduces to the logarithmic normal distribution and when $n = 0$, to the zeroth-order logarithmic distribution which we have just described. For these distributions, as pointed out above, the size parameters r_{-1} and r_0 correspond to the median and modal values, respectively.

For each value of the index n , there will be a particular parameter, r_n , occurring in the distribution which can be maintained invariant as the breadth parameter σ_n is changed. As an example, let us seek that member of the family of logarithmic distributions (eq. 18) for which the parameter r_n is the mean value, *i.e.*

$$r_n = \bar{r} = \int_0^\infty r p_n(r) dr \quad (22)$$

By eq. 19 this becomes

$$\bar{r} = G'_{(n+1)}(r)/G_n(r) \quad (23)$$

The primed value, $G'_{(n+1)}(r)$, indicates the operation

$$\int_0^\infty r^{n+m} \exp \frac{-(\ln r_n - \ln r)^2}{2\sigma_n^2} dr \quad (24)$$

where r_n and σ_n correspond to the parameters valid for $p_n(r)$ rather than for $p_{(n+m)}(r)$. Accordingly, the mean is

$$\bar{r} = r_n \exp[(2n+3)\sigma_n^2/2] \quad (25)$$

Now if $n = -3/2$, the exponential term in (25) vanishes so that $r_{(-3/2)} = r$. Hence, when $n = -3/2$, the function $p_{(-3/2)}(r)$ generates a logarithmically skewed distribution for which the parameter $r_{-3/2}$ is the mean value of r . For such a distribution, variation of $\sigma_{-3/2}$ will have the effect of altering the width of the distribution while maintaining the mean value of r invariant.

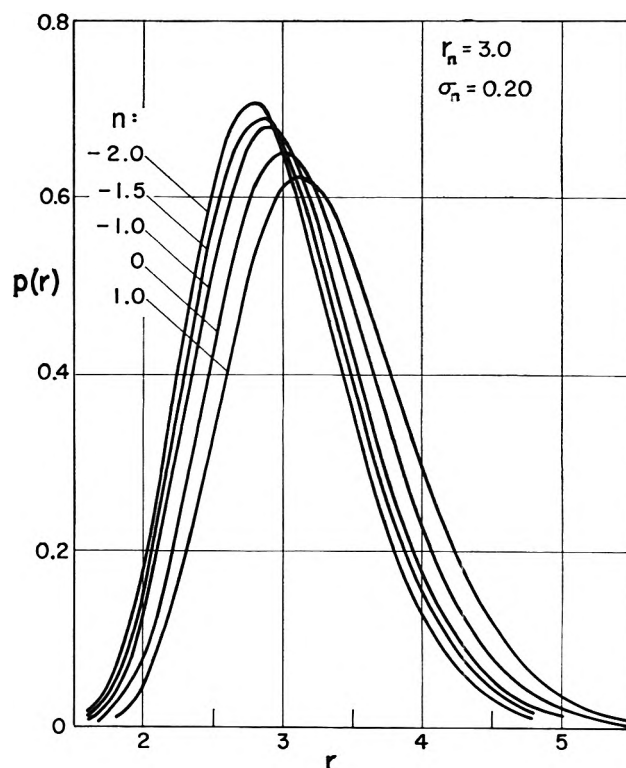


Figure 3. Distribution curves for five types of logarithmic distributions with orders 1, 0, -1, -1.5, -2. The value of r_1 , r_0 , r_{-1} , $r_{-1.5}$, and r_{-2} is 3.0, and the value of σ_1 , σ_0 , σ_{-1} , $\sigma_{-1.5}$, and σ_{-2} is 0.2.

It can be demonstrated by a similar analysis that in order to maintain the mean surface area (for spheres)

$$\bar{S} = 4\pi \int_0^\infty r^2 p_n(r) dr \quad (26)$$

invariant, the appropriate value is $n = -2$. For an invariant mean volume

$$\bar{V} = 4\pi/3 \int_0^\infty r^3 p_n(r) dr \quad (27)$$

it is necessary to set $n = -5/2$. In Fig. 3 the shape of these functions is shown for $r_n = 3.0$, $\sigma_n = 0.2$, and $n = 1, 0, -1, -1.5$, and -2 .

Appendix

Rather than evaluating the integral in eq. 13 directly, we proceed immediately to the more general integral, eq. 19. We let

$$y = (\ln r_n - \ln r) / \sqrt{2}\sigma_r \quad (A-1)$$

so that

$$G_n(r) = \sqrt{2}\sigma_n r_n^{(n+1)} \int_{-\infty}^\infty e^{\sqrt{2}\sigma_n(n+1)y} e^{-y^2} dy \quad (A-2)$$

When the first exponential is expanded, this may be written

$$G_n(r) = \sqrt{2}\sigma_n r_n^{(n+1)} \int_{-\infty}^\infty \left\{ e^{-y^2} + \frac{\sqrt{2}\sigma_n(n+1)y}{2!} e^{-y^2} + \dots \right\} dy \quad (A-3)$$

The integral

$$\int_{-\infty}^\infty y^m e^{-y^2} dy \quad (A-4)$$

which appears in this expansion for $G_n(r)$ is zero for odd values of m and is symmetrical about zero for even values of m . Accordingly, it has the value

$$2 \int_0^\infty y^m e^{-y^2} dy = \Gamma\left(\frac{m+1}{2}\right) = \Gamma(K + 1/2) \quad (A-5)$$

where m takes on all even values and $K = m/2$ assumes

all integral values. Upon substitution of (A-5) in (A-3)

$$G_n(r) = \sqrt{2}\sigma_n r_n^{(n+1)} \sum_{K=0}^\infty \frac{[\sqrt{2}\sigma_n(n+1)]^{2K} \Gamma(K + 1/2)}{(2K)!} \quad (A-6)$$

The Γ function is expanded

$$\Gamma(K + 1/2) = \frac{\sqrt{\pi}}{2^K} (2K - 1)(2K - 3)(2K - 5) \dots (1) \quad (A-7)$$

and cancelled against the factorial in the denominator, leading to

$$G_n(r) = \sqrt{2}\pi\sigma_n r_n^{(n+1)} \sum_{K=0}^\infty \frac{[(n+1)^2\sigma_n^2/2]^K}{K!} \quad (A-8)$$

which is equivalent to eq. 20. This reduces to the denominator of eq. 13 when $n = 0$.

We now derive the relation between σ_0 and the usual standard deviation, eq. 15. The standard deviation is defined by

$$\sigma^2 = \int_0^\infty (\bar{r} - r)^2 p_0(r) dr \quad (A-9)$$

where \bar{r} is the mean value of r . By expanding the square

$$\begin{aligned} \sigma^2 &= \bar{r}^2 \int_0^\infty p_0(r) dr - 2\bar{r} \int_0^\infty r p_0(r) dr + \int_0^\infty r^2 p_0(r) dr = \int_0^\infty r^2 p_0(r) dr - \bar{r}^2 = \\ &= \frac{G'_{0+2}(r)}{G_0(r)} - \bar{r}^2 \quad (A-10) \end{aligned}$$

By utilizing eq. 20 and 25 this becomes

$$\sigma^2 = r_0^2 (e^{4\sigma_0^2} - e^{3\sigma_0^2}) \quad (A-11)$$

which is identical with eq. 15 since $r_0 = r_M$. The quantity $G'_{0+2}(r)$ is defined by eq. 24.

The relation between the modal value of r (r_0 or r_M) and the mean value, \bar{r} , as given by eq. 14 can now be derived without difficulty. This simply involves substitution for $G'_{n+1}(r)$ and $G_n(r)$ in eq. 23 directly with the aid of eq. 20.

High Pressure Mass Spectrometric Study of Alkanes¹

by M. S. B. Munson, J. L. Franklin, and F. H. Field

Humble Oil and Refining Company, Research and Development, Baytown, Texas (Received July 10, 1964)

Mass spectra and ion-molecule reactions have been studied in ethane, propane, and the butanes at source pressures up to 150 μ . In all four compounds the most important reactions involve hydride ion transfer leading to the formation of the $C_nH_{2n+1}^+$ ion. With propane and the butanes this ion increases to 40–60% of the total ionization above 100 μ pressure. With propane and butane the next most important reaction involves the transfer of H_2^- to form $C_nH_{2n}^+$. $C_2H_7^+$ in small concentrations was observed in ethane and its precursor was deduced to be an excited ethane ion. Rate constants for a number of reactions have been determined. Primary ions formed with excess kinetic energy exhibit anomalous rate behavior. Several collision-induced metastable transitions occur with all four compounds.

Introduction

We have recently completed studies on ionic reactions of gaseous methane^{2a} using the wide pressure range accessible to the mass spectrometer at Humble.^{2b} As a continuation of these and earlier studies on the reactions of gaseous hydrocarbon ions, we are reporting in this paper reactions in ethane, propane, *n*-butane, and isobutane at source pressures as high as 150 μ .

The major ionic reactions in methane have been established for some time^{3–5} with good agreement of the values of the rate constants or cross sections among different workers and general agreement on the less prominent reactions and the processes occurring at high pressures.^{2a,6–8} The reactions in ethylene are more complex and the agreement among different workers^{2b,5,9,10} is not so good as in the case of methane. Ionic reactions in acetylene have also been studied at low to moderate pressures in mass spectrometers^{11–13} with fair agreement as to the general pattern of reactivity.

For the homologous series of paraffins, few data on total reactivity are available^{7,8} although hydride transfer reactions were reported for several paraffins.¹⁴ Since ionic reactions may be of importance in the radiation chemistry of hydrocarbons, we are undertaking a study of these reactions at as high pressures as possible in our mass spectrometer. Although we cannot interpret all of our data nor are the data as precise as we would like,

we feel that the observations which we are able to make will be of interest.

Experimental

The mass spectrometer was that described by Field^{2b} with an electron multiplier for ion detection. Mass spectra were obtained for different source pressures for different repeller field strengths and different electron

(1) Supported in part by Project SQUID under Contract No. Nonr-3623(S-18).

(2) (a) F. H. Field, J. L. Franklin, and M. S. B. Munson, *J. Am. Chem. Soc.*, **85**, 3575 (1963); (b) F. H. Field, *ibid.*, **83**, 1523 (1961).

(3) V. L. Tal'roze and A. K. Lyumbimova, *Dokl. Akad. Nauk SSSR*, **86**, 909 (1952).

(4) (a) D. P. Stevenson and D. O. Schissler, *J. Chem. Phys.*, **23**, 1353 (1955); (b) D. O. Schissler and D. P. Stevenson, *ibid.*, **24**, 926 (1956).

(5) F. H. Field, J. L. Franklin, and F. W. Lampe, *J. Am. Chem. Soc.*, **79**, 2419 (1957).

(6) S. Wexler and N. Jesse, *ibid.*, **84**, 3425 (1962).

(7) R. Fuchs, *Z. Naturforsch.*, **16a**, 1026 (1961).

(8) G. A. W. Derwish, A. Galli, A. Giardini-Guidoni, and G. G. Volpi, *J. Chem. Phys.*, **40**, 5 (1964).

(9) C. E. Melton and P. S. Rudolph, *ibid.*, **32**, 1128 (1960).

(10) P. Kebarle and E. W. Godbole, *ibid.*, **39**, 131 (1963).

(11) F. H. Field, J. L. Franklin, and F. W. Lampe, *J. Am. Chem. Soc.*, **79**, 2665 (1957).

(12) R. Barker, W. H. Hamill, and R. R. Williams, Jr., *J. Phys. Chem.*, **63**, 825 (1959).

(13) A. Bloch, "Advances in Mass Spectrometry," Vol. II, R. M. Elliott, Ed., Pergamon Press, Oxford, 1963, p. 48.

(14) F. H. Field and F. W. Lampe, *J. Am. Chem. Soc.*, **80**, 5587 (1958).

energies. Appearance potentials were measured by a modification of the retarding potential difference technique¹⁵ which has been described elsewhere.¹⁶ The source pressures were determined from the reservoir pressures by calibration curves for each gas obtained by the method previously described.¹⁷ The source temperature was 180–200°. Electron currents of 0.02 μ a. and electron energies of 70 e.v. were normally used, but higher currents were used in the experiments with low electron energy to give greater ion concentrations. The hydrocarbons used in these experiments were Phillips research grade (stated purity 99.9+ mole %) which were twice distilled from a Linde Molecular Sieve into carefully evacuated storage bulbs, after discarding light and heavy fractions.

Results

Ethane. Figures 1, 2, and 3 show relative concentrations of several of the ions of ethane as functions of pressure. $C_2H_5^+$ may be considered formally as involving transfer of H^- from ethane to the reactant ions but $C_3H_5^+$ must involve a complex of sufficient stability that additional C–C bonds are formed. Figure 3 shows secondary ions, $C_3H_3^+$ and $C_4H_7^+$, which perhaps react further, and $C_2H_7^+$ which is also formed by a second-order process. We did not undertake high resolution studies to verify that the mass 31 was $C_2H_7^+$ and not CH_3O^+ , but the relative concentration of mass 31 was some 50–100 times that of $32(O_2^+)$ or $19(H_3O^+)$ so we feel that the observed mass 31 was not caused by reactions of trace amounts of oxygen or water.

Protonated ethane, $C_2H_7^+$, the second of the homologous series beginning with CH_6^+ , has been observed previously in high pressure mass spectrometric studies of methane^{2a,6} and ethane⁸ and some "Cermak-type" experiments on ethane¹⁸ as well as in α -radiolysis of

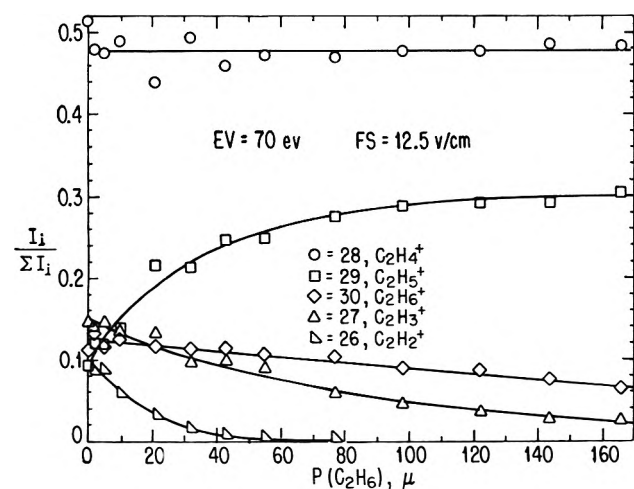


Figure 1. Relative concentrations of ions in ethane.

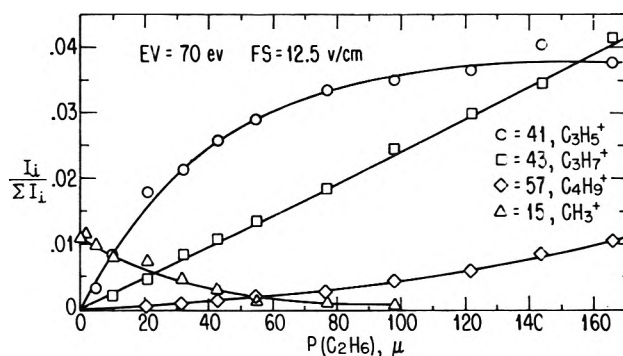


Figure 2. Relative concentrations of ions in ethane.

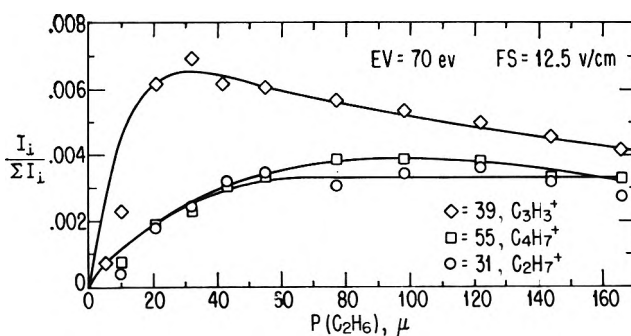


Figure 3. Relative concentrations of ions in ethane.

ethylene.¹⁰ The relative concentration of protonated ethane, $C_2H_7^+$ (about 0.3% of the total ionization for 70-e.v. electrons at about 150 μ of ethane), is much lower than that of the homologous protonated methane, CH_5^+ , under similar conditions (about 50%). The very much lower relative concentration was also noted by the other workers who observed it and is compatible with previous failures to observe this ion in ethane⁷ and ethane-hydrogen mixtures.¹⁹

The other two major product ions are $C_3H_7^+$ and $C_4H_9^+$ (Fig. 2). $C_3H_5^+$ (Fig. 2) exhibits the characteristic behavior of a second-order ion over this pressure range. The fact that the relative concentrations of $C_3H_7^+$ and $C_4H_9^+$ continuously increase over this same pressure range means that they have a higher order dependence on pressure than $C_3H_5^+$. From the shapes of these curves and the observation that I_{43}/I_{41} and I_{57}/I_{43}

(15) R. E. Fox, W. M. Hickam, D. J. Grove, and T. Kjeldaa, Jr., *Rev. Sci. Instr.*, **26**, 1101 (1955).

(16) M. S. B. Munson, J. L. Franklin, and F. H. Field, *J. Phys. Chem.*, **67**, 1542 (1963).

(17) F. H. Field and M. S. B. Munson, paper presented at 11th ASTM Conference on Mass Spectrometry, San Francisco, Calif., May, 1963.

(18) A. Henglein and G. A. Muccini, *Z. Naturforsch.*, **17a**, 452 (1962).

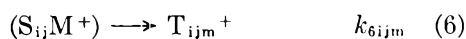
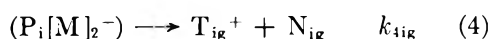
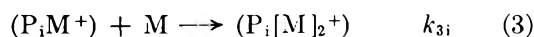
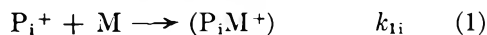
(19) V. L. Tal'roze and E. L. Frankevich, *J. Am. Chem. Soc.*, **80**, 2344 (1958).

both increase approximately linearly with ethane pressure, we conclude that $C_3H_7^+$ increases as the third power of the pressure and $C_4H_9^+$ as the fourth power, even though the stoichiometry requires only two ethane molecules. The observation that these ratios of concentrations do not pass through the origin, however, suggests that there is a small amount of both formed by second-order reactions.

Small relative concentrations of $C_3H_4^+$, $C_4H_5^+$, $C_4H_6^+$, and $C_4H_8^+$ were observed as second-order ions. Small amounts of $C_3H_6^+$ and perhaps trace amounts of $C_3H_8^+$ were observed as third-order ions. No mass 58 in excess of the ^{13}C isotope of $C_4H_9^+$ or any of the higher protonated alkanes were observed. Ions of mass as high as 78 were observed, but the relative concentrations (roughly 10^{-3} times that of $C_4H_9^+$) were too low for us to be certain that they were products of ionic reactions.

$C_2H_4^+$ is constant within $\pm 3\%$ for all of the experiments with 70-e.v. electrons at field strengths of 12.5 and 2.5 v./cm. (corresponding to a change in residence time of a factor $\sqrt{5}$). The other primary ions except $C_2H_5^+$ decrease in an approximately exponential manner as shown for $C_2H_3^+$, $C_2H_2^+$, and CH_3^+ (Fig. 1 and 2).

A reaction sequence



which involves the reaction of the intermediate complex (P_iM^+) in (3) and (4), as well as the reaction of the secondary ions in (5) and (6), to produce the tertiary ions has been analyzed by Lampe, Franklin, and Field.²⁰

For primary ions, one obtains the simple exponential decay curve

$$(P_i^+) = (P_i^+)_0 e^{-k_{1i}(M)t_i} \quad (7)$$

$(P_i^+)_0$ is the concentration of P_i^+ at zero time; k_{1i} is the rate constant for reaction of the ion P_i^+ ; (M) is the concentration of neutral species and t_i is the residence time of the ion, $(2dM_i/eF.S.)^{1/2}$; d is the ion path in the source; M_i the mass of P_i^+ ; e the electronic charge; and F.S. the field strength in the source. With the additional assumptions that ion current is proportional to ion concentration with the same factor for all ions and that the fragmentation pattern of the initially excited ion is independent of pressure, then

$$\ln(I_i/\Sigma I_i) = A_i^0 - k_i(M)t_i \quad (8)$$

since

$$(P_i^+)_0 = A_i^0 \Sigma \alpha I_i \text{ and } (P_i^+) = \alpha I_i$$

and A_i^0 is the fraction of ionization of P_i^+ at very low pressure for which no reaction occurs (which is equivalent to zero time).

Table I: Rate Constants for Reactions of Ions in Ethane

Ion	k , cc./ molecule-sec. $\times 10^9$	$Q(12.5$ v./cm.), cm. ² $\times 10^{16}$	Products
CH^+	2.6 ± 0.5	86	
CH_2^+	2.6 ± 0.7	88	
CH_3^+	1.7 ± 0.3	59	$C_2H_5^+$
C_2H^+	2.9 ± 0.6	131	
$C_2H_2^+$	2.1 ± 0.4	96	$C_2H_4^+$, $C_2H_6^+$
$C_2H_3^+$	0.48 ± 0.09	25	$C_2H_5^+$, $C_3H_6^+$
$C_2H_4^+$	0.01-0.03	0.5-1.7	
$C_2H_6^+$	0.07-0.18	3.3-8.9	$C_2H_7^+$, $C_2H_8^+$ from $C_2H_6^{++}$

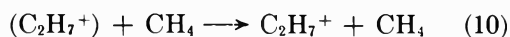
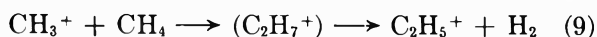
The rate constants reported in Table I are calculated from the slopes of the initial linear segments of the plots of logarithms of relative intensity against source pressure. The values of the rate constants are in sufficient agreement at field strengths of 2.5 and 12.5 v./cm. that they are listed as average values in Table I, together with the cross sections (calculated from $Q = kt/d$). From the essentially zero slope of the curve for $C_2H_4^+$ (with 70-e.v. electrons) we estimate that k_{28} cannot be greater than about 1×10^{-11} cc./molecule-sec.

The agreement of our appearance potentials for primary ions with the literature data is good, with the exception of $A(C_2H^+)$ for which we obtained 23.4 e.v. in contrast to the literature value of 27.1 e.v.²¹ $A(C_2D_7^+)$ was determined as 12.7 e.v. C_2D_6 was used rather than C_2H_6 to eliminate the complications due to the ^{13}C isotope which interferes seriously with $C_2H_7^+$ at mass 31. This value corresponds perhaps to $A(C_2H_5^+)$ (12.8 e.v.) or possibly $A(C_2H_4^+)$ (12.3 e.v.) from ethane. Henglein and Muccini¹⁸ observed $C_2H_7^+$ in ethane but did not identify its precursor. If $C_2H_6^+$ or $C_2H_4^+$ is the precursor, then $\Delta H_f(C_2H_7^+)$ is less than 193 or 170 kcal./mole, respectively. For either value the formation of $C_2H_7^+$ from $C_2H_6^+$ is exothermic and would be

(20) F. W. Lampe, J. L. Franklin, and F. H. Field, "Progress in Reaction Kinetics," Vol. I, Pergamon Press, New York, N. Y., 1961, pp. 73-79.

(21) Appearance potentials and heats of formation of ions are generally taken from F. H. Field and J. L. Franklin, "Electron Impact Phenomena," Academic Press, New York, N. Y., 1957.

expected to occur. From appearance potentials $C_2H_6^+$ (ground state) does not react to form $C_2H_7^+$. An ion with a second-order pressure dependence which saturates at high pressure cannot be formed from either $C_2H_4^+$ (which remains essentially constant with pressure) or $C_2H_5^+$ (which is a product ion itself). We are, therefore, forced to postulate that $C_2H_7^+$ is formed by reaction of excited $C_2H_6^+$, the excited state probably being that leading to the formation of the primary $C_2H_5^+$ ion. This mechanism yields $\Delta H_f(C_2H_7^+) \leq 229$ kcal./mole. The reactions involving the complex ($C_2H_7^+$) and the ions $C_2H_6^+$ and $C_2H_7^+$ in methane are probably



We observed $C_2H_7^+$ as a third-order ion in methane, but of intensity too low to prove by appearance potentials that it was formed from CH_3^+ . The observation of a small amount of $C_2H_7^+$ implies that the decomposition of $C_2H_7^+$ to $C_2H_5^+$ has an activation energy, but the very small amounts of $C_2H_7^+$ formed in CH_4 and C_2H_6 suggest that the activation energy for decomposition is very small. On the basis of all these considerations we are inclined to the opinion that $\Delta H_f(C_2H_7^+)$ is slightly less than 225 kcal./mole and that the proton affinity of ethane, $P(C_2H_6)$, is about 120 kcal./mole.

Since the appearance potential of $C_3H_7^+$ is 12.8 v. (corresponding to $C_2H_6^+$ as a primary ion) and $C_3H_7^+$ is a third-order ion and $C_2H_5^+$ is a second-order ion, we assume that $C_3H_7^+$ is formed from $C_2H_6^+$. There is, however, a small amount of $C_3H_7^+$ which is formed by a second-order reaction. From the relative concentrations involved, $C_2H_3^+$ and $C_2H_2^+$ must react to give predominantly $C_2H_5^+$ and the other ions of lower concentration may well do so. The orders of the reactions involved suggest that $C_2H_6^+$ forms $C_3H_7^+$ which then forms $C_4H_9^+$.

Experiments were also done with lower energy electrons (e.v. $\cong 12.5$ v.) with a low field strength (F.S. = 2.5 v./cm.). $C_2H_4^+$ decreased slightly under these conditions although with 70-e.v. electrons at the same field strength the relative concentration of $C_2H_4^+$ was independent of pressure. From this small decrease in $C_2H_4^+$ for which $\log(I_{28}/\Sigma I_i)$ decreased reasonably linearly in P , a value of $3.5 \pm 1.2 \times 10^{-11}$ cc./molecule-sec. was obtained for the rate constant for reaction of $C_2H_4^+$. $C_2H_2^+$ may react to form $C_2H_4^+$ exothermally and we feel that the constancy of $C_2H_4^+$ with 70-e.v. electrons is probably the result of its being formed as well as its reacting. Even this rate constant for reaction of $C_2H_4^+$ is unexpectedly low since $C_2H_4^+$ may produce several ions in exothermic reactions.

The value for the rate constant for reaction of $C_2H_6^+$ was $6.7 \pm 1.0 \times 10^{-11}$ cc./molecule-sec., lower than the value obtained with 70-e.v. electrons, 1.8×10^{-10} cc./molecule-sec. The increase in $C_2H_5^+$ concentration was about equal to the decrease in $C_2H_6^+$ concentration, but the formation of $C_2H_5^+$ from ground-state $C_2H_6^+$ is endothermic by about 20 kcal./mole. The formation of $C_2H_5^+$ from $C_2H_4^+$ is also endothermic by about 15 kcal./mole. No other primary ions are present in sufficient concentration to produce this amount of $C_2H_5^+$ so we suggest that $C_2H_5^+$ is formed from second-order reactions of excited ethane ions, probably the excited state which leads to the formation of the primary $C_2H_5^+$ ion. If excited $C_2H_6^+$ ions are the major reactive group of $C_2H_6^+$ ions, then, since the concentration of excited species will decrease relative to the ground-state species with decreasing voltage of the ionizing electrons, the apparent rate constant calculated on the assumption that all of the $C_2H_6^+$ ions react should be lower with 12.5 than with 70-e.v. electrons.

Fuchs⁷ has made a study of the ionic reactions in ethane at fairly low pressures such as that the secondary ions of molecular weight greater than the neutral species were only of the order of $1-5 \times 10^{-5}$ of that of the primary ions. He observed in the secondary spectrum of ethane that $C_3H_3^+$, $C_3H_7^+$, and $C_4H_7^+$ were about 40, 20, and 10%, respectively, of $C_3H_5^+$. From our data we estimate the ratios for second-order processes for these product ions to be about 35, 12, and 10%, respectively. He also reports a small cross section (about 1×10^{-16} cm.², each) for reaction of $C_2H_4^+$ to give $C_3H_5^+$ and $C_3H_7^+$. He attributes the other products to $C_2H_2^+$ or $C_2H_3^+$ but is unable to decide between the two reactants. The sum of the partial cross sections for the reactions which he reports is $30-60 \times 10^{-16}$ cm.², depending upon the choice of reactants.

The general pattern of reactivity of ethane in this work is the same as that given by Volpi and co-workers⁸ but the agreement of cross sections for reactions of ions is poor; our values are about twice as large as theirs although they are in about the same relative order. This disagreement is surprising since there is good agreement for the values of the rate constants for ionic reactions in methane among the different workers. Fuchs' values⁷ for reaction cross sections are also higher than those of Volpi and co-workers.⁸ Schissler and Stevenson²² report cross sections of 78 and 16×10^{-16} cm.² for reaction of $C_2H_3^+$ with C_2H_6 to give $C_3H_5^+$ at average ion energies of 0.10 and 1.0 e.v. These values are of the order of our value of 25×10^{-16} cm.² for reac-

(22) D. O. Schissler and D. P. Stevenson, *J. Chem. Phys.*, **24**, 926 (1956).

tion of $C_2H_3^+$ with ethane at an average ion energy of 1.3 e.v. and very different from Volpi's value of 4×10^{-16} cm.². Assignment of product-reactant sequences by Volpi and co-workers which are different from ours are also determined by relative concentration or "mass balance" considerations which are not conclusive in either case.

Propane. Figure 4 shows plots of the relative concentrations (as fractions of total ionization) for some of the ions in propane as a function of pressure. Obviously, the dominant reaction is that which can be considered as "hydride ion transfer" (H^-) from neutral

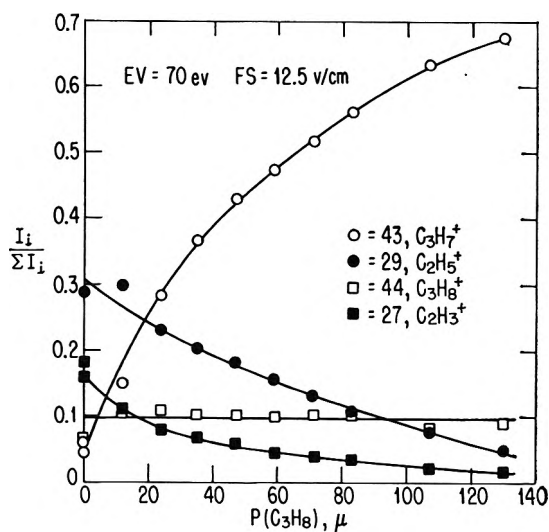


Figure 4. Relative concentrations of ions in propane.

propane to give $C_3H_7^+$. The $I_{43}/\Sigma I_i$ curve has the shape expected for a second-order ion and $C_3H_7^+$ can be formed by exothermic second-order reactions from all of the major primary ions of propane, with the possible exception of $C_3H_8^+$. The second major product is $C_3H_6^+$ (also a second-order ion) which is formed to about one-tenth the extent of $C_3H_7^+$. This process may be considered formally as involving transfer of H_2^- . $C_2H_2^+$, $C_2H_4^+$, and $C_3H_2^+$ (and perhaps $C_2H_3^+$) can react exothermally in this manner. Some C_4 species are also produced by second-order reactions, predominantly the odd mass species. The ratio $I_{57}/\Delta I_{43}$, the ratio of $C_4H_9^+$ to $C_3H_7^+$ formed by second-order processes, is substantially independent of pressure and is only 0.0046 with 70-e.v. electrons. Even though $C_4H_9^+$ can be formed exothermally by reactions of the primary ions of propane, it is not a major reaction product.

$C_3H_9^+$ is present to the extent of less than one part in 50,000 of the total ionization, if at all. Very small amounts of the ion could be masked by the ¹³C isotopes of $C_3H_7^+$ and $C_3H_8^+$. Some C_6 's are observed, pre-

dominantly the odd mass ions. These ions involve three propane molecules in their formation since the ratio I_{71}/I_{57} increases approximately linearly with an increase in pressure. The highest mass ion noted was 85, $C_6H_{13}^+$ (C_7H^+ seems highly improbable) probably formed by a third-order process. For the C_5 's and C_6 's, $C_nH_{2n+1}^+$ is the most abundant ion, which is perhaps a reflection of the lower heats of formation of these ions relative to other ions of the same carbon number, an observation which has been made for C_1-C_4 .²¹ The low ratio, $I_{57}/\Delta I_{43}$, despite the presumed permissibility of reactions to give $C_4H_9^+$, indicates that reactions of these primary ions with C_3H_8 proceed through complexes which form very weak C-C bonds and transfer H^- (similar to the $C_2H_8^+$ complex from CH_4^+ and CH_4 which forms essentially no C-C bonds¹ but rather transfers a proton¹⁸).

Table II: Reactions of Ions in Propane

Ion	k_i , cc./molecule- sec. $\times 10^9$	$Q(12.5$ v./cm.), cm. ² \times 10^{16}	Products	Fraction of second- order products
$C_2H_4^+$	0.63 ± 0.10	30	$C_3H_6^+$ $C_2H_7^+$ $C_4H_7^+$ $C_4H_8^+$ $C_4H_9^+$ $C_6H_{11}^+$	~ 0.3 ~ 0.7 < 0.0002 ≤ 0.001 ≤ 0.01 (Third-order)
$C_2H_6^+$	0.62 ± 0.13	30	$C_3H_7^+$ $C_4H_7^+$ $C_4H_8^+$ $C_4H_9^+$ $C_6H_{11}^+$	~ 1 < 0.0002 ≤ 0.001 ≤ 0.01 (Third-order)
$C_2H_3^+$	0.67 ± 0.16	32	} Not uniquely determined: mostly $C_2H_5^+$, $C_4H_7^+$, and other low intensity fragments; but probably not $C_3H_6^+$ and $C_4H_9^+$	
C_2H^+	$4.0 \pm 0.8 (?)$	180		
C_3H^+	1.6 ± 0.6	88		
$C_3H_2^+$	1.1 ± 0.2	62		
$C_3H_4^+$	$0.12 \pm 0.02 (?)$	6.9		
$C_3H_5^+$	$0.18 \pm 0.05 (?)$	10		

Rate constants are calculated from the slopes of the plots of $\log(I_i/\Sigma I_i)$ against P . Some of the primary ions did not give straight lines over a wide enough pressure range to allow an estimate of the rate constants. Table II shows the average rate constants obtained for various ions with propane. Since $C_2H_2^+$ can react with C_3H_8 to form both $C_3H_4^+$ and $C_3H_5^+$ exothermally, the apparent low rate constants for reaction of these two ions may be the net result of their formation as well as disappearance by second-order reactions. We con-

sider $C_3H_8^+$ to be essentially unreactive, although $C_2H_2^+$ may charge exchange with C_3H_8 to balance a very small reactivity.

From plots of $\log(I_{28}/\Sigma I_i)$ and $\log(I_{29}/\Sigma I_i)$ against propane pressure at low electron energies (13 e.v.) we obtained rate constants for reaction of these two ions which were substantially the same as the values obtained with 70-e.v. electrons and F.S. = 12.5 v./cm. These values were included in the average rate constants reported in Table II. $C_3H_7^+$ and $C_3H_6^+$ are well-behaved secondary ions. Since only $C_2H_4^+$ of the low voltage ions can react with propane exothermally to produce $C_3H_6^+$ we may calculate the fractional dissociation of $(C_2H_4-C_3H_8)^+$ complex to give $C_3H_6^+$ as about 0.25–0.30. From plots of $\Delta(C_3H_6^+)/C_2H_4^+$ as functions of pressure with 70-e.v. electrons we obtain similar values for the maximum value of this function, so $C_3H_6^+$ is formed predominantly from $C_2H_4^+$. $C_4H_9^+$ comes from $C_2H_4^+$ and $C_2H_5^+$, but $C_4H_7^+$ is formed from the other primary ions.

For propane, Fuchs⁷ reports the major products heavier than C_3H_8 as being $C_4H_5^+$, $C_4H_7^+$, $C_4H_8^+$, and $C_4H_9^+$ in the ratio 0.7:1.0:0.3:0.4 but was unable to assign any reactants to these products. His pressure was not high enough to enable him to calculate the total cross sections for reaction of an ion from the decrease in concentration of that ion.

n-Butane. Figure 5 shows the relative concentrations of several "primary" ions in butane. The dominant process is the formation of $C_4H_9^+$ which increases from about 2% of the total ionization at low pressures ($<1 \mu$) to greater than 50% at about 130μ where it is the most prominent ionic species. It is necessary that virtually all of the ions react to give $C_4H_9^+$ in order to account for the large increase in its relative concentration. The curve of $I_{57}/\Sigma I_i$ in Fig. 5 is not the characteristic second-order curve observed for most of the product ions for the other hydrocarbons which we have studied. That this phenomenon is not purely instrumental is indicated by a plot for $C_4H_7^+$ which shows the expected second-order behavior and the reasonably linear plots of $\log(I_i/\Sigma I_i)$ vs. P for some of the primary ions in Fig. 6. This curve for $I_{57}/\Sigma I_i$ may be expected for an ion produced by processes both second and third (or higher) order in pressure. The formation of $C_4H_9^+$ may be considered formally as involving transfer of H^- from butane to the reacting ion.

$C_3H_7^+$ exhibits an apparent slight increase followed by a gradual decrease with increasing butane pressure. The maximum, which is much more obvious in the experiments with a longer residence time, indicates that $C_3H_7^+$ is formed and also reacts. A subsequent reaction of $C_3H_7^+$ to give $C_4H_9^+$ is sufficient to give a third-

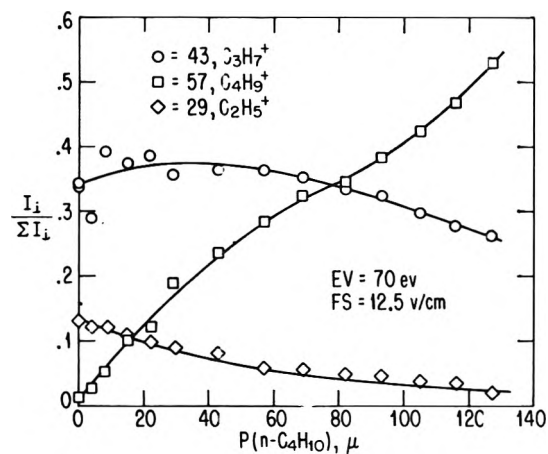


Figure 5. Relative concentrations of ions in butane.

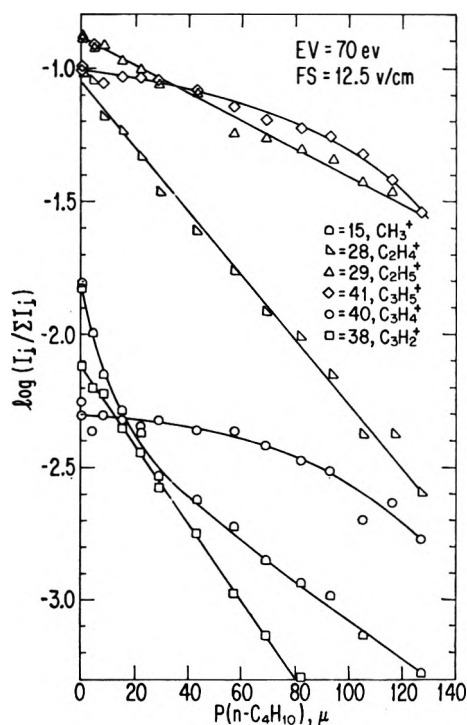


Figure 6. Logarithmic plots for reactant ions in butane.

order contribution to the formation of $C_4H_9^+$. Within our experimental error no $C_4H_{11}^+$ was detected so that we may say that the $C_4H_{11}^+$, if formed, was not produced to the extent of one part in 40,000 of the total ionization. Several ions of mass greater than C_4H_{10} were observed in very small relative concentrations. The most abundant of these, $C_5H_{11}^+$, was only about 0.05% of the total ionization at the highest pressure of these experiments. The ratio I_{71}/I_{57} increased with increasing butane pressure, but did not extrapolate to zero at zero pressure. $C_5H_{11}^+$ is formed by both

second- and third- (or higher) order processes. Of the ions of mass greater than butane, the odd mass ions are dominant and the ratios of the ion concentrations are independent of pressure. The ion of largest mass which we observed was 95, presumably $C_7H_{11}^+$. We observed no ions whose composition required participation of three molecules of butane.

Figure 6 shows logarithmic plots for the disappearance of several primary ions in butane. For some of the ions ($C_2H_5^+$, $C_2H_4^+$, $C_3H_2^+$) good straight lines were observed over the experimental pressure range from which rate constants were calculated. Others (CH_3^+) showed a continuous upward curvature without any appreciable linear portion which could be used to determine rate constants. The primary ions which showed this deviation were those which have been shown to have an average excess kinetic energy of formation.²³ One could expect any degree of upward curvature, depending upon the excess kinetic energy and the distribution of molecules containing the excess kinetic energy.

The other deviation from linearity on these logarithmic plots is shown for $C_3H_5^+$ and $C_3H_4^+$. The slight maximum for $C_3H_7^+$ in Fig. 5 is barely perceptible on a logarithmic plot. A third-order disappearance of these ions (or a combination of second-order and a larger amount of third-order reactions) and the formation and reaction of these ions by second-order reactions will give curves of essentially the same shape. From our data we are unable to distinguish between the two mechanisms. However, since $C_3H_7^+$ is apparently formed as well as reacting in these systems, and all of the ions in question may be formed exothermally by reaction of other primary ions, we conclude that the ions are being formed and reacting by second-order processes rather than disappearing by a third-order process.

The experiments at low field strength and low electron energy (2.5–5 v./cm. and 12.5 e.v.) gave rate constants for reaction of $C_2H_4^+$ and $C_2H_5^+$ which are in sufficiently good agreement with the values obtained at high electron energy that they are included in Table III.

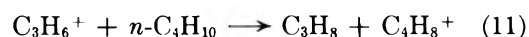
Table III: Reactions of Ions in *n*-Butane^a

P ⁺	k_i , cc./molecule- sec. $\times 10^9$	$Q(12.5 \text{ v./cm.}),$ cm. ² $\times 10^{16}$
$C_2H_3^+$	0.60 ± 0.18	28
$C_2H_4^+$	1.2 ± 0.4	58
$C_2H_5^+$	0.66 ± 0.28	32
$C_3H_2^+$	1.3 ± 0.2	73
$C_3H_3^+$	0.85	49
$C_3H_4^+$	1.2 ± 0.3	93

^a F. S. = 1.25 v. cm. and e.v. = 70.

The rate constant for reaction of $C_7H_5^+$ reported in Table III was obtained from low voltage studies for which a straight line was obtained on the appropriate logarithmic plot.

The sum of the relative concentrations of $C_3H_6^+$ and $C_4H_8^+$ is essentially constant with increasing pressure for both 70- and 12.5-e.v. electrons with different field strengths. We therefore suggest that the major reaction for the disappearance of $C_3H_6^+$ and the formation of $C_4H_8^+$ is



which is exothermic for all of the butenes.

Isobutane. The reactions of isobutane are very similar to the reactions in *n*-butane although differences are present as expected since the distribution of primary ions is different in the two gases. The major reaction is the hydride ion transfer to give $C_4H_9^+$ since the concentration of that ion increases from about 2% at very low pressures to about 35% of the total ionization at 115 μ . $C_4H_9^+$ is formed by both second- and third-order processes. $C_4H_8^+$ (by H_2^- transfer) is formed by processes which are the same order in pressure as those for $C_4H_9^+$ since $\Delta I_{56}/\Delta I_{57} = 0.076 \pm 0.004$ and 70-e.v. electrons (for *n*-butane the ratio is 0.071 with 70-e.v. electrons). $C_4H_7^+$ increases from about 0.2 to 0.6% in the manner expected for a second-order ion. $C_4H_5^+$ has a broad maximum indicating that it is both being formed and reacting (maximum concentration about 0.3%).

$C_3H_7^+$ and $C_3H_6^+$ pass through maxima in relative concentrations as the pressure increases indicating that both are being formed as well as reacting. $C_3H_3^+$ exhibits the same behavior in isobutane as in *n*-butane: a rapid initial decrease to an essentially constant value. $C_4H_{10}^+$ does not vary much with pressure. Ions of mass as high as 95 were observed in small amounts (of the order of 0.01% of the total ionization) with the odd mass ions predominant. These ions are formed by processes both second- and third-order in pressure since their increase in relative concentration with pressure is about the same as that for $C_4H_9^+$.

Rate constants are reported in Table IV for those ions for which plots of $\log(I_i/\Sigma I_i)$ vs. P are reasonably linear. We doubt that the apparent differences in the rate constants for butane (Table III) and isobutane (Table IV) are real.

For all of these compounds, particularly at high pressures, diffuse peaks occurring at nonintegral masses were noted. These so-called "metastable peaks" are

(23) J. Bracher, H. Erhard, R. Fuchs, O. Osberghaus, and R. Taubert, "Advances in Mass Spectrometry," Vol. II, R. M. Elliott, Ed., Pergamon Press, Oxford, 1963, p. 285, which also lists earlier work.

Table IV: Reactions of Ions in Isobutane^a

P ⁺	k_i , cc./molecule- sec. $\times 10^9$
C ₂ H ₃ ⁺	0.98
C ₂ H ₄ ⁺	1.8
C ₂ H ₅ ⁺	0.39
C ₃ H ₂ ⁺	1.4
C ₃ H ₅ ⁺	0.28

^a F.S. = 12.5 v./cm. and e.v. = 70.

probably collision-induced since the ratio of the diffuse peak to any presumed parent generally increased with increasing pressure. Even by operating at low electron voltages to simplify the mass spectrum, we were unable to make any unequivocal decisions about the origin of the ions. With the usual assumption that the ions are formed by collision in the analyzer and making reasonable assumptions about the precursors we calculated cross sections of $10\text{--}50 \times 10^{-16}$ cm.² for some of these collision-induced decompositions. These values seem much too high. If the processes occur in the region of the ion gun for which the pressure is much higher, essentially the same magnitude of cross section is calculated because the path is shorter in about the same proportion.

Discussion

As a rough measure of ionic polymerization we will compare, at equal pressures, the sum of all ions having more carbon atoms than the parent molecule. Thus at 100 μ pressure, with 70-e.v. electrons and 12.5 v./cm. field strength, we find for each paraffin, C_{*n*}H_{2*n*+2}, the respective values of $(\Sigma I_{C_{n+m}})/\Sigma I_{\text{total}}$: CH₄, 0.34; C₂H₆, 0.073; C₃H₈, 0.0096; *n*-C₄H₁₀, 0.0013; and *i*-C₄H₁₀, 0.0006. These data indicate a drastic decrease in the extent of ionic polymerization (under our conditions) with increasing molecular weight of the reactant molecule. This decrease in ionic polymerization with increasing molecular weight may be compared with the decrease in stability of parent ions of paraffins with increasing molecular weight and the observation that the C₃ and C₄ ions are predominant in paraffin spectra. The predominance of odd mass products for ion-molecule reactions is in general agreement with the predominance of odd mass fragments in the primary spectra of the higher paraffins.²⁴

We find for the increase in relative concentration of the parent minus one ion, C_{*n*}H_{2*n*+1}⁺: $\Delta(\text{C}_2\text{H}_5^+) = 0.40$ (from <1 to 100 μ) in ethane; $\Delta(\text{C}_3\text{H}_7^+) = 0.56$ for propane; $\Delta(\text{C}_4\text{H}_9^+) = 0.40$ in *n*-butane; and $\Delta(\text{C}_4\text{H}_9^+) =$

0.55 for isobutane. To obtain a more reliable measure of the relative amounts of hydride ion transfer or removal (the formation of C_{*n*}H_{2*n*+1}⁺) we need to consider that the reaction may be endothermic in some cases: C₂H₄⁺ and C₂H₆⁺ in ethane; formation of C₃H₇⁺ from C₃H₈⁺ in propane; and probably the formation of C₄H₉⁺ from C₄H₁₀⁺ in *n*-butane and isobutane (if one assumes that C₄H₉⁺ is the tertiary ion). Thus, if we divide the increase in C_{*n*}H_{2*n*+1}⁺ by the total initial concentration of reactants which presumably may undergo hydride ion transfer, we find 0.69 for ethane, 0.62 for propane, 0.43 for *n*-butane, and 0.55 for isobutane. Field and Lampe¹⁴ report an appreciable decrease in "effective cross sections" for hydride ion transfer in the sequence $Q(\text{C}_2\text{H}_6) > Q(\text{C}_3\text{H}_8) > Q(\textit{n}\text{-C}_4\text{H}_{10}) \cong Q(\textit{i}\text{-C}_4\text{H}_{10})$. Our somewhat smaller decrease may be the result of including processes which increase with the third power of the pressure. In neither case were direct measurements made of cross sections for reaction of specific ions. In deciding on allowable reactants we have assumed that the butyl ion was tertiary, although a simple hydride ion transfer reaction from *n*-butane could give only a primary or secondary ion. If one considers C₄H₉⁺ to be the secondary ion for *n*-butane, then the "effective cross sections" would be increased because other primary ions would be excluded.

From our observation of C₂H₇⁺ we were able to give an approximate value for the proton affinity of C₂H₆ of about 120 kcal./mole. The difference between this value and that given by Tal'roze and Frankevich¹⁹ is the result of their opinion that their failure to observe C₂H₇⁺ in ethane-hydrogen mixtures was the result of energetic considerations. Similarly, the value of $101 < P(\text{C}_2\text{H}_6) < 121$ kcal./mole given by Lampe and Field²⁵ was based primarily on the presumed nonexistence of C₂H₇⁺ as a stable ion in methane. Our value for $P(\text{C}_2\text{H}_6)$ is about the same as that for $P(\text{CH}_4)$, between 113 and 129 kcal./mole.²⁵ If we assume that C₃H₉⁺ exists, as reported by Wexler and Jesse⁶ in methane and by Kebarle and Godbole¹⁰ in ethylene, and Volpi and co-workers in ethane,⁸ we may calculate that the formation of C₃H₉⁺ from any ion in propane will be endothermic and that the decomposition of C₃H₉⁺ to C₃H₇⁺ and H₂ will be exothermic by 30 kcal./mole. In order for the decomposition of C₃H₉⁺ to C₃H₇⁺ to be about thermoneutral, $\Delta H_f(\text{C}_3\text{H}_9^+)$ should be about 190 kcal./mole. This value would give a proton affinity of propane of about 150 kcal./mole, which seems too high. While it

(24) See the discussion of J. H. Beynon, "Mass Spectrometry and its Application to Organic Chemistry," Elsevier Publishing Co., Amsterdam, 1960, Chapter 9.

(25) F. W. Lampe and F. H. Field, *J. Am. Chem. Soc.*, **81**, 3242 (1959).

Table V: k [cc./molecule-sec. $\times 10^{10}$ (F.S. = 12.5 v./cm.)]

Ion	D_2^a	CH_4^b	Neutral			
			C_2H_6	C_3H_8	$n\text{-C}_4\text{H}_{10}$	
CH_4^+	~ 0.1	10.3 ± 0.3				
CH_3^+	1.7	8.2 ± 0.3	17 ± 3			
CH_2^+	3.1	12.4 ± 1.3	26 ± 7			
CH^+	4.9	17.4 ± 1.6	26 ± 5			
C_2H_3^+		0.87 ± 0.12	4.8 ± 0.9	6.7 ± 1.6		6.0 ± 1.8
C_2H_4^+		(< C_2H_3^+)	0.35 ± 0.12	6.3 ± 1.0		12 ± 4
α^c	0.30	1.00	1.70	2.42		3.14

^a M. S. B. Munson, F. H. Field, and J. L. Franklin, *J. Am. Chem. Soc.*, **85**, 3584 (1963). ^b F. H. Field, J. L. Franklin, and M. S. B. Munson, *ibid.*, **85**, 3575 (1963). ^c Polarizability relative to CH_4 ; from H. H. Landolt and R. Bornstein, "Zahlenwerte und Funktionen," Part 3, 6th Ed., Springer-Verlag, Berlin, 1950.

is possible that C_3H_9^+ might exist at energies above that of C_3H_7^+ and H_2 , we feel that there is no convincing evidence yet available for the existence of the higher homologs of protonated methane and ethane. The other observations of masses corresponding to these ions could easily be the result of impurities.

Table V shows data for rate constants for reaction of a series of ions with different neutral species. The rate constants for CH^+ , CH_2^+ , and CH_3^+ increase about as the polarizability of the molecules for the compounds studied; C_2H_3^+ and C_2H_4^+ exhibit no recognizable pattern. The treatment based on an inverse fourth power ion-molecule interaction^{26,27} cannot predict which of the possible reaction products will be formed but it has given reasonably good agreement with rate constants for some ionic reactions. The rate constant is proportional to $(\alpha/\mu)^{1/2}$, the square root of the ratio of the polarizability of the neutral to the reduced mass of the couple. For CH_3^+ , CH_2^+ , and CH^+ this theory predicts that the rate constants should be about 15% lower for reaction of these ions with deuterium and about 15% higher for reaction with ethane than for reaction with methane. Similarly, C_2H_3^+ and C_2H_4^+ should react at essentially the same rate and the rate constants for reaction of either ion with ethane should be only 2-3% smaller than the rate constant for reaction of CH_4^+ with CH_4 . In view of the many possible theoretical and experimental complications it is not surprising that agreement between the experimental and calculated rate constants is not precise.

In this work we also noted the absence of many ions which could be produced by exothermic ionic reactions. Exothermicity is perhaps a necessary but not sufficient criterion for ionic reactions. Our postulate of reactions of an excited state of ethane ion is not without precedent since reactions of excited states of nitrogen ions²⁸ and oxygen ions²⁹ are well established. There is little convincing evidence for the necessity of postulating endo-

thermic reactions in mass spectral studies. Except that ionic reactions with alkanes generally involve transfer of small groups, H, H^+ , H^- , E_2^- , we can make no reliable predictions about which of the energetically allowed reactions will occur.

It is worthwhile to compare these data on ionic reactions with gas phase radiolysis data. Ausloos and co-workers³⁰⁻³³ have studied gas phase radiolysis of the low molecular weight alkanes and have successfully interpreted part of their data in terms of ionic reactions. In particular, they found from studies of deuterated compounds and mixtures in the presence of scavengers that much of the ethane formed in radiolysis of propane and butane and the propane formed in the radiolysis of butane was formed by hydride ion transfer reactions of C_2H_5^+ and C_3H_7^+ . This observation is in agreement with our findings, since we find that ethyl ion reacts rapidly in propane and butane and the only major product ion is $\text{C}_n\text{H}_{2n+1}^+$.

The ethylene produced in radiolysis appears to come partially from an ionic reaction as well. We find that C_2H_3^+ reacts rapidly by hydride abstraction to produce ethylene as well as by addition to give products of higher molecular weight. We cannot make a good estimate of relative amounts of these two processes. It seems entirely reasonable that H^- and H_2^- transfer

(26) H. Eyring, J. O. Hirschfelder, and H. S. Taylor, *J. Chem. Phys.*, **4**, 479 (1936).

(27) G. Gioumoussis and D. P. Stevenson, *ibid.*, **29**, 294 (1958).

(28) M. S. B. Munson, F. H. Field, and J. L. Franklin, *ibid.*, **37**, 1790 (1962).

(29) R. K. Curran, *ibid.*, **38**, 2974 (1963).

(30) P. Ausloos and S. Lias, *ibid.*, **36**, 3163 (1962).

(31) S. G. Lias and P. Ausloos, *ibid.*, **37**, 877 (1962).

(32) R. P. Borkowski and P. J. Ausloos, *ibid.*, **38**, 36 (1963).

(33) R. P. Borkowski and P. J. Ausloos, *ibid.*, **39**, 818 (1963).

reactions can account for the production of stable molecules of mass lower than the molecular weight of the parent molecule in the radiolysis of hydrocarbons.

Acknowledgment. We are very grateful to Mr. W. C. Gieger for performing these experiments with his accustomed competence.

The Radiolysis of Aqueous Perchloric Acid Solutions¹

by D. Katakis² and A. O. Allen

Chemistry Department, Brookhaven National Laboratory, Upton, New York (Received November 5 1963)

The radiolysis of aqueous perchloric acid solutions was studied as a function of concentration in the absence and presence of radical scavengers. Free radicals from water radiolysis appear not to react with perchlorate ion. Perchlorate decomposes, as reported by others, by the direct action of radiation, with a yield increasing directly with its concentration, while the yields of H₂ and other water decomposition products decrease. The major product of perchlorate ion decomposition is chlorate; most of the chloride formed arises from secondary decomposition of the chlorate ions. Excited perchlorate ions appear mainly to decompose, not to electrons and ClO₄ radicals, but to chlorate ions and oxygen atoms.

Most studies in the radiation chemistry of aqueous solutions have been concerned with relatively dilute solutions, in which the energy of the radiation is essentially all given up to the water, and solutes are affected only by reason of their reactions with active species formed by decomposition of the water. In such systems the reaction yields are independent of the solute concentration, or nearly so. At higher concentration ranges, an appreciable fraction of the radiation energy will appear as excitation of the solute molecules; the resulting reactions should appear with a yield approximately proportional to the solute concentration. Such a reaction is often called a "direct effect," as distinguished from the "indirect effect" due to reactions of active radiolysis products of the solvent. The direct effect in the radiolysis of perchloric acid in water solutions was shown in 1952 by Milling, Stein, and Weiss³ and later a more detailed study was published by Cottin.⁴ Perchlorate solutions are particularly useful in studying the radiation chemistry of metal ions in solution, because the perchlorate ions do not form complexes with the metal ions and because free radicals

generated in the water appear to act less readily with perchlorate than with other common anions such as sulfate, nitrate, or chloride. To use perchloric acid in this way, however, the direct effect of radiation on perchlorate must be understood and taken into account. In the present work, the earlier studies are extended and the reaction mechanism of the direct effect is discussed.

Experimental

Dosimetry. γ -Irradiations were made in a cylindrical Co⁶⁰ source at a dose rate of about 3.2×10^{20} e.v./l. min. Doses were determined with the Fricke dosimeter assuming $G(\text{Fe}^{+3}) = 15.5$ and an extinction coefficient of $\epsilon_{306} = 2180$ at 24°. The energy deposition in solutions was assumed to be proportional to the electron density. For solutions where both H₂SO₄

(1) Research performed under the auspices of the U. S. Atomic Energy Commission.

(2) Nuclear Research Center Democritus, Aghia Paraskevi, Attikis, Greece.

(3) B. Milling, G. Stein, and J. Weiss, *Nature*, **170**, 710 (1952).

(4) M. Cottin, *J. chim. phys.*, **53**, 903 (1956).

and HClO_4 were present it was assumed that there is no volume change on mixing solutions of the two acids.⁵ Cyclotron irradiations employed the techniques of Schuler and Allen.⁶

Reagents. Baker Analyzed perchloric acid was diluted 1:3, preirradiated to about 1 Mrad, and distilled *in vacuo* at 110°. The central cut of the distillate was used. Perchloric acid solutions were titrated with standard alkali using methyl red as indicator. The water used was triply distilled. $\text{Ce}(\text{HSO}_4)_4$ was purified by heating at *ca.* 80° in a stream of oxygen and its solutions were left to age before use. All other reagents were analytical grade and used without further purification. A Welsbach ozonizer was used to produce ozonized oxygen.

Preparation of Samples. The glassware was steam-cleaned and preirradiated. For determination of gaseous products the samples were degassed *in vacuo*. For other determinations air was removed by passing helium successively through an activated charcoal trap immersed in liquid N_2 and through the solution. Care was taken to have the irradiation vessels completely filled.

Analytical Procedures. H_2O_2 . The iodide method⁷ was used with NaI instead of KI to avoid precipitation of KClO_4 . Commercial NaI contains impurities which were destroying some of the H_2O_2 and giving consistently low results. It was found necessary to add a little H_2O_2 to the buffered I^- reagent, which gave a high blank but did not appreciably reduce the accuracy of the method. The change in the blank due to the oxidation of I^- by air was followed as a function of time and taken into consideration. The acid solutions were neutralized with NaOH before mixing with the I^- reagent. For zero dilution and a 1-cm. cell, 38.8 $\mu\text{moles/l.}$ of H_2O_2 correspond to one optical density unit.

Chlorate was determined by difference. It does not react with I^- in neutral solution. H_2O_2 was determined in an aliquot by I^- , then in another aliquot the sum of H_2O_2 and ClO_3^- was found, using Fe^{+2} in 0.7 *M* HClO_4 and determining Fe^{+3} at 240 $m\mu$ ($\epsilon_{240} = 4185$ at 23°). No change in ϵ_{240} was found by changing HClO_4 from 0.2 to 3 *M*. H_2O_2 oxidizes two ferrous ions, while ClO_3^- oxidizes six. To accelerate the reaction of Fe^{+2} and ClO_3^- , 1 drop of 0.1% cadmium sulfate solution was added and the mixture heated to 80° for about 30 min., as recommended by Cottin.⁴ An unirradiated aliquot was treated in the same way and the resulting small blank subtracted. The results were reproducible and consistent to within $\pm 2\%$. Chlorate in the presence of Ce^{IV} was determined in a similar way

by first determining Ce^{IV} and then the amount of Fe^{+2} oxidized by both ClO_3^- and Ce^{IV} .

Ce^{IV} was in 0.8 *N* H_2SO_4 and was determined at 320 $m\mu$ using $\epsilon_{320} = 5565$.⁸ Changing the perchloric acid concentration from 0.2 to 3 *M* does not have any observable effect on ϵ_{320} for Ce^{IV} . The Ce^{III} yields were determined by measuring the decrease in Ce^{IV} . Tl^+ does not interfere with the analysis.

Fe^{+3} was determined spectrophotometrically as described above. For Cl^- , the method described by Hayon and Allen⁹ was used. The Cl^- concentration was calculated from a calibration curve. For O_2 and H_2 , the low-pressure combustion method was used.¹⁰

Under the conditions of our experiments the only other possible products that are stable are Cl_2 and ClO_2 . We found neither of them up to 4 *M* HClO_4 . The test consisted in determining, in one aliquot, H_2O_2 by the I^- method, then purging another aliquot with helium and analyzing again by the I^- method. No difference was observed. A small amount of oxidizing gas (presumably Cl_2) was found in ceric solutions containing chloride ion after standing several weeks, probably because of the oxidation of Cl^- by Ce^{IV} . It was determined by passing helium through successive traps containing I^- reagent. In the experiments reported this gas was removed before irradiation. The reaction was much too slow to produce any significant autoreduction of Ce^{IV} during the irradiation period.

Results

A. Dilute Perchloric Acid Solutions— γ -Rays. 1. Air-Saturated. Figure 1 gives the H_2O_2 production in air-saturated perchloric acid solutions (10^{-2} *M* in HClO_4) without anything else added. H_2O_2 is produced initially with a *G* value of 1.25, the same as in pure water,¹¹ and then reaches a steady state at 590 μM . After 14.5 hr. (point not shown in the figure), the concentration of H_2O_2 rose slightly to 611 μM .

2. Air-Free. In the absence of air, 0.01 *M* HClO_4 showed little decomposition and was very sensitive to impurities in a way reminiscent in many respects (H_2 , CO_2 yields) of the behavior of pure water.¹²

(5) M. Usanovich, T. Sumarokova, and V. Udovenko, *Acta Physicochim. URSS*, **11**, 505 (1939).

(6) R. Schuler and A. O. Allen, *Rev. Sci. Instr.*, **26**, 1128 (1955).

(7) C. J. Hochanadel, *J. Phys. Chem.*, **56**, 587 (1952).

(8) C. M. Henderson and N. Miller, *Radiation Res.*, **13**, 641 (1960).

(9) E. Hayon and A. O. Allen, *J. Phys. Chem.*, **65**, 2181 (1961).

(10) E. R. Johnson and A. O. Allen, *J. Am. Chem. Soc.*, **74**, 4147 (1952).

(11) A. O. Allen and R. A. Holroyd, *ibid.*, **77**, 5852 (1955).

(12) H. Fricke, E. J. Hart, and H. P. Smith, *J. Chem. Phys.*, **6**, 229 (1938).

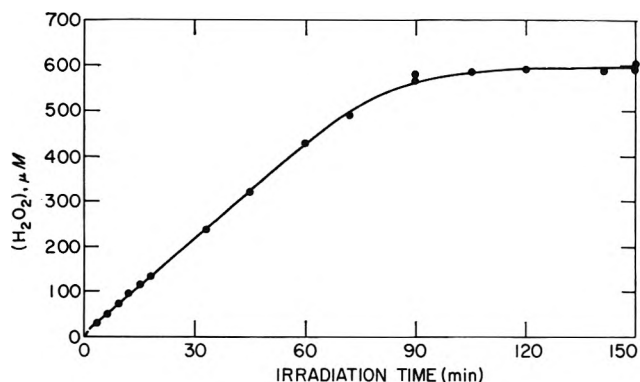


Figure 1. Hydrogen peroxide production in air-saturated 10^{-2} M HClO₄ solution. Intensity = 3.24×10^{20} e.v./l.⁻¹ min.⁻¹.

B. HClO₄ Solutions 10^{-2} M in NaCl— γ -Rays. 1. O₂ and H₂ Yields in Degassed Solutions. NaCl was added to eliminate the effect of the impurities and protect the molecular hydrogen from radical attack. It was found necessary to maintain the chloride concentration higher than usual, namely at 10^{-2} M, in order to obtain reproducible results, and concentration *vs.* dose curves having no intercept.

The hydrogen and oxygen *G* values were determined in solutions up to 11.8 M HClO₄ (Fig. 2). The concentration *vs.* dose curves were all linear up to the highest doses used (around 2.5×10^{22} e.v./l.). The oxygen yields are not too reliable because at high acid concentrations they are affected by post-irradiation reactions. Up to 3–4 M HClO₄ no post-irradiation effect occurred over a period of time much longer than that required normally to carry out the analysis. At acid concentrations above 5 M, the analysis was made after the thermal reactions were practically over. The intermediate region is uncertain. These thermal reactions were not investigated; it seems likely, however, that they involve a reaction between Cl⁻ and ClO₃⁻, which is strongly dependent on acid and gives products which rapidly oxidize H₂O₂. The discrepancy, at high acid, between our oxygen yields and those reported by Cottin⁴ may be due to these thermal reactions. The hydrogen yields are not affected by the post-irradiation reactions; the analysis gave the same results at all acid concentrations whether performed at once or 3 days after the irradiation. Addition to a solution 4.43 M in HClO₄, 10^{-2} M in NaCl, of Fe⁺² (3×10^{-4} M) and Fe⁺³ (7×10^{-4} M) resulted in a hydrogen yield of 0.25. For this acid concentration the hydrogen yield, from Fig. 2, is 0.235. The difference is only a little outside experimental error. The result indicates that the fall in *G*(H₂) with increasing HClO₄ concentration is not due to attack on the hydrogen by free radicals.

2. Cl⁻ and ClO₃⁻ Yields. The chlorate yields are given in Fig. 3 both with and without chloride added

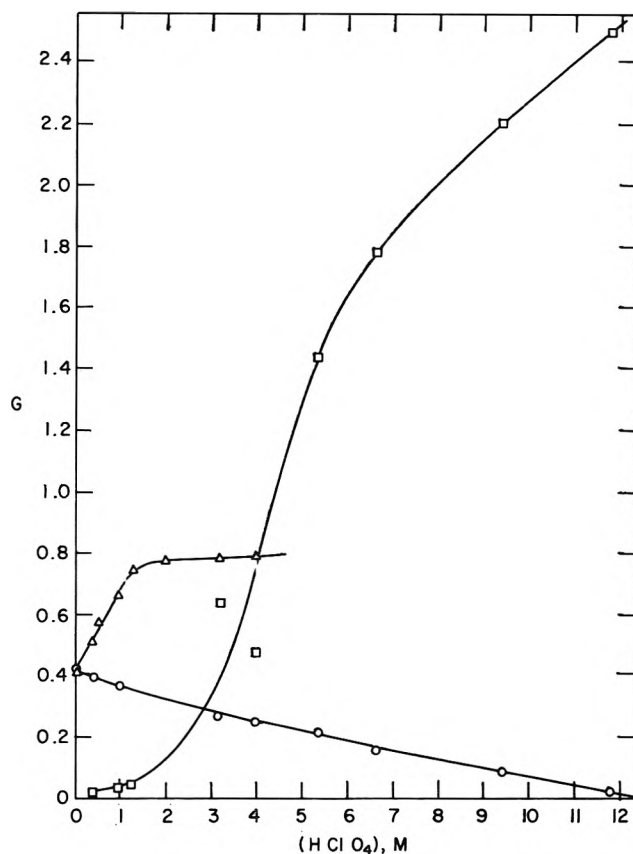


Figure 2. Effect of HClO₄ concentration on product yields in deaerated solutions containing 10^{-2} M NaCl: O, *G*(H₂); □, *G*(O₂); Δ, *G*(H₂O₂).

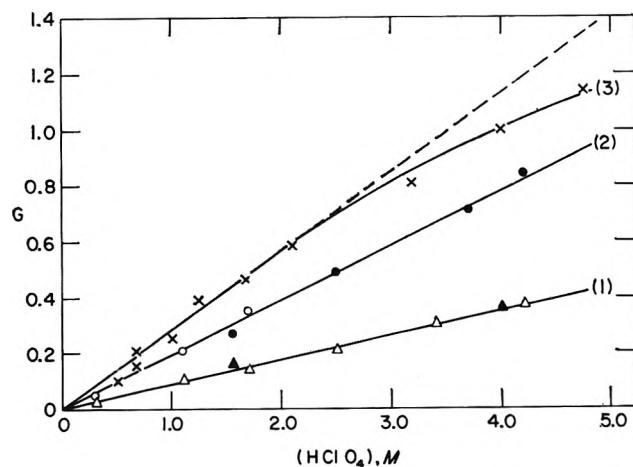


Figure 3. Effect of HClO₄ concentration on chlorate and chloride yields in deaerated solutions: ●, ClO₃⁻; ▲, Cl⁻; O, Δ, results of Cottin (ref. 4) ×, ClO₃⁻ yield with 10^{-2} M NaCl added initially. Dashed line is sum of curves 1 and 2.

initially. Cottin's results at perchloric acid concentration, 2.5 M and above, are higher than those obtained in these experiments and do not appear in the figure. Air does not affect the yield of ClO_3^- , and no difference was found at 0.515 M HClO_4 when Cl^- was replaced by Br^- .

Addition of 10^{-2} M NaCl increased the chlorate yield, and below 3 M HClO_4 , $G(\text{ClO}_3^-)$ became equal to the sum of $G(\text{Cl}^-)$ and $G(\text{ClO}_3^-)$ determined in the absence of added Cl^- (dotted curve). Above 3 M HClO_4 , $G(\text{ClO}_3^-)$ fell below the dotted curve, perhaps because of thermal reaction between ClO_3^- and Cl^- . $G(\text{Cl}^-)$ could not be determined in the presence of added NaCl. The implication is that most of the Cl^- found in the radiolysis is a secondary product, resulting from attack on ClO_3^- by free radicals in the bulk of the solution, and that added 10^{-2} M Cl^- protects ClO_3^- from this attack. To verify this idea, we irradiated an air-free solution of KClO_3 in 2.1 M HClO_4 (Fig. 4). $G(-\text{ClO}_3^-)$ was 0.22 with no chloride added and only 0.12 in the presence of 10^{-2} M NaCl. All the yields discussed in this section are constant with dose.

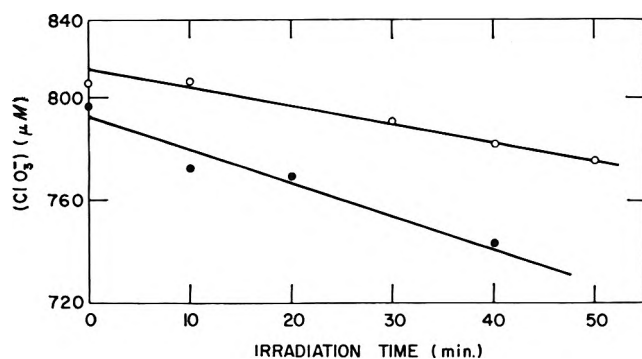


Figure 4. Chlorate disappearance in deaerated KClO_3 solutions, 2.1 M in HClO_4 : O, 10^{-2} M NaCl added; ●, no NaCl added. Intensity is 3.24×10^{20} e.v. l.⁻¹ min.⁻¹.

3. H_2O_2 Yields in Air-Saturated Solutions. The peroxide concentration rose linearly with dose to at least 250 μM . Values of G were 0.91 for 1.28 M and 0.87 for 2.5 M HClO_4 .

4. H_2O_2 Yields in Air-Free Solutions. The yields were again constant with dose. Figure 2 gives $G(\text{H}_2\text{O}_2)$ as a function of the HClO_4 concentration. Replacing Cl^- with Br^- had no effect.

C. Ce^{IV} and $\text{Ce}^{\text{IV}}\text{-Ti}^+$ Solutions. The results are given in Fig. 5. The reaction of Ce^{IV} with H_2O_2 in perchloric acid is relatively slow and not well understood. All these experiments were therefore performed in HClO_4 solutions made 0.8 N in H_2SO_4 . The

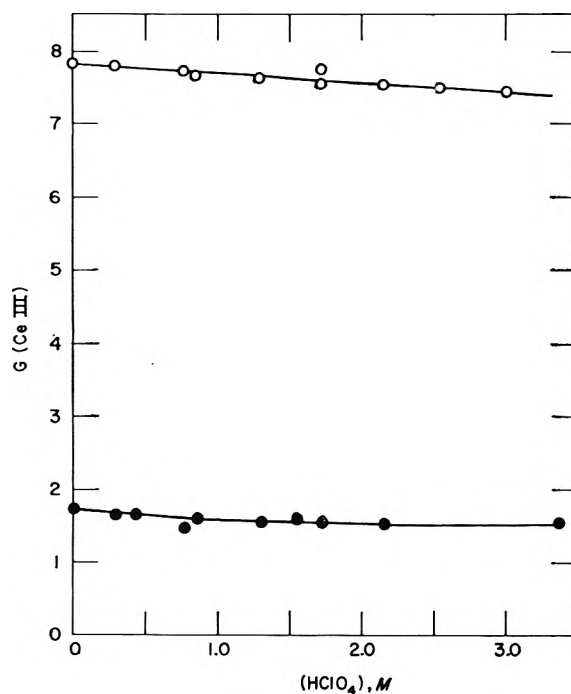


Figure 5. Cerium reduction yields in solutions containing 0.8 N H_2SO_4 , 10^{-2} M NaCl: ●, $(\text{Ce}^{\text{IV}}) \sim 3 \times 10^{-4}$ M, $(\text{Ce}^{\text{III}}) \sim 2 \times 10^{-4}$ M; O, $(\text{Ce}^{\text{IV}}) \sim 3 \times 10^{-4}$ M, $(\text{Ce}^{\text{III}}) \sim 2 \times 10^{-4}$ M, $(\text{Ti}^+) = 2 \times 10^{-4}$ M.

Ce^{IV} concentration was $2\text{--}4 \times 10^{-4}$ M and the Ce^{III} concentration 2×10^{-4} M. Ti^+ , when added, was at a concentration of 2×10^{-4} M. The irradiations were done in air-saturated solutions and the best results were obtained by irradiating a large volume of solution and taking aliquots for analysis at the desired time intervals. The concentration vs. dose curves were linear. $G(\text{Ce}^{\text{III}})$ in 0.8 N H_2SO_4 was found to be 2.4, close to the value of 2.34 found by Barr and Schuler.¹³ In 0.8 N H_2SO_4 , 10^{-2} M NaCl, $G(\text{Ce}^{\text{III}}) = 1.7$. Sworski¹⁴ finds for this chloride concentration $G(\text{H}_2\text{O}_2) = 0.95$, and since $G(\text{Ce}^{\text{III}})$ must be twice the peroxide yield $G(\text{Ce}^{\text{III}})$ should be expected to be 1.9. The difference, 0.2 unit, was attributed by Boyle¹⁵ to direct action of radiation on sulfuric acid, which yields a persulfate that appears as peroxide but does not reduce Ce^{IV} . ClO_3^- does not react with Ce^{IV} , even under the conditions of radiolysis. G values found for ClO_3^- in the presence of Ce^{IV} are the same as in HClO_4 solutions.

D. Fe^{+3} Yields in HClO_4 Solutions of Fe^{+2} . 1. Air-Saturated. One chlorate ion oxidizes six ferrous ions. The spontaneous reaction is very slow, but

(13) N. F. Barr and R. H. Schuler, *J. Phys. Chem.*, **63**, 808 (1959).

(14) T. J. Sworski, *Radiation Res.*, **2**, 26 (1955).

(15) J. W. Boyle, *ibid.*, **17**, 427 (1962).

under γ -rays formation of Fe^{+3} was found to be complete within 3 min. after irradiation; addition of CdSO_4 catalyst, with warming and standing overnight, produced no more. Since chlorate was always found as product in the absence of added ferrous salts, we conclude that radiation accelerates the $\text{Fe}-\text{ClO}_3^-$ reaction. In Fig. 6 the difference $G(\text{Fe}^{+3}) - 6G(\text{ClO}_3^-)$ is plotted against (HClO_4) . Values of $G(\text{ClO}_3^-)$ were obtained from Fig. 3. The yields were independent of the dose used. Initial concentration of Fe^{+2} was 1 mM.

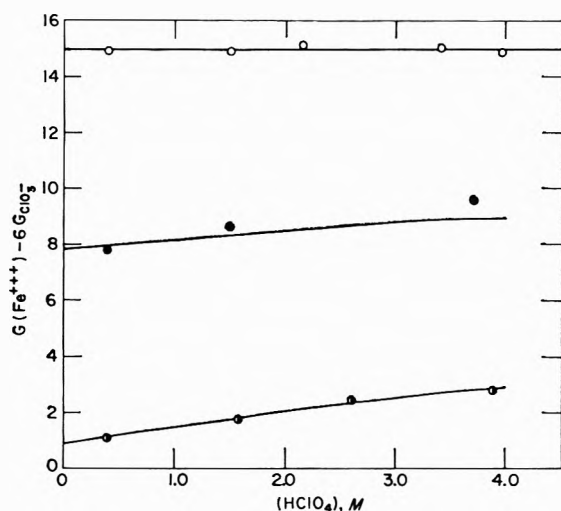


Figure 6. Ferric ion yields, corrected for ClO_3^- oxidation, in HClO_4 solutions of ferrous ion. Total iron concentration is $10^{-3} M$, $(\text{Cl}^-) = 10^{-2} M$; O, air-saturated solution; ●, initial yield in deaerated solution (no Fe^{III} added); ●, final yield in deaerated solution [$(\text{Fe}^{\text{III}})/(\text{Fe}^{\text{II}}) = 10$, initially]. The middle curve is the mean of the top and bottom curves.

2. *Air-Free Initial.* With only ferrous salt present, the concentration *vs.* dose curves (Fig. 7) were no longer linear. Accurate determination of initial yields $G_i(\text{Fe}^{+3})$ from these curves is not possible. An approximate value was obtained by use of the kinetic expression $G_i = G_{av} + 2G_H/[1 + K(\text{Fe}^{+2})/(\text{Fe}^{+3})]$, where G_{av} is the average G value over an arbitrary small time interval Δt , estimated from Fig. 7. K is estimated from Schwarz's results¹⁶ as 0.1 in $10^{-2} M$ NaCl . G_H is taken as 3.65. The points in Fig. 6, curve 2, were obtained on this basis; $G_i - 6G(\text{ClO}_3^-)$ is given for 1 mM (Fe^{+2}) .

3. *Air-Free Final.* When a tenfold excess of ferric iron is present in the solution of HClO_4 with 0.01 M Cl^- , essentially all the H atoms react with ferric iron, and the yield of oxidation of ferrous iron becomes independent of dose. Figure 6, bottom curve, gives $G_i(\text{Fe}^{+3}) - 6G(\text{ClO}_3^-)$ for solutions initially 0.1 mM in Fe^{+2} and 0.9 mM in Fe^{+3} .

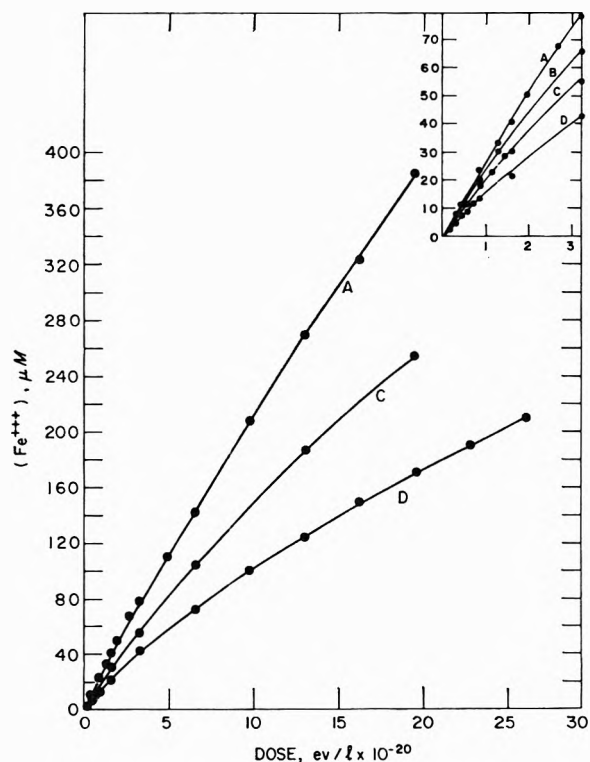


Figure 7. Ferric production in HClO_4 solutions containing $10^{-2} M$ NaCl , $10^{-3} M$ Fe^{+2} . HClO_4 concentrations: A, 3.7 M; B, 3.05 M; C, 1.5 M; D, 0.4 M.

E. Ozone Experiments. The possibility exists that atomic oxygen might be produced by the radiolysis of HClO_4 . Taube¹⁷ has shown that atomic oxygen in the ^1D state adds to H_2O to form H_2O_2 , and also that it can reduce HClO_4 to HClO_3 . By passing ozone through a HClO_4 solution we find that even O_3 itself can bring about this reduction, although the reaction seems to be slow. No further reduction to Cl^- was observed.

To see whether ozone would oxidize Tl^{I} to Tl^{II} , which reduces Ce^{IV} , or directly to Tl^{III} , which would not affect Ce^{IV} , ozonized oxygen was bubbled through a number of mixtures (Table I). The results indicate that the ozone and Tl^{I} do in fact interact, especially in the presence of chloride, to give something, presumably Tl^{II} , which reduces Ce^{IV} . However, bubbling chlorine gas through a mixture of Tl^{I} and Ce^{IV} in H_2SO_4 had no effect on the Ce^{IV} concentration; it would thus appear that Cl_2 oxidizes Tl^{I} directly to Tl^{III} . We do not know whether an O atom would behave like ozone or like chlorine.

F. Cyclotron Experiments. The experiments reported in Fig. 8 were done with ca. 33-Mev. He^{+2} ions.

(16) H. A. Schwarz, *J. Am. Chem. Soc.*, **79**, 534 (1957).

(17) H. Taube, *Trans. Faraday Soc.*, **53**, 656 (1957).

Table I: Reaction of Ozone with Thallous Ion in the Presence of Ceric Sulfate

Medium	Reaction time, min. ^a	Initial (Ce ^{IV}), M × 10 ⁴	Final (Ce ^{IV}), M × 10 ⁴
Ce ^{IV} , Cl ⁻ , Tl ⁺ , and H ₂ SO ₄ (ca. 1 N)	4	3.7	1.9
Ce ^{IV} , Cl ⁻ , Tl ⁺ , and H ₂ SO ₄	7	3.7	0.45
Ce ^{IV} , Cl ⁻ , H ₂ SO ₄	4	6.0	6.4
Ce ^{IV} , Tl ⁺ , H ₂ SO ₄	3	10.0	8.6
Ce ^{IV} , Tl ⁺ (10 ⁻² M), Cl ⁻ (10 ⁻² M), H ₂ SO ₄	4	3.7	0.25
Ce ^{III} , 1.3 × 10 ⁻³ M			
Ce ^{IV} , Tl ⁺ (10 ⁻² M), Cl ⁻ (10 ⁻²), H ₂ SO ₄	4	4.1	0.63
Ce ^{III} , 6.5 × 10 ⁻² M			
Ce ^{IV} , Tl ⁺ (10 ⁻² M), HClO ₄ (ca. 1 M)	8	11.4	1.5

^a Time that ozonized oxygen was bubbled through the solution. Rate of ozone formation was about 0.07 mmole/min.

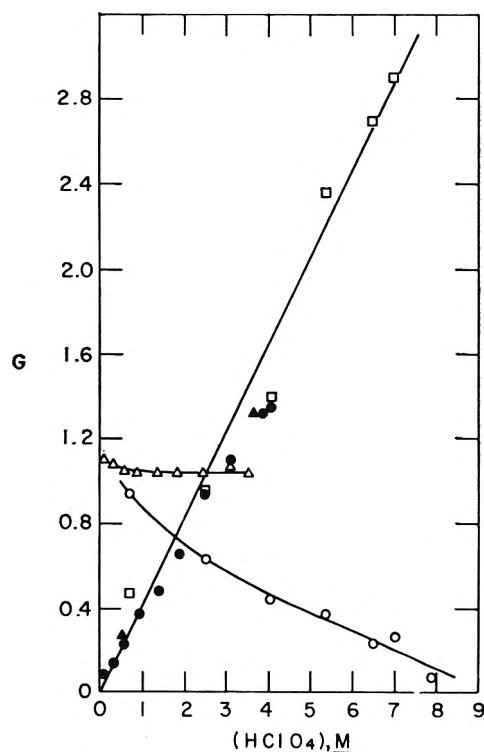


Figure 8. Product yields for 33-Mev. helium ions in 10⁻² M NaCl solutions: O, G(H₂); Δ, G(H₂O₂); □, G(O₂); ●, G(ClO₃⁻), all in deaerated solution; ▲, G(ClO₃⁻) in air-saturated solution.

All solutions were 10⁻² M in NaCl. No deviation from linearity was observed in the concentration *vs.* dose curves up to the total input employed (ca. 10²⁰ e.v.). The ClO₃⁻ yields are, within experimental error, the same in air-free and air-saturated solutions. The H₂

yields behave in a way similar to those obtained with γ-rays, although they start, as expected, at a higher value. In the H₂O₂ yields the initial increase that was observed in the γ-irradiations is missing in the helium ion results. The ClO₃⁻ yields are higher by about one-third with helium ions than with γ's. Though, as remarked above, oxygen yields are not determined as precisely as the others, comparison of Fig. 2 and 8 shows clearly that the oxygen yield is much higher with helium ions. Furthermore, the measured products show a notable excess of oxidation over reduction, given by $G(X) = G(\text{H}_2\text{O}_2) + 2G(\text{O}_2) - G(\text{H}_2) - G(\text{ClO}_3^-)$. This excess must be balanced by chloride ion formation, with $4G(\text{Cl}^-) = G(X)$. Typical values of $G(\text{Cl}^-)$ calculated by material balance from the data of Fig. 2 and 8 are given in Table II. $G(\text{Cl}^-)$ is much higher

Table II: Chloride Ion Yields Deduced from Material Balance

(HClO ₄), M	G(Cl ⁻), γ-rays	G(Cl ⁻), 33-Mev. He ⁺⁺ ions
1	0.03	0.14
2	0.03	0.29
3	0.08	0.40
4	0.27	0.55

with helium ions than with γ's; it increases linearly with concentration under helium ions but becomes appreciable with γ's only at the higher concentrations. In this respect, the α-rays appear to give qualitatively different results from the γ-rays.

Discussion

Dilute perchloric acid appears to react under irradiation in every way like pure water. In air-saturated solutions, the steady-state peroxide level is close to that found in water. According to Allen and Schwarz,¹⁸ the steady-state concentration of H₂O₂ is given by

$$\frac{\alpha}{(\text{H}_2\text{O}_2)_{\text{ss}}} = 1 - 2K \frac{G_{\text{H}_2}}{G_{\text{H}} + G_{\text{OH}}} + 2K' \left(\frac{G_{\text{H}}}{G_{\text{H}_2\text{O}_2}} - 1 \right)$$

where α is in our case 2(O₂)_{initial}, K the ratio of the rate constants for the reaction of OH with H₂ and H₂O₂, and K' the ratio for the rate constants of the reactions of H atoms with H₂O₂ and O₂. At pH 2, the hydrogen atoms are mainly in the acidic form and K' ≪ 1, so the last term on the right-hand side of the equation

(18) A. O. Allen and H. A. Schwarz, *Proc. 2nd Intern. Conf. Peaceful Uses At. Energy, Geneva*, 29, 30 (1958).

can be neglected. Taking values appropriate to this pH,¹⁹ $G_{\text{H}} = 3.35$, $G_{\text{OH}} = 2.63$, $G_{\text{H}_2} = 0.42$, and $\alpha = 520$, and from Fig. 1 (H_2O_2)_{ss} 600 μM , we find $K = 0.95$, essentially the same as in neutral solution.¹⁸ The same conclusion was reached by Hochanadel²⁰ from experiments on peroxide photolysis. In sulfuric acid solutions, by contrast, no steady state is reached, because the bisulfate ion reacts with OH to give a radical that does not react with hydrogen. Apparently, perchlorate ions do not react with H or OH and the decomposition of perchlorate in aqueous solution must be entirely due to the direct effect.

The reaction products of the perchlorate decomposition as they emerge from the spur include chlorate ion, with possibly a small amount of chloride forming at higher perchloric acid concentrations. The chloride appearing in pure perchloric acid solutions at moderate concentrations was shown to be inhibited by additional chloride and must result from the action of OH radicals on the chlorate ions. The presumptive reaction is $\text{OH} + \text{ClO}_3^- + \text{H}^+ = \text{H}_2\text{O} + \text{ClO}_3$, followed by decomposition or reduction of the radical ClO_3 to yield ultimately chloride ion. The acceleration by radiation of the oxidation of Fe^{+2} by ClO_3^- probably involves reaction of ClO_3 with Fe^{+2} initiating a series of steps that lead ultimately to formation of Cl^- and seven Fe^{+3} . To understand the system completely would require a complete study of the radiation chemistry of chlorate solutions, which we have not undertaken. Even in the presence of chloride, some of the chlorate ions emerging from the spurs may be attacked by radicals, and our values of the chlorate yield represent only a lower limit for the amount of direct action on the perchlorate ions.

The oxygen formed together with chlorate in the perchlorate decomposition might be expected to emerge from the spur in a number of different chemical forms: O_2 or H_2O_2 molecules, HO_2 or OH radicals, or O atoms. Because of the complications involving the secondary reactions with chlorate, the oxygen-peroxide system is not suitable for drawing quantitative conclusions in perchloric acid, and we turned to the use of ions of iron, cerium, and thallium as scavengers.

In aerated ferrous ion solutions, each oxygen atom would be expected to oxidize two equivalents of iron. In addition, as in the usual ferrous sulfate reaction, each H or HO_2 should oxidize three equivalents, each H_2O_2 two, and each OH one equivalent. Each chlorate ion formed will oxidize six equivalents. Thus

$$G_{\text{air}}(\text{Fe}^{+3}) - 6G(\text{ClO}_3^-) = 3G_{\text{H}} + 2G_{\text{H}_2\text{O}_2} + G_{\text{OH}} + 2G_{\text{O}} + 3G_{\text{HO}_2}$$

In air-free solutions in the presence of excess ferric ion

and of chloride ion, the hydrogen atoms react with ferric ion to reduce it in preference to oxidizing ferrous ion. Any free oxygen formed will be attacked by H atoms to form HO_2 which results in oxidation of three equivalents of ferrous ion. The combined effect of the yields of O_2 and H then will be an oxidation to the extent of $3G_{\text{O}}$, less a reduction by the balance of the H atoms, $G_{\text{H}} - G_{\text{O}}$, so the net oxidizing yield will be $4G_{\text{O}} - G_{\text{H}}$. The yield of iron oxidized under these conditions will therefore be given by

$$G_{\text{f}}(\text{Fe}^{+3}) - 6G(\text{ClO}_3^-) = -G_{\text{H}} + 2G_{\text{H}_2\text{O}_2} + G_{\text{OH}} + 2G_{\text{O}} + 3G_{\text{HO}_2} + 4G_{\text{O}}$$

In the absence of ferric ion, each O_2 formed will again pick up an H atom to form HO_2 and oxidize three equivalents of ferrous ion, but the balance of the H atoms, $G_{\text{H}} - G_{\text{O}}$, will then oxidize one equivalent of ferrous iron. The yield of oxidation resulting from the combined action of H and O_2 should then be $2G_{\text{O}} + G_{\text{H}}$. Thus the initial yields should be given by

$$G_{\text{i}}(\text{Fe}^{+3}) - 6G(\text{ClO}_3^-) = G_{\text{H}} + 2G_{\text{H}_2\text{O}_2} + G_{\text{OH}} + 2G_{\text{O}} + 3G_{\text{HO}_2} + 2G_{\text{O}}$$

We see then that the initial air-free yield should always lie just half-way between the final air-free yield and the yield obtained in the presence of air. Figure 6 shows that this appears to be the case, within the rather poor precision with which the initial yield in air-free solutions could be determined.

The significance of the yields of ceric sulfate reduction in the presence and absence of thallos ion is somewhat ambiguous as far as the behavior of the O atom is concerned. The ceric reduction yield in the absence of thallos ion is somewhat less than twice the yield of formation of peroxide in aerated perchloric acid of the same concentration, but not containing any sulfate. In the absence of cerium, the oxygen atom might be expected to destroy peroxide by the reaction $\text{O} + \text{H}_2\text{O}_2 = \text{O}_2 + \text{H}_2\text{O}$. Since the ceric reduction yield is not greater than twice the yield of H_2O_2 formed in the absence of cerium, it seems likely that if any oxygen atoms are present they must either oxidize trivalent cerium to the tetravalent form in this system, or destroy H_2O_2 before the peroxide has time to react with Ce^{IV} .

Then

$$G(\text{Ce}^{\text{III}}) = G_{\text{H}} + 2G_{\text{H}_2\text{O}_2} - G_{\text{OH}} - 2G_{\text{O}} + G_{\text{HO}_2}$$

In the presence of thallos ion we do not know if the O atom would oxidize thallium to the divalent state which

(19) A. O. Allen, "The Radiation Chemistry of Water and Aqueous Solutions," D. Van Nostrand Co., Princeton, N. J., 1962.

(20) C. J. Hochanadel, *Radiation Res.*, **17**, 286 (1962).

Table III: Effect of HClO₄ on Some Yield Relationships

(HClO ₄)	$\delta G_{OH} + G_O$	$\delta G_H - G_{O_2}$	$G_{HO_2} + G_O + G_{O_2}$	$\delta G_{H_2O_2} - G_O$	δG_{H_2}	$G_{ClO_3^-}$	G_{Cl^-}
2 M	-0.05	-0.30	0.45	-0.19	-0.1	0.57	...
3 M	-0.11	-0.45	0.66	-0.28	-0.14	0.81	0.04

reduces cerium, or directly to the trivalent state. In the latter case the yield of cerium reduction in the presence of thallose ion is

$$G(\text{Ce}^{\text{III}})_{\text{Tr}} = G_H + 2G_{\text{H}_2\text{O}_2} + G_{\text{OH}} + G_{\text{HO}_2}$$

The experiments with scavengers thus give us for any particular concentration of perchloric acid a series of relationships between the changes in yields of H, OH, and H₂O₂ produced by the perchloric acid and the yields of O₂, O, and HO₂ which may arise from the acid. If we let δG represent the yield of a water radiolysis product in the presence of any concentration of perchloric acid minus its value extrapolated to zero perchloric acid, the results may be summarized as

$$\delta G_{\text{air}}(\text{Fe}^{+3}) = 3\delta G_H + 2\delta G_{\text{H}_2\text{O}_2} + \delta G_{\text{OH}} + 2G_O + 3G_{\text{HO}_2}$$

$$\delta G_t(\text{Fe}^{+3}) = -\delta G_H + 2\delta G_{\text{H}_2\text{O}_2} + \delta G_{\text{OH}} + 2G_O + 3G_{\text{HO}_2} + 4G_{\text{O}_2}$$

$$\delta G(\text{Ce}^{\text{III}}) = \delta G_H + 2\delta G_{\text{H}_2\text{O}_2} - \delta G_{\text{OH}} - 2G_O + G_{\text{HO}_2}$$

$$\delta G(\text{Ce}^{\text{III}})_{\text{Tr}} = \delta G_H + 2\delta G_{\text{H}_2\text{O}_2} + \delta G_{\text{OH}} + G_{\text{HO}_2}$$

where the values of $G(\text{Fe}^{+3})$ have been corrected for the chlorate yield.

Since there are six unknowns and only four equations, the system is not entirely determined. However, some interesting combinations of the unknowns may be obtained

$$\delta G_{\text{OH}} + G_O = \frac{1}{2}[\delta G(\text{Ce}^{\text{III}})_{\text{Tr}} - \delta G(\text{Ce}^{\text{III}})]$$

$$\delta G_H - G_{\text{O}_2} = \frac{1}{4}[\delta G_{\text{air}}(\text{Fe}^{+3}) - \delta G_t(\text{Fe}^{+3})]$$

$$G_{\text{HO}_2} + G_O + G_{\text{O}_2} = \frac{1}{4}[\delta G_{\text{air}}(\text{Fe}^{+3}) + \delta G_t(\text{Fe}^{+3}) - 2\delta G(\text{Ce}^{\text{III}})_{\text{Tr}}]$$

$$\delta G(\text{H}_2\text{O}_2) - G_O = \frac{1}{4}[\delta G(\text{Ce}^{\text{III}}) - \delta G_{\text{air}}(\text{Fe}^{+3}) + 2\delta G(\text{Ce}^{\text{III}})_{\text{Tr}}]$$

Values of these quantities for 2 and 3 M HClO₄ are shown in Table III together with yields of chlorate and chloride and change in the yield of hydrogen. The sum of G_{O_2} , G_O , and G_{HO_2} is seen to be somewhat less than $G(\text{ClO}_3^-)$. Some of the oxygen from the perchlorate ion thus probably appears as H₂O₂ or OH. However, the sum $G_{\text{OH}} + G_{\text{H}_2\text{O}_2}$ is seen to be smaller in perchloric acid solutions than in water. The yield of

all the water decomposition products appears in fact to be decreased by perchloric acid, as expected if a considerable fraction of the energy is going to excitation of the perchlorate ions.

Since the yields all vary nearly linearly with ClO₄⁻ concentration, in both γ -ray and helium ion results, the excited perchlorate ions do not react with one another or with unexcited perchlorate; they rather react unimolecularly. One might expect the perchlorate to ionize to a ClO₄ radical and an electron, which would give rise to an H atom in acid solutions, but the results make it look very unlikely that an important fraction of the excited perchlorate reacts in this way. The yield of H atoms certainly seems to decrease with increasing perchlorate concentration. Thus the ratio $G(\text{O}_2)/G(\text{H}_2\text{O}_2)$ shown in Fig. 2 and 8 depends on the ratio of oxidizing radicals (which oxidize H₂O₂ to O₂) to H atoms (which reduce O₂ to H₂O₂); this ratio increases sharply with perchlorate concentration, while the yield of H₂, which arises from intraspur reactions of H, declines. Thus the usual fate of the excited perchlorate ions must be to decompose into ClO₃⁻ ions and O atoms. Most of the O atoms must be formed in the ground state, since Taube¹⁷ has shown that O atoms formed in the excited ¹D state react readily with water, forming H₂O₂, while $G_{\text{H}_2\text{O}_2}$ seems to decrease rather than increase with perchlorate concentration. The O atoms may emerge from the spurs as such, or react in the spurs with H to form OH, or with OH to form HO₂.

The higher yields of ClO₃⁻ and Cl⁻ in the helium ion tracks are unexpected. Again, the approximate linearity of the yields with perchlorate concentration shows that the track density effect is not due to an interaction with one another of excited perchlorate ions or radicals derived from them. The enhanced yields probably arise rather from interaction of perchlorate with the higher density of excited water molecules and free radicals. There must be many events in which an excited perchlorate ion loses its energy without decomposition or decomposes to ClO₃⁻ and O only to have these products recombine to ClO₄⁻ in the solvent cage. If, however, a neighboring water molecule is excited or has decomposed to H or OH, it can enter into the reaction and bring about generally more extensive decomposition than would have occurred had the water

excitation been located farther from the perchlorate excitation. The higher chloride yield may also arise

from secondary reactions with free radicals suffered by ClO_3^- as it diffuses out of the track.

Tritium β -Radiation-Induced Isotopic Exchange with Water Vapor

by John Y. Yang and L. H. Gevantman

U. S. Naval Radiological Defense Laboratory, San Francisco, California (Received February 24, 1964)

The rate of tritium β -decay-induced isotopic exchange between tritium gas and water vapor is found to be constant within a fourfold variation in the water vapor density, but to increase as a second-order function of the tritium concentration. Inert gases, present in large excess, appeared to function purely as moderating media for the tritium β -energy. With helium gas as the moderator and tritium concentration in the range from 0.05 to 0.7 c./l., the reaction rate in mc./l./day at the ambient temperature of $22 \pm 2^\circ$ is observed as $d(\text{HTO})/dt = 3.6 \times 10^{-5}(\text{T}_2)^2$, where (T_2) is the initial tritium concentration in mc./l. This exchange reaction is strongly inhibited by the presence of nitric oxide in the reaction mixture. The results are consistent with a reaction mechanism involving radical intermediates.

Introduction

Ever since the discovery¹ of tritium incorporation in organic compounds by exposure to tritium gas, a number of investigations devoted to detailed studies of the isotopic exchange in tritium-hydrocarbon systems have appeared in the literature.²⁻¹⁰ Although the over-all reaction mechanism appears to vary considerably with each individual system, it is generally agreed that the tritium β -radiation-induced intermediates play a major role for tritium incorporation in the organic substrate.

We chose to study the tritium-water vapor system because radiolytic processes in aqueous systems are reasonably well understood.¹¹ The effect of linear energy transfer^{12,13} and that of change to the less dense vapor phase as reaction medium¹⁴ have also been reported. It is our hope to ascertain some definite correlation between the isotopic exchange and radiation-induced reactions.

Experimental

Materials. Carrier-free tritium gas was obtained

from the Oak Ridge National Laboratory and was purified before use by passage through a liquid nitrogen trap. Research grade helium was supplied by the Matheson Company in a pressurized cylinder. Reagent grade argon, krypton, hydrogen, and nitrogen in 1-l. Pyrex flasks were purchased from the Air Reduction Co. and used without further purification. Matheson

- (1) K. E. Wilzbach, *J. Am. Chem. Soc.*, **79**, 1013 (1957).
- (2) P. Riesz and K. E. Wilzbach, *J. Phys. Chem.*, **62**, 6 (1958).
- (3) K. Yang and P. L. Gant, *J. Chem. Phys.*, **30**, 1108 (1959).
- (4) K. Yang and P. L. Gant, *ibid.*, **31**, 1589 (1959).
- (5) P. L. Gant and K. Yang, *ibid.*, **32**, 1757 (1960).
- (6) A. Y. Mottlau, *J. Phys. Chem.*, **64**, 931 (1960).
- (7) T. H. Pratt and R. Wolfgang, *J. Am. Chem. Soc.*, **83**, 10 (1961).
- (8) K. Yang and P. L. Gant, *J. Phys. Chem.*, **66**, 1619 (1962).
- (9) S. Wexler, *J. Am. Chem. Soc.*, **85**, 272 (1963).
- (10) J. Y. Yang and R. B. Ingalls, *ibid.*, **85**, 3920 (1963).
- (11) A. O. Allen, "The Radiation Chemistry of Water and Aqueous Solutions," D. Van Nostrand Co., Inc., New York, N. Y.
- (12) E. J. Hart, *Radiation Res.*, **1**, 53 (1954).
- (13) E. Collinson, F. S. Dainton, and J. Kroh, *Nature*, **187**, 475 (1960).
- (14) R. F. Firestone, *J. Am. Chem. Soc.*, **79**, 5593 (1957).

nitric oxide with a prescribed minimum purity of 99% was further purified by evacuation at liquid nitrogen temperature followed by bulb-to-bulb distillation. A standard sample of tritiated water was obtained from the National Bureau of Standards.

Tritium Exposure. A conventional high vacuum system was used throughout this investigation. A schematic diagram of the system used for the preparation and sampling of the reaction mixture is shown in Fig. 1. The reaction vessel, A, consists of a spherical

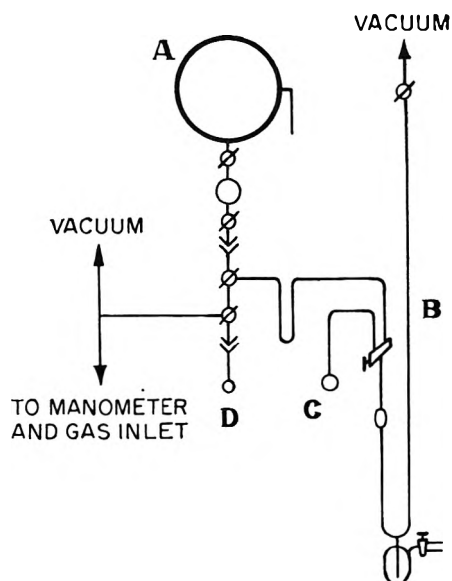


Figure 1. Schematic diagram of reaction apparatus.

flask (1 or 2 l.) with a cold finger tube on the side and a small sampling bulb (5 to 15 ml.) separated by a stopcock. The tritium-metering pipet, B, is essentially a small Toepler pump with a graduated volume coupled to a manometer. The tritium ampoule, C, was sealed to the tritium-metering pipet, and tritium gas, when not in use, was separated from the remainder of the system by raising the mercury level past the three-way stopcock. The small flask, D, was used for weighing and introduction of water samples.

For a typical run, the reaction vessel was baked at 350° for about 24 hr. while being evacuated to the order of 10^{-7} mm. A weighed amount of water was degassed and then distilled into the cold finger tube. Tritium gas was measured and expanded from the metering pipet into the reaction flask. The moderator gas was then added until the total pressure of the reaction mixture reached the desired level (350 to 650 mm.). When hydrogen or nitric oxide was used as additive, it was admitted just before the introduction of the

moderator gas. All reactions were carried out at the ambient air temperature of $22 \pm 2^\circ$.

X-Ray Irradiation. A Westinghouse 250 KVP machine operating at 15 ma. was used without filter. The reaction vessel was placed with its center at a distance of 25 cm. from the X-ray tube, where the field intensity as measured with a Victoreen thimble meter was 680 r./min.

Analysis. Samples were taken at daily intervals by admitting the reaction mixture into the sampling bulb and allowing about 30 min. for complete diffusion. A radiator-type trap coupled with a reservoir bulb containing a measured amount of carrier water was inserted between the reaction vessel and the vacuum line. After the carrier water had been properly degassed, it was warmed gently while exposed to the sampling bulb. Another hour was allowed to elapse before the reaction sample was evacuated through the water-containing trap. Several cycles of freezing and thawing were carried out, each time allowing the water to condense partly in the sampling bulb. The yield of tritiated water was analyzed by liquid scintillation counting using a Packard Tri-Carb liquid scintillation spectrometer. The use of hydrogen carrier gas to remove possible dissolved T_2 gas did not result in any subsequent lowering in the specific activity of the carrier water. Efficiency of this sampling technique was verified by the use of standard tritiated water under simulated conditions.

Results

In each of our experiments, a moderator gas was present in sufficient quantity to assure complete absorption of the tritium β -energy in the reaction system.¹⁵ The reaction rate data together with the tritiated water yields expressed as $G(\text{HTO})$, number of molecules/100 e.v. of energy, are summarized in Table I. The rate of tritiated water formation at the initial tritium concentration of 52 ± 1 mc./l. is unaffected by a nearly fourfold change in the water vapor density, whereas second-order dependence of the isotopic exchange rate on the tritium concentration is indicated from a log-log plot of the rate of tritiated water formation vs. the tritium concentration.

The use of a number of different inert gases in the reaction system caused only small changes in the reaction rate. The reaction rates at the tritium concentration of 210 ± 4 mc./l. are presented in Fig. 2, and an inverse dependence of the reaction rate on the ionization potential of the moderator is observed in the case of monatomic gases.

(15) L. M. Dorfman, *Phys. Rev.*, **95**, 393 (1954).

Table I: Tritium β -Radiation-Induced Vapor Phase Exchange between T₂ and H₂O

Moderator gas ^a	Total pressure, mm.	Vapor density, mg./l.	Initial T ₂ concn., (T ₂), mc./l.	Dose rate, e.v./l./day $\times 10^{-18}$	Additive, mm.	$R = \frac{d(\text{HTO})}{dt}$, mc./l/day	$\frac{R}{(T_2)^2} \times 10^6$	G(HTO)
He	626	9.3	714	12.7	...	16.4	3.21	2.69
He	613	9.6	380	6.76	...	5.77	3.98	1.78
He	653	9.6	207	3.69	...	1.33	4.28	1.03
He	638	12.2	102	1.82	...	0.425	4.13	0.48
He	564	17.5	52.1	0.93	...	0.095	3.49	0.21
He	627	9.4	52.6	0.94	...	0.088	3.18	0.20
He	617	5.0	51.2	0.91	...	0.083	3.17	0.19
N ₂	377	9.8	210	3.74	...	2.72	6.17	1.51
Kr	380	9.7	212	3.77	...	3.28	6.85	1.80
Ar	575	9.6	214	3.81	...	3.06	6.68	1.67
					X-Ray	11.45	25.00	...
Ar	345	9.9	210	...	X-Ray	16.68	37.82	...
He	623	9.6	194	3.45	H ₂ , 1.05	0.239	0.64	0.14
He	627	9.8	207	3.69	NO, 0.11	0.069	0.16	0.04

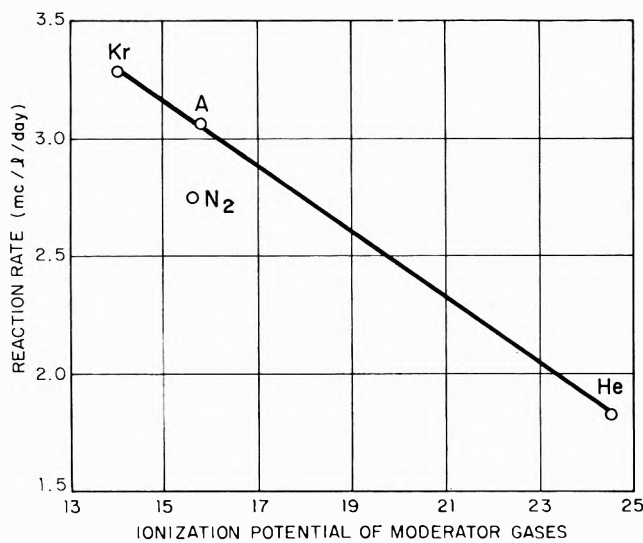


Figure 2. Effect of moderator gas.

In the presence of nitric oxide, a well-known free radical scavenger, a strong inhibition of the isotopic exchange is observed. In an experiment in which the concentration of nitric oxide was only in slight excess of that of tritium (1.58:1) the tritiated water yield was reduced to less than 4% of the normal value. Dilution with hydrogen also resulted in lowering of the tritiated water formation.

The effect of X-ray irradiation on the reaction rate has been studied and the results are presented in Fig. 3. The experiments were carried out with argon as moderator, tritium concentration at 212 ± 2 mc./l., and water vapor density at about 10 mg./l. In run A, it is shown that the reaction rate dropped

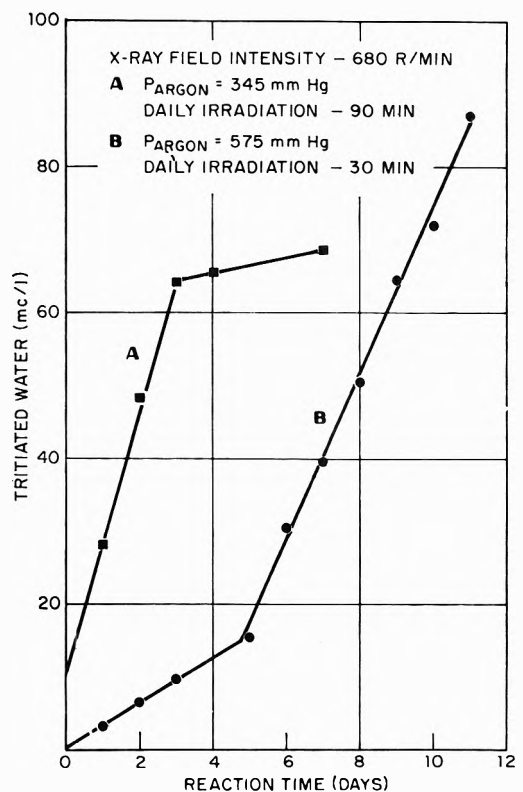


Figure 3. Effect of X-ray irradiation.

sharply upon termination of external irradiation, indicating the absence of prolonged irradiation effects. For run B, the external irradiation was applied after the tritium β -radiation-induced reaction rate had been established. The absolute X-ray irradiation dose rates were not determined, but the relative dose ab-

sorption for run A *vs.* run B can be estimated as 1.82 by assuming that the rate of radiation absorption is proportional to the total gas pressure. The relative increase in the reaction rates due to external irradiation in runs A and B was found to be 1.64. This excellent agreement gives a good indication for a first-order dependence of the isotopic exchange rate on the radiation dose rate.

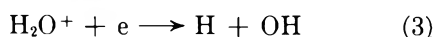
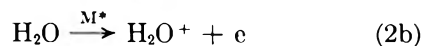
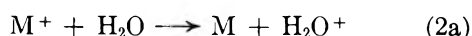
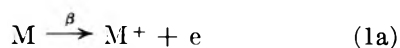
Discussion

For tritium gas exposure to light hydrocarbon molecules,^{4,5,7,8} it has been observed that the rate of tritium incorporation is of the same order as that of tritium decay, and processes initiated by the recoil ${}^3\text{HeT}^+$ particle following

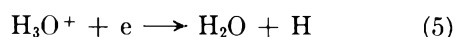
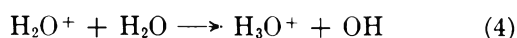


may play very important roles. Except in the presence of nitric oxide, the observed tritiated water yields in the tritium gas-water vapor system under varying conditions are much larger than the maximum contribution ($G = 0.02$) expected from ${}^3\text{HeT}^+$ -induced reactions. Tritiated water formation in the present reaction system must be attributed therefore largely to radiolytic processes initiated by tritium β -radiation.

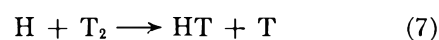
In agreement with other reports^{14,16} on the findings of radiation-induced reactions in water vapor, our results are consistent with a mechanism involving radical intermediates. Our observed dependence of the reaction rate on the ionization potential of the moderating gas reflects initial absorption of tritium β -radiation in the moderator followed by energy transfer to the water molecule¹⁷ as shown in reactions 1 and 2, and there are apparently not appreciable subexcitation electron effects¹⁸ as may be expected in the case of helium as the moderating gas. Radical intermediates may arise by dissociative neutralization of H_2O^+ as in reaction 3.



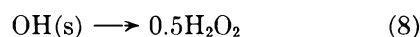
By consideration of reaction cross sections, however, reactions 4 and 5¹⁹⁻²² are more probably the processes giving rise to H atoms and OH radicals.



The tritiated water formation is then accounted by reaction 6 and accompanied by the analogous reaction 7.



As we have shown that the reaction rate is proportional to the radiation dose rate, the observed second-order dependence on tritium concentration indicates that reaction 6 is a rate-determining process and that the competing processes involving OH radical recombination such as (8) and (9) must follow the first-order reaction rate.



This latter observation is analogous to a process proposed by Firestone¹⁴ for the termination of the chain exchange reaction in water vapor above 150°.

Inhibition of the isotopic exchange by the presence of nitric oxide is clearly expected by scavenging of the OH radicals. The residual HTO formation may be accounted in part by processes initiated by the ${}^3\text{HeT}^+$ particle. The known ion-molecule reaction (10)²²



may have contributed to some extent as well. The lowering of the tritiated water yield due to tritium dilution by protium reflects an isotope effect in reaction 6 favoring protium abstraction by the OH radical. Also, it is likely that, in our experiment with protium dilution, the total hydrogen pressure is sufficiently high so that reaction 6 is no longer a rate-determining process.

In many aspects, our investigation is similar to that reported by Firestone¹⁴ on the radiation-induced exchange between deuterium and water. A rather puzzling observation in both our investigation and that by Firestone is the lack of appreciable lowering in the isotopic exchange rate in one instance even up to 30% conversion of one of the reactants. Some secondary processes such as reaction 11 must be involved in order

(16) J. H. Baxendale and G. P. Gilbert, *Discussions Faraday Soc.*, in press.

(17) R. L. Platzman, *Intern. J. Appl. Radiation Isotopes*, **10**, 116 (1961).

(18) R. L. Platzman, *Radiation Res.*, **2**, 1 (1955).

(19) H. D. Smyth and D. W. Mueller, *Phys. Rev.*, **43**, 116 (1933).

(20) M. M. Mann, A. Hustrulid, and J. T. Tate, *ibid.*, **58**, 340 (1940).

(21) K. J. Laidler, *J. Chem. Phys.*, **22**, 1740 (1954).

(22) F. W. Lampe, F. H. Field, and J. L. Franklin, *J. Am. Chem. Soc.*, **79**, 6132 (1957).



to account for results in the present reaction system.

It is interesting to note that the isotopic exchange in the T_2 - H_2O system is accounted almost entirely by reactions involving radical intermediates. On the other hand, in many tritium-hydrocarbon systems,⁷⁻¹⁰ ionic processes are found to play dominant roles. It appears that in the latter systems the abstraction of a tritium atom from a tritium molecule by organic radi-

cals is thermodynamically unfavorable and so the ionic intermediates become important for tritium incorporation.

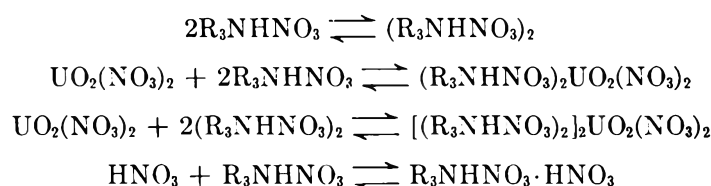
Acknowledgment. We wish to thank Dr. J. G. Burr of the North American Aviation Science Center for stimulating discussions and valuable suggestions, and we are indebted to Dr. Leon M. Dorfman of the Argonne National Laboratory for his comments on our preliminary manuscript.

Extraction of Hexavalent Uranium by Trilaurylamine Nitrate

by P. J. Lloyd^{1a} and E. A. Mason

*Department of Nuclear Engineering, Massachusetts Institute of Technology,
Cambridge, Massachusetts (Received February 24, 1964)*

The effects of amine, uranium, and hydrogen ion concentrations on the extraction of U(VI) from acidic nitrate solutions by tri-*n*-dodecylamine nitrate in toluene were studied at constant nitrate concentration. Over a wide range of these variables, it was found that the data could be correlated quantitatively on a basis of a mechanism of extraction involving equilibria between amine nitrate monomer and dimer species, extraction of uranium by both of these species, and extraction of nitric acid by the amine nitrate



By determination of the nitric acid extracted into the organic phase by the fourth equilibrium, it was possible to calculate the concentration of amine nitrate available for participation in the other equilibria. From a reported value of $K = 110 \pm 30 \text{ l. mole}^{-1}$ for the first equilibrium, values of

$$K_I = 50 \pm 10 \text{ l.}^2 \text{ mole}^{-2}$$

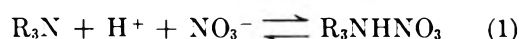
$$K_{II} = 200 \pm 50 \text{ l.}^2 \text{ mole}^{-2}$$

were estimated for the equilibria involving uranium extraction by amine nitrate monomers and dimers, respectively. Data are also presented on the variation of nitrate and hydrogen ions in the organic phase with uranium loading, from which it is concluded that no species other than the uranyl nitrate complexes are extracted. The difficulties caused by amine nitrate aggregation during studies on the mechanism of extraction of metals by other amines in other diluents are discussed.

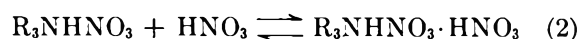
Introduction

The extraction of uranium from nitrate solutions is of interest in nuclear fuels reprocessing. The possible separation of uranium and plutonium by amine extraction was noted in 1957,^{1b} and several studies have been made of the extraction of both uranium and plutonium by alkylamines since that time.²⁻¹⁴

Of some importance, since it affects the extraction of uranium, is the behavior of amines in nitrate-nitric acid systems.¹⁵ As a first step, nitric acid is extracted to form the amine salt



The amine nitrate is capable of extracting more nitric acid



Nitric acid extracted in this fashion is referred to as "unbound" nitric acid. At very high aqueous nitric

(1) (a) South African Atomic Energy Board, Pretoria, South Africa; (b) J. C. Sheppard, Report HW-51958 (1957), and R. S. Winchester, Report LA-2170 (1958).

(2) F. Baroncelli, *et al.*, *J. Inorg. Nucl. Chem.*, **24**, 547 (1962).

(3) F. Baroncelli, *et al.*, *ibid.*, **25**, 205 (1963).

(4) U. Bertocci, Report AERE/R2933 (1959).

(5) A. Facchini, *et al.*, *Energia Nucl. (Milan)*, **9**, 681 (1962).

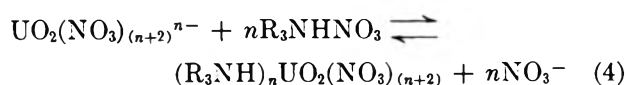
acid molarities, still more nitric acid may be extracted.¹⁰ Some water follows the nitric acid into the organic phase, but the effect is relatively slight and varies from solvent to solvent.^{10,16,17}

Except in aromatic diluents, the range of solubility of the amine nitrate in diluents is limited. This appears to be linked to aggregation of the amine nitrate in the organic phase. Infrared and light-scattering studies¹⁷⁻¹⁹ have shown aggregates in tri-*n*-octylamine nitrate-benzene, tri-*i*-octylamine nitrate-toluene, and at high concentrations of trilaurylamine nitrate in benzene. Two phase e.m.f. titrations of tridodecylamine nitrate in *m*-xylene have shown²⁰ that over the range of amine concentrations less than 20 vol. % (approximately 0.4 *M*) the amine nitrate is present mainly as monomers and dimers, with larger aggregates only forming at concentrations greater than 20 vol. %. From the data given,²⁰ a value of $K_{III} = 110 \pm 30$ l. mole⁻¹ may be derived for the equilibrium

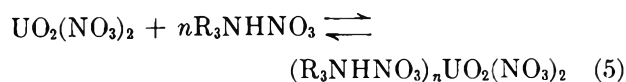


The equilibrium constant for eq. 1 is of the order of 10^6 .¹⁹⁻²² The order of magnitude of the equilibrium constant for eq. 2 is unity.^{22,23} It is of note that extraction of unbound nitric acid by eq. 2 appears to involve solvation of the molecular nitric acid by the amine nitrate. Evidence for this is in the correlation of Skavdahl and Mason; for a wide range of nitric acid-nitrate solutions the unbound nitric acid in the organic phase was a function of the molecular nitric acid activity only.²⁴

In the extraction of uranyl nitrate, two possible mechanisms may be postulated



and



The ion-exchange mechanism, eq. 4, is sometimes quoted as implying the existence of some anionic complex.^{25,26} However, the solvation mechanism of extraction, eq. 5, is thermodynamically equivalent to eq. 4, so that it is only true to say that the amine-to-metal ratio is *n*. Studies in other systems have shown that the ion-exchange mechanism is operative mainly at high salt concentrations.²⁷ Moreover, studies on anion exchange resins have shown that finite absorption occurs even under conditions where anions are not present in the aqueous phase.²⁸

It is normally assumed that only uranyl nitrate

complexes are extracted, as indicated in eq. 4 and 5, so that there should be a net increase of two nitrate ions in the organic phase for each uranyl ion transferred. However, at low acidities, hydrolyzed species are known to be present,²⁹ and it seems possible that one of these species might be extractable. Moreover, Baroncelli² has postulated that a species $HUO_2(NO_3)_3$ may be present at high nitric acid concentrations and that this species may be less extractable than pure nitrate complexes.

Difficulty arises in the determination of the ratio, *n*, of the number of amine molecules per uranium molecule in the complex in the organic phase. This is normally determined from the slope of a log-log plot of the distribution coefficient vs. free amine concentration, and nonintegral values between 0.9 and 2.5 have been found. It may be noted, in passing, that this method of determining *n* will not show whether the amine is polymerized in the metal complex. Thus if polymerized amine species are involved, it becomes difficult to make a valid correction for the amine complexed to uranium in the organic phase, in determining the free amine concentration. Moreover, in determining the free amine concentration, it is necessary

- (6) W. E. Keder, *et al.*, *J. Inorg. Nucl. Chem.*, **20**, 131 (1961).
- (7) W. E. Keder, *et al.*, *ibid.*, **12**, 327 (1959).
- (8) W. Knoch, *Z. Naturforsch.*, **16a**, 525 (1961).
- (9) V. B. Shevchenko, *Zh. Neorgan. Khim.*, **5**, 2354 (1960).
- (10) V. Vdovenko, *et al.*, *Radiokhimiya*, **3**, 403 (1961).
- (11) V. M. Vdovenko, *et al.*, *ibid.*, **3**, 636 (1961).
- (12) V. M. Vdovenko, *et al.*, *ibid.*, **3**, 555 (1961).
- (13) A. S. Wilson and W. E. Keder, *J. Inorg. Nucl. Chem.*, **18**, 259 (1961).
- (14) M. Zifferero, Report CNC-41 (1960).
- (15) U. Bertocci and G. Rolandi, *J. Inorg. Nucl. Chem.*, **23**, 323 (1962).
- (16) O. I. Zakharov, *et al.*, *Zh. Neorgan. Khim.*, **6**, 1936 (1961).
- (17) F. Baroncelli, *et al.*, *J. Inorg. Nucl. Chem.*, **24**, 405 (1962).
- (18) G. Scibona, Report CNC-43 (1960).
- (19) J. C. Peak, M. S. Thesis, Dept. of Nuclear Engineering, Massachusetts Institute of Technology, January, 1959.
- (20) E. Hogfeldt and F. Fredlund, *Trans. Roy. Inst. Technol. Stockholm*, 226 (1964).
- (21) O. I. Zakharov, *Zh. Neorgan. Khim.*, **7**, 665 (1962).
- (22) A. S. Kertes and T. T. Platzner, *J. Inorg. Nucl. Chem.*, **24**, 1417 (1962).
- (23) V. B. Shevchenko, *Zh. Neorgan. Khim.*, **5**, 1852 (1960).
- (24) R. E. Skavdahl and E. A. Mason, Report TID-16139 (1962).
- (25) S. S. Choi and D. G. Tuck, *Inorg. Chem.*, **2**, 780 (1963).
- (26) C. J. Hardy, *et al.*, *J. Inorg. Nucl. Chem.*, **7**, 257 (1956).
- (27) W. J. McDowell and C. F. Coleman, "Interface Mechanism for Uranium Extraction by Amine Sulfate," Abstract 62, p. 25K, 144th National Meeting of the American Chemical Society, Los Angeles, April, 1963, and Report ORNL-3452 (1963), p. 184.
- (28) L. I. Katzin and E. Gerbert, *J. Am. Chem. Soc.*, **75**, 801 (1953).
- (29) G. T. Seaborg and J. J. Katz, "The Actinide Elements," 1st Ed., McGraw-Hill, New York, N. Y., 1954, p. 165.

to correct for amine complexed with any unbound nitric acid extracted by eq. 2, and this can only be done by simultaneous solution of eq. 2 and 5 for the concentration of free amine nitrate.

Baroncelli and co-workers^{2,3} conclude that the effect of unbound nitric acid on the distribution of uranium is negligible. By studying the effect of amine concentration for the system tri-*n*-dodecylamine-benzene, they find values of *n* from 1.1 to 1.8 over a range of nitric acid and uranium concentrations. The data of Shevchenko⁹ for the system tri-*n*-octylamine-xylene correspond to values of *n* of 0.9 and 1.1; the correction term applied by him is, however, incorrect.^{30a} For tri-*n*-octylamine in various diluents, Vdovenko¹² found values of *n* from 1.1 to 2.2. Knoch⁸ found a value of *n* close to 1 for tri-*i*-octylamine-kerosene. The lower values of *n* appear to correspond to diluents in which the amine nitrate is more highly aggregated. For instance, Hogfeldt²⁰ found monomer and dimer trilaurylamine nitrate species in xylene, but large aggregates in *n*-octane. These should be compared to the values for *n* of 1.7 in benzene¹² and approximately 1.0 for kerosene.⁸ If, as seems likely, large aggregates are not involved in the uranium complex, then a treatment analogous to that given by Allen for the amine sulfate system^{30b} shows that such a decrease may be expected. Moreover, this variation in values of *n* is fairly typical of the extraction of metals by different amine nitrates; for instance, Brothers and Hart³¹ find values for the extraction of Pu(IV) between 1.5 and 2.0, and Baroncelli and Scibona,^{3,32} find values between 2 and 2.9; Skavdahl²⁴ found a value of 1.5 for the extraction of RuNO(III). Thus it is with this aspect of the mechanism of extraction that this paper is particularly concerned, since the results might be expected to apply to alkylamine nitrate systems in general.

Experimental

Experiments were performed by contacting an organic phase of tridodecylamine in toluene which had been pre-equilibrated with an aqueous phase of nitric acid-ammonium nitrate, with an equivalent aqueous phase containing uranyl nitrate. Equilibration was accomplished by vigorous shaking for 1 min., and slow shaking for 1 hr. at 25.0° to overcome any heat of reaction effects from the initial vigorous contact. After settling, the phases were rapidly separated, centrifuged, and decanted, to be stored at 25° before analysis. The organic phase was tri-*n*-dodecylamine, Eastman No. 7727, of 97.5% purity, dissolved in A.R. toluene, standardized by potentiometric titration against perchloric acid in dioxane. Pre-equilibration

was accomplished by contacting a single volume of organic phase with at least four fresh volumes of the relevant aqueous phase containing no uranium. Preliminary experiments showed that four such contacts were necessary to ensure no further extraction of nitrate or hydrogen ions. The pre-equilibrated organic phase was stored for no longer than 2 days at 25° before use. In this manner it was found possible to avoid change in nitric acid concentration in the organic phase which is known to occur on standing.²² Analysis for uranium was *via* the colorimetric thiocyanate method, and for nitrate by precipitation of nitron nitrate. Organic phase analysis for uranium and nitrate was by successive washings with 1 *M* Na₂CO₃ and 0.5 *M* HCl, as it was found that complete hydrolysis of the organic complex of uranium by 1 *M* Na₂CO₃ alone was slow. The washings were passed through a small Whatman No. 1 filter paper to remove amine droplets and combined. Analysis of a sample of the organic phase for hydrogen ions was by potentiometric titration in acetone *vs.* standard aqueous sodium hydroxide.

Results

The results of two sets of experiments, the one on the effect of amine concentration at constant uranium concentration in the initial aqueous phase and the other on the effect of uranium concentration at constant total amine concentration, are summarized in Tables I and II. The nitrate concentration was held approximately constant, and the hydrogen ion varied from 0.01 to 1 *M*.

Discussion

In determining the net increase in the number of nitrate ions for each uranyl ion transferred to the organic phase, it was assumed that the total nitrate in the organic phase was derived from the amine nitrate, any unbound nitric acid present, and the nitrate transferred with the uranium only, *i.e.*

$$C_{\text{NO}_3} = C_{\text{R}_3\text{N}} + C_{\text{unbound H}^+} + AC_{\text{U}} \quad (6)$$

where the organic phase concentrations of species which

(30) (a) In determining the free amine concentration, Shevchenko first corrected for the unbound nitric acid by application of a previously determined equilibrium constant for eq. 2, and then corrected for the amine complexed with the extracted uranium. However, the extraction of uranium must reduce the available amine concentration, displacing eq. 2 to the left, so that in effect Shevchenko neglected the equivalent equilibrium $2\text{R}_3\text{NHNO}_3 \cdot \text{HNO}_3 + \text{UO}_2(\text{NO}_3)_2 \rightleftharpoons (\text{R}_3\text{NHNO}_3)_2\text{UO}_2(\text{NO}_3)_2 + 2\text{HNO}_3$. The values of *n* reported by Shevchenko are consequently too low. (b) K. A. Allen and W. J. McDowell, *J. Phys. Chem.*, **64**, 877 (1960).

(31) J. A. Brothers, R. G. Hart, and W. G. Mathers, *J. Inorg. Nucl. Chem.*, **7**, 85 (1958).

(32) F. Baroncelli, *et al.*, *ibid.*, **24**, 541 (1962).

Table I: Effect of Amine Concentration on Uranium Distribution Coefficient

Amine concn., <i>M</i>	Aqueous (concn., <i>M</i>)						Organic (concn., <i>M</i>)				Phase ratio A/O	Mass bal., %	<i>D_U</i>
	Initial uranium	Initial nitrate	Initial H ⁺	Equil. uranium	Equil. nitrate	Equil. H ⁺	Equil. uranium	Equil. nitrate	Equil. total H ⁺	Equil. unbound H ⁺			
0.346 ^a	0.0170	2.72	0.010	0.00537	2.72	0.010	0.0158	0.372	0.393	Nil	4/3	101	2.91
0.210 ^a	0.0170	2.72	0.010	0.00941	2.72	0.010	0.00983	0.229	0.239	Nil	4/3	99	1.04
0.109 ^a	0.0170	2.72	0.010	0.0141	0.00357	0.116	4/3	99	0.254
0.0501 ^a	0.0170	2.72	0.010	0.0162	0.00102	4/3	100	0.0624
0.0201 ^a	0.0170	2.72	0.010	0.0168	0.00024	4/3	100	0.0141
0.0101 ^a	0.0170	2.72	0.010	0.0169	0.00005	1/1	100	0.0030
									Initial unbound H ⁺	Final unbound H ⁺			
0.339 ^b	0.0152	2.94	0.945	0.00609	2.90	0.929	0.0089	0.446	0.0584	0.0933	1/1	98	1.45
0.204 ^b	0.0152	2.94	0.945	0.0083	2.93	0.947	0.0059	0.269	0.0531	0.0512	1/1	94	0.706
0.103 ^b	0.0152	2.94	0.945	0.0128	2.95	0.945	0.00210	0.129	0.0240	0.0239	1/1	96	0.169
0.0515 ^b	0.0152	2.94	0.945	0.0140	0.00084	0.0661	0.0118	0.0118	1/1	98	0.060
0.0208 ^b	0.0152	2.94	0.945	0.0150	0.000126	...	0.0049	0.0049	1/1	100	0.0084
0.0105 ^b	0.0152	2.94	0.945	0.0152	0.000084	...	0.0025	0.0024	1/1	100	0.0006

^a Amine in equilibrium with 2.75 *M* NO₃⁻, 0.010 *M* H⁺. ^b Amine in equilibrium with 2.95 *M* NO₃⁻, 0.93 *M* H⁺.

Table II: Effect of Uranium Concentration on Distribution Coefficient

Amine concn., <i>M</i>	Aqueous (concn., <i>M</i>)						Organic (concn., <i>M</i>)				Phase ratio A/O	Mass bal., %	<i>D_U</i>
	Initial uranium	Initial nitrate	Initial H ⁺	Equil. uranium	Equil. nitrate	Equil. H ⁺	Equil. uranium	Equil. nitrate	Initial unbound H ⁺	Final unbound H ⁺			
0.346 ^a	0.0153	2.72	0.0048	0.00350	2.71	0.0048	0.0114	0.363	Nil	Nil	1/1	93	3.27
0.346 ^a	0.0374	2.74	0.0048	0.0108	2.76	0.0045	0.0256	0.387	1/1	97	2.37
0.346 ^a	0.0910	2.80	0.0046	0.0415	2.82	0.0046	0.0486	0.428	1/1	99	1.18
0.346 ^a	0.187	2.86	0.0042	0.115	2.86	0.0041	0.0687	0.474	1/1	99	0.597
0.346 ^a	0.384	2.80	0.0043	0.287	2.80	0.0041	0.0921	0.511	Nil	Nil	1/1	98	0.321
0.339 ^b	0.0383	2.90	0.945	0.0172	2.91	0.946	0.0203	0.468	0.105	0.093	1/1	98	1.18
0.339 ^b	0.0936	2.92	0.938	0.0530	2.84	0.940	0.0410	0.490	0.105	0.072	1/1	100	0.775
0.339 ^b	0.189	2.92	0.940	0.123	2.85	0.950	0.0616	0.518	0.105	0.058	1/1	98	0.503
0.339 ^b	0.405	3.22	0.941	0.312	3.16	0.956	0.0950	0.578	0.105	0.046	1/1	101	0.305
0.339 ^b	0.405	3.22	0.941	0.355	3.07	0.962	0.0996	0.582	0.105	0.042	2/1	100	0.281

^a In equilibrium with 2.72 *M* NO₃⁻, 0.0047 *M* H⁺. ^b In equilibrium with 2.90 *M* NO₃⁻, 0.940 *M* H⁺.

may be present in both the aqueous and organic phases are indicated by underlining. The unbound nitric acid was determined by titration. Typical titration curves are shown in Fig. 1. The first end point for phases in equilibrium with 1 *M* H⁺ solutions corresponds to the unbound nitric acid. The second end point, where uranium is present, corresponds to the completion of the uranium precipitation reaction, and the final end point to total hydrolysis of the amine nitrate. The precipitation of uranium as sodium diuranate requires three OH⁻ equivalents per uranium, so it is noteworthy that the total OH⁻ consumed in the titrations did correspond to the sum of the free nitric

acid, three times the uranium concentration, and the amine concentration. This is evidence that no uranyl nitrate acid, H_{x-2}UC₂(NO₃)_x, is extracted, as has been suggested previously.² In the presence of uranium it is necessary to extrapolate the curve for the nitric acid end point to the half-wave potential for the reaction in order to obtain the true end point.

A plot of (6) is given in Fig. 2. The line through the experimental points is of slope 2.0, so that there is a net increase of two nitrate ions for each uranyl ion extracted into the organic phase, as required by eq. 4 and 5. Thus it is only necessary to consider uranyl nitrate complexes in the organic phase under these

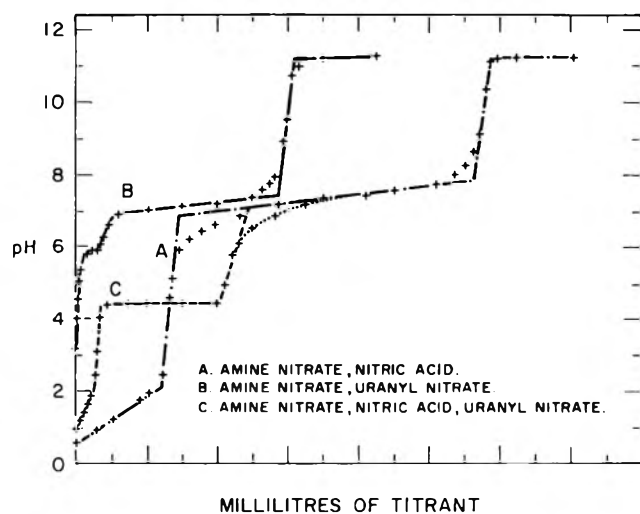


Figure 1. Titration of organic extract phases.

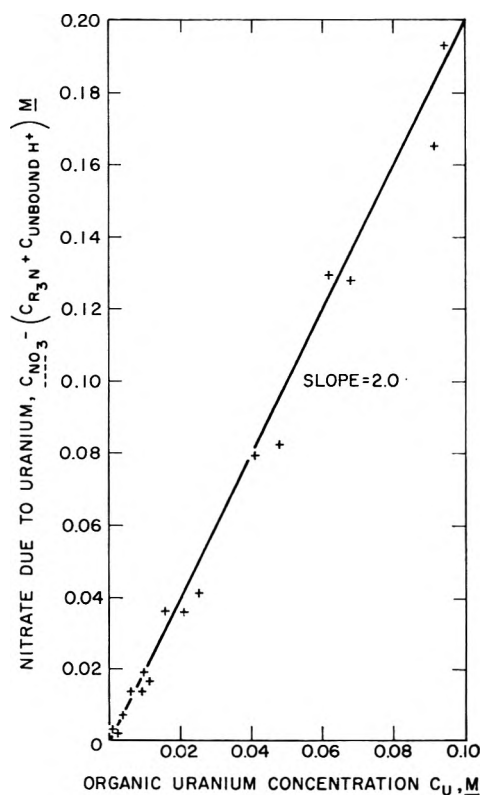
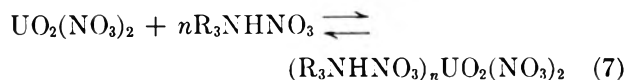


Figure 2. Plot of eq. 6.

conditions, as hydrolyzed or acidic complexes seem to be absent.

In attempting to find the amine-to-uranium ratio in the organic phase, log-log plots of distribution coefficient *vs.* free amine concentration were made for the data of Tables I and II as shown in Fig. 3 and 4. If it is assumed that the extraction of uranium is by



$$K_C = \frac{C_{\text{US}_n}}{C_{\text{U}}C_{\text{T}_i}^n}$$

and

$$D_{\text{U}} = \frac{C_{\text{US}_n}}{C_{\text{U}}} = K_C C_{\text{T}_i}^n \quad (8)$$

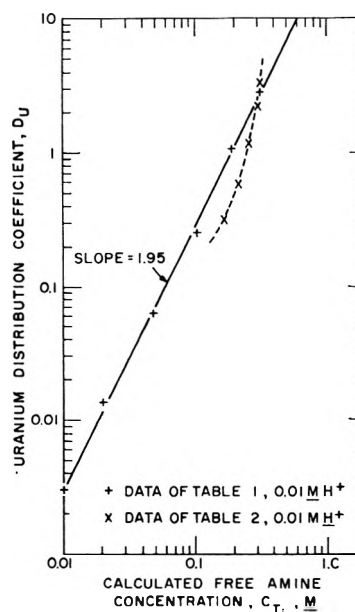
C_{T_i} is the free amine concentration, which for eq. 8 is calculated as the total amine concentration less the amine complexed to nitric acid and to uranium, *i.e.*

$$C_{\text{T}_i} = C_{\text{F}} - nC_{\text{U}} \quad (9)$$

where

$$C_{\text{F}} = C_{\text{R}_3\text{N}} - C_{\text{unbound H}^+} \quad (10)$$

If eq. 8 applies, the log-log plots in Fig. 3 and 4 should be linear and of slope n . In each figure, the data of Table I representing low and uniform uranium concentrations are consistent with a value of $n \approx 2$. However, the data of Table II representing various uranium concentrations follow quite a different trend. In order to show this difference more clearly, the isotherm for the extraction of uranium from 0.01 M H^+ by 0.346 M amine is shown in Fig. 5, together with the theoretical isotherm calculated by combining eq. 8 and 9, assuming $n = 1, 2, 3,$ and 4 , and using the values of D_{U} and $C_{\text{R}_3\text{N}}$ at point A to determine K_C .

Figure 3. Variation of uranium distribution coefficient with calculated free amine concentration, 0.01 M H^+ .

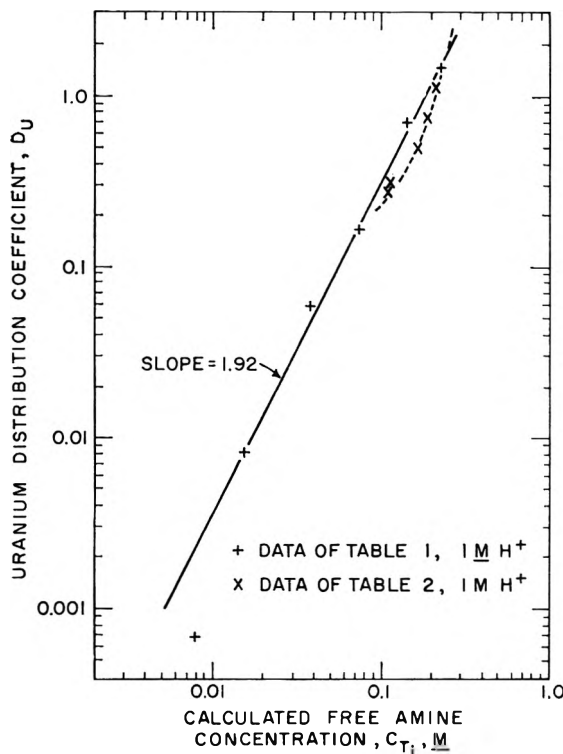


Figure 4. Variation of uranium distribution coefficient with amine concentration, 1 M H⁺.

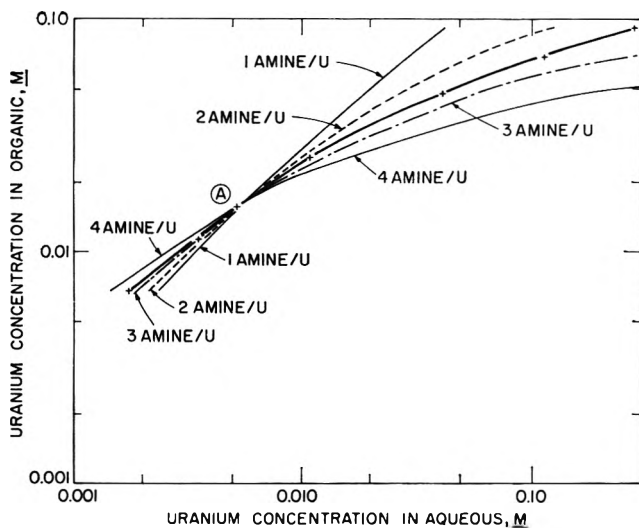
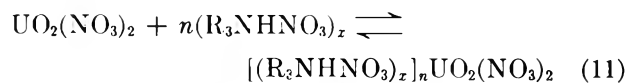


Figure 5. Comparison of experimental with theoretical extraction isotherms.

As eq. 7 did not provide an explanation to the experimental data, it was necessary to postulate a different mechanism of extraction. Similar difficulties have been encountered in previous studies,³²⁻³⁶ and a semiempirical equation of the form $D_U = K(C_F - mC_U)^n$ has been proposed for the isotherm. This could

occur if the amine is polymerized, since



$$K_C' = \frac{C_{\text{U}(\text{S}_2)_n}}{C_{\text{U}} C_{\text{T}_{ii}}^n}$$

and

$$D_U = \frac{C_{\text{U}(\text{S}_2)_n}}{C_{\text{U}}} = K_C' C_{\text{T}_{ii}}^n \quad (12)$$

where $C_{\text{T}_{ii}}$ is given by

$$C_{\text{T}_{ii}} = C_F - xnC_U \quad (13)$$

In this case, combining eq. 12 and 13 will give an equation of the same form of the semiempirical one mentioned above.³⁶ Then a plot of $D_U^{1/n}/C_F$ vs. C_U/C_F should yield a straight line, the intercept of which at $D_U^{1/n}/C_F = 0$ should be $1/xn$. Plots of this type are given in Fig. 6 and 7.

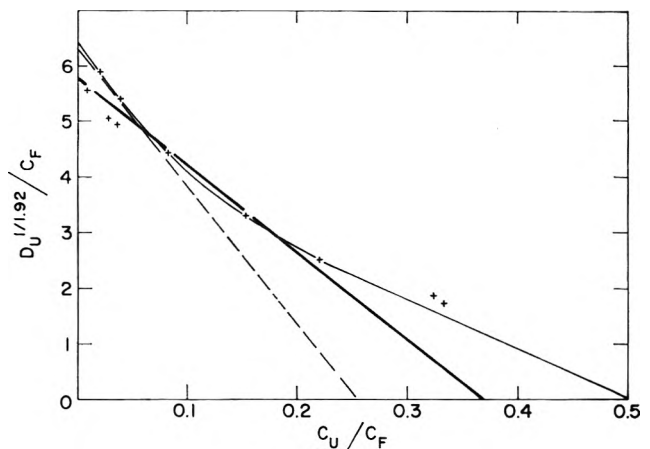


Figure 6. Plot of eq. 12 for 0.01 M H⁺.

The best straight lines through the experimental points lead to values of xn of 3 and 2.5. The scatter in the points at low values of C_U may be ascribed to the necessity of using small differences between large numbers in the calculation. However, the points at high values of C_U deviate from the straight lines drawn by more than could be expected from the slight increases in aqueous nitrate concentration associated

(33) K. B. Brown, Report CF-61-3-141 (1961).

(34) V. C. Vaughn, Report TID-12665 (1961).

(35) C. F. Coleman, *Nucl. Sci. Eng.*, **17**, 274 (1963).

(36) P. J. Lloyd and M. K. Oertel, Paper, AIME International Symposium on Hydrometallurgy, Dallas, Texas, February, 1963.

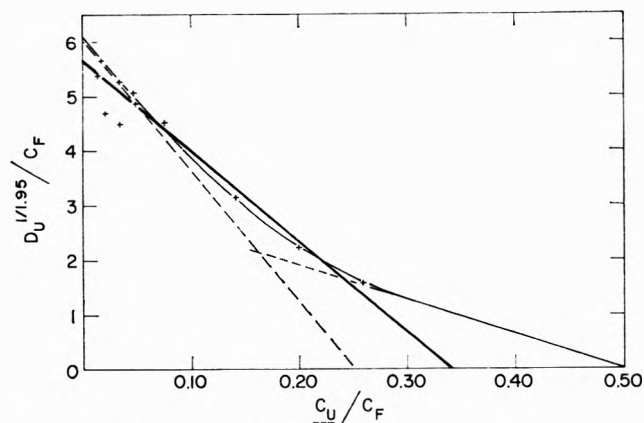


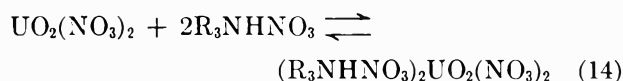
Figure 7. Plot of eq. 12 for 1 M H⁺.

with these points. Moreover, by the above mechanism which assumes a single polymeric amine species only, it is difficult to explain the range in the values of xn .

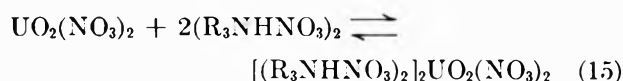
If, however, a smooth curve is drawn through the experimental points in Fig. 6 and 7, at high uranium concentrations the xn intercept tends to a value of 2 and at low concentrations to a value of $\frac{1}{2}$, in both cases. This suggests that there is some form of amine monomer-dimer equilibrium, with both species capable of extraction.

At this stage in the investigation, attention was drawn to the results of Hogfeldt²⁰ on the monomer-dimer equilibrium in the system tridodecylamine nitrate-xylene. It seemed likely his results would hold in the present system, with toluene replacing xylene as diluent.

A mechanism of extraction consistent with the results obtained above is



and



The equilibrium constants of equilibria 14 and 15 are given by

$$K_{\text{I}} = \frac{C_{\text{US}_2}}{C_{\text{U}}C_{\text{S}}^2} \quad (16)$$

$$K_{\text{II}} = \frac{C_{\text{U}(\text{S}_2)_2}}{C_{\text{U}}C_{\text{S}_2}^2} \quad (17)$$

Moreover

$$C_{\text{T}} = C_{\text{S}} + 2C_{\text{S}_2} = C_{\text{F}} - 2C_{\text{US}_2} - 4C_{\text{U}(\text{S}_2)_2} \quad (18)$$

$$K_{\text{III}} = \frac{C_{\text{S}_2}}{C_{\text{S}}^2} \quad (19)$$

and

$$D_{\text{U}} = \frac{C_{\text{US}_2} + C_{\text{U}(\text{S}_2)_2}}{C_{\text{U}}} = K_{\text{I}}C_{\text{S}}^2 + K_{\text{II}}C_{\text{S}_2}^2 \quad (20)$$

It should be possible to solve these five equations for the unknowns K_{I} , K_{II} , K_{III} , C_{S} , C_{S_2} , C_{US_2} , and $C_{\text{U}(\text{S}_2)_2}$ by simultaneous solution using various sets of values of D_{U} , C_{U} , and C_{F} obtained experimentally. In order to simplify the solution, however, the data of Hogfeldt²⁰ were used to give $K_{\text{III}} = 110 \pm 30$ l. mole⁻¹. Using the data of Table I at 0.01 M H⁺ where, as there is no extraction of excess nitric acid, $C_{\text{F}} = C_{\text{R}_3\text{N}}$, values of K_{I} and K_{II} were obtained assuming values for K_{III} of 100, 125, and 150 l. mole⁻¹. The best fit to this data was for $K_{\text{III}} = 125$, for which

$$K_{\text{I}} = 50 \pm 10 \text{ l.}^2 \text{ mole}^{-2}$$

$$K_{\text{II}} = 200 \pm 50 \text{ l.}^2 \text{ mole}^{-2}$$

To test the other data using these values of K_{I} , K_{II} , and K_{III} , and thereby to test the proposed mechanism of extraction, C_{T} was calculated for the experimental values of D_{U} , C_{U} , and C_{F} . If it was necessary to assume first that the amine nitrate-nitric acid complex exists only as the 1:1 complex and does not interact with further amine nitrate, and second that this complex is incapable as such of extracting uranium. The first assumption seems reasonable as it is known that a 1:1 amine nitrate-nitric acid complex is formed under some conditions¹⁰ while no 2:1 or higher complex has been observed. The second assumption seems reasonable both from the fact that uranium displaces unbound nitric acid from the organic phase, and by analogy with the amine sulfate system, where the amine bisulfate was shown to be unable to extract uranium.^{30b}

Figure 8 compares the observed values of the distribution coefficient with the values derived from eq. 16-20, at the same calculated free amine concentration. The values of K_{I} and K_{II} were derived only from the data at trace uranium levels and 0.01 M H⁺, yet the fit is adequate for data at high uranium concentration and 1 M H⁺. While it is clear that this is by no means a conclusive test of the assumption that the uranium is extracted by both amine monomers and dimers, it is felt that the correlation of observed and calculated distribution coefficients is sufficiently good to suggest that such a mechanism of extraction is likely.

The variation in the average number of amines associated with each uranium in the organic phase may be

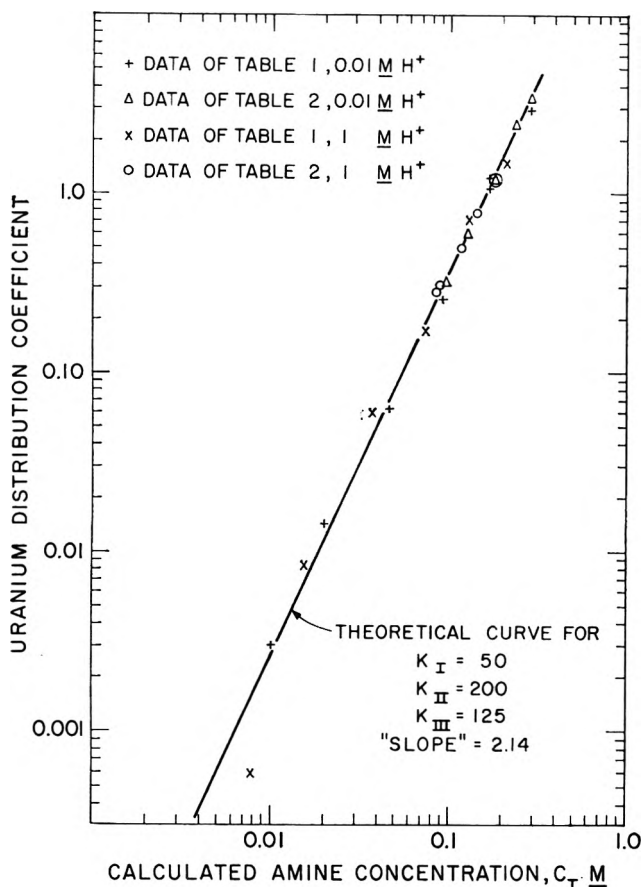


Figure 8. Comparison of the observed and calculated distribution coefficient as a function of the calculated free amine concentration.

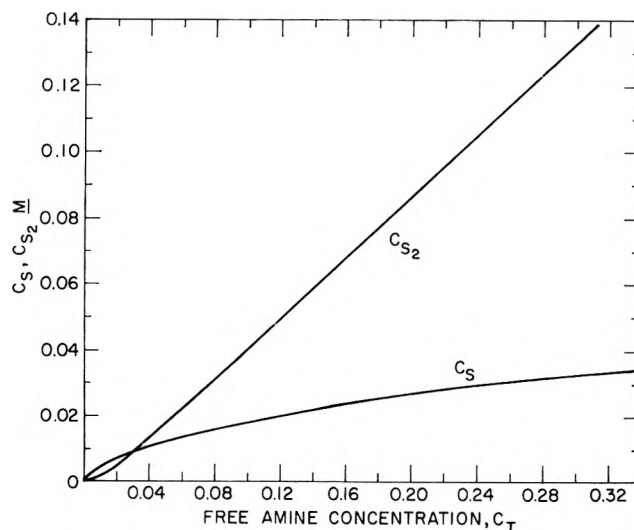


Figure 9. Variation of amine nitrate monomer and dimer concentration with free amine concentration.

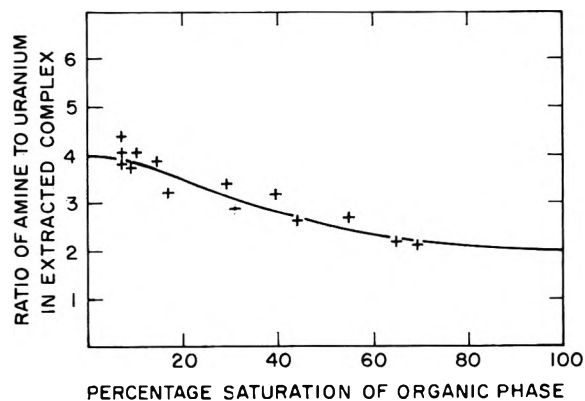


Figure 10. Variation of amine-to-uranium ratio in the extracted complex for roughly 0.3 M amine.

estimated qualitatively by considering Fig. 9, a plot of C_S and C_{S_2} vs. C_T from eq. 18 and 19 for a value of $K_{III} = 125 \text{ l. mole}^{-1}$. At a constant and relatively high total amine concentration and low uranium loading, most of the amine will be dimerized, and roughly four amines will be associated with each uranium. Increasing the uranium concentration will decrease the proportion of monomer to dimer, so in the limit two amines should be associated with each uranium, at the highest uranium concentrations. This trend is illustrated in Fig. 10, where the amine-to-uranium ratio, $(C_F - C_T)/C_U$, is plotted against the percentage saturation, $2(C_U/C_F) \times 100$, for the experimental values of C_U and C_F and the values of C_T calculated from them.

Conclusions

It appears that the assumption of an amine nitrate monomer-dimer equilibrium and the extraction of the uranyl ion by both amine monomers and dimers is capable of yielding a quantitative explanation of the

variation in the uranium distribution coefficient with varying amine, hydrogen, and uranium concentration. Values of the effective equilibrium constants K_I and K_{II} have been calculated, the uncertainties in them reflecting mainly experimental errors.

It seems probable that the only equilibria remaining to be considered in this system are those involving the effect of nitrate and hydrogen ion concentrations. However, this study was carried out under conditions of approximately constant ionic strength, and the activity coefficient of uranyl nitrate in ammonium nitrate solutions in the concentration range used here is known to be relatively constant.³⁷ Thus consideration of the equilibria involving nitrate and hy-

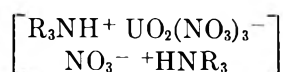
(37) I. L. Jenkins and H. A. C. McKay, *Trans. Faraday Soc.*, 50, 107 (1953).

drogen ion concentrations should only change K_I and K_{II} each by a constant factor.

Nonidealities in the organic phase are apparently sufficiently taken into account by making allowance for the monomer-dimer equilibrium of the amine nitrate. The effect of unbound nitric acid has been taken into account by direct determination of the amount present and consequent reduction in the calculated free amine nitrate concentration. This approach has proved successful in bringing together extraction data at 0.01 and 1.0 M hydrogen ion concentration in the aqueous phase. It has recently been postulated that a similar reduction in free amine salt concentration due to the extraction of unbound acid is also necessary to account for equilibria in the analogous chloride system.³⁸

The effect of diluent has not been studied, but it is probable that different amine nitrate species would have to be considered in other diluents as the aggregation of the amine nitrate varies, particularly on passing from aromatic to aliphatic hydrocarbon diluents.²⁰ Nevertheless, it seems reasonable to suppose that the variation in the ratio of amine to metal, which has been observed in other systems, also involves equilibria between various amine species and extraction of the metal by one or more of these species.

While this work has not indicated the presence of higher polymers than amine nitrate dimers, it is possible that such higher polymers are in fact present, but the techniques employed here were too insensitive to show their presence. Nevertheless, it seems likely that most of the amine nitrate is present as monomers and dimers in this diluent. The reason for the dimerization is probably quadruple interactions between the amine nitrate ion pairs. In turn, it should be mentioned that the observation of a spectrum approximately corresponding to that of the $UO_2(NO_3)_3^-$ complex⁶ by no means necessarily implies that the amine nitrate-uranium complex must be of the form $R_3NH^+UO_2(NO_3)_3^-$. Not only does there remain some doubt whether the spectrum can be conclusively identified, but also such spectral evidence can at best only give information about the inner coordination sphere of the uranyl ion. Thus ion-pair interactions between amine nitrate and amine nitrate-uranium species similar to the quadrupole interactions that lead to the formation of amine nitrate dimers, could give rise to a structure for the amine-uranium monomer complex of the type



which would also yield a spectrum similar to that of the uranyl trinitrate complex.

Nomenclature

A	Ratio of nitrate to uranium extracted into organic phase
C_F	Effective amine concentration, defined by eq. 10
C_{NO_3}	Total nitrate concentration in organic phase
C_{R_3N}	Total amine concentration in organic phase
C_S	Amine nitrate monomer concentration in organic phase
C_{S_2}	Amine nitrate dimer concentration in organic phase
C_T	Free amine nitrate concentration, calculated by eq. 18
C_{T_1}	Free amine nitrate concentration, calculated by eq. 9
C_{T_2}	Free amine nitrate concentration, calculated by eq. 13
C_U	Uranium nitrate concentration in aqueous phase
$\underline{C_U}$	Uranium nitrate concentration in organic phase
$C_{unbound\ H^+}$	Unbound nitric acid concentration in organic phase
C_{US_n}	Concentration of $(R_3NHNO_3)_nUO_2(NO_3)_2$ in organic phase
$C_{U(S_2)_n}$	Concentration of $[(R_3NHNO_3)_2]_nUO_2(NO_3)_2$ in organic phase
C_{US_2}	Concentration of $(R_3NHNO_3)_2UO_2(NO_3)_2$ in organic phase
$C_{U(S_2)_2}$	Concentration of $[(R_3NHNO_3)_2]_2UO_2(NO_3)_2$ in organic phase
D_U	Distribution coefficient of uranium = $\underline{C_U}/C_U$
K_I	Equilibrium constant for reaction 14
K_{II}	Equilibrium constant for reaction 15
K_{III}	Equilibrium constant for reaction 3
K_C	Equilibrium constant for reaction 7
K_C'	Equilibrium constant for reaction 11
n	Amine-uranium ratio determined from log-log plot of D_U vs. C_T
x	Degree of polymerization of amine nitrates

Acknowledgments. This research was jointly sponsored by the International Atomic Energy Commission through a Fellowship to P. J. L. and by Subcontract No.

(38) M. L. Good and S. E. Bryan, *J. Inorg. Nucl. Chem.*, **25**, 1167 (1963).

1327 with Union Carbide Corporation which operates the Oak Ridge National Laboratory under contract with the U. S. Atomic Energy Commission. This support is most

gratefully acknowledged. Thanks are due to A. S. Kertes for most helpful discussions during the course of this work.

Oxidation of Hydrocarbons Adsorbed on Oxide Catalysts

Induced by Cobalt-60 γ -Rays

by Harold W. Kohn

Chemistry Division, Oak Ridge National Laboratory,¹ Oak Ridge, Tennessee (Received March 30, 1964)

Radiation-induced oxidation of seventeen hydrocarbons adsorbed on silica gel, alumina and aluminosilicate catalysts was studied manometrically and by gas chromatography of oxidation product extracts. Oxygen consumption was lowest for saturated hydrocarbons on silica gel (e.g., $G(-O_2)_{\text{methane}} \cong 1$ molecule/100 e.v. absorbed) and highest for unsaturated hydrocarbons on alumina (e.g., $G(O_2)_{\text{hexene-1}} \cong 100$ molecules/100 e.v. absorbed). Based on results for two hydrocarbon-adsorbent-oxygen systems, oxidation yields were shown to be temperature independent from -195° to room temperature and to decrease with decreasing oxygen pressure and with decreasing surface coverage. Toluene oxidation products (identified by gas chromatography) were benzyl alcohol, phenol, and cresols. Xylenes, given the same treatment, yielded similar products. Toluene-alumina, when irradiated *in vacuo*, gave smaller amounts of the same products than those which contained oxygen. A postirradiation reaction followed nearly all these irradiations. A system of kinetics was developed for this postirradiation reaction. An initial step is postulated involving oxidation of the adsorbate and simultaneous reduction of the adsorbent, followed by the regeneration of the catalyst by gaseous oxygen. High G values for oxygen consumption in most systems indicate a surface chain and/or reaction of several oxygen molecules with the organic compound to give undetected products.

Introduction

When hydrocarbons adsorbed in high area solids are irradiated with γ -rays, much of the energy absorbed by the solid decomposes the hydrocarbon.²⁻⁵ The mechanism of this energy transfer is not well delineated, although it appears from work at this laboratory⁶ that, during such energy transfer processes, the adsorbent actually participates in the reaction. It was expected that by directing the reaction of the hydrocarbon along a defined path (oxidation) rather than observing several modes of simultaneous decomposition a better picture

of the energy transfer process might emerge. A previous article about the irradiation of the propane-zinc oxide-oxygen system indicated that this approach

(1) Operated by the Union Carbide Nuclear Company for the U. S. Atomic Energy Commission.

(2) J. M. Caffrey, Jr., and A. O. Allen, *J. Phys. Chem.*, **62**, 33 (1958).

(3) J. W. Sutherland and A. O. Allen, *J. Am. Chem. Soc.*, **83**, 1040 (1961).

(4) R. R. Hentz, *J. Phys. Chem.*, **65**, 1470 (1961).

(5) R. R. Hentz, *ibid.*, **66**, 1625 (1962).

(6) H. W. Kohn, *ibid.*, **66**, 1017 (1962).

should work.⁷ The present paper reports the results of experiments on the irradiation of heterogeneous systems consisting of adsorbents (silica gel, alumina, or aluminosilicate), seventeen different hydrocarbons, and oxygen or hydrogen.

Experimental

All manipulations were carried out using a conventional glass high-vacuum system, mercury diffusion pump, liquid N₂ traps, etc., capable of attaining vacua of 10⁻⁵ to 10⁻⁶ mm.

Materials. The Davison Chemical Division of W. R. Grace and Co. donated both the silica gel and the aluminosilicate used in these studies. These materials had nitrogen surface areas of 8 × 10² m.²/g. and 5 × 10² m.²/g., respectively.⁸ The aluminosilicate contained 13% alumina and was received as cylinders 0.187 × 0.187 in. The alumina was donated by the Aluminum Co. of America. It is designated Alcoa H-151, and was received as spheres 1 to 2 mm. in diameter. After degassing, its nitrogen surface area was 230 m.²/g.

The sources of the organic chemicals used in this study were: methane, Matheson, C.P.; ethane, ethylene, *n*-propane, hexene-1, Phillips Petroleum Co., research grade; naphthalene, biphenyl, cyclohexane, *o*-, *m*-, and *p*-xylenes, Matheson Coleman and Bell; cyclohexene, anthracene, mesitylene, Eastman Kodak White Label. The phenanthrene was from an unidentified source.

Gaseous and liquid hydrocarbons were stored over silica gel previously evacuated at 500°. Liquids were degassed before use by repeated freeze-pump-thaw cycles. All materials for calibrating the chromatographic unit were readily available, except for *o*- and *p*-methylbenzyl alcohol which were synthesized by the lithium aluminum hydride reduction of the corresponding ester.

Determination of $G(-O_2)$. A representation of the ampoule used is shown in Fig. 1. For convenience in handling, the side arm containing the hydrocarbon 45 to 90° angle with the manometer when viewed endwise. The volume of the ampoule was usually about 20 cc., and the weight of adsorbent was 10 g. After the adsorbent was degassed and cooled to room temperature, a measured amount of hydrocarbon was introduced from the side arm. It was necessary to distribute hydrocarbons of low vapor pressure by carefully heating with a flame. For more volatile materials (*e.g.*, toluene) the side arm could be dispensed with, and the more convenient vacuum distillation was used to introduce the organic material.

After the organic material was adsorbed and distributed, enough oxygen was let into the ampoule to

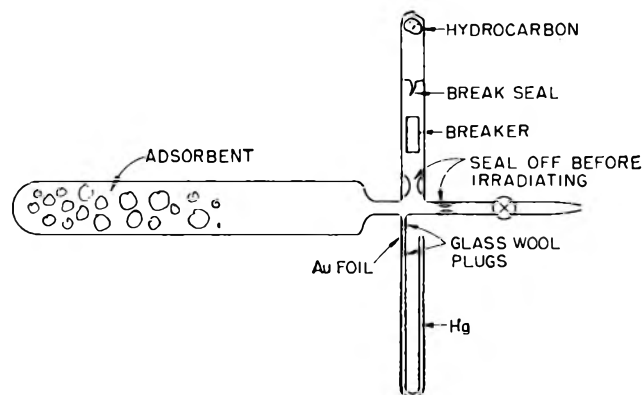


Figure 1. Irradiation ampoule.

bring the total pressure to ~80 mm. (The total pressure was limited by the size of the manometer which was, in turn, limited by the geometry of the source and shield.) The ampoule was then cooled in liquid nitrogen (as a safety precaution) and the stopcock with its standard taper joint and the side arm were sealed off (see diagram) leaving the test tube containing the reagents and the manometer. If no spontaneous reaction of hydrocarbon and oxygen occurred, the ampoule was allowed to stand overnight so that the hydrocarbon would redistribute uniformly on the surface.

The ampoule was then irradiated in a 2900-curie Co⁶⁰ γ -ray source at a dose rate of 2 × 10¹⁸ e.v. g.⁻¹ min.⁻¹ as determined by ferrous sulfate dosimetry. At suitable (1- to 5-min.) intervals, the ampoule was removed from the source and the manometer read with a cathetometer. If the irradiation was done at low temperature, the ampoule had to be warmed to room temperature before measuring the pressure because of the extensive adsorption of oxygen on these adsorbents at low temperature.

After completion of the irradiations, the ampoule was carefully cracked open, the adsorbent removed for further processing, and the ampoule volume calibrated with water. The 100-e.v. yields (defined as the G values for oxygen consumption) could then be calculated from the formula

$$G = \frac{(V - W/D)\Delta P(3.3 \times 10^{16})}{W(2 \times 10^{16})T}$$

where V is the volume of the ampoule in cc., ΔP is the change in pressure in mm., W is the weight of adsorbent in g., D is the density of adsorbent in g./cc., T is the

(7) W. H. Clingman, *Ind. Eng. Chem.*, 52, 915 (1960).

(8) The surface areas were measured by Paul G. Dake, O.R.G.D.P., Oak Ridge, Tenn.

time of irradiation in min., 3.3×10^{16} is the number of molecules in 1 cc. mm. at room temperature, and 2×10^{16} is the dose rate of the Co^{60} source in 100 e.v. $\text{g.}^{-1} \text{min.}^{-1}$.

It is assumed in this calculation that the pressure in the ampoule due to the hydrocarbon remains unchanged during irradiation, also that the oxidation products make a negligible contribution to the pressure. While these assumptions are probably true for hydrocarbons of low vapor pressure, they might well be questioned when methane, ethane, and especially benzene are the reactants.⁹

Many systematic errors are inherent in this experiment, but probably the most important is reaction occurring during the time delay between the cessation of the radiation and the reading of the manometer. For irradiations at low temperature, this error is a particularly serious one since it takes about 2 min. to warm the ampoule; furthermore, the temperature of the gas is then not well established. Attempts to repeat experiments showed that errors of the order of $\pm 20\%$ are inherent in the experiment.

Several blank experiments were indicated. Therefore the irradiation of ampoules containing oxygen plus degassed silica gel, degassed alumina, anthracene dispersed on sand, and toluene adsorbed on charcoal and on titania was examined. Only oxygen plus degassed alumina gave any appreciable decrease of pressure (initial $G(-\text{O}_2) \sim 4$, decreasing with further irradiation to ~ 2), and the experiments involving alumina, where the surface coverage was low, were corrected for this.

Separation and Identification of Products. During the course of this investigation several procedures for product recovery and identification were developed. Cresols and benzyl alcohol are strongly adsorbed by an alumina catalyst from dry ether solution. Thus, washing or even continuous extraction with ether removes little product. Products could be recovered only by destroying or hydrolyzing the catalyst surface. Therefore, the following final recovery and analysis scheme was adopted.

The adsorbent was first refluxed with 50 cc. of 1:1 ammonium hydroxide in a stream of nitrogen for 1 to 2 hr. The ammonium hydroxide solution was acidified, cooled, and extracted with several small portions of diethyl ether. Meanwhile, the adsorbent was refluxed with 50 cc. of 1:1 hydrochloric acid and in a nitrogen stream. This dissolves about half the adsorbent if it is alumina. The acid solution was then cooled and extracted with ether. The combined extracts totaling usually about 15 cc. were then evaporated to a volume of 0.05 cc. by passing a stream of nitrogen through the

solution. The liquid remaining was expected to contain the high-boiling products as well as some toluene and ether. Aliquots of this residue were examined gas chromatographically,¹⁰ and the size and position of the peaks were compared with appropriate standards. From the chromatographic data, one could calculate the amount and hence the yield of each product. If these products are the only products formed, the material balance was very poor since the recovered material could account for only about 10% of the oxygen consumed. At present it is assumed that this is because of the loss of material during the volume reduction step, although other processes such as the formation of other products cannot be ruled out. In either event, one would expect little fractionation of benzyl alcohol, cresols, and phenol during the reflux and the volume reduction steps.

Experimental Results

Oxidation (based on pressure reduction) in nearly all of the systems tested was observed. Initial yields (*i.e.*, $G(-\text{O}_2)$ from the first irradiation) varied from about one for a number of hydrocarbon-silica gel-oxygen systems to over 100 for the hexane-1-alumina-oxygen system (Table I). Following the initial irradiation, there is a slow postirradiation reaction, *i.e.*, slow compared to the reaction during irradiation (see Fig. 2). Successive irradiations again give a large rapid reduction of the oxygen pressure, but the yields from these later irradiations are usually lower than the initial yield. Within experimental error, no difference in yield was obtained when irradiations were done at -78 or at -196° . Each subsequent irradiation reaction is also followed by a slower postirradiation reaction.

The effects of oxygen pressure, surface coverage, and degassing temperature of the adsorbent were investigated in the toluene-alumina-oxygen and cyclohexane-alumina-oxygen systems. The initial yield for the toluene-alumina-oxygen system is a linear function of oxygen pressure which can be expressed by the formula

$$G(-\text{O}_2) = 12 + 0.075P_{\text{O}_2} \quad (P_{\text{O}_2} \text{ in mm.})$$

in the range 8 to 80 mm. The initial $G(-\text{O}_2)$ also increases as the surface coverage of alumina adsorbents is increased. This is true for both toluene and cyclo-

(9) Benzene is not suitable for this experiment. It shows peculiar adsorption and desorption behavior under irradiation. A small amount of phenol (identifiable chromatographically) was isolated from one of these experiments. The amount isolated shows that for benzene-alumina-oxygen, however, $G(-\text{O}_2)$ is less than 3.

(10) The author is indebted to A. D. Horton of the Analytical Division for perfecting and performing many of the gas chromatographic separations. See also V. T. Brooks, *Chem. Ind. (London)*, 1317 (1959).

Table I: Radiation Oxidation of Adsorbed Hydrocarbons^a

Adsorbate	Silica gel	Silica-alumina	Alumina
	---Total adsorbate = 50 μ moles---		
Methane	1.4	2.9	~2
Ethane	2.6	3.0	4.8
Ethylene	5.9	8.4	3.1
<i>n</i> -Propane	0.8	8.1	3.7
---Total adsorbate = 1 mmole---			
Naphthalene	3.3	1	7.0
Anthracene	28.4
-Phenanthrene	1.8	...	<Bkg. ^c
Biphenyl	1.5	<1	<Bkg. ^a
---Total adsorbate = 7.2-10 mmoles (1 ml.)---			
<i>n</i> -Hexane	6.5	14.7	2.3
Hexene-1	13	110 ^d	28 ^d
Cyclohexane	2.9	30.5	30.4
Cyclohexene	14	78 ^d	54 ^d
Toluene	3.6	11.5	18.1
<i>o</i> -Xylene	<1	12.5	40.2
<i>m</i> -Xylene	<1	19.1	29.5
<i>p</i> -Xylene	<1	10.5	36.7
Mesitylene	4.0	17.1	29.0

^a Initial $G(-O_2)$ based on energy dissipated in 10 g. of adsorbent. Adsorbent degassed overnight at $>400^\circ$. $P_{O_2} = 50-80$ mm. ^b Considerable reaction occurs also in the absence of radiation. No measurement possible. ^c Background ($G(-O_2) \cong 2$ to 4) is for the radiation reaction of oxygen and alumina with no added adsorbent. ^d Reaction occurs also in the absence of radiation.

hexane up to monolayer coverage. At coverage greater than a monolayer the results scatter badly. Initial yields are also directly proportional to the degassing temperature of the adsorbent below 300° . They are independent of degassing temperature in the 300 to 500° range. Furthermore, because of problems in handling the adsorbate (solid, liquid, or gas), reactants of each type were run at different concentrations (see Table I). The variance of vapor pressure also precluded running all experiments at the same oxygen pressure. Therefore, since $G(-O_2)$ for the representative systems was shown to depend upon both oxygen pressure and extent of surface coverage, the yields, summarized in Table I, should be accorded only a qualitative significance.

Table II shows the distribution of products obtained from the chromatographic analyses of irradiated toluene. Since product recovery did not account for all the oxygen consumed, only relative yields, referred to *o*-cresol from toluene, are given. It is noteworthy that for alumina adsorbents, the distribution of prod-

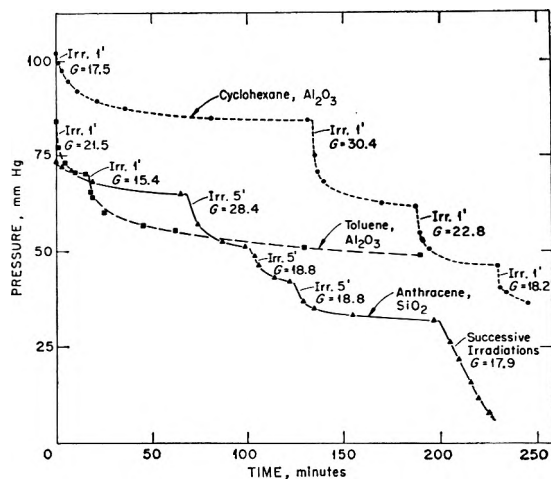


Figure 2. Radiation-induced consumption of oxygen by three hydrocarbon-adsorbent systems.

ucts for oxidations carried out in different manners (see column I) is not greatly different. *m*-Cresol always seems to be produced with a lower yield. The biggest changes in product distribution occur when the adsorbent is changed. Table IIa gives similar information for xylene-alumina-oxygen systems.

The author has previously pointed out the possible role of ionic intermediates in surface radiation chemical reactions.¹¹ In addition to the color reactions described in ref. 11 he has also observed (during the course of the present work) the formation of a pink color when mesitylene, cyclohexene, or *o*-xylene is adsorbed on aluminosilicate, or when any of these compounds is irradiated when adsorbed on silica gel. The pink coloration is, for the most part, unaffected by oxidation although some darkening is observed.

There is also a marked difference in the appearance of the organic oxidation products on different adsorbents. Most of the organic compounds when oxidized on alumina show only slight discoloration. (Anthracene is an exception and simply turns gray to black without irradiation.) An irradiated silica gel-organic-oxygen system invariably has a more marked tarry appearance than the same organic compound radiation oxidized on aluminosilicate.

None of the ampoules containing aromatic or unsaturated compounds when adsorbed and irradiated in the presence of hydrogen showed any pressure decrease.

Discussion

Yields. The most striking aspect of the radiation-induced oxidations reported here is that the energy

(11) H. W. Kohn, *J. Phys. Chem.*, **66**, 1185 (1962).

Table II: Product Distribution for Toluene-Adsorbent-Oxygen Systems

Preparative conditions	Relative concentration of products (<i>o</i> -cresol = 1)			
	Benzyl alcohol	<i>p</i> -Cresol	<i>m</i> -Cresol	Phenol
Toluene				
Irrad. 20-30 min. with C ₆ H ₅ CH ₃ , O ₂ , and Al ₂ O ₃ present	1.7 to 1.8	1.2 to 1.5	~0.5	1.5 to 2.0
Same, but adsorbent is silica-alumina	Very small	1.5 to 2.0	~0.3 to 0.4	2.0 to 3.3
Same, but adsorbent ^a is silica	~2.4	~1.0	~1.1	~0.3
Irrad. Al ₂ O ₃ <i>in vacuo</i> , add C ₆ H ₅ CH ₃ + O	0.75 to 1.0	0.5 to 0.9	~0.5	Trace to 0.5
Irrad. Al ₂ O ₃ + C ₆ H ₅ CH ₃ <i>in vacuo</i> , ^b dissolve, and extract immediately	~2 to 4	1.2 to 2.0	Trace to 0.5	1.3 to 2.4
Irrad. Al ₂ O ₃ + C ₆ H ₅ CH ₃ , add O ₂	1 to 1.5	~1	Trace	1.8 to trace
Al ₂ O ₃ , C ₆ H ₅ CH ₃ and O ₂ , no irradiation. (5 days autoxidation)	2.6	1.0	0.5	1.3

Table IIIa: Product Distributions for Xylene-Alumina-Oxygen Systems

Irrad. <i>o</i> -xylene-oxygen-alumina	<i>o</i> -methylbenzyl alcohol/ <i>o</i> -cresol = 4.1
Irrad. <i>p</i> -xylene-oxygen-alumina	<i>p</i> -methylbenzyl alcohol/ <i>p</i> -cresol = 6.5
Irrad. <i>m</i> -xylene-oxygen-alumina	<i>m</i> -methylbenzyl alcohol/ <i>m</i> -cresol = 12

^a Toluene oxidation on silica gel gives dark orange oxidation products and very little (*i.e.*, ~μg.) of the material shown in the table.

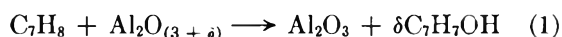
^b Very little product is obtained from this procedure, too.

absorbed by the adsorbents is transferred to the hydrocarbon resulting in its oxidation. This is particularly evident for the oxidation of adsorbed gases. $G(-O_2)$ for methane-silica gel-oxygen would be about 1200 if it were calculated on the basis of the energy absorbed by the methane. Even the systems involving most liquid adsorbates would give $G(-O_2)$ values of several hundred if calculated on the basis of energy absorbed in the liquid. Admitting that energy is transferred from adsorbent to adsorbate, one must postulate even so that each ionization event leads to the disappearance of several oxygen molecules.

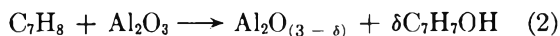
Most of the following text concerns the irradiated toluene-alumina-oxygen system although many of the salient points are equally applicable to other systems. It seems that the reaction is initiated by the adsorbent and that the adsorbent, not the atmospheric oxygen, is the oxidizing agent since some oxidation takes place in the absence of oxygen. Furthermore, silica gel is a much poorer oxidizing agent, under irradiation, than alumina. If these oxidations took place whenever a hydrocarbon was spread out on a surface and irradiated in oxygen, silica gel should be as effective as alumina for oxidation.

Much less product, of course, is formed in the absence of oxygen than in its presence. Therefore, one assumes that the alumina under irradiation, oxidizes the toluene and is itself reduced. Atmospheric oxygen reoxidizes the alumina so that it can continue its

function. In the absence of atmospheric oxygen the reduced alumina becomes incapable of oxidizing the toluene, and the reaction stops. The oxidizing power of irradiated alumina may be associated with a small amount of excess oxygen in the alumina, in which case the reaction could be represented as



This is not necessary however since

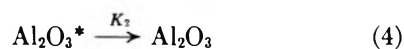
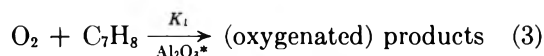


is equally plausible. These mechanisms are also consistent with the failure of hydrogen to react.

Products. Four paths for toluene oxidation can be visualized: side-chain oxidation giving benzyl alcohol, ring oxidation giving cresols, a scission followed by oxidation giving phenol plus a methyl radical oxidation product, or extensive ring oxidation. Since benzene (conspicuously absent in Table I), biphenyl, and (to a lesser extent) naphthalene seem particularly resistant to these radiation oxidations it is reasonable to assume that extensive ring oxidation does not take place in toluene either. In support of this hypothesis, the addition of side chains may increase $G(-O_2)$ (Table I). This effect is not simply a function of the number of side chains since the change in $G(-O_2)$ also depends on whether the added side chains are *ortho*, *meta*, or *para* to each other as well as on the nature of the adsorbent.

One can evaluate the ratio of scission-oxidation reactions to side-chain oxidation for toluene, *o*-, *p*-, and *m*-xylene by use of the ratios, phenol:benzyl alcohol, *o*-methylbenzyl alcohol:*o*-cresol, and *p*-methylbenzyl alcohol:*p*-cresol, respectively. Although it appears that the scission oxidation is as prevalent as side-chain oxidation for toluene, this is not true for the xylenes (Table IIa). Also noted: *o*-cresol is nearly the only cresol obtained from *o*-xylene. Similarly, *p*-cresol is obtained from *p*-xylene, etc. Hence it is concluded that little rearrangement occurs during this surface oxidation.

Postirradiation Reaction Kinetics. One may consider that the postirradiation reaction consists of two steps, as



where Al_2O_3^* is catalytically active for reaction 3. Reactions 3 and 4 can then be tested for reaction order. If 3 is zero order or slow compared with 4, and 4 is second order, the treatment is identical with that applied to adsorption kinetics by Taylor and Thon¹² and gives rise to the well-known Elovich¹³ equation

$$dq/dt = ae^{-\alpha q} \quad (5)$$

where q is the amount of material adsorbed or reacted, t is time, and a and α are experimentally determined empirical constants of the reaction.

One may also assume a first-order rate law for (3), in which case

$$-dx/dt = K_1x \quad (6)$$

where x is some measure of the amount of reactant (such as the pressure of oxygen in this case). This rate is proportional to the number of catalytic sites N

$$K_1 = K_3N \quad (7)$$

If reaction 4 is second order, *i.e.*

$$-dN/dt = K_2N^2 \quad (8)$$

upon integration of eq. 8

$$1/N = K_2t + c_1 \quad (9)$$

substitution of (7) and (9) into (6) gives

$$-dx/x = K_3/K_2 \frac{dt}{(t + c_1/K_2)} \quad (10)$$

Integration of (10) leads to

$$-\ln x = a \ln (t + b) + c \quad (11)$$

where $a = K_3/K_2$, $b = c_1/K_2$, and c is a constant of integration.¹⁴ If reaction 3 follows second-order kinetics, it can be shown by a similar series of equations that

$$1/x = a \ln (t + b) + c \quad (12)$$

The data from seven postirradiation reactions were fitted to the Elovich eq. 5 and to eq. 11, using a generalized least-square program.¹⁵ In five of the seven cases, both equations fitted the data excellently, but in the other two (which involved a different physical situation, *i.e.*, toluene and oxygen were added to preirradiated catalyst) the Elovich equation was incapable of fitting the data. Other equations [*e.g.*, (12), a first-order plot, or a log log p vs. t plot, derived on the basis of first-order site decay] gave very poor fits of the data. The results of these computations are summarized in Table III.

It is worth mentioning that for eq. 11 to have any significance, K_2 cannot be small (*i.e.*, the rate of catalyst inactivation cannot be slow) compared with K_3 , or the constants $a = K_3/K_2$ dominate the equation. The requirement of second-order catalytic site deactivation is consistent with a picture wherein the sites are associated with positive and/or negative charge entities and disappear by recombination.

Mechanism. Certain plausible mechanisms which one would first postulate are apparently not operative in this series of oxidations. If the only requirement for oxidation were organic surface ions reacting with oxygen, one would expect spontaneous oxidation of all hydrocarbons adsorbed on aluminosilicate catalysts where ions abound. Although spontaneous oxidation is observed in some cases (*i.e.*, cyclohexene, anthracene, etc., see Table I) there are other differences between the spontaneous and the irradiation-induced oxidations. Anthracene-aluminosilicate-oxygen gives a dark red product when not irradiated¹⁶ which is different from the radiation-produced product. Spontaneous cyclohexene oxidation on alumina has an activation energy (measured here) of about 10 kcal., whereas the irradiation-induced reactions have "no" activation energy. The postirradiation hydrocarbon oxidation reaction also has an activation energy.

(12) H. A. Taylor and N. Thon, *J. Am. Chem. Soc.*, **74**, 4172 (1952).

(13) S. Yu. Elovich and G. M. Zhabrova, *Zh. Fiz. Khim.*, **13**, 1761 (1939).

(14) Although one of the referees pointed out that this equation was first used by Howard and Taylor [*J. Am. Chem. Soc.*, **56**, 2259 (1934)], the equation was not derived nor elaborated upon.

(15) M. H. Lietzke, ORNL Report No. 3529.

(16) R. M. Roberts, C. Barter, and H. Stone, *J. Phys. Chem.*, **63**, 2077 (1959).

Table III: Fit of Data to Two Equations

Elovich equation, $q = (1/\alpha) \ln (a\alpha t + a\alpha t_0 + 1)$					
Expt.	$a \times 10^2$	α	t_0	var f $\times 10^5$	No. data points ^a
1	2.2 ± 0.57	5.63 ± 1.02	1.72 ± 1.99	4.4	5
2	4.6 ± 1.3	7.62 ± 0.86	1.68 ± 0.13	10	7
3	3.3 ± 0.14	5.38 ± 0.15	0.26 ± 0.19	1.4	11
4	0.32 ± 0.064	6.87 ± 0.57	1.46 ± 1.37	43	11
5	1890 ± 188	2.22 ± 1.62	-7.8 ± 2.08	9.0	8
6			would not run		
7			would not run		

This work, in $p = \ln x = a \ln (t + b) + c$					
Expt.	$-a \times 10^2$	b	c	var f $\times 10^5$	No. data points
1	12.2 ± 0.8	7.47 ± 1.2	4.0 ± 0.3	1.6	6
2	4.4 ± 0.4	2.86 ± 1.0	4.3 ± 0.02	4.5	9
3	12 ± 0.3	7.74 ± 0.6	4.7 ± 0.02	0.85	12
4	5.9 ± 0.5	5.50 ± 1.9	4.5 ± 0.02	11	12
5	2.2 ± 0.2	-7.3 ± 0.2	4.5 ± 0.001	1.4	8
6	9.1 ± 0.6	34.5 ± 4.8	4.8 ± 0.03	0.95	11
7	12 ± 2.4	93.3 ± 31	5.2 ± 0.1	0.65	9

^a It is sometimes necessary to reject the first or the first and second data points when solving the Elovich equation in order to avoid negative logarithms.

Though it is possible that during irradiation short-lived catalytic sites which promote a "zero" activation energy catalytic reaction are produced, this does not seem likely. Thus it seems doubtful that the oxidation during irradiation is due to catalytic activity of the adsorbent.

The most significant problem in this work concerns the magnitude of the G values. Previous data⁶ strongly suggest that initially about three ionizations are produced in silica gel per 100 e.v. absorbed. (One would have little reason to expect the numbers for alumina or aluminosilicate to be much different.) Now to explain a G value of 18 requires that each ionization cause the reaction of six molecules. This implies a short surface chain. If the efficiency of chain initiation is not 100%, the chains must be correspondingly longer.

The postulate of chain reactions on surfaces is somewhat startling to the average chemist, but is scarcely new. Essentially two mechanisms have been proposed. Low¹⁷ has written an exhaustive review (342 references) on the subject of material chains, and Molinari and his school¹⁸ have recently postulated the existence of "energy chains." Neither picture is entirely satisfactory as an explanation of the present data. The material chain requires the creation of surface entities in pairs. For a radiation chemical process we can logically expect these to be positive-charge entities and

their negatively charged counterparts. No explanation of how these might propagate on a surface exists. The energy chain appears unsatisfactory for the following reasons. The reaction of the H of a hydrocarbon with O₂ to give an OH releases 40-50 kcal./mole or ~2 e.v./molecule. Compared to the ~30 e.v./molecule required for an ionization this is negligible; hence, it must be considered in a separate framework to have any significance. This (amount of) energy is not enough to ionize anything. If it creates free radicals or excited species, still each oxidation should be looked on as an event. These events cannot initiate a "Molinari energy chain" unless material transport to the reaction site is sufficiently rapid. In the hydrogen or zinc oxide case, impurity conduction by electrons can handle this, but in the present hydrocarbon-alumina-oxygen system this is clearly impossible.

It must be pointed out that the mode of energy transfer has little to do with the postirradiation reaction. Beyond the demonstration that this is apparently due to catalytic activity of the solid induced by the radiation there is little which can, at present, be said about it.

Since hydrocarbons are least susceptible of all or-

(17) M. J. D. Low, *Chem. Rev.*, **60**, 267 (1960).

(18) A. Cimino, E. Molinari, and E. Cipollini, *Actes Congr. Intern. Catalyse, 2^e Paris*, 263 (1961).

ganic compounds to oxidation, it seems evident that other adsorbed organic compounds (*e.g.*, alcohols, ethers, esters, etc.) would also be oxidized by this method.

Acknowledgments. The author thanks Dr. Willis

H. Baldwin of the Chemistry Division of the Oak Ridge National Laboratory for helpful discussions, Dr. M. H. Lietzke for programming the section on postirradiation reaction kinetics, and Harvey A. Mahlman for critical review of the manuscript.

Temperature Dependence of the Unperturbed Dimensions of Polystyrene

by T. A. Orofino¹

Mellon Institute, Pittsburgh, Pennsylvania

and A. Ciferri

Chemstrand Research Center, Durham, North Carolina (Received April 6, 1964)

Results of tension-temperature studies on a cross-linked sample of bulk polystyrene and intrinsic viscosity measurements on dilute solutions of a linear polymer are reported. Both sets of data indicate a positive value, approximately $0.4 \times 10^{-3} \text{ deg.}^{-1}$, for the thermal coefficient of unperturbed end-to-end dimension $d \ln \langle r_0^2 \rangle / dT$ for atactic polystyrene. The bulk measurements were carried out at three sample elongations in the temperature interval 120–175° in accordance with techniques previously utilized. The solution studies consisted of measurements of the intrinsic viscosity $[\eta]_{\theta}$ in each of three solvents, the 1-chloro derivatives of normal decane, undecane, and dodecane, with which polystyrene displays θ -temperatures of 6.6, 32.8, and 58.6°, respectively. In view of the similarity of the solvent media selected, the increase in $[\eta]_{\theta}$ with θ observed can reasonably be attributed to the effect of temperature *per se*. The appropriateness of reported values of the thermodynamic parameters for certain polymer-solvent systems is examined in light of results of the present study.

Introduction

The average dimensions of a polymer molecule at a given temperature depend upon the thermodynamic and geometric adaptation of the individual segments to the environment provided by other parts of the chain and the external medium in which the molecule is immersed. It is constructive to associate the temperature coefficient of the polymer chain dimensions with the separate² phenomena: (1) the excluded volume effect, namely, augmentation of coil size, relative to the unperturbed state, arising from interactions between chain elements remote from one another in con-

tiguous sequence along the chain; and (2) the temperature-dependent effect of localized segment interactions on the unperturbed chain dimensions. Several procedures have been suggested and utilized in evaluation of the latter effect, which is of great interest in connection with the study of internal bond rotations in polymer chains. Values of the thermal coefficient $d \ln \langle r_0^2 \rangle / dT$, where $\langle r_0^2 \rangle$ is the mean square separation of the ends of the chain, have thus been obtained for a

(1) Chemstrand Research Center, Durham, N. C.

(2) P. J. Flory, "Principles of Polymer Chemistry," Cornell University Press, Ithaca, N. Y., 1953.

number of polymers, either directly, through suitable studies on the unperturbed molecule (a) in bulk or (b) in Θ -solution, or, indirectly, from (c) appropriate solution measurements of chain dimensions for which the excluded volume contribution (1) has been separately estimated.

Recent reviews³ of published values for $d \ln \langle r_0^2 \rangle / dT$ reveal that although satisfactory agreement between results obtained using methods (a) and (c) has been demonstrated for at least two polymer systems, in general there appear to be significant inconsistencies among the various data which call for a more detailed analysis of the entire problem.

In the present communication, values of $d \ln \langle r_0^2 \rangle / dT$ for atactic polystyrene, arrived at through independent studies of the tension-temperature relationship for a cross-linked polymer sample, method (a), and through Θ -solvent intrinsic viscosity measurements on the related linear material, method (b), are reported. To the extent that the undiluted bulk polymer and its constituent linear chains immersed in Θ -media satisfactorily approximate a common, unperturbed state of the molecule, both sets of measurements may be considered to reflect directly changes in $\langle r_0^2 \rangle$ with temperature. Recourse to dilute solution theory for independent evaluation of the excluded volume effect, required in method (c), is thus avoided. In addition, an effort has been made to circumvent a fundamental difficulty in method (b) which has not, so far,^{3a} received adequate consideration. It has been amply demonstrated⁴⁻⁸ that unperturbed dimensions in dilute solution may reflect significant specific solvent effects and, therefore, that $d \ln \langle r_0^2 \rangle / dT$ values obtained by comparing coil dimensions of a given polymer in different Θ -solvents could be seriously in error. The likelihood of this complication has been minimized in the present study through selection of polymer-solvent systems for which the relative influence of specific effects may be presumed quite small.

Within the framework of criteria adopted in the present study, an analysis of earlier data relating to evaluation of $d \ln \langle r_0^2 \rangle / dT$ for polystyrene and other systems is also presented. The need for substantial revision in currently accepted values of the thermodynamic interaction parameters for certain polymer-solvent pairs is pointed out.

Experimental

1. *Tension-Temperature Studies.* The polymer network utilized in this work was obtained⁹ by high-conversion bulk copolymerization of styrene and divinylbenzene. Soluble material extracted after prolonged swelling in benzene did not exceed 5% of the gel.

A tension-temperature analysis at six points in the range 120–175° was carried out with the unswollen polymer according to a technique described in detail elsewhere.¹⁰ The sample was stretched to the desired elongation α_e at the highest experimental temperature and allowed to relax until the tension f appeared constant. The temperature was then lowered and constant tension re-established. The procedure was repeated throughout a complete temperature cycle. No hysteresis was observed. Tension-temperature relationships established at three sample elongations are shown in Fig. 1. (Values for f have not been referred to the initial cross-sectional area of the sample, which was of the order $15 \times 10^{-3} \text{ cm.}^2$.) Pertinent numerical data are included in Table I.

Table I: Tension-Temperature Data for the Polystyrene Network

α_e	$10^3(\partial f / \partial T)_{p,L}$ (from Fig. 1)	\bar{f}_{160° , g.	$-10^3[\partial \ln (f/T) / \partial T]_{p,L}$	$10^3\beta / (\alpha_e^3 - 1)$	$10^3(d \ln \langle r_0^2 \rangle / dT)$
1.39	70.0	44.1	0.79	0.35	0.44
1.47	88.3	51.8	0.68	0.27	0.41
1.61	120.0	61.6	0.43	0.18	0.25
				Mean	0.37 deg. ⁻¹

2. *Intrinsic Viscosity Studies.* Solution viscosities of an anionically polymerized, linear polystyrene sample¹¹ ($\bar{M}_w = 4.06 \times 10^5$) in the solvents 1-chloro-*n*-decane, 1-chloro-*n*-undecane, and 1-chloro-*n*-dodecane, at four temperatures in the vicinity of each of the respective Θ -points, were determined. The data for the chloroundecane system and a description of the experimental technique employed have been presented elsewhere.⁷ An analogous investigation was carried out for the other two solvent systems.¹²

The Θ -temperatures for the polymer-solvent pairs

(3) (a) U. Bianchi, *J. Polymer Sci.*, **2A**, 3083 (1964); (b) A. Ciferri, *ibid.*, **2A**, 3089 (1964).

(4) A. R. Shultz and P. J. Flory, *ibid.*, **15**, 231 (1955).

(5) U. Bianchi, V. Magnasco, and C. Rossi, *Chim. Ind. (Milan)*, **40**, 263 (1958).

(6) K. J. Ivin, H. A. Encé, and G. Meyerhoff, *Polymer*, **3**, 129 (1962).

(7) T. A. Orofino and J. W. Mickey, Jr., *J. Chem. Phys.*, **38**, 2512 (1963).

(8) V. Crescenzi and P. J. Flory, *J. Am. Chem. Soc.*, **86**, 141 (1964).

(9) The sample was kindly provided by Dr. J. G. Pritchard, Hoffman-La Roche, Inc.

(10) A. Ciferri, *Trans. Faraday Soc.*, **57**, 846 (1961).

(11) This sample was kindly provided by Dr. F. Wenger, Celanese Corporation, and Mrs. S.-P. S. Yen, Mellon Institute. Characterization data are reported in ref. 7.

(12) T. A. Orofino, to be published.

Table II: Characterization Data for Polystyrene- Θ -Solvent Systems

Solvent	B.p., °C. (obsd.)	n_{20D} (obsd.)	% purity (chroma- tography)	Principal impurity	Θ , °C.	$[\eta]_{\Theta}$, ^c dl./g.	k_{Θ} '	δ^d
1-Chloro- <i>n</i> -decane	108.5 (18 mm.)	1.4374	99.9	...	6.6 ^a	0.497	0.80	8.2
1-Chloro- <i>n</i> -undecane	106.2 (7 mm.)	1.4406	99.6	(Undecyl alcohol)	32.8 ^b	0.501	0.68	8.2
1-Chloro- <i>n</i> -dodecane	187.3 (100 mm.)	1.4427	99.4	Dodecene	58.6 ^a	0.514	0.56	8.2

^a Estimated uncertainty, $\pm 1.5^\circ$. ^b Estimated uncertainty, $\pm 1^\circ$. ^c Estimated uncertainty, ± 0.01 . ^d Calculated solubility parameter.

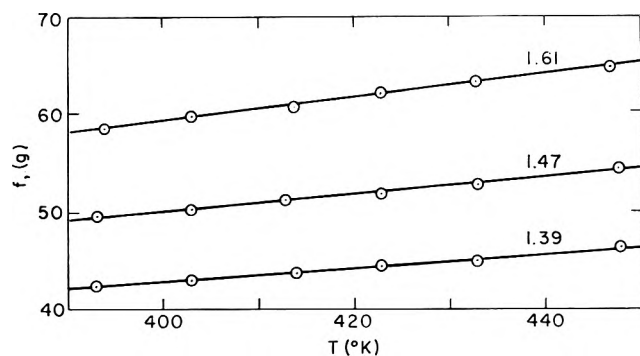


Figure 1. Tension-temperature curves at constant length for polystyrene networks. The elongation ratio, α_e (measured at 170°), is indicated.

were first estimated from precipitation studies. As described in detail for the chloroundecane system, accurate values of Θ were then established through light-scattering virial coefficient (Γ_2)-temperature measurements above and below Θ , taking as the operational definition of the latter parameter the temperature at which Γ_2 vanishes.

In Fig. 2 are plotted the observed intrinsic viscosity values $[\eta]$ vs. temperature for the three polymer-solvent systems. The trend of $[\eta]_{\Theta}$ with Θ -temperature is indicated by the dashed line.

Numerical values assigned to Θ and $[\eta]_{\Theta}$, together with the Huggins constants k_{Θ}' and characterization data for the solvents, are compiled in Table II.

Results

1. Tension-Temperature Studies. The variation of the unperturbed end-to-end distance with temperature may be determined from the data and constructions of Fig. 1 in accordance with the relationship^{10,13}

$$\begin{aligned} d \ln \langle r_0^2 \rangle / dT &= 1/T - (1/f)(\partial f / \partial T)_{p,L} - \beta / (\alpha_r^3 - 1) \\ &= -[\partial \ln (f/T) / \partial T]_{p,L} - \\ &\quad \beta' (\alpha_r^3 - 1) \quad (1) \end{aligned}$$

where β is the coefficient of cubical expansion for the

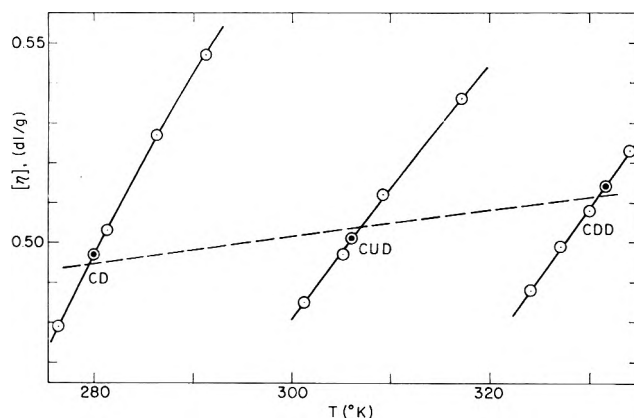


Figure 2. Plot of $[\eta]$ vs. temperature for polystyrene in 1-chloro-*n*-decane (CD), 1-chloro-*n*-undecane (CUD), and 1-chloro-*n*-dodecane (CDD). The filled circles denote interpolated $[\eta]_{\Theta}$ -values.

polymer, taken¹⁴ as $5.85 \times 10^{-4} \text{ deg.}^{-1}$. Intermediate data necessary for the calculation are compiled in Table I, together with the final results in the last column. A positive value, $(0.4 \pm 0.2) \times 10^{-3} \text{ deg.}^{-1}$, is found for the coefficient $d \ln \langle r_0^2 \rangle / dT$. This result may be considered compatible with the small value for $d \ln \langle r_0^2 \rangle / dT$ indicated in Tobolsky's earlier study¹⁵ of polystyrene networks.

2. Intrinsic Viscosity Studies. According to the Flory-Fox theory,¹⁶ the intrinsic viscosity of a linear polymer in a Θ -solvent is given by the relationship

$$[\eta]_{\Theta} = \Phi (\langle r_0^2 \rangle / M)^{1/2} M^{1/2} \quad (2)$$

where M is polymer molecular weight and Φ is a constant. In general, the unperturbed dimension $\langle r_0^2 \rangle$

(13) A. Ciferri, C. A. J. Hoeve, and P. J. Flory, *J. Am. Chem. Soc.*, **83**, 1269 (1961).

(14) M. L. Williams, *J. Appl. Phys.*, **29**, 1395 (1958); see also, T. G. Fox and S. Loshaek, *J. Polymer Sci.*, **15**, 371 (1955).

(15) A. V. Tobolsky, "Properties and Structure of Polymers," John Wiley and Sons, Inc., New York, N. Y., 1960, p. 312.

(16) P. J. Flory and T. G. Fox, Jr., *J. Am. Chem. Soc.*, **73**, 1904 (1951).

appearing in the above equation must be considered to depend upon both the temperature and the specific nature of the Θ -medium in which a particular polymer (of given molecular weight) is dissolved. In view of the close structural and chemical similarity of the Θ -media selected for the present study, the effect of the latter, relative to that operative with any given member of the solvent series, may be presumed small. Accordingly, to a first approximation, observed changes in $[\eta]_{\Theta}$ with environment may be attributed exclusively to concomitant changes in Θ -temperature. With this simplification, an expression for the thermal coefficient of $\langle r_0^2 \rangle$ is readily obtained through differentiation of eq. 2. The result is

$$d \ln \langle r_0^2 \rangle / dT = (2/3)(d \ln [\eta]_{\Theta} / d\Theta) \simeq (2/3)[\bar{\eta}]_{\Theta}(d[\eta]_{\Theta} / d\Theta) \quad (3)$$

The slope of the dashed line in Fig. 2 provides the increment $d[\eta]_{\Theta} / d\Theta$; we calculate from eq. 3 the value $0.44 \times 10^{-3} \text{ deg.}^{-1}$ for $d \ln \langle r_0^2 \rangle / dT$, in good agreement with the tension-temperature result. With respect to accountable uncertainties in the experimental data involved, the precision of the former value is estimated at $\pm 0.2 \times 10^{-3}$.

Previous studies based upon changes in $[\eta]_{\Theta}$ with temperature in various pure Θ -solvents have yielded zero¹⁷ or negative¹⁸ values for $d \ln \langle r_0^2 \rangle / dT$.¹⁹

Discussion and Conclusion

The agreement between results obtained independently from tension-temperature data and from viscosity data in structurally similar Θ -solvents demonstrated in the present study is satisfactory. In view of the limited objections which can be raised to the validity of the two methods (*cf.* introductory section and discussion below), we feel justified in concluding that a small positive value for $d \ln \langle r_0^2 \rangle / dT$, approximately $0.4 \times 10^{-3} \text{ deg.}^{-1}$, properly describes the variation of the unperturbed dimensions of atactic polystyrene with temperature. This result contrasts with some previous estimates found in the literature and it is therefore of interest to examine both the implications of our value, as well as possible sources for the disparity with earlier work.

In their analysis of viscometric data for polystyrene in various Θ -solvents of diverse structure, Schulz and Baumann¹⁷ were unable to detect any systematic variation of $\langle r_0^2 \rangle$ with temperature. Within the probable limits of uncertainty applicable, compatibility between their result and that of the present study can be adjudged. It is worth noting that agreement is even improved if, in the case of the Schulz and Baumann data, comparison is confined to values of $d \ln \langle r_0^2 \rangle / dT$

derivable from intrinsic viscosity data in Θ -solvents of related structure. Thus, with specific reference to their systems, the solvent groupings diethyl malonate-diethyl oxalate and cyclohexane-methylcyclohexane-decalin each indicate a null or slightly positive thermal coefficient for polystyrene.

Less easily reconciled are our present result for $d \ln \langle r_0^2 \rangle / dT$ and that deduced over 10 years ago in the pioneering studies of Fox and Flory.¹⁸ Their value, *ca.* $-1.5 \times 10^{-3} \text{ deg.}^{-1}$, was assigned on the basis of intrinsic viscosity data for polystyrene in two Θ -solvents, cyclohexane (34°) and ethylcyclohexane (70°). The limited scope of the original experimental study, considered together with the much less marked temperature dependence of $\langle r_0^2 \rangle$ indicated in subsequent studies on the same kinds of systems, however, subject the foregoing value to serious qualification. It seems reasonable to conclude at the present time, in fact, that the original data of Fox and Flory simply do not provide a sufficiently reliable basis for estimation of $d \ln \langle r_0^2 \rangle / dT$ for polystyrene.

With reference to the foregoing studies, it is important to note that adoption of a revised value for the temperature coefficient of $\langle r_0^2 \rangle$ in polystyrene entails also a re-evaluation of the thermodynamic parameters for certain systems. In their analysis of intrinsic viscosity-temperature data for various polystyrene-solvent pairs, Fox and Flory reported values of the interaction parameters Θ and ψ_1 calculated from the relationships¹⁶

$$\alpha^5 - \alpha^3 = 2C_M\psi_1(1 - \Theta/T)M^{1/2} \quad (4)$$

$$\alpha^3 = [\eta] / [\eta]_{\Theta}$$

where C_M appearing in the first equation is an explicit function of $\langle r_0^2 \rangle$. The latter quantity was assumed to decrease with temperature, in accordance with the viscosity results in Θ -solvents cited above. Numerical values of the thermodynamic parameters, derived from the temperature dependence of α as expressed by eq. 4, are quite sensitive to the particular choice of the associated $\langle r_0^2 \rangle$ - T relationship, especially when deduced from data at temperatures far removed from the true Θ -value of a given system. Currently accepted values for Θ and ψ_1 attributed¹⁸ to these polystyrene-solvent pairs must accordingly be viewed with the same reservations applicable to $d \ln \langle r_0^2 \rangle / dT$, the

(17) G. V. Schulz and E. Baumann, *Makromol. Chem.*, **60**, 120 (1963).

(18) T. G. Fox, Jr., and P. J. Flory, *J. Am. Chem. Soc.*, **73**, 1915 (1951).

(19) Mention should also be made of the work of U. Bianchi and V. Magnasco, *J. Polymer Sci.*, **41**, 177 (1959), who derived a negative value of $d \ln \langle r_0^2 \rangle / dT$ from viscosity data for polystyrene in mixed-solvent Θ -systems.

magnitude of which, unfortunately, plays an important role in their determination by this procedure. Results for the polystyrene-benzene pair are illustrative: Fox and Flory computed for this system the value 100°K. for the enthalpy parameter Θ . The experimental data upon which their derivation is based show a decrease in $[\eta]$ with increasing temperature and, thus, would be consistent with a null or positive value of $d \ln \langle r_0^2 \rangle / dT$ only if Θ for the system were assigned a value less than zero. The reported value of ψ_1 would likewise be subject to drastic revision.

It is opportune to point out that a situation analogous to the above may well prevail in the case of certain polyisobutylene-solvent systems for which Θ is far removed from room temperature. Values for the thermodynamic parameters, derived from intrinsic viscosity data in accordance with eq. 4, have been reported²⁰ for solutions of this polymer in *n*-heptane, 2,2,3-trimethylbutane, 2,4,4-trimethyl-2-pentene, cyclohexane, and *n*-hexadecane. In these systems, $d \ln \langle r_0^2 \rangle / dT$ for polyisobutylene was taken as *ca.* -1.2×10^{-3} , again, on the basis of the observed trend in $[\eta]_{\Theta}$ in different Θ -solvents: benzene (24°), phenetole (86°), and anisole (105°). In the light of studies subsequently undertaken, particularly the stress-temperature measurements on the bulk polymer²¹ which show $d \ln \langle r_0^2 \rangle / dT \simeq 0$, it is at present tempting to emphasize other possible interpretations of the $[\eta]_{\Theta}$ results. Intrinsic viscosity data²⁰ in the two related solvents phenetole and anisole, for example, suggest that $d \ln \langle r_0^2 \rangle / dT$ is zero, in agreement with the result of the bulk studies. In any event, as with the polystyrene system discussed above, the intimate relationship between the magnitude of the thermal coefficient of chain dimensions and the values of thermodynamic parameters derived from viscosity data should not be overlooked. Extraction of the quantity $d \ln \langle r_0^2 \rangle / dT$ from $[\eta]$ values in good solvents (method (c), opening paragraph), for example, is best attempted in cases where the required thermodynamic parameters can be independently assigned.²²⁻²⁴

The positive value for $d \ln \langle r_0^2 \rangle / dT$ indicated by our studies elicits a basic question concerning the nature of internal bond rotations in the polystyrene chain. The family of polymers for which positive values of $d \ln \langle r_0^2 \rangle / dT$ are found is increasing, and no satisfactory general interpretation for this effect exists. For polydimethylsiloxane,²⁵ a plausible explanation has been advanced based upon the occurrence of Si-O-Si bond angles differing substantially from the normal tetrahedral value. For *cis*-1,4-polybutadiene and polyisoprene,²⁶ it has been proposed recently that increase in $\langle r_0^2 \rangle$ with temperature can be ascribed to the con-

formational characteristics of single bonds adjacent to *cis* double bond elements. Ptitsyn's theory,²⁷ on the other hand, predicts zero or negative values of $d \ln \langle r_0^2 \rangle / dT$ for all vinyl polymers. In particular, this parameter is supposed to equal $-2.5 \times 10^{-3} \text{ deg.}^{-1}$ for isotactic polystyrene and to be zero for the syndiotactic form. Although the results of early dilute solution work¹⁸ were considered²⁷ to be in agreement with the Ptitsyn theory, subsequent studies, as we have seen, do not bear out these predictions. Data on stereoregular polymers would, of course, provide a basis for more significant test of the Ptitsyn theory, specifically written for tactic polymers. At the same time, a more general description of bond relations might profitably bear examination. Recent considerations²⁸ of paraffin compounds substantiate the notion that the rotational potential V about single bonds is best represented by a weighted sum involving an intrinsic potential as well as the more familiar steric contribution, *viz.*

$$V = xV_I + (1 - x)V_S \quad (5)$$

The intrinsic potential, V_I , is to be associated with the resistance of a trigonal bond to torsion, while the steric part, V_S , is to be associated with the bulk interaction of pendant atoms. For the C-C bond, $x = 1/2$. It is anticipated that for other bonds, for example C-Si, x would assume a different value.

Finally, it seems prudent to bear in mind that although reconciliation of various experimental data on polystyrene systems with the value for $d \ln \langle r_0^2 \rangle / dT$ arrived at in the present study apparently has been achieved, certain irregularities, in general, are to be expected. The selection of closely related solvents, for example, virtually mandatory in attempts at detection of changes in $\langle r_0^2 \rangle$ through variation of $[\eta]_{\Theta}$ with temperature, does not entirely eliminate the possibility of complications from specific solvent effects. It seems unlikely that the perturbing influences of solvent medium and temperature on the dimensions of the chain are independently operative. Thus, in general, the value of $d \ln \langle r_0^2 \rangle / dT$ legitimately assigned to the polymer in a given series of related Θ -solvents

(20) T. G. Fox, Jr., and P. J. Flory, *J. Am. Chem. Soc.*, **73**, 1909 (1951).

(21) A. Ciferri, C. A. J. Hoeve, and P. J. Flory, *ibid.*, **83**, 1015 (1961).

(22) P. J. Flory, A. Ciferri, and R. Chiang, *ibid.*, **83**, 1023 (1961).

(23) A. Ciferri, *Trans. Faraday Soc.*, **57**, 846 (1961).

(24) J. E. Mark and P. J. Flory, *J. Am. Chem. Soc.*, **86**, 138 (1964).

(25) P. J. Flory, V. Crescenzi, and J. E. Mark, *ibid.*, **86**, 146 (1964).

(26) G. Allegra, U. Flisi, and G. Crespi, *Makromol. Chem.*, **75**, 189 (1964).

(27) O. B. Ptitsyn, *Vysokomolekul. Soedin.*, **4**, 1445 (1962).

(28) R. L. McCullough, private communication.

may differ somewhat from that observed in bulk. Comprehensive specification of a particular system may involve even more subtle considerations, *viz.*, the possibility of fundamental changes in the geometry of the polymer chain in some temperature interval.²⁹ Expressed in another way, this would amount to failure of the convenient analytical form $d \ln \langle r_0^2 \rangle / dT$ to retain approximate constancy over a wide temperature range. We understand that aspects of the latter problem are currently under investigation.³⁰

Acknowledgment. We wish to thank Mr. John W. Mickey, Jr., for his able assistance in carrying out

some of the experimental measurements, Mr. R. J. Reitz, for contributions toward characterization of materials, Dr. John Pritchard for his interest in this work, and Professor Paul J. Flory, whose critical reading of our manuscript has resulted in a substantial improvement in the presentation. The study was financially supported, in part, by the Aeronautical Systems Division, Wright-Patterson Air Force Base, through contractual arrangements with Mellon Institute.

(29) W. R. Krigbaum, F. Mark, J. G. Pritchard, W. L. Hunter, and A. Ciferri, *Makromol. Chem.*, **65**, 101 (1963).

(30) H. Benoit, private communication.

Classical Unimolecular Rate Theory. II. Effect of the Distribution of Initial Conditions¹

by Roger C. Baetzold and David J. Wilson

Department of Chemistry, University of Rochester, Rochester, New York 14627 (Received April 6, 1964)

Current theories of unimolecular reactions assume a random distribution of initial conditions of collisionally activated molecules, *i.e.*, that the probability that a molecule is activated into a state with initial coordinates and momenta in the range $q, q + dq; p, p + dp$ depends only on the size of the volume element and the energy associated with it. The effect of this assumption is investigated by considering an alternative collision mechanism and applying it to a dissociating harmonic oscillator.

Most of the present classical theories of unimolecular reactions^{2,3} are based upon a random distribution of initial conditions in phase space of a collisionally activated molecule. These theories assume that the probability of collisional excitation for a reactant molecule into a particular volume element $d\tau$ in phase space depends on the energy associated with the volume element and is proportional to $d\tau$, but does not otherwise depend on the specific values of the coordinates and momenta in the volume element. (See, however, comments in the previous paper of this series.⁴) The pur-

pose of the present paper is to calculate the unimolecular second-order rate constant for random and nonrandom initial conditions using Slater's new approach to rate

(1) This work was supported by a grant from the National Science Foundation.

(2) (a) E. Thiele, *J. Chem. Phys.*, **36**, 1466 (1962); (b) D. Bunker, *ibid.*, **37**, 393 (1962).

(3) N. B. Sater, "Theory of Unimolecular Reactions," Cornell University Press, Ithaca, N. Y., 1959, Chapter 9.

(4) F. P. Buff and D. J. Wilson, *J. Am. Chem. Soc.*, **84**, 4063 (1962).

theory.³ A one-dimensional harmonic oscillator model is considered because of its simplicity.

A nonrandom distribution of initial states just after activating collisions in phase space results from the type of strong collision mechanism assumed. Collisions are assumed to take place during an infinitesimal time interval. The period of a molecular vibration therefore corresponds to a time interval long in comparison to the duration of a collision. Therefore, the initial states resulting immediately after the collision will be characterized by essentially no stretching or compression of the bond length and by various values of momentum, as is shown in Fig. 1. The corresponding random case has a uniform distribution of initial states around that portion of the phase space trajectory to the left of the line $q = q_c$.

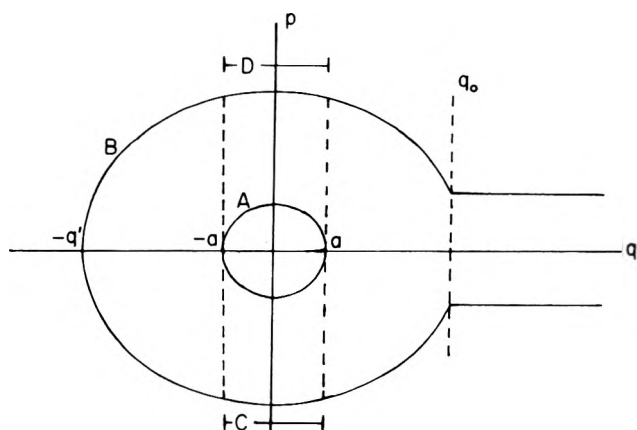


Figure 1. Phase plane diagram showing nonrandom distribution of initial states along a trajectory leading to dissociation.

Slater's formula (1) for the rate constant of a harmonic oscillator model is employed for the random case.

$$k = \phi^{-1} \int_{E_c}^{\infty} [1 - \exp(-\omega s(E))] e^{-E/\kappa T} dE \quad (1)$$

$$\phi = \frac{\kappa T}{\nu}$$

where ν is the oscillator frequency and ω is the collision frequency. The maximum time required for all of the representative points to move along a given trajectory to the critical coordinate is denoted by $s(E)$. The total time is thus twice the time required for a representative point to move from q' to q_0 as shown in Fig. 1. The equation of motion for the harmonic oscillator is integrated over this interval to obtain eq. 2.

$$s(E) = \frac{1}{2\nu} + \frac{1}{\pi\nu} \cos^{-1} \left(\sqrt{\frac{E - E_c}{E}} \right) \quad (2)$$

where E_c is the critical energy required for dissociation.

This result and the substitution $x = \sqrt{(E - E_c)/E}$ are inserted in eq. 1. The inverse cosine function is expanded to quadratic terms to obtain eq. 3.

$$k = \phi^{-1} \int_0^1 \left[1 - \exp \left\{ \frac{-4\omega\pi}{\nu} (\pi - x) \right\} \right] \times \exp \left\{ \frac{-E_c(1 + x^2)}{\kappa T} \right\} 2xE_c dx \quad (3)$$

Equation 3 is readily reduced to eq. 4, which can be machine integrated or evaluated at the high and low pressure limits.

$$k = \frac{2E_c\nu}{\kappa T} e^{-E_c/\kappa T} \int_0^1 \left[1 - \exp \left\{ \frac{-4\omega\pi}{\nu} (\pi - x) \right\} \right] \times \exp \left(\frac{-E_c x^2}{\kappa T} \right) x dx \quad (4)$$

The low-pressure rate constant is evaluated by expanding the integrand in power series and retaining only leading terms in eq. 4.

$$k = \frac{8\pi\omega E_c}{\kappa T} e^{-E_c/\kappa T} \int_0^1 (\pi - x) \exp \left(\frac{-E_c x^2}{\kappa T} \right) x dx \quad (5)$$

Equation 5 is readily integrated to yield the final expression (eq. 6) for the low-pressure rate constant, as found previously.⁴

$$k_0 = \omega e^{-E_c/\kappa T} \left[1 - \frac{1}{2} \sqrt{\frac{\kappa T}{\pi E_c}} \right] \quad (6)$$

The high-pressure rate constant is obtained by letting $\omega \rightarrow \infty$ in eq. 4. The expression is then integrated to yield eq. 7.

$$k_{\infty} = \nu e^{-E_c/\kappa T} [1 - e^{-E_c/\kappa T}] \quad (7)$$

The nonrandom case is evaluated by using many of the same techniques involved in the random case. The time required for dissociation in the nonrandom case will be less than the maximum time for the random case since motion is not required in the fourth quadrant of phase space as shown in Fig. 1.

$$s(E)_{\text{nonrandom}} = \frac{s(E)_{\text{random}}}{2} + \frac{1}{4\nu} \quad (8)$$

Equation 8 is substituted into Slater's eq. 9 to obtain eq. 10 for the rate constant.

$$k = \phi^{-1} \int_{E_c}^{\infty} \frac{\omega}{\nu} e^{-E_c/\kappa T} e^{-\omega s(E)} dE \quad (9)$$

$$k = \frac{2E_c\omega}{\kappa T} e^{-E_c/\kappa T} e^{-3\omega/4\nu} \int_0^1 e^{\left(-\frac{E_c x^2}{\kappa T} + \frac{\omega x}{2\nu} \right)} x dx \quad (10)$$

The low-pressure rate constant is calculated by expanding the terms involving ω/ν in power series. The resulting integral shown in eq. 11 is readily evaluated to yield eq. 12.

$$k = \frac{2E_c}{\kappa T} \omega e^{-E_c/\kappa T} \int_0^1 e^{-E_c x^2/\kappa T} \left\{ 1 + \frac{\omega}{\nu} \left(\frac{x}{2\pi} - \frac{3}{4} \right) \right\} x dx \quad (11)$$

$$\lim_{\omega \rightarrow 0} k = \omega e^{-E_c/\kappa T} \left\{ 1 - \frac{\omega}{\nu} \left(\frac{3}{4} - \frac{\sqrt{\kappa T}}{4\sqrt{\pi E_c}} \right) \right\} \quad (12)$$

The high pressure limiting rate constant may be obtained as follows. It can be seen from inspection that the $e^{-3\omega/4\nu}$ term in front of the integral (10) causes the rate constant to fall to zero, despite the term $\omega x/2\pi\nu$ in the integrand.

Machine calculations of k/k_0 for eq. 4,6 and 10,12 were performed on the IBM 1620 at the University of Rochester Computing Center. Results are shown in Fig. 2, where k/k_0 is plotted vs. $\log \omega/2\pi\nu$. Here $k_0 =$

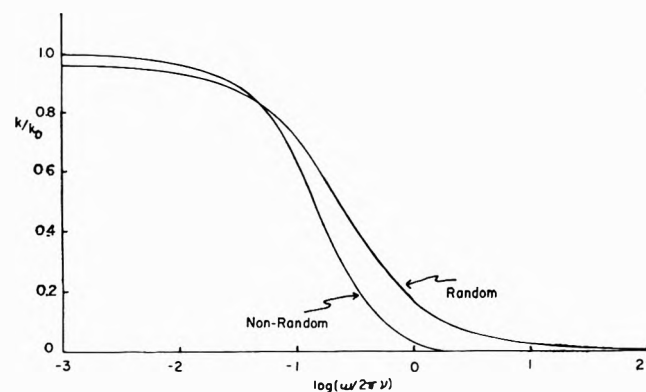


Figure 2. Plots of k/k_0 vs. $\log(\omega/2\pi\nu)$ for the random and the nonrandom models.

$\omega e^{-E_c/\kappa T}$. A clear distinction between the two situations can easily be seen. The nonrandom plot falls off rapidly while the random case shows the usual asymptotic behavior as the pressure is increased. When more complex molecules are considered, the increased lifetimes may make the differences in behavior show up at lower pressures. (Additional work on this point is needed.) For real diatomic molecules, the instantaneous collision assumption is not particularly applicable, since the periods of molecular vibration are comparable in size to the actual times of interaction during collisions. More complex molecules, on the other hand, have lifetimes much longer than the molecular vibration period. Thus the time interval in which a pair of colliding molecules are interacting is

only a small fraction of the lifetime of an activated molecule, and the assumption of nonrandom initial conditions may hold.

The ratio $E_c/\kappa T$ was varied to determine what effects the activation energy will have upon the two models. The values 40 and 20 were assigned to this parameter. Only a very minor effect was noted.

The striking difference between the random and nonrandom behavior at higher pressures can be viewed in the following light. As pressure increases, the probability per unit time that a collisionally activated molecule will suffer a deactivating collision increases proportionately to the pressure. The random case includes initial states very close to the critical surface, which can reach the critical coordinate in a short time; hence, their probability for being deactivated is very small and a fraction of them will always dissociate. This accounts for the asymptotic behavior at high pressures. The initially nonrandom representative points all have to move for a finite time interval before they can possibly cross the critical surface. The probability of collision is sufficiently great that very few points reach the critical surface. The rare constant, therefore, falls to zero.

It should be pointed out that the collision mechanism assumed violates the principle of microscopic reversibility. This is readily seen by considering the deactivation of a reactive molecule whose coordinate is distorted to a fairly large amplitude. Such a deactivation is counted, yet the reverse process, activation to reactive states from rather highly energized states, is not taken into account. This discrepancy makes the difference between the rates calculated from the two models larger than it should be. Similar difficulties arise in the application of Slater's "new approach" technique to other collision mechanisms.⁵ However, it is possible to modify Slater's method in such a way that the above difficulty can be removed. We proceed as follows

If we assume that our diatomic molecules are activated and deactivated by a strong collision mechanism with impulsive forces, then it is reasonable to assume that molecules are excited from phase plane trajectories having thermal energies (A, for example, in Fig. 1) to only such portions C of activated trajectories B which are accessible by a change of momentum p but not of coordinate q . Further, we shall assume end-on collisions, so that the instantaneous change in p upon collision is always negative. In similar fashion, collisional deactivation from B to A can only occur when the repre-

(5) We are indebted to one of the referees for a most helpful discussion of this point.

representative point is in segment D. We again utilize the truncated harmonic oscillator potential.

Let energy E' be associated with trajectory A; then $a = \sqrt{2E'/\kappa}$, where κ is the force constant of the oscillator. Let energy E be associated with trajectory B. Then $\delta(E, E')$, the time required for the representative point to traverse segment D, is given by

$$\sqrt{2E'/\kappa} = \sqrt{2E/\kappa} \sin \left[\frac{2\pi\nu\delta(E, E')}{2} \right] \quad (13)$$

where ν is the frequency of the oscillator. If $E' \ll E$, this yields

$$\delta(E, E') \cong \frac{1}{\pi\nu} \sqrt{E'/E} \quad (14)$$

We take the following expression as our choice of collisional deactivation probability per unit time from trajectories B having energies in the range $E, E + dE$ to trajectories A having energies in the range $E', E' + dE'$

$$\omega R(E, E') dE' = \omega \sqrt{E'/E} P(E') dE' \quad (15)$$

where ω is the effective collision frequency. At equilibrium, the total rate of deactivation from B to A is therefore given by

$$\omega \sqrt{E'/E} \times P(E') dE' \times P(E) dE \times A_{\text{total}} \quad (16)$$

where $P(x) = (kT)^{-1} \exp(-x/kT)$, and A_{total} is the macroscopic concentration of diatomic molecules. This expression must also be the rate of activation of molecules from A to B, from microscopic reversibility. We next integrate (16) with respect to E' to obtain the total rate of activation to trajectories having energy in the range $E, E + dE$. We assumed that the rate of activation is unaffected by the occurrence of chemical reaction. The result is

$$\Gamma^{(2/3)} \omega A_{\text{total}} \sqrt{\frac{kT}{E}} \exp(-E/kT) dE/kT \quad (17)$$

We must next calculate the probability that such a reactive molecule is not collisionally deactivated before it has an opportunity to react. It is possible for a molecule on trajectory B (see Fig. 3) to be deactivated to a nonreactive state anywhere between F and G. The time required to traverse this segment can be calculated from

$$\pm \sqrt{2E_0/\kappa} = \sqrt{2E/\kappa} \cos 2\pi\nu t$$

where E_0 is the energy associated with trajectory H. If we assume that $(E - E_0)/E_0 \ll 1$, this time is approximately

$$t' = \frac{1}{2\nu} - \frac{1}{\pi\nu} \sqrt{1 - (E_0/E)^{1/2}} \quad (18)$$

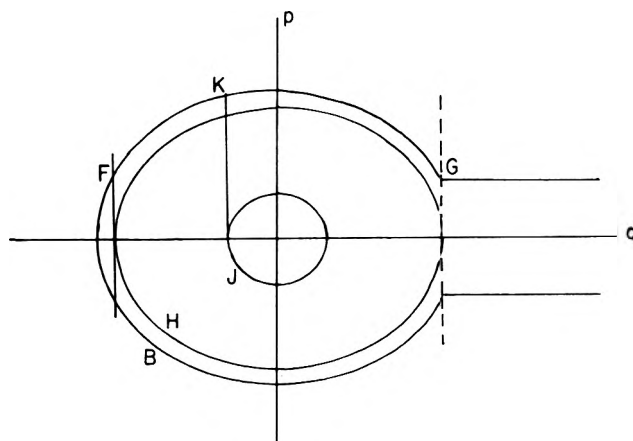


Figure 3. Phase plane diagram showing states to which deactivation can occur.

Let us assume that the representative point arrives at F at time $t = 0$, and that $P(t, E, \omega)$ is the probability that the molecule has not been deactivated in the interval $(0, t)$. We find the following equation for $P(t, E, \omega)$

$$P(t + dt, E, \omega) = P(t, E, \omega) - \omega dt \int_{E''(t)}^{E_0} R(E, x) dx P(t, E, \omega) \quad (19)$$

where $R(E, E')$ is given by eq. 15 and $E''(t)$ is given by

$$E''(t) = E \cos^2 (2\pi\nu t + \pi + \sqrt{1 - (E_0/E)^{1/2}})$$

or

$$E''(t) = E \cos^2 (2\pi\nu t + \sqrt{1 - (E_0/E)^{1/2}}) \quad (20)$$

Therefore

$$\frac{\partial P}{\partial t} (t, E, \omega) = -\omega P(t, E, \omega) \int_{E''(t)}^{E_0} \sqrt{x/E} \exp(-x/kT) \frac{dx}{kT} \quad (21)$$

$$P(0, E, \omega) = 1$$

The probability that our activated molecule escapes the hazards of collisional deactivation and is able to react is then given by $P(t'(E), E, \omega)$, where $t'(E)$ is defined in eq. 18.

We next calculate the unimolecular rate by multiplying the probability that a molecule having energy in the range $E, E + dE$ is able to react by the rate at which such molecules are formed and integrating with respect to E . This yields the following expression for the first-order rate constant

$$k = \omega \Gamma \left(\frac{3}{2} \right) \int_{E_0}^{\infty} (kT/E)^{1/2} \times \exp(-E/kT) P(t'(E), E, \omega) dE/kT \quad (22)$$

where P and t' are defined by eq. 21 and 18.

Let us next introduce some additional simplifying approximations to see if we can get some information about the qualitative behavior of k as a function of ω , since numerical evaluation by means of eq. 22 is rather difficult. Our collisional deactivation rate (15) strongly favors deactivation to low-lying energy states, such as trajectory A in Fig. 1. Let us, therefore, assume that collisional activation and deactivation take place from and to only trajectories such as A, and that the probability of collisional deactivation from segment D is independent of the exact position of the representative point on this segment. We set a in Fig. 1 equal to $\sqrt{2kT/\kappa}$. The time required for the representative point to traverse segment D is given by

$$\delta(E) \cong \frac{1}{\pi\nu} \sqrt{kT/E} \quad (23)$$

If deactivation occurs with unit efficiency for molecules whose representative points are on segment D, the rate of deactivation in the absence of chemical reaction is given by

$$A_{\text{total}} P(E) dE \omega \delta(E) / (1/\nu)$$

or

$$\frac{A_{\text{total}} \omega \exp(-E/kT) dE}{\pi \sqrt{EkT}} \quad (24)$$

This we set equal to the rate of activation in the presence of chemical reaction.

We then calculate the unimolecular rate constant by Slater's method; this yields

$$k = \frac{\omega}{\pi} \int_{E_0}^{\infty} \frac{\exp(-E/kT)}{\sqrt{EkT}} \exp \left[\frac{-\omega}{\pi\nu} \sqrt{kT/E} \right] dE \quad (25)$$

We assume that the Boltzmann factor dominates and replace E by E_0 in the remaining terms; this yields

$$k \cong \frac{\omega}{\pi} \sqrt{kT/E_0} \exp \left[\frac{-\omega}{\pi\nu} \sqrt{kT/E_0} \right] \exp(-E_0/kT) \quad (26)$$

We see that the rate constant is proportional to pressure at low pressures, but that it goes through a maximum and asymptotically approaches zero as pressure increases. Thus, the anomalous behavior of the unimolecular rate constant persists even for this more self-consistent treatment.

On Planetary Electron Corrections to Electron Diffraction Intensity Data¹

by T. Iijima and R. A. Bonham

Department of Chemistry, Indiana University, Bloomington, Indiana (Received April 20, 1964)

A new technique for correcting electron diffraction intensity data for planetary electron scattering from molecules in the gas phase is presented. The procedure does not make any assumptions about the molecular structure but still guarantees that the radial distribution will remain positive. Corrections to the peak areas in the resulting radial distribution function are discussed and the possible application of the technique to the analysis of X-ray scattering data from liquids is pointed out.

Introduction

At present there are two generally used methods for the correction of gas electron diffraction intensity data for the effect of planetary electron scattering.^{2,3} One technique makes use of a calculated correction based on a trial structure for the molecule.^{2b} The radial distribution curve obtained in this way may then be analyzed and a new planetary electron correction can be constructed from the information gained in the analysis. The procedure is then usually repeated until a self-consistent result is obtained. In a good many cases this procedure can be successfully initiated from an analysis of a radial distribution curve obtained from the intensity data without planetary electron corrections. For further details of this technique ref. 2a and 2b should be consulted.

It is possible that in precise work on large and unknown structures the previously mentioned technique may prove laborious. Bastiansen and co-workers³ have employed a different technique for correcting for planetary electron scattering effects which is superior in some respects to the one discussed above and which is the basis for the new technique to be described in this article. This method uses a theoretical background based on a scattering factor for a particular atom in the molecule and is similar in principle to the use of a unitary scattering factor for the correction of the diffraction data for planetary electron scattering effects. The technique does not assume any structural information and in a carbon-containing compound guarantees that all carbon-carbon distances will be properly corrected for planetary electron scattering if a carbon electron scattering factor is used to make the planetary electron

scattering corrections. The difficulties with this method are: (1) the peak areas for peaks other than carbon-carbon peaks in the radial distribution of the above example will be distorted, and (2) the radial distribution curve will not obey Karle's^{2a} nonnegative area criterion. Bastiansen and Strand⁴ have shown how the first difficulty may be surmounted and the second point will be the central theme of this paper.

Theory

We have made a survey of the effects on radial distribution peaks which have been corrected for planetary electrons scattering with an incorrect scattering factor and we have observed that negative areas are introduced into the radial distribution curve for all cases where the unitary scattering factor belongs to an atom of smaller atomic number than the heaviest atom involved in the peak under consideration. Of even greater importance is the fact that the converse is also true. In other words, if the planetary electron correction is based on the scattering factor for the heaviest atom in the molecule, then the resulting radial distribution curve must be essentially positive and distortions

(1) Contribution No. 1242 from the Chemical Laboratories of Indiana University; the authors wish to thank the U. S. Atomic Energy Commission, Chemistry Directorate of the Air Force Office of Scientific Research, and the Petroleum Research Fund of the American Chemical Society for their support of this work.

(2) (a) I. L. Karle and J. Karle, *J. Chem. Phys.*, **17**, 1052 (1949); (b) L. S. Bartell, L. O. Brockway, and R. H. Schwendeman, *ibid.*, **23**, 1854 (1955).

(3) A. Almenningen, O. Bastiansen, and L. Fernholt, *Kgl. Norske Videnskab. Selskabs Skrifter*, No. 3 (1958).

(4) T. G. Strand, Thesis, The Technical University of Norway, Trondheim, March, 1961.

in the radial distribution curve introduced by the process can then be accounted for by the techniques introduced by Bastiansen and Strand.⁴ This result means that the Karle nonnegative area criterion is preserved as an aid in determining the proper background as well as the data generation scheme outlined by Bonham and Momany⁵ which helps to determine the proper way of drawing the background in the small angle scattering region.

The application of this scheme is as follows. The reduced molecular intensity function $M(s)$ is given as^{2a}

$$M(s) = \frac{I(s)}{B(s)} - 1 \quad (1)$$

where $I(s)$ is the experimental intensity suitably corrected for nonlinearity of the photographic emulsion, flatness of the photographic plate, sector shape, and other pertinent experimental corrections and finally divided by the theoretical background. The function $B(s)$ is a smoothly drawn background function such that the Fourier sine transform of $M(s)$ corrected for planetary electron scattering is everywhere positive. The planetary electron correction is made by multiplying $M(s)$ as shown in eq. 2

$$M_c^1(s) = (1/s^2 f_L(s))^2 M(s) [I_A(s) / \sum (Z_k^2 + Z_k)] \quad (2)$$

where $f_L(s)$ is the unitary electron scattering factor⁶ of the largest atom. An average of the scattering factors for all the atoms in the molecule heavily weighted in favor of the largest atomic number present may also be used. The function $I_A(s)$ is the total atomic scattering given by

$$I_A(s) = s^4 \sum_k \{ f_k^2(s)^2 Z_k^2 + \left(\frac{4}{a_0^2}\right) S_k(s) \} \quad (3)$$

where the term $S_k(s)$ is the Heisenberg-Bewilogua inelastic scattering factor.⁷ A suitable average unitary scattering factor was found to be

$$f_L(s) = \frac{\sum_{i=1}^N Z_i f_i(s)}{\sum_{i=1}^N Z_i} \quad (4)$$

where the sums are taken over the different kinds of atoms present in the molecule. This definition leads to small negative contributions to the radial distribution curve for the peaks corresponding to the distances between heavier atoms, but these contributions are only a few per cent of the peak height of the peak under consideration.

The corrected reduced intensity of eq. 2 or

$$M_c(s) = \{1/[s^2 f_L(s)]^2\} M(s) [I_A(s) / \sum_k (Z_k^2 + Z_k)] \quad (5)$$

can then be inverted by use of the Fourier sine trans-

form by using the previously mentioned criteria for determining the function $B(s)$.

The areas of the peaks of the resulting radial distribution $F(r)$ given by

$$F(r) = \int_0^\infty ds s M_c(s) \sin sr \quad (6)$$

must now be characterized by correction factors based on the true scattering factors of the original atoms. Note also that a weight factor of the form e^{-os^3} can be introduced into the Fourier sine integral which simply leads to a redefinition of l_{ij}^2 in the following as $l_{ij}^2 + 2b$. A theoretical expression for an individual peak in $F(r)$ can be written in terms of a peak in the usual unmodified radial distribution function $f(r)$ where

$$f(r) = \sqrt{\frac{\pi}{8}} \frac{\sum_{i \neq j} Z_i Z_j e^{-(r - r_{ij})^2 / 2l_{ij}^2}}{\sum_k (Z_k^2 + Z_k) r_{ij} l_{ij}} \quad (7)$$

as

$$F(r) = k(ij) f(r) + \sqrt{\frac{\pi}{8}} \frac{\sum_{i \neq j} \sum_N s_N(ij) Z_i Z_j e^{-(r - r_{ij})^2 / 2[l_{ij}^2 + 2b_N(ij)]}}{\sum_k (Z_k^2 + Z_k) r_{ij} (l_{ij}^2 + 2b_N^{1/2}(ij))} \quad (8)$$

The correction sum in (8) contains terms which introduce distortions into the radial distribution curve because all peaks are not properly corrected for the planetary electron scattering. The constants $k(ij)$, $a_N(ij)$, and $b_N(ij)$ are determined from a least-squares fit of $w(s)_{ij} = f_i(s) f_j(s) / f_L(s)^2$ by a constant $k(ij)$ which is very close to unity, plus a linear combination of Gaussian terms

$$w(s)_{ij} = k(ij) + \sum_N a_N c^{-b_N s^2} \quad (9)$$

The sum over N generally takes as many terms as there are electron shells in the largest atom present in the molecule. Typical fits are shown in Fig. 1 for a molecule containing C, H, and Cl atoms. The error introduced in the analysis by this procedure is negligible as the characterization of the scattering factors is usually better than 1% and in general the corrections to the radial distribution curve are largest for the peaks which make the smallest contribution to $F(r)$ and are therefore the ones most unreliably determined by any method.

(5) R. A. Bonham and F. A. Momany, *J. Phys. Chem.*, **67**, 2474 (1963).

(6) The unitary electron scattering factor may be defined as $f(s) = (Z - F(s))/Z$, where $F(s)$ is the X-ray scattering factor of the atom.

(7) L. Bewilogua, *Physik.-Z.*, **32**, 740 (1931).

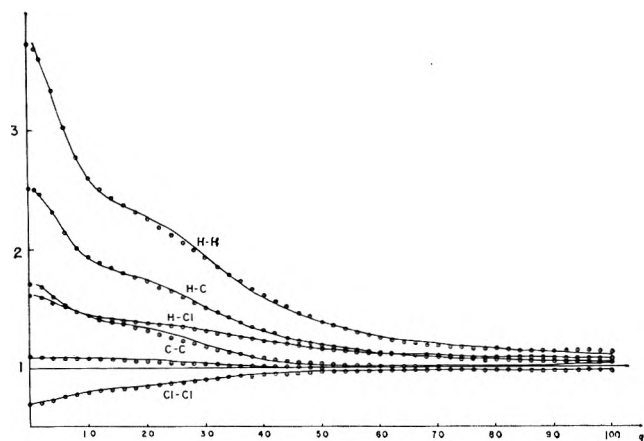


Figure 1. The least-squares fit of the $f_i f_j / f_L^2$ curve for a molecule containing C, H, and Cl (f_L was calculated from eq. 4): —, $f_i f_j / f_L^2$ calculated from form factor table; $\circ\circ\circ\circ$, fitted curves $w(q) = K + a_1 e^{-b_1 q^2} + a_2 e^{-b_2 q^2}$ ($q = (10/\pi)s$).

The main disadvantages of the procedure are two-fold. In the first place, corrections can only be made if the identity of a given peak is known. For instance, one must identify a given peak as being a carbon-hydrogen peak before the appropriate correction can be applied to it. The second point is that the $k(ij)$, $a_N(ij)$, and $b_N(ij)$ factors are not transferable to molecules which contain different elements. These parameters may be the same for all carbon-hydrogen compounds but the addition of a chlorine atom necessitates a new least-squares fit of the scattering factors to obtain the necessary factors.

The first problem pointed out above should not be too serious as most of the major peaks are usually easily identified and once a trial structure has been obtained a self-consistent procedure can be set up for the assignment of the minor peaks. The second problem is only a computational one and as long as a high-speed digital computer is available the determination of the $k(ij)$, $a_N(ij)$, and $b_N(ij)$ values from suitable atomic scattering factors⁸ should pose no problem.

X-Ray Diffraction from Liquids

One possible important application of this procedure outside the realm of gaseous electron diffraction might be in the analysis of the X-ray diffraction data from liquids.⁹ The theoretical formulas used are quite similar to the ones employed in the gas diffraction case but with the important difference that the electron scattering factors are replaced by the corresponding X-ray scattering factors.

A procedure analogous to the one outlined above can be followed with

$$I_A(s) = \sum_k [F_k^2(s) + S_k(s)] \quad (10)$$

and

$$M_x(s) = \frac{I(s)}{B(s)} - 1 \quad (11)$$

where $M_x(s)$ is the reduced molecular intensity for the X-ray case, $I_A(s)$ is the atomic background scattering, $F_k(s)$ is the X-ray scattering factor, and $I(s)$ is the experimental intensity suitably corrected for the effects encountered in the X-ray case.⁹ A corrected reduced intensity can be defined as

$$M_x^1(s) = [I_A(s) / \sum_k Z_k] M_x(s) [1 / \phi_L^2(s)] \quad (12)$$

where ϕ is the unitary X-ray scattering factor of the largest atom. A radial distribution curve may be defined as

$$f_x(r) = \int_0^\infty ds e^{-as^2} M_x^1(s) \sin sr \quad (13)$$

where the factor e^{-as^2} is an artificial convergence factor. This definition leads to the expression for the theoretical radial distribution function

$$F_x(r) = \sqrt{\frac{\pi}{8}} \sum_{i \neq j} \sum_N \frac{m_i Z_i Z_j a_N(ij) e^{-(r - r_{ij})^2 / 2(l_{ij}^2 + 2a + 2b_N(ij))}}{\sum_k Z_k r_{ij} (l_{ij}^2 + 2a + 2b_N^{1/2}(ij))} \quad (14)$$

if all interatomic vibrations are assumed to be har-

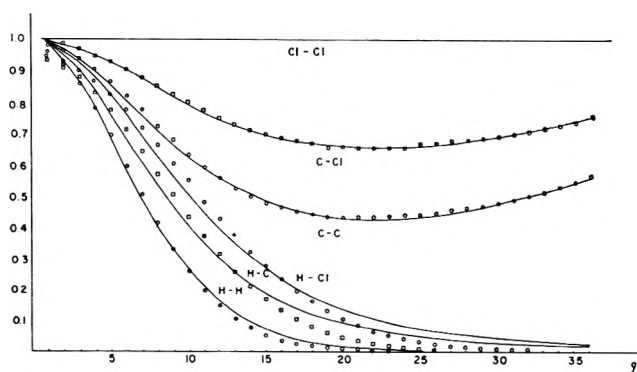


Figure 2. The least-squares fit of $\phi_i \phi_j / \phi_L^2$ curve for a molecule containing C, H, and Cl (ϕ_L was taken to be ϕ_{Cl}): —, $\phi_i \phi_j / \phi_L^2$ calculated from form factor table; $\circ\circ\circ\circ$, fitted curves: $w(q) = K + a_1 e^{-b_1 q^2} + a_2 e^{-b_2 q^2}$ for C-C and C-Cl; $w(q) = a_1 e^{-b_1 q^2}$ for H-H, C-H, and Cl-H.

(8) (a) R. A. Bonham and T. G. Strand, *J. Chem. Phys.*, **39**, 2200 (1963); (b) T. G. Strand and R. A. Bonham, *ibid.*, **40**, 1686 (1964).

(9) C. L. van Panthaleon van Eck, H. Mendel, and W. Boog, *Discussions Faraday Soc.*, No. 24, 200 (1957).

monic. The sums are over all the internuclear pairs in the solution. The $\phi_i\phi_j/\phi_L^2$ curves are shown in Fig. 2 for a molecule containing C, H, and Cl. It is noted that in the X-ray case, the least-squares fit of $\phi_{ij}\phi/\phi_L^2$ curve does not necessarily lead to a constant $k(ij)$ which is close to unity. The factor m_{ij} is the number of atom pairs present in the solution for a particular distance.

Note that hindered rotational effects in the solution have not been included in the above treatment.

Acknowledgments. The authors wish to thank Mrs. Joanne Knight for her help in preparation of the manuscript and Mr. Lao-sou Su for aiding in some of the calculations.

Chemical Properties of Carbamoylpyridinium Compounds; Ionic Decomposition in Nonhydroxylic Organic Solvents

by S. L. Johnson and K. A. Rumon

Mellon Institute, Pittsburgh, Pennsylvania 15213 (Received April 23, 1964)

The ionic adduct from dimethylcarbamoyl chloride and pyridine undergoes a decomposition reaction which produces its component parts in nonhydroxylic solvents with dielectric constants ranging from 5 to 95, but not in hydroxylic solvents with dielectric constants ranging from 11 to 80. This is because the relative nucleophilicities of chloride *vs.* pyridine are strongly affected by the chemical nature of the solvent. In hydroxylic solvents, the chloride ion can enjoy hydrogen-bonding stabilization, but in nonhydroxylic solvents, the chloride ion becomes a "hard" base.

Introduction

In an effort to synthesize less reactive acylpyridinium compounds in order to study their solvolytic behavior, some carbamoylpyridinium compounds have been prepared and their chemical properties have been studied. Diphenylcarbamoylpyridinium chloride was synthesized^{1,2} in 1907, but to date, nothing has been known chemically of this class of compounds. Since a mixture of pyridine and carbamoyl chloride is used as a carbamoylating agent, it is of interest to explore the chemical state of the carbamoylating agent.

Experimental

Preparations. 1-(N,N-Dimethylcarbamoyl)pyridinium chloride (I) was prepared in quantitative yield by allowing equimolar amounts of dimethylcarbamoyl chloride (Aldrich, redistilled) and pyridine (Eastman

White Label) to react at room temperature; a slightly exothermic reaction takes place. Purification by sublimation at 70° and 1 mm. yields colorless, extremely hygroscopic crystals, m.p. 82.8–83.5° (cor.).

Anal. Calcd. for C₈H₁₁ClN₂O: C, 51.47; H, 5.94; Cl, 19.01; N, 15.01; O, 8.57. Found: C, 51.16; H, 6.04; Cl, 18.97; N, 15.08; O, 8.47. Molecular weight determinations in water by vapor pressure osmometry yield a value of 94.3 ± 1.7; the calculated apparent molecular weight is 93.3.

Following the above procedure, but using an inert solvent, acetonitrile, to control the more exothermic reaction with the more basic pyridines 3,5-lutidine (Reilly, redistilled) and 4-picoline (Eastman White Label

(1) J. Herzog, *Ber.*, **40**, 1831 (1907).

(2) A. Nicolaus, *J. prakt. Chem.*, **82**, 526 (1910).

redistilled), the following adducts were obtained: 1-(*N,N*-dimethylcarbamoyl)-3,5-lutidinium chloride (II) as hygroscopic crystals, m.p. 92.0–94.0° (cor.) [*Anal.* Calcd. for $C_{10}H_{15}ClN_2O$: C, 55.89; H, 7.04; Cl, 16.55; N, 13.05. Found: C, 56.12; H, 7.29; Cl, 16.30; N, 12.76]; and 1-(*N,N*-dimethylcarbamoyl)-4-picolinium chloride (III) as slightly hygroscopic crystals, m.p. 137.5–138.5° (cor.). *Anal.* Calcd. for $C_9H_{13}ClN_2O$: C, 53.95; H, 6.52; Cl, 17.66; N, 13.51. Found: C, 54.09; H, 6.48; Cl, 17.41; N, 13.64. Diphenylcarbamoylpyridinium chloride (IV), m.p. 109.0–110.5° (cor.), was prepared according to published procedures.^{1,2}

The following pyridines, when mixed in equimolar quantities with dimethylcarbamoyl chloride, do not react at all, as determined by n.m.r. and infrared analysis of the equimolar mixtures—2,6-lutidine, 2,4,6-collidine, and 2,6-dimethoxy pyridine.

Physical Measurements. Proton magnetic resonance measurements were made at 37° with a Varian A-60 spectrometer operating at 59.8 Mc. Infrared measurements were made with a Perkin-Elmer 21 spectrometer and a Beckman IR-4. A Leeds and Northrup No. 4866 conductivity bridge was employed for the conductance measurements. Equilibrium constant determinations were performed with a Beckman DU spectrophotometer. The solutions were thermostated at $25.01 \pm 0.01^\circ$. The acetonitrile (Fisher reagent grade) was distilled from phosphorus pentoxide. Also, Eastman Spectrograde acetonitrile distilled from phosphorus pentoxide was used. The dimethylcarbamoyl chloride used for the equilibrium measurements was redistilled at 25 mm., b.p. 172.5°. Vapor phase chromatographic analysis of this material indicates greater than 99.8% purity. Stock solutions of the purified dimethylcarbamoyl chloride in acetonitrile kept at room temperature do not deteriorate over a 3-month period.

Results

N.m.r. Spectra. Dimethylcarbamoylpyridinium chloride (I) when dissolved in water gives a simple n.m.r. spectrum which is time independent over 24 hr. In a 0.1 *M* HCl solution, the n.m.r. spectrum is independent of time over a 1-month period. The ratio of ring hydrogens to methyl hydrogens is 5:6. There is a large displacement of all the ring protons in I to lower field compared to the positions of the corresponding ring protons in other pyridinium compounds; the displacement is largest for the α -protons. The shift of the α -proton resonance from *t*-butyl alcohol is as follows: I, 474 c.p.s.; 1-methylpyridinium bromide, 456 c.p.s.; pyridine hydrochloride, 456 c.p.s.;

pyridine hydrobromide, 455 c.p.s. All solutions were 5% by weight.

When I is dissolved in acetonitrile, the spectrum observed immediately after dissolution, shown in Fig. 1a, contains the typical pyridine pattern from τ 0.1–1.8 and two broadened methyl resonances at τ 6.83 and 7.12. After 30 min., the spectrum shown in Fig. 1b has completely changed; the pyridine proton signals are now shifted upfield by ca. 1 τ -unit and

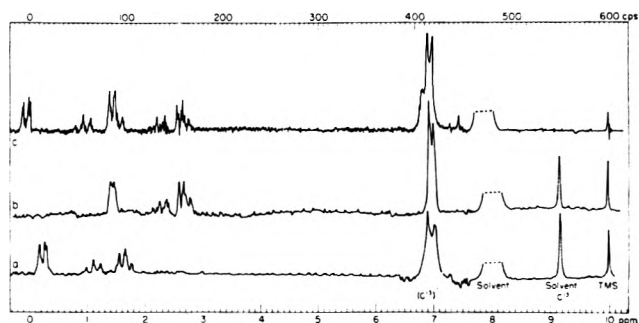
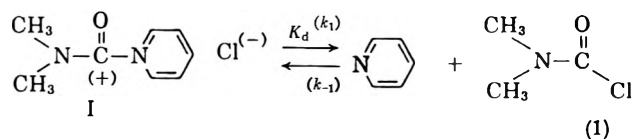


Figure 1. N.m.r. spectra of dimethylcarbamoyl chloride in acetonitrile at 37° with TMS as a reference: a, 0.725 *M*, 1 min. after mixing; b, 0.725 *M*, 30 min. after mixing; c, 5.01 *M*, 60 min. after mixing.

now occur in the region τ 1.3–2.8; the methyl resonances at τ 6.90 and 7.00 are now located at lower field and have narrowed. A 0.535 *M* solution of I gives, after 30 min., a spectrum identical with the sum of the separate spectra of 0.535 *M* pyridine and 0.535 *M* dimethylcarbamoyl chloride in acetonitrile,³ therefore, the reaction which is taking place is the decomposition of I to pyridine and dimethylcarbamoyl chloride according to eq. 1.



The equilibrium constant for the reaction according to eq. 1 is highly dependent on the initial concentration of I, indicating a large salt or medium effect upon K_d . From the integration of the proton signals of the pyridinium compound and pyridine, the following apparent equilibrium constants at 37° were calculated as a function of the total concentration of adduct: 0.75 *m*, $K_d > 30$; 3.25 *m*, $K_d = 11$; 4.42 *m*,

(3) It was necessary to use strictly the same concentrations of I, pyridine, and dimethylcarbamoyl chloride to ascertain this point as the chemical shifts of the ring protons of I and of pyridine are extremely sensitive to concentration.

$K_d = 4.0$; $5.01\text{ }m$, $K_d = 1.2$. The concentration of ions increases in this series (as calculated from the K_d values) as follows: $<0.07\text{ }m$, $0.29\text{ }m$, $1.10\text{ }m$, and $4.06\text{ }m$, respectively. Figure 1c is a reproduction of a concentrated solution spectrum ($5.01\text{ }m$) of I where the equilibrium concentration of pyridine and I may be seen clearly.

In acetonitrile as in water, a large downfield shift of all of the ring protons is experienced in dimethylcarbamoylpyridinium chloride compared to other pyridinium compounds. The average α -proton τ -values in acetonitrile solutions containing 1.5% substrate are as follows: I, -0.77 ; 1-acetylpyridinium chloride, 0.33 ; pyridine hydrochloride, 0.30 ; pyridine hydrobromide, 0.30 ; and 1-methylpyridinium bromide, 0.00 .

Decomposition of I according to eq. 1 takes place in general in nonhydroxylic solvents, as determined by the n.m.r. spectrum taken as a function of time. The forward rate in eq. 1 is quite solvent dependent. The solvents which cause $>90\%$ decomposition of $0.5\text{ }M$ solutions of I (dielectric constant in parentheses) are chloroform (5), methylene chloride (9), acetonitrile (39), dimethyl sulfoxide (47), and ethylene carbonate (95). The above solutions were 5% by weight in I.

Hydroxylic solvents, on the other hand, do not cause the ionic decomposition of I, as determined by the n.m.r. method. Slow solvolysis does, however, take place in neutral but not in acidified solutions as determined by the appearance of dimethylammonium or pyridine signals. This solvolysis is *not* due to decomposition according to eq. 1 with subsequent fast solvolysis of dimethylcarbamoyl chloride, because of a kinetic argument which will be reviewed subsequently in the Discussion. The solvents in which I is stable are (dielectric constant in parentheses) *t*-butyl alcohol (11), ethanol (25), methanol (33), and water (80).

The adducts II–IV exhibit behavior similar to I in a selected number of solvents which include acetonitrile, chloroform, dimethyl sulfoxide, water, ethanol, and methanol. The ring proton signals of II–IV are shifted downfield considerably compared to their corresponding pyridinium halides.

Infrared Spectra. Confirming evidence that I decomposes according to eq. 1 in acetonitrile was attained by an infrared study of the dissolution of I into acetonitrile to give a $0.4\text{ }M$ solution. Immediately upon dissolution, the spectrum of I resembles the solid state spectrum of I; *i.e.*, it has a strong carbonyl absorption at 1753 cm.^{-1} and a strong ring band at 1623 cm.^{-1} . Within 1 hr., a new carbonyl band at 1745 cm.^{-1} appears with noticeable intensity at the expense of the 1753 cm.^{-1} band, and the pyridinium band at

1623 cm.^{-1} is partially replaced by the strong 1578 cm.^{-1} pyridine band. After 1 day at room temperature the reaction is complete.

Of some interest are the frequencies of the carbonyl band in I, II, III, and dimethylcarbamoyl chloride, which occur at 1753 , 1757 , 1750 , and 1745 cm.^{-1} , respectively. These results are similar to those of Cook⁴ who found that the acetylpyridinium carbonyl band (1804 cm.^{-1}) is not much displaced from the acetyl chloride carbonyl band (1801 cm.^{-1}), in spite of the much stronger electron-withdrawing substituent on the carbonyl carbon of the former compound than on the carbonyl carbon of the latter.

Ultraviolet Study. In Fig. 2 is a plot of the absorbance, A (corrected for the solvent and dimethylcarbamoyl chloride absorbances), of an aged acetonitrile

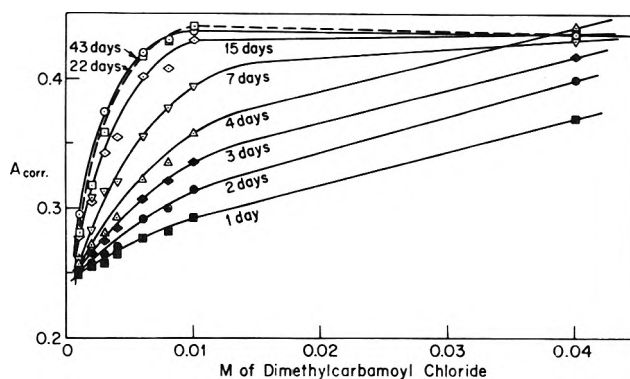


Figure 2. Absorbance at 2550 \AA . (corrected for dimethylcarbamoyl chloride and solvent absorbances) of aged acetonitrile solutions of dimethylcarbamoylpicolinium chloride (III) ($0.888 \times 10^{-4}\text{ }M$), containing varying added concentrations of dimethylcarbamoyl chloride, as a function of the time after which dimethylcarbamoyl chloride was added.

solution of dimethylcarbamoylpicolinium chloride (III) containing a constant formal concentration of III, C_F , to which various concentrations of dimethylcarbamoyl chloride, C_D , have been added. With increasing time and dimethylcarbamoyl chloride concentration, A increases. The rapid increase at low concentration of dimethylcarbamoyl chloride and its leveling off at higher concentrations indicates that an equilibrium situation involving dimethylcarbamoyl chloride is present and that the absorption coefficient for III is greater than that for 4-picoline at 2550 \AA . A plot of $\log(A_\infty - A_t)$ vs. time, where A_∞ is the 43-day absorbance reading and A_t is the absorbance at any time at constant C_D , gives a linear (pseudo) first-order kinetic plot, the slope of which is dependent upon the dimethyl-

(4) D. Cook, *Can. J. Chem.*, **40**, 2362 (1962).

carbamoyl chloride concentration. A plot of k_{obsd} , the pseudo-first-order kinetic constants, vs. the dimethylcarbamoyl chloride concentration yields a straight line indicating that the rate of appearance of III is given by eq. 2.

$$\frac{d[\text{III}]}{dt} = k_{-1}[\text{4-picoline}][\text{dimethylcarbamoyl chloride}] \quad (2)$$

The value of k_{-1} obtained from the plot is $0.638 \text{ M}^{-1} \text{ hr.}^{-1}$. This kinetic treatment is justifiable because the dimethylcarbamoyl chloride concentration is 45–113 times greater than the formal concentration of adduct, and therefore the back reaction is negligible compared to the forward reaction in the initial part of the reaction.

The equilibrium constant K_d for the decomposition of III may be obtained from the above data at constant formal concentration, C_F , but varying dimethylcarbamoyl chloride concentration C_D . We shall hereafter call this procedure method I. The K_d value is given by eq. 3 where C_A and C_P are the adduct and picoline concentrations.

$$K_d = \frac{C_P C_D}{C_A C_{C_1}} = \frac{(C_F - C_A) C_D}{(C_A)^2} \quad (3)$$

Solving eq. 3 for C_A gives

$$C_A = -C_D + \frac{(C_D^2 + 4C_D C_F K_d)^{1/2}}{2K_d} \quad (4)$$

The observed absorbance, after correction for solvent and dimethylcarbamoyl chloride is

$$\begin{aligned} A_{\text{obsd}} &= C_A \epsilon_A + C_P \epsilon_P \\ &= C_A (\epsilon_A - \epsilon_P) + C_F \epsilon_P \end{aligned} \quad (5)$$

A plot of A_{obsd} vs. C_A as calculated by eq. 4 for varying values of K_d gives a family of curves. A straight line according to eq. 5 will be obtained if the correct K_d value was chosen in calculating C_A . The intercept of this line should be $\epsilon_P C_F$ and the slope should be $(\epsilon_A - \epsilon_P)$. The K_d value which gave the best fit to eq. 5 is 20 ± 5 in one experiment and 30 ± 10 in another.

A plot of A vs. C_F for fresh solutions of III is time dependent (Fig. 3), indicating that decomposition of III is taking place. A plot of $\Delta/(\epsilon_A - \epsilon_P)$ vs. C_F^2 where Δ is the absorbance difference between 3 and 48 hr. yields a straight line with a slope of $19.7 \text{ M}^{-1} \text{ hr.}^{-1}$. This shows that the rate of decomposition of III depends upon the square of its concentration.

$$\frac{\Delta}{\epsilon_A - \epsilon_P} = \frac{-d[\text{III}]}{dt} = k_1 C_F^2 \quad (6)$$

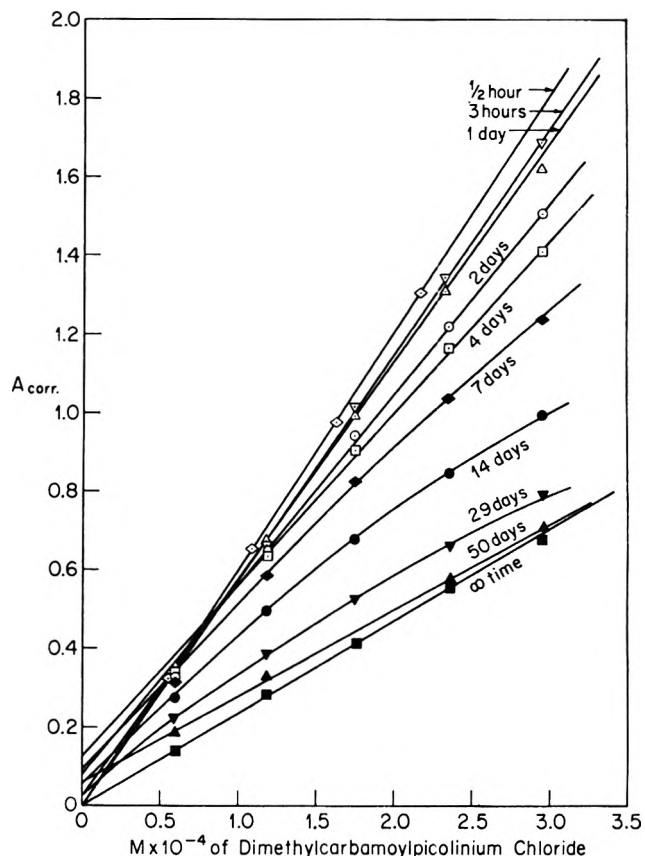


Figure 3. Absorbance at 2550 Å. (corrected for solvent absorbance) of acetonitrile solutions containing varying formal concentrations of dimethylcarbamoylpicolinium chloride (III) as a function of the time after initial preparation.

A second-order rate plot is obtained by plotting $1/C_A = (\epsilon_A - \epsilon_P)/(A_{\text{obs}} - C_F \epsilon_P)$ at any C_F value vs. time. The second-order rate constants, k_1 , are not C_F independent; there is a slight increase in k_1 as C_F decreases from 2.96×10^{-4} to $0.59 \times 10^{-4} \text{ M}$. The value of k_1 obtained from five second-order plots is $19.8 \pm 2.9 \text{ M}^{-1} \text{ hr.}^{-1}$, in good agreement with k_1 obtained from the incremental plot according to eq. 6. The method of obtaining k_1 is not completely justified because of the reversibility of the reaction. However, since k_1 is about 25 times greater than k_{-1} as estimated from the K_d values obtained by method I, the slopes of the kinetic plots obtained before the reaction has proceeded far should give reasonable values for k_1 . The ratio of k_1/k_{-1} gives 30.8 using the k_1 value from the incremental plot and gives 31.1 ± 4.5 using the k_1 value from all the second-order kinetic plots. These values of k_1/k_{-1} are in good agreement with the K_d values obtained by method I.

The K_d values can also be obtained from the infinity time Beer's law plots (method II). The slope of A_{obsd}

vs. C_F after the solution has been allowed to come to complete equilibrium should be $(\epsilon_A + \sqrt{K_d \epsilon_P}) / (\sqrt{K_d} + 1)$. Taking ϵ_A as the zero-time Beer's law slope and measuring ϵ_P separately, one can determine the value of K_d by solving the expression for the infinity time Beer's law slope. Such a solution for III yields a value of 19.3 in one experiment and 28.8 in the other experiment which is in good agreement with those values obtained by method I.

Similar studies were carried out for adduct II. A summary of the results are in Table I.

Table I: K_d Determination by Methods I and II

Compound	III	III	II
λ , Å.	2550	2550	2675
ϵ_P^a	1650	1650	3035
ϵ_A^b = slope of zero-time Beer's law plot	6000	6000	5240
$(\epsilon_A + K_d^{1/2} \epsilon_P) / (K_d^{1/2} + 1)$ = ∞ -time Beer's law slope	2457	2333	3433
K_d from ∞ -time Beer's law slope (method II)	19.3	28.8	20.6
K_d from best fit of eq. 5 (method I)	20 ± 5	30 ± 10	30 ± 5

^a ϵ_A is the absorption coefficient for the dimethylcarbamoylpyridinium compound. ^b ϵ_P is the absorption coefficient for the pyridine.

It must be borne in mind that in order to compare the ultraviolet results with the infrared and n.m.r. results, much higher concentrations ($\sim 0.5 M$) were used in the latter studies than in the former studies (10^{-3} – $10^{-4} M$). Since the decomposition rate is proportional to the square of the concentration, the complete decomposition of the adducts took place in a few hours in the latter studies compared to several weeks in the former studies.

Conductivity Behavior. Conductivity studies clearly indicate that no decomposition of I takes place in water; I behaves as a strong electrolyte in water, giving a linear, time-independent (over several days) Λ vs. $(M)^{1/2}$ plot over a concentration range of 0–0.04 M . The slope of this plot at 25° is 102, in reasonable accord with the expected slope of 87.1 calculated according to the Onsager–Fuoss equation.⁵

In acetonitrile, on the other hand, the conductivity behavior shown in Fig. 4 is time dependent; as would be expected from a slow rate of attainment of equilibrium at 25°. The conductivity curve obtained from the measurement of solutions of I in acetonitrile ca. 30 min. after preparation is a typical strong electrolyte curve. The conductivity curve obtained from the

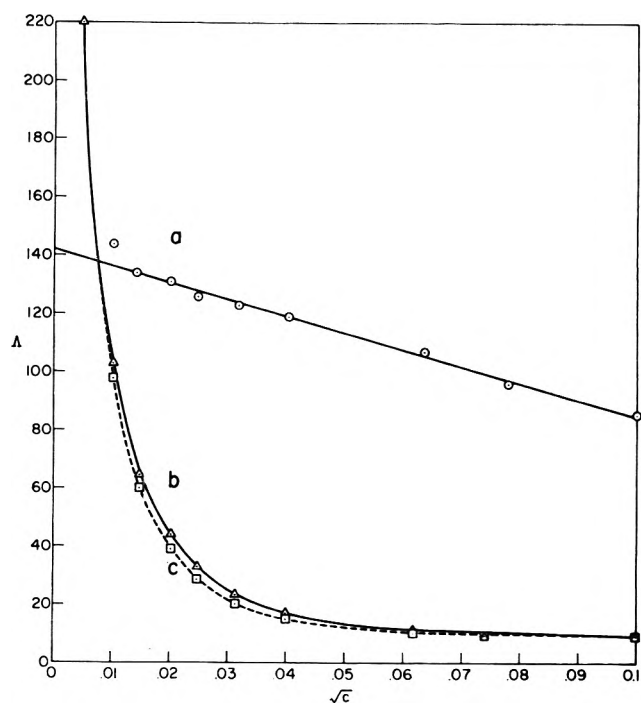


Figure 4. Equivalent conductance Λ vs. $(M)^{1/2}$ of 1-(N,N-dimethylcarbamyl)pyridinium chloride in acetonitrile at 25°: (a) data taken approximately 0.5 hr. after the solutions were prepared; (b) solid line, same solutions as (a), but data taken 3 days after initial preparation; (c) dashed line, same solutions as (a), but data taken 4 days after initial preparation.

same solutions measured 3 days after preparation is a typical weak electrolyte curve. The adduct, I, then is gradually converted to nonelectrolyte products according to eq. 1.

Discussion

From n.m.r., infrared, conductivity, and ultraviolet data all evidence points to the decomposition of carbamoylpyridinium chlorides in acetonitrile and other nonhydroxylic solvents, regardless of the dielectric solvents. This behavior is markedly different from the behavior of acylpyridinium chlorides⁶ which do not decompose in nonhydroxylic solvents and which react very rapidly with hydroxylic solvents. Furthermore, 2,6-lutidine and 2,4,6-collidine (but not 2,6-dimethoxy-pyridine) form derivatives with acetyl chloride. Dimethylcarbamoyl chloride will not form derivatives with any of the above bases.

There exists kinetic evidence that the dimethylcarbamoylpyridinium compounds do not decompose in water according to eq. 1. Dimethylcarbamoyl chlo-

(5) H. S. Harned and B. B. Owen, "The Physical Chemistry of Electrolyte Solutions," 2nd Ed., Reinhold Publishing Corp., New York, N. Y., 1950, p. 127.

(6) S. L. Johnson, unpublished results.

ride hydrolyzes in water at a rate independent of added strong nucleophilic reagents.⁷ However, carbamoylated products derived from these nucleophiles may be isolated from the reaction mixture. Therefore, the rate-controlling and product-controlling steps are separate and a two-step ionization mechanism prevails. By the principle of microscopic reversibility, then, the rate of *formation* of dimethylcarbamoyl chloride from a precursor such as I would involve the highly reactive intermediate ion $(\text{CH}_3)_2\text{NCO}^+$ and Cl^- in the slow step. However, this highly reactive ion would be expected to have low discrimination and to react with the solvent as it is formed. In support of this, large excesses of chloride ion added to aqueous solutions of I do not increase its rate of decomposition⁶ as would be expected for decomposition according to eq. 1.

The position of equilibrium of I in nonhydroxylic solvents compared to hydroxylic solvents is related to the increased energy level of halide ions in nonhydrogen-bonding solvents, *i.e.*, to the increased "hardness"⁸ of the halide ions when solvation possibilities are absent. Halide ions are known to be more nucleophilic in nonhydrogen-bonding solvents.⁹ The re-

moval of hydrogen-bonding interactions reverses the usual order of nucleophilicity of the halide ions from $\text{I}^- > \text{Br}^- > \text{Cl}^- > \text{F}^-$ in hydroxylic solvents to $\text{Cl}^- > \text{Br}^- > \text{I}^-$ in acetone¹⁰ and in dimethylformamide.¹¹ These strong hydrogen-bonding interactions of halide ions can be measured spectroscopically.¹² It therefore appears that the large solvent effect upon the equilibrium in eq. 1 is related to the large solvent effect upon the relative nucleophilicities of pyridine *vs.* the chloride ion to the dimethylcarbamoylium moiety in hydroxylic as compared to nonhydroxylic solvents.

Acknowledgment. This investigation was supported in part by Public Health Service Grant G.M. 118-34-01 from the National Institutes of Health.

(7) H. K. Hall, *J. Am. Chem. Soc.*, **77**, 5993 (1955).

(8) R. G. Pearson, *ibid.*, **85**, 3533 (1963).

(9) J. F. Bunnett, *Ann. Rev. Phys. Chem.*, **14**, 271 (1963).

(10) S. Winstein, L. G. Savedoff, S. Smith, I. D. R. Stevens, and J. S. Gall, *Tetrahedron Letters*, **9**, 24 (1960).

(11) W. Weaver and J. D. Hutchinson, *J. Am. Chem. Soc.*, **86**, 261 (1964).

(12) P. von R. Schleyer and A. Allerhand, *ibid.*, **85**, 1283 (1963).

The Effect of Substitution on the Ionization Potentials of Free Radicals and Molecules. VII. Theoretical Rationalization for Differing Correlations Found for Bond Dissociation Energies with Ionization Potentials and Electron Affinities of Organic or Inorganic Radicals

by Joyce J. Kaufman

Research Institute for Advanced Studies, Martin Company, Baltimore, Maryland 21212 (Received April 27, 1964)

The discrepancy previously noted in the relations of bond dissociation energies into organic radicals (linear with ionization potentials) or inorganic radicals (linear with the differences between ionization potential and electron affinity) has been explained on both semiempirical and theoretical grounds. In the author's earlier research on δ_K values (the effect of substitution on ionization potentials of free radicals), it was shown possible to place electronegativities, χ , of organic radicals correctly in the experimentally observed order solely on the basis of their ionization potentials. Since $\chi \sim (I + E)/2$, this dependence of χ on I alone indicated that E was small relative to I and/or varied comparatively little for a series of organic radicals. On the contrary, E for a series of inorganic radicals where the central atom can be as diverse as N, O, F, Cl, Br, etc., will vary over a much wider range. A theoretical rationalization based on Mulliken's "magic formula" gives further confirmation to the justification for the differing relationship between dissociation energies and ionization potentials or ionization potentials minus electron affinities for organic and inorganic radicals.

In a recent article by Neale,¹ bond dissociation energies $D(X-Y)$ were shown to be linearly related to the ionization potentials (I) of hydrogen and organic radicals were shown to bear a similar relation only to the differences ($I - E$) of ionization potentials and electron affinities of inorganic radicals.

$$D(X-Y) = \lambda \epsilon_X \epsilon_Y$$

where $\epsilon_A = 0.115(I_A - E_A) - 0.07$ (inorganic radicals); $\epsilon_B = 0.115I_B - 0.07$ (organic radicals (conjugated to a π e system)); and $\epsilon_C = 0.056I_C + 0.55$ (organic radicals (remaining radicals)). An explanation for this discrepancy seems straightforward in view of a relationship noted several years ago by this author in a study of the effect of substitution on the ionization

potentials of free radicals and molecules²—namely that it was possible to place $\cdot CXYZ$ radicals in correct order of electronegativity (as determined from experimentally observed chemical reactions) on the basis of the $\cdot CXYZ$ ionization potentials alone, without appeal to their electron affinities. IP and E of substituted organic radicals are inversely dependent on the substituent groups; groups which tend to lower IP almost invariably tend to raise the E and *vice versa*. Therefore, the conclusion was drawn that although electronegativities are proportional to $(I + E)/2$,

(1) R. S. Neale, *J. Phys. Chem.*, **68**, 143 (1964).

(2) J. J. Kaufman and W. S. Koski, *J. Am. Chem. Soc.*, **82**, 3262 (1960).

the E values of organic radicals are small compared to their IP values, much less affected on an absolute scale by a change in substituent group than IP values, and thus remain essentially constant for a large series of organic radicals.

This conclusion can be verified by comparison of the IP values of organic radicals which range from 7.76 e.v. for the $\text{CH}_2\text{C}_6\text{H}_5$ radical, 8.78 e.v. for the C_2H_5 radical, and 9.85, e.v. for the CH_3 radical while the E values of these radicals range only from 1.0 to 1.13 e.v. The E values are only approximately 10% of the IP values and, furthermore, the changes in the E values on substitution are only 10% of the changes in IP values and in absolute value are only about 1% of the IP value itself. On the contrary, for a series of inorganic radicals where the directly attached atoms are as diverse as Na, K, Li, N, O, F, S, Cl, Br, etc., there is a much larger difference in E (0.4 to 4 e.v.) and, hence, the effective electronegativities of the inorganic radicals will be dependent on both I and E .

In addition, there is an excellent theoretical rationalization for the differing correlations between bond dissociation energies into organic and inorganic radicals based on Mulliken's "magic formula" and its relation to the structure of bond energies.³ For a diatomic molecule $\text{X}-\text{Y}$, the bond dissociation energy, D , if an electron pair bond is broken, is given approximately by

$$D = AIS/(1 + S) \quad (1)$$

where A is an empirically determined factor, S is the overlap integral, and I is the ionization energy. Extending this approximate relation to dissociation of a polyatomic molecule R_1-R_2 into two radicals $\text{R}_1\cdot$ and $\text{R}_2\cdot$ the dissociation energy $D(\text{R}_1-\text{R}_2)$ would still be proportional to the ionization potentials of the two radicals and to the overlap integral S between the electrons in the bond between the attached atoms. In the case of the polyatomic molecules R_1-H or R_1-R_2 where $\text{R}_1\cdot$ and $\text{R}_2\cdot$ are organic radicals (especially saturated organic radicals), S will be virtually a constant varying very little between different radicals. Therefore, the bond dissociation energy $D(\text{R}_1-\text{R}_2)$ would be expected to bear a linear relation to the radical ionization potentials with a slope of $AS/(1 + S)$.

A more exact formula given in ref. 3 for energy of atomization (D_0) of a polyatomic molecule is

$$D_0 = \sum_{\text{bonds}} X_{ij} - \frac{1}{2} \sum_{\text{nonbonded pairs}} Y_{kl} + \frac{1}{2} \sum K_{mn} - P + RE \quad (2)$$

where $X_{ij} = A_p S_{ij} \bar{I}_{ij} / (1 + S_{ij})$ (\bar{I}_{ij} is here a suitably averaged ionization potential), $Y_{kl} = \nu A_k S_{kl}^2 \bar{I}_{kl}$

(these terms refer to nonbonded repulsions), K_{mn} are exchange integrals, P are the valence state promotional energies, and RE denotes resonance energies.

Exchange terms (X , Y , K) are the main terms responsible for bonding. In the case of interest here, namely the dissociation of a polyatomic molecule R_1-R_2 into two radicals $\text{R}_1\cdot$ and $\text{R}_2\cdot$, the equation for D would simplify. There would be only one term for X_{ij} (the one corresponding to the bond between R_1 and R_2) and the sums over the nonbonded pairs would only extend between nonbonded pairs in the two different radicals. The differing relations found in ref. 1 seem to follow quite naturally from an examination of eq. 2.

For dissociation into two organic radicals, the X_{ij} term is proportional to \bar{I} since $AS/(1 + S)$ remains virtually constant. The Y_{kl} and K_{mn} terms (which refer only to terms between the different R's, are smaller than the X_{ij} terms and fall off rapidly with increasing distance) do not change drastically between different R's and in addition Y_{kl} is itself proportional to \bar{I} . P is almost constant for similar organic radicals since it refers to the difference in valence state promotion energies from sp^3 (for saturated radicals) or sp^2 or sp to $\text{sp}^2\pi$ or $\text{sp}\pi\pi$ or $\text{s}\pi^2\pi$. For any specified series of organic radicals the loss in resonance energy will also be fairly constant. It is this last term, RE , which undoubtedly contributes to the changes in slopes and intercepts noted if the unpaired electron is on a carbon atom and conjugated to a π -electron system (type B, ref. 1) or if the organic radicals are of the remaining type (type C, ref. 1). In the author's earlier studies on δ_K values^{2,4,5} (a new set of constants which quantitatively measure the effect of substitution on ionization potentials of free radicals) it was noted that the ionization potentials of $\cdot\text{CY}_3$ radicals were governed by both the inductive and resonance effects of Y. If Y was a substituent capable of donating π -electrons to the half-empty π -orbital of $\cdot\text{CY}_3$ or to the empty π -orbital of CY_3 , the electron-donating resonance ability of Y could completely outweigh a very electron-attracting inductive effect. An illustrative example is the $\cdot\text{CF}_3$ radical whose ionization potential, 10.10 e.v., is only a little higher than that of the $\cdot\text{CH}_3$ radical, 9.95 e.v. The inductive effect of F would be expected to raise greatly (2.1 e.v.)⁵ the ionization potential of $\cdot\text{CF}_3$ relative to $\cdot\text{CH}_3$. Since the ionization potential of $\cdot\text{CF}_3$ is only a little higher than that of $\cdot\text{CH}_3$ it was concluded that a $\text{p}\pi\text{-p}\pi$ resonance

(3) R. S. Mulliken, *J. Phys. Chem.*, **56**, 295 (1952).

(4) J. J. Kaufman, *J. Am. Chem. Soc.*, **85**, 1576 (1963).

(5) J. J. Kaufman, *J. Chem. Phys.*, **37**, 759 (1932).

effect of F must be operative acting in the direction reverse to that of the inductive effect. This $p\pi$ - $p\pi$ electron-donating resonance effect can be operative only in the $\cdot\text{CY}_3$ radical or CY_3^+ ion; it cannot be operative when the $\cdot\text{CY}_3$ radical is attached by an electron pair bond to a $\cdot\text{CZ}_3$ radical or to an H atom. This accounts for the scatter noted in the graph of the relation between I and D for type B organic radicals. There are differing amounts of $p\pi$ - $p\pi$ resonance electron interaction between the various Y groups and the $p\pi$ -orbital of the central C atom.

For dissociation into two inorganic radicals examination of the physical origin of the terms in eq. 2 indicates why there is no longer the same linear relationship between D and \bar{I} but rather between D and $(I - E)$. A discussion of the factor $(I - E)$ in terms of the expansion of an atom and its positive (corresponding to ionization) and negative (corresponding to electron addition) ions in terms of spectroscopic term values makes it simpler to visualize conceptually the previous relationship.

As an example let us take an atom M ($s^2x^2y^2z$). The energies (ϵ) of M, M^+ , and M^- are as follows (where I are the core energies and J and K are the customary Coulomb and exchange integrals)

$$\begin{aligned} M(s^2x^2y^2z)\epsilon &= 2I_s + 2I_x + 2I_y + I_z + J_{ss} + \\ &J_{xx} + J_{yy} + 4J_{sx} + 4J_{sy} + 2J_{sz} + 4J_{xy} + 2J_{xz} + \\ &2J_{yz} - 2K_{sx} - 2K_{sy} - K_{sz} - 2K_{xy} - K_{xz} - K_{yz} \end{aligned}$$

$$\begin{aligned} M^-(s^2x^2y^2z^2)\epsilon &= 2I_s + 2I_x + 2I_y + 2I_z + J_{ss} + \\ &J_{xx} + J_{yy} + J_{zz} + 4J_{sx} + 4J_{sy} + 4J_{sz} + \\ &4J_{xy} + 4J_{xz} + 4J_{yz} - 2K_{sx} - 2K_{sy} - \\ &2K_{sz} - 2K_{xy} - 2K_{xz} - 2K_{yz} \end{aligned}$$

$$\begin{aligned} M^+(s^2x^2y^2)\epsilon &= 2I_s + 2I_x + 2I_y + J_{ss} + J_{xx} + \\ &J_{yy} + 4J_{sx} + 4J_{sy} + 4J_{xy} - 2K_{sx} - 2K_{sy} - 2K_{xy} \end{aligned}$$

$$(\epsilon_M - \epsilon_{M^+}) = I = I_z + 2J_{sz} + 2J_{xz} + 2J_{yz} - K_{sz} - K_{xz} - K_{yz}$$

$$(\epsilon_M - \epsilon_M) = E = I_z - J_{zz} + 2J_{sz} + 2J_{xz} + 2J_{yz} - K_{sz} - K_{xz} - K_{yz}$$

$$\therefore I - E = J_{zz}$$

To a rather accurate approximation

$$K_{ab} \sim 1/2S^2(J_{aa} + J_{bb})$$

$$\begin{aligned} \therefore D &\sim (I - E) + \text{const.} \sim J_{aa} + \\ &\text{const.} \sim J_{ab} - K_{ab} + \text{const.} \end{aligned}$$

(in eq. 2 K_{mn} had been arbitrarily multiplied by -1 in the original reference before inserting it into eq. 2).

For inorganic radicals E is not always as small relative to I as it is for organic radicals and the E values differ over fairly broad ranges (0.4 to 4.0 e.v.). Hence, the E terms are not negligible and they undoubtedly reflect the presence of the K_{mn} terms in the "magic formula." The P and RE terms in the general formula also would be expected to vary more with a diverse series of inorganic radicals than with a series of closely related $\cdot\text{CY}_3$ radicals.

It is encouraging that this proffered explanation for the differing behavior between D and I or $(I - E)$ for organic or inorganic radicals is based on previously noted empirical and theoretical relationships and is consistent with both of them.

Acknowledgment. This research was supported by the Air Force Office of Scientific Research of the Office of Aerospace Research, under Contract No. AF49(638)-1220.

Equation of State and Related Properties of Polymer and Oligomer Liquids¹

by V. S. Nanda² and Robert Simha

Department of Chemistry, University of Southern California,
Los Angeles, California 90007 (Received May 4, 1964)

The cell theory has been applied earlier to chain liquids by using a modified harmonic approximation to the cell potential. We discuss here the equation of state and related thermodynamic expressions derived by means of the square well approximation which forms the basis of a fairly successful description of the liquid and glassy states in terms of the free volume concept. The theoretical equation of state is in satisfactory agreement with the experimental volume-temperature data for reduced volumes up to 1.2, as compared with 1.1, obtained earlier. In terms of temperature, this extends, for polystyrene as an example, the range of the theory by about 150°. The variation of the cohesive energy density with temperature and molecular weight is also satisfactorily described. This permits a prediction of the cohesive energy density for a high polymer from the enthalpy of vaporization of a single oligomer without having recourse to swelling data. With respect to the internal pressure, however, no agreement between theory and experiment is found. Nevertheless, it is possible to establish the validity of the principle of corresponding states at low pressures with respect to such properties as the internal pressure and the compressibility.

I. Introduction

Recently the principle of corresponding states has been shown to be valid³ for several series of oligomer and high polymer liquids at atmospheric pressure. A comparison of the experimental reduced volume-reduced temperature curves with the theoretical equation of state for chain liquids, obtained by Prigogine and co-workers^{4,5} as a generalization of the Lennard-Jones-Devonshire (LJD) cell theory for monomer liquids, showed good agreement with experiment for $1 \leq \bar{V} \leq 1.1$ for the cases considered. Actually, Prigogine, *et al.*,⁴ replace the LJD cell potential by a "modified" harmonic one as an approximation. In the study of monomer liquids, however, it is convenient to adopt the square well potential as an adequate approximation to the cell potential. This approximation, moreover, provides a basis for the so-called free volume theories, which have been quite successful in the description of the liquid and glassy states. In a later publication Prigogine, *et al.*,⁵ in the deduction of the law of corresponding states for polymer liquids, also consider the square well potential as one of the simple alternatives to the actual cell potential. It appeared to us worthwhile to make a comparison of

the experimental results with the equation of state using this approximation in order to see whether a theoretical representation over a wider range of temperatures is possible. Finally, we have determined the theoretical values of the internal pressure (p_i) and the cohesive energy density (*c.e.d.*) and compared these values with the experimental results reported by Gee and co-workers^{6,7} and some additional data available in the literature. While the theory seems adequate for the description of the variation of *c.e.d.* with molecular weight for a polymer series, and even for explaining variations of *c.e.d.* with temperature for a given member, no accurate representation of p_i

(1) This work was supported by Research Grant NsG-343 of the National Aeronautics and Space Administration to the University of Southern California.

(2) On leave of absence from the Physics Department, University of Delhi, Delhi 6, India.

(3) R. Simha and A. J. Havlik, *J. Am. Chem. Soc.*, **86**, 197 (1964).

(4) I. Prigogine, N. Trappeniers, and V. Mathot, *Discussions Faraday Soc.*, **15**, 93 (1953).

(5) I. Prigogine, A. Bellemans, and C. Naar-Colin, *J. Chem. Phys.*, **26**, 75 (1957).

(6) G. Allen, G. Gee, and G. J. Wilson, *Polymer*, **1**, 456 (1960).

(7) G. Allen, G. Gee, D. Mangaraj, D. Sims, and G. J. Wilson, *ibid.*, **1**, 467 (1960).

is obtained. Nevertheless our investigation validates the principle of corresponding states with respect to internal pressure and compressibility.

II. Theoretical Expressions

The relevant theoretical expressions on the basis of cell theory, using the square well potential, can be obtained from the corresponding partition function⁵

$$Z = A_r^N g(N) (a - \sigma)^{3cN} \exp \left\{ \frac{-Nqz\epsilon^*}{(2kT) [A(v^*/v)^4 - B(v^*/v)^2]} \right\} \quad (1)$$

where A_r is a geometrical constant, $g(N)$ a combinatorial factor, $3c$ the total number of volume-dependent degrees of freedom per chain, and qz the corresponding number of intermolecular nearest neighbors on the quasi-lattice. If the coordination number z is set equal to 12, then $A = 1.011$ and $B = 2.409$. The other symbols have their usual meaning as in the cell theory of monomer liquids. However, the quantities ϵ^* , v^* , and v refer here to the chain segment. The Helmholtz free energy F is given by

$$\begin{aligned} F &= -kT \ln Z \\ &= -NkT [\ln A_r + 1/N \ln g(N)] - \\ &\quad 3cNkT \ln (a - \sigma) + Nqz\epsilon^*/2 [A(v^*/v)^4 - \\ &\quad B(v^*/v)^2] \quad (2) \end{aligned}$$

Making use of the thermodynamic relation $p = -(\partial F/\partial V)_T$, we get, after some simplification, the reduced equation of state in the form

$$\bar{p}\bar{V}/\bar{T} = (1 - 2^{-1/6}\bar{V}^{-1/6})^{-1} + \frac{(2\bar{V}^{-2}/\bar{T})(A\bar{V}^{-2} - B/2)}{\bar{T}} \quad (3)$$

where (as in ref. 3) $\bar{p} = pV^*/(qz\epsilon^*)$, $\bar{V} = V/V^*$, $\bar{T} = Tck/(qz\epsilon^*)$ while V and V^* represent the volume and the characteristic volume parameter per chain, respectively.

The internal energy U is derived from eq. 2 as

$$\begin{aligned} U &= -T^2 [\partial(F/T)/\partial T]_V \\ &= (Nqz\epsilon^*/2)(A\bar{V}^{-4} - B\bar{V}^{-2}) \quad (4) \end{aligned}$$

whence

$$p_i = T(\partial p/\partial T)_V - p = (\partial U/\partial V)_T = \frac{Nqz\epsilon^*/(V^*\bar{V})}{2} (B\bar{V}^{-2} - 2A\bar{V}^{-4}) \quad (5)$$

Noting that for a "prisoner," motion is free inside the well, we have

$$c.e.d. = \frac{Nqz\epsilon^*/(V^*\bar{V})}{2} (B\bar{V}^{-2} - A\bar{V}^{-4}) \quad (6)$$

This result should be compared with the corresponding

Prigogine expression.⁴ From eq. 5 and 6 we obtain the ratio

$$\gamma = p_i/c.e.d. = 2(B - 2A\bar{V}^{-2})/(B - A\bar{V}^{-2}) \quad (7)$$

It may be noted from eq. 5, 6, and 7 that p_i , *c.e.d.*, and γ depend explicitly on \bar{V} only.

III. Equation of State

In Fig. 1 $\log \bar{V}$ is plotted against $\log \bar{T}$ with the aid of the equation of state (3) as curve 1. Here, because of the extremely small magnitude of \bar{p} , the left-hand side has been taken to be effectively zero. Since there is no independent knowledge of the parameters in eq. 3, the experimental reduced volume-reduced temperature representation for *n*-paraffins, already reported in ref. 3, was shifted parallel to the two axes to give the best coincidence with the theoretical curve. This procedure naturally defines a new reduced coordinate system for the experimental data. The connection between the old and the new reduced variables is represented by the relations

$$\log [\bar{V}_{\text{new}}/\bar{V}_{\text{old}}] = 0.0072; \log [\bar{T}_{\text{new}}/\bar{T}_{\text{old}}] = 0.1045 \quad (8)$$

In order to show graphically the more extensive agreement with experiment obtained with the square well potential, the previous theoretical curve was shifted to the same extent along the $\log \bar{V}$ and $\log \bar{T}$ axes as the experimental data, according to eq. 8. It may be noted that we have extended here the experimental region on the low temperature side by including a point for supercooled propane.⁸ This appeared of interest especially because the two superposed theoretical curves begin to show deviations just below the experimental range covered in ref. 3. The present theoretical equation provides a satisfactory representation of the low temperature region as well. The observed range of validity is now approximately $1 \leq \bar{V} \leq 1.20$, compared with the previous range $1 \leq \bar{V} \leq 1.10$.

The experimental volume-temperature results for other polymer series, *viz.*, polystyrene, polydimethylsiloxane, and perfluorinated polymethylenes, are exhibited as inserts in Fig. 1, along with the relevant region of the theoretical curve, labeled, respectively, as 2, 3, 4. The location of the experimental points has been determined in all cases by using the shift factors defined by eq. 8 for the *n*-paraffin series. This procedure is in accord with the law of corresponding states. It should also be pointed out here that the shifting of the experimental data to the new coordi-

(8) American Petroleum Institute, "Selected Values of Physical and Thermodynamic Properties of Hydrocarbons and Related Compounds," Carnegie Press, Pittsburgh, Pa., 1953.

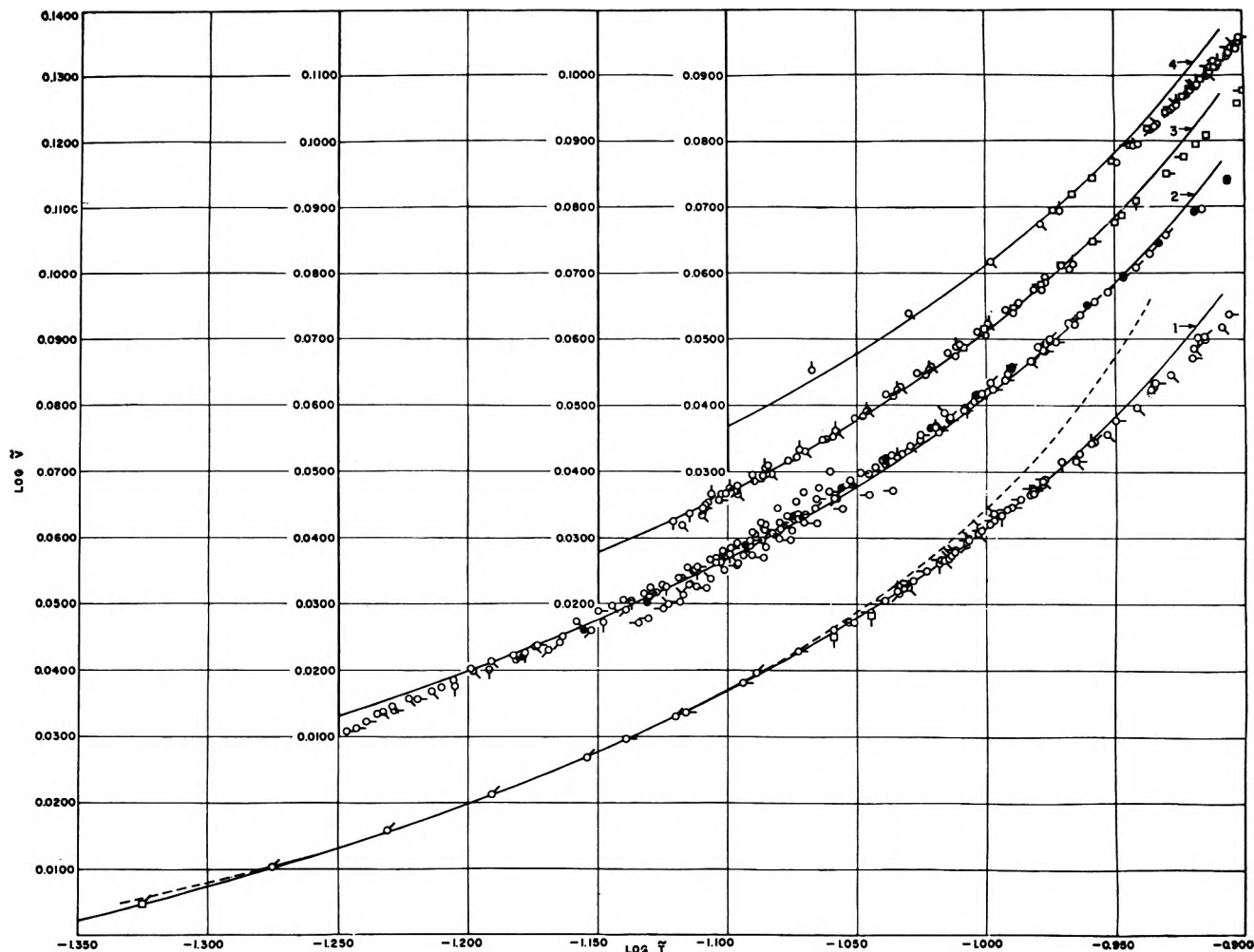


Figure 1. Reduced volume as a function of reduced temperature; solid curves 1, 2, 3, 4, theoretical equation of state, eq. 3; dashed curve, previous work (ref. 3); points show experimental data. For original sources see ref. 3. Curve 1: δ , methane; σ , propane; σ' , propane^s (supercooled); ω , heptane; α , eicosane; φ , eicosane^s (supercooled); φ , tritetracontane; ρ , tetrahexacontane; ∞ , polyethylene; ν , polymethylene. Curve 2: δ , monostyrene; σ , α , φ , ρ , polystyrene of average degree of polymerization 2, 3, 4.1, 8.1, 24.6; ∞ and ν , high polymer. Curve 3: δ , ethylene glycol; σ , diethylene glycol; ω , triethylene glycol; α , heptaethylene glycol; φ , ρ , high molecular weight polyoxyethylene; σ , octamethyltrisiloxane; ω , decamethyltetrasiloxane; φ , dodecamethylpentasiloxane; ω , tetradecamethylhexasiloxane. Curve 4: δ , f-methane, σ , f-propane; ω , f-n-butane; α , f-n-pentane; φ , f-n-hexane; ρ , f-n-heptane; ∞ , f-n-octane; ν , f-n-nonane; ω , f-n-decane; φ , (PNF₂)₃; α , (PNF₂)₄.

nate system changes, of course, the scale factors \bar{T}/T and \bar{V}/V for the infinite polymer, but does not affect the numerical values of the quantities A , B , C , and D , as defined in ref. 3, eq. 6. These quantities depend upon the ratios of the scale factors for the infinite and a given finite polymer and are therefore not altered by the transformations carried out here.

Making use of the cohesive energy density for the polymer, the quantity ϵ^* in the temperature parameter $qz\epsilon^*/(ck)$ can be separated. Except for the slight difference in the *c.e.d.* expression employed here, the procedure followed is the same as described earlier.³

In the case of polydimethylsiloxane, the temperature for the reported *c.e.d.*, 25°, is well within the theoretical range, eq. 3, and no extrapolation as in ref. 3 is required. The results are shown in Table I where the previous values are also given for comparison. The characteristic energy parameter ϵ^* has a lower value than before,³ as might have been anticipated by a comparison of the earlier and the present *c.e.d.* expressions. Since the value of the ratio T/\bar{T} is appreciably lower in the present case, the quantity $(3c/n)$ is larger than previously. However, the relative position of the four polymers is the same.

Table I: Characteristic Parameters for High Polymers

Substance	T/\bar{T}		$N_A V^*/n$, cc./mole		$(\epsilon^*s/n) \times 10^{15}$, ergs/molecule			$3c/n$		
	(a) ^a	(b) ^b	(a)	(b)	(ϵ)			(a)		
					swell.	<i>c.e.d.</i>	(b)	swell.	<i>c.e.d.</i>	(b)
Polymethylene	4247	5402	15.50	15.75	105	116	118	0.54	0.59	0.48
Polystyrene	5071	6450	47.24	48.00	397	436	443	1.70	1.87	1.50
Polydimethylsiloxane	3148	4004	33.27	33.80	234	199	276	1.61	1.38	1.50
Polytetrafluoroethylene	3766	4791	22.05	22.40	91	139 ^c	104	0.53	0.81 ^c	0.48

^a This work; *c.e.d.* values of ϵ^*s/n and $3c/n$ follow from section IV. ^b Ref. 3. ^c See Note Added in Proof.

IV. Cohesive Energy Density and Internal Pressure

Gee and co-workers^{6,7} have obtained the internal pressure for certain polymers and oligomers by direct measurement of the temperature coefficient of the pressure. They have also quoted values of p_i and *c.e.d.* for several substances from the literature and drawn some conclusions from the study of the ratio $\gamma = p_i/c.e.d.$ at 20°. They find $\gamma \approx 1$ for *n*-paraffins and other liquids of low polarity.

We have evaluated here γ for *n*-paraffins by means of eq. 7. The calculations are compared with the experimental values in Table II. Considering the approximate nature of the theory, the agreement is not unsatisfactory. However, the systematically opposite variation of γ with molecular weight suggests the need of further investigation. The approximate theory, by the very nature of the starting assumptions, might be unsuitable for the description of one or both of the quantities occurring in the ratio γ .

Table II: Comparison of Experimental⁶ and Theoretical Values of the Ratio $\gamma = p_i/c.e.d.$ for *n*-Paraffins at 20°

Substance	Theoretical	Experimental
Octane	1.15	1.11
Nonane	1.11	1.11
Decane	1.09	1.12
Dodecane	1.05	1.12
Tetradecane	1.03	1.15, 1.11
Polymethylene	0.81	1.11 ^a

^a With extrapolated p_i and *c.e.d.*

In order to examine this point, we have plotted in Fig. 2 and 3 $c.e.d./(qz\epsilon^*/V^*)$ and $p_i/(qz\epsilon^*/V^*)$ vs. \bar{V} with the aid of eq. 5 and 6, respectively. The experimental results for the *n*-paraffins are also shown for both these quantities,^{6,7} with data from additional sources.^{8,9} The value of ϵ^* , required for determining the position of the experimental data on the graph, was

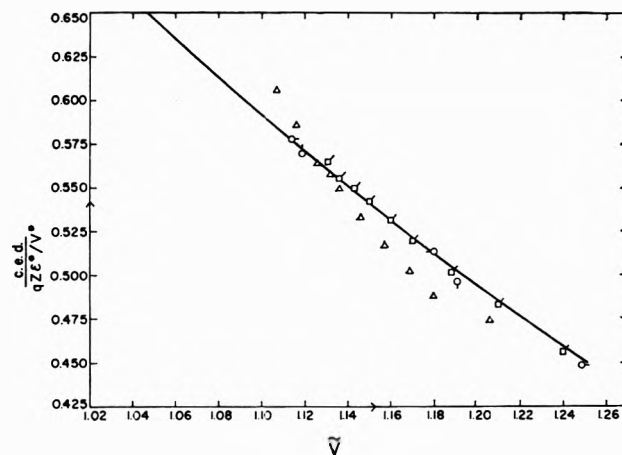


Figure 2. Cohesive energy density as a function of reduced volume. Solid curve, theory eq. 6; σ , *n*-paraffins at 20° (left to right C₁₄ to C₆); ϕ , *n*-octane; ∞ , *n*-nonane; δ , *n*-octadecane; ∞ , *n*-eicosane all at 25°; ∞ , *n*-propane⁹ at -56.7°; Δ , monostyrene, from left to right at 0, 10, 20, 25, 30, 40, 50, and 60°.¹⁰

established by equating the theoretical expression and the experimental value of *c.e.d.* for decane. This requires a computation of \bar{T} corresponding to 20° and of the corresponding \bar{V} from eq. 3 or Fig. 1. It is noted that the variation of *c.e.d.* with \bar{V} through molecular weight is represented quite well by the theory. On the other hand, no such agreement results for p_i . In fact, the trend of the theoretical curve and the experimental data is so widely different that the possibility of better representation of internal pressures through an alternative choice of $(qz\epsilon^*/V^*)$, *e.g.*, by comparison of p_i 's, can be easily ruled out.

The satisfactory representation of the *c.e.d.* values by theory over a range of molecular weights allows us

(9) "Handbook of Chemistry and Physics," Chemical Rubber Publishing Co., Cleveland, Ohio, 1962.

(10) R. H. Boundy and R. F. Boyer, Ed., American Chemical Society Monograph No. 115, Reinhold Publishing Corp., New York, N. Y., 1952, p. 55.

to predict with confidence values for the infinite polymer from the corresponding ones for oligomers. This has been done for polymethylene and polystyrene (for polydimethylsiloxane an alternative procedure will be described in the sequel). The \bar{V} are determined at 20° and the values of the ratio $c.e.d./(qz\epsilon^*/V^*)$ are read from Fig. 2 for the infinite polymer and an oligomer whose \bar{V} lies below 1.20, the high temperature limit of the theory. Making use of the experimentally known $c.e.d.$ for the oligomer, one finds by this procedure the quantity (ϵ^*/v^*) for the corresponding polymer series (for values refer to Table I). For the styrene series, enthalpies of vaporization are available for the monomer only (see below). The numerical values of ϵ/V^* are not necessarily identical for monostyrene and a styrene unit in the chain, and the result in Table I is subject to this uncertainty. The $c.e.d.$ for polymethylene and polystyrene are found to be 68 and 91 cal./cc., respectively. These values are substantially higher than those obtained from swelling data,⁷ viz., 62 and 83. The procedure for determining $c.e.d.$ from swelling in a suitable solvent involves some doubtful assumptions. Gee, *et al.*,⁷ have discussed this matter at length, and therefore we shall not pursue it here. It may however be noted that the theoretical value of 68 for $c.e.d.$ of polymethylene compares favorably with the 70 ± 1 obtained by Gee and co-workers through the extrapolation of the experimental data for the oligomers. Moreover, if we combine the internal pressure results of Gee, *et al.*, for polymethylene and polystyrene with the theoretical estimates of $c.e.d.$ given here, the ratio γ is found, respectively, to be 1.17 and 1.18. This lends further support to their expectation that $\gamma = 1.1 \pm 0.1$ for the nonpolar polymers, as is actually observed for the oligomers.

To examine the adequacy of eq. 6 further, we compare experimental and theoretical values of the $c.e.d.$ as a function of temperature. Fig. 2 shows the values for monostyrene, as obtained from the enthalpies of vaporization and the densities between 0 and 60°. We also show here the $c.e.d.$ values for some n -paraffins covering a wide range of temperature from -57 to 25°. The agreement, particularly in the case of n -paraffins, is quite satisfactory. For monostyrene, the enthalpies were derived from the vapor pressures. The small deviations from the theoretical curve cannot be ascribed to the nonideality of the vapor since appropriate corrections were made by means of an empirical equation of state.

The present theory, however, fails to provide an adequate representation for the internal pressures, as may be observed from Fig. 3. Nevertheless, the re-

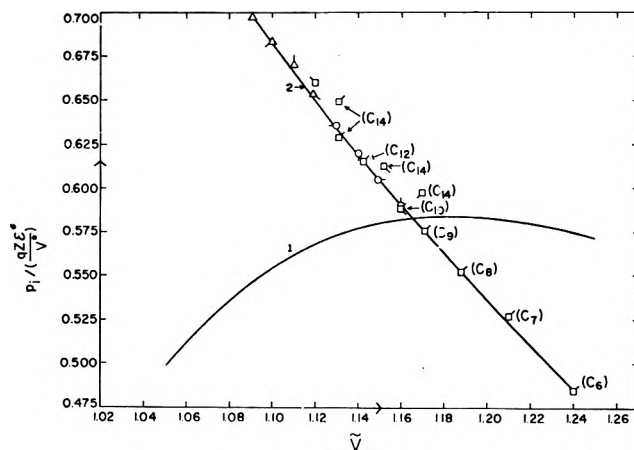


Figure 3. Internal pressure as a function of reduced volume. Curve 1, theory, eq. 7; curve 2, experimental; n -paraffins:^{6,7} \square , at 10°; σ , at 20°; α , at 40°; polydimethylsiloxane:⁷ Δ , at -20°; \blacktriangle , at -10°; \triangle , at 0°; \blacklozenge , at 10°; \circ , at 20°; \diamond , at 30°; \ominus , at 40°; δ , at 50°.

duced experimental values, over a wide range of temperature and molecular weight, for n -paraffins and polydimethylsiloxane conform to the principle of corresponding states, at least for the small external pressures considered here. The representation of polydimethylsiloxane in Fig. 3 requires the numerical value of the ratio (ϵ^*/v^*) . This was obtained independently of the swelling data by comparing the experimental values of p_i at -20° with the value of the ordinate in Fig. 3, curve 2, at the corresponding \bar{V} , as obtained from Fig. 1 (curve 3) or eq. 3. Curve 2 in Fig. 3, on the other hand, had been constructed on the basis of n -paraffin data alone. From the value of $qz\epsilon^*/V^*$ we obtain with the aid of Fig. 2 at 20° a $c.e.d.$ equal to 49 cal./cc. This is smaller than the 58 cal./cc. from swelling measurements.⁷ However, if we accept the present value of $c.e.d.$, then using the reported p_i of 57 cal./cc., the ratio γ is found to be 1.16.

We note that the failure of the theory in respect to the internal pressure extends to both the dependence on molecular weight and on temperature. Whereas experimentally p_i increases monotonically with decreasing \bar{V} , the trend should be opposite on the low temperature side according to theory. Now for small pressures p

$$p_i = (\partial U/\partial V)_T \simeq T(\partial S/\partial V)_T \quad (9)$$

The results of Fig. 3 thus imply that $(\partial S/\partial V)_T$ is in error, since the V - T relation is correctly reproduced by the theory in the major portion of the temperature range under discussion. The cell theory does not give a contribution to $(\partial S/\partial V)_T$ due to the communal entropy and hence the theoretical p_i would be less

than is observed at low temperatures. Beyond the crossover point in Fig. 3, on the other hand, the theoretical equation of state itself starts to deviate increasingly from experiment (see Fig. 1) and so no discussion of the deviations is possible here.

Finally we make use of the thermodynamic relation

$$\kappa = \alpha / (\partial p / \partial T)_V \simeq \alpha T / p_i = (\bar{\alpha} \bar{T} / \bar{p}_i) (V^* / qz\epsilon^*) \quad (10)$$

with $\bar{\alpha} = (1/\bar{V})(\partial \bar{V} / \partial \bar{T})_p$; $\bar{p}_i = \bar{T}(\partial \bar{p} / \partial \bar{T})_{\bar{V}}$. Here κ represents the isothermal compressibility. Since it has been verified earlier³ that $\bar{\alpha}$ is a function of the reduced variables only and we have found here the same to be true for \bar{p}_i , it follows that the quantity $\bar{\kappa} = \kappa(qz\epsilon^*/V^*)$ is also a function of the reduced variables.

The principle of corresponding states with respect to compressibility is thus validated for low pressures. Hijmans¹¹ has published earlier the equivalent for the *n*-paraffin series.^{12,13}

(11) J. Hijmans, *Physica*, **27**, 433 (1961).

(12) NOTE ADDED IN PROOF.—A consideration of the enthalpies of vaporization at higher reduced temperatures establishes the validity of the principle of corresponding states in respect to the *c.e.d.* for $\bar{V} = 1.6$. The (negative) deviations from eq. 6 increase monotonically with \bar{V} but do not exceed 10%. Similarly, it is possible to extend the \bar{p}_i - \bar{V} function (Fig. 2) to $\bar{V} = 1.34$. From the enthalpy of vaporization of *n*-C₁₀F₁₆, one derives, on the basis of these results for the *c.e.d.* of a (hypothetical) amorphous polytetrafluoroethylene at 25°, a value of 55 cal./cc. as compared with Scott's¹³ value of 36 cal./cc. used earlier. The resulting changes in the characteristic parameters for the polymer are indicated in Table I.

(13) R. L. Scott, *J. Am. Chem. Soc.*, **70**, 4090 (1948).

Carbon-13 Proton Spin Coupling Constants in Heteroaromatic Molecules

by Kazuo Tori and Toshio Nakagawa

Shionogi Research Laboratory, Shionogi and Co., Ltd., Fukushima-ku Osaka, Japan (Received May 19, 1964)

A number of absolute C¹³ proton spin coupling constants, J_{CH} , in heteroaromatic molecules were determined to examine the effects of the ring size and heteroatoms in the ring and to test Malinowski's additivity rule. In addition, an attempt to correlate the proton-proton spin coupling constant between *ortho* ring protons with the mean J_{CH} related to these two protons is presented. These points are discussed in comparison with aliphatic molecules.

Recently, several workers reported that the C¹³ proton spin coupling constant, J_{CH} , reflects the *s*-character of the carbon atomic orbital participating in the C-H bond.¹⁻³ When an electronegative atom is bonded to the carbon of this bond, the percentage of *s*-character increases,⁴ and accordingly an increasing J_{CH} value is observed.¹⁻³ Substituent effects on J_{CH} were found to be additive for both tetrahedrally⁵ and trigonally⁶ hybridized carbon and were interpreted theoretically.^{7,8} Further, the J_{CH} value was pointed out to increase with a decrease of the ring size of cycloalkanes¹ (sp³-CH) and cycloalkenes⁹⁻¹¹ (sp²-CH),

which corresponds to an increase of the percentage of *s*-character of the C-H bond. In the course of proton

(1) N. Muller and D. E. Pritchard, *J. Chem. Phys.*, **31**, 768, 1471 (1959).

(2) N. Muller, *ibid.*, **36**, 359 (1962).

(3) J. N. Shoolery, *ibid.*, **31**, 1427 (1959).

(4) H. A. Bent, *Chem. Rev.*, **61**, 275 (1961).

(5) E. R. Malinowski, *J. Am. Chem. Soc.*, **83**, 4479 (1961).

(6) E. R. Malinowski, L. Z. Pollara, and J. P. Larmann, *ibid.*, **84**, 2649 (1962).

(7) H. S. Gutowsky and C. S. Juan, *ibid.*, **84**, 307 (1962); C. S. Juan and H. S. Gutowsky, *J. Chem. Phys.*, **37**, 2198 (1962).

magnetic resonance studies of heteroaromatic compounds, we have had much occasion to examine the C^{13} satellites in their spectra. It is believed to be worthwhile to add some further results to Malinowski's work⁶ in this field. Thus, in this paper we present many absolute values of J_{CH} in heteroaromatic compounds to discuss the effects of the ring size and heteroatoms in the ring upon J_{CH} , and, in addition, to attempt to correlate the proton-proton spin coupling constant between adjacent CH groups, $J_{HH(ortho)}$, with the mean J_{CH} value of these C-H bonds in comparison with aliphatic molecules.

Experimental

All the spectra were recorded on a Varian A-60 spectrometer, the calibration of which was checked according to Tiers and Hotchkiss.¹² Absolute values of J_{CH} were obtained from C^{13} satellites (in natural abundance), most of which were analyzed by the first-order approximation. For the measurements of spectra, neat samples were used for liquid substances and crystalline samples were dissolved by adding a small amount of solvents. Most of the commercially available samples were used without further purification. The effect of impurities on J_{CH} was reported to be negligibly small.¹ Accuracies of the measurements are about ± 1 c.p.s. for J_{CH} and about ± 0.3 c.p.s. for J_{HH} . In most cases, our observed values were in excellent agreement with those reported in the literature (see Table I).

Results and Discussion

Table I shows the observed and reported coupling constants of heteroaromatic compounds, together with those of some other compounds for comparison. The magnitude of J_{CH} in aromatic compounds varies greatly depending on the ring size and heteroatoms in the ring in a manner similar to the case of aliphatic compounds, as expected. Malinowski's additivity rule^{5,6} is readily realized for six-membered nitrogen heterocycles as can be seen from the sixth column of Table I, when we used the following ζ' values for aromatic systems to calculate J_{CH} values according to Malinowski and co-workers⁶: $\zeta'_{CC} = 77.5$ c.p.s., $\zeta'_{CN} = 84.5$ c.p.s., and $\zeta'_{NC} = 103.0$ c.p.s. For the calculation of J_{CH} values of the other heterocycles examined, we used the following equations: ζ'' (for five-membered ring) = ζ' (for six-membered ring) + 2.5 c.p.s., $\zeta''_{CO} = 95.0$ c.p.s., $\zeta''_{OC} = \zeta''_{ON} = 121.5$ c.p.s., $\zeta''_{CS} = 82.5$ c.p.s., $\zeta''_{SC} = 101.0$ c.p.s., and $\zeta''_{NO} = 103.0$ c.p.s. Thus good correspondence between observed and calculated J_{CH} values is obtained. Although substituent effects on J_{CH} of aromatic com-

pounds are not very apparent at present, those of one methyl group produce somewhat reduced J_{CH} values in the ring (about 1-3 c.p.s.),¹³ whereas a nitro group is known to exert fairly marked effects to increase J_{CH} values (see the datum on trinitrobenzene in Table I). Further, N-oxidation usually gives larger J_{CH} values.

On the other hand, the magnitude of $J_{HH(ortho)}$ in aromatic compounds and $J_{HH(cis)}$ in aliphatic double bonds have frequently been reported to decrease with a decrease of the ring size^{10,11,14-16} and also to be correlated with electronegativity of substituted groups.^{17,18} Recently, Matsuura and Goto¹⁹ suggested that the small magnitude of J_{H_6, H_7} (1.7 c.p.s.) in pteridine may result from the two adjacent nitrogen atoms in the

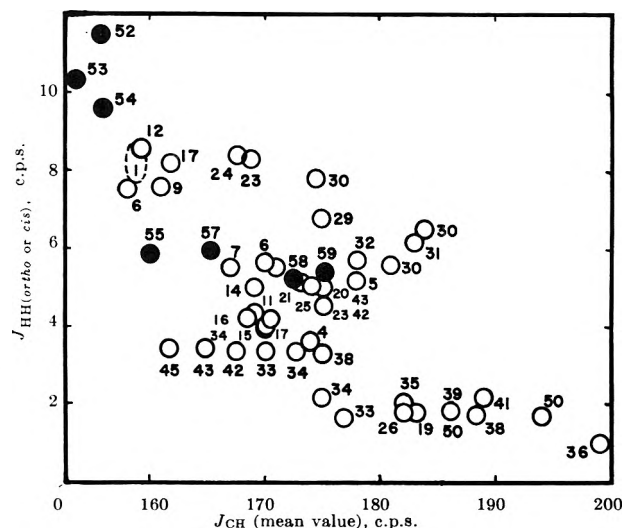


Figure 1. Plots of J_{CH} vs. $J_{HH(ortho \text{ or } cis)}$. O, aromatic molecule; ●, aliphatic double bond. Numbers show the compounds listed in Table I.

(8) Exceptions of this additivity rule were also pointed out; see N. Muller and P. I. Rose, *J. Am. Chem. Soc.*, **84**, 3973 (1962), and S. G. Frankiss, *J. Phys. Chem.*, **67**, 752 (1963).

(9) G. L. Cross, *Proc. Chem. Soc.*, 152 (1962).

(10) P. Laszlo and P. von R. Schleyer, *J. Am. Chem. Soc.*, **85**, 2017 (1963); **86**, 1171 (1964).

(11) K. Tori, R. Muneyuki, and H. Tanida, *Can. J. Chem.*, **41**, 3142 (1963).

(12) G. V. D. Tiers and D. R. Hotchkiss, *J. Phys. Chem.*, **66**, 560 (1962).

(13) Refer to C. T. Mathis and J. H. Goldstein, *ibid.*, **68**, 571 (1964).

(14) O. L. Chapman, *J. Am. Chem. Soc.*, **85**, 2014 (1963).

(15) G. V. Smith and H. Kriloff, *ibid.*, **85**, 2016 (1963).

(16) J. A. Pople, W. G. Schneider, and H. J. Bernstein, "High-Resolution Nuclear Magnetic Resonance," McGraw-Hill Book Co., New York, N. Y., 1959, Chapter 11.

(17) For example, see T. Schaefer, *Can. J. Chem.*, **40**, 1 (1962).

(18) P. F. Cox, *J. Am. Chem. Soc.*, **85**, 380 (1963).

(19) S. Matsuura and T. Goto, *J. Chem. Soc.*, 1773 (1963).

Table I: C^{13} Proton Spin Coupling Constants, J_{CH} , and Proton-Proton Spin Coupling Constants, J_{HH} , in Various Molecules

No.	Compound	Position	Solvent	J_{CH} , c.p.s.		$J_{HH(ortho)}$, c.p.s.
				Obsd.	Calcd.	
1	Benzene		Neat	158.9 (158.7 \pm 0.8) ⁱ (159) ^{i,j} (158) ⁶	155.0	(\sim 8) ¹⁶
2	Mesitylene	2, 4, 6	Neat	153.5 (154) ¹ (160) ²		
		Methyl		125.5 (126) ¹ (128) ²		
3	1,3,5-Trinitrobenzene	2, 4, 6	Acetone	(179.5 \pm 1.5) ¹		
4	Azulene	1, 3	Neat	(165) ^k	160.0	$(J_{1,2} = 3.5$ or 3.8) ¹⁶
		2		(183) ^{k,l}	160.0	
		4, 8		(158) ^k		$(J_{4,5} = 10.0)$ ¹⁶
		5, 7		(161) ^k		$(J_{5,6} = 10.0)$ ¹⁶
		6		(158) ^k		
5	Acenaphthalene	1, 2	Neat	(178 \pm 1) ¹⁰		$(J_{1,2} = 5.2)$ ¹⁰
6	Pyridine	2, 6	Neat	(179) ⁶	180.5	$(J_{2,3} = 5.5)$ ¹⁶
		3, 5		(163) ⁶	162.0	$(J_{3,4} = 7.5)$ ¹⁶
		4		(152) ⁶	155.0	
7	4-Methylpyridine ^a	2, 6	Neat	174.4		$J_{2,3} = 5.5$
		3, 5		160.0		
		Methyl		126.7		
8	3,5-Dimethylpyridine ^a	2, 6		176.0		
		4		156.6		
		Methyl		126.8		
9	2,6-Dimethylpyridine ^a	3, 5	Neat	131.0		$J_{3,4} = 7.6$
		4		131.5		
		Methyl		126.5		
10	2,4,6-Trimethylpyridine	3, 5	Neat	(158.5 \pm 0.7) ¹		
		Methyl		(126.4 \pm 0.5) ¹		
11	Quinoline ^b	2	Neat	177.5	180.5	$J_{2,3} = 4.2$ (4.2 \pm 0.1) ^m
		3		163.5	162.0	
		4			155.0	
12	2-Methylquinoline ^c	3	Neat	160.8		$J_{3,4} = 8.5$
		4		156.8		
		8		160.0		
		Methyl		126.8		
13	3-Methylquinoline ^c	2	Neat	174.8		
		Methyl		127.3		
14	4-Methylquinoline ^c	2	Neat	175.0		$J_{2,3} = 4.5$
		3		162.0		
		8		160.0		
		Methyl		127.4		
15	6-Methylquinoline ^c	2	Neat	176.6		$J_{2,3} = 4.1$ $J_{7,8} = 8.2$
		3		164.0		
		8		160.0		
		Methyl		126.8		

Table I (Continued)

No.	Compound	Position	Solvent	$J_{\text{CH, c.p.s.}}$		$J_{\text{HH(ortho), c.p.s.}}$	
				Obsd.	Calcd.		
16	7-Methylquinoline ^c	2	Neat	175.6		$J_{2,3} = 4.2$	
		8		159.8			
		Methyl		126.5			
17	8-Methylquinoline ^c	2	Neat	176.8		$J_{2,3} = 4.0$ (4.4) ⁿ (4.1) ⁿ	
		3		162.4			
		4		162.0			
		Methyl		127.0			$J_{3,4} = 8.2$ (8.3) ⁿ (7.9) ^p
18	Isoquinoline ^b	1	Neat	176.0	180.5	$J_{3,4} = 5.6$ (6.0) ^{tt}	
		3		176.0			
		4		163.0			
19	Pyrazine ^c	2, 3, 5, 6	CDCl ₃	(183.0) ^d	180.5	$(J_{2,3} = 1.8)^d$	
20	Pyrimidine ^c	2	Neat	206.0	206.0	$J_{4,5} = 5.0$ (5.0) ^p	
		4, 6		(206.0) ^p			
				182.0			
		5		(181.8) ^p			180.5
		168.0	169.0	(168.0) ^p			
21	4-Methylpyrimidine ^c	2	Neat	200.5		$J_{5,6} = 5.1$ (5.1) ^p	
		5		165.8			
		6		180.0			
		Methyl		127.4			
22	5-Methylpyrimidine ^c	2	Neat	202.5			
		4, 6		179.8			
		Methyl		127.0			
23	Pyridazine ^a	3, 6	Neat	(181.5) ^d	180.5	$(J_{3,4} = 4.5)^d$ $(J_{4,5} = 8.4)^d$	
		4, 5		(168.5) ^d			
24	3-Methylpyridazine ^d	4, 5	Neat	~167.5		$(J_{4,5} = 8.6)^d$ $(J_{5,6} = 4.7)^d$	
		6		181.0			
		Methyl		128.0			
25	4-Methylpyridazine ^d	3, 6	Neat	~181.5		$(J_{5,6} = 5.0)^d$	
		5		167.0			
		Methyl		128.5			
26	Quinoxaline ^c	2, 3	CDCl ₃	181.8	180.5	$J_{2,3} = 1.8$	
27	Phthalazine ^c	1, 4	CDCl ₃	181	180.5		
28	s-Triazine ^a	2, 4, 6	CDCl ₃	207.7	206.0		
29	4-Methylpyridine N-oxide ^b	2, 6	D ₂ O	186.5		$J_{2,3} = 6.8$	
		3, 5		163.5			
		Methyl		128.4			
30	Pyridazine N-oxide ^f	3	D ₂ O	~186		$(J_{3,4} = 5.2)^f$ $(J_{4,5} = 7.8)^f$ $(J_{5,6} = 6.5)^f$	
		4		175			
		5		174			
		6		193.0			
31	4-Methylpyridazine N-oxide ^f	3	D ₂ O	186		$(J_{5,6} = 6.2)^f$	
		5		174.5			
		6		192			
		Methyl		129.5			

Table I (Continued)

No.	Compound	Position	Solvent	J_{CH} , c.p.s.		$J_{HH(ortho)}$, c.p.s.
				Obsd.	Calcd.	
32	5-Methylpyridazine N-oxide ^f	3	D ₂ O	184.5		$(J_{3,4} = 5.6)^f$
		4		172		
		6		193.5		
		Methyl		129.5		
33	Pyrrole ^c	2, 5	Acetone + D ₂ O	184.0	185.5	$J_{2,3} = 1.6$
		3, 4		169.8	167.0	$J_{3,4} = 3.4$
34	N-Methylpyrrole ^c	2, 5	Neat	182.0		$J_{2,3} = 2.2$
		3, 4		168.5		$J_{3,4} = 4.2$
		Methyl		137.5		
35	Pyrazole ^c	3, 5	D ₂ O	185.8	185.5	$J_{3,4} = 2.0$
		4		177.8	174.0	
36	Imidazole ^c	2	D ₂ O	207.8	211.0	$J_{4,5} \sim 1.0$
		4, 5		190.0	185.5	
37	1,2,4-Triazole ^c	3, 5	D ₂ O	211.0	211.0	
38	Furan	2, 5	Neat	(201.4) ^g	201.5	$(J_{2,3} = 1.75)^g$
		3, 4		(175.3) ^g	175.0	$(J_{3,4} = 3.3)^g$
39	2-Methylfuran ^h	3	Neat	172.4		$J_{3,5} = 3.3$
		4		172.8		$(3.4)^f$
		5		200.4		$J_{4,5} = 1.8$
		Methyl		126.4		$(1.9)^f$
40	2,5-Dimethylfuran ^h	3, 4	Neat	169.8		$J_{3,4} = 3.2$
		Methyl		127.3		
41	Benzofuran	2	Neat	201.8	201.5	$J_{2,3} = 2.2$
		3		176.6	175.0	
42	Thiophene ^c	2, 5	Neat	184.5	181.0	$(J_{2,3} = 4.7)^t$
		3, 4		(187.0) ^g		
				167.5	165.0	$(J_{3,4} = 3.35)^t$
43	2-Methylthiophene	3	Neat	(163.56) ¹³		$(J_{3,4} = 3.46)^{13}$
		4		(165.50) ¹³		$(J_{4,5} = 5.20)^{13}$
		5		(184.92) ¹³		
		Methyl		(128.26) ¹³		
44	3-Methylthiophene	2	Neat	(182.36) ¹³		$(J_{4,5} = 4.88)^{13}$
		4		(164.48) ¹³		
		5		(184.92) ¹³		
		Methyl		(127.10) ¹³		
45	2,5-Dimethylthiophene	3, 4	Neat	(161.24) ¹³		$(J_{3,4} = 3.46)^{13}$
		Methyl		(162.0) ^g (128.20) ¹³		
46	Oxazole	2			227.0	
		4			200.5	
		5			208.5	
47	4-Methyloxazole	2	Neat	(231) ^u		
		5		(209) ^u		
48	Thiazole	2			206.5	
		4			188.0	
		5			188.0	

Table I (Continued)

No.	Compound	Position	Solvent	J_{CH} , c.p.s.		$J_{HH(ortho)}$, c.p.s.
				Obsd.	Calcd.	
49	4-Methylthiazole	2	Neat	(209) ^u		
		5		(187) ^u		
50	Isoxazole ^A	3	Neat	188.0	185.5	$J_{3,4} = 1.7$
		4		184.3	182.0	$J_{4,5} = 1.7$
		5		203.3	201.5	
51	3,5-Dimethylisoxazole ^A	4	Neat	178.8		
		3-Methyl		128.3		
		5-Methyl		129.3		
						$J_{HH(cis)}$
52	Ethylene	Double bond	Neat	(156.2) ^o		(11.5) ^o
				(156.4) ^o		(11.7) ^o
53	Cyclooctene	Double bond	Neat	(153.5) ¹¹		(~10) ¹¹ (10.3) ¹⁶
54	Cyclohexene	Double bond	Neat	(155.5) ¹¹		(9.60 ± 0.10) ¹⁰
				(157 ± 2) ¹⁰		(8.8) ¹⁶
				(171) ¹		
55	Cyclopentene	Double bond	Neat	(160.5) ¹¹		(~5.8) ¹¹
				(160 ± 1) ¹⁰		(5.40 ± 0.10) ¹⁰ (5.1) ¹⁶
56	3,3-Dimethylcyclopropene	Double bond	Neat	(220 ± 1) ⁹		(0.5 ~ 1.5) ¹⁰
57	Norbornene	Double bond	CDCl ₃	(165.5) ¹¹		(6.0) ¹¹
				(174 ± 1) ¹⁰		(5.80 ± 0.10) ¹⁰
58	Norbornadiene	Double bond	Neat	(172.5) ¹¹		(5.2) ¹¹
				(168 ± 1) ¹⁰		(5.05 ± 0.10) ¹⁰
59	Benzonorbornadiene	Double bond	Neat	(175.5) ¹¹		(5.4) ¹¹

^o Kindly supplied by Dr. R. Konaka. ^b Kindly supplied by Dr. T. Kubota. ^c Commercially available. ^d K. Tori and M. Ogata, *Chem. Pharm. Bull.* (Tokyo), **12**, 272 (1964). ^e Kindly supplied by Prof. E. Hayashi. ^f Kindly supplied by Dr. M. Ogata; see M. Ogata and H. Kano, *Chem. Pharm. Bull.* (Tokyo), **11**, 29, 35 (1963), and K. Tori, M. Ogata, and H. Kano, *ibid.*, **11**, 235 (1963). ^g Kindly supplied by Prof. H. Bredereck. ^h Kindly supplied by Dr. S. Sumimoto. ⁱ H. M. Hutton, W. F. Reynolds, and T. Schaefer, *Can. J. Chem.*, **40**, 1758 (1962). ^j P. C. Lauterbur, *J. Am. Chem. Soc.*, **85**, 1838 (1963). ^k H. Spiesecke and W. G. Schneider, *Tetrahedron Letters*, **14**, 468 (1961). ^l An explanation for the fairly large value of $J_{C,H}$ is not apparent. ^m W. G. Paterson and G. Bigam, *Can. J. Chem.*, **41**, 1841 (1963). ⁿ L. W. Reeves and K. O. Strømme, *ibid.*, **39**, 2318 (1961). ^o F. A. L. Anet, *J. Chem. Phys.*, **32**, 1274 (1960). ^p G. S. Reddy, R. T. Hobgood, and J. H. Goldstein, *J. Am. Chem. Soc.*, **84**, 336 (1962). ^q G. S. Reddy and J. H. Goldstein, *ibid.*, **84**, 583 (1962). ^r G. S. Reddy and J. H. Goldstein, *J. Phys. Chem.*, **65**, 1539 (1961). ^s J. H. Goldstein and G. S. Reddy, *J. Chem. Phys.*, **36**, 2644 (1962). ^t D. M. Grant, R. C. Hirst, and H. S. Gutowsky, *ibid.*, **38**, 470 (1963). ^u P. Haake and W. B. Miller, *J. Am. Chem. Soc.*, **85**, 4044 (1963). ^v D. M. Graham and C. E. Holloway, *Can. J. Chem.*, **41**, 2114 (1963). ^w R. M. Lynden-Bell and N. Sheppard, *Proc. Roy. Soc. (London)*, **A269**, 385 (1962).

molecule. Similar small values of $J_{HH(ortho)}$ are also seen in Table I. Thus, expecting some relation between J_{CH} and $J_{HH(ortho)}$, both of which are sensitive to hybridization of the participating atomic orbitals, we plot $J_{HH(ortho)}$ values together with $J_{HH(cis)}$ values for comparison, against the mean values of the relating two J_{CH} values as shown in Fig. 1. Figure 1 shows a trend for the $J_{HH(ortho \text{ or } cis)}$ value to decrease with

increasing J_{CH} value, as expected, although marked deviation is shown by several aromatic N-oxides and thiophenes indicate a reverse relationship. Besides the σ -electronic state, the π -electronic state has been reported to affect J_{HH} ,^{18,20,21} and effects of bond order

(20) K. Takahashi, *Bull. Chem. Soc. Japan*, **35**, 1046 (1962).(21) H. M. McConnell, *J. Chem. Phys.*, **24**, 460, 760 (1956); *ibid.*, **30**, 126 (1959); *J. Mol. Spectry.*, **1**, 11 (1957).

have also been discussed for aromatic systems.^{21,22} These effects might bear some relation to the plots in Fig. 1. However, Fig. 1 can, at any rate, provide a useful relationship for predicting the magnitude of $J_{HH(\text{ortho or cis})}$ values in a molecule from the J_{CH} values observed or calculated.

Acknowledgments. We are greatly indebted to

Professor H. Brederick of Technischen Hochschule Stuttgart, Professor E. Hayashi of Shizuoka Pharmaceutical College, Drs. T. Kubota, S. Sumimoto, R. Konaka, and M. Ogata of this laboratory for supplying us with several samples used.

(22) N. Jonathan, S. Gordon, and B. P. Dailey, *J. Chem. Phys.*, **36**, 2443 (1962).

Shock Tube Study of the Acetylene-Oxygen Reaction¹

by R. F. Stubbeman and W. C. Gardiner, Jr.

Department of Chemistry, The University of Texas, Austin, Texas 78712 (Received May 21, 1964)

The reaction of acetylene with oxygen was studied over the temperature range 1500–2500°K. using shock tube techniques. Observations were made of ultraviolet and visible chemiluminescence, and of the hydroxyl radical by absorption spectroscopy. The ratio of oxygen to acetylene varied from 0.34 to 7.3. Previous findings about the appearance of the chemiluminescence were in general confirmed. Comparison of the temporal behavior of OH concentration and visible chemiluminescence showed that OH appearance was substantially delayed. Consequences of the phase relationship between OH and chemiluminescence are discussed with reference to current proposals for the mechanism of the branching chain reactions. Proposals are made for the origin of the chemiluminescence which are in agreement with conclusions from other studies.

Chemical kinetic investigations of the oxidation of acetylene have been undertaken using conventional methods for many years. Spectroscopic investigations of acetylene flames, in particular, have proved fruitful in providing information about some of the possible reaction pathways. Renewed interest in this reaction has arisen with the continued development of the low-pressure flame structure and shock tube techniques at high temperatures and the discharge-flow technique at low temperatures. The combined resources of the several experimental approaches now being pursued promise that an understanding of the major elementary reactions involved, at least in the stoichiometric or lean flames at low pressure, may be found in the near future. We report here a study of the acetylene-

oxygen reaction in shock waves in the temperature range 1500–2500°K. using visible and ultraviolet emission, and OH absorption spectroscopy.

Experimental

The shock tube and associated apparatus were of conventional design. The shock tube itself was constructed of 5×10 -cm. extruded aluminum tubing. It was pumped to about 1μ before each experiment and had a leak and outgassing rate of 0.5μ hr. The principal observation station consisted of a pair of flush-mounted fused quartz plates on opposite 5-cm. sides and was located 5.2 m. from the diaphragm.

(1) Presented at the 147th National Meeting of the American Chemical Society, Philadelphia, Pa., April 5–10, 1964.

An auxiliary observation station, located at the same position in the tube, consisted of a Lucite plug flush-mounted in the center of the 10-cm. side of the tube. Nine deposited platinum heat-transfer gauges for shock velocity measurement were located at 10-cm. intervals on either side of the observation station, five of them upstream and four downstream. The gauge signals were recorded on a raster-sweep oscilloscope together with crystal-controlled time marker signals. The driver section was made from a 1.8-m. length of 15-cm. steel tubing, with a smoothly convergent nozzle converting the driver stream to a rectangular cross section at the diaphragm (0.0015–0.003-in. cellulose nitrate film). Hydrogen was used as driver gas.

Conditions in the shocked gas were obtained by interpolation on graphs of density ratio, temperature, etc., vs. shock velocity constructed from conventional one-dimensional shock wave calculations done with a digital computer. Thermochemical quantities from "JANAF Tables" (Dow Chemical Company, Midland, Mich.) were used, thus assuming vibrational equilibration in the unreacted gas. Since the concentration of reactive mixture was always small compared to the concentration of argon, no substantial temperature error would be involved if the vibrational equilibration was incomplete before onset of chemical reaction. Temperatures quoted in this paper are all no-reaction shock temperatures.

A monochromator (Beckman DU-R) was used to isolate spectral regions of light transmitted through or emitted from the experimental gas in the shock tube at the principal observation station. For emission measurements, defining slits 1 mm. wide were placed directly in front of the quartz windows, and the optical system was carefully aligned to be normal to the gas flow. For absorption measurements of OH concentration, a bismuth atomic line at 3067 Å. was excited by a 2450-Mc. discharge in argon containing a trace of bismuth trichloride.² The light passed through defining slits on both sides of the shock tube and was reflected by a concave mirror into the monochromator. The light intensity at the exit slit of the monochromator was measured by a 1P28 photomultiplier. For OH absorption measurements, the anode current of the 1P28 was matched to cable impedance by a cathode follower and recorded on an oscilloscope. For some measurements of emission, the 1P28 anode current was amplified and converted to logarithmic scale by a Kane log voltage compressor before oscilloscope recording. The over-all frequency response of the detection systems could be increased to over 1 Mc.; however, capacitive loading was used to limit the fre-

quency response to about 200 kc. in most experiments. Light emission was measured at the auxiliary observation station through glass-type and interference filters (in most of the experiments reported here a Baird-Atomic Type B1, peak 4320 Å., band width at half-peak 65 Å., peak transmission 50%) by means of another 1P28 photomultiplier. It was ascertained by observation of the same quantity (4320 Å. emission) at both stations that the alignment of the two stations corresponded to resolution of better than 1 μsec. of laboratory time. A Tektronix Type 502 or 535A, with CA or M preamplifier, was used together with oscilloscope cameras for data recording.

Experimental mixtures were prepared in a conventional vacuum system. Composition was determined by careful manometric measurements. Homogeneity of experimental mixtures was obtained by allowing several days to elapse before withdrawal of experimental gas. Argon, oxygen, and acetylene were taken from commercial cylinders. Cursory procedures were used to remove acetone from the acetylene, and the other gases were used with no purification. Mass spectrometric analyses showed no impurities. Pressures in the shock tube before each run were measured with a Dubrovin gauge. The starting pressure in virtually all experiments reported here was 5 mm.

Table I lists the composition of the experimental gases. Argon was used as inert diluent in each case.

Table I: Composition of Experimental Mixtures

Mixture no.	% C ₂ H ₂	% O ₂	[O ₂] [C ₂ H ₂]
8	0.734	5.583	7.60
9	1.326	1.940	1.46
20	1.000	1.530	1.53
21	1.000	3.235	3.235
23	1.000	7.270	7.27
24	1.000	0.342	0.34

Results

The experimental quantities reported here are induction times for appearance of OH, induction times for visible emission near 4320 Å. to rise to 0.1 of its maximum peak height, peak heights for this visible radiation, and time constants for the exponential rise of this visible radiation. Semiquantitative measurements were made of peak heights for ultraviolet radiation in the spectral region 2000–2200 Å., and induction times for this radiation were estimated by comparison with simultaneously recorded visible emission.

(2) T. Carrington, *J. Chem. Phys.*, **31**, 1418 (1959).

A sample experimental record of visible emission and OH absorption is shown in Fig. 1. The pulse form of the visible emission is in accord with the results of Hand and Kistiakowsky.³ In this record the anode current from the photomultiplier tube monitoring the intensity of the emission through the auxiliary observation station (lower trace) was converted to logarithmic

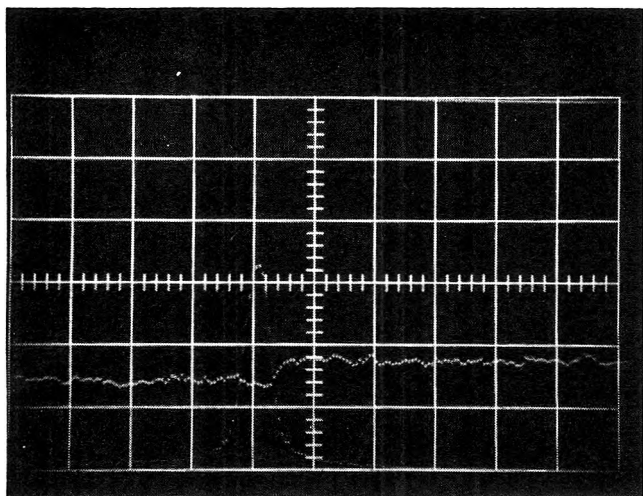


Figure 1. Sample oscillogram. Mixture 21, $[O_2]:[C_2H_2] = 3.2:1$, starting pressure 5 mm., shock temperature 1820°K., sweep rate 50 $\mu\text{sec./cm.}$ Shock arrival is after 158 $\mu\text{sec.}$ Upper trace is absorption of 3067 Å radiation by OH; lower trace is blue emission intensity converted to logarithmic scale.

scale, and the portion of the intensity increase that is actually exponential is recorded as a straight line. The curved portion of the increase before the exponential rise is still on the logarithmic portion of the response curve of the amplifier. The curvature may be due in part to a nonexponential character of the initial intensity rise, but is in any case largely attributable to scattered light. The OH absorption (upper trace) appears after the visible emission has peaked and has returned almost to the baseline. This effect, and some suggested consequences, have been reported in a preliminary communication.⁴ The constant OH concentration may or may not correspond to the equilibrium value; under the experimental conditions used, termolecular processes would be too slow to show observable effects.

Experiments were made under similar conditions with the monochromator photomultiplier at higher sensitivity and the bismuth lamp off. Small pulses of OH emission, coincident with the visible emission pulses, were observed. Since the photomultiplier signal due to OH emission was small compared to the signal due to the onset of OH absorption, it would

have only a small effect, if any, on the measured time of appearance of OH.

Other experiments were made with the monochromator set at various wave lengths in the region 2000–2200 Å., the upper wave length end of the fourth positive system of CO, which has been suggested^{5a} as the source of the ultraviolet chemiluminescence observed in the work of Kistiakowsky and Richards.^{5b} The emission was much weaker than the visible emission, but the pulses appeared to have the same form in both wave length regions and were simultaneous. The weakness of the ultraviolet emission in our experiments may be attributed to two effects. First, our detection system was more sensitive to the visible radiation, probably by a factor of ten. Second, the fourth positive system of CO fades rapidly, under excitation conditions similar to those active here, at wave lengths over 2000 Å. The relative amounts of energy radiated as ultraviolet and visible chemiluminescence may be quite different than one would conclude from the relative pulse heights in our experiments.

In one series of experiments the wave length setting of the monochromator was systematically varied through the region 2000–2200 Å. to see if any band structure could be discerned. The intensity distribution appeared to be constant. This, once again, is a combination of instrumental limitations and the nature of the emission. The bandpass of the monochromator at slit widths sufficient to collect detectable amounts of radiation was such that several lines of the CO system were necessarily passed at any setting. In addition to the experimental limitation, this measurement is faced with the difficulty that the CO fourth positive system is quite open at these wave lengths, and that the difference in line density between band-head and valley is not large.

In Fig. 2 the induction times for appearance of OH are plotted as a function of inverse temperature. The choice of $[O_2]_i$ as parameter was made to allow comparison with the results of Kistiakowsky and Richards, who in turn made this choice to allow comparison with the hydrogen-oxygen results of Schott and Kinsey⁶; it is becoming clear, however, that such presentations are misleading and not necessarily in-

(3) C. W. Hand and G. B. Kistiakowsky, *J. Chem. Phys.*, **37**, 1239 (1962); C. W. Hand, Thesis, Harvard University, 1961.

(4) R. F. Stubbeman and W. C. Gardiner, Jr., *J. Chem. Phys.*, **40**, 1771 (1964). The emission was erroneously attributed to CO + O in this communication. Spectral analysis of the visible emission (G. P. Glass, private communication) shows that CH is the principal emitter at these wave lengths.

(5) (a) C. W. Hand, *J. Chem. Phys.*, **36**, 2521 (1962); (b) G. B. Kistiakowsky and L. W. Richards, *ibid.*, **36**, 1707 (1962).

(6) G. L. Schott and J. L. Kinsey, *ibid.*, **29**, 1177 (1958).

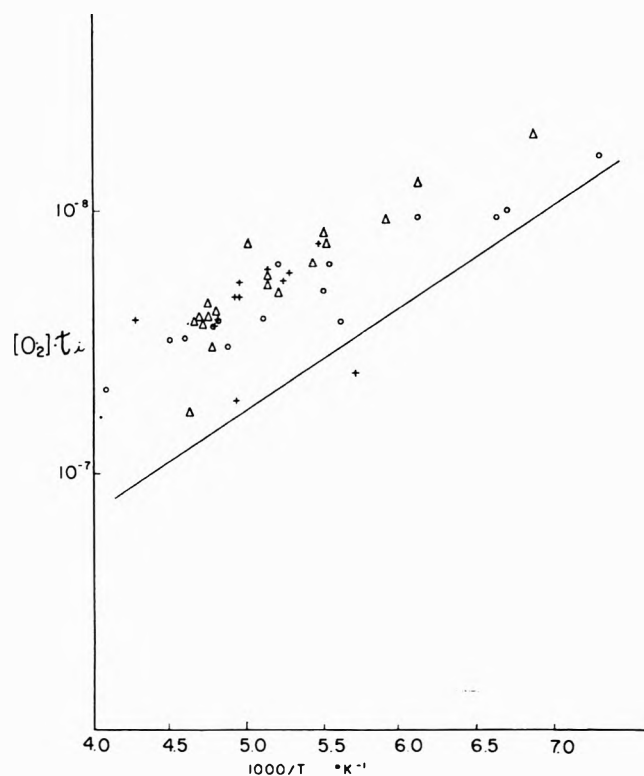


Figure 2. Induction times for appearance of OH. Solid line is the least-squares line of Kistiakowsky and Richards, determined by ultraviolet emission. Triangles are $[O_2] : [C_2H_2] = 7.4:1$. Circles are $[O_2] : [C_2H_2] = 3.2:1$. Crosses are $[O_2] : [C_2H_2] = 1.5:1$. Units of ordinate are moles/l. \times sec.

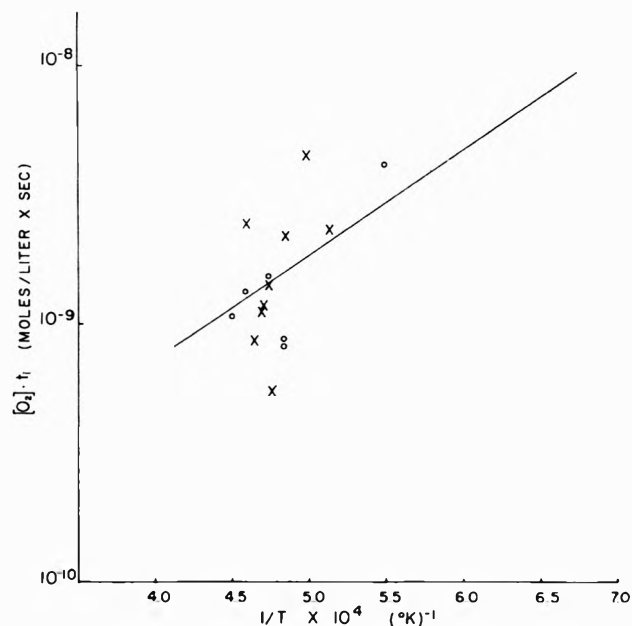


Figure 3. Induction times for blue emission to rise to 0.1 of the maximum. Solid line is the least-squares line of Kistiakowsky and Richards, determined by ultraviolet emission. Crosses are $[O_2] : [C_2H_2] = 7.3:1$. Circles are $[O_2] : [C_2H_2] = 3.3:1$.

indicative of the role of oxygen in the induction period reactions.⁷ The solid line in the figure is the least-squares line determined by Kistiakowsky and Richards from their observations of far-ultraviolet emission under experimental conditions similar to those employed in this work except for their use of starting pressures of 1 mm. compared to our starting pressure of 5 mm. It is clearly seen that the induction times for appearance of OH are substantially longer than those for onset of far-ultraviolet chemiluminescence. The data points for the leanest mixture and those for the mixture stoichiometric to CO and water appear to scatter uniformly together; those for the intermediate composition appear to correspond to shorter induction times, at least at the lower temperatures.

Defining an induction time for the onset of visible emission is a far more arbitrary affair than defining an induction time for appearance of OH. At the high sensitivities available when the logarithmic amplifier was used, scattered light began to register in some cases even before the shock wave arrived at the observation station, and the first part of the emission increase did not appear to be exponential. It was decided that

a reasonable choice would be to take the time at which the emission in a given shock rose to 0.1 of its peak height in that shock as the end of the induction zone for emission. The data are presented in Fig. 3. There is no apparent difference between the induction times for the two compositions used for these experiments. The solid line is once again the least-squares line of Kistiakowsky and Richards. The scatter of the points about this line is in accord with the previously mentioned observation that emission pulses in the visible and ultraviolet appeared to be coincident when observed in a single experiment at the two observation stations.

The peak heights of the visible emission are plotted against inverse temperature in Fig. 4. The ordinate is the output of the logarithmic amplifier, and hence a logarithmic measure of emission intensity, except at values less than about 0.02 v., where the amplifier response becomes linear rather than logarithmic. One decade corresponds to 0.11 v. The intensity is seen to be substantially higher for the 3:1 mixture than it is for the 7:1 mixture. Emission in the rich mixture is seen to be about three orders of magnitude weaker than in the 3:1 mixture. The peak intensity is strongly dependent on temperature; there is no suggestion, however, of a simple relationship.

(7) T. Asaba, W. C. Gardiner, Jr., and R. F. Stubbeman, paper presented to Tenth Symposium (International) on Combustion, Cambridge, 1964.

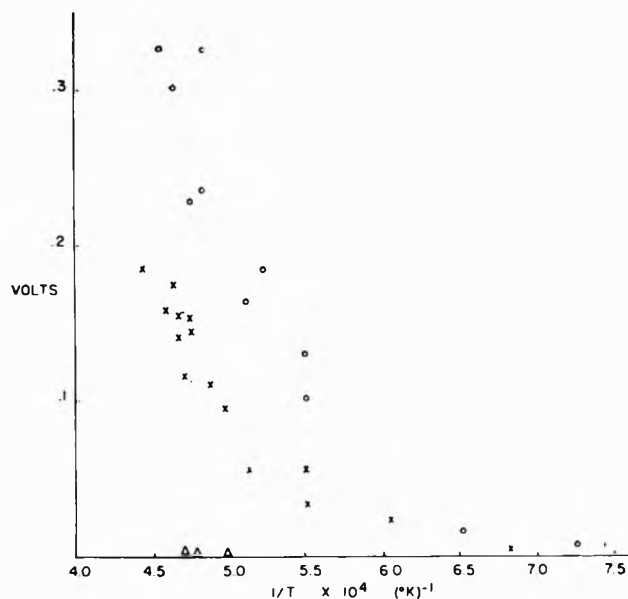
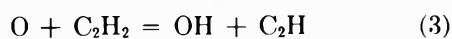
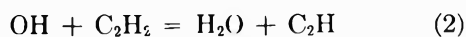


Figure 4. Peak heights for blue emission. Ordinate is voltage output of logarithmic amplifier, and therefore a logarithmic measure of emission intensity except for the lowest values (see text). Circles are $[O_2]:[C_2H_2] = 3.2:1$. Crosses are $[O_2]:[C_2H_2] = 7.3:1$. Triangles are $[O_2]:[C_2H_2] = 0.34:1$.

Time constants for the exponentially rising parts of the visible emission pulses are shown as functions of inverse temperature in Fig. 5. The time constants for decadic rise obtained directly from experimental records were converted to gas time by multiplication by the shock density ratio, converted to the base e by division by 2.3, and adjusted to 1-mm. starting pressure by multiplying by 5, which assumes that the responsible processes are first-order. This allows a comparison with the data obtained for the same quantity by Hand.³ It is seen that there is a discrepancy of about a factor of three in the two sets of data.

Discussion

The work of Kistiakowsky and Richards, combined with the time-of-flight mass spectrometric study of Bradley and Kistiakowsky,⁸ led to a proposal for the branching chain mechanism of the induction period having the form



The principal arguments advanced to support this chain were the analogy of the induction period behavior to that in the hydrogen-oxygen reaction⁶ and the dis-

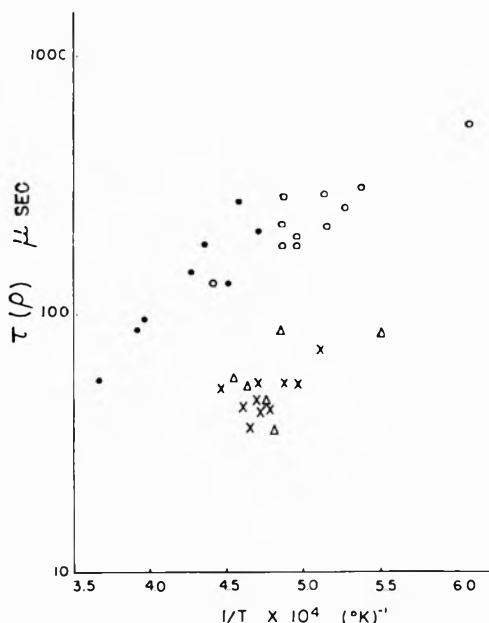
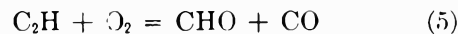
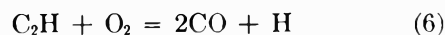


Figure 5. Time constant to base e for exponential part of intensity rise of blue emission. The data are normalized to a starting pressure of 1 mm. Circles are data of Hand for two mixtures with $[O_2]:[C_2H_2] = 1.5:1$. Triangles are our data for $[O_2]:[C_2H_2] = 3.2:1$. Crosses are our data for $[O_2]:[C_2H_2] = 7.3:1$. Starting pressures in Hand's experiments were near 1 mm., in our experiments near 5 mm.

covery of diacetylene in the mass spectrum of the shocked mixture by Bradley and Kistiakowsky. Subsequent experiments confirmed the presence of diacetylene in rich mixtures but indicated that CO was formed instead in lean mixtures⁹; it was proposed that there was a reaction of C_2H with oxygen competing with (4)



or



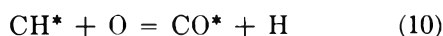
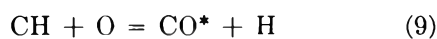
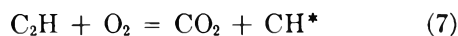
The chain-branching step 1 is here the same as in the hydrogen-oxygen reaction; its presence seems well-confirmed in light of the data of Kistiakowsky and Richards and the finding of Fenimore and Jones¹⁰ that oxygen is mostly consumed by H atoms in acetylene-oxygen flames.

(8) J. N. Bradley and G. B. Kistiakowsky, *J. Chem. Phys.*, **35**, 264 (1961).

(9) G. P. Glass, G. B. Kistiakowsky, J. V. Michael, and H. Niki, paper presented to the Tenth Symposium (International) on Combustion, Cambridge, 1964.

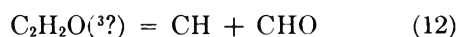
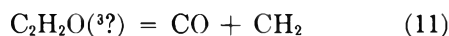
(10) C. P. Fenimore and G. W. Jones, *J. Phys. Chem.*, **63**, 1834 (1959).

A number of reactions have been proposed to account for the chemiluminescence and also for chemiionization^{11,12} in the acetylene-oxygen reaction.^{5a} We consider first for the sequence leading to the chemiluminescence in the far-ultraviolet and at 4300 Å.



The starred CH refers to either the ²Δ or the ²Π state, the starred CO to the A¹Π state.

Abstraction of H from acetylene by O may compete with attack of the triple bond itself. Evidence from a flame study¹³ suggesting that the initial attack of O may be on the carbon atom has recently been strengthened by other flame experiments¹⁴ in which the existence of a transient adduct C₂H₂O was confirmed mass spectrometrically. At shock wave or flame temperatures this adduct would decompose rapidly; two possible modes of decomposition would be

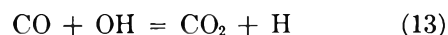


It is likely that the double valence of the oxygen atom is preserved in its reaction with acetylene¹⁵; thus, if adduct formation is the principal fate of O, then the decomposition products of the adduct should be reactive toward oxygen or acetylene molecules. The exothermic or slightly endothermic decomposition possibilities do not allow electronic excitation of the products, but they do open the possibility of the ground-state radicals CH, CHO, and CH₂ participating in the main chain-branching reaction sequence. The requirement of atomic oxygen, rather than OH or H, for producing CH chemiluminescence in acetylene has recently been demonstrated.¹⁶

Our results are in general accord with those proposals for the induction period reactions. Several additional features of the kinetics can be added by combining our results with those of previous workers.

First let us consider the temporal behavior of the visible radiation and OH concentration illustrated in Fig. 1. The question of whether the onset of chemiluminescence or the appearance of OH corresponds to the beginning of macroscopic-scale chemical reaction is easily resolved; the onset of the radiation marks the end of the induction period. The suppression of OH appearance must then be explained. For reasons discussed previously,⁴ this is probably a manifestation of the high reactivity of OH toward the reaction en-

vironment throughout the induction zone and the transition to the "recombination region."⁶ At first the only reaction partner is acetylene; when sufficient CO has been produced, the fast reaction



will continue to keep the OH concentration below the limit of detectability. The final appearance of OH can be taken to be a measure of reactions such as (13) becoming reversible. This stage, under the conditions studied in our experiments, usually corresponded also to the virtual disappearance of chemiluminescence.

The reasons for the rapid and virtually complete disappearance of the visible radiation are considerably more subtle than the reasons for the delayed appearance of OH. It is to be noted in Fig. 1 that the level of the emission falls through more than two orders of magnitude in a time comparable to the rise in concentration of OH. In experiments at higher temperatures, similar decays spanning at least four orders of magnitude can be seen. The familiar "radical overshoots" cannot begin to explain changes of this size at the temperatures of these experiments. One is then drawn to the conclusion that at least one of the reactants in the sequence leading to visible emission is at an *extremely* low concentration in the equilibrium gas, and that one of the reaction partners populating the radiating state of CH is either acetylene itself or an intermediate formed from acetylene that does not appear in the equilibrium mixture in mole fraction greater than about 0.01 of the mole fraction of CO prevailing at equilibrium. All of the oxygen-containing fragments in the main chain sequence above are present in substantial fractions of the H₂O and CO concentrations except for CHO. Unoxidized carbon-containing fragments, however, are present only at extremely low concentrations at equilibrium. Reactions such as (7) and (8), therefore, are consistent with these requirements. It would be possible to make a decision as to which type of reaction is responsible for most of the emission if the exponential rise constant could be assigned to a reaction rate involving a product of two concentrations increasing exponentially in time, or a reaction rate involving only one exponentially increasing concentration. In principle, this can

(11) G. B. Kistiakowsky and J. V. Michael, *J. Chem. Phys.*, **40**, 1447 (1964).

(12) G. P. Glass and G. B. Kistiakowsky, *ibid.*, **40**, 1448 (1964).

(13) C. P. Fenimore and G. W. Jones, *ibid.*, **39**, 1514 (1963).

(14) H. G. Wagner, private communication.

(15) W. C. Gardiner, Jr., *J. Chem. Phys.*, **40**, 2410 (1964).

(16) R. E. W. Jansson and K. D. Bayes, *Proc. Roy. Soc. (London)*, to be published.

be done by comparing the induction time for the process with the exponential rise time constant.⁶ One can then estimate the number of decades through which the concentration or concentration product has risen at the end of the induction period. Unfortunately, the present data do not give sufficiently reproducible results for this to allow a decision to be made, mainly because the temperature range of our experiments was too high for accurate comparative measurements of this kind. Careful work at lower temperatures and concentrations may allow this distinction to be made.

The above suggestions for the cause of the delayed appearance of OH do not lead immediately to any prediction about the dependence of the induction time for OH appearance upon composition, at least for the lean mixtures studied here. In Fig. 2, the data appear to indicate that the induction periods for OH appearance are shorter for the 3:1 mixture than for either of the other two mixtures. The scatter of the data points is such that this effect cannot be held to be certain, but it is indeed indicated. Two different interpretations of such an effect would be possible, one as an effect involving the main branching chain, the other as an effect involving the transition to equilibrium which appears to be the precursor to OH appearance. Since the acetylene concentration was held constant in these experiments, it is necessary to propose competitive processes in order to predict a concentration of oxygen above and below which the induction periods for OH appearance are lengthened. Such processes are not indicated in any of the heretofore proposed kinetic steps, and no likely additional steps come to mind. Since the early work on composition dependence of the induction periods for ultraviolet emission led to a weak, monotonic dependence,^{5b} we prefer to postpone any additions to the kinetic scheme that would allow interpretation of the apparent concentration dependence in Fig. 2 until the effect can be confirmed in more accurate measurements over a wide composition range.

The data for the induction time for blue emission to rise to 0.1 of its maximum are not useful for direct kinetic interpretation, but they do serve well to illustrate the coincidence of the appearance of visible and ultraviolet emission and to show the degree of agreement between our results and those of Kistiakowsky and Richards (Fig. 3). The scatter is in part due to the difficulty with scattered light, in our arrangement, and in part due to the normal variations encountered in measurements of this kind. We believe that there is no systematic error in our measurements of these data points other than that of the scattered light; it is our intention to test this in future experiments by investigating the phase relationship

between ultraviolet and visible chemiluminescence with a detector more sensitive to the ultraviolet emission than the one used in the present experiments.

The peak heights for the blue emission intensity are seen in Fig. 4 to increase very strongly on going from the 7:1 to 3:1 mixture. At the higher temperatures, the difference is practically an order of magnitude in intensity. It does not appear that this is due in large measure to a more rapid reaction in the 3:1 mixture, since the data points for the induction period to 0.1 of maximum peak height scatter uniformly together. There is a possibility that the latter stages of the induction period are accelerated by a thermal effect, but this again does not appear likely in view of the moderate exothermicity of the proposed main chain, and the fact that the more likely effect here would be in the opposite direction than observed due to the increase in heat output which would accompany favoring reactions 5 and 6 over 4. The most likely explanation would appear to be a combination of effects strongly increasing the concentration of the reduced reaction partners in (7) and (8) (or, any of the similar reactions which can be written to populate CH*) when the ratio of oxygen to acetylene is reduced from 7 to 3. It is unfortunate that our present data do not include peak height measurements extending to stoichiometric or slightly rich compositions.

The time constant for the exponential rise of the chemiluminescence intensity is intrinsically more satisfactory for comparison with predictions from a kinetic scheme for the branching chain and population of the radiating states, but suffers in our experiments from lack of accuracy due to scattered light and lack of data for higher temperature ranges. It is particularly unsatisfactory that our data for the exponential time constant disagree with the results of Hand and Kistiakowsky (Fig. 5). The data of Hand and Kistiakowsky were taken for a mixture stoichiometric to CO and H₂O (1.5:1 ratio of oxygen to acetylene) and were obtained in shock waves at starting pressures of 1 mm. Our correction for the different starting pressures was linear (multiplication by the ratio of starting pressures), and this may in fact be incorrect. If, as might seem likely, the over-all process leading to emission is approximately second-order, then a quadratic correction would be appropriate and the two sets of data would be in agreement. However, it does not seem likely that the over-all process leading to emission would be second-order in acetylene and zero-order in oxygen. It can be seen in Fig. 5 that the 7:1 and 3:1 mixtures scatter together, indicating that there is no effect as large as first-order in oxygen. Perhaps a doubling of the time constant would be observed

if the 3:1 mixture were compared with a 1.5:1 mixture. Such a change would then confirm the suggestion that the two sets of data are actually in agreement and that second-order dependence upon pressure would be observed if stoichiometric mixtures were compared. More accurate values for exponential time constant(s?) for intensity rise of visible and ultra-

violet emission studied over wider ranges of temperature and composition should be quite valuable in assigning the mechanism of the population of the radiating states to specific elementary steps.

Acknowledgment. This work was supported by the U. S. Army Research Office (Durham).

Catalytic Deuterium Exchange Reactions with Organics. XIV.¹Distinction between Associative and Dissociative π -Complex

Substitution Mechanisms

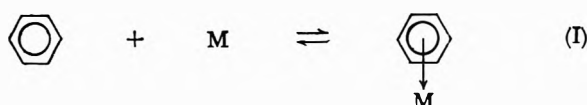
by J. L. Garnett and W. A. Sollich-Baumgartner

Department of Physical Chemistry, The University of New South Wales, Sydney, Australia (Received May 25, 1964)

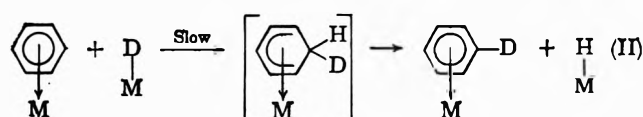
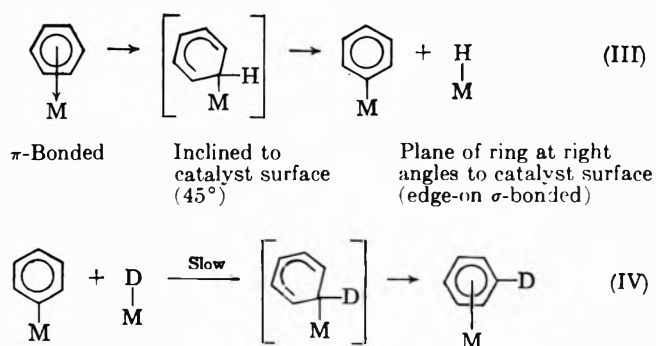
The relative importance of the associative and dissociative π -complex substitution mechanisms in group VIII transition metal catalyzed exchange reactions between heavy water and aromatic molecules has been investigated by comparing the rate of D_2O -benzene exchange reactions to the randomization rate of a mixture of normal and 98.3% deuterated benzene. Kinetic equations have been derived for the randomization process on the assumption that random deuterium incorporation occurs at all stages of the reaction. A test of these equations showed that this assumption was not valid. A semiempirical method has therefore been developed for the calculation of randomization rate constants. The results show that randomization occurs at a rate which is 70% as fast as deuterium oxide exchange. This difference in the two reaction rates is readily explained by water activation of the catalyst. It is concluded that the dissociative π -complex substitution mechanism is the predominant process by which deuterium oxide exchanges catalytically with aromatic molecules. Isotope effect studies show that the reaction between chemisorbed benzene and chemisorbed hydrogen is the rate-determining process of the exchange reaction.

Introduction

Two new reaction mechanisms, the associative and dissociative π -complex substitution mechanisms, have been proposed for group VIII transition metal catalyzed hydrogen exchange reactions between aromatic molecules and heavy water (eq. I-IV).

General π -Complex Adsorption

π -Bonded to catalyst (M) with plane of ring parallel to catalyst surface

Associative π -Complex Substitution MechanismDissociative π -Complex Substitution Mechanism

Both mechanisms involve π -complex adsorption of the aromatic reagent (*e.g.* benzene) so that the plane of the ring is parallel to the plane of the catalyst surface (eq. I). In the associative mechanism the aromatic mole-

(1) Part XIII: *Australian J. Chem.*, in press.

cule is attacked by a chemisorbed deuterium atom originating from the dissociative chemisorption of water or deuterium gas (eq. II). In the dissociative mechanism (eq. III and IV) the π -bonded aromatic reacts first with a metal radical (active site) by rotating through 90° to form a carbon-metal σ -bond so that the plane of the ring is now at right angles to the plane of the catalyst. While σ -bonded, the compound undergoes another rate-controlling² substitution reaction at the carbon-metal bond with a chemisorbed deuterium atom, so that it returns to the original π -bonded state.

From previous data³⁻⁶ it was not possible to distinguish clearly between the relative importance of these two mechanisms; however, special experiments, which are described in the present communication, were designed for this purpose. These experiments depend on the fact that π -complex adsorbed aromatics cannot furnish deuterium atoms to the catalyst. The associative mechanism requires therefore a second substance, water or deuterium gas, which can supply the attacking reagent by dissociative chemisorption. Exchange between one hydrocarbon and another (*e.g.*) benzene-*d*-diphenyl) is thus precluded by the associative mechanism, but feasible by the dissociative mechanism. Both mechanisms can operate simultaneously in benzene-deuterium oxide exchange where it has been shown that noncompetitive reagent adsorption occurs.⁷ To ascertain whether one of the two possible mechanisms is exclusively responsible for exchange, it is necessary to perform exchange reactions between a normal and a deuterated species where mutual reagent displacement effects are unimportant. This eliminates systems such as benzene-*d*-naphthalene, where no significant exchange occurs due to benzene displacement, or even benzene-*d*-diphenyl, where exchange is significantly retarded at low temperatures.² The ideal system with respect to reagent displacement is to perform exchange reactions, *i.e.*, randomization, between normal and 100% deuterated benzene. This system presents however a number of difficulties in the evaluation of the reaction rate constant. Mathematical procedures by which this randomization rate constant can be calculated and consequently compared to that of the deuterium oxide reaction are described in the following section.

Experimental

Exchange and randomization reactions were performed at 32° in evacuated ampoules with platinum catalysts by previously described procedures.⁸ The randomization mixture consisted of equimolar quantities of normal and 98.3% deuterated benzene (thiophene free), the latter being prepared from repeated exchanges

with deuterium oxide at 120° . Exchange and randomization products were analyzed mass spectrometrically (~ 10 e.v.) and the seven benzene isomers ($d_0, d_1 \dots d_6$) corrected for the contribution of the C^{13} isotope peak.

Results and Discussion

Equation for Randomization Reactions. During randomization the mass spectrum of the normal benzene-benzene-*d* (98.3%) mixture changes from that shown approximately in Fig. 1a at $t = 0$, through various intermediates (*e.g.*, Fig. 5) until it reaches the classical equilibrium distribution depicted in Fig. 2. The close agreement between the calculated and the experimental spectrum (Fig. 2) shows that isotope effects cause negligible departures from the classical equilibrium distribution.

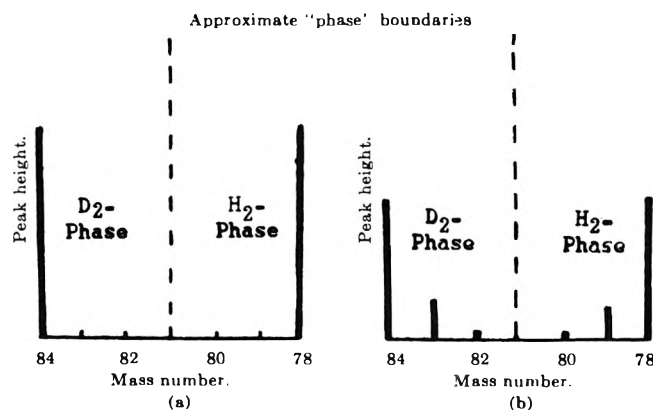


Figure 1. Approximate "phase boundaries" in the mass spectrum of an equimolar mixture of 100% deuterated benzene and normal benzene: (a) prior to commencement of reaction; (b) at early stages of randomization.

In order to calculate a reaction rate constant it is necessary to express the changes in the mass spectrum of the normal benzene-benzene-*d* (98.3%) mixture by a first-order equation. The model adopted for this purpose involves the division of the mass spectrum into two hypothetical "phases," analogous to the water and benzene phases, *viz.*, the deuterium and hydrogen "phases." In the initial stages of the randomization reactions these "phases" are visible in the mass spectrum (Fig.

(2) J. L. Garnett and W. A. Sollich, to be published.

(3) J. L. Garnett and W. A. Sollich, *Australian J. Chem.*, **14**, 441 (1961).

(4) J. L. Garnett and W. A. Sollich, *ibid.*, **15**, 56 (1962).

(5) J. L. Garnett and W. A. Sollich, *J. Catalysis*, **2**, 350 (1963).

(6) J. L. Garnett and W. A. Sollich, *Nature*, **201**, 902 (1964).

(7) T. I. Taylor, "Catalysis," P. H. Emmett, Ed., Reinhold Publishing Corp., New York, N. Y., 1957, p. 257.

(8) J. L. Garnett and W. A. Sollich, *J. Catalysis*, **2**, 339 (1963).

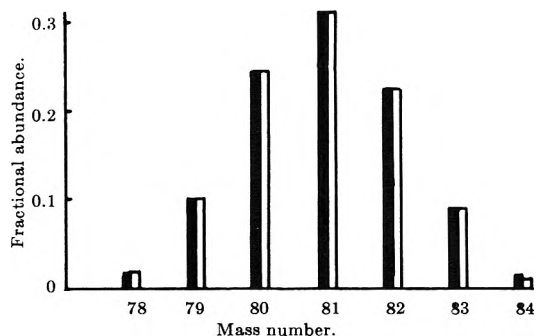


Figure 2. Mass spectrum of randomized benzene ($t \rightarrow \infty$) containing 49.06% deuterium: \square , observed; \blacksquare , calculated.

1b), and the calculation of rate constants approximates a situation where such phases really exist in the reaction vessel. Serious overlapping of "phases" occurs, however, at later stages of "exchange," and consequently the physical manifestation of these mass spectral phases disappears. The composition, however, may still be calculated by the mathematical procedures shown below, so that a theoretical "separation" of phases is still possible.

If random deuterium distribution is assumed at all stages of the randomization reaction, the spectra of the two hypothetical phases can be calculated from eq. 1

$$p_{H^{78-84}} = \frac{6!}{(6-m)!m!} P_H^m Q_H^{(6-m)} \quad (1)$$

where $p_{H^{78-84}}$ is the fractional abundance of benzene molecules containing 0, 1, . . . 6 hydrogen atoms (m) in the hypothetical hydrogen phase of the mass spectrum, giving rise to mass numbers of 84, 83, . . . 78, respectively; P_H and Q_H are the fractional abundances of hydrogen and deuterium atoms in the hydrogen "phase" at time t . An analogous equation, involving $p_{D^{78-84}}$, Q_D , and P_D , describes the deuterium "phase." Further, $P_D = (1 - P_H)$ in the case where normal and 100% deuterated species are involved.

During randomization, in which equimolar quantities of normal and 98.3% deuterated benzene are used, P_H changes exponentially from 1.0 at $t = 0$ to 0.508 at $t \approx \infty$ and can consequently be described by the first-order equation

$$\begin{aligned} \frac{-dP_H}{dt} &= k_R \frac{(P_H^0 - P_H^\infty) - (P_H^0 - P_H^t)}{(P_H^0 - P_H^\infty)} \\ &= k_R \frac{(P_H^t - P_H^\infty)}{(1 - P_H^\infty)} \end{aligned} \quad (2)$$

Integrating (2)

$$\frac{2.3(1 - P_H^\infty)}{t} \log \frac{(P_H^t - P_H^\infty)}{(1 - P_H^\infty)} = -k_R \quad (3a)$$

In order to compare the randomization rate with that of the deuterium oxide exchange reaction, the normalized rate constant k_{NR} must be calculated, *i.e.*, the rate constant expressed in terms of fractional completion of reaction per unit time.

For randomization reactions, this is given by the equation

$$-k_{NR} = \frac{2.3}{t} \log \frac{(P_H^t - P_H^\infty)}{(1 - P_H^\infty)} \quad (3b)$$

while that for exchange is

$$-k_{NE} = \frac{2.3}{t} \log \frac{(D_\infty - D_t)}{D_\infty} \quad (4)$$

where D is the deuterium content of the benzene phase.

The method by which P_H values were determined involved measuring the ratio of peaks occurring in the spectra at mass 78 and 79, *i.e.*, those corresponding to the normal and nondeuterated species. Normal benzene peaks ($p_{H+D^{78}}$) of the reaction mixture are however composed of two parts; *viz.*, one fraction is due to normal benzene in the hydrogen "phase" of the spectrum which has not yet exchanged ($p_{H^{78}}$), while the other fraction ($p_{D^{78}}$) originates from the deuterium "phase," *i.e.*, from an initially completely deuterated molecule which has exchanged all six deuterium atoms with hydrogen. Using a similar argument for the 79 peak, eq. 5 was derived which relates the peak ratio to the P_H value at time t .

$$\begin{aligned} \frac{p_{H+D^{79}}}{p_{H+D^{78}}} &= \frac{p_{H^{79}} + p_{D^{79}}}{p_{H^{78}} + p_{D^{78}}} = \\ &= \frac{6P_H^5(1 - P_H) + 6(1 - P_H)^5P_H}{P_H^6 + (1 - P_H)^6} \end{aligned} \quad (5)$$

In the early stages of the reaction, *i.e.*, with negligibly overlapping spectra, this approximates to

$$\frac{p_{H+D^{79}}}{p_{H+D^{78}}} \approx \frac{6(1 - P_H)}{P_H} \quad (6)$$

The solution of eq. 5 for a given peak ratio is complicated; consequently, the reverse procedure was adopted, *i.e.*, peak ratios were calculated for chosen P_H values. Since randomization experiments were performed with 98.3% deuterated benzene, *i.e.*, $P_D = \{(1 - P_H) + 0.017\}$, eq. 5 had to be slightly modified for residual hydrogen. Results of the calculations are shown in Fig. 3, where peak ratios are plotted against P_H values so that solutions of eq. 5 could be directly determined. The graph contains also approximate solutions as calculated from eq. 6 (dotted line). These agree satisfactorily with the exact solutions over a considerable range of the reaction.

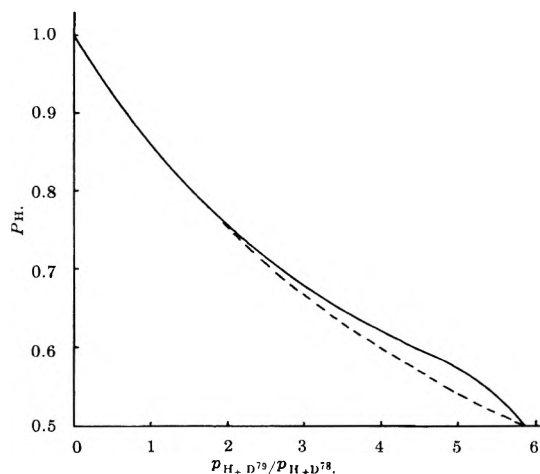


Figure 3. Theoretical peak ratios *vs.* fractional hydrogen abundance in "hydrogen phase": calculated by accurate equation (full line); calculated by approximate equation (dotted line).

Verification of Kinetic Equations. The basic assumptions involved in the derivation of the kinetic equations were subsequently investigated. The analytical procedure was confirmed by comparing experimental results with those calculated by eq. 1. The test was performed on a (49.06%) deuterated and completely randomized ($t \approx \infty$) benzene sample. Figure 2 shows an excellent agreement between the calculated and the experimentally determined spectrum. The assumption that deuterium enters benzene molecules in a random manner at all stages of the reaction ($t \neq \infty$) was examined by analyzing the products of both randomization (Fig. 4 and 5) and deuterium oxide exchange reactions (Fig. 6). In the former case the peak ratio 79/78 was measured, and the corresponding P_H value was determined from graph 3; separate spectra for hydrogen and deuterium "phases" were then calculated from P_H and P_D . These were combined and compared with the experimentally observed spectrum. The benzene spectrum from deuterium oxide exchange was calculated from the known deuterium content by eq. 1. Figures 4 and 5, which correspond to early and late stages of the randomization reaction, respectively, show poor agreement between calculated and observed spectra. These discrepancies cannot, however, be attributed to faults in the model of randomization reactions (*i.e.*, the division into hypothetical phases) since these discrepancies occur also in deuterium oxide exchange (Fig. 6) where this model does not apply. One must conclude, therefore, that deuterium does not enter benzene in a random fashion, but reaches this state only when "exchange" between the hypothetical

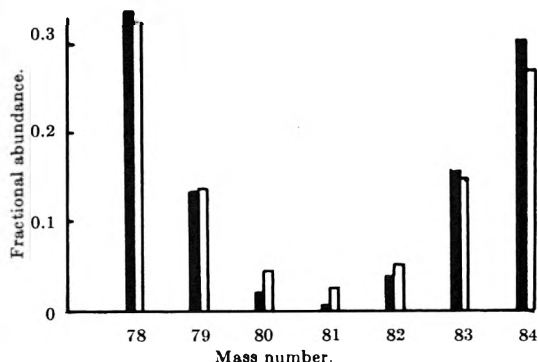


Figure 4. Benzene mass spectrum from a 4-hr. randomization reaction at 32°: □, observed; ■, calculated from $P_H = 0.938$, $Q_H = 0.062$, $P_D = 0.079$, $Q_D = 0.921$.

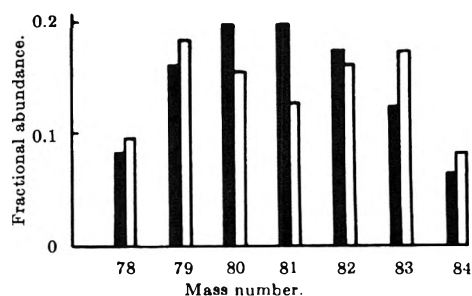


Figure 5. Benzene mass spectrum from a 17-hr. randomization reaction at 32°: □, observed; ■, calculated from $P_H = 0.765$, $Q_H = 0.235$, $P_D = 0.252$, $Q_D = 0.748$.

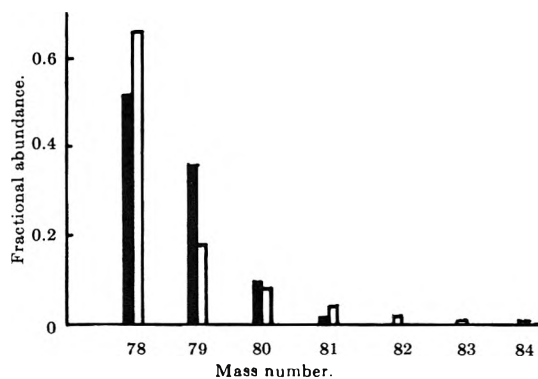


Figure 6. Benzene mass spectrum from a deuterium oxide exchange reaction at 32°: □, observed; ■, calculated; deuterium content = 10.5%.

phases, or with D_2O , has been "completed." Consequently, P_H values determined from graph 3 give only an approximate measure of the reaction progress, there being a tendency to underestimate the reaction rate.

Randomization Reactions Involving Multiple Exchange Processes. The above nonrandom deuterium distribu-

tion in benzene can be explained by the participation of multiple exchange processes.⁹ In multiple exchange, a parameter, M , may be calculated corresponding to the mean number of deuterium atoms entering each benzene molecule under initial conditions. This parameter is defined by two rate constants.

$$M = \frac{k_\phi}{k_b} \quad (7)$$

One of these, k_ϕ , was shown on theoretical grounds¹⁰ to be defined by the first-order equation

$$-\log(\phi_\infty - \phi) = \frac{k_\phi t}{2.3\phi_\infty} - \log \phi_\infty \quad (8)$$

where $\phi = u + 2v + 3w + 4x + 5y + 6z$, "u" to "z" being the percentage of total benzene present as benzene- d_1 to $-d_6$. However, the first-order equation defining k_b has no theoretical foundation, but is an empirical relationship which applies over a considerable range of a number of exchange reactions

$$-\log(b - b_\infty) = \frac{k_b t}{2.3(100 - b_\infty)} - \log(100 - b_\infty) \quad (9)$$

"b" being the percentage of total benzene present as benzene- d_0 . Equation 1 applies under conditions of random deuterium incorporation ($M = 1$). However, with increasing importance of multiple exchange, M increases, its limiting value being 6.

Before calculating M values for the empirical treatment of randomization reactions (see below) it was necessary to ascertain whether eq. 9 was applicable to deuterium oxide-benzene exchange reactions. The test was applied to the products of exchange reactions performed at 32° with two different catalysts (batches A and B). The linear relationship obtained in both cases (Fig. 7) confirmed eq. 9. M values, calculated for all points on the graph, were found to be the same ($M = 1.50 \pm 0.05$) for the two differently prerduced but identically activated⁷ catalysts.

Empirical Treatment of Randomization Reactions. The above results show that both exchange and randomization reactions, when performed at the same temperature (32°) with identically activated catalysts, deviate to approximately the same extent from random distribution. This fact suggests the possibility of obtaining more accurate randomization rate constants from an experimentally determined graph, where the progress of randomization is plotted against measured 79/78 peak ratios. Such a graph was constructed by measuring the peak ratios of a number of deuterated benzene samples derived from deuterium oxide ex-

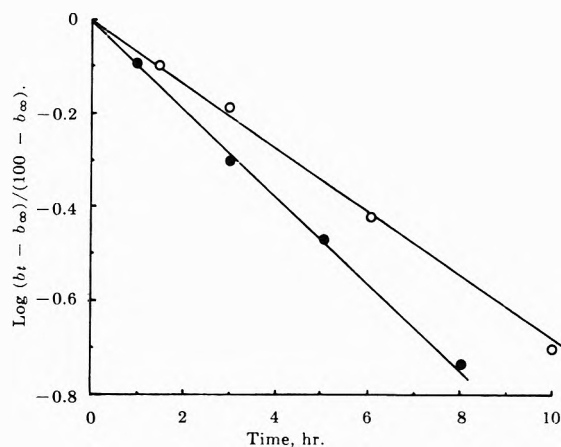


Figure 7. Disappearance of benzene- d_0 in deuterium oxide-benzene exchange reactions performed with two stable platinum catalysts: O, batch A; ●, batch B.

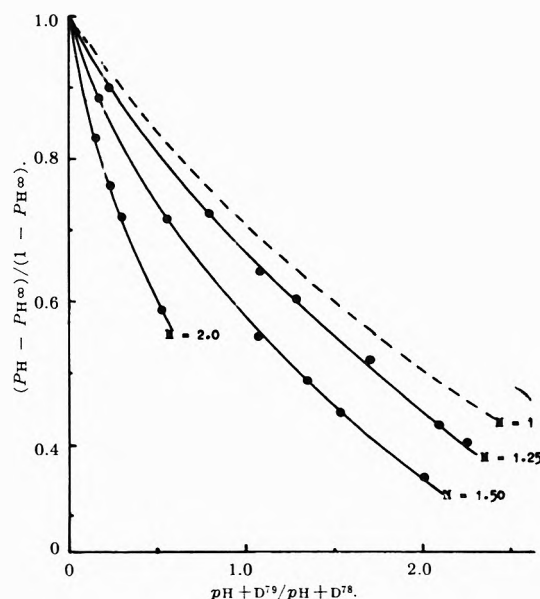


Figure 8. Experimental and calculated (dotted line) 79/78 peak ratios at different stages of benzene randomization reactions (equimolar quantities of 98.3% benzene- d and normal benzene) occurring with different M factors.

change reactions. M values were calculated and their deuterium content re-expressed in terms of the "fractional completion" of a randomization reaction involving equimolar concentrations of 98.3% deuterated and normal benzene. Values were calculated from reaction products with M factors of 1.25, 1.50, and 2.0. Results of these calculations are shown in Fig. 8 and are compared to a slightly modified version of the theoretically calculated random distribution curve, where

(9) J. R. Anderson and C. Kemball, *Advan. Catalysis*, **9**, 56 (1957).

(10) C. Kemball, *Proc. Roy. Soc. (London)*, **A217**, 376 (1953).

$M = 1$ (dotted line). With increasing M value, these graphs are seen to deviate increasingly from the random distribution curve. This would lead to considerably lower rate constants if allowance were not made for this effect.

It is now possible to make accurate comparisons of exchange and randomization rate constants and thereby to resolve the issue as to the relative importance of either the associative or dissociative π -complex substitution mechanism in aromatic- D_2O exchange reactions. Randomization reactions were performed at 32° with stable catalysts (batches A and B activated at -90°) and a benzene-catalyst weight ratio of 63, which is identical with that used in the deuterium oxide exchange reactions.

Results obtained with both catalysts (Fig. 9) gave linear plots which confirm the randomization equations. A normalized randomization rate constant (k_{NR}) of $5.9 \times 10^{-2} \text{ hr.}^{-1}$ was calculated for the reaction performed with catalyst A. The normalized deuterium oxide-benzene exchange rate constant for the same catalyst under "identical" conditions was found to be $8.60 \times 10^{-2} \text{ hr.}^{-1}$. Thus the randomization rate is only 70% that of the deuterium oxide exchange. This, however, is sufficiently large to show that exchange between aromatic hydrocarbons and water occurs mainly by the dissociative π -complex substitution mechanism. From the slightly lower result it would seem that the associative mechanism may also play a significant role; however, this is unlikely, since the faster exchange rate is probably due to the activation of the catalyst by the water-benzene mixture.⁸ It was found that catalysts undergo marked changes in physical appearance during benzene-water exchange reactions, the catalyst being transformed from a coarse and coagulated powder into a finely divided film-like state. That these changes are not merely due to the physical agitation is seen from the fact that they did not occur when each reagent was shaken with the catalyst in isolation. The mutual interaction of both reagents appears to be necessary. Several effects were found to be associated with this phenomenon. Thus, a catalyst which was pretreated with a benzene- D_2O mixture possessed (i) improved reproducibility and (ii) in some cases up to 140% higher activity. Effects (i) and (ii) are also discernible in Fig. 9 where the graphs exhibit considerably greater scatter than that usually found in deuterium oxide exchange reactions. Thus it appears most likely that the dissociative π -complex substitution is the only process by which aromatic hydrocarbons undergo significant exchange with water on group VIII transition metal catalysts.

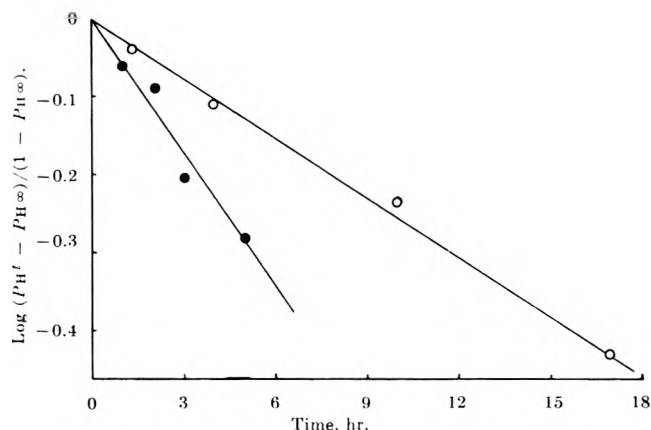
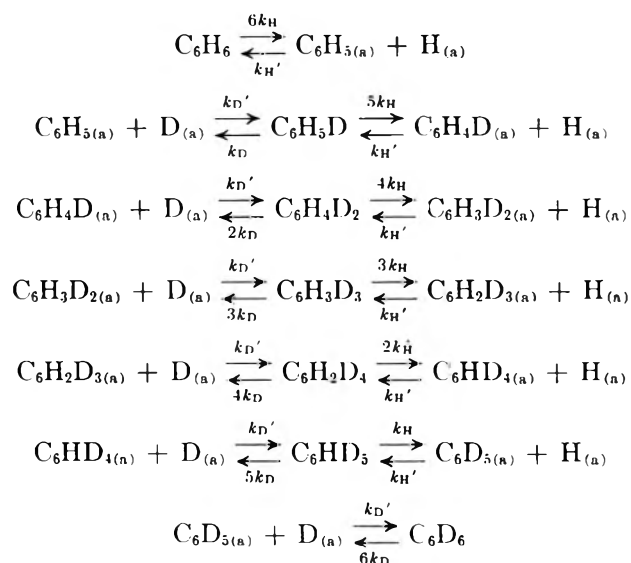


Figure 9. Randomization reactions ($M = 1.50$) of 98.7% deuterated and normal benzene at 32° with two stable catalysts: O, batch A; ●, batch B.

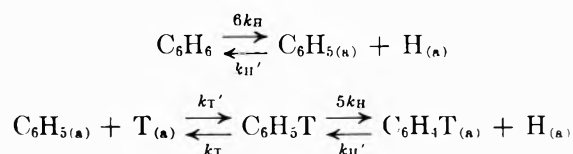
Rate-Determining Step of the Dissociative π -Complex Substitution Mechanism. The dissociative π -complex substitution mechanism having been established, it is possible to apply Gutmann's method¹¹ for the determination of the rate-controlling step of the exchange reaction. Deuterium and tritium exchange of benzene by the dissociative π -complex substitution mechanism can be represented by the following reaction scheme.

Deuterium Exchange ((a) = adsorbed)



Tritium Exchange. Only the monotritiated molecule has to be considered since tritium was used in tracer quantities.

(11) F. R. Gutmann, *Intern. J. Appl. Radiation Isotopes*, **7**, 186 (1960).



Gutmann has derived the following equations for catalytic hydrogen exchange reactions which proceed by a dissociative mechanism.

For deuterium exchange the rate is given by eq. 10

$$\frac{dD}{dt} = \frac{k_{\text{D}'}C_{\text{A}'}C_{\text{B}'}}{\epsilon \left\{ 1 - \alpha \frac{(k_{\text{H}} - k_{\text{D}})}{k_{\text{H}}} \right\}} \times [\epsilon(1 - \alpha)\beta - (1 - \beta)\alpha] \quad (10)$$

where ϵ is a thermodynamic constant related to the equilibrium constant of the system, α and β are the deuterium mole fractions in benzene and water, respectively, and C_{A} and C_{B} the surface concentration of the two reagents irrespective of isotopic composition; $k_{\text{D}'}$, k_{D} , and k_{H} are rate constants defined by the preceding equations.

The rate of tritium exchange when the isotope is present in tracer quantities is given by eq. 11

$$\frac{dT}{dt} = \frac{k_{\text{T}'}C_{\text{A}'}C_{\text{B}'}}{\epsilon} (\epsilon\beta - \alpha) \quad (11)$$

The technique of double labeling was used in the present experiment, *i.e.*, $\text{D}_2\text{O} \approx 100\%$; $\text{T}_2\text{O} \ll 1\%$. Under these initial conditions eq. 10 and 11 are considerably simplified and yield the following result for the ratio of deuterium and tritium exchange reaction rates

$$\begin{array}{l}
 \left(\frac{dD}{dt}\right) \alpha = 0; \beta = 1 \\
 \left(\frac{dT}{dt}\right) \alpha = 0; \beta \ll 1
 \end{array} = \frac{k_{\text{D}'}C_{\text{A}'}C_{\text{B}'}}{k_{\text{T}'}C_{\text{A}'}C_{\text{B}'}} = \frac{k_{\text{D}'}}{k_{\text{T}'}} \quad (12)$$

Exchange reactions with doubly labeled water and normal benzene were performed at 30° , with platinum catalysts. Deuterium was found to exchange at a faster rate than tritium, the ratio of the rate constants being 1.7 ± 0.1 . According to eq. 12 this would indicate that the union of the chemisorbed hydrogen atom with a dissociatively chemisorbed benzene molecule is the rate-determining process of the exchange reaction. In this respect the result agrees with the direct observations made by other investigators,^{12,13} namely, that unsaturated hydrocarbons chemisorb at a faster rate than their subsequent interactions with chemisorbed hydrogen.

Acknowledgment. The authors thank the Australian Institute of Nuclear Science and Engineering (Mr. E. A. Palmer) for assistance in the purchase of the heavy water, the New South Wales State Cancer Council for the use of their facilities, and Commander J. Mason for instrumentation advice. Acknowledgment is also made to the donors of The Petroleum Research Fund, administered by the American Chemical Society, for support of this research.

(12) O. Beeck, *Discussions Faraday Soc.*, 8, 118 (1950).

(13) G. I. Jenkin and E. K. Rideal, *J. Chem. Soc.*, 2490 (1955).

Isotope Effects in the Hydrogen Abstraction from Aliphatic Compounds by Radiolytically Produced Hydrogen Atoms in Aqueous Solutions

by M. Anbar and D. Meyerstein

*The Weizmann Institute of Science and the Soreq Research Establishment, Rehovoth, Israel
(Received May 26, 1964)*

The isotope effect on the abstraction of the α -hydrogen of 2-propanol by hydrogen atoms has been determined. An identical isotope effect $k_{H\alpha}/k_{D\alpha} = 7.5 \pm 1$ was found both in neutral and acid solutions, indicating the identity of the "residual hydrogen" with hydrogen atoms. The reactivity of the α -hydrogen in 2-propanol toward hydrogen atoms was found to be 110 times higher than that of the β -hydrogens. The isotope effects on hydrogen abstraction by hydrogen atoms from formate, methanol, and acetate were determined and found to be 6.5 ± 0.5 , 20 ± 1 , and 22 ± 4 , respectively. The high values for the H-D isotope effect were obtained for hydrogen abstraction reactions of a relatively low rate, where a tunneling effect may be involved.

2-Propanol has recently been applied in a number of studies as a solute in radiolyzed aqueous solutions.¹⁻³ The most characteristic reaction of 2-propanol is the abstraction of its hydrogens by hydrogen atoms, formed from hydrated electrons, and by the "residual hydrogen," which may be considered as "primary" hydrogen atoms produced in neutral solutions. It was of interest to investigate thoroughly the reactions of 2-propanol with hydrogen atoms, as these reactions were applied in the interpretation of various problems in the radiation chemistry of aqueous solutions. The understanding of the behavior of 2-propanol on reaction with hydrogen atoms involves two open questions: (a) the relative reactivity of the α - and β -hydrogens, (b) the isotope effect on the abstraction of hydrogen. The purpose of the present study was to elucidate these points.

It has been shown that for a series of similar reactions, kinetic isotope effects may be correlated to the activation energy of the reaction,⁴⁻⁶ though deviations from such a correlation may be encountered.⁷ Having measured the isotope effect on the abstraction of the α -hydrogen in 2-propanol, it was of interest to compare its value with that measured for the abstraction of the α -hydrogen in ethanol⁸ and in formate.⁹ This comparison has been extended further by measuring the isotope effects on the hydrogen abstraction from methanol and from acetate. It was found that the magnitude of

the isotope effect may be correlated with the reactivity of the given compound toward hydrogen abstraction by hydrogen atoms.

Experimental

Solutions of 2-*d*-2-propanol (Merck Sharp and Dohme Ltd., >99% deuterium) in triply distilled water were irradiated under argon (200 mm.) by Co⁶⁰ γ -rays (dose rate 11,000 rads/min.). Argon was introduced to facilitate the mass spectrometric analysis.¹⁰ The isotopic composition of small amounts of hydrogen, as low as a partial pressure of 5 μ , could be accurately measured in the presence of 10-20 times as much argon or neon. The inert gas enabled the handling of the

- (1) J. T. Allan and G. Scholes, *Nature*, **187**, 218 (1960).
- (2) J. Rabani and G. Stein, *J. Chem. Phys.*, **37**, 1865 (1962).
- (3) M. Anbar and D. Meyerstein, *J. Phys. Chem.*, **68**, 1713 (1964).
- (4) K. B. Wiberg, *Chem. Rev.*, **55**, 713 (1955).
- (5) K. B. Wiberg and L. H. Slaugh, *J. Am. Chem. Soc.*, **80**, 3033 (1958).
- (6) G. J. Buist and M. L. Bender, *ibid.*, **80**, 4308 (1958).
- (7) C. Chiltz, R. Eckling, P. Goldfinger, G. Huybrechts, H. S. Johnston, L. Meyers, and G. Verbeke, *J. Chem. Phys.*, **38**, 1053 (1963).
- (8) C. Lifshitz and G. Stein, *J. Chem. Soc.*, 3706 (1962).
- (9) A. Appleby, G. Scholes, and M. Simic, *J. Am. Chem. Soc.*, **85**, 3891 (1963).
- (10) M. Anbar and D. Meyerstein, Israel AEC Semiannual Report IA-900, 124 (1963).

minute samples as well as keeping a constant pressure of the introduced gas during the measurement.

The D₂O (Norsk Hydro Elektrisk, >99% deuterium) was triply distilled, twice from permanganate. In other experiments 2-propanol of normal isotopic composition and acetone (Fluka Puriss) were added to the irradiated solution.

Other deuterated compounds investigated were *d*₃-methanol (Merck Sharp and Dohme Ltd., >99%), *d*₃-sodium acetate (Yeda Research and Development Co. Ltd., >98% deuterium), and *d*-sodium formate (Volk Radiochemical Co., >98% deuterium); these reagents were used without further treatment. The corresponding nondeuterated compounds were Fluka Puriss grade.

To facilitate the complete degassing of the solutions, the sealed vessels contained a glass-coated magnetic stirrer, which was removed from the solution into a side arm during the irradiation. The solutions were degassed on a vacuum line. The side arm ended with a break-off tip for subsequent gas analysis. The irradiation vessels were cleaned by boiling nitric acid, rinsed with triply distilled water, and dried in a vacuum oven at 110°. After irradiation, the gases were introduced into a mass spectrometer (CEC Model 21-401) and the masses 2, 3, and 4 were measured in the sequence $\bar{2}$, $\bar{3}$, $\bar{4}$, $\bar{3}$, $\bar{2}$, $\bar{3}$, $\bar{4}$, $\bar{3}$, $\bar{2}$. From the mean values of the three parts of the measured sequence, these ratios were calculated

$$R = (\bar{3} + 2 \times \bar{4}) / (\bar{2} - \bar{4})$$

$$R' = (\bar{3} + 2 \times \bar{2}) / (\bar{4} - \bar{2})$$

The *R* values obtained showed a standard deviation of $\pm 4\%$. Mass $\bar{4}$ had to be taken into consideration owing to eventual disproportionation of HD in the ion source of the mass spectrometer to form H₂ and D₂. Mass $\bar{2}$ had also to be corrected accordingly for the contribution of H₂ which originated from HD and which was equal to the detected amount of mass $\bar{4}$. *R* is thus the true ratio of HD/H₂ in the sample, assuming that no D₂ is formed under radiolysis.

The calculation of the isotope effect from the experimental data was carried out applying the approximation of Bigeleisen.¹¹ As the total yield of hydrogen abstracted from the α -position in the case of 2-propanol was not measured directly, the following two equations were formulated.

$$\gamma = k_{H\alpha} / k_{D\alpha} = (\text{H/D})_{\text{product}} / (\text{H/D})_{\text{reactant}} =$$

$$\frac{G(\text{H}_2)_\alpha - G(\text{HD})_m}{G(\text{HD})_m} \frac{(2\text{-H-2-propanol})}{(2\text{-d-2-propanol})} \quad (\text{I})$$

$$\frac{G(\text{H}_2)_\alpha}{G_{(\text{residual hydrogen})} - G(\text{H}_2)_\alpha} = A/2(1 + \gamma) \quad (\text{II})$$

where *k_H* and *k_D* are the rate constant for abstraction of H and D atoms, respectively, at the α -position by H atoms. *G*(H₂)_α is the total yield of hydrogen originating from the α -position, and *G*(HD)_m is the observed *G* for the formation of HD in the given mixture of 2-H- and 2-d-2-propanol. The second formula is applicable to the case of a 1:1 mixture of 2-d- and 2-H-2-propanol. *A* is the ratio between abstraction at position α and abstraction at all other positions (β -position of 2-propanol and from the acetone) in a solution containing only 2-d-2-propanol and acetone.

Formula I is the mathematical expression of the Bigeleisen approximation. *G*(H₂)_α is, however, unknown because the abstraction at position α is changed by adding 2-H-2-propanol to 2-d-2-propanol. In a 1:1 mixture of 2-H- and 2-d-2-propanol the relative reactivities of positions α and β are changed by factor of 1/2(γ + 1). This is expressed in the second formula. Having two equations with two unknowns, the isotope effect (γ) could be derived.

In the case of the other organic compounds studied, only one type of hydrogen atom is involved, thus the complications of the previously cited elaborate treatment could be avoided, using $1 \times 10^{-3} M$ ZnSO₄ as an electron scavenger instead of acetone.¹² Solutions (0.05 *M*) of the deuterated compounds and of mixtures of different ratios of the deuterated and undeuterated compound, at pH 6, were irradiated.

Results and Discussion

The isotope effect involved in the abstraction of the α -hydrogen in 2-propanol was determined as follows. 2-d-2-Propanol (0.04 *M*) and acetone (0.05 *M*) in H₂O were irradiated at pH 6, yielding *R* = 0.58. In a solution containing 0.02 *M* 2-d-2-propanol, 0.02 *M* 2-H-2-propanol, and 0.05 *M* acetone, *R* = 0.068 was obtained. From these values *G*(HD) was calculated according to *G*(HD) = *G*(H₂) [*R* / (*R* - 1)] taking *G*(H₂) = 0.95.^{13,14} In the first solution *G*(HD) = 0.35 and in the second *G*(HD) = 0.061 were obtained. From these values, the value of *G*_{residual hydrogen} = 0.62 (Table I), and the ratio *A* for abstraction at position α vs. all other positions *A* = 0.35/0.27 (Table I) were derived. The isotope effect $\gamma = k_{H\alpha} / k_{D\alpha} = 7.6$ was calculated (see Experimental section).

(11) J. Bigeleisen, *J. Chem. Phys.*, **17**, 425 (1949).

(12) J. H. Baxendale and R. S. Dixon, *Proc. Chem. Soc.*, 148 (1963).

(13) J. T. Allan, M. G. Robinson, and G. Scholes, *Proc. Chem. Soc.* 381 (1962).

(14) G. Scholes and M. Simic, *Nature*, **196**, 276 (1963).

Table I: Isotope Composition of the Hydrogen Evolved from Radiolyzed Solutions of 2-*d*-2-Propanol^a

Expt. no.	pH	Isotopic composition of water	Acetone, <i>M</i>	Total dose, e.v./g. × 10 ¹⁹	<i>R</i>	<i>R'</i>	<i>G</i> (HD)
1.1	6	H ₂ O	1 × 10 ⁻³	5.9	0.88	...	0.44
1.2	6	H ₂ O	1 × 10 ⁻³	11.8	0.84	...	0.43
1.3	6	H ₂ O	1 × 10 ⁻³	23.6	0.68	...	0.38
1.4	6	D ₂ O	1 × 10 ⁻³	11.8	...	0.21	0.17
1.5	6	H ₂ O	5 × 10 ⁻²	11.8	0.58	...	0.35
1.6	6	D ₂ O	5 × 10 ⁻²	11.8	...	0.38	0.27
1.7	1	H ₂ O	...	11.8	2.02	...	2.71
1.8	1	D ₂ O	...	11.8	...	0.35	1.13

^a 2-*d*-2-Propanol, 0.04 *M*.

In acid solution 0.04 *M* 2-*d*-2-propanol in H₂O was irradiated at pH 1.0 yielding *R* = 2.02. A mixture containing 0.02 *M* 2-*d*-2-propanol and 0.02 *M* 2-H-2-propanol irradiated under the same conditions gave *R* = 0.121. Taking *G*(H₂) = 4.05 in acid solution,¹² *G*(HD) for both solutions was calculated, giving *G*(HD) = 2.71 and *G*(HD) = 0.437, respectively. Analogous to the calculation in neutral solutions, an isotope effect $\gamma = k_{H\alpha}/k_{D\alpha} = 7.0$ was derived.

In order to get information on the relative reactivity of the α - vs. β -hydrogens, solutions of 0.04 *M* 2-*d*-2-propanol and acetone were irradiated in water of different isotopic composition, and the *R* and *R'* values were determined. The results are summarized in Table I.

From the *R* values of experiments 1.1, 1.2, 1.3, and 1.5, the *G*(HD) was calculated from $G(\text{HD}) = G(\text{H}_2) \cdot [R/(R+1)]$, taking *G*(H₂) = 0.95.^{13,14} *G*(HD) for experiments 1.4 and 1.6 was obtained from $G(\text{H}_2)[R'/(R'+1)]$ where *G*(H₂) = 0.98 in D₂O was taken, after correction for the deuterium isotope effect.^{15,16} For the experiment 1.7, which was carried out in acid solution, *G*(HD) was obtained from $G(\text{H}_2)[R/(R+1)]$ taking *G*(H₂) = 4.05,¹² and for experiment 1.8, $G(\text{HD}) = G(\text{H}_2)[R'/(R'+1)]$ where *G*(H₂) in D₂O is equal to 4.35.¹⁶ From experiments 1.1 and 1.4, $G_{(\text{residual hydrogen})} = 0.61$ was calculated (the correction due to the deuterium isotope effect is less than 1% and was thus neglected). From *G*(HD) of experiments 1.1 and 1.4 the contributions of the α - and β -hydrogens of 2-propanol were calculated giving the relative reactivity $D_{\alpha}/H_{\beta} = G(\text{HD})_1/G(\text{HD})_4 = 2.58$.

Taking into account the isotope effect, $H_{\alpha}/H_{\beta \text{ total}} = 19.6$ was calculated, and from this the reactivity of H_{α}/H_{β} in neutral solutions may be derived as $6 \times 19.6 = 118$.

In complete analogy to the treatment of the neutral solutions, the relative reactivity of H_{α}/H_{β} could be calculated for acid solutions from $D_{\alpha}/H_{\beta} = 2.5$; $H_{\alpha}/H_{\beta \text{ total}} = 17.5$; $H_{\alpha}/H_{\beta} = 105$. It may be concluded, therefore, that the relative reactivities of H_{α} and H_{β} in acid and in neutral solutions are equal within the experimental error.

In all these calculations it has been assumed that hydrogen atoms do not abstract the hydroxylic hydrogen of alcohols.^{8,17}

The effect of the total dose on *G*(HD) may be calculated from experiments 1.1, 1.2, and 1.3. It is evident that *G*(HD) diminishes with dose; the effect is, however, rather small. This effect may be due to the formation of 2-H-2-propanol by disproportionation of the CH₃COHCH₃ radical.¹

In the presence of higher concentrations of acetone, *R* is diminished and *R'* is increased; this is due to hydrogen abstraction from acetone.¹⁸

It has been shown that the reactivity of the α -hydrogen in 2-propanol toward hydrogen atoms is higher than that of the β -hydrogens by a factor of about 110. The same factor is obtained in neutral and in acid solutions. Taking the rate of hydrogen abstraction for 2-propanol as 2.6×10^6 l. mole⁻¹ sec.⁻¹,¹⁹ one obtains 2.4×10^4 l. mole⁻¹ sec.⁻¹ for the rate of abstraction of one of the methyl hydrogens. This value is in satisfactory agreement with the values obtained for the rate of abstraction for one of the methyl hydrogens of acetone,¹⁸ namely 7.5×10^3 l. mole⁻¹ sec.⁻¹, of acetate,¹⁹ namely 4.7×10^3 l. mole⁻¹ sec.⁻¹, and of ethanol,^{8,9} 3.4×10^4 l. mole⁻¹ sec.⁻¹.

The complete identity, within the experimental error, obtained for the relative reactivities and isotope effects of hydrogen abstraction in neutral and acid solutions suggests that the reacting species is the same in both cases. This implies that the "residual hydrogen" is identical with H atoms. In a previous study it has been shown that hydrogen abstraction in neutral solutions by the "residual hydrogen" is affected by reactants which do not interact with hydrogen atoms.³ It may be, therefore, suggested that the species different from H, OH, and e_{aq}⁻, which was observed, is a precursor of the residual hydrogen.

The isotope effects on the hydrogen abstraction from

(15) A. A. Mahlman and J. W. Boyle, *J. Am. Chem. Soc.*, **80**, 773 (1958).

(16) K. Coatsworth, E. Collinson, and F. S. Dainton, *Trans. Faraday Soc.*, **56**, 1008 (1960).

(17) J. H. Baxendale and G. Hughes, *Z. Physik. Chem.*, **14**, 306 (1958).

(18) S. Nehari and J. Rabani, *J. Phys. Chem.*, **67**, 1609 (1963).

(19) J. Rabani, *ibid.*, **66**, 361 (1962).

methanol and from formate and acetate ions were determined; the results are summarized in Table II. In order to determine whether the high isotope effect observed for methanol and acetate is not due to some complex reactions, mixtures of different ratios between the normal and deuterated compounds were examined.

Table II: Isotope Effects in Hydrogen Abstraction by Radiolytically Produced Hydrogen Atoms^a

Substrate	k_H/k_D	$\frac{k_H - \text{substrate}}{k_H - \text{formate}}^b$
Sodium formate	6.5 ± 0.5^c	1
2-Propanol	7.5 ± 1	3.3×10^{-1}
Methanol	20.0 ± 1	1.1×10^{-2}
Sodium acetate	22.0 ± 4	1.8×10^{-3}

^a All experiments at pH 6. ^b Values calculated from ref. 9. ^c $k_H/k_D = 6.6 \pm 0.7$ for formate was measured by Appleby, *et al.*⁹

The results showed a constant isotope effect for mixtures 4:1 to 1:1.5 of the two isotopic species. It should be noted that the inaccuracy in the case of acetate is higher than in the other cases, as some exchange of deuterium

with the hydrogen of the water takes place during irradiation. To correct for this, a series of samples with different ratios between H_3 -acetate and D_3 -acetate were irradiated and the result was obtained by extrapolation.

The results clearly indicate that the kinetic isotope effect increases with a decrease in the rate of reaction for this series of reactions as was expected. As the pre-exponential factors are not expected to be equal, no linear correlation to the rate constants could be found.

From the high values of the isotope effect measured for methanol and acetate, it is clear that hydrogen tunneling is involved in these reactions.²⁰⁻²² A comparable value was obtained for the isotopic effect on the abstraction of the α -hydrogens of ethanol.⁸ It is also plausible that the contribution of a tunneling effect increases in reactions of lower rate.

Acknowledgment. The authors are thankful to Dr. J. Bigeleisen for helpful discussions.

(20) R. P. Bell, *Discussions Faraday Soc.*, **29**, 253 (1960).

(21) T. E. Sharp and H. S. Johnston, *J. Chem. Phys.*, **37**, 1541 (1962).

(22) Y. Rousseau, G. N. C. Woodall, and H. E. Gunning, *ibid.*, **37**, 2722 (1962).

A Correlation between Vibrational Isotope Shifts and Mass

Spectral Fragmentation Patterns^{1a}

by Walter J. Lehmann^{1b}

Department of Chemistry, University of California, Los Angeles, California 90024 (Received May 27, 1964)

Isotope effects on vibrational frequencies are straightforward and well understood. On the other hand, theories dealing with isotope effects on mass spectra are relatively complex and difficult to apply. Although these effects are of great concern in connection with isotope-abundance determinations, they are often disregarded; *e.g.*, for many years the "accepted" B¹¹/B¹⁰ natural-abundance ratio, 4.31, was based on the direct ratio of BF₂⁺ fragments of boron trifluoride, which the present paper shows to lead to a false ratio. The present study suggests a very simple direct correlation between vibrational frequency shifts and mass spectral isotope effects for diatomic and quasi-diatomic molecules.

In 1959 a revision of the atomic weight of boron from 10.82 to 10.811 was proposed^{2a} several years before the International Commission on Atomic Weights accepted such a change.^{2b} The Commission's report was based on work by McMullen, Cragg, and Thode,³ who reported a B¹¹/B¹⁰ ratio in the range of 4.04 to 4.07 (± 0.04), later extended to 3.95 to 4.10. (The range apparently reflects a natural variation of the boron isotope ratio.)

Those results are based on mass spectral measurements of the Na₂BO₂⁺ peaks of borax and were calibrated against synthetic mixtures prepared from B¹⁰- and B¹¹-enriched borax.

The fact that these values differed significantly from previous measurements based on *direct* comparison of B¹¹F₂⁺ and B¹⁰F₂⁺ fragments from boron trifluoride was attributed to "mass discrimination." Generally, such discrimination in mass spectrometry is ascribed to instrumental conditions. It becomes evident, however, that an entirely different type of discrimination effect is at work here—namely, an effect that is inherent in the fragmentation process itself.

Mass spectrometrists have long been familiar with isotope effects on molecular fragmentation.⁴ For example, it has been shown⁴ that in monodeuterio-methane the hydrogens fragment approximately twice as easily as the deuterium (after allowance for statistical effects). A check of the literature, however, reveals

that these effects have not been taken into consideration in many isotope-abundance determinations.⁵⁻¹¹

Consideration of molecular vibrations immediately focuses attention on such effects. The BF₂⁺ fragment is produced when the "elastic limit" is exceeded during an asymmetric vibration of the BF₃ molecule. Natu-

(1) (a) Contribution No. 1618. Presented in part at the Seventh European Congress on Molecular Spectroscopy, Budapest, Hungary, July, 1963; (b) Department of Chemistry, University of California, Riverside, Calif. 92502.

(2) (a) W. J. Lehmann and I. Shapiro, *Nature*, **183**, 1324 (1959); (b) International Commission on Atomic Weights (IUPAC Montreal, 1961); *J. Am. Chem. Soc.*, **84**, 4175 (1962).

(3) C. C. McMullen, C. B. Cragg, and H. G. Thode, *Geochim. Cosmochim. Acta*, **23**, 147 (1961).

(4) F. H. Field and J. L. Franklin, "Electron Impact Phenomena," Academic Press, Inc., New York, N. Y., 1957, pp. 204-217 and list of references therein.

(5) M. G. Inghram, *Phys. Rev.*, **70**, 653 (1946).

(6) G. M. Panchenkov and V. D. Moiseev, *Zh. Fiz. Khim.*, **30**, 1118 (1956). This paper contains a review of other boron isotope investigations.

(7) C. E. Melton, C. O. Gilpatrick, R. Baldoak, and R. M. Healy, *Anal. Chem.*, **28**, 1049 (1956).

(8) V. Shiuttse, *Soviet Phys. JETP*, **2**, 402 (1956); translated from *Zh. Eksperim. i Teor. Fiz.*, **29**, 486 (1955).

(9) N. N. Sevryugova, O. V. Uvarov, and N. M. Zhavoronkov, *J. Nucl. Energy*, **4**, 483 (1957); translated from *At. Energy*, (USSR), **1**, 113 (1956).

(10) R. W. Law and J. L. Margrave, *J. Chem. Phys.*, **25**, 1086 (1956).

(11) R. M. Abernathy, Seventh Annual Meeting of the ASTM Committee E-14 on Mass Spectrometry, Los Angeles, Calif., May, 1959.

rally, such a vibration, in which the boron atom essentially moves against three heavier fluorine atoms, is strongly isotope dependent, and this isotope dependency will be reflected in the fragmentation process, thus influencing the observed B^{11}/B^{10} ratio of BF_2^+ fragments.

The same would be expected, and is observed, for trimethylborane.¹² As a matter of fact, several apparent ratios are observed, depending on the spectral region and the fragment species under consideration. In the BC_2 region a ratio of 4.12 is obtained, but for the low-mass region 3.77 is observed. A number of other compounds similarly have been found to yield more than one apparent abundance ratio (Table I).¹²⁻¹⁶

Table I: Variation of Apparent Isotope-Abundance Ratio with Mass Group

Compound	Fragment group	B^{10}/B^{11}
B_2D_6	B_2	4.00
	B	3.85
B_5H_9	B_5	4.00
	B	3.85
Me_3B	Me_2B	4.12
	B	3.77
$Me_3B_3O_3$	$Me_3B_3O_3$	3.98
	$Me_2B_3O_3$	
	B	3.6
CCl_4		Cl^{35}/Cl^{37}
	CCl_3	3.12
	Cl	3.22

When different fragments of the same compound lead to divergent isotope ratios, obviously not both can represent a true value. But which to choose, if any? Without additional considerations we would have no basis for a choice, once errors in measurements have been eliminated.

It has previously been proposed^{12,17} that these apparent abundance ratios should be resolvable into true abundance ratios and correction factors that take into account isotope effects on fragmentation. To determine true abundance ratios, we thus seek compounds having minimal correction factors.

The principal fragments of the boron hydrides, representing successive losses of hydrogens, are produced by the vibration of the light hydrogen atoms against the heavy boron frame. Such vibrations are approximately independent of the boron mass. Like-

wise, the principal fragment, $Me_2B_3O_3^+$, of trimethylboroxine is produced by an out-of-phase vibration of the relatively light methyl group against a massive boron-oxygen ring. Vibrational motion again is concentrated in the methyl group and is very nearly independent of whether the ring contains B^{10} or B^{11} .

With these considerations in mind, it is not surprising that the principal peaks of the boron hydrides^{13,14,17-22} and of trimethylboroxine¹⁵ yield identical values, namely, an isotope ratio of 4.00, even though the boron hydrides are produced by rupture of B-H bonds, while the latter case involves breakage of a B-C linkage. (It is to be remembered that breaking of the B-C bond in Me_3B yielded an apparent ratio of 4.12.¹²)

It would be useful to have some means for at least a rough *a priori* prediction of mass spectral isotope effects, since their experimental determination is rather cumbersome. The following represents such a scheme for diatomic or "quasi-diatomic" molecules.

Consider the case of molecule AB rupturing to give fragments A and B, and its isotopic relative AB^* yielding A and B^* . AB^* will fragment less easily than AB if B^* represents the heavy isotope. For example, comparison of fragments from H_2 and D_2 shows that the protium molecule breaks up twice as easily as the deuterium molecule^{4,23}; *i.e.*, the fragmentation ratio, $f = (H^+/H_2^+)/(D^+/D_2^+)$, is approximately 2.

Table II lists experimentally determined relative fragmentation probabilities for a number of simple compounds.^{23,24} It can be seen that each f value is

(12) W. J. Lehmann, C. O. Wilson, Jr., and I. Shapiro, *J. Inorg. Nucl. Chem.*, **11**, 91 (1959).

(13) V. H. Dibeler, F. L. Mohler, L. Williamson, and R. M. Reese, *J. Res. Natl. Bur. Std.*, **43**, 97 (1949).

(14) V. H. Dibeler, F. L. Mohler, and L. Williamson, *ibid.*, **44**, 489 (1950).

(15) W. J. Lehmann, C. O. Wilson, Jr., and I. Shapiro, *J. Inorg. Nucl. Chem.*, **21**, 25 (1961).

(16) "Catalog of Mass Spectral Data," Carnegie Institute of Technology, Pittsburgh, Pa., American Petroleum Institute Research Project 44, Serial No. 603.

(17) I. Shapiro and J. F. Ditter, *J. Chem. Phys.*, **26**, 798 (1957).

(18) V. H. Dibeler and F. L. Mohler, *J. Am. Chem. Soc.*, **70**, 987 (1948).

(19) F. J. Norton, *ibid.*, **71**, 3488 (1949).

(20) J. F. Ditter and I. Shapiro, *ibid.*, **81**, 1022 (1959).

(21) S. G. Gibbins and I. Shapiro, *J. Chem. Phys.*, **30**, 1483 (1959).

(22) J. F. Ditter, E. B. Klusmann, J. C. Perrine, and I. Shapiro, *J. Phys. Chem.*, **64**, 1682 (1960).

(23) O. A. Schaeffer and J. M. Hastings, *J. Chem. Phys.*, **18**, 1048 (1950).

(24) O. Schaeffer, Proceedings of the NBS Semicentennial Symposium on Mass Spectroscopy in Physics Research, Washington, D. C., September, 1951, published in "Mass Spectroscopy in Physics Research," NBS Circular 522, January, 1953, p. 249.

numerically equal to the square of the ratio of the zero-order vibrational frequencies (4395 and 3118 cm^{-1} for H_2 and D_2 , respectively)²⁵ or the equivalent inverse ratio of the reduced masses. (The complex Franck-Condon calculation, which can be applied only to the simplest of molecules, yields 2.2 for hydrogen.^{4,23})

Admittedly, this correlation is only approximately valid for the extreme case of tritium as compared to protium, where the observed^{4,23,26} f factor is between 3.3 and 3.7, while the ratio of frequencies squared²⁵ or reduced masses is 3.0. (On the other hand, using the Franck-Condon theory, Schaeffer and Hastings calculated the equally divergent value of 4.2.^{4,23}) When smaller isotope effects are involved, such as for isotopic variants of N_2 , O_2 , and CO , reduced-mass ratios agree well with observed f values (and are at least as good as values calculated from the Franck-Condon theory).^{23,24}

The simple correlations of the present paper can be extended to polyatomic molecules which can be treated as quasi-atomic, such as diborane, B_2H_6 , which can, for the present purpose, be considered as made up of two BH_3 units (even though the borons are linked through three-center bonds with hydrogen bridges).

Because of overlapping contributions to mass spectral peaks, due to successive losses of H atoms, boron-abundance ratios in boron hydrides must be calculated through a "stripping" process^{18,19} which also yields the monoisotopic patterns. Most workers dealing

only 0.3% or less for a difference of one mass unit,^{27,28} and even in the low-mass region it is difficult to account for an instrumental discrimination effect that is 4% greater.

The value 0.25, obtained from the parent regions of a number of boron hydrides, is probably close to the true $\text{B}^{10}/\text{B}^{11}$ abundance ratio^{2a} because the difference in fragmentation probabilities between a $\text{B}^{11}\text{-H}$ and a $\text{B}^{10}\text{-H}$ bond is negligible (since the heavy boron atom participates only slightly in B-H stretching vibrations) and because the sum of B_1H_x fragments is relatively small compared to the sum of B_2H_x fragments.

On the other hand, boron isotopes should have considerable effect on B-B bond rupture. Let us say that a $\text{B}^{10}\text{-B}^{10}$ bond ruptures f times as easily as a $\text{B}^{11}\text{-B}^{11}$ bond and that the $\text{B}^{10}\text{-B}^{11}$ fragmentation factor is midway— $0.5(1 + f)$. We can calculate f by making only a few simplifying assumptions.

Probability statistics predict the compounds $\text{B}^{11}_2\text{H}_6$, $\text{B}^{11}\text{H}^{10}\text{H}_6$, and $\text{B}^{10}_2\text{H}_6$ to occur in the ratio $1:2R:\bar{R}^2$, where R is the $\text{B}^{10}/\text{B}^{11}$ ratio. For $R = 0.25$, this becomes 1:0.50:0.0625. Each B^{11}_2 rupture yields two B^{11} fragments. Each $\text{B}^{11}\text{-B}^{10}$ rupture yields one B^{11} and one B^{10} fragment, both quantities being proportional to the $\text{B}^{11}\text{B}^{10}$ abundance ($2R$) and the fragmentation factor [$0.5(1 + f)$]; i.e., $R(1 + f)$. Similarly, B^{10}_2 fragmentation produces B^{10} fragments in the relative amount of $2R^2f$. In the low-mass region, the apparent $\text{B}^{10}/\text{B}^{11}$ ratio thus is

$$R_a = [R(1 + f) + 2R^2f]/[2 + R(1 + f)]$$

Using the values of 0.25 and 0.26 for R and R_a , respectively, we find f to be 1.08.

In other words, interpretation of mass spectral data indicates that the B^{10}_2 bond ruptures 8% more readily than the B^{11}_2 bond. Again, this value corresponds closely to the square of the ratio of the B-B stretching frequencies of $\text{B}^{10}_2\text{H}_6$ and $\text{B}^{11}_2\text{H}_6$ —816 and 788 cm^{-1} , respectively²⁹—viz., 1.072. A similar value, 1.077, also is obtained from the ratio of the reduced masses of $\text{B}^{11}_2\text{H}_6$ ($\mu = 7$) and $\text{B}^{10}_2\text{H}_6$ ($\mu = 6.5$) when we consider them simply as consisting of two BH_3 groups oscillating against each other.

A word of caution: Application of this scheme is

Table II: Correlation of Fragmentation Probability with Reduced Mass or Vibrational Frequencies

Molecule	Rel. fragm. prob.	μ_2/μ_1	$(\nu_1/\nu_2)^2$
H_2 (D_2)	~1.9-2.3	2.00	1.99
N_2 (N^{15})	1.10	1.07	...
CO (C^{13})	1.04	1.05	...
$\text{BH}_3\text{-BH}_3$	1.08	1.08	1.07

with isotopically normal boron hydrides have found the value of 0.25 to be the best $\text{B}^{10}/\text{B}^{11}$ ratio for calculating monoisotopic fragmentation patterns from observed polyisotopic mass spectra in the higher mass regions.^{13,14,17-22} However, for monoboron fragments, a ratio of 0.26 has been found applicable.^{13,14}

Instrumental mass-discrimination effects alone cannot satisfactorily account for this 4% difference. The high-mass fragments, representing loss of hydrogens, do not possess much kinetic energy. Hence, mass discrimination effects here should be of the order of

(25) G. Herzberg, "Spectra of Diatomic Molecules," D. Van Nostrand Co., Inc., Princeton, N. J., 1950, p. 532.

(26) V. H. Dibeler, F. L. Mohler, E. J. Wells, Jr., and R. M. Reese, *J. Res. Natl. Bur. Std.*, **45**, 288 (1950).

(27) C. E. Berry, *Phys. Rev.*, **78**, 597 (1950).

(28) F. H. Field and J. L. Franklin, "Electron Impact Phenomena," Academic Press, Inc., New York, N. Y., 1957, p. 99.

(29) R. C. Taylor and A. R. Emery, *Spectrochim. Acta*, **10**, 419 (1958).

restricted to "quasi-diatomic" molecules in which the resulting fragments have approximately identical internal vibrational frequencies. (This is true for the fragments $B^{11}H_3$ and $B^{10}H_3$, since their vibrations involve motions of light hydrogens against essentially fixed B^{10} or B^{11} atoms.) The method must not be applied when the fragment pairs differ greatly in internal vibrational energy. For example, we cannot compare CD_3-CD_3 with CH_3-CH_3 bond rupture since

the fragments CD_3 and CH_3 have quite different vibrational energies.

To summarize, it seems that vibrational frequencies and masses can advantageously be used in a very simple manner to estimate isotope effects on mass spectral patterns of diatomic and quasi-diatomic molecules. In view of these effects, greater care should be taken in the application of mass spectral data for isotopic-abundance determinations.

Energetics of Some Gaseous Oxygenated Organic Ions^{1a}

by M. S. B. Munson^{1b} and J. L. Franklin^{1c}

Research and Development, Humble Oil and Refining Company,
Baytown, Texas, and Rice University, Houston, Texas (Received June 3, 1964)

The heats of formation of some simple oxygenated organic compounds have been measured from different sources; $\Delta H_f(CH_2OH^+) = 174$ kcal./mole and $\Delta H_f(CH_3O^+) = 202$ kcal./mole. Similar differences exist for the isomers of mass 45. The proton affinities of formic, acetic, and propionic acids were determined from rearrangement ions of esters as about 170–180 kcal./mole. The protonated acid ions are readily formed by ionic reactions in the gaseous aliphatic acids. Appearance potential data for H_3O^+ and $CH_3OH_2^+$ may be interpreted to give $P(H_2O) \cong P(CH_3OH) \cong 170$ kcal./mole.

The tabulation of appearance potentials and heats of formation of simple oxygenated ions by Field and Franklin^{1d} indicated several apparent discrepancies as well as a lack of data for certain ions. It seemed worthwhile to obtain further data on energetics of oxygenated organic ions. There were also indicated several potentially interesting variations of ion energy with structure which appeared worthy of study.

Experimental

The compounds for this study were obtained from various sources (purity about 99%) and used with only simple further purification since the fragments under study were generally prominent in the spectrum. Some of the compounds were prepared and purified by Dr. R. H. Perry of these laboratories. The mass spectrometer was that previously described by Field.² The appearance potentials reported in this paper were

obtained from the threshold of a plot of ion current *vs.* electron energy, for which the slopes of the curves of the desired ion and the calibrating ion were made about equal over a 2-v. range above the threshold or onset potential. The appearance potentials are generally the average of three or four separate determinations with two calibrating gases. Measured differences in ionization potentials of rare gases were within ± 0.1 v. of the spectroscopic differences. The pressures within the ionization chamber were not measured, but were never greater than about 10 μ . These pressures,

(1) (a) Supported in part by Project SQUID under Contract No. Nonr-3623 (S-18); (b) Humble Oil and Refining Co.; (c) Rice University; (d) F. H. Field and J. L. Franklin, "Electron Impact Phenomena and the Properties of Gaseous Ions," Academic Press, New York, N. Y., 1957.

(2) F. H. Field, *J. Am. Chem. Soc.*, **83**, 1523 (1961).

however, were high enough so that ionic reactions forming the "parent-plus-one" ion were noted.

Results and Discussion

I. Protonated Species. RCO_2H_2^+ ions as rearrange-

ment ions of esters $\text{R}'\text{-O}-\overset{\text{O}}{\parallel}{\text{C}}-\text{R}$ have been observed for $\text{R}' = \text{ethyl, propyl, or butyl}$ and $\text{R} = \text{H, methyl, ethyl, or propyl}$.³ The stoichiometry of these ions has been confirmed by high resolution mass spectrometry.⁴ Godbole and Kebarle⁵ studied deuterated ethyl and isopropyl acetates and deuterated ethyl formate and concluded that the removal of H atoms from the R' group was essentially random and that the R group remained intact. These results may also be interpreted as indicating that removal of both H atoms from the C atom β to the carbonyl group is very improbable and that β - γ removal is more probable than γ - γ removal. McLafferty⁶ reports the spectra of 2- and 3-*d-sec*-butyl acetates as involving β -, γ -, and δ -hydrogens in these rearrangement ions. Black, McFadden, and Corse⁷ in their study of deuterated *n*-butyl acetates suggested selective transfer of a γ -hydrogen followed by random selection of the other hydrogen. Their data show that hydrogens on the fourth carbon atom from the ether oxygen (ϵ -hydrogens) play little part in the rearrangement process and that very little β - β hydrogen transfer occurs.

The appearance potentials of the rearrangement ions RCO_2H_2^+ are reported in Table I, together with literature values. The value for the appearance potential of HCO_2H_2^+ from $\text{C}_2\text{H}_5\text{O}_2\text{CH}$ in this paper is lower than that of Godbole and Kebarle but gives a more consistent value for $\Delta H_f(\text{HCO}_2\text{H}_2^+)$ than their value.

Since β - β removal of hydrogen atoms is inconsequential, the C_2H_3 produced from the ethyl esters should be the vinyl radical; $\Delta H_f(\text{C}_2\text{H}_3) = 65$ kcal./mole.⁸ C_3H_5 from the propyl esters may be the allyl radical ($\dot{\text{C}}\text{H}_2-\text{CH}=\text{CH}_2$), $\Delta H_f = 30$ kcal./mole,⁹ produced by γ - δ removal of hydrogen atoms. Other possibilities are $\text{CH}_3-\text{CH}=\dot{\text{C}}\text{H}$ and $\text{CH}_3-\dot{\text{C}}=\text{CH}_2$ for which ΔH_f is estimated as about 58 kcal./mole from the assumption that the dissociation energies of the C-H bonds are 105 kcal./mole as for ethylene.⁸ The other possibility, $\dot{\text{C}}\text{H}_2-\text{CH}_2-\dot{\text{C}}\text{H}$, is the cyclopropyl radical for which ΔH_f is estimated to be 53 kcal./mole from the electron impact data of Pottie, Harrison, and Lossing.¹⁰

$\Delta H_f(\text{C}_2\text{H}_5\text{O}_2\text{CH}) = -88$ kcal./mole¹¹; therefore $\Delta H_f(\text{HCO}_2\text{H}_2^+) = 109$ kcal./mole. From the data of Gray and Williams⁹ on the heats of formation of ace-

tate esters, one may estimate an increment of -6 kcal./mole per CH_2 group of the alcohol, from which $\Delta H_f(\text{C}_3\text{H}_7\text{O}_2\text{CH})$ is estimated to be -94 kcal./mole.¹² If the neutral C_3H_5 is the allyl radical then $\Delta H_f(\text{CHO}_2\text{H}_2^+) = 130$ kcal./mole, which is not in good agreement with the previous value. However, if $\Delta H_f(\text{C}_3\text{H}_5) \cong 55$ kcal./mole, as would be the case if the other structures were formed, then $\Delta H_f(\text{CHO}_2\text{H}_2^+)$ from propyl formate would be 105 kcal./mole. Taking $\Delta H_f(\text{HCO}_2\text{H}_2^+)$ as 107 kcal./mole, one may calculate the proton affinity of formic acid, $P(\text{HCO}_2\text{H}) = 166$ kcal./mole, using $\Delta H_f(\text{HCO}_2\text{H}) = -90$ kcal./mole.¹²

$\Delta H_f(\text{C}_2\text{H}_5\text{O}_2\text{CCH}_3) = -103$ kcal./mole¹²; therefore $\Delta H_f(\text{CH}_3\text{CO}_2\text{H}_2^+) = 81$ kcal./mole. $\Delta H_f(\text{C}_3\text{H}_7\text{O}_2\text{CCH}_3)$ is probably about -111 kcal./mole.^{9,12} Taking $\Delta H_f(\text{C}_3\text{H}_5) \cong 55$ kcal./mole, one obtains $\Delta H_f(\text{CH}_3\text{CO}_2\text{H}_2^+) \cong 74$ kcal./mole. $\Delta H_f(\text{C}_3\text{H}_5) = 30$ kcal./mole gives a value of 99 kcal./mole which is above that value obtained from ethyl acetate by an amount essentially the same as in the case of the formates. This similarity increases the confidence in the assignment of the fragmentation processes. With $\Delta H_f(\text{CH}_3\text{CO}_2\text{H}_2^+) = 77$ kcal./mole, one may calculate the proton affinity of acetic acid, $P(\text{CH}_3\text{CO}_2\text{H}) = 184$ kcal./mole, using $\Delta H_f(\text{CH}_3\text{CO}_2\text{H}) = -104$ kcal./mole.¹²

$\Delta H_f(\text{C}_2\text{H}_5\text{O}_2\text{CC}_2\text{H}_5) = -111$ kcal./mole¹¹; therefore $\Delta H_f(\text{C}_2\text{H}_5\text{CO}_2\text{H}_2^+) = 65$ kcal./mole. Using $\Delta H_f(\text{C}_2\text{H}_5\text{CO}_2\text{H}) = -114$ kcal./mole,¹¹ one may calculate the proton affinity of propionic acid, $P(\text{C}_2\text{H}_5\text{COOH}) = 185$ kcal./mole. It is doubtful that the accuracy of these numbers warrants a discussion of these differences.

It was not possible with the present method of measuring pressure within the ionization chamber to determine, with sufficient accuracy, pressures of sub-

(3) A. G. Sharkey, J. L. Schultz, and R. A. Friedel, *Anal. Chem.*, **31**, 87 (1959).

(4) J. H. Beynon, R. A. Saunders, and A. E. Williams, *ibid.*, **33**, 221 (1961).

(5) E. W. Godbole and P. Kebarle, *Trans. Faraday Soc.*, **58**, 1897 (1962).

(6) F. W. McLafferty, *Anal. Chem.*, **31**, 82 (1959).

(7) D. R. Black, W. H. McFadden, and J. W. Corse, paper presented at 11th Conference on Mass Spectrometry, ASTM Committee E-14, San Francisco, Calif., May, 1963.

(8) B. E. Knox and H. B. Palmer, *Chem. Rev.*, **61**, 247 (1961).

(9) P. Gray and A. Williams, *ibid.*, **59**, 239 (1959).

(10) R. F. Pottie, A. G. Harrison, and F. P. Lossing, *J. Am. Chem. Soc.*, **83**, 3204 (1961).

(11) National Research Council of the U. S. A., "International Critical Tables," Vol. 5, McGraw-Hill Book Co., Inc., New York, N. Y., 1926, pp. 167 and 137.

(12) There is a paucity of thermodynamic data on organic oxygen compounds, and the data available frequently are in disagreement by a few kcal./mole. See J. H. S. Green, *Quart. Rev. (London)*, **15**, 125 (1961).

Table I: Appearance Potentials and Heats of Formation of RCO_2H_2^+ Ions

Molecule	Ion	A, v.		ΔH_f , kcal./mole
		These data	Lit.	
$\text{HCO}_2\text{-C}_2\text{H}_5$	HCO_2H_2^+	11.3 ± 0.1	11.73 ^a	109 (115) ^c
$\text{HCO}_2\text{-C}_3\text{H}_7$	HCO_2H_2^+	11.0		105
$\text{CH}_3\text{CO}_2\text{C}_2\text{H}_5$	$\text{CH}_3\text{CO}_2\text{H}_2^+$	10.8	10.95, ^a 11.0, ^b 10.8 ^c	81
$\text{CH}_3\text{CO}_2\text{C}_3\text{H}_7$	$\text{CH}_3\text{CO}_2\text{H}_2^+$	10.5		74
$\text{C}_2\text{H}_5\text{CO}_2\text{C}_2\text{H}_5$	$\text{C}_2\text{H}_5\text{CO}_2\text{H}_2^+$	10.4	10.77 ^a	65

^a See ref. 5. ^b Private communication from Sharkey, Hickam, and Friedel in ref. 5. ^c R. R. Bernecker and F. A. Long, *J. Phys. Chem.*, **65**, 1565 (1961).

stances which are liquid at room temperature and pressures less than 1 atm. It is easily possible, however, to introduce moderate pressures (probably as high as several tens of microns) of acid into the source to establish that RCO_2H_2^+ is formed by ionic reaction.

With formic acid a plot of I_{47}/I_{46} (the ratio of HCOOH_2^+ to HCOOH^+) increased linearly with increasing I_{46} (which should be proportional to pressure) as one would expect for the ratio of a secondary to a primary ion. In the same experiments I_{45}/I_{46} (the ratio of HCOO^+ to HCOOH^+) was independent of pressure as one would expect for the ratio of two primary ions. $A(\text{HCOOH}_2^+)$ is 11.5 ± 0.1 v. determined at high enough pressure that the C^{13} isotope of HCOOH^+ was small relative to HCOOH_2^+ . $I(\text{HCOOH}) = 11.5 \pm 0.1$ v. which value is in good agreement with the results of Morrison.¹³ The ionization efficiency curves for formic acid give no evidence for the *cis* and *trans* forms suggested by Mariner and Bleakney¹⁴ who reported 11.0 and 11.6 v. for ionization potentials of these forms of formic acid. The formation of HCOOH_2^+ from reaction of HCOOH^+ with HCOOH is exothermal. The formation of such large relative amounts of HCOOH_2^+ indicate that the rate constant for the formation must be of the order of 10^{-9} cc./molecule sec.

$\text{CH}_3\text{COOH}_2^+$ is a second-order product ion in acetic acid, whose appearance potential is 10.8 v. $I(\text{CH}_3\text{-COOH})$ was also determined as 10.8 v. in good agreement with the value reported by Morrison and Nicholson.¹⁵ The formation of $\text{CH}_3\text{COOH}_2^+$ from reaction of CH_3COOH^+ with CH_3COOH is exothermal, with a rate constant which should be of the order of 10^{-9} cc./molecule sec.

In formic acid at the highest pressure (at which $I_{46}/I_{47} = 0.12$) mass 93, $\text{H}(\text{HCOOH})_2^+$, was observed; $I_{93}/I_{47} = 2.6 \times 10^{-4}$. Mass 92—the dimer ion, $(\text{HCOOH})_2^+$ —was less than 5% of the relative concentration of $\text{H}(\text{HCOOH})_2^+$. Similarly in acetic acid

at the highest pressure (at which $I_{60}/I_{61} = 0.30$) mass 121, $\text{H}(\text{CH}_3\text{COOH})_2^+$, was observed; $I_{121}/I_{47} = 4.2 \times 10^{-3}$. These reactions seem to be analogous to those involved in the formation of $\text{H}(\text{H}_2\text{O})_n^+$ ions in water^{16,17} and suggest that clustering of polar molecules around ions will be phenomena of frequent occurrence.

It is also of interest to note that an appreciable amount of mass 103, protonated acetic anhydride, was observed as an ionic reaction product in acetic acid.

CH_3OH_2^+ . Protonated methanol appears as a rearrangement ion in 1-propanol and *n*-butanol. $A(\text{CH}_3\text{OH}_2^+)$ from *n*-propanol is 12.0 v. The neutral fragment should be the vinyl radical so that $\Delta H_f(\text{CH}_3\text{OH}_2^+) = 150$ kcal./mole. In *n*-butanol the decomposition process is less obvious since C_3H_5 has all of the possible structures mentioned earlier in the discussion of propyl esters. $A(\text{CH}_3\text{OH}_2^+)$ from 1-butanol is 11.2 v. $\Delta H_f(\text{CH}_3\text{OH}_2^+)$ is 161 kcal./mole if $\Delta H_f(\text{C}_3\text{H}_5)$ is 30 kcal./mole or 136 kcal./mole if $\Delta H_f(\text{C}_3\text{H}_5)$ is 55 kcal./mole. The agreement for $\Delta H_f(\text{CH}_3\text{OH}_2^+)$ from these two sources is not very good, but these results indicate that $\Delta H_f(\text{CH}_3\text{OH}_2^+)$ is about 150 kcal./mole. Using this value for $\Delta H_f(\text{CH}_3\text{OH}_2^+)$ one can calculate the proton affinity of methanol, $P(\text{CH}_3\text{OH}) \cong 167$ kcal./mole.

H_5O^+ . H_5O^+ is observed as a rearrangement ion in the mass spectrum of several alcohols. $A(\text{H}_5\text{O}^+)$ from ethanol is 12.6 v. This value is notably lower than the value of 14.4 v. given by Cummings and Bleakney.¹⁸ Using the value reported in this paper,

(13) J. D. Morrison, *J. Chem. Phys.*, **19**, 1305 (1951).

(14) T. Mariner and W. Bleakney, *Phys. Rev.*, **72**, 792 (1947).

(15) J. D. Morrison and A. J. C. Nicholson, *J. Chem. Phys.*, **20**, 1021 (1952).

(16) P. F. Knewstubb and A. W. Tickner, *ibid.*, **38**, 1031 (1963). report ions up to $\text{H}(\text{H}_2\text{O})_6^+$ from discharges in water.

(17) F. H. Field, J. L. Franklin, and M. S. B. Munson, unpublished work, observed ions up to $\text{H}(\text{H}_2\text{O})_4^+$ in a mass spectrometer.

one can calculate that $\Delta H_f(\text{H}_3\text{O}^+) = 169$ kcal./mole if the neutral fragment is C_2H_3 or 128 kcal./mole if the neutral fragments are C_2H_2 and H . $A(\text{H}_3\text{O}^+)$ from 2-propanol is 13.3 v. The possible neutral fragments are more numerous and a strong case for any particular process cannot be made; however, $\Delta H_f(\text{H}_3\text{O}^+)$ can be calculated as 212, 187, or 146 kcal./mole if the other products are allyl, other C_3H_5 , or C_3H_4 and H , respectively. If one chooses the low value for the heat of formation of H_3O^+ of about 140 kcal./mole, then the proton affinity of water is about 167 kcal./mole.

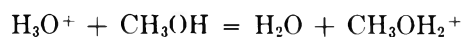
Table II shows the proton affinities from this paper and literature values. The proton affinity of water has been the subject of discussion for many years and is, unfortunately, the quantity about which these data yield the least information. Tal'roze and Frankevich¹⁹ estimated the proton affinity of water as about 169 kcal./mole based on their observing and failing to observe certain ion-molecule reactions. The nonmass spectrometric data on the existence and heat of formation of H_3O^+ are summarized by Bell.^{20a} These thermochemical cycles give values of 160–182 kcal./mole. The early appearance potential of Cummings and Bleakney gave values of $P(\text{H}_2\text{O})$ which were much lower than these values. The data reported in this paper, although hardly conclusive, show that mass spectroscopic appearance potential data are compatible with the other values for $P(\text{H}_2\text{O})$.^{20b}

Table II: Proton Affinities

X	$P(\text{X})$, kcal./mole	
	These data	Literature
H_2O	~167	169, ^a 160, ^b 180, ^b 126 ^c
CH_3OH	~167	180 ^a
HCOOH	166	156 ^d
CH_3COOH	184	180 ^d
$\text{C}_2\text{H}_5\text{COOH}$	185	176 ^d

^a See ref. 19. ^b See ref. 20a. ^c See ref. 18. ^d See ref. 5.

Estimates of the proton affinity of methanol were also made from ion-molecule reactions¹⁹; $P(\text{CH}_3\text{OH}) = 180$ kcal./mole. According to Bell,^{20a} methanol and ethanol are somewhat weaker bases than water. The value for $P(\text{CH}_3\text{OH})$ from these data is about 167 kcal./mole. It is doubtful, however, that the difference between this value and that of Tal'roze and Frankevich is significant. At present it is not possible to study in an unequivocal fashion the reaction



in the gas phase.

No nonmass spectrometric determinations of the proton affinities of the aliphatic acids are available. The discussion by Bell^{20a} of acetic and formic acids suggests that acetic acid has weaker basic properties than formic acid in addition to the much lower dielectric constant which retards dissociation. The data in this paper indicate that the proton affinity of acetic acid and formic acid are nearly the same and would not suggest any appreciable differences in basic properties.

The observation that consistent values for $\Delta H_f(\text{RCOOH}_2^+)$ can be obtained from ethyl and propyl esters if the C_3H_5 fragment corresponds not to allyl, but to a higher energy species, suggests strongly that the hydrogen atoms involved in the rearrangement process are not equivalent. This interpretation is opposite to that of Godbole and Kebarle,⁵ who considered that the hydrogens in the alcohol group were equivalent, but is still compatible with their data.

II. Other Oxygenated Ions. Mass 31. Cummings and Bleakney¹⁸ in their study on methanol and ethanol suggested that the parent-minus-one ions had the structures CH_2OH^+ and CH_3CHOH^+ . Confirmatory studies on deuterated methanol are not available, but mass spectra of deuterated ethanol²¹ and 2-*d*-2-propanol^{22,23} indicate that the hydrogen is removed from the C atom attached to the hydroxyl group for the parent-minus-H (or -D) fragment. Momigny's²¹ work also indicated that CH_2OH^+ is formed from ethanol. D'Or and Collin²⁴ measured $A(31)$ from CH_3ONO as 11.9 v. which gives $\Delta H_f(\text{CH}_3\text{O}^+)$ as 235 kcal./mole which is to be compared with $\Delta H_f(\text{CH}_2\text{OH}^+) = 175$ kcal./mole.^{1d} This major difference in heats of formation of isomeric ions appeared worthwhile substantiating. Consequently, a study was made of the appearance potentials of CH_3O^+ or CH_2OH^+ from different sources.

(18) C. S. Cummings and W. Bleakney, *Phys. Rev.*, **58**, 787 (1940).

(19) See V. L. Tal'roze, *Pure Appl. Chem.*, **5**, 455 (1962), for a summary of the work.

(20) (a) R. P. Bell, "The Proton in Chemistry," Cornell University Press, Ithaca, N. Y., 1959, Chapter III; (b) the authors' attention has been called to the work of D. Van Raalte and A. G. Harrison, *Can. J. Chem.*, **41**, 3118 (1963), which gives $\Delta H_f(\text{H}_3\text{O}^+) = 157 \pm 3$ kcal./mole and $P(\text{H}_2\text{O})$ as 151 ± 3 kcal./mole from the appearance potentials of H_3O^+ from nine compounds.

(21) J. Momigny, *Bull. Soc. Roy. Sci. Liege*, **24**, 111 (1955).

(22) F. E. Condon, H. L. McMurry, and V. Thornton, *J. Chem. Phys.*, **19**, 1010 (1951).

(23) L. Friedman and J. Turkevich, *J. Am. Chem. Soc.*, **74**, 1666 (1952).

(24) L. D'Or and J. Collin, *Bull. Soc. Roy. Sci. Liege*, **22**, 285 (1953).

Table III: Appearance Potentials and Heats of Formation of CH_3O^+ or CH_2OH^+ (Mass 31)

Source	A, v.		Neutral	$\Delta H_f(31)$, kcal./mole
	These data	Literature		
CH_3OH	1.2 ± 0.1	11.8, ^a 12.2 ^b	H	179
$\text{CH}_3\text{CH}_2\text{OH}$	11.3	11.3, ^a 11.6 ^b	CH_3	173
$\text{CH}_3-\text{CH}_2-\text{CH}_2\text{OH}$	11.1	11.1, ^c 11.6 ^b	C_2H_5	170
$\text{CH}_3-(\text{CH}_2)_2-\text{CH}_2\text{OH}$	11.4		$n-\text{C}_3\text{H}_7$	174
				174 CH_2OH^+
$\begin{array}{c} \text{O} \\ \\ \text{CH}_3-\text{O}-\text{CH} \end{array}$	12.1	12.4 ^d	CHO	197
$\begin{array}{c} \text{O} \\ \\ \text{CH}_3-\text{O}-\text{C}-\text{CH}_3 \\ \\ \text{CH}_3-\text{O}-\text{CH}_3 \end{array}$	12.7	12.9 ^d	CH_3CO	205
	12.1	12.5, ^e 12.6 ^d	CH_3	203
CH_3-ONO	11.0	11.9 ^f	NO	202 CH_3O^+
				217

^a See ref. 18. ^b L. Friedman, F. A. Long, and M. Wolfsberg, *J. Chem. Phys.*, **27**, 613 (1957). ^c T. Kambara, *J. Phys. Soc. Japan*, **5**, 31 (1950), quoted in ref. 1. ^d A. B. King and F. A. Long, *J. Chem. Phys.*, **29**, 374 (1958). ^e R. R. Bernecker and F. A. Long, *J. Phys. Chem.*, **65**, 1565 (1961). ^f See ref. 24.

Table IV: Mass 45, $\text{C}_2\text{H}_5\text{O}^+$

Source	Ion	A, v.		Neutral	$\Delta H_f(\text{ion})$, kca./mole
		These data	Literature		
$\begin{array}{c} \text{O} \\ \\ \text{CH}_3-\text{CH}_2-\text{O}-\text{CH} \end{array}$	$\text{CH}_3-\text{CH}_2-\text{O}^+$	11.4		HCO	175
				H + CO	149
$\begin{array}{c} \text{O} \\ \\ \text{CH}_3-\text{CH}_2-\text{O}-\text{C}-\text{CH}_3 \end{array}$	$\text{CH}_3-\text{CH}_2\text{O}^+$	10.8		CH_3CO	157
$\text{CH}_3-\text{CH}_2-\text{O}-\text{CH}_2-\text{CH}_3$	$\text{CH}_3-\text{CH}_2\text{O}^+$	12.3	12.5 ^a	$\text{CH}_3 + \text{CO}$	140
				CH_3-CH_2	200
				$\text{C}_2\text{H}_4 + \text{H}$	160
				$\text{C}_2\text{H}_3 + \text{H}_2$	159
$\begin{array}{c} \text{CH}_3-\text{CH}_2-\text{OH} \\ \\ \text{CH}_3-\text{O}-\text{CH}_3 \end{array}$	$\text{CH}_3-\text{CH}-\text{OH}^+$	10.9	11.0 ^{b,c}	H	143
	$\text{C}_2\text{H}_5\text{O}^+$	11.0		H	158 (168 ^a)

^a R. R. Bernecker and F. A. Long, *J. Phys. Chem.*, **65**, 1565 (1961). ^b See ref. 18. ^c L. Friedman, F. A. Long, and M. Wolfsberg, *J. Chem. Phys.*, **27**, 613 (1957).

Table III summarizes the data of this paper and available literature data. There is a difference in the heats of formation of the mass 31 ion from different sources. CH_2OH^+ , which is the ion produced from the fragmentation of the alcohols, has a heat of formation that is well established at 174 kcal./mole.

All of the other molecules should produce CH_3O^+ rather than CH_2OH^+ . $A(\text{CH}_3\text{O}^+)$ from CH_3ONO reported in this paper is notably below the value of D'Or and Collin.²⁴ Assuming that the fragmentation process gives the products indicated in Table III, one calculates $\Delta H_f(\text{CH}_3\text{O}^+) = 202$ kcal./mole, neglecting the value from CH_3ONO . Other choices for dissociation products do not give consistent values for $\Delta H_f(\text{CH}_3\text{O}^+)$. High resolution mass spectrometric studies²⁵ show that mass 31 from CH_3ONO is predominantly

CH_3O^+ and not HNO^+ . Presumably there is excess kinetic energy involved in the decomposition process.

With these values for the heats of formation of the ions and the heats of formation of the radicals by Gray and Williams,⁹ $I(\text{CH}_2\text{OH}) \cong 7.9$ v. and $I(\text{CH}_3\text{O}) \cong 8.8$ v. No direct measurements of the ionization potentials of these radicals have been made, however, for comparison.

Mass 45. Table IV shows the data for $\text{CH}_3\text{CH}_2\text{O}^+$ and CH_3CHOH^+ . The agreement among these data is not particularly good. $\Delta H_f(\text{CH}_3\text{CHOH}^+)$ is about 143 kcal./mole and $\Delta H_f(\text{CH}_3-\text{CH}_2\text{O}^+)$ is probably about 160 kcal./mole, although this value is not con-

(25) The correct mass assignment was made by E. Lumpkin and J. L. Taylor of these laboratories with an AEI MS-9 mass spectrometer.

Table V: Ionization Potentials of Aliphatic Esters

Ester	I, v.	
	These data	Literature
$\text{CH}_3\text{-O}-\overset{\text{O}}{\parallel}{\text{C}}\text{-H}$	10.4	
$\text{C}_2\text{H}_5\text{-O}-\overset{\text{O}}{\parallel}{\text{C}}\text{-H}$	10.3	
$\text{CH}_3\text{-O}-\overset{\text{O}}{\parallel}{\text{C}}\text{-CH}_3$	10.8	
$\text{C}_2\text{H}_5\text{-O}-\overset{\text{O}}{\parallel}{\text{C}}\text{-CH}_3$	10.2	10.1, ^a 9.97 ^b
$\text{C}_2\text{H}_5\text{-O}-\overset{\text{O}}{\parallel}{\text{C}}\text{-C}_2\text{H}_5$	10.2	

^a R. R. Bernecker and F. A. Long, *J. Phys. Chem.*, **65**, 1565 (1961). ^b See ref. 15.

vincingly established. The heat of formation of mass 45 from dimethyl ether is about the same as the heat of formation of $\text{CH}_3\text{-CH}_2\text{-O}^+$, suggesting the ever present possibility of rearrangement. The difference in heats of formation between $\text{CH}_3\text{-CH}_2\text{O}^+$ and $\text{CH}_3\text{-}$

CH-OH^+ is roughly the same as the difference in heats of formation of CH_3O^+ and CH_2OH^+ .

The proton affinities of formaldehyde and acetaldehyde may be calculated from the values of the heats of formation of CH_2OH^+ and CH_3CHOH^+ ; $P(\text{CH}_2\text{O}) = 163$ kcal./mole and $P(\text{CH}_3\text{CHO}) = 182$ kcal./mole. These values are about the same as values for proton affinities of other simple oxygen-containing molecules in Table II.

The ionization potentials of a series of esters are given in Table V. If, as was suggested by Cummings and Bleakney¹⁸ for alcohols, the electron is removed from the nonbonding orbitals of the oxygen atom, then these ionization potentials should be essentially the same, as they are. Except for the difference between formic acid, 11.5 v., and the formates, 10.3 and 10.4 v., the esters and acids have about the same ionization potentials,¹⁵ with the esters 0.1–0.2 v. lower.

For other ions produced from these oxygenated compounds, no heats of formation could be established for ions formed from different sources.

Acknowledgments. The authors are grateful to Mr. W. C. Gieger for performing these experiments with his usual competence.

The Nature of the Acidic Sites on a Silica-Alumina. Characterization by Infrared Spectroscopic Studies of Trimethylamine and Pyridine Chemisorption¹

by Michael R. Basila, Theodore R. Kantner, and Kee H. Rhee

Gulf Research and Development Company, Pittsburgh, Pennsylvania (Received June 16, 1964)

The chemisorption of trimethylamine and pyridine on a commercial silica-alumina catalyst was studied by infrared techniques. Trimethylamine was found to be unsuitable as an agent for differentiating between Lewis and Brønsted sites because it is dissociatively adsorbed with concomitant generation of protons which form protonated chemisorbed species. Pyridine, on the other hand, is not dissociatively adsorbed and is, therefore, useful for determining the relative numbers of Lewis and Brønsted acid sites by making use of the differences in the spectra of the pyridinium ion and coordinately bonded pyridine. Approximately equal numbers of Lewis and Brønsted sites were observed on the highly dehydrated silica-alumina. The perturbing effects of potassium poisoning and irreversible H₂O adsorption on the distribution of acid sites were studied. It was found that potassium poisoning weakens the majority of acid sites and eliminates apparent Brønsted acidity. Irreversibly adsorbed H₂O converts Lewis sites to Brønsted sites; however, the interaction is relatively weak since the H₂O can be removed by evacuation. These observations provide considerable insight into the nature of the acid sites and have led to the formulation of the following model. It is suggested that all of the primary acid sites on a silica-alumina are of the Lewis type centered on active surface aluminum atoms and that apparent Brønsted sites are produced by a second-order interaction between the molecule chemisorbed on a Lewis site and a nearby surface hydroxyl group. This model qualitatively fits the experimental observations to date.

Introduction

The question of the nature and importance of catalyst acidity with respect to catalytic reactions such as cracking and isomerization has been under intensive study for many years by a large number of workers. The various techniques for measuring catalyst acidity have been reviewed by Ryland, Tamele, and Wilson.² They can be roughly divided into two general categories, indicator techniques (with or without titration) and volumetric base adsorption techniques. Although a great deal of work has been done, little progress has been made in establishing the true nature of the catalytically important sites. One of the oldest yet still unsolved aspects of the problem is whether the acidity is of the Brønsted (protonic) or Lewis (electron acceptor) type. One can find evidence in the literature to support either of these possibilities. In recent years a number of spectroscopic tools have been ap-

plied to this problem, namely ultraviolet,³⁻⁵ infrared,⁶⁻¹⁰ and electron spin resonance.^{5,11-14} The application of these techniques has added greatly to our knowledge

(1) Presented at the symposium on "New Tools in Heterogeneous Catalytic Research," at the 145th National Meeting of the American Chemical Society, New York, N. Y., Sept. 12, 1963.

(2) L. B. Ryland, M. W. Tamele, and J. N. Wilson, "Catalysis," Vol. 7, Reinhold Publishing Corp., New York, N. Y., 1960, p. 1.

(3) (a) H. P. Leftin, *J. Phys. Chem.*, **64**, 1714 (1960); (b) H. P. Leftin and W. K. Hall, *ibid.*, **64**, 382 (1960); (c) *ibid.*, **66**, 1457 (1962); (d) *Actes Congr. Intern. Catalyse*, **2^e**, Paris, **1**, 1353 (1961).

(4) A. N. Webb, *ibid.*, **1**, 1283 (1961).

(5) A. Terenin, V. Barachevsky, E. Kotov, and V. Kalmogarov, *Spectrochim. Acta*, **19**, 1797 (1963), and references therein.

(6) J. E. Mapes and R. P. Eischens, *J. Phys. Chem.*, **58**, 1059 (1954).

(7) R. P. Eischens and W. A. Pliskin, *Advan. Catalysis*, **10**, 1 (1958).

(8) D. E. Nicholson, *Nature*, **186**, 630 (1960).

(9) I. D. Chapman and M. L. Hair, *J. Catalysis*, **2**, 145 (1963).

(10) J. B. Peri, *Actes Congr. Intern. Catalyse*, **2^e**, Paris, **1**, 1333 (1961).

(11) D. M. Brouwer, *Chem. Ind. (London)*, 177 (1961).

of the nature of catalytic surfaces; however, it has also revealed the great complexity of the problem. The question of the type of acidity still remains unresolved, although the data do seem to favor the predominance of Lewis type acidity. Recently, Parry¹⁵ has reported the utility of pyridine in the infrared study of catalyst acidity. He utilized the fact that pyridine interacting as a Lewis base (LPY) has a distinctly different spectrum from that of pyridine interacting as a Brønsted base (BPY).^{16,17} His results indicate that only Lewis sites are present on alumina while both Lewis and Brønsted sites are observed on silica-alumina.¹⁵ This agrees with the results of Eischens and co-workers^{6,7} who studied the adsorption of ammonia on silica-alumina and alumina.

In this work, the chemisorption of pyridine and trimethylamine have been studied on a typical silica-alumina cracking catalyst for the purpose of characterizing the acidic sites. In accord with the results of Parry¹⁴ and Eischens and co-workers,^{6,7} we find both Lewis and Brønsted acid sites on silica-alumina. We have also studied the perturbations of the strengths and distributions of these sites by agents such as H₂O and potassium ions to provide further enlightenment on the nature of the sites.

Experimental

Materials. The silica-alumina (SA) used in this work was the same sample of American Cyanamid Aerocat Triple A which was previously studied.¹⁸ It contains 25% alumina by weight on a dry basis and the surface area as determined by N₂ adsorption was 430 m²/g. The base exchanged sample (KSA) was also the same as was studied in our previous work.¹⁸ The KSA surface area was also 430 m²/g. It was prepared by soaking the uncalcined SA in a 1.5 M aqueous potassium acetate solution for 48 hr. Chemical analysis indicated the addition of 0.21 g.-atom of K/g.-atom of Al with the Al-Si ratio remaining the same as in the untreated sample. Deuterated silica-alumina (DSA) was prepared by repeatedly exposing the sample to D₂O vapor, evacuating between exposures, until all of the OH stretching absorption in the sample disappeared. The sample was then dehydrated by the standard technique.

The pyridine (PY) and trimethylamine (TMA) were Mallinckrodt A.R. and Eastman Kodak White Label grades, respectively. They were distilled *in vacuo* over P₂O₅ through a glass wool-P₂O₅ drying train, the heart cut being retained for use in each case.

Techniques. The sample preparation and spectroscopic techniques were identical with those previously described.¹⁸ The samples were used in wafer form and

all operations were carried out on a conventional vacuum system capable of maintaining pressures in the 10⁻⁶ mm. range. After a slow heating, with continuous evacuation, from ambient to 500° over a 3-hr. period, the samples were calcined in pure oxygen for at least 4 hr. at 500°. Following the calcination, the samples were evacuated at 500° for at least 3 hr., but generally overnight.

The addition of the nitrogen base was done, in most cases, by exposing the evacuated catalyst at 150° to the base at several mm. pressure for 1 hr. and pumping for 1 hr. at the same temperature. This procedure was followed to reduce the amount of physical adsorption. A number of additions were made at room temperature, and the results of subsequent experiments were identical with those performed on samples which had been treated at 150°.

Most of the spectra were recorded on a Perkin-Elmer Model 421 grating spectrophotometer. In a few instances a Perkin-Elmer Model 221 prism-grating instrument was used. In most samples the reference beam was attenuated during the initial part of the spectral scan, between 4000 and 2500 cm.⁻¹, after which the attenuator was removed. The spectral slit width of the Model 421 was approximately 2 cm.⁻¹ and that of the Model 221 was of the order of 4 cm.⁻¹. The spectrometers were frequency calibrated using indene and atmospheric water vapor as standards. The frequencies quoted are thought to be accurate to ±1 cm.⁻¹.

The gravimetric data were determined on a conventional quartz spiral balance having a sensitivity of 1.5 mm./mg. The catalyst samples were wafers prepared in the same manner as those used in the spectroscopic determinations.

Results

Trimethylamine Chemisorption on Silica-Alumina. The utilization of TMA as a means of distinguishing between Lewis and Brønsted sites was suggested by the NH₃ and PY techniques of other workers.^{6-8,15} The interaction of TMA with a Brønsted acid site was expected to lead to the formation of an NH⁺ group which could be detected by the characteristic NH

(12) J. J. Rooney and R. C. Pink, *Proc. Chem. Soc.*, **70**, 142 (1961); *Trans. Faraday Soc.*, **58**, 1632 (1962).

(13) W. K. Hall, *J. Catalysis*, **1**, 53 (1962).

(14) J. K. Fogo, *J. Phys. Chem.*, **65**, 1919 (1961).

(15) E. P. Parry, *J. Catalysis*, **2**, 371 (1963).

(16) N. S. Gill, R. H. Nuttall, D. E. Scaife and D. W. A. Sharp, *J. Inorg. Nucl. Chem.*, **18**, 79 (1961).

(17) D. Cook, *Can. J. Chem.*, **39**, 2009 (1961).

(18) M. R. Basila, *J. Phys. Chem.*, **66**, 2223 (1962).

stretching and deformation vibrations. The spectra of SA before and after the addition of TMA at 150° are shown in Fig. 1. The bands at 3745, 1633, and 1394 cm^{-1} in the SA spectrum have been previously assigned¹⁸ to the OH stretching vibration in surface silanol groups, an SiO overtone and a surface AlO vibration, respectively. The latter assignment is quite tentative; however, it has been shown that it is definitely a vibration of a surface group.¹⁸ The bands of interest in the spectrum of TMA chemisorbed on SA are those at 3340, 3280, 3150, and 1588 cm^{-1} which are characteristic of the NH group

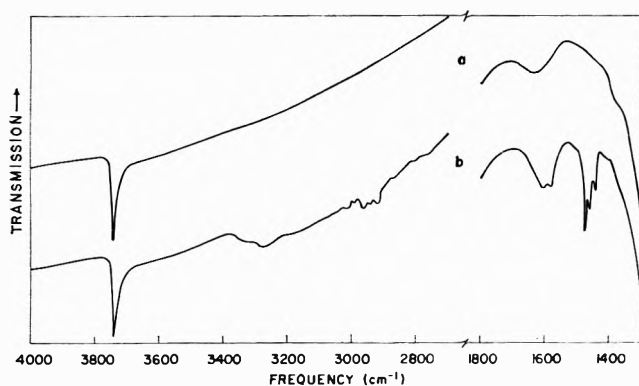


Figure 1. Trimethylamine chemisorbed on silica-alumina: (a) SA calcined and evacuated at 500°; (b) SA exposed to trimethylamine at 25 mm. and 25° for 0.5 hr. followed by 1.5-hr. evacuation at 100° and 16-hr. evacuation at 25°.

in amines, *viz.*, the NH stretching and deformation vibrations. The multiplicity of bands in the NH stretching region is typical of hydrogen-bonded NH groups^{17,19} and does not necessarily imply the presence of primary or of several types of secondary amines. It is not possible to determine on the basis of the frequencies or multiplicity of the NH stretching bands whether the NH group resides in a primary, secondary, or quaternary amine. The deformation frequency is considerably higher than is commonly observed for trimethylamine salts ($\sim 1500 \text{ cm}^{-1}$).¹⁷ It is in the center of the range quoted by Bellamy²⁰ for secondary amines and at the lower edge of the range for primary amines; however, any assignment to a particular type would be highly speculative. In any case, the source of the hydrogen atoms which form the NH groups is of particular interest. There are two possibilities: surface protons located in Brønsted acid sites or protons produced by dissociative adsorption of the TMA. In order to decide between these possibilities a sample of DSA was exposed to TMA at room temperature. As can be seen in Fig. 2a, the deuteration is essentially

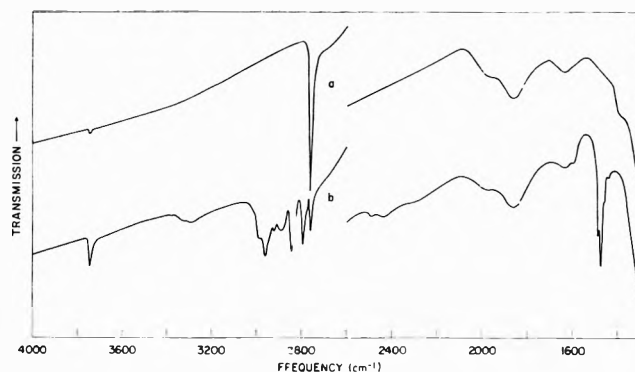


Figure 2. Trimethylamine adsorbed on deuterated silica-alumina: (a) DSA calcined and evacuated at 500°; (b) DSA exposed to trimethylamine at 25 mm. and 25° for 0.5 hr. followed by evacuation for 0.5 hr. at 25°.

complete. The spectrum of TMA on DSA in Fig. 2b exhibits bands at 3745, 3340, 3280, 3150, 2762, 2490, 2433, and 2300 cm^{-1} indicating the presence of OH, OD, NH, and ND groups. The formation of both NH and ND groups, coupled with the exchange of OD groups to form OH groups, indicates that a significant fraction of the TMA has dissociated. This conclusion is based on the expectation that only ND and OD groups would have been observed if there were no dissociation. The possibility exists that the surface OH groups were produced by direct exchange between surface OD groups and the TMA methyl groups. However, under our experimental conditions no bands due to CD stretching vibrations were observed which tends to eliminate this possibility. The above conclusion is supported by the fact that the spectrum of TMA chemisorbed on alumina is identical with Fig. 1 even though the results of Parry¹⁵ and unpublished results from this laboratory indicate that alumina has no Brønsted acidity. The possibility remains that the protons are not exchanged by the deuteration techniques used in the preparation of DSA; however, it will be shown later that this is not the case. Hence, it appears that TMA is of little value in detecting Brønsted acidity on catalytic surfaces. This result suggests the possibility that a similar dissociation occurs in the chemisorption of PY and NH_3 which gives rise to the protonated chemisorbed species which have been observed by other workers.^{6-8,15}

Pyridine Chemisorption on Silica-Alumina. The spectrum of PY adsorbed on SA at 150° by contact with 17 mm. of PY vapor for 1 hr. and pumping for 1 hr. at 150° is shown in Fig. 3b. It is evident from the

(19) L. J. Bellamy, "The Infrared Spectra of Complex Molecules," John Wiley and Sons, Inc. New York, N. Y., 1958, p. 259.

(20) L. J. Bellamy, *ibid.*, p. 249.

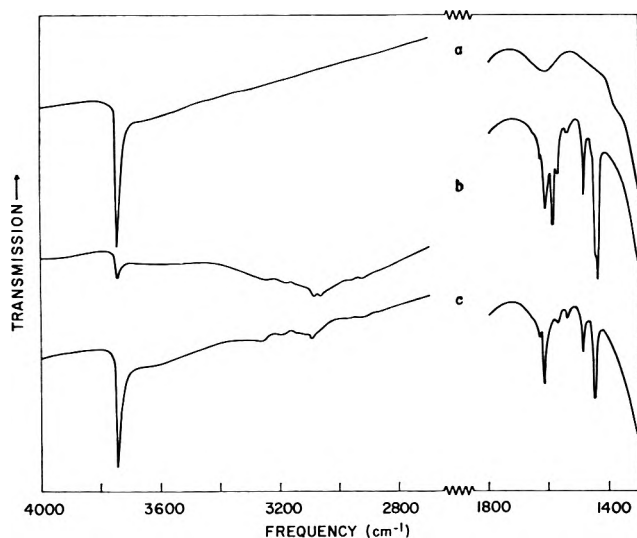


Figure 3. Pyridine adsorbed on silica-alumina: (a) SA calcined and evacuated at 500°; (b) SA exposed to 17 mm. of pyridine at 150° for 1 hr. followed by evacuation for 1 hr. at 150°; (c) evacuated an additional 16 hr. at 150°.

extent of hydrogen bonding of the surface OH groups which is indicated by the broad band centered at 3000 cm^{-1} and especially from the differences in spectra b and c that even at 150° an impressive amount of PY is physically adsorbed. In Fig. 3c virtually all of the physically adsorbed PY has been removed by extended (16 hr.) pumping at 150° as is evidenced by the lack of bands characteristic of the hydrogen-bonded species (discussed below) so that all of the bands are due to chemisorbed species. In the region 1700–1400 cm^{-1} which was studied by Parry¹⁵ our spectra are essentially identical with his. Recently, the spectra of LPY and BPY in a number of molecular complexes have been studied and vibrational assignments have been made.^{16,17} These studies are in accord with the assignments of the chemisorbed LPY and BPY made by Parry¹⁵ in the 1700–1400- cm^{-1} region. In the present work, more complete assignments of the chemisorbed species have been possible because of the wider frequency range studied. These assignments, which are based on the assignments of the molecular complexes,^{16,18} are given in Table I along with the assignment of molecular PY itself. In addition to the vibrational assignments of LPY and BPY, assignments are also given for hydrogen-bonded pyridine (HPY). These latter assignments are based on studies of the pyridine-water interaction by Sidorov.²¹ The presence of physically adsorbed PY which is apparently held on the surface by a hydrogen-bonding interaction with surface OH groups is detected by the observation of the characteristic 1593 and 1614 cm^{-1} bands as

Table I: The Assignments of Pyridine Physically and Chemically Adsorbed on Silica-Alumina

Type	PY, ^a cm^{-1}	LPY, cm^{-1}	BPY, cm^{-1}	HPY, cm^{-1}
7a ν_{NH}	3260 3188	...
20b ν_{CH}	3083	(3147)	(3147)	...
16 ν_{CH}	3054	(3114)	(3114)	3065
7b ν_{CH}	3054	(3087)	(3087)	3043
8a $\nu_{\text{CC(N)}}$	1580	1620	1638	1614
8b $\nu_{\text{CC(N)}}$	1572	1577	1620	1593
19a $\nu_{\text{CC(N)}}$	1482	1490	1490	1490
19b $\nu_{\text{CC(N)}}$	1439	1450	1545	1438

^aSee ref. 21.

well as by the broad hydrogen-bonded OH stretching vibration which is centered around 3000 cm^{-1} . The chemically adsorbed species may also be hydrogen bonded to the surface hydroxyl groups as will be shown later, but they do not give rise to the bands characteristic of the physically adsorbed species. Chemisorbed BPY is characterized by the bands at 3260 and 3188 cm^{-1} which are due to the NH^+ stretching vibration¹⁷ and by the bands at 1638 and 1545 cm^{-1} which are due to the combined C–C stretching and in-plane CH and NH bending modes.^{17,22} Chemisorbed LPY is characterized by the bands at 1452 and 1577 cm^{-1} which are due to the combined C–C stretching and in-plane CH bending modes.^{16,22} As previously mentioned, the assignments of the 1638, 1577, 1545, 1490, and 1450 cm^{-1} bands are in accord with those of Parry.¹⁵ The additional assignments in Table I serve to corroborate his evidence that both Lewis and Brønsted acidity are present on the surface of a silica-alumina. This conclusion agrees with the results of Eischens and co-workers^{6,7} and Nicholson⁸ on the chemisorption of NH_3 on silica-alumina.

It should be mentioned that the CH stretching vibrations of LPY and BPY are indistinguishable; thus, the assignments of these vibrations shown in Table I are the same for each species and are quite tentative as indicated by the parentheses. One further point of interest in Table I is the fact that ν_{19a} has the same frequency in both LPY and BPY and is shifted only slightly (8 cm^{-1}) from its normal position in unperturbed PY.

It was indicated earlier that the chemisorbed species are engaged in hydrogen-bonding interactions with

(21) A. N. Sidorov, *Opt. i Spektroskopiia*, **8**, 51 (1960).

(22) G. Zerbi, B. Crawford, and J. Overend, *J. Chem. Phys.*, **38**, 127 (1963).

surface OH groups. This is evident from the results of a series of desorption experiments in which the chemisorbed PY is removed in stages by evacuation for a number of hours (four or more) at a series of temperatures. After each evacuation, the sample was cooled to room temperature and spectra were recorded. The results of these measurements are shown in Fig. 4. The relative amount of PY remaining on the surface was determined by measuring the peak absorbance of the 1450-, 1490-, and 1620-cm.⁻¹ bands and averaging the results to reduce the scatter. The LPY and BPY are apparently desorbed with equal probability. This is indicated by the identical functional dependence on temperature of the 1450-cm.⁻¹ band which is characteristic of LPY as compared to the 1490- and 1619-cm.⁻¹ bands which contain contributions from both LPY and BPY. The number of free (nonhydrogen-

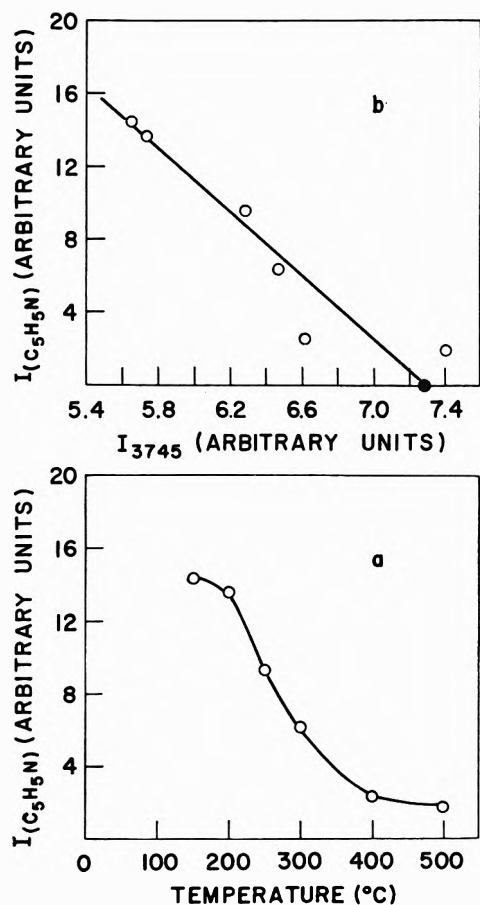


Figure 4. Pyridine desorption from silica-alumina: (a) the amount of pyridine remaining after evacuation at elevated temperature vs. temperature; (b) the amount of pyridine remaining after evacuation at elevated temperatures vs. the number of nonhydrogen-bonded surface OH groups. The solid point represents the number of OH groups prior to pyridine chemisorption.

bonded) surface OH groups relative to the number which were present prior to the PY chemisorption was determined by measuring the peak absorbance of the 3745 cm.⁻¹ band. It was evident that roughly 10% of the surface OH groups remained hydrogen bonded after all of the HPY was removed. Figure 4a is a plot of the amount of chemisorbed PY remaining after evacuation at a given temperature vs. the temperature, and Fig. 4b is a plot of the amount of chemisorbed PY remaining vs. the relative number of free surface OH groups after evacuation at a given temperature. It is seen in Fig. 4b that the removal of a portion of the chemisorbed PY is accompanied by an increase in the number of free (nonhydrogen-bonded) surface OH groups indicating that a hydrogen-bonding interaction exists between these two surface species. Furthermore, the relationship is linear, suggesting that the ratio of PY to surface OH groups engaged in the interaction is constant. It has been possible to estimate this ratio by combining gravimetric adsorption measurements with the spectroscopic results. These experiments indicate that the chemisorbed PY-hydrogen-bonded surface OH ratio is approximately one; *i.e.*, on the average, each chemisorbed PY molecule is hydrogen bonded to a single surface OH group. It should be noted that the surface OH group concentration after the 500° evacuation is greater than that on the original surface. This increase is undoubtedly due to the decomposition of chemisorbed PY at the highest temperatures with subsequent generation of surface OH groups.

It remains to be shown that the chemisorbed BPY is not produced by decomposition of chemisorbed PY at low temperature with subsequent proton generation as was observed in the case of TMA. PY was chemisorbed on DSA at 150° and only OD and ND vibrations were observed; hence, no detectable decomposition occurred. This experiment also shows that the surface hydrogen atoms which give rise to the BPY species are exchanged by the deuteration technique used, thus supporting the conclusion that TMA is dissociatively adsorbed.

Pyridine Chemisorbed on Base-Exchanged Silica-Alumina. Alkali metals are known to have a detrimental effect on the cracking activity of silica-alumina catalysts.^{23,24} In certain cases the addition of potassium has completely destroyed cracking activity.²⁴ In Fig. 5 the spectrum of PY chemisorbed on KSA is given. It is evident from the absence of the char-

(23) D. Stright and J. E. Danforth, *J. Phys. Chem.*, **57**, 448 (1953).

(24) G. A. Mills, E. R. Boedeker, and A. G. Oblad, *J. Am. Chem. Soc.*, **72**, 1554 (1950).

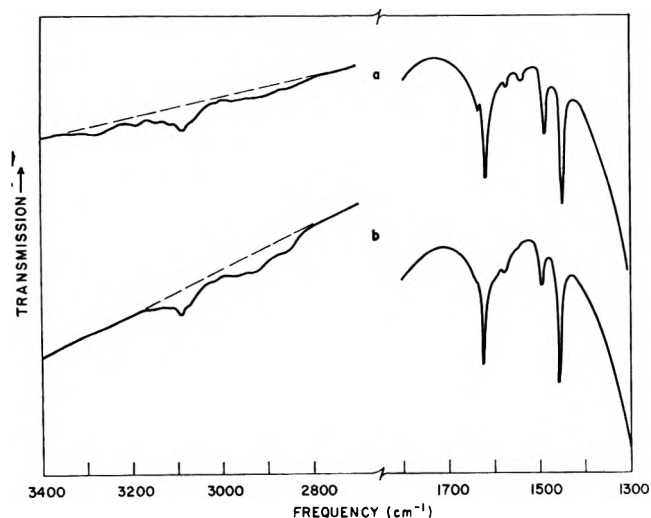


Figure 5. Effect of K-poisoning on the chemisorption of pyridine on silica-alumina: (a) SA exposed to pyridine at 17 mm. and 150° for 1 hr. followed by evacuation for 16 hr. at 150°; (b) KSA exposed to pyridine at 17 mm. and 150° for 1 hr. followed by evacuation for 16 hr. at 150°.

acteristic NH vibrations of BPY at 3260, 3188, and 1545 cm^{-1} that K-poisoning has resulted in the elimination of the Brønsted acid sites. It should also be noted that the concentration of surface OH groups is not markedly reduced on KSA. This agrees with the results of Haldeman and Emmett.²⁵ Further insight into the effect of K-poisoning is provided by a study of the desorption of PY from KSA in stages as previously described. Gravimetric measurements indicate that the amount of PY initially adsorbed on KSA is somewhat less than that adsorbed on SA, *i.e.*, after exposure to 17 mm. of PY vapor for 1 hr. at 150° and evacuation for 1 hr. at the same temperature, SA retained 7.35×10^{-2} mg./m.² of PY, and KSA retained 5.37×10^{-2} mg./m.². Upon subsequent heating with evacuation at a series of temperatures, it was evident that the PY was much less tenaciously held on KSA than on SA. This finding is illustrated in Table II. The desorption was followed spectroscopically rather than gravimetrically utilizing the intensities, I , of the 1450 and 1620 cm^{-1} bands of chemisorbed PY. Since the intensities give only relative concentrations (upon comparison with the initial intensity), it was necessary to form ratios of the intensity of the band at two temperatures in order that the two sets of data for SA and KSA be comparable. Thus, in Table II, the intensity ratio of each band at two temperatures, I_{T_2}/I_{T_1} , represents the ratio of the PY retained after evacuation at T_2 to that previously retained after evacuation at T_1 . One obtains the same information for each band so that the I_{T_2}/I_{T_1} ratios should be identical and the extent

of agreement between the sets of data is a measure of the internal consistency of the data. It is evident that the ratios are smaller for KSA than for SA, especially in going from 200 to 250°. Hence, it appears that K-poisoning severely weakens the acidic sites on SA. This agrees with the similar conclusions of Hirschler²⁶ and Hall, *et al.*²⁷ This explains our previous observation¹⁸ that the amount of H₂O irreversibly adsorbed at 150° on KSA is considerably less than that adsorbed on SA.

Table II: Desorption of Pyridine from SA and KSA

T_1 , °C.	T_2 , °C.	$(I_{T_2}/I_{T_1})_{1450}$		$(I_{T_2}/I_{T_1})_{1620}$	
		SA	KSA	SA	KSA
150	200	0.93	0.77	0.94	0.71
200	250	0.76	0.26	0.75	0.24

It should be pointed out that the degree of alkali metal poisoning may vary over a considerable range. For example, Parry¹⁵ observes only a partial poisoning of the Brønsted sites on silica-alumina. Similar differences in degree occur with respect to the activity of the poisoned catalyst.²⁶ In some earlier work¹⁸ we have observed the disappearance of the 1394 cm^{-1} band of Triple A silica-alumina as a result of K-poisoning. We have subsequently found that, in cases where this band does not completely disappear, some Brønsted acid sites remain. Thus, one must be careful about interpreting the results of alkali metal poisoning unless the extent of poisoning has been established.

Distribution of Lewis and Brønsted Acid Sites. One of the most difficult problems in spectroscopic studies of chemisorbed molecules is in the determination of absorption coefficients of the bands of interest in their spectra. In cases where the adsorption experiment gives rise to two or more species, the situation is almost hopeless. The problem is not that the absorption coefficient of a band in a chemisorbed species would be drastically different from that in a comparable molecular species, but that it generally happens that the comparable molecular species is not available for evaluation.

In the present case, one is faced with the evaluation of absorption coefficients of characteristic bands of chemisorbed LPY and BPY in order to determine the

(25) R. G. Haldeman and P. H. Emmett, *J. Am. Chem. Soc.*, **78**, 2917 (1956).

(26) A. E. Hirschler, *J. Catalysis*, **2**, 428 (1963).

(27) W. K. Hall, F. E. Lutinski, and H. R. Gerberich, *ibid.*, in press.

relative numbers of Lewis and Brønsted acid sites. If equal absorption coefficients are assumed for the 1450 and 1545 cm^{-1} bands, the ratio of the number of Lewis to the number of Brønsted sites would simply be the ratio of the observed intensities, *viz.*, 10.5:1. As will be seen later, this value is incorrect. While it is true that a number of molecular complexes of LPY and BPY can be prepared, it is generally the case that these complexes are crystalline and essentially insoluble in the available infrared transparent solvents. One hesitates to use solvents of very high polarity because of the problem of the solvent effect on the absorption coefficients. The direct determination of absorption coefficient is thus not possible. However, we have been able to evaluate the relative absorption coefficients of the 1545- and 1450- cm^{-1} bands by an indirect method based on the assumption that the absorption coefficients of the ν_{19a} mode of chemisorbed BPY and LPY are the same. It was noted earlier that the frequency of this mode is identical (1490 cm^{-1}) in LPY, BPY, and HPY and only slightly displaced from the normal frequency in unperturbed PY which suggests that the vibration is not sensitive to complex formation at the N atom. Having made this assumption the absorption coefficients were calculated by making use of the selective elimination of BPY on KSA. The ratio of the intensities of the 1490- cm^{-1} band to that of the 1450- cm^{-1} band on KSA was taken to be identical with the comparable ratio of chemisorbed LPY. One can then combine this ratio with the ratios of the 1490- cm^{-1} band to the 1450- and 1545- cm^{-1} bands from the spectrum of PY chemisorbed on SA to obtain the ratio of the absorption coefficients of the characteristic LPY and BPY bands. The ratio of the absorption coefficient of the 1450- cm^{-1} band to that of the 1545- cm^{-1} band is

$$\frac{\epsilon_{1450}}{\epsilon_{1545}} = 8.8$$

The magnitude of this ratio was checked by a study of the molecular complexes of PY with BF_3 and HCl at low temperature. The assumption that the absorption coefficient of the 1490- cm^{-1} band is the same in LPY, BPY, and PY was necessary in this determination, also. The value obtained for the ratio was within 15% of that given above. The ratio obtained from the chemisorbed species, themselves, is obviously preferred for use in subsequent measurements. This ratio is combined with the relative intensity data to yield a value of 1.25 for the ratio of the number of Lewis sites to the number of Brønsted sites on the SA surface which is considerably different than the value of 10.5

which was obtained by assuming equal absorption coefficients. Hence, there appear to be approximately equal numbers of Lewis and Brønsted acid sites on the SA surface which has been prepared by calcination and evacuation at 500°. The validity of this result is, of course, subject to the assumption that the absorption coefficient of ν_{19a} is the same in LPY and BPY. Since ν_{19a} does not involve a vibration of the NH group in BPY and the interaction is taking place at the N atom in both cases (which would presumably lead to about the same inductive effect on the intensity) it is felt that this assumption is reasonable. It is to be noted, however, that a deviation from the assumed equal absorption coefficients will produce an inversely proportional change in the ratio of Lewis to Brønsted sites.

Effect of Irreversibly Adsorbed H₂O on the Acidity of Silica-Alumina. It has been shown that small amounts of H₂O irreversibly adsorbed on silica-alumina enhance the catalyst activity for cracking,^{28,29} isomerization,²⁰ and exchange reactions.^{29,30} Mapes and Eischens⁶ have observed the conversion of chemisorbed NH₃ to NH₄⁺ upon exposure of a silica-alumina sample which contained chemisorbed NH₃ to H₂O vapor. Parry¹⁵ has observed a similar conversion of chemisorbed LPY to BPY upon contact with H₂O vapor. Thus, the net effect of the added water appears to be the conversion of Lewis to Brønsted acid sites.

In Fig. 6 the results of our studies of the dual adsorption of PY and H₂O on SA are shown. It was found that the order of adsorption does not affect the results so that only one set of experiments is shown. In this set, PY was chemisorbed at 150° giving the spectrum a in Fig. 6. Upon exposure to 15 mm. of H₂O at 150° for 1 hr. followed by evacuation for 1 hr. at the same temperature, spectrum b results. Further contact with 15 mm. of H₂O at room temperature for 1 hr. with subsequent pumping for 1 hr. yields spectrum c. Evacuation at 150° for 16 hr. removes most of the H₂O and yields spectrum d which is almost identical with the original spectrum a. It is evident from the increase in the intensity of the bands at 1490, 1545, and 1638 cm^{-1} with accompanying decrease in the 1450- cm^{-1} band that the concentration of BPY is increasing at the expense of LPY. These observations are in agreement with those of Mapes and Eischens⁶ and Parry¹⁵ suggesting that the H₂O is converting the Lewis acid sites to Brønsted sites. This implies that the H₂O

(28) R. C. Hansford, *Ind. Eng. Chem.*, **39**, 849 (1947).

(29) S. G. Hindin, A. G. Oblad, and G. A. Mills, *J. Am. Chem. Soc.*, **77**, 535 (1955).

(30) R. G. Haldeman and P. H. Emmett, *ibid.*, **78**, 2922 (1956).



Figure 6. Dual adsorption of pyridine and H_2O on silica-alumina: (a) SA exposed to pyridine at 17 mm. and 150° for 1 hr. followed by evacuation at 150° for 16 hr.; (b) exposure to H_2O at 15 mm. and 150° for 1 hr. followed by evacuation at 150° for 1 hr.; (c) exposure to H_2O at 15 mm. and 25° for 1 hr. followed by evacuation for 1 hr. at 25° ; (d) evacuation for 16 hr. at 150° .

displaces the PY from a primary interaction with the surface acid sites such that the PY engages in a secondary interaction with the site through the chemisorbed H_2O by the formation of BPY. It is surprising, therefore, that the H_2O is removed upon pumping at 150° , whereas the amount of PY removed is negligible

(Fig. 6d). As indicated above, the order of adsorption has no effect on the results so that, in truth, PY displaces H_2O . It is also to be noted that the addition of H_2O is accompanied by an increase in the number of hydrogen-bonded surface OH groups as indicated by the decrease on the 3745-cm.^{-1} band and concomitant increase in the broad band centered at 3500 cm.^{-1} . This is a significant departure from the normal behavior of irreversibly adsorbed H_2O on SA (which is adsorbed under the same conditions used in obtaining spectrum b) which engages in little (if any) hydrogen bonding to surface OH groups.¹⁸ Thus, it would appear that the H_2O interacts simultaneously with chemisorbed PY and a surface OH group, but does not displace the PY from the acid site; however, it is difficult to establish whether the primary interaction is with the PY or the surface OH.

Similar effects of H_2O on the electronic spectra of chemisorbed carbonium ions have been observed by Leftin and Hall^{3c,d} and others^{4,5} wherein the characteristic absorption band of the chemisorbed carbonium ion disappears upon the addition of H_2O and reappears after brief evacuation at room temperature which desorbs the H_2O . On the other hand, NH_3 addition permanently eliminated the carbonium ion absorption by displacing it from the site so that it is desorbed.^{3c,d,4} It had been suggested by Leftin and Hall^{3d} that the H_2O is physically adsorbed and that it acts as a co-catalyst to effect the desorption of the carbonium ion; however, recent work on an ether-triphenyl carbonium ion complex in solution by Smith and Rao³¹ has shown that the ether-carbonium ion adduct does not exhibit the characteristic spectrum of the carbonium ion. Hall³² has suggested that a similar complex is formed between H_2O and chemisorbed triphenylmethyl carbonium ion which causes the disappearance of the absorption band. Thus, it is probable that the carbonium ion is not desorbed upon contact with H_2O vapor, which is consistent with our experiments on the PY- H_2O system. Since it cannot be easily pumped off in 1 hr. at 150° , but does eventually desorb on long pumping at the same temperature, it is evident that the interaction of H_2O with PY is stronger than that observed with the carbonium ion.

Dual Adsorption of H_2O and Pyridine on Base-Exchanged Silica-Alumina. It has been shown in our earlier work¹⁸ that K-poisoning leads to a severe reduction in the amount of irreversibly adsorbed H_2O .

(31) W. B. Smith and P. S. Rao, *J. Org. Chem.*, **26**, 254 (1961).

(32) W. K. Hall, private communication. The authors are grateful to Dr. Hall for calling attention to ref. 31 and for suggesting its significance with respect to his earlier work.^{3c,d}

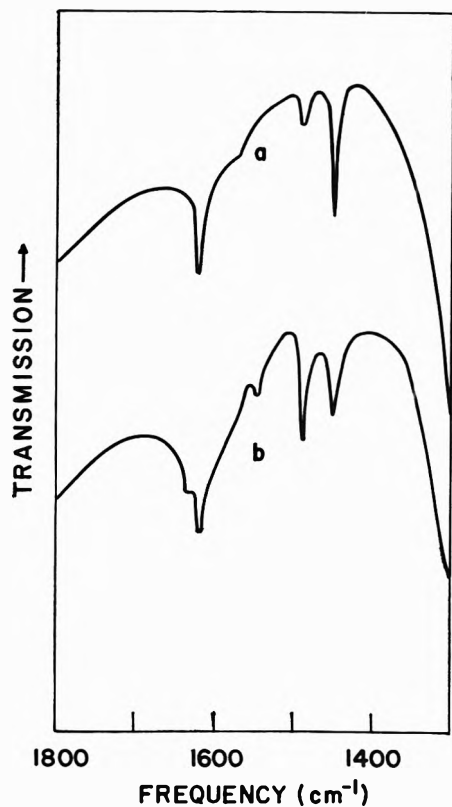


Figure 7. Dual adsorption of pyridine and H_2O on K-poisoned silica-alumina: (a) KSA exposed to pyridine at 17 mm. and 150° for 1 hr. followed by evacuation for 16 hr. at 150° ; (b) exposed to H_2O at 15 mm. and 150° for 1 hr. followed by evacuation for 1 hr. at 150° .

Since the Brønsted acidity is eliminated by K-poisoning, it was of interest to examine the effect of irreversibly adsorbed H_2O on PY chemisorbed on KSA. In Fig. 7 the spectra of PY chemisorbed on KSA before and after contact with 15 mm. of H_2O vapor at 150° (1-hr. exposure and 1-hr. evacuation) are shown. Again the addition of H_2O leads to the conversion of LPY to BPY.

Discussion

Nature of the Acid Sites on Silica-Alumina. A number of conclusions concerning the nature of the acid sites on SA can be drawn from the results described in the foregoing sections and from our previous study of SA.¹⁸ Before proceeding further it is worthwhile to review the pertinent experimental observations to be taken into consideration:

(1) There are very few, if any surface OH groups attached to Al atoms.^{18,33}

(2) The adsorption of NH_3 and PY on silica-alumina indicates that both Lewis and Brønsted acidity are present on the surface.^{6-8,15} Our measure-

ments indicate approximately equal numbers of each type.

(3) On the average, each chemisorbed PY is hydrogen bonded to one surface OH group.

(4) The desorptions of LPY and BPY exhibit the same functional dependence on temperature.

(5) K-poisoning weakens the majority of the acid sites and eliminates apparent Brønsted acidity.

(6) Irreversibly adsorbed H_2O converts LPY to BPY on both SA and KSA. This interaction is reversible and relatively weak since the H_2O can be pumped away.

(7) In the dual adsorption of H_2O and PY on SA, the PY is the stronger base and remains on the acid site. The H_2O interacts with surface OH as well as with the chemisorbed PY.

In order to facilitate the interpretation of the above observations, the distribution of groups on the surface of SA has been estimated. For example, the approximate number of surface Al atoms has been determined by an acid leaching technique¹⁸; hence, the ratio of O/Al at the surface can be estimated by a knowledge of the surface area and the assumption that the surface O atoms are close-packed. The value obtained, 6.62, is identical with that obtained by assuming a homogeneous distribution of the Al throughout the bulk of the solid. In Table III a compilation of data which approximates the average distribution of surface groups is given. These data indicate that there are roughly two surface Al atoms and five or six surface Si atoms per surface OH group. It is also evident that only a small fraction of the surface O atoms are situated in surface OH groups; similarly, only a small proportion of the surface Al atoms are located in acidic sites strong enough to chemisorb PY at 150° .

The most striking of the experimental observations

Table III: Average Distribution of Surface Groups on a Silica-Alumina^a

$(OH)_s/Al_s$	= 0.55 ^b
O_s/Al_s	= 6.62
Si_s/Al_s	= 2.50
$(OH)_s/O_s$	= 0.084
K/Al_s	≥ 0.6 ^c
C_5H_5N/Al_s	= 0.087 ^d

^a Subscript S indicates a surface species. ^b Based on a value of 1.24×10^{-4} surface OH/cm² for Triple A silica-alumina.³⁴ ^c For KSA only.¹⁸ ^d Chemisorbed at 150° .

(33) W. K. Hall, H. P. Leftin, F. J. Cheselske, and D. E. O'Reilly, *J. Catalysis*, 2, 506 (1963).

(34) D. S. MacIver, private communication.

is the conversion of LPY to BPY through a relatively weak interaction with H_2O . This reminds one of the weak interaction between NH_3 and H_2O in solution to form ammonium hydroxide. However, Sidorov²¹ has shown that the interaction between PY and H_2O in solution is a typical hydrogen-bonding interaction. It is significant that no evidence for the formation of BPY was found in his study.²¹ The formation of BPY on the SA surface is, thus, a manifestation of the activation of the PY by the acid site. This observation is the basis of the following descriptive model which appears to qualitatively fit the experimental observations quite satisfactorily.

It is proposed that all of the primary acid sites on a silica-alumina are of the Lewis type centered on active surface Al atoms. Brønsted acidity occurs by a "second-order" interaction between the molecules chemisorbed on the Lewis type site and a nearby surface OH group. This interaction between the surface OH group and the chemisorbed molecule is essentially a hydrogen-bonding interaction. The strength of this interaction depends upon the interaction distance, the nature of the chemisorbed molecule and the degree of activation of the molecule by the acid site. A critical dependence of the fraction of apparent Brønsted acid sites upon the strength of the primary Lewis sites and the critical interaction distance, CID (maximum interaction distance to produce the protonated chemisorbed species), is predicted from the model. In the preceding sections it has been concluded that an approximately equal distribution of LPY and BPY exists on SA, despite the fact that, on the average, each PY molecule is hydrogen bonded to a surface OH group. It was also found that this distribution is altered by the adsorption of H_2O which significantly increases the number of BPY at the expense of LPY. These observations imply (in terms of the above model) that the interaction distance of roughly half of the chemisorbed PY was greater than the CID and that the addition of H_2O increased the fraction of BPY by providing OH groups to interact with the chemisorbed PY at less than the CID. On the other hand, one observes no apparent Brønsted acidity on KSA, and it was further shown that the effect of K-poisoning was to reduce the strength of the acid sites. Thus, while the interaction distances are essentially the same as on SA, the decrease in strength of the site has resulted in a drastic decrease in the amount of BPY. The subsequent addition of H_2O produces an increase in BPY suggesting that the decrease in strength of the acid site has resulted in a smaller CID than can be achieved by the surface OH groups, but which can occur with adsorbed H_2O .

The model thus qualitatively accounts for the effect of H_2O on the distribution of Lewis and apparent Brønsted sites. The initial distribution of acid sites can also be rationalized in terms of the model. One must first have a rough idea of the geometrical arrangement of the surface groups. A possible representation of the relative distributions of the surface groups is shown in Fig. 8. This representation is not thought to be a valid model of the surface, but intended merely

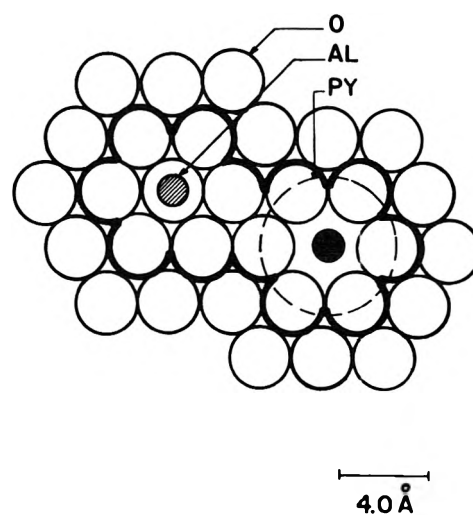


Figure 8. Model of the basic structural unit of a silica-alumina surface.

to provide a rough idea of the surface geometry. The surface is assumed to consist of several atomic layers, the outermost layer consisting of close-packed O atoms under which is a layer containing Si and Al atoms. The structural unit of interest consists of 13 O atoms, two Al atoms, five or six Si atoms, and one H atom (located in a surface OH). It is further presumed that the acidic aluminum is exposed by removal of an O atom from the close-packed structure. Only the Al and O atoms are shown in Fig. 8 since the location of the Si atoms are not of particular interest. The hydrogen atom can be located on any of the 13 O atoms in the structural unit; it is equally probable that it may be located adjacent to the acidic Al atom, or to the nonacidic partner Al atom. A considerable variation in interaction distance is thus possible. The relative size of a PY molecule is also shown in Fig. 8 where it is depicted as a circular molecule centered on the acidic Al. It is most probable that the PY interacts through the N atom,³⁵ so that its circle of influence is expected to be somewhat larger than shown in Fig. 8. It is also

(35) L. R. Snyder, *J. Phys. Chem.*, **67**, 2344 (1963).

probable that the BPY is produced by the interaction of the OH with the N atoms rather than with the π -electrons of PY. The interaction with the π -electrons would give simple hydrogen bonding.³⁶ From this crude representation it is evident that the sites most likely to give BPY are those which have the OH group adjacent to the acidic Al atom. Since it is equally probable that the OH group would be adjacent to the acidic Al or the nonacidic Al, one would predict an equal distribution of BPY and LPY, which is experimentally observed.

Thus the model can be used qualitatively to rationalize the experimental results on the adsorption of nitrogen bases on silica-alumina. The catalytic importance of the apparent Brønsted acidity is still open to question, however. From the gravimetric measurement of PY chemisorption on SA at 150°, the number of acid sites per cm.² is estimated to be 5.6×10^{13} . It is becoming evident that the number of catalytically active sites is considerably smaller than this. Recent estimates by Hall and co-workers^{27,37} places the number in the 1×10^{12} to 5×10^{12} site/cm.² range which is an order of magnitude smaller than the number estimated by PY adsorption. This discrepancy can probably be attributed to the difference in basicity between PY and hydrocarbons. PY, being a much stronger base, can adsorb on weakly acidic sites which presumably would be too weak to be catalytically active. The role (in terms of the above model) of apparent Brønsted sites on catalytic reactions is also strongly dependent on this factor. Since the production of an apparent Brønsted site depends on the degree of activation of the adsorbed molecule by the pri-

mary Lewis site, it is quite possible that the relative importance of these protonic sites would vary over a considerable range from one reaction to another.

One might logically attempt to apply this model to the acidic sites on an alumina surface. However, the adsorption of PY on alumina is significantly different than on SA. Parry¹⁵ has shown that only LPY is observed and that the addition of H₂O does not convert LPY to BPY on alumina. We repeated these experiments on a γ -alumina and obtained the same results. We have not been able to rationalize these differences in behavior between SA and alumina, especially the lack of a conversion from LPY to BPY upon H₂O adsorption since alumina is known to have strong acidic sites.³⁸

Conclusion

The infrared spectroscopic study of pyridine chemisorbed on a typical silica-alumina cracking catalyst has led to the conclusion that there are essentially equal numbers of Lewis and Brønsted acid sites present on the surface. A model has been proposed in which all of the primary acid sites are of the Lewis type, and apparent Brønsted sites are produced by the second-order interaction between the molecule chemisorbed on the primary Lewis site and a nearby surface OH group. This model is consistent with the experimental observations to date and is felt worthy of further evaluation.

(36) M. R. Basila, *J. Chem. Phys.*, **35**, 1151 (1961).

(37) W. K. Hell, J. G. Larson, and H. R. Gerberich, *J. Am. Chem. Soc.*, **85**, 3711 (1963).

(38) H. Pines and W. O. Haag, *ibid.*, **82**, 2471 (1960).

Spin-Spin Coupling in the Tetrafluoroborate Ion^{1a}

by Karl Kuhlmann^{1b} and David M. Grant

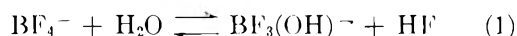
Department of Chemistry, University of Utah, Salt Lake City, Utah 84112 (Received June 16, 1964)

The B¹¹-F¹⁹ spin-spin coupling in BF₄⁻ has been found to vary between 1 and 5 c.p.s. in various aqueous solutions. This value is dependent upon both a concentration and specific cationic effect, which is explained by ion-pair formation. The equilibrium constant for the association in NaBF₄ solutions is about 0.2 M⁻¹, and the infinite dilution coupling constant for the BF₄⁻ ion in water is 1.13 ± 0.07 c.p.s. The average coupling constant in the ion-pair species depends markedly upon the cation involved in the association.

Introduction

The B¹¹-F¹⁹ spin-spin coupling constant in the BF₄⁻ ion, which was reported previously to be 4.8 c.p.s.,^{1c} has been found in this laboratory to depend upon the nature of the associated cation and, in general, upon the concentration of the ionic species. To explain this variation the observed splitting value is considered to be an average of coupling constants for two or more species in rapid equilibrium. Proposed alterations in the equilibrium conditions by various cations and changing concentrations are sufficient to account for the variation in coupling constants.

The chemistry of aqueous fluoroborate solutions has been extensively studied by several workers,²⁻⁵ and the reaction



was found to occur to the extent of about 5.5% in a 5.4 M solution of HBF₄.⁴ Furthermore, there has been only meager evidence for the existence of the species BF₂(OH)₂⁻ and BF(OH)₃⁻ in these solutions, and we also have found no evidence for their existence in measurable quantities in our solutions. The kinetic data^{4,5} indicate that the reaction is fast enough to ensure that BF₃(OH)⁻ will be present in all of our samples, but the rate is too slow to average the coupling constants of BF₄⁻ and BF₃OH⁻. The previous work, therefore, supports the hypothesis that the averaging process does not involve fluoroborate ions other than BF₄⁻. The rapid averaging process then involves equilibrium interactions of BF₄⁻ with positively charged ions and the solvent. The data are discussed in terms of a simplified three-parameter ion-pair model.

Experimental

The n.m.r. spectra were taken on a Varian V-4311 spectrometer system equipped with standard accessories and operating at 56.4 Mc./sec. for F¹⁹ and 15.085 Mc./sec. for B¹¹. The spectra were calibrated with a Hewlett-Packard 200 CD audio oscillator and a Hewlett-Packard 524C counter. The spectrum of each sample was recorded no fewer than seven times and the splittings and shifts averaged.

The F¹⁹ magnetic resonance spectra were measured for 0.23 to 7.0 M solutions of NaBF₄ and for 0.39 to 2.1 M solutions of NH₄BF₄. In addition, multiplet splittings were measured for 0.50 M solutions of NaBF₄ containing concentrations ranging from 0.99 to 7.1 M of NaNO₃, NH₄NO₃, LiNO₃, and HNO₃, and for a 1 M solution of NaBF₄ which was 6 M in NaClO₄. Since hydrolysis is considerably accelerated by elevated temperature^{3,5} the fluoroborates were purified by recrystallization at room temperature. A saturated aqueous solution of sodium or ammonium fluoroborate was prepared from commercial technical grade material, and the undissolved matter was removed by filtration

(1) (a) This is an essential portion of a thesis submitted to the Chemistry Department, University of Utah, in partial fulfillment of the requirements for a Doctor of Philosophy degree; (b) NDEA Title IV Fellow, 1959-1962; (c) R. C. Chambers, H. C. Clark, L. W. Reeves, and C. J. Willis, *Can. J. Chem.*, **39**, 258 (1961).

(2) H. S. Booth and D. R. Martin, "Boron Trifluoride and Its Derivatives," John Wiley and Sons, Inc., New York, N. Y., 1949, p. 87.

(3) I. G. Ryss, *Compt. rend. Acad. Sci. URSS*, **52**, 417 (1946); *Zavodskaya Lab.*, **12**, 651 (1946).

(4) C. A. Wamser, *J. Am. Chem. Soc.*, **70**, 1209 (1948); **73**, 409 (1951).

(5) M. Anbar and S. Guttmann, *J. Phys. Chem.*, **64**, 1896 (1960).

through washed charcoal. The solution was then evaporated in a rotating inclined dish in a stream of filtered air for 2 to 3 hr. until little liquid remained. The crystals were collected in a sintered glass filter and the process repeated. The crystals were then dried for 2 weeks over anhydrous magnesium perchlorate. The other compounds used were reagent grade.

The sample solutions were made by diluting an accurately weighed sample to 10 ml. in a volumetric flask. All chemical shifts and most coupling measurements were made using Wilmad semiprecision 5-mm. glass sample tubes. Chemical shifts were measured relative to neat trifluoroacetic acid as an external standard. The reference sample was contained in a sealed, thin-wall capillary. The same reference capillary was used for each sample. The chemical shift data were not corrected for differences in the bulk magnetic susceptibility.

Dissolved oxygen was removed from the samples by passing a fine stream of pure nitrogen through the filled sample tube for about 10 min. The nitrogen used was previously passed through another tube of sample solution in order to reduce changes in concentration by evaporation. After degassing, the sample tubes were covered with tight-fitting polyethylene caps. In order to minimize uncertainties in the concentrations due to hydrolysis the sample solutions were run as soon as possible after preparation. When it was necessary to keep samples more than 1 day, they were frozen until they could be used. The samples were run in a random order so that the age of a sample would not be related to its stoichiometric concentration.

Results

Figure 1 contains both the B^{11} and F^{19} spectra of a 7.0 *M* $NaBF_4$ solution. The sharp 1:4:6:4:1 quintet in the B^{11} spectrum (Fig. 1A) clearly exhibits that the B^{11} is coupled to four equivalent F^{19} nuclei, and the 4.6 ± 0.1 c.p.s. splitting observed for this multiplet is in agreement with the coupling observed in the sharp quartet of lines found in the corresponding fluorine spectrum (Fig. 1B). The fluorine 1:1:1:1 quartet results from the four spin states of the B^{11} nucleus, which has a total spin of $3/2$ and a natural abundance of 81%. This multiplet is considerably more pronounced than the less intense septet resulting from coupling to the B^{10} nuclei of spin 3 and 19% natural abundance. Only four of the smaller peaks of the septet can be observed as the multiplet is interlaced among the three lower field components of the quartet which obscure several of the peaks. In $NaBF_4$ and NH_4BF_4 solutions of lower concentration where the boron-fluorine couplings are smaller, the

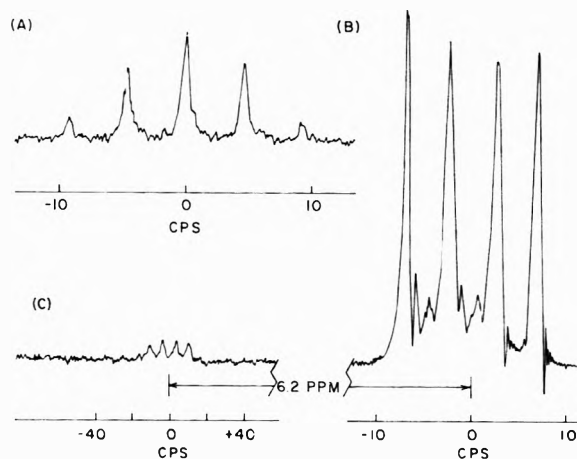


Figure 1. Spectra of a 7.0 *M* $NaBF_4$ solution. (A) The 1:4:6:4:1 quintet found in B^{11} spectrum is attributed to the BF_4^- ion. (B) The F^{19} spectrum of BF_4^- contains a prominent 1:1:1:1 multiplet due to spin-spin coupling with the B^{11} isotope and interlaced with these signals is the septet resulting from the less abundant B^{10} nuclei. (C) The F^{19} spectrum of BF_3OH^- exhibits the quartet due to the B^{11} splittings. The B^{10} induced multiplet, however, is obscured in the noise.

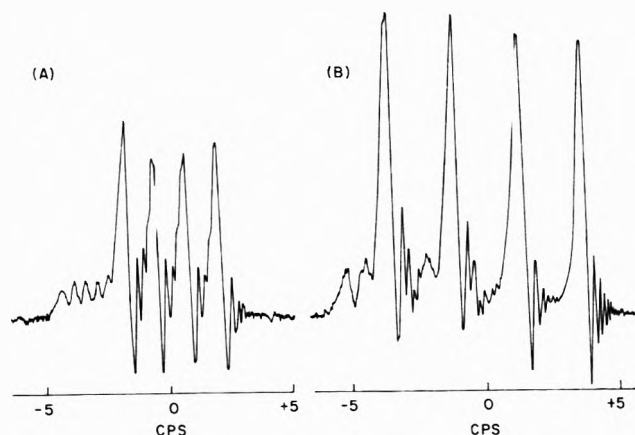


Figure 2. The F^{19} spectrum of (A) 2.1 *M* NH_4BF_4 and (B) 2.0 *M* $NaBF_4$. The B^{10} septet can be recognized readily in these spectra.

B^{10} and B^{11} fluorine multiplets are more readily identified as can be observed in Fig. 2. The assumption that the two multiplets are due to the two naturally occurring isotopes of boron is confirmed from ratios of splittings and intensities observed for the two sets of lines. The isotopic shift of 0.050 ± 0.002 p.p.m. was found to be essentially independent of the concentration of the BF_4^- solutions.

A broad quartet (Fig. 1C) of low intensity, found 6.2 p.p.m. downfield from the fluorine resonance in BF_4^- , is assigned to the BF_3OH^- ion. To increase the concentration of this species, a 5 *M* solution of $NaBF_4$

was treated with a small amount of CaCO_3 to remove fluoride and boiled for about 1 hr. This treatment significantly enhanced the intensity of the quartet, and the splitting was determined to be 12.7 ± 0.2 c.p.s. As in the case of BF_4^- , this multiplet also shows concentration and specific cationic effects. To confirm the identity of the BF_3OH^- species the B^{11} spectrum of the hydrolyzed NaBF_4 solution is given in Fig. 3 at higher radiofrequency power. Three of the four peaks expected for the 1:3:3:1 quartet in BF_3OH^- are clearly evident, and the lowest field peak is overlapping the more intense BF_4^- quintet. The much sharper lines observed in the quintet transitions indicates the lack of quadrupole broadening in the highly symmetrical tetrahedral BF_4^- ion. This broadening is clearly evident in the less symmetrical BF_3OH^- ion.

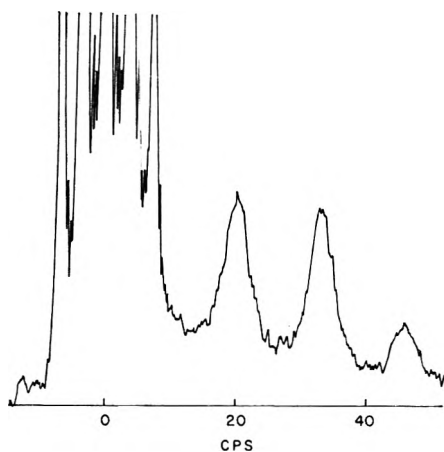


Figure 3. The sharp B^{11} quintet of BF_4^- overlaps the lower field peak of the broad B^{11} quartet of BF_3OH^- . The difference in line widths of the two multiplets is attributed to quadrupolar broadening in the asymmetrical BF_3OH^- species which apparently is absent in the highly symmetrical BF_4^- species.

Figure 4 shows the dependence of J , the observed B^{11} - F^{19} coupling constant in BF_4^- , on the concentration of NaBF_4 and NH_4BF_4 . This figure clearly exhibits both the specific cation and total concentration effects. In NaBF_4 solutions J is strongly dependent on the total concentration, undergoing better than a threefold change over the concentration range studied. In contrast, the splittings in NH_4BF_4 solutions are essentially independent of concentration up to the limits of solubility. This marked cationic effect suggests that cation-anion interactions are responsible for the variations in splitting. Fluorine-19 chemical shift data in these compounds exhibit a similar and

specific ion and concentration dependence as noted for the spin-spin coupling constant, and this plot is given in Fig. 5.

Further evidence for a specific ion effect is portrayed in Fig. 6 for a constant NaBF_4 concentration of 0.5 M and various added nitrates. While the effect of the ammonium and hydronium ion is relatively concentration independent, the lithium ion, like the so-

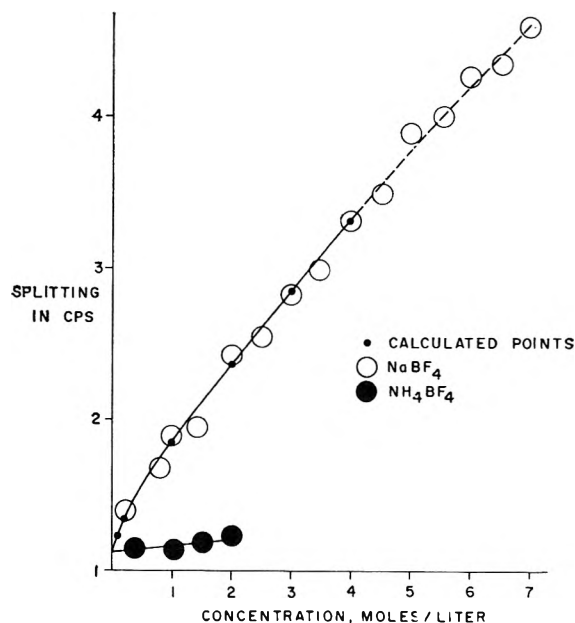


Figure 4. The concentration dependence of the B^{11} - F^{19} coupling constant in BF_4^- is shown for NaBF_4 and NH_4BF_4 .

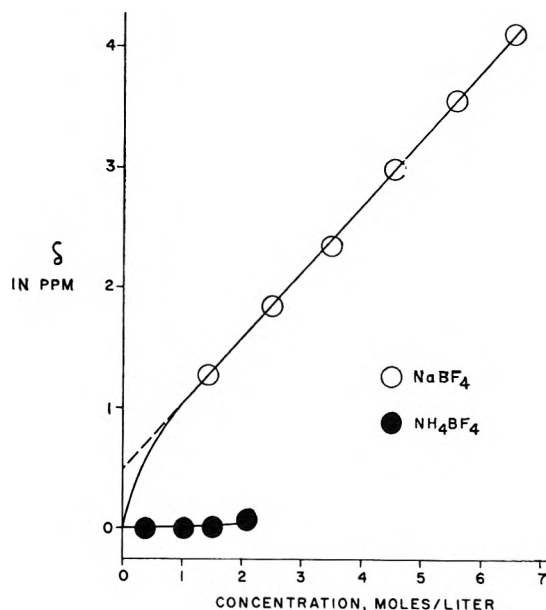


Figure 5. The dependence of the F^{19} chemical shift of the BF_4^- resonance is shown as a function of concentration.

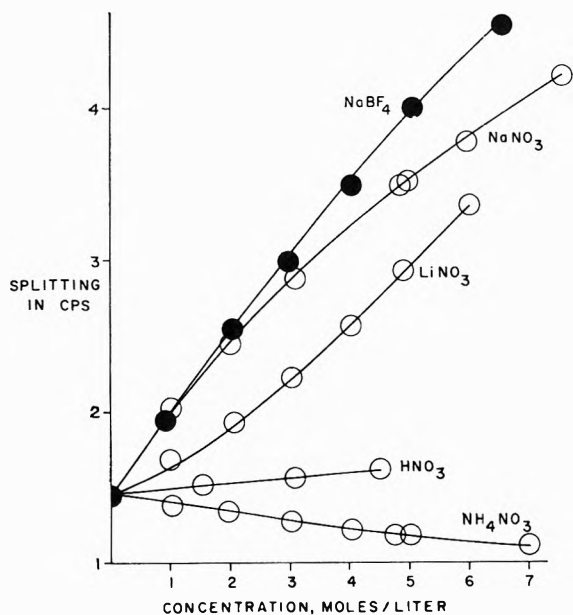
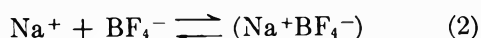


Figure 6. The $B^{11}\text{-F}^{19}$ coupling constant for 0.5 M NaBF_4 dissolved in nitrate solutions of various concentrations exhibits the specific ion effect noted for this constant. The data for NaBF_4 are plotted vs. the concentration in excess of 0.5 M in order that all the data would be directly comparable.

dium ion, has a prominent effect upon the coupling constant. Also found in Fig. 6 for reference is the splitting data given for NaBF_4 in Fig. 4 plotted vs. the concentration of pure NaBF_4 in excess of 0.5 M .

Discussion

A clue to the nature of the specific cation effect is afforded by comparing the infinite dilution splittings predicted by an assumed linear dependence on concentration. The extrapolated value for NH_4BF_4 is 1.15 c.p.s., whereas for NaBF_4 the value is 1.37 c.p.s. It is only reasonable to assume that concentration effects for various salts should disappear at infinite dilution, yet the discrepancy between the NH_4BF_4 and NaBF_4 values given by linear extrapolation is well outside the experimental error (± 0.07 c.p.s.) in the measurements. This suggests that the curve of J vs. concentration for NaBF_4 turns down at lower concentrations and intercepts the axis near 1.15 c.p.s. Behavior of this sort is possible from a labile equilibrium of the form



where each species is understood to be hydrated to some extent. If BF_4^- and $(\text{Na}^+\text{BF}_4^-)$ have different coupling constants, J_o and J_p , respectively, the observed splitting will be a weighted average of the individual couplings according to

$$J = J_p(1 - \alpha) + J_o\alpha \quad (3)$$

where α is the degree of dissociation of $(\text{Na}^+\text{BF}_4^-)$ into Na^+ and BF_4^- . The degree of dissociation is related to the stoichiometric concentration, c , by the formation constant, K , as follows

$$K = \frac{[(\text{Na}^+\text{BF}_4^-)]}{[\text{Na}^+][\text{BF}_4^-]} = \frac{1 - \alpha}{\alpha^2\gamma_{\pm}^2c} \quad (4)$$

where γ_{\pm} is the mean activity coefficient of the ions. The activity coefficient of the ion pair has been assumed to be unity. While the advisability of this assumption is somewhat questionable⁶ for very concentrated solutions, it is made here for the sake of simplicity. Unfortunately, no experimental values of γ_{\pm} for NaBF_4 solutions are available, so as an approximation the activity coefficients for NaClO_4 ⁷ were used. It is not expected that the correspondence will be exact, but since the solubilities⁸ and structures⁹ of the two salts are similar, it is plausible to assume that semiquantitative agreement can be expected in their mean ionic activities in solution. To test this assumption J was measured for a solution 1 M in NaBF_4 and 6 M in NaClO_4 and found to be 4.9 c.p.s., only slightly higher than the 4.6 c.p.s. value for 7 M NaBF_4 .

Equations 3 and 4 may be combined to give an expression of the form

$$y = J_px + 2J_o \quad (5)$$

where

$$y = \frac{-4K\gamma_{\pm}^2cJ}{1 - \sqrt{1 + 4K\gamma_{\pm}^2c}} \quad (6)$$

and

$$x = -1 + \sqrt{1 + 4K\gamma_{\pm}^2c} \quad (7)$$

Using a given value of K , eq. 5 gives values for J_p and J_o from the data by the method of least squares. The value of K for which the variance of the least-squares fit is a minimum may be taken to be the most probable value of K .¹⁰ This procedure was applied to the NaBF_4 data for concentrations in which the NaClO_4 activity coefficients⁷ are known, *i.e.*, up to 4.5 M . The activity coefficients were expressed in terms of molar concentrations obtained from the densities of NaClO_4 solutions given in the International

(6) D. R. Rosseinsky, *J. Chem. Soc.*, 785 (1962).

(7) J. H. Jones, *J. Phys. Chem.*, 51, 516 (1947).

(8) E. Wilke-Dorfurt, *Z. angew. Chem.*, 37, 712 (1924).

(9) N. V. Sidgwick, "The Chemical Elements and Their Compounds," Vol. I, Oxford University Press, London, 1950, p. 410.

(10) C. A. Bennett and N. L. Franklin, "Statistical Analysis in Chemistry and the Chemical Industry," John Wiley and Sons, Inc., New York, N. Y., 1954, p. 238.

Critical Tables.¹¹ The parameters derived in this way are $K = 0.22 \pm 0.1 M^{-1}$, $J_p = 11 \pm 2$ c.p.s., and $J_o = 1.13 \pm 0.07$ c.p.s. The limits of error given were calculated assuming that the intercept J_o would have the same probable error as the average probable error of the individual measurements of J . The empirical curve calculated using these parameters is given in Fig. 4. The agreement with the data over the concentration range treated is very good, and the curve can be extrapolated smoothly through the remaining data.

The splitting at infinite dilution, J_o , predicted by this model is in excellent agreement with the value given by linear extrapolation of the NH_4BF_4 data. This close agreement is good evidence for the correctness of the model.

In agreement with the ion-pair model proposed, the data for various nitrate mixtures (Fig. 6) show specific dependence on the cation, and the curve for NaNO_3 shows a definite common ion effect. The generally lower J for solutions with NaNO_3 instead of NaBF_4 probably results from a combination of lower activity coefficients for the nitrate and competition between $(\text{Na}^+\text{BF}_4^-)$ and $(\text{Na}^+\text{NO}_3^-)$ for the available sodium ions. The same effect would account for the lowering of J with increasing concentration of NH_4NO_3 .

The different behavior of the ammonium and hydronium cations probably is due to the fundamentally different nature of these ions. The ion-pair model can account for the lack of appreciable concentration dependence in two ways. If the association constant, K , is very small (*i.e.*, $4K\gamma_{\pm}^2c \ll 1$) for all concentrations of interest then $\alpha \cong 1 - K\gamma_{\pm}^2c$, and eq. 3 becomes

$$J = (J_p - J_o)K\gamma_{\pm}^2c + J_o \quad (8)$$

The slope of the J vs. c curve now will be appreciable only if J_p differs enormously from J_o . On the other hand, if J_p is nearly equal to J_o no concentration effect will be observed even if K is fairly large. In the case of the hydronium and ammonium ions the effective radius of these cations may be so large that the anion is not perturbed enough on association to change the coupling constant, and furthermore the hydrogen-bonded type of ion-pair interactions expected for NH_4^+ and H_3O^+ would not differ appreciably from that expected for the hydrated ion in aqueous solution.

There is an interesting correlation between the behavior of the curves of Fig. 6 and the concentration dependence of mean ionic activity coefficients in the pure nitrates. The activity coefficients of the nitrates and perchlorates of cations used in this study are shown in Fig. 7. The lower activity coefficients of

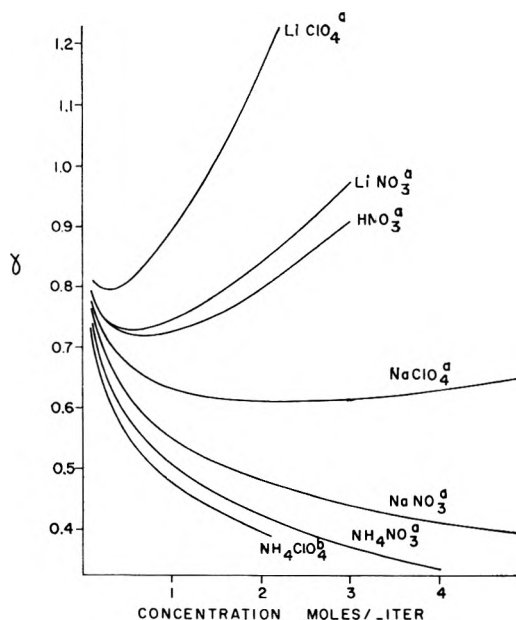


Figure 7. The concentration dependence of activity coefficients for some nitrates and perchlorates. See (a) H. S. Harned and B. B. Owen, "The Physical Chemistry of Electrolytic Solutions," 3rd Ed., Reinhold Publishing Corp., New York, N. Y., 1958, p. 383, and (b) O. E. Esvall and S. Y. Tyree, Jr., *J. Phys. Chem.*, **66**, 940 (1962).

NaNO_3 with respect to NaClO_4 are reflected in the lowering of J when ClO_4^- is replaced by NO_3^- . The upswing of the lithium nitrate activity coefficients is clearly reflected in the curve of J vs. the lithium nitrate concentration in Fig. 6.

The curvature of the F^{19} chemical shift vs. concentration plot given in Fig. 5 is negligible at higher concentrations, but again the infinite dilution values obtained by linear extrapolation of the NaBF_4 and NH_4BF_4 plots disagree far more than the experimental error would permit. Thus the NaBF_4 chemical shift curve like the splitting plot must turn down for dilute solutions. This is just the sort of behavior found by Freeman and co-workers¹² for the thallium chemical shifts in thallos salts. They concluded that higher order associations were responsible for the linearity of the chemical shifts in concentrated solutions. Apparently the chemical shift of the ion pair is being affected in a slightly different manner than noted for the coupling constant. This is not too surprising in view of the generally greater sensitivity of chemical shifts to medium effects.

(11) "International Critical Tables of Numerical Data, Physics, Chemistry and Technology," Vol. III, McGraw-Hill Book Co., Inc., New York, N. Y., 1926, p. 51.

(12) R. Freeman, R. P. H. Gasser, R. E. Richards, and D. H. Wheeler, *Mol. Phys.*, **2**, 75 (1959).

The ion-pair model proposed here is admittedly oversimplified. At the concentrations studied there would be higher order associations, and the value of the parameters K and J_p can only be considered to be demonstrative. However, the value of 11 c.p.s. obtained for J_p is reasonable. If the anion is considered to be momentarily distorted by the cation along the axis of one B-F bond, one would expect the coupling constant of the remaining three fluorines to be somewhat similar to that in compounds of the type BF_3X^- . The compound of this type expected to be most like the ion pair would be BF_3OH^- which was observed in this study to have a coupling constant of about 13 c.p.s.

It would appear that no single coupling mechanism can account for both the anomalously low $\text{B}^{11}\text{-F}^{19}$ coupling constant and the several-fold variation in this value for solutions of differing concentration. This position is substantiated if one compares the 1-5 c.p.s. $\text{B}^{11}\text{-F}^{19}$ coupling constant in BF_4^- with the 259 c.p.s. $\text{C}^{13}\text{-F}^{19}$ coupling recorded¹³ for the iso-electronic CF_4 molecule. In the directly bonded $\text{C}^{13}\text{-F}^{19}$ coupling, shown by Tiers¹⁴ to be negative, mechanisms other than that due to the Fermi contact terms are undoubtedly important. This is necessary as the directly bonded Fermi contact term should render the coupling positive. Likewise, it is attractive

to explain the small $\text{B}^{11}\text{-F}^{19}$ coupling in BF_4^- with large but opposing coupling mechanisms as ion-pair formation might well effect minor changes in large but nearly equal coupling terms of opposite sign. This in turn could lead to large relative changes in the observed difference. To attempt an explanation of the several-fold variation in these small coupling constants with a single mechanism would require that the electronic structure of the BF_4^- ion be altered substantially by ion-pair formation. This seems unlikely when electronic energies are compared with the relatively small association energy of the ion pair.

Without considerably more information regarding the nature and the structure of the ion pair complex represented by $(\text{Na}^+\text{BF}_4^-)$ it is not possible to discuss the details of the alteration in the coupling mechanism as the ion pair is formed. Nevertheless, further studies of the n.m.r. spectra of fluoroborate solutions may give considerable insight into the nature of electrolytic solutions as well as additional data for understanding the detailed mechanism of spin-spin coupling.

Acknowledgment. The work was supported in part by the NSF and NDEA Title IV.

(13) R. K. Harris, *J. Phys. Chem.*, **66**, 768 (1962).

(14) G. V. D. Tiers, *J. Am. Chem. Soc.*, **84**, 3972 (1962).

Radiolysis of Cyclohexene. III. Cyclohexene- d_{10} ¹

by B. R. Wakeford and G. R. Freeman

Department of Chemistry, University of Alberta, Edmonton, Alberta, Canada (Received June 17, 1964)

The γ -radiolysis of liquid cyclohexene- d_{10} gave the following product yields. The corresponding yields from light cyclohexene are given in parentheses: hydrogen, 0.65 (1.28); cyclohexane, 0.66 (0.95); 2,2'-dicyclohexenyl, 1.36 (1.90); 3-cyclohexylcyclohexene, 0.66 (0.58); dicyclohexyl, 0.47 (0.21); unidentified dimer, 0.32 (0.22). The over-all rate of decomposition of cyclohexene- d_{10} is quite similar to that of light cyclohexene, although the product distribution is quite different. Moderately large isotope effects (~ 3.6) are evident in the over-all radiolytic reaction. Considering the activated species that produce hydrogen, activation transfer occurs from the $c\text{-C}_6\text{D}_{10}$ species to $c\text{-C}_6\text{H}_{10}$, as well as to 1,3- and 1,4-cyclohexadiene and to benzene.

Introduction

The radiolysis of liquid cyclohexene- d_{10} , in the presence and absence of inhibitors and of light cyclohexene, has been studied in an attempt to elucidate the mechanism of radiolysis of cyclohexene.²

Experimental

The cyclohexene- d_{10} , obtained from Merck Sharp and Dohme of Canada, Ltd., contained up to 12% $\text{C}_6\text{D}_9\text{H}$, depending on the sample, $\sim 0.3\%$ cyclohexane and $\sim 1\%$ benzene. The cyclohexane and benzene were removed from the cyclohexene by vapor phase chromatography (v.p.c.).

1,3-Cyclohexadiene (1,3-D) and 1,4-cyclohexadiene (1,4-D) were obtained from Aldrich Chemical Co. and were purified by vacuum distillation followed by v.p.c.

Research grade benzene from Phillips Petroleum Co. was used as supplied.

The total hydrogen yield was determined by low-temperature distillation and pressure-volume measurement. The H_2 , HD, and D_2 contents of the gases were measured using a Metropolitan-Vickers MS-2 mass spectrometer that was calibrated with H_2 , D_2 , and a mixture of H_2 , D_2 , and HD.

Other pertinent experimental details have been reported earlier.²

Results

The product yields from cyclohexene- d_{10} are given in column 1 of Table I, with the corresponding results

from light cyclohexene^{2a} given in parentheses. The yields of heavy hydrogen, cyclohexane, and 2,2'-dicyclohexenyl from deuterated cyclohexene were less than the yields of their light counterparts from protonated cyclohexene, while the yields of heavy dicyclohexyl, 3-cyclohexylcyclohexene, and the unidentified dimer D-1^{2a} were greater than those of the corresponding light compounds (see column 2, Table I).

The yields of products from a dilute solution of light 1,3-D (electron fraction of 1,3-D, $\epsilon_{1,3\text{-D}} = 0.0013$) in heavy cyclohexene are given in column 3 of Table I. The results for a corresponding light cyclohexene solution, obtained by interpolation of earlier results,^{2b} are given in parentheses. The relative efficiencies of interfering with the formation of the various products in the heavy and light cyclohexene systems are indicated in column 4. The relative amounts of inhibition in the heavy and light systems are essentially the same, with two exceptions. Cyclohexane formation is much more readily inhibited in the heavy than in light cyclohexene, while the unidentified dimer D-1 is somewhat less readily inhibited in the deuterated system.

The rate of 1,3-D consumption was higher in the cyclohexene- d_{10} solution than in the light cyclohexene solution (column 3, Table I). The yield of dicyclohexadiene was higher in the cyclohexene- d_{10} solution,

(1) This work was supported in part by The National Research Council of Canada.

(2) B. R. Wakeford and G. R. Freeman: (a) part I, *J. Phys. Chem.*, **68**, 2635 (1964); (b) part II, *ibid.*, **68**, 2992 (1964).

Table I: Product Yields from Cyclohexene-*d*₁₀ in the Presence and Absence of a Trace of Inhibitor^a

Product	(1)	(2)	(3)	(4)
	<i>G</i> ε _{1,3-D} = 0.0000	heavy yield/ light yield (uninhibited)	<i>G</i> ε _{1,3-D} = 0.0013	column 3/ column 1
Hydrogen	0.65 (1.28)	0.51	0.62 (1.23)	0.95 (0.96)
Cyclohexane	0.66 (0.95)	0.70	0.43 (0.88)	0.65 (0.93)
2,2'-Dicyclohexenyl	1.36 (1.90)	0.72	1.15 (1.64)	0.85 (0.86)
3-Cyclohexylcyclohexene	0.66 (0.58)	1.14	0.56 (0.49)	0.85 (0.85)
Dicyclohexyl	0.47 (0.21)	2.24	0.38 (0.18)	0.81 (0.86)
Dimer D-1	0.32 (0.22)	1.46	0.30 (0.18)	0.94 (0.82)
Dicyclohexadiene			1.5 (0.7)	
Total C ₁₂ hydrocarbon ^b	2.7 (3.2)	0.84	3.8 (3.7)	1.4 (1.2)
1,3-D			-4.3 (-1.6)	

^a Values in parentheses are those for the corresponding light cyclohexene system. Dose = 1×10^{20} e.v./g. Dose rate = 8×10^{18} e.v./g. hr. ε_{1,3-D} = electron fraction of 1,3-D in solution. ^b Average of two values obtained using different v.p.c. columns.

Table II: H₂, D₂, and HD Yields from Solutions of Cyclohexene, 1,3-D, 1,4-D, and Benzene in Cyclohexene-*d*₁₀^a

Electron fractions of components in solutions					<i>G</i> values				
<i>c</i> -C ₆ D ₁₀	<i>c</i> -C ₆ D ₉ H ^b	<i>c</i> -C ₆ H ₁₀	1,3- <i>c</i> -C ₆ H ₈	1,4- <i>c</i> -C ₆ H ₈	C ₆ H ₆	H ₂	HD	D ₂	Total
0.880	0.120					~0.008	0.039	0.604	0.65
0.813	0.086	0.003	0.098			0.030	0.092	0.238	0.36
0.359	0.038	0.018	0.585			0.142	0.073	0.025	0.24
0.790	0.108			0.102		0.087	0.229	0.374	0.69
0.347	0.047			0.606		0.690	0.242	0.039	0.97
0.789	0.108				0.103	~0.007	0.063	0.440	0.51
0.343	0.047				0.610	0.025	0.052	0.083	0.16
0.440	0.060	0.500				0.463	0.378	0.129	0.97
0.396	0.054	0.453	0.098			0.292	0.206	0.062	0.56
0.174	0.024	0.216	0.585			0.227	0.055	0.008	0.29

^a Dose rate = 7.65×10^{18} e.v./g. hr. Dose range = 1.02 - 1.54×10^{20} e.v./g. ^b Cyclohexene-*d*₁₀ contained 12.0% *c*-C₆D₉H (batch 1) and 9.6% *c*-C₆D₉H (batch 2).

but the increase in the yield of this product was much too small to explain the much greater rate of disappearance of 1,3-D. This probably means that the polymer yield was greater in the heavy than in the light solution under these conditions.

The hydrogen yields were measured for binary solutions of benzene, 1,4-D, and 1,3-D in cyclohexene-*d*₁₀. Also, a 50-50 solution of heavy and light cyclohexene was irradiated with and without added 1,3-D. The total hydrogen yields from these solutions are given in Fig. 1. The dash-dot lines represent the corresponding hydrogen yields for the light cyclohexene system. The H₂, HD, and D₂ contents of the hydrogen products are given in Table II.

Discussion

The over-all consumption of cyclohexene, based on the measured C₆ and C₁₂ hydrocarbon product yields, was reduced by only about 10% by deuteration. How-

ever, the distribution of the product yields was considerably altered, which indicates that moderately large kinetic isotope effects occur in this system.

It appears that the 2,2'-dicyclohexenyl, 3-cyclohexylcyclohexene, and dicyclohexyl are formed by the combination of free radicals in the cyclohexene radiolysis system.^{2a} It is possible to write several mechanisms for the formation of the free radicals and for the formation of hydrogen. Some of the possible mechanisms involve atoms and radicals, others involve ions, and others involve excited molecules. The present work shows that, whatever the mechanism is, it is subject to moderately large kinetic isotope effects. For the sake of simplicity, only an atom-radical mechanism will be used to illustrate the effects.

The hydrogen yield was reduced and the yields of dicyclohexyl and 3-cyclohexylcyclohexene were increased by deuteration of the cyclohexene. These

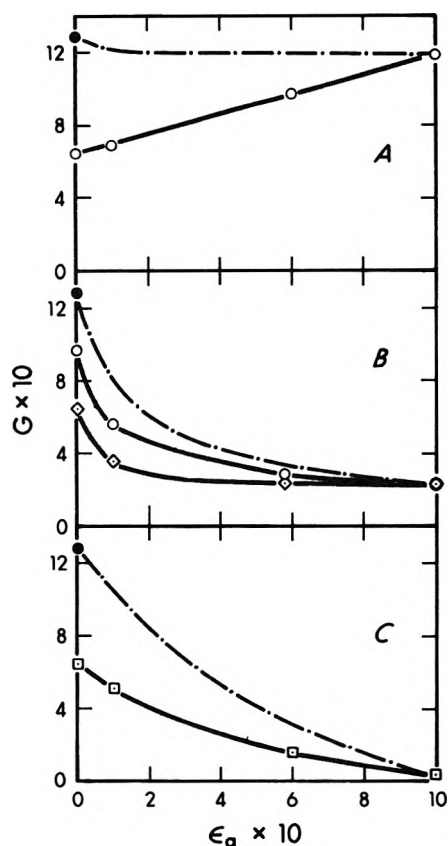
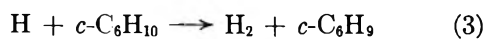
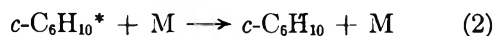
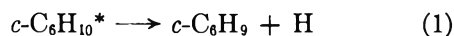


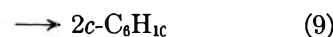
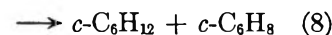
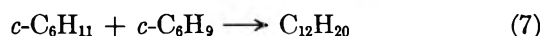
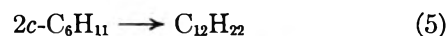
Figure 1. Hydrogen yields from liquid cyclohexene- d_{10} solutions; dose rate = 7.6×10^{18} e.v./g. hr.; dose = 1.0 – 1.5×10^{20} e.v./g.; ϵ_a = electron fraction of additive: ●, hydrogen yield from pure light cyclohexene; ----, yields from corresponding light cyclohexene solutions. A: 1,4-D solutions. B: ◇, 1,3-D solutions; O, 1,3-D added to a 50–50 solution of cyclohexene and cyclohexene- d_{10} . C: benzene solutions.

facts are consistent with the isotope effects that would be expected in the reactions



Substitution of D for H in cyclohexene would be expected to decrease the values of the ratios k_1/k_2 and k_3/k_4 . The results in Fig. 1 indicate that k_1/k_2 is reduced by about 14% when M in reaction 2 is 1,3-D and by about 4% when M is benzene. The initial slopes of the curves were calculated using the points at $\epsilon_a = 0.0$ and 0.1. These effects are relatively small (recall also that, based on the C_6 and C_{12} product yields in pure cyclohexene, the over-all consumption of cyclohexene was reduced by roughly 10% when D was sub-

stituted for H). However, based upon the yields of hydrogen, dicyclohexyl, and 3-cyclohexylcyclohexene, k_3/k_4 is reduced about 3.6-fold by substitution of $c\text{-C}_6\text{D}_{10}$ for $c\text{-C}_6\text{H}_{10}$. According to this mechanism, $k_3 \propto G(\text{H}_2)$ and $k_4 \propto G(c\text{-C}_6\text{H}_{11}) \propto G(\text{C}_{12}\text{H}_{22} + \text{C}_{12}\text{H}_{20})$ because the cyclohexyl radicals generated by reaction 4 react according to steps 5–9.



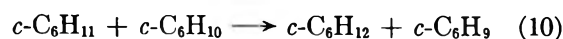
In liquid cyclohexane, $k_6/k_5 = 1.3^3$ and it will be assumed to have the same value in liquid cyclohexene. In liquid cyclohexene, $k_8/k_7 < 0.2^{2a}$ and, considering the relative exothermicities of reactions 8 and 9, it is probable that $k_9/k_7 < 0.2$. If it is assumed that $(k_8 + k_9)/k_7 = 0.2$, then $k_3/k_4 = G(\text{H}_2)/G(c\text{-C}_6\text{H}_{11}) = 1.28/1.67 = 0.77$. If it is assumed that $(k_8 + k_9)/k_7 = 0.0$, then $k_3/k_4 = 0.83$. Using the same assumptions for the cyclohexene- d_{10} system, $k_3/k_4 = 0.22$ and 0.23, respectively. The respective values of the isotope effect in k_3/k_4 are 3.5 and 3.6. This assumes that the disproportionation to combination ratios are the same for $c\text{-C}_6\text{H}_{11}$ and $c\text{-C}_6\text{D}_{11}$ radicals. Even if the disproportionation to combination ratio were zero for $c\text{-C}_6\text{D}_{11}$ radicals, the apparent reduction in k_3/k_4 would be 2.0-fold, so a moderately large isotope effect is evident.

The smaller yield of 2,2'-dicyclohexenyl in the deuterated system is consistent with the smaller expected yield of cyclohexenyl radicals (reactions 1 and 3).

Other isotope effects are evident from Table II. The cyclohexene- d_{10} contains 1.2 atomic % H, yet the product hydrogen contains 4.2 atomic % H. This constitutes an over-all isotope effect of 3.5.

More detailed isotope effects could be calculated from the hydrogen results, but the reaction mechanism is not sufficiently well known to make this worthwhile. The preceding discussion clearly illustrates that the reactants that produce cyclohexyl radicals and hydrogen are of sufficiently low energy that they suffer moderately large kinetic isotope effects.

It was concluded in part I,^{2a} that the reaction



does not occur to an appreciable extent under the present conditions of irradiation. This is consistent

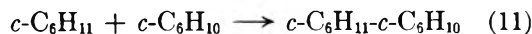
(3) C. E. Klots and R. H. Johnson, *Can. J. Chem.*, **41**, 2702 (1963).

Table III: Relative Abundances of Ions in Mass Spectra of $c\text{-C}_6\text{H}_{10}$ and $c\text{-C}_6\text{D}_{10}$ ^a

m	n	$C_mH_n^+$	$C_mD_n^{+b}$	$C_mH_n^+ / C_mD_n^+$
6	10	1.00	1.00	1.0
6	9	0.30	0.20	1.5
6	8	0.03	0.02	1.5
6	7	0.17	0.10	1.7
6	6	0.05	0.05	1.0
6	5	0.15	0.11	1.4
5	7	2.67	2.69	1.0
4	6	2.09	2.38	0.9
\sum_0^6	\sum_0^{10}	11.48	11.71	0.98

^a The height of a peak at a given mass to charge ratio is reported relative to that of the parent peak. The total sensitivity of each compound was obtained by summing the heights of all the peaks in its mass spectrum and dividing the sum by the pressure of the compound in the reservoir. The ratio of total sensitivities was $c\text{-C}_6\text{H}_{10}/c\text{-C}_6\text{D}_{10} = 1.06$. The ratio of the parent peak heights, per micron of pressure in the reservoir, was $C_6H_{10}^+/(C_6D_{10}^+ + C_6D_9H^+) = 1.08$. ^b Includes $C_mD_{n-1}H^+$ from $c\text{-C}_6\text{D}_9\text{H}$ impurity.

with the present results because, although the yield of cyclohexyl radicals increased, the yield of cyclohexane decreased when cyclohexene- d_{10} was substituted for cyclohexene. These facts are not explained by a competition between reactions 10 and 11 because a



self-consistent mechanism that included reaction 11 could not be devised which would explain the observed product distribution.

Cyclohexane is formed by the disproportionation of radicals and by some other mechanism.^{2a} When $c\text{-C}_6\text{D}_{10}$ was substituted for $c\text{-C}_6\text{H}_{10}$, the cyclohexane yield decreased while the dicyclohexyl yield increased. These changes cannot be due entirely to isotope effects in the disproportionation to combination ratios of the radicals because, in the cyclohexene- d_{10} system, cyclohexane formation is more readily inhibited than is the formation of dicyclohexyl (column 4, Table I). The increased facility of inhibition of cyclohexane formation is consistent with its lower yield in the deuterated system because both facts indicate that the cyclohexane formation reaction occurs with greater difficulty in the deuterated than in the nondeuterated system.

The present work points out a great need for information about isotope effects in disproportionation-combination reactions and in ion-molecule reactions.

Isotope effects are evident in mass spectra. Gordon and Burton⁴ compared the mass spectra of benzene and benzene- d_6 and found the ratio of the abundances of the ions, $C_6H_n^+/C_6D_n^+$ ($n = 3, 4, \text{ or } 5$), to be about

1.7. For the production of ions by C-C bond cleavage, the effect of substituting D for H was much smaller ($C_mH_n^+/C_mD_n^+ = 1.0\text{--}1.3$). Similar effects are observed in the mass spectra of cyclohexene and cyclohexene- d_{10} (see Table III).

All the mass spectra in the present work were obtained using 70-v. electrons. The total sensitivity of a compound was obtained by summing the heights of all the peaks in its mass spectrum and dividing the sum by the pressure of the compound in the reservoir. The total sensitivity of cyclohexene was 6% greater than that of cyclohexene- d_{10} . The difference was probably mostly due to a secondary type of mass discrimination in the mass spectrometer because the value of the ratio of the gas phase diffusion coefficients of the two compounds is 1.06. This conclusion was confirmed by showing that the values of the ratios of the total sensitivities of C_2H_4/C_2D_4 and C_2H_6/C_2D_6 were nearly the same as the ratios of their diffusion coefficients (Table IV). Jesse,⁵ using a simple ion chamber,

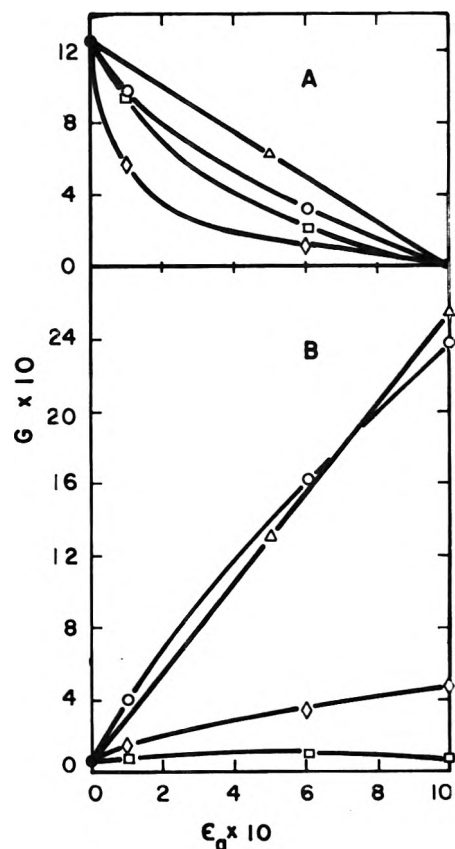


Figure 2. H and D content of the hydrogen from the $c\text{-C}_6\text{D}_{10}$ solutions; ϵ_a = electron fraction of additive: Δ , $c\text{-C}_6\text{H}_{11}$; \square , 1,4-D; \circ , benzene; \diamond , 1,3-D. A filled point is common to a set of curves. A: $2G(D_2) + G(HD)$. B: $2G(H_2) + G(HD)$.

(4) S. Gordon and M. Burton, *Discussions Faraday Soc.*, **12**, 88 (1952).

(5) W. P. Jesse, *J. Chem. Phys.*, **38**, 2774 (1963).

found that the total ionization produced by β -particles of several kev. energy in C_2H_4 or C_2H_6 was 1% less than that produced in C_2D_4 or C_2D_6 , respectively. The measurement of total ionization using a mass spectrometer gives a false picture because the instrument evidently discriminates against molecules (or perhaps their ions) according to their diffusion coefficients. It is not clear at what stage of the mass spectrometric process this discrimination occurs, but

measurements with our instrument indicate that it occurs before the ions reach the analyzing magnetic field.

The D and H content of the hydrogen from the cyclohexene- d_{10} solutions are shown in Fig. 2. The $c-C_6D_{10}$ - $c-C_6H_{10}$ plots are linear. Attempts to explain this behavior by a simple atomic hydrogen mechanism, using isotope effects of various assumed magnitudes, failed. If the end points of the H and D curves in Fig. 2 are fixed, the atomic hydrogen mechanism requires a value of the H:D ratio, in the hydrogen produced from the solutions, that is lower than is observed experimentally. The results indicate that, for the activated species that produce hydrogen, activation transfer occurs from the $c-C_6D_{10}$ species to $c-C_6H_{10}$. However, so little is known about the ion-molecule reactions of olefins that it would not be useful to speculate further about the mechanism of production of hydrogen at this time.

For reasons similar to those mentioned previously, the curves in Fig. 2 indicate that, for the activated species which produce hydrogen, activation transfer occurs from cyclohexene to 1,4-D, to benzene, and to 1,3-D in their respective solutions.

Table IV: Mass Spectrometric Total Sensitivities

	TS^a	$TS-h/TS-d^b$	$D-h/D-d^c$
$c-C_6H_{10}$	78.8	1.06	1.06
$c-C_6D_{10}$	74.5		
C_2H_4	37.3	1.05	1.07
C_2D_4	35.6		
C_2H_6	45.2	1.11	1.10
C_2D_6	40.9		

^a Total sensitivity, mm. peak height per micron pressure in the reservoir. ^b Ratio of the TS value of the light isomer to that of the heavy isomer. ^c Ratio of the gas phase diffusion coefficient of the light isomer to that of the heavy isomer.

A Surface Tension Study of the Interaction of Dimethyldodecylamine Oxide with Potassium Dodecanesulfonate in Dilute Aqueous Solution

by Milton J. Rosen, David Friedman, and Michael Gross

Department of Chemistry, Brooklyn College of the City University of New York, Brooklyn 10, New York (Received June 17, 1964)

A study has been made of the interaction of *N,N*-dimethyldodecylamine oxide (DMDAO) with potassium dodecanesulfonate (KDSO₃) in aqueous solution below the critical micelle concentration of either solute. It is shown that the protonated dimethyldodecylamine oxide cation, formed by the reaction of DMDAO with water, reacts with the dodecanesulfonate anion to form a salt, C₁₂H₂₅N(CH₃)₂O⁺H · -O₃SC₁₂H₂₅ (B). The infrared spectrum of this salt indicates that the cation and anion are strongly hydrogen bonded *via* the ionizable hydrogen. Equations are developed for calculating the activity of B in aqueous solutions containing B as the only solute and in aqueous mixtures of DMDAO and KSO₃. The coincidence of the γ -activity of B curve for solutions containing B as the only solute with that for aqueous KDSO₃-DMDAO mixtures indicates that the activity of B determines the γ of these mixtures. The slope of the γ -activity of B curve indicates a close-packed arrangement of the hydrocarbon chains of B at the air-solution interface.

Introduction

During the past few years, there has been a good deal of interest in the use of long-chain amine oxides as foam stabilizers in solutions of detergents and a number of papers have been published describing some of the properties of these amine oxides.¹⁻⁴ This paper presents the results of an investigation whose object was to determine the nature of the interaction between an amine oxide, dimethyldodecylamine oxide (DMDAO), and an anionic surfactant, potassium dodecanesulfonate (KDSO₃), in order to elucidate the mechanism of this foam stabilization.⁵

The nature of the interaction between two surface-active solutes in dilute (aqueous) solution may be determined from surface tension measurements. For a system containing two surface-active solutes, if the interface is located so that the surface excess of the solvent, $\Gamma_0 = 0$

$$-d\gamma = RT\Gamma_1 d \ln a_1 + RT\Gamma_2 d \ln a_2 \quad (1)$$

where Γ_1 and Γ_2 refer to the respective surface excess of the two solutes. Assuming that, in dilute solution below the critical micelle concentrations of the two solutes, concentrations can be substituted for activities

$$-d\gamma = RT\Gamma_1 d \ln c_1 + RT\Gamma_2 d \ln c_2 \quad (2)$$

Hutchinson⁶ has shown that the average area/molecule at the air-solution interface

$$\text{area/molecule} = \frac{1}{N(\Gamma_1 + \Gamma_2)} \quad (3)$$

where N = Avogadro's number, Γ_1 = surface excess of solute 1, and Γ_2 = surface excess of solute 2, can be calculated from the slopes of the surface tension-concentration curves obtained by holding the concentration of one solute constant and varying the concentration of the other, since

- (1) K. W. Hermann, *J. Phys. Chem.*, **66**, 295 (1962).
- (2) D. G. Kolp, R. G. Laughlin, F. R. Krause, and R. E. Zimmerer, *ibid.*, **67**, 51 (1963).
- (3) D. B. Lake and G. L. K. Hoh, *J. Am. Oil Chemists' Soc.*, **40**, 628 (1963).
- (4) T. P. Matson, *ibid.*, **40**, 640 (1963).
- (5) The work of Kolp and co-workers (ref. 2) on the interaction of dimethyldodecylamine oxide with sodium dodecylbenzenesulfonate came to the attention of the authors only after the work on this project had been completed.
- (6) E. Hutchinson, *J. Colloid Sci.*, **3**, 413 (1948).

$$\Gamma_1 = -\frac{1}{RT} \left(\frac{\partial \gamma}{\partial \ln c_1} \right)_{c_2, T} \quad (4)$$

and

$$\Gamma_2 = -\frac{1}{RT} \left(\frac{\partial \gamma}{\partial \ln c_2} \right)_{c_1, T} \quad (5)$$

A plot of the average area/molecule at the air-solution interface *vs.* the molar ratio of the two solutes, either in the bulk phase, $C_{\text{KDSO}_3}/C_{\text{DMDAO}}$, or at the interface, $\Gamma_{\text{KDSO}_3}/\Gamma_{\text{DMDAO}}$, can then be used to determine whether interaction between these two materials is a maximum at some particular molar ratio, as evidenced by a minimum (or maximum) in the curve. However, if interaction occurs to form a new component, B, which is much more strongly adsorbed at the air-solution interface than either of the reactants, then the lowering of the surface tension of the solvent may be due almost entirely to the adsorption of component B, and

$$-d\gamma \cong RT d \ln a_B \quad (6)$$

Results and Discussion

Surface Tension of DMDAO-KDSO₃ Mixtures.

Initial surface tension measurements on mixtures of DMDAO and KDSO₃ in dilute aqueous solution indicated that strong interaction was occurring between these two solutes. Mixtures of these two materials show marked lowering of the surface tension of water at solute concentrations at which these materials, individually, produce only insignificant decreases in the surface tension of water (Table I).

Table I: Surface Tensions of DMDAO and KDSO₃ Solutions and Their Mixtures

C_{DMDAO}^a	$C_{\text{KDSO}_3}^a$	γ_{25}° , dynes/cm.
...	5.05×10^{-4}	>69
6.7×10^{-5}	5.05×10^{-4}	24.1
6.7×10^{-5}	...	61.1
...	5.05×10^{-5}	>70
2.02×10^{-5}	5.05×10^{-5}	38.4
2.02×10^{-5}	...	66.7
...	3.03×10^{-4}	>70
2.02×10^{-5}	3.03×10^{-4}	48.0
2.02×10^{-5}	...	>70.6

^a These refer to initial concentrations.

valid for this system. The average area/molecule at the interface, as calculated from eq. 3, 4, and 5, at constant surface pressure is independent of changes in the molar ratio of the two reactants either in the bulk phase, $C_{\text{KDSO}_3}/C_{\text{DMDAO}}$, or at the interface, $\Gamma_{\text{KDSO}_3}/\Gamma_{\text{DMDAO}}$.

Instead, the data showed that the surface tension of these dilute aqueous mixtures of DMDAO and KDSO₃ was related to the product of the initial concentrations of DMDAO and KDSO₃ and decreased with increasing H⁺ content of the mixture (Tables II and III). These observations indicated that a third component, B, was being formed by a 1:1 reaction of the protonated dimethyldodecylamine oxide cation (DMDAOH⁺) with the dodecanesulfonate anion (DSO₃⁻).

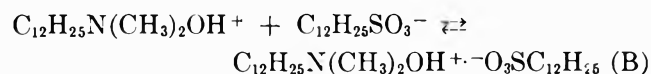


Table II: Relationship between Surface Tension and Product of Initial Concentrations of DMDAO and KDSO₃ in Dilute Aqueous Solution

γ_{25}° , dynes/ cm.	C_{DMDAO}^a	$C_{\text{KDSO}_3}^a$	$C_{\text{DMDAO}} \times C_{\text{KDSO}_3}^a$
38	2.02×10^{-5}	5.25×10^{-5}	1.06×10^{-9}
38	1.01×10^{-5}	1.01×10^{-4}	1.02×10^{-9}
38	0.670×10^{-5}	1.47×10^{-4}	1.17×10^{-9}
38	0.596×10^{-5}	2.02×10^{-4}	1.20×10^{-9}
38	0.457×10^{-5}	3.03×10^{-4}	1.39×10^{-9}
49	2.28×10^{-5}	2.02×10^{-4}	4.60×10^{-10}
49	3.57×10^{-5}	1.01×10^{-4}	3.60×10^{-10}
49	5.70×10^{-5}	0.505×10^{-4}	2.88×10^{-10}

^a These refer to initial concentrations.

Table III: pH Dependence of the Surface Tension of Dilute Aqueous Mixtures of KDSO₃ and DMDAO

C_{DMDAO}^a	$C_{\text{KDSO}_3}^a$	pH	γ_{25}° , dynes/ cm.
4.19×10^{-5}	1.47×10^{-5}	6.24 ₀	63.8
4.19×10^{-5}	1.47×10^{-5}	6.22 ₃	62.8
4.19×10^{-5}	1.47×10^{-5}	5.81 ₀	56.4
4.19×10^{-5}	1.47×10^{-5}	4.62 ₀	47.7
8.22×10^{-6}	2.88×10^{-5}	6.23 ₈	55.9
8.22×10^{-6}	2.88×10^{-5}	5.43 ₅	45.5
8.22×10^{-6}	2.88×10^{-5}	4.30 ₈	38.4
8.22×10^{-6}	2.88×10^{-5}	4.27 ₅	37.2

^a These refer to initial concentrations.

Treatment of the surface tension data by the method of Hutchinson⁶ indicated that this approach is not

This confirms the work of Kolp and co-workers,² who have shown that the analogous compound is formed by

the interaction of DMDAOH⁺ and sodium dodecylbenzenesulfonate. Subsequent investigation indicates that B is the sole component determining the surface tension of dilute aqueous mixtures of DMDAO and KDSO₃; the unreacted KDSO₃ and DMDAO or DMDAOH⁺ have no significant effect on this property.

Nature of C₁₂H₂₅N(CH₃)₂OH⁺-O₃SC₁₂H₂₅. This compound is formed in quantitative yield when a solution of DMDAO in dilute sulfuric acid is treated with the stoichiometric amount of potassium dodecanesulfonate in aqueous solution. Analyses for N and S confirm the empirical formula. Its infrared spectrum indicates that this compound is rather unusual in that the two ions are tightly hydrogen bonded *via* the ionizable hydrogen. Two bands in the infrared spectrum are assignable, *via* deuteration, to the O-H group: a broad band of strong intensity in the vicinity of 3.82 μ (2610 cm.⁻¹) due to O-H stretching and a band of medium intensity at 6.43 μ (1555 cm.⁻¹) due to O-H in-plane bending. Both of these bands are missing in the deuterated compound, formed by equilibrating B with D₂O. They are also missing from the infrared spectra of the free amine oxide and the sulfate salt of the amine oxide, (C₁₂H₂₅N(CH₃)₂OH⁺)₂SO₄⁻². The decrease in the frequency of the O-H stretching absorption from the usual position above 3000 cm.⁻¹ to the 2500-2700-cm.⁻¹ region is indicative of a strongly hydrogen-bonded OH group.⁷ This is confirmed by the higher-than-usual frequency of the O-H in-plane bending frequency. That this is *not* due to hydrogen bonding between the protonated amine oxide cations themselves, but due to hydrogen bonding between the protonated amine oxide cation and the dodecanesulfonate anion is indicated by the absence of these bands from the spectrum of the sulfate salt of the amine oxide, (C₁₂H₂₅N(CH₃)₂OH⁺)₂SO₄⁻².

Surface Tension-Activity Relationship of B. The activity of B, [B], in a dilute aqueous solution in which it is the only solute, can be calculated as follows: The equilibria involved in the formation of B are



The respective equilibrium constants for (7) and (8) are

$$K_b = \frac{[\text{DMDAOH}^+][\text{OH}^-]}{[\text{DMDAO}]} \quad (9)$$

and

$$K_{\text{assoc}} = \frac{[\text{B}]}{[\text{DMDAOH}^+][\text{DSO}_3^-]} \quad (10)$$

where the quantities in brackets are the equilibrium activities relative to a standard state in which, at infinite dilution, the activity equals the concentration in moles/l.

From (9) and (10)

$$K_b K_{\text{assoc}} = \frac{[\text{B}][\text{OH}^-]}{[\text{DMDAO}][\text{DSO}_3^-]} \quad (11)$$

and

$$[\text{B}] = K_b K_{\text{assoc}} \frac{[\text{DMDAO}][\text{DSO}_3^-]}{[\text{OH}^-]} \quad (12)$$

For dilute aqueous solutions containing B as the only solute, since $\text{B} \rightleftharpoons \text{DMDAOH}^+ + \text{DSO}_3^-$

$$[\text{B}] = B - x$$

$$[\text{DSO}_3^-] = x$$

$$[\text{DMDAO}] = x - [\text{DMDAOH}^+]$$

$$= x - \frac{K_b [\text{DMDAO}]}{[\text{OH}^-]}$$

where B = initial molar concentration of B and x = equilibrium molar concentration of B decomposed to DMDAOH⁺ and DSO₃⁻, whence

$$[\text{DMDAO}] = \frac{x}{1 + \frac{K_b}{[\text{OH}^-]}}$$

From (12)

$$[\text{B}] = \frac{K_b K_{\text{assoc}}}{[\text{OH}^-]} \frac{x^2}{\left(1 + \frac{K_b}{[\text{OH}^-]}\right)} = B - x$$

or

$$x^2 + \left(\frac{[\text{OH}^-] \left\{ 1 + \frac{K_b}{[\text{OH}^-]} \right\}}{K_b K_{\text{assoc}}} \right) x - \frac{B[\text{OH}^-] \left(1 + \frac{K_b}{[\text{OH}^-]} \right)}{K_b K_{\text{assoc}}} = 0$$

whence

(7) L. J. Bellamy, "The Infrared Spectra of Complex Molecules," Methuen, London, 1962, p. 164.

$$x = \frac{-\left(\frac{[\text{OH}^-] \left\{1 + \frac{K_b}{[\text{OH}^-]}\right\}}{K_b K_{\text{assoc}}}\right) + \sqrt{\left(\frac{[\text{OH}^-] \left\{1 + \frac{K_b}{[\text{OH}^-]}\right\}}{K_b K_{\text{assoc}}}\right)^2 + \frac{4B[\text{OH}^-] \left(1 + \frac{K_b}{[\text{OH}^-]}\right)}{K_b K_{\text{assoc}}}}}{2} \quad (13)$$

and

$$[\text{B}] = B + \frac{[\text{OH}^-] \left(1 + \frac{K_b}{[\text{OH}^-]}\right)}{K_b K_{\text{assoc}}} - \sqrt{\left(\frac{[\text{OH}^-] \left\{1 + \frac{K_b}{[\text{OH}^-]}\right\}}{K_b K_{\text{assoc}}}\right)^2 + \frac{4B[\text{OH}^-] \left(1 + \frac{K_b}{[\text{OH}^-]}\right)}{K_b K_{\text{assoc}}}} \quad (14)$$

The activity of B in these solutions, [B], can therefore be calculated from the initial concentration of B, the pH of the solution, and two constants, K_b and K_{assoc} . The value of the $K_b K_{\text{assoc}}$ product is obtained by neutralizing approximately half of a solution of B with a known amount of strong base (NaOH) and determining the pH of the resulting mixture: $\text{C}_{12}\text{H}_{25}\text{N}(\text{CH}_3)_2\text{OH}^+ \cdot \text{O}_3\text{SC}_{12}\text{H}_{25} + \text{OH}^- \rightleftharpoons \text{C}_{12}\text{H}_{25}\text{N}(\text{CH}_3)_2\text{O} + \text{O}_3\text{SC}_{12}\text{H}_{25} + \text{H}_2\text{O}$. From (11)

$$K_b K_{\text{assoc}} = \frac{(B - x)(\text{OH}^-) \left(1 + \frac{K_b}{[\text{OH}^-]}\right)}{x^2} \quad (15)$$

Using a value of $K_b = 7.94 \times 10^{-10}$, calculated from the acidity constant, $K_A = 10^{-4.90}$, of Kolp and co-workers,² a value of $K_b K_{\text{assoc}} = 1.14 \pm 0.02 \times 10^{-4}$ was obtained and is used in all subsequent calculations.

Table IV lists the surface tension and the activity of B, as calculated by this method, for solutions containing various initial concentrations of B. Figure 1 shows the relationships between the surface tension and the activity of B in dilute aqueous solutions. The straight-line portion of the curve ($\gamma < 55$ dynes/cm.) was fitted to the data by the method of least squares, following Acton.⁸

Surface Tension-Activity Relationship of B in Mixtures of DMDAO and KDSO₃. The activity of B in dilute aqueous mixtures of DMDAO and KDSO₃ may be calculated in analogous fashion, again assuming that concentrations may be substituted for activities. Since $\text{DMDAOH}^+ + \text{DSO}_3^- \rightleftharpoons \text{B}$

$$[\text{DSO}_3^-] = S - [\text{B}]$$

where S = initial molar concentration of KDSO₃ and

$$\begin{aligned} [\text{DMDAO}] &= A - [\text{B}] = [\text{DMDAOH}^+] \\ &= A - [\text{B}] - \frac{K_b [\text{DMDAO}]}{[\text{OH}^-]} \end{aligned}$$

where A = initial molar concentration of DMDAO, whence

Table IV: Surface Tension and Calculated Activity of B for Dilute Aqueous Solutions of B

Initial concn. of B, M	pH	[B], calcd. from eq. 14	γ_{25}° , dynes/cm.
3.134×10^{-5}	4.86	1.651×10^{-5}	29.2
2.495×10^{-5}	5.07	1.110×10^{-5}	32.8
1.663×10^{-5}	5.15	5.92×10^{-6}	40.1
1.663×10^{-5}	5.20	5.71×10^{-6}	40.6
1.423×10^{-5}	5.18	4.59×10^{-6}	44.2
1.109×10^{-5}	5.39	2.57×10^{-6}	48.8
1.109×10^{-5}	5.38	2.58×10^{-6}	49.0
8.317×10^{-6}	5.21	1.927×10^{-6}	53.1
7.129×10^{-6}	5.49	1.074×10^{-6}	57.0
4.990×10^{-6}	5.32	7.21×10^{-7}	59.7
3.564×10^{-6}	5.47	3.20×10^{-7}	65.0
3.557×10^{-6}	5.42	3.44×10^{-7}	65.9
2.668×10^{-6}	5.61	1.486×10^{-7}	66.3
3.064×10^{-6}	5.69	1.668×10^{-7}	67.9
1.188×10^{-6}	5.70	2.65×10^{-8}	71.5

$$[\text{DMDAO}] = \frac{A - [\text{B}]}{1 + \frac{K_b}{[\text{OH}^-]}}$$

Thus, from (12)

$$[\text{B}] = \frac{K_b K_{\text{assoc}}}{[\text{OH}^-]} \left(\frac{A - [\text{B}]}{1 + \frac{K_b}{[\text{OH}^-]}} \right) (S - [\text{B}])$$

or

$$[\text{B}]^2 - \left(S + A + \frac{\left\{1 + \frac{K_b}{[\text{OH}^-]}\right\} [\text{OH}^-]}{K_b K_{\text{assoc}}} \right) [\text{B}] + (A)(S) = 0$$

whence

(8) F. S. Acton, "Analysis of Straight-Line Data," John Wiley and Sons, Inc., New York, N. Y., 1959, pp. 9-14.

$$[B] = \frac{\left(S + A + \frac{\left\{ 1 + \frac{K_b}{[\text{OH}^-]} \right\} [\text{OH}^-]}{K_b K_{\text{assoc}}} \right) - \sqrt{\left(S + A + \frac{\left\{ 1 + \frac{K_b}{[\text{OH}^-]} \right\} [\text{OH}^-]}{K_b K_{\text{assoc}}} \right)^2 - 4AS}}{2} \quad (16)$$

Table V lists the surface tension and the activity of B, as calculated by this method, for dilute aqueous mixtures of DMDAO and KDSO₃, at various initial concentrations of DMDAO and KDSO₃, and at various pH values.

Table V: Surface Tension and Calculated Activity of B for Dilute Aqueous Mixtures of DMDAO and KDSO₃ at Various pH Values

Initial concn. of DMDAO, M	Initial concn. of KDSO ₃ , M	pH of mixture	[B] calcd. from eq. 16	γ ₂₀ ^o , dynes/cm.
1.069 × 10 ⁻⁴	1.125 × 10 ⁻³	6.859	6.65 × 10 ⁻⁶	23.1
6.106 × 10 ⁻⁴	2.143 × 10 ⁻⁴	7.265	5.47 × 10 ⁻⁶	23.5
3.562 × 10 ⁻⁴	1.250 × 10 ⁻⁴	6.730	4.89 × 10 ⁻⁶	23.4
8.549 × 10 ⁻⁵	1.5001 × 10 ⁻⁴	6.407	2.93 × 10 ⁻⁵	24.7
8.549 × 10 ⁻⁵	1.5001 × 10 ⁻⁴	6.431	2.84 × 10 ⁻⁵	26.6
6.106 × 10 ⁻⁵	2.143 × 10 ⁻⁴	6.429	2.66 × 10 ⁻⁵	27.3
8.549 × 10 ⁻⁶	1.5001 × 10 ⁻⁴	6.590	2.29 × 10 ⁻⁵	25.8
3.813 × 10 ⁻⁵	2.676 × 10 ⁻⁵	4.295	1.85 × 10 ⁻⁵	27.5
3.810 × 10 ⁻⁵	2.674 × 10 ⁻⁵	4.612	1.77 × 10 ⁻⁶	30.6
3.810 × 10 ⁻⁵	2.674 × 10 ⁻⁶	5.512	1.15 × 10 ⁻⁶	32.7
3.685 × 10 ⁻⁵	7.759 × 10 ⁻⁶	6.400	8.58 × 10 ⁻⁶	36.8
8.220 × 10 ⁻⁶	2.885 × 10 ⁻⁶	4.308	5.95 × 10 ⁻⁶	38.4
3.816 × 10 ⁻⁵	2.679 × 10 ⁻⁵	6.20	4.95 × 10 ⁻⁶	42.2
4.191 × 10 ⁻⁶	1.471 × 10 ⁻⁵	4.620	3.90 × 10 ⁻⁶	47.7
8.211 × 10 ⁻⁶	2.881 × 10 ⁻⁵	5.435	3.69 × 10 ⁻⁶	45.5
3.816 × 10 ⁻⁶	2.679 × 10 ⁻⁶	6.412	3.47 × 10 ⁻⁶	45.6
8.220 × 10 ⁻⁶	2.885 × 10 ⁻⁵	6.238	1.22 × 10 ⁻⁶	55.9
4.186 × 10 ⁻⁶	1.469 × 10 ⁻⁵	5.810	7.52 × 10 ⁻⁷	56.4
4.191 × 10 ⁻⁶	1.471 × 10 ⁻⁶	6.223	3.58 × 10 ⁻⁷	62.8
4.191 × 10 ⁻⁶	1.471 × 10 ⁻⁶	6.240	3.46 × 10 ⁻⁷	63.8

Figure 2 shows the relationship between the surface tension of dilute aqueous mixtures of DMDAO and KDSO₃ and the activity of B, as calculated by this method. The points from Fig. 1, showing the relationship between surface tension and activity of B in dilute aqueous solutions containing B as the only solute, are also included in this same figure. The straight-line portion of the curve (24–55 dynes/cm.) was fitted to the combined data for solutions containing only B as the

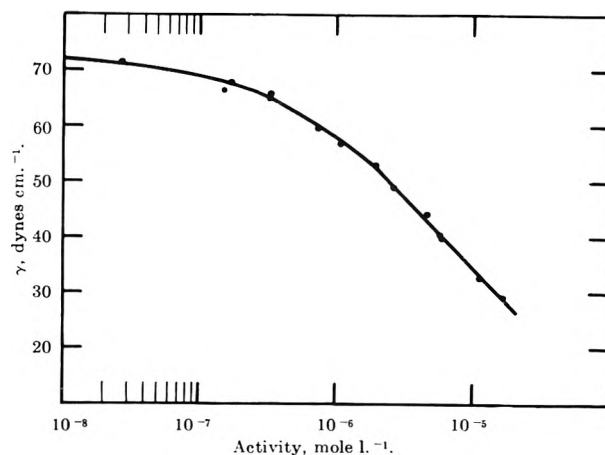


Figure 1. Relationship between surface tension and activity of B in dilute aqueous solutions of B.

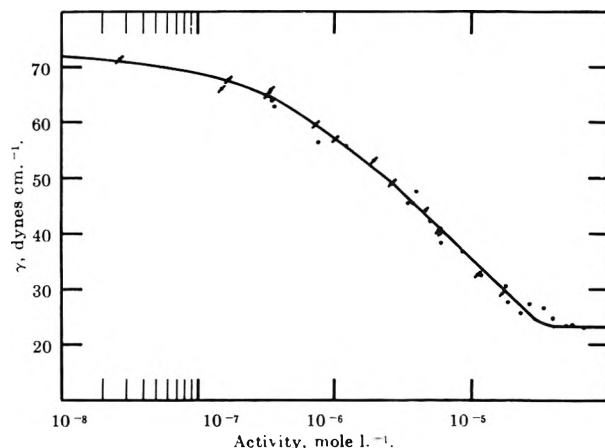


Figure 2. Relationship between surface tension and activity of B in dilute aqueous solutions of B and in dilute aqueous mixtures of DMDAO and KDSO₃: ●, aqueous solutions of B; ■, aqueous mixtures of DMDAO and KDSO₃.

solute and for mixtures containing both DMDAO and KDSO₃ as solutes (Tables IV and V, respectively) by the least-squares method, following Acton.⁸ Statistical analysis of the data⁹ indicates that fitting two lines to the data rather than one results in no significant reduction in variance ($F < 1$). This portion of the curve follows the equation $\gamma = 23.4 \log [B] - 81.9$. It is apparent, therefore, that the surface tension of dilute aqueous mixtures of DMDAO and KDSO₃ is for all practical purposes dependent solely upon the activity of their interaction product, B, and that the unreacted DMDAO and KDSO₃ and DMDAOH⁺ present have no significant effect upon it.

The area per molecule of B at the air-solution inter-

(9) F. S. Acton, ref. 8, pp. 80–83.

face at 25°, as calculated from the slope of the straight-line portion of the curve in Fig. 2

$$\text{area/molecule} = \frac{1}{N\Gamma_B} = \frac{-2.303RT}{N \left(\frac{\partial \gamma}{\partial \log [B]} \right)_T} = \frac{947.4}{23.4}$$

is 40.5 Å.² or 20.3 Å.²/hydrocarbon chain, indicating a close-packed arrangement of the molecules at the interface. This close-packed arrangement may account for the foam stabilization produced upon the addition of this amine oxide to solutions of anionic surfactants. This aspect is currently being investigated.

Experimental

N,N-Dimethyldodecylamine Oxide (DMDAO). The dimethyldodecylamine oxide used was a research sample obtained as a solution in aqueous isopropyl alcohol from Armour Industrial Chemical Co. through the courtesy of Dr. S. H. Shapiro. After removal of the solvent at <55° under reduced pressure, the residue was recrystallized several times from benzene-hexane mixture at temperatures below 65° until further recrystallization produced no change in the γ -concentration curve in the vicinity of the critical micelle concentration. The m.p. of the hygroscopic final product was 135.8–137.5° after drying *in vacuo* for 3 days over P₂O₅. *Anal.* Calcd. for C₁₄H₃₁NO: C, 73.30; H, 13.71. Found: C, 73.87; H, 13.88. The critical micelle concentration of the product was 1.6 × 10⁻³ at 25 ± 0.05°.

Potassium Dodecanesulfonate (KDSO₃). Potassium dodecanesulfonate was synthesized from *n*-dodecyl bromide and potassium sulfite, using aqueous dimethyl sulfoxide as the reaction medium, as described below. The *n*-dodecyl bromide, b.p. 155.5° at 21 mm., *n*_D²⁵ 1.4561, was prepared from *n*-dodecyl alcohol, *n*_D³⁰ 1.4387, b.p. 157.5° at 26 mm., obtained by fractionation of commercial dodecyl alcohol of 98% minimum purity through a 42-plate Todd column at 50:1 reflux ratio. Then 24.9 g. (0.1 mole) of *n*-dodecyl bromide, 79.1 g. (0.5 mole) of potassium sulfite dissolved in 80 g. of water, and 20 g. of dimethyl sulfoxide were heated and stirred under reflux on a steam bath for 60 hr. The reaction mixture was cooled and filtered. The insoluble material was washed several times on the filter with petroleum ether, then extracted a few times with 400-ml. portions of boiling 95% ethyl alcohol. The combined alcoholic extracts were filtered to remove inorganic salts; the volume was reduced to about 300 ml. and filtered again. Then the mixture was cooled to precipitate the potassium dodecanesulfonate. The sulfonate was recrystallized from ethyl

alcohol two additional times, then recrystallized twice from 60–70 ml. of water. The yield of product was 19.2 g. (66.6% of theory).

This partially purified product showed a small minimum in its γ -concentration curve near the critical micelle concentration. It was extracted several times by grinding with ethyl ether in a mortar, yielding 0.2 g. of extract. It was then extracted with hexane for several days in a Soxhlet apparatus.

The resulting product showed no minimum in its γ -concentration curve in the vicinity of its critical micelle concentration. The critical micelle concentration was 8.6 × 10⁻³ M at 25.00 ± 0.05°. Lin¹⁰ has reported a value of 9.0 × 10⁻³; Williams, *et al.*,¹¹ have reported a value of 8.1 × 10⁻³ for the sodium salt.

Surface Tension Measurements. All surface tension measurements were made by the Wilhelmy vertical plate technique, using a sand-blasted platinum plate of approximately 5-cm. perimeter, which was calibrated against quartz-distilled water (conductivity, 2.0 × 10⁻⁶ ohm⁻¹ cm.⁻¹) each day measurements were made. The plate was suspended from a dial-type torsion balance capable of being read to 0.2 mg. All solutions to be tested were immersed in a constant temperature bath at 25.00 ± 0.05° and aged for at least 0.5 hr. before measurements were made. Measurements were repeated at 20-min. intervals until no significant change occurred. To minimize changes in pH during the measurements, KDSO₃-DMDAO mixtures were buffered at various pH values by use of 0.001 M ammonium acetate or 0.001 M ammonium acetate-acetic acid mixtures as solvent.

pH Measurements. All pH measurements were made with a DELTA-matic Model 135A pH-mv. electrometer (Instrumentation Laboratory, Inc., Boston, Mass.) with a rated accuracy and repeatability of better than 0.003 pH.

C₁₂H₂₅N(CH₃)₂OH⁺·⁻O₃SC₁₂H₂₅ (B). Exactly 1.1470 g. (5 mmoles) of dimethyldodecylamine oxide (DMDAO) was dissolved in 100 ml. of 0.1 N H₂SO₄ and the clear solution treated with a solution of 1.4425 g. (5 mmoles) of potassium dodecanesulfonate (KDSO₃) in 50 ml. of H₂O. The white, crystalline precipitate which formed upon cooling the mixture was removed by filtration, washed twice on the filter with cold water, and dried *in vacuo* over P₂O₅. The m.p. of the product was 113.8–114.8°. One additional recrystallization from water yielded a product melting at 113.4–114.5°. A subsequent recrystallization from hexane yielded

(10) W.-C. Lin, *J. Chinese Chem. Soc.*, **4**, 28 (1957).

(11) R. J. Williams, J. N. Phillips, and K. J. Mysels, *Trans. Faraday Soc.*, **51**, 728 (1955).

2.162 g. (90%) of product melting at 113.7–114.7°. *Anal.* Calcd. for $C_{28}H_{57}O_4NS$: N, 2.92; S, 6.68. Found: N, 2.92; S, 6.74.

Calculation of Activity of B. Activity of B was calculated from eq. 14 and 16 by use of an IBM 1620 computer.

Acknowledgment. This investigation was supported in part by Undergraduate Science Education Program Grants GE-141 and GE-2920, National Science Foundation. The authors gratefully acknowledge the assistance of Messrs. Joel Blatt and David Solan in the preliminary stages of this investigation.

Hydrogen Bonding in Nitro Compounds¹

by H. E. Ungnade, E. M. Roberts, and L. W. Kissinger

*University of California, Los Alamos Scientific Laboratory,
Los Alamos, New Mexico (Received June 18, 1964)*

Experimental evidence from infrared and n.m.r. spectra indicates the existence of a weak hydrogen bond between nitro groups and alcoholic hydroxyl groups. Other findings from ultraviolet absorption spectra can be accounted for by an interaction between hydroxyl oxygens and nitro groups.

An investigation of the absorption spectra of β -nitro alcohols has shown that the absorption bands due to the nitro group can be explained without assuming an internal hydrogen bond in these compounds,² and preliminary examinations of the infrared spectra of nitromethane solutions of alcohols have given evidence for an interaction but no satisfactory explanation of the type of bond.² The small shift of the alcohol hydroxyl band from carbon tetrachloride to nitromethane solution has been regarded as doubtful evidence for a hydrogen bond in the past.³ More recent investigators disagree on its significance. Thus, the hydroxyl band of water in nitromethane is said to fall on the Kirkwood–Bauer–Magat plot⁴ and to deviate from such a plot.⁵ Careful studies of frequency shifts and band widths for several A–H stretching modes in a number of solvents have established, however, that there is a smooth progression of these parameters between polar and nonpolar solvents and, therefore, an interaction which differs from one solvent to another in degree rather than kind.⁶

The problem has been reinvestigated by different methods. Since absorption intensities and band widths

are generally more sensitive to hydrogen-bonding effects than frequency shifts, these have been determined for the hydroxyl bands of four alcohols in several solvents under comparable conditions. The results (Table I) show that, while the shift of the methanol hydroxyl band from carbon tetrachloride to nitromethane is small, the apparent molar absorptivity and half-band width are increased. Similar increases are observed with nitrobutane and nitrobenzene and a much larger one with triethylamine. Better proton donors such as heptafluorobutanol give more intense absorption ($\epsilon \times \Delta\nu^{1/2}$) while poorer proton donors like *t*-butyl alcohol have weaker hydroxyl bands in

(1) This work was performed under the auspices of the U. S. Atomic Energy Commission.

(2) H. E. Ungnade and L. W. Kissinger, *Tetrahedron, Suppl.* 1, 19, 121 (1963).

(3) W. Gordy, *J. Chem. Phys.*, 7, 93 (1939).

(4) E. Greinacher, W. Luttke, and R. Mecke, *Z. Elektrochem.*, 59, 23 (1955).

(5) P. Saumagne and M. L. Josien, *Bull. soc. chim. France*, 813 (1958).

(6) L. J. Bellamy, H. E. Hallam, and R. L. Williams, *Trans. Faraday Soc.*, 54, 112 (1958).

nitromethane. A plot of band shifts of the methanol hydroxyl bands against half-band widths for nitro compounds and other solvents (including established proton acceptors) is a straight line. The combined evidence indicates that nitro compounds form weak hydrogen bonds with alcohols.

Table I: Hydroxyl Bands of Alcohols

Alcohol	Solvent	Mole/l.	Thick-ness, cm.	ν , cm.^{-1}	ϵ	$\Delta\nu^{1/2}$, cm.^{-1}	$\Delta\nu^a$, cm.^{-1}
MeOH	CCl_4	0.005	1.00	3640	66	25	0
MeOH	MeNO_2	0.1	0.05	3600	110	60	40
MeOH	BuNO_2	0.1	0.05	3600	100	60	40
MeOH	PhNO_2	0.1	0.05	3600	106	60	40
MeOH	Et_3N	0.1	0.05	3240	120	170	400
<i>n</i> -BuOH	CCl_4	0.005	1.00	3636	68	26	0
<i>n</i> -BuOH	MeNO_2	0.1	0.05	3595	100	60	41
<i>t</i> -BuOH	CCl_4	0.005	1.00	3616	72	19	0
<i>t</i> -BuOH	MeNO_2	0.1	0.05	3578	80	52	38
<i>n</i> - $\text{C}_3\text{F}_7\text{CH}_2\text{OH}$	CCl_4	0.005	1.00	3616	130	25	0
<i>n</i> - $\text{C}_3\text{F}_7\text{CH}_2\text{OH}$	MeNO_2	0.1	0.05	3544	104	116	72

^a Band shift.

A study of the methanol hydroxyl band in carbon tetrachloride with varying amounts of nitromethane with a high-resolution infrared spectrophotometer has established that the shift of the hydroxyl band from carbon tetrachloride to nitromethane is actually due to the formation of a new band (Fig. 1).⁷ The infrared absorption bands in 0.1 *M* methanol solutions can be assigned to monomer, tetramer, and polymer, and it is observed (Fig. 1) that the addition of nitromethane causes the polymer band to be decreased in intensity while the tetramer band remains largely unchanged. In more concentrated solutions (0.5 *M*) so much polymer is present that the small tetramer band can no longer be observed. N.m.r. studies of these same solutions show that the nitromethane peak remains unchanged relative to the methyl peak of the methanol and that, therefore, in neither molecule are the methyl protons involved in any interaction. In 0.5 *M* methanol solutions, the hydroxyl proton is shifted upfield by about 50 cycles as the concentration of nitromethane is increased from 0 to 3 *M*. In 0.1 *M* methanol, the hydroxyl proton is shifted slightly upfield upon the first addition of nitromethane. For concentrations greater than 0.1 *M* the shift is downfield (Fig. 2). The upfield shifts of the hydroxyl protons are in agreement with the assumption that hydrogen-bonded methanol polymer is depolymerized to form the complex between methanol and nitromethane. There is

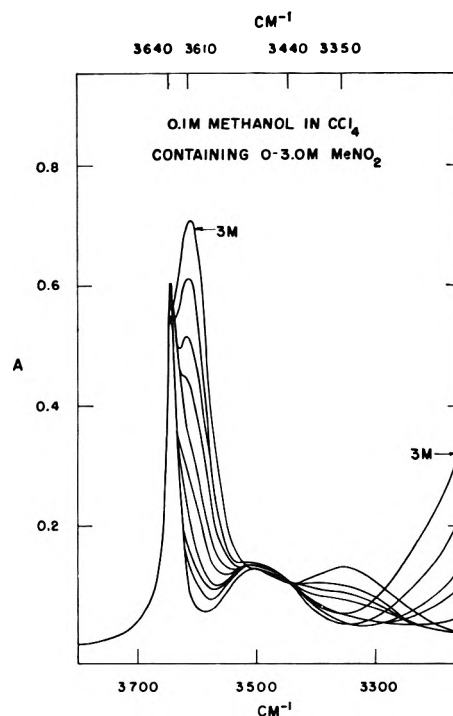


Figure 1. Hydroxyl stretching bands in methanol solutions.

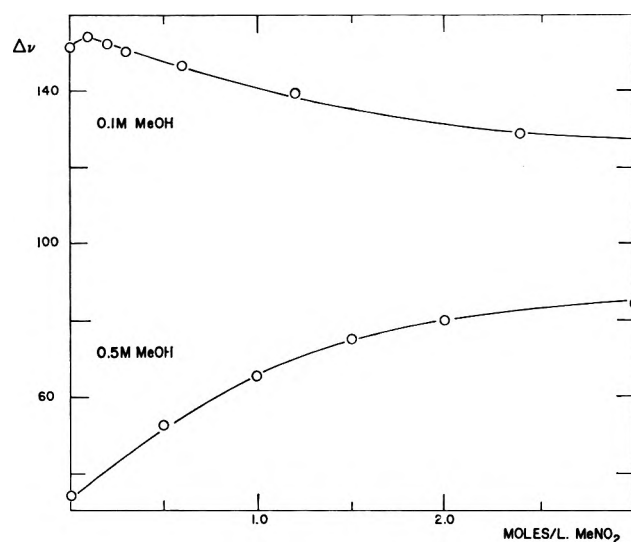


Figure 2. Chemical shifts of the hydroxyl proton in methanol solutions with reference to the methyl peak of methanol.

such an excess of polymer in the 0.5 *M* solution that this trend is not reversed. In the 0.1 *M* solutions, the downfield shift is due to the removal of monomer

(7) Since the completion of these investigations, high-resolution spectra have been determined also by P. J. Krueger and H. D. Mettee [*Can. J. Chem.*, 42, 288 (1964)] and by W. F. Baitinger, P. von R. Schleyer, T. S. S. R. Murty, and L. Robinson (the authors are indebted to Dr. P. von R. Schleyer for a preprint of their manuscript).

(for complexing with the nitromethane) while the concentration of the tetramer remains approximately constant. The addition of nitromethane to methanol solutions has the additional effect of considerably narrowing the initially broad methyl and hydroxyl resonance peaks. This line-narrowing is regarded as evidence that the nitromethane-methanol complex is favored over the methanol polymer. The infrared data further indicate that the complex is intermediate in strength between methanol tetramer and polymer.

Other experimental findings confirm that the interaction is weak. The frequency of the *as*-nitro band in nitromethane is virtually identical in methanol and carbon tetrachloride (Table II). The apparent molar absorptivities are affected by solvents but the change is in the same direction for a tertiary amine which cannot form a hydrogen bond with the nitro group and an alcohol which can. It is, therefore, unlikely that studies of the nitro stretching frequencies will give information about hydrogen bonding in nitro compounds.

Table II: Nitro Bands of Nitromethane

Solvent	ν		ν	
	<i>as</i> -NO ₂	ϵ	<i>sym</i> -NO ₂	ϵ
CCl ₄	1563	550	1373	110
CHCl ₃	1563	600	1374	140
CH ₂ Cl ₂	1563	610	1374	140
Et ₃ N	1563	412
MeOH	1562	425 ^a

^a This value may be somewhat low because of solvent absorption near the maximum. It was determined in 0.002-cm. cells.

Further information about the interaction between hydroxyl and nitro groups has been derived from a study of the low intensity absorption band of nitro compounds near 280 m μ . This band is quite sensitive to solvents, with respect to both position and intensities. New measurements of this band in water, methanol, and hexane (Fig. 3) confirm the blue shift with increasing solvent polarity with reference to hexane and gas.⁸ In the case of pyridazine and benzophenone the blue shift of the $n \rightarrow \pi^*$ transition has been traced to hydrogen bonding with the solvent.⁹ Nitromethane does absorb at the shortest wave lengths in the solvents which can form the strongest hydrogen bonds, *i.e.*, water and heptafluorobutanol (Table III). There is, however, a simultaneous decrease in the electron density on the oxygen of these solvents, which also may affect the position of the band.¹⁰ For this reason the

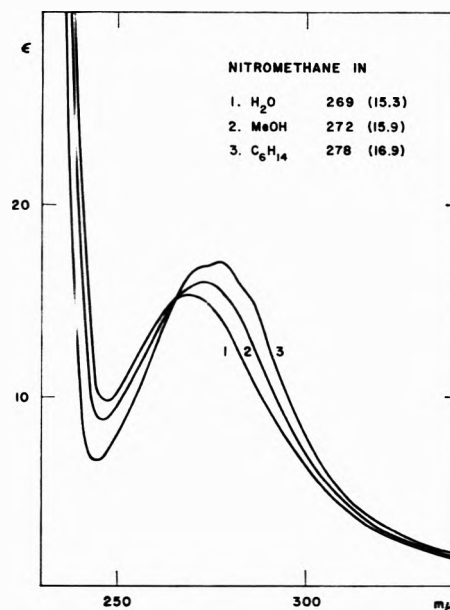


Figure 3. Ultraviolet absorption spectra of nitromethane.

absorption intensities of the ultraviolet band have been examined. It was established previously that dioxane can increase the intensity of this transition over "inactive" solvents such as hydrocarbons¹¹ and that nitrogen-containing solvents give even larger increases which fall in the order of their electron-donor tendencies.¹² The interaction which occurs can be recognized by an increase in the intensity of the 280-m μ band, a small apparent red shift of the intense band at shorter wave lengths,¹³ and a pronounced increase in the absorption at the minimum (near 250 m μ). We have now observed that an increase in the electron-donor properties of ethers similarly enhances the complex formation with nitro compounds (Table III), thus, the last two criteria for such an interaction give the ether series $(\text{ClCH}_2\text{CH}_2)_2\text{O} < \text{Et}_2\text{O} < (\text{MeOCH}_2\text{CH}_2)_2\text{O} < \text{dioxane}$.¹⁴

(8) N. S. Bayliss and E. G. McRae, *J. Phys. Chem.*, **58**, 1006 (1954).

(9) G. J. Brealy and M. Kasha, *J. Am. Chem. Soc.*, **77**, 4462 (1955).

(10) Such a change could be expected if the solvent were to alter the electron density on the nitrogen. It has been shown that frequency shifts in RNO_2 are in the Baker-Nathan order: $\text{Me} > \text{Et} > i\text{-Pr} > t\text{-Bu}$ [A. Balasubramanian and C. N. R. Rao *Chem. Ind. (London)*, 1025 (1960)]. A similar order was found in the present investigation, both in polar and nonpolar solvents (Table III).

(11) N. S. Bayliss and C. J. Brackenridge, *J. Am. Chem. Soc.*, **77**, 3959 (1955).

(12) H. E. Ungnade, E. D. Louzhran, and L. W. Kissinger, *J. Phys. Chem.*, **64**, 1410 (1960).

(13) Because of solvent absorption only a small portion of this band can be observed; *cf.* also ref. 11.

(14) The somewhat higher intensity at the maximum for the chloroethyl ether is ascribed to the effect of the chlorine which finds a parallel in the case of carbon tetrachloride.¹¹

Table III: Ultraviolet Absorption Bands in Aliphatic Nitro Compounds

Compound	Solvent	λ_{\min}	ϵ	λ_{\max}	ϵ
MeNO ₂	MeCN	246	7.0	272	15.0
MeNO ₂	H ₂ O	247.5	9.2	269	15.3
MeNO ₂	<i>n</i> -C ₃ F ₇ CH ₂ OH	246	8.3	268	15.4
MeNO ₂	MeOH	247.5	8.5	272.5	15.9
MeNO ₂	EtOH	248	9.7	272.5	16.9
MeNO ₂	<i>n</i> -PrOH	248	9.5	273	17.3
MeNO ₂	<i>i</i> -PrOH	248	9.5	273	17.5
MeNO ₂	<i>n</i> -BuOH	248	9.8	273.5	17.9
MeNO ₂	<i>t</i> -BuOH	248	9.7	273.5	18.2
MeNO ₂	(ClCH ₂ CH ₂) ₂ O	248	9.6	276	19.5
MeNO ₂	Et ₂ O	250	10.4	275	17.1
MeNO ₂	(MeOCH ₂ CH ₂) ₂ O	252.5	14.0	276	20.2
MeNO ₂	Dioxane	265	22.6	272	22.9
EtNO ₂	MeOH	248	9.9	275	18.9
PrNO ₂	MeOH	248	9.1	275	20.1
BuNO ₂	MeOH	248	9.4	276	23.7
MeNO ₂	C ₆ H ₁₄	246	6.5	278	16.9
EtNO ₂	C ₆ H ₁₄	246	6.8	278	19.4
PrNO ₂	C ₆ H ₁₄	246	6.8	279	22.1
BuNO ₂	C ₆ H ₁₄	246	7.1	279	23.0

In the case of alcohol solutions the band intensities are in the order *n*-C₃F₇CH₂OH < MeOH < EtOH < *n*-PrOH < *i*-PrOH < *n*-BuOH < *t*-BuOH, which corresponds to the electron-donor properties of these solvents. In the related carbonyl absorption band, the formation of hydrogen bonds causes an increase in intensity,¹⁵ *i.e.*, the solvent order is reversed, so that such bonding cannot account for the observed results if the solvation processes are strictly comparable.^{16,17} It is proposed, therefore, that alcohols can act also as electron donors toward nitro compounds. Further evidence for such interaction comes from a consideration of absorption at the minimum. Hydrocarbons and heptafluorobutanol, which are poor electron donors, have nearly identical absorption below the minimum while the other alcohols ROH all show an apparent red shift of 1.5–2.0 μ of the high-intensity band and an increased absorption at the

minimum. This behavior is similar to that of the ethers but the interaction is weaker in this case, as would be expected.

Experimental

Infrared Absorption Spectra. Carefully weighed amounts of alcohols and nitro compounds were made up to exact volumes, and the solutions were run in matched sodium chloride cells in a Perkin-Elmer Mod 421 infrared spectrophotometer. For the determination of absorbance each solution was run two or three times under the same conditions. The listed intensity values represent the average.

Ultraviolet Absorption Spectra. The observed differences in intensities and wave lengths were smaller than differences between instruments and it was, therefore, not possible to use literature data. The purest available specimens of nitro compounds (99.9+%) were weighed out into volumetric flasks and dissolved in Spectrograde solvents. Absorption spectra were determined in silica cells 0.2 cm. thick (to minimize solvent absorption) with a Cary Model 14 spectrophotometer at 25°. The intensities in the present investigation were reproducible to within 0.5%.

N.m.r. Spectra. Freshly prepared solutions with the same concentrations as those used for the infrared determinations were run within 1 hr. on a Varian DP-60 spectrometer. The chemical shifts were measured by the side-band technique. In 0.5 *M* methanol solution cyclohexane was used as external reference while in 0.1 *M* methanol solutions tetramethylsilane was used as internal reference. All data in Fig. 2, however, are reported with reference to the methyl peak of methanol. The temperature of the probe was 30°.

(15) C. N. R. Rao, G. K. Goldman, and A. Balasubramanian, *Can. J. Chem.*, **38**, 2508 (1960).

(16) N. S. Bayliss and E. G. McRae, *J. Phys. Chem.*, **58**, 1002, 1006 (1954).

(17) Polarization effects which depend on the solvent refractive index are probably obscured since they would lead to the order *n*-Bu > *t*-Bu, opposite to the experimental findings.

Vaporization Reactions in the Copper Chloride-Chlorine System

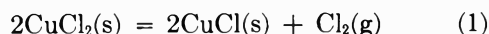
by Robert R. Hammer and N. W. Gregory

Department of Chemistry, University of Washington, Seattle, Washington (Received June 19, 1964)

An effusion study of the equilibrium pressures of cuprous chloride and chlorine above solid cupric chloride has been made. The condensation coefficients for both species are relatively large and the effusion method is quite satisfactory for study of this system. The vapor pressure of cupric chloride above its solid in chlorine atmospheres has also been measured by transpiration. Thermodynamic constants for these processes are given and the results compared with related studies.

We have been interested in the study by effusion of vaporization processes in which several chemically distinguishable species effuse simultaneously from the cell. In the case of iron(III) chloride, for example, dimeric ferric chloride vapor, by vaporization, and chlorine, by decomposition of the ferric chloride to ferrous chloride, have comparable equilibrium pressures.¹ Chlorine effusion pressures are well below expected equilibrium values, however, while ferric chloride pressures gave good equilibrium data. Hence in this system the condensation coefficients for the two processes, both originating on the ferric chloride surface, are vastly different.

We now wish to report results of an effusion and transpiration study of the vaporization processes occurring when solid copper(II) chloride is heated. The reaction



and the corresponding reaction above the melting point of the mixture have been studied by a number of workers, most of whom have used manometric methods at higher temperatures.²⁻⁷ Phase studies of the CuCl_2 - CuCl system show that the two solids are not significantly soluble in each other.⁵ Some rather limited results on the vaporization of copper(I) chloride below its melting point (425°)^{8,9} and on the vaporization of CuCl_2 ¹⁰ above its melting point have also been reported. These results suggest that the equilibrium constant for reaction 1 and the vapor pressure of solid cuprous chloride can be measured in the same effusion experiment. We have also studied, by transpiration, the vaporization of CuCl_2 under a sufficient pressure of chlorine to prevent the decomposition into $\text{CuCl}(\text{s})$.

Experimental

CuCl_2 was prepared by reaction of electrolytic copper with commercial chlorine, previously dried over P_2O_5 . The chlorine was first condensed into a cold finger attached to the vacuum line and then redistilled; the first and last 20% of the sample was discarded. The copper sample was held at 450° under a chlorine pressure of from 60 to 350 mm. for a 48-hr. period. Samples of CuCl_2 were transferred to the effusion cells in a drybox. The geometrical characteristics of the effusion cells (described previously)¹¹ are shown in Table I.

Effusion runs were initiated by placing a preheated furnace around the evacuated Pyrex effusion cell, maintained at less than 10^{-5} mm. background pressure. Temperatures were held constant within $\pm 1^\circ$ during the 2- to 30-hr. effusion periods. The effused cuprous

(1) R. R. Hammer and N. W. Gregory, *J. Phys. Chem.*, **66**, 1705 (1962).

(2) C. G. Maier, U. S. Bureau of Mines Technical Paper No. 360, U. S. Govt. Printing Office, Washington, D. C., 1925.

(3) J. Kustinson, *Z. Elektrochem.*, **44**, 537 (1938).

(4) S. A. Shechukarev and M. A. Oranskaya, *J. Gen. Chem. USSR*, **24**, 1926 (1954).

(5) W. Blitz and W. Fisher, *Z. anorg. allgem. Chem.*, **166**, 290 (1927).

(6) F. Ephraim, *Ber.*, **50**, 1078 (1917).

(7) K. Jellinek and R. Koop, *Z. physik. Chem.*, **145**, 305 (1929).

(8) P. I. Fedorov and M. N. Shakova, *Izv. Vysshikh Uchebn. Zavedenii, Khim. i Khim. Tekhnol.*, **4**, 550 (1961).

(9) D. W. McGee, *Dissertation Abstr.*, **16**, 35 (1956).

(10) D. N. Tarasenkov and L. L. Klyachko-Guvich, *J. Gen. Chem. USSR*, **6**, 305 (1936).

(11) J. H. Stern and N. W. Gregory, *J. Phys. Chem.*, **61**, 1226 (1957).

Table I

Cell	Orifice area $a_o \times 10^3 \text{ cm.}^2$	Ratio of a_o and cell cross-sectional area, a_s $a_o \times 10^3/a_s$	Orifice Clausing factor K
2	7.34	3.1	0.98
5	16.7	13.5	0.96
6	4.23	0.6	0.97

chloride condensed at the edge of the furnace on a glass insert tube, *ca.* 25-mm. o.d., which fitted snugly against the wall of the vacuum line and against an inner wall which contained the effusion orifice. The effused chlorine was collected in a liquid nitrogen-cooled trap. At the end of an effusion period, the furnace was quickly removed; after cooling, dry air was admitted and the insert tube quickly replaced, *via* a standard taper joint, by a duplicate and the system re-evacuated.

Initial samples were varied in composition from 67 to 99% CuCl_2 (with CuCl). In some cases decomposition was continued until virtually pure CuCl remained. No dependence of pressures on the relative amounts of solids was observed.

It was recognized that the measured chlorine pressures would appear lower than true values if recombination of chlorine with the condensed cuprous chloride occurred. However, the color of the condensate indicated that negligible amounts of chlorine had recombined; furthermore, the amount of CuCl collected was considerably less than the quantity of chlorine released; even if all of the sample of CuCl had been chlorinated, the values of $\log P_{\text{Cl}_2}$ would have been reduced by less than 5%. Hence we believe error from this source to be negligible.

The sample of CuCl was washed from the insert tube with an ammonia solution and was subsequently oxidized by addition of nitric acid. The excess nitric acid was removed by addition of urea. KI was then added to the solution, acidified with H_2SO_4 , and the liberated iodine, formed by reduction of cupric ion, determined by the amperometric dead-stop end-point method.^{12,13} The trapped chlorine sample was also dissolved in potassium iodide solution, and the liberated iodine was determined by the same method.

The vapor pressure of cuprous chloride above CuCl(s) was also measured by torsion effusion. The torsion constant (3.24×10^{-2} mm. deg.⁻¹) of the 30-cm. 1-mil tungsten wire was determined by calibration with zinc.¹ The total orifice (two) area was 2.09×10^{-3} cm.². Baker's Analyzed CuCl (95%) was sublimed under high vacuum and then transferred to the cell in a drybox.

In the transpiration study, chlorine gas, which was allowed to vaporize from the condensed liquid held at various slush bath temperatures to give the desired pressure, was caused to flow over the sample of CuCl_2 by freezing out the gas in a liquid nitrogen-cooled trap at the exit end. The flow rate was controlled by means of interchangeable capillary orifices, placed between the reaction vessel and the exit trap. Pressures of chlorine were measured with a Pyrex diaphragm gauge; the quantity of gas flowing across the sample was determined by measuring the volume and pressure of Cl_2 collected during the run. Runs were initiated by placing a preheated furnace around the reaction vessel; while the sample was coming to equilibrium, gas flow was reversed in direction. During the run, the vaporized CuCl_2 condensed in the exit tube just outside the furnace. On completion of the run, this tube was removed, the CuCl_2 dissolved in excess KI solution, and the liberated iodine again determined by the dead-stop method.

Results and Discussion

Steady-state effusion pressures of chlorine above $\text{CuCl}_2(\text{s})$ and $\text{CuCl}(\text{s})$, calculated from the equation $P_{\text{mm}} = (17.14n(MT)^{1/2})/(a_o t K)$ where n is the number of moles of molecular weight M effusing in time t at $T^\circ\text{K.}$, are shown in Fig. 1. Equilibrium values of these pressures constitute the equilibrium constant for reaction 1. Cells 2 and 6, with the smaller a_o/a_s factors, gave indistinguishable results; pressures from

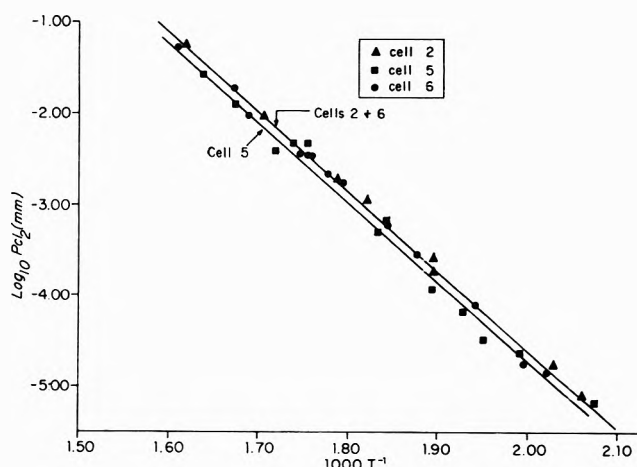


Figure 1. Chlorine effusion pressures produced by the reaction $2\text{CuCl}_2(\text{s}) = 2\text{CuCl}(\text{s}) + \text{Cl}_2(\text{g})$.

(12) A. R. Olson, C. W. Koch, and G. C. Pimentel, "Introductory Quantitative Analysis," Freeman and Co. San Francisco, Calif., 1956, pp. 369-373.

(13) W. B. Fortune and M. G. Mellon, *Ind. Eng. Chem., Anal. Ed.*, 10, 60 (1938).

these two cells were combined in a least-squares treatment and gave the equation $\log P_{\text{Cl}_2}(\text{mm.}) = 12.741 - 8672T^{-1}$. Cell 5 pressures were slightly lower and gave the equation $\log P_{\text{Cl}_2}(\text{mm.}) = 12.602 - 8665T^{-1}$. The similarity of pressures from three cells, which have significantly different orifice diameters, leads us to conclude that the condensation coefficient α for reaction 1, calculated from the simple approximation¹¹ $P_e = P_s(1 + a_o/a_s\alpha)$, is larger than 0.04; α shows no detectable variation with temperature. Pressures from cells 2 and 6 have been assumed to represent equilibrium values. Effusion pressures of chlorine were not noticeably dependent on sample size or on the percentage decomposition; equilibrium values were maintained until virtually all of the material had decomposed.

A second-law treatment of the experimental data gives $\Delta H^\circ = 39.7$ kcal. and $\Delta S^\circ = 45.1$ cal. deg.⁻¹ mole⁻¹ at the mean reaction temperature of 285°. A "third-law" treatment shows the data to have good consistency. Kelley and King¹⁴ recommend a value of S°_{298} for CuCl(s) of 20.8 cal. mole⁻¹ deg.⁻¹ based on the results of Watanabe.¹⁵ Lewis, Randall, Brewer, and Pitzer¹⁶ also quote this value and give -22.2 as the free energy function at 500°K. Based on the heat capacity data of Stout and Chisholm,¹⁷ Brewer, Somayajulu, and Brackett¹⁸ give the values of -25.83 at 298.2°K. and -28.0 at 500°K. for the free energy functions of CuCl₂(s). Combined with the well-known free energy function of chlorine, we derive the equation

$$\Delta H^\circ_{298} = 43.29T - 0.003(T - 298)T - RT \ln P_{\text{Cl}_2}(\text{atm.})$$

for the temperature range of our experiments. Calculated values of ΔH°_{298} are shown in Fig. 2a and give an average value 38.6 kcal. mole⁻¹, somewhat larger than that indicated by data in NBS Circular 500 (34 kcal.)¹⁹ but which corresponds well with the second-law result.

Earlier work on reaction 1 has been largely at temperatures above the melting point of the CuCl₂-CuCl eutectic mixture. Our results are considerably below those of the Russian workers and of Maier over the solid phases. A manometric method was used by Maier and little confidence was expressed in the small pressures measured at the lowest temperatures. Figure 3 compares the results of the various workers. The effect on the chlorine pressures of formation of liquid solutions at the higher temperatures cannot be evaluated without detailed information on the activities and enthalpies of both CuCl₂ and CuCl.

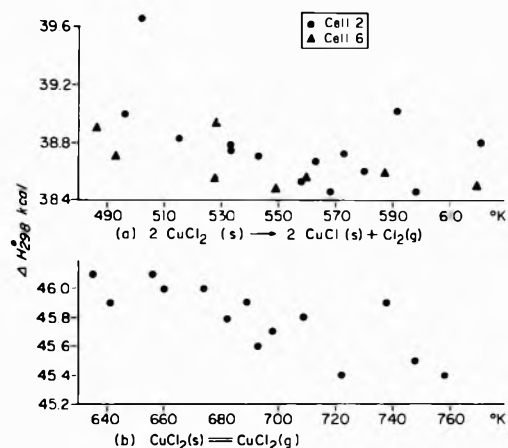


Figure 2. Correlation of ΔH°_{298} with free energy functions.

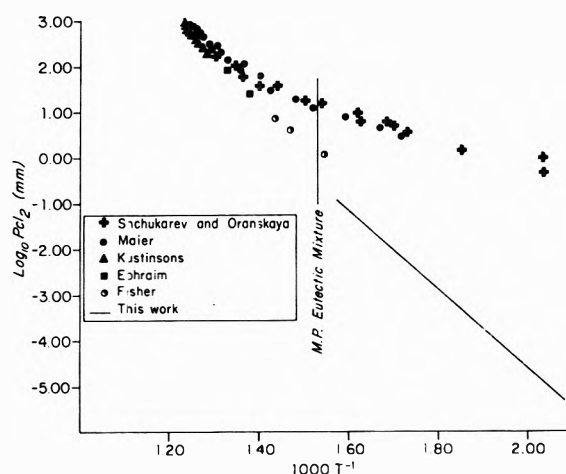


Figure 3. Comparison of results of various investigators for chlorine pressures over mixtures of CuCl₂ and CuCl.

Effusion pressures of cuprous chloride from reaction 1, determined in the same experiment used for the chlorine data are shown in Fig. 4. The molecular form of the vapor has been assumed for simplicity to be Cu₃Cl₃. A comparison of ordinary effusion (by analysis of condensed effusate) and of the torsion effusion study of pure CuCl(s) (shown as crosses in

(14) K. K. Kelley and E. G. King, U. S. Bureau of Mines Bulletin 592, U. S. Govt. Printing Office, Washington, D. C., 1961.

(15) M. Watanabe, *Sci. Rept. Tohoku Univ.*, **22**, 423 (1933).

(16) G. N. Lewis, M. Randall, L. Brewer, and K. S. Pitzer, "Thermodynamics," 2nd Ed., McGraw-Hill Book Co., Inc., New York, N. Y., 1961.

(17) J. W. Stout and R. C. Chisholm, *J. Chem. Phys.*, **36**, 979 (1962).

(18) L. Brewer, G. R. Somayajulu, and E. Brackett, *Chem. Rev.*, **63**, 111 (1963).

(19) D. D. Wagman, W. H. Evans, S. Levine, and I. Jaffey, National Bureau of Standards Circular 500, U. S. Govt. Printing Office, Washington, D. C., 1952.

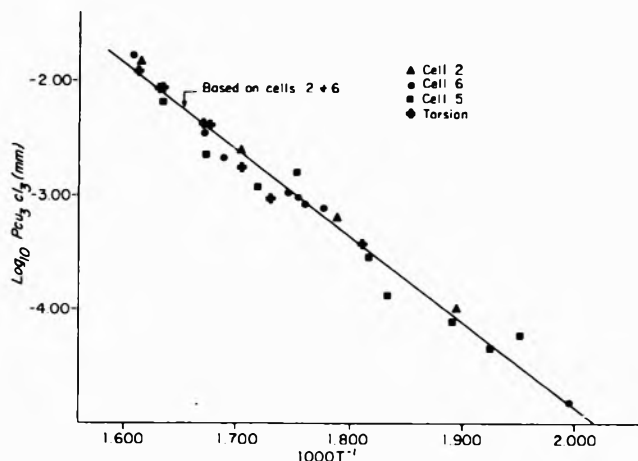


Figure 4. Effusion pressures of cuprous chloride (calculated as Cu_3Cl_3) produced by the reaction $2\text{CuCl}_2(\text{s}) = 2\text{CuCl}(\text{s}) + \text{Cl}_2(\text{g})$ (torsion effusion values were obtained with pure $\text{CuCl}(\text{s})$).

Fig. 4; torsion pressures are independent of assumed molecular weight) indicated a molecular weight close to that of the trimer. A similar observation is also reported by McGee⁹; studies at considerably higher temperatures by Brewer and Lofgren²⁰ show that between 988 and 1343°K. the monomer and trimer are the principal species. Fedorov and Shakova⁸ suggest that the hexamer may be an important vapor species at lower temperatures; their results were obtained at temperatures somewhat above our range and are generally consistent with an extrapolation of our curve. In view of the torsion effusion evidence, we have reported pressures on an assumed basis that Cu_3Cl_3 is the principal molecular form in the vapor phase. Values may be recalculated if subsequent studies confirm that the vapor composition is more complex.

Results, shown in Fig. 4, again show close agreement between cells 2 and 6, with those in cell 5 only slightly less at the highest temperatures. Least-squares treatment of the combined results from cells 2 and 6 gave the equation $\log P_{\text{Cu}_3\text{Cl}_3}(\text{mm.}) = 10.290 - 7574T^{-1}$ which we take to represent equilibrium values of the pressure. The equilibrium expression gives $\Delta H^\circ = 34.6$ kcal. and $\Delta S^\circ = 33.9$ cal. mole⁻¹ deg.⁻¹ for the mean temperature of 285°.

The apparent value of the condensation coefficient is *ca.* 0.1; the scatter of points for cell 5 is such as to make estimation of α difficult.

Results of the transpiration experiments on the vaporization of CuCl_2 in chlorine atmospheres are shown in Fig. 5. The pressures were found independent of flow rate, varied between 87 and 15 cc./min., and independent of chlorine pressure, varied from 6 to

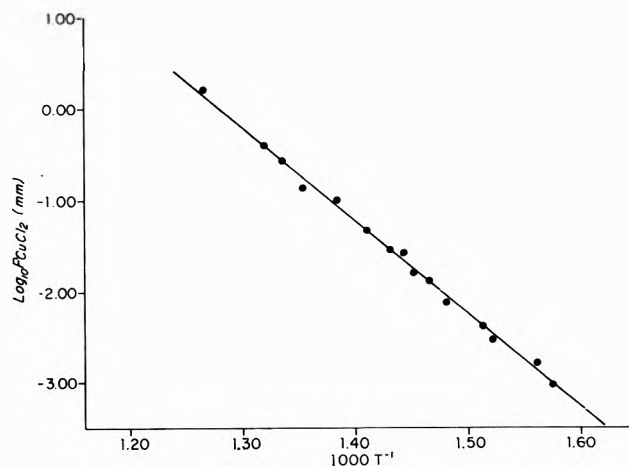


Figure 5. Transpiration pressures of CuCl_2 (calculated as monomer) in chlorine over $\text{CuCl}_2(\text{s})$.

57 cm. mercury. Only the higher chlorine pressures were used at the highest temperatures; the calculated partial pressure of cuprous chloride was negligible relative to that of cupric chloride in all experiments. The equation of the least-squares line shown is

$$\log P_{\text{CuCl}_2}(\text{mm.}) = 12.941 - 10,119T^{-1}$$

The constants correspond to values of $\Delta H^\circ = 46.3$ kcal. mole⁻¹ and $\Delta S^\circ = 46.0$ cal. mole⁻¹ deg.⁻¹ at the mean temperature of 440°. Calculated pressures are dependent on the assumed molecular weight. Results have been given, for simplicity and because of agreement with free energy function calculations, on the basis that the monomer is the principal species of copper(II) chloride in the vapor phase in these experiments. Because of the need for relatively large chlorine pressures to repress formation of Cu_3Cl_3 , it is difficult, by the usual methods, to obtain direct evidence for the molecular form of the vapor. Klemperer and co-workers,²¹ in a recent spectral study, have found evidence for two major species in the vapor phase above CuCl_2 in an atmosphere of chlorine at 600°. Extrapolation of our equilibrium expressions indicates that, if the chlorine pressure is taken as 1 atm., the pressure of cuprous chloride polymer exceeds that of cupric chloride at 600° (no allowance was made in the extrapolation for the fact that 600° exceeds the melting point). Hence the spectral evidence may not necessarily indicate a large proportion of CuCl_2 polymeric species.

(20) L. Brewer and N. L. Lofgren, *J. Am. Chem. Soc.*, **72**, 3038 (1950).

(21) G. E. Leroi, T. C. James, J. T. Hougen, and W. Klemperer, *J. Chem. Phys.*, **36**, 2879 (1962).

We find our data based on monomer as the principal species to give a satisfactory third-law correlation using free energy functions for $\text{CuCl}_2(\text{s})$ and $\text{CuCl}_2(\text{g})$ from Brewer, Somayajulu, and Brackett.¹⁸ The temperature dependence of these functions leads to the equation

$$\Delta H_{298}^{\circ} = 46.2T - 0.005(T - 500)T - RT \ln P_{\text{atm}}$$

Values of ΔH_{298}° calculated from each pressure shown on Fig. 5 are plotted in Fig. 2b; an average value of 45.8 kcal. is obtained. The very slight trend of points with temperature is easily within experimental error and the uncertainty in the free energy functions.

It can be seen from these results that the contribution of CuCl_2 to the effusion pressures at lower temperatures can be neglected. An extrapolation of our equation is generally consistent with the three pressure values reported by the Russian workers¹⁰; their data are not sufficiently extensive to permit a quantitative comparison of thermodynamic constants.

The condensation coefficients for chlorine and for cuprous chloride in the vaporization of CuCl_2 at low temperatures are sufficiently large so that the effusion method is satisfactory as a means of studying reaction 1, and simultaneously, the vapor pressure of $\text{CuCl}(\text{s})$. The reaction analogous to (1) in the copper bromide system was also studied by the effusion method.²² Although the effusion method was also satisfactory in the CuBr_2 case, a more marked dependence of pressures with degree of decomposition and sample size was observed. In the latter, temperatures at which the

bromine pressure was in the effusion range were so low that cuprous bromide was not appreciably volatile. The condensation coefficient for bromine on CuBr appeared to be of a similar magnitude to that found here for chlorine on CuCl . The behavior of these and related systems suggests that the effusion method is most likely to be successful for the study of decomposition reactions in cases where both solid phases have vapor pressures in or near the effusion range at the temperature of the study. The volatility of the ferrous halides in similar reactions in the iron halide systems¹ is very low, and near equilibrium pressures were not obtained.

In the present study, only cell 5 gave pressures which were appreciably less than equilibrium and even here the deviation is so small that estimate of the condensation coefficient and its temperature dependence is difficult. The slope of the steady-state pressure line for chlorine from cell 5 is virtually the same as that of the equilibrium line, indicating that the activation energy for condensation is virtually zero. α appears to decrease with increasing temperature for Cu_3Cl_3 although the scatter of points is such that an attempt to estimate activation energies seems unjustified.

Acknowledgment. This work was supported in part by the National Science Foundation (NSF G-20631) and by the National Aeronautics and Space Administration (NSG-484).

(22) R. R. Hammer and N. W. Gregory, *J. Phys. Chem.*, **68**, 314 (1964).

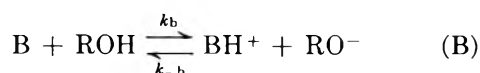
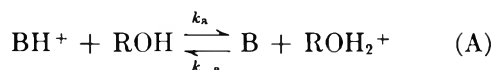
Acid Dissociation and Proton Transfer of *p*-Toluidinium Ion and Dimethylphenylphosphonium Ion in Methanol

by M. Cocivera, Ernest Grunwald, and Charles F. Jumper

Bell Telephone Laboratories, Incorporated, Murray Hill, New Jersey 07971 (Received June 19, 1964)

Acid dissociation constants, K_a , and rate constants, k_a and k_{-a} , in methanol have been measured over a wide temperature range; $K_a = k_a/k_{-a}$. For *p*-toluidinium ion at 25°, $k_a = 2.92 \times 10^3 \text{ sec.}^{-1}$, $k_{-a} = 1.04 \times 10^{10} \text{ sec.}^{-1} M^{-1}$, $K_a = 2.8 \times 10^{-7} (M)$; $\Delta H_a^\circ (-28^\circ) = 13.7 \text{ kcal. mole}^{-1}$, $\Delta S_a^\circ (-28^\circ) = 16 \text{ e.u.}$ For dimethylphenylphosphonium ion at 25°, $k_a = 3.7 \times 10^3 \text{ sec.}^{-1}$, $k_{-a} = 1.3 \times 10^8 \text{ sec.}^{-1} M^{-1}$, $K_a = 2.8 \times 10^{-5} (M)$; $\Delta H_a^\circ (-22^\circ) = 10.2 \text{ kcal. mole}^{-1}$, $\Delta S_a^\circ (-22^\circ) = 13 \text{ e.u.}$, $\Delta H_a^* (0^\circ) = 11.3 \text{ kcal. mole}^{-1}$, $\Delta S_a^* (0^\circ) = -4 \text{ e.u.}$ Kinetic data for the symmetrical proton exchange, $BH^+ + CH_3OH^* + B \rightarrow B + HOCH_3 + H^*B^+$, are as follows. For $B = p$ -toluidine, $k_2 (25^\circ) = 8.1 \times 10^7 \text{ sec.}^{-1} M^{-1}$, $\Delta H_2^* (-28^\circ) = 2.33 \text{ kcal. mole}^{-1}$, $\Delta S_2^* (-28^\circ) = -14.4 \text{ e.u.}$ For $B = \text{dimethylphenylphosphine}$, $k_2 (25^\circ) < 10^4 \text{ sec.}^{-1} M^{-1}$. The data provide a further example that proton transfer involving phosphorus acids and bases is appreciably slower than that involving nitrogen acids and bases.

For acid and base dissociation in hydroxylic solvents



the rate constants for reaction in the direction of decreasing standard free energy are of considerable current interest. If B is an oxygen or nitrogen base and ROH is water, data are available for a number of substrates and suggest that such reaction takes place at each encounter of suitable geometry.¹⁻⁴ On the other hand, if B is a phosphorus base, this conclusion may not be justified; however, kinetic measurements have been reported for only one system, trimethylphosphine in water.⁵

To be specific, let us compare rate constants for trimethylphosphine with those for the nitrogen analog, trimethylamine. The following data refer to reaction in water in the direction of decreasing standard free energy: for trimethylamine, $k_{-a} = 2.7 \times 10^{10} \text{ sec.}^{-1} M^{-1}$ at 25°, and $k_{-b} = 2.1 \times 10^{10} \text{ sec.}^{-1} M^{-1}$ at 20°^{3,4}; for trimethylphosphine, $k_{-a} = 5 \times 10^9 \text{ sec.}^{-1} M^{-1}$ at 22° and $k_{-b} = 4.6 \times 10^7 \text{ sec.}^{-1} M^{-1}$ at

22°.⁵ For comparison, the specific rates for encounters between reactant molecules⁶ in these processes are about $4 \times 10^{10} \text{ sec.}^{-1} M^{-1}$.

On the basis of these data, if reaction were taking place at each encounter of suitable geometry, the geometrical factors would be about 0.5 for the processes measured by k_{-a} and k_{-b} , in the case of trimethylamine, but only 0.1 or less in the case of trimethylphosphine. While geometrical factors of the order of 0.5 are plausible for diffusion-controlled processes,^{1b} values much below this figure are not. Therefore, for trimethylphosphine the process measured by k_{-a} is probably,

(1) (a) M. Eigen and L. DeMaeyer, *Proc. Roy. Soc. (London)*, **A247**, 505 (1958); (b) M. Eigen and K. Kustin, *J. Am. Chem. Soc.*, **82**, 5952 (1960).

(2) W. J. Albery and R. P. Bell, *Proc. Chem. Soc.*, 169 (1963).

(3) (a) M. T. Emerson, E. Grunwald, and R. A. Kromhout, *J. Chem. Phys.*, **33**, 547 (1960); (b) E. Grunwald, *J. Phys. Chem.*, **67**, 2208 (1963).

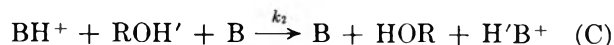
(4) A useful tabulation of data has been given by M. Eigen and L. DeMaeyer, in "Rates and Mechanisms of Reactions," S. L. Friess, E. S. Lewis, and A. Weissberger, Ed., Part II, Interscience Publishers, New York, N. Y., pp. 1031-1050.

(5) B. Silver and Z. Luz, *J. Am. Chem. Soc.*, **83**, 786 (1961).

(6) Calculated from eq. 18 and 19 of ref. 2a, assuming a collision diameter of 4.8 Å.

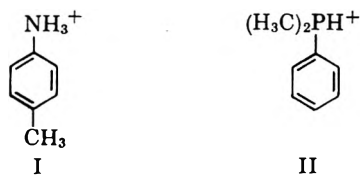
and that measured by k_{-b} is almost certainly, activation-controlled.

When phosphonium ion and phosphine both participate in a proton transfer process, the reduction in reactivity relative to that of the nitrogen analogs appears to be very striking indeed. Thus, for the symmetrical exchange reaction C, which involves a solvent molecule (ROH)



the values of k_2 in water at 25° are $3 \times 10^8 \text{ sec.}^{-1} M^{-1}$ and $\leq 1.2 \times 10^2 \text{ sec.}^{-1} M^{-1}$, respectively, when B is trimethylamine^{3b} and trimethylphosphine.⁶

In order to extend the rate measurements for reactions A–C to other hydroxylic solvents and to extend the comparison of phosphorus with nitrogen bases to other structures, we now report a kinetic and equilibrium study of acid dissociation and proton transfer for *p*-toluidinium ion (I) and dimethylphenylphosphonium ion (II)



over a wide temperature range in buffered and unbuffered methanol solutions. The measurements were made by nuclear magnetic resonance techniques. The kinetic data demonstrate again the high reactivity characteristic of nitrogen acids and bases and the relatively low reactivity of the phosphorus analog. The K_a measurements enable us not only to evaluate both k_a and k_{-a} in (A) but also to elucidate a discrepancy of long standing concerning the absolute value of K_a for *p*-toluidinium ion.

Experimental

Materials. Commercial reagent grade methanol was dried by treatment with magnesium⁷ and distilled, the first and final quarter being discarded. A small quantity (ca. 50 mg./l.) of benzoic acid was added to the middle fraction, and the resulting solution was redistilled, only the middle portion being collected.

Dimethylphenylphosphine was prepared in the following manner. Dichlorophenylphosphine (obtained commercially) was added to an ether solution of methylmagnesium iodide under a nitrogen atmosphere and at Dry Ice–methanol temperature. The crude product was fractionally distilled at reduced pressure in a nitrogen atmosphere on a spinning band column. The fraction with b.p. 65.0° at 8 mm. was collected.

This fraction was redistilled at reduced pressure under a nitrogen atmosphere in an all-glass system. The fraction with b.p. 70.0° at 12 mm. was collected.

Eastman Kodak White Label *p*-toluidinium chloride was recrystallized first from pure methanol to which a small amount of HCl was added, and finally from pure, neutral methanol. The resulting crystals were pure white and were stored over anhydrous $\text{Mg}(\text{ClO}_4)_2$ in an evacuated desiccator. For experiments involving acid–base ratios in excess of 100, this recrystallized material was further purified by zone refining in a nitrogen atmosphere.

Solutions. Solutions of dry HCl in methanol, NaOMe in methanol, and the various buffers in methanol were prepared using standard quantitative methods. The dimethylphenylphosphine buffers were in outgassed solutions while those for the toluidine buffers were air-saturated. Whenever possible, those concentrations that were made up by weight were checked by titration with standard acid or base.

N.m.r. Measurements. Measurements were made on Dr. S. Meiboom's n.m.r. spectrometer, using spin-echo and slow passage techniques. For further details, see previous papers.^{3–10}

Chemical Shifts. Pertinent n.m.r. line positions at constant field and at a nominal resonance frequency of 60 Mc./sec. for *p*-toluidinium ion in methanol at 25° were found to be as follows: CH_3 protons of methanol (internal reference), 0.0 c.p.s.; OH protons, 94.1 c.p.s.; NH_3^+ protons, 405.4 c.p.s. In the presence of up to 8.5 *M* HCl, the OH line position was $94.1 + 44.7[\text{HCl}] - 0.13[\text{HCl}]^3$ c.p.s. The chemical shift of the NH_3^+ protons was measured directly at –80° (407.5 c.p.s.) and at –60° (407.1 c.p.s.). Because of proton exchange, the NH_3^+ protons are not directly observable at 25°, except in very strong acid. The value given above was obtained from the low-temperature data by linear extrapolation; direct measurement at 25° in 6.4 *N* HCl gave a value of 390 c.p.s. Under all conditions where direct measurement was possible, the NH_3^+ proton resonance was a single line; that is, spin–spin interaction with N^{14} was effectively averaged out to a value approaching zero by T_1 relaxation of the N^{14} nucleus.

Pertinent n.m.r. line positions for dimethylphenylphosphonium ion and the conjugate phosphine are

(7) N. Bjerrum and L. Zechmeister, *Ber.*, 56, 894 (1923).

(8) (a) E. Grunwald, C. F. Jumper, and S. Meiboom, *J. Am. Chem. Soc.*, 84, 4664 (1962); (b) E. Grunwald, C. F. Jumper, and S. Meiboom, *ibid.*, 85, 522 (1963).

(9) S. Meiboom and D. Gill, *Rev. Sci. Instr.*, 29, 688 (1958).

(10) S. Alexander, *ibid.*, 32, 1C66 (1961).

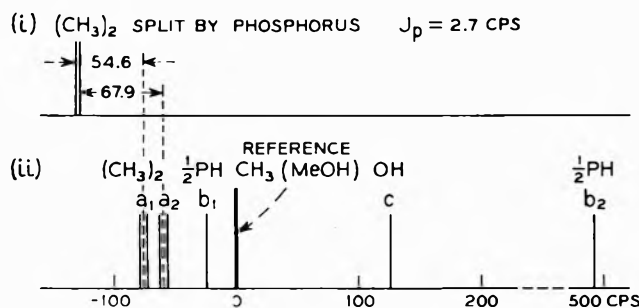


Figure 1. Pertinent n.m.r. line positions, in c.p.s., at -42.7° and 60 Mc./sec. (i) 0.3 *M* dimethylphenylphosphine in methanol. (ii) 0.3 *M* dimethylphenylphosphonium chloride in methanol containing 1 *M* hydrochloric acid. Precise line positions, relative to CH_3 of methanol, are as follows: a_1 , -74.5 ; a_2 , -59.6 ; $J_{\text{P-CH}_3}$, 14.9; $J_{\text{CH}_3\text{-PH}}$, 4.4; b_1 , -24.6 ; b_2 , 491.7; c , $107.8 - 0.533t - 0.00096t^2$; t is temperature in $^\circ\text{C}$.

shown schematically in Fig. 1, and precise values for these line positions at -42.7° and 60 Mc./sec. are stated in the caption. All positions were measured directly under these conditions in methanol solution, except for the PH line labeled b_1 . Its position was determined by assuming that the phosphorus-hydrogen spin-coupling constant has the same value in methanol as in 6 *M* aqueous HCl, where it could be measured directly at -1° . The chemical shifts (relative to the CH_3 protons of methanol) were measured also at -63.0° and at -21.8° and, with the exception of that for the OH protons, were independent of the temperature.

Results

p-Toluidinium Ion. Proton exchange rates of the OH protons of methanol were measured by means of the CH_3 proton resonance of methanol, as described previously.⁸ Measurements were made at 25° and at -81.6° , in buffered solutions containing *p*-toluidinium ion (BH^+) and *p*-toluidine (B). Data at both temperatures are represented accurately by the rate eq. 1, where R denotes the rate of exchange of OH protons, in g.-atom/l. sec., and $[\text{BH}^+]$ and $[\text{B}]$ denote molar concentrations. The latter were varied over wide ranges.

$$R = k_2[\text{BH}^+][\text{B}] + Q[\text{BH}^+]/[\text{B}] \quad (1)$$

Sample data are shown in Table I, and values of the parameters k_2 and Q are given in Table II. These values of the parameters reproduce 15 data sets at -81.6° to $\pm 8\%$, and 7 data sets at 25° to $\pm 5\%$.

Our interpretation of eq. 1 is that k_2 is the rate constant for reaction C, and that $Q[\text{BH}^+]/[\text{B}]$ is the rate of proton exchange catalyzed by CH_3OH_2^+ .

Table I: Sample Kinetic Data for Proton Exchange between *p*-Toluidinium Ion and Methanol

$[\text{C}_7\text{H}_7\text{NH}_3^+]$	Other solutes	R or R' , g.-atom/l. sec.	
		(obsd.)	(calcd.)
1. From CH_3 proton resonance at -81.6°			
0.545		2260	2550 ^a
0.439		1690	1720
0.330	$[\text{C}_7\text{H}_7\text{NH}_3^+] =$	1110	1060
0.188	780 $[\text{C}_7\text{H}_7\text{NH}_2]$	490	470
0.133		280	290
2. From OH-NH proton system at 24.9°			
0.00999	$[\text{HCl}] = 0.000463$	31.7	33.8 ^b
0.00999	0.00139	30.5	30.4
0.00999	0.00417	29.0	29.3
0.00999	0.0125	29.6	28.7
0.00999	0.0375	28.7	27.8
0.00999	0.1126	24.6	25.5

^a $R = 6.2 \times 10^6[\text{BH}^+][\text{B}] + 8.9 \times 10^{-3}[\text{BH}^+]/[\text{B}]$. ^b $R' = 2890[\text{BH}^+] \text{ antilog}(-0.48[\text{HCl}]) + 22.8[\text{EH}^+]^2/[\text{HCl}]$.

Table II: Kinetic and Thermodynamic Results for Acid Dissociation and Proton Transfer of *p*-Toluidinium Ion in Methanol

Temp., $^\circ\text{C}$.	24.8	-81.6
$k_{\text{MeOH}_2^+}$, sec. ⁻¹ ^a	8.79×10^{10e}	1.2×10^{10g}
Q , sec. ⁻¹ <i>M</i> ^b	2.47×10^{4e}	8.9×10^{-3j}
K_a , <i>M</i>	2.81×10^{-7e}	7.2×10^{-13g}
k_2 , sec. ⁻¹ <i>M</i> ⁻¹	8.1×10^{7j}	6.2×10^{5e}
k_2' , sec. ⁻¹ <i>M</i> ⁻¹	9.0×10^{7e}	...
$k_1' = k_a$, sec. ⁻¹ ^c	2.92×10^{3e}	...
k_{-a} , sec. ⁻¹ <i>M</i> ⁻¹ ^d	1.04×10^{10e}	...
ΔH_a° (kcal., at ca. -28°)		13.7 ± 0.7
ΔS_a° (e.u., at ca. -28°)		16.1 ± 2.5
ΔH_2^* (kcal., at ca. -28°)		2.33 ± 0.15
ΔS_2^* (e.u., at ca. -28°)		-14.4 ± 0.6

^a Ref. 8a. ^b See eq. 1. ^c Extrapolated to zero ionic strength. Actual values: $[\text{BHCl}] = 0.01$, $k_1' = 2890$; $[\text{BHCl}] = 0.11$, $k_1' = 2640$. ^d k_1'/K_a . ^e Accuracy $\pm 10\%$ or better. ^f Accuracy ± 10 – 20% . ^g Accuracy below $\pm 20\%$.

On that basis, $Q = K_a k_{\text{MeOH}_2^+}$, where K_a is the acid dissociation constant of BH^+ and $k_{\text{MeOH}_2^+}$ the rate constant for proton exchange of CH_3OH_2^+ . Values for the latter have been reported^{8a}; hence, K_a can be evaluated. The results are included in Table II. The accuracy of K_a is limited by that of $k_{\text{MeOH}_2^+}$. We estimate that at 25° , K_a is accurate to better than 10% , but at -81.6° the value is probably only semi-quantitative.

While the CH_3 proton resonance measures the exchange rate of OH protons of methanol in a com-

pletely nonspecific way, the rate of exchange of OH protons specifically with NH_3^+ protons of *p*-toluidinium ion can be derived from resonance measurements on the $\text{NH}_3^+\text{-OH}$ proton system under acidic conditions where the CH_3 resonance is a sharp, fully exchange-narrowed single line. The method is analogous to that described previously for solutions of benzoic acid in methanol.^{8b} Let R' denote the rate of exchange, in g.-atom/l. sec., of OH protons with NH_3^+ protons. We measured R' at 25° , either in the presence of excess HCl or at buffer ratios in excess of 50. The data are reproduced by the empirical equation

$$R' = k_2'[\text{BH}^+][\text{B}] + k_1'[\text{BH}^+] \quad (2)$$

Some sample data are included in Table I, and values of the parameters k_2' and k_1' are listed in Table II.

Strictly speaking, the presence of a term $k_1'[\text{BH}^+]$ in (2) is inconsistent with the absence of an analogous term in (1). However, we must remember that eq. 1 and 2 are empirical rate equations. Under the conditions of relatively low $[\text{BH}^+]$ and high $[\text{B}]$ under which R is measured at 25° , the kinetic term $k_1'[\text{BH}^+]$ would be small compared to the experimental error.

Examination of Table II shows that, within experimental error, k_2' (which is based on R') is equal to k_2 (which is based on R). This equality completes the proof that the underlying process is reaction C. The concentration dependence proves participation by one molecule each of BH^+ and B. The appearance of this kinetic term in the expression for R proves participation by one or more molecules of methanol. The equality, $k_2' = k_2$, proves that the number of methanol molecules is one.¹¹

The term $k_1'[\text{BH}^+]$ most probably measures the rate of acid dissociation, that is, $k_1' = k_a$. It has been found that in water, k_a , in contrast to k_2 , is subject to rather large salt effects.^{3a,12} Within the limited scope of the present data, the same appears to be true in methanol. In the range of ionic strength covered by this investigation, $0 < \mu < 0.22$, k_1' varies with $[\text{HCl}]$ and $[\text{BHCl}]$ according to (3).

$$\log k_1' = \log (2920) - 0.48[\text{HCl}] - 0.40[\text{BHCl}] \quad (3)$$

The coefficients, -0.48 and -0.40 , have only semi-quantitative significance. However, it is clear that the coefficient of $[\text{HCl}]$ is of the same order of magnitude as that of $[\text{BHCl}]$.

In a previous kinetic analysis of proton exchange resulting from the acid dissociation of trimethylammonium ion in water,¹² an unusually large negative salt effect of HCl was interpreted in terms of the for-

mation of a relatively stable (lifetime $\sim 10^{-10}$ sec.) hydrogen-bonded solvation complex, $\text{B}\cdot\text{HOH}$. The failure to observe an unusually large negative salt effect for HCl in the present system suggests that the solvation complex $\text{C}_7\text{H}_7\text{NH}_2\cdot\text{HOCH}_3$ has a lifetime well below 10^{-10} sec., resembling in this respect the complex $\text{CH}_3\text{NH}_2\cdot\text{HOH}$ in water.¹³

Dimethylphenylphosphonium Ion. The kinetic analysis is based on measurements of the resonance of the CH_3 protons of methanol (rate = R), the OH-PH proton system (rate = R'), the $(\text{CH}_3)_2$ protons of dimethylphenylphosphonium ion (rate = R'') and the $(\text{CH}_3)_2$ proton system of dimethylphenylphosphonium ion-dimethylphenylphosphine (rate = R'''). The results are less precise than those for *p*-toluidinium ion because $1/T_1$, which we used as a measure of the line width in the absence of exchange, had an erratic dependence on the concentrations of the phosphonium ion (BH^+) and the phosphine (B). Although the values of $1/T_1$ were significantly greater than that for pure solvent, they seemed to approach a steady value for each solution soon after preparation. Increases in the value of $1/T_1$ are sometimes the result of the presence of free radicals but electron spin resonance measurements gave negative results. We did not investigate this complication further because it did not prevent us from deducing the kinetics of proton exchange, and because we found the phosphine to have unpleasant physiological effects.

A consistent interpretation of all data can be given on the following basis.

(1) In the dilute buffer solutions in which R is slow enough to be measurable, contributions to R from kinetic terms involving the buffer components are negligible. The only significant kinetic term is proportional to methyloxonium ion. As a result, $R = k_{\text{MeOH}_2} \cdot K_a [\text{BH}^+]/[\text{B}]$, and the measurements afford K_a with an estimated accuracy of $\pm 30\%$. Results are listed in Table III.

(2) Measurements of R' were made in the presence of HCl as well as in buffered solutions. The PH proton fraction was sufficiently small to base the rate calculations on the treatment of Meiboom for the special case of one dominant line.¹⁴ The final equation is

(11) For a full discussion, see ref. 8b.

(12) E. Grunwald, *J. Phys. Chem.*, **67**, 2211 (1963).

(13) M. T. Emerson, E. Grunwald, M. L. Kaplan, and R. A. Kromhout, *J. Am. Chem. Soc.*, **82**, 6307 (1960).

(14) S. Meiboom, *J. Chem. Phys.*, **34**, 375 (1961), especially pp. 387 and 388.

Table III: Kinetic and Thermodynamic Results for Acid Dissociation of Dimethylphenylphosphonium Ion in Methanol

Temp., C°.	-42.7	-1.0	24.8
$k_{MeOH_2^+}$, sec. ⁻¹ ^a	3.1×10^{16}	6.2×10^{10}	...
$k_{MeOH} \cdot K_a$	$(5.6 \pm 1.7) \times 10^3$	$(3.2 \pm 0.9) \times 10^5$...
K_a , M	$(1.8 \pm 0.6) \times 10^{-7}$	$(5.2 \pm 1.5) \times 10^{-6}$	$(2.8 \times 10^{-5})^f$
$k_1' = k_a$, sec. ⁻¹	$(9.0 \pm 2.0)^d$	$(4.8 \pm 0.9) \times 10^2$	$(3.7 \pm 0.7) \times 10^{3e}$
k_{-a} , sec. ⁻¹ M^{-1b}	0.5×10^8	0.9×10^8	1.3×10^8
k_2 , sec. ⁻¹ M^{-1}	<10 ⁴
ΔH_a° (kcal., at ca. -22°)		10.2 ± 1.1	
ΔS_a° (e.u., at ca. -22°)		13 ± 4	
ΔH_a^* (kcal., -43° to +50°)		11.3 ± 0.5^f	
ΔS_a^* (e.u., -43° to +50°)		-4 ± 2	

^a Reference 8a. ^b k_1'/K_a . ^c Extrapolated from data at lower temperatures. ^d Based on measurement of R'' . ^e Additional data at 50.2° give $k_1' = (1.2 \pm 0.4) \times 10^4$ sec.⁻¹. ^f $\log k_1' = \log k_a = 12.200 - 2587/T$, -43° to +50°.

$$\frac{1}{T_2'} - \frac{1}{T_1} = \frac{p\tau}{2} \left[\frac{\delta_1^2}{1 + \delta_1^2\tau^2} + \frac{\delta_2^2}{1 + \delta_2^2\tau^2} \right] \quad (4)$$

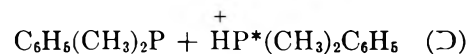
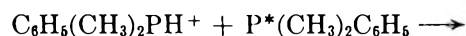
where $1/T_2'$ is the transverse relaxation time of the dominant line in the OH-PH proton system (measured by spin-echo), $p = [BH^+]/([BH^+] + [CH_3OH])$, $1/\tau = R'/[BH^+]$, and δ_1 and δ_2 (in radians/sec.) denote the line separations b_{1c} and b_{2c} in Fig. 1.

The data at all temperatures are consistent, within their experimental error of $\pm 20\%$, with the first-order rate law, $R' = k_1'[BH^+]$. We considered the possibility of a small contribution to R' from a second-order kinetic term, $k_2[BH^+][B]$; an estimate of the upper limit to k_2' is 10^4 sec.⁻¹ M^{-1} at 25°. As before, we interpret k_1' as the rate constant for acid dissociation, that is, $k_1' = k_a$. Results are given in Table III.

(3) Measurements of R''' provide a further check on the insignificance of the second-order kinetic terms. These measurements were made at -1.6° on a solution of 0.153 M BH^+ and 0.0670 M B . Under these conditions the splitting of the $(CH_3)_2P$ protons due to spin-spin interaction with the PH proton in BH^+ is effectively averaged to zero by exchange. Referring to Fig. 1, we therefore need to consider four lines, d_1 and d_2 for the phosphine and the dashed lines a_1 and a_2 for the phosphonium ion. Because the spin of the phosphorus nucleus is unaffected by the addition or removal of a proton, we can divide these four lines into two independent pairs, a_1-d_1 and a_2-d_2 . As a result of proton exchange, the phosphorus atom to which the methyl groups are attached is phosphonium part of the time and phosphine the rest of the time. Hence, the resonance of the $(CH_3)_2$ proton exchanges between an a-line and the corresponding d-line.

As a matter of fact, the resonance of the $(CH_3)_2$ protons consists of two partially overlapping broad lines. One of these lines has its maximum at the

weighted average position of a_1 and d_1 , the second at that of a_2 and d_2 . The widths of the lines lead to the following rates: $R_1''' = 59.5$ and $R_2''' = 60.3$ g.-atom/l. sec., which are in excellent agreement. By comparison, $k_1'[BH^+]$ under the same conditions is 73.7 g.-atom/l. sec. The discrepancy of 20% between the two methods is well within the combined experimental errors. Besides strengthening the conclusions based on the measurements of R' , this agreement shows that the rate of direct proton transfer (D) which does not involve solvent is negligible.



Since reaction D does not involve the solvent, it makes no contribution to R and R' .

(4) R'' was determined from the $(CH_3)_2$ proton resonance of dimethylphenylphosphonium ion in the presence of excess HCl at -42.7° . Under these conditions, resonances a_1 and a_2 in Fig. 1 are each a lifetime-broadened spin-spin doublet due to interaction with the PH proton, as indicated by the solid lines. The spectra were interpreted as described in other papers dealing with spin-spin doublets.^{8a,15}

The results were interpreted on the basis of $R'' = k_1''[BH^+]$. The value obtained for k_1'' at -42.7° , when combined with data for k_1' obtained in the temperature range -1.6 to 50° , gave a single smooth activation plot.

The final averaged results for dimethylphenylphosphonium ion are summarized in Table III.

Discussion

Acid Dissociation Constants. The problem of obtaining absolute values for acid dissociation constants

(15) A. Loewenstein and S. Meiboom, *J. Chem. Phys.*, **27**, 1067 (1957).

has not been solved nearly as accurately in nonaqueous solvents as in water. In methanol, the most comprehensive measurements leading to absolute K_a values have originated in the laboratories of Goldschmidt¹⁶ and Kilpatrick.¹⁷ Goldschmidt's measurements were made by a conductance method, Kilpatrick's by colorimetry. While the two laboratories are in good agreement concerning K_a for benzoic acid and its derivatives, there is a consistent discrepancy of about 50% concerning K_a for anilinium ion and its derivatives. For example, for *p*-toluidinium ion at 25°, the reported values are 2.80×10^{-7} (Goldschmidt, *et al.*¹⁶) and 4.60×10^{-7} (Kilpatrick, *et al.*¹⁷). Our value, recorded in Table II, is 2.81×10^{-7} , in almost exact agreement with Goldschmidt's.

For acid dissociation equilibria of the charge type shown in eq. A, it has often been assumed that medium effects are very nonspecific.¹⁸ However, Gutbezahl and Grunwald pointed out some time ago that in ethanol-water mixtures, this assumption can lead to errors of more than one order of magnitude in K_a .¹⁹ The pK_a values for dimethylphenylphosphonium ion, when compared with those for the structurally similar dimethylanilinium ion, provided a further striking example of such specificity. For the phosphonium ion at 25°, $pK_a = 6.3$ in water²⁰ and 4.6 in methanol (Table III); $\Delta pK_a = -1.7$. For the anilinium ion at 25°, $pK_a = 5.15$ in water²¹ and 5.20 in methanol^{16b}; $\Delta pK_a = +0.05$.

Rate Constants for Acid Dissociation. In this section we wish to consider whether the reaction of methyloxonium ion with *p*-toluidine and with dimethylphenylphosphine is diffusion-controlled. Using the diffusion coefficient of methyloxonium ion²² and estimating diffusion coefficients for the bases from data for other substituted anilines,²³ we calculate⁶ that the specific rate of encounters is about $2 \times 10^{10} \text{ sec.}^{-1} M^{-1}$

in both systems. On the basis of the reaction of hydrogen ion with phenoxide ion, a plausible geometric factor is 0.5,²⁴ leading to a rate constant of $10^{10} \text{ sec.}^{-1} M^{-1}$ if the reaction is diffusion-controlled. Values obtained for k_{-a} at 25° are 1.04×10^{10} for *p*-toluidine and 1.3×10^8 for dimethylphenylphosphine. Apparently the former reaction is diffusion-controlled while the latter is activation-controlled. This pattern of reactivity is similar to, but more definitive than, that obtained in aqueous solution for trimethylamine^{3b} vs. trimethylphosphine.⁵

The present data for reaction C also resemble those obtained in water.^{3b,5} For B = *p*-toluidine, the rate constant is large, and ΔH_2^* , 2.3 kcal., is only slightly greater than ΔH_{visc}^* , 1.7 kcal., for viscous flow of the solvent.²⁵ On the other hand, for B = dimethylphenylphosphine the rate constant is immeasurably smaller, with an estimated upper limit that is only 1/10,000 of the rate constant for B = *p*-toluidine.

(16) (a) H. Goldschmidt and F. Aas, *Z. physik. Chem.*, **112**, 423 (1924); (b) H. Goldschmidt and E. Mathiesen, *ibid.*, **119**, 439, 465 (1926).

(17) (a) M. Kilpatrick and C. A. Arenberg, *J. Am. Chem. Soc.*, **75**, 3812 (1953); (b) M. Kilpatrick and W. H. Mears, *ibid.*, **62**, 3047 (1940).

(18) This assumption is implicit in all applications of the acidity function H_0 . See, for example, L. P. Hammett, "Physical Organic Chemistry," McGraw-Hill Book Co., Inc., New York, N. Y., 1940, p. 267.

(19) B. Gutbezahl and E. Grunwald, *J. Am. Chem. Soc.*, **75**, 559 (1953).

(20) C. A. Streuli, *Anal. Chem.*, **32**, 985 (1960).

(21) H. P. Marshall and E. Grunwald, *J. Am. Chem. Soc.*, **76**, 2000 (1954).

(22) A. G. Ogston, *Trans. Faraday Soc.*, **32**, 1679 (1936); R. E. Jervis, D. R. Muir, J. P. Butler, and A. R. Gordon, *J. Am. Chem. Soc.*, **75**, 2855 (1953).

(23) G. Thovert, *Ann. phys.*, **2**, 369 (1914).

(24) M. Eigen and K. Kustir, *J. Am. Chem. Soc.*, **82**, 5952 (1960).

(25) J. R. Partington, R. F. Hudson, and K. W. Bagnall, *J. chim. phys.*, **55**, 77 (1958).

The Heat Capacity of and the Entropy Change in a Monolayer of Oxygen Chemisorbed on Platinum Black from 15 to 300°K.^{1a}

by R. A. Fisher,^{1b} H. Chon, and J. G. Aston

Contribution No. 125 from the Cryogenic Laboratory of The Pennsylvania State University, University Park, Pennsylvania (Received June 22, 1964)

The heat capacity of a monolayer of oxygen chemisorbed on platinum black has been measured from 15 to 300°K. These heat capacity data were used to evaluate the entropy change in the oxygen monolayer. A thermally indicated titration, using hydrogen to remove the chemisorbed oxygen, demonstrated that there was a one-to-one correspondence between the atoms of chemisorbed oxygen and the surface platinum atoms. An analysis of the heat capacity and entropy data showed that below 90°K. the chemisorbed oxygen was strongly localized on the platinum surface. Above 90°K., cooperative interactions between the adsorbed oxygen seemed to be involved in a transition from localized chemisorption to chemisorption where at least some of the oxygen molecules have restricted motion within the monolayer. Some evidence is presented that indicates hindered mobility would be expected for oxygen chemisorbed on platinum only at monolayer coverages where cooperative interactions are greatest, and, as a consequence, can operate to lower potential barriers to motions within the surface monolayer. On the basis of the heat capacity and entropy data, it was not possible to decide if the chemisorbed oxygen was present on the surface in a diatomic or monatomic form.

Introduction

In recent series of experiments in this laboratory, a technique was developed for cleaning a platinum surface, using the recombination of hydrogen and oxygen on platinum, by a thermally indicated titration.² This experimental technique allows the preparation of a platinum surface either free of chemisorbed molecules or with a known amount of adsorbed hydrogen or oxygen present. Since an adiabatic calorimeter, capable of high accuracy, had been used for the titration experiments, it was decided to attempt a measurement of the heat capacity of a monolayer of adsorbed oxygen. A subsequent analysis of the heat capacity data for the adsorbed monolayer has enabled some conclusions to be drawn concerning the mobility of the adsorbed molecules, as well as giving some insight into the nature of the surface bonding.

Experimental

Apparatus and Materials. The adiabatic calorimeter assembly and the related measuring apparatus

and equipment, as well as the purification procedure used for the various gases used in the experiments, has been extensively described elsewhere.^{2,3a,b} The temperature scale used was in terms of a strain-free platinum resistance thermometer (ice-point resistance, 25 absolute ohms) which had been compared with laboratory standards.^{4a} Temperatures are given in terms of the NBS scale.^{4b}

Surface Preparation. In the experiments described below, the surface of the 163.4-g. platinum black sample was always prepared using a thermally indicated titra-

(1) (a) This work was supported in part by the Office of Ordnance Research; (b) presently at the Low Temperature Laboratory of the University of California, Berkeley, Calif.

(2) H. Chon, R. A. Fisher, and J. G. Aston, *J. Am. Chem. Soc.*, **82**, 1055 (1960).

(3) (a) R. A. Fisher, Ph.D. Dissertation, The Pennsylvania State University, University Park, Pa., 1961; available from University Microfilms, Ann Arbor, Mich.; (b) J. Greyson and J. G. Aston, *J. Phys. Chem.*, **61**, 610 (1957).

(4) (a) G. W. Moessen, J. G. Aston, and R. H. Asch, "Temperature," Reinhold Publishing Corp., New York, N. Y., 1962, p. 91; (b) H. J. Hoge and F. G. Brickwedde, *J. Res. Natl. Bur. Std.*, **22**, 362 (1939).

tion with hydrogen or oxygen, followed by water desorption, using the methods described previously.²

Determination of the surface area of the platinum black was accomplished using standard B.E.T. techniques to evaluate the area from a nitrogen isotherm taken at the boiling point of liquid nitrogen. (The area of a nitrogen molecule was taken as 16.3 \AA^2 .) From B.E.T. surface area measurements the number of surface sites (platinum atoms present at the surface) could be estimated provided the area per surface site was known. The average area per platinum site is obtainable from the lattice constant and the indices of the surface crystallographic planes. The lattice constant for platinum (f.c.c.) is 3.91 \AA and the assumption was made that the platinum black surface had only low index (100, 110, and 111) crystallographic planes present, each with equal probability. Using this as a basis gave a calculated average area per platinum site of 8.37 \AA^2 .

In estimating the number of surface platinum atoms and the volume of gas necessary to form a monolayer the following equations were used.

$$V_M(\text{g}) = 22.4(n_{\text{Pt}}/fN_0) \text{ (in l. at STP)} \quad (1)$$

$$n_{\text{Pt}} = S_{\text{Pt}}/s_{\text{Pt}} \quad (2)$$

$$S_{\text{Pt}} = (N_0 s_{\text{N}_2}/22.4)V_M(\text{N}_2) \text{ (in \AA}^2\text{)} \quad (3)$$

Here $V_M(\text{N}_2)$ is the nitrogen monolayer volume, $V_M(\text{g})$ the monolayer volume of the chemisorbed gas, n_{Pt} the number of surface platinum sites, S_{Pt} the total platinum surface area, s_{Pt} the surface area of a single platinum site, s_{N_2} the area of an adsorbed nitrogen molecule, 22.4 the molar volume in l. mole⁻¹, N_0 Avogadro's number (6.023×10^{23} molecules mole⁻¹), and f the number of platinum sites needed for each adsorbed gas molecule.

Heat Capacity of Oxygen Chemisorbed on Platinum Black. A B.E.T. determination of the platinum black surface area yielded a monolayer volume for nitrogen of 1.09 l. of N_2 at STP. A calculation, using the procedure and equations outlined above, gave 1.06 l. at STP as the expected monolayer volume for O_2 or H_2 using the assumption that there was one adsorbed atom per surface site.

Following the B.E.T. determination, with a monolayer of oxygen adsorbed, the calorimeter was outgassed to a pressure of less than 10^{-6} mm. Purified helium gas was then admitted to the calorimeter to a pressure of 1 cm. at room temperature to serve as an exchange gas. Heat capacities for this system were then obtained between 15 and 300°K . Following these heat capacity determinations, the chemisorbed oxygen was removed by a thermally indicated titration with hydrogen.² The oxygen removal by this procedure resulted in a

40% decrease in the platinum black surface area as shown by a B.E.T. nitrogen surface area determination.

The heat capacity of the resulting platinum black sample, with an essentially clean surface, was determined in a manner similar to that for the sample with a monolayer of chemisorbed oxygen. It was assumed that the surface area reduction produced a negligible change in the heat capacity. This assumption was justified by the results.

To obtain the heat capacity due to the adsorbed oxygen, the data from both heat capacity determinations were plotted and smooth curves drawn through the points. Differences between these two curves were then taken at even temperature intervals. Between 15 and 90°K . there was no detectable heat capacity contribution from the chemisorbed oxygen. From 90 to 170°K . the heat capacity rose rapidly to a maximum and then fell off slowly in going from 170 to 300°K . The entropy change associated with the heat capacity for the chemisorbed oxygen was obtained from the relationship

$$\Delta S = \int_0^T C_p/T \, dT \quad (4)$$

using a Simpson's rule integration of the heat capacity data.

Table I lists the heat capacity and entropy data for the chemisorbed oxygen at even temperature intervals. Column two of the table gives the heat capacities for the actual amount of oxygen chemisorbed on the platinum surface (0.0473 mole of O_2). Columns one, three, and four list, respectively, temperature, molal heat capacities, and related molal entropies on the basis of 1 g. mole of chemisorbed oxygen. Columns five and six are the heat capacities and related entropies on the

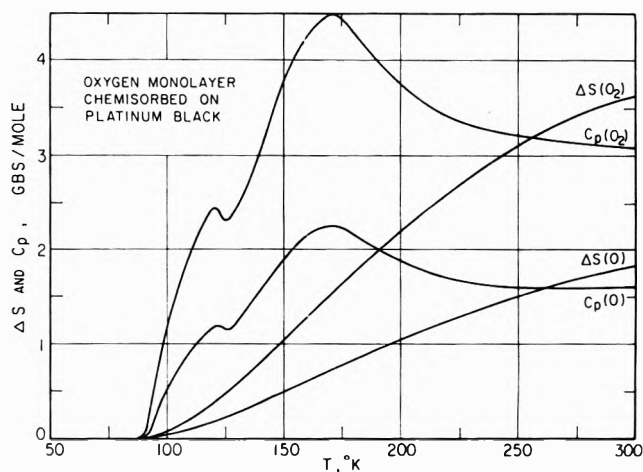


Figure 1. Experimental heat capacity and related entropy change data for oxygen chemisorbed on platinum black.

basis of 1 g.-atom of chemisorbed oxygen. Figure 1 is a graph of the molar data of Table I.

Table I: Experimental Heat Capacities and Related Entropy Changes for Oxygen Chemisorbed on Platinum Black^a

T , K°.	ΔC_p , gibbs	C_n —gibbs/mole of O ₂ —	ΔS	C_p —gibbs/g.-atom of O—	ΔS
0 to 90	0.000	0.00	0.00	0.00	0.00
92.5	0.015	0.33		0.16	
95	0.031	0.66	0.02	0.33	0.01
97.5	0.041	0.87		0.44	
100	0.051	1.09	0.06	0.55	0.03
105	0.067	1.42		0.71	
110	0.087	1.85	0.20	0.92	0.10
115	0.103	2.18		1.09	
120	0.113	2.39	0.39	1.20	0.20
125	0.111	2.28		1.14	
130	0.113	2.39	0.57	1.20	0.28
135	0.123	2.60		1.30	
140	0.144	3.02	0.77	1.51	0.39
145	0.164	3.48		1.74	
150	0.175	3.70	1.01	1.85	0.50
155	0.190	3.93		1.97	
160	0.206	4.35	1.26	2.18	0.63
165	0.211	4.46		2.23	
170	0.216	4.56	1.53	2.28	0.77
175	0.211	4.46		2.23	
180	0.206	4.35	1.79	2.18	0.90
190	0.195	4.14		2.07	
200	0.180	3.80	2.22	1.90	1.11
210	0.173	3.64		1.82	
220	0.170	3.58	2.56	1.79	1.28
230	0.164	3.48		1.74	
240	0.159	3.37	2.86	1.68	1.43
250	0.154	3.26		1.63	
260	0.152	3.21	3.13	1.60	1.56
270	0.150	3.17		1.58	
280	0.149	3.14	3.36	1.57	1.68
290	0.149	3.14		1.57	
300	0.148	3.13	3.58	1.56	1.79

^a One monolayer equals 0.0473 mole of O₂.

The average deviations of the experimental data from smooth curves through them for the two sets of heat capacities is: 0.2% from 15 to about 20°K., 0.1% from 20 to about 190°K., and 0.2% from 190 to 300°K. The corresponding precision of the heat capacities for the chemisorbed oxygen is, on the average, 0.2 gibbs (mole of O₂)⁻¹. (Here the convention is used, as originated by Giaque⁵ and used by him, of defining the gibbs as: 1 gibbs = 1 defined cal./defined °K.) The precision in all cases is understood to be both positive and negative.

Since the original particle size of the platinum black sample was about 100 Å. on a side before the oxygen removal,^{2,3a} and because sintering occurred upon re-

moval of the chemisorbed oxygen, the question arises as to the possibility of heat capacity contributions due to surface and particle size effects.^{6,7} Lien and Phillips⁸ have shown that for MgO particles about 100 Å. on a side, the heat capacity at low temperatures (in the liquid helium range) is quite different than that for bulk MgO. Their results are in qualitative agreement with those predicted from theory.^{6,7} For the present case of the platinum black-oxygen system, no detectable heat capacity existed for the chemisorbed oxygen below 90°K. It may be concluded from this that sintering of the platinum black to larger particles, with correspondingly lower surface areas, resulted in no detectable change in the heat capacity above 15°K. due to this effect.

Near room temperature, contributions to the heat capacity would be expected from any water adsorbed on the platinum surface. This water would be present because of incomplete removal following the thermally indicated hydrogen titration. In the event that any water were present and did lead to contributions to the heat capacity, then the heat capacity for the sample, with an assumed bare surface, would be too high. Consequently, the heat capacity due to chemisorbed oxygen would be too low. However, due to the outgassing conditions following the titration, it is unlikely that much water remained on the surface. From the measured quantity of water removed, the maximum amount remaining on the surface could have been no more than 50 cc. at STP (0.0002 mole of H₂O). Heat capacity contributions, in the temperature range of interest, from an amount of water this small would be expected to be low.

Discussion

Theoretical. Gas molecules adsorbed on a surface tend to occupy sites, or regions, of minimum potential energy. The variation of the potential energy from point to point on the surface leads to potential barriers V between adjacent sites. These potential barriers hinder motion from one site to another. Three cases arise: (I) $V \ll kT$, the variation in potential in passing from site to site is unimportant and the surface is effectively a continuum. Consequently, the adsorbed molecules have two-dimensional mobility. (II) $V \gg kT$, the variation of the potential from site to site is large. As a result, the adsorbed molecules are localized and vibrate about the minima of the potential wells.

(5) W. F. Giaque, E. W. Hornung, J. E. Kunzler, and T. R. Rubin, *J. Am. Chem. Soc.*, **82**, 62 (1960).

(6) E. W. Montroll, *J. Chem. Phys.*, **18**, 185 (1950).

(7) G. Jura and K. S. Pitzer, *J. Am. Chem. Soc.*, **74**, 6030 (1952).

(8) W. H. Lien and N. E. Phillips, *J. Chem. Phys.*, **29**, 1415 (1958).

(III) $V \approx kT$, hindered surface migration may take place from one site to another by passage over (or through by quantum mechanical tunneling) the potential barriers. Cooperative interactions between molecules adsorbed on a surface may lead to lowering of the potential barriers, V . That is, there may be a mutual interaction of the adsorbed molecules, due to their motions, so that the net result is a lowering of the potential barriers to this motion.

When a gas molecule is diatomic, the degrees of freedom relating to the internal motions of the atoms relative to one another are usually altered upon adsorption. In the extreme case dissociation will take place at the surface. For the nondissociative case the rotational degree of freedom for in-plane rotation may have a potential barrier associated with it so that free rotation is restricted. Likewise, the out-of-plane rotation and the vibrational motion of the atoms relative to one another may have barriers associated with them. These barriers related to the internal degrees of freedom of the molecule may all be lowered by cooperative interactions.

The heat capacity of adsorbed molecules will depend on the population changes with temperature of the various energy levels associated with external and internal degrees of freedom for the adsorbed molecules. The external degrees of freedom, which are related to motions of the centers of mass of the molecule, lead to translational and/or vibrational heat capacity contributions. Degrees of freedom associated with internal motions of the atoms of the molecule relative to one another, when the molecule is polyatomic, give rise to rotational and/or vibrational heat capacity contributions. Rotational and translational degrees of freedom may be so highly hindered that they go over into vibrational degrees of freedom. Cooperative phenomena involving a degree of freedom will lead to a rapid change with temperature of the heat capacity associated with the degree of freedom. A maximum in the heat capacity *vs.* temperature curve results from cooperative interactions. The sharpness of the curve increases with increasing cooperation, and, in the limit of complete cooperation, the heat capacity-temperature curve goes over into a λ -type anomaly.

The entropy change at temperature T accompanying the localization of gas molecules on an adsorbent surface may be represented by

$$\Delta S_{loc} = [S(g) - S_{loc}(ad)] \quad (5)$$

while the entropy change for mobile adsorption may be written as

$$\Delta S_{mob} = [S(g) - S_{mob}(ad)] \quad (6)$$

Here the subscripts *loc* and *mob* refer, respectively, to localized and mobile adsorbed phases, while $S(g)$ is the entropy of the molecules in the gas phase and $S(ad)$ the entropy of the adsorbed molecules. Transition from localized to mobile adsorption involves an entropy change which is given by

$$\Delta S_{m.l} = [\Delta S_{mob} - \Delta S_{loc}] = [S_{mob}(ad) - S_{loc}(ad)] \quad (7)$$

For the entropy change to be expected in a transition from localized to mobile adsorption $\Delta S_{m.l}$ may be written as

$$\Delta S_{m.l} = [S_c(ad) - {}_2S_t(ad)] \quad (8)$$

where the term ${}_2S_t(ad)$ is the entropy associated with free two-dimensional translational motion and $S_c(ad)$ is the configurational entropy for the adsorbed molecules. $S_c(ad)$ is a function of the surface coverage θ and for monolayer coverages is equal to zero.

Heat Capacity and Entropy of Oxygen Chemisorbed on Platinum Black. From an examination of Fig. 1, several valuable conclusions can be drawn concerning the state of the chemisorbed oxygen on the platinum black surface. The negligible heat capacity contribution from the chemisorbed oxygen below 90°K., and the rapid rise in the heat capacity to a maximum in going from 90 to 170°K., points to hindered mobility, with cooperative interactions between oxygen atoms or molecules, above 90°K. Localized adsorption below 90°K. explains the negligible heat capacity contribution in this region of temperature.

From previous work² on the thermally indicated hydrogen titration of oxygen chemisorbed on platinum black, it was shown that the heat of reaction changed by about 11 kcal. (mole of H_2)⁻¹ in removing the first 10% of the adsorbed oxygen. Removal of the remaining 90% chemisorbed oxygen gave practically a constant heat of reaction. The high initial heats indicate less tightly bound oxygen. Removal of a small fraction of the chemisorbed oxygen decreases the cooperative interactions between the adsorbed oxygen. This causes the chemisorbed oxygen to become localized and, as a consequence, more tightly bound to the platinum surface. Thus, the drop in the heat of reaction by 11 kcal. (mole of H_2)⁻¹ shows that hindered motions within the layer loosen the surface bonds.

It is interesting to compare the experimental heat capacity and entropy change data at 300°K. with the heat capacity and entropy associated with various unhindered motions of oxygen molecules or atoms on the adsorbent surface. This comparison is made in Table II for both the case of diatomic and atomic oxygen

chemisorbed on the surface. In the table, the subscripts to the right (t, r, and v) refer, respectively, to translation, rotation, and vibration, while the subscripts to the left denote the number of degrees of freedom to be associated with each.

Table II: Comparison of Experimental Heat Capacity and Entropy for Oxygen Chemisorbed on Platinum Black, with the Heat Capacity and Entropy Associated with Various Unhindered Degrees of Freedom. The Comparison is Made at 300°K.

	Exptl.		Caled.				
	C_p	S	$2C_t$	$1C_r$	$1C_v$	$2S_t$	$1S_r$
Diatomic oxygen	1.6R	1.8R	R	R/2	R	8.3R	1.4R
Atomic oxygen	0.8R	0.9R	R	...	R	6.9R	...

The entropies $2S_t$ and $1S_r$ were calculated from equations taken from Trapnell⁹

$$2S_t = R(\ln MTA + 33.12) \quad (9)$$

and

$$1S_r = R/2(1 + \ln IT - \ln \sigma + 87.28) \quad (10)$$

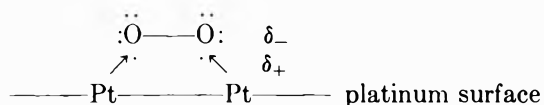
In the two above equations R is the gas constant (1.987 gibbs mole⁻¹), M the molecular weight of the adsorbed molecules, A the area in cm.² occupied by each adsorbed molecule, I is the moment of inertia for the rotating group in g. cm.², and σ is the symmetry number for the rotation.

In the preparation of Table II the following constants were used. For atomically adsorbed oxygen, A was taken as 8.37×10^{-16} cm.² and M as 16. For diatomically adsorbed oxygen, A was taken as 16.7×10^{-16} cm.² (this is twice the average area per platinum site because of the experimentally found one-to-one correspondence between oxygen atoms and surface platinum atoms) and M as 32. The moment of inertia used was that of a gaseous oxygen molecule (7.3×10^{-40} g. cm.²) with a rotational symmetry number of 2.

Since a monolayer of oxygen was chemisorbed on the platinum surface, $S_r(\text{ad})$ is zero, and the *minimum* entropy change to be expected in a transition from localized to mobile adsorption would be $2S_t(\text{ad})$. From an examination of Table II it is clear that if the oxygen is chemisorbed as atoms, then only a fraction of them are on sites with potential barriers sufficiently low that a transition to hindered mobility can take place. If the oxygen is diatomically adsorbed, it is not possible to say

whether the entropy change is associated with hindered rotational degrees of freedom, hindered translational degrees of freedom, or a combination of both. Contributions from vibrational degrees of freedom, other than those associated with in-plane vibrations of the centers of mass (which go over into hindered translational or rotational motion), would be expected to be low for both diatomically and atomically chemisorbed oxygen at 300°K. This would also be expected for contributions from out-of-plane torsional vibrations associated with one of the rotational degrees of freedom for the diatomic case.

The question as to whether or not the chemisorbed oxygen is atomic or diatomic cannot, unfortunately, be answered by the heat capacity and entropy data. It is known that oxygen chemisorbed on most metals is dissociated into atoms.¹⁰ On the other hand, an oxygen molecule in the gaseous state possesses two unpaired electron spins. Thus, it is possible that upon adsorption a platinum-oxygen complex could result from formation of bonds between the surface platinum orbitals and these unpaired electron spins. This picture of in-plane diatomic oxygen chemisorption is not inconsistent with the relative electronegativities for oxygen and platinum given by Pauling,¹¹ or with the sign of the surface dipole.¹² A type of surface compound which might be formed from diatomic chemisorption of oxygen on platinum can be schematically shown as



where the arrows indicate electron transfer toward the oxygen atoms from the platinum atoms in the surface. For this type of configuration, the oxygen would be in the state of hybridization similar to that found in peroxides.

Appendix

A treatment of hindered two-dimensional surface translation has been given by Hill.¹³ Hill's attack on the problem is analogous to Pitzer's treatment of the hindered rotation problem.¹⁴

(9) B. M. W. Trapnell, "Chemisorption," Academic Press, New York, N. Y., 1955, p. 210.

(10) B. M. W. Trapnell, *ibid.*, p. 180.

(11) L. Pauling, "Nature of the Chemical Bond," Cornell University Press, New York, N. Y., 1945, p. 65.

(12) C. W. Oatley, *Proc. Phys. Soc. (London)*, **51**, 318 (1939); see also ref. 9, p. 181.

(13) T. L. Hill, "Introduction to Statistical Thermodynamics," Addison-Wesley, New York, N. Y., 1960, p. 172.

(14) K. S. Pitzer, "Quantum Chemistry," Prentice-Hall, New York, N. Y., 1953, p. 492.

For the simple case of noninteracting, monatomic molecules, adsorbed on a simple cubic lattice, a periodic potential U_{XY} at the adsorbent surface may be approximated by

$$U_{XY} = U_z^0 + V/2[1 - \cos(2\pi X/a - \cos(2\pi Y/a)] \quad (11)$$

In eq. 11, X and Y are coordinates in the surface plane and Z the coordinate perpendicular to the surface, U_z^0 is the depth of the potential in U_{XY} , V the potential barrier separating potential minima, and a is the nearest neighbor spacing for the adsorbent lattice.

The partition function for a system of N noninteracting particles of mass m is given by

$$Q_{XY} = (q_{XY})^N/N! \quad (12)$$

where q_{XY} is the partition function for an individual particle. It may be calculated using the potential of eq. 11 and using the approximation that

$$q_{XY} = q_{\text{classical}}[q_{\text{HO-QM}}/q_{\text{HO-classical}}] \quad (13)$$

where HO stands for harmonic oscillator and QM means quantum mechanical.

After some mathematical manipulation q_{XY} is obtained

$$q_{XY} = \frac{(2\pi mu)I_0^2(u) \exp(-2u - 2Ku)}{(1 - \exp(-Ku))^2} \quad (14)$$

where

$$K = (2h^2/ma^2V)^{1/2} \quad (15)$$

and

$$u = V/2kT \quad (16)$$

In the above equations k is the Boltzmann constant (1.380×10^{-16} erg/°K.) and h Planck's constant (6.625×10^{-27} erg sec.).

Q_{XY} is evaluated, and in the usual way the heat capacity is found to be given by

$$2C_v/Nk = -1 + 2u[u - I_1(u)/I_0(u) - u(I_1(u)/I_0(u))^2] + \frac{2K^2u^2 \exp(-Ku)}{(1 - \exp(-Ku))^2} \quad (17)$$

using the relationship

$$C/Nk = \frac{\partial}{\partial T} \left[T^2 \frac{\partial \ln Q}{\partial T} \right] \quad (18)$$

In the preceding, $I_0(u)$ and $I_1(u)$ are, respectively, the modified Bessel functions of the first and second kind.¹⁵ The potential barrier V may be obtained from the relation

$$V = 5kT_M \quad (19)$$

T_M is the temperature where the heat capacity maximum of eq. 17 occurs.

Although the oxygen heat capacity data would not be expected to follow any such simple theoretical heat capacity curve as that obtained from eq. 17, it is interesting to see just how closely the data do fit.

Figure 2 shows the experimental heat capacity and entropy change data, as points, for a mole of chemisorbed O_2 molecules. Curve A is the theoretical heat capacity calculated from eq. 17. Taking T_M equal to

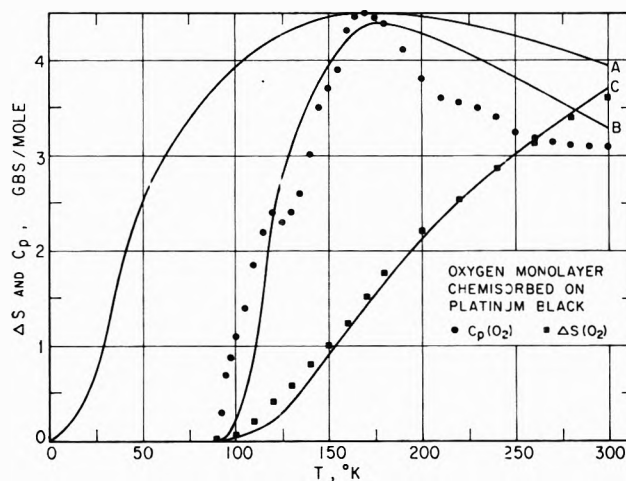


Figure 2. Comparison of experimental heat capacity and entropy change data with calculated values.

170°K., the potential barrier V is 1700 cal. (mole of O_2)⁻¹ using eq. 19. The parameter a for platinum is 2.76 Å. It is quite evident, as was to be expected, that curve A does not fit the experimental heat capacity data except at the maximum. Qualitatively, however, the calculated curve exhibits similar characteristics.

Since curve A has the general shape of the experimental heat capacity data, an empirical method for fitting the data suggests itself. Curve B was computed using the following artifice. Transformation of the temperature coordinate was made according to the following definition

$$T' = T - T_0 \quad (20)$$

where T_0 is taken as the experimental temperature where heat capacity contributions first become detectable. A potential barrier V' is then calculated using

$$V' = 5kT'_M \quad (21)$$

By use of eq. 20, 21, and 17 curve B was obtained. T_0

(15) A table of the various Bessel functions is given in "British Association Mathematical Tables X," Part II, Cambridge University Press, London, 1952.

was taken as 90°K . which gave T'_M as 80°K . The potential barrier V' was $800 \text{ cal. (mole of O}_2\text{)}^{-1}$.

The entropy change at 300°K ., obtained from an integration of curve A gave $8.5 \text{ gibbs (mole of O}_2\text{)}^{-1}$, while curve B gave $3.7 \text{ gibbs (mole of O}_2\text{)}^{-1}$. The experimental change of entropy at 300°K . is $3.6 \text{ gibbs (mole of O}_2\text{)}^{-1}$. Curve C is a plot of the entropy change obtained from an integration of curve B.

The fit of curves B and C to the experimental heat capacity and entropy change data on the basis of a mole of chemisorbed O_2 is surprisingly good. However, it must be emphasized that use of eq. 20 has no known theoretical justification, and it is used in an entirely empirical manner. (The introduction of T_0 is some-

what analogous to the introduction of the Weiss Δ into the equation for magnetic susceptibility, $\psi = C/(T - \Delta)$.)

If the assumption is made that the oxygen is atomically chemisorbed, and that only a fraction of it, about 50%, occupies sites with barriers which can become sufficiently lowered through cooperative interactions, then the heat capacity data can also be fit using the empirical method embodied in eq. 20 and 21.

The same empirical method may be applied to hindered rotational degrees of freedom which involve cooperative interactions. (For calculating hindered rotational heat capacities and associated entropy changes, the tables given by Pitzer are useful.¹⁴)

A Calorimetric Study of the Transformation of Some Metastable

Modifications of Alumina to α -Alumina

by T. Yokokawa and O. J. Kleppa

Department of Chemistry and Institute for the Study of Metals, The University of Chicago, Chicago, Illinois 60637 (Received June 26, 1964)

The heats of solution, in a lead-cadmium-borate melt at 705° , of α -alumina (corundum) and of several metastable modifications of aluminum oxide have been investigated. From the measured heats of solution we obtained the following enthalpies of transformation: $\text{Al}_2\text{O}_3(\gamma) = \text{Al}_2\text{O}_3(\alpha)$, $\Delta H = -5.3 \text{ kcal./mole}$; $\text{Al}_2\text{O}_3(\kappa) = \text{Al}_2\text{O}_3(\alpha)$, $\Delta H = -3.6 \text{ kcal./mole}$; $\text{Al}_2\text{O}_3(\delta) = \text{Al}_2\text{O}_3(\alpha)$, $\Delta H = -2.7 \text{ kcal./mole}$.

Introduction

Crystalline alumina (Al_2O_3) is known to occur in a series of different structural modifications. Among these only the α -modification (corundum) is thermodynamically stable. The various metastable forms are denoted β , γ , δ , κ , η , θ , χ and have been characterized by X-ray powder diagrams only. The conditions under which they form are not well understood. Characteristically they are obtained on the ignition of aluminum compounds, and the appearance of a particular phase depends on a variety of factors such as im-

purity content, temperature, particle size, quenching speed, etc.¹

All the various metastable modifications can be converted to the stable corundum form by ignition at sufficiently high temperatures. The conditions required for complete conversion change from one sample to another.

We have found no reliable information in the published literature on the heat of transformation of the

(1) See, e.g., M. Plummer, *J. Appl. Chem.* (London), **8**, 35 (1958); H. P. Roothsby, *ibid.*, **8**, 44 (1958).

various metastable forms to the stable corundum modification. This is not surprising since the conversion process is quite sluggish. Also corundum dissolves only with great difficulty in calorimetric solvents near room temperature. Thus the heat of transformation cannot be obtained from conventional solution calorimetry.

We were alerted to the interesting problems associated with the energy of transformation of the metastable aluminas to corundum through two considerations. On the one hand it has been noted on many occasions that the end product in the combustion calorimetry of aluminum compounds sometimes is a mixture of corundum with differing amounts of a metastable form.² As a consequence there is at times some uncertainty associated with the adopted value of the heat of combustion of aluminum. On the other hand, we have recently become interested in the thermodynamics of spinel formation, and it is known that one of the metastable forms of alumina (γ - Al_2O_3) has a defect spinel structure.³

In the present communication we report the results of a calorimetric study of the heats of solution of α -, γ -, δ -, and κ -alumina in a lead-cadmium-borate melt at 705°. From these results we have derived the heats of transformation of these metastable modifications to the α -form.

Experimental and Materials

The solvent used in the present work was prepared from reagent grade lead(II) oxide, cadmium(II) oxide, and boric acid, in the ratio 9PbO:3CdO:4B₂O₃. Forty grams of this mixture was melted down prior to each run in a platinum dish. Near the liquidus temperature (about 500°) this melt is very viscous. However, it is quite fluid at 700°, and at this temperature it dissolves alumina at a satisfactory rate. In our early work we attempted to use a pure lead borate solvent of composition 3PbO·B₂O₃, which melt has been used for the growing of single crystals of various oxides. However, we found that this melt attacked our gold and platinum containers.

Our alumina samples were prepared from three different starting materials. One sample (alumina-P) was obtained by ignition of aluminum hydroxide, which was precipitated from an aqueous solution of aluminum nitrate (Merck reagent grade, total non-volatile impurities <0.25%) with ammonium hydroxide. A second sample (alumina-C) was prepared by igniting a commercial preparation of aluminum hydroxide ($\text{Al}(\text{OH})_3 \cdot n\text{H}_2\text{O}$, Fisher Certified reagent). A third sample (alumina-A) was prepared by thermal decomposition of ammonium alum ($\text{NH}_4\text{Al}(\text{SO}_4)_2 \cdot$

12H₂O, Merck reagent grade). A sample of α - Al_2O_3 (Baker's Analyzed reagent) was used as a reference material. This oxide was sifted, and the finest material (-200 mesh) was used in our experiments in order to achieve a fast dissolution reaction. Finally, through the courtesy of Drs. G. T. Armstrong and R. C. King of the National Bureau of Standards, we obtained a small sample of δ - Al_2O_3 , which had been obtained as a reaction product in a bomb-calorimetric study of Al_4C_3 .

The samples of metastable alumina, contained in a platinum crucible, were heated in air. Most ignitions were carried out in a muffle furnace suitable for temperatures up to 1200°. In addition, two samples of alumina-A were ignited in a high frequency induction furnace at 1350 and 1450°. After each stage of heat treatment the samples were examined by X-ray powder diffraction, and the phase(s) present identified by comparison with patterns reported in the literature.⁴

The calorimeter was the same, and the experimental procedures similar to those adopted by Yokokawa and Kleppa⁵ in their recent calorimetric study of the PbO-V₂O₅ system. The only significant modification in procedure involved the method for adding the solid sample to the melt at 705°. In the present work the solid powder was contained in a shallow platinum spoon which was maintained before the reaction just above the surface of the melt. Dissolution of the sample was facilitated by moving the spoon up and down in the melt a few times. The temperature of the calorimeter was maintained at 705 ± 2° throughout the present work. Calibration was achieved by dropping small pieces of gold wire into the calorimeter from room temperature. The calibrating heat effects were computed from the heat content equation for gold given by Kelley.⁶ Small corrections were applied for the heat generated in the mixing operation and for the heat pickup of the gold pieces during the drop. The solvent was renewed after each two consecutive solution experiments. In the concentration range used (up to 150 mg. of Al_2O_3 /40 g. of solvent) we observed no concentration dependence of the heat of solution.

Results and Discussion

We present in Fig. 1 a graph of the experimental values of the heat of solution (kcal./mole of Al_2O_3)

- (2) G. T. Armstrong and R. C. King, private communication.
- (3) A. F. Wells, "Structural Inorganic Chemistry," 3rd Ed., Oxford University Press, 1962.
- (4) X-Ray Powder Data File, American Society for Testing Materials.
- (5) T. Yokokawa and O. J. Kleppa, *Inorg. Chem.*, **3**, 954 (1964).
- (6) K. K. Kelley, U. S. Bureau of Mines Bulletin 584, U. S. Government Printing Office, Washington, D. C., 1960.

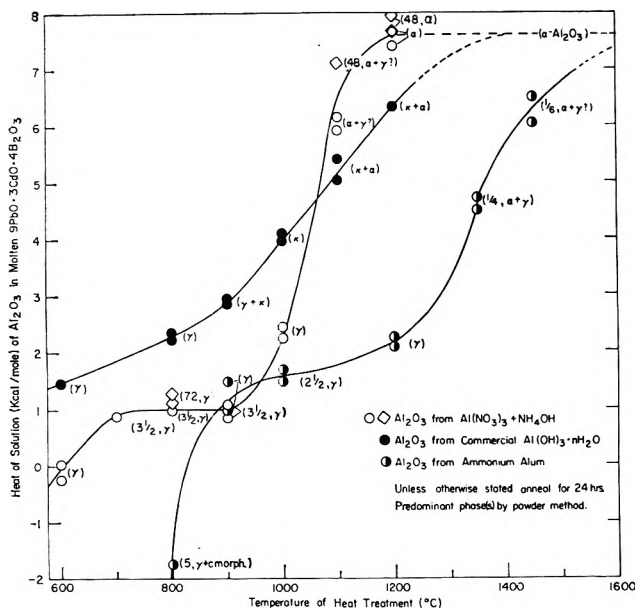


Figure 1. Enthalpies of solution for different heat treatments of three samples of alumina in a lead-cadmium-borate melt at 705°. Open symbols refer to alumina-P, filled circles to alumina-C, and semifilled circles to alumina-A.

plotted as a function of the temperature of heat treatment. Actually the transformation of the various metastable phases is quite sluggish and depends both on temperature and on the period of ignition. Unless otherwise indicated in the figure we used a standard 24-hr. period of heat treatment.

In Fig. 1 we have drawn three separate curves, which connect the experimental points relating to a common starting material. We also indicate in this figure the predominant phase(s) present in each sample, as shown by the X-ray powder pattern. Note, however, that the X-ray pattern for γ -alumina is quite diffuse because of the small particle size and the extent of crystal imperfection. Therefore, positive identification of this phase was difficult in many cases, even when the presence of the γ -phase was indicated by the heat of solution data.

The figure shows certain general features, which apply to all the three starting materials used. Thus, we see that alumina-A, -C, and -P form γ -alumina at low ignition temperatures. The samples of this phase are associated with small positive, and in some cases even with negative, enthalpies of solution. On the other hand we note that all samples, as expected, transform to α at high ignition temperatures. This phase has the largest positive enthalpy of solution.

When the temperature of ignition of γ -alumina is raised, the enthalpy of solution becomes more positive. We attribute this to the energy release associated with

crystal growth, to the removal of gross lattice imperfections, and possibly also to the removal of small amounts of volatile impurities. However, the latter effect undoubtedly is a minor one, since the weight losses on ignition were found to be quite small.

It will be noted also that usually the transformation from one modification to another seems to occur within a fairly narrow temperature range, different for each starting material. Thus, 3 days heating of alumina-P at 800° did not significantly affect its heat of solution. However, when the same material was heated at 1100°, the heat of solution was found to increase with increasing length of ignition time. As for alumina-A, ignition at 1200° for 24 hr. gave no significant transformation to α , while in 15 min. at 1350° almost half of the γ -alumina was converted to the α -form. Alumina-C did show a less sharp transformation behavior, possibly because of the appearance of the intermediate κ -phase between γ and α .

The heat of solution of Baker's Analyzed Al_2O_3 (corundum) was found to be +7.6 kcal./mole with a standard deviation for four separate experiments of ± 0.2 kcal./mole. α - Al_2O_3 from alumina-P, ignited at 1200°, and from δ - Al_2O_3 , ignited for 0.5 hr. at 1450° (not shown in Fig. 1), also gave heats of solution within the range 7.6 ± 0.2 kcal./mole. Thus, the heat of solution of α - Al_2O_3 in the solvent used must be considered to be fairly well established.

On the other hand, as already discussed above, the results for γ -alumina scattered over a fairly wide range. However, for each starting material, the highest heat of solution before the appearance of a new phase, was of comparable magnitude. The values are +2.4 kcal. for alumina-P, +2.3 kcal. for alumina-C, and +2.2 for alumina-A. Presumably at this stage γ -alumina has the most highly developed crystals with the least "stored" energy in the surface and in imperfections. We therefore have adopted the mean of these values, 2.3 kcal./mole, as the enthalpy of solution of γ - Al_2O_3 . Based on this result we have for the enthalpy of transformation, $\Delta H_{\gamma \rightarrow \alpha} = -5.3$ kcal./mole.

Turning next to κ -alumina, this phase was found only in alumina-C, and a definite arrest of the heat of solution curve was not observed. We estimate from our results the heat of solution of the κ -form to be +4 kcal./mole, *i.e.*, intermediate between the values for α and γ . Thus, we have $\Delta H_{\kappa \rightarrow \alpha} = -3.6$ kcal./mole.

In addition to the results plotted in Fig. 1, we carried out solution experiments with δ - Al_2O_3 . The mean of four separate experiments was 4.9 ± 0.3 kcal./mole. We accordingly obtain for the transformation of δ to α : $\Delta H_{\delta \rightarrow \alpha} = -2.7$ kcal./mole.

We did not in the present work observe the other metastable forms such as η , θ , or β .

Acknowledgment. This work has been supported in part by National Science Foundation Grant GP-1993.

Heat Capacity of Cobalt(II) Bromide from 74 to 450° and a Structural Change in the Vicinity of 370°

by Theodore J. Wydeven and N. W. Gregory

Department of Chemistry, University of Washington, Seattle 5, Washington (Received July 3, 1964)

The heat capacity of $\text{CoBr}_2(\text{s})$ has been measured over the range 74 to 450°. A minor reversible transition occurs in the stable form in the vicinity of 370°. Below the transition the heat capacity may be expressed as a function of temperature by the equation $C_P = 18.07 + 3.25 \times 10^{-3}T$ cal. mole⁻¹ deg.⁻¹. X-Ray powder pattern evidence indicates that the transition involves a change in crystal structure from what appears to be a $P\bar{3}m1$ (halogens in HCP array) form to an apparent $R\bar{3}m$ (CCP array) form. A modification in which the halogen layers are packed randomly has also been prepared; this form does not undergo a transition under similar conditions. The structural relationship of these various forms is discussed.

Recent investigations in this laboratory have shown a thermal anomaly at about 360° in the heat capacity of FeBr_2 .¹ The anomaly is believed to be associated with a change from the hexagonal close-packed $\text{Cd}(\text{OH})_2$ layer type crystal structure to the cubic close-packed CdCl_2 type structure.² We have also observed an anomaly in the heat capacity of CoBr_2 which is apparently associated with a crystal transformation similar to that found in FeBr_2 .

Experimental

Cobalt bromide was prepared from Baker's analyzed cobaltous carbonate and Mallinckrodt Analytical Reagent 48% hydrobromic acid. The solution formed by the reaction was dehydrated in air on a steam bath until crystals of cobalt bromide hexahydrate appeared. Dehydration, completed under vacuum at 130°, was followed by two vacuum sublimations at 550° (background pressure 10^{-5} mm.). A negligible amount of residue remained after the second sublimation.

The sample was analyzed for cobalt by electrodeposition as cobalt metal.³ Bromine was determined by precipitation as AgBr . Results of the analysis of three samples follow.

Anal. Calcd. for CoBr_2 : Co, 26.94; Br, 73.06. Found: Co, 26.91, 27.00; Br, 73.11, 73.09, 73.10.

X-Ray fluorescence analysis of a sample indicated only a trace amount of nickel in addition to cobalt and bromine.

A continuous heating adiabatic vacuum calorimeter, with only minor modifications from that described previously, was used to measure the heat capacity.^{4,5}

(1) N. W. Gregory and H. E. O'Neal, *J. Am. Chem. Soc.*, **81**, 2649 (1959).

(2) N. W. Gregory and T. Wydeven, *J. Phys. Chem.*, **67**, 927 (1963).

(3) J. L. Hague, E. E. Maczkowsek, and H. A. Bright, *J. Res. Natl. Bur. Std.*, **53**, 353 (1954).

(4) H. E. O'Neal and N. W. Gregory, *Rev. Sci. Instr.*, **30**, 434 (1959).

(5) T. J. Wydeven, Ph.D. Thesis, University of Washington, Seattle, Wash., 1964.

In the present work the calorimeter was calibrated electrically and checked by measurement of the heat capacity of $\alpha\text{-Al}_2\text{O}_3$. Results were compared with those published by the National Bureau of Standards.⁶ The standard deviation of our experimental points from the NBS curve was $\pm 2\%$. The total energy input between room temperature and 500° was reproducible to within $\pm 0.6\%$. A heating rate of about $0.88 \text{ deg. min.}^{-1}$ was found to be satisfactory.

The average energy input, corrected for lead losses, for the empty cell and the filled cell, respectively, was measured for similar heating rates at the end of each $70\text{-}\mu\text{v.}$ (Pt—Pt—10% Rh thermocouple) increment of temperature, except for intervals where an anomaly existed in which case increments ranging from 10 to $35 \mu\text{v.}$ were used. These values were then summed for four $70\text{-}\mu\text{v.}$ increments (except in the anomaly region) and the average energy per microvolt plotted vs. the average sample temperature for each $280\text{-}\mu\text{v.}$ interval. A representative plot of data from four of thirteen runs is shown in Fig. 1. The smooth curve drawn was obtained by least squares of all data. In the region of a thermal anomaly no such summations were made; here the corrected average energy input per microvolt was obtained for each of the 10 to $35\text{-}\mu\text{v.}$ increments of temperature.

Heat capacities were calculated by subtracting the contribution of the empty cell and multiplying by the calibrated thermocouple conversion factors to change the values from calories per microvolt to calories per degree. A plot of such values, corresponding to those in Fig. 1, is shown in Fig. 2. An equation corresponding to the behavior in the interval where no anomaly exists was fitted by least squares. In previous work using this calorimeter,⁴ heat capacities were calculated from smoothed curves of the form shown in Fig. 1. The present method is believed to give a better representation of the experimental data.

The cobalt bromide was transferred in a drybox from the sublimation tube to the calorimeter cell which was then attached to the vacuum line (ultimate background pressure 10^{-5} mm) and heated at 475° for several hours to remove traces of moisture. Then 200 mm. pressure of dry argon gas was introduced before scaling off. The cobalt bromide sample weighed 211.00 g.

CoBr_2 , resublimed as described and cooled to room temperature, forms crystals (with the $\text{Cd}(\text{OH})_2$ -type structure, apparently $P\bar{3}m1$) in which the halogen atoms are in a hexagonal close-packed (HCP) array. The heat capacity measurements were made with this material. It was found that samples in which the halogen layers are stacked randomly are formed on dehydra-

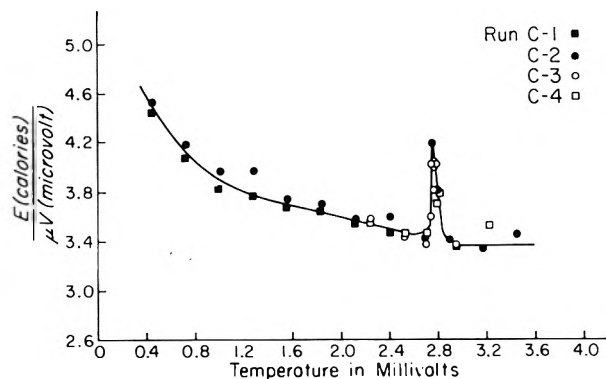


Figure 1. Energy per microvolt (Pt—Pt—Rh thermocouple) for cell filled with cobalt bromide.

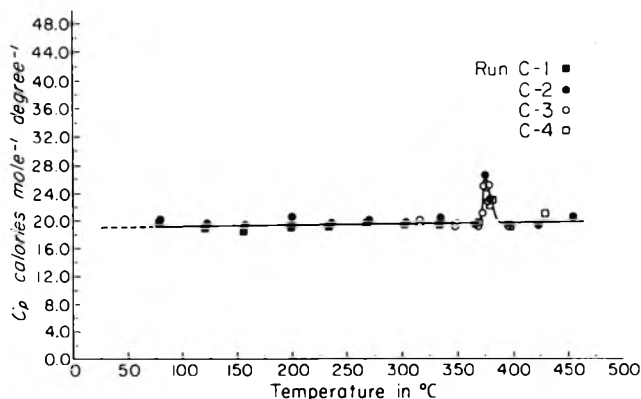


Figure 2. Heat capacity as a function of temperature for cobalt bromide.

tion of cobalt bromide hexahydrate under vacuum at 130° . The heat capacity of this material was not measured but its behavior was studied by X-ray powder and differential cooling thermal analysis experiments.

High temperature X-ray powder photographs were taken with an apparatus described previously.^{1,5} $\text{Mo K}\alpha$ radiation was used and scattering detected on a rotating flat photographic plate approximately 4.5 cm. from the sample, sealed in a Pyrex capillary filled with 200 mm. pressure of dry argon gas. Exposure times of about 72 hr. were required. Room temperature X-ray patterns were also taken with a conventional Debye—Scherrer powder camera. Whereas a single crystal X-ray study will be needed to determine the structures of these various forms with certainty, the powder data are adequate to show the nature of the packing of the halogen atoms in the various forms.

Results and Discussion

Heat capacity data for four representative runs (from a total of thirteen) on ordered crystals of cobalt

(6) G. T. Furukawa, T. B. Douglas, R. E. McCoskey, and D. C. Ginnings, *J. Res. Natl. Bur. Std.*, **57**, 67 (1956).

Table I: Powder Pattern Results for Cobalt Bromide

Room temperature ordered form (Cd(OH) ₂ type) <i>a</i> = 3.68 Å., <i>c</i> = 6.12 Å. (18.36 Å.)					Room temperature random form <i>a</i> = 2.13 Å., <i>c</i> = 6.12 Å.					443 ± 20° ordered form (CdCl ₂ type) <i>a</i> = 6.61 Å. (3.76 Å.), <i>c</i> = 33° 2' (<i>c</i> = 18.73 Å.)				
<i>hkl</i>	<i>d</i> , obsd.	<i>d</i> , calcd.	<i>I</i> ₀ ^a	<i>I</i> _c (rel.)	<i>hkl</i>	<i>d</i> , obsd.	<i>d</i> , calcd.	<i>I</i> ₀ ^a	<i>I</i> _c (rel.)	<i>hkl</i>	<i>d</i> , obsd.	<i>d</i> , calcd.	<i>I</i> ₀ ^a	<i>I</i> _c (rel.)
001 (003)	5.85	6.12	vs	51	001 (003)	5.94	6.12	m	51	222 (006)	3.17	3.13	m	10
100 (100)	3.17	3.19	w	0.3						110 (012)	3.12	3.08	m	30
002 (006)	3.01	3.06	s	27	... (103)	-2.798	2.830	m	...	211 (104)	2.70	2.67	vs	100
101 (103)	2.798	2.830	vs	42						332 (018)	1.88	1.90	vs	38
102 (106)	2.197	2.208	m	21	100 (110)	1.842	1.842	vs	100	101 (110)				
110 (110)	1.845	1.842	m	100	101 (113)	1.762	1.764	vw	6					
111 (113)	1.762	1.764	w	13						433 (1010)	1.60	1.62	m	5
103 (109)	1.718	1.719	m	66	102 (116)	1.575	1.578	w	13	220 (024)	1.53	1.54	m	20
112 (116)	1.576	1.578	w	26	104 (0012)	1.529	1.530	w	18	111 (021)	1.45	1.46	vw	1
004 (0012)	1.528	1.530	s	18						331 (027)	1.38	1.40	vw	1
202 (206)	1.412	1.415	vw	18					432 (119)	1.38				
203 (209)	1.262	1.257	vw	4						422 (208)	1.33	1.34	w	3
005 (0015)	1.222	1.224	vw	0.6						544 (1013)	1.32	1.32	w	0.8
211 (213)	1.182	1.183	vs	6	104 (1112)	1.177	1.177	s	23	310 (214)	1.19	1.19	w	17
114 (1112)		1.177		46							431 (128)	1.07	1.09	vw
105 (1015)	1.145	1.143	vw	3					300 (303)	1.07	1.07			
212 (216)	1.123	1.122	vw	16	110 (300)	1.067	1.064	vw	16					
300 (300)	1.072	1.064	vw	16						200 (220)	0.9258	0.9214	vw	10
301 (303)	1.046	1.048	vw	1						114 (3012)	0.8761	0.8735	m	6
006 (0018)	1.020	1.020	vw	1										
115 (1115)		1.019		2										
205 (2015)	0.9723	1.9709	m	9										
310 (310)	0.8807	0.8850	m	0.2										

^a vs, very strong; s, strong; m, medium; w, weak; vw, very weak.

bromide are shown in Fig. 2. A thermal anomaly, beginning at about 366° and extending over a temperature range of 18°, can be seen clearly in both Fig. 1 and 2. The heat of transition indicated by graphical integration is 40 ± 15 cal. mole⁻¹; for example, values of 54, 51, and 26 were obtained in three successive runs on the same sample. The corresponding values for the entropy of transition, also obtained by graphical integration, were 0.08, 0.08, and 0.04 cal. deg.⁻¹ mole⁻¹. The anomaly was observed each time after several heating and cooling cycles with no apparent difference (within experimental error) in the measured heat of transition. No thermal anomalies were observed in the temperature range 74–366°. The heat capacity in this interval can be expressed by the equation $C_P = 18.07 + 3.25 \times 10^{-3}T$, where C_P is in defined calories per mole degree and T is in °K. The heat capacity for CoBr₂ at 298.15°, obtained by linear extrapolation, is 19.04 cal./mole deg. The estimated uncertainty is ± 3%.

Since a continuous heating method was used, it is difficult to determine whether the transition occurs at a fixed temperature and involves a latent heat or whether it occurs over a temperature interval. The temperature gradient across the cell was only *ca.* 7° in the region of the transition, whereas the anomaly appears to be spread over an interval of about 18°. The transition is of minor importance in its effect on the enthalpy and entropy of cobalt bromide.

X-Ray powder photographs of CoBr₂ taken at a sample temperature of 443 ± 20° were definitely not of the HCP type characteristic at room temperature,⁷ but could be correlated on the basis of a CdCl₂ type structure (apparently R $\bar{3}m$); see Table I. The unit cell constants in parentheses and the indices *hkl* in parentheses are for a nonprimitive hexagonal cell which is convenient for comparison of the room temperature and high temperature structures. Only

(7) A. Ferrari and F. Giorgi, *Rend. accad. Lincei*, **9**, 1134 (1929).

those reflections are observed in the high temperature structure for which the nonprimitive hexagonal cell indices satisfy the condition $-h + k + l = 3n$. The observed d -spacings agree with those calculated to within ± 0.02 Å. (the high temperature apparatus was not designed for high precision) with good agreement between the calculated and observed relative intensities. The cell constants for the high temperature structure correspond to those for the low temperature form if one assumes a linear thermal expansion of about 2%.

Powder patterns of CoBr_2 taken at a sample temperature of $280 \pm 20^\circ$, below the transition temperature, indicated the same HCP type structure observed at room temperature.

X-Ray pattern characteristics of the random-packed material, formed by dehydration of the hydrate at 130° , are also shown in Table I. Again the cell constants and the indices in parentheses are for the nonprimitive hexagonal cell. With the exception of one weak reflection (corresponding to the 101 reflection of HCP CoBr_2) the "random" patterns could be indexed on the basis of the small cell shown, which is to be expected for a truly random-packed structure. A similar result has also been observed for CdBr_2 .⁸

Random-packed CoBr_2 did not appear, from X-ray powder photographs taken at a sample temperature of $415 \pm 20^\circ$ during a 72-hr. exposure, to transform to an ordered structure. Neither could evidence for a transition be found in differential cooling thermal analysis experiments between 500° and room temperature.⁵ Samples were converted to an ordered structure by annealing at 525° for 15 hr. These results suggest that the conversion of random-packed samples to the ordered structures takes place only through recrystallization, possibly *via* vaporization, and that the transformation to the CCP structure does not occur as readily as for the HCP form. An explanation for this behavior may be suggested as follows.

In each of these crystalline modifications metal "ions" are "sandwiched" in between alternate layers of close-packed halogen "ions." Consider the representation of idealized HCP and CCP forms shown in Table II (X represents bromine atoms, M cobalt atoms;

the symbols A, B, and C are the common notations used to designate the various layers of a close-packed

Table II

HCP	CCP
$X_A (0, 0, 0)$	$X_A (0, 0, 0)$
$M (2/3, 1/3, 1/12)$	$M (2/3, 1/3, 1/12)$
$X_B (1/3, 2/3, 2/12)$	$X_B (1/3, 2/3, 2/12)$
$X_A (0, 0, 4/12)$	$X_C (2/3, 1/3, 4/12)$
$M (2/3, 1/3, 5/12)$	$M (1/3, 2/3, 5/12)$
$X_B (1/3, 2/3, 6/12)$	$X_A (0, 0, 6/12)$
$X_A (0, 0, 8/12)$	$X_B (1/3, 2/3, 8/12)$
$M (2/3, 1/3, 9/12)$	$M (0, 0, 9/12)$
$X_B (1/3, 2/3, 10/12)$	$X_C (2/3, 1/3, 10/12)$

structure; the fractions in parentheses are the atomic positions (x, y, z) as fractions of the nonprimitive hexagonal cell dimensions (see Table I).

To transform the HCP structure into the CCP structure the second and third sandwiches may be shifted as a whole (by $2/3$ in the x value and $1/3$ in the y value for the second and by $1/3$ in the x value and $2/3$ in the y value for the third). This only involves disruption of van der Waals interactions between the sandwich units and does not necessarily require the rearrangement of metal-halogen bonds. However for the transformation of a random-packed structure to an ordered form it will be necessary, in the general case, to realign the layers which constitute the "minimal" sandwich,^{9,10} that is to disrupt the halogen-metal bonds. The latter process may be expected to require a considerably greater activation energy than the HCP to CCP transition and would seem to account for the different behavior of the random packed form.

Acknowledgment. This work was supported by a grant from the U. S. Army Research Office (Durham) which is acknowledged with thanks.

(8) J. M. Bijvoet and W. Nieuwenkamp, *Z. Krist.*, **86**, 466 (1933).

(9) A. J. Forty, *Phil. Mag.*, **43**, 377 (1952).

(10) G. Hagg, *Arkiv Kemi*, **B16**, No. 3, 1 (1943).

Flash Photolysis in Thin Films of Gelatin and Other Polymers¹

by A. V. Buettner

Research Laboratories, Eastman Kodak Company, Rochester, New York 14650 (Received July 3, 1964)

The kinetics of the decay of the triplet states of molecules at room temperature may be studied conveniently by flash photolysis of solutions of the molecules in thin polymeric films. The samples can be deoxygenated by merely passing nitrogen over the surface of the film. The permeability of some polymers to oxygen is low enough so that oxygen quenching is restricted to the point where triplets have measurable lifetimes even with the film in contact with air. A comparison of the decay rates in such a polymer when the film is in equilibrium with air with those when the film is in equilibrium with nitrogen reveals whether or not any significant oxygen quenching remains after deoxygenation. The absorption spectra and decay kinetics of the triplet states of anthracene, 2-naphthol, and three xanthene dyes were examined. The rates of decay at room temperature were from two to four times higher than the lowest reported rates in glasses at 77°K. Despite triplet concentrations as high as $6 \times 10^{-4} M$, no triplet self-quenching was observed.

Introduction

It is well known that in the flash photolysis of liquid solutions, it is necessary to remove dissolved oxygen from the solution by careful degassing. Oxygen molecules react efficiently with free radicals and excited electronic states, so that even traces of oxygen may greatly reduce the lifetimes of transient species from their intrinsic value. In the course of studies of the photographic process by flash photolysis, we have been able to follow, at room temperature, the transients accompanying the flashing of certain dyes and other compounds dissolved in thin films of gelatin and other polymeric matrices. It appears that, even if such films are photolyzed in air, access of oxygen to the transient species in some films is sufficiently inhibited to allow these species not only to have measurable decay times, but, if their intrinsic lifetime is relatively short, to decay practically uninfluenced by oxygen quenching. Consistent with this is the work of Meluish and Hardwick² on the flash photolysis of anthracene in Lucite plastic blocks at room temperature, of Moore and Windsor,³ Oster and co-workers,⁴ and El-Sayed⁵ on the phosphorescence of aromatic compounds in various polymers at room temperature, and of Iwaki⁶ on the lifetimes of dye-gelatin phosphors.

If the transient species has a measurable rate of decay when the sample is in equilibrium with air, a com-

parison of this rate with the rate when the sample is in equilibrium with nitrogen reveals the extent of oxygen quenching in air and whether any significant oxygen quenching remains after deoxygenation with nitrogen. Because of the large ratio of surface to volume for the films, equilibrium with a nitrogen atmosphere can be readily achieved.

Experimental Methods

Material. Eastman Grade 2-naphthol, General Aniline Histological Grade erythrosin and eosin, and Eastman anthracene (special grade for blue-violet fluorescence) were used without further purification. Eastman rose bengal, technical grade, was recrystallized from hot water.

Eastman Grade purified calfskin gelatin (pH 4.7, isoelectric point 4.8), Du Pont polyvinyl alcohol 72-60 (PVA), General Aniline polyvinylpyrrolidone (PVP),

(1) Presented in part at Photochemistry Symposium, University of Rochester, March, 1963.

(2) W. H. Meluish and R. Hardwick, *Trans. Faraday Soc.*, **58**, 1908 (1962).

(3) R. S. Moore and M. W. Windsor, *Spectrochim. Acta*, **18**, 1364 (1962).

(4) G. Oster, N. Geacintov, and A. Ullah Khan, *Nature*, **196**, 1089 (1962).

(5) M. A. El-Sayed, *J. Opt. Soc. Am.*, **53**, 797 (1963).

(6) (a) R. Iwaki, *Nippon Kagaku Zasshi*, **74**, 503 (1953); (b) R. Iwaki, *ibid.*, **75**, 843 (1954).

and sodium acrylate-ethyl acrylate copolymer (PNaEA), which was prepared in these laboratories, were used without purification. Koppers 8X polystyrene was precipitated from hot cyclohexane before use. Nitrogen was Airco H.P. dry.

Preparation of Films. Approximate 1% solutions of PVA, PVP, or PNaAEA in water and 10% solutions of polystyrene in toluene were prepared. The solutes were then dissolved in these dopes, which were poured on glass or Vycor plates to a depth of about 1 mm. or more and allowed to dry. To get reasonable optical quality, the films must dry slowly (overnight). An inverted Petri dish was placed over the polystyrene film to slow the drying.

Six-per-cent aqueous solutions were prepared by allowing the necessary amount of gelatin to swell in water for a few hours and heating the gelatin to $\sim 40^\circ$ until it dissolved. Solute was added and the warm solution poured on a glass plate. On cooling to room temperature, the solution gelled and could then be dried quite rapidly. Since it gelled before it dried, there was little migration of either the solute or the polymer toward the edges of the film during drying, as there was with the other media.

Most films when dry were from 10 to 40 μ thick, although some thicker ones were used.

Apparatus and Measurements. The flash-photolysis apparatus was similar to those described by Livingston and Tanner⁷ and by Linschitz and Sarkanen.⁸ The change of the optical density was measured photoelectrically at a selected wave length and displayed on a Tektronix 535 oscilloscope as a function of time. Changes of density of ± 0.001 were reliably measured. The energy per flash was 10 joules (0.2 μ f., 10 kv.); the flash was triggered by a spark gap in series with the flashtube. The gap was broken down by a high-voltage ignition pulse, which, in turn, was triggered by the low-voltage, "delayed-trigger" output pulse from the oscilloscope. The flash could therefore be set to fire at any time during the sweep of the oscilloscope. The ignition pulse was generated by discharging a 0.5- μ f. capacitor charged to 270 v. through the primary of a UTC, PF-3 ignition coil in series with a silicon-controlled rectifier. Since the impedance of the silicon-controlled rectifier was too low to be triggered directly by the output pulse from the oscilloscope, the oscilloscope and the silicon-controlled rectifier were coupled through an emitter follower. To provide d.c. isolation between the ignition coil and the high voltage on the trigger electrode, the secondary of the coil was coupled to the trigger electrode through two 500- μ f., 30-kv. capacitors in series. A General Electric FT-110 xenon flashtube, with a glass envelope, was used for

most of the work, but the General Electric FT-127, with a quartz envelope, was used for films containing 2-naphthol, for which excitation farther into the ultraviolet region was needed. Both flashes had a half-width of 3 μ sec., but the FT-110 had a shorter tail, dropping to 1% intensity in less than 25 μ sec.

The flashtube was enclosed in a metal box lined with barium sulfate. To follow the transient changes in optical density in the flashed film, measuring light from the small filament of a tungsten lamp (G.E. No. 1594) was collimated, passed through the box by means of windows at each end, through the sample, which was placed over the exit window, and then focused on the entrance slit of the monochromator. The flashtube was placed near one side of the box so as not to interfere with the measuring beam. A selected wave length of the measuring beam was passed through the monochromator to an RCA 1P28 photomultiplier tube, coupled to the oscilloscope through a cathode follower. The measuring lamp was powered by an Electro D-612T filtered d.c. supply and the photomultiplier tube by a Northeast Scientific RE-1602 regulated high-voltage supply (300-1600 v.).

When a nitrogen atmosphere was desired, the film was placed in a flat cell, through which nitrogen was passed, and the cell was positioned on the window of the box. Nitrogen continued to flow over the sample during the flashing.

To measure phosphorescence from a sample, the film on its support was placed inside the box, parallel to the flashtube, with one edge of the support in the exit window. The support acts as a light-guide conveying the luminescence of the film to the edges, and the brightly illuminated edge of the support was imaged on the entrance slit of the monochromator. The light from the flash was prevented from reaching the photomultiplier tube by a photographic shutter (Kodak, No. 2 Supermatic). With the flash synchronization set on M delay, the shutter contacts closed 12 msec. before the shutter opened. The closing contacts triggered the oscilloscopic trace, and the "delayed-trigger" output pulse was set to delay the flash 10 msec. after the start of the trace to minimize the time between the flash and the opening of the shutter. Unfortunately, both flashlamps emitted a slow phosphorescence of their own, with a lifetime of ~ 10 msec.; it was much too dim to affect the flash-photolysis measurements but it prevented the measurement of phosphorescence until 50 msec. after the flash.

(7) R. Livingston and D. W. Tanner, *Trans. Faraday Soc.*, **54**, 765 (1958).

(8) H. Linschitz and K. Sarkanen, *J. Am. Chem. Soc.*, **80**, 4826 (1958).

Results and Discussion

1. *2-Naphthol*. The absorption spectrum of the triplet state of 2-naphthol in degassed solutions of water and liquid paraffin was observed by Jackson and Porter⁹ by means of flash photolysis; the maximum absorption was at 433 m μ in liquid paraffin and 432 m μ in water. No decay times were reported, except that the triplet absorption was "measurable" for 0.5 msec.

Figure 1 summarizes a series of decay curves for the transient absorption induced by successive 10-joule flashes of a rather thick (120- μ), air-dried film of 2-naphthol in gelatin on Vycor. The sample was positioned with the Vycor support toward the flash. In the spectral region where the exciting light was absorbed, the optical density averaged about 2, so that most of the excited molecules were close to the support and relatively few were near the free surface. The transient species produced by the first flash decayed according to first-order kinetics with a mean life, τ , of 15 msec. No phosphorescence could be seen as a result of this flash, but it would not be detectable in our present apparatus during the short lifetime of the transient formed by the first flash because of the phosphorescence from the walls of the flashtube. A second flash produced the same amount of transient, which then decayed with slow and fast components, and, with increasing number of flashes, the proportion of

transient decaying by the slower process (or processes) increased. After about seven flashes, a steady state was reached, unchanged by further flashing. With the sample in this steady state, the transient decayed principally by a first-order process with τ 0.47 sec., and a small amount decayed by a much faster process. The transient absorption spectrum with a maximum at 443 m μ was unchanged during the decay, indicating that only one labile species was involved.

After a few flashes in such a series, a bright green phosphorescence could be seen, increasing in intensity until the steady state was reached. As is shown in Fig. 1, the phosphorescence and the transient absorption decayed at the same rate, consistent with the identification of the transient as the triplet state.

These observations, along with others to be described, suggest that the changes in the rate of decay of the triplet state of 2-naphthol in the films largely depended on the changes of the oxygen content of the films during the sequence of flashes. The film was initially saturated with oxygen in equilibrium with atmospheric oxygen and the fast decay associated with the first flash was the result of oxygen quenching at the saturated oxygen content of the gelatin. During the exposures, the dissolved oxygen was photochemically consumed more rapidly than it could be replaced by diffusion from the surface; in the steady state, much less oxygen quenching occurs than initially. Since the energy per flash was only 10 joules, it is probable that a single 100-joule flash, as is used in many flash apparatus, would be sufficient to bring such a sample to the steady state.

Figure 2 shows the decay of the 2-naphthol triplet in the same film taken to the steady state by successive flashing, left in air for a time, and then subjected to a single flash. After standing for 4 hr., no change in decay was observed, but after 1 day there was considerably more fast decay than slow decay, and after 5 days there was only first-order decay with τ 15 msec. The series of decays suggests that the oxygen diffuses into the film from the air, first producing an inhomogeneous quenching of the triplet in the oxygen concentration gradient set up in the film, and ultimately causing homogeneous quenching as oxygen equilibrium is attained throughout the film.

Figure 3 shows the decay of the 2-naphthol triplet when the same sample as was used to obtain the data in Fig. 1 and 2 was reversed so that the free gelatin surface, instead of the Vycor surface, faced the flash. Most of the exciting radiation was therefore absorbed in the film near the gelatin-air surface, where photo-

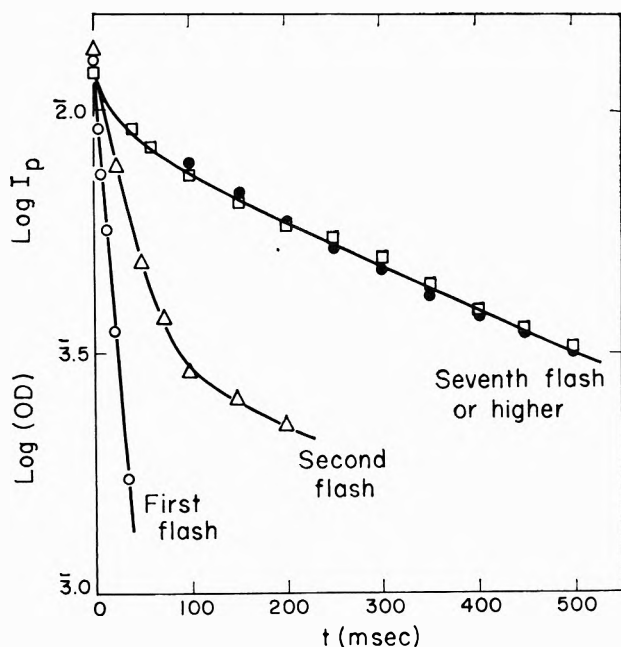


Figure 1. Decay of the triplet state of 2-naphthol in a 120- μ thick gelatin film, on Vycor, in air, Vycor surface facing the flash: O, Δ , and \square , optical density at 440 m μ ; \bullet , relative phosphorescence intensity at 530 m μ .

(9) G. Jackson and G. Porter, *Proc. Roy. Soc. (London)*, **A260**, 13 (1961).

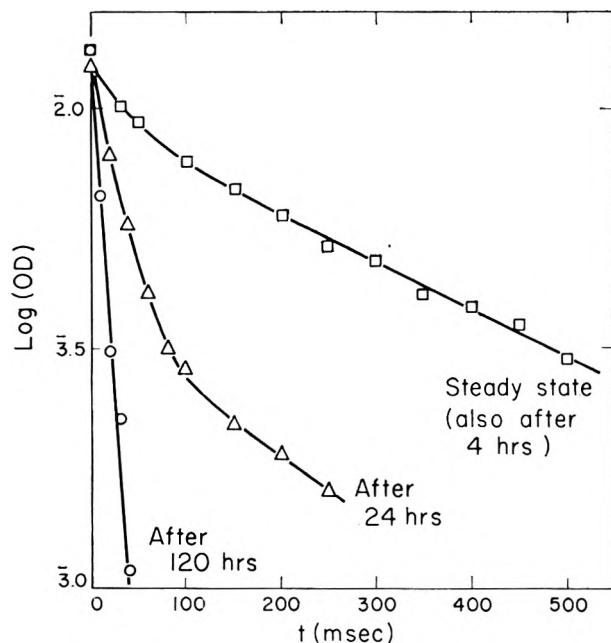


Figure 2. Decay of the triplet state of 2-naphthol in a 120- μ thick gelatin film, on Vycor, in air, Vycor surface facing the flash; $\lambda = 443 \text{ m}\mu$. Excitation was by the first flash a given time after the sample had been brought to the steady-state condition by successive flashes.

chemically consumed oxygen could be replaced more easily than under the conditions of Fig. 1 and 2, where oxygen had to diffuse through the thickness of the film to reach the photoexcited molecules. Hence, as shown in Fig. 3, repeated flashing again resulted in a steady state, but this state showed a greater component of the first decay of the triplet, and, when the film was left in air, the steady state persisted for a much shorter time than that shown in Fig. 2.

There was very little permanent change in the sample; after over 100 flashes, the absorption spectrum showed less than 3% loss of 2-naphthol and a small increase (0.03) in optical density throughout the blue and the near-ultraviolet regions.

A thinner film ($\sim 20 \mu$) with approximately double the naphthol concentration had an average O.D. of ~ 0.6 and absorbed exciting radiation throughout the thickness of the film, so that even with excitation through the Vycor backing, much of the radiation was absorbed near the air surface. Under these conditions the thinner film behaved very much like a thicker film exposed from the front.

When such a thin film was dried in a current of nitrogen for 1 day, the first flash produced a triplet which decayed in the same way as a thick film after multiple flashes. Also, bright green phosphorescence was observed after the first flash. Successive flashing

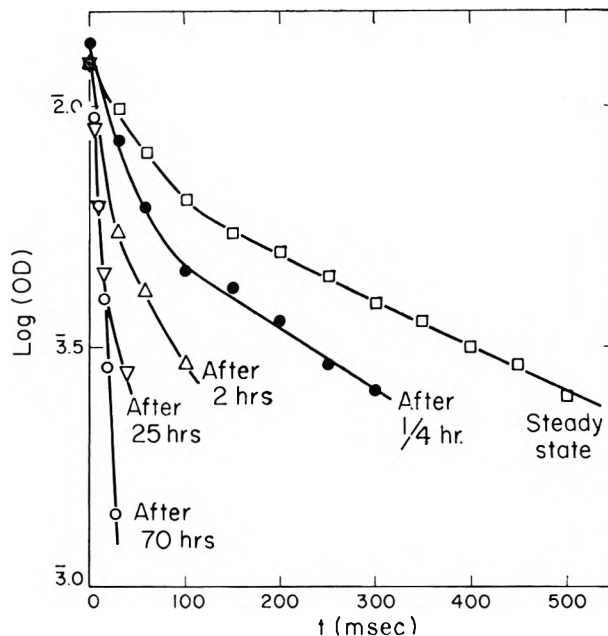


Figure 3. Decay of the triplet state of 2-naphthol in a 120- μ thick gelatin film on Vycor, in air, gelatin surface facing the flash; $\lambda = 443 \text{ m}\mu$. Excitation was by the first flash a given time after the sample had been brought to the steady-state condition by successive flashes.

and continuation of the nitrogen flow for 2 more days did not increase τ , which was 0.47 sec. The film could also be dried in air and brought into equilibrium with nitrogen by passing nitrogen over it for 1 day, after which the first flash produced a similar effect. The effect of nitrogen is not merely one of drying the gelatin matrix^{6a} but of removal of oxygen. Nitrogen which had been bubbled through a saturated solution of NaBr in water to give a relative humidity of $\sim 57\%$ did not give a significantly different effect from that of dry nitrogen.

We conclude that 0.47 sec., corresponding to the first-order decay constant $k_1 = 2.1 \text{ sec.}^{-1}$, is the mean life of the triplet state of 2-naphthol at room temperature, free from oxygen quenching. At 77°K. in a rigid glass, McClure found, from phosphorescent decay, that the mean life was 1.3 sec.¹⁰

2. *Xanthene Dyes.* Transient bleaching of the ground singlet accompanied by transient absorption of a labile species has been observed in gelatin films containing eosin (2,4,5,7-tetrabromofluorescein), erythrosin (2,4,5,7-tetraiodofluorescein), and rose bengal (2,4,5,7-tetraiodo-3',6'-dichlorofluorescein). These transients probably are the triplet state of these dyes.

The transient spectral changes of the erythrosin in

(10) D. S. McClure, *J. Chem. Phys.*, **17**, 905 (1949).

gelatin film are shown in Fig. 4. The conversion with a 10-joule flash is assumed to be 44%. If a conversion of 5% greater or less than this is assumed, the spectrum of the triplet would be quite similar except that a sharp peak or dip (dotted lines in Fig. 4) would appear at 538 m μ , the position of the ground singlet peak. Such a coincidence of a peculiar spectral feature of the triplet with the absorption peak of the dye is improbable and the abnormalities are almost certainly the results of over- and underestimates of the conversion. The absorption of the species is diffuse, with a peak overlapping that of the ground singlet. Similar transient spectra were found for eosin and rose bengal. However, the mean life of these labile species decreases

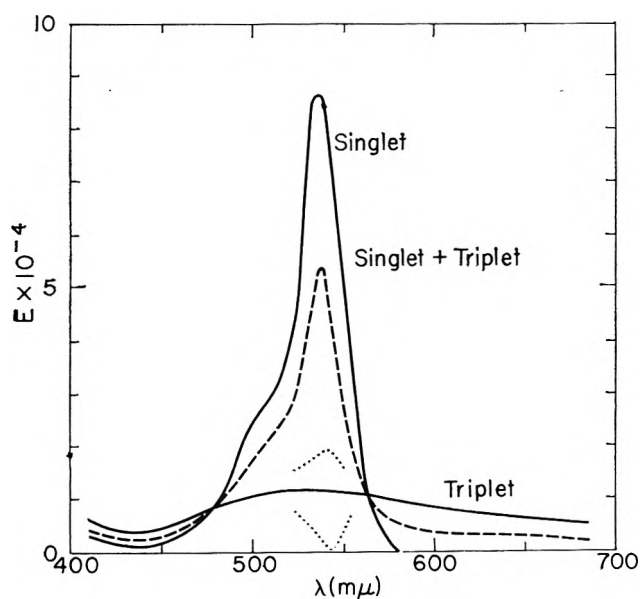


Figure 4. Absorption spectra, erythrosin in gelatin.

with increasing atomic weight of the substituents: eosin, 4.2 msec.; erythrosin, 0.63 msec.; and rose bengal, 0.32 msec. This sequence is consistent with the "heavy-atom effect" and is evidence of the production of triplet states. These values for τ of the eosin and erythrosin transients are roughly half those reported by Forster and Dudley¹¹ for the mean life of the phosphorescence of eosin (9.4 msec.) and erythrosin (1.3 msec.) in a rigid glass at 77°K. Also consistent with the identification as the triplet state is the extreme permanence of the samples, despite over 40% conversion per flash. If free radicals were produced, some permanent destruction of the dye should have occurred.

Since oxygen quenching of the triplet state is usually a very efficient process, occurring at nearly every encounter, the observed oxygen-quenched decay of 2-

naphthol, with τ about 15 msec., is probably about the general value to expect for oxygen quenching of triplets formed in air-saturated gelatin films at room temperature. Triplets whose natural decay time is much less than 15 msec. are therefore expected not to be greatly influenced by oxygen quenching in gelatin films flashed in air. In fact, the lifetime of the triplet state of erythrosin in gelatin was not increased significantly after placing the film in a stream of nitrogen for 18 hr.

Figure 5 shows the decay of the triplet state of erythrosin in different matrices, as measured by transient bleaching of the ground-state absorption.

In polyvinyl alcohol (PVA) film in air, the triplet decay is, within the limits of experimental error, the same as that in gelatin, with τ equal to 610 μ sec., and, as expected, it does not increase significantly in nitrogen.

In films of the sodium salt of the copolymer of ethyl acrylate and acrylic acid (PNaAEA), the transient of erythrosin decayed with τ 660 μ sec. after drying in nitrogen overnight, and this is scarcely changed after the film has been kept in a stream of nitrogen for 3 days. After standing in air for 40 min., the film which had

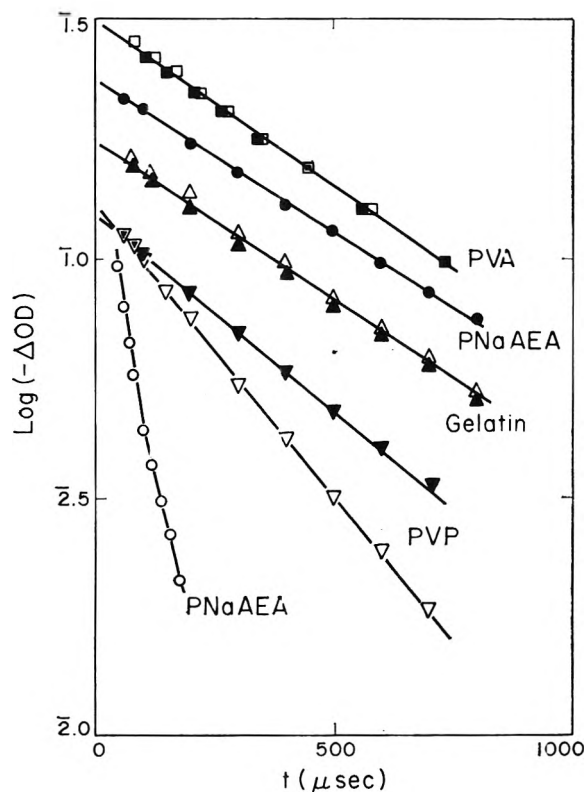


Figure 5. Decay of the triplet state of erythrosin in various matrices: O, \square , Δ , and ∇ , sample in air; \bullet , \blacksquare , \blacktriangle , and \blacktriangledown , sample in nitrogen.

(11) L. S. Forster and D. Dudley, *J. Phys. Chem.*, **66**, 838 (1962).

been freed from oxygen by 3-days' passage of a stream of nitrogen showed a mean life of 80 $\mu\text{sec.}$; this does not decrease with a longer time in air. A higher oxygen permeability for the film of this polymer than for gelatin or PVA is indicated. Because of this permeability, a correspondingly short purging of the air-equilibrated film for 20 min. in nitrogen increased the mean life of the erythrosin triplet to 650 $\mu\text{sec.}$ This 650- $\mu\text{sec.}$ mean life is not greatly different from the mean life in gelatin or PVA in air or in nitrogen and represents the triplet decay uninfluenced by oxygen quenching. Since the nitrogen purging increased τ by a factor of less than ten, whereas it must have decreased the oxygen concentration to less than 1/1000 of the value in air, any effect of oxygen on the longer τ must be negligible.

Erythrosin in polyvinyl pyrrolidone (PVP) showed some oxygen quenching (τ 320 $\mu\text{sec.}$) in air, but on flushing with nitrogen for 7 min., τ increased to 530 $\mu\text{sec.}$ and did not increase significantly after 1–1.5 hr. more.

Thus, even though the oxygen is removed, the rate of decay is greater in PVP than in the other matrices. This is probably connected with the fact that the spectrum of the erythrosin ground state undergoes a pronounced red shift in PVP, with the absorption maximum at 553 $m\mu$. In the other matrices the peak is at 538–540 $m\mu$, similar to its position in alcohol solvent. This shift and the accompanying increase in the rate of decay of the triplet state may be due to the molecules being "bound" to the polymer.¹²

Repeated flashing did not increase the mean life of the triplet state of erythrosin, eosin, or rose bengal in any of the matrices. When the gelatin films containing 2-naphthol or erythrosin were wet in contact with air, no transients were observed, probably because of much freer passage of oxygen through the samples.

Although the mean life of the triplet state of eosin in gelatin, 4.2 msec., is long enough so that measurable oxygen quenching might be expected, passing nitrogen over a film of eosin in gelatin for 24 hr. did not change the rate of decay of the triplet state. The mean life remained 4.2 msec., which is roughly twice that reported for the eosin triplet in fluid solvents at room temperature (1.7 msec. in ethanol, 2.4 msec. in glycerol,¹³ 2.4 msec. in water¹⁴) and half that reported in glasses at 77°K. (9.3 msec. in ethanol, 10.7 msec. in glycerol,¹³ 9.4 msec. in EPA¹¹).

3. *Anthracene.* For compounds not soluble in gelatin, such as anthracene, polystyrene was used as a medium. Since the films, which are $\sim 150 \mu$ thick, were made from a polystyrene-toluene dope, there was no danger of the solute being either attacked during polymerization or incorporated in the polymer chains. In air, flash excitation produced no observable labile

species, but after nitrogen was passed over the surfaces of the film for 50 min., a transient was observed with a sharp absorption peak at 433 $m\mu$ and a first-order decay with a mean life of 26 msec. ($k_1 = 38 \pm 1 \text{ sec.}^{-1}$). Repeated flashing did not increase the lifetime of the transient, which is tentatively identified as the triplet state of anthracene. The position of the absorption maximum is about that to be expected in a medium with the refractive index (1.59) of polystyrene.¹⁵ When nitrogen was passed over the surface of the sample for 3 hr. before the first flash, the results were the same as with the shorter exposure to nitrogen. When the film in equilibrium with nitrogen was placed in a stream of air for 1 min., the triplet state was quenched to a point where it could not be detected by our apparatus. Since k_1 in air is too great to measure, it cannot be compared to k_1 in nitrogen, so that it remains doubtful whether any residual oxygen quenching is associated with the value of $k_1 = 38 \text{ sec.}^{-1}$. However, the reproducibility of the result with different nitrogen samples is indicative of, at most, very little oxygen quenching.

The rate of anthracene triplet decay in polystyrene film at room temperature compares with Meluish and Hardwick's² $53 \pm 1 \text{ sec.}^{-1}$ in Lucite blocks² and Linschitz, Steel, and Bell's¹⁶ $56 \pm 76 \text{ sec.}^{-1}$ in hexane and $0 \pm 40 \text{ sec.}^{-1}$ in tetrahydrofuran; also, with Livingston and Ware's¹⁷ extrapolated, relatively temperature-independent (from 350 to 200°K.) "intrinsic decay" of $49 \pm 25 \text{ sec.}^{-1}$ in toluene and $45 \pm 25 \text{ sec.}^{-1}$ in hexane, and with Hilpern, Porter, and Stief's¹⁸ extrapolated room temperature rates of 69 sec.^{-1} in isopentane and 40 sec.^{-1} in propylene glycol.

The reported rate constants for anthracene triplet at 77°K. are $35 \pm 4 \text{ sec.}^{-1}$ in Lucite,² $24 \pm \text{sec.}^{-1}$ in EPA glass,¹⁷ and 10.9 sec.^{-1} in isopentane¹⁸; all were measured by flash photolysis.

4. *Triplet Decay at Room Temperature and -25° :* In all cases, the rate of decay of the triplet state at room temperature was never more than four times higher than the lowest reported in glasses at liquid nitrogen temperature. In the case of erythrosin, it is only half again as great as the lowest reported value at 77°K.

(12) G. Oster, *J. Polymer Sci.*, **16**, 235 (1955).

(13) C. A. Parker and C. G. Hatchard, *J. Phys. Chem.*, **66**, 2506 (1962).

(14) E. F. Zwicker and L. I. Grossweiner, *ibid.*, **67**, 549 (1963).

(15) G. Jackson, R. Livingston, and A. C. Pugh, *Trans. Faraday Soc.*, **56**, 1635 (1960).

(16) H. Linschitz, C. Steel, and J. A. Bell, *J. Phys. Chem.*, **66**, 2574 (1962).

(17) R. Livingston and W. R. Ware, *J. Chem. Phys.*, **39**, 2593 (1963).

(18) J. W. Hilpern, G. Porter, and L. J. Stief, *Proc. Roy. Soc. (London)*, **A277**, 437 (1964).

This is indicative of a very low energy of activation for the triplet decay, of the order of a few hundred calories per mole or less. Preliminary measurements of the triplet decay of erythrosin in gelatin and anthracene in polystyrene at room temperature and -25° bear this out. The rates at the lower temperatures are only slightly less than those at room temperature and correspond to an apparent energy of activation of 310 ± 180 cal./mole for erythrosin and 150 ± 90 cal./mole for anthracene.

Conclusions

The results indicate that flash photolysis in solid films is a simple and effective means of studying the properties of transient species free of translational molecular motion and the resulting self-quenching. Despite triplet concentrations of $6 \times 10^{-4} M$ and $>2 \times 10^{-5} M$ with the halogenated fluoresceins and 2-naphthol in

gelatin, and $>5 \times 10^{-5} M$ with anthracene in polystyrene, no self-quenching was observed. This restricted motion also minimizes the effects of impurities in the solute and matrix itself, and obviates the need for extensive purification of either. The lack of triplet self-quenching does not necessarily preclude oxygen quenching when the sample is in air. Anthracene in polystyrene is a good example of this. However, the diffusion of oxygen is restricted enough so that by simply passing nitrogen over the sample, the effect of oxygen can be greatly lessened or eliminated, and, by comparing the rates in air and nitrogen, it can be determined whether or not any significant oxygen quenching remains.

Acknowledgment. The author wishes to thank Dr. W. West for his encouragement and for much helpful advice and criticism.

The Crystal Structure of Strontium Bromide Monohydrate

by Maurice Dyke and Ronald L. Sass

Department of Chemistry, William March Rice University, Houston, Texas (Received July 8, 1964)

The structure of strontium bromide monohydrate has been determined by X-ray single crystal diffraction techniques. The strontium ion was found to have an environment similar to the environment of the barium ion in the anhydrous barium halides.

Introduction

In 1939 Kamermans,¹ on the basis of a single crystal X-ray diffraction investigation, reported the crystal structure of a substance which he identified as strontium bromide. The space group of the structure is D_{2h}^{16} -Pnma with $a = 11.42 \text{ \AA}$, $b = 4.3 \text{ \AA}$, and $c = 9.20 \text{ \AA}$. If Kamermans' notation is transformed into the international standard form. Recently, Sass, Brackett, and Brackett² have shown that a sample of hydrated strontium bromide kept under vacuum at room temperature for several hours will yield an X-ray powder diffraction pattern showing a single phase with an orthorhombic unit cell identical with the one reported by Kamermans

for strontium bromide. They have also found that when a weighed sample of this material is heated under vacuum at 200° there is a weight loss corresponding to 1 mole of water per mole of compound on the basis of an original sample composition of $\text{SrBr}_2 \cdot \text{H}_2\text{O}$. An X-ray powder diffraction pattern of the new substance showed a single phase with a tetragonal unit cell. Sass, *et al.*, have identified this material as strontium bromide and have determined the crystal structure by X-ray powder diffraction. We have now completed a single crystal

(1) M. A. Kamermans, *Z. Krist.*, **101**, 406 (1939).

(2) R. Sass, T. Brackett, and E. Brackett, *J. Phys. Chem.*, **67**, 2862 (1963).

X-ray diffraction study of strontium bromide monohydrate.

Experimental

An anhydrous sample of strontium bromide was obtained by heating hydrated strontium bromide crystals obtained from Matheson Coleman and Bell at 200° under vacuum for 12 hr. A weighed sample of anhydrous strontium bromide and a mole equivalent of water were each placed into separate beakers. The uncovered beakers were immediately placed in a sealed jar and allowed to equilibrate. The beaker containing the water became empty within 24 hr. The material from the other beaker was dissolved in absolute ethanol to form a saturated solution of $\text{SrBr}_2 \cdot \text{H}_2\text{O}$. Anhydrous ethyl acetate was slowly added from a dropping funnel to the saturated solution maintained at 45° to prevent the formation of the strontium bromide ethyl alcoholate complex.¹ Crystallization of the $\text{SrBr}_2 \cdot \text{H}_2\text{O}$ was finished after the ethyl acetate had been added for 12 hr. After crystal formation the supernatant liquid was quickly decanted off and the crystals were immediately covered with paraffin oil and heated at 50° until all traces of solvent had evaporated. If an unprotected crystal is exposed directly to the air it will turn cloudy from further hydration. A crystal 0.19 mm. in diameter was mounted in a thin-walled glass capillary of 0.20-mm. diameter. The remaining space in the capillary was filled with paraffin oil. One end of the capillary had to be left unsealed to prevent it from exploding upon prolonged exposure in the X-ray beam. These explosions were probably due to expansion of the paraffin oil in the capillary and were not caused by any change in crystal structure since no change in the diffraction pattern of the crystal could be detected upon extensive exposure in the X-ray beam.

Rotation and Weissenberg photographs show the unit cell to be orthorhombic with $a = 11.38 \text{ \AA}$, $b = 4.28 \text{ \AA}$ (rotation axis), and $c = 9.19 \text{ \AA}$. The following systematic absences are observed: $0kl$ absent if $k + l = 2n + 1$, and $hk0$ absent if $h = 2n + 1$. The preceding data indicate that the space group is D_{2h}^{16} - Pnma or C_{2v}^9 - Pn2a . Our initial assumption that the former space group is the correct one for crystalline $\text{SrBr}_2 \cdot \text{H}_2\text{O}$ is verified by the final results obtained in the structure refinement. The experimental density reported by Kamermans is 3.8 while the calculated density is 3.93 assuming four molecules of $\text{SrBr}_2 \cdot \text{H}_2\text{O}$ per unit cell. This allows the molecules to be in the fourfold special positions $x, 1/4, z; \bar{x}, 3/4, \bar{z}; 1/2 - x, 3/4, 1/2 + z;$ and $1/2 + x, 1/4, 1/2 - z$. Weissenberg photographs of the $k = 0$ and $k = 1$ layers were used to determine the intensities of 222 independent reflections by visual com-

parison with standard intensity strips. The intensities were corrected for absorption by the method of Bradley³ using a linear absorption coefficient of 389 cm.^{-1} . In making the absorption correction, the slender wedge-shaped crystal was assumed to have cylindrical symmetry in order to simplify the calculations. Corrections were also made for the Lorentz, polarization, and Tunnell effects.

The data from the 0-layer were least-squared using as trial parameters for the strontium and bromine atoms the values reported by Kamermans and given in Table I. A two-dimensional electron density projection was constructed using the observed ($h0l$) data with signs assigned from the least-squares analysis. The electron density map showed three peaks which might be due to the oxygen of the water molecule. However, in two of these positions there was not sufficient space for the packing of an oxygen atom into the crystal lattice and thus the position of the oxygen atom was assigned to the coordinates of the third peak. A final least-squares refinement was done on each layer using the parameters obtained from the electron density projection giving an R of 18% for the 0-layer and an R of 19% for the first layer. Table II contains the observed and calculated structure factors for strontium bromide monohydrate.

Table I: $\text{SrBr}_2 \cdot \text{H}_2\text{O}$ Atomic Parameters

Atom	Source	X	Y	Z
Sr	Kamermans	0.311	1/4	0.392
	This paper	0.3094	1/4	0.3845
Br(1)	Kamermans	0.103	1/4	0.119
	This paper	0.1019	1/4	0.1143
Br(2)	Kamermans	0.614	1/4	0.842
	This paper	0.6150	1/4	0.8456
O	This paper	0.325	1/4	0.879

A two-dimensional ($h0l$) electron density difference synthesis was attempted in order to obtain stronger evidence for the position of the water oxygen atom. The difference projection contained numerous extraneous features and was not of particular use in locating the oxygen atom. The poor resolution of the water molecule in the difference synthesis and the inability to obtain lower R values in the least-squares refinements were probably due to the inexactness of our absorption corrections.

Results and Discussion

Table I contains the final parameters obtained from the least-square refinements. The nearest-neighbor

(3) A. J. Bradley, *Proc. Phys. Soc. (London)*, **47**, 879 (1935).

Table II: Structure Factors for Strontium Bromide Monohydrate

h	l	F_{calcd}	$ F_{\text{obsd}} $	h	l	F_{calcd}	$ F_{\text{obsd}} $	h	l	F_{calcd}	$ F_{\text{obsd}} $	h	l	F_{calcd}	$ F_{\text{obsd}} $
$h0l$				$h0l$				$h1l$				$h1l$			
2	0	-14.81	14.49	6	5	4.31	4.63	2	0	-28.76	21.73	0	5	-3.61	4.98
4	0	-46.75	49.14	7	5	8.74	7.78	4	0	-51.70	54.06	1	5	-3.33	4.37
6	0	-6.11	7.40	9	5	-8.61	7.81	6	0	50.04	62.01	2	5	-5.97	5.88
8	0	1.59	3.30	10	5	-5.52	5.53	8	0	21.52	21.89	3	5	24.97	28.09
10	0	29.67	36.35	11	5	-10.76	11.72	10	0	-21.60	30.08	4	5	11.31	14.26
12	0	-6.76	6.63	12	5	-5.21	4.81	12	0	-5.32	7.92	6	5	4.11	3.01
14	0	-15.27	19.73	13	5	9.42	8.68	14	0	-5.83	4.16	7	5	-24.29	20.88
1	1	12.05	20.73	1	6	-3.94	3.92	0	1	-12.06	19.66	8	5	-14.03	13.91
2	1	15.65	19.35	2	6	4.66	5.94	1	1	15.85	19.56	9	5	5.62	4.29
3	1	-12.64	15.46	3	6	26.79	27.13	2	1	10.11	11.90	11	5	1.52	2.70
4	1	-17.39	19.91	4	6	-8.52	7.45	3	1	-14.91	15.69	12	5	4.89	5.51
5	1	8.52	11.34	6	6	-3.57	3.81	4	1	-8.15	9.17	1	6	26.18	27.93
6	1	2.92	3.81	7	6	-27.41	21.30	5	1	-7.67	10.10	2	6	-13.20	15.55
7	1	-14.20	19.56	8	6	11.02	9.80	6	1	-2.93	3.13	3	6	-27.00	26.90
10	1	4.00	4.58	9	6	7.06	5.43	7	1	14.47	19.82	4	6	6.54	7.98
11	1	12.01	14.77	10	6	-1.54	1.49	8	1	17.37	24.01	5	6	-2.93	4.05
12	1	5.19	4.56	11	6	3.82	5.89	9	1	-4.14	3.15	7	6	-7.07	4.74
13	1	-4.39	3.94	12	6	-4.31	5.66	10	1	-9.89	11.28	9	6	9.34	9.30
14	1	-10.13	10.42	1	7	-4.63	4.56	11	1	6.11	6.78	10	6	-3.74	3.05
2	2	-2.85	5.02	2	7	11.59	10.80	12	1	-4.52	5.99	11	6	13.63	12.64
3	2	-57.76	49.40	3	7	1.97	2.46	13	1	-5.38	5.83	12	6	-4.65	4.37
4	2	5.87	5.58	4	7	19.13	17.10	14	1	1.89	1.46	1	7	9.93	10.25
7	2	49.83	53.75	5	7	9.62	7.40	1	2	-54.49	49.02	2	7	-5.39	4.69
8	2	-5.94	6.73	6	7	-20.27	15.97	2	2	8.54	14.07	3	7	3.88	3.87
9	2	-11.18	13.46	7	7	-6.20	3.81	3	2	50.84	44.78	4	7	-15.40	15.08
10	2	0.33	2.03	8	7	-7.74	6.91	4	2	-2.99	4.05	5	7	-5.40	4.43
11	2	-10.39	15.00	9	7	-5.14	4.63	5	2	13.06	16.14	6	7	-4.35	3.50
12	2	2.33	2.76	10	7	7.16	7.09	6	2	-2.46	2.22	7	7	-2.89	2.45
13	2	-4.38	4.91	11	7	3.87	3.33	7	2	7.89	7.18	10	7	17.86	16.69
1	3	3.89	4.25	0	8	25.39	20.20	9	2	-18.99	26.12	11	7	6.84	5.51
2	3	-3.64	3.10	1	8	-10.40	10.65	10	2	2.18	2.07	2	8	-1.79	3.76
4	3	-23.78	26.62	2	8	-6.52	4.85	11	2	-18.70	23.08	3	8	-1.82	2.19
5	3	-15.86	18.25	4	8	-8.46	7.60	12	2	2.43	2.35	4	8	-19.04	15.37
6	3	16.92	18.66	5	8	6.23	6.07	13	2	21.00	19.34	5	8	9.89	9.06
7	3	12.74	12.77	8	8	-5.52	3.15	14	2	-2.92	2.44	6	8	15.42	12.38
8	3	5.88	7.55	10	8	11.45	11.70	0	3	-33.80	54.59	7	8	-6.83	5.19
9	3	6.40	7.63	1	9	17.13	13.62	1	3	-18.93	25.28	8	8	7.19	5.57
10	3	-2.87	2.82	2	9	6.08	4.81	2	3	8.90	12.08	9	8	-5.36	5.41
11	3	-8.85	8.81	3	9	-15.43	12.34	4	3	7.70	8.59	10	8	-6.54	9.49
13	3	-0.87	5.89	5	9	-6.18	5.38	5	3	9.68	11.47	0	9	3.15	3.02
14	3	-8.51	7.24	6	9	-2.49	2.10	8	3	10.22	10.23	3	9	-21.35	17.73
0	4	-68.01	57.33	7	9	-4.04	3.20	10	3	-17.25	20.19	4	9	-5.21	4.00
1	4	12.22	16.74	8	9	-1.70	1.14	11	3	-10.10	11.02	7	9	21.59	16.48
2	4	11.02	15.69	9	9	9.28	10.14	13	3	3.52	3.11	8	9	5.36	3.64
3	4	4.20	3.56	0	10	2.39	3.02	1	4	3.85	3.37	9	9	-4.65	3.60
4	4	29.63	30.68	1	10	6.11	3.71	2	4	16.29	22.21	1	10	-7.90	5.33
5	4	-6.85	7.93	2	10	-3.57	3.10	4	4	38.25	38.29	2	10	7.41	6.36
6	4	3.27	3.22	3	10	-7.55	5.86	5	4	-10.82	11.18	3	10	9.73	6.81
10	4	-23.12	23.29	4	10	3.85	2.97	6	4	-36.39	33.65	4	10	-6.82	6.09
11	4	5.77	4.97	5	10	-3.31	2.39	7	4	6.16	5.67	5	10	-3.06	5.06
12	4	4.36	3.81	6	10	2.21	2.12	8	4	-16.23	17.44	7	10	5.12	3.35
1	5	-21.43	24.93	7	10	9.34	7.58	9	4	6.02	6.78	0	11	-23.67	16.43
2	5	-15.59	17.56	1	11	1.35	1.19	10	4	16.10	18.23	1	11	-1.95	1.06
3	5	19.22	22.17	2	11	-8.46	7.58	11	4	-4.77	6.04	2	11	2.50	1.70
4	5	6.48	6.58	4	11	-11.44	10.62	12	4	3.27	4.53	3	11	-1.55	1.07
5	5	3.58	3.87	5	11	-2.19	1.21	13	4	-2.06	1.95	4	11	12.25	9.06

environment of the strontium ion in strontium bromide monohydrate is analogous to the environment of the barium ion in BaCl_2 , BaBr_2 , and BaI_2 ,⁴ except that two of the nearest halide ions around a barium ion are replaced by water molecules around the strontium ion. Each strontium atom is surrounded by three nearest-neighbor bromine atoms in the same crystallographic mirror plane and by two bromine atoms and one water molecule on each of the equivalent mirror planes above and below. The distance from a strontium atom to a nearest-neighbor bromine atom ranges from 3.13 to 3.38 Å, while each nearest-neighbor oxygen atom is at a distance of 2.63 Å. Thus, in strontium bromide monohydrate and in the barium halides each metal cation has nine nearest neighbors. Since in strontium bromide each strontium atom has only eight nearest neighbors,² the strontium ion is probably not large enough to allow the stable coordination of nine bromide ions as nearest neighbors. However, as oxygen is smaller than bromine, a strontium ion is large enough to allow the stable coordination of seven bromide ions and two water mole-

cules. It thus seems likely that the greater stability of $\text{SrBr}_2 \cdot \text{H}_2\text{O}$ over SrBr_2 is due primarily to the increase in coordination number of the strontium ion by the water molecule to allow the same type of stabilization as found in the barium halide crystal lattices.

Each bromine atom of type 1 has for nearest neighbors three oxygen atoms at distances of 3.35 Å (2) and 3.34 Å, four strontium atoms with distances ranging from 3.25 to 3.43 Å, and seven bromine atoms with distances varying from 3.79 to 4.23 Å. Each bromine atom of type 2 has for nearest neighbors one oxygen atom at a distance of 3.31 Å, three strontium atoms at distances of 3.13 Å (2) and 3.32 Å, and seven bromine atoms with distances ranging from 3.89 to 4.36 Å.

Acknowledgments. This work was supported by grants from the National Aeronautics and Space Administration and The Robert A. Welch Foundation of Texas.

(4) R. Sass, T. Brackett, and E. Brackett, *J. Phys. Chem.*, **67**, 2132 (1963).

Significant Structure Theory of Transport Phenomena

by Teresa S. Ree, Taikyue Ree, and Henry Eyring

Department of Chemistry, University of Utah, Salt Lake City, Utah (Received July 9, 1964)

By applying the significant structure theory of liquids to transport phenomena, the equation for viscosity is derived for rigid-sphere systems. When the Enskog theory of viscosity is compared to the present theory, close agreement between the two theories is found. The diffusion coefficient is also derived in terms of viscosity and V_s , the solid molar volume at the melting point. For simple liquids, viscosities and diffusion coefficients are calculated from the theory without using any adjustable parameters. The agreement between theory and experiment is satisfactory.

I. Introduction

There are three major theoretical approaches to the study of transport phenomena of liquids and dense gases. One of these theoretical approaches was introduced by Enskog.¹ Although the Enskog theory is

derived for rigid-sphere systems, it has been applied to real dense gases in excellent agreement with experi-

(1) (a) S. Chapman and T. G. Cowling, "The Mathematical Theory of Non-Uniform Gases," Cambridge University Press, Cambridge, 1939, Chapter 16; (b) *ibid.*, Chapter 10.

ment. A second approach was made by Kirkwood.² Starting from the Liouville equation, he obtained exact expressions for the flux vectors in terms of the so-called nonequilibrium radial distribution function. Certainly this approach to the study of transport phenomena is more satisfying from a theoretical viewpoint than any other. At present, however, only a very few calculations have been carried out, so that the method is still not developed for practical work. The third approach was made by Eyring, Ree, and co-workers³⁻⁵ by applying the theory of absolute reaction rates to various transport phenomena. Since the flow of a liquid is a rate process, insofar as it takes place with a definite velocity under a given condition, it is justifiable to apply the theory of absolute reaction rates to the problems of transport phenomena. In this paper, we derive the equation of viscosity for rigid spheres from Eyring's rate process approach, and we compare the results with Enskog's theory. Further, we derive the equation for diffusion, and we apply our theory to real liquids. The theory is very successful.

II. Theory

The significant structure theory of liquids of Eyring, Ree, and co-workers^{5,6} is based on the concept of a quasi-lattice theory containing highly mobile vacancies randomly distributed. Such a mobile vacancy confers gas-like properties on the molecule which jumps into it. These vacancies also give rise to a positional degeneracy for neighboring solid-like molecules. The numbers of solid-like and gas-like molecules are NV_s/V and $N(V - V_s)/V$, respectively, where V is the molar volume of the liquid, V_s is the molar volume of the solid at the melting point, and N is Avogadro's number.

The significant structure theory of liquids has implicit in it a general theory of transport properties. Since there are solid-like and gas-like degrees of freedom in the liquid, both must be taken into account in calculating the viscosity. If a fraction, x_s , of the shear plane is covered by solid-like molecules and the remaining fraction, x_g , by gas-like molecules, then the viscosity, η , which is the ratio of shear stress, f , to rate of strain, \dot{s} , is^{4,5}

$$\eta = \frac{f}{\dot{s}} = (x_s f_s + x_g f_g) / \dot{s} = x_s \eta_s + x_g \eta_g = \frac{V_s}{V} \eta_s + \frac{V - V_s}{V} \eta_g \quad (1)$$

Here, the subscripts, s and g, indicate that the quantity belongs to the solid-like and the gas-like molecules, respectively. In the last equality of eq. 1, it is assumed that x_s equals the fraction of the solid-like molecules, V_s/V , and consequently that $x_g = (V - V_s)/V$.

The term η_g in eq. 1 is taken as equal to the rigid-sphere viscosity at infinite dilution and is equal to^{1b}

$$\eta_g = \frac{5}{16d^2} \left(\frac{mkT}{\pi} \right)^{1/2} \quad (2)$$

where d is the molecular diameter. The quantity η_s in eq. 1 is calculated in accord with Eyring's earlier procedure⁷ as^{4,5}

$$\eta_s = \frac{f_s}{\dot{s}} = f_s / \left[\sum_i \left(\frac{\lambda \cos \theta_i}{\lambda_i} \right) k_i \exp \frac{\lambda_2 \lambda_3 \lambda f_s \cos \theta_i}{2kT} \right] \quad (3)$$

In the above equation, as shown in Fig. 1, $\lambda_2 \lambda_3$ is the area occupied by a molecule on which the shear stress, f_s , is acting; λ_1 is the distance between two successive molecular layers, one of which slips with the shear

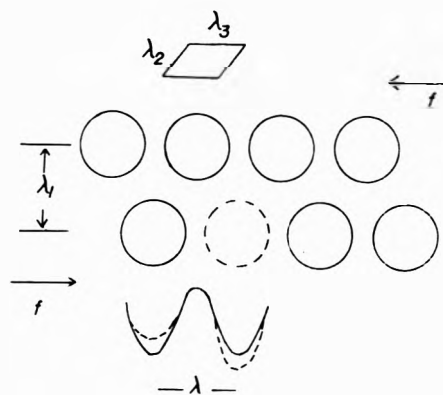


Figure 1. Distances between molecules in a liquid. λ is the distance between two successive equilibrium positions; λ_1 is the distance between two successive molecular layers.

rate, s , with respect to the other; the distance for one jump along the direction of f_s is then $\lambda \cos \theta_i$, θ_i being the angle between the direction of stress and the direction of jumping; k_i is the jumping frequency of the molecule to the i th neighboring hole when $f_s = 0$ and is assumed to be equal to k' for every position i . Expanding the exponential of eq. 3, we obtain

$$\eta_s = f_s / \left[\frac{k'}{\lambda_1} \sum_i \left(\cos \theta_i + \frac{f_s \lambda_2 \lambda_3 \lambda \cos^2 \theta_i}{2kT} \right) \right] \quad (4)$$

(2) J. G. Kirkwood, *J. Chem. Phys.*, **14**, 180 (1946).

(3) H. Eyring, D. Henderson, B. Stover, and E. Eyring, "Statistical Mechanics and Dynamics," John Wiley and Sons, Inc., New York, N. Y., 1964, Chapter 16.

(4) T. S. Ree, T. Ree, and H. Eyring, *Proc. Natl. Acad. Sci. U. S. A.*, **48**, 501 (1962).

(5) H. Eyring and T. Ree, *ibid.*, **47**, 526 (1961).

(6) (a) T. S. Ree, T. Ree, and H. Eyring, *J. Phys. Chem.*, **68**, 1163 (1964); (b) R. Marchi and H. Eyring, *J. Chem. Educ.*, **40**, 526 (1963).

Since the sites are randomly distributed over a solid angle, we may take the averages of $\cos \theta_i$ and $\cos^2 \theta_i$. Thus

$$\begin{aligned}\Sigma \cos \theta_i &= 0 \quad (5) \\ \Sigma \cos^2 \theta_i &= Z \frac{V - V_s}{V} (1/3)\end{aligned}$$

where Z is the number of nearest neighbors and is equal to 12 when there is hexagonal packing; $Z(V - V_s)/V$ is the number of holes in the immediate vicinity of a molecule.

In eq. 3 we are able to correlate molecular dimensions, λ_1 , λ_2 , λ_3 , and λ to V_s for hexagonal packing as follows (cf. Fig. 2)

$$\begin{aligned}\lambda_2 \lambda_3 &= \frac{\sqrt{3}}{2} a^2 \\ \lambda_1 &= \frac{\sqrt{3}}{2} a \quad (6) \\ \lambda &= a \\ \frac{a^3}{\sqrt{2}} &= \frac{V_s}{N}\end{aligned}$$

where a is the distance between two nearest neighbors. In eq. 4, k' is written in accord with Eyring's reaction rate theory⁷ as

$$k' = \kappa \frac{kT}{h} \frac{F^*}{F} \exp \frac{-\epsilon_0}{kT} \quad (7)$$

where κ is the transmission coefficient, and F and F^* are the partition functions for the molecule in the initial and activated complex states, respectively, and are given by⁸⁻¹⁰

$$F = \frac{(2\pi mkT)^{3/2}}{h^3} v_f \left[\exp \frac{-Z\phi(a)}{2kT} \right] J(T) \quad (8)$$

$$F^* = \frac{(2\pi mkT)}{h^2} a_f \left[\exp \frac{-Z\phi(a)}{2kT} \right] J(T) \quad (9)$$

where v_f and a_f are the free volume and the free area, respectively; $J(T)$ is the partition function for the internal degrees of freedom, and for the hexagonal packing lattice $\phi(a)$ is given by¹⁰

$$\phi(a) = \epsilon \left[1.0109 \left(\frac{N\sigma^3}{V_s} \right)^4 - 2.4090 \left(\frac{N\sigma^3}{V_s} \right)^2 \right] \quad (10)$$

Here ϵ and σ are the energy and the distance characteristic of the system and are listed in the literature.¹¹ In eq. 7 ϵ_0 is the activation energy and is written as

$$\epsilon_0 = - \frac{a' Z \phi(a)}{2} \frac{V_s}{V - V_s} \quad (11)$$

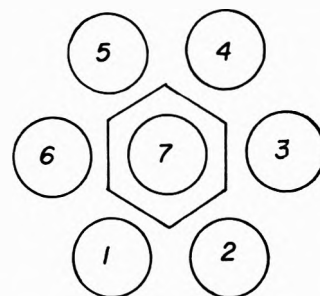


Figure 2. Hexagon normal to the direction of diffusion in a liquid or hexagonal packing. Molecule 7 is diffusing forward, hence f is acting upward. $\lambda_2 \lambda_3$ is the area occupied by a pair of molecules 7 and 1 in the direction normal to the paper. The other molecular pairs, 7-2, 7-3, 7-4, 7-5, and 7-6, also occupy the area of $\lambda_2 \lambda_3$ for each.

where a' is a proportionality constant, and it is assumed that the activation energy is proportional to $\phi(a)$ and inversely proportional to the number of holes $(V - V_s)/V_s$.

Hence, substituting eq. 5 through 9 into eq. 4, η_s is written as

$$\eta_s = \frac{V}{V_s} \frac{(\pi mkT)^{1/2} N l_f}{2(V - V_s) \kappa} \exp \left[\frac{-a' V_s Z \phi(a)}{V - V_s 2kT} \right] \quad (12)$$

In the above equation Z is taken as 12 and l_f is a free length and equal to v_f/a_f . Substituting eq. 2 and 12 into eq. 1 leads to

$$\eta = \frac{(\pi mkT)^{1/2} N l_f}{2(V - V_s) \kappa} \left[\exp \frac{-a' V_s Z \phi(a)}{V - V_s 2kT} \right] + \frac{V - V_s}{V} \frac{5}{16d^2} \left(\frac{mkT}{\pi} \right)^{1/2} \quad (13)$$

If in the above equation the rigid sphere condition is introduced, *i.e.*

$$\begin{aligned}\phi(a) &= 0 \\ l_f &= 2(a - d) \\ \kappa &= 1 \quad (14)\end{aligned}$$

then the viscosity for the rigid spheres becomes

(7) S. Glasstone, K. J. Laidler, and H. Eyring, "The Theory of Rate Processes," McGraw-Hill Book Co., Inc., New York, N. Y., 1941, Chapter 9.

(8) D. Henderson, *J. Chem. Phys.*, **39**, 1857 (1963).

(9) T. S. Ree, T. Ree, and H. Eyring, *ibid.*, **41**, 524 (1964).

(10) R. H. Wentoff, R. J. Buehler, J. O. Hirschfelder, and C. F. Curtiss, *ibid.*, **18**, 1484 (1950).

(11) J. O. Hirschfelder, C. F. Curtiss, and R. B. Bird, "Molecular Theory of Gases and Liquids," John Wiley and Sons, Inc., New York, N. Y., 1964, pp. 1110-1112.

Table I: Comparison of Calculated and Experimental Viscosities for Simple Liquids

Substances and parameters	T , °K.	ρ , g./cc.	$\eta_{\text{exptl.}}$, mpoise	$\eta_{\text{theor.}}$, mpoise	Substances and parameters	T , °K.	ρ , g./cc.	$\eta_{\text{exptl.}}$, mpoise	$\eta_{\text{theor.}}$, mpoise
Ar	84.25	1.414 ^b	2.82 ^b	2.72	Cl ₂	197.7	1.658 ^f	7.29 ^f	8.43
$d = 2.944 \text{ \AA.}$	86.25	1.397	2.62	2.50	$d = 3.546 \text{ \AA.}$	199.2	1.653	7.10	8.02
$V_s = 24.98 \text{ (cc./mole)}^a$	86.90	1.392	2.56	2.44	$V_s = 40.455 \text{ (cc./mole)}^e$	202.7	1.646	6.80	7.53
	87.30	1.39	2.52	2.42		207.4	1.635	6.49	6.86
	90.0	1.37	2.32	2.21		207.8	1.634	6.46	6.81
	99.5	1.31	1.62	1.78		213.0	1.623	6.16	6.27
	111.0	1.22	1.37	1.35		213.2	1.622	6.10	6.22
	120	1.16	1.16	1.17		220.2	1.606	5.69	5.58
	127	1.10	1.00	1.02		220.8	1.604	5.66	5.51
	133.5	1.02	0.77	0.86		228.1	1.587	5.30	4.98
	138.7	0.95	0.70	0.76		229.1	1.585	5.24	4.92
	143	0.88	0.63	0.67		237.8	1.564	4.94 ^g	4.40
	147	0.78	0.56	0.57		273.2	1.468	3.85 ^g	2.96
	149	0.70	0.50	0.50	CH ₄	91	0.452 ^f	2.1 ^g	1.32
N ₂	64.8	0.861 ^d	2.22 ^d	2.05	$d = 3.257 \text{ \AA.}$	94	0.448	1.86	1.26
$d = 3.142 \text{ \AA.}$	71.8	0.832	1.67	1.60	$V_s = 31.06 \text{ (cc./mole)}^e$	98.5	0.442	1.61	1.17
$V_s = 29.31 \text{ (cc./mole)}^c$	78.07	0.798	1.33	1.27		103	0.436	1.45	1.10
	90.65	0.746	0.95	0.97		109	0.428	1.25	1.01
	99.43	0.69	0.77	0.76		111	0.425	1.18	0.99
	109.3	0.63	0.62	0.62		131	0.395	0.94	0.76
	113.4	0.60	0.60	0.56		148.5	0.364	0.68	0.61
	122.5	0.50	0.43	0.41		161	0.338	0.59	0.52
	123.8	0.47	0.37	0.38		166.5	0.325	0.56	0.48
	125.08	0.43	0.37	0.34		180	0.277	0.51	0.37
	126	0.38	0.31	0.30	C ₂ H ₆	273.2	0.9001 ^h	9.12 ⁱ	7.70
					$d = 4.506 \text{ \AA.}$	283.2	0.8895	7.58	6.22
					$V_s = 82.826 \text{ (cc./mole)}^e$	293.2	0.8790	6.52	5.23
						303.2	0.8685	5.64	4.52
						313.2	0.8576	5.03	3.96
						323.2	0.8466	4.42	3.53
						333.2	0.8357	3.92	3.18
						343.2	0.8248 ^j	3.58	2.90
						353.2	0.8145 ^j	3.29	2.68

^a See ref. 16. ^b See ref. 17. ^c See ref. 18. ^d See ref. 19. ^e See ref. 20. ^f See ref. 21. ^g See ref. 22. ^h See ref. 23. ⁱ See ref. 15. ^j See ref. 24.

$$\eta = (\pi mkT)^{1/2} N \frac{\left[\left(\sqrt{2} \frac{V_s}{N} \right)^{1/2} - d \right]}{V - V_s} + \frac{V - V_s}{V} \frac{5}{16d^2} \left(\frac{mkT}{\pi} \right)^{1/2} \quad (15)$$

The diffusion coefficient also may be calculated by means of the following equation which has been obtained by Eyring and Ree⁵

$$D = \frac{kT}{\xi \frac{\lambda_2 \lambda_3}{\lambda_1} \eta} \quad (16)$$

Where ξ is the effective number of neighboring molecules of the diffusing molecule lying in the same plane and perpendicular to the direction of diffusion. For

hexagonal packing, it is six (cf. Fig. 2). Substituting eq. 6 into 16 we obtain

$$D = \frac{kT}{6 \left(\frac{\sqrt{2} V_s}{N} \right)^{1/2} \eta} \quad (17)$$

III. Calculations

In order to carry out numerical calculations of the rigid-sphere viscosity of eq. 15, we use V_s from the result of machine calculations by Alder and Wainwright.¹² According to these authors, the phase transition from solid to liquid is observed at $1.5V_0 < V_s < 1.7V_0$, where V_0 is the closest packing volume, being equal to $Nd^3/$

(12) (a) B. J. Alder and T. E. Wainwright, *J. Chem. Phys.*, **27**, 1208 (1957); (b) *ibid.*, **33**, 1439 (1960).

$\sqrt{2}$. When we take the mean value $V_s = 1.6V_0$, eq. 15 becomes

$$\frac{\eta}{\eta_s} = 1 - 0.540 \left(\frac{b}{V}\right) + \left(\frac{b}{V}\right) \frac{0.811}{1 - 0.540 \left(\frac{b}{V}\right)} \quad (18)$$

where

$$b = \frac{2\pi}{3} d^3 N \quad (19)$$

The viscosity based on the Enskog theory is written as^{1a}

$$\frac{\eta}{\eta_s} = \frac{b}{YV} [1 + 0.8Y + 0.761Y^2] \quad (20)$$

where $Y = (PV/NkT) - 1$. In order to calculate the preceding equation, we use PV/NkT obtained by Thiele¹³ for the compressibility equation of rigid spheres

$$\frac{PV}{NkT} = \frac{1 + X + X^2}{(1 - X)^2} \quad (21)$$

where $X = b/4V$.

In Fig. 3 we compare the hard sphere viscosities calculated from our eq. 18 with those calculated from Enskog's theory (eq. 20). As shown in this figure, the

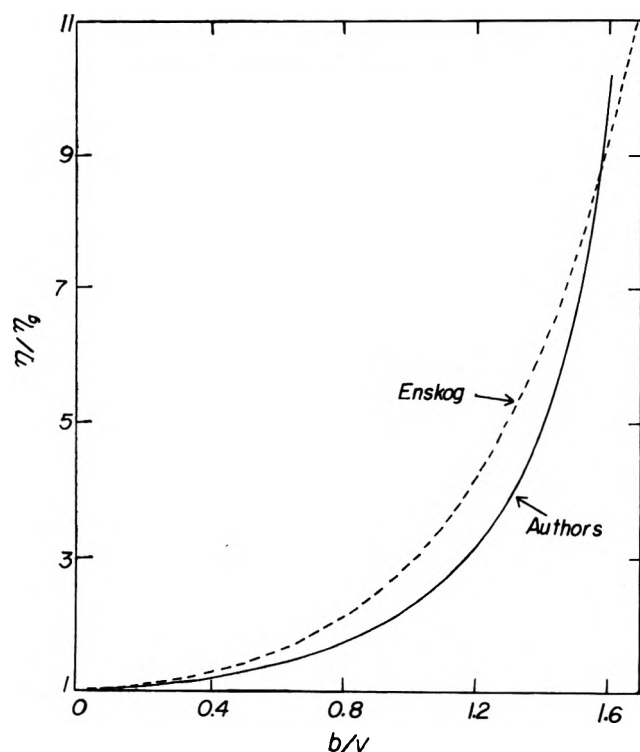


Figure 3. Comparison of Enskog's theory with the authors' theory.

agreement between the two theories is quite good. It is interesting to note that we obtain the virial expansion from both eq. 18 and 20, in which all of the virial coefficients are positive.

Through the studies of the Enskog theory¹ and the work by Longuet-Higgins and Pople,¹⁴ it is well established that even though the rigid sphere condition is imposed for deriving the viscosity equation, the calculated results from the latter agree excellently with experimental viscosities of simple liquids. Therefore, in Table I¹⁵⁻²⁴ we compare the viscosities calculated

Table II: Comparison of Calculated and Experimental Diffusion Coefficients for Simple Liquids

Substance and V_s	$T, ^\circ\text{K.}$	$\eta \times 10^3$ poise	$D_{\text{expt}} \times 10^6$ $\text{cm.}^2/\text{sec.}$	$D_{\text{theo}} \times 10^6$ $\text{cm.}^2/\text{sec.}$
Ar $V_s = 24.98$ (cc./mole) ^a	84.31 ± 0.13	2.82 ^b	2.67 ± 0.06 ^c	1.77
	90	2.32 ^d	2.43 ^d	2.30
	100	1.7	3.54	3.48
	110	1.40	4.80	4.65
	120	1.14	6.06	6.23
	130	0.90	7.45	8.54
	140	0.69	8.72	12.0
CH ₄ $V_s = 31.06$ (cc./mole) ^e	100	1.45 ^f	3.0 ^d	3.7
	110	1.18	4.2	5.0
	120	1.02	6.0	6.6
C ₆ H ₆ $V_s = 82.826$ (cc./mole) ^e	130	0.94	7.8	8.5
	287.7	7.08 ^g	1.6 ^h	1.61
	288.2	6.96	1.88 ± 0.01	1.64
	298.2	5.99	2.15 ± 0.05	1.98
CCl ₄ $V_s = 87.1$ (cc./mole) ⁱ	308.2	5.30	2.40 ± 0.03	2.31
	318.2	4.60	2.67 ± 0.06	2.75
	298.2	8.88 ^g	1.41 ^j	1.31
	308.2	7.70	1.75	1.56
	318.2	6.90	1.99	1.80

^a See ref. 16. ^b See ref. 17. ^c See ref. 25. ^d See ref. 26. ^e See ref. 20. ^f See ref. 22. ^g See ref. 23. ^h See ref. 27. ⁱ See ref. 29. ^j See ref. 28.

(13) E. Thiele, *J. Chem. Phys.*, **39**, 474 (1963).

(14) H. G. Longuet-Higgins and J. A. Pople, *ibid.*, **25**, 884 (1956).

(15) "Handbook of Chemistry and Physics," 41st Ed., C. D. Hodgman, Editor-in-Chief, Chemical Rubber Publishing Co., Cleveland, Ohio, 1959-1960.

(16) K. Clausius, *Z. physik. Chem.*, **B31**, 459 (1936).

(17) N. F. Zhadanova, *Soviet Phys. JETP*, **4**, 749 (1957).

(18) F. Simon, M. Ruhemann, and W. Edwards, *Z. physik. Chem.*, **B6**, 331 (1930).

(19) N. F. Zhadanova, *Soviet Phys. JETP*, **4**, 19 (1957).

(20) S. Chang, H. Pak, W. Paik, S. Park, M. S. John, and W. S. Ahn, *J. Korean Chem. Soc.*, **8**, 33 (1964).

(21) "International Critical Tables," E. W. Washburn, Editor-in-Chief, McGraw-Hill Book Co., New York, N. Y., 1926.

(22) A. F. Gerf and G. I. Galkov, *Soviet Phys.-Tech. Phys.*, **10**, 725 (1941).

from eq. 15 with the measured values for several types of liquids over a range of temperatures. The experimental viscosities are given in column 4, and the computed viscosities are in column 5. The molecular diameter, d , listed in column 1 is calculated from the van der Waals constant, b , available in the literature¹⁶ according to eq. 19. The agreement between experiment and theory is striking for viscosities of Ar and N₂, and for Cl₂, CH₄, and C₆H₆ the agreement is quite good. If V_s and d used in the calculations were to be fixed by using the experimental viscosities, the agreement would have been excellent in the latter three cases also.

In Table II, we compare the diffusion coefficient calculated by using eq. 17 with the experimental data.²⁵⁻²⁸ For calculating D we use the experimental viscosity as

listed in column 3. Agreement with theory and experiment is very good in general.

Acknowledgment. The authors express appreciation to the National Science Foundation for financial support of this research under Grant No. GP-415.

(23) J. Timmermans, "Physico-Chemical Constants of Pure Organic Compounds," Elsevier Publishing Co., Inc., New York, N. Y., 1950.

(24) "Landolt-Bornstein Tabellen," Verlag von Julius Springer, Berlin, 1923.

(25) J. W. Corbet and J. H. Wang, *J. Chem. Phys.*, **25**, 422 (1956).

(26) J. Naghizadeh and S. A. Rice, *ibid.*, **36**, 2710 (1962).

(27) K. Graupner and E. R. S. Winter, *J. Chem. Soc.*, 1145 (1952).

(28) H. Watts, B. J. Alder, and J. H. Hildebrand, *J. Chem. Phys.*, **23**, 659 (1955).

(29) H. Sackmann and G. Kloos, *Z. physik. Chem.*, **209**, 319 (1958).

Kinetic Studies of the Selectivity of Xylene Isomerization over Silica-Alumina Catalyst¹

by A. J. Silvestri and C. D. Prater

Research Department, Socony Mobil Oil Company, Princeton, New Jersey (Received February 5, 1964)

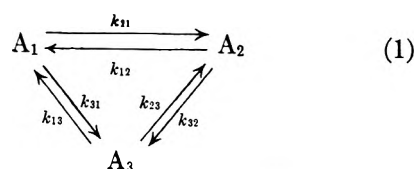
The theoretical studies of Wei and Prater provide tools for transforming highly coupled complex systems of monomolecular and pseudo-monomolecular reactions into completely uncoupled hypothetical systems amenable to solution. In this paper the results obtained by Wei and Prater are applied to the study of the kinetics of xylene isomerization over a silica-alumina catalyst. This chemical system provides an example of a chemically perturbed pseudo-monomolecular system. The perturbation is in the form of six bimolecular disproportionation reactions which accompany the isomerization. Despite the perturbation, it is still found possible to employ the methods of Wei and Prater to study the isomerization subsystem of the total reaction system and for the determination of the relative rate constants for the isomerization reactions. Approximate values are also obtained for the six second-order relative rate constants for the disproportionation subsystem through the use of standard techniques. The latter study illustrates the necessity of mapping the error sensitivity of the composition space before using curve-fitting methods for the determination of kinetic parameters.

Introduction

Xylene isomerization has been studied by various investigators.²⁻⁴ In this paper the methods of Wei and Prater⁵ will be applied to the kinetics of the gas phase isomerization of xylene over a porous silica-alumina catalyst. In general, kinetic studies on highly coupled systems of reactions are made by evaluating the parameters of a mathematical model which is assumed to describe the system. This is often done by curve-fitting techniques applied either to the analytical solution of the differential equations or to the differential equations themselves. The difficulties inherent in such a procedure have been pointed out by Lanczos⁶ and by Wei and Prater⁵; they will be illustrated later in the paper. Furthermore, the insensitivity of the observed data to the particular sequence of surface reactions assumed in the model is not always realized. This lack of sensitivity is demonstrated by the impossibility of ruling out a 1-3 alkyl migration from steady-state kinetic data alone.

Wei and Prater⁷ have shown that a highly coupled monomolecular (or pseudo-monomolecular) reaction system with n species A_i can be transformed into an

equivalent completely uncoupled monomolecular reaction system with n hypothetical new species B_i . For example, the general three-component monomolecular reaction system



(1) Presented in part at the Symposium on New Tools in Heterogeneous Catalytic Research at the 145th National Meeting of the American Chemical Society, New York, N. Y., September 9-13, 1963. The title of presentation was "Application of Monomolecular Rate Theory to the Mass-Action Kinetics of Xylene Isomerization over Silica-Alumina."

(2) P. M. Pitts, J. E. Connor, and L. N. Leum, *Ind. Eng. Chem.*, **47**, 770 (1955).

(3) E. R. Boedeker and W. E. Erner, U. S. Patent 2,719,183 (1955).

(4) T. Amemiya, E. Tsunetomi, E. Nakamura, and T. Nakazawa, *Bull. Japan Petrol. Inst.*, **3**, 14 (1961).

(5) J. Wei and C. D. Prater, *Advan. Catalysis*, **13**, 203 (1962).

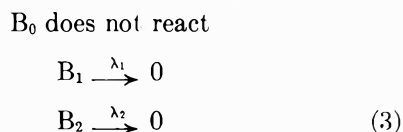
(6) C. Lanczos, "Applied Analysis," Prentice-Hall, Inc., Englewood Cliffs, N. J., 1956.

(7) The Wei and Prater (WP) article (ref. 5) will be used as a running reference through this paper in order to assist the reader who is not familiar with this method.

with rate equations, in terms of the concentrations a_i of the i th species, given by

$$\begin{aligned}\frac{da_1}{dt} &= -(k_{21} + k_{31})a_1 + k_{12}a_2 + k_{13}a_3 \\ \frac{da_2}{dt} &= k_{21}a_1 - (k_{12} + k_{32})a_2 + k_{23}a_3 \\ \frac{da_3}{dt} &= k_{31}a_1 + k_{32}a_2 - (k_{13} + k_{23})a_3\end{aligned}\quad (2)$$

can be transformed into the equivalent system



with rate equations given by

$$\begin{aligned}\frac{db_0}{dt} &= 0 \\ \frac{db_1}{dt} &= -\lambda_1 b_1 \\ \frac{db_2}{dt} &= -\lambda_2 b_2\end{aligned}\quad (4)$$

This latter set of differential equations is completely uncoupled. The solution for the hypothetical B system can be obtained readily. Then the solution to the set of equations for the A system can be obtained by transforming the B solution back to the A system through the use of transforms determined from experimental data.

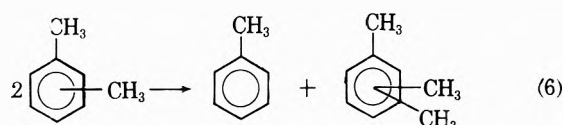
It has been shown that if certain conditions are fulfilled,⁸ heterogeneous reactions that take place on a solid surface will be pseudo-monomolecular. A reaction is said to be pseudo-monomolecular if the rate equation for the i th species is of the form

$$\frac{da_i}{dt} = \varphi[-\sum_j \theta_{ji} a_j + \sum_j \theta_{ij} a_j] \quad (5)$$

where θ_{ij} is the pseudo-first-order rate constant for the reaction from the j th to the i th species and φ is a function of composition and time which is the same for all rate equations in the system. Wei and Prater have called the term in brackets in eq. 5 the mass-action term, and it is the elucidation of this term, for xylene isomerization, with which this paper is concerned. The mass-action term determines the selectivity behavior of the catalyst. By selectivity is meant the particular composition sequences that are produced from a given initial composition. The selectivity is completely de-

termined when the relative values of the rate constants are known. Because only the relative values of the rate constants are needed and the function φ is the same for all the rate equations in the system, the selectivity behavior exhibited by a pseudo-monomolecular system is identical with the selectivity behavior of a monomolecular system.

Generally for xylene isomerization over a silica-alumina catalyst, the problem is complicated by the fact that the pseudo-monomolecular isomerization is accompanied by a significant amount of bimolecular disproportionation. There are six possible disproportionation reactions of the form



Under the conditions employed here, only a small amount of disproportionation has occurred when the xylene isomerization system has reached the neighborhood of its equilibrium; consequently, the reverse transalkylation reaction was considered to have a negligible effect on the results.

To illustrate this system geometrically, consider a tetrahedron which represents the reaction simplex⁹ for the total system (Fig. 1). One face of the tetrahedron is the reaction simplex for the isomerization reaction. In the ideal case with no side reaction the reaction paths will all lie on the isomerization plane outlined by the solid lines. The actual reaction paths will, however, fall away from the isomerization face into the interior of the tetrahedron since disproportionation accompanies the isomerization. In the general case, the projections of these reaction paths onto the isomerization plane (obtained by simply normalizing the xylene concentrations) will be distorted from those expected if there were no disproportionation.

Experimental

The reactions were carried out in a high-pressure glass flow reactor. The glass reactor system is totally enclosed in a metal bell. High-pressure operation is made possible by pressurizing the space outside the glass reactor system and inside the bell with nitrogen to a pressure essentially equal to that inside the glass

(8) See WP (ref. 5), section VI, p. 313.

(9) The composition of an n -component system can be expressed as a vector in n -dimensional composition space. The constraints of conservation of mass and nonnegativity of mass confine the composition vector to an $n - 1$ dimensional space lying in the positive orthant of the n -dimensional composition space. The $n - 1$ dimensional space to which the composition vector is confined is called the reaction simplex.

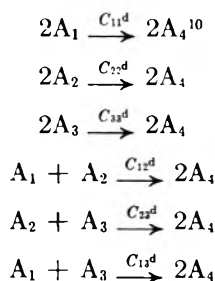
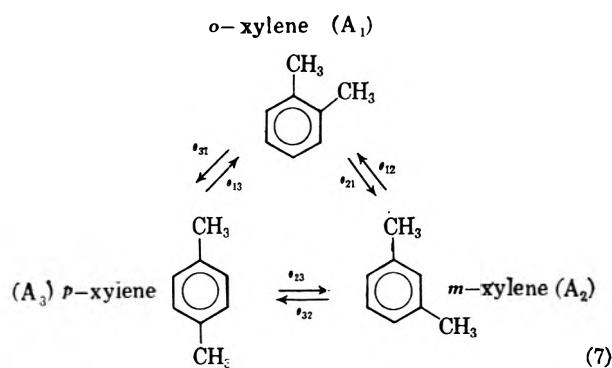
reactor system. The flow through the reactor system is in turn controlled by the bell pressure exerted on the reference side of the diaphragm in a back-pressure regulator.

The xylene isomers employed were Phillips pure grade hydrocarbons. The catalyst was a commercial silica-alumina bead-type cracking catalyst manufactured by the Socony Mobil Oil Co. It had a surface area of 409 m.²/g. and an Al₂O₃ content of 9.8 wt. %. This catalyst (100–200 mesh) was dispersed in 100–200 mesh Pyrex to give a total bed size of 10 cc. The amount of catalyst used varied from 2 to 100 vol. % of the catalyst bed. The reaction conditions employed were: temperature, 510°; hydrogen to hydrocarbon molar ratio, 10:1; and pressure, 200 p.s.i.g. Each datum point in the composition diagrams was obtained from a separate experiment. Each experiment included a 30-min. stabilizing period to stabilize reaction conditions, followed by a 30-min. reaction period. The product from the stabilizing period was discarded, and that from the reaction period was analyzed.

The analyses were made by gas chromatography using a flame ionization detector and a 45.7-m. × 0.025-cm. capillary column coated with oxybis(2-ethylbenzoate).

Results and Discussion

I. General. The composition sequences for the system studied are identical with those obtained from the scheme



where the parameters θ_{ij} are the pseudo-first-order rate constants for isomerization and C_{mn}^d are pseudo-

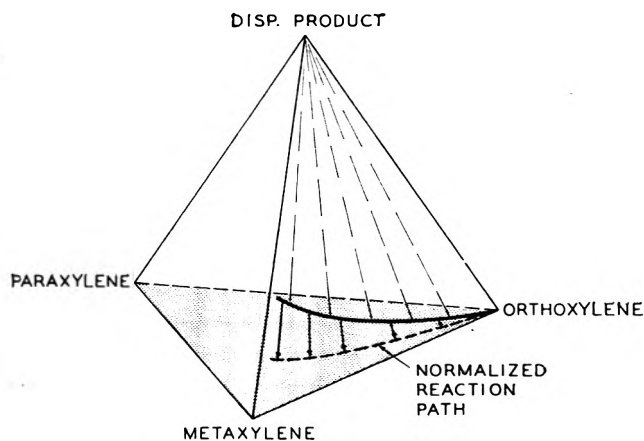


Figure 1. Reaction simplex for isomerization and disproportionation of xylene.

second-order rate constants for disproportionation. Since there is no increase in the number of molecules in this system, the set of rate equations for the system (7) can be written in terms of mole fractions if new rate constants are defined such that

$$\theta_{mn}^d = C_{mn}^d(a_1 + a_2 + a_3 + a_4) \quad (8)$$

This gives

$$\begin{aligned}
 \frac{da_1}{dt} &= -(\theta_{21} + \theta_{31})a_1 + \theta_{12}a_2 + \theta_{13}a_3 - \\
 &\quad \theta_{11}^d(a_1)^2 - \theta_{12}^da_1a_2 - \theta_{13}^da_1a_3 \\
 \frac{da_2}{dt} &= \theta_{21}a_1 - (\theta_{12} + \theta_{32})a_2 + \theta_{23}a_3 - \\
 &\quad \theta_{22}^d(a_2)^2 - \theta_{12}^da_1a_2 - \theta_{23}^da_2a_3 \quad (9) \\
 \frac{da_3}{dt} &= \theta_{31}a_1 + \theta_{32}a_2 - (\theta_{13} + \theta_{23})a_3 - \\
 &\quad \theta_{33}^d(a_3)^2 - \theta_{23}^da_2a_3 - \theta_{13}^da_1a_3 \\
 \frac{da_4}{dt} &= \theta_{11}^d(a_1)^2 + \theta_{22}^d(a_2)^2 + \theta_{33}^d(a_3)^2 + \\
 &\quad 2\theta_{12}^da_1a_2 + 2\theta_{13}^da_1a_3 + 2\theta_{23}^da_2a_3
 \end{aligned}$$

where a_i is the mole fraction of the i th species. Mole fractions will be used throughout the remainder of this paper.

The isomerization mass-action kinetics are studied by normalizing the actual composition points back to the isomerization plane of the reaction simplex and then

(10) $2A_4$ = toluene + trimethylbenzenes. As stated previously, the reverse reaction will be considered to have a negligible effect for the condition of the experiment. Hence it is not necessary to distinguish between toluene and trimethylbenzene in the above mathematical model nor is it necessary to consider isomerization among the three possible trimethylbenzene isomers.

applying the methods of Wei and Prater to the normalized data (see Fig. 1).

It is convenient to determine a sufficient condition that will cause the isomerization reaction paths to be unchanged from pseudo-first-order behavior when projected onto the isomerization plane by normalization of the mole fractions of the isomers. The composition vector for the isomerization system in the A system of coordinates is defined as

$$\mathbf{a} = \begin{pmatrix} a_1 \\ a_2 \\ a_3 \end{pmatrix} = \begin{pmatrix} o\text{-xylene mole fraction} \\ m\text{-xylene mole fraction} \\ p\text{-xylene mole fraction} \end{pmatrix} \quad (10)$$

The matrix rate equation which accounts for the effect of disproportionation on the isomerization reaction system is then

$$\frac{d\mathbf{a}}{dt} = (\Theta + \Psi)\mathbf{a} \quad (11)$$

where Θ is the relative pseudo-first-order rate constant matrix for the isomerization system and is given by

$$\Theta = \begin{pmatrix} -(\theta_{21} + \theta_{31}) & \theta_{12} & \theta_{13} \\ \theta_{21} & -(\theta_{12} + \theta_{32}) & \theta_{23} \\ \theta_{31} & \theta_{32} & -(\theta_{13} + \theta_{23}) \end{pmatrix} \quad (12)$$

and Ψ is the diagonal matrix

$$\Psi = - \begin{pmatrix} (\theta_{11}^d a_1 + \theta_{12}^d a_2 + \theta_{13}^d a_3) & 0 & 0 \\ 0 & (\theta_{12}^d a_1 + \theta_{22}^d a_2 + \theta_{23}^d a_3) & 0 \\ 0 & 0 & (\theta_{13}^d a_1 + \theta_{23}^d a_2 + \theta_{33}^d a_3) \end{pmatrix} \quad (13)$$

If all the disproportionation constants are equal and have the value θ_d , the matrix Ψ becomes

$$\Psi = -c(t)\theta_d \mathbf{I} \quad (14)$$

where $c(t)$ is $(a_1 + a_2 + a_3)$ at time t and \mathbf{I} is the identity matrix. For this case eq. 11 becomes

$$\frac{d\mathbf{a}}{dt} = (\Theta - c(t)\theta_d \mathbf{I})\mathbf{a} \quad (15)$$

The characteristic vectors \mathbf{x}_i of the matrix Θ and \mathbf{I} are the same since any vector is a characteristic vector of \mathbf{I} . Hence

$$[\Theta - c(t)\theta_d \mathbf{I}]\mathbf{x}_i = -[\lambda_i + c(t)\theta_d]\mathbf{x}_i \quad (16)$$

where $-\lambda_i$ is the i th characteristic value of the matrix Θ . Therefore

$$\begin{aligned} \frac{d\mathbf{X}^{-1}\mathbf{a}}{dt} &= \mathbf{X}^{-1}[\mathbf{c}' - c(t)\theta_d \mathbf{I}]\mathbf{X}\mathbf{X}^{-1}\mathbf{a} \\ &= [\mathbf{X}^{-1}\Theta\mathbf{X} - c(t)\theta_d \mathbf{X}^{-1}\mathbf{I}\mathbf{X}]\mathbf{X}^{-1}\mathbf{a} \end{aligned} \quad (17)$$

where \mathbf{X} is the matrix of characteristic vectors of the matrix Θ . This gives

$$\frac{d\mathbf{b}}{dt} = [\Lambda - c(t)\theta_d \mathbf{I}]\mathbf{b} \quad (18)$$

where \mathbf{b} is the composition vector in terms of the characteristic species and Λ is the matrix of characteristic values of the matrix Θ .

Equation 18 can be integrated to give

$$\mathbf{b}(t) = e^{-\Lambda t} e^{-[\theta_d \int_0^t c(t) dt] \mathbf{I}} \mathbf{b}(0) \quad (19)$$

where $e^{-\Lambda t}$ and $e^{-[\theta_d \int_0^t c(t) dt] \mathbf{I}}$ are diagonal matrices given by

$$e^{-\Lambda t} = \begin{pmatrix} 1 & 0 & 0 \\ 0 & e^{-\lambda_1 t} & 0 \\ 0 & 0 & e^{-\lambda_2 t} \end{pmatrix} \quad (20)$$

and

$$e^{-[\theta_d \int_0^t c(t) dt] \mathbf{I}} = \left(\exp \left[-\theta_d \int_0^t c(t) dt \right] \right) \mathbf{I} \quad (21)$$

Hence, eq. 19 may be written

$$\mathbf{b}(t) = e^{-\theta_d \int_0^t c(t) dt} e^{-\Lambda t} \mathbf{b}(0) \quad (22)$$

According to eq. 22, each element of the vector \mathbf{b} , including the equilibrium composition b_0 , decays by the

factor $\exp \left[-\theta_d \int_0^t c(t) dt \right]$. Hence, if all components of \mathbf{b} are renormalized by the factor required to return $b_0(t)$ to its original value $b_0(0)$, eq. 22 becomes

$$\Phi \mathbf{b}(t) = e^{-\Lambda t} \mathbf{b}(0) \quad (23)$$

where $\Phi \mathbf{b}(t)$ is the renormalized $\mathbf{b}(t)$. (Since the vector $\mathbf{b}(t)$ will always be renormalized in the remainder of this paper, the distinction between these two vectors will be discontinued and the renormalized vector will also be designated $\mathbf{b}(t)$.) This operation is equivalent to renormalizing $a_1 + a_2 + a_3$ to unity. Consequently, when the disproportionation constants are all equal and the isomer mole fractions are renormalized to unity for each composition point, the reaction paths in the isomerization subspace are unchanged regardless of the extent of disproportionation.

In general, the larger the departure from equality of the disproportionation rate constants the larger the departure of the reaction paths from those characteristic of a pure isomerization system. In these studies the over-all reaction was first examined to determine the

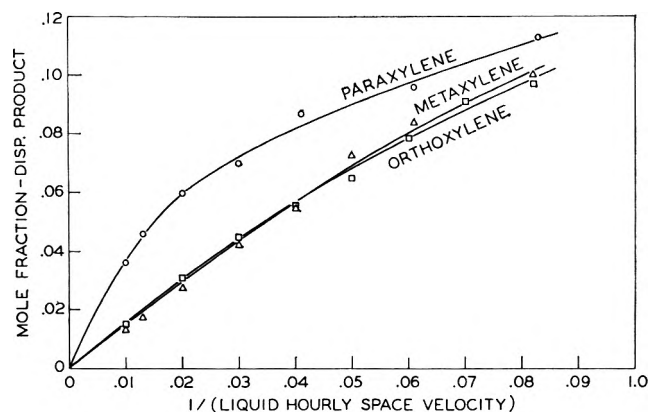
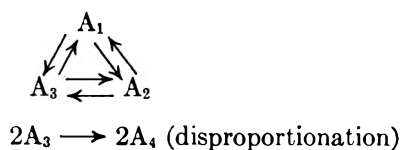


Figure 2. Comparative disproportionation of three xylene isomers.

relative importance of the disproportionation reaction. The results given in Fig. 2 show that the amount of disproportionation of the *p*-xylene isomer is somewhat higher than that of the *ortho* or *meta* isomer. It is also true that approximately 10% of the starting xylene is disproportionated on going from one corner of the isomerization plane to the neighborhood of isomerization equilibrium. In order to test qualitatively the possible effect of unequal disproportionation on the isomerization subspace in this particular study, a computer analysis was carried out on the model



The rate constant for the single disproportionation step was adjusted in such a way that when a reaction path had reached a point greater than 90% of the distance to isomerization equilibrium, the amount of A_4 produced was approximately 10 mole % of the mixture. Even with the one-sided disproportionation it was found that the perturbation of the projected reaction paths was small. Hence the Wei-Prater monomolecular model should provide an excellent approximation to the mass-action kinetics of xylene isomerization under the conditions used here. Of course, the justification for this is *a posteriori*; that is, normalized isomerization composition sequences have actually been found to fulfill the requirements of a pseudo-monomolecular reaction within experimental error.

II. Mass Action Isomerization Kinetics. A. Determination of the Equilibrium Vector. The equilibrium vector for the isomerization reaction alone will be designated \mathbf{a}^* with elements a_i^* . Taylor and co-workers¹¹ have determined the equilibrium composition of the

xylene system at 510° from thermodynamic data to be

$$\mathbf{a}^* = \begin{pmatrix} 0.253 \\ 0.514 \\ 0.233 \end{pmatrix} \quad (24)$$

We determined its value experimentally by allowing a mixture having a composition given by eq. 24 to react at various, progressively decreasing velocities of flow through the catalyst bed. The results gave

$$\mathbf{a}^* = \begin{pmatrix} 0.246 \\ 0.514 \\ 0.240 \end{pmatrix} \quad (25)$$

The value given by eq. 25 will be used in this paper for the first or equilibrium characteristic vector.

B. Determination of the Other Characteristic Vectors. The *o*-xylene reaction path was chosen as a convenient starting point for the determination of the first straight line reaction path (see WP (ref. 5), p. 227). The results are shown in Fig. 3. The approximately straight

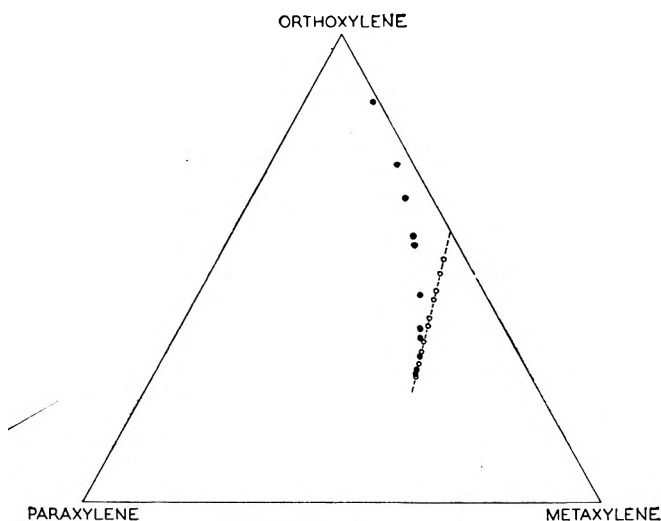


Figure 3. Location of first straight line reaction path:

- , composition points for $\mathbf{a}(0) = \begin{pmatrix} 1 \\ 0 \\ 0 \end{pmatrix}$,
- , composition points for $\mathbf{a}(0) = \begin{pmatrix} 0.580 \\ 0.420 \\ 0 \end{pmatrix}$.

line portion of the reaction path near equilibrium is extrapolated back to the reaction triangle to give a new starting composition.

(11) W. J. Taylor, D. D. Wagman, M. G. Williams, K. S. Pitzer, and F. D. Rossini, *J. Res. Natl. Bur. Std.*, **37**, 95 (1946).

$$\mathbf{a}(0) = \begin{pmatrix} 0.580 \\ 0.420 \\ 0.000 \end{pmatrix} \quad (26)$$

This composition is used as a new starting composition and its reaction path determined. It can be seen from Fig. 3 that this reaction path is very near the straight line reaction path. Hence least-squares methods are used to fit the nine composition points given in Table I to a straight line. Since the straight line must pass through the equilibrium point and the latter is considered to be more accurate than other composition points, the least-squares expressions are of the form

$$\frac{a_m - a_m^*}{a_j - a_j^*} = \frac{\langle a_m \rangle - a_m^*}{\langle a_j \rangle - a_j^*} \quad (27)$$

where a_m^* is the equilibrium value of a_m and $\langle a_m \rangle$ is the average value of a_m in the composition points included in the least-squares fit.

Treatment of the data in Table I by this method gives

$$\mathbf{a}_{x_1}(0) = \begin{pmatrix} 0.581 \\ 0.419 \\ 0.000 \end{pmatrix} \quad (28)$$

Table I: Composition Points for Determination of Straight Line Reaction Path

<i>o</i> -Xylene	<i>m</i> -Xylene	<i>p</i> -Xylene
0.491	0.445	0.064
0.456	0.454	0.090
0.435	0.459	0.106
0.395	0.472	0.133
0.379	0.476	0.145
0.347	0.485	0.168
0.325	0.492	0.183
0.298	0.500	0.202
0.270	0.507	0.223
Av. 0.3773	0.4767	0.1460

Since this value is so close to the above starting composition, it will be taken as the second characteristic composition vector. This gives for the second characteristic vector^{12a}

$$\begin{aligned} \mathbf{x}_1 &= \mathbf{a}_{x_1} - \mathbf{x}_0 \\ &= \begin{pmatrix} 0.581 \\ 0.419 \\ 0.000 \end{pmatrix} - \begin{pmatrix} 0.246 \\ 0.514 \\ 0.240 \end{pmatrix} = \begin{pmatrix} 0.335 \\ -0.095 \\ -0.240 \end{pmatrix} \quad (29) \end{aligned}$$

The third characteristic vector \mathbf{x}_2 can be computed from the values of the characteristic vectors \mathbf{x}_0 and \mathbf{x}_1

by use of the orthogonality relations given by Wei and Prater.^{12b} The value obtained is¹³

$$\mathbf{x}_2 = \begin{pmatrix} 0.177408 \\ -0.514000 \\ 0.336591 \end{pmatrix} \quad (30)$$

The value of the third characteristic composition vector $\mathbf{a}_{x_2}(0)$ is given by

$$\mathbf{a}_{x_2}(0) = \mathbf{x}_2 + \mathbf{x}_0 = \begin{pmatrix} 0.423408 \\ 0.000000 \\ 0.576591 \end{pmatrix} \quad (31)$$

The vectors \mathbf{x}_0 , \mathbf{x}_1 , and \mathbf{x}_2 are combined to form the matrix \mathbf{X} .

$$\mathbf{X} = \begin{pmatrix} 0.246000 & 0.335000 & 0.177408 \\ 0.514000 & -0.095000 & -0.514000 \\ 0.240000 & -0.240000 & 0.336591 \end{pmatrix} \quad (32)$$

The inverse matrix \mathbf{X}^{-1} is computed by use of eq. 44 and 46 from the paper of Wei and Prater. Its value is

$$\mathbf{X}^{-1} = \begin{pmatrix} 1 & 1 & 1 \\ 1.907915 & -0.258947 & -1.401037 \\ 0.647371 & 0.897667 & 1.253944 \end{pmatrix} \quad (33)$$

C. Determination of the Relative Rate Constant Matrices for the Characteristic and Natural Systems. The rate constant matrix for the characteristic system (eq. 3) is given by the diagonal matrix

$$\Lambda = \begin{pmatrix} 0 & 0 & 0 \\ 0 & -\lambda_1 & 0 \\ 0 & 0 & -\lambda_2 \end{pmatrix} \quad (34)$$

The rate constant matrix (34) can be converted into the relative rate constant matrix Λ' such that $\Lambda = \lambda_2 \Lambda'$, where

$$\Lambda' = \begin{pmatrix} 0 & 0 & 0 \\ 0 & -\lambda_1/\lambda_2 & 0 \\ 0 & 0 & -1 \end{pmatrix} \quad (35)$$

A plot of $\ln(b_1)$ vs. $\ln(b_2)$ has the slope of λ_1/λ_2 and the matrix Λ' can be determined from composition sequences alone. For this determination, the curved reaction path with

$$\mathbf{a}_0 = \begin{pmatrix} 0.700 \\ 0.000 \\ 0.300 \end{pmatrix} \quad (36)$$

was used. The composition points \mathbf{a} in the A system were converted to the composition points \mathbf{b} in the B

(12) (a) See WP (ref. 5), eq. 54; (b) p. 239.

(13) Six figures are carried to maintain internal consistency and to reduce the accumulation of errors caused by the computation procedure.

system by use of the matrix \mathbf{X}^{-1} . These data are shown in Table II. In Fig. 4, $\ln b_1$ is plotted against

Table II: Composition Points for Determination of λ_1/λ_2

a	$\mathbf{X}^{-1}\mathbf{a} = \mathbf{b}$
(0.700)	(1)
(0.000)	(0.9152)
(0.300)	(0.8308)
(0.664)	(1)
(0.054)	(0.8578)
(0.282)	(0.7364)
(0.658)	(1)
(0.066)	(0.8516)
(0.276)	(0.7142)
(0.631)	(1)
(0.104)	(0.8057)
(0.265)	(0.6488)
(0.577)	(1)
(0.181)	(0.7149)
(0.242)	(0.5157)
(0.535)	(1)
(0.240)	(0.6433)
(0.225)	(0.4142)
(0.522)	(1)
(0.257)	(0.6197)
(0.221)	(0.3854)
(0.492)	(1)
(0.296)	(0.5650)
(0.212)	(0.3197)
(0.457)	(1)
(0.337)	(0.4960)
(0.206)	(0.2527)
(0.435)	(1)
(0.363)	(0.4529)
(0.202)	(0.2100)

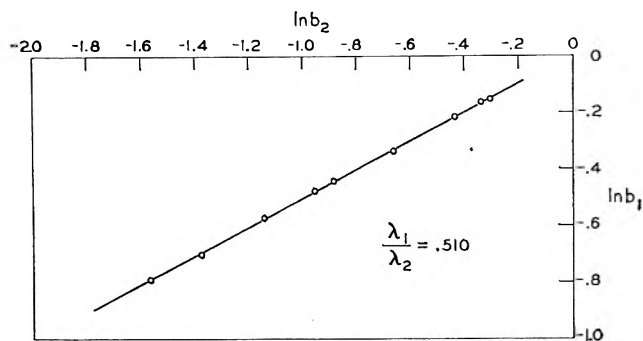
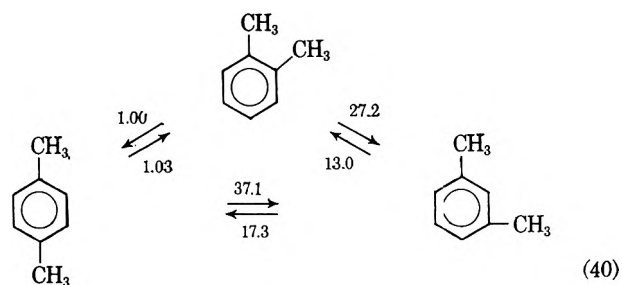


Figure 4. Plot of $\ln b_1$ vs. $\ln b_2$.

order to normalize θ_{31} to unity, the set of relative pseudo-first-order rate constants is obtained.



D. Calculation of Reaction Paths. Since the decay in the B system is represented by the set of eq. 4, the theoretical reaction paths can be calculated for any initial composition using the equations

$$\mathbf{b}(0) = \mathbf{X}^{-1}\mathbf{a}(0)$$

$$\mathbf{b}' = \begin{pmatrix} 1 & 0 & 0 \\ 0 & e^{-(\lambda_1/\lambda_2)t} & 0 \\ 0 & 0 & e^{-t} \end{pmatrix} \mathbf{b}(0) \quad (41)$$

$$\mathbf{a}' = \mathbf{X}\mathbf{b}'$$

for any arbitrary set of times. An even more convenient way of calculating reaction paths is provided by the \mathbf{T} matrix.¹⁵

The calculated paths along with the experimentally determined composition points are shown in Fig. 5. The only experimental data that have been used in the determination of the rate constants for the theoretical calculations are the equilibrium concentration of the isomerization reactions, the initial composition for the straight line reaction path indicated by the star, and data from the single curved reaction path indicated by the arrow in Fig. 5. It can be seen that the agreement is excellent in all regions of the isomerization subspace. Most important is the fact that the reaction studied

(14) See WP (ref. 5), eq. 67.

(15) See WP (ref. 5), eq. 77 and 78.

In b_2 . The slope of the straight line is determined by applying least-squares methods. The value of the slope, λ_1/λ_2 , is 0.510; hence

$$\Lambda' = \begin{pmatrix} 0 & 0 & 0 \\ 0 & -0.510 & 0 \\ 0 & 0 & -1 \end{pmatrix} \quad (37)$$

In the natural or A system, the relative rate constant matrix is given by eq. 12. This is calculated from Λ' by the equation¹⁴

$$\Theta = \mathbf{X}\Lambda'\mathbf{X}^{-1} \quad (38)$$

which gives

$$\Theta = \begin{pmatrix} -0.4408 & 0.2035 & 0.0160 \\ 0.4252 & -0.4739 & 0.5792 \\ 0.0156 & 0.2704 & -0.5952 \end{pmatrix} \quad (39)$$

Dividing all the off-diagonal elements by 0.0156 in

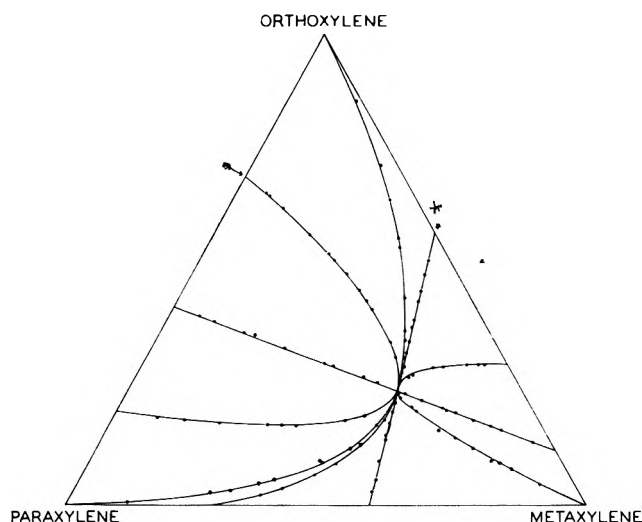


Figure 5. Experimental points and calculated reaction paths for xylene isomerization.

has been shown to follow the selectivity required by a pseudo-monomolecular model in *all* regions of the reaction simplex. Some of the consequences of this will be discussed in section IV.

III. Mass-Action Disproportionation Kinetics. In section II, it was shown that under the conditions used in this study, the isomerization of xylene over silica-alumina catalyst is quite accurately pseudo-monomolecular. Nevertheless, the isomerization is perturbed by the bimolecular disproportionation. Therefore, either the disproportionation does not appreciably disturb the pseudo-monomolecular character of the isomerization or it interacts with the isomerization kinetics to give the pseudo-monomolecular behavior. Although the qualitative hypothetical computer study discussed in section I reduces the possibility of the latter it is convenient to elucidate the structure of the disproportionation subspace and obtain a set of values for the rate constants for the six possible disproportionation reactions. Then, having the set of disproportionation rate constants, it is possible to evaluate quantitatively the perturbation of isomerization kinetics caused by the disproportionation kinetics. The set of differential equations which governs the total reaction simplex (isomerization and disproportionation) within the region of interest is given by eq. 9.

It appeared that the simplest and most accurate way of obtaining values for the three constants θ_{ii}^d is from the initial slopes of graphs of A_4 (disproportionated product) vs. time for each of the three xylene isomers. This is possible since at this point

$$\frac{da_4}{dt} = \theta_{ii}^d (a_i)^2 \quad (42)$$

and $(a_i)^2 = 1$; hence the slope is equal to θ_{ii}^d . The time data are the most difficult to reproduce in catalytic experiments. It is therefore desirable to carry out the necessary calculations solely on the basis of composition sequences using a hypothetical time scale. This places the set of disproportionation constants on the same relative basis as the set of isomerization rate constants. For example, the procedure for obtaining the value of θ_{22}^d follows. From the experimental data for an initial composition of *m*-xylene (Fig. 6) a curve is drawn giving

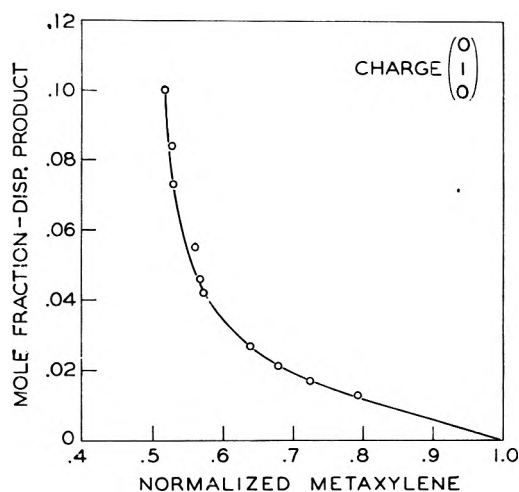


Figure 6. Disproportionated product vs.

normalized *m*-xylene for $\mathbf{a}(0) = \begin{pmatrix} 0 \\ 1 \\ 0 \end{pmatrix}$.

the variation of disproportionated product (A_4) as a function of normalized *m*-xylene. Then by using the set of relative rate constants already determined for isomerization, a set of isomerization composition points for an initial charge of *m*-xylene is calculated using a time scale that is characteristic of a set of real rate constants equal to the relative set given by scheme 40. With these data (Table III) a graph of A_4 vs. this time scale is constructed and θ_{22}^d obtained from the initial slope of this curve (Fig. 7). This process is repeated for an initial composition of *o*-xylene to obtain θ_{11}^d and an initial composition of *p*-xylene to obtain θ_{33}^d . The results are

$$\begin{aligned} \theta_{11}^d &= 1.3 \\ \theta_{22}^d &= 1.6 \\ \theta_{33}^d &= 4.3 \end{aligned} \quad (43)$$

In principle, it should be possible to obtain the three remaining constants θ_{ij}^d by using the appropriate xylene mixture of two isomers for each of the three possible

Table III: Hypothetical Time Scale for *m*-Xylene Reaction Path

$T \times 10^{-2}$	<i>o</i> -Xylene	<i>m</i> -Xylene	<i>p</i> -Xylene
0.05	0.006	0.985	0.009
0.1	0.013	0.971	0.016
0.2	0.025	0.943	0.032
0.3	0.036	0.917	0.047
0.4	0.047	0.893	0.060
0.5	0.057	0.870	0.073
0.6	0.066	0.849	0.085
0.8	0.084	0.810	0.106
1.0	0.099	0.775	0.126
1.2	0.113	0.745	0.142
1.4	0.126	0.718	0.156
1.6	0.137	0.694	0.169
1.8	0.147	0.674	0.179
2.0	0.157	0.655	0.188

combinations. In these cases the initial slopes of the graphs of A_4 vs. time are given by

$$\frac{da_4}{dt} = \theta_{i1}^d(a_i)^2 + \theta_{j1}^d(a_j)^2 + 2\theta_{ij}^d a_i a_j \quad (44)$$

However, since three reactions are involved and, particularly, since $a_i a_j$ is always ≤ 0.25 , the error magnification¹⁶ is quite large. Consequently, other methods were used to obtain these values.

The values of the three constants θ_{ij}^d are best obtained by fitting the reaction paths for the total composition space in the region of interest. The method employed is the generalized curve-fitting procedure of Howland and Vaillancourt.¹⁷ Since the data are in terms of composition sequences, time is removed from the set of eq. 9 and a_4 is made the independent variable

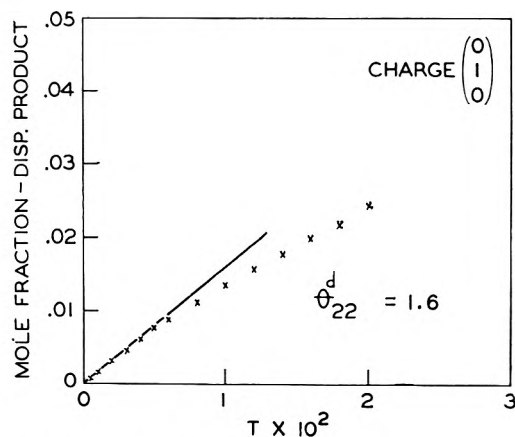


Figure 7. Disproportionated product vs. hypothetical time scale for $\mathbf{a}(0) = \begin{pmatrix} 0 \\ 1 \\ 0 \end{pmatrix}$.

to give a new set of three primary differential equations

$$\begin{aligned} \frac{da_1}{da_4} &= f_1(a_1, a_2, a_3) \\ \frac{da_2}{da_4} &= f_2(a_1, a_2, a_3) \\ \frac{da_3}{da_4} &= f_3(a_1, a_2, a_3) \end{aligned} \quad (45)$$

The differential equations of "variation" are of the form

$$\frac{d}{da_4} \frac{\partial a_1}{\partial \theta_{ij}^d} = f \left(a_1, a_2, a_3, \frac{\partial a_1}{\partial \theta_{ij}^d}, \frac{\partial a_2}{\partial \theta_{ij}^d}, \frac{\partial a_3}{\partial \theta_{ij}^d} \right) \quad (46)$$

The number of equations of variation is always equal to the number of primary equations times the number of variable parameters.

At first a three-parameter variation was carried out on the reaction path with

$$\mathbf{a}(0) = \begin{pmatrix} 1 \\ 0 \\ 0 \end{pmatrix} \quad (47)$$

That is, all three rate constants¹⁸ θ_{12}^d , θ_{23}^d , and θ_{13}^d were allowed to vary simultaneously in obtaining a fit of this reaction path. The best least-squares values obtained were

$$\begin{aligned} \theta_{12}^d &= 0.85 \\ \theta_{13}^d &= 4.1 \\ \theta_{23}^d &= -1.7 \end{aligned} \quad (48)$$

The negative value for θ_{23}^d is clearly not admissible. It arises in this case because the three-parameter variation method is relatively insensitive to the values of some of the rate constants. This is shown by the fact that many sets of values could be obtained that differ greatly from the set of "best values" but which simulate the experimental data with almost the same root-mean-square deviation. For example

$$\begin{aligned} \theta_{12}^d &= 1.35 \\ \theta_{13}^d &= 0.20 \\ \theta_{23}^d &= 0.10 \end{aligned} \quad (49)$$

(16) It can easily be seen that even if there are no errors in θ_{ij}^d and θ_{jj}^d , the error in the slope will be multiplied by at least a factor of four in determining $2\theta_{ij}^d$, since $a_i a_j \leq 0.25$.

(17) J. L. Howland and R. Vaillancourt, *J. Soc. Ind. Appl. Math.*, **9**, 165 (1961).

(18) In these regression calculations, which were carried out to determine the three constants θ_{ij}^d , the six isomerization rate constants and the three constants θ_{ii}^d were always taken to be known parameters.

It becomes apparent that the system with such complex coupling contains too many degrees of freedom for a meaningful three-parameter fit on one reaction path.

The solution would not be improved significantly by fitting all the reaction paths separately and averaging the results. The reason is that arithmetic averaging of the sets of parameters determined in this type of computation makes the *a priori* assumption that different reaction paths from different regions of the simplex are all equally sensitive to each of the rate constants in the set. This is not the case since a particular reaction path may be extremely sensitive to a particular rate constant, say θ_{12}^d , whereas some other reaction path may be almost insensitive to the same rate constant.

To circumvent these difficulties, a numerical integration procedure was used to determine the sensitivity of various regions of the reaction simplex to each of the three rate constants; that is, the error sensitivity of the various regions of the reaction simplex was mapped. This was done in the following way. For each region a reaction path was obtained for the case where all three constants θ_{ij}^d were zero. Then each of the constants θ_{ij}^d was individually allowed to vary from zero to some reasonable upper limit. By observing the effect on the curve, it was possible to determine if that reaction path had a significant sensitivity to the rate constant that was varied.

It was found that the reaction path with

$$\mathbf{a}(0) = \begin{pmatrix} 1 \\ 0 \\ 0 \end{pmatrix}$$

was quite sensitive to θ_{12}^d and that the two reaction paths with

$$\mathbf{a}(0) = \begin{pmatrix} 0 \\ 0 \\ 1 \end{pmatrix}; \quad \mathbf{a}(0) = \begin{pmatrix} 0 \\ 0.3 \\ 0.7 \end{pmatrix}$$

were fairly sensitive to θ_{23}^d . In addition, it was found that only those paths having their origin on the *ortho-para* leg of the isomerization plane showed any significant sensitivity to θ_{13}^d .

Using this information, an iterative procedure employing a series of three one-parameter variations was developed. This is shown schematically in Fig. 8. In those cases where more than one initial composition was used for the determination of a rate constant, the results were arithmetically averaged since error sensitivities were approximately equal. The results of this iterative procedure are shown in Table IV. The values obtained for the three rate constants are

$$\begin{aligned} \theta_{12}^d &= 0.7 \\ \theta_{23}^d &= 0.45 \\ \theta_{13}^d &= 3.0 \end{aligned} \quad (50)$$

The total set of 12 rate constants is then used in a numerical integration to calculate the theoretical reaction paths in the tetrahedral space (isomerization and disproportionation) in the region of interest. Each reaction path is of course a curve in three-dimensional space, but each path can be represented as a set of three curves in a two-dimensional space. These two-dimensional representations are given in Fig. 9

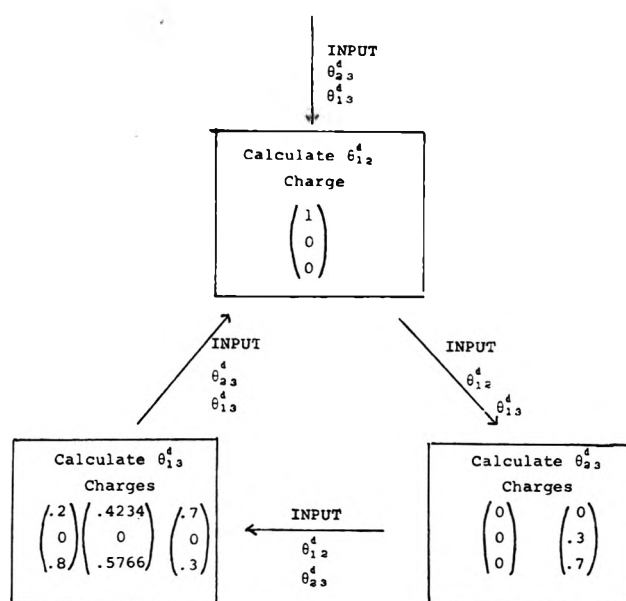


Figure 8. Iterative procedure for calculation of θ_{ij}^d . The set of six isomerization constants and the three θ_{ij}^d are considered as known in these calculations.

Table IV: Iterative Results in Calculation of θ_{ij}^d

Iteration	Variable rate constant	Input ^a			Output ^a
		θ_{12}^d	θ_{23}^d	θ_{13}^d	
1	θ_{12}^d	...	1.25	1.25	0.9
	θ_{23}^d	0.9	...	1.25	0.65
	θ_{13}^d	0.9	0.65	...	2.75
2	θ_{12}^d	...	0.65	2.75	0.7
	θ_{23}^d	0.7	...	2.75	0.45
	θ_{13}^d	0.7	0.45	...	2.95
3	θ_{12}^d	...	0.45	2.95	0.7
	θ_{23}^d	0.7	...	2.95	0.45
	θ_{13}^d	0.7	0.45	...	3.0
4	θ_{12}^d	...	0.45	3.0	0.7
	θ_{23}^d	0.7	...	3.0	0.45
	θ_{13}^d	0.7	0.45	...	3.0

^a The numbers appearing in this table have been rounded off. In the actual calculations one or two more places were carried.

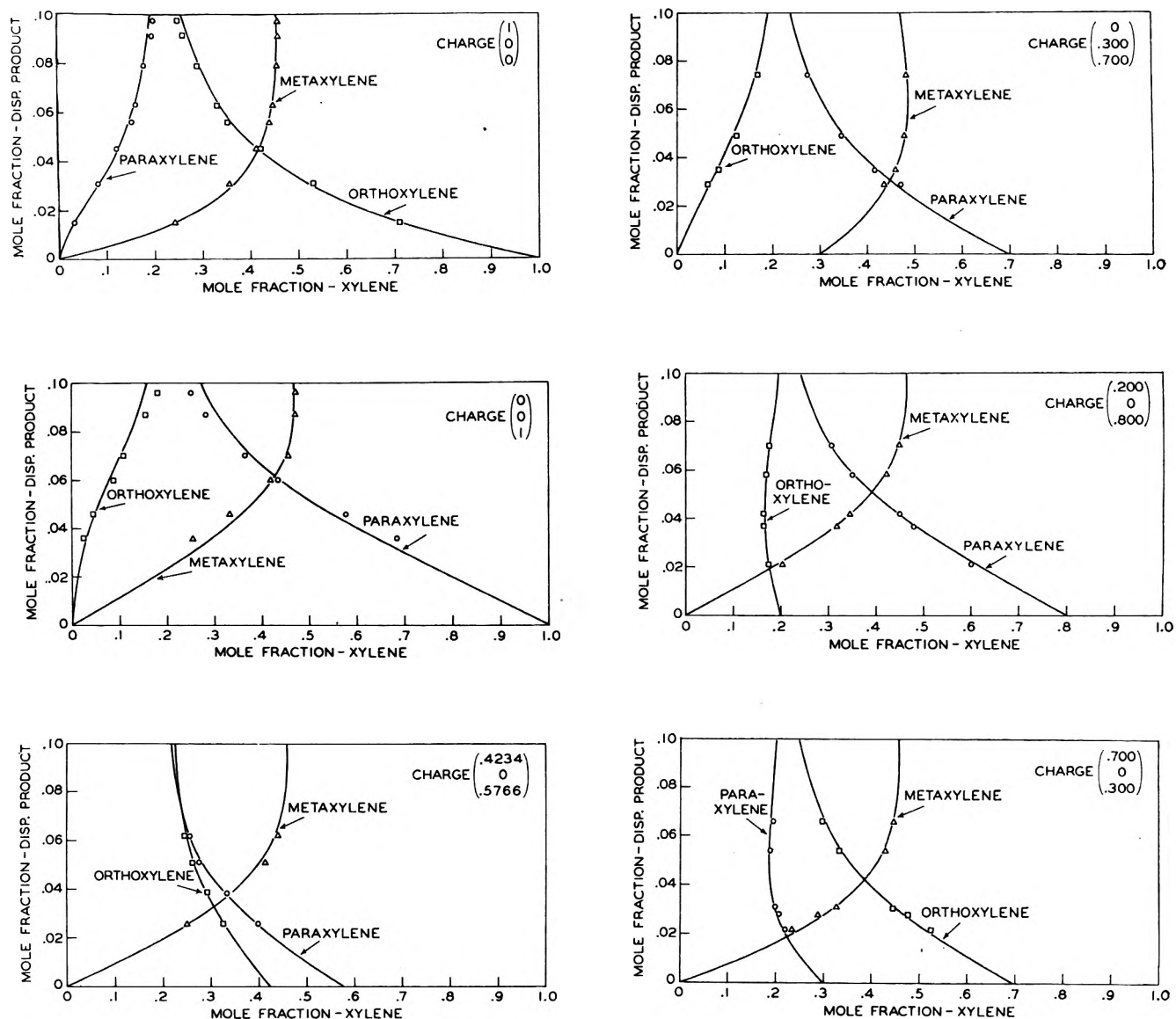


Figure 9. Experimental points and calculated reaction paths for initial compositions used in iterative procedure.

and 10 together with the experimentally determined points for the eleven reaction paths studied.

As expected, in the case of those initial compositions from which data were used in the iterative procedure, the experimental points agree quite well with the calculated reactions paths (Fig. 9). The remaining reaction paths given in Fig. 10 were *not* used in the regression calculations. Nevertheless, the agreement between the experimental points and the calculated reaction paths is as good as for those used in the calculations. Furthermore, the reaction paths not used in the regression calculations are from different regions of the reaction simplex than those used in the iterative procedure. This is shown in Fig. 11.

Having the set of disproportionation rate constants

it is possible to evaluate quantitatively the perturbation of isomerization kinetics caused by the disproportionation kinetics. Hence the calculated total reaction paths (isomerization and disproportionation) were projected (by normalization) onto the isomerization plane of the reaction simplex. This is illustrated in Fig. 12, where the reaction paths which would exist if there were no disproportionation reaction are shown as lines and some of the calculated projections of the total reaction paths are shown as crosses. It can be seen that the deviation is very slight. Therefore, it can be concluded that disproportionation does not appreciably disturb the pseudo-monomolecular character of the isomerization reaction.

IV. Relation of Pseudo-Rate Constants to Mechanism.

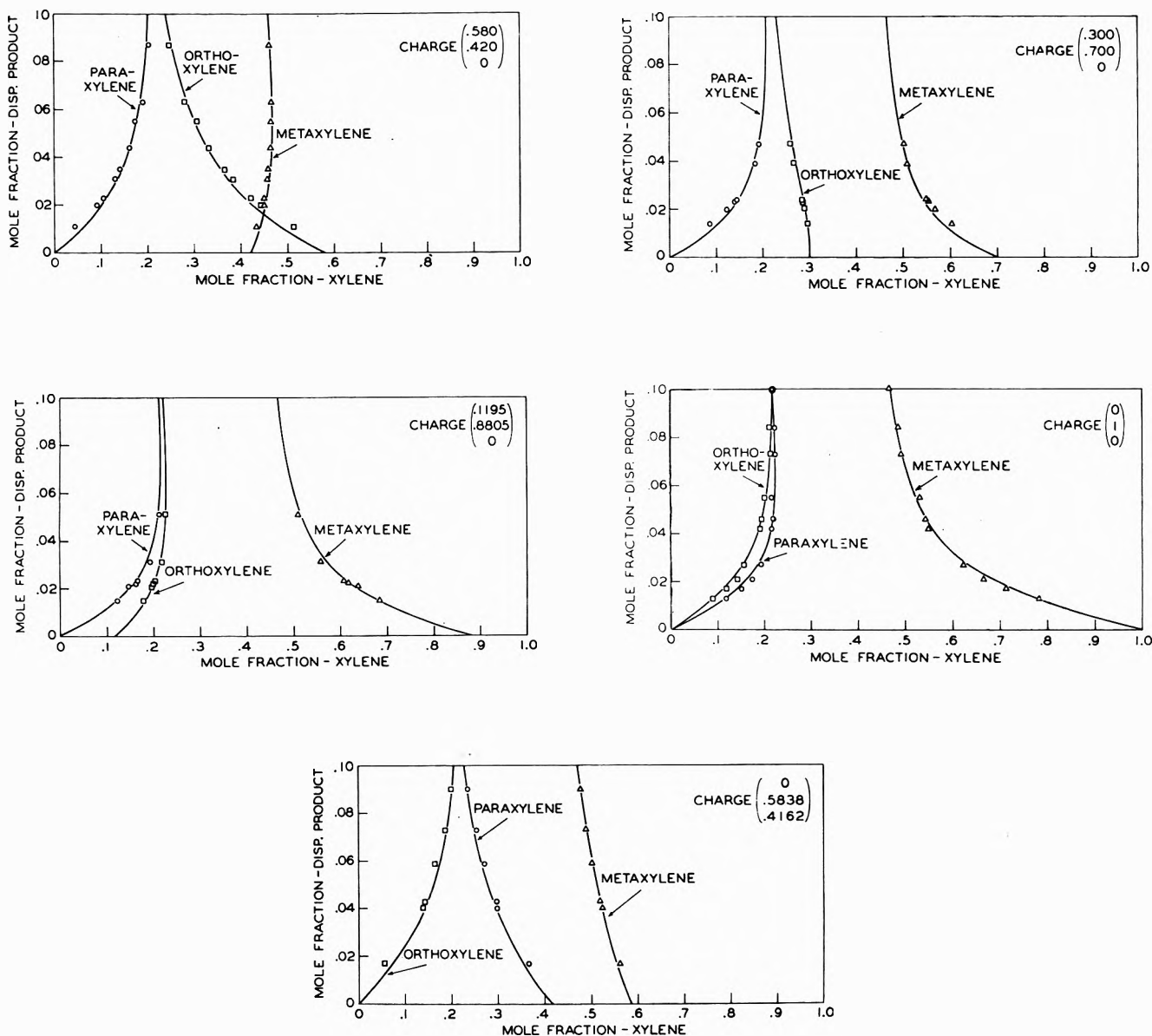
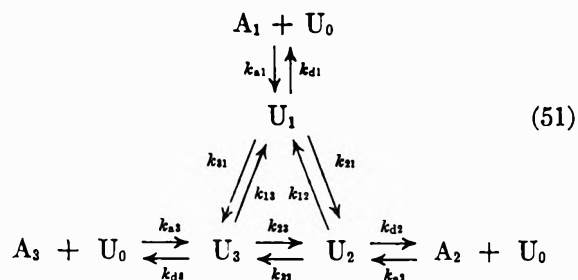


Figure 10. Experimental points and calculated reaction paths for initial compositions not used in iterative procedure.

Let us examine the explicit relations between the pseudo-rate constants and the true rate constants for this system. The selectivity behavior of the isomerization reactions is consistent with the monomolecular behavior given by eq. 7. If the selectivity behavior of a heterogeneous catalytic system is like that of a monomolecular system, Wei and Prater¹⁹ have shown that one of the following conclusions must hold. Either only a single type of catalytically active site is present on the catalyst to any appreciable extent or, if more than one type of active site is present, either (a) the adsorption properties of all free molecular species are such that only the linearly increasing portions of their adsorption isotherms are involved or (b) the strengths of all adsorption

on all types of active sites are equal. The most likely case is that a single site exists; for this case, the isomerization system can be represented by the detailed scheme



where k_{a_i} is the rate of adsorption of A_i , k_{d_i} is the rate of desorption of A_i , U_0 is the free active site, and U_i is the adsorbed species corresponding to A_i .

Using the method of Wei and Prater,²⁰ to obtain the kinetic equations, the following matrices are defined

$$\mathbf{U} = \begin{pmatrix} (k_{21} + k_{31}) & -k_{12} & -k_{13} \\ -k_{21} & (k_{12} + k_{32}) & -k_{23} \\ -k_{31} & -k_{32} & (k_{13} + k_{23}) \end{pmatrix} \quad (52)$$

and

$$\mathbf{G} = \begin{pmatrix} (k_{d1} + k_{21} + k_{31}) & -k_{12} & -k_{13} \\ -k_{21} & (k_{d2} + k_{32} + k_{12}) & -k_{23} \\ -k_{31} & -k_{32} & (k_{d3} + k_{23} + k_{13}) \end{pmatrix} \quad (53)$$

Then by using the equation²¹

$$\theta_{ij} = -k_{a_i} |\mathbf{G}^{ij}| \quad (54)$$

where \mathbf{G}^{ij} is the matrix found by replacing the j th row of \mathbf{G} by the i th row of \mathbf{U} one can find the desired relations. These are

$$\begin{aligned} \theta_{12} &= k_{a2}k_{d1}[k_{12}(k_{d3} + k_{23} + k_{13}) + k_{32}k_{13}] \\ \theta_{13} &= k_{a3}k_{d1}[k_{13}(k_{d2} + k_{32} + k_{12}) + k_{12}k_{23}] \\ \theta_{21} &= k_{a1}k_{d2}[k_{21}(k_{d3} + k_{23} + k_{13}) + k_{23}k_{31}] \\ \theta_{23} &= k_{a3}k_{d2}[k_{23}(k_{d1} + k_{21} + k_{31}) + k_{13}k_{21}] \\ \theta_{32} &= k_{a2}k_{d3}[k_{32}(k_{d1} + k_{21} + k_{31}) + k_{31}k_{12}] \\ \theta_{31} &= k_{a1}k_{d3}[k_{31}(k_{d2} + k_{32} + k_{12}) + k_{21}k_{32}] \end{aligned} \quad (55)$$

Chemical experience²² indicates that for xylene isomerization $k_{31} \approx k_{13} \approx 0$ or that the isomerization

takes place in a series of 1,2-methyl shifts without any significant 1,3-alkyl migration. Since the question arises as to whether the small values of θ_{31} and θ_{13} relative to the values of the remaining pseudo-first-order rate constants are directly indicative of a 1,2-methyl shift mechanism, let us investigate whether the kinetic data can be used to support or deny the existence of a 1,3-methyl migration. Setting k_{13} and k_{31} equal to zero in the set of eq. 55 and using the observed values of the rate constants θ_{ij} , one obtains eq. 56.

$$\begin{aligned} \frac{\theta_{23}}{\theta_{13}} &= \frac{k_{d2}k_{d1} + k_{d2}k_{21}}{k_{d1}k_{12}} = 36.0 \\ \frac{\theta_{21}}{\theta_{31}} &= \frac{k_{d2}k_{d3} + k_{d2}k_{23}}{k_{d3}k_{32}} = 27.2 \end{aligned} \quad (56)$$

Thus, if k_{31} and k_{13} are zero, then

$$\begin{aligned} k_{d1}k_{12} &\ll k_{d2}(k_{d1} + k_{21}) \\ k_{d3}k_{32} &\ll k_{d2}(k_{d3} + k_{23}) \end{aligned} \quad (57)$$

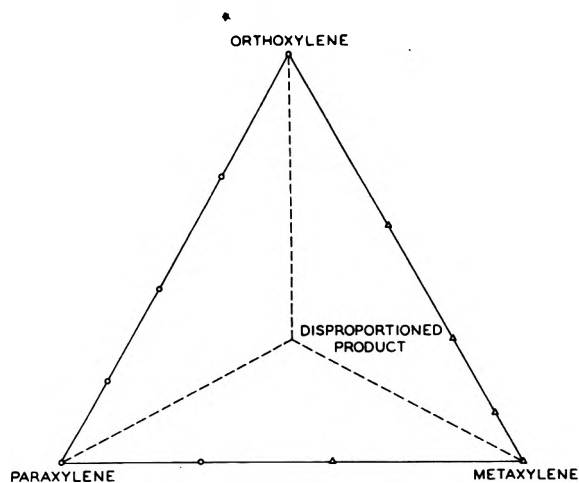


Figure 11. Initial compositions of reaction paths: O, initial compositions used in iterative procedure; Δ , initial compositions not used in iterative procedure.

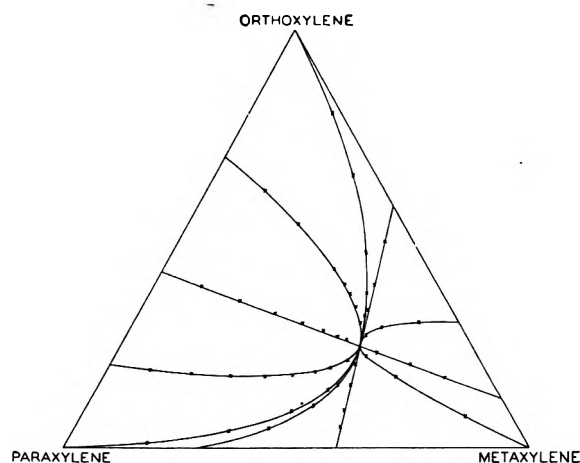


Figure 12. Reaction paths for isomerization and projections of reaction paths for isomerization and disproportionation.

However, these conditions may not apply and require experimental verification. One way in which the condition (57) can be satisfied is

- (19) See WP (ref. 5), p. 333.
 (20) See WP (ref. 5), eq. 321 and 322.
 (21) See WP (ref. 5), eq. 333.
 (22) H. C. Brown and H. Jungk, *J. Am. Chem. Soc.*, **77**, 5579 (1955)

$$k_{di} \gg k_{ij} \quad (58)$$

The assumption that the rates of adsorptions and desorptions are so much faster than the rates of surface reactions, that is the gas phase species are essentially in adsorption equilibrium with their corresponding surface species, is consistent with condition (58). This assumption is often made without sufficient experimental justification and may not be applicable.

Some of the hazards of reasoning directly from such kinetic studies to mechanistic conclusions in heterogeneous systems will be further illustrated. The values of the rate constants θ_{ij} can be such as to indicate a direct path between two species where there actually is none. For example, in the above case if $k_{13} = k_{31} = 0$, and $k_{d1}, k_{d3} \gg k_{d2}$ then θ_{31} and θ_{13} can take significant values relative to the values of the remaining rate constants θ_{ij} . Conversely, the values of the rate constants θ_{ij} can be such as to indicate the absence of a direct path between two species where there actually is one. For example, in the above case the small relative values of θ_{31} and θ_{13} are not necessarily indicative of the absence of a direct path between U_1 and U_3 . Let us consider what form the set of eq. 56 takes if k_{13} and k_{31} are not set equal to zero. From the set of eq. 55, one obtains

$$\begin{aligned} \frac{\theta_{23}}{\theta_{13}} &= \frac{k_{d2}[k_{23}(k_{d1} + k_{21} + k_{31}) + k_{13}k_{21}]}{k_{d1}[k_{13}(k_{d2} + k_{32} + k_{12}) + k_{12}k_{23}]} \\ \frac{\theta_{21}}{\theta_{31}} &= \frac{k_{d2}[k_{21}(k_{d3} + k_{23} + k_{13}) + k_{23}k_{31}]}{k_{d3}[k_{31}(k_{d2} + k_{32} + k_{12}) + k_{21}k_{32}]} \end{aligned} \quad (59)$$

These can easily be rearranged to give

$$\begin{aligned} \frac{\theta_{23}}{\theta_{13}} &= \frac{k_{d2}k_{d1}k_{23} + k_{d2}[k_{23}(k_{21} + k_{31}) + k_{13}k_{21}]}{k_{d2}k_{d1}k_{13} + k_{d1}[k_{13}(k_{32} + k_{12}) + k_{12}k_{23}]} \\ \frac{\theta_{21}}{\theta_{31}} &= \frac{k_{d2}k_{d3}k_{21} + k_{d2}[k_{21}(k_{23} + k_{13}) + k_{23}k_{31}]}{k_{d3}k_{d1}k_{31} + k_{d3}[k_{31}(k_{32} + k_{12}) + k_{21}k_{32}]} \end{aligned} \quad (60)$$

It is now apparent that if the rate constants k_{ij} are approximately equal and it is also true that $k_{ij}, k_{d2} \gg k_{d1}, k_{d3}$, then the values of θ_{13} and θ_{31} will be relatively small compared to the values of θ_{21} and θ_{23} .

This will occur in spite of the fact that k_{13} and k_{31} have values essentially equal to those of the remaining rate constants k_{ij} . Hence, the apparent kinetic behavior of a heterogeneous catalytic reaction as viewed from the gas phase does not, in general, mirror directly the kinetic behavior of the surface reaction and care must be taken in drawing conclusions from such studies. Knowledge concerning the adsorption steps is required. This may be obtained from a study of the isotherm or φ term of the rate equation (5). In addition, examination of the structure of the φ -term, for the general case, shows that transient studies may be required before kinetic experiments alone are sufficient to determine the sequence of a surface reaction.

Acknowledgment. The authors wish to thank Mr. R. J. Kelly of this laboratory for making available the numerical integration program and for suggesting the use of the Howland-Vaillancourt procedure and making available the program necessary for its application.

Spin-Free Quantum Chemistry. II. Three-Electron Systems^{1a}

by F. A. Matsen

Molecular Physics Group, The University of Texas, Austin, Texas (Received April 22, 1964)

There exists a spin-free formulation of the quantum mechanics of any polyelectronic system with a spin-free Hamiltonian. This was discussed in paper I of this series.^{1b} In the present paper, we briefly summarize the conclusions of I and explore the three-electron problem in considerable detail. As examples, we consider three hydrogen atoms, Rydberg states of lithium, and the effect of paramagnetic molecules on "spin-forbidden" transitions.

1. Introduction

The spin-free formulation of quantum chemistry^{1b} is based on the commutation of a spin-free Hamiltonian with the $N!$ permutations on the space coordinates² of the N electrons. The spin-free formulation makes use of the theorems of the permutation group and the permutation group algebra. We formulate the quantum mechanics in terms of a permutation vector space of $N!$ dimensions. The permutation vector space is decomposed into subspaces, called permutation states, each characterized by a partition³ of N and each lying in one-to-one correspondence with the irreducible representations of the permutation group. Certain permutation states are excluded by the Pauli principle. For electrons, the allowed permutation states are characterized by partitions each of which are specified by a single integer called the permutation quantum number. The permutation quantum number for a particular permutation state is equal to the number of electron pairs in that state.

Each allowed vector subspace is spanned by a structure basis whose elements lie in one-to-one correspondence with the canonical chemical structures. Each state vector lies wholly in a subspace and is represented by a linear combination (*e.g.*, a resonance hybrid) of the canonical structure basis elements which span the subspace. The coefficients of the eigenvector and its eigenvalue are determined from a secular equation appropriate to the subspace. An equivalent basis for any vector subspace is the matrix basis. This basis offers certain mathematical advantages but lacks direct connection with chemical structures.

In computational quantum mechanics the spin-free formulation yields eigenvalues which are identical

with those obtained by the conventional antisymmetrized space-spin formulation. In this article we are not concerned with the computational aspects of the problem. Instead, we seek out those relationships which arise from the permutational symmetry.

There have been voiced several objections to a spin-free quantum chemistry. We present both the objections and our rebuttals.

(1) Spin is an intrinsic property of the electron and so should not be neglected in any discussion of electronic properties.

A complete relativistic treatment of two or more electrons has not been formulated. For these systems, it is necessary to assume the separability of space and spin coordinates. With this approximation, the results for a spin-free Hamiltonian are identical in the spin-free and in the antisymmetric space-spin formulation. It should be pointed out that many effects attributed to spin should in fact be attributed to the permutational symmetry which is induced on the space function by the Dirac identity coupled with the antisymmetry principle. It should be noted that the formulation of a spin-free quantum chemistry does not constitute a denial of the existence of spin.

(2) The spin-free formulation requires a knowledge of group theory.

(1) (a) This research was supported by the Robert A. Welch Foundation of Houston, Texas, and the National Aeronautics and Space Administration; (b) F. A. Matsen, "Advances in Quantum Chemistry," Vol. I, P. O. Lowdin, Ed., Academic Press, New York, N. Y., in press. See also, F. A. Matsen, "Finite Group Algebras and Quantum Mechanics," Technical Report, Molecular Physics Group, The University of Texas, October, 1962.

(2) Space coordinate here is shorthand for coordinates in Euclidian three-space, *e.g.*, x , y , and z . This space does not contain spin coordinates.

(3) A set of integers whose sum is N .

Group theory is now a standard course in the graduate schools of our large universities. The treatment of the permutation group requires a small addition to the conventional point group course.

(3) The spin-free formulation is abstract and does not relate to chemistry.

With the development of the structure operator this criticism is no longer valid. The structure operators, and the spin-free structure functions they project, lie in one-to-one correspondence with the classical chemical structures. The structure functions, since they are spin-free, give a clearer view of the forces which operate in our chemical systems.

A brief summary of the relevant group algebra is presented in Appendices I, II, and III. Further details can be found in ref. 1b.

2. The Permutation Vector Space. Its Regular Basis⁴

In the quantum mechanical application of group algebra,⁴ the algebraic elements are applied to functions of the space coordinates of the N electrons. We are not interested in the detailed form of the functions. We are interested only in the way in which the functions transform under the algebraic operators and in the relationships which the permutational symmetry induces among matrix elements over these functions. It is convenient to represent these relationships in terms of a permutation vector space. We use Dirac kets as vectors, bras as their duals, and the bracket as the scalar product.

The permutation vector space for N objects is a space spanned by the $N!$ kets

$$\eta^r = \{|1\rangle, \dots |a\rangle, \dots |N!\rangle\} \quad (2.1)$$

where

$$|a\rangle = P_a|g\rangle \quad (2.2)$$

The ket $|1\rangle = |g\rangle$ is called the primitive ket. The basis η^r is called the regular basis of the vector space.

For $N = 3$

$$\eta^r = \{|g\rangle, |(12)\rangle, |(13)\rangle, |(23)\rangle, |(123)\rangle, |(132)\rangle\}$$

In quantum mechanical calculations the primitive ket assigns arbitrarily numbered electrons to the physical space of the system.

For $N = 3$, two examples of primitive kets are (i) the orbital product for three hydrogen atoms

$$|g\rangle = a(1)b(2)c(3)$$

(ii) the James and Coolidge function⁵ for lithium

$$|g\rangle = \sum c(i, j, k, l, m, n) r_1^i r_2^j r_3^k r_{12}^l r_{13}^m r_{23}^n \exp[-(\alpha r_1 + \beta r_2 + \gamma r_3)]$$

Let

$$X = \sum_a (X)_a P_a \quad (2.3)$$

be an element in the permutation algebra. Corresponding to each X is a vector in the permutation vector space.

$$|X\rangle \equiv X|g\rangle = \sum_a (X)_a P_a|g\rangle = \sum_a (X)_a |a\rangle \quad (2.4)$$

The dual vector space is spanned by the bras

$$\langle a| = \langle g|P_a^{-1} \quad (2.5)$$

A scalar product (bracket) in the permutation vector space is written

$$\begin{aligned} \langle a|b\rangle &= \langle g|P_a^{-1}P_b|g\rangle \\ &= \langle g|P_c|g\rangle \\ &= \langle g|c\rangle \\ &= \langle d|g\rangle \end{aligned} \quad (2.6)$$

Here $P_a^{-1}P_b = P_c = P_a^{-1}$. Note that

$$\langle a|a\rangle = \langle g|g\rangle \quad (2.7)$$

Since $X|b\rangle$ is also a ket, we can form the scalar product $\langle a|X|b\rangle$. The set of elements $\langle a|X|b\rangle$ where $a, b = 1$ to $N!$ is called the representation of X in the regular basis. Since $\langle a|b\rangle = \langle a|g|b\rangle$, the set of the elements $\langle a|b\rangle$ where $a, b = 1$ to $N!$ is the representation of the identity operator in the regular basis.

For $N = 3$ we set $\langle g|g\rangle \equiv q$, $\langle(12)|g\rangle \equiv a$, $\langle(13)|g\rangle \equiv b$, $\langle(23)|g\rangle \equiv c$, $\langle(123)|g\rangle \equiv d$. Note that if the kets are real, $\langle(123)|g\rangle = \langle(132)|g\rangle$.⁶ The matrix of the identity operator in the regular basis is

	$ g\rangle$	$ (12)\rangle$	$ (13)\rangle$	$ (23)\rangle$	$ (123)\rangle$	$ (132)\rangle$
$\langle g $	q	a	b	c	d	d
$\langle(12) $	a	q	d	d	c	b
$\langle(13) $	b	d	q	d	a	c
$\langle(23) $	c	d	d	q	b	a
$\langle(123) $	d	c	a	b	q	d
$\langle(132) $	d	b	c	a	d	q

The Hamiltonian is a linear operator in the permutation vector space. Thus $H|b\rangle$ is a ket lying in the vector space. Its scalar product with a bra $\langle a|$ is

(4) See Appendix I.

(5) See, for example, E. A. Burke, *Phys. Rev.*, **130**, 1871 (1963).

(6) This equality has been pointed out by J. L. Calais, Preprint No. 71, Quantum Chemistry Group, Uppsala, Sweden, December, 1961.

$$\begin{aligned}
 \langle a|H|b\rangle &= \langle g|P_a^{-1}P_bH|g\rangle \\
 &= \langle g|P_cH|g\rangle \\
 &= \langle g|H|c\rangle \\
 &= \langle d|H|g\rangle \quad (2.8)
 \end{aligned}$$

This $N! \times N!$ matrix $[\langle a|H|b\rangle]$ is called the representation of the Hamiltonian in the regular basis.

For $N = 3$ we set $Q \equiv \langle g|H|g\rangle$, $\alpha \equiv \langle(12)|H|g\rangle$, $\beta \equiv \langle(13)|H|g\rangle$, $\gamma \equiv \langle(23)|H|g\rangle$, $\delta \equiv \langle(123)|H|g\rangle = \langle(132)|H|g\rangle$. The matrix of the Hamiltonian in the regular basis is

$ g\rangle$	Q	α	β	γ	δ	δ
$\langle(12) $	α	Q	δ	δ	γ	β
$\langle(13) $	β	δ	Q	δ	α	γ
$\langle(23) $	γ	δ	δ	Q	β	α
$\langle(123) $	δ	γ	α	β	Q	δ
$\langle(132) $	δ	β	γ	α	δ	Q

The eigenkets are

$$|K\rangle = \sum_a^{N!} \langle a|K\rangle |a\rangle \quad (2.9)$$

Their coefficients are formally determined from the set of simultaneous equations

$$\sum_a^{N!} (\langle b|H|a\rangle - E_K \langle b|a\rangle) \langle a|K\rangle = 0 \quad b = 1 \text{ to } N! \quad (2.10)$$

The $N!$ eigenvalues E_K are obtained from the secular equations

$$\langle b|H|a\rangle - E \langle b|a\rangle = 0 \quad a, b = 1 \text{ to } N! \quad (2.11)$$

We discuss eigenvalues and the eigenkets in subsequent sections.

3. The Permutation Vector Space. Its Matrix Basis⁷

The application of group theory to quantum mechanics accomplishes the following results. (1) It introduces zeros into the representation of the Hamiltonian. (2) It provides a labeling for the eigenstates. (3) For these states, it specifies the degeneracy which arises from the symmetry of the Hamiltonian. In the present case, we are interested in permutational symmetry.

These features are clearly exhibited if we take as the basis for the permutation vector space, the matrix basis

$$\begin{aligned}
 \eta^m &= \{ \dots | \alpha r s \rangle \dots \} \\
 \alpha &= 1 \text{ to } p(N), r, s = 1 \text{ to } f^\alpha \quad (3.1)
 \end{aligned}$$

where

$$\begin{aligned}
 |\alpha r s\rangle &= N_s^\alpha e_{r_s}^\alpha |g\rangle \\
 &= N_s^\alpha (f^\alpha / N!) \sum_a [P_a^{-1}]_{sr}^\alpha |a\rangle \quad (3.2)
 \end{aligned}$$

Here N_s^α is a normalization factor, and the $e_{r_s}^\alpha$ are matrix basis elements. See Appendix A2.

For $N = 3$

$$\begin{aligned}
 \eta^m &= \{ \{ |1^3\rangle 11 \}, \{ |2,1\rangle 11 \}, \{ |2,1\rangle 12 \}, \{ |2,1\rangle 21 \}, \\
 &\quad \{ |2,1\rangle 22 \}, \{ |3\rangle 11 \} \} \\
 \{ |1^3\rangle 11 \} &= (N_1^{(1^3)}/6) \{ |g\rangle - |(12)\rangle - |(13)\rangle - |(23)\rangle + \\
 &\quad |(123)\rangle + |(132)\rangle \} \\
 \{ |2,1\rangle 11 \} &= (N_1^{(2,1)}/3) \{ |g\rangle + |(12)\rangle - (1/2)|(13)\rangle - \\
 &\quad (1/2)|(23)\rangle - (1/2)|(123)\rangle - (1/2)|(132)\rangle \} \\
 \{ |2,1\rangle 12 \} &= (N_2^{(2,1)}/2\sqrt{3}) \{ 0 + 0 + |(13)\rangle - |(23)\rangle - \\
 &\quad |(123)\rangle + |(132)\rangle \} \\
 \{ |2,1\rangle 21 \} &= (N_1^{(2,1)}/2\sqrt{3}) \{ 0 + 0 + |(13)\rangle - |(23)\rangle + \\
 &\quad |(123)\rangle - |(132)\rangle \} \\
 \{ |2,1\rangle 22 \} &= (N_2^{(2,1)}/3) \{ |g\rangle - |(12)\rangle + \\
 &\quad (1/2)|(13)\rangle + (1/2)|(23)\rangle - (1/2)|(123)\rangle \\
 &\quad - (1/2)|(132)\rangle \} \\
 \{ |3\rangle 11 \} &= (N_1^{(3)}/6) \{ |g\rangle + |(12)\rangle + |(13)\rangle + |(23)\rangle + \\
 &\quad |(123)\rangle + |(132)\rangle \}
 \end{aligned}$$

The matrix kets transform according to the irreducible representations of the permutation group. Thus by (A2.6)

$$P_a |\alpha r s\rangle = \sum_{r'}^{f^\alpha} [P_a]_{r'r}^\alpha |\alpha r' s\rangle \quad (3.3)$$

Since the irreducible representations are unitary and the Hamiltonian commutes with all permutations, we have with (A2.5)

$$\begin{aligned}
 H_{ss'}^\alpha &\equiv \langle \alpha r s | H | \alpha' r' s \rangle \\
 &= N_s^\alpha N_{s'}^{\alpha'} \langle g | e_{r_s}^\alpha e_{r'_s}^{\alpha'} H | g \rangle \\
 &= \delta^{\alpha\alpha'} \delta_{rr'} N_s^\alpha N_{s'}^{\alpha'} \langle g | e_{s_s}^\alpha H | g \rangle \\
 &= \delta^{\alpha\alpha'} \delta_{rr'} N_s^\alpha N_{s'}^{\alpha'} \sum_a [P_a]_{s's}^\alpha \langle a | H | g \rangle \quad (3.4)
 \end{aligned}$$

This $N! \times N!$ matrix is called the representation of the Hamiltonian in the matrix basis.

For $N = 3$ the matrix of the Hamiltonian in the matrix basis is

(7) See Appendix A2.

	$ \{1^3\}11\rangle$	$ \{2,1\}11\rangle$	$ \{2,1\}12\rangle$	$ \{2,1\}21\rangle$	$ \{2,1\}22\rangle$	$ \{3\}11\rangle$
$\langle\{1^3\}11 $	$H_{11}^{(1^3)}$	0	0	0	0	0
$\langle\{2,1\}11 $	0	$H_{11}^{(2,1)}$	$H_{12}^{(2,1)}$	0	0	0
$\langle\{2,1\}12 $	0	$H_{21}^{(2,1)}$	$H_{22}^{(2,1)}$	0	0	0
$\langle\{2,1\}21 $	0	0	0	$H_{11}^{(2,1)}$	$H_{12}^{(2,1)}$	0
$\langle\{2,1\}22 $	0	0	0	$H_{21}^{(2,1)}$	$H_{22}^{(2,1)}$	0
$\langle\{3\}11 $	0	0	0	0	0	$H_{11}^{(3)}$

$$H_{11}^{(1^3)} = ((N_1^{(1^3)})^2/6)(Q - \alpha - \beta - \gamma + 2\delta)$$

$$H_{11}^{(2,1)} = ((N_1^{(2,1)})^2/3)(Q + \alpha - (1/2)\beta - (1/2)\gamma - \delta)$$

$$H_{12}^{(2,1)} = (N_1^{(2,1)}N_2^{(2,1)}/2\sqrt{3})(\beta - \gamma)$$

$$H_{21}^{(2,1)} = (N_1^{(2,1)}N_2^{(2,1)}/2\sqrt{3})(\beta - \gamma)$$

$$H_{22}^{(2,1)} = ((N_2^{(2,1)})^2/3)(Q - \alpha + (1/2)\beta + (1/2)\gamma - \delta)$$

$$H_{11}^{(3)} = ((N_1^{(3)})^2/6)(Q + \alpha + \beta + \gamma + 2\delta)$$

Similarly, the matrix elements for the identity operator in the matrix basis are

$$S_{ss'}^\alpha = \langle\alpha rs|\alpha' r' s'\rangle = \delta^{\alpha\alpha'} \delta_{rr'} N_s^\alpha N_{s'}^\alpha \sum_a [P_a]_{r's'}^\alpha \langle a|g\rangle \quad (3.5)$$

For $N = 3$ we have, on taking the kets to be normalized

$$S_{11}^{(1^3)} = (N_1^{(1^3)})^2/6(q - a - b - c + 2d) = 1$$

$$S_{11}^{(2,1)} = (N_1^{(2,1)})^2/3(q + a - (1/2)b - (1/2)c - d) = 1$$

$$S_{12}^{(2,1)} = (N_1^{(2,1)}N_2^{(2,1)}/2\sqrt{3})(b - c)$$

$$S_{21}^{(2,1)} = (N_1^{(2,1)}N_2^{(2,1)}/2\sqrt{3})(b - c)$$

$$S_{22}^{(2,1)} = ((N_2^{(2,1)})^2/3)(q - a + (1/2)b + (1/2)c - d) = 1$$

$$S_{11}^{(3)} = ((N_1^{(3)})^2/6)(q + a + b + c + 2d) = 1$$

The matrix of $S_{ss'}^\alpha$ has the same form as the matrix of $H_{ss'}^\alpha$.

We see that the use of the matrix basis factors the representation of the Hamiltonian into $p(N)^8$ blocks each of which is in turn factored into f^α identical blocks of dimensions $(f^\alpha)^2$. The secular equation for each distinct block is solved separately.

For $N = 3$ the eigenvalues are

$$E_K^{(1^3)} = H_{11}^{(1^3)}$$

$$E_K^{(2,1)} = \frac{H_{11}^{(2,1)} + H_{22}^{(2,1)} - 2S_{12}^{(2,1)}H_{12}^{(2,1)}}{2 - 2(S_{12}^{(2,1)})^2} \pm$$

$$\frac{\{(H_{11}^{(2,1)} - H_{22}^{(2,1)})^2 + 4(H_{12}^{(2,1)} - S_{12}^{(2,1)}H_{11}^{(2,1)})(H_{12}^{(2,1)} - S_{12}^{(2,1)}H_{22}^{(2,1)})\}^{1/2}}{2 - 2(S_{12}^{(2,1)})^2}$$

$$E_K^{(3)} = H_{11}^{(3)}$$

If $S_{12}^{(2,1)} = 0$ and $N_1^{(2,1)} = N_2^{(2,1)}$, then

$$E_K^{(2,1)} = Q - \delta \pm (1/\sqrt{2})\{(\alpha - \beta)^2 + (\alpha - \gamma)^2 + (\beta - \gamma)^2\}^{1/2}$$

This becomes the familiar London-Eyring formula⁹ if we set δ , the multiple exchange integral, equal to zero.

The matrix elements vanish unless $\alpha = \alpha'$ and $r = r'$ so the matrix elements are independent of r . Consequently, to obtain a state vector we need consider only a particular (α, r) subspace of the permutation vector space. It is spanned by the f^α matrix kets $|\alpha rs\rangle$, $s = 1$ to f^α . For each α there occur f^α eigenvalues each of which occurs f^α times. The K th eigenket from the (α, r) th subspace is

$$|K\rangle = |K\alpha r\rangle = \sum_s^{f^\alpha} |\alpha rs\rangle \langle \alpha s|K\rangle \quad r = 1 \text{ to } f^\alpha$$

For $N = 3$ the eigenkets $|K\rangle$ are given by (for $\alpha = \{1^3\}$)

$$|1\rangle = |1\{1^3\}1\rangle = |\{1^3\}11\rangle$$

and (for $\alpha = \{2,1\}$, $r = 1, 2$)

$$|1\rangle \equiv |1\{2,1\}r\rangle = |\{2,1\}r1\rangle \langle\{2,1\}1|1\rangle + |\{2,1\}r2\rangle \langle\{2,1\}2|1\rangle$$

$$|2\rangle \equiv |2\{2,1\}r\rangle = |\{2,1\}r1\rangle \langle\{2,1\}1|2\rangle + |\{2,1\}r2\rangle \langle\{2,1\}2|2\rangle$$

where

$$\frac{\langle\{2,1\}1|K\rangle}{\langle\{2,1\}2|K\rangle} = -\frac{H_{12} - S_{12}E_K}{H_{11} - E_K} = -\frac{H_{22} - E_K}{H_{12} - S_{12}E_K}$$

For $\alpha = \{3\}$

$$|1\rangle = |1\{3\}1\rangle = |\{3\}11\rangle$$

An eigenket characterized by the partition α is said to lie in the α th permutation state. By (3.3) an eigenket transforms under a permutation as

$$P_a|K\alpha r\rangle = \sum_{r'} [P_a]_{r'r}^\alpha |K\alpha r'\rangle \quad (3.6)$$

(8) $p(N)$ is the number of partitions of N .

(9) See H. Eyring, J. Walter, and G. Kimball, "Quantum Chemistry," John Wiley and Sons, Inc., New York, N. Y., 1944, p. 245 ff.

Thus the eigenkets transform under permutation according to the irreducible representations of the permutation group. This is a particular example of the theorem that eigenfunctions of a Hamiltonian which commutes with a finite group transform according to the irreducible representations of that group.¹⁰

Let us consider a primitive ket $|g\rangle$ such that the elements $|a\rangle$ are not linearly independent. For such a ket and with the proper choice of matrix basis, certain matrix basis kets vanish. This is called the "algebraic exclusion principle" since it can be shown to arise entirely from algebraic considerations.^{1b}

Example 1

$$|g\rangle = |(12)\rangle, |(13)\rangle = |(123)\rangle, |(23)\rangle = |(132)\rangle$$

A specific example is $|g\rangle = a(1)a(2)b(3)$

Then

$$(13)a(1)a(2)b(3) = a(3)a(2)b(1) = b(1)a(2)a(3)$$

and

$$(123)a(1)a(2)b(3) = (13)(12)a(1)a(2)b(3) = \\ (13)a(2)a(1)b(3) = a(2)a(3)b(1) = b(1)a(2)a(3)$$

Similarly

$$(23)a(1)a(2)b(3) = (132)a(1)a(2)b(3) = a(1)b(2)a(3)$$

$$\begin{aligned} |\{1^3\}11\rangle &= 0 \\ |\{2,1\}11\rangle &= N_1^{12,11}/3\{2|g\rangle - |(13)\rangle - |(23)\rangle\} \\ |\{2,1\}21\rangle &= N_1^{12,11}/3\{2|(13)\rangle - 2|(23)\rangle\} \\ |\{2,1\}12\rangle &= |\{2,1\}22\rangle = 0 \\ |\{3\}11\rangle &= N_1^{131}/6\{2|g\rangle + 2|(13)\rangle + 2|(23)\rangle\} \end{aligned}$$

Example 2

$$|g\rangle = |(22)\rangle = |(13)\rangle = |(23)\rangle = |(123)\rangle = |(132)\rangle$$

A specific example is $|g\rangle = a(1)a(2)a(3)$

$$\begin{aligned} |\{1^3\}11\rangle &= |\{2,1\}11\rangle = |\{2,1\}12\rangle = |\{2,1\}21\rangle \\ &= |\{2,1\}22\rangle = 0 \end{aligned}$$

$$|\{3\}11\rangle = N_1^{131}|g\rangle/6$$

4. The Exclusion Principle

As a consequence of the antisymmetry principle and the fact that there exist two spin states for an electron, the only permutation states^{1b} which occur in nature are those for which

$$\alpha = \{2^p, 1^{N-2p}\}, \quad 0 \leq p \leq N/2 \quad (4.1)$$

For these we can replace the partition α by the single integer p . We call p the permutation quantum number. It identifies the p th permutation state. The spin

quantum number to be associated with the p th permutation state is

$$S = N/2 - p \quad (4.2)$$

The number f^p of basis kets in the p th permutation state is given by

$$f^\alpha = f^p = N!(N - 2p + 1)/p!(N - p + 1)! \quad (4.3)$$

For $N = 3$ the allowed permutation states for electrons are

$$\alpha = \{1^3\}, p = 0 (S = 3/2); f^p = 1$$

$$\alpha = \{2,1\}, p = 1 (S = 1/2); f^p = 2$$

The permutation state $\alpha = \{3\}$ is excluded.

The Pauli and the algebraic exclusion principles together exclude primitive kets which are invariant under the permutation groups of order higher than two. This excludes as primitive kets orbital products in which more than two electrons are assigned to the same orbital.

For $N = 3$, let $|g\rangle = a(1)a(2)a(3)$. Now, $e_{rs}^\alpha|g\rangle = 0$ for $\alpha = \{1^3\}$ and $\{2,1\}$, so $\alpha = \{1^3\}$ and $\alpha = \{2,1\}$ are excluded by the algebraic exclusion principle. $\alpha = \{3\}$ is excluded by the Pauli exclusion principle. Thus no allowed matrix basis elements can be constructed from $|g\rangle = a(1)a(2)a(3)$ so it is an excluded primitive ket.

5. The Permutation Vector Space.

Its Structure Basis¹¹

We have shown that the (p,r) th subspace of the permutation vector space is spanned by a matrix basis consisting of the f^p matrix basis kets $|prs\rangle$, $s = 1$ to f^p . While the matrix basis has many useful properties, it suffers from the disadvantage that it is not simply related to chemical structures.

A second basis for the (p,r) th subspace, called the structure basis, is composed of f^p kets $|\kappa\rangle$, $\kappa = 1$ to f^p , which lie in one-to-one correspondence with chemical structures. Each ket is said to represent a pure valence state of the system. A graphical realization of a structure is a structure diagram D_κ^p . A structure diagram for the p th permutation state consists of N numbered points arranged clockwise around a circle with p tie lines connecting pairs of points.

(10) E. P. Wigner, "Group Theory," Academic Press, New York, N. Y., 1959, p. 108.

(11) See Appendix 3.

For $N = 3$

$$p = 0$$

$$\kappa = \text{I}$$

$$D_{\kappa}^p = \begin{array}{c} 1 \quad .2 \\ 3. \end{array}$$

3.

$$p = 1$$

$$\kappa = \text{I} \quad \text{II} \quad \text{III}$$

$$D_{\kappa}^p = \begin{array}{ccc} 1 \quad .2 & 1 \quad .2 & 1 \quad .2 \\ 3. & 3 \quad .2 & 3 \quad .2 \end{array}$$

The diagram in which, for $p = 1$, one is tied to two or, for $p = 2$, one is tied to two, three to four, etc., is labeled I.

The structure kets are projected from the primitive ket by the structure operators (see Appendix 3). Thus

$$\begin{aligned} |\kappa\rangle &= \kappa|g\rangle \\ &= \sum_a (\kappa)_a P_a |g\rangle \\ &= \sum_a (\kappa)_a |a\rangle \end{aligned} \quad (5.1)$$

For $N = 3$

$$p = 0$$

$$|\text{I}\rangle = |g\rangle - |(12)\rangle - |(13)\rangle - |(23)\rangle + |(123)\rangle + |(132)\rangle$$

$$p = 1$$

$$|\text{I}\rangle = |g\rangle + |(12)\rangle - |(13)\rangle - |(123)\rangle$$

$$|\text{II}\rangle = -|g\rangle + |(13)\rangle - |(23)\rangle + |(132)\rangle$$

$$|\text{III}\rangle = |(12)\rangle - |(23)\rangle - |(123)\rangle + |(132)\rangle$$

Note that $|\text{III}\rangle = |\text{I}\rangle + |\text{II}\rangle$

The matrix of the Hamiltonian in the structure basis has elements $\langle \kappa | H | \kappa' \rangle$.

For $N = 3$

$$p = 0 \quad (S = 3/2)$$

$$\langle \text{I} | H | \text{I} \rangle = 6\{Q - \alpha - \beta - \gamma + 2\delta\}$$

$$p = 1 \quad (S = 1/2)$$

$$\langle \text{I} | H | \text{I} \rangle = 2(2Q + 2\alpha - \beta - \gamma - 2\delta)$$

$$\langle \text{I} | H | \text{II} \rangle = \langle \text{II} | H | \text{I} \rangle = 2(-Q - \alpha + 2\beta - \gamma + \delta)$$

$$\langle \text{II} | H | \text{II} \rangle = 2(2Q - \alpha - \beta + 2\gamma - 2\delta)$$

$$\langle \text{III} | H | \text{III} \rangle = 2(2Q - \alpha + 2\beta - \gamma - 2\delta)$$

$$\langle \text{II} | H | \text{III} \rangle = 2(Q - 2\alpha + \beta + \gamma - \delta)$$

Note that

$$\langle \text{I} | H | \text{I} \rangle = 4H_{11}^{(2,1)} / ((N_1^{(2,1)})^2/3) \quad (5.2)$$

These matrix elements are the same as obtained by conventional methods.⁹

6. Three Hydrogen Atoms. The Jahn-Teller Effect¹²

We consider here the $p = 1$ ($S = 1/2$) states(s) for a system of three hydrogen atoms. We label the hydrogen atoms a, b, and c and the internuclear distances r_{ab} , r_{ac} , and r_{bc} . We restrict ourselves to changes in the internuclear distances such that

$$r_{ab} + r_{ac} + r_{bc} \equiv \rho, \text{ constant}$$

A convenient set of coordinates are the symmetry coordinates

$$\begin{aligned} x &= (r_{ac} + r_{bc} - 2r_{ab})/\sqrt{6} \\ y &= (r_{ac} - r_{bc})/\sqrt{2} \\ z &= \rho/\sqrt{3} \end{aligned} \quad (6.1)$$

These coordinates are conveniently plotted on a triangular graph (see Fig. 1). The three vertices of the triangle are $r_{ab} = 0$, $x = \rho/\sqrt{6}$, $y = 0$; $r_{bc} = 0$, $x = -\rho/2\sqrt{6}$, $y = \rho/\sqrt{2}$; $r_{ac} = 0$, $x = -\rho/2\sqrt{6}$, $y = -\rho/\sqrt{2}$. The midpoint is $r_{ab} = r_{ac} = r_{bc}$, $x = y = 0$. Here the configuration is that of an equi-

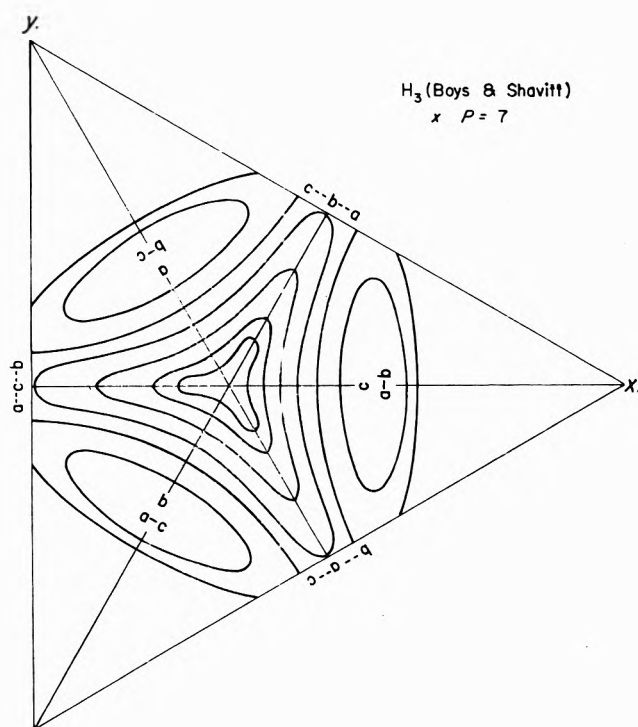


Figure 1.

(12) A. D. Liear, *J. Phys. Chem.*, **67**, 414 (1963); G. Herzberg and H. C. Longuet-Higgins, *Discussions Faraday Soc.*, **35**, 77 (1963), and a comment on this paper by Professor C. A. Coulson.

lateral triangle (D_{3h}). Along each edge the configuration is linear ($C_{\infty v}$). At the midpoint of each edge, the configuration is linear and symmetrical ($D_{\infty h}$). On a line passing through the midpoint and perpendicular to an edge, the atoms have the configuration of an isosceles triangle (C_{2v}). Between the midpoint and vertex the isosceles triangle is acute. Between the midpoint and the edge the isosceles triangle is obtuse. For the line $y = 0$, *i.e.*, $r_{ao} = r_{bc}$

$$x = (\rho - 3r_{ab})/\sqrt{6} \quad (6.2)$$

We will wish also to use the polar coordinates

$$R = \{x^2 + y^2 + z^2\}^{1/2} = \{(r_{ab} - r_{ac})^2 + (r_{ab} - r_{bc})^2 + (r_{ac} - r_{bc})^2\}^{1/2}/\sqrt{6}$$

$$\tan \theta = y/x = \sqrt{3}(r_{ao} - r_{bo})/(r_{ao} + r_{bo} - 2r_{ab}) \quad (6.3)$$

The following configurations are of particular interest.

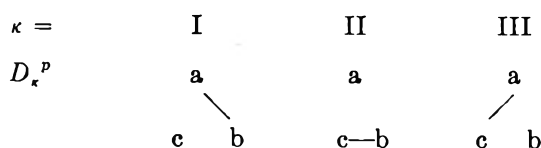
	θ
$r_{ab} = r_{ao} = r_{bo}$	$0 - 2\pi(R = 0)$
$r_{ac} = r_{bc} > r_{ab}$	0
$r_{ab} = r_{bc} < r_{ao}$	60
$r_{ab} = r_{ao} > r_{bc}$	120
$r_{ao} = r_{bc} < r_{ab}$	180
$r_{ab} = r_{bc} > r_{ao}$	240
$r_{ab} = r_{ao} < r_{bc}$	300

For $R = 0$, the configuration is D_{3h} . For $\theta = n \times 60^\circ$ the configuration is C_{2v} .

We turn now to a quantum mechanical formulation of the H_3 problem. We write the primitive ket

$$|g\rangle = a(1)b(2)c(3) \quad (6.4)$$

The ket is to be interpreted as an assignment of electron one predominantly to the vicinity of atom a, etc. In its simplest form it is the product of three orbitals centered on atoms a, b, and c. The pairing between electrons is then to be interpreted as bonding between atoms and the structure diagrams become bond diagrams. For $p = 1$



The structure kets are

$$|I\rangle = a(1)b(2)c(3) + a(2)b(3)c(2) - a(3)b(2)c(1) - a(2)b(3)c(1) \quad (6.5)$$

$$|II\rangle = -a(1)b(2)c(3) + a(3)b(2)c(1) - a(1)b(3)c(2) + a(3)b(1)c(2) \quad (6.6)$$

$$|III\rangle = a(2)b(1)c(3) - a(2)b(3)c(1) - a(1)b(3)c(2) + a(3)b(1)c(2) \quad (6.7)$$

The three structure kets projected out of $|g\rangle$ are not linearly independent since

$$|III\rangle = |I\rangle + |II\rangle$$

Any pair can be used as a basis for a description of the $p = 1$ state. There are two eigenvalues E_K and two eigenkets $|K\rangle$ associated with each configuration.

We consider now the formulation for the equilateral configuration $r_{ab} = r_{ao} = r_{bc}$, *i.e.*, $x = 0$. The point group is $D_{3h} = \{g, C_3, C_3^2, S_3, S_3^2, \sigma_h, \sigma_a, \sigma_b, \sigma_c, C_2', C_2'', C_2'''\}$. We show that the structure kets $|\kappa\rangle$ are the bases for irreducible representations of D_{3h} .

For example

$$C_3|g\rangle = C_3a(1)b(2)c(3) = c(1)a(2)b(3) = a(2)b(3)c(1)$$

Further

$$C_3|I\rangle = c(1)a(2)b(3) + c(2)a(1)b(3) - c(3)a(2)b(1) - a(3)b(1)c(2) = |III\rangle$$

The table summarizes the transformation properties of the structure kets

$ \kappa\rangle/R$	R_{κ}					
	g	C_3	C_3^2	σ_a	σ_b	σ_c
$ I\rangle$	$ I\rangle$	$ III\rangle$	$ II\rangle$	$- III\rangle$	$ II\rangle$	$ I\rangle$
$ II\rangle$	$ II\rangle$	$ I\rangle$	$ III\rangle$	$ II\rangle$	$ I\rangle$	$- III\rangle$
$ III\rangle$	$ III\rangle$	$ II\rangle$	$ I\rangle$	$- I\rangle$	$ III\rangle$	$- II\rangle$

The effect of σ_b is identical with g, S_3 to C_3, S_3^2 to C_3, C_2' to σ_a, C_2'' to σ_b , and C_2''' to σ_c .

If we take any pair of kets as a basis for a representation of D_{3h} the characters of the transformations are

x	g	C_3	C_3^2	σ_a	σ_b	σ_c
	2	1	-1	0	0	0

For example

$$C_3\{|I\rangle, |II\rangle\} = \{|III\rangle, |I\rangle\} = \{|I\rangle + |II\rangle, |III\rangle\} = \{|I\rangle, |II\rangle\} \begin{bmatrix} 1 & 1 \\ 1 & 0 \end{bmatrix}$$

then

$$[C_3] = \begin{bmatrix} 1 & 1 \\ 1 & 0 \end{bmatrix} \text{ and } x(C_3) = 1$$

These are the characters of the degenerate representation E' so the eigenstate for $p = 1$ in the configuration

D_{3h} of the wave function is doubly degenerate. The assignment of E' to the D_{3h} configuration agrees with the molecular orbital assignment

$$\begin{aligned}\psi(A_1) &= \phi_a + \phi_b + \phi_c \\ \psi(E') &= \begin{cases} 2\phi_a - \phi_b - \phi_c \\ \phi_b - \phi_c \end{cases}\end{aligned}$$

The ground state is $\psi(A_1)^2\psi(E')$ which transforms according to E' .

We note that

$$\langle R_\kappa | H | R_\kappa \rangle = \langle \kappa | H | \kappa \rangle \text{ and } \langle R_\kappa | R_\kappa \rangle = \langle \kappa | \kappa \rangle \quad (6.8)$$

so that

$$\begin{aligned}\langle I | H | I \rangle &= \langle II | H | II \rangle = \langle III | H | III \rangle \text{ and } \langle I | I \rangle \\ &= \langle II | II \rangle = \langle III | III \rangle\end{aligned} \quad (6.9)$$

On comparison with section 5, (6.9) requires that

$$\alpha = \beta = \gamma \text{ and } a = b = c$$

Then with $|II\rangle$ and $|III\rangle$ as a basis

$$E_1 = \frac{\langle II | H | II \rangle + \langle II | H | III \rangle}{\langle II | II \rangle + \langle II | III \rangle} = \frac{Q - \delta}{q - d}$$

and

$$E_2 = \frac{\langle II | H | II \rangle - \langle II | H | III \rangle}{\langle II | II \rangle - \langle II | III \rangle} = \frac{Q - \delta}{q - d}$$

As noted above, the state is twofold degenerate.

We consider next the configurations $r_{ac} = r_{bc} \neq r_{ab}$. The point group is $C_{2v} = \{g, \sigma_c, C_2''', \sigma_v (= \sigma_b)\}$.

We see that

$$\begin{aligned}\langle II | H | II \rangle &= \langle III | H | III \rangle, \beta = \gamma \quad (6.10) \\ \langle II | II \rangle &= \langle III | III \rangle, b = c\end{aligned}$$

$$E_1 = \frac{\langle II | H | II \rangle + \langle II | H | III \rangle}{\langle II | III \rangle + \langle II | III \rangle} = \frac{Q - \alpha + \beta - \delta}{q - a + b - d}$$

$$|I\rangle = |II\rangle + |III\rangle$$

Now $\sigma_c|1\rangle = -|III\rangle - |II\rangle = -|1\rangle$ so $|1\rangle$ belongs to irreducible representation B_2 of C_{2v} .

$$\begin{aligned}E_2 &= \frac{\langle II | H | II \rangle - \langle II | H | III \rangle}{\langle II | II \rangle - \langle II | III \rangle} = \frac{Q + \alpha - \beta - \delta}{q + a - b - d} \\ |2\rangle &= |II\rangle - |III\rangle = -|I\rangle\end{aligned}$$

Now $\sigma_c|2\rangle = |2\rangle$ so $|2\rangle$ belongs to irreducible representation A_1 of C_{2v} .

From actual computation, it appears that most of the variation in E_K with change in configuration resides in the transposition integrals α , β , and γ . Accordingly, we define

$$E_{K'} = \bar{E}_K \langle K | K \rangle - Q + \delta$$

For the C_{2v} configuration with $\beta = \gamma$

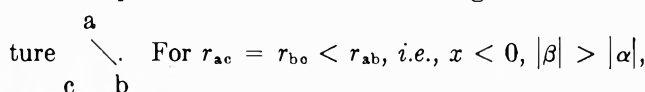
$$E_{1'} = -\alpha + \beta$$

$$E_{2'} = \alpha - \beta$$

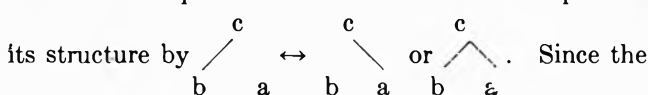
For the D_{3h} configuration

$$E_{1'} = E_{2'} = 0$$

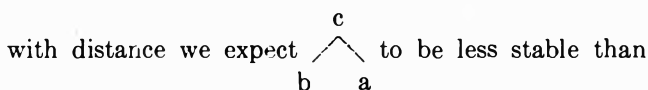
The transposition integrals appear to be negative and drop off rapidly with distance. For $r_{ac} = r_{bc} > r_{ab}$, i.e., $x > 0$, we conclude that $|\alpha| > |\beta|$, $E_{2'} < E_{1'}$, and the ground state ket is $|2\rangle = |II\rangle - |III\rangle = -|I\rangle$. This is a pure valence state and we assign it the struc-

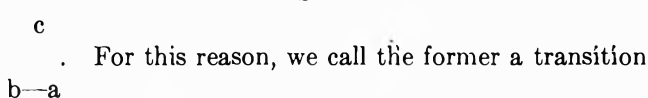
ture . For $r_{ac} = r_{bc} < r_{ab}$, i.e., $x < 0$, $|\beta| > |\alpha|$,

$E_{1'} < E_{2'}$, and the ground ket is $|2\rangle = |II\rangle + |III\rangle$. This is not a pure valence state. We can represent

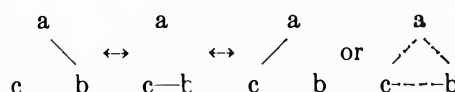
its structure by . Since the

transposition integrals are assumed to drop off rapidly

with distance we expect  to be less stable than

. For this reason, we call the former a transition

state. For $r_{ac} = r_{bc} = r_{ab}$, i.e., $x = 0$, $E_{1,2} = 0 > -\alpha + \beta$ or $-\beta + \alpha$. Thus the doubly degenerate state as $x = 0$ lies above the ground states of C_{2v} configuration. We represent its structure by



It too is a transition state.

In Fig. 2 we have plotted the quantity

$$E_{K''} = E_K(r_{ab}) + 1.6523$$

for $r_{ac} = r_{bc}$ and $\rho = 7.0$ a.u. The values of E_K for $r_{ab} = 2.33$ and 3.5 a.u. were calculated by Boys and Shavitt.¹³ Boys and Shavitt did not calculate the point $r_{ab} = 1.4$, $r_{ac} = r_{bc} = 2.8$. We have assigned it the value of -1.6523 a.u., the value which Boys and Shavitt calculated for $r_{ab} = 1.4$, $r_{ac} = r_{bc} = \infty$.

Since the energy of the upper state is given in terms of the same parameters as the lower states, its approximate shape can be inferred from the lower curves.

(13) S. F. Boys, G. B. Cook, C. M. Reeves, and I. Shavitt, *Nature*, **178**, 1207 (1956); S. F. Boys and I. Shavitt, Technical Report WIS-AF-13, University of Wisconsin, 1959.

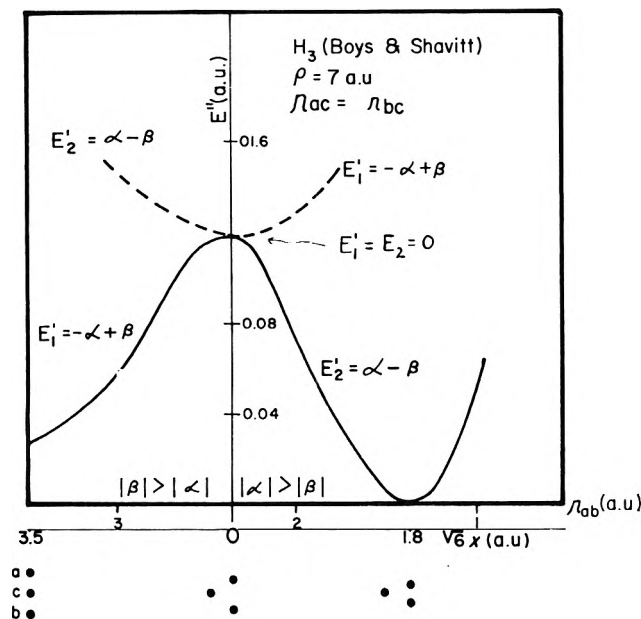


Figure 2.

Note that E_1' and E_2' change sign and reverse their order in passing through the midpoint ($x = 0$). For $x > 0$ the ground state $|2\rangle$ is A_1 and the excited state $|1\rangle$ is B_2 of C_{2v} . For $x < 0$ the ground state $|1\rangle$ is B_2 and the excited state $|2\rangle$ is A_1 of C_{2v} . Since $E_{K'}$ changes sign through the origin, it follows that its leading term is odd in x . It follows that the E' state of D_{3h} is unstable against distortion, *i.e.*, the system exhibits a Jahn-Teller effect.

An identical energy profile obtains for any of the perpendicular bisectors. In Fig. 1 we plot an approximate potential energy diagram for the lower energy surface or sheet.

We wish to traverse the lower sheet keeping R fixed and varying from zero to 2π with no discontinuous change in phase. In this traverse we alternate between acute and obtuse configurations and between valence and transition structures. (See Table I.)

It will be noted that the wave function changes sign on the traversal from $\theta = 0$ to $\theta = 2\pi$. In this it duplicates the behavior of the antisymmetrized space-spin function which was shown by Herzberg and Longuet-Higgins.

In a reaction, a hydrogen atom can approach a hydrogen molecule on a line bisecting and perpendicular to the internuclear axis. For example, the representative point of the system can move along the x axis in Fig. 1. If reaction is to occur, the representative point must exit along one of the other two bisectors. The system can, as Coulson has suggested, side-step the

Table I

e	$E_{K'}$	Ground state $ K\rangle$	Structure
0	$E_2' = \alpha - \beta$ $ \alpha > \beta = \gamma $	$ 2\rangle = II\rangle - III\rangle = - I\rangle$	a c b
60	$E_2' = \alpha - \beta$ $ \beta < \alpha = \gamma $	$ 2\rangle = - I\rangle + II\rangle$	c--b--a
120	$E_2' = -\alpha + \gamma$ $ \gamma > \alpha = \beta $	$ 2\rangle = - I\rangle + III\rangle = II\rangle$	b c a
180	$E_1' = -\alpha + \beta$ $ \alpha < \beta = \gamma $	$ 1\rangle = II\rangle + III\rangle$	b--c--a
240	$E_1' = -\alpha + \beta$ $ \beta > \alpha = \gamma $	$ 1\rangle = I\rangle + II\rangle = III\rangle$	c b e
300	$E_1' = \alpha - \gamma$ $ \gamma < \alpha = \beta $	$ 1\rangle = I\rangle + III\rangle$	b--a--c
360	$E_2' = \alpha - \beta$ $ \alpha > \beta = \gamma $	$ 2\rangle = I\rangle$	b a c

midpoint in which case it takes a lower energy path. It can also proceed directly to the midpoint ($x = 0$). Here it can pass directly to one of the other two bisectors or it can pass on to the upper sheet in an inverse Jahn-Teller effect. After this, it can undergo a normal Jahn-Teller effect and exit along one of the bisectors. In this instance, the upper sheet is acting as a transition state.

The configuration which is usually discussed in kinetics is the linear one. If a transition state is invoked for the linear configuration, it is located at the midpoint of an edge. This hypothetical transition state is not related to the upper energy sheet which we discussed in the previous paragraph.

7. Perturbation Theory

We consider here systems of three electrons in which one electron is essentially detached from a core containing the other two. Examples are systems with one highly excited electron or with one electron attached to an atom widely separated from the core. For such systems a perturbation treatment is indicated.

We decompose the Hamiltonian as

$$H = H^0 + H' \quad (7.1)$$

where

$$H^0 = H(12) + H(3) \tag{7.2}$$

is the zero-order Hamiltonian. It commutes with the subgroup $\pi_2 = \{g, (12)\}$ of π_3 . The matrix basis elements of this subgroup are

$$e_{11}^{(1^2)} = (1/2)(g - (12)) \tag{7.3}$$

and

$$e_{11}^{(2)} = (1/2)(g + (12)) \tag{7.4}$$

From a three-electron primitive ket we project normalized π_2 matrix basis kets

$$|a\rangle \equiv |g; \{1^2\}11\rangle = N_a e_{11}^{(1^2)} |g\rangle = (N_a/2) \{ |g\rangle - |(12)\rangle \} \tag{7.5}$$

$$|s\rangle \equiv |g; \{2\}11\rangle = N_s e_{11}^{(2)} |g\rangle = (N_s/2) \{ |g\rangle + |(12)\rangle \} \tag{7.6}$$

The zero-order energies are

$$E_a \equiv \langle a | H^0 | a \rangle = \epsilon_a + \epsilon \tag{7.7}$$

and

$$E_s \equiv \langle s | H^0 | s \rangle = \epsilon_s + \epsilon \tag{7.8}$$

Here ϵ_a and ϵ_s are core energies and ϵ is the energy of the third electron. The π_2 matrix basis kets transform under π_3 as

$$\begin{aligned} |g; a\rangle &= -|(12); a\rangle & |g; s\rangle &= |(12); s\rangle \\ |(13); a\rangle &= -(123); a\rangle & |(13); s\rangle &= |(123); s\rangle \\ |(23); a\rangle &= -(132); a\rangle & |(23); s\rangle &= |(132); s\rangle \end{aligned}$$

The matrix elements are given below in terms of the π_2 matrix basis brackets and the regular basis brackets.

$$\begin{aligned} Q^{aa} &\equiv \langle g; a | H | g; a \rangle = -\langle (12); a | H | g; a \rangle \tag{7.9} \\ &= (N_a^2/2)(Q - \alpha) \end{aligned}$$

$$\begin{aligned} \beta^{aa} &\equiv \langle (13); a | H | g; a \rangle = -\langle (23); a | H | g; a \rangle \\ &= -\langle (123); a | H | g; a \rangle = -\langle (132); a | H | g; a \rangle \\ &= (N_a^2/4)(\beta + \gamma - 2\delta) \end{aligned}$$

$$\begin{aligned} Q^{ss} &\equiv \langle g; s | H | g; s \rangle = \langle (12); s | H | g; s \rangle \tag{7.10} \\ &= (N_s^2/2)(Q + \alpha) \end{aligned}$$

$$\begin{aligned} \beta^{ss} &\equiv \langle (13); s | H | g; s \rangle = \langle (23); s | H | g; s \rangle \\ &= \langle (123); s | H | g; s \rangle = \langle (132); s | H | g; s \rangle \\ &= (N_s^2/4)(\beta + \gamma + 2\delta) \end{aligned}$$

$$\begin{aligned} Q^{as} = Q^{sa} &\equiv \langle g; s | H | g; a \rangle = \langle (12); s | H | g; a \rangle \\ &= \langle g; s | H | (12); a \rangle \tag{7.11} \end{aligned}$$

$$\begin{aligned} &= -\langle g; s | H | g; a \rangle = 0 \\ \beta^{as} = \beta^{sa} &\equiv \langle (13); s | H | g; a \rangle = \langle (123); s | H | g; a \rangle \\ &= \langle g; s | H | (132); a \rangle = -\langle g; s | H | (23); a \rangle \\ &= -\langle (23); s | H | g; a \rangle = -\langle (132); s | H | g; a \rangle \\ &= (N_a^2 N_s^2/2)(\beta - \gamma) \end{aligned}$$

We next form π_3 matrix basis kets from the π_2 matrix basis kets. The nonvanishing kets are

$$\begin{aligned} |S\rangle &\equiv \begin{cases} \{ |1^3; 11; a\rangle = (N_a \{1^3\}/3) \{ |g; a\rangle - |(13); a\rangle - |(23); a\rangle \} \\ |2, 1; 11; s\rangle = (N_s/3) \{ 2|g; s\rangle \} |(13); s\rangle - |(23); s\rangle \\ |2, 1; 21; s\rangle = (N_s/\sqrt{3}) \{ |(13); s\rangle - |(23); s\rangle \} \end{cases} \\ |A\rangle &\equiv \begin{cases} |2, 1; 12; a\rangle = (N_a/\sqrt{3}) \{ |(13); a\rangle - |(23); a\rangle \} \\ |2, 2; 22; a\rangle = (N_a/3) \{ 2|g; a\rangle + |(13); a\rangle + |(23); a\rangle \} \end{cases} \end{aligned}$$

We now restrict our attention to the $p = 1 (S = 1/2)$ permutation states. The matrix elements in terms of the π_2 matrix basis brackets and the regular basis brackets are

$$\begin{aligned} H_{SS} &= (2N_s^2/3)(Q^{ss} - \beta^{ss}) \\ &= (N_s^2 N_a^2/3)(Q + \alpha - 1/2\beta - 1/2\gamma - \delta) \\ &= H_{11}^{(2,1)} \tag{7.12} \end{aligned}$$

$$\begin{aligned} H_{AA} &= (2N_a^2/3)(Q^{aa} - \beta^{aa}) \\ &= N_a^2 N_s^2 (Q - \alpha + (1/2)\beta + (1/2)\gamma - \delta) \\ &= H_{22}^{(2,1)} \tag{7.13} \end{aligned}$$

$$\begin{aligned} H_{AS} = H_{SA} &= \langle S | H | A \rangle \\ &= (N_a N_s (4\sqrt{3}/3)) \beta^{sa} \\ &= ((N_a N_s N_a N_s) (2\sqrt{3}/3)) (\beta - \gamma) \\ &= H_{12}^{(2,1)} = H_{21}^{(2,1)} \end{aligned}$$

The secular equation is

$$\begin{vmatrix} H_{SS} - E & H_{SA} - S_{SA} E \\ H_{SA} - S_{SA} E & H_{AA} - E \end{vmatrix} = 0$$

The eigenkets are

$$\begin{aligned} |1\rangle &= |S\rangle \langle S|1\rangle + |A\rangle \langle A|1\rangle \\ |2\rangle &= |S\rangle \langle S|2\rangle + |A\rangle \langle A|2\rangle \end{aligned}$$

where

$$\frac{\langle S | K \rangle}{\langle A | K \rangle} = \frac{H_{SA} - S_{SA} E_K}{H_{SS} - E_K}$$

We consider three cases.

Case I. Zero Order

$$\begin{aligned} \beta, \gamma, \delta, \beta^{ss}, \beta^{aa}, \beta^{as}, H_{AS} &= 0 \\ b, c, d, b^{ss}, b^{aa}, b^{as}, S_{AS} &= 0 \\ E_1 = H_{AA} = E_a; |1\rangle &= |A\rangle \\ E_2 = H_{SS} = E_s; |2\rangle &= |S\rangle \end{aligned} \quad (7.14)$$

Case II. First Order

$$\begin{aligned} \beta, \gamma, \beta^{as}, H_{AS} &= 0 \\ b, c, b^{as}, S_{AS} &= 0 \\ E_1 = H_{AA} = E_a + \langle A|H'|A\rangle; |1\rangle &= |A\rangle \\ E_2 = H_{SS} = E_s + \langle S|H'|S\rangle; |2\rangle &= |S\rangle \end{aligned} \quad (7.15)$$

For case I and case II, $E_2 = \langle I|H|I\rangle/\langle I|I\rangle$. That is, state $|2\rangle$ may be described as a pure valence state with structure I. Note

$$(12)|S\rangle = |S\rangle$$

and

$$(21)|I\rangle = |I\rangle \quad (7.16)$$

Case III. Second Order

$$\begin{aligned} \alpha, b, c, d, S_{AS} &= 0, H_{AS} \text{ small,} \\ E_1 \sim E_a, E_2 \sim E_s \end{aligned} \quad (7.17)$$

Here

$$\begin{aligned} E_1 = H_{AA} - \frac{H_{AS}^2}{\Delta} \quad |1\rangle &= |A\rangle - \frac{H_{AS}}{\Delta}|S\rangle \\ E_2 = H_{SS} + \frac{H_{AS}^2}{\Delta} \quad |2\rangle &= |S\rangle + \frac{H_{AS}}{\Delta}|A\rangle \end{aligned}$$

where

$$\Delta \equiv E_s - E_a$$

In terms of the regular brackets

$$H_{AS} = \sqrt{3}/2(\beta - \gamma)$$

We apply these results in the three succeeding sections.

8. A Hydrogen Molecule and a Hydrogen Atom

The interaction between a widely separated hydrogen atom and a hydrogen molecule can be treated by perturbation theory. We take the zero-order Hamiltonian to be

$$H^0 = H(R;12) + H(3) \quad (8.1)$$

where $H(R;12)$ is the Hamiltonian for a hydrogen molecule with an internuclear separation of R and

$$H(3) = (1/2)\nabla_3^2 - 1/r_{3c} \quad (8.2)$$

The perturbation is

$$H' = -1/r_{1c} - 1/r_{2c} - 1/r_{3a} - 1/r_{3b} + 1/r_{13} + 1/r_{23} \quad (8.3)$$

We take the primitive ket to be

$$|g;s\rangle = \phi(R;12)\Psi(3) \quad (8.4)$$

where $\phi(R;12)$ is an exact eigenfunction for H_2 and $\Psi(3)$ is a hydrogen function. The zero-order energy is in atomic units.

$$E_s(R) = \epsilon_s(R) - 1/2 \quad (8.5)$$

where $\epsilon_s(R)$ is the exact electronic energy for H_2 . From section 7 we choose for the zero-order wave function

$$|S\rangle = (N_s/3)\{2|g;s\rangle - |(13);s\rangle - |(23);s\rangle\} \quad (8.6)$$

Then to the first order

$$E_s(R) = \langle S|H|S\rangle = N_s^{2(2/3)}\{Q^{ss} - \beta^{ss}\} = \frac{Q^{ss} - \beta^{ss}}{q^{ss} - b^{ss}} \quad (8.7)$$

Now

$$\begin{aligned} Q^{ss} &= \langle g;s|H|g;s\rangle = \langle (12);s|H|g;s\rangle \\ &= E_s(R)q^{ss} + \langle g;s|H'|g;s\rangle \end{aligned} \quad (8.8)$$

and

$$\begin{aligned} \beta^{ss} &= \langle (13);s|H|g;s\rangle = \langle (23);s|H|g;s\rangle \\ &= \langle (123);s|H|g;s\rangle = \langle (132);s|H|g;s\rangle \\ &= E_s(R)b^{ss} + \langle (13);s|H'|g;s\rangle \end{aligned} \quad (8.9)$$

so

$$E_s(R) = E_s(R) + \frac{\langle g;s|H'|g;s\rangle - \langle (13);s|H'|g;s\rangle}{q^{ss} - b^{ss}} \quad (8.10)$$

To avoid three-center integrals, we can approximate $\phi(R;12)$ by a one-center expansion for each R about the midpoint of H_2 .

9. The Effect of Paramagnetic Molecules on the Intensity of a Spin-Forbidden Absorption Band

The so-called spin-forbidden electric dipole transitions are, in fact, forbidden by the permutation symmetry. The dipole moment operator is

$$\vec{\tau} = \sum_{i=1}^N \vec{r}_i \quad (9.1)$$

where \vec{r}_i is the vector from the origin to the i th electron is a function of space coordinates. Now $\vec{\tau}$ commutes with every permutation of the space coordinates so we

can evaluate its matrix elements between two permutation states by means of an equation similar to (3.4). Thus

$$\langle \alpha r s | \vec{r} | \alpha' r' s' \rangle = \delta^{\alpha\alpha'} \delta_{rr'} \langle \alpha s' s | \vec{r} | g \rangle \quad (9.2)$$

The selection rules for permutation states are then

$$\begin{aligned} \alpha &\rightarrow \alpha \\ \alpha &\not\rightarrow \alpha' \text{ for } \alpha' \neq \alpha \end{aligned} \quad (9.3)$$

Since each α uniquely identifies a spin state this selection rule is the analog of the more familiar rule which states that transitions between states of different spin multiplicities are forbidden.

Evans¹⁴ has shown that paramagnetic species, *e.g.*, O₂ and NO, enhance the singlet-triplet transition in many organic molecules. Murrell¹⁵ has carried out a model three-electron calculation using the conventional space-spin formulation. We repeat Murrell's treatment in the spin-free formulation.

Let $|gs\rangle$, $|es\rangle$, and $|ea\rangle$ be the symmetric ($p = 1$, singlet) ground state, symmetric ($p = 1$, singlet) excited state, and antisymmetric ($p = 0$, triplet) kets for a chromophore R to which has been assigned electrons 1 and 2. The dipole moment operator is

$$\vec{r}_{(2)} = \vec{r}_1 + \vec{r}_2 \quad (9.4)$$

then

$$\langle gs | r_{(2)} | es \rangle = T_s \neq 0 \quad (9.5)$$

$$\langle gs | r_{(2)} | ea \rangle = 0 \quad (9.6)$$

Let $|q\rangle$ be the ket for the paramagnetic species to which has been assigned electron 3. The three-electron primitive kets are

$$\begin{aligned} |gsq\rangle &= |gs\rangle|q\rangle \\ |esq\rangle &= |es\rangle|q\rangle \\ |eaq\rangle &= |ea\rangle|q\rangle \end{aligned} \quad (9.7)$$

We neglect the perturbation of the ground state $|gs\rangle$ by the paramagnetic species. For the excited states we generate $N = 3$, $p = 1$ (doublet) matrix basis kets

$$|eS\rangle = N_S e_{r_1}^{(2,1)} |es\rangle|q\rangle \quad (9.8)$$

$$|eA\rangle = N_A e_{r_2}^{(2,1)} |ea\rangle|q\rangle \quad (9.9)$$

The transition moments for the complex are

$$\langle gsq | \vec{r}_{(2)} | eS \rangle \approx \langle gs | \vec{r}_{(2)} | es \rangle = T_s \neq 0 \quad (9.10)$$

$$\langle gsq | \vec{r}_{(2)} | eA \rangle \approx \langle gs | \vec{r}_{(2)} | ea \rangle = 0 \quad (9.11)$$

If H_{AS} is small we can use perturbation theory.

Then the wave function for the perturbation triplet state is

$$|1\rangle = |eA\rangle - \frac{H_{AS}}{\Delta} |eS\rangle \quad (9.12)$$

The transition moment between this state and the ground state is

$$\begin{aligned} \langle gsq | \vec{r}_{(2)} | 1 \rangle &= \langle gsq | \vec{r}_{(2)} | eA \rangle - \frac{H_{AS}}{\Delta} \langle gsq | r_{(2)} | eS \rangle \\ &= -\frac{H_{AS} T_s}{\Delta} \end{aligned} \quad (9.13)$$

or

$$|\langle gsq | \vec{r}_{(2)} | 1 \rangle|^2 = 3/4 \left(\frac{\beta - \gamma}{\Delta} \right)^2 |T_s|^2 \quad (9.14)$$

which is Murrell's result. It shows that a paramagnetic substance permits a triplet function to assume some singlet character. Thus the paramagnetic molecule permits the singlet-triplet transition to steal intensity from the singlet-triplet transition. Note that while the effect is usually described in terms of spin language, the origin of the effect is in spin-free quantum chemistry.

10. The Rydberg States of Lithium

For the zero-order Hamiltonian we take

$$H = H(12) + H(3) \quad (10.1)$$

where $H(12)$ is the Hamiltonian for the lithium ion and

$$H(3) = -1/2 \nabla_3^2 - 1/r_3 \quad (10.2)$$

The perturbation is then

$$H' = -(Z-1)/r_3 + 1/r_{13} + 1/r_{23} \quad (10.3)$$

The zero-order eigenfunction is

$$|g;s\rangle = \phi(12) \Psi_n(3) \quad (10.4)$$

where $\phi(12)$ is the singlet ground state for Li⁺ and $\Psi_n(3)$ is a hydrogen orbital with the principal quantum number n . The zero-order energy is

$$E_s = \epsilon_s - 1/2n^2 \quad (10.5)$$

where ϵ_s is the energy of the lithium ion in its ground $p = 1$ (singlet) state. The eigenfunctions and energy expressions are identical with those of section 8.

Following Coulson and Stamper¹⁶ we approximate $|g;s\rangle$ as

(14) D. F. Evans, *Nature*, **178**, 534 (1956).

(15) J. N. Murrell, *Mol. Phys.*, **3**, 319 (1960).

(16) C. A. Coulson and J. G. Stamper, *Mol. Phys.*, **6**, 609 (1963).

$$\begin{aligned}\phi(12) &= 1s(1)1s(2) \\ \Psi_n(3) &= np(3)\end{aligned}\quad (10.6)$$

so that $q^{ss} = 1$ and $b^{ss} = 0$. Further

$$\begin{aligned}\langle g; s | H' | g; s \rangle &= -(Z-1) \int \frac{np^2(3)}{r_3} d\tau_3 + \\ \iint \frac{np^2(3)s^2(1)}{r_{13}} d\tau_1 d\tau_3 &+ \iint \frac{np^2(3)s^2(2)}{r_{23}} d\tau_2 d\tau_3\end{aligned}\quad (10.7)$$

$$\langle (13); s | H' | g; s \rangle = \int \frac{np(1)s(3)np(3)s(1)}{r_{13}} d\tau_1 d\tau_3 \quad (10.8)$$

The second and third integrals in (10.7) are identical. The total energy to the first order is

$$\begin{aligned}E_s &= \epsilon_s - 1/2n^2 - (Z-1) \int \frac{np^2(3)}{r_3} d\tau_3 + \\ 2 \iint \frac{np^2(3)s^2(1)}{r_{13}} d\tau_1 d\tau_3 &- \int \frac{np(1)s(3)np(3)s(1)}{r_{13}} d\tau_1 d\tau_3\end{aligned}$$

in agreement with Coulson and Stamper.

11. Conclusion

We have shown that the spin-free formulation reproduces the results obtained by the conventional space-spin formulation for systems with three electrons.

Appendix¹⁷

A1. The Permutation Algebra. Its Regular Basis.

The $N!$ permutations on N objects form a group $\pi_N = \{P_1, \dots, P_a, \dots, P_{N!}\}$.

α	f^α	$P_a =$	g	(12)	(13)	(23)	(123)	(132)
$\{1^3\}$	1		[1]	[-1]				
$\{2,1\}$	2		$\begin{bmatrix} 1 & 0 \\ 0 & 1 \end{bmatrix}$	$\begin{bmatrix} 1 & 0 \\ 0 & -1 \end{bmatrix}$	$\begin{bmatrix} -a & b \\ b & a \end{bmatrix}$	$\begin{bmatrix} -a-b \\ -b & a \end{bmatrix}$	$\begin{bmatrix} -a-b \\ b & -a \end{bmatrix}$	$\begin{bmatrix} -a & b \\ -b & -a \end{bmatrix}$
$\{3\}$	1		[1]	[1]	[1]	[1]	[1]	[1]

For $N = 3$, $\pi_N = \{g, (12), (13), (23), (123), (132)\}$. Its multiplication table is

g	g	(12)	(13)	(23)	(123)	(132)
(12)	(12)	g	(132)	(123)	(23)	(13)
(13)	(13)	(123)	g	(132)	(12)	(23)
(23)	(23)	(132)	(123)	g	(13)	(12)
(123)	(123)	(13)	(23)	(12)	(132)	g
(132)	(132)	(23)	(13)	(13)	g	(123)

The set of all linear combinations of the $N!$ permutations is the permutation group algebra, A . A typical element of A is

$$X = \sum_a (X)_a P_a \quad (A1.1)$$

where $(X)_a$ is a numerical coefficient. The zero element $((X)_a = 0$ for all a) is also an element in A . The set of $N!$ permutations is called the regular basis of A .

Any set of $N!$ linearly independent elements of A can serve as a basis for A . The basis which best displays the symmetry relations of A is its matrix basis.

A2. The Permutation Algebra. Its Matrix Basis.

The matrix basis of A is the set of $N!$ matrix basis elements

$$e_{rs}^\alpha = (f^\alpha/N!) \sum_a^{N!} [P_a^{-1}]_{sr}^\alpha P_a, \quad r, s = 1 \text{ to } f^\alpha \quad (A2.1)$$

Here α is one of the $p(N)$ partitions of N . A partition is a set of integers whose sum is N . A partition is usually written

$$\alpha = \{ \dots, g^{\alpha_g}, \dots, 2^{\alpha_2}, 1^{\alpha_1} \} \quad (A2.2)$$

where α_g is the number of times the integer g occurs in the partition. For $N = 3$, $p(N) = 3$ and $\alpha = \{1^3\}, \{2,1\}, \{3\}$. The symbol $[P_a^{-1}]_{sr}^\alpha$ is the s, r th element in the α th irreducible representation of P_a^{-1} . The dimension of the α th irreducible representation is f^α . The number of matrix basis elements is

$$\sum_\alpha^{p(N)} (f^\alpha)^2 = N! \quad (A2.3)$$

We consider only orthogonal representations, *i.e.*, representations for which

$$[P_a]_{rs}^\alpha = [P_a^{-1}]_{sr}^\alpha \quad (A2.4)$$

For $N = 3$, the irreducible representations are

$$a = 1/2; \quad b = \sqrt{3}/2$$

The multiplication rule between matrix basis elements is

$$e_{rs}^\alpha e_{tu}^\beta = \delta^{\alpha\beta} \delta_{st} e_{ru}^\beta \quad (A2.5)$$

The Kronecker deltas between α and β and between s and t make the matrix basis a very useful one.

For $n = 3$, the matrix basis multiplication table is

	$e_{11}^{\{1^3\}}$	$e_{11}^{\{2,1\}}$	$e_{12}^{\{2,1\}}$	$e_{21}^{\{2,1\}}$	$e_{22}^{\{2,1\}}$	$e_{11}^{\{3\}}$
$e_{11}^{\{1^3\}}$	$e_{11}^{\{1^3\}}$	0	0	0	0	0
$e_{11}^{\{2,1\}}$	0	$e_{11}^{\{2,1\}}$	$e_{12}^{\{2,1\}}$	0	0	0
$e_{12}^{\{2,1\}}$	0	0	0	$e_{11}^{\{2,1\}}$	$e_{12}^{\{2,1\}}$	0
$e_{21}^{\{2,1\}}$	0	$e_{21}^{\{2,1\}}$	$e_{22}^{\{2,1\}}$	0	0	0
$e_{22}^{\{2,1\}}$	0	0	0	$e_{21}^{\{2,1\}}$	$e_{22}^{\{2,1\}}$	0
$e_{11}^{\{3\}}$	0	0	0	0	0	$e_{11}^{\{3\}}$

The product of a permutation P_a and a matrix basis element is given by

$$P_a e^{\alpha}_{r_s} = \sum_{r'}^{j\alpha} [P_a]_{r'r'}^{\alpha} e^{\alpha}_{r's} \quad (A2.6)$$

A typical algebraic element expressed in the matrix basis is

$$X = \sum_{\alpha}^{p(N)} \sum_r^f \sum_s^{\alpha} [X]_{rs}^{\alpha} e^{\alpha}_{rs} \quad (A2.7)$$

A3. Structure Operators

Associated with each structure diagram D_{κ}^p is a structure operator

$$\kappa = \sum_{\alpha} (\kappa)_{\alpha} P_{\alpha} \quad (A3.1)$$

The rules for the construction of a structure operator follow.

(1) Arrange the integers in two rows of lengths $N - p$ and p , respectively, so that the paired integers lie in the same row. The arrangement for D_{κ}^p is labeled T_{κ}^p .

For $N = 3$

$p = 0$

$$\kappa = \text{I}$$

$$T_{\kappa}^p = \begin{bmatrix} 1 \\ 2 \\ 3 \end{bmatrix}$$

$p = 1$

$$\kappa = \begin{matrix} \text{I} & \text{II} & \text{III} \\ T_{\kappa}^p = \begin{bmatrix} 1 & 2 \\ 3 \end{bmatrix} & \begin{bmatrix} 2 & 3 \\ 1 \end{bmatrix} & \begin{bmatrix} 1 & 3 \\ 2 \end{bmatrix} \end{matrix}$$

(2) Find the permutation $\sigma_{I_{\kappa}}$ which rearranges the integers in T_{I^p} so as to convert it into $T_{\kappa I^p}$. That is, $T_{I^p} = \sigma_{I_{\kappa}} T_{\kappa}^p$.

$$\kappa = \begin{matrix} \text{I} & \text{II} & \text{III} \\ \sigma_{I_{\kappa}} & (g) & (132) & (23) \\ \epsilon(\sigma_{I_{\kappa}}) & +1 & +1 & -1 \end{matrix}$$

(3) Form structure element I^p by multiplying the antisymmetric sum N_{I^p} of the operators that permute integers down the column by P_{I^p} , the symmetric sum of the operators that permute the integers along the rows in T_{I^p} .

$$I = N_{I^p} P_{I^p}$$

$p = 0$

$$I^p = [g - (12) - (13) - (23) + (123) + (132)][g] = g - (12) - (13) - (23) + (123) + (132)$$

$p = 1$

$$I^p = [g - (13)][g + (12)] = g + (12) - (13) - (123)$$

(4) Form structure element κ from the formula

$$\kappa^p = \epsilon(\sigma_{I_{\kappa}}) I^p \sigma_{I_{\kappa}} \quad (A3.2)$$

$N = 3$

$$\kappa \quad \sigma_{I_{\kappa}} \quad \kappa^p$$

$$p = 0$$

$$\text{I} \quad g \quad g - (12) - (13) - (23) + (123) + (132)$$

$$p = 1 \quad \text{I} \quad g \quad g + (12) - (13) - (123)$$

$$\text{II} \quad (132) \quad -g + (13) - (23) + (132)$$

$$\text{III} \quad (13) \quad (12) - (23) - (123) + (132)$$

Note that $\text{III}^p = I^p + \text{II}^p$.

The structure elements are linear combinations of matrix basis elements

$$\kappa^p = \sum (\kappa)_{rs} e^{\alpha}_{rs} \quad (A3.3)$$

For $N = 3$

$$I^p = (\sqrt{3})e_{21}^{[2,1]} + 3e_{22}^{[2,1]}$$

$$\text{II}^p = (\sqrt{3})e_{21}^{[2,1]} - 3e_{22}^{[2,1]}$$

Note that these are the matrix basis elements which differ from those of section 5 by interchanging the integers 2 and 3 in the permutations. That is $(12) \rightarrow (13)$, $(123) \rightarrow (132)$, etc.

A.4. The Conventional Space-Spin Formulation in the Matrix Basis

The conventional formulation consists of antisymmetrizing the products of a primitive ket and the eigenfunctions Θ of S^2 . By the Dirac identity matrix, spin functions are eigenfunctions of S^2 . That is

$$S^2 \Theta^{SM_{rs}} = S(S + 1) \hbar^2 \Theta^{SM_{rs}} \quad (A4.1)$$

where

$$\Theta^{SM_{rs}} = N_{S_{rs}} e^{\tilde{\alpha}}_{rs} \Theta^M \quad (A4.2)$$

Here for $e^{\tilde{\alpha}}_{rs}$ we take

$$[P_a]_{rs}^{\tilde{\alpha}} = \epsilon_a [P_a]_{rs}^{\tilde{\alpha}} \quad (A4.3)$$

with $\epsilon_a =$ plus or minus one for an even or odd permutation. Again $\alpha = \{2^p, 1^{N-2p}\}$ and $S = N/2 - p$. The matrix spin functions are normalized and orthogonal. We take $M = 0$ or $+1/2$ and $\Theta^M = \alpha(1)\alpha(2)\dots\beta(N)$. Then

(17) For further details, consult ref. 1 and additional references listed there.

$$\Theta^{SM_{r_1}} = \delta_{s_1} \Theta^{SM_{r_1}} \quad (\text{A4.4})$$

$$\text{For } N = 3, \Theta^M = \alpha(1)\alpha(2)\beta(3)$$

$$S = 3/2$$

$$\Theta^{SM_{11}} = 1/\sqrt{3}(\alpha(1)\alpha(2)\beta(3) + \beta(1)\alpha(2)\alpha(3) + \alpha(1)\beta(2)\alpha(3))$$

$$S = 1/2$$

$$\Theta^{SM_{11}} = 1/\sqrt{6}(2\alpha(1)\alpha(2)\beta(3) - \beta(1)\alpha(2)\alpha(3) - \alpha(1)\beta(2)\alpha(3))$$

$$\Theta^{SM_{21}} = 1/\sqrt{2}(\beta(1)\alpha(2)\alpha(3) - \alpha(1)\beta(2)\alpha(3))$$

by (3.6) and (A4.3)

$$\begin{aligned} P_a \Theta^{SM_{r_1}} &= N_a^{\bar{\alpha}} P_a e^{\bar{\alpha}} \Theta^M \\ &= N_a^{\bar{\alpha}} \sum_t [P_a]^{\bar{\alpha}} e^{\alpha}_{tr} \Theta^M \\ &= \epsilon_a \sum_t [P_a]^{\alpha}_{tr} \Theta^{SM_{11}} \end{aligned} \quad (\text{A4.5})$$

We antisymmetrize and neglect multiplicative constants

$$\begin{aligned} \Omega^{SM_r} &= \sum_a \epsilon_a P_a |g\rangle P_a \Theta^{SM_{r_1}} \\ &= \sum_a \sum_t \epsilon_a [P_a]^{\bar{\alpha}} e^{\alpha}_{tr} |a\rangle \Theta^{SM_{11}} \\ &= \sum_a \sum_t [P_a]^{\alpha}_{tr} |a\rangle \Theta^{SM_{11}} \\ &= \sum_t |\alpha tr\rangle \Theta^{SM_{11}} \end{aligned} \quad (\text{A4.6})$$

For $N = 3$

$$S = 3/2$$

$$\begin{aligned} \Omega^{S_1} &= |\{1^3\}11\rangle(1/\sqrt{3})(\alpha(1)\alpha(2)\beta(3) + \beta(1)\alpha(2)\alpha(3) + \alpha(1)\beta(2)\alpha(3)) \\ &= (1/6\sqrt{3})\{[1g] - |(12)\rangle - |(13)\rangle - |(23)\rangle + |(123)\rangle + |(132)\rangle\}\alpha(1)\alpha(2)\beta(3) + [1g] - |(12)\rangle - |(13)\rangle - |(23)\rangle + |(123)\rangle + |(132)\rangle\}\beta(1)\alpha(2)\alpha(3) + [1g] - |(13)\rangle - |(23)\rangle + |(123)\rangle + |(132)\rangle\}\alpha(1)\beta(2)\alpha(3) \end{aligned}$$

$$S = 1/2$$

$$\begin{aligned} \Omega^{S_1} &= |\{2,1\}11\rangle(1/\sqrt{6})(2\alpha(1)\alpha(2)\beta(3) - \beta(1)\alpha(2)\alpha(3) - \alpha(1)\beta(2)\alpha(3)) + |\{2,1\}21\rangle(1/\sqrt{2})(\beta(1)\alpha(2)\alpha(3) - \alpha(1)\beta(2)\alpha(3)) \end{aligned}$$

$$\begin{aligned} &= (1/\sqrt{6})\{[2|\{2,1\}11\rangle]\alpha(1)\alpha(2)\beta(3) + [-|\{2,1\}11\rangle + \sqrt{3}|\{2,1\}21\rangle]\beta(1)\alpha(2)\alpha(3)\} + [-|\{2,1\}11\rangle - \sqrt{3}|\{2,1\}21\rangle]\alpha(1)\beta(2)\alpha(3) \\ &= 1/\sqrt{6}\{[(1/3)(2|g\rangle + 2|(12)\rangle - |(13)\rangle - |(23)\rangle - |(123)\rangle - |(132)\rangle)]\alpha(1)\alpha(2)\beta(3) + [(1/3)[-|g\rangle - |(12)\rangle + 2|(13)\rangle - |(23)\rangle + 2|(123)\rangle - |(132)\rangle]\beta(1)\alpha(2)\alpha(3) + [(1/3)[-|g\rangle - |(12)\rangle - |(13)\rangle + 2|(23)\rangle - |(123)\rangle + 2|(132)\rangle]\alpha(1)\beta(2)\alpha(3)\} \end{aligned}$$

$$\begin{aligned} \Omega^{S_2} &= |\{2,1\}12\rangle(1/\sqrt{6})(2\alpha(1)\alpha(2)\beta(3) - \beta(1)\alpha(2)\alpha(3) - \alpha(1)\beta(2)\alpha(3) + |\{2,1\}22\rangle(1/\sqrt{2})(\beta(1)\alpha(2)\alpha(3) - \alpha(1)\beta(2)\alpha(3)) \\ &= (1/\sqrt{6})\{[2|\{2,1\}12\rangle]\alpha(1)\alpha(2)\beta(3) + [-|\{2,1\}12\rangle + \sqrt{3}|\{2,1\}22\rangle]\beta(1)\alpha(2)\alpha(3) \\ &= (1/\sqrt{6})\{[(1/\sqrt{3})(|(13)\rangle - |(23)\rangle - |(123)\rangle + |(132)\rangle)]\alpha(1)\alpha(2)\beta(3) + [(1/\sqrt{3})(|g\rangle - |(12)\rangle - |(23)\rangle - |(132)\rangle)]\beta(1)\alpha(2)\alpha(3) + [(1/\sqrt{3})(|g\rangle - |(12)\rangle - |(13)\rangle + |(123)\rangle)]\alpha(1)\beta(2)\alpha(3)\} \end{aligned}$$

The expanded form for $S = 1/2$ has been given by Burke.⁶

The space-spin state vector is

$$\phi^{S_K} = \sum_r \langle r|K\rangle \Omega^{SM_r} \quad (\text{A4.7})$$

The secular equation is

$$|\langle \Omega^{S'M_r} | H | \Omega^{SM_r} \rangle - E \langle \Omega^{S'M_r} | \Omega^{SM_r} \rangle| = 0$$

Now by (3.4) and since the spin functions are normalized,

$$\begin{aligned} \langle \Omega^{S'M_r} | H | \Omega^{SM_r} \rangle &= 1/f^{\alpha} \sum_{t'} \sum_t \langle \alpha' t' r' | H | \alpha tr \rangle \langle \Theta^{S'M_{t'}} | \Theta^{SM_{11}} \rangle \\ &= \delta^{S'S'} \langle \alpha r r' | H | g \rangle \end{aligned} \quad (\text{A4.8})$$

We see that the secular equations are identical in the conventional and spin-free formulations. It follows that the eigenvector coefficients $\langle \alpha tr | K \rangle$ are identical also.

The Radiation Chemistry of Organic Liquid Mixtures. II

by J. F. Merklin² and S. Lipsky

Department of Chemistry, University of Minnesota, Minneapolis 14, Minnesota (Received April 24, 1964)

Studies have been made of the hydrogen yields produced by γ -irradiation of (a) mixtures of benzene with the cycloalkanes: methylcyclohexane, ethylcyclohexane, and bicyclohexyl, (b) mixtures of benzene with the arylcycloalkanes: 1-methyl-4-phenylcyclohexane and 1-phenyl-2-cyclohexylethane, and (c) mixtures of methylcyclohexane and ethylcyclohexane with their respective aryl derivatives: 1-methyl-4-phenylcyclohexane and 1-phenyl-2-cyclohexylethane. Both methylcyclohexane and ethylcyclohexane exhibit sharp reduction in their hydrogen yields on addition of traces of benzene. The mechanism responsible for this effect seems to saturate at about 0.05 *M* benzene, and further addition of benzene reduces the hydrogen yield with much lower efficiency. The effect at low concentration is attributed to scavenging of thermal H atoms by benzene, and on the basis of this assumption a kinetic analysis leads to calculated thermal H atom yields at zero dose of $G(\text{H}) = 1.4 \pm 0.4$ for methylcyclohexane and $G(\text{H}) = 2.3 \pm 0.4$ for ethylcyclohexane. The "protection" efficiency at high benzene concentrations in both liquids is found to be the same as exhibited by benzene in cyclohexane mixtures at all benzene concentrations suggesting that thermal H atoms are produced with yield not exceeding 0.2 ± 0.4 in radiolysis of cyclohexane. A comparison of the dose dependence of $G(\text{H}_2)$ from cyclohexane, methylcyclohexane, and ethylcyclohexane is consistent with this interpretation. For cycloalkane-arylcycloalkane mixtures at high arylcycloalkane concentrations, the "protective" effect is qualitatively similar to that exhibited by benzene. However, at low concentrations, the arylcycloalkane is much less efficient than benzene in reducing $G(\text{H}_2)$ in methylcyclohexane and ethylcyclohexane. A comparison is made of $G(\text{H}_2)$ from pure arylcycloalkane liquid with $G(\text{H}_2)$ from physical mixtures of benzene and the corresponding cycloalkane at equivalent electron fractions. In all cases, the yield from the mixture is at least two times greater than from the pure compound.

1. Introduction

In cyclohexane radiolysis, there is evidence from the work of Dyne and Jenkinson³ for both a unimolecular and a bimolecular route to hydrogen production. Both processes seem to be inhibited to the same extent by the addition of either benzene or iodine, suggesting that thermal H atoms are not involved to any significant extent in the bimolecular process.^{4,5} Inhibition is postulated to occur by interaction of the additive with some precursor of both the unimolecular and the bimolecular process.³⁻⁵ Neither the identity of the precursor nor the nature of the process is known. However, for the case of benzene, stationary-state kinetic analysis indicates that the process at high benzene concentration (*ca.* $>0.5 M$) is first order in benzene with a

specific rate $k_5 \approx 0.6\tau^{-1}$ to $1.0\tau^{-1}$ l./mole sec. where τ is the lifetime of the precursor.⁶⁻⁸

(1) Work supported by the U. S. Atomic Energy Commission under Contract AT(11-1)-913. The material presented here is taken from a dissertation presented to the University of Minnesota by J. F. Merklin in partial fulfillment of the requirements for the Ph.D. degree in June, 1963.

(2) E. I. du Pont de Nemours and Co., Predoctorate Summer Fellow, 1960 and 1962.

(3) P. J. Dyne and W. M. Jenkinson, *Can. J. Chem.*, **38**, 539 (1960).

(4) P. J. Dyne and W. M. Jenkinson, *ibid.*, **39**, 2163 (1961).

(5) J. A. Stone and P. J. Dyne, *Radiation Res.*, **17**, 353 (1962).

(6) G. R. Freeman, *J. Chem. Phys.*, **33**, 71 (1960).

(7) G. Meshitsuka, F. Takemura, T. Sakai, and K. Hirota, *Ann. Rept. Tokyo Metropol. Isotope Center*, **1**, 61 (1962).

(8) J. F. Merklin and S. Lipsky, "Biological Effects of Ionizing Radiation at the Molecular Level," International Atomic Energy Agency, Vienna, Austria, 1962, p. 73.

At lower benzene concentrations, results from various laboratories disagree. For benzene concentrations less than 0.5 *M*, Freeman⁶ has reported evidence for a considerably more efficient "protective" process whereas earlier measurements by Burton, Chang, Lipsky, and Reddy⁹ give no indication of such a difference. The more efficient process is attributed to a scavenging of thermal H atoms by benzene with a yield, in absence of benzene, of $G(H) = 2.4$. This value is in reasonable agreement with a value that would be predicted from the measured HI yield in mixtures of cyclohexane with iodine on the basis of the assumption that I₂ also scavenges H atoms.^{10,11} In addition, the nature and yields of liquid products from cyclohexane radiolysis has suggested the production of thermal H atoms in approximately this same yield.¹¹⁻¹³ The presence of thermal H atoms has also been suggested from kinetic analysis of $G(H_2)$ from cyclohexane-benzoquinone mixtures.¹⁴ However, the results of Dyne and Jenkinson³⁻⁵ are unequivocal and cannot simply be reconciled with the existence of a substantial thermal H yield from cyclohexane. These authors have questioned, therefore, the propriety of the kinetic analysis that indicates the presence of H atoms.

In a recent publication⁸ (hereafter referred to as paper I), we re-examined the cyclohexane system. The addition of trace amounts (*ca.* 10⁻⁴ *M*) of either benzene or phenylcyclohexane seemed to sensitize rather than depress $G(H_2)$. At concentrations greater than 0.05 *M* our results were in agreement with those reported from other laboratories. The anomalous results at low concentration have not been possible to repeat. The behavior consistently obtained now is a monotonic decrease in $G(H_2)$ with increasing benzene or phenylcyclohexane concentration. No evidence is found for enhanced sensitivity to benzene at low concentrations. This is discussed in greater detail in a later section of this paper.

In the case of radiolysis of methylcyclohexane-benzene mixtures, Freeman¹⁵ has again reported evidence for enhanced sensitivity of $G(H_2)$ to benzene at low benzene concentrations. In paper I, this result was qualitatively confirmed although our absolute hydrogen yields differed considerably. In view of the difficulty experienced with the cyclohexane system, we have extensively repeated these measurements. However, we find no substantial change in these results nor in any other of the results reported in paper I.

In this paper we report new measurements on the effect of benzene and arylcycloalkanes on $G(H_2)$ from ethylcyclohexane and bicyclohexyl. In addition, results are presented for the effect of benzene on the arylcycloalkanes. In paper I, phenylcyclohexane and

bicyclohexyl were the only arylcycloalkanes employed. We now include measurements with 1-methyl-4-phenylcyclohexane and 1-phenyl-2-cyclohexylethane. Aside from their use as "protection" solutes, these compounds are also employed to estimate the efficacy of a chemical bond in the aromatic "protection" effect. A comparison is made of $G(H_2)$ from the pure arylcycloalkanes with $G(H_2)$ from an equivalent physical mixture of benzene and the corresponding cycloalkane.

2. Experimental

Materials. Source and purification of benzene, cyclohexane, and methylcyclohexane have been previously reported.⁸

Ethylcyclohexane (Matheson Coleman and Bell, White Label) was purified either by chromatography through a 1-m. silica gel column or, more frequently, by treatment with fuming sulfuric acid. In either case, this was followed by distillation in a 20-theoretical plate column retaining a middle fraction of about 40% with a normal boiling point of 131.9° (lit. 131.78°).¹⁶ The optical density of an air-equilibrated sample of the liquid in a 1-cm. cell did not exceed 0.7 at 2100 Å: nor 0.15 at 2260 Å.

Bicyclohexyl (Eastman Kodak practical grade) was first treated with fuming sulfuric acid and then vacuum distilled. A middle fraction of about 40% was retained, having a boiling point of 79° at 3 mm. This fraction was accepted for use if its optical density in a 1-cm. cell did not exceed 1.0 at 2100 Å. nor 0.15 at 2260 Å.

p-Dicyclohexylbenzene (Eastman Kodak White Label) was purified by a single recrystallization from methanol. The recrystallized sample melted in the range 103.2-103.3° (lit. 100°).¹⁷

1-Methyl-4-phenylcyclohexane was synthesized from 4-methylcyclohexanone by Grignard reaction with phenylmagnesium bromide followed by dehydration with H₂SO₄. The product, 1-methyl-4-phenylcyclohexane, was hydrogenated in a Paar bomb under 40

(9) M. Burton, J. Chang, S. Lipsky, and M. P. Reddy, *Radiation Res.*, **8**, 203 (1958).

(10) G. Meshitsuka and M. Burton, *ibid.*, **10**, 499 (1959).

(11) L. J. Forrestal and W. H. Hamill, *J. Am. Chem. Soc.*, **83**, 1535 (1961).

(12) H. A. Dewhurst, *J. Phys. Chem.*, **63**, 813 (1959).

(13) T. D. Nevitt and L. P. Remsburg, *ibid.*, **64**, 969 (1960).

(14) G. E. Adams, J. H. Bauxendale, and R. D. Sedgwick, *ibid.*, **63**, 854 (1959).

(15) G. R. Freeman, *J. Chem. Phys.*, **36**, 1542 (1962).

(16) American Petroleum Institute, "Selected Values of Hydrocarbons and Related Compounds," Project 44, 1959.

(17) J. von Braun, *Ber.*, **60**, 1180 (1927).

lb./cm.² of H₂ with 10% charcoal-palladium catalyst for 72 hr. The product was vacuum distilled at 120–122° and 10 mm.

1-Phenyl-2-cyclohexylethane was synthesized from cyclohexane-acetyl chloride by Friedel-Crafts condensation with benzene followed by Wolff-Kishner reduction with hydrazine. The product was vacuum distilled at 117° and 4 mm.

Sample Preparation. Pyrex cells were sealed to a high vacuum manifold and baked during evacuation. The cells were then filled with dry nitrogen, opened, filled with the solutions, cooled to liquid nitrogen temperature, and sealed under a nitrogen atmosphere. The solutions were degassed by four freeze-thaw cycles.

Radiation. Sample irradiation was performed at the University of Minnesota 1000-c. Co⁶⁰ γ -ray facility. Dose rate determinations were made with the Fricke dosimeter, using a value of 15.6 for $G(\text{Fe}^{+3})$.¹⁸ To obtain dose rates in the organic solutions, the values obtained for the Fricke dosimeter were multiplied by the ratio of the electron density of the organic solution to the electron density of the dosimeter solution. In the case of cyclohexane, for example, this ratio is taken as 0.785. Dose rates employed in this work varied from about 2.0×10^{19} to 5.0×10^{19} e.v./min.¹⁹ In studies of pure compounds, total doses ranged from about 1.2×10^{21} to 200×10^{21} e.v./l.

Analysis. Products volatile at -126° were removed from the irradiated liquids by refluxing in a small vacuum still.²⁰ The number of moles of volatile product was determined by compression into the calibrated volumes of a Saunders-Taylor apparatus. The composition of the gas was then determined by analysis on a modified CEC 21-401 mass spectrometer.

3. Results

Pure Cycloalkanes. Hydrogen and methane yields from pure liquid cyclohexane (C₆H₁₂), methylcyclohexane (C₆H₁₁CH₃), ethylcyclohexane (C₆H₁₁C₂H₅), and bicyclohexyl (C₆H₁₁-C₆H₁₁) were obtained as functions of absorbed dose. Results for $G(\text{H}_2)$ and $G(\text{CH}_4)$ are shown in Fig. 1 and 2, respectively. The severity of the dose dependence in the compounds C₆H₁₁CH₃, C₆H₁₁C₂H₅, and C₆H₁₁-C₆H₁₁ makes extrapolation of either $G(\text{H}_2)$ or $G(\text{CH}_4)$ to zero dose somewhat uncertain. Lower estimates of these extrapolated yields are presented in Table I.

Our dose dependence for cyclohexane is similar to that previously reported by Freeman⁶ (dose range $2\text{--}26 \times 10^{22}$ e.v./l.) and Guentner, Hardwick, and Nijak²¹ (dose range $5\text{--}200 \times 10^{22}$ e.v./l.). In all three cases the dose dependence is linear to $ca. 20 \times 10^{22}$ e.v./l. and the slopes comparable at $ca. -1 \times 10^{-26}$ l./e.v.²

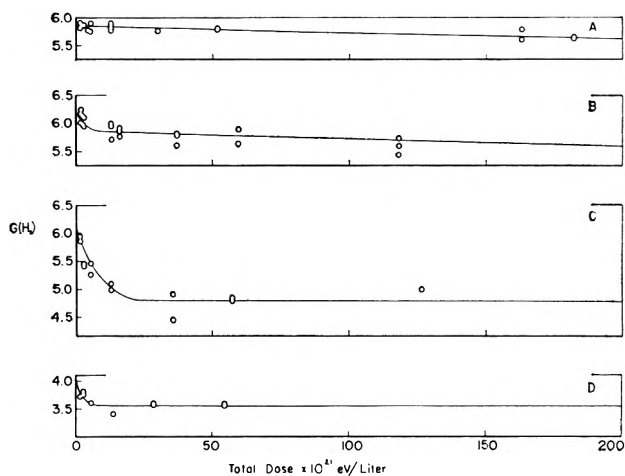


Figure 1. $G(\text{H}_2)$ as a function of absorbed dose: A, cyclohexane; B, methylcyclohexane; C, ethylcyclohexane; D, bicyclohexyl.

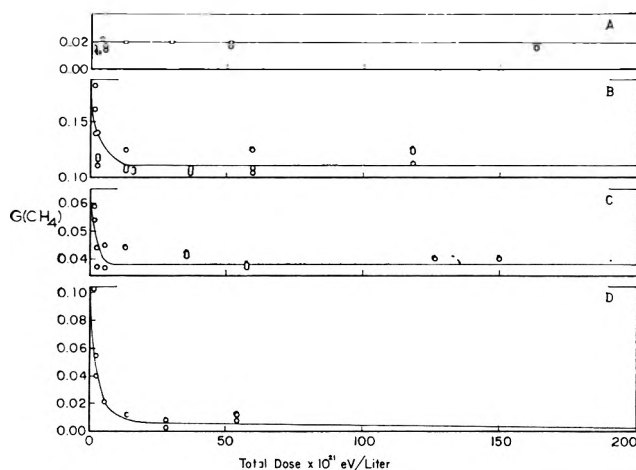


Figure 2. $G(\text{CH}_4)$ as a function of absorbed dose: A, cyclohexane; B, methylcyclohexane; C, ethylcyclohexane; D, bicyclohexyl.

Dyne and Stone,²² however, working over a more extensive dose range from $ca. 0.2\text{--}100 \times 10^{22}$ e.v./l. report concave upward behavior with an initial slope about six times larger than ours. However, within the G value uncertainties of $ca. 0.05\text{--}0.1$ G unit, this discrepancy is not a very serious one at low doses. It should be noted, for comparison, that the initial slopes for $G(\text{H}_2)$ from C₆H₁₁CH₃ and C₆H₁₁C₂H₅ are several

(18) J. Saldick and A. O. Allen, *J. Chem. Phys.*, **22**, 438 (1954).

(19) All dose rates, doses, and G values reported in this work refer to energy absorbed by the organic solution.

(20) V. Van Dusen, Jr., and W. H. Hamill, *J. Am. Chem. Soc.*, **84**, 3648 (1962).

(21) W. S. Guentner, T. J. Hardwick, and R. P. Nijak, *J. Chem. Phys.*, **30**, 601 (1959).

(22) P. J. Dyne and J. A. Stone, *Can. J. Chem.*, **39**, 2381 (1961).

Table I: Extrapolated Zero Dose Hydrogen and Methane Yields from Pure Cycloalkanes and Pure Aromatics

Compound	$G_0(\text{H}_2)$		$G_0(\text{CH}_4)$	
	This work	Lit.	This work	Lit.
C_6H_{12}	5.83 ± 0.06	$5.37\text{--}5.85^a$	0.02	$0.02\text{--}0.09^a$
$\text{C}_6\text{H}_{11}\text{CH}_3$	6.25 ± 0.1	4.80^b	0.17	0.08^b
$\text{C}_6\text{H}_{11}\text{C}_2\text{H}_5$	6.1 ± 0.1	...	0.06	
$(\text{C}_6\text{H}_{11})_2$	4.0 ± 0.1	...	0.10	
C_6H_6	0.045 ± 0.003	$0.036\text{--}0.044^c$		

^a See ref. 6, 9, 11, 24. ^b See ref. 15. ^c See ref. 23.

orders of magnitude larger than the initial slope for cyclohexane.

Benzene. The hydrogen yield from benzene is also presented in Table I. No dose dependence was noted.²³

Cycloalkane-Benzene Mixtures. In paper I, we reported an anomalous increase in $G(\text{H}_2)$ from mixtures of benzene (or phenylcyclohexane) with cyclohexane at aromatic concentrations between 1.1×10^{-4} and $1.4 \times 10^{-2} M$. As mentioned in the Introduction, attempts to reproduce these measurements have failed using techniques seemingly identical with those employed at that time. Our hydrogen yields in this concentration region are now found to extrapolate smoothly to the yield obtained in the absence of the aromatic. At aromatic concentrations greater than $1.4 \times 10^{-2} M$, present values for $G(\text{H}_2)$ agree well with those previously reported (see Fig. 1A, B in paper I).

Hydrogen yields from methylcyclohexane-benzene mixtures were reported in paper I at benzene concentrations varying from 10^{-5} to $11.2 M$ and at an absorbed dose of 4.6×10^{21} e.v./l. A very rapid decrease in $G(\text{H}_2)$ was found at low benzene concentrations. At $4.2 \times 10^{-2} M$ benzene, for example, $G(\text{H}_2)$ is reduced from 5.95 to 4.9, whereas in the case of cyclohexane the same concentration of benzene results in a reduction of $G(\text{H}_2)$ from 5.8 to 5.5. These measurements have now been repeated with the same results as previously reported (see Fig. 2A and Table II in paper I). The methylcyclohexane-benzene mixtures have also been studied at a higher dose of 11×10^{21} e.v./l. These results are presented in Fig. 3A showing $G(\text{H}_2)$ from the mixture as a function of benzene electron fraction, ϵ_B .

In Fig. 3B and 3C is shown $G(\text{H}_2)$ vs. benzene electron fraction, ϵ_B , for ethylcyclohexane-benzene mixtures at doses of 2.3×10^{21} e.v./l. and 26×10^{21} e.v./l., respectively. Exceedingly high sensitivity to low benzene concentrations has been found particularly at the low dose. Values for $G(\text{H}_2)$ for benzene concentrations less than $4.5 \times 10^{-2} M$ are presented in Table II.

Table II: $G(\text{H}_2)$ from Ethylcyclohexane-Benzene Mixtures

[Benzene], ^a mole/l.	2.3×10^{21} e.v./l. ^b	26×10^{21} e.v./l. ^b
0.00	5.60	4.80
9.35×10^{-4}	4.80	4.80
1.2×10^{-2}	...	4.16
4.58×10^{-2}	4.15	4.07

^a To convert from concentration in mole/l. to electron fraction divide by 10.4. ^b Estimated errors ± 0.1 ; standard deviation of the average ± 0.05 .

The effect of benzene on $G(\text{H}_2)$ from bicyclohexylbenzene mixtures at a dose of 14×10^{21} e.v./l. is similar to that found for cyclohexane. No sharp decrease in $G(\text{H}_2)$ is observed at low benzene concentrations. Results are shown in Fig. 4A. At a benzene concentration of $5.34 \times 10^{-4} M$ (not shown in Fig. 4A), $G(\text{H}_2) = 3.5$.

Pure Arylcycloalkanes. Hydrogen yields from phenylcyclohexane ($\text{C}_6\text{H}_{11}\text{--C}_6\text{H}_5$) and benzylcyclohexane ($\text{C}_6\text{H}_{11}\text{CH}_2\text{--C}_6\text{H}_5$) were reported in paper I. Values for $G(\text{H}_2)$ have now also been obtained for 1-methyl-4-phenylcyclohexane ($\text{CH}_3\text{C}_6\text{H}_{10}\text{--C}_6\text{H}_5$), 1-phenyl-2-cyclohexylethane ($\text{C}_6\text{H}_{11}\text{C}_2\text{H}_4\text{--C}_6\text{H}_5$), and *p*-dicyclohexylbenzene ($\text{C}_6\text{H}_{11}\text{--C}_6\text{H}_4\text{--C}_6\text{H}_{11}$). No dose dependence was found for total doses varying from 4.8×10^{21} to 130×10^{21} e.v./l. The results for all arylcycloalkanes are presented in Table III. The *p*-dicyclohexylbenzene was studied both as a liquid at 110° and as a solid at 25° .

Cycloalkane-Arylcycloalkane Mixtures. Measurements of $G(\text{H}_2)$ from mixtures of cyclohexane- $\text{C}_6\text{H}_{11}\text{--C}_6\text{H}_5$ and methylcyclohexane- $\text{C}_6\text{H}_{11}\text{CH}_2\text{C}_6\text{H}_5$ have been reported in paper I. In Fig. 4B and 4C are presented results for $G(\text{H}_2)$ from methylcyclohexane- $\text{CH}_3\text{C}_6\text{H}_{10}\text{--}$

(23) S. Gordon and M. Burton, *Discussions Faraday Soc.*, **12**, 88 (1952); R. H. Schuler, *J. Phys. Chem.*, **60**, 381 (1956); S. Gordon, A. R. Van Dyken, and T. F. Doumani, *ibid.*, **62**, 20 (1958).

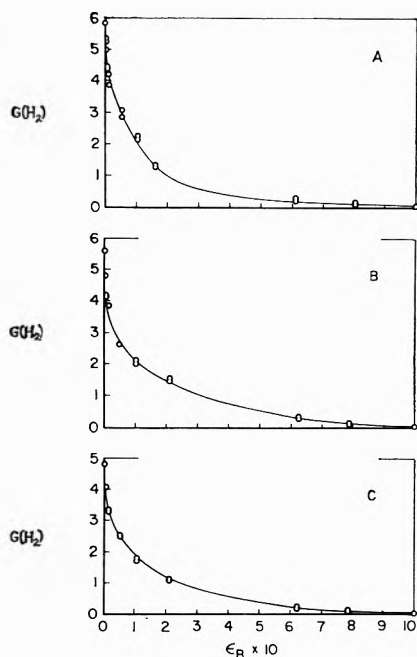


Figure 3. Dependence of $G(\text{H}_2)$ on electron fraction of aromatic: A, methylcyclohexane-benzene mixtures (dose: 11×10^{21} e.v./l.); B, ethylcyclohexane-benzene mixtures (dose: 2.3×10^{21} e.v./l.); C, ethylcyclohexane-benzene mixtures (dose: 26×10^{21} e.v./l.).

Table III: Hydrogen Yields from Pure Arylcycloalkanes

Compounds	$G(\text{H}_2)$
$\text{C}_6\text{H}_{11}-\text{C}_6\text{H}_6$	0.26 ± 0.01
$\text{C}_6\text{H}_{11}\text{CH}_2-\text{C}_6\text{H}_5$	0.29 ± 0.02
$\text{CH}_3\text{C}_6\text{H}_{10}-\text{C}_6\text{H}_5$	0.29 ± 0.02
$\text{C}_6\text{H}_{11}\text{C}_2\text{H}_4-\text{C}_6\text{H}_5$	0.37 ± 0.02
$\text{C}_6\text{H}_{11}-\text{C}_6\text{H}_4-\text{C}_6\text{H}_{11}$ (liq., 110°)	0.20 ± 0.01
$\text{C}_6\text{H}_{11}-\text{C}_6\text{H}_4-\text{C}_6\text{H}_{11}$ (solid, 25°)	0.32 ± 0.02

C_6H_5 mixtures at 11×10^{21} e.v./l. and from ethylcyclohexane- $\text{C}_6\text{H}_{11}\text{C}_2\text{H}_4\text{C}_6\text{H}_5$ mixtures at 2.3×10^{21} e.v./l., respectively. It will be noted that these arylcycloalkane solutes have much less effect on $G(\text{H}_2)$ at low concentrations than was apparent in the corresponding benzene mixtures. This is more clearly presented in Tables IV and V. A similar effect accompanying the replacement of benzene by $\text{C}_6\text{H}_{11}\text{CH}_2-\text{C}_6\text{H}_5$ in mixtures with methylcyclohexane was reported in paper I.

Arylcycloalkane-Benzene Mixtures. In paper I, it was reported that addition of benzene to either $\text{C}_6\text{H}_{11}-\text{C}_6\text{H}_5$ or $\text{C}_6\text{H}_{11}\text{CH}_2-\text{C}_6\text{H}_5$ resulted in a linear decrease in $G(\text{H}_2)$ with increasing benzene concentration. Similar linear dependence is now found for mixtures of ben-

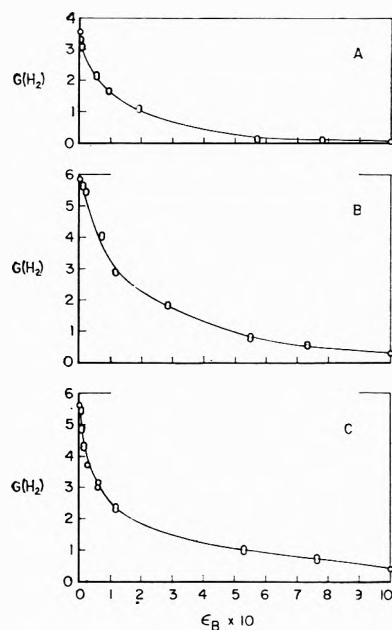


Figure 4. Dependence of $G(\text{H}_2)$ on electron fraction of aromatic: A, bicyclohexyl-benzene mixture (dose: 14×10^{21} e.v./l.); B, methylcyclohexane-1-methyl-4-phenylcyclohexane mixtures (dose: 11×10^{21} e.v./l.); C, ethylcyclohexane-1-phenyl-2-cyclohexylethane mixtures (dose: 2.3×10^{21} e.v./l.).

Table IV: $G(\text{H}_2)$ from $\text{CH}_3\text{C}_6\text{H}_{11}-\text{CH}_3\text{C}_6\text{H}_{10}\text{C}_6\text{H}_5$ Mixtures (Dose: 11×10^{21} e.v./l.)

$[\text{CH}_3\text{C}_6\text{H}_{10}\text{C}_6\text{H}_5]^a$ mole/l.	$G(\text{H}_2)^b$
0.00	5.85
6.40×10^{-4}	5.81
6.40×10^{-3}	5.75
2.85×10^{-2}	5.69

^a To convert from concentration in mole/l. to electron fraction divide by 4.57. ^b Estimated error ± 0.1 ; standard deviation of the average $\leq \pm 0.05$.

Table V: $G(\text{H}_2)$ from $\text{C}_6\text{H}_{11}\text{C}_2\text{H}_5-\text{C}_6\text{H}_{11}\text{C}_2\text{H}_4\text{C}_6\text{H}_5$ Mixtures (Dose: 2.3×10^{21} e.v./l.)

$[\text{C}_6\text{H}_{11}\text{C}_2\text{H}_4\text{C}_6\text{H}_5]^a$ mole/l.	$G(\text{H}_2)^b$
0.00	5.60
4.62×10^{-4}	5.54
5.04×10^{-3}	5.47
2.52×10^{-2}	4.85

^a To convert from concentration in mole/l. to electron fraction, divide by 4.20. ^b Estimated error ± 0.1 ; standard deviation of the average $\leq \pm 0.05$.

zene with either $\text{CH}_3\text{C}_6\text{H}_{10}-\text{C}_6\text{H}_6$ or $\text{C}_6\text{H}_{11}\text{C}_2\text{H}_4-\text{C}_6\text{H}_6$. These results are presented in Fig. 5.

4. Discussion

Dose Dependence. As presented in Fig. 1 and 2, yields of hydrogen and methane from methylcyclohexane, ethylcyclohexane, and bicyclohexyl exhibit a much more severe dependence on dose, at low doses, than is found for these yields from cyclohexane. At higher doses, the dose dependence exhibited by the substituted cyclohexanes becomes essentially the same as found for cyclohexane. Dose dependence of a product yield is most plausibly attributed to the accumulation of a substance capable of somehow inhibiting product formation. In the radiolysis of cyclohexane, this substance is believed to be cyclohexene.²⁴ It is likely that

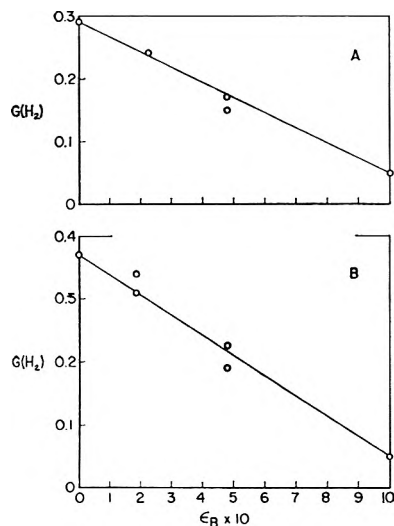
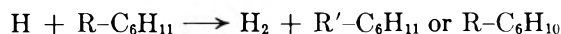


Figure 5. Dependence of $G(\text{H}_2)$ on electron fraction of benzene: A, 1-methyl-4-phenylcyclohexane-benzene mixtures; B, 1-phenyl-2-cyclohexylethane-benzene mixtures.

olefin production is also responsible for the dose dependence observed in the substituted cyclohexanes. A plausible mechanism for olefin interference with H_2 production is, of course, *via* H atom scavenging. However, the measured differences in olefin yields between cyclohexane and the substituted cyclohexanes^{6,15} seems insufficient to explain the observed differences in dose dependence, unless one is prepared to accept a strong dependence of H atom scavenging efficiency on slight differences in the structure of the olefin. For example, in the case of methylcyclohexane the major olefin is 1-methylcyclohexene-1, with smaller amounts of 3-methylcyclohexene-1 and 4-methylcyclohexene-1. These are to be compared with cyclohexene in H atom scavenging efficiency. Although no information is

available for such a comparison in these systems, it is known that the specific rates for H atom addition to butene-2 (*cis*) and to trimethylethylene differ only by 8%.²⁵ Assuming that in the substituted cyclohexanes, the marked dose dependence at low doses is indeed attributable to H atom scavenging by accumulated olefin, it would then seem to follow that the absence of a marked dose dependence in cyclohexane indicates absence of thermal H atoms as precursors of molecular hydrogen. Alternatively, it may be argued that H atoms are precursors of molecular hydrogen in both cyclohexane and the substituted cyclohexanes, but that the olefin scavenging reaction competes more efficiently with the reaction



than with the reaction



However, in general, where similar comparisons have been made, just the reverse behavior is found, namely, that abstraction from the substituted alkane is somewhat²⁶ more rapid.

Absence of thermal H atoms in cyclohexane and their presence in the radiolysis of the substituted cyclohexanes seems also to be consistent with the results we obtain for the effect of benzene on $G(\text{H}_2)$. This will be discussed in the following sections.

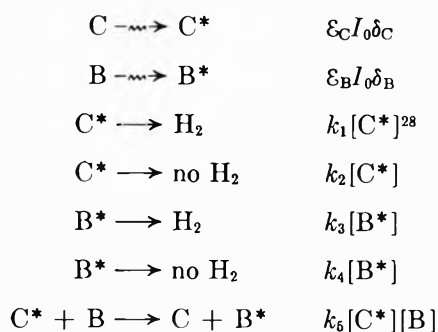
Radiolysis of Mixtures. In order to permit a comparison of protection effects observed in the various mixtures, it is convenient to attempt a description of the processes pertinent to hydrogen production in terms of some kinetic sequence. The simple sequence adopted in paper I has proven useful for this purpose and we continue to employ it. It is assumed that (a) two components in a mixture each absorb energy proportional to their electron fraction²⁷; (b) the aromatic reduces the hydrogen yield by reaction with some intermediate (ultimately the source of all hydrogen from the aliphatic) in a process kinetically first order in aromatic concentration; (c) the aromatic is itself activated as a result of this reaction and subsequently behaves as if it had been primarily activated. On this basis, we then write

(24) P. J. Dyne and J. W. Fletcher, *Can. J. Chem.*, **38**, 851 (1960); *ibid.*, **39**, 2381 (1961).

(25) H. W. Melville and J. C. Robb, *Proc. Roy. Soc. (London)*, **A202**, 181 (1950).

(26) E. R. W. Steacie, "Atomic and Free Radical Reactions," 2nd Ed., Vol. II, Reinhold Publishing Corp., New York, N. Y., 1954.

(27) This assumption has been discussed in paper I.



where C and B refer to cycloalkane and aromatic (benzene or arylcycloalkane), respectively, ϵ_C and ϵ_B refer to their electron fractions, I_0 is rate of total energy absorption per unit volume, and δ_C and δ_B refer to the number of activated species C^* and B^* produced on the average per unit of energy absorbed in C and B. Employing the usual steady-state approximation for C^* and B^* , it follows that^{23,30}

$$\eta \equiv \frac{\epsilon_C(G_C - G_B)}{G - G_B} = \frac{1 + \alpha[B]}{1 + \gamma[B]} \quad (1)$$

where G , G_C , and G_B refer to 100-e.v. hydrogen yields from the mixture, pure cycloalkane, and pure aromatic (benzene or arylcycloalkane), $\alpha = k_5/(k_1 + k_2)$,²⁸ and $\gamma = (\delta_C/\delta_B - 1)(G_C - G_B)^{-1}\alpha G_B$.

Benzene as Solute. Empirically, it is found that for all cycloalkane-benzene mixtures at $6M \gtrsim [B] \gtrsim 0.05M$, the experimental quantity η , defined in eq. 1, is adequately represented by the two-parameter equation

$$\eta = A(1 + \alpha[B]) \quad (2)$$

where both A and α are independent of $[B]$. For mixtures of benzene with cyclohexane and bicyclohexyl, eq. 2 is found to have an even wider range of validity extending to the lowest benzene concentrations studied ($[B] \simeq 10^{-4}M$). In Fig. 6, the dependence of η on $[B]$ is presented for cyclohexane-benzene mixtures (dose: 11.8×10^{21} e.v./l.) and bicyclohexyl-benzene mixtures (dose: 14×10^{21} e.v./l.). The line drawn in Fig. 6 with unit intercept, $A = 1$, and ratio of slope to intercept of $\alpha = 0.84$ l./mole adequately represents the results for both liquids.

For mixtures of benzene with either methylcyclohexane or ethylcyclohexane, it is already apparent from the dependence of $G(H_2)$ on benzene concentration (see Fig. 3A, B, and C) that eq. 2 will not adequately describe the results for both high and low benzene concentrations. A considerably more efficient protective mechanism seems to operate at low benzene concentrations. In Fig. 7, η vs. $[B]$ is presented for ethylcyclohexane-benzene (Fig. 7A, dose: 2.3×10^{21} e.v./l.) and methylcyclohexane-benzene (Fig. 7B, dose: 4.6

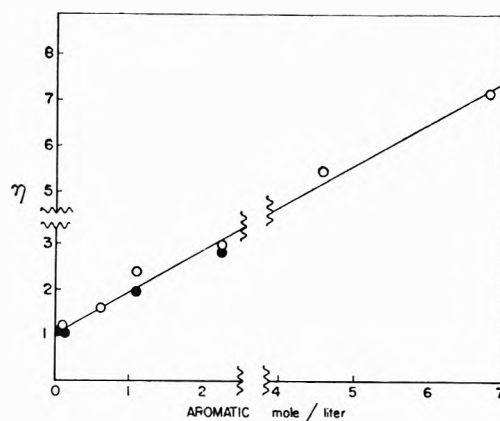


Figure 6. Dependence of η on concentration of benzene: O, cyclohexane-benzene mixtures (dose: 11.8×10^{21} e.v./l.); ●, bicyclohexyl-benzene mixtures (dose: 14×10^{21} e.v./l.).

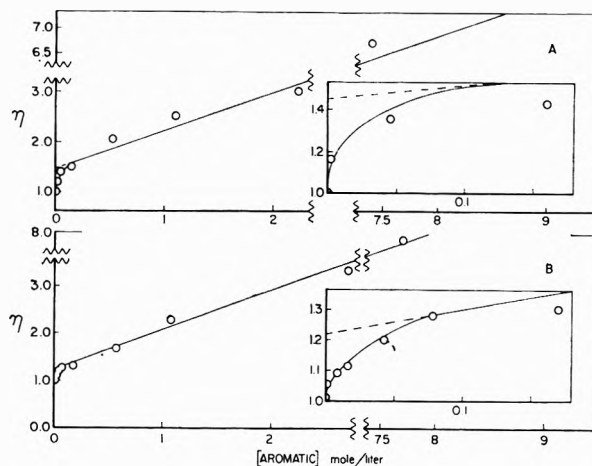


Figure 7. Dependence of η on concentration of aromatic: A, ethylcyclohexane-benzene mixtures (dose: 2.3×10^{21} e.v./l.); B, methylcyclohexane-benzene mixtures (dose: 4.6×10^{21} e.v./l.).

$\times 10^{21}$ e.v./l.). Values of η for both $[B] < 0.2M$ are shown on expanded scales in the two inserts. For $[benzene] \gtrsim 0.05M$, eq. 2 adequately represents the data with parameters $A \simeq 1.2$, $\alpha \simeq 0.7$ l./mole for methylcyclohexane and $A \simeq 1.45$, $\alpha \simeq 0.5$ l./mole for ethylcyclohexane. At higher doses (ethylcyclohexane dose: 26×10^{21} e.v./l., Fig. 8A; methylcyclohexane

(28) k_1 may be a function of aliphatic concentration if, for example, the precursor C^* is an H atom.

(29) If assumption c were dropped and the kinetic sequence suitably modified, eq. 1 would be altered to $(\epsilon_C G_C)/(G - \epsilon_B G_B) = 1 + \alpha[B]$. For the case of benzene as solute, G_B is not sufficiently large to permit adequate distinction between these equations. However, for the arylcycloalkane solutes, the data at high solute concentration are somewhat better represented by eq. 1. Assumption c has therefore been retained for all mixtures.

(30) In paper I, η was defined somewhat differently as $\epsilon_C/(G - G_B)$.

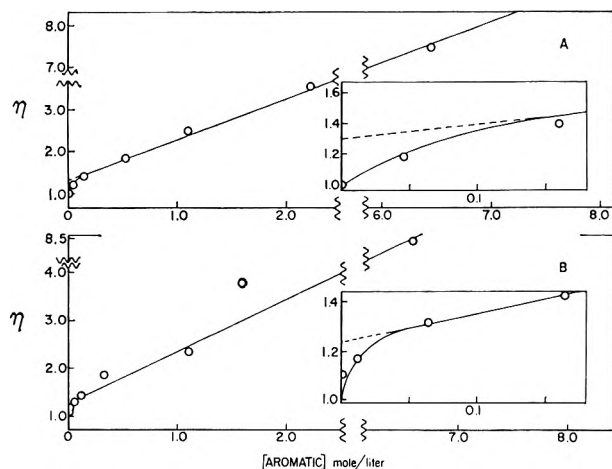


Figure 8. Dependence of η on concentration of aromatic: A, ethylcyclohexane-benzene mixtures (dose: 26×10^{21} e.v./l.); B, methylcyclohexane-benzene mixtures (dose: 11×10^{21} e.v./l.).

dose: 11×10^{21} e.v./l., Fig. 8B) similar results are obtained with $A \simeq 1.2$, $\alpha \simeq 0.9$ l./mole for methylcyclohexane and $A \simeq 1.3$, $\alpha \simeq 0.8$ l./mole for ethylcyclohexane.

Granting the validity of our stated assumptions, the parameter α is interpreted as a measure of the strength of the protective interaction. Since α remains relatively constant for all cycloalkane-benzene mixtures, it is concluded that the same protective mechanism operates in all mixtures at high benzene concentrations.

The deviation from linearity at low concentrations is perhaps most plausibly attributed to failure of our assumption b. It was assumed here that the yield of hydrogen arises exclusively from a single precursor. We now modify this somewhat by permitting the presence of two precursors, C^\dagger and C^* , and associate with each one separately reactions such as 1, 3, and 5. Further, we will assume that precursor C^\dagger is much more sensitive to the presence of benzene than C^* (i.e., $[k_5/k_1 + k_2]^\dagger \gg [k_5/k_1 + k_2]^*$). Thus if one studies effects at high benzene concentrations one measures essentially the reaction of benzene with C^* . In this case, the dependence of G on $[B]$ becomes

$$G = \frac{\epsilon_c G^*}{1 + \alpha^* [B]} \quad (3)$$

where we have set G_B and therefore γ in eq. 1 equal to zero to simplify the further discussion and where G^* is the yield of hydrogen from precursor C^* at $[B] = 0$. G^* is to be determined experimentally by linearly extrapolating a plot of ϵ_c/G vs. $[B]$ from high concentrations to $[B] = 0$.

Alternatively, if one studies effects at low benzene concentrations, ($\epsilon_c \simeq 1$), one measures essentially the reaction of benzene with C^\dagger . In this case, the dependence of G on $[B]$ becomes

$$G = \frac{G^\dagger}{1 + \alpha^\dagger [B]} + G^* \quad (4)$$

where G^\dagger is the yield of hydrogen from precursor C^\dagger . If, indeed, as we assume, there are but two precursors, then G_c should be equal to the sum of G^\dagger and G^* permitting eq. 4 to be transformed to

$$\frac{1}{G_c - G} = \frac{1}{G^\dagger \alpha^\dagger} \left(\frac{1}{[B]} \right) + \frac{1}{G^\dagger} \quad (5)$$

Thus G^\dagger can be determined either as $G_c - G^*$ or, if the precision of the data permits, by linearly extrapolating a plot of $1/(G_c - G)$ vs. $1/[B]$ from low benzene concentrations to $1/[B] = 0$.

In Fig. 6, 7, and 8 our data have been presented essentially according to eq. 3 and thus from the point of view of high concentrations (i.e., benzene reacting with C^*). Values of G^* are obtained from these figures as the ratio of $G_c - G_B$ to the linearly extrapolated intercept (see eq. 1). The following values of G^* result: cyclohexane (11.8×10^{21} e.v./l.), $G^* = 5.6 \pm 0.3$; bicyclohexyl (14×10^{21} e.v./l.), $G^* = 3.5 \pm 0.2$; methylcyclohexane ($4.6, 11 \times 10^{21}$ e.v./l.), $G^* = 4.8 \pm 0.3$; ethylcyclohexane ($2.3, 26 \times 10^{21}$ e.v./l.), $G^* = 3.9, 3.7 \pm 0.3$. Values for the yields of the more sensitive precursor, C^\dagger , are calculated by difference, $G^\dagger = G_c - G^*$: cyclohexane, $G^\dagger = 0.2 \pm 0.4$ ³¹; bicyclohexyl, $G^\dagger = 0.4 \pm 0.3$; methylcyclohexane, $G^\dagger = 1.4 \pm 0.4$ ³²; ethylcyclohexane, $G^\dagger = 2.2, 2.4 \pm 0.4$.

It appears, therefore, from our results that the yield of the "sensitive" precursor C^\dagger is much larger in both methylcyclohexane and ethylcyclohexane than in

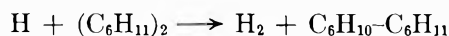
(31) We use for G_c the values at zero dose. This is consistent with our view that C^\dagger is also inhibited by certain radiolytic products.

(32) Freeman,⁶ using an analysis very similar to ours for cyclohexane and benzene mixtures obtains directly $G^* = 3.0 \pm 0.4$ and by difference $G^\dagger = 2.4 \pm 0.4$. The discrepancy is large and considerably outside of random experimental error. However, his reported value for $\alpha = 0.78$ is in good agreement with our value of 0.84. Stone and Dyne⁵ report data for cyclohexane-benzene from $[B] = 0.003$ to $0.3 M$. Their data from 0.06 to $0.3 M$ when treated from the point of view of eq. 3 result in a value for $G^* = 4.6$, and therefore by difference $G^\dagger = 0.95$. In the lower concentration region, ca. 0.003 to $0.02 M$, they treat their data according to eq. 5 and obtain thereby directly $G^\dagger = 0.95$. Our value of $G^\dagger = 0.2 \pm 0.4$ is thus barely within experimental error equivalent to their value and it is likely that there exists a small, but real, difference in our respective results.

(33) Freeman¹⁶ using an analysis similar to ours reports for methylcyclohexane-benzene, $G^\dagger = 3.0 \pm 0.3$. By difference from $G_c = 4.8$ he obtains $G^* = 1.8 \pm 0.3$. It will be noted that his value for G_c is considerably lower than our extrapolated value of 6.2 ± 0.1 . However, we both agree reasonably closely on values for α . He reports 0.58 as compared to our value of 0.7.

either bicyclohexyl or cyclohexane. The low benzene concentration at which this precursor, $C\ddagger$, seems to be completely removed suggests its identification with a thermal H atom and $k_5\ddagger$ with a mechanism involving the scavenging of such atoms by benzene. Since in both cyclohexane and bicyclohexyl $G\ddagger$ is relatively so small, the implication is that for these substances the protective mechanism operating at high benzene concentrations is also predominantly responsible for protection at low concentrations. Stated otherwise, in these solvents, benzene does not appear to scavenge H atoms. Since cyclohexane is not expected to compete with benzene for H atoms more efficiently than methylcyclohexane or ethylcyclohexane, we are inclined to conclude that thermal H atoms are produced, if at all, in very low yield in cyclohexane.

The presence of bicyclohexyl of two tertiary C-H bonds may result in sufficient H atom lability to make the reaction



more competitive with H atom scavenging by benzene than the similar reactions in methylcyclohexane and ethylcyclohexane. Thus, the low value of $G\ddagger$ in this system does not necessarily imply low probability for primary production of thermal H atoms.

Dose dependence of $G(H_2)$ in the cycloalkanes is commonly attributed to some form of interference with H_2 production occasioned by the buildup of unsaturation. On this basis, the increasingly abrupt dose dependence of $G(H_2)$ in the order cyclohexane, methylcyclohexane, and ethylcyclohexane is consistent with the increasing sensitivity of these compounds to low concentrations of benzene and may, therefore, be similarly attributed to increasing yields of $G(H)$. This comparison loses some validity, of course, if G (unsaturation) increases markedly from cyclohexane to ethylcyclohexane. Since the scavenging efficiency is not markedly dependent upon the nature of the unsaturation,²⁵ the measured difference in G (cyclic unsaturation) for cyclohexane and methylcyclohexane of about 1.56 units^{6,15} seems insufficient to explain the observed differences in dose dependence.

Bicyclohexyl clearly is anomalous in this comparison. $G(H_2)$ exhibits a strong dose dependence, but low sensitivity to traces of benzene. However, the explanation for this may again be related to the requirement for an H atom scavenger than can effectively compete with abstraction from bicyclohexyl. Radiolytically produced olefins may be superior to benzene in this respect.³⁴

Arylcycloalkane Solutes. With the exception of $C_6H_{11}C_2H_4-C_6H_5$, all arylcycloalkane solutes studied

satisfy eq. 2 for $[B] \geq 3 M$.³⁵ At higher concentrations, η becomes concave downward as predicted by eq. 1. The apparently greater value of γ for these solutes as compared to benzene is related both to their larger intrinsic hydrogen yields (G_B) and to a somewhat larger value for α .

Results for cyclohexane-phenylcyclohexane mixtures (dose: 11.8×10^{21} e.v./l.) and methylcyclohexane- $C_6H_{11}CH_2C_6H_5$ mixtures (dose: 4.6×10^{21} e.v./l.) have been reported in paper I. For comparison with the other arylcycloalkanes solutes, these results are presented again in Fig. 9A in the form of a plot of η vs.

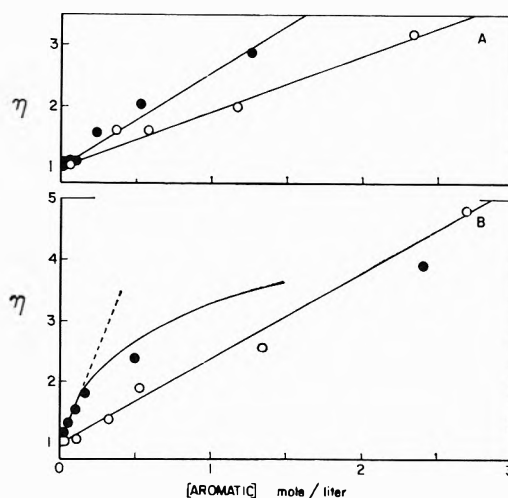


Figure 9. Dependence of η on concentration of aromatic. A: O, cyclohexane- $C_6H_{11}C_6H_5$ mixtures (dose: 11.8×10^{21} e.v./l.); ●, methylcyclohexane- $C_6H_{11}CH_2C_6H_5$ mixtures (dose: 4.6×10^{21} e.v./l.). B: O, methylcyclohexane- $CH_3C_6H_{10}C_6H_5$ mixtures (dose: 11×10^{21} e.v./l.); ●, ethylcyclohexane- $C_6H_{11}C_2H_4C_6H_5$ mixtures (dose: 2.3×10^{21} e.v./l.).

[B]. In Fig. 9B, η vs. [B] is presented for methylcyclohexane- $CH_3C_6H_{10}C_6H_5$ (dose: 11×10^{21} e.v./l.) and ethylcyclohexane- $C_6H_{11}C_2H_4C_6H_5$ (dose: 2.3×10^{21} e.v./l.).

Phenylcyclohexane seems to be equivalent to benzene in its action on cyclohexane. In both cases $A = 1$ and $\alpha \approx 0.9$ l./mole. As discussed in paper I, the cyclohexyl ring apparently neither inhibits nor enhances the "protective" efficiency of the aromatic part of the molecule.

In methylcyclohexane mixtures with either $C_6H_{11}CH_2-C_6H_5$ or $CH_3C_6H_{10}-C_6H_5$ as solutes, $A = 1$ and $\alpha \approx 1.4$ l./mole. Unlike the effect of benzene, these

(34) T. J. Hardwick, *J. Phys. Chem.*, **65**, 101 (1961).

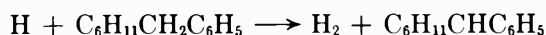
(35) As in the case of benzene as solute, this upper limit is about two-thirds the molar density of the pure liquid.

Table VI: Comparison of Inter- and Intramolecular Effects

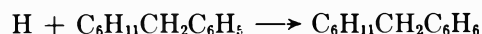
Compound	G_B	ϵ_B	Mixture	G_m
$C_6H_{11}-C_6H_5$	0.26	0.47	$C_6H_{12} + C_6H_6$	0.57 ^a
$C_6H_{11}CH_2-C_6H_5$	0.29	0.43	$C_6H_{11}CH_3 + C_6H_6$	0.70 ^b
$CH_3C_6H_{11}-C_6H_5$	0.29	0.43		
$C_6H_{11}C_2H_4-C_6H_5$	0.37	0.395	$C_6H_{11}C_2H_5 + C_6H_6$	0.82 ^c
$C_6H_{11}-C_6H_4-C_6H_{11}$	0.20	0.30	$\left\{ \begin{array}{l} C_6H_{12} + C_6H_6 \\ (C_6H_{11})_2 + C_6H_6 \end{array} \right.$	$\left. \begin{array}{l} 1.0^a \\ 0.75^d \end{array} \right.$

^a Dose: 11.8×10^{21} e.v./l. ^b Dose: 4.6×10^{21} e.v./l. ^c Dose: 2.3×10^{21} e.v./l. ^d Dose: 14×10^{21} e.v./l.

solutes give no evidence for thermal H atom scavenging at low concentrations. However, this is not unexpected in view of the presence, in these solutes, of hydrogen more labile to radical attack.³⁶ Abstraction reactions such as



if sufficiently competitive with H atom addition to the aromatic ring



would effectively reduce the scavenging probability per solute-H atom encounter. It is suggested that this probability is sufficiently reduced to allow the mechanism responsible for protection at high concentration to dominate at all concentrations.

The behavior of ethylcyclohexane- $C_6H_{11}C_2H_4C_6H_5$ mixtures shown in Fig. 9B seems to present a case intermediate to those already discussed. In the case of ethylcyclohexane or methylcyclohexane-benzene mixtures, we interpret the abrupt change in slope of the η vs. [B] plot as evidence for two mechanisms, H atom scavenging predominating at low concentrations and perhaps some form of energy transfer at the higher concentrations. In cyclohexane-benzene or phenylcyclohexane mixtures it is suggested that no thermal H atoms are involved, and therefore only one protection mechanism obtains, presumably of the same energy transfer type. In ethylcyclohexane- $C_6H_{11}C_2H_4C_6H_5$ mixtures, it is suggested that both protection mechanisms are of approximately comparable importance throughout the measured range of solute concentration. Scavenging of H atoms by $C_6H_{11}C_2H_4-C_6H_5$ is presumably reduced in efficiency again due to the presence of hydrogen with high reactivity to radical attack.

Inter- and Intramolecular Effects. In Table VI, we compare hydrogen yields from an arylcycloalkane with the yields from an equivalent physical mixture of ben-

zene and the related cycloalkane. In column 2 of this table is presented the hydrogen yield, G_B , of the pure arylcycloalkane; in column 3, the electron fraction, ϵ_B , of the aromatic ring (C_6H_6 or C_6H_4) in the compound; in column 4, the equivalent physical mixture; and in column 5 the hydrogen yield, G_m , from the mixture at the aromatic electron fraction listed in column 3. It will be noted that in all cases, the yield from the compound is substantially less than the yield from the equivalent physical mixture. A similar result has been reported in the comparison of radical yields from *n*-octylbenzene and a physical mixture of *n*-octane-benzene.³⁷

The kinetic sequence used to define the parameter α for the intermolecular process may be formally applied to define a similar parameter for the interaction between benzene and the cycloalkane when they are chemically bonded in the arylcycloalkane. However, the ambiguity in assigning a value to [B] in the intramolecular process makes the significance of such an analysis doubtful.⁸

Reference to Fig. 5 shows that addition of benzene to the arylcycloalkane depresses the hydrogen yield only by simple dilution effect. These arylcycloalkanes seem, therefore, to be already maximally self-protected. Addition of another phenyl ring to these compounds is not expected to reduce their hydrogen yields significantly.

Acknowledgment. The authors wish to thank Mr. Eugene Wewerka for help in the syntheses of phenylcyclohexylmethane, 1-methyl-4-phenylcyclohexane, and 1-phenyl-2-cyclohexylethane, and Mr. Adrian Swanson for help with mass spectrometer analyses.

(36) D. H. Hey, B. W. Pengilly, and G. H. Williams, *J. Chem. Soc.*, 1463 (1956).

(37) K. S. Bagdasar'yan, N. S. Izrailevich, and V. A. Krogauz, *Dokl. Akad. Nauk SSSR*, 141, 887 (1961).

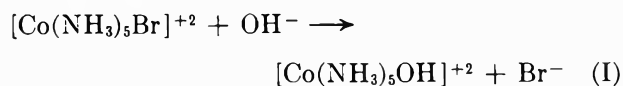
Kinetic Salt Effects in Concentrated Solutions of Supporting Electrolyte. The Reaction between the Bromopentaamminecobalt(III) and Hydroxyl Ions¹

by Berta Perlmutter-Hayman and Yael Weissmann

Department of Physical Chemistry, Hebrew University, Jerusalem, Israel (Received April 25, 1964)

The kinetics of the substitution of Br⁻ by OH⁻ in the bromopentaamminecobalt(III) complex has been investigated spectrophotometrically in the presence of ten different supporting electrolytes, at concentrations up to 2.7 M. The influence of electrolytes having univalent anions can be represented by a classical expression, whereas no quantitative explanation has been found for the influence of SO₄⁻². The connection between the salt effect and the possible existence of a rapid pre-equilibrium is discussed. The classical salt effect in this reaction between two ions of unlike sign is contrasted with the specific ionic effects found in reactions between anions.

The reaction between the bromopentaamminecobalt(III) and hydroxyl ions, *viz.*



was first studied by Brønsted and Livingston.² It was among the first reactions to be adduced as evidence for the classical Debye-Hückel-Brønsted equation for the primary kinetic salt effect.^{3,4} It also figures prominently in the attack of Olson and Simonson⁵ on this classical theory. The reaction was subsequently brought in line with Mayer's equation for activity coefficients^{6,7} by assuming a slight error in the concentration of the hydroxide used by Olson and Simonson. The influence of supporting electrolytes has been discussed in detail by Davies.^{8,9} The reaction has not been investigated at ionic strengths higher than about 0.11. In view of the continued interest in the field of the kinetic salt effect⁹ we thought it worthwhile to extend both the range of concentrations and the variety of electrolytes employed and to examine to what extent the results can be explained theoretically.

Experimental

The supporting salts were all reagent grade. Sodium hydroxide solutions were freshly prepared for each series of experiments by diluting an ~0.1 M stock solution with fresh "triple-distilled" water whose known, low carbon dioxide content allowed the calculation of OH⁻.

Nevertheless, the uncertainty in the OH⁻ concentration, caused by contamination with carbon dioxide, constitutes the chief source of error in our experiments. On the other hand, the concentration of sodium carbonate was always negligible for the purpose of the calculation of the ionic strength.

Bromopentaamminecobalt(III) nitrate was prepared from cobalt(II) nitrate by a procedure analogous to that described for the iodide.¹⁰

In most cases, the reaction was started by mixing

(1) This paper forms part of a thesis to be submitted to the Senate of the Hebrew University by Y. Weissmann in partial fulfillment of the requirements for a Ph.D. degree.

(2) J. N. Brønsted and R. Livingston, *J. Am. Chem. Soc.*, **49**, 435 (1927).

(3) J. N. Brønsted, *Z. physik. Chem.*, **102**, 169 (1922); **115**, 337 (1925); N. Bjerrum, *ibid.*, **108**, 82 (1924); J. A. Christiansen, *ibid.*, **113**, 35 (1924).

(4) R. Livingston, *J. Chem. Educ.*, **7**, 2887 (1930); V. K. La Mer, *Chem. Rev.*, **10**, 179 (1932); E. S. Amis, "Kinetics of Chemical Change in Solution," The Macmillan Co., New York, N. Y., 1949, p. 71 ff.

(5) A. R. Olson and T. R. Simonson, *J. Chem. Phys.*, **17**, 348, 1167, 1322 (1949).

(6) G. Scatchard, "Electrochemical Constants," National Bureau of Standards Circular 524, U. S. Government Printing Office, Washington, D. C., 1953, p. 185.

(7) J. E. Mayer, *J. Chem. Phys.*, **18**, 1426 (1950).

(8) C. W. Davies and I. W. Williams, *Trans. Faraday Soc.*, **54**, 1547 (1958).

(9) C. W. Davies in "Progress in Reaction Kinetics," Vol. I, G. Porter, Ed., Pergamon Press, Inc., New York, N. Y., 1961, p. 161 ff.

(10) F. Basclo and R. K. Murmann, *Inorg. Syn.*, **4**, 171 (1953).

appropriate thermostated solutions of bromopentaamminecobalt nitrate and supporting electrolyte and of sodium hydroxide, to give reactant concentrations of $\sim 4 \times 10^{-5}$ and $\sim 10^{-3}$ *M*, respectively. A sample of the reaction mixture was transferred into a silica spectrophotometric cell thermostated with the aid of "thermospacers." The reaction was followed by measuring, at suitable time intervals, the optical density at 250 *mμ*, using a Beckman DU spectrophotometer.

In the absence of supporting electrolyte, the reaction was too fast for this procedure. The solutions of the reactants were mixed in the spectrophotometric cell itself, which was already in its place in the cell compartment. A syringe which contained the hydroxide solution together with a little air was found to mix the two solutions satisfactorily.¹¹ The progress of the reaction was then followed with the aid of a recorder ("Speedomax," Type G, indicating per cent transmission).

Since the alkali is always in large excess, the reaction is a pseudo-first-order one; its rate constant can be calculated from a plot of $\log(D_t - D_\infty)$ vs. time, where D_t and D_∞ are the optical densities at times t and ∞ , respectively. The spectrum of bromopentaamminecobalt has a peak at 250 *mμ*. We found ϵ_{250} 15.00×10^3 , whereas previous authors report a value which is 10% higher. For the reaction product in alkaline solution, we found $\epsilon_{250} \sim 1.80 \times 10^3$ to be compared with $\sim 2.00 \times 10^3$ found previously.⁴ However, since the reaction is first order, and since D_∞ was determined experimentally for each run, the exact values of the molar absorption coefficients are immaterial for the kinetic results. The temperature was 25°.

Results

The first order with respect to the bromopentaamminecobalt was checked by varying its concentration between 2 and 8×10^{-5} *M*. The rate constant remained uninfluenced.

Five experiments carried out at OH⁻ concentrations varying between 1.0 and 3.2×10^{-3} *M* showed a slight decrease in the rate constant with increasing concentration.

The supporting electrolytes employed, together with the range or their concentrations, are listed in Table I. The results are shown in Fig. 1, where the logarithm of the rate constant is plotted against the square root of the ionic strength, calculated from the stoichiometric concentrations. The results of all the experiments where the supporting anion is univalent, are represented by a single line, curve I. In several cases, experiments carried out with three or more electrolytes at the same concentration coincided to such a degree that

Table I: List of Supporting Electrolytes

Electrolyte	Range of molarity
NaCl	0.027–2.67
KCl	0.007–0.67
NaBr	0.007–0.33
KBr	0.007–1.00
LiBr	0.007–0.27
KF	0.133–0.80
KNO ₃ ^a	0.013–0.13
NaAc	0.007–0.67
BaCl ₂	0.013–0.80
Na ₂ SO ₄	0.003–2.00

^a The concentration of KNO₃ which can be employed is limited by the absorption of NO₃⁻ at 250 *mμ*. According to D. Meyerstein and A. Treimin (*Trans. Faraday Soc.*, **57**, 2104 (1961)), $\epsilon_{250} \approx 8.5$.

they can only be represented by a single point (full circles). Curve II shows the results with sodium sulfate.

Discussion

In order to test the applicability of classical formulas to the reaction in the presence of univalent anions, the logarithm of the rate constant has been plotted against $\sqrt{\mu}/(1 + \sqrt{\mu})$ in Fig. 2. The straight line in this figure has been plotted with the "theoretical" slope of 2.036 and is seen to represent the experimental results very satisfactorily. This means that the expression¹²

$$\log k_0' \equiv \log k - 2z_A z_B A \sqrt{\mu}/(1 + \sqrt{\mu}) \quad (1)$$

(where z_A and z_B are the valencies of the reactants and A the Debye-Hückel limiting slope) is strictly constant. We found (for k in mole⁻¹ l. sec.⁻¹)

$$\log k_0' = 0.996 \pm 0.031 \text{ (std. dev.)}$$

as a mean of 58 experiments, including those in the absence of supporting electrolyte, with no trend with either the concentration or the character of the electrolyte, not even the barium ion (the only bivalent cation which can be employed in the presence of OH⁻) showing any specific effect. The value of k_0' can therefore be identified with k_0 , the rate constant at zero ionic strength.

In other reactions between ions of unlike sign $\log k_0'$

(11) D. Pouli and W. MacF. Smith, *Can. J. Chem.*, **38**, 567 (1960).

(12) E. A. Guggenheim and J. E. Prue, "Physico-Chemical Calculations," North Holland Publishing Co., Amsterdam, 1955, p. 466; A. Indelli, G. Nolan, and E. S. Amis, *J. Am. Chem. Soc.*, **82**, 3233 (1960); A. Indelli, *J. Phys. Chem.*, **65**, 240 (1961); F. Bell, R. Gill, D. Holden, and W. F. K. Wynne-Jones, *J. Phys. Colloid Chem.*, **55**, 874 (1951).

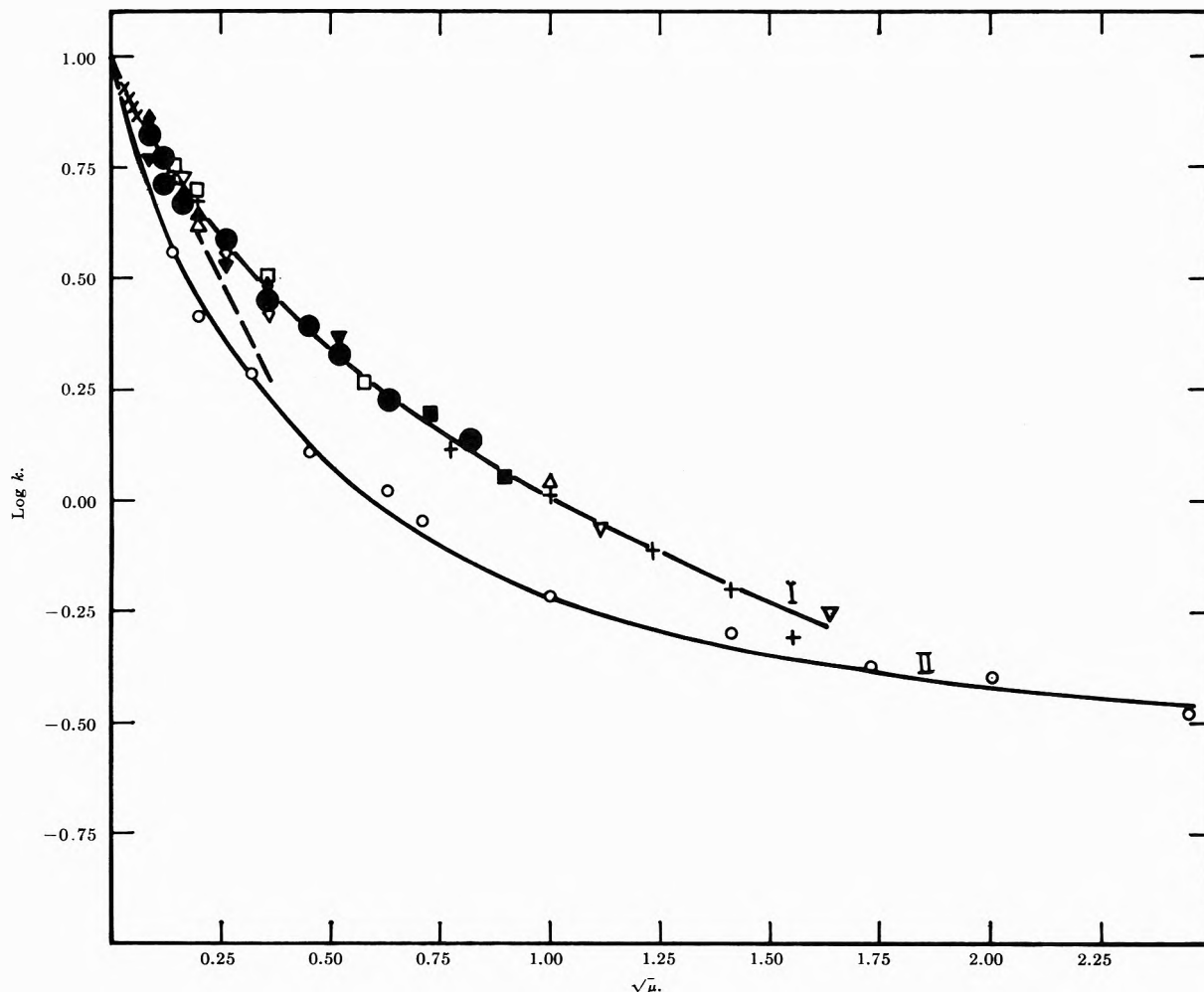


Figure 1. The logarithm of the rate constant as a function of the square root of the ionic strength. Curve I: univalent anions (crosses), no added electrolyte; open inverted triangles, NaCl; filled inverted triangles; KCl; open squares, N₂Br; open triangles, KBr; filled diamonds, LiBr; filled squares, KF; filled triangles, KNO₃; diamonds, CH₃COONa; plus signs, BaCl₂; filled circles, three different electrolytes coinciding (except at $\sqrt{\mu} = 0.26$ and 0.52 when they represent four, and at $\sqrt{\mu} = 0.37$, five). Curve II: Na₂SO₄. Dashed line: Debye-Hückel limiting slope.

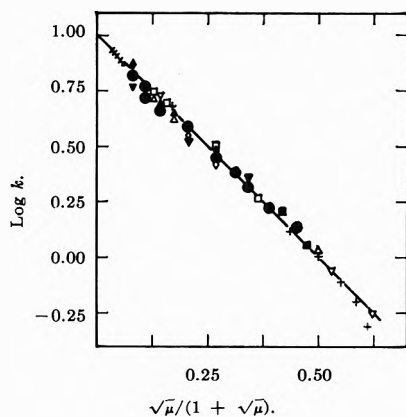


Figure 2. The logarithm of the rate constant vs. $\sqrt{\mu}/(1 + \sqrt{\mu})$ for univalent electrolytes. (Meaning of points as in Fig. 1.)

as defined by eq. 1 has been found to vary linearly with the ionic strength with a small positive or negative slope.^{12,13} Our case where the slope is zero is therefore in line with previous results.

(13) We recalculated the results obtained for two reactions which are very similar to ours, namely the substitution of Ni^{2+} and NO_2^- by OH^- in the analogous pentaamminecobalt ions. (G. C. Lalor and E. A. Moelwyn-Hughes, *J. Chem. Soc.*, 156) (1963); G. C. Lalor and J. Lang, *ibid.*, 5620 (1963).) We found that the extremely good fit obtained by the authors' using the formula

$$\log k = \log k_0 - 2z_A z_B A' \sqrt{\mu} + b' \mu$$

(where A' and b' are parameters, A' being almost identical with the limiting Debye-Hückel slope) is practically equalled by the fit we could obtain with

$$\log k = \log k_0 - 2z_A z_B A \sqrt{\mu}/(1 + \sqrt{\mu}) - b \mu$$

where b is a free parameter which may be positive or negative. These experimental results refer to very low ionic strengths, in the absence of supporting electrolytes.

When the equation suggested by Davies¹⁴ for the activity coefficients of nonassociating electrolytes is combined with the Brønsted kinetic equation, the expression

$$\log k = \log k_0 + 2z_A z_B A [\sqrt{\mu}/(1 + \sqrt{\mu}) - 0.20\mu] \quad (2)$$

is obtained. For reactions between ions of unlike sign $\log k_0'$ as defined by eq. 1 should thus increase linearly with increasing μ , with a slope equal to $0.2036|z_A z_B|$. According to Davies, a slope smaller than this, or negative, shows that ion-pair formation takes place.⁸⁻¹⁰ This leads to the somewhat improbable conclusion that *all* the monovalent anions employed by us should associate to the same extent with the bivalent bromopentaamminecobalt ion. It might be preferable to consider the linear relationship between $\log k_0'$ and the ionic strength as a semiempirical one.

We also recalculated the results of Olson and Simonson in the presence of low concentrations of bromide⁵ and found that again $\log k_0'$ shows much less trend with concentration than does $\log k_0$ as calculated from eq. 2.

While the principle of ionic strength is thus strictly adhered to as long as we consider only univalent anions, the situation is different with respect to the divalent sulfate ion. For any given ionic strength, its retarding influence is much more pronounced than that of the univalent ions (see Fig. 1). (This becomes even more apparent when we take the formation of NaSO_4^- into account which makes the true ionic strength considerably lower than that calculated from the stoichiometric concentration.)

Davies^{8,9} has quantitatively explained the strong specific influence of sodium sulfate at low concentrations⁵ by assuming the existence of two parallel reaction paths, one of them involving an ion pair formed from the divalent bromopentaamminecobalt and sulfate ions, and the other, the unassociated reactant. The ion pair, being electrically neutral, has the lower rate constant, whereas its relative concentration increases with increasing sulfate concentration, hence the strong decrease in the observed rate constant.

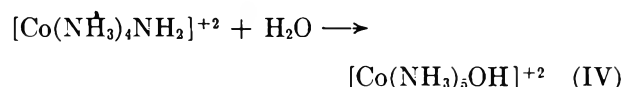
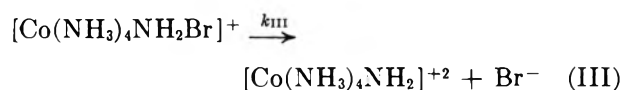
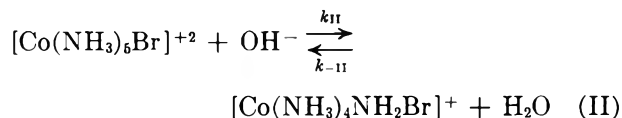
We have not been able to explain our results on this basis. No reasonable assumption about the rate and equilibrium constants and about their dependence on ionic strength enabled us to explain the steepness of the decrease of the observed rate constant with increasing sulfate concentration.

It seems to us an oversimplification to assume two independent reaction paths involving two sharply defined entities: an ion pair which behaves like an uncharged particle, on the one hand, and a completely "free" ion, on the other. Instead, a continuous series of reaction paths, involving the divalent anion to a

lesser or higher degree, might be nearer the truth.¹⁵ In any case it is hardly surprising that the simple assumption of *two* reaction paths should break down under our conditions where the calculated contribution of the ion pair to the observed rate should actually predominate over that of the unassociated reactant. Indeed, Davies himself⁹ commented upon the discrepancy between calculated and observed rate constants at his highest sulfate concentration, *viz.*, 0.03 *M*.

It would be interesting to investigate the influence of other bivalent anions. Unfortunately, no suitable such ions seem to be available. The HPO_4^{-2} ion, for instance, acts as a buffer and decreases the concentration of hydroxyl ions strongly, and in a way which, in the absence of data on activity coefficients in concentrated phosphate solutions, cannot be calculated with sufficient accuracy. Similarly, the chromate ion *increases* the hydroxyl ion concentration.

According to Basolo and Pearson,¹⁶ reaction I proceeds in the steps



with reaction III rate determining. The observed rate constant is thus a composite quantity, *viz.*, $k_{II}k_{III}/k_{-II}$. The values of k_{II} and k_{-II} should be affected only slightly, and both to a similar extent, by the ionic strength. The influence of the ionic strength is thus thrown chiefly onto k_{III} ; what we investigate, therefore, would be the *salt effect on the first, bimolecular step although this is not the rate-determining one*. Alternatively, neglecting the salt effect on k_{III} , it may be argued that we are not dealing here with a primary salt effect at all, but with a *secondary* one; the concentration of a participant in the rate-determining step is changed because of the influence of ionic strength on the rapid pre-equilibrium II.

The question then arises whether there should be any fundamental difference between the effect of ionic

(14) C. W. Davies, "Ion Association," Butterworths Scientific Publications Ltd., London, 1962, p. 39.

(15) B. Perlmutter-Hayman and G. Stein, *J. Phys. Chem.*, **63**, 734 (1959).

(16) F. Basolo and R. G. Pearson, "Mechanisms of Inorganic Reactions," John Wiley and Sons, Inc., New York, N. Y., 1958, p. 129.

strength on an equilibrium constant and on a rate constant. Complete analogy seems to have been taken for granted by Olson and Simonson,⁵ whereas the possibility of a difference in behavior has been mentioned recently.¹⁷

On the basis of absolute reaction-rate theory, the rate constant is proportional to K^* , the "equilibrium constant" between the reactants and the activated complex. When the Debye-Hückel-Brønsted equation is derived from that theory^{18a} the only property of the activated complex which is taken into account is the charge type, and there should, therefore, be no difference between the environmental effects on K^* and on an ordinary chemical equilibrium constant. This may be expected to constitute a good approximation in most cases.¹⁹

Equilibrium constants might be influenced differently from rate constants for yet another reason, namely, the inapplicability of absolute reaction rate theory, which, strictly speaking, holds only under equilibrium conditions. It is, however, generally assumed^{18b} that even in a unidirectional reaction—provided it is not too fast—the concentration of the activated complexes moving to the right is practically equal to that corresponding to equilibrium with the reactants at the given concentration. It has been argued that absolute reaction-rate theory might be especially liable to break down for reactions between ions in solution because it has to be assumed that the activated complex has its equilibrium ionic atmosphere in spite of its short lifetime.^{18a} This argument is, however, somewhat weakened when we remember that the so-called ionic atmosphere, in fact, constitutes an *average*, and ions do not have at every moment the ionic atmosphere which corresponds *exactly* to their charge type. The activated complex will be preferentially formed from those reactants whose ionic atmospheres favor its formation. On the other hand, somewhat more energetic reactants may be able to form an activated complex whose ionic atmosphere deviates considerably from the average.

We thus come to the conclusion that the effect of ionic strength on the observed rate constant should be essentially the same, no matter whether the reaction takes place in a single bimolecular step^{5,13} (reaction I) or whether it proceeds *via* a rapid pre-equilibrium as proposed by Basolo and Pearson¹⁶ (reactions II and III). This conclusion is not affected by the fact that the

equilibrium reaction II is probably diffusion-controlled. Although absolute reaction rate theory cannot be applied to such reactions and diffusion-controlled reactions between ions have been shown to be influenced by ionic strength differently from ordinary reactions,²⁰ the position of the equilibrium is necessarily independent of the mechanism by which it is reached.

We are, therefore, inclined to attribute the nature of the ionic effect on our reaction to its charge type, and not to its mechanism. As we have already pointed out,²¹ there seems to be a fundamental difference between reactions involving ions of *like* sign, where the ion of sign opposite to that of the reactants exerts a marked specific effect,^{21,22} and reactions involving ions of *unlike* sign, where the salt effect can essentially be expressed in terms of ionic strength. It is only in the presence of a bivalent *anion* that the principle of ionic strength breaks down in our reaction between a bivalent cation and a monovalent anion, a feature which is somewhat analogous to the effect of polyvalent anions on the solubility of salts having polyvalent cations.²³

Whereas a *quantitative* treatment of the specific effects would be very difficult at the present stage, the behavior of both types of reactions can be understood *qualitatively* on the basis of the principle of the "specific interaction of ions of unlike sign."²⁴

Acknowledgment. We are indebted to Dr. H. J. G. Hayman for helpful discussion.

(17) A. Indelli and G. Sglietto, *Trans. Faraday Soc.*, **58**, 1033 (1962).

(18) (a) See, e.g., A. A. Frost and R. G. Pearson, "Kinetics and Mechanism," 2nd Ed., John Wiley and Sons, Inc., New York, N. Y., 1961, pp. 150, 151; (b) *ibid.*, pp. 89, 90.

(19) However, strictly speaking, K^* is not an ordinary equilibrium constant, but rather the equilibrium constant between the reactants and a hypothetical "stiff" complex whose vibrational partition function along the reaction coordinate is unity. (See, e.g., H. J. G. Hayman, *Bull. Res. Council Israel*, **A10**, 120 (1961).) Thus, owing to the *absence* of one vibrational partition function in K^* which is present in the ordinary equilibrium constant, this approximation might lead to erroneous conclusions when the reaction can take place *via* more than one reaction path.

(20) P. Debye, *Trans. Electrochem. Soc.*, **82**, 265 (1942); J. Q. Umberger and V. K. La Mer, *J. Am. Chem. Soc.*, **67**, 1099 (1945).

(21) B. Perlmutter-Hayman and G. Stein, *J. Chem. Phys.*, **40**, 848 (1964).

(22) V. K. La Mer and R. W. Fessenden, *J. Am. Chem. Soc.*, **54**, 2351 (1932).

(23) J. N. Brønsted and A. Petersen, *ibid.*, **43**, 2235 (1921); V. K. La Mer and C. F. Mason, *ibid.*, **49**, 410 (1927); V. K. La Mer and R. G. Cook, *ibid.*, **51**, 2622 (1929); V. K. La Mer and F. H. Goldman, *ibid.*, **51**, 2632 (1929).

(24) J. N. Brønsted, *ibid.*, **44**, 877 (1922).

Relative Cation Mobilities in Potassium Chloride-Lithium Chloride Melts^{1a,b}

by Cornelius T. Moynihan and Richard W. Laity

Frick Chemical Laboratory, Princeton University, Princeton, New Jersey (Received May 13, 1964)

Hittorf-type transference experiments have been used to determine the relative mobilities of Li^+ and K^+ , taking Cl^- as reference, over a wide composition range of the KCl-LiCl system at 640° . Combining these with conductivity data yields equivalent conductance isotherms for each cation that show monotonously decreasing behavior with increasing concentration of K^+ . The Li^+ mobility decreases much more rapidly, crossing that of K^+ at 20 mole % KCl and eventually reaching 0.2 of its value in pure LiCl . Comparison with other systems indicates that similar behavior may be rather general and is consistent with a model previously proposed to explain thermodynamic observations. The model is based on the relative abilities of different-sized cations to polarize large anions. The observed effect of temperature on ionic mobilities is predicted by the model, as is the behavior of viscosity in KCl-LiCl melts.

It is well known that conductivity isotherms in binary fused salt mixtures usually exhibit negative deviations from the "ideal" behavior defined by connecting the equivalent conductances of the pure salts with a straight line. The work of Van Artsdalen and Yaffe² showed that in alkali halide systems, which should be the most ionic of all melts, such deviations are greatest when the conductivities of the pure salts differ by the greatest amount. Thus, in KCl-LiCl where the latter salt has almost twice the conductivity of the former, the effect is so large that the isotherm actually passes through a minimum at about 80 mole % KCl . Van Artsdalen and Yaffe's results on this system have subsequently been confirmed in this laboratory³ and elsewhere.⁴ The present study of relative cation mobilities in KCl-LiCl melts was initiated in the hope that a better understanding of this curve would be provided by resolving it into ionic components.

Preliminary results of this investigation, as well as a review of some previous measurements on systems of this type reported in the literature, were described in an earlier report.⁵ Results up to that point had been consistent with a rather remarkable generalization: the mobilities of like-charged ions in binary fused salt mixtures were found to be equal (within about 15%) at all concentrations. It will be seen in the present communication that this "rule" no longer

applies to KCl-LiCl when the experiments are extended beyond 50 mole % KCl and a correction is made in one of our earlier results. Instead, it must be replaced by a less restrictive generalization, whose implications are nonetheless significant and will be discussed herein. Some results showing the effect of temperature will also be included. We begin, however, with a fuller explanation of the method used in the experiments.

Hittorf Method in Fused Salts. The procedure employed in this investigation resembles the Hittorf method for determining transference numbers in electrolytic solutions, providing a measure of mobilities of ionic species relative to components of the electrolyte. It should not be confused with experiments in which a porous disk or other external reference is used to define the transference numbers.⁶ In our experiments a binary fused salt mixture initially having uniform composition throughout the cell is electrolyzed

(1) (a) Part of a paper presented at the Symposium on Electrolytic Solutions and Fused Salts, 145th National Meeting of the American Chemical Society, New York, N. Y., September, 1963; (b) this work is supported through a contract with the U. S. Atomic Energy Commission. Financial assistance from an NSF predoctoral fellowship is also gratefully acknowledged.

(2) E. R. Van Artsdalen and I. S. Yaffe, *J. Phys. Chem.*, **59**, 118 (1955).

(3) E. D. Wolf, S. Petrucci, and R. W. Laity, to be published.

(4) F. R. Duke and C. L. Bissell, *J. Electrochem. Soc.*, **3**, 717 (1964).

(5) R. W. Laity and C. T. Moynihan, *J. Phys. Chem.*, **67**, 723 (1963).

with a measured number of coulombs, giving rise to concentration changes in the vicinity of the electrodes. If some means is taken to confine the entire region of concentration change around each electrode so as to prevent mixing with the bulk of the melt, the relative difference in mobilities of the two like-charged ions may be calculated from analysis of either isolated region. In our case the melt about the electrode was confined in a glass tube, the end of which was closed by a porous glass disk. It is assumed that the pores of the disk are sufficiently large so that the properties of the melt that relate to relative cation mobilities remain unchanged from those in the bulk of the melt. The porous disk serves merely as a barrier to convective mixing.

Results of such experiments in $\text{AgNO}_3\text{-NaNO}_3$ mixtures were reported by Aziz and Wetmore⁷ in terms of a "transport function" ϕ defined by the relation

$$\phi = 1 - t_1 - E_1 t_3$$

where E_1 is the equivalent fraction of cation 1 in the bulk of the melt, and the two t 's are cationic and anionic transference numbers, respectively. The actual values of these transference numbers are arbitrary, so long as both refer to a common reference frame.⁶ Thus, if the anion itself is chosen for reference, *i.e.*, if its mobility is taken equal to zero, it is seen that ϕ is equal to the transference number of cation 2. In this paper we will designate the ϕ of Aziz and Wetmore by ϕ_2 , and define a corresponding transport function ϕ_1 by

$$\phi_1 = t_1 + E_1 t_3$$

With electrodes reversible to the anion, as was the case in the present work, the latter is related to experimental quantities as

$$\phi_1 = E_1 - n_3(E_1' - E_1)/z \quad (1)$$

where E_1' is the final equivalent fraction of cation 1 in a quantity of anolyte containing n_3 equivalents of the anion, and z is the number of faradays passed.

There is as yet no unambiguous way of assigning unique electrical mobilities to each ionic species. Choosing the anion as reference, however, provides a useful basis for comparison of the two cations. The conductances of ions 1 and 2 relative to 3 are given by

$$\lambda_{13} = \phi_1 \Lambda / E_1; \quad \lambda_{23} = \phi_2 \Lambda / E_2 \quad (2)$$

where Λ is the equivalent conductance of the mixture whose composition is specified by $E_1 (= 1 - E_2)$. Thus, the value of Λ is related to the two cation conductances by

$$\Lambda = E_1 \lambda_{13} + E_2 \lambda_{23} \quad (3)$$

and becomes identical with the pure salt conductances at the extremes of the isotherm. Although the individual conductances are more informative than the value of ϕ alone, a knowledge of Λ is required to evaluate them. A useful alternative when the latter is lacking is the *per cent mobility difference* Q defined by

$$Q = 100(\lambda_{13} - \lambda_{23})/\lambda_{23}$$

It can be evaluated from the results of a Hittorf experiment using the following relation

$$Q = 100(\phi_1 - E_1)/\phi_2 E_1 \quad (4)$$

Both Q and the individual cation conductances, λ_{13} and λ_{23} , will be used to express results of the present work.

Experimental

Materials. Baker and Adamson reagent grade KCl and LiCl were used in all experiments. The mixtures were dried under vacuum in a furnace which had been heated slowly to a temperature of 300° and maintained at this temperature for a period of 1 to 2 days. They were subsequently kept under an atmosphere of dry nitrogen.

Chlorine gas from a cylinder (Matheson) was dried over magnesium perchlorate before being passed into the cell.

Apparatus. The transference cell is shown in Fig. 1. The electrolysis vessel was made of Vycor glass joined by a graded seal to a Pyrex O-ring connector at the top. All other glassware was Pyrex for experiments done below 600° and Vycor for those above 600°. Except for one determination in which a coarse porosity was used to determine the possible effect of pore size, the fritted disks were 10-mm. fine porosity Pyrex or Vycor. The latter disks were prepared by alternately passing tetraethyl orthosilicate and concentrated hydrochloric acid through a medium porosity disk until the disk was stopped up, and then baking for several hours at 700°. The amount of time needed to pass 5 ml. of water through the disk under water aspirator suction was used as a porosity criterion; the pores were considered fine enough to prevent significant flow losses during the experiment when this time was greater than 100 sec.

The cathode was a 25-cm. long 0.635-cm. o.d. hollow graphite tube with a porous graphite plug at one end.⁸

(6) For a discussion of this distinction see the article "Fused Salt Transport Numbers" in "The Encyclopedia of Electrochemistry," C. A. Hampel, Ed., Reinhold Publishing Corp., New York, N. Y., 1964, pp. 653-659.

(7) P. M. Aziz and F. E. W. Wetmore, *Can. J. Chem.*, **30**, 779 (1952).

(8) Such tubes were obtained from Union Carbide Research Laboratories at Parma, Ohio, through the courtesy of S. Senderoff.

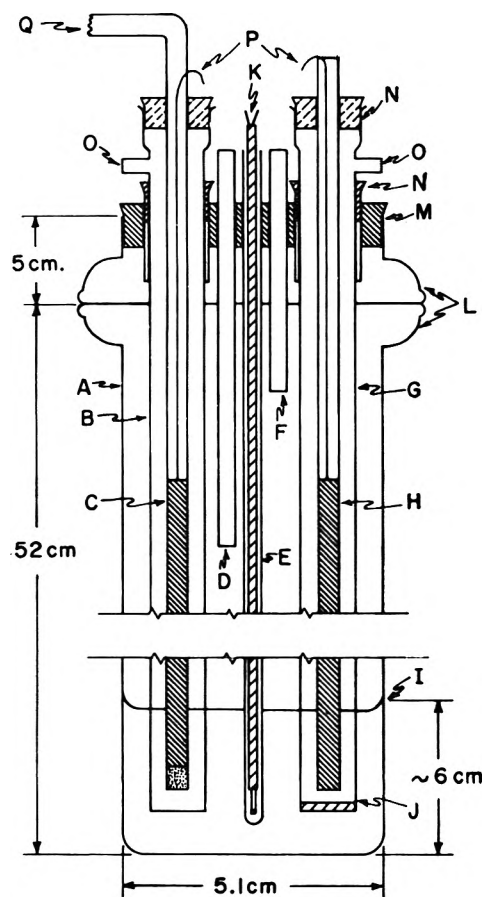


Figure 1. Electrolysis cell: A, main electrolysis vessel; B, 13-mm. o.d. cathode sheath; C, cathode; D, N_2 inlet; E, thermocouple sheath; F, N_2 outlet; G, 13-mm. o.d. anode compartment; H, anode; I, melt level; J, fritted disk; K, chromel-alumel thermocouple; L, O-ring connectors; M, no. 10.5 rubber stopper; N, no. 1 silicone rubber stoppers; O, Cl_2 outlet; P, Pt-lead wires; Q, Cl_2 inlet.

The anode was a 25-cm. long 0.635-cm. o.d. graphite rod. These electrodes were cemented into the ends of 9-mm. glass tubing with Sauereisen cement. A tube furnace containing a heavy-walled nickel tube inside the alundum core to help minimize thermal gradients was used to maintain constant temperature during the runs. Temperature control was effected by a thyatron controller incorporated in the external circuit of the furnace. Although the arrangement has been found in this laboratory to be capable of maintaining temperatures constant within $\pm 0.1^\circ$, the variations were nearer to $\pm 1^\circ$ in these experiments. Heating caused by the electrolysis current, which was not rapidly compensated by the controller due to the large thermal lag of the system, was the source of these fluctuations. Temperature was measured by a Vycor-sheathed chromel-alumel thermo-

couple dipping into the melt and connected to a Leeds and Northrup No. 8657-C thermocouple potentiometer.

Procedure. After the salt mixture to be studied had been melted and brought to the desired temperature under a nitrogen atmosphere, a sample was pipetted out and dissolved in water for determination of the initial composition. The anode compartment was inserted and allowed to fill by leakage of the melt through the porous disk. The cathode sheath and electrodes, which had been heated to red heat in a Bunsen burner flame, were also inserted. Chlorine gas was passed through the cathode at a rate of about 10 ml./min., and electrolysis was started. The time of electrolysis was between 1 and 2 hr. and was accurately measured. Current was held constant during this period at a value between 300 and 360 ma. by placing large resistors in series with the cell and using a 110-v. d.c. source.

Upon completion of electrolysis the anode compartment was removed and the salt contained therein allowed to freeze. This salt was then dissolved in water. The resulting solution, as well as that containing the sample of the original composition, was analyzed for chloride and potassium ion content. The chloride analysis consisted of titration with silver nitrate solution to a silver chromate end point. Potassium was determined gravimetrically as potassium tetraphenylboron.⁹ In concentration regions where appreciable cation mobility difference could be detected, the composition of the anode compartment after electrolysis was found to have changed by as much as 1 to 2 mole % from the original melt composition.

Some corrosion of the glass, whether Vycor or Pyrex, was generally observed, especially at high LiCl concentrations. At temperatures above 600° the graphite cathode was also attacked and partially fell to pieces during the electrolysis. A possible explanation is that some alkali metal deposited in spite of the excess chlorine being bubbled through the melt. After every run, the solutions to be analyzed were first tested for basicity with phenolphthalein as a possible indication of hydrolysis; in no case did this test show a detectable amount of base.

Results and Discussion

The results of all our transference measurements on the molten KCl-LiCl system are summarized in Table I. The quantities ϕ_K and Q were calculated from eq. 1 and 4, taking $1 = K^+$, $2 =$

(9) H. Flaschka and A. J. Barnard, Jr., in "Advances in Analytical Chemistry and Instrumentation," Vol. I, C. N. Reilly, Ed., Interscience Publishers, Inc., New York, N. Y., 1960, p. 1.

Li⁺, and 3 = Cl⁻. The ranges of accuracy indicated are based on the assumption that the limiting error is the uncertainty in the analytical determinations, indicated by the precision obtained with several samples. It is apparent that at high Li⁺ concentrations the lithium ion is more mobile; at high K⁺ concentrations the potassium ion is more mobile. The mobility cross-over point occurs around 80 mole % Li⁺ at 640°. This can be compared with the corresponding cross-over points observed in LiBr-KBr melts (70 mole % Li⁺ at 450°) and LiBr-NaBr melts (75 mole % Li⁺ at 540°).¹⁰ The only transference datum previously available for the KCl-LiCl system was a single measurement reported by Klemm and his co-workers.¹¹ Their result at 630° was $Q = -13$ at $E_1 = 0.0224$, in fair agreement with our figures. These workers used finely powdered glass to separate their electrode compartments, which indicates the results were not strongly influenced by the nature of the separator.

Table I: Transport Data for Molten KCl-LiCl Mixtures

Run	Temp., °C.	E_K	ϕ_K	Q
1	640	0.0323	0.0270 ± 0.0003	-17 ± 1
2	636	0.201	0.200 ± 0.002	0 ± 1
3	624	0.203	0.203 ± 0.006	0 ± 3
4	639	0.204	0.202 ± 0.005	-1 ± 2
5	638	0.302	0.318 ± 0.008	8 ± 3
6	708	0.309	0.326 ± 0.007	8 ± 3
7	509	0.311	0.307 ± 0.009	-2 ± 4
8	504	0.313	0.311 ± 0.011	-1 ± 5
9	438	0.410	0.434 ± 0.004	10 ± 2
10	640	0.496	0.528 ± 0.004	14 ± 2
11	731	0.646	0.699 ± 0.010	27 ± 4
12	645	0.656	0.717 ± 0.010	33 ± 5
13	642	0.662	0.731 ± 0.009	39 ± 4
14	713	0.795	0.862 ± 0.015	61 ± 11

Further evidence that these results were not affected by possible ionic interaction with the walls inside the porous disk is provided by comparing the results of runs 12 and 13. A coarse porosity disk was used in the former, a very fine porosity disk in the latter. The compositions were almost the same, and the agreement of Q values is within experimental error (but indicative that there may have been a slight leakage through the coarse disk).

While Q is clearly a function of composition, its value at a particular concentration is only weakly dependent on temperature. Runs 5 and 6 show that this is especially true when the mobility difference is small, although a gradual shift in the cross-over point

with changing temperature is indicated by comparing runs 2 through 5 with runs 7 through 9. Even though the somewhat larger variation of Q observed in runs 11 and 13 appears to be outside the range of error, the temperature dependence is in general small enough that we can use all of the data taken between 636 and 642° to construct a "640° isotherm." This isotherm is shown in Fig. 2, where the point at $E_K = 0.795$ (run 14) has been added for good measure, despite the higher temperature at which this measurement was made.

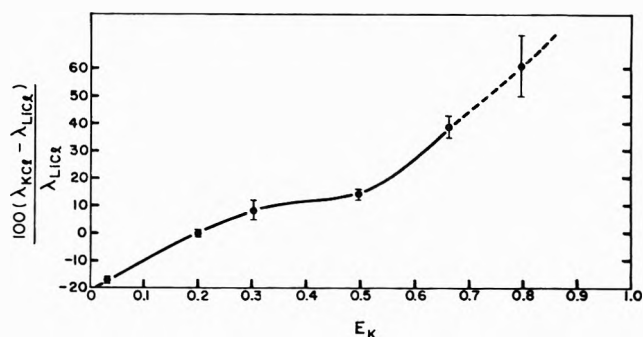


Figure 2. Per cent difference in mobilities of K⁺ and Li⁺ ions in KCl-LiCl melts at 640°.

The dashed line indicates that this part of the curve is actually below the melting point, the data referring to a hypothetical supercooled liquid mixture. The flat portion of this curve at $E_K = 0.5$ and below was the basis for the conclusion in our earlier communication.⁵ At that time it appeared even flatter due to replacement of the point shown at the lowest concentration by an earlier value not included in Fig. 2 due to the much larger experimental uncertainty of that run.

Figure 3 shows isotherms of equivalent conductance for each of the two cations at 640°, again taking the chloride ion as reference. The points were calculated by eq. 2 from the transference results shown in Fig. 2 and the conductance data of Van Artsdalen and Yaffe.² Beyond $E_K = 0.7$ the latter data were extrapolated to the hypothetical liquid at 640°. Although this represents a rather lengthy extrapolation for pure KCl, the shapes of these curves apparently are not very sensitive to temperature. This is indicated by combining the transference results of runs 6 and 14 with conductance data for both mixtures and the pure salts at 710°. The extrapolation required for KCl is now very much shorter, but the shapes of the "710° isotherms" are remarkably similar to those in Fig. 3.

(10) J. Perie, M. Chemla, and M. Gignoux, *Bull. soc. chim. France*, 1249 (1961).

(11) A. Klemm, H. Hintenberger, and P. Hoernes, *Z. Naturforsch.*, 2a, 245 (1947).

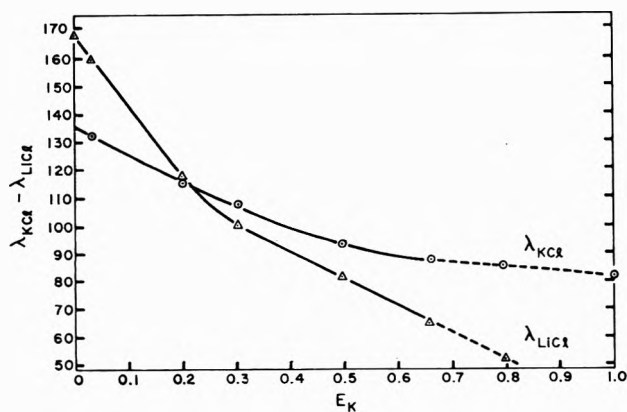


Figure 3. Relative conductances of K^+ and Li^+ ions in KCl-LiCl melts at 640° .

Several features of these curves are worth noting. First, the mobilities of *both* cations monotonously change in the same direction as the conductivity of the melt varies from its value in one pure salt to that in the other. This seems to be a less restrictive version of our earlier generalization that the mobilities of both like-charged ions are equal at all concentrations.⁵ In the present form it covers all of the examples cited in that communication, as well as the exceptions subsequently noted by Berlin and co-workers.¹² At first sight the steady decrease in the mobilities of both Li^+ and K^+ relative to Cl^- may appear inconsistent with the existence of a minimum in the isotherm of equivalent conductance Λ for the melt as a whole. Equation 3 shows that there is no inconsistency when the effect of concentration is taken into account. In other words, the lithium ion is such a poor conductor in nearly pure KCl that the primary effect of adding LiCl to the melt is simply to dilute it, thereby lowering its total conductance.

We note further that changing the composition has a much greater effect on the mobility of Li^+ than on that of K^+ . Such behavior may also turn out to be rather general in mixtures of this type. When the concentration effect is large enough, it leads to the mobility cross-over shown in Fig. 3 and cited above for two other alkali halide systems. In addition to these examples, an extensive series of mobility results for binary mixtures of alkali metal nitrates recently reported by Honig¹³ and a determination of the temperature dependence of ion mobilities in KNO_3 - $NaNO_3$ by Lantelme and Chemla¹⁴ revealed a crossing over of cation mobilities in every one of ten systems for which data were reported, although the latter workers found no cross-over at the lowest of their temperatures. In the present work the change in conductance with concentration of the lithium ion is so rapid at low

concentrations of KCl that it would fall to zero by about 70 mole % KCl if the trend were continued. A rough extrapolation of the actual curve for the lithium ion in Fig. 3 indicates that at infinite dilution in (hypothetical) pure liquid KCl the conductance of lithium ion is only about 0.2 its value in pure LiCl at the same temperature. It should further be noted that if any part of these conductances is assigned to the chloride ion, the lithium ion conductance must be even smaller and its per cent change with concentration even greater.

The change of ion mobility with composition in alkali halide systems has been discussed by Chemla and co-workers^{10,14} in terms of complex ion formation. Although this viewpoint seems rather extreme for simple ionic melts, we feel that the generality of the type of behavior observed here can be understood in terms of a relatively simple model involving a kind of cation-anion association. The essential features of this model are contained in the more detailed version proposed by Lumsden to explain the observed heats of mixing in binary alkali halide systems.¹⁵ Lumsden stated that when all the cations are the same, the environment of the anion is on the average symmetrical. When cations of unequal size are mixed, however, some of the anions (considering for the moment a colinear group like $Li^+Cl^-K^+$) find themselves between electric fields of differing intensities. In such circumstances the electron cloud of a large anion like Cl^- tends to become polarized in the direction of the smaller of the two cations. Lumsden pointed out that this effect gives a net stability to the mixture which is consistent with the exothermic nature of the mixing process. This simple model was found to give remarkably quantitative correlation of experimental data with calculations based solely on ionic size and anion polarizability parameters.

It is difficult to apply the Lumsden model quantitatively to any transport process. Qualitatively, however, it is apparent that a strengthening of the attractive force between a cation and an anion should lower the mobility of the former relative to the latter. The addition of a single potassium ion to pure LiCl can affect a substantial number of lithium ions in this way,

(12) A. Berlin, F. Mén's, S. Forcheri, and C. Monfrini, *J. Phys. Chem.*, **67**, 2505 (1963). This communication erroneously criticizes the use of liquid junction potentials to draw conclusions about relative ion mobilities. The objection apparently is based on the false assumption that ion mobilities must be assumed constant over a very large range of concentration in order to interpret such data. Cf. the explanation by K. H. Stern, *ibid.*, **63**, 741 (1959).

(13) J. A. A. Ketelaar and E. P. Honig, *ibid.*, **68**, 1596 (1964).

(14) F. Lantelme and M. Chemla, *Bull. soc. chim. France*, 2200 (1963).

(15) J. Lumsden, *Discussions Faraday Soc.*, **32**, 138 (1961).

by inducing polarization in each of the chloride ions in its immediate coordination sphere. Hence the very rapid initial drop in lithium ion mobility as KCl is added. At higher concentrations of KCl, it is clear that the additional asymmetry introduced by addition of further potassium ions is somewhat smaller, and the lithium ion mobility falls less rapidly. As for the potassium ion itself, its attraction to chloride is *weakened* by addition of lithium ions. The weakening of its attachment to just one chloride in its coordination sphere does not greatly increase its ability to move, however. Hence, starting from pure KCl, we see that the potassium ion mobility rises only slowly until a substantial fraction of chlorides in the neighborhood of each potassium have become polarized by having also a lithium neighbor.

If changes in relative mobility are to be attributed to changes in the cation-anion bond energy, it is reasonable to expect a corresponding change in the activation energy for conductance. Although accurate evaluations of activation energy are not permitted by the uncertainties in our data, we have combined the results of runs 5-8 and those of runs 11 and 13 with the conductance data of Van Artsdalen and Yaffe² to obtain the rough estimates listed in Table II. The heats

Table II: Approximate Heats of Activation for Relative Cation Conductances in KCl-LiCl

E_K	ΔH^*_{KCl} , cal. mole ⁻¹	ΔH^*_{LiCl} , cal. mole ⁻¹
0.000	...	2000
0.310	3500	2800
0.650	3500	5100
1.000	3700	...

of activation ΔH^* were calculated from the equations $\lambda_{KCl} = A_K \exp(-\Delta H_{KCl}/RT)$ and $\lambda_{LiCl} = A_{Li} \exp(-\Delta H_{LiCl}/RT)$. The apparent increase in ΔH^* for each cation with increasing KCl concentration is consistent with the model, as is the greater *rate of increase* for Li⁺.

It is appropriate to consider the concentration dependence of other transport properties in the light of this model. It is known that the viscosity of KCl-LiCl mixtures actually shows a negative deviation from additivity of the pure salt values.¹⁶ In view of the behavior of Λ , this is the opposite of what would be predicted by Walden's rule. A microscopic picture of viscous flow in fused salts, however, does not require cations and anions to move relative to one another, so long as there are some bonds weak enough to permit relative motion of adjacent layers. Specifically, the strengthening of the Li-Cl bond need not inhibit flow substantially, since the two ions can move along together. The weakening of the K-Cl bond does enhance the flow process, nevertheless, by providing points at which successive layers can shear. Thus the polarization of the anion in fused mixtures also accounts qualitatively for the behavior of viscosity.

Similar predictions can be anticipated for the case of self-diffusion, where again, in contrast with electrical mobility, cations are not required, by the definition of the transport property, to move relative to their anion neighbors in order to contribute to the total observed flux. Hence, the diffusion mobility of lithium ion in this system would not be expected to show such a strong decrease with increased potassium ion concentration. Experiments are under way in this laboratory to test this hypothesis. Some indication of its validity is provided by the self-diffusion results in molten NaNO₃-KNO₃ mixtures reported by Lantelme and Chemla.¹⁷ The concentration dependencies of both cation diffusion mobilities appear to be linear, while the electrical conductance of the system shows the usual negative deviation from additivity. The effects in these nitrate mixtures are too small to be unambiguous, however, so that further confirmation of the applicability of the Lumsden model in explaining transport phenomena should be sought in other systems.

(16) S. V. Karpachev, A. Stromberg, and V. N. Podchainova, *Zh. Obshch. Khim.*, **5**, 1517 (1935).

(17) F. Lantelme and M. Chemla, *Bull. soc. chim. France*, 969 (1963).

Transient Species Observed in the Catalyzed Decomposition of Ammonia

by Charles E. Melton^{1a} and Paul H. Emmett^{1b}

*Chemistry Division, Oak Ridge National Laboratory,^{1c} Oak Ridge, Tennessee, and
The Johns Hopkins University, Baltimore, Maryland (Received June 6, 1964)*

A research mass spectrometer has been used in the study of the catalytic decomposition of ammonia over a platinum wire over the pressure range 10^{-4} to 1 mm. and a temperature range 75 to 1300°. Three free radicals, N, NH, and NH₂, have been observed in the gas phase and, hence, must have desorbed from the surface of the catalyst. The radical NH₂ was studied as a function of temperature. In addition to the radicals, the ions NH₄⁺ and NH₂⁻ were observed in the gas phase. These ions were apparently produced by the hot surface of the catalyst; no ionizing electrons were utilized in their production. NH₄⁺ was observed at catalyst temperatures as low as 500°. NH₃D⁺ was obtained from an ammonia-deuterium mixture. The activation energy for ammonia decomposition from a 1:5 H₂-NH₃ mixture was found to be 52 kcal./mole of ammonia. Measurable quantities of N, NH, and NH₂ were found in the gas phase when an iron filament was used as a catalyst at 1000°.

It has already been shown^{2a,b} that transient species (ions, free radicals, etc.) evolving from the surface of a catalyst during the course of catalyzed reactions at pressures as high as 1 mm. can be identified by mass spectrometry.³ These previously developed apparatus and methods have now been utilized to investigate the platinum-catalyzed decomposition of ammonia. A few measurements have also been made on an iron catalyst.

Experimental

The research mass spectrometer utilized in this study has been described previously in detail.^{2a} Transient species were produced and detected by essentially the same techniques as those described for the initial CO₂-D₂ study. Briefly, the sample under investigation passed through the reaction chamber containing the catalyst in the form of a filament. Pressure in the reaction chamber (ionization chamber) was varied over the range from 10^{-8} to 1 mm. as measured by the techniques previously discussed.⁴ Intermediates evolving from the catalyst were detected and identified by suitably adjusting the electron energy so as to ionize only the desired species. The concentration of these could be monitored for either steady-state or for transient conditions. At temperatures above about 600°, the temperature of the catalyst was measured with an

optical pyrometer. The lower temperatures were calculated from the known value of the heating current flowing through the catalyst.

In the present investigation, several experiments were carried out, with the ionizing electron beam off, to search for possible charged species evolving from the surface of the hot catalyst. A background spectrum was determined at high pressure (to 1 mm.), with the catalyst cold, to rule out possible ionization by stray electrons during the period in which the electron beam was turned off. Therefore, any ions observed with the electron beam off had to be produced by the hot catalyst.

(1) (a) Chemistry Division, Oak Ridge National Laboratory, Oak Ridge, Tenn.; (b) The Johns Hopkins University, Baltimore, Md.; (c) operated for the U. S. Atomic Energy Commission by the Union Carbide Corp.

(2) (a) C. E. Melton, *J. Chem. Phys.*, **35**, 1751 (1961); (b) C. E. Melton, *J. Am. Chem. Soc.*, **84**, 1491 (1962).

(3) As pointed out in ref. 2a, all previous mass spectrometric measurements of radicals formed by decomposition or pyrolysis on hot filaments were limited to the pressure range 10^{-8} to 10^{-4} mm. Furthermore, the formation of radicals in previous work has usually not been permitted to take place directly in the ionization chamber. The present apparatus is unique in that it permits radical formation and ionization by an electron beam to take place in the same chamber and at pressures as high as 1 mm. See ref. 2a for a list of references to previous work.

(4) C. E. Melton, "Mass Spectrometry of Organic Ions," F. W. McLafferty, Ed., Academic Press, Inc., New York, N. Y., 1962, p. 78.

Matheson anhydrous ammonia (99.99%) used in this investigation was condensed in liquid nitrogen and evacuated to a pressure of 10^{-7} mm. to remove possible noncondensable impurities. Hydrogen (Matheson ultra pure, 99.99%) and deuterium (Stuart Oxygen Co.) were used without further purification.

Results and Discussion

All of the species containing nitrogen observed during the course of the catalyzed decomposition of ammonia are tabulated in Table I. Products from ion-molecule reactions^{4,5} although observed are not tabulated. The NH_4^+ and NH_2^- shown in Table I were produced by the hot catalyst rather than by either ion-molecule reactions or electron bombardment of possible neutral precursors as will be shown later in the paper. Steady-state concentrations of the transient species are based on the following estimates, and assumptions and may be in error by one or more orders of magnitude.

(1) Equal ionization and collection efficiencies for N, NH, and NH_2 for ionization by 16, 14, and 13 e.v. electrons, respectively. These energies are considerably lower than those needed to produce N^+ , NH^+ , and NH_2^+ by the dissociative ionization of NH_3 . (See Table II.) (2) Equal collection efficiencies (about 1 in 1000) for the ions NH_4^+ and NH_2^- . (The NH_2^- ion was measured by reversing the polarity of both the analyzer magnet and the accelerating voltage.) (3) An efficiency of 1 in 10^7 for the production and collection of NH_2^+ produced from NH_2 by 13-e.v. electrons. This is probably the least accurate of the three assumptions.

Table I: Concentration of Species Containing N, Observed in the Catalytic Decomposition of NH_3 over Pt at 0.1 mm. and 1200°

Species	Concn. ^a
N	100
NH	1,000
NH_2	10,000
N_2	100,000,000 ^b
NH_2^- ^c	1
NH_4^+ ^c	10,000

^a May be in error by one or more orders of magnitude. ^b 10% NH_3 decomposition. ^c No electron beam used.

The detailed experimental evidence for the occurrence of each of the transient species listed in Table I is as follows:

NH_4^+ . A typical curve showing the increase and decrease in the concentration of NH_4^+ in the gas phase is presented in Fig. 1. The temperature of the catalyst

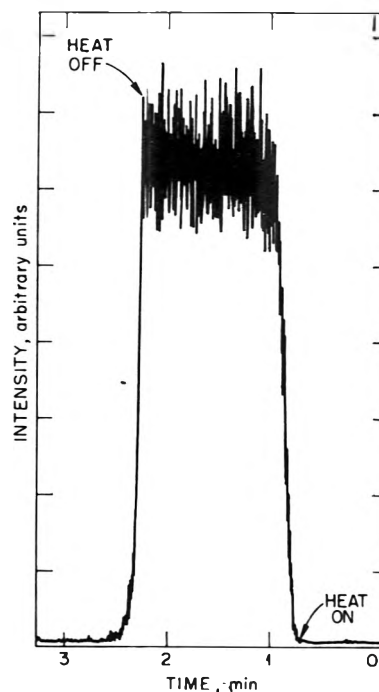


Figure 1. NH_4^+ ion released from Pt catalyst in the catalytic decomposition of NH_3 .

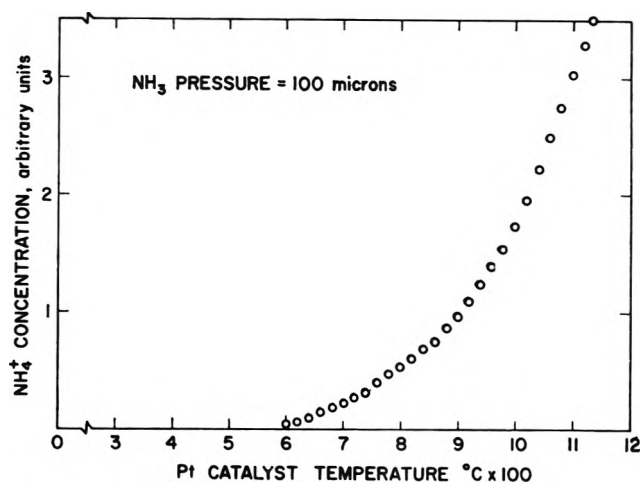


Figure 2. NH_4^+ concentration as a function of catalyst temperature in the catalytic decomposition of NH_3 over Pt.

was suddenly changed from 75 to 1000° to obtain these data. No ionizing electrons were present during this run. The behavior of the concentration of NH_4^+ with temperature is shown more fully in Fig. 2. The catalyst temperature was changed by small increments over the 600 to 1100° range. Although the concentra-

(5) C. E. Melton, Chemistry Division Annual Progress Report ORNL, 1962.

Table II: Energetics of the Ionization and Dissociation of NH_3

m/e	Ion	Reaction	Appearance potential, e.v.	Reaction	Appearance potential, e.v.
14	N^+	$\text{N} + e \rightarrow \text{N}^+ + 2e$	14.5	$\text{NH}_3 + e \rightarrow \text{N}^+ + 3\text{H} + 2e$	25.0
15	NH^+	$\text{NH} + e \rightarrow \text{NH}^+ + 2e$	~ 12	$\text{NH}_3 + e \rightarrow \text{NH}^+ + 2\text{H} + 2e$	19.5
16	NH_2^+	$\text{NH}_2 + e \rightarrow \text{NH}_2^+ + 2e$	~ 11	$\text{NH}_3 + e \rightarrow \text{NH}_2^+ + \text{H} + 2e$	15.8
17	NH_3^+			$\text{NH}_3 + e \rightarrow \text{NH}_3^+ + 2e$	10.5

tion of NH_4^+ is not given below a temperature of 600° , this ion was detectable at temperatures as low as 500° .

In previous work, it was shown that NH_4^+ is probably formed by a surface reaction between NH_3 and H_2 molecules. In Fig. 3 is given the variation of NH_4^+ concentration with the pressure for constant catalyst temperature of 1200° . These data are corrected for the partial pressure of hydrogen produced from NH_3 by decomposition. When D_2 rather than H_2 was added to the system, NH_3D^+ was observed. The concentration of this species as a function of D_2 pressure is also given in Fig. 3. The values for the NH_4^+ curve are equal approximately to those for NH_3D^+ multiplied by $\sqrt{2}$. This suggests that the difference in concentration of the NH_4^+ and NH_3D^+ ions is due to the relative collision frequency for H_2 and D_2 .

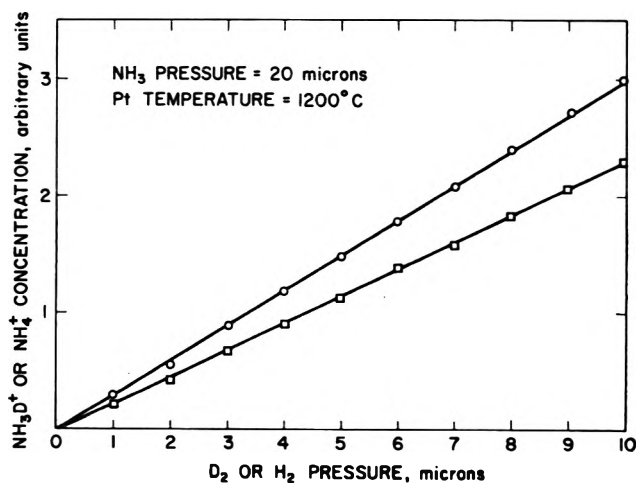


Figure 3. Concentration of NH_3D^+ , open squares, and NH_4^+ , open circles, as a function of D_2 and H_2 pressure.

The formation of an NH_3D species in an NH_3 - D_2 system is consistent with the observations of Kemball⁶ for the ammonia-deuterium exchange reaction on platinum. His results showed that the initial exchange product is always NH_2D and that NHD_2 and ND_3 are formed by subsequent independent reactions. If the intermediate in this exchange reaction were indeed the

NH_3D species, the initial product would always be NH_2D because the intermediate on dissociation would give either $\text{NH}_2\text{D} + \text{H}$ or $\text{NH}_3 + \text{D}$. The results given in Fig. 4 for a 35 D_2 -65 NH_3 mixture clearly show that little NH_2D_2^+ is formed and desorbed from the hot catalyst. This is in accord with Kemball's conclusion that species with more than one D atom attached are formed by secondary reactions. Since the data in Fig. 4 were taken at 1000° , NH_4^+ was also being formed by a reaction of NH_3 with hydrogen molecules resulting from the NH_3 decomposition. Consequently, a large NH_4^+ peak was observed as well as the NH_3D^+ peak.

NH_2^- . Negative ions were not detected in the absence of an electron beam at temperatures below 1200° . Therefore, only qualitative studies of the concentration of NH_2^- evolving from the surface could be made because the reaction chamber was not designed to operate

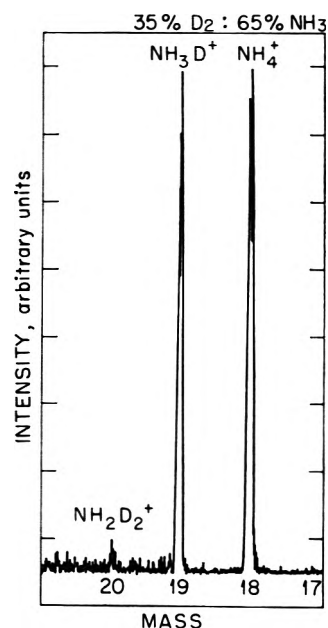


Figure 4. Ionic species formed from a mixture of 35% D_2 and 65% NH_3 over a platinum catalyst at 1000° .

(6) C. Kemball, *Proc. Roy. Soc. (London)*, **A217**, 376 (1953).

at filament temperatures higher than 1300°. At temperatures above 1200°, NH₂⁻ concentrations seemed to increase exponentially with temperature. However, it is possible that at this high temperature some of the ions were formed by electrons emitted from the hot catalyst.

NH₂ and NH. Of the neutral transient species, NH₂ was the most abundant. The time and temperature dependence of this species is shown in Fig. 5 and 6. In the run represented by Fig. 5, the temperature was sud-

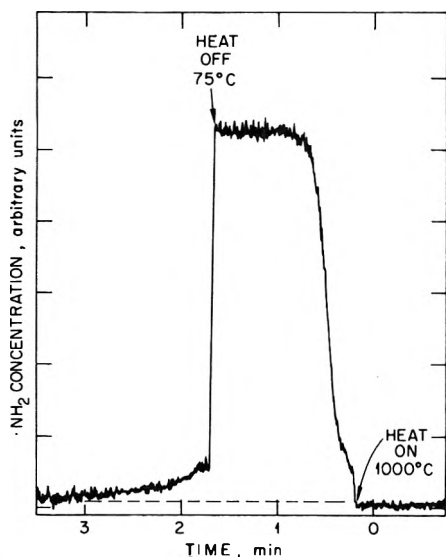


Figure 5. NH₂ radicals produced by the catalytic decomposition of NH₃ over Pt.

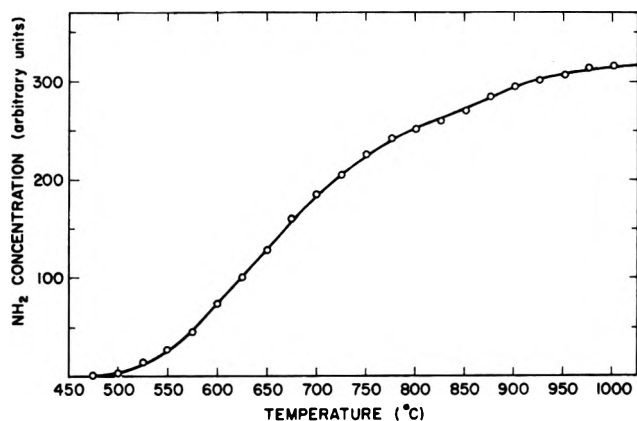


Figure 6. NH₂ concentration as a function of temperature in the catalytic decomposition of NH₃ over Pt.

denly increased from 75 to 1000° at a constant partial pressure of ammonia of 0.1 mm. The NH₂ concentration increased gradually and reached a steady-state concentration about 20 sec. after the temperature was

increased. By contrast, when the temperature was decreased suddenly the concentration of NH₂ decreased abruptly to a very low value and then slowly approached zero. The leveling off of the NH₂ yield at the higher temperature (Fig. 6) probably indicates a decrease in the steady-state concentration of surface NH₂ groups due to an increasing tendency for the NH₂ to decompose on the surface as the temperature is raised.

The results for NH were much more qualitative than those for NH₂ since the concentration of the former species was about a factor of 20 less than that for the latter. The behavior of NH with a sudden increase and decrease of temperature was similar to that of NH₂.

N. The ratio of atoms of nitrogen to molecules of nitrogen in the gas phase decreased markedly with an increase in the partial pressure of ammonia as shown in Fig. 7. Qualitatively, this is reasonable since the

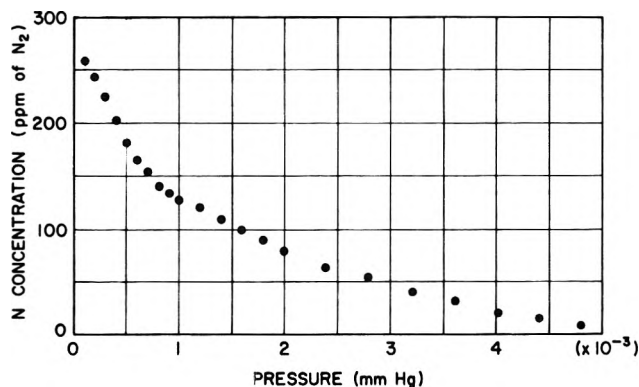


Figure 7. Concentration of N as a function of NH₃ pressure in the catalytic decomposition of NH₃ over Pt.

probability of nitrogen being removed as molecules should depend on a higher power of the concentration of chemisorbed nitrogen atoms than the probability of it being removed as atoms. However, since over the pressure range of ammonia used in getting the data for Fig. 7 the rate of formation of nitrogen molecules is proportional to the partial pressure of ammonia, it is apparent that the absolute rate of nitrogen atom evolution goes through a maximum at about 2 × 10⁻³ mm. of ammonia and then decreases rapidly with an increase in the partial pressure of ammonia. Possibly at the higher pressure of NH₃, many nitrogen atoms are reacting in the gas phase with ammonia molecules before reaching the electron beam or are being diverted to the wall of the reaction vessel where they might react with adsorbed ammonia. In any event, the marked de-

crease in the number of nitrogen atoms being evolved at partial pressures of ammonia higher than about 2×10^{-3} is very striking. Incidentally, it should be noted that the concentration of this species as a function of temperature was not quantitatively measured because of possible decomposition of N_2 at higher temperatures.

In the course of the present work, it seemed worthwhile to determine the kinetics and temperature coefficient of ammonia decomposition for comparison with similar data in the literature. Accordingly, a few observations were made relative to the dependence of the rate of decomposition on temperature and on the partial pressures of ammonia and hydrogen.

The nitrogen concentration and, hence, the amount of ammonia decomposed as a function of temperature are given in Fig. 8.

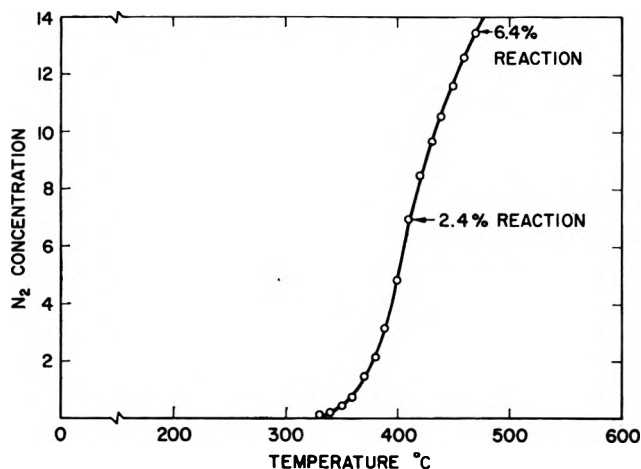


Figure 8. Concentration of N_2 as a function of temperature from the catalytic decomposition of NH_3 over Pt.

Since it was known that the decomposition of ammonia over platinum is inhibited by hydrogen, it seemed best to measure the temperature coefficient with an ammonia-hydrogen mixture with such a small percentage decomposition that the partial pressures of hydrogen and of ammonia may be assumed to be essentially constant throughout the experiments. Results of such a series of measurements of a 5:1 ammonia-hydrogen mixture are shown in Table III.

The value of 52 kcal./mole of ammonia decomposed for the apparent energy of activation is in reasonable agreement with the value of 59 kcal. obtained by mass spectrographic analysis by Logan and Kemball. It is, of course, recognized that these apparent temperature coefficients are larger than they would be if it were possible to keep a constant amount of inhibitor (hydrogen) on the catalyst surface at the various temperatures

Table III: Activation Energy of Ammonia Decomposition

Pressure of NH_3 - H_2 mixture, μ	Activation energy, kcal./mole	Maximum % decomposition
5	52,880	1.4
5	52,600	1.3
10	52,700	1.1
15	52,600	1.0

^a The mixture contained 16.6% hydrogen.

employed. Insufficient information, relative to the heats of adsorption of ammonia and hydrogen on the platinum surface, is available for correcting this apparent temperature coefficient to an energy of activation calculated on the basis of a constant number of ammonia molecules adsorbed on the catalyst surface.

The absolute rate of ammonia decomposition was found in the present work to be proportional to the partial pressure of ammonia in the pressure range at and below 10^{-3} mm. (Fig. 9). It was also found to

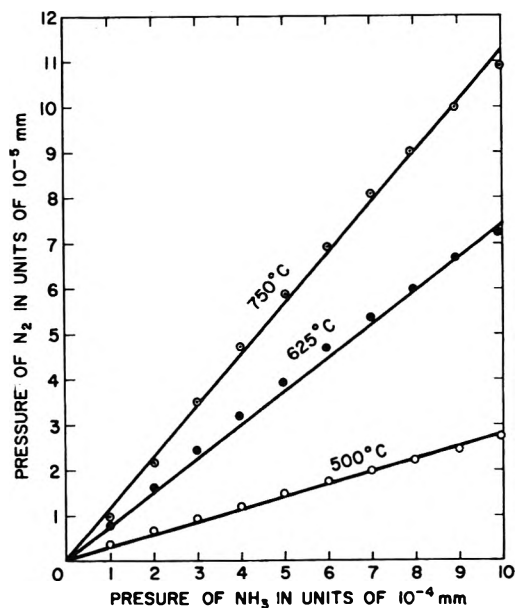


Figure 9. Decomposition of NH_3 by Pt as a function of pressure.

be slowed down by adding hydrogen. Figure 10 indicates the decomposition to be approximately inversely proportional to the partial pressure of added hydrogen. Actually, the inhibitive action of hydrogen is probably a little greater than that corresponding to the first power of hydrogen since some hydrogen is always formed during the decomposition of ammonia. In

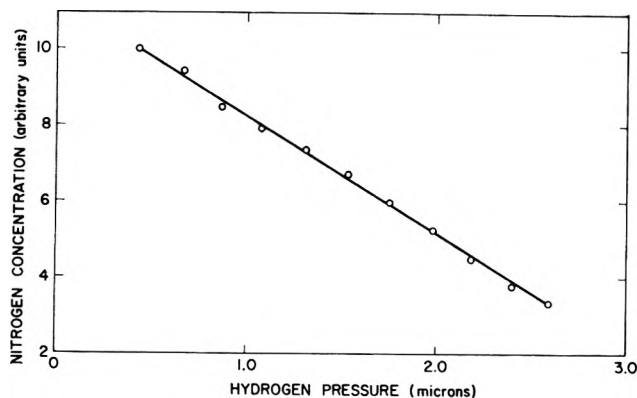


Figure 10. Concentration of N_2 as a function of H_2 pressure in the decomposition of NH_3 over Pt at 400° and $10 \mu NH_3$ pressure.

other words, the curve in Fig. 10 would be even steeper if average partial pressures of hydrogen were used rather than the pressure of added hydrogen. These kinetic results are considered to be in satisfactory agreement with those of Logan and Kemball who found the rate of ammonia decomposition proportional to the 0.96 power of ammonia and inversely proportional to the 1.6 power of hydrogen.

Recently⁷ some work was published in Russia in which argon ions were used to bombard a platinum ribbon. In the presence of ammonia, both secondary ions from the argon bombardment and the ionization of the gas by an electron beam could be detected. The authors conclude that the decomposition of ammonia occurs primarily by the reaction



Pending a more detailed publication of their data, one must reserve judgment as to whether their experiments really show evidence for this mechanism. Certainly the present measurements do not point to such a mechanism. The relative yields of NH_2 , NH , and N radicals in the present work would suggest instead the presence of more NH_2 groups than NH groups on the surface. However, until one has values for the relative energies of activation for the desorption of N , NH , and NH_2 radicals, one cannot conclude from the observed emissions the relative surface concentrations of these groups. The present experiments seem, however, to afford definite evidence of the presence of N , NH , and NH_2 and presumably NH_4 or NH_4^+ ions on the surface of the platinum during the catalytic decomposition of ammonia in the temperature range 500 to 1000° .

Finally, a few very qualitative experiments concerning the decomposition of NH_3 over iron were carried out. Results from this work are given in Fig. 11. No

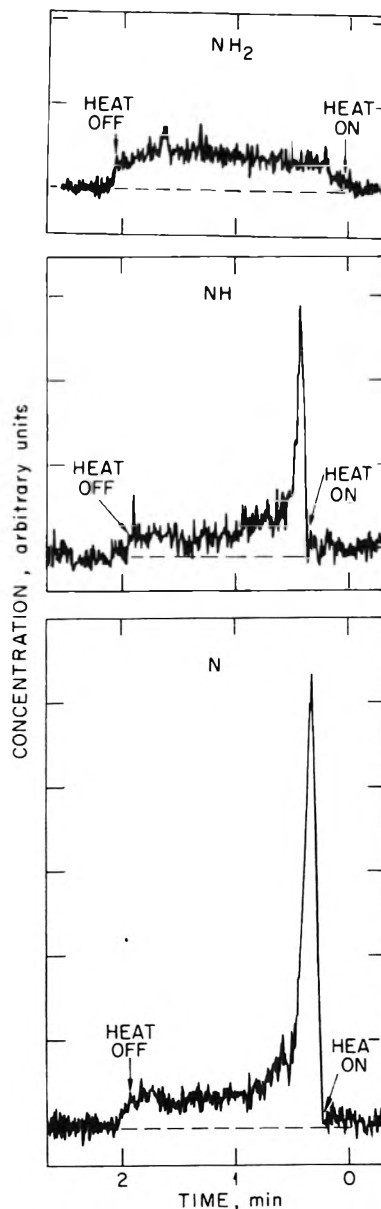


Figure 11. Radicals produced by the catalytic decomposition of NH_3 over Fe. The steady-state ratio of N to NH is between 10 and 20. The ordinate scales have been altered for convenience of presentation.

attempt was made to observe charged transient species such as NH_4^+ . The behavior of the observed transient species N , NH , and NH_2 was quite different from that observed for these species evolving from Pt. When the temperature of the catalyst was suddenly increased from 75 to 1000° , a burst of N and NH atoms was observed after which the concentration of these species

(7) Ya. M. Fcgel, B. T. Nadykto, V. F. Rybalko, R. P. Siabospitskii, and I. E. Kōrobchanskaya, *Dokl. Akad. Nauk SSSR*, **147**, 414 (1962).

decreased to a steady-state value. The number of N atoms in the burst was estimated to be from 10 to 20 times the number of NH radicals. As shown in Fig. 11, no burst of NH₂ radicals was observed.

It seems very probable that the burst of N atoms may be interpreted as resulting from the formation of some Fe₄N at low temperature as the temperature is being raised from room temperature to 1000°. Such a nitride is known to form rapidly at low temperature and is also known to decompose at temperatures above 500°. The evolution of NH in such large quantities initially is a little puzzling. If the Fe₄N contained from 5–10% of a compound Fe₄NH, as an impurity, the burst of NH radicals would be accounted for.⁸ Such NH groups have never been reported in connection with the formation of iron nitrides. It is quite possible, however, that the presence of this small amount of NH could have been overlooked.

It is interesting to note that at steady state, the evolution of N, NH, and NH₂ reach small but finite

steady-state levels. It would appear on the basis of approximate calibrations that the number of nitrogen atoms is five- to tenfold greater at steady state than the number of NH groups though this ratio must still be taken as an approximation.

The presence of a high concentration of nitrogen atoms on the surface of an iron catalyst is consistent with the current theories of ammonia synthesis and decomposition. The presence of NH groups on well-reduced catalysts is perhaps less well established than the presence of nitrogen atoms although, when certain promoters such as alumina are present, considerable evidence exists that NH and perhaps NH₂ groups are also to be found as intermediates on the surface of an active iron catalyst. The observations here made, therefore, in regard to an iron wire at 1000° seem to be entirely reasonable.

(8) The referee pointed out that FeNH may also be formed.

Substituent Effects on Intramolecular Energy Transfer. II. Fluorescence Spectra of Europium and Terbium β -Diketone Chelates

by N. Filipescu, W. F. Sager, and F. A. Serafin

Department of Chemistry, The George Washington University, Washington 6, D. C. (Received June 12, 1964)

The fluorescence spectra of europium and terbium β -diketone chelates are modified significantly on changing substituents in the organic ligand. The relative intensity, spectral distribution, shifting, and splitting of the fluorescence lines are discussed in relation to the nature of substituents, their position, molecular configuration, and the over-all intramolecular energy transfer.

Introduction

Sharp-line emission and absorption characteristic to the rare earth ions imbedded in crystalline solids consists primarily of electric-dipole transitions between the levels of certain multiplets that can be built from the inner f-electrons that these ions possess. The

clearly expressed discrete structure is closely related to the immediate environment surrounding the ion, and, therefore, the ions of the rare earth elements can serve as sensitive probes introduced in systems being investigated. The spectra of rare earth ions incorporated in inorganic single crystals have been success-

fully interpreted by considering the crystalline field as a perturbation on the free ion Hamiltonian.¹ The Zeeman effect, paramagnetic studies, and polarized light have also been used to elucidate the behavior of these ions in different environments.² Rare earth ions incorporated in organic complexes by coordination through a donor atom such as oxygen or nitrogen, when excited with light absorbed by the ligand, exhibit narrow-line emission at approximately the same frequencies as the inorganic single crystal system. This phenomenon is the result of an intramolecular energy transfer from the electronic states associated with the organic complex to localized intra-4f shell energy levels of the ions.³ In a previous paper of this series⁴ the ultraviolet absorption spectra of a number of substituted rare earth β -diketone chelates and the phosphorescence spectra of the gadolinium complexes have been analyzed. The present work is concerned with the fluorescence spectra of the europium and terbium β -diketonates and the over-all intramolecular energy transfer governing the absorption-emission process.

Experimental

The preparation of different β -diketones and the rare earth chelates has been described previously.⁴ The fluorescence spectra of europium and terbium complexes were recorded on a Cary Model 14 spectrophotometer using the fluorescence attachment. The compounds were dissolved at a concentration of $\sim 10^{-5} M$ in EPA (5 parts diethyl ether, 5 parts 3-methylpentane, and 2 parts absolute ethanol by volume). The diethyl ether and the methylpentane were distilled from metallic sodium ribbon, and the reagent grade ethanol was distilled from magnesium ethoxide. The fresh solutions of europium or terbium chelates were introduced into 10-mm. quartz tubes and immersed in liquid nitrogen in a transparent quartz dewar. The frozen samples were irradiated with two sources: a beam from the internal mercury vapor lamp in the Cary 14 spectrophotometer illuminating the sample from the front and one from an external mercury vapor lamp 9W, Model SL 3660 (Ultraviolet Products, Inc.) normal to the sample-slit beam. For all the aromatic β -diketone chelates the exciting light was filtered through an aqueous CuSO_4 solution and a Corning 5840 filter (3000–4000-Å. transmission range), whereas for the aliphatic β -diketonates (acetylacetonates, trifluoroacetylacetonates, and hexafluoroacetylacetonates) the internal Cary 14 ultraviolet source was filtered through a NiSO_4 water solution and a Corning 9863 filter and coupled with an external short wave ultraviolet lamp 9W, Model SL 2537, perpendicular to the sample-beam direction. The log scale was used on the recorder, and all the fluorescence spectra

were extrapolated to an equivalent 0.5-mm. slit for comparison. A semiquantitative evaluation of the relative intensities is possible by comparing the area under the curve of a given peak on a linear R.I. = $f(\nu)$ scale.

Results and Discussion

The ground state of both europium and terbium trivalent ions is a 7F state. The lowest excited states inside the 4f-shell are the 5D_0 , 5D_1 , and 5D_2 levels for europium and the 5D_4 level for terbium. Under the influence of the electric field of the surrounding crystal lattice or ligand, the excited states as well as the ground 7F levels will separate into a number of states with different energy. The number of sublevels resulting from the splitting and the extent of their separation are understood rather well for rare earth ions situated in a field of known symmetry in ionic crystals, but the calculations made attempting to explain the experimental intensities can at best be described as semiquantitative.¹ The theoretical problems encountered are difficult to treat not only because they involve simultaneous interaction among radiation, matter, and phonons but also because crucial specific details of the wave functions are not known.⁵ For rare earth ions, the difficulty in estimating intensities of electric dipole transitions is that they arise from the admixture into $4f^n$ of transitions of opposite parity. To calculate such admixtures, not only must the energies and eigenfunctions of configurations such as $4f^n-5d$ be known, but also that part of the ligand or crystal field potential responsible for the admixing.^{1f} For an ion in a chelate, similar to an ion in a crystal, the influence of the field of the surrounding atoms on this ion will be great for all

(1) (a) J. Van Vleck, *J. Phys. Chem.*, **41**, 57 (1937); (b) H. Bethe, *Ann. Physik*, **3**, 133 (1929); (c) B. R. Judd, *Proc. Roy. Soc. (London)*, **A228**, 120 (1955); (d) G. S. Ofelt, *J. Chem. Phys.*, **37**, 511 (1962); (e) J. D. Axe, *ibid.*, **39**, 1154 (1963); (f) B. R. Judd, *Phys. Rev.*, **127**, 750 (1962); (g) S. Freed, S. I. Weissman, and F. E. Fortress, *J. Am. Chem. Soc.*, **63**, 1079 (1941); (h) S. Freed and S. I. Weissman, *J. Chem. Phys.*, **6**, 297 (1938).

(2) (a) P. Selwood, *J. Am. Chem. Soc.*, **56**, 2392 (1934); (b) A. Schmillen, *Ann. Physik*, **39**, 502 (1941); (c) S. Freed, *J. Chem. Phys.*, **8**, 291 (1940); (d) F. Spedding, *Phys. Rev.*, **38**, 2083 (1931); (e) E. H. Carlson and G. H. Dieke, *J. Chem. Phys.*, **34**, 1602 (1961); (f) A. Friedrich, K. H. Hellwege, and H. Lammermann, *Z. Physik*, **159**, 524 (1960).

(3) (a) S. I. Weissman, *J. Chem. Phys.*, **10**, 214 (1942); (b) G. A. Crosby and M. Kasha, *Spectrochim. Acta*, **10**, 377 (1958); (c) G. A. Crosby, R. E. Whan, and R. M. Alire, *J. Chem. Phys.*, **34**, 743 (1961); (d) R. E. Whan and G. A. Crosby, *J. Mol. Spectry.*, **8**, 315 (1962); (e) N. Filipescu, M. R. Kagan, N. McAvoy, and F. A. Serafin, *Nature*, **196**, 467 (1962); (f) G. A. Crosby and R. E. Whan, *J. Chem. Phys.*, **35**, 863 (1962); (g) H. Samelson, A. Lempicki, V. A. Brophy, and C. Brecher, *ibid.*, **40**, 2547, 2553 (1963); (h) N. McAvoy, N. Filipescu, M. R. Kagan, and F. A. Serafin, *J. Phys. Chem. Solids*, **25**, 461 (1964).

(4) W. F. Sager, N. Filipescu, and F. A. Serafin, paper I of this series, *J. Phys. Chem.* (in press).

(5) D. L. Dexter, *J. Chem. Phys.*, **21**, 836 (1953).

the outer 6s- and 5d-electrons and considerably smaller for the internal electrons of the 4f-shell. The spectra of europium and terbium ions in chelates, as in crystals, possess a pronounced discrete structure which is naturally explained as due to transitions between levels of the f-shell. The prohibition for electric dipole transitions between levels of one parity is related to the presence in the free ion of a center of symmetry which coincides with the nucleus. But if, upon chelation of the ion, its nucleus ceases to be a center of symmetry, then "forced" dipole transitions between levels of one parity appear. These emission lines characteristic of intra-4f parity-forbidden transitions are observed with high intensity for both europium and terbium in β -diketone chelates. It has been shown that noncentrosymmetry due to oscillatory motion¹ is minor compared to field distortion introduced by the β -diketone structure and substituents attached to these rare earth chelates.

The departure from regular octahedral symmetry in the β -diketone chelates investigated is due to a number of reasons: (1) The oxygen atom orbitals involved in bonding to the metallic ion do not have axial symmetry along the bond because of resonance with the enolate ring, a feature which annihilates the molecular center of symmetry; (2) different radicals attached to the chelating ring affect both the metal-oxygen distance and the electron density associated with the oxygen atoms bound to the ion; (3) solvent molecules of high polarity may tend to associate with the ion introducing new (but probably much weaker) perturbing effects and possibly slight modification of the regular arrangement of the nearest neighbors. As a rule, the less symmetrical the geometric arrangement surrounding the ion, the more numerous the lines appearing in the spectrum due to internal Stark splitting of the "unperturbed" ionic levels. The distribution of the nearest neighbors around a trivalent ion in β -diketone chelates is very close to a configuration of O_h symmetry, whereas the whole molecule of a symmetrically substituted β -diketonate belongs to the C_{3v} group symmetry. The number of sublevels in which the individual ionic levels are split under the influence of internal Stark fields of known symmetry is easily predicted as dependent on the total angular momentum quantum number J .⁶ The maximum number of lines to be observed for individual transitions from 5D_0 , 5D_1 (or 5D_4) to the low-lying 7F levels of europium (or terbium) ion in an O_h or C_{3v} field is given in Table I.

Generally, the number of lines in the fluorescence spectra of europium and terbium β -diketonates agrees with a distorted octahedral field about the ion approaching a C_{3v} symmetry depending on substituents.

Table I

Eu ³⁺	5D_0 to	7F_0	7F_1	7F_2	7F_3	7F_4	7F_5	7F_6
max. number	O_h	1	1	2	3	4	4	6
of lines	C_{3v}	1	2	3	5	6	7	9
Eu ³⁺	5D_1 to	7F_0	7F_1	7F_2	7F_3	7F_4	7F_5	7F_6
max. number	O_h	1	1	2	3	4	4	6
of lines	C_{3v}	2	4	6	10	12	14	18
Tb ³⁺	5D_4 to	7F_0	7F_1	7F_2	7F_3	7F_4	7F_5	7F_6
max. number	O_h	4	4	8	12	16	16	24
of lines	C_{3v}	6	12	18	30	36	42	54

Appreciable variation is observed in relative intensity and number of individual lines in the fluorescence spectra of differently substituted europium and terbium β -diketone chelates. The various substituents change both the symmetry and the strength of the molecular field surrounding the ion and modify the interaction of the inner 4f-shell of the ion with its environment. The differences in the emission spectra of europium or terbium chelates grouped in series A (*meta*- and *para*-substituted dibenzoylmethides) indicate a significant interaction through the aromatic benzene ring between distantly appended substituents and the enolate chelate ring.

The successive steps of the over-all intramolecular energy transfer, the result of which is the ionic fluorescence, are affected by the substituents as given in the following paragraphs.

Absorption in the Near-Ultraviolet ($S \rightarrow S'$). Substituents directly attached to the β -diketone chelate ring (series B) or more distantly (series A) shift λ_{max} of the main molecular absorption peak. The absorption intensity does not vary significantly on changing substituents. The energy of the excited singlet (which changes on replacing substituents) does not affect directly the energy transfer from the organic ligand to the chelated ion.

Intersystem Crossing ($S' \rightsquigarrow T$). This radiationless process depends markedly on the substituents; different efficiencies were observed for the various chelates investigated. The efficiency was evaluated from the phosphorescence spectra ($T \rightarrow S$) of the gadolinium chelates at 77°K. in a solid matrix, when quenching of the triplet state is negligible. Competing processes are the organic fluorescence ($S' \rightarrow S$) and the radiationless deactivation of the excited singlet as thermal energy. The organic fluorescence has a low yield so that the amount of energy available at the triplet level depends on the efficiency of $S' \rightsquigarrow T$ intersystem crossing

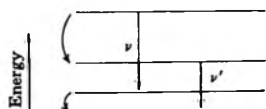
(6) (a) H. Bethe, *Ann. Physik*, **3**, 133 (1929); (b) H. Gobrecht, *ibid.*, **28**, 673 (1937).

which competes with an intramolecular radiationless deactivation.

Triplet State. The energy of the triplet state is directly dependent on the substituents. The requirement for an efficient migration of energy to the ion is that the triplet state be equal or above the resonance level of the chelated ion. Apparently shifting, splitting, or line width of individual transitions are not dependent on the energetic location of the triplet.

Energy Transfer from the Organic Triplet to the Rare Earth Ion. This is a balance-like process in that the organic part goes by a radiationless transition to the ground-state configuration, as the ionic 4f-electron is raised to an excited state. The mechanism of energy transfer to the ion involves a strong interaction between the triplet state or a vibrational level of the chelate in the triplet configuration with the resonance level of the ion. Consequently, the closer the triplet state to the emitting level of the rare earth ion, the more efficient is the coupling between the two states and the migration of energy to the ion. Attached substituents affect this step through their influence on the energetic location of the triplet and the nature of the metal-oxygen bond since the donor capability of the oxygen atoms depends on the substituents through resonance or inductive effects in both singlet and triplet states. Competing processes are the organic phosphorescence ($T \rightarrow S$) and the thermal dissipation of the triplet state energy through vibrational coupling to the surroundings (solvent). For chelates having the triplet state near (equal or above) the emitting level of the chelated ion, the organic phosphorescence is negligible which shows efficient transfer to the ion. Solvent quenching of the triplet state is also insignificant in the rigid matrix at 77°K.³ Figures in the previous paper of this series⁴ illustrate the relative positions of the triplet states of different chelates (as determined from the phosphorescence of the gadolinium β -diketonates) and the resonance levels of europium (5D_0 and 5D_1) and terbium (5D_4).

The fluorescence emission of the excited europium ion depends on the perturbing field of the ligand which varies from chelate to chelate. On increasing interaction between the 4f shell and the nearest neighbors, *i.e.*, an increase in the internal electric field, both the lower and the upper combining levels are displaced downward.



The displacement of the upper levels, the less shielded levels, is usually greater, and, hence, the lines are dis-

placed with an increase in the molecular field, as a rule, in the direction of longer wave lengths ($\nu' < \nu$). Of particular interest is the zero line $^5D_0 \rightarrow ^7F_0$ in europium ion which is not split in electric fields. This transition from an upper level with $J = 0$ to the lower 7F level corresponding also to $J = 0$ which is strictly forbidden for the free ion becomes possible for the ion in the chelate, since the quantum number J only approximately preserves its meaning. Displacement of the zero line gives an indication of the magnitude of the internal electric field.

According to the observed structure of the band (splitting), it is possible to estimate the symmetry of the field, which is directly related to the number of lines corresponding to purely electronic transitions. The magnitude of the splitting is related to the magnitude of the electric field. Superposition of oscillatory transitions upon the purely electronic transitions in the fluorescence spectra of Eu^{3+} , Gd^{3+} , and Tb^{3+} , has been found to be negligible. In β -diketonates, europium ion transitions are observed between unsplit levels, between levels of which only one is split, and between upper and lower levels where both are split by the internal electric field. The fluorescence spectrum of terbium consists of transitions originating at a level with $J = 4$, which is highly split in both O_h and C_{3v} field symmetry, and terminating at highly split levels with $J = 6, 5, 4, 3$.

The line width is temperature dependent, but the fluorescence spectra were recorded at the same temperature (77°K.) for all chelates. The dependence of the line width and line contour of surroundings is obvious on comparing spectra of the rare earth ions in different crystals, glasses, and solutions at the same temperature. Line broadening is associated with irregular distribution of ions in static electric fields of different magnitude and symmetries as in glasses, or superposition of oscillatory transitions on purely electronic transitions. In rare earth chelates the line width may also depend on the location of the triplet state of the ligand *vs.* the emitting level of the ion and the existence of stereoisomers. Some general considerations on the fluorescence spectra of europium chelates are summarized below.

General Considerations on Fluorescence Spectra of Europium Chelates

(1) The requirement for energy migration to the ion is that the triplet state be close to or above the resonance level of the europium ion. The shifting, splitting, and line width of individual transitions are not dependent on the energetic location of the triplet.

(2) The relative intensity of the fluorescence lines is not directly dependent only on the amount of energy

available at the triplet state and transferred to the ion but primarily on the probability of radiative deactivation compared to nonradiative dissipation of energy from the excited ion. This probability is very sensitive to changes in substituents in the ligand.

(3) The molecular electric field surrounding the ion is affected strongly by substituents, determining important variation in line intensity, line width, shifting, and splitting of the individual lines. The intensity of this molecular field is changed to some extent on replacing substituents, but the symmetry of the field is modified significantly and seems to determine the spectroscopic behavior of the chelated ion.

(4) The ratio of intensity of two different transitions originating from the same resonance level varies greatly for different chelates, indicating that once energy is transmitted to the ionic resonance level (5D_1 or 5D_0), transitions to different low-lying 7F levels are not in the same statistical ratio for europium ions in any chelates, but that very different transition probabilities for transitions from the same level are determined by the surroundings (substituents).

(5) The parity-forbidden intra-4f shell transitions in europium ion are strong in the investigated chelates; this indicates the existence of a noncentrosymmetrical field about the ion. The $^5D_0 \rightarrow ^7F_0$ line which would be strictly forbidden in a regular octahedral field is more intense for asymmetrically substituted β -diketonates than for those with symmetrical substituents in both series studied, showing that the departure from O_h symmetry is substituent dependent. (Similar behavior has been observed for other transitions.) The shifting of the unsplit $^5D_0 \rightarrow ^7F_0$ line shows minor changes in the molecular field intensity, so that the major cause for differences in fluorescence spectra of europium chelates is the change in symmetry of the internal Stark field.

(6) Electron-donor methoxy groups substituted on dibenzoylmethide chelate increase the amount of energy transferred from the triplet state of the ligand to the ion, probably by an increased orbital overlap in the metal-oxygen bond. An opposite effect, decrease in total ionic emission, was observed for the electron-withdrawing nitro substituents, attached in both *meta* and *para* positions.

(7) An increase in the conjugated system by attaching aromatic substituents (*p*-phenyldibenzoylmethide, dinaphthoylmethides) resulted in enhanced ionic emission.

(8) The aliphatic β -diketonates (acetylacetonate, trifluoroacetylacetonate, and hexafluoroacetylacetonates) showed a weak ionic fluorescence, and this was attributed to the existence of a large gap between the resonance levels of the europium ion and the triplet

state of the ligand, causing inefficient transfer to the ion.

(9) Combinations of aromatic-aliphatic substituents on β -diketonates (benzoylacetonate, benzoyltrifluoroacetate, theonyltrifluoroacetate) showed a strong ionic emission. This was attributed to efficient energy migration to the trivalent ion coupled with high radiative transition probability between the excited state and the low-lying 7F levels due to an increased asymmetry about the ion.

(10) The distribution of the energy transferred to the ion among the individual possible transitions originating at the two 5D_1 and 5D_0 levels and terminating at different 7F levels cannot be correlated with the location of the triplet state of the ligand. Thus, aryl-alkyl substituted β -diketonates (BA, BTA, TTA) fluoresce stronger from the 5D_0 level (the $^5D_0 \rightarrow ^7F$ transition represents more than 60% of total emission) although the triplet state lies at wave lengths shorter than the corresponding diaryl β -diketonates (DBM, DTM) which in turn emit more strongly from the 5D_1 level ($^5D_1 \rightarrow ^7F_4 > 65\%$).

(11) The splitting of the fluorescence lines corresponds to molecular electric fields having a distorted O_h symmetry, but not exceeding in number of lines the C_{3v} symmetry. The $^5D_0 \rightarrow ^7F_1$ line is split into a doublet in asymmetrical ligands in both series A and B and is singlet in symmetrical chelates, showing a greater departure from octahedral symmetry in unsymmetrically substituted diketonates (the line should be a singlet in a field of O_h symmetry and doublet in a field of C_{3v} symmetry).

(12) The line width of the fluorescence transitions is substituent dependent. A regular variation of the line width of the weak $^5D_0 \rightarrow ^7F_0$ and $^5D_1 \rightarrow ^7F_3$ transitions is observed in series A where monophenyl substitution on dibenzoylmethide sharpened these lines and *para* disubstitution of either CH_3O , NO_2 , or F had a broadening effect. If stereoisomers are formed in the case of asymmetrically substituted chelates, they have essentially equivalent electric fields surrounding the ion. Otherwise, line broadening would result from emission at very close different frequencies. This is not observed.

(13) The strong $^5D_0 \rightarrow ^7F_2$ and $^5D_1 \rightarrow ^7F_4$ lines are broadened significantly on *para* substitution of electron-withdrawing groups (nitro, fluoro) on the dibenzoylmethide chelate in series A, whereas not much change is observed on *meta* substitution of either methoxy or nitro groups or *para* methoxy substitution.

Following is a more detailed discussion of the individual lines in the fluorescence spectra of europium β -diketonates.

The total relative intensities of ionic fluorescence for europium chelates (regardless of how this emission is distributed among individual transitions) varied with the chelate as given in the two series in Table II (the total intensity of europium dibenzoylmethane was taken as unity).

Table II

Series A		
<i>p</i> -Phenyldibenzoylmethide	(<i>p</i> Ph)	4.6
Di- <i>m</i> -methoxydibenzoylmethide	(<i>DmM</i>)	1.81
<i>m</i> -Methoxydibenzoylmethide	(<i>mM</i>)	1.13
Dibenzoylmethide	(DBM)	1
<i>p</i> -Methoxydibenzoylmethide	(<i>pM</i>)	0.95
<i>p</i> -Nitrodibenzoylmethide	(<i>pN</i>)	0.75
Di- <i>p</i> -methoxydibenzoylmethide	(<i>DpM</i>)	0.62
<i>m</i> -Nitrodibenzoylmethide	(<i>mN</i>)	0.23
Di- <i>m</i> -nitrodibenzoylmethide	(<i>DmN</i>)	0.23
Di- <i>p</i> -nitrodibenzoylmethide	(<i>DpN</i>)	0.12
Di- <i>p</i> -fluorodibenzoylmethide	(<i>DpF</i>)	0.04
Series B		
Di-2-naphthoylmethide	(D2NM)	14.01
Theonyltrifluoroacetate	(TTA)	9.12
Di-1-naphthoylmethide	(D1NM)	9.12
Benzoylacetate	(BA)	4.38
Difuroylmethide	(DFuM)	3.24
Benzoyltrifluoroacetate	(BTA)	1.32
Dibenzoylmethide	(DBM)	1
Di-theonylmethide	(DTM)	0.37
Diisonicotylmethide	(DPyM)	0.15
Hexafluoroacetylacetate	(HFAcA)	0.10
Trifluoroacetylacetate	(TFAcA)	0.01
Acetylacetate	(AcA)	0.01

The over-all fluorescence intensity characteristic to the ion depends on the amount of energy available at the organic triplet and on the efficiency of energy transfer to the ion. These two factors vary for different appended substituents. Thus, *methoxy* groups, substituted in *meta* position on dibenzoylmethide chelates, tend to enhance the ionic emission, whereas *para*-methoxy substitution decreases the europium fluorescence. The effect is more pronounced for the di- than for monomethoxy-substituted dibenzoylmethides. The phosphorescence-relative intensities of the Gd chelates indicate a more efficient intersystem crossing for *para*-methoxy-substituted dibenzoylmethide than for the *meta* isomers. The reverse order in ionic fluorescence (*m*-CH₃O > *p*-CH₃O) can be explained in part by the exclusive inductive effects of methoxy groups in *meta* position, whereas in *para*-substituted dibenzoylmethides resonance effects tend to decrease the efficiency of energy from the organic triplet to the ionic. The inductive effect of the electron-donor methoxy group at-

tached to a dibenzoylmethide system increases the electron density in the conjugated system, and possibly in the metal-oxygen bond, with the result of a higher orbital overlap and consequently an easier transfer of energy to the ion.

An opposite effect is expected and observed for the nitro-substituted dibenzoylmethides of europium. The electron-attracting nitro groups appended *para* or *meta* decrease the total ionic emission of europium. The effect is more powerful for di- than for monosubstituted dibenzoylmethides. *para*-Monosubstitution of a CH₃O or NO₂ group in europium dibenzoylmethide decreases slightly the over-all ionic emission intensity but on *para*-disubstitution of either CH₃O or NO₂ (or F) the intensity is significantly decreased. This indicates that resonance effects of *para* substituents opposing energy transfer to the ion slightly overcome the asymmetry effects introduced by *meta* substitution which favor ionic emission. When asymmetry effects are removed by *para*-disubstitution, only the (opposing) resonance effects remain, decreasing the ionic emission significantly. Europium *p*-phenyldibenzoylmethide has a special position in this series. Its strong ionic fluorescence indicates that an increase in the aromatic system enhances the amount of energy transferred to the europium ion (the organic triplet of the chelate is not significantly shifted compared to dibenzoylmethide). This fact is also confirmed by the two naphthyl-substituted diketones in series B which have substantially higher ionic emission than the dibenzoylmethide chelate (14.01 and 9.12).

In series B the location of the triplet state varies over a wider range. The weak ionic fluorescence from aliphatic β -diketone chelates (AcA, TFAcA, and HFAcA) can be explained by the existence of a large gap between the resonance levels of europium ion (⁵D₁, ⁵D₀) and the triplet level of the chelates (more than 3500, 2000, and 1000 cm⁻¹, respectively).

Combinations of aromatic-aliphatic substituents on β -diketones (TTA, BTA, BA) result in an increased Eu³⁺ fluorescence, compared to the parent symmetrical aromatic (DTM, DBM) or aliphatic (HFAcA, AcA) diketone chelates. On replacing one substituent in a diaromatic β -diketone (DBM, DTM) with a CH₃ or CF₃ group (BA, BTA, TTA), the energy of the triplet state is displaced toward shorter wave lengths, further above the ⁵D₀ and ⁵D₁ levels of Eu³⁺ ion. This displacement should not increase the efficiency of the energy transfer to the ion. The strong ionic emission in asymmetrical aryl-alkyl-substituted β -diketone chelates (TTA, BA, BTA) results from an efficient energy migration to the trivalent europium ion coupled with a

high transition probability between the two excited levels 5D_0 and 5D_1 and the low-lying 7F multiplet.

The amount of energy transferred to the ion depends on substituent influence in the $S' \rightsquigarrow T$ intersystem crossing (amount of energy available at T), in the energetic location of the triplet *vs.* ionic resonance levels, and in the efficiency of transfer through the metal-oxygen bond to the ion. But the relative fluorescence intensity of the ion is the energy dissipated radiatively from the excited level, a process which competes with a nonradiative degradation process. The competition between the radiative process and quenching, probably *via* vibronic coupling to the ligands and thence to the surroundings, depends upon other factors such as temperature, solvent, energy gap, etc., which are more or less equivalent for all chelates and on the transition probabilities for the radiative process. The fluorescent lines from Eu^{3+} ion correspond to intra-4f shell "forbidden" transitions, which become more allowed, the more the internal electric field due to the particles surrounding the ion is distorted from a symmetry configuration where the ion occupies the center of symmetry. This departure from centrosymmetry (in this case O_h) is dependent on substituents and expected to be greater for unsymmetrical β -diketones. This would explain the higher relative intensity of BA, BTA, and TTA compared to DBM, DTM, AcA, and TFAC. There is no apparent reason to consider

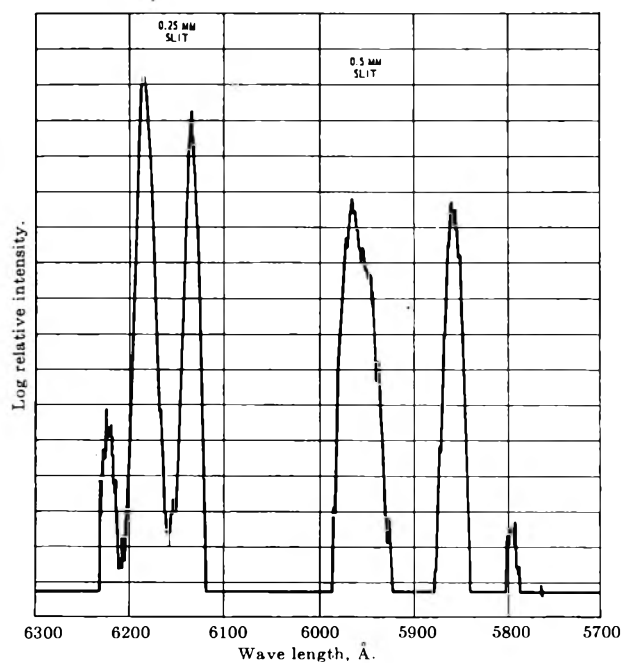


Figure 1. Fluorescence spectrum of europium tris(dibenzoylmethane) (EuDBM); $10^{-5} M$ in EPA, $77^\circ K$, 5 \AA./sec.

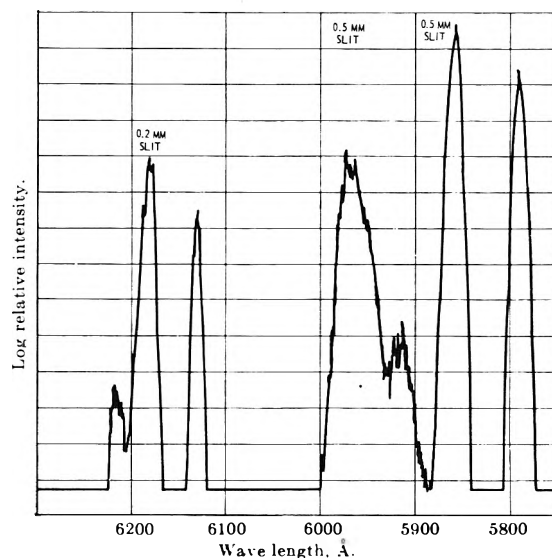


Figure 2. Fluorescence spectrum of europium tris(*p*-methoxydibenzoylmethane) (EupM); $10^{-5} M$ in EPA, $77^\circ K$, 5 \AA./sec.

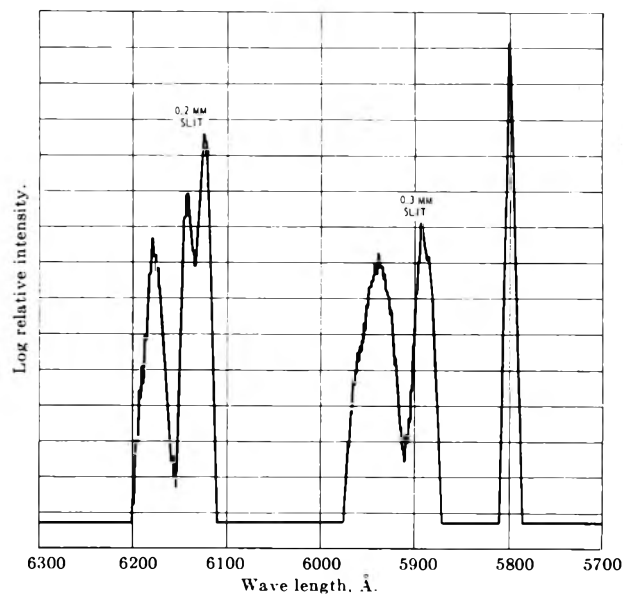


Figure 3. Fluorescence spectrum of europium tris(*di-m*-methoxydibenzoylmethane) (EuDmM); $10^{-5} M$ in EPA, $77^\circ K$, 5 \AA./sec.

that the aliphatic substituent increases the amount of energy transferred to the ion. Instead, it creates a more unsymmetrical field in combination with an aromatic substituent, thus increasing the transition probability of the radiative process in the Eu ion which competes more favorably with the nonradiative energy dissipation.

Another distinction is made here between the different europium β -diketone chelates. The "symmetrical"

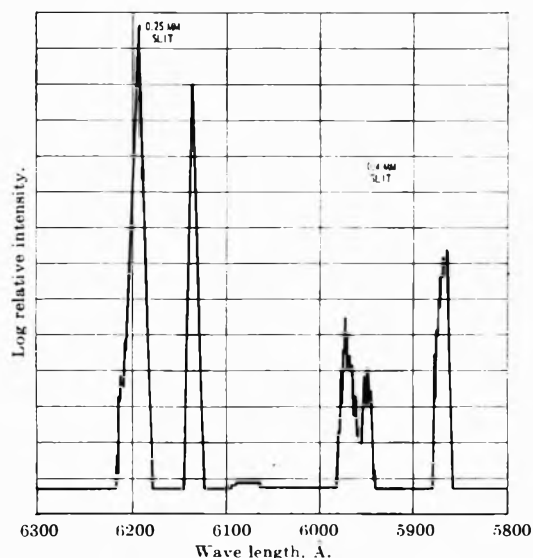


Figure 4. Fluorescence spectrum of europium tris(di-2-theonylmethane) (EuDTM); $10^{-5} M$ in EPA, $77^{\circ}K.$, 5 \AA./sec.

180° around the diketone ring-substituent bond, an identical configuration results. Group (a) includes DBM, *DpM*, *DpN*, *DpF*, *DPyM*, AcA, and HFAcA. The second group includes all the symmetrical diketones where 180° rotation of the substituent brings about a different steric configuration. Group (b) consists of *DFuM*, *DTM*, *DmM*, *DmN*, *DINM*, and *D2NM*. These chelates are the "less symmetrical" of the symmetrical β -diketones. Resonance in a β -diketone chelate involves only one substituent at a time and the chelating ring. One substituent in this group may be rotated out of the chelate ring plane and "frozen" in that position in the solid matrix at $77^{\circ}K.$ A substituent of this "less symmetrical" type would need a much larger energy to rotate back in the chelating plane compared to a phenyl, *p*-methoxyphenyl, methyl, etc. (group a). The resulting "fixed" configuration is rather unsymmetrical for the europium ion. The remaining chelates are the asymmetrical ones having two chemically different substituents attached to the

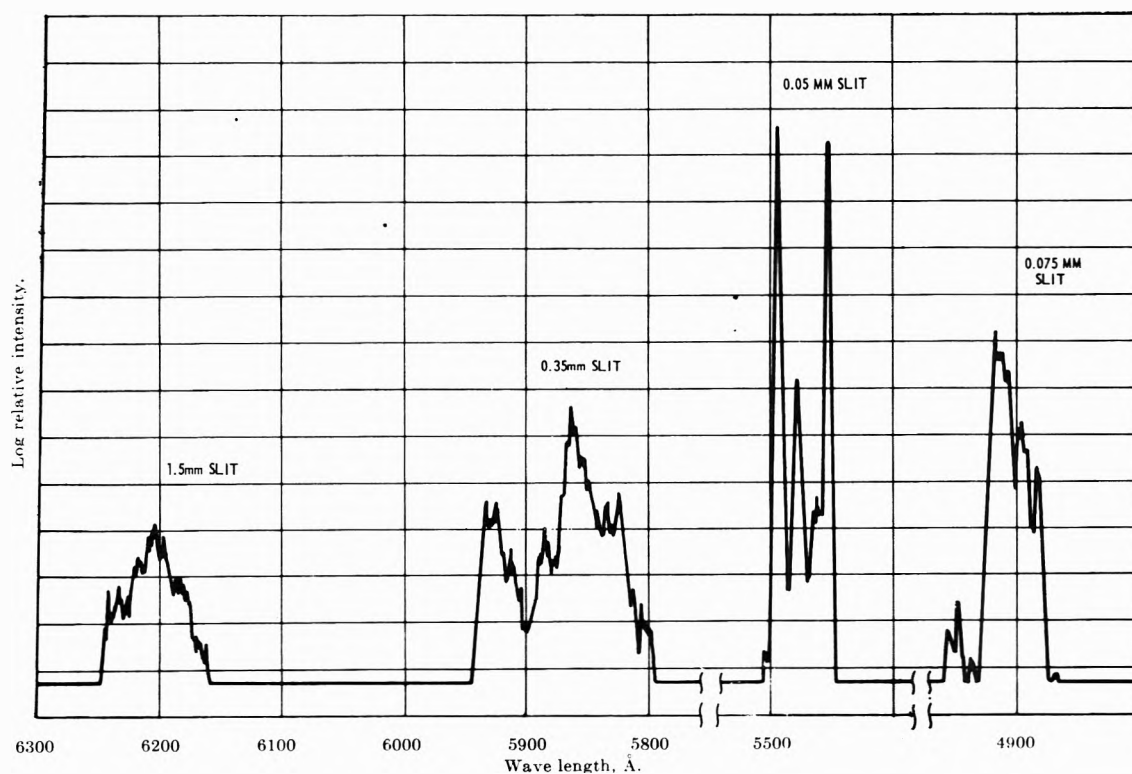


Figure 5. Fluorescence spectrum of terbium tris(dibenzoylmethane) (TbDBM); $10^{-5} M$ in EPA, $70^{\circ}K.$, 5 \AA./sec.

complexes (*DFuM*, DBM, *DTM*, *DpM*, *DmM*, *DmN*, *DpN*, *DpF*, *DINM*, *D2NM*, AcA, HFAcA, *DPyM*) are divided into two groups which behave differently spectroscopically. In the first group are considered those chelates, where on rotating a substituent by

chelating ring. Group (c) includes *pM*, *pN*, *mM*, *mN*, *pPh*, TTA, BA, BTA, and TFAcA.

An increased ionic fluorescence is observed on replacing CH_3 groups with CF_3 in the AcA, TFAcA, HFAcA series. This trend may be easily explained

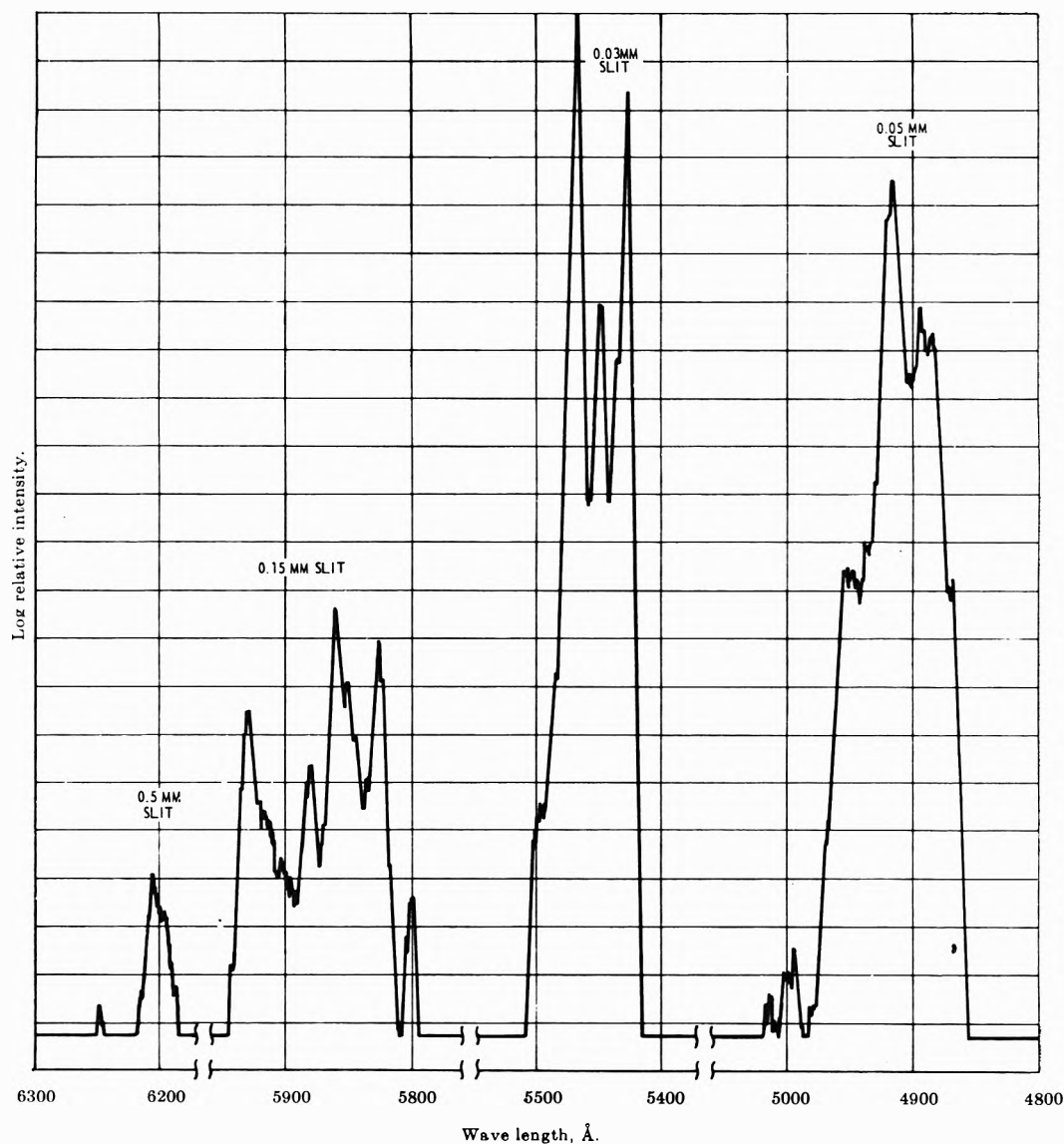


Figure 6. Fluorescence spectrum of terbium tris(di-*p*-fluorodibenzoylmethane) (TbDpF); 10^{-8} M in EPA, 77°K., 5 Å./sec.

by the lowering of the triplet state energy of the ligand, thus decreasing the gap to the 5D_1 ionic level from more than 3500 to approximately 1000 cm^{-1} . No such enhanced fluorescence is observed on replacing a methyl with a trifluoromethyl group in BA (to BTA), the triplet level being lowered by only 300 cm^{-1} .

The total fluorescence intensity in symmetrical aromatic β -diketones decreased in the following order: 1-naphthyl > 2-naphthyl > furyl > phenyl > thienyl > 4-pyridyl.

From these findings one may predict an expected relative ionic fluorescence intensity of Eu^{3+} in β -diketone chelates with different attached substituents. An alkyl substituent combined with a large aromatic

radical (naphthyl, biphenyl, phenanthryl, etc.) attached on a $\text{R-CO-CH}_2\text{-CO-R}'$ system would probably offer the combination of efficient transfer of energy to the ion and high transition probability for the radiative process, provided the triplet state has the proper location *vs.* the ionic resonance level. Both alkyl (straight chain, branched chain, haloalkyl, substituted alkyl, etc.) and aryl (aromatic mono- or polynuclear hydrocarbons, linearly linked or condensed, heterocyclic radicals, etc.) may be selected to provide the most adequate $\text{S}' \rightarrow \text{T}$ intersystem crossing, location of triplet state, and transfer to the ion. Chelates having from poor to very bright ionic fluorescence can be prepared from ligands with various substituents. The fluores-

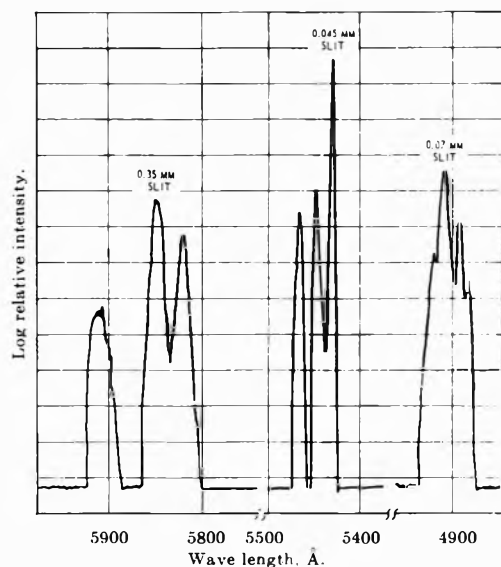


Figure 7. Fluorescence spectrum of terbium tris(benzoyltrifluoroacetate) (TbBTA); $10^{-6} M$ in EPA, $77^{\circ}K.$, 5 \AA./sec.

cence spectra of europium and terbium chelates are illustrated in Fig. 1-8⁷ and the data are listed in Tables III and IV.

Individual Lines in Eu Chelates: Splitting of Electronic Levels

The only transitions observed in the fluorescence spectra were from the two resonance levels 5D_1 and 5D_0 to the lower four levels ${}^7F_0, \dots, {}^7F_4$ of the ground multiplet. Transitions to 7F_5 and 7F_6 ($\Delta J \geq 4$) are very weak and therefore were unobserved by the phototube detector which had a limited sensitivity at wave lengths greater than 7000 \AA.

The ${}^5D_0 \rightarrow {}^7F_0$ line is singlet for all europium chelates investigated, as expected for a $J = 0 \rightarrow J = 0$ transition, unsplit by fields of any symmetry. The spectral purity of this transition is remarkable. The noncentrosymmetrical configuration in chelates allows this strictly "forbidden" transition with a high probability. In general, any change in the dibenzoylmethide structure resulted in increased relative intensity for the $0 \rightarrow 0$ line (expressed as percentage of total fluorescence).

The variation of the relative intensity of the ${}^5D_0 \rightarrow {}^7F_0$ transition in europium chelates is expressed in Table V (in % of total emission) for series A and B.

The ${}^5D_0 \rightarrow {}^7F_1$ transition terminates on a level with $J = 1$ which is unsplit in a field of O_h symmetry but splits into two levels under the perturbing field of ligands having a less symmetrical arrangement such as C_{3v} . This line, corresponding to the ${}^5D_0 \rightarrow {}^7F_1$ transition, is a singlet for all essentially symmetrical β -diketones

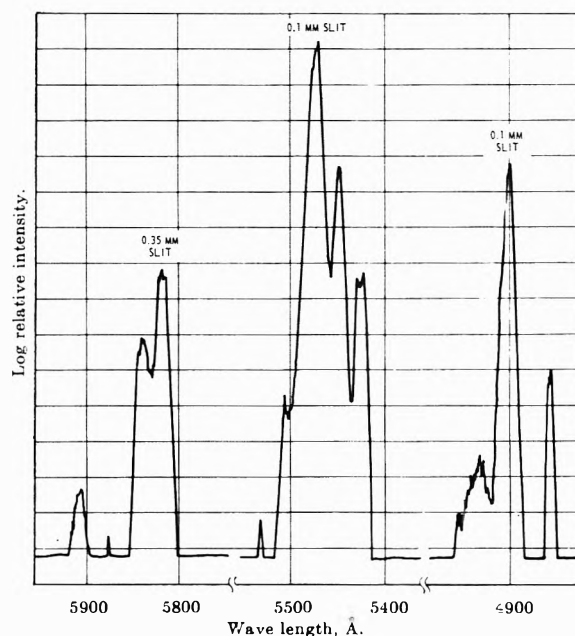
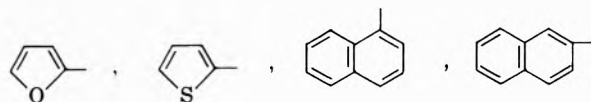


Figure 8. Fluorescence spectrum of terbium tris(trifluoroacetylacetonate) (TbTFAcA); $10^{-6} M$ in EPA, $77^{\circ}K.$, 5 \AA./sec.

and doublet for the unsymmetrical ones, even if differences in ligands are marginal, as in series A where only distant substituents are changed. This is a very significant indication that the departure from O_h symmetry is substituent dependent.

Some other information can be drawn from close examination of the ${}^5D_0 \rightarrow {}^7F_1$ lines of the chelates. The amount of splitting ($\Delta\nu$) could be taken as a qualitative measure of the distortion from centrosymmetrical O_h configuration. *para*- and *meta*-monosubstituted (CH_3O or NO_2) dibenzoylmethides have a greater splitting than asymmetrical β -diketones in series B (BA, TTA, BTA, etc.). Substituents which are not symmetrical on free rotation around the bond with the chelating ring



generate a small but distinct doublet for the ${}^5D_0 \rightarrow {}^7F_1$ transition. (This type of substituent belongs to

(7) Figures 1-4 (europium chelates) and 5-8 (terbium chelates) are illustrated in the paper. The entire collection of fluorescence spectra (44 diagrams) has been deposited as Document No. 8150 with the ADI Auxiliary Publication Project, Photoduplication Service, Library of Congress, Washington 25, D. C. A copy may be secured by citing the Document Number and by remitting \$6.25 for photoprints or \$2.50 for microfilm in advance payment by check or money order payable to: Chief, Photoduplication Service, Library of Congress.

Table III: Individual Fluorescence Lines of Europium Chelates

Europium ion transition	ν_{\max} , cm. ⁻¹	$\Delta\nu'$ at $1/2\nu_{\max}$, cm. ⁻¹	$\Delta\nu$, ^a cm. ⁻¹	λ_{\max} , ^b R.U.	Relative intensity, A.U. ^c	Percentage total emission, %	J-Level splitting, cm. ⁻¹
Europium Dibenzoylmethide $\text{Eu}(\text{C}_6\text{H}_5\text{COCHCO-C}_6\text{H}_5)_3$ (EuDBM)							
${}^5\text{D}_1 \rightarrow {}^7\text{F}_4$	16,077	48	64	$10^{1.3}$	798	63.0	99
	16,176	40	149	$10^{2.4}$	14,381		
${}^5\text{D}_0 \rightarrow {}^7\text{F}_2$	16,308	27	129	$10^{2.2}$	7,251	30.1	...
${}^5\text{D}_0 \rightarrow {}^7\text{F}_1$	16,773	81	170	$10^{1.1}$	1,046	4.3	...
${}^5\text{D}_1 \rightarrow {}^7\text{F}_3$	17,065	39	96	$10^{1.1}$	548	2.3	...
${}^5\text{D}_0 \rightarrow {}^7\text{F}_0$	17,256	33	85	$10^{0.2}$	60	0.2	...
Europium <i>p</i> -Methoxydibenzoylmethide $\text{Eu}(\text{CH}_3\text{O-C}_6\text{H}_4\text{COCHCO-C}_6\text{H}_4)_3$ (EupM)							
${}^5\text{D}_1 \rightarrow {}^7\text{F}_4$	16,090	39	83	$10^{1.8}$	2,540	72.7	83
	16,173	37	152	$10^{2.4}$	14,193		
${}^5\text{D}_0 \rightarrow {}^7\text{F}_2$	16,305	27	81	$10^{2.1}$	4,253	18.5	...
${}^5\text{D}_0 \rightarrow {}^7\text{F}_1$	16,750	95	196	$10^{0.9}$	767	4.1	153
	16,903	95	115	$10^{0.4}$	192		
${}^5\text{D}_1 \rightarrow {}^7\text{F}_3$	17,073	50	110	$10^{1.3}$	1,047	4.6	...
${}^5\text{D}_0 \rightarrow {}^7\text{F}_0$	17,277	42	110	$10^{1.2}$	769	3.3	...
Europium Di- <i>p</i> -methoxydibenzoylmethide $\text{Eu}(\text{CH}_3\text{O-C}_6\text{H}_3(\text{OCH}_3)\text{COCHCO-C}_6\text{H}_3(\text{OCH}_3))_3$ (EuDpM)							
${}^5\text{D}_1 \rightarrow {}^7\text{F}_4$	16,090	26	49	10	253	1.7	...
${}^5\text{D}_0 \rightarrow {}^7\text{F}_2$	16,292	16	84	$10^{2.7}$	14,535	96.0	...
${}^5\text{D}_0 \rightarrow {}^7\text{F}_1$	16,835	108	225	$10^{0.3}$	220	1.5	...
${}^5\text{D}_1 \rightarrow {}^7\text{F}_3$	17,036	139	174	$10^{0.01}$	45	0.3	...
${}^5\text{D}_0 \rightarrow {}^7\text{F}_0$	17,301	97	150	10^0	86	0.6	...
Europium <i>p</i> -Nitrodibenzoylmethide $\text{Eu}(\text{O}_2\text{N-C}_6\text{H}_4\text{COCHCO-C}_6\text{H}_4)_3$ (EupN)							
${}^5\text{D}_1 \rightarrow {}^7\text{F}_4$	16,064	32	49	$10^{0.8}$	178	27.4	117
	16,181	53	136	$10^{1.9}$	4,806		
${}^5\text{D}_0 \rightarrow {}^7\text{F}_2$	16,313	81	151	$10^{2.2}$	12,402	68.2	...
${}^5\text{D}_0 \rightarrow {}^7\text{F}_1$	16,736	81	87	$10^{0.7}$	312	3.1	127
	16,863	81	94	$10^{0.6}$	255		
${}^5\text{D}_1 \rightarrow {}^7\text{F}_3$	17,079	39	61	$10^{0.6}$	138	0.8	...
${}^5\text{D}_0 \rightarrow {}^7\text{F}_0$	17,241	33	41	$10^{0.6}$	85	0.5	...
Europium Di- <i>p</i> -nitrodibenzoylmethide $\text{Eu}(\text{O}_2\text{N-C}_6\text{H}_3(\text{NO}_2)\text{COCHCO-C}_6\text{H}_3(\text{NO}_2))_3$ (EuDpN)							
${}^5\text{D}_1 \rightarrow {}^7\text{F}_4$	16,181	87	173	$10^{1.3}$	1,713	57.8	...
${}^5\text{D}_0 \rightarrow {}^7\text{F}_2$	16,287	73	96	$10^{1.2}$	959	32.0	...
${}^5\text{D}_0 \rightarrow {}^7\text{F}_1$	16,793	135	208	$10^{0.13}$	161	5.4	...
${}^5\text{D}_1 \rightarrow {}^7\text{F}_3$	17,010	120	135	$10^{0.02}$	98	3.3	...
${}^5\text{D}_0 \rightarrow {}^7\text{F}_0$	17,241	55	64	$10^{0.1}$	44	1.5	...
Europium Di- <i>m</i> -methoxydibenzoylmethide $\text{Eu}(\text{C}_6\text{H}_3(\text{CH}_3\text{O})_2\text{COCHCO-C}_6\text{H}_3(\text{OCH}_3)_2)_3$ (EuDmM)							
${}^5\text{D}_1 \rightarrow {}^7\text{F}_4$	16,181	53	128	$10^{2.2}$	9,272	21.2	...
${}^5\text{D}_0 \rightarrow {}^7\text{F}_2$	16,273	48	102	$10^{2.4}$	12,434	58.7	38
	16,311	32	69	$10^{2.6}$	13,240		
${}^5\text{D}_0 \rightarrow {}^7\text{F}_1$	16,835	86	211	$10^{1.4}$	2,405	5.5	...
${}^5\text{D}_1 \rightarrow {}^7\text{F}_3$	17,001	51	107	$10^{1.8}$	2,080	4.8	...
${}^5\text{D}_0 \rightarrow {}^7\text{F}_0$	17,241	17	74	$10^{2.2}$	4,280	9.8	...

Table III (Continued)

Europium ion transition	ν_{\max} , cm. ⁻¹	$\Delta\nu'$ at $1/2\nu_{\max}$, cm. ⁻¹	$\Delta\nu$, ^a cm. ⁻¹	h_{\max} , ^b R.U.	Relative intensity A.U., ^c	Percentage total emission, %	J-Level splitting, cm. ⁻¹
Europium <i>m</i> -Methoxydibenzoylmethide $\text{Eu}(\text{C}_6\text{H}_4(\text{CH}_3\text{O})\text{COCHCO-C}_6\text{H}_5)_3$ (EumM)							
⁶ D ₁ → ⁷ F ₄	16,090	68	77	10 ^{1.7}	2,669	39.8	112
	16,155	65	74	10 ²	5,100		
	16,202	32	60	10 ²	3,100		
⁶ D ₀ → ⁷ F ₂	16,265	16	59	10 ^{2.6}	9,050	47.0	59
	16,324	30	60	10 ^{2.1}	3,780		
⁶ D ₀ → ⁷ F ₁	16,722	38	48	10 ^{0.8}	196	5.6	204
	16,892	67	76	10 ^{1.2}	832		
	16,926	54	59	10 ^{1.1}	526		
⁶ D ₁ → ⁷ F ₃	17,065	30	64	10 ^{1.1}	391	1.43	...
⁶ D ₀ → ⁷ F ₀	17,241	55	101	10 ^{1.7}	1,668	6.1	...
Europium <i>m</i> -Nitrodibenzoylmethide $\text{Eu}(\text{C}_6\text{H}_4(\text{O}_2\text{N})\text{COCHCO-C}_6\text{H}_5)_3$ (EumN)							
⁶ D ₁ → ⁷ F ₄	16,064	39	50	10 ^{0.7}	161	53.9	167
	16,132	39	52	10 ^{1.5}	1,028		
	16,171	42	54	10 ^{1.6}	1,374		
	16,231	48	50	10 ^{1.1}	460		
⁶ D ₀ → ⁷ F ₂	16,329	32	90	10 ^{1.6}	1,217	21.67	...
⁶ D ₀ → ⁷ F ₁	16,734	59	87	10 ^{0.6}	204	9.7	124
	16,858	73	127	10 ^{0.7}	343		
⁶ D ₁ → ⁷ F ₃	16,987	67	137	10 ^{0.9}	539	9.6	...
⁶ D ₀ → ⁷ F ₀	17,241	33	80	10 ^{0.9}	290	5.2	...
Europium Di- <i>m</i> -nitrodibenzoylmethide $\text{Eu}(\text{C}_6\text{H}_4(\text{O}_2\text{N})\text{COCHCO-C}_6\text{H}_4(\text{NO}_2))_3$ (EuDmN)							
⁶ D ₁ → ⁷ F ₄	16,069	53	54	10 ^{1.0}	400	60.1	154
	16,129	48	55	10 ^{1.4}	948		
	16,173	48	54	10 ^{1.6}	1,186		
	16,223	53	54	10 ^{1.3}	798		
⁶ D ₀ → ⁷ F ₂	16,329	34	89	10 ^{1.4}	986	17.8	...
⁶ D ₀ → ⁷ F ₁	16,722	73	70	10 ^{0.5}	171	7.5	130
	16,852	65	115	10 ^{0.6}	244		
⁶ D ₁ → ⁷ F ₃	16,992	65	136	10 ^{0.9}	529	9.5	...
⁶ D ₀ → ⁷ F ₀	17,235	33	80	10 ^{0.9}	290	5.2	...
Europium <i>p</i> -Phenyldibenzoylmethide $\text{Eu}(\text{C}_6\text{H}_4\text{-C}_6\text{H}_4\text{-COCHCO-C}_6\text{H}_5)_3$ (EupPh)							
⁶ D ₁ → ⁷ F ₄	16,108	34	82	10 ³	37,500	67.3	60
	16,168	53	81	10 ^{2.9}	37,138		
⁶ D ₀ → ⁷ F ₂	16,369	48	121	10 ^{2.3}	10,823	9.8	...
⁷ D ₀ → ⁷ F ₁	16,689	51	78	10 ^{1.4}	1,130	10.1	223
	16,912	51	152	10 ^{2.2}	10,064		
⁶ D ₁ → ⁷ F ₃	16,992	48	80	10 ^{1.7}	2,205	8.5	79
	17,071	33	79	10 ^{2.3}	7,252		
⁶ D ₀ → ⁷ F ₀	17,280	27	105	10 ^{0.4}	100	0.1	...
⁶ D ₀ → ⁷ F ₃	15,420	230	260	10 ⁰	180	0.2	...
⁶ D ₁ → ⁷ F ₁	18,500	138	160	10 ^{1.1}	1,373	4.0	334
	18,675	97	140	10 ^{1.3}	1,666		
	18,834	111	150	10 ^{1.2}	1,474		

Table III (Continued)

Europium ion transition	ν_{\max} , cm. ⁻¹	$\Delta\nu'$ at $1/2\nu_{\max}$, cm. ⁻¹	$\Delta\nu$, ^a cm. ⁻¹	h_{\max} , ^b R. U.	Relative intensity, A. U. ^c	Percentage total emission, %	<i>J</i> -Level splitting, cm. ⁻¹
Europium Di- <i>p</i> -fluorodibenzoylmethide $\text{Eu}(\text{F} \text{ \text{COCHCO} \text{ \text{F})_3$ (EuDpF)							
⁵ D ₁ → ⁷ F ₄	16,129	105	186	10 ^{0.8}	625	55.4	...
⁵ D ₀ → ⁷ F ₂	16,308	92	141	10 ^{0.3}	162	14.4	...
⁵ D ₀ → ⁷ F ₁	16,906	139	175	10 ^{0.1}	143	12.7	...
⁵ D ₁ → ⁷ F ₃	17,053	92	91	10 ^{0.1}	86	7.6	...
⁵ D ₀ → ⁷ F ₀	17,271	58	109	10 ^{0.3}	112	9.9	...
Europium Difuroylmethide $\text{Eu}(\text{ \text{COCHCO} \text{ })_3$ (EuDFuM)							
⁵ D ₁ → ⁷ F ₄	16,113	32	72	10 ²	3,400	36.3	53
	16,166	27	72	10 ^{2.0}	25,024		
⁵ D ₀ → ⁷ F ₂	16,279	19	60	10 ^{2.8}	15,460	31.3	45
	16,324	27	60	10 ^{2.6}	9,011		
⁵ D ₀ → ⁷ F ₁	16,773	22	68	10 ^{1.6}	1,115	3.3	62
	16,835	40	72	10 ^{1.6}	1,513		
⁵ D ₁ → ⁷ F ₃	16,992	27	71	10 ^{2.3}	6,234	8.0	...
⁵ D ₀ → ⁷ F ₀	17,241	22	90	10 ^{2.4}	8,415	10.8	...
⁵ D ₀ → ⁷ F ₃	15,372	194	300	10 ⁰	172	0.2	...
⁵ D ₁ → ⁷ F ₁	18,587	116	150	10 ^{1.6}	6,026	10.1	157
	18,744	111	150	10 ^{1.3}	1,855		
Europium Dithionylmethide $\text{Eu}(\text{ \text{COCHCO} \text{ })_3$ (EuDTM)							
⁵ D ₁ → ⁷ F ₄	16,142	16	133	10 ^{2.2}	6,538	72.8	...
⁵ D ₀ → ⁷ F ₂	16,313	13	69	10 ^{1.9}	1,887	21.0	...
⁵ D ₀ → ⁷ F ₁	16,736	40	65	10 ^{0.7}	182	3.5	171
	16,807	41	54	10 ^{0.6}	135		
⁵ D ₁ → ⁷ F ₃	17,036	32	55	10 ^{0.9}	237	2.6	...
Europium Di-1-naphthoylmethide $\text{Eu}(\text{ \text{COCHCO} \text{ })_3$ (EuD1NM)							
⁵ D ₁ → ⁷ F ₄	16,207	73	134	10 ^{2.7}	35,084	16.0	...
⁵ D ₀ → ⁷ F ₂	16,335	29	162	10 ^{3.3}	109,725	50.0	...
⁵ D ₀ → ⁷ F ₁	16,793	57	84	10 ²	4,950	13.1	90
	16,883	81	139	10 ^{2.6}	23,794		
⁵ D ₁ → ⁷ F ₃	16,978	53	95	10 ^{2.6}	15,889	7.2	...
⁵ D ₀ → ⁷ F ₀	17,241	11	90	10 ³	28,000	12.7	...
⁵ D ₀ → ⁷ F ₃	15,347	208	260	10 ⁰	169	0.1	...
⁵ D ₁ → ⁷ F ₁	18,553	81	120	10 ^{0.8}	445
	18,657	55	100	10 ^{1.1}	662	0.9	138
	18,691	55	126	10 ^{1.2}	935		

Table III (Continued)

Europium ion transition	ν_{\max} , cm. ⁻¹	$\Delta\nu'$ at $1/2\nu_{\max}$, cm. ⁻¹	$\Delta\nu$, ^a cm. ⁻¹	$h\nu_{\max}$, ^b R.U.	Relative intensity A.U., ^c	Percentage total emission, %	J-Level splitting, cm. ⁻¹
Europium Di-2-naphthoylmethide $\text{Eu}(\text{C}_{10}\text{H}_7\text{COCHCO})_3$ (EuD2NM)							
⁵ D ₁ → ⁷ F ₄	16,194	81	155	10 ^{3.1}	99,855	29.6	...
⁵ D ₀ → ⁷ F ₂	16,273	48	50	10 ^{3.1}	45,990	40.4	62
	16,300	48	50	10 ^{3.1}	45,990		
	16,335	46	50	10 ^{3.1}	44,730		
⁵ D ₀ → ⁷ F ₁	16,749	46	84	10 ^{2.5}	13,915	12.4	37
	16,821	55	80	10 ^{2.4}	11,932		
	16,886	57	90	10 ^{2.5}	16,126		
⁵ D ₁ → ⁷ F ₃	16,972	73	100	10 ^{2.2}	9,748	6.4	93
	17,065	33	83	10 ^{2.5}	11,790		
⁵ D ₀ → ⁷ F ₀	17,241	36	112	10 ^{2.9}	36,542	10.8	...
⁵ D ₀ → ⁷ F ₃	15,337	200	360	10 ^{0.02}	190	0.1	...
⁵ D ₁ → ⁷ F ₂	17,841	139	200	10 ^{0.5}	379	0.2	226
	18,067	166	200	10 ^{0.5}	422		
Europium Diisonicotylmethide $\text{Eu}(\text{N}_2\text{C}_6\text{H}_4\text{COCHCO})_3$ (EuDPyM)							
⁵ D ₁ → ⁷ F ₄	16,163	84	196	10 ^{1.3}	1,815	49.9	...
⁵ D ₀ → ⁷ F ₂	16,308	79	117	10	395	10.9	...
⁵ D ₀ → ⁷ F ₁	16,889	122	213	10 ^{0.6}	458	12.6	...
⁵ D ₁ → ⁷ F ₃	16,978	108	159	10 ^{0.7}	471	13.0	...
⁵ D ₀ → ⁷ F ₀	17,256	44	110	10	495	13.6	...
Europium Benzoylacetate $\text{Eu}(\text{C}_6\text{H}_5\text{COCHCOCH}_3)_3$ (EuBA)							
⁵ D ₁ → ⁷ F ₄	16,213	54	92	10 ^{2.6}	15,810	15.0	...
⁵ D ₀ → ⁷ F ₂	16,281	43	72	10 ^{2.9}	31,379	59.4	48
	16,329	43	72	10 ^{2.9}	31,379		
⁵ D ₀ → ⁷ F ₁	16,764	59	99	10 ^{1.8}	3,423	9.9	99
	16,863	81	120	10 ²	7,053		
⁵ D ₁ → ⁷ F ₃	16,978	54	110	10 ^{1.9}	4,329	5.0	72
	17,050	50	81	10 ^{1.3}	902		
⁵ D ₀ → ⁷ F ₀	17,241	29	94	10 ^{2.4}	9,546	9.0	...
⁵ D ₀ → ⁷ F ₃	15,347	160	160	10 ⁰	120	0.1	...
⁵ D ₁ → ⁷ F ₂	17,841	138	150	10 ⁰	106	0.2	216
	18,057	128	150	10 ⁰	139		
⁵ D ₁ → ⁷ F ₁	18,553	108	130	10 ^{1.1}	1,090	1.4	139
	18,692	108	140	10 ^{0.7}	447		
Europium Benzoyltrifluoroacetate $\text{Eu}(\text{C}_6\text{H}_5\text{COCHCOF}_2)_3$ (EuBTA)							
⁵ D ₁ → ⁷ F ₄	16,181	43	102	10 ^{2.3}	9,377	29.4	...
⁵ D ₀ → ⁷ F ₂	16,281	27	89	10 ^{2.6}	14,236	44.6	...
⁵ D ₀ → ⁷ F ₁	16,779	57	189	10 ^{1.7}	3,797	11.9	...
⁵ D ₁ → ⁷ F ₃	16,998	43	104	10 ^{1.6}	1,891	5.9	...
⁵ D ₀ → ⁷ F ₀	17,224	50	91	10 ^{0.3}	95	0.3	...
⁵ D ₁ → ⁷ F ₂	18,308	57	140	10 ^{1.4}	1,595	5.0	...
⁵ D ₁ → ⁷ F ₁	18,553	100	160	10	900	2.8	...

Table III (Continued)

Europium ion transition	ν_{\max} , cm. ⁻¹	$\Delta\nu'$ at $1/2A_{\max}$, cm. ⁻¹	$\Delta\nu$, ^a cm. ⁻¹	h_{\max} , ^b R.U.	Relative intensity, A.U. ^c	Percentage total emission, %	J-Level splitting, cm. ⁻¹
Europium Theonyltrifluoroacetate $\text{Eu}(\text{C}_5\text{H}_4\text{S})\text{COCHCOCF}_3)_3$ (EuTTA)							
$^5D_1 \rightarrow ^7F_4$	16,126	21	60	$10^{2.7}$	12,781	25.7	50
	16,176	52	71	10^3	43,750		
$^5D_0 \rightarrow ^7F_2$	16,287	30	102	$10^{3.4}$	101,736	54.5	26
	16,313	22	70	$10^{2.8}$	17,984		
$^5D_0 \rightarrow ^7F_1$	16,770	38	65	$10^{2.4}$	8,835		
	16,827	38	65	$10^{2.3}$	7,032	9.2	99
	16,869	38	65	$10^{2.1}$	4,442		
$^5D_1 \rightarrow ^7F_3$	17,007	24	94	$10^{2.7}$	17,793	8.1	...
$^5D_0 \rightarrow ^7F_0$	17,241	22	54	$10^{1.9}$	1,946	0.9	...
$^5D_0 \rightarrow ^7F_3$	15,267	179	260	$10^{0.01}$	155	0.1	...
$^5D_1 \rightarrow ^7F_1$	18,560	72	160	$10^{1.6}$	3,026	1.5	181
	18,741	54	100	$10^{0.7}$	261		
Europium Acetylacetonate $\text{Eu}(\text{CH}_3\text{COCHCOCH}_2)_3$ (EuAcA)							
$^5D_1 \rightarrow ^7F_4$ and $^5D_0 \rightarrow ^7F_2$	16,292	197	221	$10^{0.04}$	61	13.0	...
$^5D_0 \rightarrow ^7F_1$ and $^5D_1 \rightarrow ^7F_3$	16,906	240	262	$10^{0.01}$	186	39.7	...
$^5D_1 \rightarrow ^7F_2$	18,315	167	370	$10^{0.1}$	222	47.3	...
Europium Trifluoroacetylacetonate $\text{Eu}(\text{CF}_3\text{COCHCOCH}_2)_3$ (EuTFAcA)							
$^5D_1 \rightarrow ^7F_4$ and $^5D_0 \rightarrow ^7F_2$	16,179	147	194	$10^{0.1}$	171	46.1	...
$^5D_0 \rightarrow ^7F_1$ and $^5D_1 \rightarrow ^7F_3$	16,949	102	120	$10^{0.1}$	102	27.5	...
$^5D_1 \rightarrow ^7F_2$	18,298	122	356	$10^{0.2}$	98	26.4	...
Europium Hexafluoroacetylacetonate $\text{Eu}(\text{CF}_3\text{COCHCOCF}_2)_3$ (EuHFAcA)							
$^5D_1 \rightarrow ^7F_4$ and $^5D_0 \rightarrow ^7F_2$	16,228	55	158	$10^{1.2}$	1,062	40.7	...
$^5D_0 \rightarrow ^7F_1$ and $^5D_1 \rightarrow ^7F_3$	16,878	102	183	$10^{0.9}$	769	29.5	...
$^5D_1 \rightarrow ^7F_2$	17,986	166	360	$10^{0.05}$	194	17.1	312
	18,298	138	358	$10^{0.2}$	254		
$^5D_1 \rightarrow ^7F_1$	18,632	250	380	$10^{0.18}$	330	12.6	...

^a The width of the spectral range covered by the entire band. ^c Arbitrary units (recorder units \times cm.⁻¹).

^b The height of the peak on a linear scale, in (arbitrary) recorder units.

the "less symmetrical" group b). The amount of splitting ($\Delta\nu$) of the $^5D_0 \rightarrow ^7F_1$ transition varies as a function of substituents as: $pPh > mM > pM > D-2NM > DmN > pN > mN > BA > TTA > D1NM > DTM > DFuM$; unsplit: DBM, DpM, DpN, DmM, DpF; no transition: AcA, TFAC, HFAC.

The line splitting is not due to stereoisomers. The magnitude of splitting is around 100 cm.⁻¹, and the symmetrical DFuM, DTM, D1NM, D2NM, and DmN europium chelates show the same range of $^5D_0 \rightarrow ^7F_1$ line-splitting.

Expressing the relative intensity of the $^5D_0 \rightarrow ^7F_1$

Table IV: Individual Fluorescence Lines of Terbium Chelates


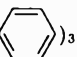
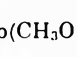
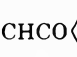
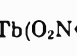
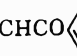
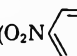
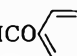
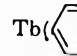
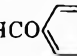
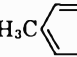
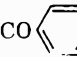
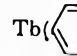
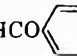
Terbium ion transition	ν_{\max} , cm. ⁻¹	λ_{\max} , R.U. ^a	$\Delta\nu$, cm. ⁻¹	Relative intensity, A.U. ^b	Percentage total emission, %	Terbium ion transition	ν_{\max} , cm. ⁻¹	λ_{\max} , R.U. ^a	$\Delta\nu$, cm. ⁻¹	Relative intensity, A.U. ^b	Percentage total emission, %
Terbium Dibenzoylmethide						Terbium Di- <i>p</i> -methoxydibenzoylmethide					
Tb( COCHCO ) ₃ (TbDBM)						Tb(CH ₃ O  COCHCO  OCH ₃) ₃ (TbDpM)					
⁵ D ₄ → ⁷ F ₆	20,539	10 ^{2.6}				⁵ D ₄ → ⁷ F ₆	20,513	10 ²			
	20,470	10 ^{3.4}					20,450	10 ^{2.1}			
	20,458 (sh) ^c	10 ^{3.4}					20,346	10 ²			
	20,442	10 ^{3.5}					20,284	10 ²			
	20,367 (sh)	10 ^{3.6}	378	238,140	26.4		20,202 (sh)	10 ^{1.7}	473	18,880	24.6
	20,346	10 ^{3.7}					20,040 (sh)	10 ^{1.1}			
	20,243	10 ^{2.5}				⁵ D ₄ → ⁷ F ₅	18,443	10 ³			
	20,202	10 ^{2.66}					18,416 (sh)	10 ^{2.7}	178	56,159	73.3
	20,161	10 ^{2.6}					18,355 (sh)	10 ^{2.1}			
⁵ D ₄ → ⁷ F ₅	18,430	10 ^{4.3}					18,298	10 ^{3.4}			
	18,382	10 ^{3.66}				⁵ D ₄ → ⁷ F ₄	17,138	10 ^{0.5}	372	1,488	1.9
	18,349	10 ^{3.9}	165	659,352	73.3		16,891	10 ^{1.3}			
	18,298	10 ^{4.4}				⁵ D ₄ → ⁷ F ₃	16,276	10 ^{0.02}	264	133	0.2
	18,265	10 ^{3.2}				Terbium <i>p</i> -Nitrodibenzoylmethide					
	17,227	10 ^{0.5}				Tb(O ₂ N  COCHCO ) ₃ (Tb _p N)					
	17,167	10 ^{0.8}					20,305	10	1,000	5,000	63.4
	17,138	10 ^{0.8}					(organic)				
	17,065	10	378	1,140	0.1		18,433 (sh)	10 ^{0.1}	100	50	0.6
	17,992	10 ^{0.7}					(organic)				
	16,920	10 ^{0.66}				⁵ D ₄ → ⁷ F ₅	18,302	10 ^{1.8}	90	2,835	36.0
	16,878	10 ^{0.8}				Terbium Di- <i>p</i> -nitrodibenzoylmethide					
	16,849	10 ^{0.8}				Tb(O ₂ N  COCHCO  NO ₂) ₃ (Tb _{Dp} N)					
⁵ D ₄ → ⁷ F ₃	16,234 (sh)	10 ⁰					20,305	10 ^{1.3}	550	5,500	67.7
	16,181 (sh)	10 ⁰					(organic)				
	16,129	10 ^{0.01}	208	104	0.01		18,433	10 ^{0.7}	250	625	7.7
	16,077 (sh)	10 ⁰					(organic)				
	16,051 (sh)	10 ⁰				⁵ D ₄ → ⁷ F ₆	18,298	10 ^{1.7}	80	2,000	24.6
	16,026 (sh)	10 ⁰				Terbium <i>m</i> -Methoxydibenzoylmethide					
Terbium <i>p</i> -Methoxydibenzoylmethide						Tb( COCHCO ) ₃ (Tb _m M)					
Tb(CH ₃ C  COCHCO ) ₃ (Tb _p M)						Tb( COCHCO ) ₃ (Tb _m M)					
							CH ₃ O				
⁵ D ₄ → ⁷ F ₆	20,534 (sh)	10 ³				⁵ D ₄ → ⁷ F ₆	20,504 (sh)	10 ^{2.7}			
	20,483	10 ^{3.6}					20,450	10 ^{3.1}			
	20,429	10 ^{3.6}					20,367	10 ^{3.1}	464	146,392	39.7
	20,354	10 ^{3.9}	606	381,780	12.5		20,284	10 ³			
	20,194	10 ^{3.2}					20,202	10 ^{2.9}			
	20,020	10 ^{2.3}					20,040 (sh)	10 ^{2.5}			
	19,928	10 ^{2.3}				⁵ D ₄ → ⁷ F ₅	18,433 (sh)	10 ^{3.5}			
⁵ D ₄ → ⁷ F ₅	18,433	10 ^{4.9}					18,382	10 ^{3.7}			
	18,399	10 ^{4.1}	135	2,667,940	87.4		18,332	10 ^{3.8}	110	219,010	59.4
	18,352	10 ^{4.3}					18,298	10 ^{4.5}			
	18,298	10 ^{6.1}					18,132	10 ^{2.5}			
⁵ D ₄ → ⁷ F ₄	17,212	10				⁵ D ₄ → ⁷ F ₄	17,135	10 ^{1.4}	372	2,975	0.8
	17,167	10 ^{1.5}					16,978	10 ^{0.9}			
	17,065	10 ^{1.6}				⁵ D ₄ → ⁷ F ₃	16,114	10 ⁰	174	87	0.02
	17,001	10 ^{1.4}	354	3,540	0.1						
	16,920 (sh)	10 ^{1.3}									
	16,892 (sh)	10 ^{1.4}									
	16,858	10 ^{1.6}									
⁵ D ₄ → ⁷ F ₃	16,116	10 ^{0.02}	190	96	0						

Table IV (Continued)

Terbium ion transition	ν_{\max} , cm. ⁻¹	λ_{\max} , R.U. ^a	$\Delta\nu$, cm. ⁻¹	Relative intensity, A.U. ^b	Percentage total emission, %	Terbium ion transition	ν_{\max} , cm. ⁻¹	λ_{\max} , R.U. ^a	$\Delta\nu$, cm. ⁻¹	Relative intensity, A.U. ^b	Percentage total emission, %
Terbium Di- <i>m</i> -methoxydibenzoylmethide						Terbium Di- <i>p</i> -fluorodibenzoylmethide					
 Tb(COCHCO) ₃ (TbDmM)						 Tb(FCOCHCO) ₃ (TbDpF)					
⁵ D ₄ → ⁷ F ₆	20,429 (sh)	10 ^{2.6}				⁵ D ₄ → ⁷ F ₆	20,429	10 ^{4.7}			
	20,395	10 ^{2.7}					20,442	10 ^{4.8}			
	20,346	10 ^{2.7}					20,346	10 ^{5.1}			
	20,305 (sh)	10 ^{2.5}	309	38,808	19.7		20,202	10 ^{4.3}	564	3,553,200	11.0
	20,202 (sh)	10 ^{2.1}					20,026	10 ^{3.6}			
	20,120 (sh)	10 ^{1.8}					20,000	10 ^{3.4}			
⁶ D ₄ → ⁷ F ₅	18,433	10 ^{3.7}				⁶ D ₄ → ⁷ F ₅	18,426	10 ^{6.1}			
	18,365 (sh)	10 ^{3.0}	168	167,580	85.1		18,399 (sh)	10 ^{5.2}			
	18,305	10 ^{3.4}					18,349	10 ^{5.6}	228	28,636,800	88.9
⁶ D ₄ → ⁷ F ₄	17,138	10 ^{0.6}	255	384	0.2		18,298	10 ^{6.6}			
	16,978	10 ^{0.4}					18,198 (sh)	10 ⁴			
⁶ D ₄ → ⁷ F ₃	16,103	10 ⁰	179	89	0.04	⁶ D ₄ → ⁷ F ₄	17,241	10 ^{1.9}			
							17,167	19 ^{2.3}			
							17,057	10 ^{2.4}			
							17,004	10 ^{2.1}	372	20,916	0.06
							16,949 (sh)	10 ^{1.8}			
							16,915 (sh)	10 ^{1.9}			
							16,869	10 ^{2.2}			
						⁶ D ₄ → ⁷ F ₃	16,116	10 ^{0.3}	181	144	0
							16,008	10 ^{0.07}			
Terbium <i>m</i> -Nitrodibenzoylmethide						Terbium Difuroylmethide					
 Tb(COCHCO) ₃ (TbmM)						 Tb(COCHCO) ₃ (TbDFuM)					
⁵ D ₄ → ⁷ F ₆	20,304	10 ^{0.7}	190	475	4.1	⁶ D ₄ → ⁷ F ₆	20,325 (sh)	10 ^{0.2}			
...	20,060	10 ^{0.7}	500	1,250	10.7		20,284 (sh)	10 ^{0.3}			
	(organic)						20,243	10 ^{0.4}			
	18,977	10 ^{0.3}	350	350	2.9		20,202	10 ^{0.6}	392	588	0.2
	(organic)						20,120 (sh)	10 ^{0.4}			
⁶ D ₄ → ⁷ F ₅	18,416	10 ^{1.5}	193	9,650	82.3		20,040 (sh)	10 ^{0.3}			
	18,305	10 ^{2.6}					20,000 (sh)	10 ^{0.2}			
Terbium Di- <i>m</i> -nitrodibenzoylmethide						Terbium Di- <i>p</i> -fluorodibenzoylmethide					
 Tb(COCHCO) ₃ (TbDmN)						 Tb(FCOCHCO) ₃ (TbDpF)					
...	20,060	10 ²	500	25,000	58.8	⁶ D ₄ → ⁷ F ₅	18,443	10 ^{3.8}			
	(organic)						18,392	10 ^{3.4}			
	18,832	10 ^{1.2}	300	2,400	5.6		18,355	10 ^{3.7}	150	375,900	99.8
	(organic)						18,298	10 ^{4.2}			
⁶ D ₄ → ⁷ F ₅	18,423	10 ^{1.8}	190	15,105	35.5						
	18,298	10 ^{2.6}									
Terbium <i>p</i> -Phenyldibenzoylmethide						Terbium Ditheonylmethide					
 Tb(COCHCO) ₃ (TbpPh)						 Tb(COCHCO) ₃ (TbDTM)					
...	19,900	10 ²	600	30,000	66.5	...	19,493	10 ^{2.3}	250	25,000	77.9
	(organic)						(organic)				
⁶ D ₄ → ⁷ F ₅	18,443	10 ^{1.8}	190	15,105	33.5	⁶ D ₄ → ⁷ F ₅	18,308	10 ^{1.8}	90	2,835	8.8
	18,298	10 ^{2.7}					18,083	10 ^{1.6}	200	4,000	12.5
							(organic)				
						⁶ D ₄ → ⁷ F ₄	17,406	10 ^{0.4}	200	252	0.8

Table IV (Continued)

Terbium ion transition	ν_{\max} , cm.^{-1}	h_{\max} , R.U. ^a	$\Delta\nu$, cm.^{-1}	Relative intensity, A.U. ^b	Percentage total emission, %	Terbium ion transition	ν_{\max} , cm.^{-1}	h_{\max} , R.U. ^a	$\Delta\nu$, cm.^{-1}	Relative intensity, A.U. ^b	Percentage total emission, %
Terbium Di-1-naphthoylmethide $\text{Tb}(\text{C}_{10}\text{H}_7\text{COCHCO})_3$ (TbD1NM)						Terbium Benzoylacetate $\text{Tb}(\text{C}_6\text{H}_5\text{COCHCOCH}_3)_3$ (TbBA)					
...	19,212	$10^{0.6}$	400	800	88.3	$^5\text{D}_4 \rightarrow ^7\text{F}_6$	20,513	10^4			
	(organic)						20,471	$10^{3.7}$			
$^5\text{D}_4 \rightarrow ^7\text{F}_5$	18,308	$10^{0.2}$	70	56	6.2		20,396 (sh)	$10^{3.1}$		433	272,160
$^5\text{D}_4 \rightarrow ^7\text{F}_4$	17,322	$10^{0.01}$	100	50	5.5		20,367	$10^{3.3}$			2.9
							20,255	10^3			
							20,202	10^3			
							20,080 (sh)	10^2			
						$^5\text{D}_4 \rightarrow ^7\text{F}_6$	18,433	$10^{4.2}$			
							18,416	$10^{4.2}$			
							18,392	$10^{3.8}$	168	1,331,400	81.6
							18,342	$10^{4.2}$			
							18,275	$10^{4.6}$			
						$^5\text{D}_4 \rightarrow ^7\text{F}_4$	17,164	10^3			
							17,123	$10^{2.6}$			
$^5\text{D}_4 \rightarrow ^7\text{F}_6$	18,298	$10^{1.7}$	75	1,850	8.1		17,079 (sh)	$10^{2.2}$			
...	18,050	10	180	900	4.0		17,036	$10^{2.2}$	364	28,938	1.8
	(organic)						16,892	$10^{1.7}$			
							16,810	$10^{1.4}$			
						$^5\text{D}_4 \rightarrow ^7\text{F}_3$	16,103 (sh)	10^0	181	91	0
							16,064	$10^{0.01}$			
Terbium Diisonicotylmethide $\text{Tb}(\text{N} \langle \text{C}_6\text{H}_4 \rangle \text{COCHCO})_3$ (TbDPM)						Terbium Benzoyltrifluoroacetate $\text{Tb}(\text{C}_6\text{H}_5\text{COCHCOCF}_3)_3$ (TbBTA)					
$^5\text{D}_4 \rightarrow ^7\text{F}_6$	20,513	10^2				$^5\text{D}_4 \rightarrow ^7\text{F}_6$	20,475	$10^{2.6}$			
	20,408	$10^{2.2}$	528	16,632	20.6		20,442	$10^{2.7}$	145	36,144	14.6
	20,202 (sh)	$10^{1.6}$					20,367	$10^{2.9}$			
	20,141	$10^{1.6}$					20,325	$10^{2.6}$			
$^5\text{D}_4 \rightarrow ^7\text{F}_5$	18,433	$10^{3.1}$	128	64,000	79.1		18,420	$10^{4.1}$			
	18,305	$10^{2.9}$				$^5\text{D}_4 \rightarrow ^7\text{F}_6$	18,365	$10^{3.7}$	70	220,850	85.6
$^5\text{D}_4 \rightarrow ^7\text{F}_4$	17,167	$10^{0.1}$					18,305	$10^{3.6}$			
	17,036 (sh)	$10^{0.01}$					17,188	$10^{1.3}$			
	16,949	$10^{0.05}$	347	174	0.2	$^5\text{D}_4 \rightarrow ^7\text{F}_4$	17,106	$10^{1.4}$	117	928	0.4
	16,915 (sh)	$10^{0.01}$					16,915	10^0			
	16,883 (sh)	10^0									
$^5\text{D}_4 \rightarrow ^7\text{F}_3$	16,155	10^0	180	90	0.1						
Terbium Theonyltrifluoroacetate $\text{Tb}(\text{C}_4\text{H}_3\text{S}\text{COCHCOCF}_3)_3$ (TbTTA)						Terbium Acetylacetonate $\text{Tb}(\text{CH}_3\text{COCHCOCH}_3)_3$ (TbAcA)					
$^5\text{D}_4 \rightarrow ^7\text{F}_6$	20,500	$10^{2.6}$				$^5\text{D}_4 \rightarrow ^7\text{F}_6$	20,513	$10^{2.6}$			
	20,442	$10^{2.7}$	187	46,686	7.7		20,367	$10^{2.6}$			
	20,362	$10^{2.9}$					20,300 (sh)	$10^{2.3}$	413	32,360	23.6
$^5\text{D}_4 \rightarrow ^7\text{F}_5$	18,416	$10^{4.3}$					20,177 (sh)	$10^{1.9}$			
	18,359	10^4	141	556,080	92.1		20,121 (sh)	$10^{1.8}$			
	18,298	$10^{3.9}$				$^5\text{D}_4 \rightarrow ^7\text{F}_5$	18,440	$10^{3.3}$			
	18,275	$10^{3.5}$					18,345 (sh)	$10^{2.9}$			
$^5\text{D}_4 \rightarrow ^7\text{F}_4$	17,182	$10^{0.9}$					18,315	$10^{3.1}$	268	106,396	76.1
	17,100	$10^{0.9}$	345	1,038	0.2		18,265 (sh)	$10^{2.9}$			
	16,929	$10^{0.6}$					18,172	$10^{2.3}$			
						$^5\text{D}_4 \rightarrow ^7\text{F}_4$	17,182	$10^{0.6}$	320	489	0.4
							16,935	$10^{0.3}$			

Table IV (Continued)

Terbium ion transition	ν_{\max} , cm. ⁻¹	h_{\max} , R. U. ^a	$\Delta\nu$, cm. ⁻¹	Relative intensity, A.U. ^b	Percentage total emission, %
Terbium Trifluoroacetylacetonate Tb(CH ₃ COCHCOCF ₃) ₃ (TbTFAcA)					
⁶ D ₄ → ⁷ F ₆	20,534	10 ^{3.6}	332	831,992	16.5
	20,408	10 ^{4.6}			
	20,284	10 ^{3.6}			
	20,202 (sh)	10 ^{3.3}			
⁵ D ₄ → ⁷ F ₅	18,433	10 ^{4.6}	366	4,220,160	83.5
	18,399	10 ^{4.5}			
	18,349	10 ^{4.8}			
	18,282	10 ^{6.2}			
	18,165	10 ⁴			
	18,067	10 ^{3.6}			
⁵ D ₄ → ⁷ F ₅	17,188	10 ^{1.2}	320	960	0.01
	17,138	10			
	17,021	10 ^{0.4}			
	16,935	10 ^{0.6}			
Terbium Hexafluoroacetylacetonate Tb(CF ₃ COCHCOCF ₃) ₃ (TbHFAcA)					
⁶ D ₄ → ⁷ F ₆	20,471	10 ⁴	229	1,145,000	30.8
	20,429	10 ^{4.1}			
	20,367 (sh)	10 ^{3.9}			
⁵ D ₄ → ⁷ F ₅	18,467	10 ^{4.4}	205	2,562,240	69.0
	18,423	10 ^{4.7}			
	18,355	10 ^{4.6}			
	18,298	10 ^{4.3}			
	18,268 (sh)	10 ^{4.1}			
⁵ D ₄ → ⁷ F ₄	17,100	10 ²	125	6,250	0.2

^a The height of the peak on a linear scale in (arbitrary) recorder units. ^b Relative intensity taken as $1/2\Delta\nu h_{\max}$ in arbitrary units (recorder units \times cm.⁻¹). The average height of a band h_{\max} is taken as $10\sum h_i/n_i$ where h_i is the height of the individual peak on the log $I = f(\nu)$ scale and n_i the number of peaks in a band. (Only the relative intensity of the strongest band is tabulated.) ^c (sh) designates shoulder.

transition as percentage of total emission, the decreasing order in the two series (A and B) is given in Table VI.

The ⁵D₀ → ⁷F₂ line is the most intense line originating from the ⁵D₀ level for all chelates. The terminating level having $J = 2$ can be split into two sublevels in a field of O_h symmetry or into three sublevels in a C_{3v} field. The recorded fluorescence spectra show singlets for the chelates investigated,⁸ except for *mM*, *DmM*, *DFuM*, *BA*, *TTA* (doublet), and *D2NM* (triplet), all belonging to the asymmetrical c group or "less symmetrical" b group.

In series A, the ⁵D₀ → ⁷F₂ transition is generally sharpened and intensified by methoxy substitution in

Table V

Series A	Series B
	DPyM (13.6)
	D1NM (12.7)
	D2NM (10.8)
	DFuM (10.8)
<i>DpF</i> (9.9)	
<i>DmM</i> (9.8)	
	BA (9.0)
<i>mM</i> (6.1)	
<i>mN</i> (5.2)	
<i>DmN</i> (5.2)	
<i>pPh</i> (4.0)	
<i>pM</i> (3.3)	
<i>DpN</i> (1.5)	
	TTA (0.9)
<i>DpM</i> (0.6)	
<i>pN</i> (0.5)	
	BTA (0.3)
<i>DBM</i> (0.2)	
	DBM (0.2)
	DTM (0.0)
	HFAcA (0.0)
	TFAcA (0.0)
	AcA (0.0)

Table VI

Series A	Series B
	D1NM (13.1)
<i>DpF</i> (12.7)	
	DPyM (12.6)
	D2NM (12.4)
	BTA (11.9)
<i>pPh</i> (10.1)	
	BA (9.9)
<i>mN</i> (9.7)	
	TTA (9.2)
<i>DmN</i> (7.5)	
<i>mM</i> (5.6)	
<i>DmM</i> (5.5)	
<i>DpN</i> (5.4)	
<i>DBM</i> (4.3)	
<i>pM</i> (4.1)	
	DBM (4.3)
	DTM (3.5)
<i>pN</i> (3.1)	
<i>DpM</i> (1.5)	
	DFuM (3.3)
	HFAcA (0.0)
	TFAcA (0.0)
	AcA (0.0)

both *para* or *meta* on dibenzoylmethane. A reverse effect (broadening and decrease in intensity) is observed on *para* or *meta* nitro substitution. If the rela-

(8) It is possible, and in some cases very probable, that further resolution of the fluorescent bands (*i.e.*, by lowering the temperature) would reveal a band structure finer than the one observed.

tive intensity of the ${}^5D_0 \rightarrow {}^7F_2$ is expressed as percentage of total emission, the europium chelates arrange as shown in Table VII.

Table VII

Series A	Series B
DpM (96.0)	
pN (68.2)	
DmM (58.7)	BA (59.4)
	TTA (54.5)
mM (47.0)	D1NM (50.0)
	BTA (44.6)
DpN (32.0)	D2NM (40.4)
DBM (30.1)	DFuM (31.3)
mN (21.7)	DBM (30.1)
	DTM (21.0)
pM (18.5)	
DmN (17.8)	
DpF (14.4)	
	DPyM (10.9)
pPh (9.8)	

No pure ${}^5D_0 \rightarrow {}^7F_2$ transition was observed for AcA, TFAcA, and HFAcA, but a broad band with λ_{\max} located somewhere between the expected wave lengths of ${}^5D_1 \rightarrow {}^7F_4$ and ${}^5D_0 \rightarrow {}^7F_2$. The band may be a resultant of the two, but the resolution of the band structure does not permit confirmation or rejection of this possibility.

Fluorescent bands corresponding to the ${}^5D_0 \rightarrow {}^7F_3$ transition were recorded for only six chelates (pPh, DFuM, D1NM, D2NM, BA, and TTA), all of low relative intensity, and no bands were observed corresponding to the ${}^5D_0 \rightarrow {}^7F_4$, ${}^5D_0 \rightarrow {}^7F_5$, or ${}^5D_0 \rightarrow {}^7F_6$ transitions.

From the fluorescent lines corresponding to transitions originating at the 5D_1 level, only those terminating at 7F_4 and 7F_3 lower levels were consistently observed. In a few cases (pPh, DFuM, D1NM, BTA, TTA, and HFAcA) one, two, or three bands were recorded in the ${}^5D_1 \rightarrow {}^7F_1$ frequency range.

The ${}^5D_1 \rightarrow {}^7F_4$ line is the most intense line originating from the 5D_1 level, for all chelates. The terminating level having $J = 4$ can be split into four sublevels in a field of O_h symmetry or into six sublevels in a C_{3v} field, whereas the 5D_1 level is unsplit in O_h and doubly split in C_{3v} symmetry. Actually not all the possible lines are observed either because the difference in energy between the sublevels is too small for the re-

solving power of the spectrophotometer to be distinguished or because they may overlap. This transition was recorded as singlet for DpM, DpN, mM, DpF, DTM, D1NM, D2NM, DPyM, BA, BTA, AcA, TFAcA, and HFAcA; doublet for DBM, pM, pN, pPh, DFuM, and TTA; triplet for DmM; and quadruplet for mN and DmN. The intensity of the ${}^5D_1 \rightarrow {}^7F_4$ transition being expressed in percentage of total intensity, the order in the two series is shown in Table VIII.

Table VIII

Series A	Series B
	DTM (72.8)
pM (72.7)	
pPh (67.3)	
DBM (63.0)	DBM (53.0)
DmN (60.1)	
DpN (57.8)	
DpF (55.4)	
mN (53.9)	
	DPyM (49.9)
	TFAcA (46.1)
	HFAcA (40.7)
mM (39.8)	
	DFuM (36.3)
	D2NM (29.6)
	BTA (29.4)
pN (27.4)	
DmM (21.2)	TTA (25.7)
	D1NM (16.0)
	BA (15.0)
	AcA (13.0)
DpM (1.7)	

The ${}^5D_1 \rightarrow {}^7F_3$ transition is weaker than ${}^5D_1 \rightarrow {}^7F_4$, but has been observed for all chelates investigated except the aliphatic diketones (AcA, TFAcA, HFAcA). The recorded line was a doublet (pPh, D2NM, and BA) or singlet (all the rest).

The relative intensity (percentage of total emission) is given in Table IX.

Line Splitting in Fluorescence Spectra on Europium Chelates

The different transitions in the europium ion are affected in different ways by changing substituents in the surrounding ligand. The number of lines resulting from the splitting of an individual transition and the magnitude of this splitting are given in Table X.

In series A, monosubstitution in *para* results in splitting of the ${}^5D_0 \rightarrow {}^7F_1$ transition into a doublet with a separation of 153 cm^{-1} for pM, 127 cm^{-1} for pN,

and 223 cm^{-1} for *pPh*, whereas the same transition for DBM and the two *para*-disubstituted *DpM* is a singlet. Similarly the $^5D_1 \rightarrow ^7F_4$ transition is a doublet for *pM* and *pN*, whereas for the disubstituted *DpM* and *DpN* it is a singlet. The $^5D_0 \rightarrow ^7F_2$ line is split into a doublet only for the two *meta*-methoxy-substituted dibenzoylmethides (*mM* and *DmM*). *pPh* is quite different (as number of lines and magnitude of splitting) compared to the other substituted dibenzoylmethides.

Line Width of Fluorescence Transitions in Europium Chelates

The line widths of the fluorescence lines are primarily dependent on the nature of the ligand, namely on the substituents attached to the β -diketone chelate ring, and not on the location of the triplet state level or the efficiency of transfer to the ion.

A similar variation is observed for the two transitions $^5D_0 \rightarrow ^7F_0$ (singlet) and $^5D_1 \rightarrow ^7F_3$ (singlet with a few exceptions). The line width decreases on *para*-phenyl substitution of dibenzoylmethide for the $^5D_0 \rightarrow ^7F_0$ line, and does not change for the $^5D_1 \rightarrow ^7F_3$ line. Significant line-broadening takes place on *para* disubstitution. The broadest $^5D_0 \rightarrow ^7F_0$ and $^5D_1 \rightarrow ^7F_3$ lines in series A are those from *DpN*, *DpF*, and *DpM*. Mononitro substitution in *para* does not change the line width of either $^5D_0 \rightarrow ^7F_0$ or $^5D_1 \rightarrow ^7F_3$ transitions, and only a small broadening is observed on *para*-monomethoxy substitution. *DmM* has the sharpest $^5D_0 \rightarrow ^7F_0$ transition in series A, whereas *mM* has the sharpest $^5D_1 \rightarrow ^7F_3$ line.

Actually, such a variation was not expected. For asymmetrical β -diketone chelates probably a mixture of stereoisomers is formed during synthesis, and due to slight differences in the molecular field of these isomers, line broadening was expected, resulting from the emission of very close different frequencies. The observed result seems to indicate that either no stereoisomers are formed, and there are no obvious reasons to sustain this supposition, or, more probably, that the internal electric fields in different stereoisomers are essentially equivalent. The $^5D_1 \rightarrow ^7F_3$ line in the aliphatic diketonates is narrower for the unsymmetrical TFACa than for the other two symmetrical AcA and HFACa. The strong $^5D_1 \rightarrow ^7F_4$ and $^5D_0 \rightarrow ^7F_2$ transitions are affected by substituents in a different way than $^5D_0 \rightarrow ^7F_0$ and $^5D_1 \rightarrow ^7F_3$. Although their line width is more difficult to analyze due to splitting, some observations can be made. *para*-Substitution of electron-withdrawing groups (*pN*, *DpN*, *DpF*) on dibenzoylmethide broadens the $^5D_1 \rightarrow ^7F_4$ and $^5D_0 \rightarrow ^7F_2$ transitions considerably, whereas methoxy (in both *para* or *meta*) or *meta*-nitro substitution does not change the line width significantly (*pM*, *DpM*, *mM*, *DmM*, *mN*, *DmN*). A continuous narrowing of this strong transition is observed for the aliphatic β -diketonates on replacing methyl with trifluoromethyl from AcA to TFACa and HFACa. This trend is probably due to a decrease of the large gap between the organic triplet and the 5D_1 level of the ion from 5000 to 4000 and 3000 cm^{-1} , respectively.

The three five-membered heterocyclic ring-substituted

Table IX

Series A	Series B
	AcA (39.7)
	HFACa (29.5)
	TFACa (27.5)
	DPyM (13.0)
<i>mN</i> (9.6)	
<i>DmN</i> (9.5)	
<i>pPh</i> (8.5)	
	TTA (8.1)
	DFuM (8.0)
<i>DpF</i> (7.6)	
	D1NM (7.2)
	D2NM (6.4)
	BTA (5.9)
	BA (5.0)
<i>DmM</i> (4.8)	
<i>pM</i> (4.6)	
<i>DpN</i> (3.3)	
	DTM (2.6)
DBM (2.3)	DBM (2.3)
<i>mM</i> (1.4)	
<i>pN</i> (0.8)	
<i>DpM</i> (0.3)	

In series B, the variations from one chelate to another are even greater.

It does not seem to be a continuous change or obvious correlation with the different substituents, even for ligands having only different distant substituents. The only similar spectra were those of *mN* and *DmN*, and the three aliphatic diketones (AcA, TFACa, HFACa). Changes in number of lines observed and magnitude of splitting are very significant on going from one chelate to another. No general rule relating the number of lines or the magnitude of splitting is obvious. On the other hand, it is very possible that some of the individual lines, components of split transitions, are overlapping or very weak compared to those observed. This would make Table X a rather incomplete basis for this discussion.

Table X: Splitting in Fluorescence Spectra of Europium Chelates. Number of Observed Lines and Magnitude of Splitting

Europium chelate	⁵ D ₁ → ⁷ F ₄		⁵ D ₀ → ⁷ F ₂		⁵ D ₀ → ⁷ F ₁		Transition ⁵ D ₁ → ⁷ F ₃		⁵ D ₁ → ⁷ F ₂		⁵ D ₁ → ⁷ F ₁		⁵ D ₀ → ⁷ F ₃		⁵ D ₀ → ⁷ F ₀	
	N.l.o. ^a	$\Delta\nu, \text{cm.}^{-1}$	N.l.o.	$\Delta\nu, \text{cm.}^{-1}$	N.l.o.	$\Delta\nu, \text{cm.}^{-1}$	N.l.o.	$\Delta\nu, \text{cm.}^{-1}$	N.l.o.	$\Delta\nu, \text{cm.}^{-1}$	N.l.o.	$\Delta\nu, \text{cm.}^{-1}$	N.l.o.	$\Delta\nu, \text{cm.}^{-1}$	N.l.o.	$\Delta\nu, \text{cm.}^{-1}$
DBM	2	99	1	...	1	...	1	...	0	...	0	...	0	...	1	...
pM	2	83	1	...	2	153	1	...	0	...	0	...	0	...	1	...
DpM	1	...	1	...	1	...	1	...	0	...	0	...	0	...	1	...
pN	2	117	1	...	2	127	1	...	0	...	0	...	0	...	1	...
DpN	1	...	1	...	1	...	1	...	0	...	0	...	0	...	1	...
mM	1	...	2	38	1	...	1	...	0	...	0	...	0	...	1	...
DmM	3	112	2	59	3	204	1	...	0	...	0	...	0	...	1	...
mN	4	167	1	...	2	124	1	...	0	...	0	...	0	...	1	...
DmN	4	154	1	...	2	130	1	...	0	...	0	...	0	...	1	...
pPh	2	60	1	...	2	223	2	79	0	...	3	334	1	...	1	...
DpF	1	...	1	...	1	...	1	...	0	...	0	...	0	...	1	...
DFuM	2	53	2	45	2	62	1	...	0	...	2	157	1	...	1	...
DTM	1	...	1	...	1	...	1	...	0	...	0	...	0	...	0	...
D1NM	1	...	1	...	2	90	1	...	0	...	3	138	1	...	1	...
D2NM	1	...	3	62	3	37	2	93	2	226	0	...	1	...	1	...
DPyM	1	...	1	...	1	...	1	...	0	...	0	...	0	...	1	...
TTA	2	50	2	26	3	99	1	...	0	...	2	181	1	...	1	...
BA	1	...	2	48	2	99	2	72	2	216	2	139	1	...	1	...
BTA	1	...	1	...	1	...	1	...	1	...	1	...	0	...	1	...
AcA	1	...	0	...	0	...	1	...	1	...	0	...	0	...	0	...
TFAcA	1	...	0	...	0	...	1	...	1	...	0	...	0	...	0	...
HFAcA	1	...	0	...	0	...	1	...	2	512	1	...	0	...	0	...

^a Number of lines observed. ^b Magnitude of splitting.

diketonates (DFuM, DTM, and TTA) have slightly sharper lines in general, compared to the others.

No direct correlations between substituents and line broadening due to superposition of oscillatory transitions on pure electronic transitions could be made.

General Considerations on Fluorescence Spectra of Terbium Chelates

Fluorescence emission was observed for all terbium chelates investigated, although in some cases the triplet state of the ligand lies below the ⁵D₄ resonance level of the ion. In such cases the ionic emission was much weaker compared to the other chelates where the organic triplet was equal to or above the ⁵D₄ level. When the ionic emission was weak, the broad-band organic phosphorescence was intense, approaching the intensity values recorded for Gd chelates.

The most intense fluorescence band was that corresponding to the ⁵D₄ → ⁷F₅ transition for all chelates. Bands associated with transitions to low-lying ⁷F levels with J = 6, 5, 4, and 3 were recorded for several complexes, but no transitions to ⁷F₂, ⁷F₁, and ⁷F₀ were observed. The fluorescence bands are highly split in numerous individual lines as expected for transitions between levels with high J number. The intensity was evaluated in arbitrary area units equivalent to the area under the curve recorded, which was

estimated as being approximately equal to 1/2 Δν h̄_{max} (Δν is the spectral range of the observed band in cm.⁻¹ and h̄_{max} is the average height of the band equal

to $\sum_{i=1}^n h_i/N$, h_i = 10^{n_i}, n_i being the height—in recorder units—of the individual lines of a band).

The total intensity of fluorescence decreased in the two series investigated as given in Table XI (total intensity expressed as arbitrary area units).

The very strong total emission of terbium ion in DpF and pM chelates (series A) could be interpreted as due to the ideal location of the 0 → 0 band of the organic triplet vs. the ⁵D₄ resonance level, that is almost the same frequency and slightly above. This would imply a very efficient transfer of energy to the metallic ion. The comparatively poor ionic emission of DBM, pN, DpN, mM, DmM, mN, DmN, and pPh chelates is primarily due to cisadvantageous location of the organic triplet, below the ⁵D₄ terbium level. It is observed that nitro substitution decreases significantly the ionic emission in both meta and (more) in para positions. Disubstitution decreases the intensity more than mononitro substitution. This effect has also been observed for europium chelates, although for terbium the triplet states lie below the emitting level of the ion. Monomethoxy substitution in both meta

Table XI

Series A		
Di- <i>p</i> -fluorodibenzoylmethide	(D <i>p</i> F)	32,211,060
<i>p</i> -Methoxydibenzoylmethide	(<i>p</i> M)	3,053,356
Dibenzoylmethide	(DBM)	898,736
<i>m</i> -Methoxydibenzoylmethide	(<i>m</i> M)	368,465
Di- <i>m</i> -methoxydibenzoylmethide	(D <i>m</i> M)	196,861
Di- <i>p</i> -methoxydibenzoylmethide	(D <i>p</i> M)	76,660
<i>p</i> -Phenyldibenzoylmethide	(<i>p</i> Ph)	15,105
Di- <i>m</i> -nitrodibenzoylmethide	(D <i>m</i> N)	15,105
<i>m</i> -Nitrodibenzoylmethide	(<i>m</i> N)	10,123
<i>p</i> -Nitrodibenzoylmethide	(<i>p</i> N)	2,835
Di- <i>p</i> -nitrodibenzoylmethide	(D <i>p</i> N)	2,000
Series B		
Trifluoroacetylacetonate	(TFAcA)	5,053,112
Hexafluoroacetylacetonate	(HFAcA)	3,713,490
Benzoylacetonate	(BA)	1,632,589
Dibenzoylmethide	(DBM)	898,736
Theonyltrifluoroacetonate	(TTA)	603,804
Difuroylmethide	(DFuM)	376,488
Benzoyltrifluoroacetonate	(BTA)	257,922
Acetylacetonate	(AcA)	139,845
Diisonicotylmethide	(DPyM)	80,896
Ditheonylmethide	(DTM)	19,000
Di-2-naphthoylmethide	(D2NM)	1,850
Di-1-naphthoylmethide	(D1NM)	56

or *para* leads to more intense fluorescence than the respective disubstitution, among other reasons being the increased asymmetry of the molecular field.

In series B, the poor ionic emitters DTM, D1NM, and D2NM chelates have the organic triplet well below the 5D_4 ionic level. It is interesting to observe that even in such situations some energy is transferred to the ion, although most of it is radiated as organic phosphorescence, which approaches the values obtained for Gd chelates. The partial transfer of energy in those cases may take place from higher triplet states formed by $T \rightarrow T'$ absorption.

The asymmetrical TFAcA is a more powerful ionic emitter than the symmetrical HFAcA, although the latter has the organic triplet closer to the 5D_4 ionic level. The other aliphatic β -diketonate (AcA) is a comparatively poor emitter justified by its large energy gap between the organic triplet and 5D_4 level. Just as for europium chelates, BA has a more intense fluorescence than BTA, probably because the trifluoromethyl group tends to increase the ionic character of the metal-oxygen bond through negative inductive effects.

The splitting of the fluorescence bands is rather extensive as expected for transitions involving levels of high J value with much overlapping between individual lines, many of which, however, are remarkably sharp.

Acknowledgment. Part of this work has been carried out at Melpar, Inc., in Falls Church, Va.

Chronopotentiometric Study of Anionic Diffusion in the Potassium-Liquid Ammonia System¹

by Roger P. Gordon and Benson Ross Sundheim

Department of Chemistry, New York University, Washington Square, New York, N. Y. 10003
(Received February 18, 1964)

A chronopotentiometric study was made of anion diffusion in solutions of potassium in liquid ammonia ranging in concentration from 0.01 to 0.1 *M* in the presence of excess KI. Diffusion coefficients for the electron of the order of 5×10^{-5} cm.² sec.⁻¹ were obtained. Measurements were also made in the absence of supporting electrolyte and led to apparent integral diffusion coefficients of the order of 5×10^{-4} cm.² sec.⁻¹. The capacitance of the double layer was determined by the "galvanostatic charging" method and found to be 65 μ f./cm.². Diffusion activation energies were calculated and found to vary both with concentration and with temperature from 2 to 7 kcal./mole.

I. Introduction

Because of the fact that metal-ammonia and metal-amine solutions occupy a unique position between electrolytic and metallic conductors, these systems are again being widely and actively investigated. The basic nature of metal-ammonia solutions seems to be well established, and, since many excellent reviews are available,²⁻⁶ no elementary description is presented here.

Conductance studies indicate that the most important charge carrier is the electron species, *e*, which carries about 87% of the total current in very dilute solutions, increasing to almost 100% in highly concentrated solutions. The mechanism by which ions, particularly electronic ions, move through the solution is of the highest interest and importance. As far as is known, no specific investigation of the anionic diffusion process in metal-amine solutions has previously been made. The theory and experimental method of chronopotentiometry are now fairly well known.^{7,8} The method appears to be admirably suited to the determination of diffusion coefficients.

II. Experimental

Scrupulous purification procedures were followed throughout. All experiments were performed in a baked, evacuated, all-glass system without stopcocks or mercury seals. Details of experimental procedures

and fuller treatment of other points may be found in the dissertation of Gordon.⁹

The circuit employed to generate constant current pulses is shown in Fig. 1. The high-speed relay is a C. P. Clare¹⁰ Type HG-1002 with mercury-wetted contacts. The cell voltage and the voltage across the standard resistors were presented on a Tektronix¹¹ Type 545A oscilloscope, using a Type CA dual-input preamplifier, and photographed as needed. The experimental cell is shown in Fig. 2 and 3. The center electrode is the probe, made by grinding the tip flat

(1) Based on a Thesis presented by R. P. Gordon to the Graduate School of Arts and Science in partial fulfillment of the requirements of the degree of Doctor of Philosophy.

(2) (a) W. L. Jolly, *Progr. Inorg. Chem.*, **1**, 235 (1959); (b) G. Lepoutre and J. F. Dewald, *J. Am. Chem. Soc.*, **76**, 3369 (1954); **78**, 2592 (1956); (c) T. P. Das, *Advan. Chem. Phys.*, **4**, 303 (1962).

(3) M. C. R. Symons, *Quart. Rev. (London)*, **13**, 99 (1959).

(4) C. A. Kraus, *J. Chem. Educ.*, **30**, 83 (1953).

(5) C. A. Kraus, *J. Franklin Inst.*, **212**, 537 (1931).

(6) L. Paoloni, *Gazz. chim. ital.*, **90**, 1682 (1960); **91**, 121, 412, 518, 529, 787, 1063 (1961).

(7) H. J. S. Sands, *Phil. Mag.*, **1**, 45 (1901) (correct equations obtained despite error in derivation).

(8) P. Delahay, "New Instrumental Methods in Electrochemistry," Interscience Publishers, Inc., New York, N. Y., 1954, and many later references on improvements and modifications.

(9) R. P. Gordon, Ph.D. Thesis, New York University, Department of Chemistry, 1963.

(10) C. P. Clare and Co., Chicago, Ill.

(11) Tektronix, Inc., Beaverton, Ore.

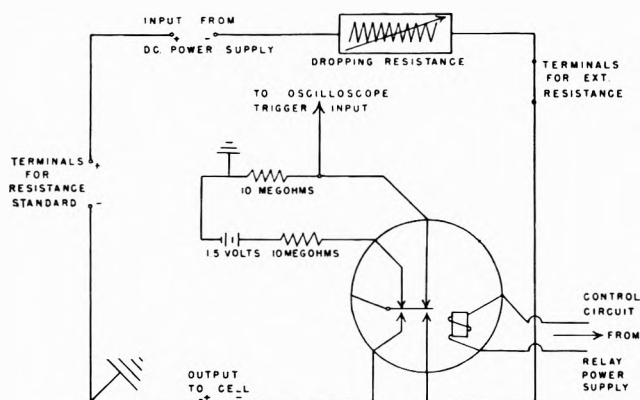


Figure 1. Constant current pulse generator for anodic chronopotentiometry.

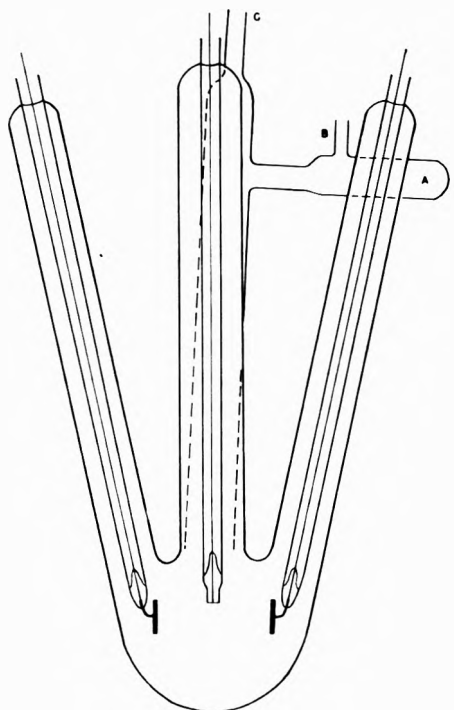


Figure 2. Cell, front view.

so that only the cross section of known area of the sealed-in platinum is exposed. The other two electrodes are heavy disks, one of which serves as the working electrode and the other as the reference. This latter is effectively an electron electrode.¹² Details of the electrodes are shown in Fig. 4.

A series of capillary tubes holding carefully purified potassium metal was lowered into arm D of the cell (Fig. 2, 3). Thoroughly dried KI was weighed into A through B. Liquid ammonia was distilled into the cell from a thermostated buret.

To initiate a cycle of measurements, the thermostated cell was tilted to introduce the KI, and a mag-

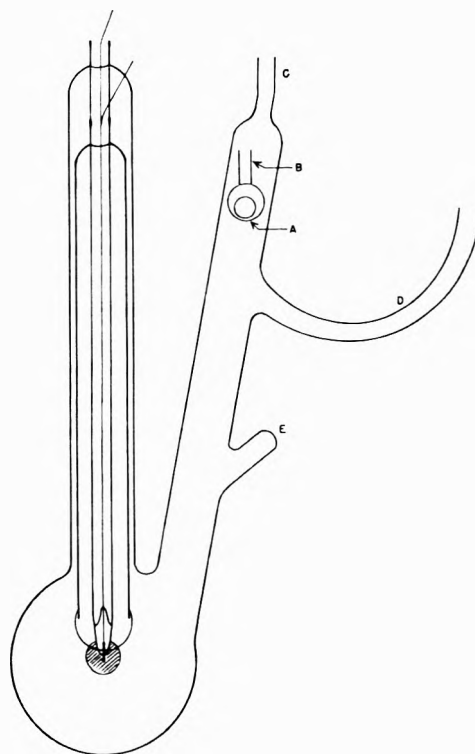


Figure 3. Cell, side view.

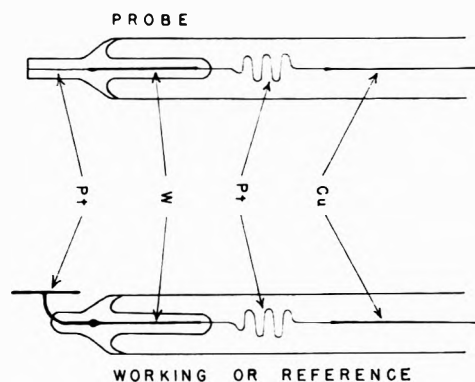


Figure 4. Electrode detail.

netic plunger was operated to drop the first of the potassium capsules into the liquid ammonia. Chronopotentiograms were run at a series of temperatures. The next potassium capsule dropped into the solution, and another set of chronopotentiograms was obtained at the prescribed temperatures. Three or more concentrations were ordinarily studied in a given experiment.

III. Results

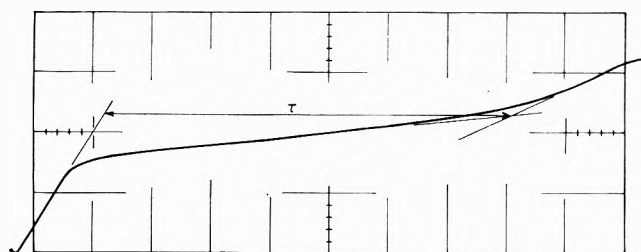
In each experiment a chronopotentiometric wave was located which started from zero potential (neglect-

(12) D. J. G. Ives and G. J. Janz, Eds., "Reference Electrodes," Academic Press, New York, N. Y., and London, 1961, p. 456.

ing internal resistance drop and capacitor voltage). The $i_0\tau^{1/2}$ product followed the changes in the potassium concentration quite closely, although not exactly. On this base the wave is taken to be due to the oxidation of the electron species in liquid ammonia solution.

A chronopotentiogram typical of the better-shaped curves is shown in Fig. 5, which also illustrates the graphical construction employed to locate the transition time. While this method is arbitrary,^{13,14} it has been recommended¹³ as reasonably consistent and in agreement with other electrochemical methods.

Since the electrodes were unshielded and were located as shown in Fig. 2, the transition time constant (TTC) varied with i .¹⁵ This variation is shown in Fig. 6. The shape of these curves seems typical of those found in aqueous investigations.¹⁵ However, the rise of the TTC past the minimum is unusually rapid. This is apparently due to the remarkable density difference between pure ammonia and metal-ammonia solutions¹⁶ and to the fact that the viscosity



VERTICAL AXIS: 1 VOLT / MAJOR DIVISION
HORIZONTAL AXIS: 2 MSEC / MAJOR DIVISION

Figure 5. Typical chronopotentiogram. The initial rise is due, in part, to a combination of internal resistance drop and capacitive charging. The placement of the electrode was not ideal.

of liquid ammonia is an order of magnitude lower than that of water. Comparison of the curves of Fig. 6 rules out an explanation based on a preliminary slow dissociation since the transition time increases with concentration. From Fig. 6 it is seen that the current should be adjusted so as to give transition times close to 16 msec.

This choice may not adequately allow for double-layer charging.¹⁷ It is possible that a systematic error is introduced in D by this procedure. Errors of this sort are not important in the conclusions drawn in the discussion.

The data were interpreted by means of the Sands equation

$$i_0\tau^{1/2} = \frac{1}{2}\pi^{1/2}n\mathfrak{F}D_0^{1/2}C^0 \quad (1)$$

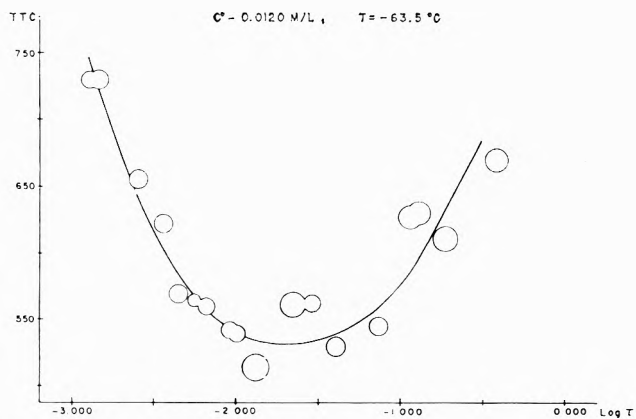


Figure 6a. Plot of TTC vs. $\log \tau$.

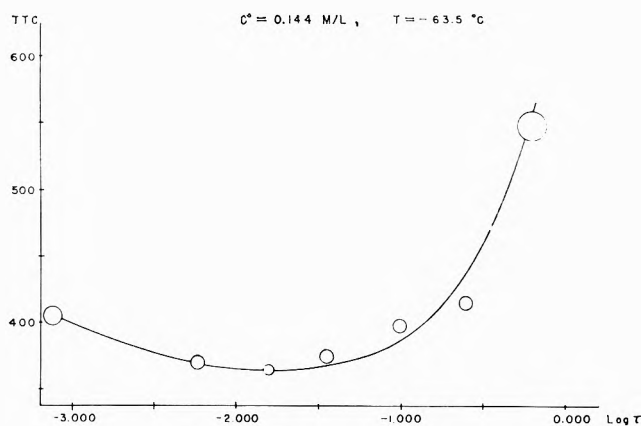


Figure 6b. Plot of TTC vs. $\log \tau$.

where i_0 is the current density, τ the transition time, n the number of electrons transferred in the electrode reaction, \mathfrak{F} the faraday, D_0 the diffusion coefficient, and C^0 the bulk concentration of the species reacting at the electrode. All results obtained with potassium-ammonia solutions containing excess potassium iodide are presented in Table I. The first entry in the table is doubtful, as it was obtained in an early exploratory experiment.

Further data in the low concentration region were unobtainable because of an unfortunate circumstance: as the concentration becomes lower and the temperature higher, the shape of the latter part of the $E-t$ curve changes in such a way as to prevent reliable determinations of the transition time. This was the case with those entries marked *b* in Table I. This

(13) W. H. Reinmuth, *Anal. Chem.*, **33**, 485 (1961).

(14) P. Delaunay and G. Mamantov, *ibid.*, **27**, 487 (1955).

(15) A. J. Bard, *ibid.*, **33**, 11 (1961).

(16) E. C. Evers and A. M. Filbert, *J. Am. Chem. Soc.*, **83**, 3337 (1961).

(17) (a) S. V. Tatwawade and A. J. Bard, *Anal. Chem.*, **36**, 2 (1964).

(b) H. A. Laitinen and L. M. Chambers, *ibid.*, **36**, 5 (1964).

Table I: Integral Diffusion Coefficients of Electron Species in Potassium-Ammonia Solutions Containing Excess KI

D_0 , cm. ² /sec.	C^0 , mole/l.	Temp., °C.	(KI), moles/l.
13.0×10^{-5a}	0.00834	-63.5	0.562
4.76×10^{-6}	0.00965	-63.5	1.66
6.64×10^{-5b}	0.00965	-45.2	1.66
7.06×10^{-5b}	0.00965	-36	1.66
3.87×10^{-5}	0.0120	-63.5	0.578
2.26×10^{-6}	0.0668	-63.5	1.66
3.56×10^{-6}	0.0668	-45.2	1.66
4.34×10^{-6}	0.0668	-36	1.66
1.82×10^{-6}	0.144	-63.5	1.66
3.16×10^{-6}	0.144	-45.2	1.66
3.54×10^{-6}	0.144	-36	1.66

^a Unreliable value (see text). ^b Estimated from $t_{1/4}$ (see text).

effect is also known to occur in aqueous chronopotentiometry and polarography.¹⁸ Evidence has been obtained which indicates that the change in shape may be due, at least in part, to the influence of electrode geometry. The differential method has been shown¹⁸ to be of value in coping with this situation. If the early part of the curve still remains near to the theoretical shape, the readily-derived equation

$$D_0^{1/2} = \left[\frac{RT}{nF} \left(\frac{dE}{dt} \right)_t^{-1} + 2t \right] (C^0 n \bar{v} \pi^{1/2} t^{1/2} / i_0)^{-1} \quad (2)$$

may be used in place of eq. 1. However, in the present investigation the values marked "b" were obtained from estimates of the quarter-time point. They must thus be regarded as somewhat uncertain.

Further progress into the high concentration region was blocked by problems of phase separations.¹⁹

In considering measures of precision, it is necessary to estimate the errors involved in determining current density, transition time, and concentration. Employing the usual techniques,²⁰ we find that the precision of the diffusion coefficients in Table I is approximately 2.4%, except as noted above.

Efforts were made to obtain chronopotentiograms with pure potassium-ammonia solutions (no KI). Diffusion coefficients obtained in this way refer to the electrolyte as a whole. A transport number factor, $(1 - \eta)$, where η is the transport number of the species reacting at the electrode, multiplies the left side of eq. 1. The necessary transport numbers were interpolated from the data of Dye, *et al.*²¹ The computed results are shown in Table II.

The reproducibility of these data was not very good; the precision was approximately $\pm 10\%$, due probably to the disturbing effects of Joulean heating. At the

Table II: Integral Diffusion Coefficients Obtained in Pure Potassium-Ammonia Solutions

D_0 , cm. ² /sec.	C^0 , mole/l.	Temp., °C.
0.774×10^{-5}	0.0809	-63.5
1.28×10^{-5}	0.0809	-45.2
1.12×10^{-5}	0.0809	-36
0.350×10^{-5}	0.164	-63.5
0.603×10^{-5}	0.164	-45.2
0.661×10^{-5}	0.164	-36

higher concentrations, the latter part of the chronopotentiograms appeared to show the onset of boiling. Approximate calculations show that a temperature rise on the order of 30° is possible at the end of the transition region in experiments employing the highest current densities.

The "galvanostatic charging" method²² was used to evaluate the double layer capacity, using the relation

$$C = i \left(\frac{dE}{dt} \right)_{t \rightarrow 0}^{-1} \quad (3)$$

The results are shown in Table III. They are, in es-

Table III: Double Layer Capacitances^a

C^0 , mole/l.	Temp., °C.	C_{dl} , f./cm. ²
0.00834	-63.5	64.6
0.00834	-45.2	35.6
0.01524	-45.2	68.5
0.01524	-36	62.8

^a Concentration of KI was 0.562 M; current density ranged from 1.2 to 4.8 amp./cm.²

sence, zero-voltage differential capacitances of the platinum-ammoniacal solution interface. The data showed a scatter of about 10%. The value of 35.6 $\mu\text{f./cm.}^2$ is apparently anomalous but cannot be discarded.

After the cell was filled with ammonia and sealed, it was kept immersed in a Dry Ice-acetone bath until needed. After some time, the ammonia would be partially solid and partially liquid, indicating that it was just at its melting point of -77.7°. At this tem-

(18) R. T. Iwamoto, *Anal. Chem.*, **31**, 1062 (1959).

(19) D. D. Cubicciotti, *J. Phys. Colloid Chem.*, **53**, 1302 (1949).

(20) O. F. Steinbach and C. V. King, "Experiments in Physical Chemistry," American Book Co., New York, N. Y., 1950, pp. 1-10.

(21) J. L. Dye, R. F. Sankuer, and G. E. Smith, *J. Am. Chem. Soc.*, **82**, 4797 (1960).

(22) W. Mehl and J. O'M. Bockris, *Can. J. Chem.*, **37**, 190 (1950).

perature, the vapor pressure of ammonia is 45 torr.²³ It was observed that the potassium in arm D (Fig. 2) would, in the course of several days, extrude from its tube, appearing somewhat spongy, but having a clean surface. The ammonia also penetrated into the tube, as shown by the changes which could be seen through the wall. The rate at which the ammonia moved through the solid potassium (at room temperature) was estimated at about 2.5 mm./day. The preceding is in accord with the observation of Kraus,²⁴ who noted that ammonia dissolved in liquid Na-K alloy and reacted slowly with it, forming amides and hydrogen. The phenomenon appears comparable to the diffusion of hydrogen through palladium and merits further investigation.

IV. Computations and Discussions

The most important source of inaccuracy in the calculated quantities is the inapplicability of eq. 1, which was derived directly from Fick's second law, which contains the assumption that D is a constant over the entire concentration range. Since the present values, which may be termed "chronopotentiometric integral diffusion coefficients," vary by several hundred per cent over the concentration range, the analysis should be based on the form of Fick's law which includes the concentration dependence of D . The problem would require the solution of

$$\frac{\partial^2 C(x,t)}{\partial x^2} - \frac{1}{D(C)} \frac{\partial C(x,t)}{\partial t} + \frac{1}{D(C)} \frac{\partial D(C)}{\partial C} \left(\frac{\partial C(x,t)}{\partial x} \right) = 0 \quad (4)$$

where $D(C)$ is the true differential coefficient, an *a priori* unknown function, subject to the boundary conditions

$$\left(\frac{\partial C(x,t)}{\partial x} \right)_{x=0} = i/(nF)D(C) = \text{constant} \quad (5)$$

and

$$C(x,t) \rightarrow C^0 \text{ as } x \rightarrow \infty \quad (6)$$

Since this problem is too formidable for analytic solution and since the accuracy and precision of the data do not justify computer solution, we restrict ourselves to the following comments. The initial buildup of the gradient on application of a current pulse will be almost independent of $D(C^0)$ until mass transport by diffusion becomes important. Thus, eq. 1 tends to emphasize the low-concentration differential diffusion coefficients over the high-concentration coefficients in producing the measured "chrono-

potentiometric integral diffusion coefficients." This effect will, of course, become less important at low bulk concentrations, C^0 .

Considering the figures of Table I, it is likely that the values of D at the lowest concentrations are nearly correct, though possibly somewhat too large. The correct values for the two highest concentrations are probably much lower than the tabulated values. However, the bias will always be upward, and at each concentration, the percentage increase will be nearly the same at each temperature (see below).

We assume that the diffusion coefficients vary with temperature according to the usual equation

$$D = A \exp(-Q/RT) \quad (7)$$

The general pattern can be seen in Fig. 7. The important features are as follows: the diffusion coefficients at a given temperature fall off as the concentration

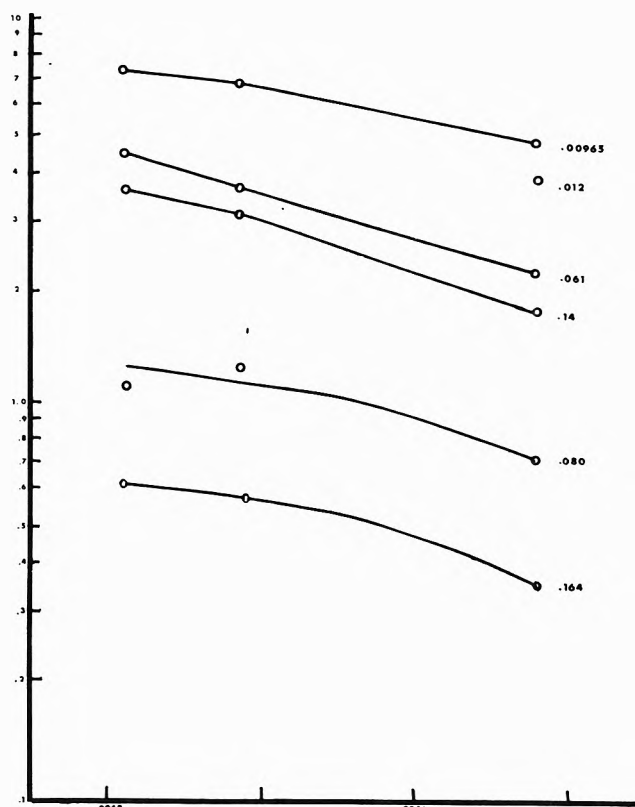


Figure 7. Observed diffusion coefficient $\times 10^5$ (abscissa) as a function of $1/T^\circ\text{C}$. (ordinate). The top three curves refer to experiments made in the presence of supporting electrolytes; the bottom two, in the absence of supporting electrolytes. The numbers near the curves refer to the concentrations of the alkali metal.

(23) G. A. Burrell and I. W. Robertson, *J. Am. Chem. Soc.*, **37**, 2482 (1915).

(24) C. A. Kraus, *ibid.*, **43**, 749 (1921).

rises, both for the electron and the neutral combination; the diffusion coefficient of the electron is about five times larger than that of the metal at near 0.15 *M*; the heats of activation are rather similar, being somewhat lower for the electron in the most dilute solutions and all decreasing with increasing temperature. Approximate values of the heats of activation are given in Table IV. It should be noted that these

Table IV: Average Diffusion Activation Energies

C°, mole/l.	Activation energy, cal.	
	237.2–228.0° K.	228.0–209.7° K.
0.00965	2129	5418
0.0668	2331	7266
0.144	1325	8866

are rather insensitive to systematic errors in the diffusion coefficients.

Comparisons with conductivity data must be made with caution. In the infinitely dilute solution, the Nernst–Einstein limiting relation may be used.

$$D_{NE}^0 = RT\lambda^0/|z|\mathfrak{F}^2 \quad (8)$$

Here λ^0 and z are the limiting equivalent conductance and the valence, respectively, of the given ion. Adjusting the data of Dye, *et al.*,²¹ to -36° , we have $\lambda^0 = 824 \text{ cm.}^2 \text{ ohm}^{-1} \text{ equiv.}^{-1}$. From eq. 8, $D_{NE}^0 = 17.4 \times 10^{-5} \text{ cm.}^2/\text{sec.}$ However, this refers to pure ammonia as solvent, while we wish to compare it with a value obtained in 0.6 *M* KI solution. To a first approximation, the necessary correction is the viscosity ratio. Apparently no measurements have been made for NH_3 -KI solutions.

The theoretical and experimental variation of diffusion coefficients with concentration is well known. At very low concentrations all systems approach the Onsager–Fuoss limiting law²⁶

$$D = D^0 - S_D\sqrt{C} \quad (9)$$

When the present data were plotted in accordance with eq. 9 and a long extrapolation made to infinite dilutions, it was found that D^0 at -36° is approximately $14.5 \times 10^{-5} \text{ cm.}^2/\text{sec.}$ Thus, assuming a reasonable value for the viscosity ratio, we conclude that the experimental value found here is in satisfactory agreement with the computed Nernst–Einstein value.

The magnitude of the diffusion coefficient for the electron compared with that for the neutral combination indicates that, although the electron is the more mobile species, its mobility and, hence, probably its mechanism of diffusion are not essentially different from that of the slower partner. Similarly, the activation energies for diffusion are not greatly different for the electron and the neutral combination. A conduction band as proposed^{2a,b} for concentrated solutions, about 0.83 e.v. above the level of an electron bound in an e_1 cavity, implies a temperature coefficient of conductance of diffusion of 15–20%. The value observed for conductance is about 2%, and that found here for diffusion is about 2.3% at 0.07 *M*. Thus, there is no evidence for the unusual mode of transport suggested for concentrated solutions.^{2a,b} It is not clear whether the tunneling mechanism^{2b} described by Dewald and Lepoutre would have an activation energy at all. The results of this work support the view that the electron in dilute solution shows no evidence of unique transport properties.

Acknowledgment. We are pleased to acknowledge support from the Office of Naval Research (Contract Nonr-285-37) and the U. S. Atomic Energy Commission (Contract AT-30-1-1837).

(25) H. S. Harned and B. B. Owen, "The Physical Chemistry of Electrolytic Solutions," Reinhold Publishing Corp., New York, N. Y., 1950, p. 179.

Heats of Formation of Some Hexavalent Uranium Compounds

by E. H. P. Cordfunke

Reactor Centrum Nederland, Petten, The Netherlands (Received May 13, 1964)

The heat of formation of the UO_2^{2+} ion was determined by measuring the heat of solution of $\gamma\text{-UO}_3$ in nitric acid calorimetrically. From the known heat of formation of $\gamma\text{-UO}_3$, the heat of formation of the UO_2^{2+} ion in 6 *N* HNO_3 was found to be: $-\Delta H_{298} = 242.2 \pm 1.0$ kcal./mole. This value was used for the determination of the heats of formation of the modifications of UO_3 , the hydrates of UO_3 , the hydrates of uranyl nitrate, and the uranates of ammonium by heat of solution measurements in nitric acid.

Uranium trioxide is known to exist in at least five crystalline modifications and an amorphous form. Recent studies by Hoekstra and Siegel¹ have shown the complexity of this system. As most of the thermochemical data of UO_3 are prior to 1920, little characterization of the materials used was possible. Moreover, new compounds in these systems have been found since. Apparent inconsistencies in the data available, as pointed out by Rand² and by Rand and Kubaschewski,³ and the absence of some essential data, have made it worthwhile to determine the heat of formation of the phases in the above-mentioned systems. The results obtained are presented in this paper.

Experimental

The Calorimeter. A constant-temperature-environment calorimeter was used for the determination of the heats of solution. The calorimeter consisted of a dewar vessel, placed in a well-stirred, thermostated water bath, the temperature of which was fixed at $25.0 \pm 0.1^\circ$.

The dewar vessel was closed with a Perspex stopper (covered with a brass cap), through which a Ni-Cr heating element, a stirrer, a calibrated Beckmann thermometer (provided with a lens), and a thin-walled glass tube, containing the sample, were fitted. For further details we refer to a similar apparatus described by Skinner.⁴

When starting the experiments, the bath and the calorimeter were heated to the required temperatures, the latter being lower in temperature than the former by about half the expected temperature change in the calorimeter. The measurements were started when

a stationary condition was reached, which required 1 to 2 hr.

The heats of solution of the uranium compounds were determined by dissolving 2.000 g. of UO_3 (or equivalent molar amounts for the other compounds) in 200 ml. of 6.0 *N* nitric acid. The measurements were carried out at least in triplicate. All samples investigated dissolved in less than 10 min., which is sufficiently fast for the heats of solution to be measured with good accuracy. The energy equivalent of the system was determined by electrical heating, the current being measured by the potential drop across a standard resistance with a potentiometer. The calorimetric quantities are expressed in terms of the defined calorie, which is equal to 4.1840 absolute joules. In the case of uranium trioxide, a series of 15 determinations of the energy equivalent gave a value of 197.1 ± 0.4 cal./deg., the uncertainty being twice the standard deviation of the mean.

The absolute reliability of the calorimeter was tested by the determination of the heat of solution of potassium chloride in water. The value found, $-\Delta H_{298} = -4.18$ kcal./mole ($7 \times 10^{-4} M$), is in good agreement with data from literature, extrapolated to the same dilution.⁵

(1) H. R. Hoekstra and S. Siegel, *J. Inorg. Nucl. Chem.*, **18**, 154 (1961).

(2) M. H. Rand, Proceedings, Symposium on Thermodynamics of Nuclear Materials, International Atomic Energy Agency, Vienna, 1962, p. 71.

(3) M. H. Rand and O. Kubaschewski, "The Thermochemical Properties of Uranium Compounds," Oliver and Boyd, Ltd., Edinburgh and London, 1963, p. 36.

(4) H. A. Skinner, Ed., "Experimental Thermochemistry," Vol. II, Interscience Publishers, Inc., New York, N. Y., 1952, p. 189.

Materials. The samples used were carefully prepared in order to obtain a high purity and a sufficient crystallinity. The purity was determined both by chemical analysis (ignition to U_3O_8 at 800°) and by X-ray analysis. A high degree of crystallinity of the samples was ensured by prolonged heating in order to avoid corrections for the heat of crystallization. In some cases (*e.g.*, β - UO_3 prepared by decomposition of ammonium uranate at 500°) heating times of about 1 month were used.

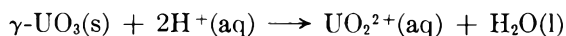
The polymorphic modifications of UO_3 were, in general, prepared as described by Hockstra and Siegel,¹ with the exception of α - UO_3 , the preparation of which was reported recently.⁶ The preparation of the hydrates of UO_3 and of the uranates of ammonium has also been described elsewhere.^{7,8}

The hydrates of uranyl nitrate were prepared as follows. $UO_2(NO_3)_2 \cdot 6H_2O$ (Merck, p.a.) was recrystallized from water several times and then placed over 40% H_2SO_4 until a constant water content was obtained. Chemical analysis (with oxine) showed it to be of the correct composition. The trihydrate was prepared by recrystallization from a saturated solution of uranyl nitrate, which is about 20 *N* with respect to HNO_3 . This hydrate was kept over 70% H_2SO_4 according to the data given by Vdovenko, *et al.*⁹

Results

Heat of Formation of the Uranyl Ion. The heat of formation of the uranyl ion was determined by Fontana¹⁰ in 0.5 *M* $HClO_4$. Recalculation of this data by Rand² gave a value of $-\Delta H_{298} = 250$ kcal./mole. Rand and Kubaschewski,³ however, have shown that this value leads to inconsistencies in the data for the heats of formation of several uranium compounds. These authors suggest that the value for the uranyl ion may be too positive by about 6 kcal./mole. We have determined the heat of formation of γ - UO_3 by dissociation pressure measurements.¹¹ Using the known heat capacity of γ - UO_3 , the heat of formation of γ - UO_3 at room temperature was calculated to be: $-\Delta H_{298} = 293.5 \pm 1.0$ kcal./mole. This value is in good agreement with the value ($-\Delta H_{298} = 293.0$ kcal./mole) suggested by Rand and Kubaschewski.³

Samples of γ - UO_3 of a high crystallinity were used for the determination of the heat of solution in 6 *N* HNO_3 . A series of three different samples of γ - UO_3 (Table I) gave an average value of $-\Delta H_{298} = 17.04 \pm 0.03$ kcal./mole for the reaction



Using the heat of formation of $H_2O(l)$, $-\Delta H_{298} = 68.32$ kcal./mole, the heat of formation of the UO_2^{2+}

Table I: Heat of Solution of γ - UO_3

Wt. of γ - UO_3 , g.	Purity, wt. % UO_3	Δt , $^\circ C$.	Heat of soln., ^a kcal./mole
1.99975	99.51	0.601	17.03
2.00060	99.51	0.600	17.00
1.99955	99.66	0.602	17.04
1.99965	99.66	0.600	16.98
2.00000	99.49	0.603	17.09
1.99970	99.49	0.602	17.06
2.00005	99.49	0.603	17.09
Mean:			17.04 ± 0.03

^a Energy equivalent of the calorimeter system, 197.1 ± 0.4 cal./deg.

ion in 6 *N* HNO_3 was found to be $-\Delta H_{298} = 242.2 \pm 1.0$ kcal./mole. It is evident that this value is only a formal one, as part of the uranyl ions is present in the form of uranyl nitrate complexes. For this reason, the value given may strictly only be used for the same UO_2^{2+} and HNO_3 concentrations.

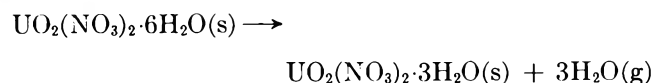
The heats of solution of $UO_2(NO_3)_2 \cdot 6H_2O$ and of $UO_2(NO_3)_2 \cdot 3H_2O$ in 6 *N* HNO_3 have been determined (Table II) also. From the results obtained, the heat of

Table II: Heats of Formation of Uranyl Nitrate

Substance	Heat of solution in 6 <i>N</i> HNO_3 ($-\Delta H_{298}$), kcal./mole	Heat of formation ($-\Delta H_{298}$), kcal./mole	
		Present investigation	Literature
$UO_2^{2+}(aq)$		242.2	250 ^a
$UO_2(NO_3)_2(aq)$...	342.8 ^a
$UO_2(NO_3)_2 \cdot 6H_2O$	-9.53	762.3	764.3 ^b
			759 ± 3^a
$UO_2(NO_3)_2 \cdot 3H_2O$	-2.75	550.5	552.3 ^b
			547 ^a

^a See ref. 3. ^b W. M. Latimer, "Oxidation Potentials," Prentice-Hall, Inc., New York, N. Y., 1952.

transition of the equilibrium



(5) J. Coops, A. N. Balk, and M. W. Tolck, *Rec. trav. chim.*, **75**, 75 (1956).

(6) E. H. P. Cordfunke, *J. Inorg. Nucl. Chem.*, **23**, 285 (1961).

(7) E. H. P. Cordfunke and P. C. Debets, *ibid.*, **26**, 1671 (1964).

(8) E. H. P. Cordfunke, *ibid.*, **24**, 303 (1962).

(9) V. M. Vdovenko and A. P. Sokolov, *Radiokhimiya*, **1**, 117 (1959).

(10) B. J. Fontana, T.I.D. report 5290 (1947).

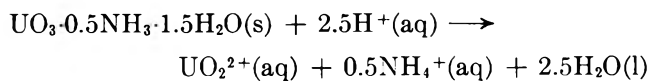
(11) E. H. P. Cordfunke and P. Aling, *Trans. Faraday Soc.*, in press.

was calculated as $-\Delta H_{298} = -38.3$ kcal./mole. This value is in good agreement with the values obtained independently from vapor pressure measurements by Vdovenko, *et al.*⁹ ($-\Delta H_{298} = -38.7$ kcal./mole), and in this laboratory¹² ($-\Delta H_{298} = -38.53$ kcal./mole).

Using the heat of formation of the aqueous uranyl nitrate solution,³ the heats of formation of the hydrates of uranyl nitrate can be calculated. Table II gives a survey of the results. A comparison with the literature shows a reasonable agreement.

The System $UO_3-H_2O-NH_3$. At least three determinations of the heat of solution in 6.0 *N* nitric acid were made on each compound in the ternary system $UO_3-H_2O-NH_3$ investigated. In the case of uranium trioxide a small correction was necessary for the impurities, mainly present as moisture and residual nitrogen. The results are listed in Table III, together with the heats of formation derived from the heat of solution data with the heat of formation of the uranyl ion.

In the case of the ammonium uranates, *e.g.*, $UO_3 \cdot 0.5NH_3 \cdot 1.5H_2O$ (ADU-III⁸), dissolving according to the equation



the heat of formation of the NH_4^+ ion is necessary for the calculation of the heats of formation of the uranates of ammonium. Therefore, the heat of solution of solid $NH_4NO_3(IV)$ was determined in a solution of uranyl nitrate in 6 *N* HNO_3 , so that the same final concentra-

Table III: Heats of Solution in 6 *N* HNO_3 at 25° and Heats of Formation

Substance	Heat of solution, $-\Delta H_{298}$, kcal./mole	Heat of formation, $-\Delta H_{298}$, kcal./mole
α - UO_3	18.61 ± 0.05	291.8
β - UO_3	17.89	292.6
γ - UO_3	17.04	293.5
δ - UO_3	...	290 ^a
ϵ - UO_3	18.65	291.8
A- UO_3	20.8	289.6
$UO_{2.92}$	18.43	292.0
α - $UO_3 \cdot 0.85H_2O$	11.15	357.4
β - $UO_3 \cdot H_2O$	11.40	367.4
ϵ - $UO_3 \cdot H_2O$ (ref. 7)	11.97	366.8
ADU	$UO_3 \cdot 2H_2O$ (I)	437.3
	$UO_3 \cdot \frac{1}{3}NH_3 \cdot 1\frac{1}{3}H_2O$ (II)	423.0
	$UO_3 \cdot \frac{1}{2}NH_3 \cdot 1\frac{1}{2}H_2O$ (III)	415.6
	$UO_3 \cdot \frac{2}{3}NH_3 \cdot 1\frac{1}{3}H_2O$ (IV)	406.6

^a Estimated value for δ - UO_3 , based on the heat of solution of a mixture of δ - UO_3 and α - UO_3 (see Discussion).

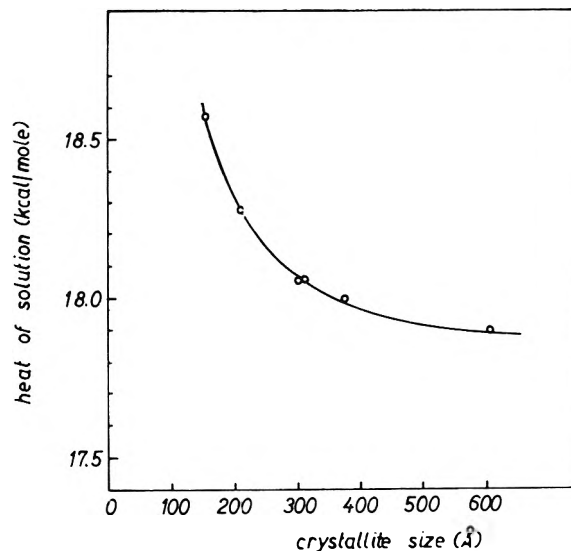


Figure 1. Heats of solution of β - UO_3 in 6 *N* HNO_3 as a function of crystallite size.

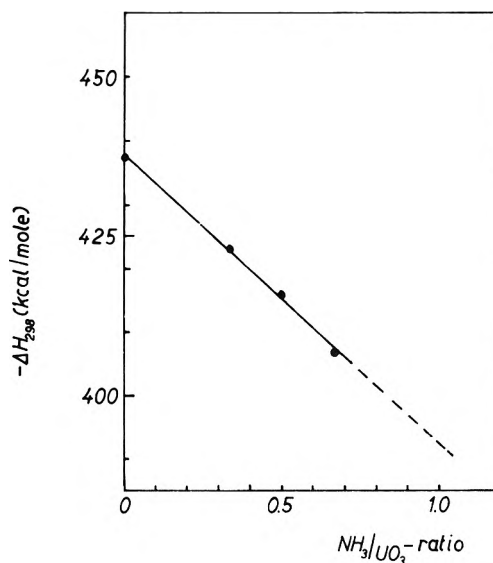


Figure 2. Heats of formation of uranates of ammonium.

tions were obtained, as is the case for dissolving the uranate in nitric acid. From the heat of solution thus obtained ($-\Delta H_{298} = -4.17 \pm 0.02$ kcal./mole), the heat of formation of the NH_4^+ ion was calculated as $-\Delta H_{298} = 32.60$ kcal./mole, using the heat of formation of solid $NH_4NO_3(IV)$ recommended by the National Bureau of Standards¹³ ($-\Delta H_{298} = 87.27$ kcal./mole) and the heat of formation of the NO_3^- ion ($-\Delta H_{298} = 50.5$ kcal./mole), derived from the heat of for-

(12) Unpublished results.

(13) National Bureau of Standards Circular 500, U. S. Government Printing Office, Washington, D. C., 1952.

mation of $\text{UO}_2(\text{NO}_3)_2(\text{aq})$. The heats of formation of the uranates of ammonium found in the ternary system $\text{UO}_3\text{-H}_2\text{O-NH}_3$ ⁸ are listed in Table III.

Discussion

The heats of solution obtained in the present investigation cannot be compared directly with those of other authors because of the marked effect of the conditions in the solution. Measurements on the hydrates of uranyl nitrate, for instance, have only been carried out in water. The heats of formation derived from these measurements and those from ours (Table II) are in good agreement. This is also the case for the hydrates of UO_3 for which only old data were available³ until now.

The heats of solution of UO_3 preparations depend to a marked extent on the mode of preparation and on the starting material. "Active" preparations might have a heat of solution up to 1.0 kcal./mole higher than that of the inactive preparations. The differences in energy content may be due to incomplete ordering of the crystal lattice, as is probably the case for $\epsilon\text{-UO}_3$,⁷ or to differences in particle size. The influence of the degree of crystallinity on the heat of solution is shown for $\beta\text{-UO}_3$ in Fig. 1, in which the crystallinity is expressed as the crystallite size (\AA) calculated from the X-ray line broadening. Further, the measurements of the heats of solution of uranium trioxide are very sensitive to hydration of the samples because of the large differences in the values for the hydrates and the oxides. In order to prevent hydra-

tion during the measurements (preperiod), the tube containing the sample was provided with a small vessel filled with P_2O_5 .

The heats of solution of UO_3 listed in Table III are reasonably consistent with those by Hoekstra and Siegel,¹ who have carried out their measurements in 300 ml. of 5 *N* HNO_3 . Comparison with their data is possible if 0.1 kcal./mole is added to our data, as was found by us experimentally. The only serious disagreement is the value for $\delta\text{-UO}_3$. It was found previously⁷ that this oxide is difficult to obtain in a pure form. In fact, $\delta\text{-UO}_3$ is always contaminated with either amorphous UO_3 or with $\alpha\text{-UO}_3$. From samples of $\delta\text{-UO}_3$, containing approximately 30 wt. % of $\alpha\text{-UO}_3$, a heat of formation of $\delta\text{-UO}_3$ was estimated (290 kcal./mole) from the heat of solution of the mixture (19.9 kcal./mole).

Figure 2 shows the heats of formation of the compounds in the system $\text{UO}_3\text{-H}_2\text{O-NH}_3$ as a function of the NH_3/UO_3 ratio. From this, the heat of formation of the compound $(\text{NH}_4)_2\text{U}_2\text{O}_7$ (ammonium diuranate or ADU) could be found by extrapolation.

$$-\Delta H_{298} = 393 \pm 1 \text{ kcal./mole}$$

It was reported previously^{8,14} that this compound could not be prepared.

Acknowledgment. The author wishes to thank Miss B. J. M. de Boer for experimental assistance.

(14) P. C. Debets and B. O. Loopstra, *J. Inorg. Nucl. Chem.*, **25**, 945 (1963).

Mercaptan Inhibition of the Decay of a Smooth Platinum Cathode¹

by Joel Jacknow, Henry Eyring, and Terrell N. Andersen

Department of Chemistry, University of Utah, Salt Lake City, Utah (Received May 13, 1964)

The open circuit decay of a cathodically charged smooth platinum electrode in aqueous oxidizing solutions was studied in the presence and absence of *n*-alkyl mercaptans. Removal of hydrogen was measured by means of the open circuit potential. The decay time, which was controlled by mass transfer of the oxidant (hydrogen peroxide) to the electrode, was considerably lengthened by the addition of mercaptan inhibitors. The inhibition, which was due to competitive adsorption between mercaptan and oxidant, indicated that the amounts of inhibitors adsorbed were generally in agreement with Traube's rule, *i.e.*, that adsorption is greatest for the least soluble substances. Departures from Traube's rule can be explained on the basis of oxidation of the adsorbed mercaptan by the hydrogen peroxide.

Maxted² has shown that the adsorption of a series of *n*-alkyl thiols increases with increasing length of the alkyl chain. This result is expected from Traube's rule which originally applied to the decrease in surface tension with chain length of a series of compounds adsorbed at the liquid-air interface. Freundlich's extension of this rule to the solid-liquid interface has been verified in many different experimental systems.³⁻⁶ An increase of adsorption with chain length is to be expected because the negative heat of adsorption and thus the surface coverage increases with chain length.⁷ Thus, surface reactions occurring in the presence of saturated chain compounds would be expected to proceed with less current efficiency as the chain length is increased. However, measurement by both Hackerman and co-workers^{8,9} and Ostrowski¹⁰ on the inhibition of the corrosion of steel by a series of *n*-alkyl amines have shown that there is a maximum effect of inhibition at the 12 to 14 carbon chain length of the amine. The present paper explains this as due to oxidation of the adsorbed inhibitor at the metal surface due either to dissolved air or to purposely added oxidants. Such oxidation effects will be shown to have a dependence on inhibitor chain length, the reverse of that predicted by Traube's rule. The inhibition can be maximized by adjustments of chain length, pH, or acetic acid concentration.

Experimental

The equipment and procedure used have been essentially described by Andersen and Eyring.¹¹ The

cell, a 200-ml. stoppered electrolytic beaker, contained 100 ml. of solution which was stirred at a speed of 500 r.p.m. with a magnetic stirring bar. Solutions were prepared from water, doubly distilled from basic permanganate solution, and reagent grade chemicals. High purity nitrogen (99.997%) was bubbled through the electrolyte to effect deoxygenation, and the temperature of the cell was $24.5 \pm 1.5^\circ$. The solutions of varying pH were 0.45 *M* H₂SO₄, 0.0045 *M* H₂SO₄ + 0.1 *M* (NH₄)₂SO₄, 0.1 *M* (NH₄)SO₄, and 0.1 *N* KOH. The mercaptans were the best grade available from Eastman Kodak.

The handling of the mercaptans was crucial in obtaining reproducible data. Stock solutions of approximately 10^{-2} *M* were made up by pipetting a known amount of mercaptan into 100-ml. glass-stoppered flasks containing 90 ml. of nitrogen-saturated, doubly

(1) This is an essential portion of the thesis submitted by J. J. to the Chemistry Department, University of Utah, in partial fulfillment of the requirements for a Ph D. degree.

(2) E. B. Maxted, *Advan. Catalysis*, **3**, 165 (1951).

(3) H. N. Holmes and J. B. McKelvey, *J. Phys. Chem.*, **32**, 1522 (1928).

(4) R. S. Hansen and R. P. Craig, *ibid.*, **58**, 211 (1954).

(5) R. S. Hansen and B. H. Clambitt, *ibid.*, **58**, 909 (1954).

(6) R. J. Meckins, *J. Appl. Chem.*, **13**, 339 (1963).

(7) Y.-F. Yu Yao, *J. Phys. Chem.*, **67**, 2055 (1963).

(8) N. Hackerman and E. L. Cook, *J. Electrochem. Soc.*, **97**, 1 (1950).

(9) H. F. Finley and N. Hackerman, *ibid.*, **107**, 259 (1960).

(10) A. Ostrowski, *Acta Chim. Acad. Sci. Hung.*, **20**, 215 (1959).

(11) T. N. Andersen and H. Eyring, *J. Phys. Chem.*, **67**, 92 (1963).

distilled water. The flasks were then shaken vigorously for a few minutes and the shorter hydrocarbon chain (2–4 CH₂ groups) solutions were used immediately. However, it was found that the time for equilibration of the saturated solutions increased with the chain length of the homolog. Therefore, the higher alkyl mercaptan solutions were allowed to stand at room temperature, being vigorously shaken every few hours. Equilibration was considered to be reached when the inhibition due to the mercaptan was at a maximum.

After checking the reaction rate in the absence of mercaptan (which was reproducible to within $\pm 10\%$), a known amount of mercaptan was added to the cell; a cathodic bias of 0.80 ma. cm.⁻² was applied to the platinum test electrode for 1 min. and then switched off. (The time of the cathodic bias, if kept low enough so as to not change the H₂O₂ concentration, did not affect the decay curves.) The resulting potential vs. time decay curve was recorded.

Results and Discussion

I. Uninhibited Process. Typical decay curves in $6 \times 10^{-4} M$ H₂O₂ for the uninhibited and inhibited process are denoted as curves a and b, respectively, in Fig. 1. Both curves have essentially the same profile except for longer elapsed times in the inhibited system.

Andersen and Eyring¹¹ have reviewed the pertinent literature for the uninhibited process. Their conclusions concerning the mechanisms for the two different parts of the curve BC and CD¹² (using Fe³⁺, MnO₄⁻, Ce⁴⁺, Fe(CN)₆⁻³, and Cr₂O₇⁻² as oxidant) are these.

1. The potential change from B to C is controlled by the transfer of oxidant at its limiting current, i_{lim} , to the surface where it reacts with adsorbed hydrogen. The mechanism is the same in the present work as shown by (a) a large stirring effect, (b) the decay times being comparable to those in the above¹¹ case, and (c) oxidant concentration effects. For the platinum test electrode on open circuit, we may write

$$i_{ext} = 0 = \frac{d(CE)}{dt} + \Sigma i_{cath} - \Sigma i_{anod} \quad (1)$$

where C is the effective electrode capacity (including the pseudo-capacity), Σi_{cath} is the current due to cathodic processes, and Σi_{anod} that due to anodic processes. The hydrogen oxidation and hydrogen ion reduction reactions are in equilibrium and hence equal; the reductant \rightarrow oxidant reaction rate is negligible because of the negative potential, and the rate of reduction of oxidant is equal to i_{lim} . Therefore, the rate of potential change from B to C (Fig. 1) is given by

$$\frac{d(CE)}{dt} = i_{lim} = \frac{K}{\tau} \quad (2)$$

where K is a constant and τ is the time lapse between potentials E_B and E_C (C , the capacity, is a function of the potential). From eq. 2, it can be seen that the reaction rate or the reciprocal decay time (τ^{-1}) should be proportional to the oxidant concentration; *i.e.*, considering a diffusion layer model,¹³ we have

$$i = \frac{nFD}{\delta} (a_0 - a_1) \quad (3)$$

where nF is the number of coulombs per mole of reduction, D is the diffusion coefficient of the oxidant, and a_0 and a_1 are the bulk and pre-electrode activities, respectively. For the case of $a_1 \ll a_0$, $i = i_{lim}$. Table I shows approximately the expected oxidant concentration effect as predicted by eq. 2 and 3.

2. The controlling steps as the voltage passes from C to D in Fig. 1 are the mass transport of oxidant onto and the reductant away from the electrode surface. Especially at the higher potentials, near D in Fig. 1, the Nernst equation can be applied to predict,¹¹ for a reversible couple, *e.g.*, $e + Fe^{+3} \rightleftharpoons Fe^{+2}$, the potential vs. time relaxation with the diffusion layer thickness as a parameter.

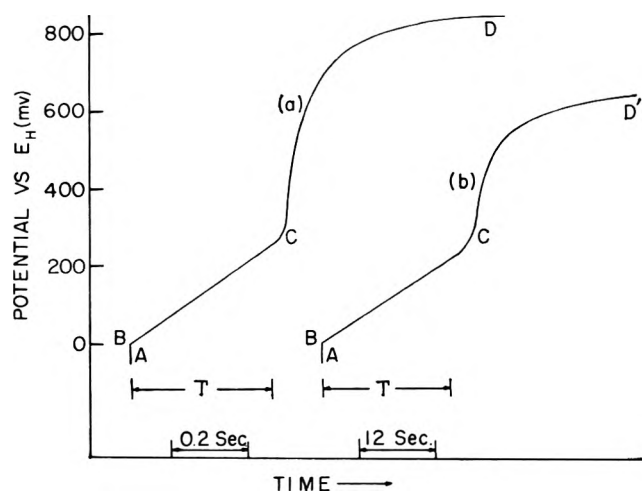


Figure 1. Typical decay curves for uninhibited (a) and inhibited (b) reaction. The solution was 50% acetic acid by volume. The inhibition was produced by $6.5 \times 10^{-6} M$ *n*-decyl thiol.

(12) $E_C = E_H + 350$ to 400 m.v. in 0.1 N KOH and is also dependent on the chemical nature of the solution. A most comprehensive review of the general area of the adsorption and overvoltage of hydrogen on platinum is given by A. N. Frumkin in "Advances in Electrochemistry and Electrochemical Engineering," Vol. III, Interscience Publishers, 1963.

(13) J. J. Lingane and P. J. Lingane, *J. Electroanal. Chem.*, 5, 411 (1963).

Table I: Depolarization Time, τ , to go from B to C in Fig. 1 for the Uninhibited Reaction as a Function of pH and Oxidizer Concentration

Concn. of H ₂ O ₂ , M	Time, sec.		
	pH 0.7 0.45 M H ₂ SO ₄	pH 5.0 0.1 M (NH ₄) ₂ SO ₄	pH 12.8 0.1 M KOH
2×10^{-4}	1.4	1.2	1.2
6×10^{-4}	0.40	0.35	0.36
12×10^{-4}	0.18	0.16	0.17

Potential D is the oxidation-reduction potential of the oxidizer couple. In H₂O₂ solutions, this potential is¹⁴ $E_D = (E_H + 835) \pm 5$ mV. and is independent of the H₂O₂ concentration above 10^{-6} M.

II. Inhibited Process. The prolongment of the decay time when mercaptan is present indicates that the surface sites for H₂O₂ reduction are blocked to a greater extent than the sites for hydrogen adsorption. (Experimental verification of this will be shown in section IV.) To account for this, the area of effective oxidation sites must be considered in eq. 3, *i.e.*

$$\frac{d(CE)}{dt} = i'_{lim}(A) = \phi i_{lim} \quad (4)$$

where A is the sum total of oxidative sites (in area), i'_{lim} is the limiting current density in the absence of inhibitor, and ϕ is the fraction of the sites which are effective in the reduction of H₂O₂ when inhibitor is present. Since the charge, Q , removed from the electrode is decreased to a less extent than is ϕ , dQ/dt ($=d(CE)/dt$) is decreased by the presence of mercaptan. The effect of oxidant concentration on the reaction remains the same as in the noninhibited case as shown in Table II. The observed deviation from

Table II: Depolarization Time, τ , of Section BC of Inhibited Reaction as a Function of Oxidizer Concentration. Inhibitor Was 5×10^{-5} M Decyl Thiol in 50% Acetic Acid

Concn. of H ₂ O ₂ , M	τ , sec.	$(\tau) \times$ concn.
2×10^{-4}	45.0	90
6×10^{-4}	14.0	84
12×10^{-4}	7.0	84
18×10^{-4}	3.9	70

proportionality between concentration of H₂O₂ and reaction rate (τ^{-1}) is due to reaction between mercaptan and H₂O₂ which lowers the effective H₂O₂ concentration. In fact, the removal of mercaptan from the platinum can be followed experimentally at the higher

oxidizer concentrations. As the mercaptan is oxidized and desorbed from the surface² and replaced by the peroxide, the open circuit "steady-state" potential drifts in a positive direction toward the potential existing without mercaptan in solution (from potential D' in Fig. 1b to D in Fig. 1a). The depression of the steady-state oxidation-reduction potential is due to (1) charge transferred across the double layer by mercaptan dipoles of the type¹⁵ $R^{\delta+}SH^{\delta-}$ and (2) the competitive adsorption by the mercaptan on sites previously occupied by the oxidant.

III. Solvent Effect on the Inhibited Reaction. The degree of inhibition of a particular mercaptan was measured by the lengthening of the duration, τ , of the linear step BC of the depolarization curve. More specifically, the ratio of the duration with mercaptan in solution to that without mercaptan in solution indicated the extent of the inhibition. This term was designated the "ratio of durations," τ/τ_0 , and was plotted *vs.* the acetic acid concentrations and the pH in Fig. 2 and 3 at a concentration of 6.5×10^{-5} M mercaptan. Both figures are plotted so as to have the mercaptan solubility increase from left to right. Figure 4 represents typical data for the degree of inhibition as a function of mercaptan concentration. The concentration of H₂O₂ is kept constant at 6.0×10^{-4} M in all of these experiments.

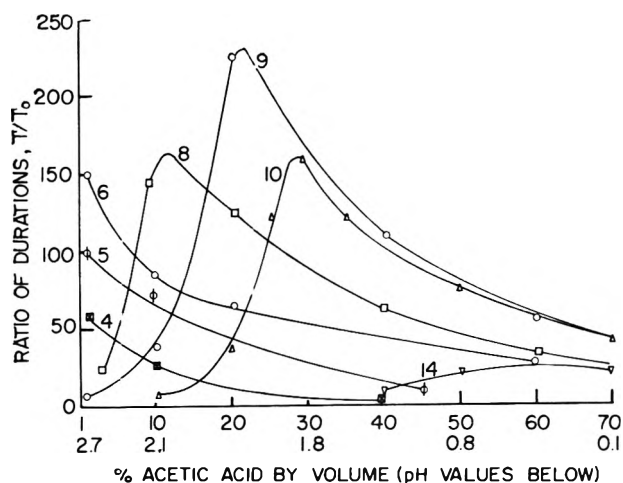


Figure 2. Ratio of durations τ/τ_0 as a function of acetic acid concentration for different n -mercaptans. The numbers on the curves indicate the number of carbon atoms in the mercaptan. Concentration of mercaptan = 6.5×10^{-5} M; H₂O₂ concentration = 6.0×10^{-4} M.

(14) J. O'M. Bockris and L. F. Oldfield, *Trans. Faraday Soc.*, **51**, 249 (1955).

(15) M. H. Dilke, D. E. Fley, and E. B. Maxted, *Nature*, **161**, 804 (1948).

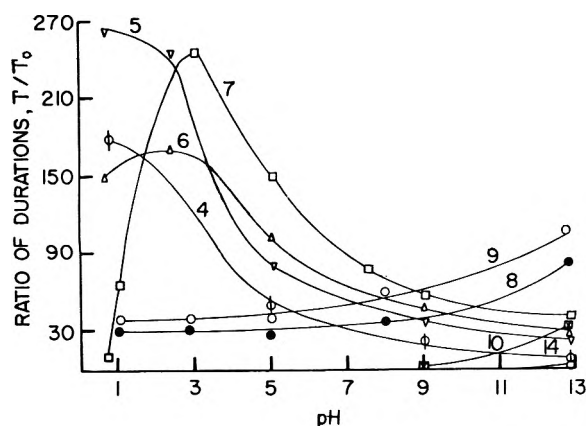


Figure 3. Ratio of durations τ/τ_0 as a function of pH for different n -mercaptans. The numbers on the curves indicate the number of carbon atoms in the mercaptan. Concentration of mercaptan = $6.5 \times 10^{-5} M$; H_2O_2 concentration = $6.0 \times 10^{-4} M$.

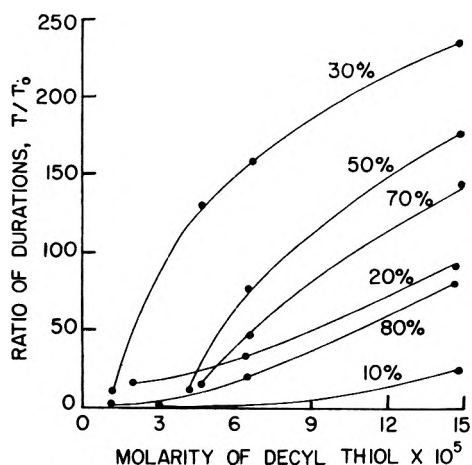


Figure 4. Effect of mercaptan concentration on the degree of inhibition. The numbers on the curves indicate the per cent by volume of acetic acid. Concentration of H_2O_2 is $6.0 \times 10^{-4} M$.

A steady state will be reached such that the rate of migration of mercaptan to the platinum test electrode balances its rate of oxidation (by H_2O_2) there, *i.e.*, if adsorbed mercaptan is in equilibrium with that (desorbed) in the pre-electrode layer, then

$$D\delta^{-1}(C_0^M - C_A^M) = \phi^M K_0 \phi^{ox} \quad (5)$$

where D is the diffusion coefficient of mercaptan in solution, δ is the diffusion layer thickness, C_0^M is the concentration of mercaptan in bulk, C_A^M is the pre-electrode concentration of mercaptan, and ϕ^M and ϕ^{ox} are the surface coverage with mercaptan and oxidant, respectively; K_0 is a constant including the reaction rate constant for the H_2O_2 + mercaptan reaction and geometrical constants of the surface (*i.e.*, the number of adsorption sites per square centimeter and

the reaction layer thickness). C_A^M is related to ϕ^M through an isotherm which we shall take as that describing the adsorption of butyl mercaptan on mercury¹⁶ (a competitive Langmuir adsorption between the mercaptan and water), *i.e.*

$$\phi^M = \frac{C_A^M \exp\left(-\frac{\Delta F_{ads}^\circ}{RT}\right)}{0.0555} \quad (6)$$

where ΔF_{ads}° is the standard free energy of adsorption of the mercaptan, including the desorption of water which is necessary to make room for the adsorbing organic. From (5) and (6) we have

$$\phi^M = \frac{D\delta^{-1}C_0^M}{K_0\phi^{ox} + 0.055D\delta^{-1} \exp\left(-\frac{\Delta F_{des}^\circ}{RT}\right)} \quad (7)$$

where $\Delta F_{des}^\circ = -\Delta F_{ads}^\circ$. In order to rationalize maximum inhibition at an intermediate number of carbon atoms, n , on the mercaptan chain, let us consider the various factors in eq. 7. D , δ , and K_0 would not be expected to vary greatly with n . However, ΔF_{des}° increases with an increase in n since the larger homologs are adsorbed more strongly, and this term tends to increase ϕ^M as n increases. C_0^M , the concentration driving the diffusion of inhibitor to the surface, decreases with n (and hence tends to decrease ϕ^M) since saturation takes place at lower concentrations for higher n values¹⁷; *i.e.*, when mercaptan is added to the cell beyond the saturation amount, the excess goes into droplets which do not increase the concentration diffusing to the electrode. For the case $K_0\phi^{ox} \ll 0.055D\delta^{-1} \exp(-\Delta F_{des}^\circ/RT)$, the denominator decreases faster than the numerator with an increase in n , and hence ϕ^M increases indefinitely with n corresponding to Traube's law. This is the case observed for the lower molecular weight mercaptans. Finally, as n increases and $K_0\phi^{ox}$ (where such a term is important) becomes comparable with and overtakes $0.055D\delta^{-1} \exp(-\Delta F_{des}^\circ/RT)$, the numerator decreases relatively faster than the denominator, and ϕ^M decreases as the length of the carbon chain on the inhibitor, n , increases. This is the condition evident in the present work (Fig. 2 and 3) for the higher n -valued inhibitors, and it is this condition which gives a maximum ϕ^M and inhibition at intermediate values of n .

For calculating purposes, the parameters in eq. 7 may be approximated as: $D = 2 \times 10^{-5} \text{ cm}^2 \text{ sec}^{-1}$

(16) E. Blomgren, J. O'M. Bockris, and C. Jesch, *J. Phys. Chem.*, **65**, 2000 (1961).

(17) D. L. Yarbrough, *Ind. Eng. Chem.*, **32**, 257 (1940).

(an intermediate value of diffusion coefficients in liquid); $\delta = 10^{-3}$ cm. (typical of δ -values obtained in stirred solutions obtained by limiting currents).¹¹ C_0^M as added to the solution (Fig. 2 and 3) was 6.5×10^{-5} M; however, the solubility limited this to diminished values for the longer chain mercaptan, so C_0^M is taken as the concentration of the solution composed of 6.5×10^{-5} mole of mercaptan in a liter of the solution mercaptan plus water. The C_0^M values corresponding to the various n values are¹⁷ $n = 4, 5, 6,$ and 7 . $C_0^M = 6.5 \times 10^{-5}$ M; $n = 8$, $C_0^M = 1.7 \times 10^{-5}$; $n = 9$, $C_0^M = 3.5 \times 10^{-6}$; $n = 10$, $C_0^M = 8 \times 10^{-7}$. ΔF_{des}° values are not available for mercaptans on platinum. However, from Traube's rule, it can be shown¹⁸ that ΔF_{des}° increases 0.6 kcal mole⁻¹ for each increasing carbon on the alkyl chain. ΔF_{des}° for n -butyl mercaptan on mercury has been measured¹⁶ and is used (along with Traube's rule) in the present case for platinum. This approximation is justified considering that dispersion interactions are the principal forces involved in such adsorption, and these vary little with the metal substrate.¹⁹ $K_0\phi^{ox}$ could not be approximated to sufficient accuracy from the literature, so it was varied as a parameter, the values being chosen as required by the data. Figure 5 shows plots of ϕ^M vs. n as given by eq. 7 for $\phi^{ox}K_0 = 10^{-7}, 10^{-8}, 10^{-9}$, and 10^{-10} (in c.g.s. units).

Within the limitations of the values chosen for constants in eq. 7, Fig. 5 is seen to describe the experimental findings of maximum inhibition at intermediate chain lengths of the inhibitor. It is to be noted that the value of the surface coverage for n -butyl mercaptan compares favorably with that on mercury.¹⁶ From the low ϕ^M values and the large amount of inhibition, it appears that the fraction of sites suitable for H_2O_2 reduction is small, and that these are the sites most favorable for inhibitor adsorption. Also important may be the fact that reaction between adsorbed oxidant and inhibitor is rapid compared to reduction of the oxidant; thus, although ϕ^M is low, each adsorbed mercaptan may react with several neighboring H_2O_2 molecules and thus multiply its own coverage in inhibition effectiveness. In all the curves of Fig. 5 a maximum is noted for $n = 7$. The n value at which ϕ^M is a maximum varies with the solution since the variation of solvent determines at which chain length saturation begins (and hence at which n value C_0^M decreases). In more basic solutions and at higher acetic acid concentrations, the mercaptans are more soluble, and hence Traube's rule is followed to higher n values (see Fig. 2 and 3).

A decrease of ϕ^{ox} with an increase of n is expected but not taken into account in testing eq. 7. This

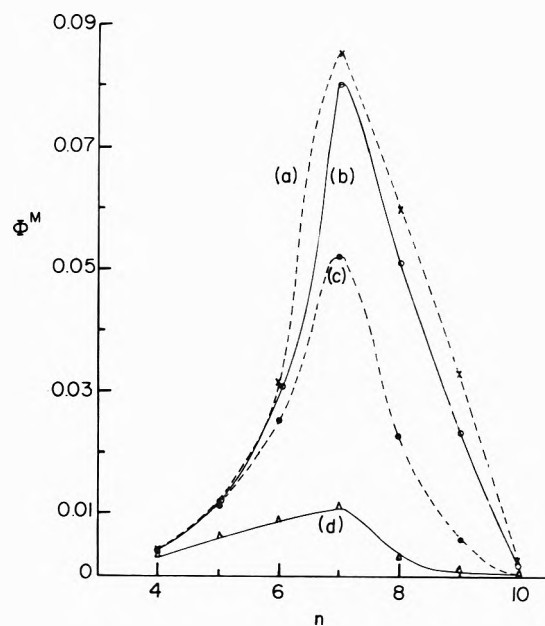


Figure 5. Plot of the surface coverage of mercaptan, ϕ^M , vs. the number of carbon atoms in the mercaptan chain, n , calculated from eq. 7. The values of $\phi^{ox}K_0$ are (a) 10^{-10} ; (b) 10^{-9} ; (c) 10^{-8} ; (d) 10^{-7} .

effect would tend to shift the ϕ^M -value to successively higher curves in Fig. 5 as n increases. The result of this may shift $\phi_{(max)}^M$ to $n = 8$ or 9 but would surely not affect the relative positions of $n \geq 10$.

IV. Mechanistic Interpretation. Because H, H_2O_2 , and mercaptan are all competing for sites, it is difficult to assess separately the electrode coverage by each. However, the system can be separated so that the mercaptan, hydrogen, and hydrogen peroxide will not interfere with each others' adsorption isotherm. This was done by placing the hydrogen peroxide in beaker 1 with a connecting platinum wire dipping into an adjoining beaker 2. Hydrogen was plated out on the platinum wire in beaker 2. Also connecting both beakers was a salt bridge. The solution, stirring rates, etc., were the same in both beakers. In order for the hydrogen on the cathode in beaker 2 to be oxidized, electrons released by the reaction, $H_{ads} \rightarrow H^+ + e$, must be used by the reduction of H_2O_2 on the cathode in beaker 1. Thus, unoccupied sites are seen to be sites where electron transfer to the peroxide can take place. In other words, empty sites on which the peroxide is reduced do not have to be available next to adsorbed hydrogen in order for the hydrogen to be

(18) A. W. Adamson, "Physical Chemistry of Surfaces," Interscience Publishers, New York, N. Y., 1960.

(19) J. O'M. Bockris and D. A. J. Swinkels, *J. Electrochem. Soc.*, **111**, 736 (1964).

oxidized. The electrode is simply acting as an electron-transfer medium. The role of the mercaptan is to reduce the number of available sites for electron transfer. These conclusions have been further substantiated by the following experiments using the above system with the two beakers.

A depolarization curve was obtained without inhibitor added to either beaker in 50% acetic acid solution under the conditions previously described in the experimental procedure. The solution in beaker 2 where the hydrogen is plated was then made $5 \times 10^{-5} M$ with decyl thiol. The cathodic bias was applied for 10 sec. and a new depolarization curve was obtained. The rate of depolarization was tripled (*i.e.*, τ was one-third as long).

The solution of hydrogen peroxide in beaker 1 was now made $5 \times 10^{-5} M$ with decyl thiol, and a depolarization curve was obtained after plating hydrogen for

10 sec. The depolarization slowed down to a rate one-sixth of the previous rate and to one-half of the rate without mercaptan added to either beaker.

Mercaptan speeds up the reaction when added to beaker 2 as it reduces the capacity of the cathode for adsorbed hydrogen, without interfering with the electron-transfer process. However, from the above experiment and Fig. 2-4, it is seen that the major role in the mechanism of the inhibition is the adsorption of mercaptan on those sites on which electron transfer to the peroxide takes place and the reaction of the inhibitor with peroxide.

Acknowledgment. The authors wish to express appreciation for financial support of this work to the Atomic Energy Commission under Contract AT-(11-1)-1144. We also wish to thank P. H. Lewis of the Texaco Research Laboratory, Beacon, N. Y., for his help with the manuscript.

Faradaic Impedance at Platinum Microelectrodes.

Behavior of the Iodide–Iodine Oxidation–Reduction Couple

by A. B. Thomas¹ and R. J. Brodd

Union Carbide Corporation, Consumer Products Division, Research Laboratory, Parma 30, Ohio
(Received May 25, 1964)

Using carefully purified reagents and controlled surface preparation, it was possible to obtain accurate and reproducible impedances at platinum electrodes for the iodine–iodide oxidation–reduction couple. Proper electrode construction was found to be very important. It was possible to prepare and activate single crystal platinum electrodes of known surface area and reproducible faradaic impedance. The diffusion coefficients of iodine and triiodide deduced from the faradaic impedance were shown to be in agreement with measurements using rotating disk electrodes. It was shown that the electrode process follows the path proposed by Vetter with α of about 0.6. In low concentration iodide solution, a process parallel to the main reaction scheme was found that was tentatively ascribed to an adsorption of iodide ions on the electrode surface.

Introduction

Several studies of the electrode kinetic behavior of the iodine–iodide oxidation–reduction couple at platinum electrodes have been made. Those using faradaic impedance methods are the work of Vetter^{2a} and Llopis, *et al.*^{2b} A study using the rotating disk electrode has been reported by Newson and Riddiford,³ who supported the rate-determining step proposed by Vetter.^{2a} The differences between the various investigations may be ascribed as the difficulty of establishing a characterizable surface state on the solid electrode surface. A method for the preparation of a reproducible, characterizable platinum surface is described which is comparable with a mercury surface for electrokinetic investigations.

Experimental Details

Impedance measurements were made with the α -series resistance–capacitance bridge with the experimental cell composing one arm of the bridge. The bridge could be balanced at all frequencies to 1% or better when standard resistors and capacitors were substituted for the experimental cell. Impedances of the test electrodes were measured at 2000, 800, 500, 400, 350, 300, 250, 200, and 150 c.p.s. and were reproducible to $\pm 5\%$.

Distilled water was redistilled from alkaline potassium permanganate solutions. The middle fraction was redistilled and stored in seasoned Pyrex flasks. Reagent grade potassium sulfate was heated in a casserole over a Meeker burner and recrystallized twice from the triple-distilled water. The product was vacuum dried over phosphorus pentoxide. Reagent grade iodine was freshly sublimed from a mixture of potassium iodide and barium oxide. Reagent grade potassium iodide was recrystallized twice from triple-distilled water and vacuum dried over phosphorus pentoxide. Double-distilled 70% perchloric acid was mixed with 10 to 20% concentrated nitric acid and distilled at atmospheric pressure. The middle fraction was retained and chlorine was removed by pumping with a water aspirator and/or bubbling dry purified nitrogen through for several hours. The final product gave no test for chloride ion.

(1) Deceased.

(2) (a) K. J. Vetter, *Z. physik. Chem. (Leipzig)*, **199**, 285 (1952); (b) J. Llopis and F. Colom, *Anales Fis. Quim.*, **52A**, 233 (1956); J. Llopis, J. Fernandes-Biarge, and M. Perez-Fernandes, *ibid.*, **55A**, 93 (1959); J. Llopis, J. Fernandes-Biarge, and M. Perez-Fernandes, *Electrochim. Acta*, **1**, 130 (1959).

(3) J. D. Newson and A. C. Riddiford, *J. Electrochem. Soc.*, **108**, 699 (1961); D. P. Gregory and A. C. Riddiford, *J. Chem. Soc.*, 3756 (1956).

Tank nitrogen was purified by bubbling through Oxorbent solution, concentrated sulfuric acid, and either drying towers of phosphorus pentoxide and magnesium perchlorate or triple-distilled water prior to use.

Solutions were prepared as needed by weighing reagents. No stock solutions were used.

Pure platinum wire and sheet (American Platinum Works) were used to prepare electrodes. Four types of electrodes, spherical, wire loop, plain sheet, and flat ground, were used in this study. Counter electrodes were 1-cm. diameter disks of sheet platinum placed 1 cm. beneath the microelectrodes. The proper sealing of platinum to glass was critical in obtaining reproducible electrode impedances. Pyrex and cobalt glass seals were not dependable but were occasionally satisfactory for wire of less than 0.2-mm. diameter. Uniformly dependable seals were obtained with lead glass and soft glass when the wire diameter was less than 0.5 mm.

Wire loop and sheet electrodes were prepared by sealing appropriate platinum pieces into soft glass tubing using lead glass. Flat polished electrodes prepared by grinding sealed wires carefully to a final polish with 0.1- μ alumina were not reliable.

Spherical electrodes were produced by sealing appropriate lengths of platinum wire into soft glass tubing with lead glass and carefully fusing the platinum in a gas-oxygen flame. Natural cooling in air yielded mirror-bright spheres, varying less than 5% in diameter. Electrodes prepared in this way were 0.015 to 0.1 cm. in diameter or 0.0010 to 0.04 cm.² in area. X-Ray diffraction patterns revealed that such electrodes were single crystals when the diameter was less than 0.05 cm., and were composed of only two to five grains if larger in diameter. A convenient procedure for revealing grain boundaries and other crystal characteristics was to etch with a 50-c.p.s. alternating current at a current density of 20 to 50 ma./cm.² in a solution of 0.5 M NaCl-0.5 M HCl for 15 to 60 min.⁴ An etched sphere 0.1 cm. in diameter is shown in Fig. 1. Notice the grain boundary and diamond figure revealing one crystal face.

Two different methods were used to prepare the electrodes for the measurements. In the first method, the test electrodes were allowed to stand in the test solution overnight (*i.e.*, 16 hr. or longer) with low amplitude (10 mv.) 15 to 20 c.p.s. field applied between the electrodes. This corresponds to Vetter's pretreatment of his electrodes. The other activation method consisted of preparing an oxide film on the electrode by anodic polarization at 1.0 v. positive to a saturated calomel electrode and then reducing the oxide film



Figure 1. Platinum microelectrode showing presence of several grains developed by the etching process.

by cathodic polarization at 0.5 v. positive to a saturated calomel electrode on the test electrode in 1 M HClO₄ as described by Laitinen and Enke.⁵ The test electrode was then transferred to the test solution. The impedance of these electrodes reached steady-state values after 2 to 5 min. This method of activation is similar to that of Llopis, *et al.*^{2b}

The resistance of the solution and the capacitance of the electrical double layer were determined by measuring the cell impedance in the absence of the iodine-iodide oxidation-reduction couple. All electrode impedances with the exception of the flat ground electrodes were reproducible to $\pm 5\%$. The electrode area determined by double layer capacitance was in excellent agreement with the apparent electrode area for all except the flat ground electrodes.

Results and Discussion

The results of studies in high concentration iodide solution are given in Table I. Only results using loop,

(4) E. Raub and G. Buss, *Z. Elektrochem.*, **46**, 195 (1940).

(5) H. A. Laitinen and C. G. Enke, *J. Electrochem. Soc.*, **107**, 773 (1960); H. A. Laitinen and J. E. B. Randles, *Trans. Faraday Soc.*, **51**, 54 (1955).

Table I: Faradaic Impedance of High Concentration Iodide-Iodine Solutions in 0.5 M K₂SO₄

Concn. of KI ₃ , mole/l.	Concn. of KI, mole/l.	$I_0 \times 10^2,^a$ amp./cm. ²	$\left(\frac{\sigma_{RA}}{C_0 + C_R}\right) \times 10^{-6}$, ohm-cm. ^{2a}	$\left(\frac{\sigma_{XA}}{C_0 + C_R}\right) \times 10^{-6}$, ohm-cm. ^{2a}
0.001	0.1	2.1	15.4	15.2
0.001	0.2	2.7	14.6	14.9
0.002	0.2	3.2	14.6	16.0
0.002 ^b	0.2 ^b	3.8	14.8	14.6
0.004	0.4	4.6	15.4	15.2

^a Based on apparent electrode area. ^b 1 M HClO₄ supporting electrolyte.

spherical, and sheet electrodes are included since the impedances of the flat ground electrodes were not reproducible. Faradaic impedance and its relation to electrode kinetics have been given theoretical attention in recent years.⁶⁻⁹ For electrode processes which are diffusion controlled, it has been shown that

$$R_s = \theta + R_1 = \theta + \sigma/\sqrt{\omega} \quad (1)$$

$$C_s = C_1 = 1/\sigma\sqrt{\omega} \quad (2)$$

$$X_1 = \frac{1}{\omega C_1} = R_1 \quad (3)$$

$$I_0 = \frac{RT}{\lambda F \theta A} \quad (4)$$

where R_s and C_s are the series resistive and capacitive components, θ is the transfer resistance associated with the electrochemical reaction, and A is the electrode area. R_1 , C_1 , and X_1 are associated with the Warburg or diffusion impedance, ω is the angular frequency (radians/sec.), and I_0 is the exchange current. The Warburg coefficient σ for the iodine oxidation-reduction electrode is given by

$$\sigma = \frac{RT}{\sqrt{2n^2F^2A}} \left[\frac{1}{(C_{I_2^-} + C_{I^-})\sqrt{D}} + \frac{2}{C_{I_3^-}\sqrt{D}} \right] \quad (5)$$

The diffusion coefficients, D , of I₂, I⁻, and I₃⁻ are assumed to be equal. Measurements³ at rotating disk electrodes which gave $D_{I_3^-} = 1.13 \times 10^{-5}$ cm.²/sec. and $D_{I_2^-} = 1.15 \times 10^{-5}$ cm.²/sec. at 25° justify this assumption for the present system. The grand average value of σ for both the resistive and reactive portions of the Warburg impedance was 15.2×10^{-6} ohm/cm.², and the average value of D was 0.96×10^{-5} cm.²/sec. in the 0.5 M K₂SO₄ solutions. This value is in satisfactory agreement with that reported by Riddiford, *et al.*, and in fair agreement with the value of D

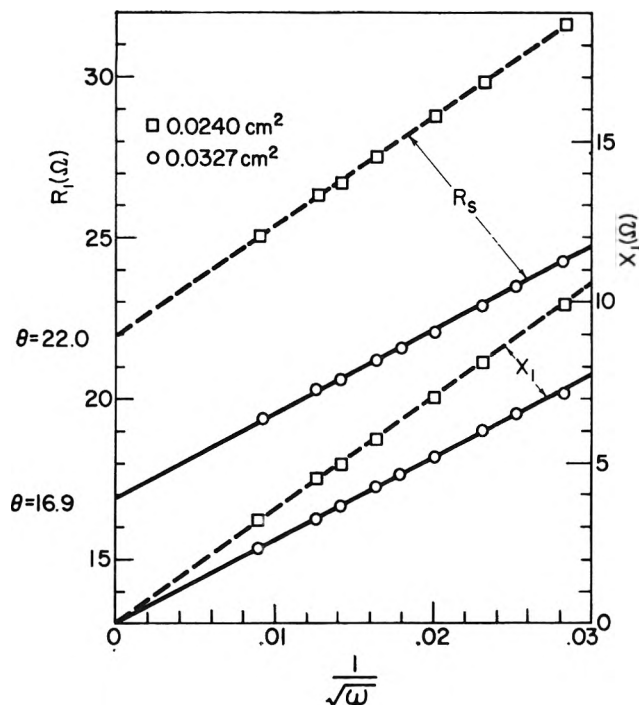


Figure 2. Impedance data for two platinum electrodes in 0.002 M KI₃ + 0.20 M KI solution.

determined by Vetter,^{2a} 0.42×10^{-5} cm.²/sec. The presence of supporting electrolyte may result in a depression of D below the values of Riddiford, whose ionic strength was much lower.

Small deviations from expected behavior of the Warburg impedance can be noted in Table I and Fig. 2. The linearity of the resistance and reactance lines with $\omega^{-1/2}$ was obeyed. It might be noted that the diffusion coefficient calculated from the resistive component (0.99×10^{-5} cm.²/sec.) is slightly larger than that calculated from the reactive component (0.94×10^{-5} cm.²/sec.). There was good agreement between the two methods of surface preparation as noted by the results in 0.2 M KI-0.002 M KI₃ solutions.

The difficulty in reproducibly preparing a solid electrode surface is a crucial problem. Transfer resistances that were reproducible and independent of electrode history could not be obtained either with anodic or cathodic polarization below or above gas evolution potentials or with a.c. polarization at various frequencies with gas evolution. Any of these methods of activation produced electrodes whose impedance

(6) J. E. B. Randles, *Discussions Faraday Soc.*, 1, 11 (1947).

(7) B. V. Eishler, *Zh. Fiz. Khim.*, 22, 683 (1948).

(8) H. Gerischer, *Z. physik. Chem. (Leipzig)*, 198, 286 (1951); 201, 55 (1952); *Z. Elektrochem.*, 55, 98 (1951); *Z. physik. Chem. (Frankfurt)*, 1, 278 (1954).

(9) D. C. Grahame, *J. Electrochem. Soc.*, 99, 370C (1952).

drifted rapidly with time to an arbitrary static value. Immediately after anodic or cathodic "activation" below gas evolution or with H_2 evolution, the electrode impedance was very low and consisted essentially of the Warburg impedance. The impedance of these electrodes approximated the impedances reported by Llopis, *et al.*,^{2b} for thin activated electrodes. The electrode impedance then increased slowly with time to an arbitrary static value. Anodic "activation" with oxygen evolution produced anomalous electrode impedances.

The results in dilute iodine solutions of impedance measurements using electrodes activated by the Laitinen and Enke technique are given in Tables I and II. The

Table II: Faradaic Impedance of Low Concentration Iodine-Iodide Solutions in 1 M $HClO_4$

Concn. of I_2 , mole/l.	Concn. of NaI, mole/l.	$I_0 \times 10^2$, amp./cm. ²	$R_{ads}A$, ohm-cm. ²	C_{ads}/A , $\mu f./cm.^2$	$R_{ads}C_{ads} \times 10^4$, sec.	S (eq. 6)
0.0005	0.001	0.86	1.32	175	231	0.003
0.001	0.002	1.2	0.60	311	186	0.007
0.002	0.004	1.7	0.38	509	225	0.011
0.003	0.006	2.0	0.29	685	199	0.014

analysis indicated that a classical faradaic circuit did not apply to the dilute solutions as it did to the more concentrated solutions. It was reported by Newson and Riddiford³ that no satisfactory kinetic plots could be obtained in very dilute solution. The parallel adsorption path circuit proposed by Laitinen and Randles⁵ shown in Fig. 3 appeared to resolve the data. Attempts to fit the data, assuming two series-connected reactions, were not successful. It is not clear that the "adsorption" branch of the proposed circuit is a true adsorption process. It is possible that the triiodide-iodine equilibrium or some other surface reaction is responsible for the observed behavior.

The theory for the adsorptive branch requires that the product $R_{ads}C_{ads}$ should be constant. The results in Table II show $R_{ads}C_{ads}$ to be roughly constant. If it is assumed that the Langmuir adsorption isotherm applies here, the adsorption isotherm on the electrode surface is given by

$$S = \frac{(C_{ads}/A)}{(C_{ads}/A)^*} = \frac{(R_{ads}A)^*}{(R_{ads}A)} = \frac{kC_{I^-}}{1 + kC_{I^-}} \quad (6)$$

where S is the coverage computed from the adsorptive resistance or reactance. The terms $(R_{ads}A)^*$ and $(C_{ads}/A)^*$ represent the values of the terms at maximum coverage. Equation 6 was confirmed by plotting

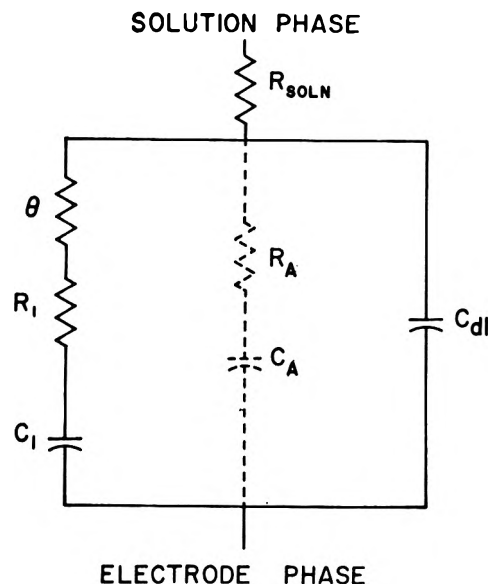


Figure 3. An equivalent circuit for electrode-solution interfaces.

$(R_{ads}A)C_{I^-}$ vs. C_{I^-} and $C_{I^-}/(C_{ads}/A)$ vs. C_{I^-} . The concentrations of iodine, iodide, and triiodide were calculated using the equilibrium constant¹⁰

$$768 = \frac{C_{I_3^-}}{C_{I^-}C_{I_2}}$$

Straight-line plots for both resistive and capacitive components were obtained only when the concentration of iodide ions was used in eq. 6. It should be noted that since data are available only for a limited range of S , it is not possible to distinguish conclusively whether the Langmuir or Temkin adsorption isotherm is applicable in the present case.

It has been reported that the iodide adsorption on platinum¹¹ becomes irreversible after prolonged contact with iodide solutions. Since Vetter^{2a} aged his electrodes for long periods, his results in dilute solutions would not contain an adsorptive impedance branch. The impedances reported here were constant for over 1 hr., but if an electrode was allowed to remain in contact with the solution for long periods (1 day or longer) the adsorptive branch did disappear and the impedance plots were linear as reported by Vetter.^{2a} The electrode could be returned to its initial active state by repeating the electrochemical pretreatment in 1 M $HClO_4$ solution.

From Table I it is seen that the exchange current density for the 0.001 M KI_3 , 0.1 M KI , 0.5 M K_2SO_4 solution is 2.1×10^{-2} amp./cm.². For 1 N sulfuric

(10) M. Davies and E. Gwynne, *J. Am. Chem. Soc.*, **74**, 2748 (1952).

(11) N. Balashova, *Zh. Fiz. Khim.*, **32**, 2266 (1958)

acid solutions with the same iodine-triiodide concentration, Vetter^{2a} found 0.4×10^{-2} amp./cm², while Riddiford³ reported about 0.04×10^{-2} amp./cm² in the absence of supporting electrolyte. The differences between the various investigations may be ascribed tentatively to variations in surface uniformity. The results given in Tables I and II appear to conform with the mechanism postulated by Vetter^{2a} with slow electron transfer to an iodine atom as the rate-determining step, if the transfer coefficient, α , is taken to be approximately 0.6. There was no evidence to support the two-electron-transfer step.¹²

Recent adsorption and kinetic studies¹³⁻¹⁵ indicate that the kinetic reaction mechanisms may occur on the platinum surface which is covered with strongly adsorbed iodide and iodine. Even though the adsorbed species in the first layer do not exchange with the solution species,¹³ it is still possible to have unimpeded electron transfer through the very thin adsorbed layer.

The low values of surface coverage in Table II may be associated with a second layer of adsorbed species since the surface is almost saturated at iodine and iodide concentrations of 10^{-4} mole/l. In view of the large exchange currents, it is conceivable that the first adsorbed layer acts as a bridging agent and facilitates electron transfer to the electrode.

Acknowledgment. The authors thank Drs. S. Senderoff, R. A. Powers, and H. A. Laitinen for their stimulating discussions in the course of this work. Also, appreciation must be expressed to Miss Sharon P. LeMoine, who performed much of the experimental work.

(12) J. Jordan and R. A. Javik, *J. Am. Chem. Soc.*, **80**, 1264 (1958).

(13) R. Osteryoung, G. Lauer, and F. C. Anson, *Anal. Chem.*, **34**, 183 (1962); R. Osteryoung and F. C. Anson, *ibid.*, **36**, 975 (1964).

(14) S. Schuldiner and C. H. Presbrey, Jr., *J. Electrochem. Soc.*, **111**, 457 (1964).

(15) M. W. Breiter, *Electrochim. Acta*, **8**, 925 (1963).

Extensions of the Steady-State Rate¹ Law for the Fumarase Reaction

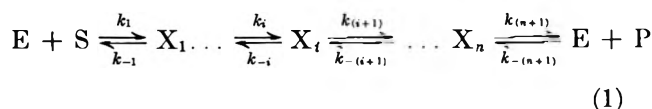
by Mildred Taraszka and Robert A. Alberty

Department of Chemistry, University of Wisconsin, Madison, Wisconsin (Received June 1, 1964)

When steady-state and relaxation rates for the fumarase reaction are measured with both fumarate and L-malate present, it is found that there is a term in the denominator of the rate law which is proportional to the product of fumarate and L-malate concentrations. The coefficient of this term was measured at three pH values. At the high substrate and product concentrations required to make this denominator term important, numerator terms which represent substrate and product activation must also be taken into account. These experimental data are discussed in terms of a mechanism which provides for the binding of substrate or product molecules at a neighboring site so that the properties of the enzymatic site are altered. This mechanism may readily be extended to represent other experimental data on the fumarase reaction, namely competitive inhibition and pH effects.

Introduction and Theory

The steady-state rate equation^{2a,b} for a mechanism of the type



can be written as

$$v = -\frac{d(S)}{dt} = \frac{d(P)}{dt} = \frac{(V_S/K_S)(S) - (V_P/K_P)(P)}{1 + (S)/K_S + (P)/K_P} \quad (2)$$

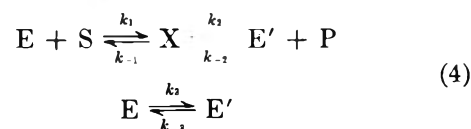
where V_S and V_P are maximum velocities and K_S and K_P are Michaelis constants. Assuming that the time required to reach a steady state is negligible in comparison with the elapsed time,³ eq. 2 may be integrated to yield

$$\frac{(P)}{t} = \frac{V_S/K_S + V_P/K_P}{1/K_S - 1/K_P} + \left[\frac{1 + \frac{(S)_0}{K_P}}{1/K_S - 1/K_P} + \frac{(S)_0}{1 + K_{eq}} \right] \frac{1}{t} \ln \left[\frac{(P)_{eq} - (P)}{(P)_{eq}} \right] \quad (3)$$

According to this equation, plots of $(P)/t$ vs. $(1/t) \ln [1 - (P)/(P)_{eq}]$ should be linear.

For the fumarase reaction it is found that such plots are not linear, especially at higher substrate concentra-

tions. This indicates that rate eq. 2, and therefore mechanism 1, does not adequately represent the steady-state behavior of this enzymatic reaction. The nature of the deviations suggests that there is an additional term of the form of $(S)(P)/K_{SP}$ in the denominator of the rate equation, written in the form of eq. 2. The simplest mechanism which requires such a term is mechanism 4. The enzyme E' has to undergo an isomerization to regenerate the original form E before it can react with another molecule of substrate S .



The steady-state rate equation for mechanism 4 is

$$v = \frac{(V_S/K_S)(S) - (V_P/K_P)(P)}{1 + (S)/K_S + (P)/K_P + (S)(P)/K_{SP}} \quad (5)$$

where

$$V_S = \frac{k_2 k_{-3} (E)_0}{k_{-3} + k_2} \quad V_P = \frac{k_{-1} k_3 (E)_0}{k_3 + k_{-1}}$$

$$K_S = \frac{(k_{-1} + k_2)(k_3 + k_{-2})}{k_1(k_2 + k_{-3})}$$

(1) This research was supported by grants from the National Science Foundation and the National Institutes of Health.

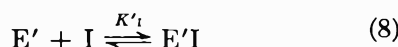
(2) (a) J. B. S. Haldane, "Enzymes," Longmans, Green and Co., London, 1930, p. 81; (b) L. Peller and R. A. Alberty, *J. Am. Chem. Soc.*, **81**, 5907 (1959).

(3) W. Miller and R. A. Alberty, *ibid.*, **80**, 5146 (1958).

$$K_P = \frac{(k_{-1} + k_2)(k_3 + k_{-3})}{k_{-2}(k_{-1} + k_3)}$$

$$K_{SP} = \frac{(k_{-1} + k_2)(k_3 + k_{-3})}{k_1 k_{-2}} \quad (6)$$

If this type of mechanism is to be used to rationalize kinetic data for the fumarase reaction it must be possible to extend it to give a satisfactory representation of the experimental facts about competitive inhibition, substrate activation, the effect of pH, etc. The salts of a number of dicarboxylic acids have been found⁴⁻⁷ to be competitive inhibitors of fumarase, and the same values of the inhibition constant have been obtained whether fumarate or L-malate is used as substrate. If the following steps are added to mechanism 4



the rate equation may still be written in the form of eq. 5, but the apparent maximum velocities and Michaelis constants are now given by

$$V_S = \frac{k_2 k_{-3} (E)_0}{k_{-3} + k_2 [1 + (I)/K_I]}$$

$$V_P = \frac{k_{-1} k_3 (E)_0}{k_3 + k_{-1} [1 + (I)/K_I]}$$

$$K_S = \frac{(k_{-1} + k_2) \{k_3 [1 + (I)/K'_I] + k_{-3} [1 + (I)/K_I]\}}{k_1 \{k_{-3} + k_2 [1 + (I)/K'_I]\}}$$

$$K_P = \frac{(k_{-1} + k_2) \{k_3 [1 + (I)/K'_I] + k_{-3} [1 + (I)/K_I]\}}{k_{-2} \{k_3 + k_{-1} [1 + (I)/K_I]\}}$$

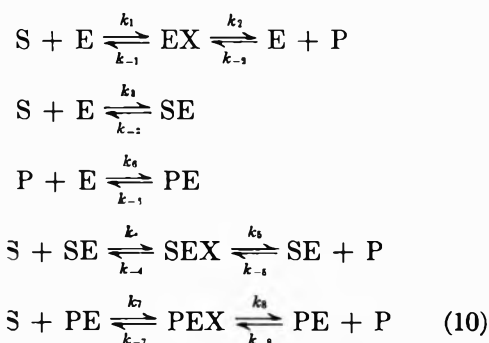
$$K_{SP} = \frac{(k_{-1} + k_2) \{k_3 [1 + (I)/K'_I] + k_{-3} [1 + (I)/K_I]\}}{k_1 k_{-2}} \quad (9)$$

The inhibition constants K_I and K'_I are defined as dissociation constants.

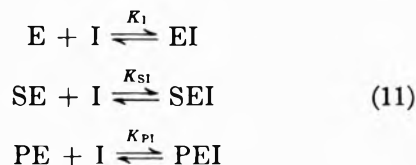
In general V_S and V_P will be functions of (I) so that the inhibition will not be competitive. If the inhibitor can combine with only one form of the enzyme, either K_I or K'_I will be infinite and the corresponding maximum velocity will be independent of (I) . However, since the other maximum velocity will be dependent on (I) , this mechanism is not consistent with competitive inhibition for both substrate and product. If $k_{-3} \gg k_2$ and $k_3 \gg k_{-1}$, that is, if the step involving enzyme isomerization is a rapid equilibrium, V_S and V_P become independent of (I) , and K_S and K_P show the same dependence on (I) in accordance with competitive

inhibition, but the $(S)(P)/K_{SP}$ term is no longer required in the steady-state rate equation. Thus mechanism 4 does not account for the experimental facts of the fumarase reaction.

A second mechanism, which leads to a K_{SP} term is one involving substrate and product activation or inhibition. At high concentrations both fumarate and L-malate act as activators of fumarase.^{8,9} This is in contrast with substrate inhibition which is frequently observed at high substrate concentrations for some other enzymes.¹⁰ For the fumarase reaction substrate activation has been attributed to the binding of substrate at sites on the enzyme which have an activating effect upon the enzymatic sites. Mechanism 10 provides for both substrate and product activation.



Competitive inhibition by I may be provided for by adding the steps



where the equilibrium constants are defined as dissociation constants. The steady-state rate equation for mechanism 10 with the three additional reactions with I can be written as

$$v = \frac{[(V_S/K_S)(S) - (V_P/K_P)(P)][1 + \theta_S(S) + \theta_P(P)]}{1 + (S)/K_S + (P)/K_P + (S)(P)/K_{SP} + (S)^2/K_{S_2} + (P)^2/K_{P_2}} \quad (12)$$

- (4) V. Massey, *Biochem. J.*, **55**, 172 (1953).
- (5) C. Frieden, Ph.D. Thesis, University of Wisconsin, 1955, p. 25.
- (6) G. G. Hammes and R. A. Alberty, *J. Am. Chem. Soc.*, **82**, 1564 (1960).
- (7) P. W. Wigler and R. A. Alberty, *ibid.*, **82**, 5482 (1960).
- (8) R. A. Alberty and R. M. Bock, *Proc. Natl. Acad. Sci. U. S.*, **39**, 895 (1953).
- (9) R. A. Alberty, V. Massey, C. Frieden, and A. R. Fuhlbrigge, *J. Am. Chem. Soc.*, **76**, 2485 (1954).
- (10) M. Dixon and E. C. Webb, "Enzymes," Academic Press, Inc., New York, N. Y., 1958, pp. 81-91.

where

$$\begin{aligned}
 V_S &= \frac{k_1 k_2 k_{-3} (E)_0}{k_1 k_{-3} + k_3 (k_{-1} + k_2) [1 + (I)/K_{SI}]} \\
 V_P &= \frac{k_{-1} k_{-2} k_{-6} (E)_0}{k_{-2} k_{-6} + k_6 (k_{-1} + k_2) [1 + (I)/K_{PI}]} \\
 K_S &= \frac{k_{-3} (k_{-1} + k_2) [1 + (I)/K_I]}{k_1 k_{-3} + k_3 (k_{-1} + k_2) [1 + (I)/K_{SI}]} \\
 K_P &= \frac{k_{-6} (k_{-1} + k_2) [1 + (I)/K_I]}{k_{-2} k_{-6} + k_6 (k_{-1} + k_2) [1 + (I)/K_{PI}]} \\
 \theta_S &= \frac{(k_{-1} + k_2) k_3 k_4 k_6}{k_1 k_2 k_{-3} (k_{-4} + k_6)} \\
 \theta_P &= \frac{k_6 k_{-7} k_{-8} (k_{-1} + k_2)}{k_{-1} k_{-2} k_{-6} (k_{-7} + k_8)} \\
 K_{SP} &= \frac{k_{-3} k_{-6} (k_{-4} + k_6) (k_{-7} + k_8) [1 + (I)/K_I]}{k_3 k_{-6} k_{-6} (k_{-7} + k_8) + k_{-3} k_6 k_7 (k_{-4} + k_6)} \\
 K_{S_1} &= \frac{k_{-3} (k_{-4} + k_6) [1 + (I)/K_I]}{k_3 k_4} \\
 K_{P_1} &= \frac{k_{-6} (k_{-7} + k_8) [1 + (I)/K_I]}{k_6 k_{-8}} \quad (13)
 \end{aligned}$$

Both V_S and V_P are functions of (I) instead of being independent of (I) as observed for fumarase, unless the inhibitor dissociation constants K_{SI} and K_{PI} are much larger than the inhibitor concentrations used. All the competitive inhibition data for fumarase have been obtained under experimental conditions with no apparent product or substrate activation; that is, the squared terms in eq. 12 were negligible. If insignificant concentrations of the complexes SE and PE are formed under these conditions, it is reasonable to assume that the concentrations of SEI and PEI are also insignificant so that the inhibition steps with dissociation constants K_{SI} and K_{PI} may be neglected. Under these conditions V_S and V_P are independent of (I) , and K_S and K_P are linear functions of (I) and will yield the same inhibition constant K_I . Therefore, mechanism 10 can satisfactorily represent the competitive inhibition data for fumarase.⁴⁻⁷

Mechanism 10 can represent any combination of activation or inhibition by substrate and product. At high concentrations of substrate and product the squared and cross product terms in (S) and (P) will be of significance and, depending on the ratio of their coefficients, either activation or inhibition will result.

Two mechanisms suggested by Kistiakowsky and Rosenberg¹¹ lead to K_{SP} terms. The first involves two types of enzymatic sites which are independent

but have different values for the rate constants. The second involves enzymatic sites which are identical but interact in pairs. The first mechanism can be eliminated on the basis of arguments about competitive inhibition which are similar to those given above. The second mechanism is a real possibility but will not be discussed here because it involves the rather special circumstance of pairwise interaction.¹²

Experimental Procedure

Crystalline fumarase was prepared from pig heart muscle by the method described in ref. 13 and was stored as crystals suspended in 50% saturated ammonium sulfate solution at 0°. Fumaric and L-malic acids were purified by methods described earlier.¹⁴ Tris(hydroxymethyl)aminomethane, "Tris," used for "Tris" acetate buffers, was primary grade Sigma 121. All solutions were prepared with conductivity water made with a Barnstead conductivity water still.

A Cary 14 recording spectrophotometer with a scale of 0-0.2 absorbancy unit was used to obtain the initial velocities and the relaxation times. All solutions were thermostated at 25.5°, except the buffered fumarase solution which was kept at 0° in order to keep the decay of enzymatic activity to a minimum. The initial velocity and relaxation time for each reaction mixture were corrected to an enzyme concentration which would give a change of 0.0550 absorbancy unit/min. at 230 m μ when 0.5 ml. of buffered enzyme solution was added to 25 ml. of 204 μM L-malate, 0.02 M "Tris" acetate, at pH 7.50 and 25.5°.

The initial velocity for each reaction mixture is an average of five determinations. The relaxation times were determined in triplicate for a given substrate concentration and were measured from both sides of the equilibrium, that is, excess fumarate in one experiment and excess malate in the other.

Results of Steady-State Velocity Experiments

Initial velocities measured with L-malate and fumarate at pH 7 are shown in Fig. 1. The maximum velocities and Michaelis constants calculated from the linear parts of these graphs and from similar data at other pH values are summarized in Table I. It is evident that, with both fumarate and L-malate, substrate activation is encountered at the higher substrate con-

(11) G. B. Kistiakowsky and A. J. Rosenberg, *J. Am. Chem. Soc.*, **74**, 5020 (1952).

(12) For further details see M. Taraszka, Ph.D. Dissertation, University of Wisconsin, 1962.

(13) C. Frieden, R. M. Bock, and R. A. Alberty, *J. Am. Chem. Soc.*, **76**, 2482 (1954).

(14) C. Frieden, R. G. Wolfe, Jr., and R. A. Alberty, *ibid.*, **79**, 1523 (1957).

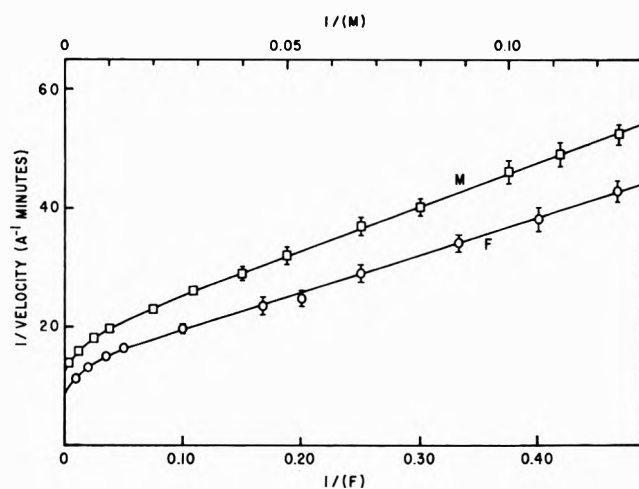


Figure 1. Plot of reciprocal initial velocity vs. reciprocal initial fumarate concentration and reciprocal L-malate concentration for pH 7.00, 0.02 M "Tris" acetate, and 25°. The initial velocity is expressed in absorbancy units/min. for a 10-cm. cuvette at 230 m μ . The substrate concentrations in both cases are given in μ molar units.

Table I: Kinetic Parameters for the Fumarase Reaction in 0.02 M "Tris" Acetate Buffer at 25°^a

Parameter	pH 6.50	pH 7.00	pH 7.50
V_B , mM min. ⁻¹	2.35 ± 0.09	1.63 ± 0.07	0.94 ± 0.05
V_P , mM min. ⁻¹	0.76 ± 0.03	1.26 ± 0.04	1.38 ± 0.09
K_B , μ M	5.4 ± 0.6	4.6 ± 0.5	4.8 ± 0.07
K_P , μ M	8.9 ± 0.8	16.3 ± 1.6	29.4 ± 2.8
$V_B K_P / V_P K_B$	5.1	4.6	4.2
K_{SP} , μ M ²	300 ± 100	250 ± 100	400 ± 150
θ_B , μ M ⁻¹		10 ⁻³	
θ_P , μ M ⁻¹		10 ⁻⁴	

^a S = fumarate; P = L-malate.

centrations. As required by eq. 2 and 12 the quantity $V_F K_M / V_M K_F$ is equal to the directly determined equilibrium ratio of L-malate to fumarate, which is 4.53 in this buffer at 25° and pH 7.

When the product concentration is negligible eq. 12 becomes

$$v = \frac{(V_S/K_S)(S)[1 + \theta_S(S)]}{1 + (S)/K_S + (S)^2/K_{S_2}} \quad (14)$$

The fact that substrate activation is observed (Fig. 1) indicates that the numerator term in substrate concentration squared is more important than the corresponding denominator term. The values of V_S and K_S were calculated from the linear portions of plots of the type of Fig. 1. Then the value of θ_S required to give the best fit of the nonlinear portion was determined. The values $\theta_S = 10^{-3} \mu$ M⁻¹ and

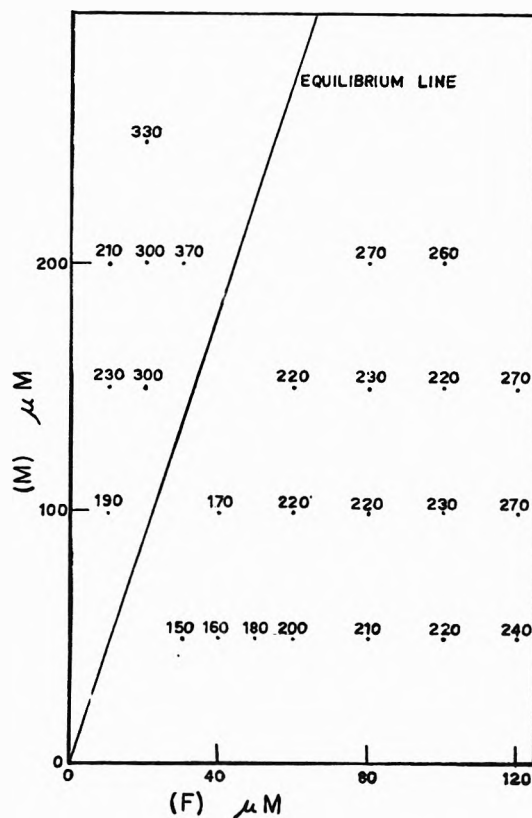


Figure 2. Grid of K_{MF} values for pH 7.00, 0.02 M "tris" acetate, and 25°. The K_{MF} values were calculated using eq. 12, $\theta_B = 10^{-3} \mu$ M⁻¹, $\theta_P = 10^{-4} \mu$ M⁻¹, $K_S^2 = K_M^2 = \infty$, and the kinetic parameters V_B , V_P , K_B , and K_P given in Table I.

$\theta_P = 10^{-4} \mu$ M⁻¹ are found to represent the data at pH 7. For the fumarase reaction we will let S represent fumarate and P represent L-malate.

The steady-state velocities for various mixtures of fumarate and malate were then used to calculate K_{SP} using eq. 12, the values of all of the other parameters being known. The values of K_{SP} obtained at pH 7 are shown in a grid in Fig. 2. These values increase from approximately 150 to 300 μ M² as the total concentration of fumarate and malate is increased from 80 to 300 μ M, but it would not have been expected that a very accurate determination of this parameter could be made, especially in view of the approximate values of θ_S , θ_P , K_{S_2} , and K_{P_2} . As can be seen from Table I nothing can be said about the pH dependence of K_{SP} due to the large experimental error.

Only the initial velocities for solutions in which the sum of the concentrations of fumarate and L-malate was less than 300 μ M were considered so that the ionic strength contribution of fumarate plus L-malate was less than 5% of the total ionic strength. Experimental data require an (S)(P) term rather than an (S)²(P)

term or $(S)(P)^2$ term, and this is in agreement with the proposed mechanism. If the term were $(S)^2(P)$, the observed value of K_{SP} would equal $K_{SP}/(S)$ and the value of K_{SP} would decrease to half its value when (S) is doubled.

Steady-State Relaxation Theory and Results

The form of the complete steady-state rate law may also be investigated by studying the rate of approach to equilibrium starting with a mixture which differs only slightly from the equilibrium mixture. This relaxation method⁶ has already been used to study the fumarase reaction. If the initial displacement of the substrate concentration from equilibrium, $[\Delta(S)]_0$, is sufficiently small, the difference between the substrate concentration at any time and its equilibrium concentration is given by

$$\Delta(S) = [\Delta(S)]_0 e^{-t/\tau_{SS}} \quad (15)$$

where τ_{SS} is the steady-state relaxation time. Using procedures described earlier it may be shown that for rate eq. 12, corresponding with mechanism 10, the expression for the relaxation time is

$$\tau_{SS} = \frac{1 + (\bar{S})/K_S + (\bar{P})/K_P + (\bar{S})(\bar{P})/K_{SP} + (\bar{S})^2/K_{S_2} + (\bar{P})^2/K_{P_2}}{(V_S/K_S + V_P/K_P)[1 + \theta_S(\bar{S}) + \theta_P(\bar{P})]} \quad (16)$$

where the bars indicate equilibrium concentrations. Introducing $K_{eq} = (\bar{P})/(\bar{S}) = V_S K_P / V_P K_S$ and $(S)_0 = (\bar{S}) + (\bar{P})$ this equation may be rewritten

$$\tau_{SS} = \frac{1 + [(S)_0/(1 + K_{eq})](1/K_S + K_{eq}/K_P) + [(S)_0^2/(1 + K_{eq})^2](K_{eq}/K_{SP} + 1/K_{S_2} + K_{eq}^2/K_{P_2})}{(V_S/K_S + V_P/K_P)\{1 + [(S)_0/(1 + K_{eq})](\theta_S + K_{eq}\theta_P)\}} \quad (17)$$

For the simple reversible Michaelis-Menten mechanism this reduces to

$$\tau_{SS} = \frac{1 + [(S)_0/(1 + K_{eq})](1/K_S + K_{eq}/K_P)}{V_S/K_S + V_P/K_P} \quad (18)$$

which has been confirmed experimentally for the fumarase reaction at low total substrate concentrations. As may be seen from eq. 17, a nonlinear dependence of τ_{SS} on $(S)_0$ would be expected at higher concentrations. This nonlinear dependence is illustrated in Fig. 3. To evaluate τ_{SS} a smooth line was drawn through the spectrophotometer tracing and Guggenheim¹⁵ plots of $\ln(A_t + \Delta t - A_t)$ vs. time were used to obtain relaxation times since the rate of re-

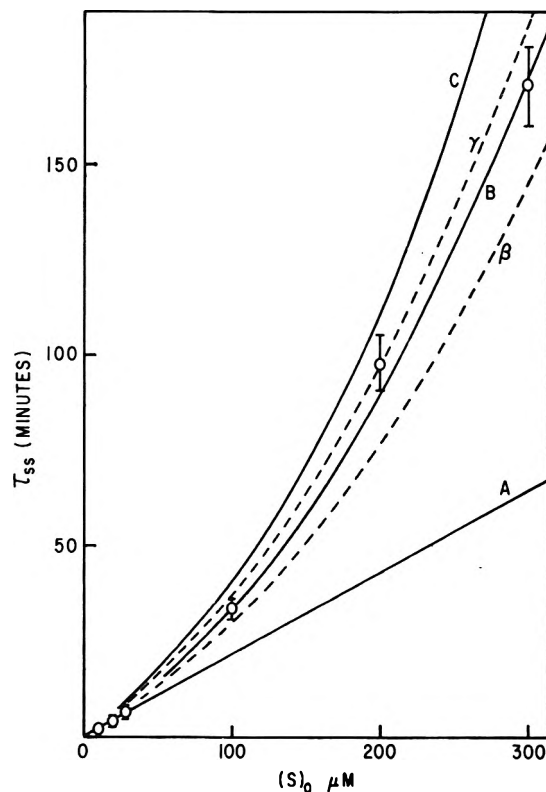


Figure 3. Plot of steady-state relaxation time vs. total substrate concentration, $(S)_0 = (S) + (P)$, for pH 7.00, 0.02 M "Tris" acetate, and 25°. The points are experimental. Curves A, B, C, β , and γ are all obtained by using V_S , K_S , V_P , K_P , and K_{eq} determined by initial velocity experiments. Curve A is a plot of eq. 18; curves B and C are plots of eq. 17 with K_{SP} equal to 300 and 200 μM^2 , respectively; curves β and γ are plots of eq. 17 with $\theta_S = 10^{-3} \mu M^{-1}$, $\theta_P = 10^{-4} \mu M^{-1}$, and $K_{SP} = 300$ and 200 μM^2 , respectively.

action is proportional to the displacement from equilibrium. A_t is the absorbancy at time t and $A_t + \Delta t$ is the absorbancy of t plus Δt , where Δt is a constant time interval. The relaxation time is equal to the negative reciprocal of the slope of such a plot. All experimental τ_{SS} values were corrected to the enzyme activity used for the initial velocity data so they can be compared with the values calculated from the parameters determined in initial velocity experiments. The corrected experimental τ_{SS} values are plotted vs. $(S)_0$ in Fig. 3 where $(S)_0$ is the total concentration of fumarate plus L-malate. The graph shows that at low substrate concentrations, $(S)_0 < 50 \mu M$, the data may be represented by eq. 18, which applies to the simple reversible Michaelis-Menten mechanism. At high substrate concentrations the experimental τ_{SS} values are in agreement with eq. 17 with the initial

(15) E. A. Guggenheim, *Phil. Mag.*, 2, 538 (1926).

velocity parameters from Table I and $\theta_S = 10^{-3} \mu M^{-1}$ and $\theta_P = 10^{-4} \mu M^{-1}$.

Discussion

This paper illustrates the fact that more thorough studies of the kinetics of an enzymatic reaction generally disclose further terms in the rate law which in turn require extension of the mechanism. There are at least two ways of explaining the present results, but mechanism 10 has the advantage that it represents a simple extension of the mechanism which is generally used to account for substrate activation and substrate inhibition effects. The extension consists of providing for effects of both substrate and product. Actually, mechanism 10 has been extended to include more intermediates to provide for the effect of pH on the steady-state rates of the fumarase reaction.¹² Since the effect of pH on various kinetic parameters is not discussed in this article, this extension is not necessary here and would only increase the complexity of the rate equation.

There are several difficulties in the determination of further kinetic parameters of the type discussed here. First, since the substrate is an electrolyte, the range of substrate concentration which can be used must be well below the buffer concentration. As the substrate concentration approaches the buffer concentration, the medium effects on the kinetics change appreciably as the substrate concentration is varied. Second, since the rate equation is not linear, it is difficult to devise objective methods for evaluating all of the kinetic parameters at one time. In the method used here, errors in the values of the Michaelis constants and maximum velocities determined at low concentrations lead to larger errors in kinetic parameters such as K_{SP} . An analysis of the effect of these errors indicates that K_{SP} is uncertain by about $\pm 40\%$.

An important conclusion from this study is that initial velocity studies with only substrate or product present are not sufficient to reveal all of the terms that may be present in the complete rate law for an enzymatic reaction.

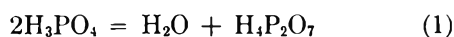
Self-Dissociative Equilibria in Molten Phosphoric Acid

by Ronald A. Munson

General Electric Research Laboratory, Schenectady, New York (Received June 6, 1964)

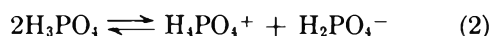
Stoichiometric orthophosphoric acid dissociates extensively to produce pyrophosphate, H_4PO_4^+ , and H_2PO_4^- ions. The concentrations of these ions, which have been determined by cryoscopic and electromotive force measurements, are $[\text{H}_4\text{PO}_4^+]_0 = 0.54 m$, $[\text{H}_2\text{PO}_4^-]_0 = 0.26 m$, and $[\text{H}_3\text{O}^+]_0 = [\text{pyrophosphate}]_0 = 0.28 m$ at 38° . Water acts as a base and perchloric and sulfuric acids have been found to behave as strong monoprotic acids in phosphoric acid. Pyrophosphoric acid appears to be a diprotic acid. The fivefold greater conductivity of stoichiometric orthophosphoric acid over that of sulfuric acid results from the greater concentration of charge carriers in phosphoric acid while the protonic mobility in phosphoric acid is appreciably smaller.

The self-dissociation properties of most of the major inorganic acids have been investigated, and those of sulfuric acid¹ are particularly well established. Phosphoric acid, however, is relatively less well understood. This lack of knowledge is due, in part, to experimental difficulties caused by the sluggish character of the orthophosphoric-pyrophosphoric interconversion in the neighborhood of room temperature. Without the intent of specifying the degree of ionization, this interconversion may be represented by



Ion-exchange elution and filter paper chromatography have provided estimates of the degree of pyrophosphate formation.^{2,3} However, it has not previously been fully appreciated that the extent of pyrophosphate formation is somewhat temperature dependent and that solutions equilibrated at higher temperatures tend to "freeze in" a higher concentration of pyrophosphate (unless several weeks are allowed for equilibration) when cooled to room temperature.

Although molten stoichiometric orthophosphoric acid has an equilibrium composition of a few mole per cent pyrophosphate, crystalline anhydrous phosphoric acid is apparently completely ortho.⁴⁻⁶ Both crystalline and freshly fused anhydrous phosphoric acid exhibit an appreciable ionic conductivity which suggests extensive autoprotolysis according to eq. 2.



The conductivity of phosphoric acid is anomalously

high ($K_{26} = 4.596 \times 10^{-2} \text{ ohm}^{-1} \text{ cm.}^{-1}$) for Stokesian diffusion when its high viscosity ($\eta_{25} = 178 \text{ c.p.}$) is taken into consideration. Greenwood and Thompson⁷ correctly interpreted this to mean that a protonic Grotthuss chain conduction mechanism was responsible for the high ionic conductivity. They tested their hypothesis by showing that the transport number for potassium ion (which must conduct by Stokesian migration) was less than 0.002. Arguing by analogy from the sulfuric acid system and by the choice of a reasonable value for the chain mobility, these workers estimated the concentration of each of the products of autoprotolysis to be about $0.1 m$ at 25° .

Experimental

Phosphoric acid (100.1%) was prepared from analytical reagent 85% phosphoric acid by water removal under vacuum.⁸ Crystalline melting points (Fig. 1) proved to be the best criterion of purity and water content. By their use, the 100.0% acid was prepared. Some 100.0% acid, which was used in some of the

- (1) R. J. Gillespie, *Rev. Pure Appl. Chem.*, **9**, 1 (1959).
- (2) A. L. Huhti and P. A. Gartaganis, *Can. J. Chem.*, **34**, 785 (1956).
- (3) R. F. Jameson, *J. Chem. Soc.*, 752 (1959).
- (4) A. Simon and G. Schulze, *Z. anorg. allgem. Chem.*, **242**, 315 (1939).
- (5) S. Fuberg, *Acta Chem. Scand.*, **9**, 1557 (1955).
- (6) J. P. Smith, W. E. Brown, and J. R. Lehr, *J. Am. Chem. Soc.*, **77**, 2728 (1955).
- (7) N. N. Greenwood and A. Thompson, *J. Chem. Soc.*, 3485 (1959).
- (8) *Inorg. Syn.*, **1**, 101 (1960).

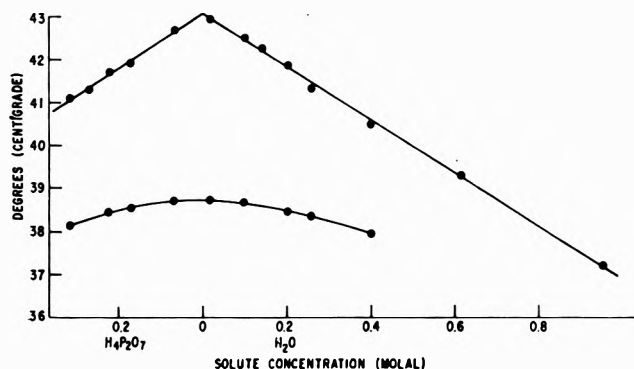


Figure 1.—Crystalline (upper data) and equilibrium melting points of the system water-phosphorus pentoxide in the vicinity of the composition of phosphoric acid.

e.m.f. determinations, was prepared conveniently from Phospholeum (105% phosphoric acid) and distilled water. This batch of acid had a slight straw color and considerably greater light absorption in the ultraviolet region. Although it was considered to be less pure than the acid prepared by water removal, it gave e.m.f. values consistent with those obtained with the phosphoric acid of greater purity. Sulfuric acid (100.0%) was prepared from analytical reagent fuming sulfuric acid and distilled water. A solution 19.0% by weight perchloric acid and 80.8% phosphoric acid was prepared at 120° by stirring analytical reagent phosphorus pentoxide with analytical reagent 70% perchloric acid. Lithium perchlorate was prepared by neutralizing lithium carbonate with analytical reagent perchloric acid. Just prior to use it was heated to 300°, and it analyzed 92.9% (93.5) ClO_4^- . Lithium dihydrogen phosphate (99.0%) was also prepared from lithium carbonate. Reagent potassium bisulfate (100.1%) and potassium dihydrogen phosphate (99.4%) as well as the other salts were stored in a vacuum desiccator at 100°. All open manipulations were carried out in a drybox furnished with dry N_2 and P_2O_5 .

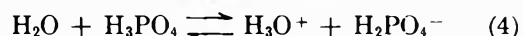
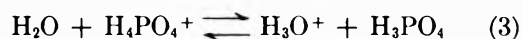
E.m.f. Measurements. An H-type cell contained a hydrogen on platinum and a silver-silver chloride half-cell. Ultrapure hydrogen was bubbled through 100% phosphoric acid before passing into the hydrogen half-cell. The temperature was maintained to $\pm 0.01^\circ$, and a K-3 Leeds and Northrup Universal potentiometer was employed. All solutions were saturated with silver chloride, which is very insoluble below 100°. Brief anodic polarization of the hydrogen electrode with a third electrode was found to be beneficial to its stability.

Melting Point Determinations. The modified Beckmann method employed in the cryoscopy of sulfuric acid⁹ could not be used owing to the presence of a vary-

ing amount of pyrophosphate which was dependent upon the past thermal history of the sample. Rather, samples were sealed in 0.159-cm. diameter, thin-walled, glass capillary tubes, and the tubes were placed on Beckmann thermometers in constant temperature baths so that the tubes could be frequently rotated. The thermometers were standardized to within 0.005° by comparison with a platinum resistance thermometer calibrated at the National Bureau of Standards. Melting points were accurate to $\pm 0.05^\circ$. Two types of melting points were determined. For the crystalline melting points, the sample remained completely crystalline for at least 2 days at room temperature in order to shift the equilibrium back to 100% orthophosphoric acid. The lowest temperature at which the entire sample would melt with agitation within 1 hr. was taken as the melting point. One hour is somewhat arbitrary, but it is short enough to avoid significant pyrophosphate formation and long enough for thermal equilibrium. For the equilibrium melting points the sample was maintained in the bath for at least 3 weeks before the final melting point was obtained. The equilibrium melting point was taken to be the lowest temperature at which all crystals disappeared.

Results and Discussion

Figure 1 exhibits the crystalline melting point depressions occasioned by the presence of water (molal melting point depression, $k_m = 6.19$) and pyrophosphoric acid ($k_m = 6.36$). The heat of fusion of phosphoric acid is 3.1 kcal./mole,¹⁰ which corresponds to a one-particle cryoscopic constant of 6.28 deg. m^{-1} . This apparent one-particle/molecule depression may be interpreted as indicating that neither water nor pyrophosphoric acid dissociates in phosphoric acid. Alternatively, they may act as a base and acid, respectively, but, in the presence of a high degree of autoprotolytic dissociation, the autoprotolytic equilibrium shifts in a manner which keeps the number of cryoscopically active particles nearly constant. This situation may be represented by the simultaneous occurrence of reactions 3 and 4



where the amounts of H_4PO_4^+ consumed and H_2PO_4^- produced are the more nearly equal, the greater the degree of self-dissociation (so long as excess H_3PO_4 is present). The latter interpretation is experimentally

(9) R. J. Gillespie, E. D. Hughes, and C. K. Ingold, *J. Chem. Soc.*, 2473 (1950).

(10) E. P. Egan and Z. T. Wakefield, *J. Phys. Chem.*, 61, 1500 (1957).

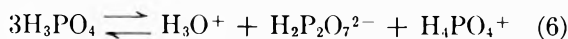
supported by the nearly one-particle/molecule depressions found for bases and acids [$k_m(\text{KH}_2\text{PO}_4) = 7.5$; $k_m(\text{LiH}_2\text{PO}_4) = 8.7$; $k_m(\text{HClO}_4) = 8.7$] which may be contrasted with the two-particle depressions found for KHSO_4 ($k_m = 11.7$) and LiClO_4 ($k_m = 12.7$) as may be expected for 1-1 salts. The roles of water and pyrophosphoric acid in phosphoric acid appear to be analogous to those of water and pyrosulfuric acid in sulfuric acid,¹¹ except, as will be shown below, pyrophosphoric acid is a much stronger acid than pyrosulfuric in their respective solvents.

If we assume that orthophosphoric acid sufficiently obeys Raoult's law, then the degree of dissociation (α_0)¹² is given by

$$\alpha_0 = (-k_m/m_1)(T'')_0 \quad (5)$$

where m_1 is the orthophosphoric acid molal concentration and T''_0 the second derivative of the melting temperature with respect to the water concentration at $m_2 = 0$. Equation 5 presumes the formation of two cryoscopically active particles (water and pyrophosphoric acid) from two molecules of solvent since the further dissociation of these species does not produce a substantial cryoscopic effect. From Fig. 2 we find $(T'')_0 = -11.3 \text{ deg./}m^2$, $\alpha_0 = 0.055$, and, therefore, stoichiometric orthophosphoric acid contains 0.28 m hydronium ion and pyrophosphate ion, each at equilibrium in the vicinity of its melting point. This result differs from those of others^{2,3,13-15} who found pyrophosphate concentrations of 0.4 to 0.7 m . However, none of these investigators allowed sufficient time for equilibration at a constant temperature following sample preparation (3 weeks are required at 40°). They appear to have measured that amount of pyrophosphate which happened to be "frozen in" during their cooling process.

For the determination of the H_4PO_4^+ concentration, e.m.f. measurements were made on a series of hydrogen silver-silver chloride cells at 25 and 80° (Fig. 3 and 4). If pyrophosphate ion is formed according to reaction 6, then the equilibria in phosphoric acid



may be represented by (7) and (8). Solving (7) and

$$[\text{H}_4\text{PO}_4^+][\text{H}_2\text{PO}_4^-] = K_1 \quad (7)$$

$$[\text{H}_2\text{P}_2\text{O}_7^{2-}]^2[\text{H}_4\text{PO}_4^+] = K_2 \quad (8)$$

(8) for the relation between $[\text{H}_4\text{PO}_4^+]$ and the concentration of added base (x) or acid ($-x$) we obtain

$$x[\text{H}_4\text{PO}_4^+] + [\text{H}_4\text{PO}_4^+]^2 - K_1 = \sqrt{K_2[\text{H}_4\text{PO}_4^+]} \quad (9)$$

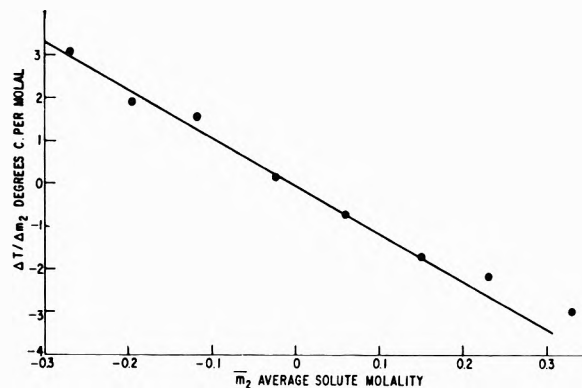


Figure 2. First derivative of the equilibrium melting points as a function of average water content.

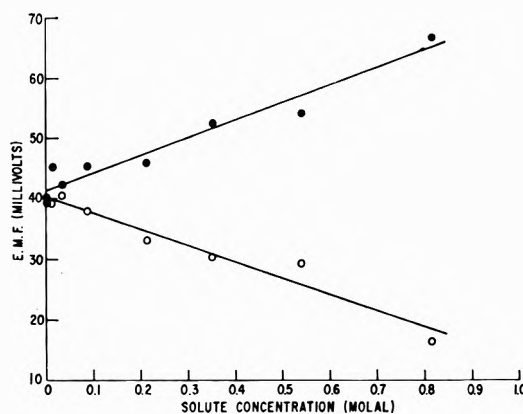


Figure 3.—E.m.f. vs. solute concentration at 25°: ●, KH_2PO_4 ; ○, H_2SO_4 ; $9.8 \times 10^{-4} m$ KCl.

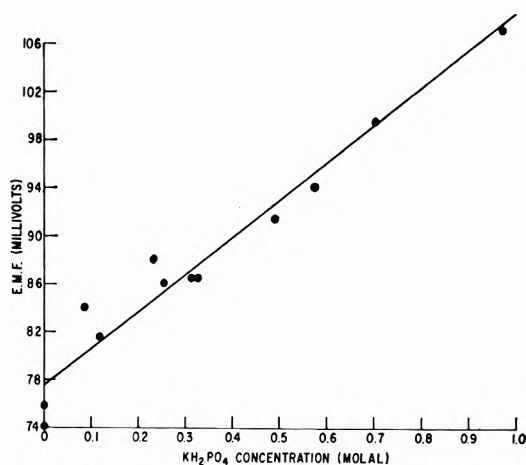


Figure 4.—E.m.f. vs. KH_2PO_4 concentration at 80°; $6.1 \times 10^{-4} m$ KCl.

(11) R. H. Flowers, R. J. Gillespie, and E. A. Robinson, *Can. J. Chem.*, **38**, 1363 (1960).

(12) P. A. H. Wyatt, *Trans. Faraday Soc.*, **52**, 806 (1956).

(13) R. N. Bell, *Ind. Eng. Chem.*, **40**, 1464 (1948).

(14) C. E. Higgins and W. H. Baldwin, *Anal. Chem.*, **27**, 1780 (1955).

(15) J. C. Guffy and G. R. Miller, *ibid.*, **31**, 1895 (1959).

Linearizing for relatively small changes in H_4PO_4^+ concentration we find

$$\Delta[\text{H}_4\text{PO}_4^+] = \frac{x}{2[1 - (\sqrt{K_2})/(4[\text{H}_4\text{PO}_4^+]_0)^{1/2}]} \quad (10)$$

By neglecting activity coefficient changes for small changes in concentrations we obtain the expression for the electromotive force at low solute concentration

$$\begin{aligned} \text{e.m.f.} &= E^\circ + (RT/F) \ln [\text{H}_4\text{PO}_4^+] = \\ &E^\circ + (RT/F) \ln (1 + \\ &\Delta[\text{H}_4\text{PO}_4^+]/[\text{H}_4\text{PO}_4^+]_0) \quad (11) \end{aligned}$$

$$\begin{aligned} \text{e.m.f.} &= E^{\circ'} + \\ &\frac{RTx}{2F[\text{H}_4\text{PO}_4^+]_0(1 - (\sqrt{K_2})/(4[\text{H}_4\text{PO}_4^+]_0)^{1/2})} \quad (12) \end{aligned}$$

At 25° we find an average slope of $27.7 \text{ mv. } m^{-1}$ and at 80° a slope of $31.0 \text{ mv. } m^{-1}$. This increase in slope corresponds nearly to the temperature change in RT/F so that $[\text{H}_4\text{PO}_4^+]_0$ must be only weakly temperature dependent. We may, therefore, employ the results of the e.m.f. measurements with the melting point depression curvature data at approximately 38° to obtain $K_1 = 0.14$, $K_2 = 0.042$, $[\text{H}_4\text{PO}_4^+]_0 = 0.54$, and $[\text{H}_2\text{PO}_4^-]_0 = 0.26 \text{ m}$. Had it been assumed that the $\text{H}_3\text{P}_2\text{O}_7^-$ ion was not involved in an equilibrium with the H_4PO_4^+ ion, then the plot of e.m.f. vs. acid or base concentration could not be expected to remain linear beyond 0.6 m . Since such deviations are not observed, eq. 6 and 8 appear justified.

It has been assumed throughout that the activity coefficients effectively remain constant under the con-

ditions investigated and that their role may be neglected. None of the data suggests that we have entered into considerable error as a result of this simplification. Indeed, e.m.f. measurements on phosphoric acid solutions of salts indicate that activity coefficient effects are one order of magnitude less important than the results discussed. The relatively high dielectric constant of phosphoric acid,¹⁶ as well as its high intrinsic ionic strength, tend to minimize the electrostatic influence on activities.

Comparison with Sulfuric Acid. The autodissociation of sulfuric acid is considerably less extensive¹⁷ ($[\text{pyrosulfate}] = 0.0088 \text{ m}$, $[\text{H}_3\text{SO}_4^+]_0 = 0.0135 \text{ m}$, and $[\text{HSO}_4^-]_0 = 0.0178 \text{ m}$) than that of phosphoric acid. Despite its 20 to 30 times greater charge carrier concentration, phosphoric acid exhibits just a five-fold conductivity increase over sulfuric acid. The proton-jump mobility in phosphoric acid must be of the order of one-fifth as large as it is in sulfuric acid. The reduced mobility may be ascribed to the greater ion atmosphere retarding forces at the higher ionic concentration and to slower solvent orientation to form hydrogen bonds suitable for current-carrying proton jumps in phosphoric acid.

Acknowledgment. The author is indebted to Professors N. N. Greenwood and R. J. Gillespie for stimulating discussions. A. D. Warner graciously supplied him with a least-squares curve-fitting program which was used in analyzing the data.

(16) R. A. Munson, *J. Chem. Phys.*, **40**, 2044 (1964).

(17) R. H. Flowers, R. J. Gillespie, E. A. Robinson, and C. Solomons, *J. Chem. Soc.*, 4327 (1960).

Solute Diffusional Specificity in Hydrogen-Bonding Systems¹

by Samuel B. Horowitz and I. Robert Fenichel

Laboratory of Cellular Biophysics, Albert Einstein Medical Center Research Laboratories, Philadelphia, Pennsylvania 19141 (Received June 8, 1964)

The diffusion coefficients of 18 H-bonding aliphatic organic nonelectrolytes were measured in water-swollen (5–25°) and formamide-swollen (15.3°) dextran gels. Variation in coefficient is attributable to molecular size and at least two other sources. The first of these, solute-solvent H-bond formation, has the effect of selectively slowing the diffusion of stronger H-bonding solutes; this appears to be a general property of H-bonding solvents. The second source is probably confined to water and relatively unmodified aqueous systems. It arises from the ability of water to form stabilized structures ("icebergs") through interaction with nonpolar groups and has the effect of selectively slowing the diffusion of solutes bearing such groups. Solute diffusional specificity in water represents a superimposition of these two processes; additional evidence for this is provided by data on the temperature dependence of diffusion and the correlation of diffusion coefficients with entropies of vaporization.

Introduction

The study of the diffusion of small organic nonelectrolytes in H-bonded systems can be an important source of information for the understanding of these materials. Among the types of systems—liquid, gel, and crystalline—technical considerations have largely limited study to the first two. A few theoretical approaches to the data have been made, but none has had more than limited success unless it relied heavily on empirical correction. One of the least satisfying aspects of the problem is the lack of a coherent picture of the effect on diffusion, in a given solvent, of variation of the solute species. Thus, Eyring's theory² fails almost entirely to predict variation of the diffusion coefficient, D , among different solutes in water. Arnold,³ with fairly good success, accounted for solute variation in water and other H-bonding solvents using both molecular size parameters and solute "association factors," while Wilke,⁴ using only the solute molal volume, obtained an equally good correlation of the same data for water, but poorer results for other solvents when the possibility of H-bond interaction existed.

It was felt that a clarification of solute specificity in diffusion in H-bonding systems required a body of data incorporating a systematic variation of solute parameters, both molecular size and chemical composition. The present work describes such a study, using two

solvent systems, both strongly H-bonding: water-swollen and formamide-swollen dextran gels.

Experimental

The experimental methods, materials, and analysis were essentially the same for both formamide and water gels. The slight differences in procedure are detailed in the appropriate places.

Materials. Spherical G-34 Sephadex[®] beads⁵ of 1.25–1.91-mm. dry diameter were used. Dry beads were selected under a microscope for size, spherical shape, and surface smoothness. They were weighed and swollen for at least 48 hr. in an excess of the appropriate solvent. The swollen beads were reweighed and the solvent content was calculated. The formamide-

(1) This work was supported by National Science Foundation Grants GB 665 and GB 1794 and by Public Health Service Research Grant GM 11070-01 from the Division of General Medical Sciences. Part of this work was done at The Institute of Physiology, University of Uppsala, Uppsala, Sweden.

(2) A. E. Stearn, E. M. Irish, and H. Eyring, *J. Phys. Chem.*, **44**, 981 (1940).

(3) J. H. Arnold, *J. Am. Chem. Soc.*, **52**, 3937 (1930).

(4) C. R. Wilke, *Chem. Eng. Progr.*, **45**, 218 (1949).

(5) Sephadex[®] is the trade mark of AB Pharmacia, Uppsala, for epichlorohydrin cross-linked dextran, a high molecular weight poly- α -1,6-glucoside. The properties of the material are reviewed by P. Flodin, "Dextran Gels and Their Application in Gel Filtration," Pharmacia, Uppsala, Sweden, 1962. The beads used in these experiments were provided by the manufacturer through the courtesy of Doc. B. Gelotte.

swollen beads were $86.3 \pm 0.5\%$ solvent. The water-swollen beads were $81.7 \pm 0.9\%$ solvent. The radius, a , of the swollen bead, required for the evaluation of diffusion coefficients, was calculated from the wet weight taking the bead density as 1.1 for water-swollen beads⁶ and 1.2 for formamide-swollen beads.⁷

The radioisotopically labeled solutes and their sources were acetone-C¹⁴, ethyl acetate-C¹⁴, methanol-C¹⁴, ethanol-C¹⁴, 2-propanol-C¹⁴, 1-propanol-C¹⁴, 1-butanol-C¹⁴, 1-pentanol-C¹⁴, formamide-C¹⁴, acetamide-C¹⁴, propionamide-C¹⁴, methylurea-C¹⁴, glycerol-H³, water-H³, and thiourea-S³⁵ from New England Nuclear Corp., Boston, Mass.; thiourea-C¹⁴, methylthiourea-S³⁵, ethylthiourea S³⁵, and urea-C¹⁴ from the Radiochemical Centre, Amersham, England. The compounds were used as supplied by the manufacturer with no additional purification. The unlabeled forms of the above compounds were reagent grade. The substituted thioureas were synthesized from Eastman isothiocyanates by the method of Moore and Crossley.⁸

The formamide (Eastman No. 565) was used as received. Formamide is hygroscopic, and some uptake of atmospheric water occurred. This uptake was monitored by refractometry and found to increase in the course of an experiment. However, the water uptake was similar in each experiment and always small, rarely exceeding 1.5% by weight. No correction for this uptake was applied.

Method. A single swollen bead was transferred from solvent to an excess of 20 mM (50 mM in the case of thiourea in water) solution of the unlabeled solute for at least 4 hr. at room temperature. The bead was then transferred to a 1-ml. portion of solution containing the labeled solute at the same concentration and was allowed to equilibrate overnight at the temperature of the experiment. Temperature was maintained to $\pm 0.05^\circ$.

The bead was removed from the radioactive solution, blotted to remove excess liquid, and immersed, with stirring, successively in 10.0-ml. (7.0 ml. in the water experiments) portions of the nonradioactive solution. This provided a dilution factor of not less than 350, adequate to assure that the tracer concentration in each wash-out bath, except the final one, was negligible relative to that in the bead. Stirring was accomplished by having the bead held in a fine copper wire holder which was mounted eccentrically by a friction cuff to the shaft of a variable-speed stirring motor. Seven wash-out baths were used in each run. Transfer of the bead between baths was done at 100, 300, 600, 900, 1200, and 1500 sec. (for some of the formamide experiments an 1800-sec. bath was added). Each transfer was accomplished in 3–4 sec. The bead was allowed to remain

in the final wash-out bath at least 2 hr. at room temperature to recover all remaining tracer.

Analysis. A 1.0-ml. aliquot of wash-out bath was pipetted into a 22-ml. counting vial with 20 ml. of scintillation fluid⁹ and counted in a 314EX or 3214 Packard liquid scintillation spectrometer at 2°. The standard error of the count was kept below 1.5%.

Data were analyzed as follows. Let n_i represent the number of counts per minute, less background, in a 1.0-ml. aliquot from the i th wash-out bath, V , the volume of a wash-out bath, and N , the total number of wash-out baths. The amount of tracer remaining in the bead at the end of the experiment is negligible (less than 0.3%) in comparison to the amount in any of the wash-out baths. Then $V \sum_{i=1}^N n_i$ represents the total counts in the bead at the start of the experiment, and $C_0 = V \sum_{i=1}^N n_i / (\text{wt. of bead})$ represents the initial total bead concentration in c.p.m./g. At the end of the first wash-out period, Vn_1 counts have left the bead, and so the mean bead concentration at this time is $\bar{C}(t_1) = V \sum_{i=2}^N n_i / \text{wt.}$ Similarly, at the end of the j th wash-out period, the mean concentration is $V \sum_{i=j+1}^N n_i / \text{wt.}$ At any time, the relative mean concentration $\bar{C}(t_j)/C_0$ is given by

$$\bar{C}(t_j)/C_0 = \frac{\sum_{i=j+1}^N n_i}{\sum_{i=1}^N n_i} \quad (1)$$

This is plotted semilogarithmically against time. The curve conforms to the equation describing diffusion from a spherical bead into a medium free of tracer

$$\frac{\bar{C}(t)}{C_0} = \frac{6}{\pi^2} \sum_{k=1}^{\infty} \frac{1}{k^2} \exp[-k^2 \pi^2 D t / a^2] \quad (2)$$

For large times this becomes asymptotic to a line of slope

$$\sigma = -\frac{\pi^2 D}{a^2} \quad (3)$$

The diffusion coefficient was assessed from this equation. The independence of D from bead weight (Tables

(6) P. Flodin, ref. 5, p. 28.

(7) Calculated from the densities of pure formamide and dried Sephadex® (Flodin, ref. 5) assuming no volume change on mixing.

(8) M. L. Moore and F. S. Crossley in "Organic Syntheses," Coll. Vol. III, E. C. Horning, Ed., John Wiley and Sons, Inc., New York, N. Y., 1955, p. 617.

(9) PPO (2,5-diphenyloxazole) (7 g.), 250 mg. of POPOP (1,4-bis-2-(5-phenyloxazolyl)benzene), and 150 g. of naphthalene in 1 l. of *p*-dioxane.

I and II) shows that no significant surface process is involved in the flux.

Results and Discussion

Formamide-Swollen Beads. Diffusion coefficients in formamide-swollen beads at $15.3 \pm 0.05^\circ$ are given in Table I. To facilitate comparison, the mean values of D are displayed in Fig. 1, as a function of M^{-1} , the reciprocal of the solute molecular weight, with members of each homologous series joined by a line.¹⁰ While

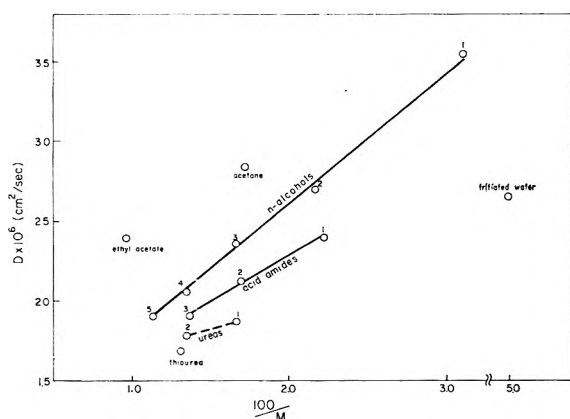


Figure 1. Mean diffusion coefficients at 15.3° in formamide-swollen dextran gel as a function of solute reciprocal molecular weight. Members of series are specified by number of C atoms, given next to each point.

there is a general tendency toward smaller D at larger molecular weight, at any molecular weight a solute containing fewer or weaker H-bonding groups¹¹ diffuses more rapidly than one with more or stronger groups. As a class the alcohols diffuse more rapidly than the amides, which, in turn, are faster than the ureas. Consistent with this, acetone and ethyl acetate, relatively weak proton acceptors which are also unable to donate protons, diffuse especially rapidly. On the other hand, water, which can form several strong H-bonds, diffuses more slowly than the larger methanol and acetone. The same specificity pattern has previously been shown to occur in methanol and ethanol, and evidence has been presented for it in cytoplasm as well.^{12,13}

The question arises as to whether the dependence of D on chemical composition reflects a direct effect of solute H-bonding ability or whether some molecular size parameter alone can account for the differences among the series. The latter alternative would imply that, among the compounds studied, the better H-bonder at any molecular weight is geometrically larger. While there are certainly shape differences which may influence D , the conventional measures of molecular size show the opposite relation to be true. For example,

plotting D against solute molal volume, as done by Wilke,⁴ substantially increases the separation among the series.

It seems necessary, therefore, to invoke a differential slowing effect arising from solute-solvent interaction. This may be ascribed to H-bonding, the greater the number and strength of bonds which form, the slower the diffusion.¹⁴ The effect of the solute-solvent H-bonding on diffusion may be viewed as arising in any of several ways: the unit diffusional process may involve the rupture of the solute-solvent bonds, or the H-bonded solute and solvent molecules may tend to move in the unit process as a single complex, effectively a larger molecule.

Among molecules having the same functional group, the larger diffuses more slowly. It is interesting to note that, though we have used M^{-1} in Fig. 1, any one of a number of different solute size parameters would have given as acceptable a linear function. Others we have considered are $M^{-1/2}$, $V_m^{-1/3}$, $V_m^{-0.6}$, and Arnold's size parameter $(1/M + 1/M')^{1/2}[V_m^{1/3} + (V_m')^{1/3}]^{-2}$, where M and M' are the solute and solvent¹⁵ molecular weights, and V_m and V_m' the molal volumes. The only effect of using parameters other than M^{-1} is to change the slopes and intercepts of the lines.

The success of a linear function in Fig. 1 does not necessarily imply that the addition of methylene groups influences diffusion only through an increase in molecular size. One would expect other effects of the addition, such as steric interference with H-bonding, shape factors, and inductive influences on the H-bonding group, to be involved. The existence of such additional factors is supported by the different slopes and intercepts in the different homologous series.

Water-Swollen Beads. The experimental diffusion

(10) The line joining urea and methylurea is dotted to indicate that the series is not quite homologous, in that the addition of the alkyl group is to a nitrogen rather than a carbon. The same consideration applies to thiourea and methylthiourea used in the water-swollen bead series.

(11) The relative proton donating and accepting strengths of the various polar radicals were taken to be those given by S. Mizushima, "Structure of Molecules and Internal Rotation," Academic Press, Inc., New York, N. Y., 1954, pp. 131-134.

(12) I. R. Fenichel and S. B. Horowitz, *Acta Physiol. Scand.*, *Suppl.*, **221**, 1 (1963).

(13) There is also evidence for this pattern in the proton-accepting solvent benzene; for example, ethyl ether ($M = 74.1$), a nondonating solute, diffuses 1.48 times as rapidly as the smaller molecule 1-propanol ($M = 60.0$) which is both proton donor and acceptor. However, solute dimerization must be considered in this solvent.

(14) This is applicable to both solute-formamide and solute-dextran H-bonding. For the present purpose of demonstrating specificity based on H-bonding it is unnecessary to distinguish between these.

(15) M' and V_m were taken as those of pure formamide. This is equivalent to assuming the polymer effect to be independent of solute size for these small solutes, an assumption which is supported by the data for water-swollen gel, below.

Table I: Diffusion of 14 Nonelectrolytes in Formamide-Swollen Dextran Gel at 15.3°

Compound	Bead wt., mg.	10 ³ σ , sec. ⁻¹	10 ⁶ \bar{D} , cm. ² /sec.
Water (HTO)	15.45	1.24	2.66
	14.79	1.29	2.69
	19.29	1.05	2.61
	13.00	1.37	2.62
			$\bar{D} = 2.64$
Formamide	18.22	1.03	2.47
	19.05	0.979	2.41
	12.85	1.22	2.31
			$\bar{D} = 2.40$
Acetamide	15.60	0.968	2.09
	14.90	0.989	2.07
	18.25	0.930	2.23
			$\bar{D} = 2.13$
Propionamide	15.02	0.916	1.93
	15.44	0.892	1.91
	16.29	0.859	1.91
			$\bar{D} = 1.92$
Methanol	22.19	1.26	3.45
	19.35	1.43	3.57
	17.50	1.56	3.64
			$\bar{D} = 3.56$
Ethanol	19.06	0.917	2.26
	19.72	1.15	2.89
	19.75	1.16	2.93
			$\bar{D} = 2.69$
1-Propanol	17.49	1.09	2.53
	14.17	1.14	2.27
	16.79	1.01	2.29
			$\bar{D} = 2.36$
1-Butanol	15.18	0.900	1.91
	17.80	0.904	2.13
	19.18	0.866	2.14
			$\bar{D} = 2.06$
1-Pentanol	14.94	0.920	1.93
	17.20	0.820	1.89
	15.61	0.891	1.92
			$\bar{D} = 1.91$
Urea	15.60	0.865	1.87
	19.20	0.768	1.90
			$\bar{D} = 1.88$
Methylurea	14.06	0.889	1.79
	13.98	0.884	1.77
	18.87	0.738	1.80
			$\bar{D} = 1.79$
Thiourea	18.49	0.759	1.83
	15.88	0.741	1.62
	15.87	0.744	1.62
			$\bar{D} = 1.69$
Acetone	18.90	1.17	2.86
	17.76	1.19	2.79
	15.04	1.37	2.88
			$\bar{D} = 2.84$
Ethyl acetate	16.56	0.951	2.13
	16.89	1.14	2.59
	16.26	1.11	2.47
			$\bar{D} = 2.40$

coefficients are presented in Table II, together with the temperature at which they were determined and the bead weights. Within the experimental error, the temperature dependence of D is described by an Arrhenius equation of the form

$$\ln D = \ln D_0 - E/RT \quad (4)$$

The least-squares activation energy E and interpolated D at 15° are also given with their standard errors in Table II.

The diffusion coefficient in the gel varies with both the molecular size and chemical composition of the solute, as shown in Fig. 2. As in the formamide-swollen gel, in each homologous series of compounds, D de-

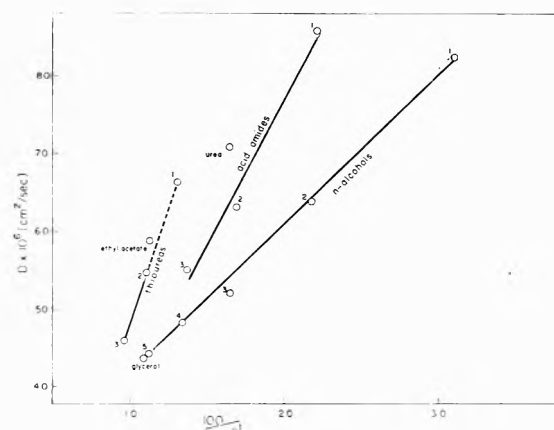


Figure 2. Least-squares-fitted diffusion coefficients at 15° in water-swollen dextran gel as a function of solute reciprocal molecular weight. Members of series are specified by number of C atoms, given next to each point. The point for ethyl acetate is the average D at 15.2°.

creases as M increases through the addition of alkyl groups; the lines joining members of the series tend to converge as chain length increases. The relation of D to chemical composition, on the other hand, is different in the water-swollen gel. Except for glycerol and ethyl acetate, the poorer H-bonding solute at a given molecular weight diffuses more slowly than the better. As a class, the alcohols diffuse more slowly than the amides of comparable weight, and the amides more slowly than urea and the thioureas.

In Table III, D' , the solute diffusion coefficients in dilute aqueous solution, are compared with the interpolated values of D in the gel. The large value of the ratio D/D' and its constancy with respect to size, chemical grouping, and temperature indicates that the effect of the polymer is largely a nonspecific obstruction of the diffusional paths of the small molecules. Moreover, the constancy of D/D' shows that the same speci-

Table II: Diffusion of 16 Nonelectrolytes in Water-Swollen Dextran Gel

Compound	t , °C.	Bead wt., mg.	$10^6 D$, cm. ² /sec.	$10^6 D_{16}$, cm. ² /sec.	E , kcal./mole
Water (HTO)	5.5	13.62	9.53		
	5.7	15.09	8.94		
	15.1	13.45	12.4		
	15.3	21.96	12.5		
	25.2	11.40	15.4	12.1 ± 0.2	4.4 ± 0.4
Methanol	4.0	12.10	6.00		
	15.2	14.78	8.35		
	24.0	10.36	10.4	8.24 ± 0.03	4.5 ± 0.1
Ethanol	3.8	12.56	4.55		
	4.2	9.60	4.33		
	15.1	10.97	6.02		
	16.1	9.60	7.07		
	24.1	15.28	8.25		
	24.2	11.75	8.53	6.37 ± 0.13	5.2 ± 0.4
1-Propanol	4.0	14.17	3.52		
	4.2	14.18	3.82		
	15.1	9.32	4.52		
	15.3	15.14	5.33		
	24.0	10.94	6.70		
2-Propanol	24.2	12.14	7.92	5.21 ± 0.21	5.5 ± 0.8
	3.8	9.56	3.51		
	4.8	23.07	3.63		
	4.8	16.64	3.84		
	4.8	8.81	3.71		
	15.4	14.33	5.31		
1-Butanol	24.2	12.57	7.14	5.27 ± 0.00	5.7 ± 0.0
	4.0	12.52	3.28		
	5.6	23.14	3.54		
	5.8	22.54	3.65		
	18.1	11.88	5.34		
1-Pentanol	24.7	9.76	6.68	4.84 ± 0.05	5.4 ± 0.2
	4.2	10.81	3.01		
	15.2	11.68	4.33		
Formamide	24.2	11.50	6.24	4.44 ± 0.09	5.9 ± 0.4
	4.2	16.84	6.18		
	15.2	17.56	8.55		
Acetamide	24.3	10.91	11.3	8.58 ± 0.06	4.8 ± 0.1
	4.0	16.80	4.52		
	4.1	12.39	4.60		
	15.1	8.98	6.40		
	15.2	11.67	6.34		
Propionamide	24.1	17.81	8.30		
	24.4	9.60	7.93	6.31 ± 0.05	4.7 ± 0.2
	4.1	8.00	3.84		
	4.2	8.90	3.72		
	5.0	23.14	4.14		
	5.4	24.82	4.07		
	5.7	22.54	4.26		
	15.3	10.55	5.60		
	15.3	8.85	5.64		
Thiourea	24.2	10.43	7.31		
	24.3	12.62	7.34	5.55 ± 0.05	5.2 ± 0.2
	4.1	8.03	4.64		
	5.0	22.54	4.74		
	5.5	23.14	5.26		
	5.8	24.82	5.23		
	15.3	12.04	6.78		
24.4	12.54	8.53	6.64 ± 0.13	4.7 ± 0.3	

Table II (Continued)

Compound	t , °C.	Bead wt., mg.	$10^6 D$, cm. ² /sec.	$10^6 D_{15}$, cm. ² /sec.	E , kcal./mole
Methylthiourea	4.0	12.20	3.94		
	15.3	18.00	5.75		
	24.3	14.26	6.96	5.51 ± 0.09	4.7 ± 0.3
Ethylthiourea	4.0	16.97	3.38		
	15.3	8.96	4.62		
	24.3	9.54	5.89	4.60 ± 0.03	4.5 ± 0.1
Urea	4.1	17.87	5.30		
	15.1	14.50	6.88		
	24.3	11.06	9.23	7.09 ± 0.14	4.4 ± 0.4
Glycerol	4.1	9.66	3.18		
	15.1	11.05	4.39		
	24.1	15.54	5.58	4.37 ± 0.02	4.5 ± 0.1
Ethyl acetate	15.2	15.42	6.24		
	15.2	18.93	5.54		

$$(\bar{D}_{15.2} = 5.89)$$

ficity pattern, as is seen in the dextran gel, prevails in liquid water, so that data from the two systems can be used jointly. This permits an additional homologous series, the alkanes, to be added to those we have studied. This is shown in Fig. 3 in which a variety of D' values, expressed as the ratio to D' for water,¹⁶ are plotted as a function of M^{-1} . The position of the alkanes, relative to the alcohols, shows them to be the most slowly diffusing of the nonelectrolytes in water, a position corresponding to their nonpolar nature.

Figure 3, when considered with Fig. 2, suggests the over-all complexity of the specificity in water. The relationship among the four homologous series does not carry over to such molecules as ethyl acetate, acetone, and glycerol. The behavior of these is more like that seen in formamide; glycerol is a good H-bonder and diffuses slowly, while the others are relatively poor and diffuse rapidly.

Because of the extensive solute-solvent H-bonding in water one would anticipate the type of diffusional retardation described for formamide-swollen gel to occur in water as well. Since the effect of this is to slow the diffusion of H-bonding solutes, the inverse pattern observed in water among the alkanes, alcohols, amides, and thioureas can only be reconciled if an additional mechanism is operative, one opposite in effect and, for these solutes, of greater influence. The unusual solute-solvent interactions in water do, in fact, suggest such a mechanism. As pointed out by Frank and Evans,¹⁷ nonpolar solutes (*e.g.*, noble gases and alkanes) and, to a lesser extent, weakly polar solutes (*e.g.*, alcohols, ethers, and ketones) show unusually large negative entropies of solution and positive partial molar heat capacities in aqueous solution. To explain these it was suggested

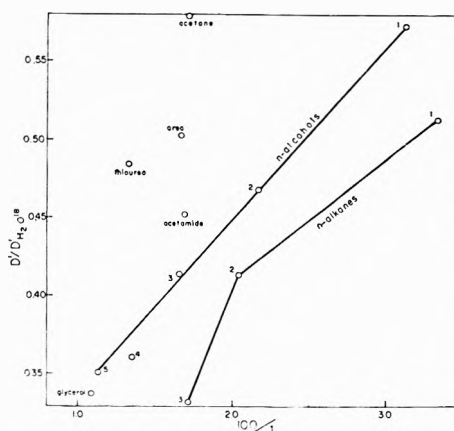


Figure 3. Normalized diffusion coefficients in water as a function of solute reciprocal molecular weight. Members of series are specified by the number of C atoms, given next to each point. Sources of the data are given in footnotes 16 and 17.

that increased association of water molecules occurs in the vicinity of a nonpolar solute or radical (*e.g.*, the alkyl chain of an alcohol) with the production of a local

(16) In order to compare D' values obtained by a variety of workers at different temperatures, the values have been normalized by expressing the diffusion coefficient as a ratio to that for H_2O ¹⁸ (J. H. Wang, C. V. Robinson, and I. S. Edelman, *J. Am. Chem. Soc.*, **75**, 466 (1953)). The errors introduced due to the different temperature coefficients for the various solutes are insufficient to affect the conclusions.

Of the numerous organic nonelectrolytes whose diffusion in water has been studied, for simplicity only a few have been included: those in which data are available in both water and Sephadex, other homologous series, and compounds for which ΔS_s is available (see below). This sampling is, however, sufficient to provide a picture of the range of organic nonelectrolyte diffusional behavior. Sources of the data are those cited in Table III and also: acetone, H. Lemonde, *Ann. phys.*, **9**, 539 (1938); *n*-alkanes, D. N. Saraf and P. A. Witherspoon, *Science*, **142**, 955 (1963).

(17) H. S. Frank and M. W. Evans, *J. Chem. Phys.*, **13**, 507 (1945).

Table III: Comparison of Diffusion in Free Aqueous Solution with That in Water-Swollen Dextran Gel

Compound	t , °C.	$D' \times 10^5$, cm. ² /sec.	D/D'
Methanol	15	1.26 ^a	0.66
	20	1.37 ^b	0.69
	27	1.56 ^c	0.73
Ethanol	10	0.84 ^a	0.65
	15	1.00 ^a	0.64
	18	1.09 ^a	0.64
	20	1.20 ^b	0.62
	25	1.24 ^d	0.70
1-Propanol	11	0.77 ^a	0.60
	15	0.87 ^a	0.60
	20	1.07 ^b	0.59
1-Butanol	15	0.77 ^a	0.63
	20	0.90 ^b	0.63
	25	0.956 ^c	0.70
1-Pentanol	20	0.85 ^b	0.62
Acetamide	15	0.96 ^f	0.65
	25	1.25 ^g	0.67
Urea	15	0.94 ^f	0.75
	25	1.38 ^h	0.67
Thiourea	25	1.33 ⁱ	0.66
Glycerol	15	0.72 ^f	0.61
	20	0.81 ^b	0.62
Water (HTO)	5	1.39 ^j	0.65
	15	1.83 ^j	0.65
	25	2.44 ^j	0.63

^a H. Lemonde, *Ann. phys.*, **9**, 539 (1938). ^b F. H. Garner and P. J. M. Marchant, *Trans. Inst. Chem. Engrs.* (London), **39**, 397 (1961). ^c G. Seimel and A. L. Babb, unpublished data cited by P. A. Johnson and A. L. Babb, *Chem. Rev.*, **56**, 387 (1956). ^d B. R. Hammond and R. H. Stokes, *Trans. Faraday Soc.*, **49**, 890 (1953). ^e P. A. Lyons and C. L. Sandquist, *J. Am. Chem. Soc.*, **75**, 3896 (1953). ^f J. Thovert, *Ann. chim. phys.*, [7] **26**, 366 (1902). ^g A. Biancheria and G. Kegeles, *J. Am. Chem. Soc.*, **79**, 5908 (1957). ^h L. J. Gosting and D. F. Akeley, *ibid.*, **74**, 2058 (1952). ⁱ D. B. Ludlum, R. C. Warner, and H. W. Smith, *J. Phys. Chem.*, **66**, 1540 (1962). ^j J. H. Wang, C. V. Robinson, and I. S. Edelman, *J. Am. Chem. Soc.*, **75**, 466 (1953).

stabilized domain. These domains have been referred to as "icebergs," and the concept has been applied to a variety of equilibrium and kinetic¹⁸ properties of aqueous solutions.

The stabilized domains may be expected to influence diffusional rates as well, slowing the movement of the solute with which they are associated. The direction of the effect would be such as to give rise to the specificity seen among the four homologous series: for solutes of equal size, that containing the larger hydrocarbon radical will have the larger (or more stable) domain and suffer the greater depression of mobility. The specificity of diffusion in water in respect to chemical grouping, then, represents a superimposition of the

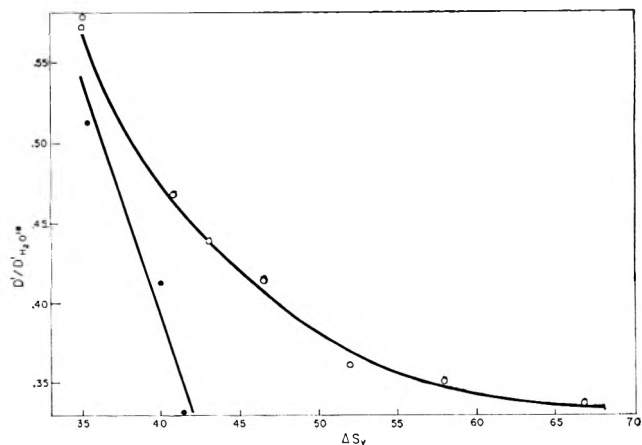


Figure 4. Normalized diffusion coefficients in water as a function of the reciprocal of the entropy of vaporization from dilute aqueous solution at 25°. D'/D'_{H_2O} ¹⁸ for ethyl acetate was calculated from data in water-swollen dextran gel. The points for the alkanes are solid circles, those for the polar solutes are open. Entropy data from Frank and Evans¹⁸ and Claussen and Polglase.²¹

effects of solute-solvent H-bonding and iceberg formation. These interactions are also reflected in ΔS_v , the entropy of vaporization of the nonelectrolyte from water, and it is of interest to examine the relationship of ΔS_v to diffusion. In Fig. 4, D'/D'_{H_2O} is plotted as a function of ΔS_v . Solute which are able to form H-bonds—*n*-alcohols, acetone, ethyl acetate, and glycerol—fall on a single curve which includes a substantial range of both size and polarity.¹⁹ The alkanes fall on a second curve, diffusing more slowly at any value of ΔS_v than the H-bonding solutes.

An explanation for some of the features of this correlation, and in particular for the difference between the H-bonding solutes and the alkanes, can be provided by an examination of differences in the rotational component of ΔS_v . A molecule held by an H-bond to the water lattice will suffer a restriction of rotational freedom about axes perpendicular to the H-bond, and a large part of the ΔS_v may reflect the release of this constraint. The importance of this increases with solute size among solutes having similar H-bond interaction since the rotational entropy in the vapor phase increases with size both absolutely and as a fraction of the total entropy. Thus, the effect of the H-bond on ΔS_v is greater for 1-pentanol than for methanol. It is

(18) F. S. Feates and D. J. G. Ives, *J. Chem. Soc.*, 2798 (1956); H. S. Frank, *Proc. Roy. Soc. (London)*, **A247**, 481 (1958).

(19) Similar correlations have been noted for other kinetic properties: between the molal fluidity elevation of ions and their ΔS_v (H. S. Frank and M. W. Evans, ref. 17) and between the activation energy for viscous flow and the entropy of dilution of aqueous solutions of amino acids (L. S. Mason, P. M. Kampmeyer, and A. L. Robinson, *J. Am. Chem. Soc.*, **74**, 1287 (1952)).

unlikely, however, that the effect of the H-bond on D increases with solute size in the same manner. While the rotational ΔS_v , as a measure of the restriction of motion due to the H-bond, may, to some extent, be an index to the magnitude of the diffusional activation barrier, it is unlikely that the activated state of a molecule such as 1-pentanol necessitates its free rotation about all axes. One would expect rather that the effect of an H-bond on diffusion is relatively independent of the size of the molecule so that ΔS_v should increase more rapidly with size than D decreases, leading to the curvature of the D - ΔS_v line for the H-bonding solutes.

The alkanes, on the other hand, do not suffer rotational restriction in the condensed phase due to the steric requirements of an H-bond. One would expect an alkane to have substantially more rotational entropy in aqueous solution than a polar molecule of similar size. This is especially likely if, as has been suggested,²⁰ the alkanes are enclosed in relatively large cavities formed by certain water structures, in which they can undergo only slightly restricted rotation.²¹ The measured ΔS_v for the alkanes would then include only a small rotational component and not involve the large component unrelated to diffusion which is seen in the H-bonding solutes. At any value of ΔS_v , then, an alkane would diffuse more slowly than an H-bonding solute, as the data show. The behavior of argon, a monatomic substance having no rotational entropy, supports this formulation; the values of ΔS_v , 30.2 cal./deg.,¹⁷ and $D'/D'_{\text{H}_2\text{O}}$, 0.532,²² place this substance to the left of both the H-bonding and alkane lines in Fig. 4.

The temperature dependence of diffusion provides additional evidence for the involvement of icebergs. As Table II shows, among the solutes devoid of a hydrocarbon chain (*e.g.*, methanol, formamide, thiourea, urea, and glycerol), E is independent of size and is similar to that of the self-diffusion of water. On the other hand, solutes for which iceberg formation is most significant—the higher alcohols—have larger values of E . This is the counterpart of the large partial molar heat capacities of nonpolar solutes and reflects the breakdown or "melting" of the icebergs as temperature increases. The temperature coefficients of D for hydro-

carbon-bearing solutes will, as a result, include a contribution from the melting of the icebergs.²³ A rough estimate of this contribution may be made by subtracting $E_{\text{H}_2\text{O}}$, 4.4 kcal., from the observed value of E .

The presence of icebergs which slow the diffusion of solutes bearing nonpolar groups and of solute-solvent bonding which slows the diffusion of H-bonding solutes results in a mutual masking of specificity. The recognition of this permits an explanation of the rather good correlation observed by Wilke⁴ between D in water and the solute molal volume, V_m . In the case of diffusion in formamide, it was noted that the use of V_m in Fig. 1 rather than M would have increased the separation between homologous series. On the other hand, in water, in which an inverted specificity order tends to prevail, the use of V_m will bring the series together, so that differences between compounds of the same V_m can be seen in most cases only by careful examination of the data. The success of the correlation of V_m with D in water must therefore be viewed as of limited significance to understanding solute diffusional specificity.

NOTE ADDED IN PROOF. Evidence has been presented,²⁴ based on viscosity and activity data, that urea and amides disrupt normal water structure. As in the case of the monovalent cations,²³ such structure breaking may be associated with increased solute mobility and thus contribute to the specificity seen in water. However, the corollary decrease of E to a value smaller than that of water itself, which occurs with the large cations, is not seen with any solute in the present study.

Acknowledgments. We wish to thank Dr. Nigel V. B. Marsden for help and advice during the course of this study. We thank Dr. Gilbert N. Ling and Prof. Torsten Teorell for valuable discussions and Mrs. M. Miller and Mrs. V. Wasylszyn for technical assistance.

(20) W. F. Claussen and M. F. Polglase, *J. Am. Chem. Soc.*, **74**, 4817 (1952).

(21) Cf. V. McKoy and O. Sinanoğlu, *J. Chem. Phys.*, **38**, 2946 (1963).

(22) R. E. Smith, E. T. Friess, and M. F. Morales, *J. Phys. Chem.*, **59**, 382 (1955).

(23) The opposite effect, a decrease of E due to breakdown of normal water structure, has been described in ionic solutions by J. H. Wang, *ibid.*, **58**, 686 (1954).

(24) J. A. Rupley, *ibid.*, **60**, 2002 (1964).

The Nucleation of Long-Chain Molecules¹

by L. Mandelkern, J. G. Fatou, and C. Howard

*Department of Chemistry and Institute of Molecular Biophysics,
Florida State University, Tallahassee, Florida (Received June 10, 1964)*

A theory pertinent to the nucleation of long-chain molecules of finite molecular weight has been developed. Although, for very high molecular weights, the free energy of nucleus formation and the critical dimensions of nuclei assume the same values as in the usually employed infinite molecular weight approximation, in the molecular weight range of usual interest, significant differences are observed as a function of molecular weight and of temperature. In particular, it is found that the critical number of repeating units per chain, that are required to form a nucleus, does not become infinite at the melting temperature. Moreover, when the molecular nature of the nucleus and mature crystallite differ, it becomes theoretically possible, depending on the situation, for the homogeneous steady-state nucleation rate to vanish either below or above the equilibrium melting temperature of the system.

Introduction

The important role played by nucleation processes in the liquid-crystal transformation of long-chain molecules has been strongly emphasized in the past. Nucleation theory has been important in analyzing and understanding the kinetics of isothermal crystallization from the melt and the temperature coefficient of this process.^{2a,b} It also appears very likely that the observed dependence of morphology and crystalline texture on the crystallization temperature stems from considerations of the dimensions of critical size nuclei and their free energy of formation.³⁻⁵ In treating the nucleation of long-chain molecules, the nucleus has been taken to have an asymmetric geometry with different arrangements of the polymer chains within the nucleus being assumed.^{1,6,7} However, the assumption has always been made, explicitly or otherwise, that one is dealing with a chain of infinite molecular weight. In this approximation, the equations which describe the critical condition for nucleation (irrespective of detailed model) have the same analytical form as the equations derived for a collection of monomeric molecules with a similar geometric arrangement in the nucleus.⁸

In the present paper, we re-examine the nucleation theory pertinent to chains of large but finite molecular length. By avoiding the infinite molecular weight approximation we observe significant departures from monomer theory in the molecular weight range of usual

interest. Furthermore, a connection can be made between the nucleation of long-chain molecules of precisely the same chain length, wherein the formation of molecular crystals is theoretically possible under certain circumstances,⁹ and the case where the required uniformity of chain length cannot be attained, even for a molecular weight fraction. Our discussion will be limited to three-dimensional homogeneous nucleation since we shall be concerned solely with the effect of the finite chain length. The results obtained can be easily extended to other types of nucleation when pertinent.

Results and Discussion

In developing a nucleation theory appropriate to

(1) This work was supported by a grant from the U. S. Army Research Office (Durham) and a contract with the Division of Biology and Medicine, Atomic Energy Commission.

(2) (a) L. Mandelkern, F. A. Quinn, Jr., and P. J. Flory, *J. Appl. Phys.*, **25**, 830 (1954); (b) L. Mandelkern, "Growth and Perfection of Crystals," R. H. Doremus, B. W. Roberts, and D. Turnbull, Ed., John Wiley and Sons, Inc., New York, N. Y., 1958.

(3) P. J. Flory and A. D. McIntyre, *J. Polymer Sci.*, **18**, 592 (1955).

(4) L. Mandelkern, *ibid.*, **47**, 494 (1960).

(5) J. D. Hoffman and J. J. Weeks, *J. Res. Natl. Bur. Std.*, **A66**, 13 (1962).

(6) L. Mandelkern, *J. Appl. Phys.*, **26**, 443 (1955).

(7) J. D. Hoffman and J. I. Lauritzen, *J. Res. Natl. Bur. Std.*, **A64**, 73 (1960); **A65**, 297 (1961).

(8) L. Mandelkern, "Crystallization of Polymers," McGraw-Hill Book Co., New York, N. Y., 1964, p. 248.

(9) P. J. Flory and A. Vrij, *J. Am. Chem. Soc.*, **85**, 3548 (1963).

chain molecules we shall adopt the same classical procedures that have been used for monomeric systems. The expression for the free energy of forming a small crystallite or nucleus from the melt is composed of two types of terms. One term is the bulk free energy of fusion which characterizes the crystalline phase of finite size. Of opposite sign are terms which represent the excess surface free energies contributed by the interfaces present. It is thus tacitly assumed that the nucleus is sufficiently large so that its interior is homogeneous and that the exterior surfaces (real or effective) can be defined. The resulting free energy surface is then examined, by standard methods, for the conditions of stability of nuclei and of mature crystallites. We need make no assumptions at present in regard to the molecular nature of the mature crystallites that are eventually evolved.

With the above stipulations, the free energy change in forming a cylindrically arranged crystalline array of ζ units long and ρ sequences in cross section for a pure system containing N polymer molecules each comprised of x repeating units is given by^{6,10}

$$\Delta F = 2\pi^{1/2}\rho^{1/2}\zeta\sigma_u - \rho RT \ln D - \zeta\rho\Delta f_u - RT \left\{ \frac{xN}{x} \ln \left[1 - \frac{\zeta\rho}{xN} \right] - \rho \ln \left[\frac{x - \zeta + 1}{x} \right] \right\} \quad (1)$$

where σ_u is the lateral interfacial free energy per molecule and D is defined as $\exp\{-2\sigma_c/RT\}$, where σ_c is the excess interfacial free energy per repeating unit as it emerges from the crystal face normal to the chain direction. The free energy of fusion per repeating unit for a chain of infinite molecular weight is given by Δf_u . The first two terms in eq. 1 represent the positive contribution to the total free energy change of the interfaces present. The third term represents the bulk free energy of fusion for the $\zeta\rho$ units involved in the transformation, behaving as though they were part of an infinite molecular weight chain. The latter two terms result from the finite length of the chains. The first of these terms expresses the entropy gain which results from the increased volume available to the ends of the molecule after melting. The last term results from the fact that only a portion of the chain units of a given molecule are involved in the nucleus. It represents the entropy gain that arises from the number of different ways a sequence of ζ units can be located in a chain x units long with the terminal units being excluded from the sequence in question.^{9,10} The inclusion of this latter term is of prime importance to the present discussion, for it introduces the effect of a finite chain. Equation 1 can be recognized as the net free energy of fusion, previously calculated by Flory,¹⁰ but devoid of the

stipulations that equilibrium with respect to the crystallite size and amount of crystallinity prevails. The inherent assumption has been made that each sequence in the ordered array which comprises the nucleus is denoted by a different chain.

Since we shall only be concerned with the development of small amounts of crystallinity, the first term of the series expansion of $\ln [1 - \zeta\rho/xN]$ can be used so that

$$\Delta F = 2\pi^{1/2}\rho^{1/2}\zeta\sigma_u + 2\rho\sigma_e + \frac{RT}{x}\zeta\rho - \rho\zeta\Delta f_u - \rho RT \ln \left[\frac{x - \zeta + 1}{x} \right] \quad (2)$$

The surface described by eq. 2 possesses neither a maximum nor minimum but does contain a saddle point. The coordinates of the saddle point are defined by $(\partial\Delta F/\partial\rho)_\zeta$ and $(\partial\Delta F/\partial\zeta)_\rho = 0$, which also prescribe the dimensions of a nucleus of critical size. These dimensions are given by the relations

$$\rho^{*1/2} = \frac{2\pi^{1/2}\sigma_u}{\Delta f_u - RT/x - RT/(x - \zeta^* + 1)} \quad (3)$$

and

$$\frac{\zeta^*}{2} \left[\Delta f_u - \frac{RT}{x} + \frac{RT}{x - \zeta^* + 1} \right] = 2\sigma_e - RT \ln \left(\frac{x - \zeta^* + 1}{x} \right) \quad (4)$$

where the asterisks denote the critical dimensions at the saddle point. The value of the free energy change at the saddle point, obtained by substituting eq. 3 and 4 into eq. 2, is found to be

$$\Delta F^* = \pi^{1/2}\zeta^*\rho^{*1/2}\sigma_u \quad (5)$$

Equation 5 is identical with that obtained for the infinite molecular weight polymer, as well as for a nucleus composed of monomers arranged in a similar geometric array. If x is very large and $\zeta^* \ll x$ then eq. 3 and 4 also reduce to the results previously obtained in the infinite molecular weight approximation. However, if these latter conditions are not fulfilled then significant differences exist for the dependence of the critical dimensions on the molecular weight and on the crystallization temperature.

In order to specify the dependence of the critical dimensions and ΔF^* on molecular weight and the crystallization temperature, it becomes necessary to stipulate the manner in which the melting temperature T_m depends on the chain length. Two choices of models exist which will allow for this calculation. One of these

(10) P. J. Flory, *J. Chem. Phys.*, 17, 223 (1949).

models is similar to the formation of molecular crystals. The completely ordered chains are arranged in a regular array with the terminal unit of one molecule paired with its neighbor. In order to achieve this type of arrangement it is obviously required that all the chains be precisely of uniform length. Even if this hypothetical structural situation could be achieved it is theoretically possible that, for sufficiently high molecular weight chains, the thermodynamically most stable situation would be depicted by the partial melting or unpeeling of a specified number of chain units from the ends.⁹ We take this latter model, with disorder at the ends of the molecule, to represent the case of a molecular weight fraction since it is not possible to achieve complete uniformity of chain lengths in a real system. For this model it has been shown that¹⁰

$$\frac{1}{T_m} - \frac{1}{T_m^0} = \frac{R}{\Delta H_u} \left(\frac{1}{x} + \frac{1}{x - \zeta_e + 1} \right) \quad (6)$$

where T_m^0 is the melting point of the infinite molecular weight chain, ΔH_u is the heat of fusion per repeating unit, and ζ_e is the length of a crystalline sequence at total equilibrium. The latter quantity is given by the relation¹⁰

$$2\sigma_e = RT \left\{ \frac{\zeta_e}{x - \zeta_e + 1} + \ln \left(\frac{x - \zeta_e + 1}{x} \right) \right\} \quad (7)$$

The simplifying assumption has been made that the value of the interfacial energy σ_e for the mature equilibrium crystallite is the same as for the nucleus. (As will be seen subsequently this assumption is not required but it does allow for a simplification in the initial analyses.)

With this set of premises we can examine the behavior of the critical dimensions at the melting point, T_m , characteristic of a given chain length. At the melting temperature, a solution of eq. 4 is $\zeta^* = \zeta_e$. The denominator of eq. 3 thus becomes identically equal to zero so that ρ^* and ΔF^* become infinite at T_m . These latter conditions are the same as deduced from the infinite molecular weight theory or for the nucleation of monomeric systems. However, we do observe a fundamental difference for the nucleation of a chain of finite length. Although stable nucleus formation at the melting temperature requires an infinite number of chains or crystalline sequences, only a finite number of ordered units per chain are needed. In the infinite molecular weight approximation or for an asymmetric nucleus of a monomeric substance, all the dimensions of concern would become infinite at the melting temperature.

Because of the nature of their analytical form, a detailed study of the behavior of eq. 3-5 at temperatures

below the melting temperature can best be made by treating a system to which a specific set of parameters has been assigned. For this purpose we shall take linear polyethylene as our example and assign the values $T_m^0 = 145.5^\circ$,⁹ $\sigma_u = 100$ cal./mole,¹¹ and $\sigma_e = 4600$ cal./mole. The value for σ_u is taken from the study of the nucleation kinetics of low molecular weight hydrocarbons by Turnbull and Cormia.¹¹ The unusually high value for σ_e , which can be ascribed to the unique nature of the interface involved, is deduced from three independent types of study. These are nucleation kinetics of polyethylene droplets,¹² the equilibrium melting of copolymers,¹³ and an interpretation of the low-angle diffraction maxima in polyethylene as a function of temperature.¹⁴ We shall also utilize the approximation that $\Delta f_u = \Delta H_u(T_m^0 - T)/T_m^0$ and take for ΔH_u 950 cal./mole of CH_2 units.¹⁵

Values of ζ^* for this model system, calculated according to eq. 4, are plotted in Fig. 1 as a function of the temperature variable $T_m - T$ for different chain lengths. The quantity $T_m - T$ is the undercooling, based on the calculated melting temperature of the finite chain. From conventional nucleation theory we would expect that $\zeta^* = 4\sigma_e T_m / [\Delta H_u(T_m - T)]$, and this function is represented by the dashed curve in the

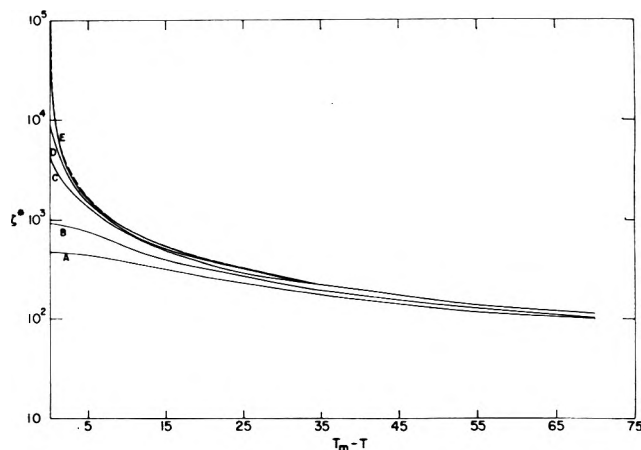


Figure 1.—Plot of ζ^* against $T_m - T$ for different chain lengths, x . Curve A, $x = 500$; curve B, $x = 1000$; curve C, $x = 5000$; curve D, $x = 10,000$; curve E, $x = 100,000$. Dashed curve represents infinite molecular weight approximation.

(11) D. Turnbull and R. L. Cormia, *J. Chem. Phys.*, **34**, 820 (1961).

(12) R. L. Cormia, F. P. Price, and D. Turnbull, *ibid.*, **37**, 1333 (1962).

(13) M. J. Richardson, P. J. Flory, and J. B. Jackson, *Polymer*, **4**, 221 (1963).

(14) L. Mandelkern, A. S. Posner, A. F. Diorio, and D. E. Roberts, *J. Appl. Phys.*, **33**, 237 (1962).

(15) F. A. Quinn, Jr., and L. Mandelkern, *J. Am. Chem. Soc.*, **80**, 3178 (1958).

figure. For $x \geq 10^5$ there is no appreciable difference, at temperatures less than T_m , between ζ^* from the infinite molecular weight theory (or monomer theory) and that calculated for the finite chain. For polyethylene, this limiting value corresponds to a molecular weight of 1.4×10^6 . However, for molecular weights less than this value significant departures from the classical relation are observed. These deviations become more pronounced at the lower undercoolings and the lower molecular weights. Not only are smaller values of ζ^* calculated, but the temperature dependence is also quite different at the lower undercoolings. Hence, it is clear that if the conventional equation is utilized to calculate ζ^* , even if the effect of chain length on the melting temperature is taken into account, erroneous conclusions will result.

In Fig. 2, the calculated values of ζ^* are plotted against the number of repeating units in the chain for various temperatures. For the high molecular weights, at a fixed temperature, ζ^* is essentially independent of

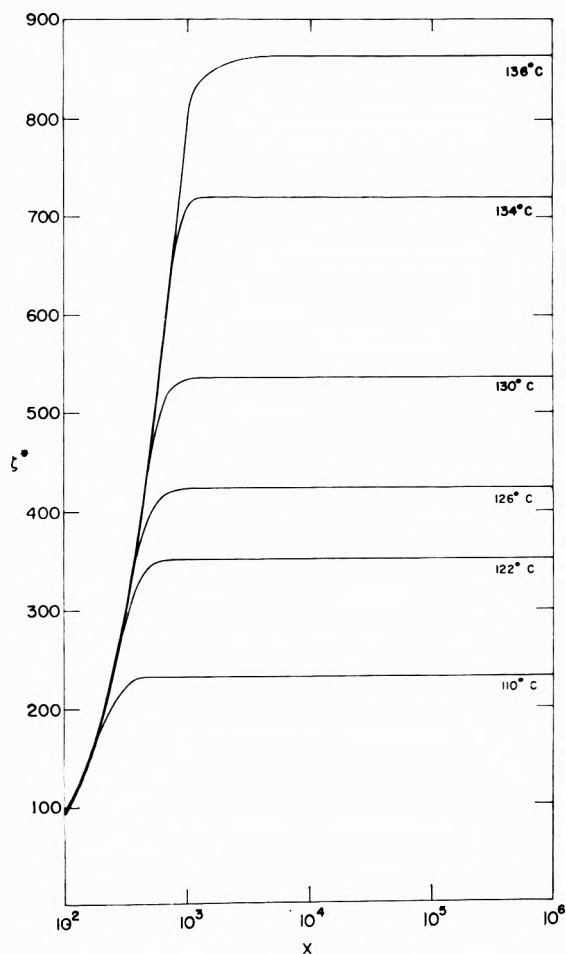


Figure 2.—Plot of ζ^* against chain length, x , for various temperatures indicated.

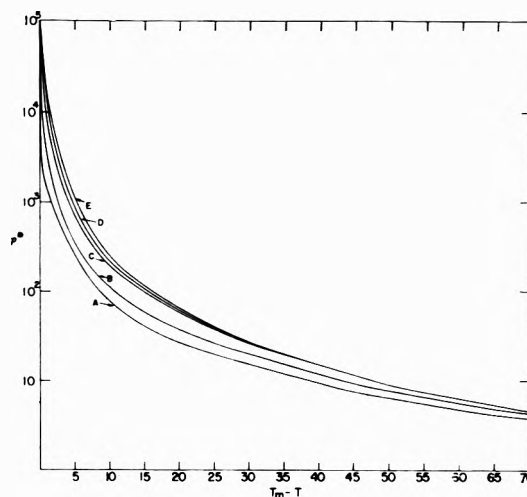


Figure 3.—Plot of ρ^* against $T_m - T$ for different chain lengths, x . Designation of curves same as in Fig. 1.

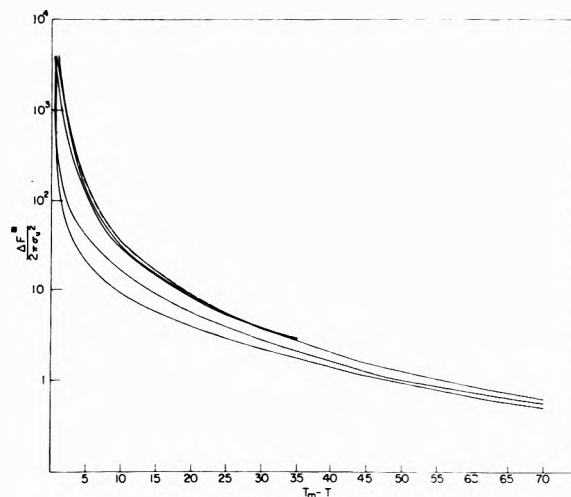


Figure 4.—Plot of quantity $\Delta F^*/(2\pi\sigma_u)^2$ against $T_m - T$ for different chain lengths. Designation of curves same as in Fig. 1. Dashed curve represents infinite molecular weight approximation.

x . The molecular weight range over which this constancy of ζ^* is observed increases as the temperature is lowered. Hence ζ^* can, to a good approximation, be taken to be independent of molecular weight when comparison is made at the same crystallization temperature. In other words, when compared at the same undercooling, calculated from the melting temperature of the infinite molecular weight polymer, ζ^* becomes independent of molecular weight at the larger undercoolings.

In Fig. 3, ρ^* , calculated according to eq. 3, is also plotted against $T_m - T$. Although ρ^* becomes infinite at the melting temperature for each molecular

weight, the rate of change of ρ^* as the temperature is lowered is strongly dependent on the chain length. For the higher chain lengths ($x \geq 10^5$) the results can again be expressed by the classical expression

$$\rho^* = \frac{4\pi\sigma_u^2 T_m^2}{\Delta H_u(T_m - T)^2} \quad (8)$$

From eq. 5 and the values of ζ^* and ρ^* , ΔF^* can be calculated for this system as a function of T and x . The results of this calculation are plotted in Fig. 4 as $\Delta F^*/(2\pi\sigma_u^2)$ against $T_m - T$. The dashed line again represents the standard or conventional relation

$$\frac{\Delta F^*}{2\pi\sigma_u^2} = \frac{4\sigma_u T_m^2}{\Delta H_u^2(T_m - T)^2} \quad (9)$$

Again, only at the very high molecular weights is this expression obeyed when undercoolings are calculated from the equilibrium melting temperature of the finite chain. The major discrepancies are again observed at the lower undercoolings and lower molecular weights, although ΔF^* still goes to infinity at each T_m . However, in Fig. 5 the same data are plotted as a function of molecular weight at various temperatures. As the temperature is lowered, the dependence of ΔF^* on molecular weight becomes less pronounced, and an approximate constancy of ΔF^* is obtained. In effect, therefore, if the conventional expression for ΔF^* were to be used, undercoolings based on the melting temperature of the infinite molecular weight polymer would more accurately reflect the correct values. However, appreciable error would still persist at the lower undercoolings in the molecular weight range of interest.

In terms of the model discussed, it is clear that significant errors will be committed, for molecular weight fractions less than 10^6 , if the nucleation parameters are calculated from the intuitive relations based on the melting temperatures of the finite chains. These errors would then reflect themselves in the analysis of crystallization kinetics in general and nucleation rates specifically, as well as in any interpretation of the dependence of morphological form and crystallite size on the crystallization temperature.

The nucleation of long-chain molecules presents a very unique situation since it is possible for the molecular nature of the nucleus to be quite different from that of the equilibrium crystallite. For example, we can consider the hypothetical case of a collection of long-chain molecules of perfectly uniform length which, at equilibrium in the crystalline state, form a collection of end-paired molecular crystals.⁹ The equilibrium melting temperature of such an ordered array can be calculated from the relation given by Flory and Vrij.⁹

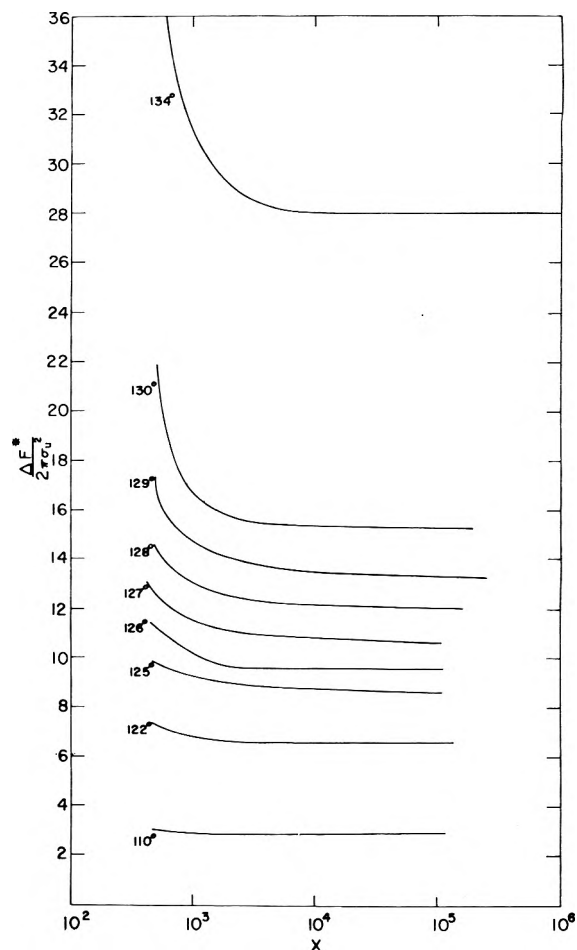


Figure 5.—Plot of quantity $\Delta F^*/(2\pi\sigma_u^2)$ against chain length, x , for various temperatures indicated.

However, for sufficiently long chains, only a portion of each of the molecules will participate in the formation of a nucleus, despite the equilibrium requirements. In these circumstances the critical requirement for nucleus formation is still given by eq. 3 and 4. However, a very interesting and unique situation now results. Neither ρ^* nor ΔF^* becomes infinite at the equilibrium melting temperature of the system. Instead, numerical calculations show that the point at which ρ^* and ΔF^* do become infinite occurs at a temperature which corresponds to the melting temperature of the ordered array in which terminal units are not paired. Since the end-pairing model has been assumed to be more stable in this instance, this latter temperature will be less than the equilibrium melting temperature for the system. Hence, since the steady-state nucleation rate is proportional to $\exp\{-\Delta F^*/RT\}$,¹⁶ a temperature interval exists below the true melting temperature

(16) D. Turnbull and J. C. Fisher, *J. Chem. Phys.*, **17**, 71 (1949).

wherein nucleation by this mechanism will be theoretically impossible. For nucleation to occur at a finite rate in this temperature interval another kind of molecular mechanism would need to be invoked.

A similar situation exists for the unpaired equilibrium model, if σ_c for the nucleus and the crystallite are different. If the interfacial energy of the nucleus is greater than that for the mature crystallite, ΔF^* again becomes infinite at a temperature below the equilibrium melting temperature of the system. Numerical analysis indicates that this temperature is very close to the melting temperature for the equilibrium crystallite that is characterized by the value of the interfacial energy of the nucleus. Conversely, for the hypothetical situation of the interfacial energy for the nucleus being less than that for the crystal, ΔF^* becomes infinite at the equilibrium melting temperature of the crystal characterized by the smaller value of the interfacial

energy. Since this temperature is greater than the equilibrium melting temperature of the system, homogeneous nucleation will become theoretically possible above the melting temperature in this instance.

In summary, we have observed generally that the nucleation theory for infinite molecular weight chains, which is formally equivalent to that for monomeric systems, serves as a poor approximation when the number of chain bonds is less than about 10^5 . In this molecular weight range, irrespective of the molecular nature of the form of the equilibrium crystal, appropriate cognizance must be taken of the finite length of the chain in treating nucleus formation. In particular, we also see the unique possibility, depending on the relative values of the interfacial energies involved, of the homogeneous steady-state nucleation rate vanishing at a temperature below the equilibrium melting temperature of the system or being finite at a temperature above it.

Kinetics of the Acid-Catalyzed Hydrolysis of Acetal in Dimethyl Sulfoxide–Water Solvents at 15, 25, and 35°

by Richard K. Wolford

National Bureau of Standards, Washington, D. C. 20254 (Received June 15, 1964)

Rate constants for the acid-catalyzed hydrolysis of acetal in binary solvent mixtures composed of dimethyl sulfoxide and water have been determined as a function of solvent composition and temperature. The rate decreases as the dimethyl sulfoxide content increases. The pK value of *m*-nitroaniline and the acidity function $p_w(a_{H^+})$ were determined in the same solvents, and these measures of acidity were compared with the kinetic results. The reaction rate as a function of solvent composition is discussed in terms of changes in the internal structure of the solvent. Specific solute–solvent interactions apparently play a very important role in determining the kinetic and the equilibrium behavior. The isocomposition activation energy passes through a minimum in solvents of high water content where the temperature coefficient of the dielectric constant passes through a maximum. Acetal hydrolysis rates are compared for various water–organic solvent mixtures, and it is concluded that the basicity is the solvent property which is most important in determining the rate of the acid-catalyzed hydrolysis.

Introduction

The purpose of this study was to determine the effects of change in the solvent composition and temperature on the rate of the acid-catalyzed hydrolysis of acetal, $CH_3CH(OC_2H_5)_2$, in dimethyl sulfoxide–water solvents and to compare these results with those obtained for the same reaction in other water–organic solvent mixtures.^{1,2} A comparison of the kinetic behavior for acetal hydrolysis was made with other measures of acidity obtained from equilibrium studies in the same solvents.

Although the effect of a solvent change on the acid-catalyzed hydrolysis of esters has been studied extensively,³ acetals have received little attention.⁴ Acetal hydrolysis in aqueous solutions is extremely sensitive to hydrogen ion and appears to undergo specific hydrogen ion catalysis.⁵ Other reasons for choosing this reaction for study are that the reaction products do not affect the acidity of the solution, the uncatalyzed reaction is negligible, and the reaction goes to completion in all the solvent mixtures studied here.

Experimental

The rate of the reaction was determined by observing the change in density of the solution using a dilatometric procedure.² The rate of the reaction



is given by $k_1c_A = k_2c_Ac_H^+$ where k_1 is the first-order rate coefficient in sec^{-1} , c_A the molar concentration of acetal, c_H^+ the stoichiometric molar concentration of hydrochloric acid, and k_2 the second-order rate co-

(1) R. K. Wolford, *J. Phys. Chem.*, **67**, 632 (1963).

(2) R. K. Wolford and R. G. Bates, *ibid.*, **66**, 1496 (1962).

(3) E. Tommila and A. Hella, *Ann. Acad. Sci. Fennicae, Ser. A II*, **53**, 3 (1954); H. S. Harned and A. M. Ross, *J. Am. Chem. Soc.*, **63**, 1993 (1941); the papers of E. S. Amis and co-workers are summarized in *Anal. Chem.*, **27**, 1672 (1955).

(4) P. Salomaa, *Acta Chem. Scand.*, **11**, 461 (1957); J. Koskikallio and I. Tarvainen, *ibid.*, **16**, 263 (1962).

(5) J. N. Bronsted and W. F. K. Wynne-Jones, *Trans. Faraday Soc.*, **25**, 59 (1929).

(6) The values of k_2 were corrected for expansion of the solvent due to temperature change. By using 25° as reference, the magnitude of this correction is well within the experimental error, not amounting to more than 1%.

Table I: Hydrolysis Rates for Acetal in Hydrochloric Acid-Water-Dimethyl Sulfoxide Mixtures and Dielectric Constants for Water-Dimethyl Sulfoxide Solvents at Various Temperatures

Mole % DMSO	10 ⁴ c _{HCl} , moles l. ⁻¹	k ₂ , l. mole ⁻¹ sec. ⁻¹	c(acetal), mole l. ⁻¹	D
t = 15°				
0	...	0.391 ^a	...	81.95 ^b
7.7	0.989, 2.967	0.218	0.0700	81.23
13.1	4.951	0.1303	0.0700	80.16
16.6	4.945	0.0908	0.0700	79.25
19.4	4.948	0.0583	0.0700	78.39
30.13	74.56 ^c
40.7	19.92, 38.79	0.0137	0.0486	70.46
44.82	68.79 ^c
62.79	61.46 ^c
66.1	26.59, 44.35	0.00800	0.0348	60.17
81.54	54.36 ^c
89.4	25.94	0.00902	0.0204	51.50
100.00	47.64 ^c
t = 25°				
0	...	1.462 ^d	...	78.30 ^b
7.7	0.982	0.762	0.0696	77.49
13.1	0.981	0.454	0.0696	76.41
16.6	1.962	0.323	0.0696	75.56
19.5	1.963	0.215	0.0696	74.74
30.13	71.31 ^c
40.8	4.935	0.0478	0.0483	67.46
44.82	65.94 ^c
62.79	59.15 ^c
66.2	9.886	0.0271	0.0345	57.95
81.54	52.58 ^c
89.3	25.81	0.0284	0.0202	49.95 (46.4) ^e
100.00	46.36 ^c
t = 35°				
0	74.83 ^b
7.7	0.4861	2.53	0.0693	74.09
13.1	0.4927	1.423	0.0692	73.09
16.6	0.6851	1.000	0.0691	72.24
19.4	0.975	0.778	0.0691	71.49
30.13	68.17 ^c
40.5	1.950	0.164	0.0478	64.64
44.82	63.15 ^c
62.79	56.90 ^c
66.7	4.895	0.0867	0.0342	55.58
81.54	50.81 ^c
89.3	5.578	0.0975	0.0200	48.37
100.00	45.10 ^c

^a See ref. 1. ^b C. G. Malmberg and A. A. Maryott, *J. Res. Natl. Bur. Std.*, **56**, 1 (1956). ^c See ref. 9. (Specific conductivity of dimethyl sulfoxide is 2×10^{-8} ohm⁻¹ cm.⁻¹, m.p. 18.483°.)
^d See ref. 2. ^e See ref. 10.

efficient in l. mole⁻¹ sec.⁻¹. Values of k₂ can be obtained with an uncertainty not greater than ±2%. Thus the uncertainty in values of the activation energy is ±0.4 kcal. mole⁻¹. For solutions containing 66 and

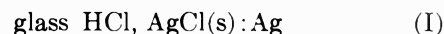
92.5 mole % dimethyl sulfoxide, it was shown that the acetal hydrolysis reaction went to completion. This was done by comparing the ultraviolet absorption spectrum of the reaction mixture with that of solutions containing known amounts of acetaldehyde. There was no indication of any reaction between dimethyl sulfoxide and hydrochloric acid, or between dimethyl sulfoxide and the reactants or products of the acetal hydrolysis.

The pK of the acid form of *m*-nitroaniline for dimethyl sulfoxide-water solvents was determined from the equation

$$pK = \log \frac{(A_B - A)}{(A - A_{BH^+})} - \log c_{HCl}$$

where A_B is the absorbance of *m*-nitroaniline, A_{BH⁺} that of its protonated form, and A is the absorbance of a solution containing *m*-nitroaniline and hydrochloric acid at a molar concentration, c_{HCl}. A Cary Model 14 spectrophotometer was used to obtain all spectra; the cell was maintained at a constant temperature of 25.0 ± 0.1°.

The e.m.f. of the cell



with dimethyl sulfoxide-water solvents was measured with a pH meter utilizing a chopper-type amplifier.⁷

Dimethyl sulfoxide of the best commercial grade was distilled through an efficient column packed with glass helices at about 5 mm. pressure. The low-conducting fractions were fractionally frozen several times to give a product having a freezing point of 18.471° (as determined with a platinum resistance thermometer) and a specific conductivity less than 1×10^{-7} ohm⁻¹ cm.⁻¹. By analyzing the cooling curve⁸ and using a cryoscopic constant of 4.36° for dimethyl sulfoxide, the sample was found to contain approximately 0.002 mole of impurity.

Dielectric constants of dimethyl sulfoxide-water mixtures (determined by a bridge method) are listed in Table I.⁹ Values of the dielectric constant, D, for the solvent mixtures used in the kinetic studies were interpolated from a plot of (D - 1)/ρ against the mole fraction of dimethyl sulfoxide, where ρ is the density of the dimethyl sulfoxide-water solvent. The values of D obtained by Lindberg and Kenttämää¹⁰ by a

(7) It was necessary to employ the glass electrode because stable readings could not be obtained with the hydrogen electrode.

(8) A. R. Glasgow, A. J. Streiff, and F. D. Rossini, *J. Res. Natl. Bur. Std.*, **35**, 355 (1945).

(9) From the data of C. G. Malmberg, unpublished results, National Bureau of Standards.

(10) J. J. Lindberg and J. Kenttämää, *Suomen Kemistilehti*, **33B**, 104 (1960).

resonance method for the same solvent system at 25° do not deviate from the above plot by more than 0.3 in D . The densities are given by $\rho = b_0 - b_1(10^{-3})t - b_2(10^{-6})t^2$ which can be used for temperatures from 0 to 75°. The constants have the values given in Table II.

Table II

x_{DMSO}	b_0	b_1	b_2
1.0000	1.12048	1.00442	0
0.8154	1.12156	0.96538	0.2068
0.6279	1.12229	0.92437	0.3915
0.4482	1.11955	0.86171	0.6839
0.3013	1.10725	0.7200	1.50

Results

Data for the hydrolysis of acetal in aqueous hydrochloric acid-dimethyl sulfoxide solutions are presented in Table I. The values of the second-order rate coefficient can be considered to be those at infinite dilution in the given solvent. The pK values at infinite dilution in the given solvents for m -nitroanilinium ion are listed in Table III. The values for 65.0, 80.2,

Table III: Values of pK for m -Nitroanilinium Ion in Dimethyl Sulfoxide-Water Solvents at 25° and Wave Lengths where Maximum Absorbance of m -Nitroaniline Occurs

$100x_{\text{DMSO}}$	Max. $m\mu$	pK	$100x_{\text{DMSO}}$	Max. $m\mu$	pK
0	360	2.440	65.04	396	0.70
6.24	363	2.109	80.18	398	0.82
14.51	370	1.669	92.73	398	0.96
23.33	381	1.225	100.00	399	1.15
42.26	392	0.778			

and 92.7 mole % dimethyl sulfoxide are extrapolated values, whereas those for the other solvent mixtures are the average of determinations made at different acid concentrations.

Activation Energy at Constant Composition, ΔE . These values are calculated from the Arrhenius equation using the k_2 values of Table I. The values obtained for the temperature range 15 to 25° are 21.4, 21.3, 21.7, 22.3, 21.4, 20.9, and 19.6, and for the temperature range 25 to 35° the values are 21.9, 20.8, 20.6, 23.5, 22.5, 21.2, and 22.5 kcal. mole⁻¹ for the solvents containing dimethyl sulfoxide at mole fractions of 0.077, 0.131, 0.166, 0.195, 0.408, 0.662, and 0.893,

respectively. The value for aqueous solution¹ is 22.4 kcal. mole⁻¹, which is in good agreement with the value 22.3 obtained by others.¹¹

Activation Energy at Constant Dielectric Constant, ΔE_D . From the data of Table I, plots of $\log k_2$ against D were drawn for the three temperatures. From these, values of $\log k_2$ at constant D were obtained by interpolation. Values of ΔE_D could then be calculated from the Arrhenius equation. For the temperature range 15 to 25° these values are 35.3, 27.6, 25.0, 22.9, 21.4, 20.4, and 19.0, and for the range 25 to 35° they are 48.5, 32.9, 28.7, 25.0, 23.0, 21.6, and 21.3 kcal. mole⁻¹ for $D = 74, 69, 66, 62, 59, 56,$ and $51,$ respectively. As a check, the same procedure was repeated by employing a plot of $\log k_2$ against $(1/D)$. For the temperature range 15 to 25°, $\Delta E_D = 34.3, 28.1, 24.8, 20.9,$ and $19.0,$ and for the temperature range 25 to 35°, $\Delta E_D = 45.1, 34.4, 29.3, 22.2,$ and 21.4 kcal. mole⁻¹ for $D = 73.5, 69.4, 65.8, 57.5,$ and $51.0,$ respectively.

Discussion

Hydrolysis Rate and Mechanism. A generally accepted mechanism for the acid-catalyzed hydrolysis of acetals in aqueous solution¹² consists of a fast pre-equilibrium step between solvated proton, acetal, and the protonated form of acetal, followed by the rate-determining unimolecular formation of a carbonium ion from the protonated acetal. There is evidently a dispersion of charge in forming the transition state. That this mechanism governs the rate when dimethyl sulfoxide is added has not been clearly established. The entropy of activation, ΔS^* , and the enthalpy of activation, ΔH^* , appear to change in the same manner when the solvent composition is varied,¹³ *i.e.*, ΔH^* is a linear function of ΔS^* within the experimental error.

This observation might be interpreted as indicating a constancy of mechanism although it should be noted that the experimental error in these quantities is rather large. The manner in which the pK of m -nitroaniline changes with solvent composition may lend some support to this mechanism in the mixed solvents. The

(11) L. C. Riesch and M. Kilpatrick, *J. Phys. Chem.*, **39**, 561 (1935).

(12) F. A. Long and M. A. Paul, *Chem. Rev.*, **57**, 935 (1957).

(13) From the theory of absolute reaction rates (see S. Glasstone, K. J. Laidler, and H. Eyring, "The Theory of Rate Processes," McGraw-Hill Book Co., Inc., New York, N. Y., 1941, p. 199) one can calculate ΔS^* . Thus $(\Delta S^*/2.3R) = \log k_2 + (\Delta E/2.3RT) - 0.434 - \log (RT/Nh)$ for a standard state of unit hydrochloric acid concentration. For the temperature range 15 to 25° and $T = 298^\circ\text{K}$., the values of ΔS^* for $x_{\text{DMSO}} = 0, 0.077, 0.131, 0.166, 0.195, 0.408, 0.662,$ and 0.893 are 16, 11, 10, 10, 11, 6, 3, and -1 cal. deg.⁻¹ mole⁻¹, respectively. Since $\Delta H^* = \Delta E - RT$, values of ΔH^* are readily obtainable.

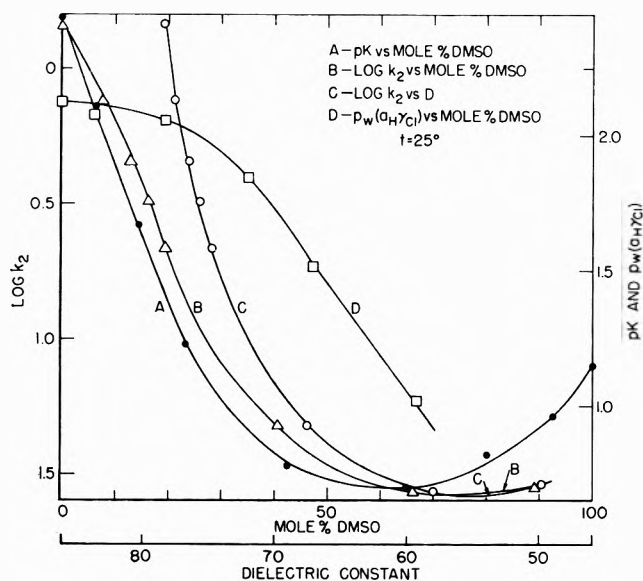


Figure 1. $\log k_2$ for acetal hydrolysis, pK_{BH^+} for *m*-nitroanilinium ion, and $p_w(a_{H\gamma Cl})$ as a function of solvent composition for dimethyl sulfoxide-water solvents.

values for pK are listed in Table III, and they can be compared with $\log k_2$ (Fig. 1). The change in $\log k_2$ with solvent composition is similar to that for the change in pK except that the relatively broad minimum in $\log k_2$ occurs at $x_{DMSO} = 0.76$ to 0.77 whereas the sharper minimum in pK occurs at $x_{DMSO} = 0.6$. This general similarity in behavior probably means that the pre-equilibrium step in the assumed mechanism is an acid-base reaction of the same charge type as the dissociation of *m*-nitroanilinium ion. Hence the equilibrium constants for the two reactions respond in the same manner to changes in solvent composition. To be more specific, one can write

$$p_s K = p_w K + \log (m_{y_B} / m_{y_{BH^+}}) + \log m_{y_H}$$

where $p_s K$ is referred to infinite dilution in the given dimethyl sulfoxide-water solvent (the symbols $p_s K$ and pK are often used interchangeably) and $p_w K$ refers to the infinitely dilute solution in water. The terms m_{y_i} are medium effect activity coefficients,¹⁴ and the subscripts B and BH^+ refer to *m*-nitroaniline and the protonated form of *m*-nitroaniline, respectively. Assuming the mechanism for acetal hydrolysis is $A + H^+ \rightleftharpoons AH^+$ followed by the rate-determining step, $AH^+(H_2O) \rightarrow x^*$ (where A = acetal and the parentheses indicate that water may or may not participate directly as a nucleophile) one can derive the equation¹⁵

$$\log k_2 = \text{constant} + \log (m_{y_A} / m_{y_{x^*}}) + \log m_{y_H}$$

when the rate-determining step is unimolecular.

Comparing the $\log k_2$ equation with the pK equation suggests that a plot of $\log k_2$ against pK might be a straight line of *unit slope*. Such a plot is not linear, although it can be divided into three parts: a linear segment with slope = 0.75 for solvents containing 0 to 20 mole % dimethyl sulfoxide, another linear segment with slope = 1.12 between 20 and 50 mole %, and finally the portion between 50 and 90 mole % where the curve reverses itself. One can conclude that (1) the activity coefficient ratios change in a different manner with solvent composition or (2) water participates in a rate-determining bimolecular step, or both.

Specific solute-solvent interaction between *m*-nitroaniline and dimethyl sulfoxide is indicated by the shift in the maximum of the absorption spectra to longer wave lengths (Table III). A similar spectral shift has been found for aniline,¹⁶ along with an indication (from other data) of compound formation between the amine and the sulfoxide. No interaction of this sort (H-bonding or dipole-dipole) is expected to occur between acetal and dimethyl sulfoxide. Thus, a difference in behavior of m_{y_B} and m_{y_A} as solvent changes is not unexpected.

The quantity¹⁷

$$p_w(a_{H\gamma Cl}) \equiv -\log (m_{H^+}) \times \\ w(\gamma_H \cdot \gamma_{Cl^-}) = \frac{E - wE^\circ}{0.05916} + \log m_{Cl^-}$$

and the e.m.f. values of cell I are listed in Table IV.

Table IV: The Quantity $p_w(a_{H\gamma Cl})$ Calculated from the E.m.f. Values of the Cell, Glass HCl, AgCl:Ag for Dimethyl Sulfoxide-Water Solvents

100x _{DMSO}	Mv.	$p_w(a_{H\gamma Cl})$	Mv.	$p_w(a_{H\gamma Cl})$
	$c_{HCl} = 0.0532 M$		$c_{HCl} = 0.00887 M$	
0	308.8	1.431	222.4	2.132
5.9	309.4	1.419	223.6	2.078
19.4	309.7	1.384	224.4	2.059
35.3	320.0	1.205	235.6	1.847
47.3	337.6	0.899	254.6	1.524
66.8	363	0.477	284.7	1.017

(14) R. G. Bates, "Determination of pH," John Wiley and Sons, Inc., New York, N. Y., 1964, p. 190.

(15) This derivation follows closely that given by Long and Paul, ref. 12.

(16) J. Kenttämä and J. J. Lindberg, *Suomen Kemistilehti*, **34B**, 117 (1961).

(17) R. G. Bates and R. Gary, *J. Res. Natl. Bur. Std.*, **65A**, 495 (1961).

The subscript w refers to the solvent water and m_{Cl^-} is the molality of the chloride ion. This acidity function changes in a completely different manner with solvent composition than does either pK or $\log k_2$. This is not surprising since this function has a form that one might expect to follow equilibria of the type $BH \rightleftharpoons B^- + H^+$.

Solvent Structure and the Change in Rate. The following properties of water–dimethyl sulfoxide mixtures at 25° may help to form some picture of the nature of the solvent in these mixtures. (1) Although the density passes through a relatively broad maximum at $x_{DMSO} = 0.6$, the point of greatest deviation from a straight line connecting the density of pure water with that of pure dimethyl sulfoxide occurs at $x_{DMSO} = 0.33$.^{18a,b} (2) The viscosity maximum and the point of greatest deviation from a straight line between the pure solvents occur at $x_{DMSO} = 0.3$ – 0.4 .^{18b,19} (3) The heat of mixing per mole of solution has an exothermic maximum between $x_{DMSO} = 0.3$ and 0.4 .^{18b,20} (4) The thermodynamic excess function $T\Delta S^E$ is negative for all dimethyl sulfoxide–water solutions and passes through a minimum value at $x_{DMSO} = 0.3$ – 0.4 .²¹ (5) Finally, the temperature coefficient ($d \ln D/dT$) for the temperature range 15 to 35° is relatively insensitive to solvent change until x_{DMSO} reaches 0.3 to 0.4. Above $x = 0.4$, however, the temperature coefficient decreases rapidly with increasing dimethyl sulfoxide content.⁹ The composition $x = 0.33$ corresponds to a compound, $DMSO \cdot (H_2O)_2$. The freezing point–composition curve shows only the presence of a eutectic at $x_{DMSO} = 0.33$. This indicates that one is probably not dealing with such a compound in these solutions. On the basis of the above information one is tempted to consider dimethyl sulfoxide–water solvents as consisting of three zones of differing solvent structure: one from 0 to around 30 mole %, the next from 30 to about 40 or 50 mole %, and, finally, one after 50 mole % dimethyl sulfoxide.

There appears to be a parallelism between the changes in solvent structure and the kinetic behavior. This could be due to relative changes in solvation of the initial and transition states for the acetal hydrolysis reaction. Thus, the slope of the plot $\log k_2$ against x_{DMSO} increases until about $x = 0.20$ (Fig. 1), then it decreases until $x = 0.75$. The three segments into which the deviations of the $\log k_2$ – pK plot from a unit slope are divided correspond roughly to the solvent zones above. The activation energy, ΔE , passes through a minimum in the region 0 to 20 mole % dimethyl sulfoxide.

That there is a greater degree of association in

dimethyl sulfoxide–water solvents than in the pure solvent components seems apparent. If it is assumed that the interactions are due to H-bonding only, then we might conclude that the $-OH \cdots OS<$ bond is stronger than the $-HO \cdots HO-$ bond, which is a conclusion that is opposite to that reached by others.²² In addition, dipole–dipole interactions between water and dimethyl sulfoxide molecules appear to play a role. Evidence for this comes from Raman spectra of dimethyl sulfoxide–water mixtures²³ and from a comparison of heat of mixing data with n.m.r. spectra of dimethyl sulfoxide–water mixtures.²²

Self-association between dimethyl sulfoxide molecules must also be considered. Thus, chain polymers appear to form due to dipole–dipole interactions in benzene solutions.²⁴ This conclusion appears to receive support from the fact that the infrared spectrum of dimethyl sulfoxide in carbon tetrachloride is not concentration dependent up to 100% dimethyl sulfoxide. Self-association by H-bonding,²⁵ therefore, seems unlikely.

Relation between ΔE and ΔE_D . The manner in which the activation energy at constant composition (ΔE) and the activation energy at constant dielectric constant (ΔE_D) change with solvent composition is illustrated by Fig. 2. These quantities were calculated from data at 15 and 25°. When ΔE and ΔE_D are calculated from data at 25 and 35° a plot similar to that of Fig. 2 results. Starting from the differential of $\ln k_2 = f(T, D)$, an expression for this relationship can be derived.^{1,26} Thus

$$\Delta E_D - \Delta E = 2.3bDRT^2 \left(\frac{\partial \log k_2}{\partial D} \right)_T \quad (1)$$

where b is the slope of a plot of $\ln D$ against T for the temperature range 15 to 35°. Table V shows the results of a test of this equation. Values for the quantities on the right-hand side of eq. 1 for the median temperatures 20 and 30° were used.

(18) (a) Results from this paper; (b) J. M. G. Cowie and P. M. Toporowski, *Can. J. Chem.*, **39**, 2240 (1961).

(19) R. G. LeBel and D. A. I. Goring, *Chem. Eng. Data Ser.*, **7**, 100 (1962).

(20) J. Kenttämää and J. J. Lindberg, *Suomen Kemistilehti*, **33B**, 3 (1960).

(21) J. Kenttämää and J. J. Lindberg, *ibid.*, **33B**, 98 (1960).

(22) W. Drinkard and D. Kivelson, *J. Phys. Chem.*, **62**, 1494 (1958).

(23) J. J. Lindberg and C. Majani, *Acta Chem. Scand.*, **17**, 1477 (1963).

(24) J. J. Lindberg, J. Kenttämää, and A. Nissema, *Suomen Kemistilehti*, **34B**, 156 (1961).

(25) A. Allerhand and P. von R. Schleyer, *J. Am. Chem. Soc.*, **85**, 1715 (1963).

(26) W. J. Svirbely and J. C. Warner, *ibid.*, **57**, 1883 (1935).

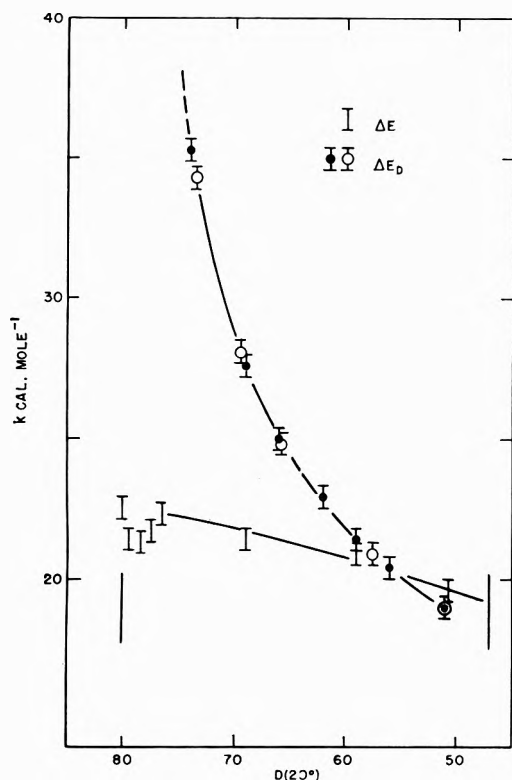


Figure 2. The activation energies, ΔE_D and ΔE , for the hydrolysis of acetal in aqueous hydrochloric acid-dimethyl sulfoxide solutions as a function of the dielectric constant of the solvent. The values of D used for ΔE are those for 20°. The calculation of ΔE and ΔE_D is from rate data at 15 and 25°.

Table V

D	—($\Delta E_D - \Delta E$) 15-25°—		—($\Delta E_D - \Delta E$) 25-35°—	
	Calcd.	Obsd.	Calcd.	Obsd.
74	12.7	13.0
70	7.3	7.1	12.8	12.5
66	3.8	3.7	6.9	6.5
56	0	0	0	0

The point at which the curves intersect corresponds to the value of D at which the plot of $\log k_2$ against D passes through a minimum. On the high D side of the minimum $\Delta E_D > \Delta E$, and on the low D side the reverse is true, because $(\partial \log k_2 / \partial D)$ has changed sign.

When the activation energy at constant composition is plotted against x_{DMSO} , the minimum is observed at mole fractions of dimethyl sulfoxide between 0.1 and 0.2. The activation energy at constant dielectric constant apparently does not exhibit a maximum as solvent composition is varied. Although b passes through a maximum value for $0.1 < x_{\text{DMSO}} < 0.2$ (b is the only other factor in eq. 1 that exhibits

maximum or minimum behavior in this solvent composition range), the relative magnitude of this maximum is not sufficient to cause the minimum in ΔE . According to eq. 1, ΔE is determined by the difference in ΔE_D and the quantity on the right-hand side of eq. 1. Both of these factors decrease at different rates as x_{DMSO} increases, and this, possibly, causes the minimum in ΔE .²⁷

Comparison of Acetal Hydrolysis Rates in Various Water-Organic Solvent Mixtures. Figure 3 compares some of the results of this paper with some data of ref. 1 and 2. One interpretation of this comparison

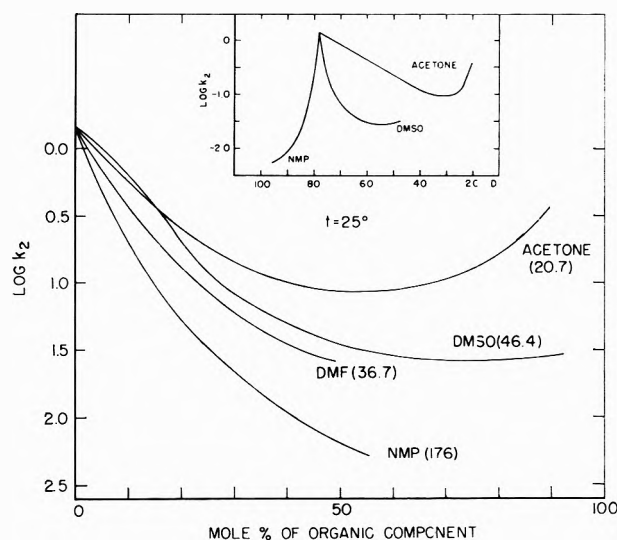


Figure 3. $\log k_2$ for the hydrolysis of acetal for aqueous-organic binary solvent mixtures as a function of the concentration of the organic component and as a function of the dielectric constant of the binary solvent (DMSO = dimethyl sulfoxide, DMF = *N,N*-dimethylformamide, and NMP = *N*-methylpropionamide). The numbers in parentheses give the dielectric constant of the pure organic component at 25°.

is that it gives an indication of the relative basicities of the various solvent mixtures. It is interesting to note that the order of decreasing rate of solvolysis of *p*-methoxyneophyl toluenesulfonate in the pure solvents is $\text{H}_2\text{O} > \text{DMSO} > \text{DMF} > \text{acetone}$.²⁸ Since this is also the order of decreasing ionizing power and decreasing dielectric constant of the solvent, the results indicated in Fig. 3 must indicate that some other sol-

(27) The minimum in ΔE might be explained in terms of the specific solvation model employed by J. B. Hyne, R. Wills, and R. E. Wonkka, *J. Am. Chem. Soc.*, **84**, 2914 (1962); J. B. Hyne, *ibid.*, **82**, 5129 (1960). Since the mechanism of the reaction in these solvents is not known with certainty, one is hesitant to explain the ΔE behavior in terms of preferential solvation of an initial or transition state by the more polar component of the binary solvent mixture.

(28) S. G. Smith, A. H. Fainberg, and S. Winstein, *ibid.*, **83**, 618 (1961).

vent property is more important for the acid-catalyzed hydrolysis of acetal, and that property is apparently the solvent basicity. It appears that the point where the minimum occurs in the $\log k_2$ -solvent composition plot will shift toward pure organic solvent as the basicity of the organic solvent component increases.

Comparison of Acid-Catalyzed Hydrolysis Rates. The acid hydrolysis of ethyl acetate in dimethyl sulfoxide-water solvents has been studied recently.²⁹ The following statements compare these results with the present results for acetal hydrolysis. (1) The second-order rate coefficient for acetal experiences its greatest decrease for solvents containing 0 to 25 mole % dimethyl sulfoxide and passes through a broad minimum in solvents containing 50 to 100 mole % dimethyl sulfoxide, whereas that for ethyl acetate increases and passes through a maximum in the first composition range and experiences its greatest decrease in the second. (2) The ΔF^* values for the various solvents are about 5 kcal. greater for ethyl acetate, and the ΔE values are about 6 kcal. less than those for acetal. The reason for this is that values of ΔS^* for ethyl acetate are about 34 e.u. more negative than those for acetal. (3) Ethyl acetate hydrolysis proceeds faster in water-dimethyl sulfoxide solvents than it does in acetone-water for most of the solvent composition range. The reverse is true for acetal hydrolysis.

The mechanisms for the ester and the acetal hydrolysis both involve a fast pre-equilibrium protonation step before the rate-determining step. While the protonated substrate for acetal apparently undergoes unimolecular decomposition, that for the ester reacts with water to form a tetrahedral intermediate³⁰ which then reacts further in one of three ways depending on which bond is broken. Thus, a hydrolytic reaction and a carbonyl oxygen exchange can occur concurrently, and the magnitudes of the respective rate coefficients will depend on the partitioning of the intermediate which in turn will depend on the solvent composition. The experimental rate coefficient and the activation parameters derived from it will reflect contributions from all three sources. To draw conclusions from a comparison of the activation parameters for the acetal and ester reactions is thus risky. Nevertheless, the difference in the magnitudes of ΔS^* for the two reactions may indicate a greater degree of freezing or restriction of water molecules during the course of the ester hydrolysis. This fact and the actual magnitudes of the ΔS^* values for acetal are consistent with a unimolecular rate-determining step for acetal hydrolysis.

(29) E. Tommila and M. Murto, *Acta Chem. Scand.*, **17**, 1957 (1963).

(30) M. Bender, *Chem. Rev.*, **60**, 54 (1960); J. F. Bunnett, *J. Am. Chem. Soc.*, **83**, 4978 (1961); R. B. Martin, *ibid.*, **84**, 4130 (1962).

Water Adsorption on Molybdenum Disulfide Containing

Surface Contaminants

by R. R. M. Johnston and A. J. W. Moore

*Division of Tribophysics, Commonwealth Scientific and Industrial Research Organization,
Parkville N.Z., Victoria, Australia (Received June 23, 1964)*

MoS₂ was quantitatively analyzed for traces of sulfate and hexavalent molybdenum ions, and the results were compared with pH changes during neutralization of an aqueous slurry of MoS₂ in NaOH and with the acidity of an aqueous Soxhlet extract of MoS₂. The presence of adsorbed sulfuric acid and molybdenum trioxide was indicated quantitatively. With a silica helix balance, the losses in weight while heating MoS₂ at various temperatures up to 1000° under vacuum were measured, and in the same apparatus water vapor isotherms at 30° were determined. Physical adsorption of water occurred on MoS₂ as received, but not on MoS₂ previously heated to 350° under vacuum when sulfuric acid would have been removed. However, chemisorption of water still occurs, and it is associated with the MoO₃ still present. On MoS₂ heated under conditions in which MoO₃ would have been volatilized, chemisorption is reduced. The significance of these results on the lubricating behavior of MoS₂ is briefly discussed.

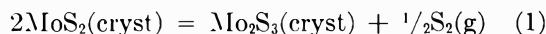
Introduction

The lubricating behavior of graphite^{1,2} and MoS₂³⁻⁶ is profoundly affected by water vapor. With graphite, Campbell and Kozak² observed smooth sliding in an atmosphere with a water vapor content very similar to one in which Savage¹ observed wear. This lack of agreement has been much discussed,⁷ but the observations that water adsorption by graphite⁸ and, therefore, its lubricating behavior depend on the degree of surface oxidation have so far received little attention. There is the possibility that the graphite used by the former workers was rendered hydrophilic by heating in air prior to experiment, while that used by the latter was made hydrophobic by heating *in vacuo*. Similar considerations might apply to MoS₂, but with this substance, unlike graphite for which adsorption properties have been studied in great detail, very little gas adsorption work has been done. Moreover, previous work has been difficult to interpret because the nature of the contaminant layer produced by atmospheric oxidation of the MoS₂ surface has not been sufficiently understood.

Ballou and Ross⁹ determined nitrogen and water adsorption isotherms on MoS₂ powder before and after it

had been treated for oxide removal. Their results suggested that the oxide-free surface is hydrophobic and that water adsorption is promoted by the presence of surface oxide. However, they removed oxides from MoS₂ powder by wet chemical methods, and there is, therefore, some doubt as to whether all contaminants have been removed or even that new ones may have been introduced. An alternative method of removal, that of volatilization of surface contaminants by heating *in vacuo*, has been proposed,¹⁰ but the effects of thermal dissociation of MoS₂ by the reaction

- (1) R. H. Savage, *J. Appl. Phys.*, **19**, 1 (1948).
- (2) W. E. Campbell and R. Kozak, *Trans. Am. Soc. Mech. Eng.*, **70**, 491 (1948).
- (3) M. B. Peterson and R. L. Johnson, National Advisory Committee for Aeronautics Technical Note 3055, 1953.
- (4) Yu P. Toporov, *J. Eng. Phys. BSSR Minsk.*, **4**, 44 (1960).
- (5) V. R. Johnson and G. W. Vaughn, *J. Appl. Phys.*, **27**, 1173 (1956).
- (6) A. J. Haltner and C. S. Oliver, G. E. Res. Lab. Report 63-RL-3495C, Nov., 1963.
- (7) E. R. Braithwaite, *Nuclear Eng.*, **2**, 107 (1957).
- (8) P. H. Emmett and R. B. Anderson, *J. Am. Chem. Soc.*, **67**, 1492 (1945).
- (9) E. V. Ballou and S. Ross, *J. Phys. Chem.*, **57**, 653 (1953).
- (10) P. Cannon, *Nature*, **183**, 1612 (1959).



must be considered.¹¹

Ross and Sussman¹² found that MoS_2 which had been comminuted in air contained just the amount of water-soluble sulfate (SO_4^{-2}) and ammonia-soluble hexavalent molybdenum (Mo(VI)) that would have been produced by complete oxidation of the outer S-Mo-S layer. The rate of surface oxidation was found to be enhanced in humid air but was generally slow at room temperature, and it was suggested that MoO_3 and H_2SO_4 are present on the sulfide surface.

It was our aim to establish the nature of the surface contaminants on the MoS_2 surface and by selective removal to ascertain their effect on its adsorption of water vapor.

Experimental

Molybdenum Disulfide. The powder was supplied by Molybond Laboratories Pty. Ltd., Melbourne, and had been prepared from natural molybdenite mined in north Queensland. After comminution the MoS_2 was purified by treating the powder with hydrofluoric acid and drying in a stream of air. This reduced the silica content to $<0.02\%$. Subsequent qualitative micro-analysis¹³ showed no trace of hydrofluoric acid in the sample. The particles in the sample had an average maximum dimension of about 2μ . This "as received" sample of MoS_2 will be referred to as A.

Quantitative Analysis of Surface Contaminants. The ammonia-soluble molybdenum(VI) and water-soluble sulfate (SO_4^{-2}) content of A was determined by stirring separate 2.5-g. samples for 0.5 hr. in 25 ml. of 0.3 *M* ammonium hydroxide and in 25 ml. of distilled water, respectively. In each case, the MoS_2 (insoluble) was filtered off. Sulfate ion was precipitated and weighed as barium sulfate,¹⁴ and the molybdenum(VI) was precipitated with oxine and weighed as $\text{MoO}_2(\text{C}_9\text{H}_6\text{ON})_2$.¹⁵

pH Titration of Total Acidity. Samples of 1 g. of A were stirred for 0.5 hr. with 20 ml. of ca. 0.05 *M* sodium hydroxide under an atmosphere of nitrogen, excess alkali being back-titrated with standard hydrochloric acid. The pH of the mixture during the course of titration was followed with a Radiometer 4 pH meter and plotted against the volume of standard acid added.

Acidity of Soxhlet Water Extract. Samples of 10 g. of A were placed in 2.5-cm. diameter Soxhlet thimbles and refluxed with 150 ml. of water in an all-Pyrex Quickfit extractor for 4 hr. The pH of the cooled extract was measured. This procedure conforms with U. S. Specification MIL-M-7866A(ASG).¹⁶

Thermogravimetry and Adsorption. A McBain-Bakr¹⁷ quartz helix balance was used to perform thermo-

gravimetric and adsorption experiments on the one sample without removing it from the apparatus. Weight losses during heating under vacuum were measured, and then, after cooling and admitting humidified air, adsorption was followed. The apparatus consisted of a vertical tube, Fig. 1 (a), which could be evacuated to less than 10^{-5} torr. The upper half (Pyrex) housed the helix balance, while the lower half (silica) contained the platinum sample bucket which hung on a fine platinum wire (24 cm. long) from the bottom of the helix.

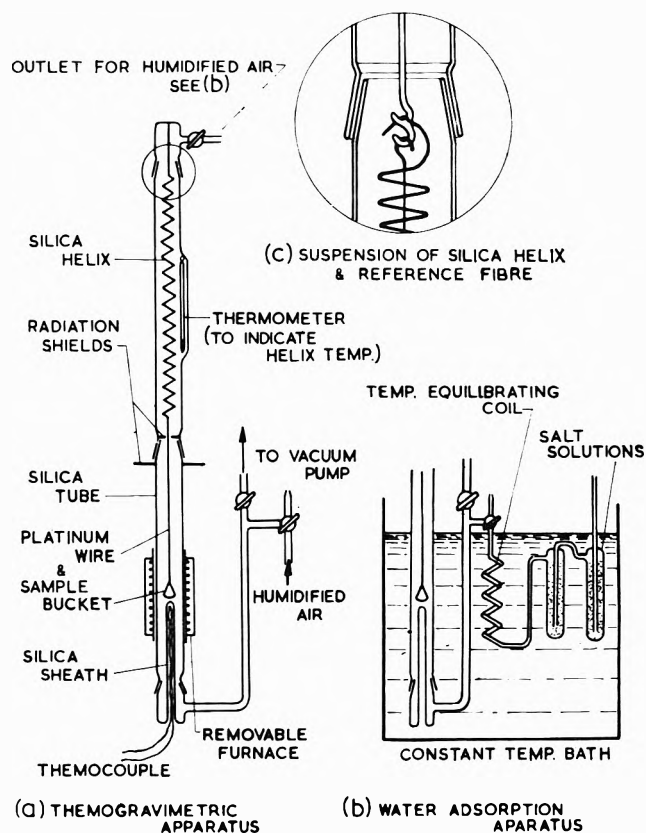


Figure 1. Thermogravimetric and water adsorption apparatus.

(11) J. R. Stubbles and F. D. Richardson, *Trans. Faraday Soc.*, **56**, 1460 (1960).

(12) S. Ross and A. Sussman, *J. Phys. Chem.*, **59**, 889 (1955).

(13) F. Feigl, "Spot Tests in Inorganic Analysis," 5th Ed., Elsevier Publishing Co., London, 1958, pp. 269-275.

(14) I. M. Kolthoff and E. B. Sandell, "Text Book of Quantitative Inorganic Analysis," 3rd Ed., The Macmillan Co., New York, N. Y., 1959, p. 322.

(15) A. I. Vogel, "Quantitative Inorganic Analysis," 2nd Ed., Longmans Green and Co., London, 1951, pp. 439, 441.

(16) Custodians U. S. Navy (Bureau of Aeronautics), U. S. Air Force.

(17) J. W. McBain and A. M. J. Bakr, *J. Am. Chem. Soc.*, **48**, 690 (1926).

The quartz helices were constructed by the method of Ernsberger and Drew.¹⁸ A typical helix had a diameter of 28 mm. and consisted of 58 turns of quartz fiber, 0.28 mm. in diameter. The sensitivity at 25° was 0.514 mm./mg., extension being proportional to load. Extensions, measured with a cathetometer reading to ± 0.015 mm., were taken relative to the end of a quartz reference fiber which was suspended on the same mounting as the helix, Fig. 1 (c), and reached almost to its lower end. This eliminated any error arising from expansion of the Pyrex supporting envelope. The reversible contraction of the quartz helix, as its temperature is raised at constant load,¹⁸ is probably due to a change with temperature of Young's modulus for silica and was corrected by converting the extension at an observed helix temperature to that corresponding to 25°. The helix temperature was obtained from a thermometer hanging alongside it inside the Pyrex envelope, the contraction rate of 0.055 mm./deg. being practically constant over the range of loads concerned. The final accuracy was $\pm 0.03\%$ for a 200-mg. sample.

During thermogravimetry experiments the sample was heated by a resistance furnace placed around the silica section of the envelope. Direct radiation and thermal gradients from the furnace to the silica helix in the upper envelope were reduced by the use of appropriately placed bright aluminum shields. The sample temperature was obtained by means of a chromel-alumel thermocouple inserted in a silica sheath which projected upward into the envelope to within 1 cm. of the platinum bucket. On completion of a thermogravimetric run, the furnace could be replaced by a water bath thermostated at $30 \pm 0.05^\circ$ for adsorption measurements, Fig. 1 (b).

The carrier gas for water adsorption was oil-free air from a water pump. From this, dry air was obtained by the use of a train of tubes containing silica gel and P_2O_5 . Humidification was achieved by bubbling the air through saturated aqueous salt solutions contained in tubes immersed in the thermostat bath. Before admission to the sample, the air was passed through a long copper coil, also immersed in the bath, to ensure thermal equilibrium and then through a three-way tap which enabled the connecting tubes to be flushed out whenever the humidity was being changed. The values of relative humidity of the saturated salt solutions were taken from tables compiled by Fionnuala and O'Brien.¹⁹

Results

Quantitative Analysis of Surface Contaminants. The results of analysis carried out on sample A for water-soluble sulfate ion (SO_4^{-2}) and ammonia-soluble molybdenum(VI) are shown in Table I.

Table I

Sample number	Moles of sulfate, g. of MoS_2	Moles of Mo(VI), g. of MoS_2
i	3.3×10^{-5}	2.5×10^{-6}
ii	4.5×10^{-5}	2.6×10^{-6}
iii	3.9×10^{-5}	
Mean	3.9×10^{-5}	2.55×10^{-6}

If it is assumed that the sulfate ions are present in the MoS_2 as H_2SO_4 and the molybdenum(VI) as MoO_3 , the proportion of the weight of the sample due to the oxide layer is MoO_3 , 0.37 wt. %, and H_2SO_4 , 0.38 wt. %, giving a total of 0.75 wt. %.

pH Titration of Total Acidity. Sample A neutralized $13 (\pm 2) \times 10^{-5}$ mole of hydroxyl ion/g. Apart from a very slight kink at pH 6.5 due to the presence of carbonate impurity, the plot of volume of standard acid added against the pH of NaOH which had been stirred with MoS_2 showed only a single point of inflection (curve II in Fig. 2). However, at pH less than 5, the pH curve showed a more gradual change of slope compared with the pH curve for the neutralization of pure sodium hydroxide (curve I). A similar titration of an aliquot of sodium hydroxide containing H_2SO_4 and resublimed MoO_3 in the quantities shown in Table I, is shown as curve III, and within the experimental error it reproduces curve II.

pH of Soxhlet Water Extract. The results are shown in Table II.

Table II

Sample number	pH of distilled water	pH after refluxing 4 hr. in 150 ml. of water	
		Soxhlet thimble	Thimble + sample A
i	6.5	7.3	2.7
ii	6.5	5.8	2.6

Weight Loss under Vacuum. The thermogravimetric behavior of MoS_2 powder was studied *in vacuo* up to 1000°. The temperature was raised at a rate of approximately 2°/min., but at various intervals the sample temperature was maintained constant ($\pm 2^\circ$) for periods of up to several hours.

(18) F. M. Ernsberger and C. M. Drew, *Rev. Sci. Instr.*, **24**, 117 (1953).

(19) E. M. Fionnuala and M. A. O'Brien, *J. Sci. Instr.*, **25**, 73 (1948).

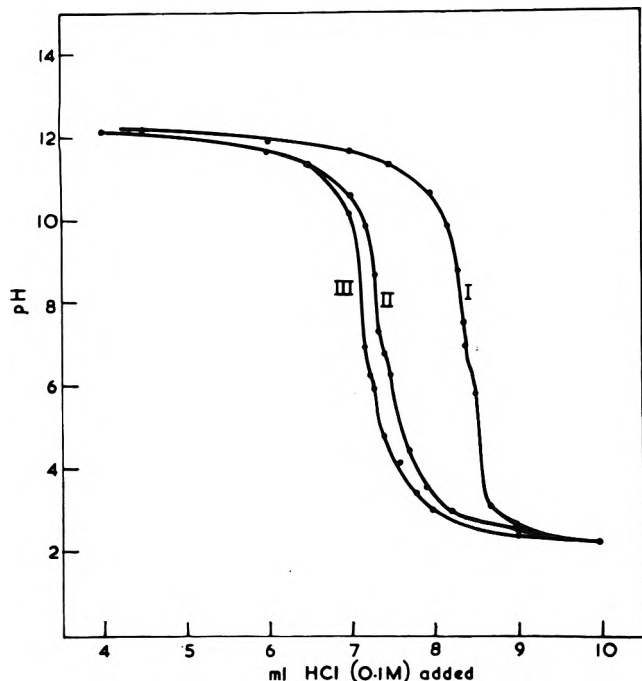


Figure 2. Change of pH during titration with HCl of 20 ml. of ca. 0.05 *M* NaOH (curve I), of 20 ml. of NaOH which had been stirred with 1 g. of MoS_2 (curve II), and of 20 ml. of NaOH to which 3.9×10^{-6} mole of H_2SO_4 and 2.55×10^{-6} mole of MoO_3 (resublimed) had been added.

(a) *Room Temperature to 800°*. The weight lost by MoS_2 (sample A) when it was heated up to 800° was found to depend on temperature, and a typical example is shown in Fig. 3. At any given temperature, constant weight was attained in less than 5 min., and at 350 and 800° , the temperature was held, after constant weight had been reached, for 5 and 3.5 hr., respectively, without further detectable weight loss. This behavior indicates the presence of sorbed species having a distribution of binding energies.²⁰ The weight loss up to 800° was 0.9%. When the product of heating at a temperature below 800° (sample B in Fig. 3) was cooled *in vacuo* and then reheated *in vacuo*, no further weight loss occurred below this temperature. On the other hand, if B was first heated for about 1 hr. between 200 and 250° in humid air, then an increase in weight of about 1% occurred, and subsequent thermogravimetric behavior *in vacuo* was virtually identical with that exhibited by sample A.

(b) *800 to 1000°*. If the MoS_2 was held at any given temperature between 800 and 1000° , a constant weight was not attained rapidly but there was a continuous loss of weight which, in its initial stages, was approximately proportional to time. The rate of weight loss was not reproducible, and later observations indicated that this was probably due to the distribution of the

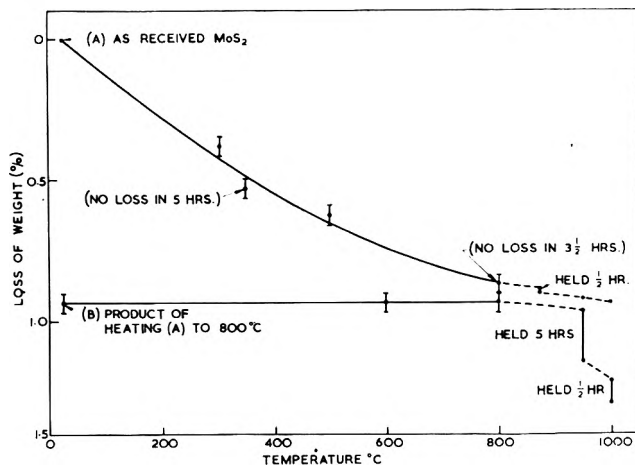


Figure 3. Weight loss of MoS_2 on heating under vacuum at a rate of $2^\circ \text{ min.}^{-1}$.

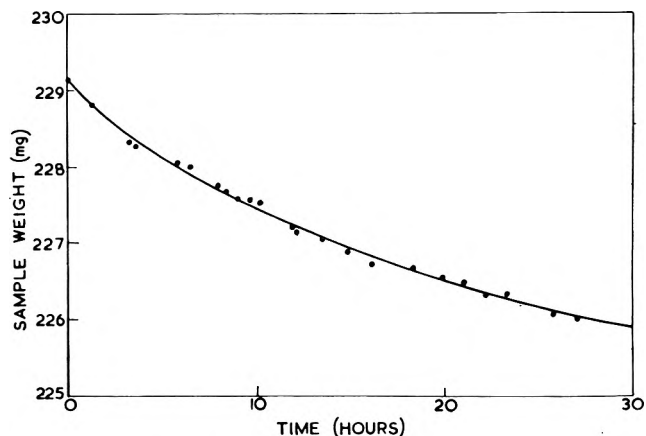


Figure 4. Weight loss of MoS_2 on heating *in vacuo* at 950° . The full line corresponds to a logarithmic decrement of 0.05 hr.^{-1} and an asymptote at 225 mg.

powder in the bucket which would affect the area of the powder exposed. An indication of the rates of weight loss is shown in Fig. 3, and it is plotted in detail for a specimen held at 950° in Fig. 4. It would appear that the loss would reach 2% in about 50 hr. By the choice of 225 mg. as the value of the asymptote in Fig. 4, the loss can be shown to be logarithmic with a time constant of 0.05 hr.^{-1} . When the sample which had been heated *in vacuo* at 950° for 30 hr. was cooled, a thin, friable, and sintered crust completely covered the surface of the powder. The MoS_2 beneath the surface was not sintered.

Water Adsorption. (a) *Water Adsorption on MoS_2 (as Received)*. The water adsorption isotherm at 30° for MoS_2 as received (sample A) is shown in Fig. 5.

(20) S. J. Gregg, "Chemisorption," W. E. Garner, Ed., Butterworth and Co., Ltd., London, 1957, pp. 68-75.

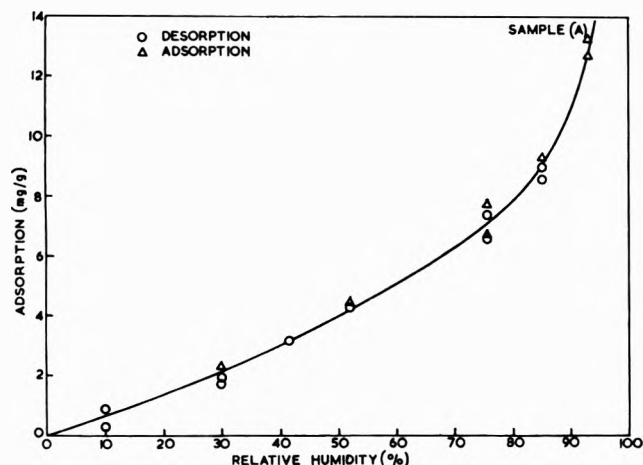


Figure 5. The adsorption and desorption of water vapor at 30° on MoS₂ sample A (as received).

The points on the curve represent series of adsorption and desorption measurements made on two separate samples. As all the points are satisfied by a single line, it can be concluded that the adsorption is completely reversible, and that, so far as adsorption measurements are concerned, the surface of sample A is quite stable. The isotherm is of type III of the Brunauer, *et al.*,²¹ classification and gives a good B.E.T. plot which would correspond to a surface area of 12 m.²/g.

Sample A, after having been in contact with air dried over P₂O₅, was later held under vacuum (5×10^{-6} torr) at room temperature for several hours. When dry air was readmitted subsequent to evacuation, the sample was the same weight. If there are water molecules present other than those which are reversibly adsorbed from humid air, then they are not readily removed.

(b) *Water Adsorption on MoS₂ Degassed at 350°.* When sample A was heated under vacuum at 350°, it lost 0.5% by weight. The powder so produced will be referred to as sample C, and its water adsorption isotherm is shown in Fig. 6. The lower half of the curve represents the first adsorption branch, while the upper half represents the first desorption branch. A large proportion of the water vapor taken up during the first adsorption is not desorbed when the relative humidity is reduced to zero. The second adsorption-desorption cycle taken up to 52% relative humidity followed the upper half of the curve, and, thus, the irreversibility of the first adsorption was absent from subsequent cycles. The 1.3 mg./g. of water adsorbed irreversibly could only be quantitatively desorbed by heating *in vacuo* at 10^{-5} torr between 350 and 370°; even at 250° 0.6 mg./g. of water remained adsorbed, and no weight loss was detected in 2 hr. Thus the conditions required for the removal of this chemisorbed water were similar to

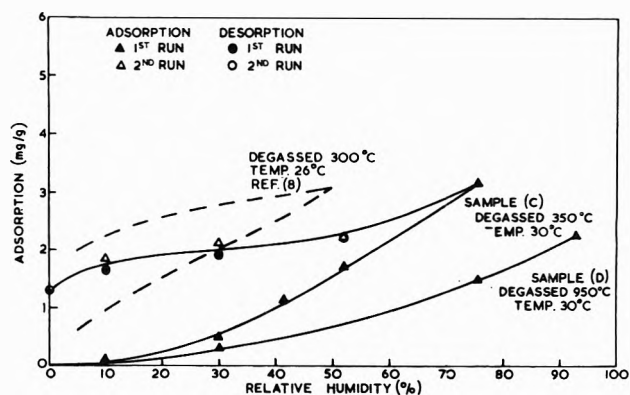


Figure 6. The adsorption and desorption of water vapor on MoS₂ heated to 350° *in vacuo* and the adsorption on MoS₂ heated to 950° *in vacuo*.

those employed in the preparation of the initial surface of C. In considering the isotherm for C, it may be noted that when the 1.3 mg./g. of irreversible water is taken as part of the weight of the adsorbent, the upper branch is of type II²¹ and provides a B.E.T. plot which would correspond to a surface area for this adsorption of 2 m.²/g.

Ballou and Ross⁹ determined the water adsorption isotherm *in vacuo* on a sample of MoS₂ powder which was considered to contain surface oxides and which they had degassed at 300° and 10^{-4} torr for 3 hr. This is shown as a broken line in Fig. 6 and is remarkably similar to the isotherm for sample C. However, these workers carried out only a single adsorption-desorption run and did not show measurements below a relative pressure of 0.05. They were, therefore, unable to distinguish between a reversible hysteresis loop and the irreversibility arising from true chemisorption.

(c) *Water Adsorption on MoS₂ Degassed at 950°.* Sample A was heated under vacuum at 950° for 5 hr. This caused a total weight loss of 1.3%, and the sample so produced will be referred to as D. Electron microscope examination showed no evidence of sintering. The water adsorption isotherm at 30° is shown in Fig. 6. Only adsorption measurements were carried out. Comparison with the isotherm obtained with sample C shows that at 75.5% relative humidity, sample D had adsorbed little more than 1.3 mg./g. of water, and, if desorption had been carried out from that point, then the slope of the desorption branch would have to be practically zero for the irreversibility to be the same (1.3 mg./g.) as for sample C. Thus, the irreversibility produced by degassing at 950° cannot be greater than that produced by degassing at 350° and is probably less.

(21) S. Brunauer, L. S. Deming, W. E. Deming, and E. Teller, *J. Am. Chem. Soc.*, **62**, 1723 (1940).

Discussion

The Nature of the Surface Contaminants. The MoS_2 in the "as received" condition has been shown by gravimetric analyses to contain 3.9×10^{-5} mole of sulfate ions and 2.55×10^{-5} mole of molybdenum(VI)/g. The total acidity was neutralized by $13 (\pm 2) \times 10^{-5}$ mole of NaOH /g., and, if this neutralization produced Na_2SO_4 and Na_2MoO_4 from H_2SO_4 and MoO_3 , respectively, then the total acidity value is in good agreement with the gravimetric analyses

$$\begin{aligned} 3.9 \times 10^{-5} \text{ mole of } \text{H}_2\text{SO}_4 &= && 7.8 \times 10^{-5} \text{ mole of NaOH} \\ 2.55 \times 10^{-5} \text{ mole of } \text{MoO}_3 &= && 5.1 \times 10^{-5} \text{ mole of NaOH} \\ \text{total} & && 12.9 \times 10^{-5} \end{aligned}$$

The titration of the synthetic mixture of sulfuric and molybdic acids was carried out to show that the presence of both acids was not inconsistent with a single point of inflection in the pH curve obtained for the MoS_2 slurry. If, as seems likely, molybdic acid is a weaker acid than sulfuric then this would account for the rounding of the tail of the pH curve.

Acidity of Soxhlet Extract. Assuming that all of the sulfate found by analysis is derived from H_2SO_4 , then the acidity due to this alone would give a pH of 2.3. The measured value thus appears to be too alkaline by 0.3 pH unit. However, it has been shown that 2.55×10^{-5} mole of molybdenum(VI)/g. of MoS_2 is also present, and the condensation of molybdate anions which may be expected in acid solution would use up hydroxonium ions and lead to a slightly higher pH.

In the past this "acidity of Soxhlet extract" has been considered to reflect the amount of surface oxide present in MoS_2 samples, and measurements have been published¹⁶ of acidities of a series of synthetic mixtures of MoS_2 and MoO_3 . However, if an approximately equivalent quantity of H_2SO_4 is present as a contaminant on the sulfide surface, its effect on pH would be much greater than that of MoO_3 . Therefore, acceptance tests based on pH measurements would have to be interpreted with caution.

Thermogravimetry. When the MoS_2 powder (as received) was heated under vacuum up to 800° , a weight loss of 0.9% occurred. On reheating the sample under vacuum through the same temperature range, a second weight loss similar to the first could be brought about only if, prior to the reheating, the sample had been subject to conditions favorable to surface oxidation (*i.e.*, heated at about 200° in humid air). This indicates that these weight losses are due to the volatilization of the products of surface oxidation, and the analytical

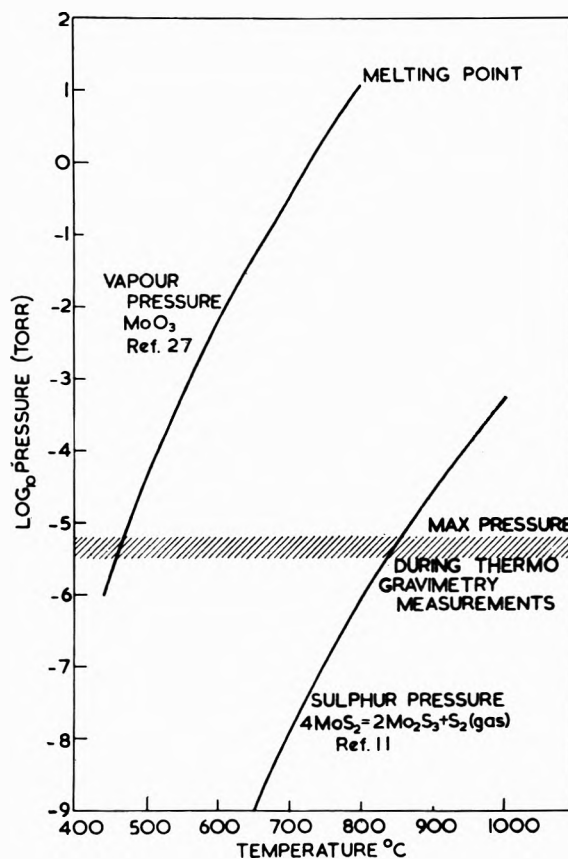


Figure 7. The vapor pressure of MoO_3 and the pressure of sulfur above MoS_2 as a function of temperature.

evidence suggests that these are molybdenum trioxide and sulfuric acid. Figure 7 shows that at about $450\text{--}500^\circ$ the vapor pressure of MoO_3 is greater than that maintained in the thermogravimetric apparatus (10^{-5} torr), and at 800° it reaches 10 torr. There seems, therefore, little doubt that MoO_3 would be driven off from the MoS_2 surface below 800° . Sulfuric acid and water form a mixture which has a constant boiling point of 338° under a pressure of 1 atm.,²² and, hence, it may be expected to be lost from the sulfide surface below this temperature at pressures of the order of 10^{-5} torr. Although the molybdenum trioxide and sulfuric acid determined gravimetrically amount to only 0.75 wt. %, as will be discussed under Adsorption, it seems that the discrepancy of 0.15 wt. % can be accounted for as chemisorbed water.

Figure 7 also shows the pressure of sulfur, essentially in the form of S_2 molecules, above a mixture of MoS_2 and Mo_2S_3 .¹¹ When the sulfur pressure is above the pres-

(22) H. Remy, "Treatise on Inorganic Chemistry," Vol. 1, Elsevier Publishing Co., London, 1956, p. 709.

sure maintained in the apparatus, *i.e.*, above 850° , the dissociation described in eq. 1 may be expected to proceed more rapidly, and, if the formation of Mo_2S_3 went to completion, a loss of weight of 20% is to be expected. In this work at 950° , the loss, initially proceeding at a constant rate, slowly became asymptotic at about 2%, and at this stage a sintered crust formed on the surface of the powder mass. Apparently, McCabe²³ has experienced a similar phenomenon with MoS_2 , and he considers that such sintering can prevent the escape of sulfur into the gas phase. Clearly, once the pressure of S_2 molecules in the interstices of the powder became sufficient, thermal dissociation would cease and there could be a limiting loss of weight considerably less than the equilibrium value. The 2% loss observed here probably represents the evolution of sulfur from only the uppermost layers of the powder mass. It seems not unreasonable that sintering accompanies thermal dissociation as eutectic formation between MoS_2 and Mo_2S_3 has been proposed.²⁴ The possibility that the 2% weight loss reported by Cannon,¹⁰ on heating MoS_2 under vacuum under similar conditions, is also due to thermal dissociation should be considered, and it may be noted that the formation of an impervious crust might explain why he could not detect sulfur in the gas phase at temperatures up to 1800° .

Adsorption. Surface areas of MoS_2 powder determined from nitrogen isotherms suffered no reduction after the powder had been degassed at 300° for 6 hr.,⁸ while other samples degassed at temperatures up to about 750° ²⁵ have similarly shown no evidence of sintering. Thus, in the present work, degassing at 350° should not have caused any loss of geometrical surface area, and the reduction in the reversible adsorption of water vapor must be attributed to removal of surface contaminants. The presence on the surface of a solid of ionic or hygroscopic contaminants can greatly enhance its physical adsorption of water vapor,²⁶ and the hydrophilic nature of sulfuric acid is well known.

Vapor pressure data²⁷ indicate that degassing at 350° could not have caused any appreciable volatilization of the molybdenum trioxide, and the 0.5% weight loss (see Fig. 3) must be due to evolution of the sulfuric acid and chemisorbed water. Indeed the 1.3 mg./g. (0.13 wt. %) of water sorbed irreversibly by sample C (Fig. 6) is just sufficient to make up the difference between the percentage loss at 350° and the amount of sulfuric acid found gravimetrically. When experimental error is considered, this irreversible water is probably sufficient to account for the discrepancy between the amounts of molybdenum trioxide and sulfuric acid and the weight loss up to 800° , also. This suggests that, during degassing at 350° , all of the original chemisorbed water

was driven off and that a similar quantity of water was "resorbed" when the degassed sample (C) was subsequently exposed to humid air.

Gregg²⁰ reported similar water adsorption behavior with certain hydrous oxides, and he postulated the existence of highly localized sites, each having a specific adsorption energy which remains unchanged for the repeated adsorption and desorption of successive water molecules. It is possible that localized adsorption sites on the MoS_2 surface may be provided by the contaminant molybdenum trioxide. The required distribution of binding energies, enabling water to be desorbed up to about 350° , might be satisfied by the formation of some hydrated forms of molybdic acid in which water molecules are held by more than one type of binding. Molybdenum trioxide is the end product of heating any form of molybdic acid, and this would comply with the concept of sites having adsorption energies which remain unchanged during repeated adsorption-desorption cycles.

Recently, Haltner²⁸ has shown that the coefficient of friction of MoS_2 remains low even after having been baked out under a pressure of 10^{-9} torr, thus showing that, unlike graphite, its good lubricating properties do not depend on adsorbed films. In fact, the presence of water vapor increases the coefficient of friction of MoS_2 films on steel.³⁻⁶ In the present work, experiments have shown how pretreatment of MoS_2 can alter the amount of adsorbed water, and there is, therefore, the possibility that MoS_2 could be prepared, which, for a time at least, would show a low coefficient of friction in a humid atmosphere.

Summary

This phenomenological study of surface contamination of molybdenum disulfide indicates that MoS_2 which has been exposed to damp air will contain, in addition to physically adsorbed water, sulfuric acid, molybdenum trioxide, and chemisorbed water as surface contaminants. The adsorption measurements indicate that physical adsorption of water is promoted by sulfuric acid contamination. The MoO_3 promotes chemisorption of water.

(23) C. L. McCabe, *Trans. A.I.M.E.*, **203**, 61 (1955).

(24) W. G. Scholtz, D. V. Doane, and G. A. Timmons, *ibid.*, **221**, 356 (1961).

(25) E. R. Braithwaite, *Research (London)*, **14**, 24 (1961).

(26) F. P. Bowden and W. R. Throssel, *Proc. Roy. Soc. (London)*, **A209**, 297 (1951).

(27) "Landolt-Bornstein Tables," Springer, Berlin, Vol. 2, Part 2a, 1960, pp. 45, 56.

(28) A. J. Haltner, *Wear*, **7**, 102 (1964).

Acknowledgment. We wish to thank H. C. Sleight Ltd. for support of this work by a grant which was

given as a contribution to investigations into Australian raw materials.

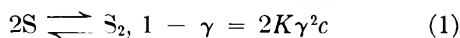
Dipole Association¹

by Claude Treiner,² James F. Skinner,³ and Raymond M. Fuoss

Contribution No. 1763 from the Sterling Chemistry Laboratory of Yale University, New Haven, Connecticut (Received July 2, 1964)

Dimerization of dipolar solutes in solvents of low dielectric constant is proposed, and a method of determining association constants (and dipole moments) from dielectric constants and densities is derived. In dioxane, *p*-nitroaniline, *m*-nitrophenol, and pyridinium dicyanomethylide were found to have association constants of 0.37, 0.8, and 3, respectively. The logarithms of these constants are linear in the square of the dipole moments (4.38, 6.91, and 9.2) as expected from theory.

When two polar molecules approach to contact in a nonpolar solvent, dimer formation due to dipole-dipole attraction might be expected, if their mutual potential energy u is sufficiently larger than kT to stabilize the dipole pair. For two point dipoles with moments of 5 D. at a distance of 5 Å. in a medium of dielectric constant 2.0, the ratio u/kT is about 5. Depending on the geometry of the molecule (oblate or prolate ellipsoid), the stable configurations would be with the dipole axes parallel or antiparallel. Interaction of this sort could be formally described by a mass action equation



where K is the association constant (l./mole), c is concentration, γ is the fraction of solute present as monomer, and activity coefficients of monomer and dimer are approximated by unity. In order of magnitude, K should be given by

$$K \approx 10^{-3}Na^3 \exp(-u/kT) \quad (2)$$

where N is Avogadro's number and a^3 is the volume occupied by a pair. The latter is of the order of one to several hundred cubic Ångströms, so we might expect to find dimerization constants of the order 0.1–1.0 for reasonably polar molecules in benzene or dioxane.

If dimers in the antiparallel position are formed, the volume polarization should increase less rapidly with increasing concentration than would be observed for no interaction between solute dipole molecules. Measurement of dielectric constants as a function of concentration should therefore show whether such interaction occurs.

The purpose of this paper is to present dielectric data for solutions of several polar solutes (*p*-nitroaniline, *m*-nitrophenol, and pyridinium dicyanomethylide) in dioxane, which show behavior which can be accounted for by the hypothesis of dimerization due to electrostatic attraction. A method of analyzing the data in order to obtain dimerization constants is presented, which simultaneously evaluates the dipole moment of the monomer.

Experimental

Materials. Matheson Coleman and Bell *p*-nitroaniline (PNA) was first recrystallized from water (1

(1) This work was partially supported by the Directorate of Chemical Sciences, Air Force Office of Scientific Research Grant No. AF-AFOSR-244-63.

(2) Du Pont Postdoctoral Research Fellow, 1963–1964; on leave of absence from the University of Paris.

(3) Sterling Research Fellow, 1963–1964.

g./100 ml.) and then from methanol (1 g./10 ml.); m.p. 146.6–146.8°. Eastman *m*-nitrophenol (MNP) was recrystallized from *n*-hexane; a hot solution of 2.1 g. in 800 ml. was filtered and evaporated to 600 ml. The needles which separated were dried overnight at 70° and 5 μ ; m.p. 114.4°. Pyridinium dicyanomethylide⁴ (PDM), C₅H₅N⁺·C⁻(CN)₂, was very kindly furnished by Dr. William J. Linn of E. I. du Pont de Nemours and Co. Matheson Coleman and Bell *p*-dioxane was used as received; density, 1.0280; specific conductance, 10⁻¹³ mho; dielectric constant, 2.233; n_D , 1.4209. Small variations in density and dielectric constant were noted; these were probably due to erratic moisture absorption. For calculating each run, the observed $c = 0$ properties of the solvent for that run were used.

Densities and refractive indices were linear in concentration over our working range: $\rho = \rho_0 + \beta c$; $n_D = n_{D0} + \beta'c$. For PNA in dioxane, $\beta = 0.0406$ based on densities 1.02796, 1.02872, and 1.02956 at $c = 0.0$, 0.01885, and 0.03867. For MNP, $\beta = 0.0348$, based on a density 1.03204 at $c = 0.1286$. For PDM, $\beta = 0.019$ from a density 1.02813 at $c = 0.00946$. For PNA, $\beta' = 0.034$ from n_D 1.4238 at $c = 0.0849$. For MNP and PDM, the $\beta'c$ term was neglected in our final calculations because it is absorbed in the total dielectric constant in the final analysis of the data.

Apparatus and Method. Capacities of solutions in dioxane were measured in a guarded cell with platinum electrodes of design similar to that described by Mead and Fuoss⁵; the air capacity was 12.64 pf. The cell was sealed to a glass-capped erlenmeyer flask so that a series of dilutions could be made on one sample of solute. Measurements were made at 400 v. and 500 cycles on the guarded Schering bridge.⁶ Indices of refraction were measured with a Spencer Abbé-type refractometer, using a sodium lamp. All measurements were made at $25 \pm 0.01^\circ$. The dielectric data are summarized in Table I, where c is concentration as moles/l.

Discussion

In dilute solutions in solvents of low dielectric constant, the volume polarization may be approximated by the Debye–Clausius–Mosotti equation

$$(\epsilon - 1)/(\epsilon + 2) = (4\pi/3)\Sigma_i n_i \alpha_i \quad (3)$$

where ϵ is dielectric constant, n_i is the number of molecules of species i per unit volume, and α_i is their polarization. The latter is given by

$$\alpha_i = \alpha_{i0} + \mu_i^2/3kT \quad (4)$$

where α_{i0} is the electronic polarization and μ_i is the dipole moment. Subscripts are defined as: s for solvent,

Table I: Dielectric Constants of Solutions

c	ϵ	c	ϵ
PNA		MNP	
0.00000	2.233	0.00000	2.237
0.02492	2.379	0.01935	2.271
0.03838	2.456	0.03017	2.290
0.05348	2.545	0.04589	2.317
0.07273	2.660	0.1142	2.436
0.00000	2.232	0.1512	2.501
0.01999	2.349	PDM	
0.03021	2.405	0.000000	2.233
0.04128	2.471	0.003635	2.271
0.06239	2.595	0.005133	2.288
0.1088	2.870	0.006935	2.306
0.1626	3.203	0.009456	2.333
		0.004706	2.283
		0.005552	2.292
		0.006869	2.305

1 for monomer, and 2 for dimer. For a solute which dimerizes, (3) then becomes

$$(\epsilon - 1)/(\epsilon + 2) = 4\pi n_s \alpha_s / 3 + (4\pi N / 3000)(c_1 \alpha_1 + c_2 \alpha_2) \quad (5)$$

where

$$c_1 = \gamma c = 1000 n_1 / N \quad (6)$$

and

$$c_2 = (1 - \gamma)c/2 = 1000 n_2 / N \quad (7)$$

are concentrations (moles/l.) of monomer and dimer, respectively, and c is the stoichiometric concentration of the polar solute. The problem then is, given dielectric constants and densities at a series of concentrations, to find the association constant K and the dipole moment μ_1 . We shall show that (5) can be transformed into a function of concentration and dielectric constant such that a linear plot results, with μ_1 determined by the intercept at zero concentration and K by the slope of the line. The transformation essentially amounts to eliminating the properties of the solvent from (3), so that the properties of the solute can be seen directly.

The number n_s of solvent molecules per unit volume is

$$n_s = (N/M_s)(\rho - cM/1000) \quad (8)$$

(4) W. J. Linn, O. W. Webster, and R. M. Benson, *J. Am. Chem. Soc.*, **85**, 2032 (1963).

(5) D. J. Mead and R. M. Fuoss, *ibid.*, **61**, 2047 (1939).

(6) D. Edelson, W. N. Maclay, and R. M. Fuoss, *J. Chem. Educ.*, **27**, 644 (1950).

where M_s and M are molecular weights of solvent and solute. In the pure solvent

$$n_s^0 = N\rho_s/M_s \quad (9)$$

Up to moderate concentrations

$$\rho = \rho_s + \beta c \quad (10)$$

At zero concentration from (3) and (9)

$$(\epsilon_s - 1)/(\epsilon_s + 2) = (4\pi\alpha_s/3)(\rho_s N/M_s) \quad (11)$$

Now subtract (11) from (5) and substitute (10) for the density; after rearrangement, the result is

$$\begin{aligned} (\epsilon - \epsilon_s)/(\epsilon + 2) = \\ (\epsilon_s - 1)(\beta - M/1000)c/3\rho_s + \\ 4\pi N(\epsilon_s + 2)\Sigma_i c_i \alpha_i / 9000 \quad (12) \end{aligned}$$

Define a function $F(\epsilon)$ of the observed dielectric constants (and concentrations) as

$$F(\epsilon) = [9000/4\pi N(\epsilon_s + 2)]\{(\epsilon - \epsilon_s)/(\epsilon + 2) - [(\epsilon_s - 1)(\beta - M/1000)c/3\rho_s]\} = \quad (13a)$$

$$[1.1890 \times 10^{-21}/(\epsilon_s + 2)]\{f_1(\epsilon, \epsilon_s) - f_2(\epsilon_s, \beta, M, \rho_s)c\} \quad (13b)$$

This function summarizes the data in a way which reduces determination of the constants μ_1 and K to a simple linear plot, because also

$$F(\epsilon) = c_1\alpha_1 + c_2\alpha_2 \quad (14)$$

Substituting for c_1 and c_2 from (6) and (7), and rearranging

$$F(\epsilon)/c - \alpha_2/2 = \gamma(\alpha_1 - \alpha_2/2) \quad (15)$$

Define the quantity on the left side of (15) as $G(\epsilon)$ and define a constant A by

$$1/\epsilon = \alpha_1 - \alpha_2/2 \quad (16)$$

so that

$$\gamma = AG \quad (17)$$

Using the mass action eq. 1, we finally obtain the extrapolation function

$$1/G = A + 2KA^2cG \quad (18)$$

A plot of the reciprocal of G against cG should be linear; the intercept at zero concentration evaluates the polarization difference (16), and this quantity and the slope, in turn, give the association constant K .

For molecules which dimerize antiparallel, μ_2 is zero, so α_2 reduces to α_{20} , the electronic polarization of the dimer, which can simply be set equal to $2\alpha_{10}$. Then

$$G(c) = F(\epsilon)/c - \alpha_{10} \quad (19)$$

and

$$\mu^2 = 3kT/A \quad (20)$$

because from (17)

$$G(0) = 1/A = \alpha_1 - \alpha_{10} \quad (21)$$

From the data of Table I and the values of β , the function (19) was calculated for the three polar compounds. The corresponding plots are shown in Fig. 1. (Note that the scales are different for the three compounds.) For *p*-nitroaniline and *m*-nitrophenol, excellent straight lines are obtained. Due to the low solubility in dioxane, the maximum $\Delta\epsilon$ obtainable for the ylide was only 0.072; the points therefore scatter somewhat, but an average line can be drawn. A typical calculation, to show the magnitude of the various terms, is given for *p*-nitroaniline in Table II, and the derived constants are summarized in Table III. The electronic polarizations were estimated as follows: for MNP, the molar refraction was estimated as that of nitrobenzene plus phenol minus benzene; for PNA,

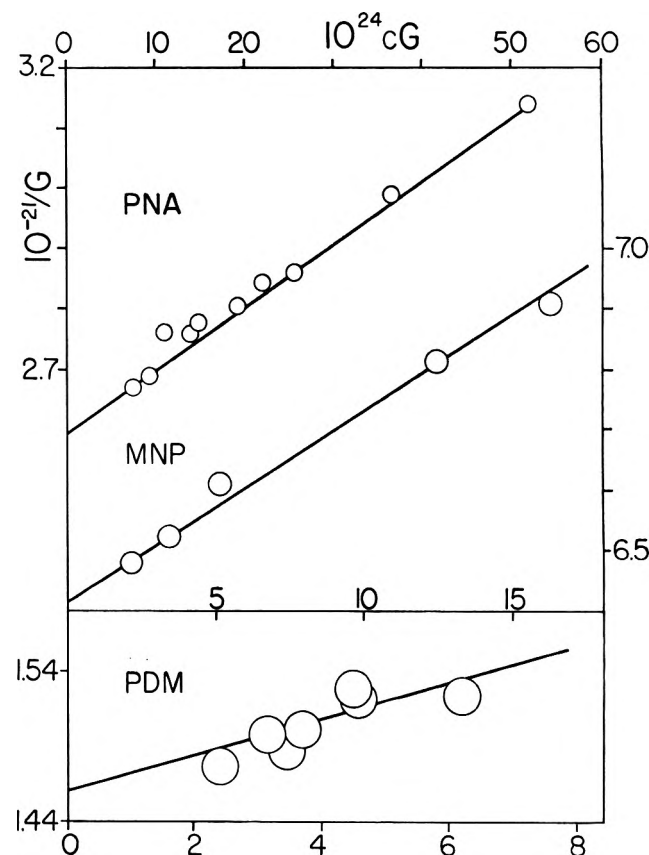


Figure 1. Extrapolation function (18); PNA, cG scale at top, G^{-1} scale at upper left; MNP, cG scale under MNP line, G^{-1} scale at right center; PDM, cG scale at bottom, G^{-1} scale at lower left.

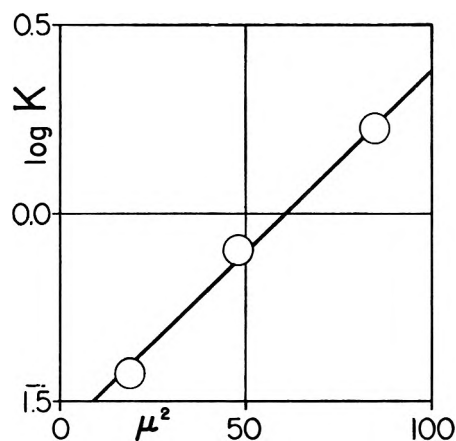


Figure 2. Dependence of association constants on dipole moments.

nitrobenzene plus aniline minus benzene; and for PDM, pyridine plus malononitrile. Included in Table III are also the values of the moments obtained by Halverstadt's⁷ and by Guggenheim's⁸ methods. The values of μ_1 by the different methods agree with each other, and, for *p*-nitroaniline, also with the literature value.⁹ For *m*-nitrophenol, the moment in benzene is given⁹ as 3.90; moments in dioxane usually are somewhat higher than moments found in benzene.

The dimerization constants are of the expected order of magnitude. Furthermore, as shown in Fig. 2, a plot of $\log K$ against the square of the moments is ap-

Table II: Calculations for *p*-Nitroaniline

c	f_1	f_2	$10^{24}F(\epsilon)$	$10^{-21}/G(\epsilon)$
0.0200	0.0269	0.0008	7.78	2.67
0.0302	0.0393	0.0012	11.37	2.77
0.0413	0.0535	0.0016	15.47	2.78
0.0624	0.0790	0.0025	22.89	2.84
0.1088	0.1310	0.0043	38.00	2.99
0.1626	0.1866	0.0064	54.21	3.14

Table III: Derived Constants

Compound	$10^{24}\alpha_1$	$10^{24}\alpha_0$	μ_1^7	μ_1^8	μ_1	K
MNP	169	14	4.38	4.40	4.38	0.37
PNA	401	15	6.87	6.91	6.91	0.8
PDM	701	16	9.4	9.3	9.2	3

proximately linear, as would be expected from eq. 2, because the potential energy u varies as μ^2/a^3 , and the three molecules are all about the same size, and from their geometry they would be expected to form anti-parallel dimers.

(7) I. F. Halverstadt and W. D. Kumler, *J. Am. Chem. Soc.*, **64**, 2988 (1942).

(8) E. A. Guggenheim, *Trans. Faraday Soc.*, **47**, 573 (1951).

(9) L. G. Wesson, "Tables of Electric Dipole Moments," Massachusetts Institute of Technology, 1947.

Classical Model for Free Radical Formation

by H. Shin

Department of Chemistry, Cornell University, Ithaca, New York (Received July 13, 1964)

By use of an idealized model, the probability of radical formation for a reaction of the type $\text{RH} + \text{H} \rightarrow \text{R}\cdot + \text{H}_2$ is formulated classically. The average probability of the radical formation is $\langle P(V_0/kT) \rangle = (V_0/kT)^{1/2} \exp(-V_0/kT) + (1/2) \operatorname{erfc}(V_0/kT)$, where V_0 is the potential barrier and $\operatorname{erfc}(V_0/kT)$ is 1 minus the error function. A simple numerical computation shows that the formation is very effective when $V_0/kT = 0-0.5$.

Introduction

Some years ago, Widom¹ developed a model of the string oscillator to describe the relaxation of collisionally excited particles. In a recent article, Rubin² obtained some valuable results for the isotope effects in energy transfer and particle exchange reactions by applying the method of images which was originally formulated by Jepsen and Hirschfelder.³ When the masses of the colliding particles are identical, as in the case of Widom's work, the collisional process can be completely analyzed. Such a case can be exemplified by the collision of a hydrogen atom which is attached to a massive molecule by an incident hydrogen atom, *e.g.*, a reaction of the type $\text{RH} + \text{H} \rightarrow \text{R}\cdot + \text{H}_2$. Once the probability of momentum exchange or of energy transfer is calculated, the average probability of the radical R· formation can be evaluated. This problem is considered in this paper.

In the present paper we assume a model of a collinear collision between RH and H on an idealized potential energy surface. For the calculation of the probability of momentum exchange per collision, we treat the relative motion of the colliding atoms classically in terms of a rectilinear motion of the configuration point in the region of a constant potential.

Model and Method

If the H atom of RH, which we denote by $\text{H}_{(1)}$, is hit along its line of motion by the incident H atom, $\text{H}_{(2)}$, in which the interaction is impulsive, the system will involve either one impact or two impacts, depending on the law of force of the oscillator RH as well as its phase at the beginning of the collision. In the former case there is complete exchange of momentum, while in the latter case there is no net momentum change.

Since the mass of R is, in general, much greater than that of H, we assume that during the collisional process the position of R is practically unchanged so that only $\text{H}_{(1)}$ moves back and forth between $x = 0$ and l as shown in Fig. 1. There are assumed to be three regions in which the potential energy is constant

$$\begin{aligned} V &= \infty & x < 0 \\ V &= V_0 & 0 < x < l \\ V &= 0 & x > l \end{aligned}$$

Therefore, the dissociation of RH to form the R· radical requires the crossing of the potential energy barrier V_0 .

Either when $\text{H}_{(1)}$ reaches the left extreme position $x = 0$ or when $\text{H}_{(1)}$ is hit by $\text{H}_{(2)}$, the interaction is infinitely repulsive. Hence, the motion of $\text{H}_{(1)}$ and $\text{H}_{(2)}$ can be expressed in a potential surface of the region $\triangle OPl$ shown in Fig. 2.

Because the potential energy in $0 < x < l$ is constant, the relative motion of $\text{H}_{(1)}$ and $\text{H}_{(2)}$ is characterized by rectilinear motion of the configuration point in $\triangle OPl$. The impact between $\text{H}_{(1)}$ and $\text{H}_{(2)}$ is equivalent to the crossing of the configuration point through *line* \overline{OP} . On the other hand, when $\text{H}_{(1)}$ reaches $x = 0$, it can be equivalently expressed by the crossing of the configuration point through *line* \overline{Ol} .

To discuss the collision process effectively, we introduce a method of the generation of images in which the rectilinear motion of a configuration point can be extended. This is similar to the method of Jepsen and Hirschfelder³ and to a more recent study by Rubin.²

(1) B. Widom, *J. Chem. Phys.*, **28**, 918 (1958).

(2) R. J. Rubin, *ibid.*, **40**, 1069 (1964).

(3) D. W. Jepsen and J. O. Hirschfelder, *ibid.*, **30**, 1032 (1959).

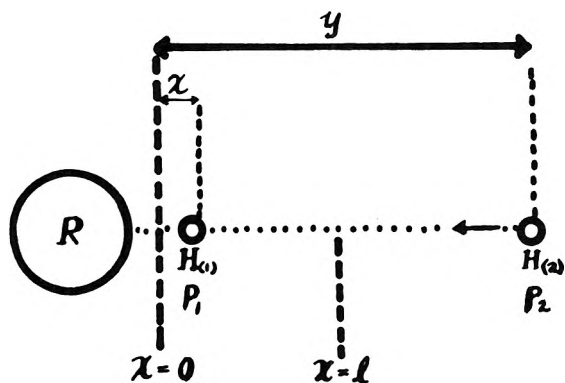


Figure 1. Collision coordinates.

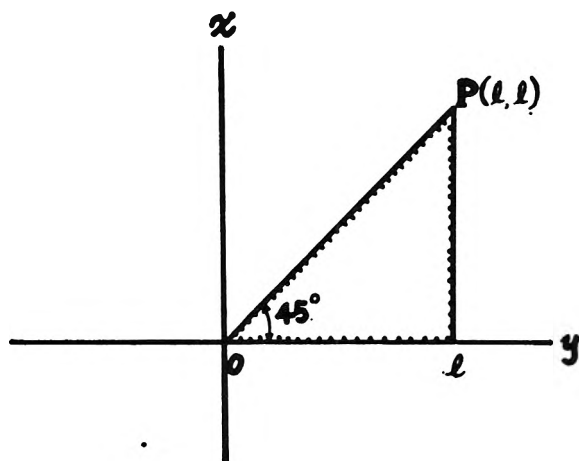


Figure 2. The potential energy surface in the x,y -coordinate system. All collisions take place in the triangular region ΔOPl .

However, for the present case it is more convenient to use the potential energy surface of Fig. 2 than use a new coordinate system as the above investigators have done. When the masses of the colliding particles are not identical, we can still use the 45° diagram as Fig. 2, but a configuration point now proceeds with a different angle when it hits an impact line. This refraction is a function of the mass ratio.

As shown in Fig. 3, ΔOPl and its images produce a pattern of eightfold symmetry filling the plane of 360° . The configuration point which originally started from $\bar{l}P$ moves in the plane $\square PP_1P_2P_3$ rectilinearly, and it may cross the impact line PP_2 , P_1P_3 , or the reflection line $\bar{l}l_2$, $\bar{l}l_3$. When we take PP_2 as an image axis ΔOPl_1 is the first image generated. Next, for the image axis P_1P_3 , the two images ΔOP_2l_2 and ΔOP_2l_3 result. Then, reflection through $\bar{l}l_2$ or $\bar{l}l_3$ produces four additional image regions to complete the eightfold symmetry.

Obviously, at the moment of impact $H_{(1)}$ is moving either right or left while H_2 is always moving left. In

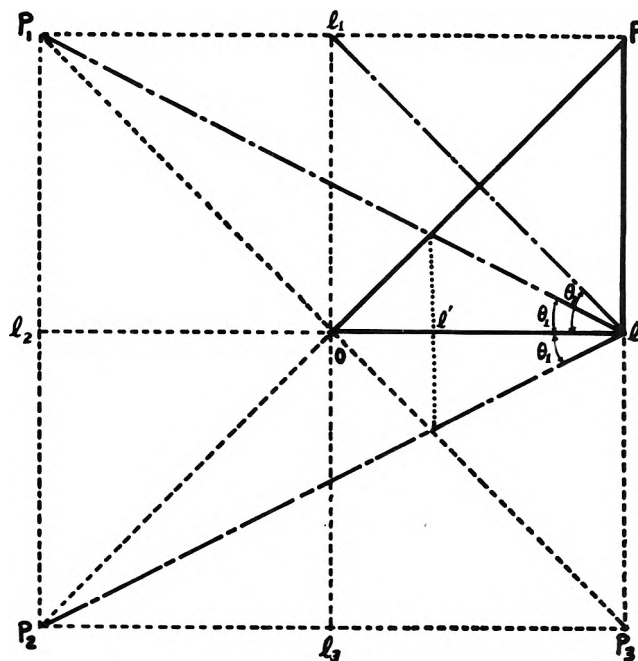


Figure 3. Motion of the configuration points representing $RH + H \rightarrow R + H_2$.

Fig. 3, the case of $H_{(1)}$ -right and $H_{(2)}$ -left is represented by an upward configuration point starting from $\bar{l}P$, while the case of $H_{(1)}$ -left and $H_{(2)}$ -left is shown by a downward configuration point. In the former case, the configuration point always crosses the impact line first, while in the latter case, the configuration point always crosses the reflection line first, if $\theta > 45^\circ$.

We first consider a configuration point which starts at l with an upward motion. From Fig. 3, it is then seen that all configuration points which proceed with angles greater than θ_1 always cross only one impact line \overline{OP} . In this case we have three possibilities.

(1) If $\theta_1 < \theta < \theta_2$, the configuration point also crosses a reflection line $\overline{Ol'}$. This is the case that after an impact both $H_{(1)}$ and $H_{(2)}$ reverse their direction, in which $H_{(1)}$ is now moving with the momentum of $H_{(2)}$, p_2 . Since p_2 is not sufficiently greater than p_1 , $H_{(2)}$ moves out from the interaction region $\langle Ol \rangle$ before $H_{(1)}$ hits again. Hence, $H_{(2)}$ continues its oscillatory motion in $\langle Ol \rangle$ with p_2 , and there is a net energy change $|p_2^2 - p_1^2|/2m$, where m is the mass of the hydrogen atom.

(2) If $\theta_2 < \theta < \pi/2$, after the impact $H_{(2)}$ moves out from $\langle Ol \rangle$ before $H_{(1)}$ reaches $x = 0$. Therefore, the situation is the same as above.

(3) We now consider an upward motion of the configuration point with $0 < \theta < \theta_1$. After the first impact $H_{(1)}$ with P_2 reaches $x = 0$, catches up with $H_{(2)}$, and causes it to suffer another impact. Therefore, there is no momentum interchange. However, a configuration

point can start from anywhere between P and l in Fig. 3. Thus a motion with ℓ less than θ_1 can also result in a one-impact collision.

In the upward motion these three cases account for all possible impact processes. From the kinematics shown in Fig. 3, it can be readily seen that $\theta = p_1/p_2$. Furthermore $\theta = \langle Ol \rangle / \langle l' l \rangle = 1/2$. Therefore, when $p_2 < 2p_1$, the momenta of the two hydrogen atoms are always interchanged. On the other hand, if $p_2 > 2p_1$, there is a small probability of the interchange and the probability is a function of the momentum ratio and the phase of $H_{(1)}$. It is worthwhile to point out two extreme cases, *i.e.*, when $\theta = 0$ and 90° . In the former case $p_2 \gg p_1$, and, irrespective of the position of $H_{(1)}$, $H_{(2)}$ always hits $H_{(1)}$ twice. However, in the latter case the configuration point moves parallel to $l\bar{P}$. In this case $p_1 \gg p_2$, and the collision system always involves one impact.

When $H_{(1)}$ is moving left at the moment of impact, the configuration point in Fig. 3 moves downward. In this case there are two possibilities.

(1) If $\theta > 45^\circ$, the configuration point always crosses only one impact line, \overline{OP}_3 . This corresponds to $p_1 > p_2$ and the momenta are interchanged. When $45^\circ > \theta > \theta_1$, the configuration point sometimes crosses only one impact line \overline{OP}_3 depending on the initial phase of $H_{(1)}$. This case corresponds to $p_2 > p_1 > p_2/2$.

(2) If $\theta_1 > \theta > 0^\circ$, the configuration point crosses two impact lines, \overline{OP}_3 and \overline{OP}_2 or \overline{OP} and \overline{OP}_1 . Therefore, $H_{(1)}$ always suffers two impacts when $p_2/2 > p_1 > 0$.

Probability of Radical Formation

We now sum the ranges of the initial position of $H_{(1)}$ when $H_{(2)}$ reaches $x = l$, which result in a one-impact collision. For the right motion of $H_{(1)}$ at the moment of impact, if $p_1 > p_2/2$, the system involves only one impact irrespective of the position in $\langle Ol \rangle$. However, if $p_1 < p_2/2$, only $H_{(1)}$ which is in the range $2\langle Ol \rangle p_1/p_2$ suffers one impact. For the left motion of $H_{(1)}$, on the other hand, if $p_1 > p_2$, $H_{(1)}$ suffers only one impact regardless of its initial position in $\langle Ol \rangle$. If $p_2 > p_1 > p_2/2$, only $H_{(1)}$ in the range $2\langle Ol \rangle p_1/p_2 - \langle Ol \rangle$ suffers one impact.

Another important aspect of breaking the R-H bond is that p_2 must be greater than p_1 . Therefore, the necessary conditions for the breaking are that $H_{(1)}$ and $H_{(2)}$ must collide only once and $p_1 > p_2$. Then the ratio of the range in which these conditions are satisfied to $\langle Ol \rangle$ is the probability that $H_{(1)}$ will undergo the change in state $p_1 \rightarrow p_2$ with a net energy change $|p_2^2 - p_1^2|/2m$ upon the collision. From these arguments, we can write the probability by

$$P(p_1, p_2) = \frac{2\langle Ol \rangle \frac{p_1}{p_2} - \langle Ol \rangle + \langle Ol \rangle}{2\langle Ol \rangle} = \frac{p_1}{p_2}; \quad p_2 > p_1 > \frac{p_2}{2} \quad (1)$$

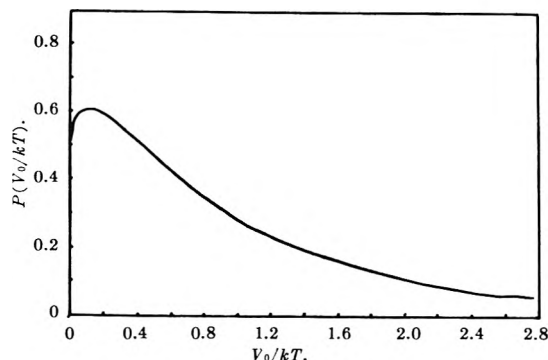


Figure 4. Plots of the average probability as a function of V_0/kT .

When $p_2 > \sqrt{2mV_0}$, $H_{(1)}$ dissociates from the molecule. Thus $P(p_1, p_2)$, in which $p_2 > \sqrt{2mV_0}$, is the probability that the radical R· is formed by a collinear collision with an incident hydrogen atom. Assuming that RH and H are in thermal equilibrium, we calculate the temperature average of the probability for the radical formation

$$\langle P(V_0/kT) \rangle = \frac{\int_0^\infty e^{-\frac{p_1^2}{2mkT}} dp_1 \int_{\sqrt{2mV_0}}^\infty p_2^3 P(p_1, p_2) e^{-\frac{p_2^2}{2mkT}} dp_2}{\int_0^\infty e^{-\frac{p_1^2}{2mkT}} dp_1 \int_0^\infty p_2^3 e^{-\frac{p_2^2}{2mkT}} dp_2} \quad (2)$$

where the p_1 integral is proportional to the probability that the velocity of $H_{(1)}$ is p_1/m and the p_2 integral is proportional to the number of collisions per unit time suffered by each $H_{(1)}$. The evaluation of eq. 2 yields

$$\langle P(V_0/kT) \rangle = \sqrt{\frac{V_0}{\pi kT}} e^{-V_0/kT} + 1/2 \operatorname{erfc}(V_0/kT) \quad (3)$$

where

$$\operatorname{erfc}(V_0/kT) = \frac{2}{\sqrt{\pi}} \int_{\sqrt{V_0/kT}}^\infty e^{-x^2} dx \rightarrow \begin{cases} 1 - \frac{2}{\sqrt{\pi}} \sqrt{\frac{V_0}{kT}}, \frac{V_0}{kT} \rightarrow 0 \\ \sqrt{\frac{kT}{V_0\pi}} \left[1 - 1/2 \left(\frac{kT}{V_0} \right) \right] e^{-(V_0/kT)}, \frac{V_0}{kT} \rightarrow \infty \end{cases}$$

The result of the average probability calculation is shown in Fig. 4 as a function of V_0/kT . The maximum of $\langle P(V_0/kT) \rangle$ occurs at the solution of

$$V_0/kT + \sqrt{V_0/kT} - 0.5 = 0$$

which is $V_0/kT \simeq 0.14$. For $kT \gg V_0$ the one-impact collision is a rare event, but the collision almost always results in the dissociation of the R-H bond. The most effective case of the dissociation is when $H_{(1)}$ barely missed two impacts with $p_1 < p_2$, *i.e.*, near the upper limit for the one-impact process. The average probability is proportional to the classical rate constant, and the effective formation of the radical $R\cdot$ comes from the

V_0/kT values between 0 and 0.5. For the potential barrier larger than kT , $\langle P(V_0/kT) \rangle \simeq (V_0/kT)^{1/2} \exp(-V_0/kT)$. For example, if $V_0/kT = 4.0$ and 6.0, $\langle P(V_0/kT) \rangle = 0.020$ and 0.003, respectively.

The model studied in the present paper is admittedly simplified, but it is hoped that the results which are obtained by a very simple scheme will still be helpful in calculating the radical formation in the thermal systems of hydrocarbon and hydrogen atom.

Acknowledgment. The author thanks M. P. Hanson for reading the manuscript and for making several helpful suggestions.

Dynamic Mechanical Properties of Cross-Linked Rubbers. I.

Effects of Cross-Link Spacing in Natural Rubber¹

by John D. Ferry, Ralph G. Mancke, Etsuji Maekawa,
Yasuji Ōyanagi, and Ray A. Dickie

Department of Chemistry, University of Wisconsin, Madison, Wisconsin (Received August 3, 1964)

The complex shear compliances of five samples of natural rubber cross linked by dicumyl peroxide and three samples cross linked by sulfur, covering a broad range of average cross-link spacing, have been measured over a frequency range of 0.1 to 1000 c.p.s. and a temperature range from -18 to 55° . The data were all reduced to 25° by shift factors calculated from an equation of the WLF type. In the transition zone of frequencies, the viscoelastic functions were closely similar; the loss tangents of the dicumyl peroxide vulcanizates were identical within experimental error, and those of the sulfur vulcanizates were shifted somewhat to the left on the logarithmic frequency scale with increasing degree of vulcanization. In the rubbery zone, the losses persisted to much lower frequencies than could be expected from configurational rearrangements within individual strands on the basis of current molecular theories, reflecting slow relaxation mechanisms whose presence has also been deduced from other measurements. The magnitude of the loss tangent at a given frequency in this zone (e.g., 1.6 c.p.s.) increases substantially with the average spacing between cross links in both dicumyl peroxide and sulfur vulcanizates. The possible role of trapped coupling entanglements as a source of the slow relaxation mechanisms is discussed.

Introduction

Measurements of dynamic viscoelastic properties of cross-linked rubbers,²⁻⁴ as well as of stress relaxation,^{5,6} have revealed slow relaxation mechanisms with relaxation times much too long to attribute to configurational rearrangements within individual network strands on the basis of current molecular theories. A satisfactory explanation of these mechanisms has not been achieved. In dynamic measurements, they are manifested by mechanical losses which persist to very low frequencies.

In an earlier study,⁴ we noted differences between natural rubber vulcanizates cross linked by sulfur and by other agents such as dicumyl peroxide or γ -radiation and inferred that the chemical nature of the cross link was important in determining the low-frequency losses. However, the spacing between cross links varied somewhat in that series of vulcanizates. We have now studied two series of samples, cross linked by dicumyl peroxide and by sulfur, respectively, with different

cross-link spacings. The average molecular weight of the network strands is found to have an important influence on the low-frequency losses.

Experimental

Materials. The cross-linked rubbers were generously prepared for us in the laboratory of Dr. P. Thirion, Institut Français du Caoutchouc, Paris; identical preparations have been used in some of his stress relaxation studies.^{7,8} The dicumyl peroxide vulcanizates,

(1) Part XLVII of a series on mechanical properties of substances of high molecular weight.

(2) W. Philippoff, *J. Appl. Phys.*, **24**, 685 (1953).

(3) A. R. Payne in "Rheology of Elastomers," P. Mason and N. Wookey, Ed., Pergamon Press Ltd., London, 1958, p. 86.

(4) R. A. Stratton and J. D. Ferry, *J. Phys. Chem.*, **67**, 2781 (1963); *Rev. gen. caoutchouc*, **41**, 635 (1964).

(5) P. Thirion and R. Chasset, Proceedings of the Fourth Rubber Technology Conference, London, 1962, p. 338.

(6) A. N. Gent, *J. Appl. Polymer Sci.*, **6**, 433 (1962).

(7) P. Thirion, "Proceedings of the Fourth International Congress on Rheology," Interscience Publishers, New York, N. Y., in press.

Series 98, all contained three parts of dicumyl peroxide (DCP) per 100 parts of smoked sheet rubber with a very low content of inorganic impurities. They were vulcanized for different times at 135° as shown in Table I. The molecular weight between cross links, M_c , was determined by Thirion and Chasset from swelling measurements in benzene, using a value of 0.444 for the thermodynamic parameter μ ; the latter was obtained, in turn, from the swelling of samples whose M_c had been calculated from tensile stress-elongation measurements on two samples in a highly swollen state. The sulfur vulcanizates, Series 74, had the same composition as that numbered 74 in ref. 4: 5 parts of ZnO, 1 part of phenylcyclohexyl-*p*-phenylenediamine, 1 part of stearic acid, 3.25 parts of sulfur, and 1.25 parts of diphenylguanidine per 100 parts of smoked sheet rubber. They were vulcanized for different times at 140° as shown in Table I. The value of M_c is available only for sample 60 which has already been described in ref. 4.

The equilibrium shear compliances, J_e , were measured in the torsion pendulum as previously described⁴ with a maximum shear strain of about 0.007 and are also given in Table I. In view of the slow relaxation processes described by Thirion,^{7,8} these may be too low by several per cent, even though the samples were equilibrated under stress for several hours; for the samples identified as F and G, the error is probably

obtained by an empirical analysis of the relaxation function^{7,8} which amounts to extrapolation to infinite time.

In the DCP series, M_c varies over a factor of 3.7, but the range of J_e is somewhat smaller; this difference is associated with well-known deviations from the simple theory of rubber-like elasticity, as a result of which J_e and M_c are not directly proportional. However, J_e is an indirect measure of the spacing between cross links, and in the sulfur series it is the only measure available.

Methods. As in previous studies,⁴ the Fitzgerald transducer was used for measurements of the storage (J') and loss (J'') components of the dynamic shear compliance in the range from 30 to 1000 c.p.s., and the Plazek torsion pendulum in the range from 0.1 to 1.3 c.p.s. The logarithmic decrement was determined from the recorder tracings of the torsion pendulum by a method of direct matching to exponential envelopes which will be described elsewhere. The maximum temperature range was from -18 to 55°. The more highly cross-linked samples could be taken to lower temperatures without encountering crystallization; any data showing the symptoms of crystallization (drop in magnitude of J' and J'' , failure to superpose with reduced variables at different temperatures) were rejected. The disk-shaped samples were 1.75 cm. in diameter; the thickness was about 0.13 cm. for the transducer measurements and 0.64 cm. for the torsion pendulum.

Since the question had been raised in discussion with other investigators as to whether friction effects at the interface between sample and either the top or bottom plate of the torsion pendulum could influence the observed damping, a series of measurements was undertaken on several samples of the same rubber with different thicknesses. The rubber was a sulfur vulcanizate denoted as 77 in ref. 4, which had been stored at -5° since the measurements by Stratton 3 years previously. A single disk, 0.218 cm. thick, was used, and combinations of two and three such disks layered on each other, as well as a combination of one such disk with a thinner one to give a total thickness of 0.297 cm., were also taken. A very slight tackiness provided satisfactory adherence of the disks to each other and to the upper and lower torsion pendulum plates. The disks were compressed *in situ* about 2.4% in every case. Measurements taken at 15, 25, and 35°, reduced to 25° by the method of reduced variables as described below, agreed very closely with each other,

Table I: Characteristics of Cross-Linked Rubbers

Agent	Sample code ^a	Vulcanization time, min.	$M_c \times 10^{-3}$	Log J_e from direct shear measurements, cm. ² /dyne	Log J_e from equilibrium extension, ^b cm. ² /dyne
DCP (98)	F	20	20.0	-6.36	-6.29
	G	30	14.8	-6.42	-6.41
	H	40	11.4	-6.40	-6.51
	I	75	7.6	-6.58	-6.65
	J	150	5.4	-6.65	-6.75
S (74)		30	...	-6.54	
		45	...	-6.63	
		60 ^c	4.7	-6.70	

^a Identification used in ref. 7 and 8. ^b From data of ref. 7 and 8. ^c Sample 74 of ref. 4.

greater. An alternative calculation of J_e is obtained from the stress relaxation data of Thirion,^{7,8} taking the extrapolated ratio of $F_e/(\lambda - \lambda^{-2})$ to vanishing tensile strain as one-third of Young's modulus E_e , and using the relation $J_e = 3/E_e$. Here F_e , the equilibrium force per unit area at a given extension ratio λ , is

(8) R. Chasset and P. Thirion, "Proceedings of the International Conference on Non-Crystalline Solids," North Holland Publishing Co., Amsterdam, in press.

as well as with the earlier measurements of Stratton.⁴ The loss tangents ϵ_r are plotted against the logarithm of reduced frequency in Fig. 1; a similar plot of the storage modulus showed equally good agreement. It may be concluded that there are no anomalies due to interfacial effects.

Although the loss tangents measured in the torsion pendulum are sometimes very small, the background loss in the pendulum is believed to be far smaller; its oscillatory behavior with no sample indicates that the background is never more than 1% of the magnitude measured with the samples described here.

Results

For plotting with reduced variables, the storage and loss compliances, J' and J'' , were reduced in magnitude by the usual factor $T\rho/T_0\rho_0$, where ρ and ρ_0 are the densities at the temperature of measurement T and the reference temperature of $T_0 = 298.2^\circ\text{K}$.; the application of this factor is denoted by the subscript p . For this purpose the thermal expansion coefficient of the rubber was taken as $7.1 \times 10^{-4} \text{ deg}^{-1}$. The frequency shift factor a_T was calculated by the equation⁴

$$\log a_T = -5.94(T - 298.2) / (151.6 + T - 298.2) \quad (1)$$

In Fig. 2, J' and J'' are plotted logarithmically in this manner for two dicumyl peroxide vulcanizates with low (30) and high (150) cross-link densities. The low-frequency data from the torsion pendulum and the high-frequency data from the transducer match satisfactorily for J' , indicating that the sample coefficients based on sample geometry are correctly determined (as is not always the case⁴). For J'' , the low-frequency losses appear higher in the transducer, but these are believed to be less reliable because the driving tube loss correction is substantial when the loss is so small, and there is no known source of a negative error in the loss measured by the torsion pendulum. Hence the J''_p curves at low frequencies have been based on the torsion pendulum measurements. In comparing the two samples, that with the shorter spacing between cross links (150) has a somewhat smaller J' at low frequencies, as would be expected, and a much smaller J'' , indicating that the unexplained low-frequency losses diminish with reduction in cross-link spacing.

The same conclusion is reached by comparing the sulfur vulcanizates. In Fig. 3, J' and J'' for sample 60 are reproduced from ref. 4; the data for the other two samples with larger cross-link spacings show larger values of J'' at low frequencies.

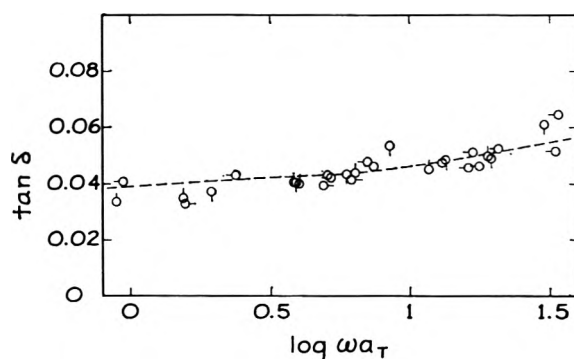


Figure 1. Loss tangent plotted against logarithm of reduced frequency at 25° for sulfur vulcanizate 77 of Stratton and Ferry⁴ for different sample thicknesses as follows: pip left, single disk, 0.218 cm.; pip down, two disks, total 0.297 cm.; pip right, two disks, total 0.433 cm.; pip up, three disks, total 0.646 cm. Points include measurements at 15, 25, and 35° . Curve is reproduced from earlier measurements by Stratton in 1961.

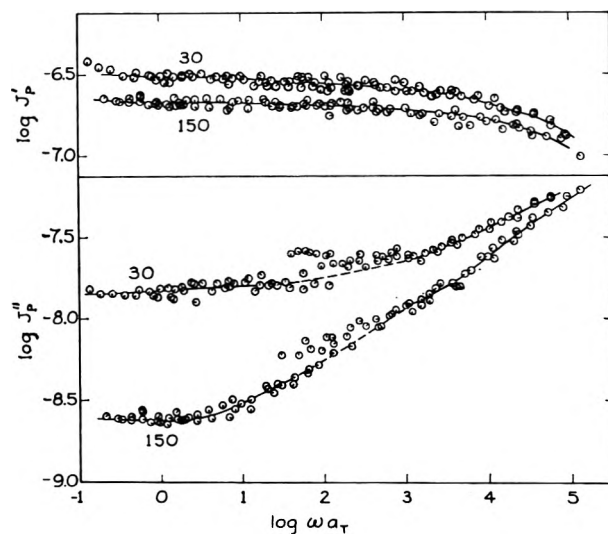


Figure 2. Storage and loss compliance reduced to 25° and plotted logarithmically against reduced radian frequency for two samples cross linked by dicumyl peroxide, identified by vulcanization times (Table I). Pips denote different temperatures, spaced at about 5° intervals from -6.7 (sample 30) and -17.9 (sample 150) to -5° , and then 10° intervals from -5 to 54.5° .

The most direct measure of relative loss is the loss tangent, $\tan \delta = J''/J'$. This quantity is plotted logarithmically against frequency for all the dicumyl peroxide vulcanizates in Fig. 4 and the sulfur vulcanizates in Fig. 5. At low frequencies the level of $\tan \delta$ falls markedly with increasing degree of vulcanization.

Discussion

The Transition Zone. Although the primary interest of this study is the rubbery zone at low frequencies, it

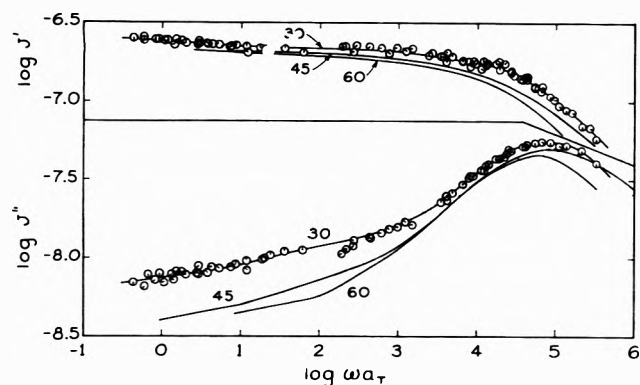


Figure 3. Storage and loss compliance reduced to 25° and plotted logarithmically against radian frequency for three samples cross linked by sulfur, identified by vulcanization times (Table I). Pips denote different temperatures, spaced at about 5° intervals from -12.2 to 5.3° and then 10° intervals to 35°.

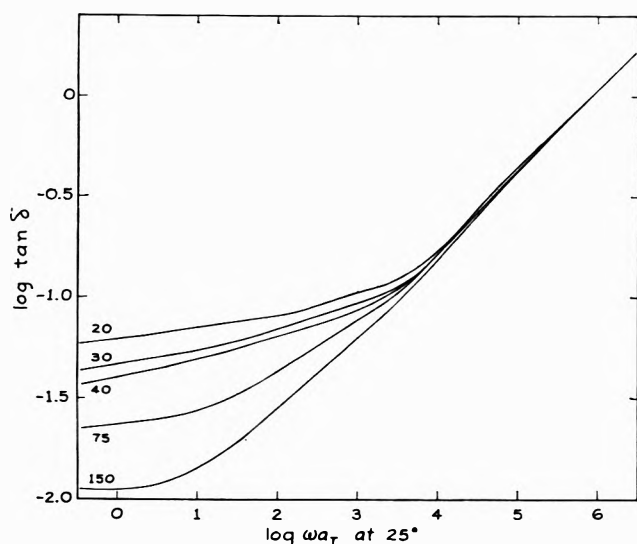


Figure 4. Loss tangents of dicumyl peroxide vulcanizates plotted logarithmically against radian frequency reduced to 25°. Numbers denote vulcanization times in Table I.

may be remarked that in the transition zone where $\tan \delta$ becomes of the order of unity the position on the logarithmic frequency scale is determined primarily by the local friction coefficient which will be more sensitive to differences in chemical constitution than to the degree of cross linking. In agreement with this expectation, all the dicumyl peroxide vulcanizates, for which the cross-linking process is unaccompanied by side reactions influencing the composition of the polymer, converge to a single curve for $\tan \delta$ as the transition zone is entered.⁹ On the other hand, sulfur vulcanization is accompanied by side reactions which increase the friction coefficient at a given temperature¹⁰; the

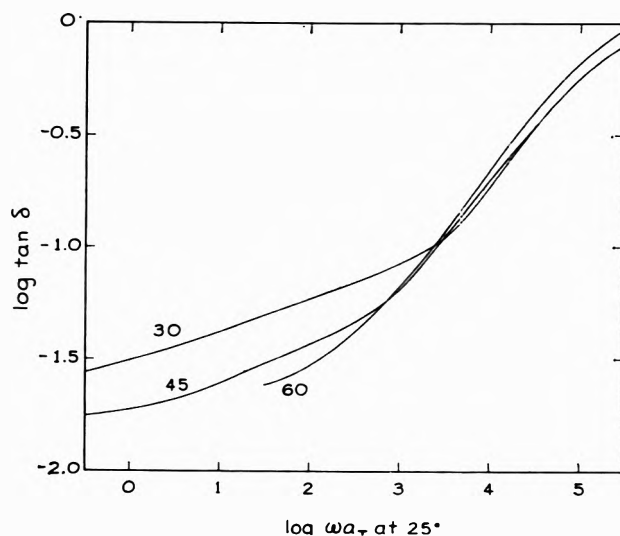


Figure 5. Loss tangents of sulfur vulcanizates plotted logarithmically against radian frequency reduced to 25°. Numbers denote vulcanization times in Table I.

position of the curve on the frequency scale in the transition zone is, accordingly, shifted to the left with increasing degree of vulcanization (Fig. 5).

The Rubbery Zone. At present, the complete effect of cross-link spacing on losses in the rubbery zone in Fig. 4 and 5 cannot be adequately interpreted because there is no guiding theory. The Rouse theory,¹¹ modified for networks^{12,13} and taking into account strand length distribution,⁴ predicts a rapid decrease in $\tan \delta$ with decreasing frequency and no curvature convex to the abscissa axis. For a partial quantitative description, the value of $\log \tan \delta$ at a fixed frequency of 10 radians/sec. or about 1.6 c.p.s. is plotted in Fig. 6, both against $\log M_c$ (dicumyl peroxide series only) and against $\log J_c$ as an alternative measure of cross-link density (both series). It is evident that the effect of cross-link spacing in determining the magnitude of the loss is much more important than that of the chemical nature of the cross link.

Possible Role of Entanglements. It is suggestive that the average spacing between coupling entanglements in the polymer before cross linking, M_e' , is in the range of M_c covered in these vulcanizates. Only a very rough estimate of M_e' can be obtained for

(9) Measurements of diffusion through rubber networks (S. P. Chen, unpublished experiments) indicate that there is a small dependence of the friction coefficient on density of cross linking, insufficient to be clearly distinguished in Fig. 4.

(10) H. D. Heinze, K. Schmieder, G. Schnell, and K. A. Wolf, *Kautschuk Gummi*, **14**, 208 (1961).

(11) P. E. Rouse, Jr., *J. Chem. Phys.*, **21**, 1272 (1953).

(12) M. Mooney, *J. Polymer Sci.*, **34**, 599 (1959).

(13) R. B. Blizard, *J. Appl. Phys.*, **22**, 730 (1951).

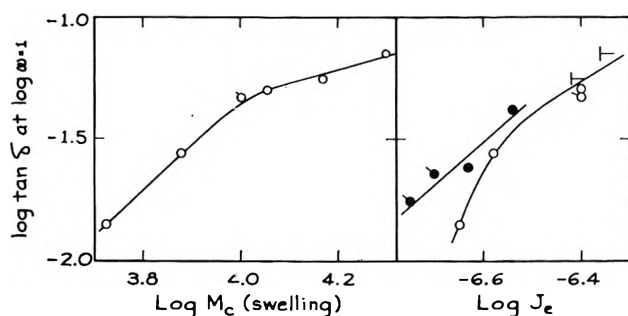


Figure 6. Loss tangent at $\log \omega \tau = 1$, plotted logarithmically against molecular weight between cross links determined from swelling (left) and equilibrium compliance (right). Open circles, dicumyl peroxide vulcanizates; black circles, sulfur vulcanizates. Tags denote data from ref. 4.

natural rubber, from the pseudo-equilibrium plateau in the modulus of a linear polymer of high molecular weight¹⁴; it is 5000 to 7000. In analyzing the relation between the density of physically effective cross links and the density of chemical cross links introduced in the vulcanization process, Mullins¹⁵ has deduced that trapped entanglements with a molecular weight spacing of about 14,000 contribute to the equilibrium modulus in natural rubber vulcanizates. The treatment tacitly identifies these entanglements with coupling loci already present before cross linking rather than the topological entanglements caused by the cross linking as discussed by Flory.¹⁶ A similar treatment of entanglements in polybutadiene networks has been given by Kraus.¹⁷ It can hardly be expected that exact agreement between the entanglement spacings in the linear and cross-linked polymers would be obtained, even if they do represent the same loci, since both estimations are very rough; the network calculations may be subject to several corrections.^{18,19}

The very long relaxation times revealed by the low-frequency losses may thus be associated with readjustments of configurational distributions coupled through trapped entanglements and extending over relatively long distances through the network volume. When

$M_c > M_e'$, as is almost certainly the case for sample 20 of the DCP series, some strands will have two or more entanglements and there will be a substantial number of such coupling sequences. When $M_c < M_e'$, as in sample 150 of the DCP series, many of the strands will have no entanglements, and such sequences will be rare. Qualitatively, this picture is in accord with the dependence of losses on cross-linking spacing, but a more precise formulation is needed. The probable role of trapped entanglements in slow relaxation mechanisms in rubber networks has also been deduced by Kraus²⁰ from stress relaxation experiments and by Plazek²¹ from creep.

There are, however, other possible sources of slow relaxation mechanisms, such as network strands with free ends and unattached molecules ("sol fraction"). These will be investigated subsequently. The relation of our dynamic measurements to transient measurements by Thirion on samples of identical composition will be discussed in more detail elsewhere.

Acknowledgment. We are grateful to Drs. P. Thirion and R. Chasset for preparation of samples, examination of their unpublished data, and valuable discussions. This work was supported in part by the U. S. Army Research Office (Durham), in part by the National Science Foundation, and in part by the Research Committee of the Graduate School of the University of Wisconsin. We are indebted to Miss Monona Rossol and Miss Marilyn Etzelmueller for help with calculations.

(14) H. Markovitz, T. G. Fox, and J. D. Ferry, *J. Phys. Chem.*, **66**, 1567 (1962).

(15) L. Mullins, *J. Appl. Polymer Sci.*, **2**, 1 (1959).

(16) P. J. Flory, "Principles of Polymer Chemistry," Cornell University Press, Ithaca, N. Y., 1953, pp. 461-464.

(17) G. Kraus, *J. Appl. Polymer Sci.*, **7**, 1257 (1963).

(18) J. A. Duizer and A. J. Staverman, "Proceedings of the International Conference on Non-Crystalline Solids," North Holland Publishing Co., Amsterdam, in press.

(19) W. Prins, *ibid.*, in press.

(20) G. Kraus and G. A. Moczygemba, *J. Polymer Sci.*, **A2**, 277 (1964).

(21) D. J. Plazek, private communication.

Viscosity of Metallic Mercury (and Its Saturated Vapor) over Its Entire Liquid Range, *i.e.*, from Its Melting Point (234.3°K.) to Its Critical Point (1733°K.), and an Estimate of Its Critical Viscosity¹

by A. V. Grosse

The Research Institute of Temple University, Philadelphia, Pennsylvania (Received August 6, 1964)

The viscosities of both liquid metallic mercury and its saturated vapor have been determined experimentally up to about 900°K. Using Andrade's equation, correlating viscosity, temperature, and specific volume, and from the known specific volumes of mercury up to the critical temperature, the viscosity of mercury and its saturated vapor are extrapolated to the critical point (1733°K.). Advantage is also taken of the experimental straight-line relations for the mean viscosity, *i.e.*, $\frac{1}{2}(\eta_{\text{liq}} + \eta_{\text{satd vap}})$, *vs.* temperature in the critical region. The critical viscosity of mercury is estimated to equal 0.4₁ cp.

Since some liquid metals can be heated up to very high temperatures, being elementary substances,² and methods of containing them up to temperatures of over 4500°K. have been developed,³ it becomes of increasing interest to be able to estimate their more important physical properties at as high a temperature as possible.

Of all the 80 elementary metals known, mercury is the only one whose critical temperature has been determined experimentally and whose liquid densities or specific volumes are known up to the critical point.²

The so-called transport properties of fluids, *i.e.*, viscosity, diffusion, and thermal conductivity, are interrelated. Statistical mechanics gives mathematical expressions for these properties, in terms of molecular parameters and intermolecular forces, for the dilute gases with reasonable accuracy. The theory of the same properties for condensed fluids is much more complicated.⁴ Particularly in recent years, a number of papers by physicists and chemical physicists⁵⁻¹³ have appeared attacking this problem, especially for the simplest case, namely, monatomic liquids having a spherically symmetrical field of force, such as the liquid noble gases.

However, agreement between theory and experiment and lack of precise experimental data, even in the simplest case of liquid argon, leave much to be desired.

In the case of liquid *metals*, the relationships are further complicated by the metallic bonding forces in contrast to the much more readily understood van der Waals forces of homopolar substances. This complication is indicated, for example, by the fact that the thermal conductivity of a normal liquid (such as liquid argon, krypton, or xenon) *decreases* with temperature; in the case of liquid metals some behave normally—for example sodium and potassium—and others, *in contrast*, have thermal conductivities increasing with temperature, exemplified by lithium and mercury.

(1) This work supported by the U. S. Atomic Energy Commission under Contract No. AT(30-1)-2082.

(2) A. V. Grosse, *J. Inorg. Nucl. Chem.*, **22**, 23 (1961).

(3) A. V. Grosse, *Science*, **140**, 781 (1963).

(4) See J. O. Hirschfelder, C. F. Curtiss, and R. B. Bird, "Molecular Theory of Gases and Liquids," John Wiley and Sons, Inc., New York, N. Y., 1954.

(5) P. Gray and S. A. Rice, *J. Chem. Phys.*, **40**, 3671 (1964).

(6) B. A. Lowry, S. A. Rice, and P. Gray, *ibid.*, **40**, 3673 (1964).

(7) H. Friedmann and W. A. Steele, *ibid.*, **40**, 3669 (1964).

(8) G. Boato, G. Casanova, and A. Levi, *ibid.*, **40**, 2419 (1964).

(9) J. Naghizadeh and S. A. Rice, *ibid.*, **36**, 2710 (1962).

(10) E. Helfand and S. A. Rice, *ibid.*, **32**, 1642 (1960).

(11) H. Reiss, H. L. Frisch, E. Helfand, and J. L. Lebowitz, *ibid.*, **32**, 119 (1960).

(12) G. Ciui-Castagnoli and F. P. Ricci, *ibid.*, **32**, 13 (1960).

(13) H. Mori, *Phys. Rev.*, **112**, 1829 (1958).

The thermal conductivity of liquid metals is directly related to electrical conductivity by the Wiedemann-Franz law. We are particularly interested to estimate electrical conductivities of liquid metals, at as high temperatures as possible, since they can now be heated to high temperatures by simple ohmic resistance, because the "pinch" effect can be readily overcome in a centrifugally rotating electrical furnace.¹⁴ Attempts to develop the transport theory for electron-phonon interactions in metals are being made.¹⁵

In view of the present state of theory we are forced to rely on experiments and on empirical methods, which will be developed herewith.

In our previous papers on the viscosity of liquid metals^{16,17} we used the *first* Andrade equation, namely

$$\eta = ae^{H\eta/RT} \quad (1)$$

to describe the change with temperature over a comparatively narrow temperature range (of about 500°K.). In his often-cited paper of 1934 on the theory of liquid viscosity, Andrade¹⁸ emphasized that for a wider temperature range, the change in density or specific volume of the liquid should be taken into account and developed his *second* equation, *i.e.*

$$\eta v^{1/3} = Ae^{c/vT} \quad (2)$$

where A and c are constants of a particular liquid, η (in poises) is its viscosity, and v (in cm^3/g .) is its specific volume at the temperature, T , in °K. In its logarithmic form, *i.e.*, plotting $\log(\eta v^{1/3})$ vs. $1/vT$, this equation is a straight line. Andrade applied his equation to mercury also and obtained the following values for his constants¹⁸

$$A = 2.67 \times 10^{-6}; c = 21.0 \quad (3)$$

All of the viscosity data on mercury up to 1960 are conveniently tabulated and critically evaluated in the mercury volume of the Gmelin handbook.¹⁹ The data of Erk²⁰ cover the range from the melting point to ~500°K., while Chalilov²¹ extended his measurements to 900°K. and also determined the viscosity of saturated mercury vapor.

Table I contains the pertinent data on viscosity¹⁹; also given are the experimental specific volumes of mercury from the melting point to the critical point, smoothed out according to our best present estimates (see ref. 2). The values of Andrade's variables, *i.e.*, $\eta v^{1/3}$ and $1/vT$, are also given in Table I.

They are plotted in Fig. 1; one can readily see that Andrade's straight-line relationship holds for the whole experimental range. The equation of this line is

$$\log(\eta v^{1/3}) = \log(2318 \times 10^{-6}) + 0.43429 \times 22.76/vT \quad (4)$$

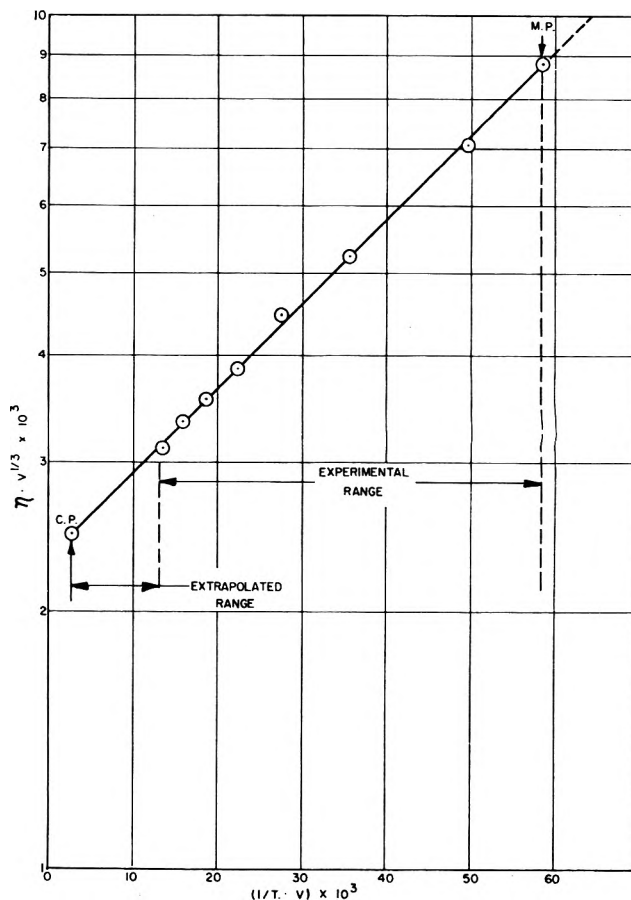


Figure 1. Viscosity, η , of Hg_{liq} using the second Andrade equation.

Our constants A and c are practically identical with the 30-year earlier ones of Andrade. Since the critical temperature of mercury²² is 1733°K. and the critical density² is known, the Andrade line was extended to the critical point (see Fig. 1). The viscosities for set values of temperature were calculated from our Andrade equation since the corresponding specific volumes are known (see Table I); the calculated η -values cover the range from 973°K. to the critical point (the four significant figures given for η_{calcd} should not imply the precision of these values).

(14) See A. V. Grosse, ref. 2, p. 787, Fig. 8.

(15) R. E. Prange and L. P. Kadanoff, *Phys. Rev.*, **134**, A566 (1964).

(16) A. V. Grosse, *J. Inorg. Nucl. Chem.*, **25**, 317 (1963); *Science*, **140**, 788 (1963).

(17) A. V. Grosse, *J. Inorg. Nucl. Chem.*, **23**, 233 (1961).

(18) E. N. daC. Andrade, *Phil. Mag.*, **17**, 698 (1934).

(19) "Gmelin's Handbook," Mercury, No. 34, Section 1, Verlag Chemie, GmbH., Weinheim, West Germany, 1960, pp. 312-317.

(20) S. Erk, *Z. Physik*, **47**, 886 (1928).

(21) Ch. Chalilov, *Zh. Tekhn. Fiz.*, **8**, 1249 (1938).

(22) F. Birch, *Phys. Rev.*, **41**, 641 (1932).

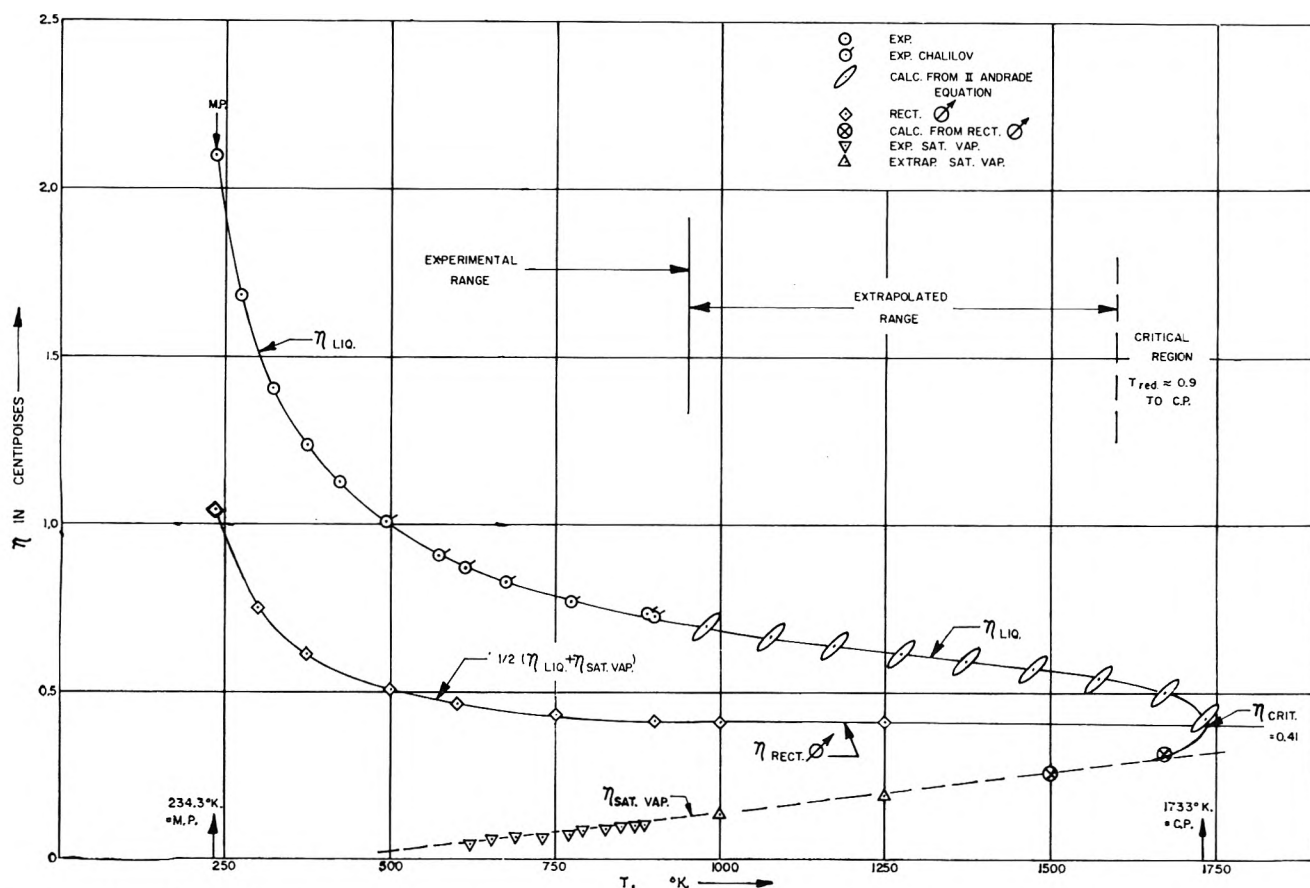


Figure 2. Viscosity, η , of mercury vs. T from the melting point (234.3°K .) to the critical point (1733°K .).

Finally, all values of viscosity in Table I are plotted over the entire range from melting point to critical point in Fig. 2; the *average* values of Erk and Chalilov (see Table I) are plotted in their range of overlap (*i.e.*, from 493 to 613°K .).

In addition to the data of Table I, we have also plotted in Fig. 2 the *experimental* values of Chalilov^{19,21} for the *viscosity of saturated vapor*, in equilibrium with liquid mercury, in the temperature range of his measurements, namely, from 350 to 610° . In contrast to dilute gases where the viscosity increases proportionally to the \sqrt{T} , the η of saturated vapor (because of the much greater pressure) is essentially a straight line function of T , as Fig. 2 shows. Thus, an extrapolation to higher temperatures can be readily made.

An additional empirical fact helps us to correlate the viscosity of the liquid and the viscosity of saturated vapor. In 1908, Phillips²³ was the first to investigate the viscosity of CO_2 , both of the liquid and the saturated vapor *in the critical region*, and established the main features of the behavior of η vs. T and P in the critical region. It could be demonstrated that the change of

viscosity of liquid and its saturated vapor vs. T showed a similar relationship to the density, namely the law of rectilinear diameter of Mathias and Cailletet (see ref. 2). Thus, the *mean* viscosity, *i.e.*

$$\frac{1}{2}(\eta_{\text{liq}} + \eta_{\text{satd vap}}) \quad (5)$$

is a straight-line function of temperature in the region of $T_{\text{red}} = 0.75$ to the critical point. In contrast to the mean density, *i.e.*, $\frac{1}{2}(D_{\text{liq}} + D_{\text{satd vap}})$, which can be extrapolated on a straight line all the way back to 0°K ., the mean viscosity curves upward toward the melting point on a *hyperbolic curve*, as Fig. 2 shows.

Recent and precise measurements on *ethane* and *propane* in the critical region by Starling, *et al.*,²⁴ confirmed this regularity for these two gases. Chalilov's

(23) P. Phillips, *Proc. Roy. Soc. (London)*, **A83**, 265 (1908); see also D. M. Newitt, "The Design of High Pressure Plant and the Properties of Fluids at High Pressures," Clarendon Press, Oxford, 1940, pp. 407-409.

(24) K. E. Starling, B. E. Eakin, J. P. Dolan, and R. T. Ellington; "Progress in International Research on Thermodynamic and Transport Properties," American Society of Mechanical Engineers, New York, N. Y., 1962, pp. 530-540.

Table I: The Viscosity and Specific Volume of Liquid Mercury from the Melting Point to the Critical Point

T , °K.	η , cp.	v , cm. ³ /g.	$\eta^{1/2}$, poise cm./g. ^{1/2} $\times 10^3$	$1/vT$, g./cm. ³ °K. $\times 10^3$
M.p. 234.3	2.10	0.073041	8.7782	58.433
273	1.685	0.073554	7.0600	49.801
323	1.407			
373	1.240	0.074870	5.2262	35.808
423	1.130			
473	1.052	0.076233	4.4606	27.733
493	1.027 ^a	1.008		
523	0.995			
543	0.985	0.9570		
573	0.950	0.9091	0.077655	3.8786
613	0.921	0.8728		
653		0.8405		
673		0.8285	0.079164	3.5510
693		0.8165		
733	0.7941			
773	0.7746	0.080802	3.3488	16.010
813	0.7596			
853	0.7444			
873	0.7385	0.082630	3.2166	13.863
898	0.7304			
973	0.6987	0.084083	3.0610	12.223
1073	0.6661	0.087306	2.9550	10.675
1173	0.6407	0.090212	2.8737	9.450
1273	0.6178	0.093624	2.8055	8.390
1373	0.5943	0.098348	2.7432	7.406
1473	0.5702	0.104613	2.6865	6.490
1573	0.5472	0.113766	2.6495	5.588
1673	0.4995	0.135135	2.5632	4.423
C.p. 1733	0.4249	0.197941	2.4765	2.915

^a The data in the left column are due to Erk (ref. 20); those in the right column are Chalilov's (ref. 21).

measurements (see Fig. 2 and ref. 19) established it *experimentally* for mercury, at least with some degree of accuracy at temperatures of about 900°K.

With all these facts and considerations in mind, we can first extrapolate the viscosity of liquid mercury on the one hand and its saturated vapor on the other to a temperature of about 1600°K. Both extrapolations are essentially straight lines because there are no abrupt changes in either viscosity or in specific volume with T ; thus the decrease of η from 900 to 1500°K. is only 0.7 cp. The calculated Andrade formula extrapolation and that of Chalilov's saturated vapor measurements give a mean rectilinear diameter viscosity of 0.41 cp. at 1000 and 1250°K. The critical region, which may be defined as the range from $T_{red} = 0.9$ (or $\sim 1600^\circ\text{K}$.) to the critical point, is where one has to expect a comparatively rapid decrease in η_{liq} coupled with the rapid increase in $\eta_{satd\ v\ a\ p}$. From the second Andrade equation the viscosity of the critical point is estimated to equal 0.42 cp. (see Table I);

the law of rectilinear diameter gives the nearly identical and, to us, preferable value of 0.41 cp.

To anyone who has observed or measured the rapid, that is manifold, change in viscosity over a narrow temperature range of *nearly all* chemical substances, it may seem foolhardy to extrapolate viscosities over a range of 800°K. However, it should be emphasized that our case is an exceptional one in that the critical viscosity is "self-bracketing"; this is to say that the liquid viscosity has to *decrease* constantly from the already low value of 0.73 cp. at 900°K. and, on the other hand, the $\eta_{satd\ v\ a\ p}$ has to increase *constantly* from the experimental value of 0.11 cp. at 900°K. From the known behavior of *all thermally stable* substances which do not undergo chemical change—and mercury is an element²⁵—it is known that the two functions *must*

(25) The only possible change at high temperatures, i.e., ionization of the saturated vapor, sets in, according to the Saha equation and the known ionization potential of mercury at the very much higher temperatures.

meet at the known critical point of 1733°K. Independently, the law of rectilinear diameter leads one to practically the same value. We thus consider the critical viscosity of mercury equal to 0.41 cp. at 1733°K. to be a good estimate. To illustrate this further, water has the viscosity equal to 1.00 cp. at 20°; thus mercury, at the critical point, is 2.5 times as fluid as water at 20°.

Since the critical density² is equal to 5.0 g./cm.³, the critical *kinematic* viscosity of mercury equals 0.082 centistoke.

The same method may be used to estimate the critical viscosity of a number of other metals whose η_{liq}

and $\eta_{satd\ vap}$ are known over a substantial temperature range. Such is the case of the alkali metals; the critical temperatures and densities of sodium, potassium, rubidium, and cesium have been estimated (see ref. 3).

Self-diffusion is another transport property which is closely related to viscosity. In a number of papers of the author²⁶ it has been stressed that the values of the diffusion constant, D , of metals can be obtained from η thanks to the Stokes-Einstein relation.

(26) The latest one is A. V. Grosse, *Science*, **145**, 50 (1964).

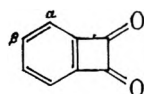
NOTES

An Electron Spin Resonance Study of the Anion Radical of Benzocyclobutadienoquinone

by David H. Geske and Alan L. Balch

Department of Chemistry, Cornell University, Ithaca, New York
(Received June 4, 1964)

The considerable investment of experimental effort by organic chemists in attempts to synthesize cyclobutadiene and its derivatives has borne fruit in the case of a number of quinones related to cyclobutadiene. The preparation of phenylcyclobutenedione by Smutny and Roberts^{1,2} was followed by the synthesis of diphenylcyclobutenedione,³ dihydroxycyclobutenedione,⁴ and dimethylcyclobutenedione.⁵ Recently Cava and co-workers⁶ have secured benzocyclobutadienoquinone (I). This paper reports on an electron spin resonance (e.s.r.) study of the anion radical of I.



(I)

A polarographic study of millimolar solutions of I in acetonitrile (0.1 M in tetraethylammonium perchlorate as supporting electrolyte) shows a reduction wave at -1.20 v. *vs.* aqueous s.c.e. The diffusion

current constant of $4.1 \mu a. \text{ mg.}^{-2/3} \text{ sec.}^{1/2} \text{ mM}^{-1}$ is the same as that for the known one-electron reduction of nitrobenzene in acetonitrile.⁷ The shape of the polarographic wave is close to that for a reversible one-electron reaction; $E_{1/4} - E_{3/4}$ is -65 mv. compared with the value of -56 mv. for a reversible process.

The anion radical of I, which is conveniently secured by *intra muros* electroreduction⁷ of I, is pale yellow. The e.s.r. spectrum obtained on reduction of a 1 mM solution of I in acetonitrile is shown in Fig. 1. The line width is 0.1 gauss and the g value is 2.0040.

The seven-line spectrum is readily assigned to isotropic proton coupling constants of 1.87 gauss and 3.74 gauss for two sets of two equivalent protons. The assignment of these coupling constants to molecular positions is shown in Table I. This assignment is supported by comparison with the accepted assignments for several other *ortho*-disubstituted anion

(1) E. J. Smutny and J. D. Roberts, *J. Am. Chem. Soc.*, **77**, 3420 (1955).

(2) E. J. Smutny, M. C. Caserio, and J. D. Roberts, *ibid.*, **82**, 1793 (1960).

(3) A. T. Blomquist and E. A. LaLancette, *ibid.*, **83**, 1387 (1961); **84**, 220 (1962).

(4) S. Cohen, J. R. Lacher, and J. D. Park, *ibid.*, **81**, 3480 (1959).

(5) A. T. Blomquist and R. A. Vierling, *Tetrahedron Letters*, 655 (1961).

(6) M. P. Cava and D. R. Napier, *J. Am. Chem. Soc.*, **79**, 3606 (1957); M. P. Cava, D. R. Napier, and R. J. Pohl, *ibid.*, **85**, 2076 (1963).

(7) D. H. Geske and A. H. Maki, *ibid.*, **82**, 2671 (1960).

Table I: Ring Coupling Constants in Anion Radicals

Structure	$\Sigma a_{ring} $, GAUSS	Ref.
	11.2	a
	9.2	a
	9.1	b
	5.6 ^c	d
	4.1	e

^a M. Adams, M. S. Blcis, Jr., and R. H. Sands, *J. Chem. Phys.*, **28**, 774 (1958). ^b P. H. Rieger, I. Bernal, W. H. Reinmuth, and G. K. Fraenkel, *J. Am. Chem. Soc.*, **85**, 683 (1963). The phthalonitrile anion radical was also observed by A. Carrington and P. F. Todd, *Mol. Phys.*, **6**, 161 (1963), who found ring proton coupling constants of 4.24 and 0.33 gauss for the radical in tetrahydrofuran. ^c The phthalaldehyde anion radical exists in the *meso* form as shown in Table I. Consequently there are not two sets of exactly equivalent proton coupling constants; the actual values are 2.91, 2.19, 0.49, and <0.24 gauss. ^d E. W. Stone and A. H. Maki, *J. Chem. Phys.*, **38**, 1999 (1963). ^e A. H. Maki and D. H. Geske, *ibid.*, **33**, 825 (1960). The ring proton coupling constants for this radical in dimethylformamide solution are 1.72 and 0.114 gauss: P. H. Rieger and G. K. Fraenkel, *ibid.*, **39**, 609 (1963), and J. H. Freed and G. K. Fraenkel, *ibid.*, **40**, 1815 (1964).

radicals. Assignments for the *o*-dinitrobenzene⁸ and phthalaldehyde⁹ anion radicals were established on the basis of deuteration studies. Molecular orbital calculations have been used to support the assignment for the *o*-benzoquinone¹⁰ and phthalonitrile¹¹ anion radicals. Preliminary Hückel molecular orbital (HMO) calculations for the benzocyclobutadienoquinone anion radical emphasized the sensitivity of the calculated spin densities to the choice of coulomb and resonance integrals used to describe the dicarbonyl group. Selection of such parameters is particularly arbitrary in the present case where nothing is known of bond lengths and bond angles for the group. It was felt that comparison of coupling constants in the anion of I with those in related radicals (Table I) represented a more convincing basis for assigning coupling constants to molecular positions than did HMO calculations.

The usual relationship¹² between ring coupling con-

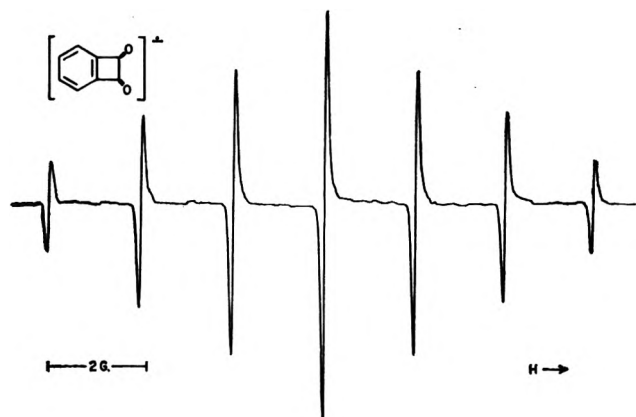


Figure 1. Derivative electron spin resonance spectrum of anion radical of benzocyclobutadienoquinone as obtained by electrolysis of a 1 mM solution of benzocyclobutadienoquinone in acetonitrile solution.

stant, a_H , and π -electron spin density on the adjacent carbon atom, ρ_C^π , as stated in eq. 1 may be used to

$$a_H = Q_{CH}^H \rho_C^\pi \quad (1)$$

estimate spin density values in the anion of I. Taking the value of $|Q_{CH}^H|$ as 24 gauss the π -electron spin density is estimated as 0.078 at the α -position and 0.156 at the β -position. Unfortunately no information is available on the distribution of spin density over the remaining six atoms.

A qualitative indication of the electrophilic nature of the *ortho* substituents is afforded by the magnitude of the ring proton coupling constants. For convenience, the sum of the absolute values of the four ring proton coupling constants is tabulated in Table I. Clearly the *o*-nitro groups are the best electron acceptors, and the dicarbonyl group in the anion of I is a relatively poor acceptor.¹³

Experimental

Benzocyclobutadienoquinone, as kindly supplied by Professor M. P. Cava, was recrystallized twice from an ethyl acetate-petroleum ether mixture. The melting point was 128–130° compared with the literature value⁶ of 132–135°. Details of the electron spin resonance and polarographic measurements were described previously.¹⁴

(8) A. H. Maki and D. H. Geske, *J. Chem. Phys.*, **33**, 825 (1960).

(9) E. W. Stone and A. H. Maki, *ibid.*, **38**, 1999 (1963).

(10) G. Vincow and G. K. Fraenkel, *ibid.*, **34**, 1333 (1961); G. Vincow, *ibid.*, **38**, 917 (1963).

(11) P. H. Rieger and G. K. Fraenkel, *ibid.*, **37**, 2795 (1962).

(12) H. M. McConnell and D. B. Chestnut, *ibid.*, **28**, 107 (1958).

(13) The possibility that some of the small coupling constants may actually be associated with negative spin densities does not perturb the over-all picture.

Acknowledgment. The financial support of the National Science Foundation through grant NSF-CP-1985 is gratefully acknowledged.

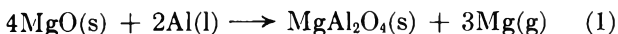
(14) D. H. Geske, J. L. Ragle, M. A. Bambenek, and A. L. Balch, *J. Am. Chem. Soc.*, **86**, 987 (1964).

Heat of Formation of $MgAl_2O_4$

by Robert L. Altman¹

Rice University, Houston, Texas (Received June 4, 1964)

Grjotheim, Herstad, and Toguri² report a ΔH°_{298} of 1.1 kcal./mole and a ΔS°_{298} of 10.1 e.u. for the formation of $MgAl_2O_4$ from MgO and Al_2O_3 . These values were obtained by a second-law treatment of experimental Mg vapor pressure data according to the reaction



A third-law treatment of the same data by this author³ yielded a ΔH°_{298} value of -8 ± 2 kcal./mole. The third-law entropy of formation of $MgAl_2O_4$ from the oxides at 298°K. is 0.53 e.u.⁴

This note reports weight loss results in transpiration experiments similar to those of Grjotheim, *et al.*,² and also the results of experiments in which argon was transpired over heated mixtures of Al and $MgAl_2O_4$.

Experimental

Mullite boats were loaded with 0.25-g. Al-MgO or Al- $MgAl_2O_4$ samples. The source and preparation of the MgO and $MgAl_2O_4$ powders are described elsewhere.³ The boat was pushed into a preheated Pt-Rh wire-wound tube furnace⁵ into which argon gas flowed in the opposite direction. The mullite furnace tube was closed at one end by a Pyrex optical flat through which the temperature of the boat was read with a Leeds and Northrup optical pyrometer. The pyrometer temperatures, corrected for the light absorbed by the optical flat, were in fair agreement with readings obtained from a chromel-alumel thermocouple attached to the mullite boat.

After heating in flowing argon for 3 to 7 hr. at pressures of ~ 1.5 -2 atm. and flow rates of ~ 100 cc./min., the boat was moved to the colder part of the furnace and cooled in the flowing gas before being removed from the furnace and reweighed. The weight loss results for both series of runs are given in Fig. 1.

Discussion

Transpiration runs, not shown in Fig. 1, have also been carried out using helium at flow rates of 160-240 cc./min. as the carrier. In eight out of ten of these experiments the boats gained weight. X-Ray crystallographic examination of a white residue on the outside

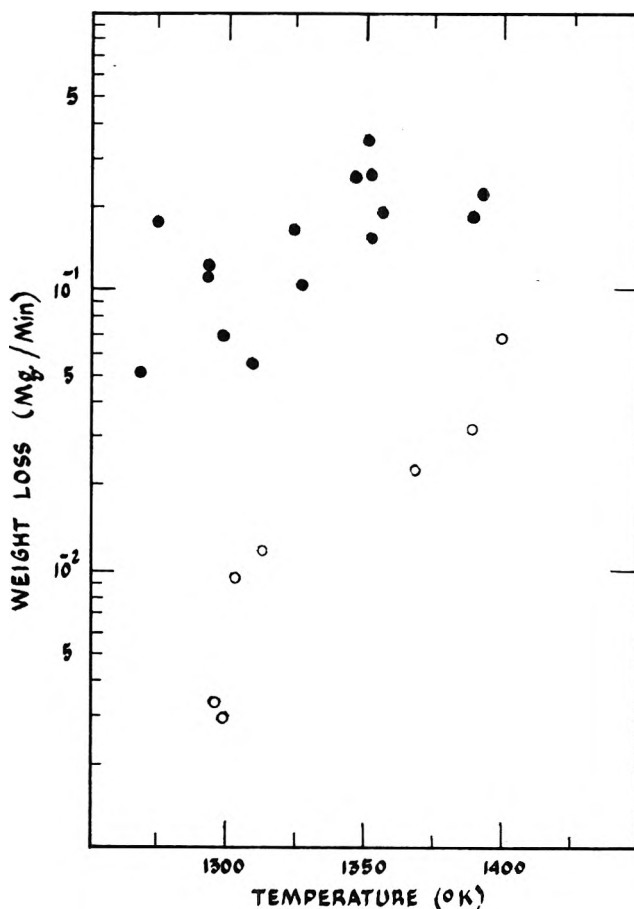


Figure 1. Transpiration weight loss of Al-MgO (●) and Al- $MgAl_2O_4$ (○) in flowing argon.

of the boat showed it to be MgO and similar examination of the contents of the boat showed Al_2O_3 . The weight gain can be attributed to oxidation of the gaseous magnesium product and aluminum starting material by diffusion of air through the wall of the mullite furnace tube.

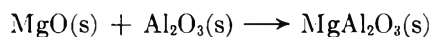
- (1) California State College at Hayward, Calif.
- (2) K. Grjotheim, O. Herstad, and J. M. Toguri, *Can. J. Chem.*, **39**, 443 (1961).
- (3) R. L. Altman, *J. Phys. Chem.*, **67**, 366 (1963).
- (4) E. G. King, *ibid.*, **59**, 218 (1955).
- (5) R. T. Grimley, Ph.D. Thesis, University of Wisconsin, 1958, p. 16.

Of thirty-one runs with the argon carrier, twenty-eight lost weight. However, at argon flow rates as low as 50 cc./min. the boats gained weight and only those runs with argon flow rates between 100 and 200 cc./min. are shown in Fig. 1.

The magnesium vapor pressures calculated from the data in Fig. 1 are about one order of magnitude lower than those of Grjotheim, *et al.*² X-Ray examination of several successful Al-MgO runs showed Al₂O₃ among the contents of the boat. Again, the difference between all these runs and the results of Grjotheim, *et al.*, can be attributed to partial oxidation of the aluminum starting material.

Similar examination of successful Al-MgAl₂O₄ runs showed the presence of Al, Al₂O₃, and the spinel phase. However, the back-reflection lines of this spinel phase were somewhat broader than for the unheated MgAl₂O₄. The incorporation of excess Al₂O₃ in the spinel lattice reduces the lattice parameter,^{6,7} while similar incorporation of MgO increases it.⁸ The Al-MgAl₂O₄ weight loss data suggest that some of the aluminum present in the Al-MgO heatings was incorporated into the spinel lattice.

As shown in Fig. 1, weight loss in the Al-MgAl₂O₄ system is negligible at temperatures below 1300°K. Since weight loss in the Al-MgO heatings is still significant at these temperatures, the composition of the spinel phase must be close to MgAl₂O₄. The third-law treatment of the lowest temperature runs will give the most meaningful heat for reaction 1. A ΔH°_{298} of 131 kcal./mole was obtained from such a treatment of the Grjotheim results for temperatures as low as 1150°K.³ This value yields an upper limit for the heat of formation of MgAl₂O₄, -551 kcal./mole, and a ΔH°_{298} for the reaction



of -7 kcal./mole. This last value is in agreement with previous Knudsen effusion data.³

Acknowledgments. The author wishes to thank Professor John L. Margrave for his interest and for having made possible this experimental work at Rice University during the summer of 1963. Financial support was provided through a grant from the National Aeronautics and Space Administration.

(6) G. L. Clark, E. E. Howe, and A. E. Badger, *J. Am. Ceram. Soc.*, **17**, 7 (1934).

(7) D. M. Roy, R. Roy, and E. F. Osborn, *Am. J. Sci.*, **251**, 337 (1953).

(8) A. M. Alper, R. N. McNally, P. H. Ribbe, and R. C. Doman, *J. Am. Ceram. Soc.*, **45**, 263 (1962).

A Solid Benzene-Tetra-*n*-butylammonium Nitrate Complex¹

by Thomas J. Plati and Edward G. Taylor

Thompson Chemical Laboratory, Williams College, Williamstown, Massachusetts (Received June 27, 1964)

Following up an earlier observation² that tetra-*n*-butylammonium nitrate crystals contain benzene when recrystallized from this solvent, we have established the existence of a solid 1:1 mole ratio complex between the two compounds. Vapor pressure-temperature measurements have been used to determine ΔH for the dissociation.

Experimental

Materials. Tetra-*n*-butylammonium iodide was prepared in the usual manner from fractionated tri-*n*-butylamine and *n*-butyl iodide and was converted into the nitrate by metathesis with silver nitrate in ethanol solution. The nitrate was purified by multiple recrystallizations from benzene and melted at 120° after vacuum drying at 90°. Benzene was either of reagent or spectrophotometric quality and was used without further purification.

Procedure. The vapor pressure-composition diagram was determined at 25° in a simple type of apparatus consisting of a flask attached to an open end manometer leading to a vacuum pump. Starting with approximately 5 g. of the nitrate and 10 g. of benzene in the flask, the usual procedure of evacuation followed by equilibration and subsequent weighing of the flask plus contents was carried out. A step curve, shown in Fig. 1, was obtained, the sudden break establishing the existence of a 1:1 mole ratio complex.

The vapor pressures of the molecular complex were measured at a series of temperatures using a flask to which was attached a closed end manometer. In this way it was possible to submerge most of the apparatus in the thermostat. After equilibration the difference in the mercury levels was observed using a cathetometer; it is estimated that the vapor pressure measurements are good to within ± 0.2 mm.

Solubility measurements were carried out by scaling the appropriate mixtures of benzene and the nitrate in heavy walled glass tubing. The tubes were attached to a wrist action shaking device and immersed in a

(1) Abstracted from the Honors Thesis of T. J. Plati, Williams College, 1964.

(2) N. L. Cox, C. A. Kraus, and R. M. Fuoss, *Trans. Faraday Soc.*, **31**, 749 (1935).

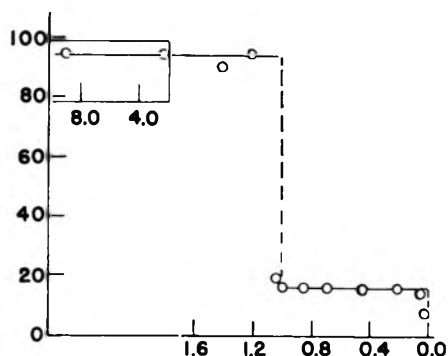


Figure 1. Vapor pressure-composition curve for the system benzene-tetra-*n*-butylammonium nitrate at 25°.

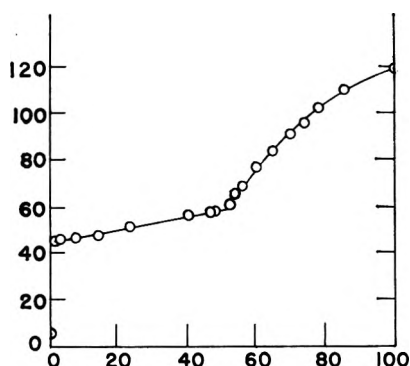


Figure 2. Phase diagram for the system $C_6H_6-(n-C_4H_9)_4NO_3$.

thermostat. The temperature of the latter was raised very slowly until the last trace of solid phase disappeared, at which point the temperature was recorded. Corrections for the amount of benzene in the vapor phase were negligible.

Infrared spectra of the solid complex in Nujol (kindly obtained for us by Mr. S. Traiman of Hoffman-LaRoche, Inc., Nutley, N. J.) were made on a Beckman IR-5 instrument. Confirmatory spectra were run in this laboratory using a Perkin-Elmer Model 137 Infracord.

Results

The method of least squares was applied to the vapor pressure-temperature data, giving the expression

$$\log p \text{ (mm.)} = -3.41 \times 10^3/T + 12.62$$

with a calculated probable error in the slope of 53, while that for the intercept is 0.17. Thus ΔH for the dissociation is 15.6 kcal./mole, $\Delta G^\circ_{298} = -1.6$ kcal./mole, and the entropy increase is 58 e.u./mole. The solubility data are plotted as the phase equilibrium diagram of Fig. 2. It is seen that the solid complex exhibits a congruent melting point of approximately 58° and

that it is largely dissociated in the fused state. Infrared data for the solid complex in Nujol show one new absorbance peak at 14.4 μ , which could perhaps be ascribed to a C-H out-of-plane bending vibration.

Kinetics of *n*-Paraffin Sorption in the Natural Zeolite Erionite

by R. M. Barrer and D. L. Peterson^{1a}

Physical Chemistry Laboratories, Chemistry Department, Imperial College, London, S.W. 7 (Received April 29, 1964)

Dehydrated crystalline zeolites have large intracrystalline volumes of molecular dimensions, access to which is limited to molecules having less than a critical size.^{1b} When the narrowest constrictions governing diffusion in the zeolitic channel network are rings of eight (Al,Si)O₄ tetrahedra, *n*-paraffins, but not branched-chain, aromatic, or naphthenic hydrocarbons, are sorbed; zeolites known to exhibit such selectivity are Sieve A in the calcium form,² chabazite,^{1b} and erionite.³ However, the rate of sorption of *n*-paraffins in the normal temperature range is much higher in Ca-A than in chabazite. This may be due, in part, to the smaller minimum free diameter (the distance between the peripheries of the nearest opposed pair of oxygen atoms) of eight-membered rings in the latter (3.7 Å. compared with 4.3 Å.). Erionite contains a channel network closely related to that of chabazite, with distorted eight-membered rings of 3.6-Å. minimum free diameter.⁴ In the present communication we report some preliminary observations of the rate of sorption of *n*-paraffins in erionite.

In Fig. 1 the kinetics of sorption of *n*-butane at 25° in specimens of natural and Ca²⁺-exchanged erionite (sample 1) are compared with those observed previously in chabazite.⁵ Because in the early stage the rate of sorption is inversely proportional to the crystallite diameter,⁶ which might have been somewhat larger for the chabazite specimen, the difference in intrazeolitic

(1) (a) 1005 Miller Ave., Berkeley 8, Calif.; (b) R. M. Barrer *Ann. Rept. Progr. Chem.*, **41**, 31 (1944).

(2) D. W. Breck, W. G. Eversole, R. M. Milton, T. B. Reed, and T. C. Thomas, *J. Am. Chem. Soc.*, **78**, 5964 (1956).

(3) P. E. Eberly, Jr., *Am. Mineralogist*, **49**, 30 (1964).

(4) R. M. Barrer and I. S. Kerr, *Trans. Faraday Soc.*, **55**, 1915 (1959).

(5) R. M. Barrer and D. A. Ibbitson, *ibid.*, **40**, 206 (1944).

(6) R. M. Barrer, "Diffusion in and Through Solids," Cambridge University Press, London, 1941, Chapter 1.

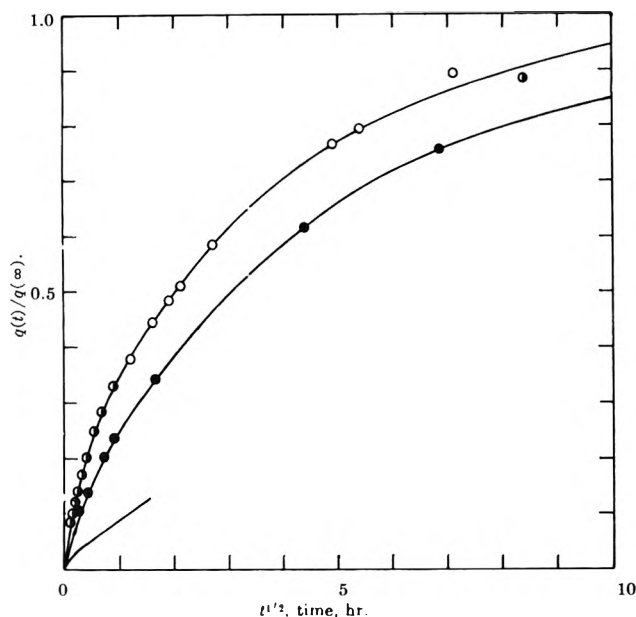


Figure 1. Kinetics of sorption of *n*-butane at 25° and ca. 40 cm. pressure: (a) erionite sample 1, without treatment (open circles) and after washing (half-filled circles); (b) erionite sample 1 after Ca⁺² exchange (filled circles); (c) natural chabazite⁶ (lower curve).

diffusivity might be less than implied by Fig. 1. The rate of sorption of *n*-butane in this erionite sample is thus certainly more nearly equal to that in chabazite than to that in Ca-A which, in the coordinates of Fig. 1, would be depicted by a curve lying very near to the vertical axis. Further, the observed rate was only moderately affected by Ca⁺² exchange, as was the equilibrium capacity (from 0.060 to 0.067 g. per g. of out-gassed erionite).

However, in another natural erionite (sample 2), having a crystallite size comparable with that of sample 1, *n*-pentane was found to be sorbed at nearly the same rate⁷ as in Ca-A, this rate being two orders of magnitude higher than in sample 1, whether in the native or a Ca⁺²-exchanged form. Since a difference in crystal size was apparently not the cause, the rate difference was thought to require further consideration. This rate difference is further emphasized because it was the longer *n*-pentane molecule which was more rapidly sorbed (in sample 2) than was the shorter *n*-butane molecule (in sample 1).

In Table I the compositions of the two erionite specimens are given and compared with that of the material characterized by Staples and Gard.⁸ The greater rate is seen from Table I to be associated with the more aluminous specimen, in which the total cation density is higher. Normally one expects sorption rate to decrease with increasing cation density,⁹ since cations

Table I: Compositions of Erionite Samples

	Fraction of total cations, equiv.				Si:Al
	Na	K	Mg	Ca	
Sample 1	0.6	0.2	0.1	0.1	3.73
Ca ⁺² -exchanged sample 1	...	0.2	0.1	0.7	...
Sample 2	0.7	0.2	...	0.1	3.45
Ca ⁺² -exchanged sample 2	0.1	0.2	...	0.7	...
Staples and Gard ⁸	0.3	0.2	0.1	0.4	3.02

tend partially to obstruct intracrystalline channels.

Another possibility is that the higher the silica content the more restricted are the eight-ring windows through which diffusion must occur, because Si-O bonds are slightly shorter than Al-O bonds. Isomorphous replacements NaAl \rightleftharpoons Si do cause small but detectable changes in the unit cells of Linde Sieve A,¹⁰ or in faujasite-type crystals,¹¹ but no change in unit cell could be detected in our erionites.

In order further to examine the role of the free dimensions of the eight-rings in Sieve A, chabazite, and erionite, we have calculated the energy of interaction φ between individual eight-rings in the three zeolites, and a portion of an *n*-paraffin chain passing through these rings (Fig. 2). The Lennard-Jones 6:12 potential was employed, and the dispersion energy constants between methylene groups and anionic oxygens were calculated using London's formula.¹² The polarizabilities α and characteristic energies E used were $-\text{CH}_2-$, $\alpha = 1.83 \times 10^{-24} \text{ cm.}^3$ per radical, $E = 10.80 \text{ e.v.}$; and $-\text{O}-$, $\alpha = 1.65 \times 10^{-24} \text{ cm.}^3$ per atom,¹³ $E = 13.55 \text{ e.v.}$ The equilibrium separation between a methylene group and a framework oxygen atom was taken to be 3.55 Å. Interactions were summed between all eight oxygen atoms of a given eight-ring and three methylene groups of an *n*-paraffin chain. The following assumptions were employed.

(a) The saddle point in the interaction energy surface occurs whenever a methylene radical in the *n*-paraffin chain passes through the "plane" of the ring (a plane from which the sum of the normal distances from the

(7) D. L. Peterson, unpublished results.

(8) L. W. Staples and J. A. Gard, *Mineral. Mag.*, **32**, 261 (1959).

(9) R. M. Barrer and J. W. Baynham, *J. Chem. Soc.*, 2892 (1956).

(10) G. T. Kerr and G. T. Kokotailo, *J. Am. Chem. Soc.*, **83**, 4675 (1961).

(11) G. Bergerhoff, W. H. Baur, and W. Nowacki, *Neues Jahrb. Mineral. Monatsh.*, 193 (1958).

(12) F. London, *Z. physik. Chem.*, **B11**, 222 (1930).

(13) R. M. Barrer and D. L. Peterson, *Proc. Roy. Soc. (London)*, **A280**, 466 (1964).

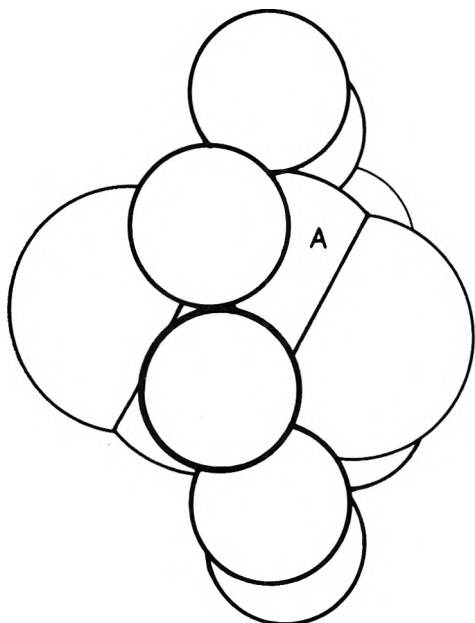


Figure 2. An *n*-butane molecule in the calculated position of the saddle point in an eight-membered ring of erionite. The methylene group labeled A is in the "plane" of the ring (see text).

center of the $-\text{CH}_2-$ to the oxygen atoms of the ring is a minimum (see Fig. 2).

(b) The rings are rigid and have the free dimensions and configurations found for the hydrated zeolites⁴ (that these may differ appreciably in the dehydrated form has been shown for chabazite by Smith,¹⁴ but it is not known whether, for a zeolite rich in another guest molecule, hydrated or dehydrated ring dimensions are more appropriate).

(c) The *relative* magnitudes of φ are adequately defined for the three kinds of eight-ring when only the three $-\text{CH}_2-$ groups most centrally placed through the eight-ring (as in Fig. 2) are considered. The values of φ at the saddle points for the eight-rings in Linde Sieve A, chabazite, and erionite are shown in Fig. 3 as the values of φ at the zero of the abscissa. The saddle point is highest for erionite, lowest for Sieve A, and the saddle points are energetically rather clearly separated. If it can be assumed that for an *n*-paraffin in an equilibrium position inside the largest cavity the energy of sorption is nearly the same for all three zeolites, and that this is the initial state for a unit act of diffusion, then the energies of activation for diffusion would be in the sequence: erionite > chabazite > Sieve A.

Figure 3 also shows the influence upon φ of small equal displacements, δr , of all ring oxygens, toward ($\delta r < 0$) or away ($\delta r > 0$) from the ring center. In this way the dependence of φ upon an idealized change

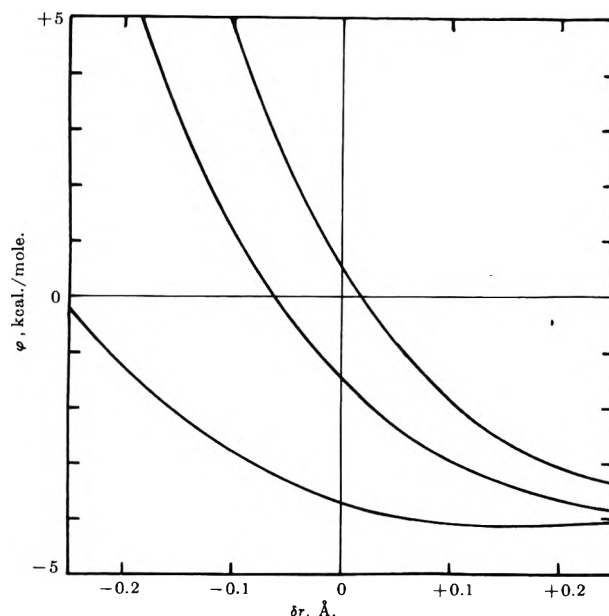


Figure 3. Variation of the interaction potential at the saddle point between an *n*-paraffin chain and the oxygen atoms of eight-membered rings in erionite (upper curve), chabazite (middle curve), and Sieve A (lower curve) with changes in the distances of the oxygen atoms from the centers of the rings.

in ring dimensions was approximated, such as might accompany a change in an Al-Si ratio, or stretching of the ring by the molecule traversing it. For no values of $\pm \delta r$ do the φ vs. δr curves for the three zeolites cross. For erionite to give a lower energy of activation than chabazite it would be necessary to assume that whereas the chabazite ring resisted distortion, the erionite ring was more easily deformable as the *n*-paraffin passed through it, or that distortion was not necessarily uniform for all oxygens in the ring.

Although $d\varphi/dr$ at the zero of the abscissa is greatest for erionite, this does not necessarily explain the different kinetic behavior of the two erionite specimens examined. The presence to various extents of a hydrolyzed skin on the surface of the crystals, perhaps rendered somewhat glassy during outgassing, or of entrained salts or other impurities, still remain as possible causes of the difference. Washing of the zeolite produced no alteration in rate (Fig. 1), so that salts, if present, must be firmly entrained in the intracrystalline channels.

Acknowledgment. D. L. P. wishes to acknowledge the award of a Fellowship from the National Science Foundation, during the tenure of which part of this work was carried out.

(14) J. V. Smith, *Acta Cryst.*, 15, 835 (1962).

Proton-Proton Spin Coupling Constants in Ethyl Derivatives

by S. Ebersole, S. Castellano, and A. A. Bothner-By

Mellon Institute, Pittsburgh, Pennsylvania 15213
(Received June 15, 1964)

Interest in the theoretical understanding of spin-spin coupling continues to be strong. Central to the formulation and testing of theories is the availability of accurate values for coupling constants in simple compounds, for example ethyl compounds. The values now mostly cited for these substances are those reported in 1956 by one of us and Glick,¹ using a method of measurement dictated by experimental expediency, which took no account of second-order splitting and therefore yielded some suspect values.

We have recently remeasured with great care the spectra of several ethyl compounds, and analyzed the spectra exactly by the method of least squares. The improved values which were obtained are given in Table I, along with probable errors, obtained by statistical analysis using the computer program²

taining 1% tetramethylsilane, introduced into 5-mm. o.d. n.m.r. tubes, degassed by repeatedly freezing and thawing under vacuum, and sealed under vacuum.

Spectra were recorded on a Varian A-60 spectrometer, using the 50 c.p.s. scale. The spectra were individually calibrated using audiofrequency side bands; the audiofrequency was determined with a Hewlett-Packard 522B counter. The spectrum of each multiplet was recorded four times, twice with increasing field, twice with decreasing field. The line positions used in the final computation were thus the averages of four independent determinations; line positions showed standard deviations in the range 0.01–0.08 c.p.s. The larger deviations were usually associated with lines broadened through some further interaction (*e.g.*, coupling with ring protons in ethylbenzene, coupling across the oxygen in diethyl ether, or with the acetyl methyl in ethyl acetate, etc.).

Spectral Analysis. Computation of the best parameters was performed with the iterative least-squares program LAOCOON II on IBM 704 and 7090 computers. Final values of the RMS error in fitting calculated to observed transition frequencies ranged from 0.022 (3,3-dimethylpentane) to 0.082 c.p.s. (ethyl bromide). The probable errors quoted in Table I

Table I: Chemical Shifts and Coupling Constants of Ethyl Derivatives

Compound	τ_{CH_2} , p.p.m.	τ_{CH_3} , p.p.m.	$J_{\text{CH}_2-\text{CH}_3}$, c.p.s.
$(\text{CH}_3\text{CH}_2)_2\text{C}(\text{CH}_3)_2$	8.7939 \pm 0.0006	9.2023 \pm 0.0007	7.524 \pm 0.030
$(\text{CH}_3\text{CH}_2)_3\text{C}$	8.8291 \pm 0.0006	9.2724 \pm 0.0005	7.528 \pm 0.026
$\text{CH}_3\text{CH}_2\text{C}_6\text{H}_5$	7.3941 \pm 0.0015	8.7757 \pm 0.0010	7.619 \pm 0.045
$\text{CH}_3\text{CH}_2\text{C}\equiv\text{N}$	7.6892 \pm 0.0008	8.7111 \pm 0.0007	7.605 \pm 0.035
$\text{CH}_3\text{CH}_2\text{COCH}=\text{CH}_2$	7.4595 \pm 0.0008	8.9327 \pm 0.0008	7.316 \pm 0.034
$(\text{CH}_3\text{CH}_2)_2\text{O}$	6.6308 \pm 0.0011	8.8639 \pm 0.0009	6.973 \pm 0.045
$\text{CH}_3\text{CH}_2\text{OCOCH}_3$	5.9539 \pm 0.0011	8.7680 \pm 0.0007	7.120 \pm 0.034
$(\text{CH}_3\text{CH}_2)_3\text{N}$	7.5747 \pm 0.0009	9.0303 \pm 0.0008	7.127 \pm 0.035
$\text{CH}_3\text{CH}_2\text{I}$	6.8454 \pm 0.0007	8.1407 \pm 0.0007	7.446 \pm 0.034
$\text{CH}_3\text{CH}_2\text{Br}$	6.6338 \pm 0.0010	8.3233 \pm 0.0011	7.327 \pm 0.049
$\text{CH}_3\text{CH}_2\text{Cl}$	6.4947 \pm 0.0008	8.5118 \pm 0.0008	7.232 \pm 0.040

LAOCOON II. The values, in general, are more in line with expectations based on recent studies of vicinal coupling constants.^{3,4} Sizable variation in the coupling constant is observed within the group of compounds containing an ethyl group attached to carbon.

Experimental

Recording of Spectra. Compounds of commercial provenance were used throughout; absence of extraneous peaks in the n.m.r. spectrum was taken as a sufficient criterion of purity. All samples were made up as 10% (v./v.) solutions in carbon tetrachloride con-

are obtained from the equation

$$E_j = 0.6745 \sqrt{(m_{jj} \Sigma \Delta^2) / (\det \mathbf{M} (N_1 - N_p))}$$

where \mathbf{M} is the matrix of the normal equations in the method of least squares, m_{jj} is the minor of the element M_{jj} in this matrix, $\Sigma \Delta^2$ is the total squared

(1) R. E. Glick and A. A. Bothner-By, *J. Chem. Phys.*, **25**, 362 (1956).

(2) To be described elsewhere.

(3) R. J. Abraham and K. G. R. Pachler, *Mol. Phys.*, **7**, 165 (1963).

(4) M. Karplus, *J. Am. Chem. Soc.*, **85**, 2870 (1963).

error in line fitting, and N_l and N_p are the number of lines matched and the number of parameters determined (3).

Acknowledgment. This work was supported by the Air Force Office of Scientific Research under grant AFOSR (199-63). Computation on the 7090 computer was performed with partial support of the National Science Foundation. We are indebted to Mr. J. Lorenc for technical assistance.

Interchange of *cis* and *trans* Chemical Shifts in Symmetrically Substituted Amides

by A. Greenville Whittaker,^{1a} D. W. Moore,^{1b} and S. Siegel^{1a}

Aerospace Corporation, El Segundo, California, and Naval Ordnance Test Station, China Lake, California (Received April 30, 1964)

It has been known for some time that the chemical shift ($\delta\omega$) at room temperature of the methyl resonances observed because of hindered internal rotation in *N,N*-dimethylformamide (DMF) is significantly larger than the corresponding shift associated with the CH_2 protons in *N,N*-diethylformamide (DEF).^{1c} A study of the variation of these chemical shifts over a wide temperature range which has been made by two of the present authors (A. G. W. and S. S.) shows that the latter observation also prevails for the relative values of $\delta\omega$ for temperatures down to -40° (compare Fig. 3 and Table I). However, the same study has shown that the magnitudes of the corresponding values of $\delta\omega$ for the CH resonances from *N,N*-diisopropylformamide (DIPF) are somewhat larger than those in DMF, as shown in Table I.² The experimental results indicate that the values of $\delta\omega$ for the protons either go through a minimum as the alkyl substituent is changed in this series of molecules or that the *cis* and *trans* resonances change relative positions in such a manner that the CH_2 resonance in DEF happens to occur near the "cross-over point." In the latter case, there would be no true minimum.

To investigate the possibility of a change in the relative positions of the *cis* and *trans* resonances, the n.m.r. spectra of methyl deuterated *N,N*-diethylformamide- d_6 and *N,N*-diisopropylformamide- d_{12} were examined.³ In these molecules the deuterons can be decoupled from the neighboring protons leaving only the hyperfine coupling between the α protons and the

Table I: Temperature Dependence of the Chemical Shift Due to Hindered Rotation

DIPF ^a (CH Resonance)		DMF ^b	
T, °K.	Chemical shift ^c	T, °K.	Chemical shift
387	0.0 ^d	395	0.0 ^d
378	11.1	391	4.56
375	15.8	390	5.50
361	16.1	389	6.97
353	15.8	381	7.79
342	15.4	363	8.59
302	12.6	337	8.82
247	10.2	305	9.42
		249	9.93

^a DIPF, diisopropylformamide. ^b DMF, dimethylformamide. ^c Chemical shift in c.p.s. at 56.4 Mc.; the precision of each value is approximately ± 0.1 c.p.s. ^d May not be exact coalescence temperature.

formyl protons. The latter decoupling was accomplished using a high resolution Varian 40-Mc. n.m.r. spectrometer and a Varian spin-decoupling unit. The decoupled spectra obtained are shown in Fig. 1 and 2. Figure 1 shows that the hyperfine splitting in DEF was not resolved. Attempts to sharpen the line by the addition of about 30% D_2O were not successful.⁴ However, the two lines are not equally sharp. Their widths at half-height were 1.7 and 2.0 c.p.s. with the low field line being broader; the increased breadth of the latter line indicates that this line has a larger unresolved hyperfine interaction. The spectrum of DIPF in Fig. 2 shows good resolution of the hyperfine splitting.⁵ The J values for the lines are 0.6 and 0.4

(1) (a) Aerospace Corp., El Segundo, Calif.; (b) Naval Ordnance Test Station, China Lake, Calif.; (c) J. V. Hatton and R. E. Richards, *Mol. Phys.*, **5**, 139 (1962); also, private communications with workers in the field indicated that this observation was made in several laboratories quite a few years before 1962.

(2) While it is true that the relative chemical shifts in DIPF and DMF are approaching each other at low temperatures, it is felt that the maximum shown by the CH chemical shift in DIPF is due to intermolecular association effects which predominate at low temperatures. At the higher temperatures where the association effect should be minimized, the fact that the chemical shift due to internal rotation is larger for the CH groups in DIPF than for the CH_2 groups in DMF is well established by the data.

(3) The deuterated compounds were obtained from Merck Sharp and Dohme Ltd. of Canada.

(4) V. J. Kowalewski and D. G. de Kowalewski, *J. Chem. Phys.*, **32**, 1272 (1960).

(5) The reason that the hyperfine splitting was resolved in DIPF and not in DEF was probably due to the fact that the DEF spectrum was taken at -40° while that of DIPF was taken at 29° . The reduced temperature distorts the plastic structure holding the field homogeneity shim coils. This makes it impossible to get comparable resolution at all temperatures. Also, the increased viscosity at low temperature broadens the lines somewhat. It is unfortunate that it is necessary to go to low temperature to separate clearly the CH_2 resonances in DEF.

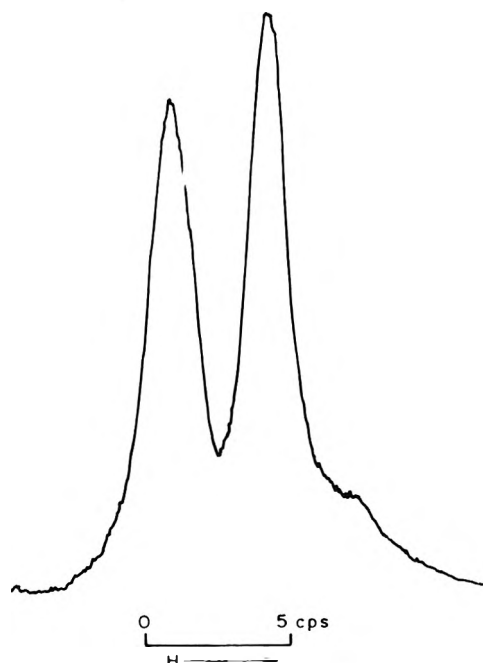


Figure 1. N.m.r. proton spectrum of methyl deuterated N,N-diethylformamide- d_6 at 40.0 Mc. and -40° with deuterons decoupled. Field strength increases from left to right.

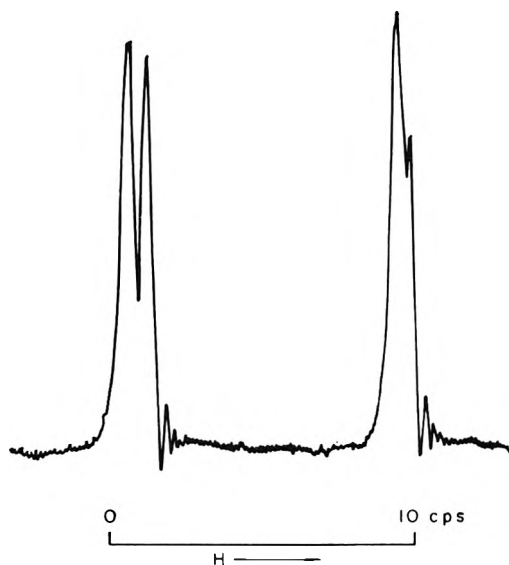


Figure 2. N.m.r. proton spectrum of methyl deuterated N,N-diisopropylformamide- d_{12} at 40.0 Mc. and 29° with deuterons decoupled. Field strength increases from left to right.

c.p.s. with the low field line showing the greater splitting. If it is assumed that the *trans* coupling remains greater than the *cis* (as found for DMF⁴ and for the C=C type molecules⁵) in this series of compounds, then

it follows that the resonance of the protons *trans* to the formyl proton occurs at the lower field in these two molecules. However, in DMF, the high field line is due to the protons *trans* to the formyl proton.³ This is clear evidence that the *cis* and *trans* resonances cross over in this series of compounds rather than the chemical shift going through a minimum.

It is not immediately clear why the protons on the carbon α to the nitrogen and *cis* to the carbonyl group are less shielded than the corresponding *trans* protons in DEF and DIPF while the reverse is true in DMF. However, the origin of the latter effect may be related to the fact that these protons in DEF and DIPF show very unusual behavior when their chemical shift due to internal rotation is measured as a function of temperature. These results are shown in Fig. 3. In DEF the relative chemical shifts of the methyl protons show what appears to be normal behavior, and they yield an activation energy of about 15 kcal./mole using the method of Gutowsky and Holm.⁷ On the other hand, the chemical shift of the CH_2 protons shows abnormal behavior in that it increases linearly as the temperature decreases. In DIPF the chemical shift of the CH protons goes through a maximum at about 90° ; but the resonance for the methyl groups is still coalesced down to -32° (the freezing point of DIPF). These results serve as

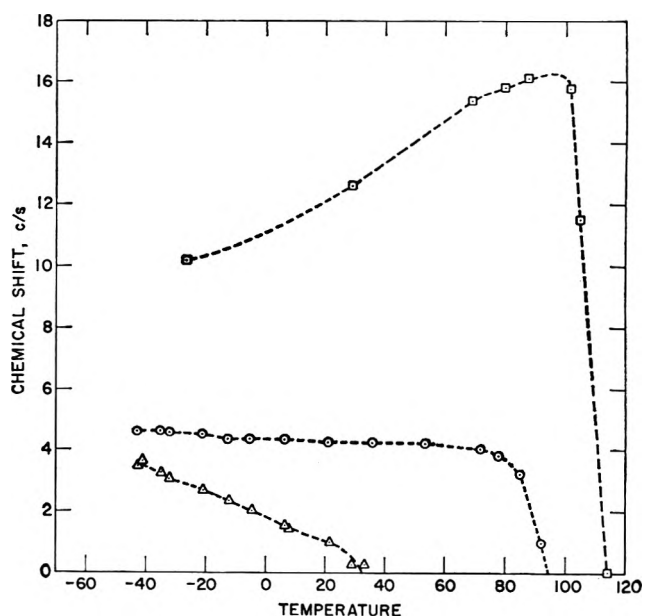


Figure 3. Chemical shift at 56.4 Mc. vs. temperature for N,N-diisopropylformamide (DIPF) and N,N-diethylformamide (DEF): \square , CH chemical shift in DIPF; \circ , CH_3 chemical shift in DEF; \triangle , CH_2 chemical shift in DEF.

(6) M. Karplus, *J. Chem. Phys.*, **30**, 11 (1959).

(7) H. S. Gutowsky and C. H. Holm, *ibid.*, **25**, 1228 (1956).

good evidence that the protons on the carbon α to the nitrogen are being strongly perturbed. Studies currently underway on solvent effects in amide solutions suggest that strong dipolar association exists between amide molecules and that the anomalous results illustrated in Fig. 3 arise from this type of intermolecular interaction. It is not unlikely that changes in the extent of the dipolar interaction may cause significant changes in the magnetic anisotropy in the carbonyl bond because of induced resonance effects, among others. This, in turn, could bring about changes in the relative shielding of the protons on the α -carbon atom, which could easily be structure sensitive as was experimentally observed.

A cursory search was made for a possible isotope effect in DEF- d_6 and DIPF- d_{12} , even though no such effect was expected. A 50 mole % solution of DEF- d_6 in acetone- d_6 was studied over a temperature range of -50 to 15° . The chemical shifts due to hindered rotation in this compound were found to be the same within experimental error as those found for normal DEF under corresponding conditions. Similar results were obtained from a 60 mole % solution of DIPF- d_{12} in acetone- d_6 over the temperature range -30 to 115° . Indeed, the points agreed well with the curve for neat DIPF shown in Fig. 3. The position of the maximum chemical shift was unaltered. These results confirm the expectation that the barrier to hindered rotation is not significantly altered by substitution of deuterons for protons in the methyl positions.

Acknowledgment. This work was supported by the U. S. Air Force under contract No. AF04(695)-469.

Surface Tensions of Binary Mixtures of Isooctane with Benzene, Cyclohexane, and *n*-Dodecane at 30° ¹

by Hiram Butler Evans, Jr., and
H. Lawrence Clever

Department of Chemistry, Emory University,
Atlanta, Georgia 30322 (Received June 1, 1964)

The surface tension-composition plots of ideal binary mixtures are usually convex due to Gibbs enrichment of the surface in the component of lower surface tension. The data can often be fitted with a symmetrical equation containing the pure component surface tensions

and a single size parameter if the molecules do not differ too much in size and shape.

This work was undertaken to study the effect of varying molecular size on the mixture surface tension. The component of lower surface tension (isooctane) was mixed with liquids of both higher surface area (*n*-dodecane) and lower surface area (benzene, cyclohexane). In general the data can be fitted to ideal-like equations but only by using unreasonably large molecular surface areas.

Experimental

All of the hydrocarbons were Phillips Petroleum pure grade (99 mole %). The benzene, cyclohexane, and *n*-dodecane were shaken with concentrated sulfuric acid, water-washed until neutral, and dried over metallic sodium. The benzene and cyclohexane were distilled on a 50-plate spinning band column. The *n*-dodecane was purified in 10-ml. lots by passage through a preparative gas chromatograph with column temperature about 10° above the normal boiling point. The isooctane (2,2,4-trimethylpentane) was distilled on the spinning band column and stored over sodium. The refractive index,² density,² and surface tension³⁻⁸ of the purified materials checked well with accepted values.

The mixtures were prepared by weight in glass-stoppered weighing bottles. The surface tensions were measured by the maximum bubble pressure technique on apparatus built and described by Quayle.⁹ The temperature was controlled at $30.0 \pm 0.05^\circ$. The surface tension bubbler air was presaturated with vapor from the liquid mixture to prevent evaporation losses and cooling of the surface during the measurement.

Densities of the isooctane-*n*-dodecane system were determined at 30° in a 5-ml. pycnometer previously calibrated with freshly boiled distilled water.

The isooctane-cyclohexane densities were assumed linear with mole fraction since Danusso¹⁰ reports an

(1) This work is part of a research program supported by NSF-G-7357. Mr. Evans was an undergraduate research participant supported by NSF-GE-1011.

(2) F. D. Rossini, *et al.*, "Selected Values of Properties of Hydrocarbons," National Bureau of Standards Circular 461, U. S. Government Printing Office, Washington, D. C., 1947.

(3) R. E. Donaldson, Ph.D. Thesis, Emory University, 1950.

(4) R. E. Donaldson and O. R. Quayle, *J. Am. Chem. Soc.*, **72**, 35 (1950).

(5) O. R. Quayle, R. A. Day, and G. M. Brown, *ibid.*, **66**, 938 (1944).

(6) A. E. Robinson, Ph.D. Thesis, Emory University, 1950.

(7) A. I. Vogel, *J. Chem. Soc.*, 133 (1946).

(8) J. P. Wibaut, *Rec. trav. chim.*, **58**, 375 (1939).

(9) O. R. Quayle, *Chem. Rev.*, **53**, 439 (1953).

(10) F. Danusso as quoted in J. C. Rowlinson, "Liquids and Liquid Mixtures," Academic Press, New York, N. Y., 1959, p. 143.

excess volume of only 0.04 ml./mole at 0.5 mole fraction. Wood and Sandus¹¹ report densities of the isooctane-benzene system at 25°. We determined several isooctane-benzene densities at 30° and constructed a large scale plot of density against mole fraction that paralleled the Wood and Sandus values. Required mixture densities were taken from the plot.

Results and Discussion

The surface tensions of the three mixtures are presented in Table I along with densities and excess volumes for the isooctane-*n*-dodecane system. The excess

Table I: Surface Tension of Some Binary Mixtures of Isooctane with Benzene, Cyclohexane, or *n*-Dodecane at 30°

Isooctane, mole fraction	Surface tension, dynes/cm.			Density, g./cm. ³	Excess volume, cm. ³ /mole <i>n</i> -Dodecane
	Benzene	Cyclohexane	<i>n</i> -Dodecane		
0.0000	27.53	23.77	24.47	0.6837	0.00
0.1860	23.40
0.2290	22.99	0.6972	-0.11
0.2741	22.47
0.2784	..	21.03
0.3211	22.34	0.7042	-0.17
0.3775	21.21
0.4221	21.68	0.7113	-0.25
0.4829	20.29
0.4838	..	19.88
0.5172	21.18	0.7174	-0.32
0.5827	19.70
0.6192	20.39	0.7225	-0.29
0.6452	19.32
0.6799	..	13.99
0.7192	19.80	0.7274	-0.26
0.7937	18.74
0.8271	19.07	0.7320	-0.15
1.0000	17.89	17.89	17.89	0.7423	0.00

volumes are negative and unsymmetrical with the minimum occurring between 0.5 and 0.6 mole fraction of isooctane. The related isooctane-*n*-hexadecane system is reported¹² to have an excess volume of -0.49 cm.³/mole at 0.5 mole fraction.

Guggenheim¹³ has derived a symmetrical, single-parameter equation for the surface tension of an ideal mixture of molecules of similar size

$$\exp\left(\frac{\gamma a}{kT}\right) = X_1 \exp\left(\frac{-\gamma_1 a}{kT}\right) + X_2 \exp\left(\frac{-\gamma_2 a}{kT}\right)$$

where γ , γ_1 , and γ_2 are surface tensions of the mixture, pure component 1, and pure component 2, respectively; a is the average surface area per molecule, kT the ther-

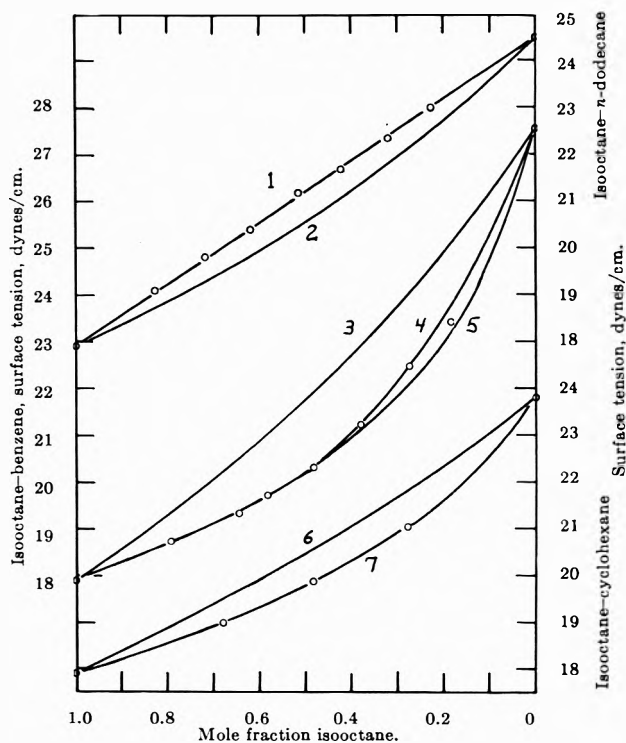


Figure 1. Surface tension vs. composition. Isooctane-*n*-dodecane: 1 linear, 2 ideal with a 48.6; isooctane-benzene: 3 ideal with a 35.4, 4 ideal-like with a 112, 5 unsymmetrical with a_1 136 and a_2 45; isooctane-cyclohexane: 6 ideal with a 38.4, 7 ideal-like with a 109.3.

mal energy, and X_1 and X_2 the mole fractions of components 1 and 2.

Figure 1 shows the ideal behavior (curves 2, 3, and 6) using for a the average surface area per molecule for each mixture. Surface areas, assuming spherical molecules, are benzene, 28.2; cyclohexane, 34.2; isooctane, 42.6; and *n*-dodecane, 52.6 Å.²/molecule.

Considering the differences in size of the molecules it is not surprising that none of the three systems is fit by the ideal equation using the average surface area. However, the isooctane-cyclohexane system can be fitted to the ideal equation when a surface area of 109.3 Å.²/molecule is used. The equation

$$\exp\left(\frac{-\gamma}{-3.828}\right) = X_1 \exp\left(\frac{-\gamma_1}{3.828}\right) + X_2 \exp\left(\frac{-\gamma_2}{3.828}\right)$$

(11) S. E. Wood and O. Sandus, *J. Phys. Chem.*, **60**, 801 (1956).

(12) J. H. van der Waals, *Trans. Faraday Soc.*, **52**, 916 (1956).

(13) E. A. Guggenheim, *ibid.*, **41**, 150 (1945); "Mixtures," Clarendon Press, Oxford, 1952, Chapter IX.

(where X_1 is the mole fraction of isooctane and X_2 the mole fraction of cyclohexane) reproduces the isooctane-cyclohexane data at 30° with an average deviation of 0.06 dyne/cm.

An a of 112 Å.²/molecule in the ideal equation reproduces the isooctane-benzene surface tensions with an average deviation of 0.14 dyne/cm. (Fig. 1, curve 5). The fit is poor at the benzene-rich end of the curve. A better fit is obtained if the three terms of the equation

$$\gamma = X_1\gamma_1 + X_2\gamma_2 - \frac{1}{2} \frac{(\gamma_1 - \gamma_2)^2}{kT} (X_1a_1 + X_2a_2)X_1X_2 + \dots$$

developed by Hildebrand and Scott¹⁴ by an expansion of the Guggenheim equation to take into account the different size molecules in a mixture is used. The terms above were manipulated and fitted to the data to get the equation

$$\gamma = 17.89 + 9.64X_3 - 5.00X_1X_3 - 10.11X_1X_3^2$$

where X_1 is isooctane mole fraction and X_3 the benzene mole fraction (Fig. 1, curve 4). The equation reproduces the seven isooctane-benzene surface tensions with an average deviation of 0.06 dyne/cm. The surface areas that make this fit are isooctane, 136, and benzene, 45 Å.²/mole, which are much larger and of different ratio than the actual areas.

No effort was made to fit the isooctane-*n*-dodecane data to the ideal equations. The slope-intercept equation

$$\gamma = 24.47 - 6.58X_1$$

(where X_1 is the isooctane mole fraction) reproduces the experimental points with an average deviation of 0.03 dyne/cm. (Fig. 1, curve 1). In this system isooctane, the component of lower surface tension, certainly enriches in the surface, but even after the surface enrichment possibly the larger *n*-dodecane molecule is so oriented as to cover such a surface fraction that the mixture surface tension is linear against bulk mole fraction. There should be systems where this difference in size leads to a concave surface tension-composition plot, and we are presently studying some systems where we expect such behavior.

Thermodynamics of Ionization and Tautomerism of Aqueous Pyridine Monocarboxylic Acids

by Frank J. Millero, J. C. Ahluwalia, and Loren G. Hepler

Department of Chemistry, Carnegie Institute of Technology, Pittsburgh, Pennsylvania (Received June 9, 1964)

This investigation of the thermodynamics of ionization of aqueous α -picolinic acid, β -picolinic acid (nicotinic acid), and γ -picolinic acid (isonicotinic acid) was undertaken as a continuation of a program aimed at the determination of such data for a variety of organic acids in water. A general interest in the picolinic acids derives from the physiological activity (vitamins, antituberculosis drugs, etc.) of a number of derivatives. A more immediate interest concerns the uncertainty as to which of the tautomeric forms, $^+HNR-COO^-$ or $NR-COOH$, is more important in aqueous solution.

Experimental

The calorimeter used is patterned after one previously described,¹ except that a Leeds and Northrup Mueller G-2 bridge and HS galvanometer were used with a nickel wire resistance thermometer for temperature measurements. Also, the resistance thermometer and calibration heater were contained in a glass spiral filled with mineral oil rather than wound on a silver cylinder. All of the calorimetric work reported here was carried out with 950 ml. of H₂O in the calorimeter at 25.0 ± 0.1°.

Nicotinic and isonicotinic acids were obtained from Fisher Scientific Co. in high purity and were used without further purification. Practical grade picolinic acid from Fisher was recrystallized three times from 95% ethanol and then vacuum dried. The melting point was 137–138°.

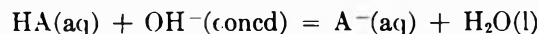
Sodium hydroxide solutions were prepared and standardized by common procedures.

Results and Calculations

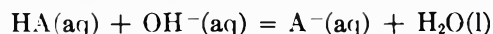
Heats of ionization were determined by measuring the heats of reaction of the aqueous acids with aqueous NaOH. Aliquots (10 ml.) of 4.946 *M* NaOH were mixed with 950 ml. of H₂O containing a known amount of acid. A general reaction equation for this process is

(14) J. H. Hildebrand and R. L. Scott, "Solubility of Nonelectrolytes," Reinhold Publishing Corp., New York, N. Y., 1950, Chapter XXI.

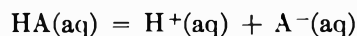
(1) W. F. O'Hara, C. H. Wu, and L. G. Hepler, *J. Chem. Educ.*, **38**, 519 (1961).



Separate determination of the total heat associated with breaking the bulb containing NaOH and diluting the NaOH permitted us to calculate heats for the reactions



These values, designated ΔH_n , are listed in Tables I-III. Combination of these heats of neutralization with $\Delta H^\circ = 13.34$ kcal./mole for the heat of ionization of water^{2,3} leads to the desired heats of ionization; that is, ΔH° for



These heats of ionization are listed in Table IV. Free energies of ionization that were calculated from pK values⁴ are also listed there, along with entropies of ionization calculated from ΔH° and ΔG° values.

Table I: Heats of Neutralization of Isonicotinic Acid by NaOH

Moles of acid/950 ml.	$-\Delta H_n$, kcal./mole ^a
0.004477	10.30
0.006488	10.30
0.008492	10.37
0.009452	10.35
0.010676	10.37
0.014101	10.36
0.018729	10.34

$$^a \Delta H_n^\circ = -10.34 \pm 0.05 \text{ kcal./mole.}$$

Table II: Heats of Neutralization of Nicotinic Acid by NaOH

Moles of acid/950 ml.	$-\Delta H_n$, kcal./mole ^a
0.004413	10.80
0.006471	10.76
0.008215	10.75
0.008526	10.80
0.010308	10.75
0.012476	10.75
0.016466	10.78

$$^a \Delta H_n^\circ = -10.77 \pm 0.05 \text{ kcal./mole.}$$

Discussion

Hughes, Jellinek, and Ambrose⁵ made measurements on aqueous solutions of nicotinic acid that led them to conclude that zwitterion species $^+\text{HNR}^-\text{COO}^-$

Table III: Heats of Neutralization of Picolinic Acid by NaOH

Moles of acid/950 ml.	$-\Delta H_n$, kcal./mole ^a
0.004912	10.85
0.006977	10.91
0.009521	10.91
0.009998	10.91
0.010856	10.88
0.012928	10.91
0.015985	10.91

$$^a \Delta H_n^\circ = -10.89 \pm 0.05 \text{ kcal./mole.}$$

Table IV: Thermodynamics of Ionization of Aqueous Pyridine Monocarboxylic Acids

Acid	ΔG° , kcal./mole	ΔH° , kcal./mole	ΔS° , cal./deg. mole
Picolinic	7.22	2.45	-16.0
Nicotinic	6.51	2.57	-13.2
Isonicotinic	6.60	3.00	-12.1

are not present. Later investigations by Evans, Herington, and Kynaston⁶ led to reliable pK values (macroconstants) but did not give microconstant values that would permit calculation of the relative prevalence of the tautomeric species $^+\text{HNR}^-\text{COO}^-$ and NR^-COOH in solutions of the three pyridine monocarboxylic acids. Jaffé's theoretical considerations,⁷ based on the Hammett equation, led him to suggest that the zwitterion $^+\text{HNR}^-\text{COO}^-$ is more, rather than less, prevalent than the tautomer NR^-COOH . Green and Tong⁴ then determined macroconstant pK values for the three pyridine carboxylic acids and evaluated microconstants by combining macroconstant pK values with separately determined pK values for the methyl esters (Wegscheider-Ebert method). Their results⁴ indicate that the pyridine monocarboxylic acids are present in aqueous solution as $^+\text{HNR}^-\text{COO}^-$ to an extent of more than 90% and as NR^-COOH to an extent of less than 10%.

(2) J. Hale, R. M. Izatt, and J. J. Christensen, *J. Phys. Chem.*, **67**, 2605 (1963).

(3) C. F. Vanderzee and J. A. Swanson, *ibid.*, **67**, 2608 (1963).

(4) R. W. Green and H. K. Tong, *J. Am. Chem. Soc.*, **78**, 4896 (1956).

(5) E. B. Hughes, H. H. G. Jellinek, and B. A. Ambrose, *J. Phys. Colloid. Chem.*, **53**, 414 (1949).

(6) R. F. Evans, E. F. G. Herington, and W. Kynaston, *Trans. Faraday Soc.*, **49**, 1284 (1953).

(7) H. H. Jaffé, *J. Am. Chem. Soc.*, **77**, 4445 (1955).

Previous investigations of thermodynamics of ionization of aqueous carboxylic acids in which there is no possibility of zwitterion formation indicate that entropies of ionization can be expected to be about -20 cal./deg. mole. The entropy of ionization of benzoic acid, which should be comparable to that of the pyridine monocarboxylic acids in the form NR₂COOH, is -18.9 cal./deg. mole.⁸ Entropies of ionization of amino acid zwitterions are considerably less negative, often being about -10 cal./deg. mole.^{9,10}

Entropies of ionization reported in Table IV are clearly less negative than expected for NR₂COOH species and therefore support the work of Jaffé⁷ and Green and Tong⁴ which led them to conclude that the pyridine monocarboxylic acids exist largely in the zwitterion form $^+HNR_2COO^-$ in aqueous solution. The entropy of ionization of picolinic acid is considerably more negative than ΔS° values for nicotinic and isonicotinic acids, which indicates that the charges in the zwitterion of picolinic acid are so close together that, from the point of view of nearby water molecules, there is only a little difference between $^+HR_2NCOO^-$ and RN₂COOH.

Acknowledgment. We are grateful to the National Institutes of Health for support of this research.

(8) L. P. Fernandez and L. G. Hepler, *J. Phys. Chem.*, **63**, 110 (1959).

(9) R. N. Diebel and D. F. Swinehart, *ibid.*, **61**, 333 (1957).

(10) J. T. Edsall and J. Wyman, "Biophysical Chemistry," Vol. I, Academic Press, Inc., New York, N. Y., 1958.

A Steady-State at Initial Concentration

Method of Studying Reaction Rates

by Homer Jacobson and Herbert Dubno

Department of Chemistry, Brooklyn College,
City University of New York, Brooklyn 10, New York
(Received January 17, 1964)

This communication describes a method of measuring reaction rate kinetics in a stirred-flow system with a steady state which does not vary from the initial conditions. Known methods using flow systems to study kinetics in the gas phase¹ or in solution²⁻⁴ give a steady state within the reaction chamber. Where there is a longitudinal flow path, the steady state will vary along it; in the stirred-flow reaction methods, the steady state is substantially constant, once attained, but cannot be specified in advance and must be measured by

"freezing" the reaction and analyzing aliquots from the flow. The recent development of servo-controlled burets^{5,6} has allowed measurement of reaction rates as a function of the flow rate of the reactant (typically H⁺) added (or of H⁺ product removed by addition of OH⁻). In the described method, the entire reaction mixture is rigidly maintained in a steady state determined in advance, at concentrations initially put into the system. The reaction rate is determined by measuring the flow rate of input reactants, as needed to maintain the steady state.

A servo device is basic for attainment of correct flow rate to keep the steady state. A careful adjustment of the relative quantities of reactants, as determined by reaction stoichiometry, and of concentrations of added reactants, and, if desired, an overflow device to keep the volume of the system constant (the flow rate will otherwise increase exponentially with the volume) constitute, in principle, the requirements of the steady state at initial concentration, or SIC, kinetics method.

Any servo system which responds to a null device primarily activated by a change in concentration of one component of the mixture can suffice to adjust the reaction rate. The pH-Stat, responding to changes in [H⁺], is frequently convenient and commercially available. Let such a reaction including proton transfer for study be represented in generalized form by the equation



(generalization to proton-producing reactions, using OH⁻ instead of H⁺ in the compensating buret, is entirely analogous and needs no separate treatment). Let the initial concentration of reactant or product Y be designated [Y_i]. At the reaction rate needed to match an input of reactants, reaction stoichiometry demands a mole ratio of $a:b:h:c:d$ for the reactants added and products produced, respectively. The servo system needed to maintain the match must supply these reactants in compensation in the mole ratios $a:b:h$. We define the generalized compensatory concentration [X] such that the servo burets supply A, B, and H⁺ in concentrations of $a[X]$, $b[X]$, and $h[X]$, respectively. In addition, however, a supply of solutions of the reagents must also compensate for their

(1) M. Bodenstein and S. Wolgast, *Z. physik. Chem.*, **61**, 422 (1908).

(2) K. G. Denbigh, *Trans. Faraday Soc.*, **40**, 352 (1944).

(3) H. H. Young and L. P. Hammett, *J. Am. Chem. Soc.*, **72**, 280 (1950).

(4) J. Saldick and L. P. Hammett, *ibid.*, **72**, 283 (1950).

(5) J. J. Lingane, *Anal. Chem.*, **21**, 497 (1949).

(6) C. F. Jacobsen and J. Leonis, *Compt. rend. trav. Lab. Carlsberg; Ser. Chim.*, **27**, 333 (1951).

dilution of the reaction mixture by the solvent present. This means that the additional concentrations of $[A_i]$, $[B_i]$, and $[H_1^+]$ must be added to the compensatory concentrations above, since addition of solutions at the same concentration will not dilute, making the corrective concentrations of the three reactants equal to $[A_i] + a[X]$, $[B_i] + b[X]$, and $[H_1^+] + h[X]$, respectively.

There are further constraints, if absolute constancy of conditions is desired. There is ordinarily likely to be a buildup of products, and certainly so if none are present in the initial reaction mixture. This buildup can be prevented if products are initially added to the system, taking advantage of the diluting action of the solvent in the added reactant solutions, using a prescribed initial concentration of products, *i.e.*, $[C_i]$ and $[D_i]$, in the mole ratio of $c:d$. If, now, $[C_i]$ and $[D_i]$ are taken equal to $c[X]$ and $d[X]$, then the conversion of reactants to products can be simply shown to be exactly matched by a sufficient addition of solvent to keep the concentration of products the same.

We have described the addition of the compensatory reactants as though a single such solution were added. Such a solution would, of course, be unstable, and in practice the material must be added with at least two separate burets to prevent reaction. The concentrations given for compensation above would have, for instance, to be doubled if added in two equal but separate solutions from two burets.

Reactions other than proton transfer can, of course, be studied by the SIC method. A separate electrode system, sensitive to changes in any other reactant or product concentration, *e.g.*, an oxidation-reduction electrode, or one more or less specific for a given reactant or product ion, used with the pH-Stat electronics and burets, will give the same kind of compensation.

Reaction rates cannot be obtained by the full SIC method for solutions without some products initially present, as well as reactants. Where the reverse reaction or presence of products plays no role, a partial SIC can be used, with the ratio of $[X]$ to product concentrations arbitrary. Where the reverse reaction is important, however, the minimum amount of initial product concentrations present is determined by how low $[X]$ can go practically. At low enough values, the ratio of $[X]$ to the initial reactant concentrations is so small that setting the compensation by the concentrations in the buret becomes inaccurate. Moreover, the rate of the reaction may become large compared with the mixing and diffusion rate at low values of $[X]$.

Unreacting substances whose effect on the kinetics of the reaction of interest, such as salts or variable solvent, can be simply present at one constant concentra-

tion in the initial solution and in all compensating burets.

Comparison of the SIC method with the stirred-flow methods of Hammett and co-workers^{3,4} shows the advantages of avoidance of any sampling or measurements on the system other than that implicit in the null device, furnishing of data directly on a linear plot or record, estimation of the accuracy of the determined rate and the freedom from side reactions from the linearity of the plot, lack of waste of reactants during the almost instantaneous setting up of the steady state, and, above all, determination of the rate of reaction at an unchanging and previously set group of concentrations. It shares the disadvantage with stirred-flow methods of giving only a single point on a kinetics curve per run, although the variable of the null device can be changed during the measurement if desired; in addition, the demand for clean and known reaction stoichiometry and the requirement that mixing be rapid relative to the reaction rate measured place limits on the type of reaction which can be studied by the SIC method. In the variation of Saldick and Hammett, in which continuous titration of the effluent of the stirred reactor is made, one sees something very close to the discovery of the SIC method (the Saldick-Hammett work was unknown to the authors prior to this). The simple switching of the titrator to the input of the reactor would have, along with the compensatory concentrations demanded, given the essence of SIC.

Acknowledgment. We acknowledge with thanks support from N.I.H. on Grant GMS-09023.

Reaction of Hydroxylamine with Thioesters

by R. Bruce Martin and Laura P. Henkle

Cobb Chemical Laboratory, University of Virginia,
Charlottesville, Virginia (Received June 19, 1964)

Two studies of the reaction of hydroxylamine with thioesters at room temperature have given apparently conflicting results. The reaction of hydroxylamine with acetylthioglycolic acid has been found to be first order in hydroxylamine at pH 5.4.¹ On the other hand, a second-order reaction in hydroxylamine has been reported for the reaction of hydroxylamine with butyl thiolacetate at pH 5.4-7.5.² In this note further

(1) L. H. Noda, S. A. Kuby, and H. A. Lardy, *J. Am. Chem. Soc.*, **75**, 913 (1953).

(2) T. C. Bruce and L. R. Fedor, *ibid.*, **86**, 738 (1964).

experimental results on the reaction of hydroxylamine with butyl thiolacetate resolve this contradiction. A new disagreement of our results with a previous interpretation is introduced and proposed solutions are discussed. Two previous studies agree that the main reaction is formation of acetohydroxamic acid and butyl mercaptan.^{1,3}

Experimental

n-Butyl thiolacetate was prepared by the addition of acetyl chloride to butyl mercaptan.⁴ A hydrochloride salt of hydroxylamine was used for most of the runs; however, some of the low concentration runs at pH 5.31 were made on a sulfate salt. Points for both salts appear in Fig. 1. Butyl thiolacetate disappearance was followed by measuring the decrease in absorption at 235 m μ on a Cary 14 spectrophotometer and calculating the observed first-order rate constants from initial slopes in the case of slow runs or from half-lives in the case of more rapid runs. Runs with intermediate rates gave nearly the same values by both methods. The ester concentration was usually about 2×10^{-4} M. Hydrolysis is negligible compared to aminolysis for all except the slowest runs. All experiments were performed at 25.0° and ionic strength 0.90 controlled with NaCl. Solutions were self-buffered by hydroxylamine and the pH was within ± 0.01 unit of recorded values.

Because the interpretation is sensitive to the value of the acid ionization constant of hydroxylammonium ion, K_a , used in the calculations, we determined pK_a at several acid-to-base ratios at 25.0° and ionic strength 0.90 controlled in two different ways. In the first, low concentrations of $\text{NH}_2\text{OH}\cdot\text{HCl}$, about 0.1 M, were used, and the ionic strength was made up to 0.90 with NaCl. In the second, pK_a was determined from solutions containing several ratios of $\text{NH}_2\text{OH}\cdot\text{HCl}$ and NH_2OH made by addition of NaOH to yield a total ionic strength of 0.90. Both types of ionic strength control yielded the same result of $pK_a = 6.03$. All pH readings were taken on a Radiometer TTT1a pH meter.

Results

Observed first-order rate constants, k' , for the disappearance of butyl thiolacetate divided by the total molar concentration of hydroxylamine in both acidic and basic forms, C , vs. total molar hydroxylamine concentration at three pH values are presented in Fig. 1. The results yield three straight lines with different slopes and with different intercepts. They may be represented by an equation of the form

$$k'/C = k_1(\text{H}_2\text{O})f + k_2Cf^2 \quad (1)$$

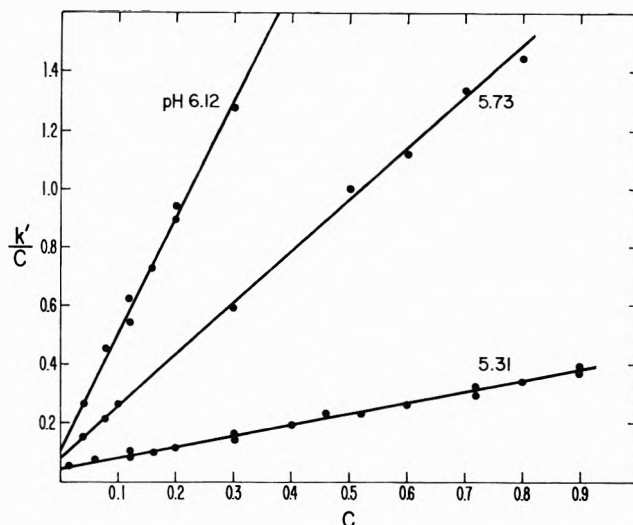


Figure 1. Observed first-order rate constants in min.^{-1} divided by total molar concentration of hydroxylamine, C , vs. C for reaction of butyl thiolacetate and hydroxylamine at three indicated pH values.

where the fraction of hydroxylamine in the free base form $f = K_a/[K_a + (\text{H}^+)]$ and $pK_a = 6.03$ for the cation of hydroxylamine at 25.0° and 0.9 ionic strength. This equation conforms to general base catalysis of the reaction of butyl thiolacetate with hydroxylamine. Water is the general base in the first term on the right of eq. 1 and NH_2OH in the second. Multiplication of the total molar hydroxylamine concentration by the fraction $f = K_a/[K_a + (\text{H}^+)]$ yields the molar concentration of free base NH_2OH .

Quantitative verification of the above equation over a sixfold range of (H^+) is obtained. Division of the intercept at each pH value by the corresponding value of f yields $k_1(\text{H}_2\text{O}) = 0.25, 0.24,$ and $0.22 \text{ min.}^{-1} \text{ M}^{-1}$ at pH 5.31, 5.73, and 6.12, respectively. Division of the slopes in Fig. 1 at each pH value by the appropriate value of f^2 yields $k_2 = 14.7, 15.9,$ and $13.0 \text{ min.}^{-1} \text{ M}^{-2}$ at the same three pH values. The water and hydroxylamine general base catalyzed reactions yield a Brønsted exponent of about 0.45, similar to that obtained for other ester aminolyses.⁵ This value indicates negligible hydroxide ion catalysis under our conditions, and none was observed.

Discussion

The results of Fig. 1 are simply interpreted by the single step reaction

(3) T. C. Bruice and L. R. Fedor, *J. Am. Chem. Soc.*, **86**, 739 (1964).

(4) F. W. Wenzel, Jr., and E. E. Reid, *ibid.*, **59**, 1089 (1937).

(5) R. B. Martin, A. Parcell, and R. I. Hedrick, *ibid.*, **86**, 2406 (1964).

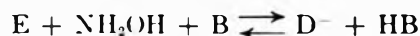


where E represents thiol ester and B a general base catalyst, which may be water or a second molecule of free base hydroxylamine under the conditions of this study. At low pH the line in Fig. 1 is nearly horizontal and general base catalysis by a second molecule of amine may go undetected. At high pH and any but the lowest amine concentrations general base catalysis by amine is much more important than that of water and the reaction may appear roughly as second order in hydroxylamine. The reaction is not simply second order in hydroxylamine, however, because the intercepts of Fig. 1 are significant and different for each pH value studied.

A tetrahedral addition intermediate has been strongly indicated in a displacement reaction at a thiol ester bond by the tripartite nature of the pH-rate profile in the acetyl transfer reaction of S-acetyl- β -mercaptoethylamine.⁶ In order to account for the pH-rate profile it was recognized that both acidic and basic forms of metastable intermediates are involved in any kinetic scheme.⁵ Furthermore, a tetrahedral intermediate has been suggested to account for the results in an aminolysis study of amino acid carboxylic acid esters.⁵ Since the straight lines of Fig. 1 give no evidence of leveling off, and since eq. 1 quantitatively accounts for the results, the formulation of reaction 2 is all that may be inferred and no positive information concerning formation of tetrahedral addition intermediates or the nature of the rate-limiting step can be gained from the pH studies reported here. Over the pH range (5.3–6.1) of this study Bruice and Fedor have interpreted their results as a general acid catalyzed reaction.² The results reported in Fig. 1 cannot be made to fit a general acid catalyzed formulation; only the general base catalyzed eq. 1 describes the results. The reaction of hydroxylamine with δ -thiolvalerolactone also appears to be general base catalyzed.⁷

At pH >6.1, Bruice and Fedor² report that the reaction of hydroxylamine with butyl thioacetate proceeds more slowly than eq. 1 would indicate. We are not well equipped to measure accurately the rapid rates at these relatively high pH values. Though the results are less precise than those presented in Fig. 1, what few results we have obtained tend to indicate that eq. 1 may not account for the data at pH >6.1. Accepting the data of Bruice and Fedor,² it is necessary to merge their results at pH >6.1 with our demonstration of general base catalysis at pH 5.3–6.1 rather than with general acid catalysis, as their interpretation implies.

Two mechanisms which yield apparent general base catalysis at low pH and an inhibition of the rate in more basic solutions are



and



where DH_2^+ , DH, and D^- represent a tetrahedral addition intermediate in various stages of protonation. It may easily be shown that application of the steady-state assumption to the addition intermediates in both mechanisms yields rate expressions with the appropriate requirements. At low pH the mechanisms describe apparent general base catalysis with the first step rate-limiting in the first mechanism and the second step rate-determining in the second. At high pH the second step is rate-limiting in the first mechanism and the first step in the second. In both mechanisms the high pH limit predicts apparent general acid catalysis in contrast to the demonstrated general base catalysis at low pH. The prediction of apparent general acid catalysis at high pH remains to be established experimentally. The reaction of hydroxylamine with butyl thioacetate appears to be the third class of reactions for which metastable tetrahedral addition intermediates in at least two stages of protonation appear to play a role. Other examples are transacetylation in S-acetyl- β -mercaptoethylamine⁶ and semicarbazone, oxime, and Schiff base formation and hydrolyses.⁸

Comparison of the general base catalyzed rates for the reactions of hydroxylamine and other amines such as glycine⁹ with thioesters demonstrates that the reactivity of hydroxylamine is comparatively high. Evidently the α -effect¹⁰ of special reactivity also applies in the reaction of hydroxylamine with straight-chain aliphatic thioesters.

Acknowledgment. This research was supported by a grant from the National Science Foundation.

(6) R. B. Martin and R. I. Hedrick, *J. Am. Chem. Soc.*, **84**, 106 (1962).

(7) T. C. Bruice, J. J. Bruno, and W. S. Chou, *ibid.*, **85**, 1659 (1963).

(8) R. B. Martin, *J. Phys. Chem.*, **68**, 1369 (1964).

(9) V. V. Koningsberger and J. Th. G. Overbeek, *Koninkl. Ned. Akad. Wetenschap. Proc.*, **B58**, 49 (1955).

(10) J. O. Edwards and R. G. Pearson, *J. Am. Chem. Soc.*, **84**, 16 (1962).